BIOCHIMICA ET BIOPHYSICA ACTA

BBA

3

MOLECULAR BASIS OF DISEASE

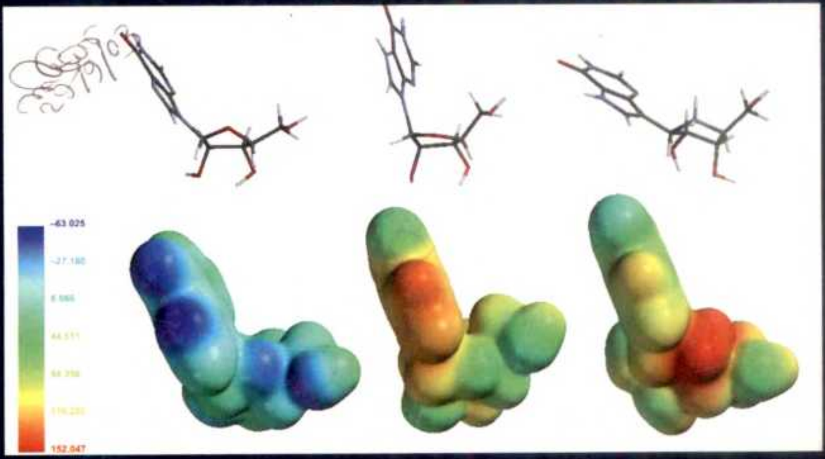

Special Issue:
Molecular Aspects of Chemotherapy

Guest Editor:
David Shugar

ELSEVIER

BIOCHIMICA ET BIOPHYSICA ACTA

BBA

Founded in 1947 by H.G.K. Westenbrink
Managing Editor, 1947-1964

HONORARY EXECUTIVE EDITOR
E.C. Slater (Southampton, UK)

EDITOR-IN-CHIEF: Peter C. van der Vliet (Utrecht, The Netherlands)

EXECUTIVE EDITORS:

Bioenergetics (including *Reviews on Bioenergetics*): **P.R. Rich** (London, UK) and **M. Wikström** (Helsinki, Finland)
Biomembranes (including *Reviews on Biomembranes*): **A.G. Lee** (Southampton, UK) and **P.L. Yeagle** (Storrs, CT, USA)
Molecular and Cell Biology of Lipids: **D.E. Vance** (Edmonton, AB, Canada) and **F. Spener** (Münster, Germany)
Protein Structure and Molecular Enzymology: **A. Fink** (Santa Cruz, CA, USA), **Y. Lindqvist** (Stockholm, Sweden) and **F. Lottspeich** (Martinsried bei München, Germany)
Molecular Cell Research: **E.L.F. Holzbaur** (Philadelphia, PA, USA) and **N. Pfanner** (Freiburg, Germany)
Gene Structure and Expression: **C.L. Peterson** (Worcester, MA, USA) and **P.C. van der Vliet** (Utrecht, The Netherlands)
Molecular Basis of Disease: **P.E. Fraser** (Toronto, ON, Canada) and **J.R. Riordan** (Scottsdale, AZ, USA)
General Subjects: **M. Fukuda** (La Jolla, CA, USA) and **C.G. Gahmberg** (Helsinki, Finland)
Reviews on Cancer: **N.C. Jones** (Manchester, UK)

Publication information: *Biochimica et Biophysica Acta* full subscription for 2002 consists of Volumes 1553-1603. Subscription prices are available upon requ from the Publisher or from the Regional Sales Office nearest you or from this journal's website (http://www.bba-direct.com). Further information is available this journal and other Elsevier Science products through Elsevier's website (http://www.elsevier.com). Subscription are accepted on a prepaid basis only and entered on a calendar year basis. Issues are sent by standard mail (surface within Europe, air delivery outside Europe). Priority rates are available upon reque Claims for missing issues should be made within six months of the date of dispatch.

BBA – Publication schedule for 2002
BBA is published according to a volume-numbering scheme that embraces all section of the journal.
Full subscription: 51 volumes

BIO-ENERGETICS including Reviews on Bioenergetics	BIO-MEMBRANES including Reviews on Biomembranes	GENE STRUCTURE AND EXPRESSION	GENERAL SUBJECTS	MOLECULAR AND CELL BIOLOGY OF LIPIDS	MOLECULAR BASIS OF DISEASE	MOLECULAR CELL RESEARCH	PROTEIN STRUCTURE AND MOLECULAR ENZYMOLOGY	REVIEW ON CANCER
5 volumes:	10 volumes:	6 volumes:	6 volumes:	6 volumes:	3 volumes:	5 volumes:	8 volumes:	2 volumes:
1553–1557 (15 issues)	1558–1567 (20 issues)	1574–1579 (18 issues)	1568–1573 (18 issues)	1580–1585 (18 issues)	1586–1588 (9 issues)	1589–1593 (15 issues)	1594–1601 (16 issues)	1602–160 (4 issues)

Submission
Authors should submit their manuscripts (four copies) to one of the appropriate Executive Editors at either of the following Editorial Offices:
BBA Editorial Secretariat, P.O. Box 1345, 1000 BH Amsterdam, The Netherlands. Tel.: (+31) 20 4853510; Fax: (+31) 20 4853506; E-mail: bba@elsevier.c
BBA Editorial Secretariat, 275 Washington Street, Newton, MA 02458, USA. Tel.: (+1) (617) 630-2244; Fax: (+1) (617) 630-2245; E-mail: us_bba@elsevier.c

Although most published *Review* articles are submitted on the invitation of the Executive Editor(s), authors of suitable (mini) reviews may also submit th work unsolicited (four copies) by sending their paper(s) to one of the Executive Editors of the appropriate section.

For detailed instructions on the preparation of electronic artwork, consult the Author Gateway from Elsevier Science at http://authors.elsevier.com

Author enquiries
For enquiries relating to the submission of articles (including electronic submission where available) please visit the Author Gateway from Elsevier Scienc http://authors.elsevier.com. The Author Gateway also provides the facility to track accepted articles and set up e-mail alerts to inform you of when an artic status has changed, as well as detailed artwork guidelines, copyright information, frequently asked questions and more.

Contact details for questions arising after acceptance of an article, especially those relating to proofs, are provided after registration of an article for publicatio

Authors in Japan please note: Upon request, Elsevier Science K.K. will provide authors with a list of people who can check and improve the English of t paper (*before submission*). Please contact our Tokyo office: Elsevier Science K.K., 9-15 Higashi-Azabu 1-chome, Minato-ku, Tokyo 106-0044; Tel.: (03)-5 5032; Fax: (03)- 5561-5045.

Colour figures
Colour figures are published at the author's expense: €340 for the first page and € 227 each subsequent page, excluding sales tax.

BBA has no page charges and 25 offprints are provided free to the corresponding author of each published paper.

Vol. 1587 Index (2-3)

BIOCHIMICA ET BIOPHYSICA ACTA

BBA

3

CUL- H05434-3-P25704

VOL. 1587
(2002)

P, 25, 704

BIOCHIMICA ET BIOPHYSICA ACTA

Founded in 1947 by H.G.K. Westenbrink, Managing Editor, 1947-1964

HONORARY EXECUTIVE EDITOR: E.C. Slater (Southampton, UK)

EDITOR-IN-CHIEF: Peter C. van der Vliet (Utrecht, The Netherlands)

EXECUTIVE EDITORS:

Bioenergetics (including *Reviews on Bioenergetics*): **P.R. Rich** (London, UK) and **M. Wikström** (Helsinki, Finland)
Biomembranes (including *Reviews on Biomembranes*): **A.G. Lee** (Southampton, UK) and **P.L. Yeagle** (Storrs, CT, USA)
Molecular and Cell Biology of Lipids: **D.E. Vance** (Edmonton, AB, Canada) and **F. Spener** (Münster, Germany)
Protein Structure and Molecular Enzymology: **A. Fink** (Santa Cruz, CA, USA), **Y. Lindqvist** (Stockholm, Sweden) and **F. Lottspeich** (Martinsried bei München, Germany)
Molecular Cell Research: **E.L.F. Holzbaur** (Philadelphia, PA, USA) and **N. Pfanner** (Freiburg, Germany)
Gene Structure and Expression: **C.L. Peterson** (Worcester, MA, USA) and **P.C. van der Vliet** (Utrecht, The Netherlands)
Molecular Basis of Disease: **P.E. Fraser** (Toronto, ON, Canada) and **J.R. Riordan** (Scottsdale, AZ, USA)
General Subjects: **M. Fukuda** (La Jolla, CA, USA) and **C.G. Gahmberg** (Helsinki, Finland)
Reviews on Cancer: **N.C. Jones** (Manchester, UK)

A.D. Albert (Storrs, CT, USA)
J.M. Allen (London, UK)
T.M. Allen (Edmonton, AB, Canada)
K. Altendorf (Osnabrück, Germany)
T. Arakawa (Thousand Oaks, CA, USA)
P.A. Baeuerle (Martinsried, Germany)
C. Balny (Montpellier, France)
U. Beisiegel (Hamburg, Germany)
D.J. Benos (Birmingham, AL, USA)
P. Bernardi (Padua, Italy)
H. Beug (Vienna, Austria)
C.L. Bevins (Cleveland, OH, USA)
C. Birchmeier (Berlin, Germany)
C. Borner (Freiburg, Germany)
I. Braakman (Utrecht, The Netherlands)
U. Brandt (Frankfurt am Main, Germany)
R.J. Bridges (Pittsburgh, PA, USA)
C.L. Brooks, III (La Jolla, CA, USA)
D.D. Busath (Provo, UT, USA)
M. Busslinger (Vienna, Austria)
F. Carrière (Marseille, France)
J.E. Celis (Copenhagen, Denmark)
G. Ceve (München Germany)
H. Chap (Toulouse, France)
A.H. Chishti (Boston, MA, USA)
R. Cogdell (Glasgow, UK)
N.H. Colburn (Frederick, MD, USA)
H.W. Cook (Halifax, NS, Canada)
P.F. Cook (Norman, OK, USA)
C. Cooper (Colchester, UK)
W.A. Cramer (West Lafayette, IN, USA)
B. de Crombrugghe (Houston, TX, USA)
R.D. Cummings (Oklahoma, OK, USA)
D.T. Curiel (Birmingham, AL, USA)
D.A. Day (Canberra, Australia)
J.P. Dekker (Amsterdam, The Netherlands)
B. De Strooper (Leuven, Belgium)
B. Desvergne (Lausanne, Switzerland)
G. Dickson (Egham, UK)
K.T. Douglas (Manchester, UK)
H.B. Dunford (Edmonton, AB, Canada)
D.H. Ellison (Portland, OR, USA)
T. Endo (Tokyo, Japan)
R.M. Epand (Hamilton, ON, Canada)
J. Fidy (Budapest, Hungary)
A. Fontana (Padua, Italy)
M. Fontecave (Grenoble, France)
J.-C. Fruchart (Lille, France)
J.T. Gallagher (Manchester, UK)
G. Geba (New Haven, CT, USA)
R. Geyer (Giessen, Germany)
T.E. Golde (Jacksonville, FL, USA)
Y. Goto (Osaka, Japan)
L.I. Grossman (Detroit, MI, USA)
A.P. Halestrap (Bristol, UK)
T.D. Heath (Madison, WI, USA)
J. Heberle (Jülich, Germany)
J. Horwitz (Los Angeles, CA, USA)
R.A. Houghten (San Diego, CA, USA)
G. Hübner (Halle/Saale, Germany)
R.C. Hughes (Mill Hill, UK)
S.W. Hui (Buffalo, NY, USA)
M. Ikeda-Saito (Cleveland, OH, USA)
A.N. Imbalzano (Worcester, MA, USA)
T. Iwatsubo (Tokyo, Japan)
R.L. Juliano (Chapel Hill, NC, USA)
W. Junge (Osnabrück, Germany)
T. Kiefhaber (Basel, Switzerland)
J.A. Killian (Utrecht, The Netherlands)
K. Kimata (Aichi Japan)
K.H. Kinne (Dortmund, Germany)
M. Kiso (Gifu, Japan)
W.N. Konings (Groningen, The Netherlands)
J.M. Kooter (Amsterdam, The Netherlands)
S.S. Krag (Baltimore, MD, USA)
I. Kudo (Tokyo, Japan)
K. Kuwajima (Tokyo, Japan)
W. Lamers (Amsterdam, The Netherlands)
T. Levade (Toulouse, France)
R. Lührmann (Göttingen, Germany)
G.I. Makhatadze (Lubbock, TX, USA)
B. Mannervik (Uppsala, Sweden)
W. Mäntele (Frankfurt am Main, Germany)
W.F. Marzluff (Chapel Hill, NC, USA)
R.N. McElhaney (Edmonton, AB, Canada)
M.G. McNamee (Davis, CA, USA)
R. Mendelsohn (Newark, NJ, USA)
J. Moody (Plymouth, UK)
C.P. Moran Jr. (Atlanta, GA, USA)
O.G. Mouritsen (Odense, Denmark)
S. Nagata (Osaka, Japan)
P.E. Nielsen (Copenhagen, Denmark)
K.H. Nierhaus (Berlin, Germany)
B. Nordén (Gothenburg, Sweden)
N. Oppenheimer (San Francisco, CA, USA)
J.F. Oram (Seattle, WA, USA)
N. Osheroff (Nashville, TN, USA)
R.P. Oude Elferink (Amsterdam, The Netherlands)
E. Padan (Jerusalem, Israel)
S. Parthasarathy (Atlanta, GA, USA)
C.L. Peters-Golden (Ann Arbor, MI, USA)
D.W. Pettigrew (College Station, TX, USA)
J. Philo (Thousand Oaks, CA, USA)
J.J.H.H.M. de Pont (Nijmegen, The Netherlands)
T. Pozzan (Padua, Italy)
N.C. Price (Glasgow, UK)
U.R. Rapp (Würzburg, Germany)
J.-L. Rigaud (Paris, France)
G.T. Robillard (Groningen, The Netherlands)
S. Rose-John (Kiel, Germany)
E. Rozengurt (Los Angeles, CA, USA)
F. Sachs (Buffalo, NY, USA)
M.S.P. Sansom (Oxford, UK)
S. Schuldiner (Jerusalem, Israel)
H.H. Schulz (New York, NY, USA)
K. Schulze-Osthoff (Münster, Germany)
J.M. Seddon (London, UK)
R. Serrano (Valencia, Spain)
D.L. Severson (Calgary, AB, Canada)
T. Shimizu (Tokyo, Japan)
H. Sjöström (Copenhagen, Denmark)
S.T. Smale (Los Angeles, CA, USA)
S. Spiegel (Washington, DC, USA)
W.D. Stein (Jerusalem, Israel)
B. Svensson (Copenhagen, Denmark)
G. Tigyi (Memphis, TN, USA)
K.F. Tipton (Dublin, Ireland)
J. Travis (Athens, GA, USA)
L.-C. Tsui (Toronto, ON, Canada)
B. Tümmler (Hannover, Germany)
G. van Meer (Amsterdam, The Netherlands)
M.H. Vos (Palaiseau, France)
E. Wahle (Halle/Saale, Germany)
M.J. Waring (Cambridge, UK)
D. Wemmer (Berkeley, CA, USA)
R. Wetzel (Knoxville, TN, USA)
G.R. Willsky (Buffalo, NY, USA)
D.C. Wilton (Southampton, UK)
R.F.A. Zwaal (Maastricht, The Netherlands)

Reviews on Cancer has its own independent Editorial Advisory Board.

BIOCHIMICA ET BIOPHYSICA ACTA

BBA

INTERNATIONAL JOURNAL OF BIOCHEMISTRY, BIOPHYSICS
AND MOLECULAR BIOLOGY

VOL. 1587 (2–3) (2002)

MOLECULAR BASIS OF DISEASE

Executive Editors: P.E. Fraser (Toronto, Canada) and
J.R. Riordan (Scottsdale, AZ, USA)

Section Editors:
C.L. Bevins
R.J. Bridges
B. De Strooper
G. Dickson
D.H. Ellison
G. Geba
T.E. Golde
R.A. Houghten
T. Iwatsubo
R.P. Oude Elferink
B. Tümmler

ELSEVIER
Amsterdam – London – New York – Oxford – Paris – Shannon – Tokyo

© 2002 Elsevier Science B.V. All rights reserved.

This journal and the individual contributions contained in it are protected under copyright laws by Elsevier Science B.V., and the following terms and conditions apply to their use:

Photocopying
Single photocopies of single articles may be made for personal use as allowed by national copyright laws. Permission of the Publisher and the payment of a fee is required for all other photocopying, including multiple or systematic copying, copying for advertising or promotional purposes, resale, and all forms of document delivery. Special rates are available for educational institutions that wish to make photocopies for non-profit educational classroom use.

Permissions may be sought directly from Elsevier Science via their homepage (http://www.elsevier.com) by selecting "Customer support" and then "Permissions". Alternatively you can send an e-mail to: permissions@elsevier.co.uk, or fax to: (+44) 1865 853333.

In the USA, users may clear permissions and make payments through the Copyright Clearance Center, Inc., 222 Rosewood Drive, Danvers, MA 01923, USA; phone: (+1) (978) 7508400, fax: (+1) (978) 7504744, and in the UK through the Copyright Licensing Agency Rapid Clearance Service (CLARCS), 90 Tottenham Court Road, London W1P 0LP, UK; phone: (+44) 20 7631 5555; fax: (+44) 20 7631 5500. Other countries may have a local reprographic rights agency for payments.

Derivative Works
Subscribers may reproduce tables of contents of prepare lists of articles including abstracts for internal circulation within their institutions. Permission of the Publisher is required for resale or distribution outside the institution.
Permission of the Publisher is required for all other derivative works, including compilation and translations.

Electronic Storage or Usage
Permission of the Publisher is required to store or use electronically any material contained in this journal, including any article or part of an article.

Except as outlined above, no part of this publication may be reproduced, stored in a retrieval system of transmitted in any form of by any means, electronic, mechanical, photocopying, recording or otherwise, without prior written permission of the Publisher.

Address permission requests to: Elsevier Science Global Rights Department, at the mail, fax and e-mail addresses noted above.

Notice
No responsibility is assumed by the Publisher for any injury and/or damage to persons or property as a matter of products liability, negligence or otherwise, or from any use or operation of any methods, products, instructions or ideas contained in the material herein. Because of the rapid advances in the medical sciences, in particular, independent verification of diagnoses and drug dosages should be made.

Although all advertising material is expected to conform to ethical (medical) standards, inclusion in this publication does not constitute a guarantee or endorsement of the quality or value of such product or of the claims made of it by its manufacturer.

Advertising Information
Advertising orders and enquiries can be sent to **USA, Canada and South America**: Mr Tino de Carlo, The Advertising Department, Elsevier Science Inc., 655 Avenue of the Americas, New York, NY 10010-5107, USA; phone: (+1) (212) 633 3815; fax: (+1) (212) 633 3820; e-mail: t.decarlo@elsevier.com. **Japan**: The Advertising Department, Elsevier Science K.K., 9-15 Higashi-Azabu 1-chome, Minato-ku, Tokyo 106-0044, Japan; phone: (+81) (3) 5561 5033; fax: (+81) (3) 5561 5047. **Europe and ROW**: Rachel Leveson-Gower, The Advertising Department, Elsevier Science Ltd., The Boulevard, Langford Lane, Kidlington, Oxford, OX5 1GB, UK; phone: (+44) (1865) 843565; fax: (+44) (1865) 843976; e-mail: r.leveson-gower@elsevier.co.uk.

Orders, claims, and product enquiries: please contact the Customer Support Department at the Regional Sales Office nearest you:
New York: Elsevier Science, PO Box 945, New York, NY 10159-0945, USA; phone: (+1) (212) 633 3730 [toll free number for North American customers: 1-888-4ES-INFO (437-4636)]; fax: (+1) (212) 633 3680; e-mail: usinfo-f@elsevier.com
Amsterdam: Elsevier Science, PO Box 211, 1000 AE Amsterdam, The Netherlands; phone: (+31) 20 4853757; fax: (+31) 20 4853432; e-mail: nlinfo-f@elsevier.nl
Tokyo: Elsevier Science, 9-15 Higashi-Azabu 1-chome, Minato-ku, Tokyo 106-0044, Japan; phone: (+81) (3) 5561 5033; fax: (+81) (3) 5561 5047; e-mail: info@elsevier.co.jp
Singapore: Elsevier Science, No. 1 Temasek Avenue, #17-01 Millenia Tower, Singapore 039192; phone: (+65) 434 3727; fax: (+65) 337 2230; e-mail: asiainfo@elsevier.com.sg
Rio de Janeiro: Elsevier Science, Rua Sete de Setembro 111/16 Andar, 20050-002 Centro, Rio de Janeiro - RJ, Brazil; phone: (+55) (21) 509 5340; fax: (+55) (21) 507 1991; e-mail: elsevier@campus.com.br [Note (Latin America): for orders, claims and help desk information, please contact the Regional Sales Office in New York as listed above]

USA mailing notice: *Biochimica et Biophysica Acta (Molecular Basis of Disease)* (ISSN 0925–4439) is published monthly except in February, May and September by Elsevier Science B.V. (P.O. Box 211, 1000 AE Amsterdam, The Netherlands).
Annual subscription price in the USA US$ 1165.00 (valid in North, Central and South America), including air speed delivery. Second class Periodicals postage paid at Jamaica, NY 11431.
USA POSTMASTER: Send address changes to *Biochimica et Biophysica Acta (Molecular Basis of Disease)*, Publications Expediting, Inc., 200 Meacham Avenue, Elmont, NY 11003.
AIRFREIGHT AND MAILING in the USA by Publications Expediting, Inc., 200 Meacham Avenue, Elmont, NY 11003.

Printed in The Netherlands
⊗ The paper used in this publication meets the requirements of ANSI/NISO Z39.48-1992 (Permanence of Paper).

Special Issue

Molecular Aspects of Chemotherapy

(8th International Symposium, Gdańsk, Poland, September 5-9, 2001)

Guest Editor:

David Shugar
Institute of Biochemisry & Biophysics, Polish Academy of Sciences,
and
Department of Biophysics, Institute of Experimental Physics, University of Warsaw, Warsaw, Poland

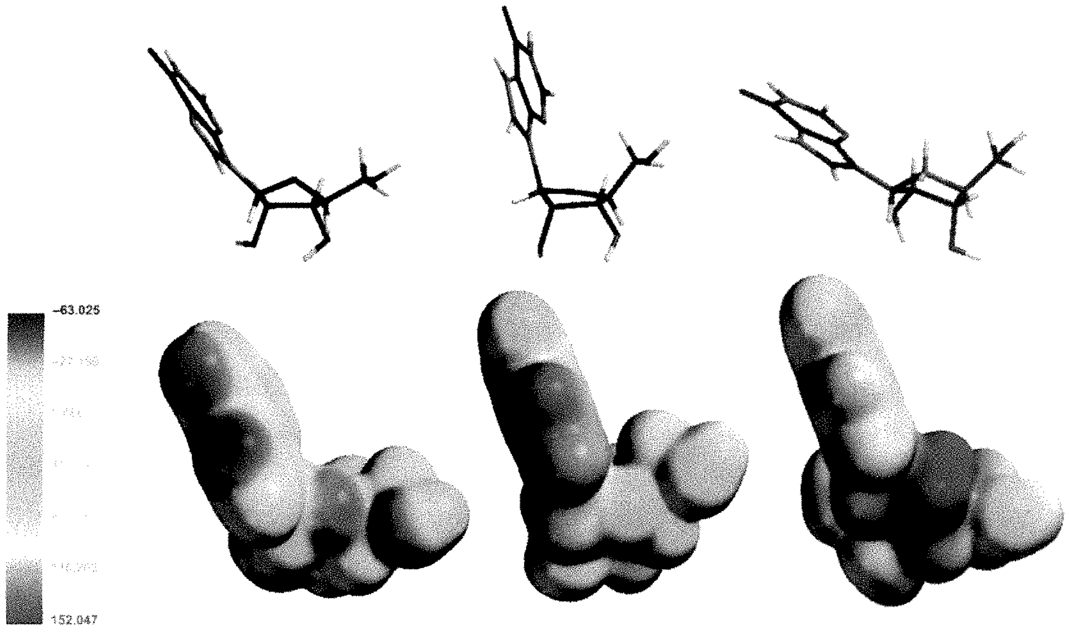

Molecular electrostatic potential surfaces for inosine (left), inosine at the transition state of purine nucleoside phosphorylase (center) and immucillin-H, a transition state analogue inhibitor (right).

8th International Symposium

on

MOLECULAR ASPECTS OF CHEMOTHERAPY

Gdańsk, Poland, September 5-9, 2001

Under the auspices of :

International Society of Chemotherapy
European Federation for Medicinal Chemistry
International Union Against Cancer

Organized by

Committee on Drug Research, Polish Academy of Sciences
Chemical Faculty, Technical University of Gdansk
Centre of Excellence in Molecular Biotechnology, Institute of Biochemistry & Biophysics, Polish Academy of Sciences, Warszawa

Organizing Committee:

Edward Borowski (Chairman)
Maria M. Bontemps-Gracz (Secretariat)
Marek Gniazdowski, Jerzy Konopa, Tadeusz Kulikowski, Bogdan Lesyng, Slawomir Milewski, Wojciech Rode, David Shugar

International Advisory Board: Federico M. Arcamone (Italy), Tom Bergan (Norway), Joseph R. Bertino (USA), Erik De Clercq (Belgium), William A. Denny (New Zealand), Paul Janssen (Belgium), Paolo Lombardi (Italy), J. Andrew McCammon (USA), Stephen Neidle (UK), Satoshi Omura (Japan), Hans-Hartwig Otto (Germany), Rajendra Prasad (India), Maria N. Preobrazhenskaya (Russia), Waldemar Priebe (USA), William H. Prusoff (USA), Alan C. Sartorelli (USA), Waclaw Szybalski (USA), Zhen-yi Wang (People's Republic of China), Witold Zatoński (Poland), Franco Zunino (Italy), Harald zur Hausen (Germany).

Sponsors: Professor E. Borowski, on behalf of the Organizing Committee, expresses appreciation to the following for financial support: Committee on Drug Research, Polish Academy of Sciences, Warszawa; Technical University of Gdańsk, Gdańsk, Poland; Centre of Excellence in Molecular Biotechnology, Institute of Biochemistry & Biophysics, Polish Academy of Sciences, Warszawa; Ministry of National Education, Warszawa; Taiho Pharmaceutical Co., Ltd., Saitama, Japan; Ingenieurburo Becker, Prisdorf, Germany; Polish Society of Cytometry, Warszawa; Sigma-Aldrich Sp. z.o.o., Poznań, Poland; Chrysalon S. A., Lyon, France; LONTZA-NATA S.C., Gdańsk, Poland; PROKOM Software S. A., Gdynia, Poland.

ELSEVIER
Biochimica et Biophysica Acta 1587 (2002) vii
BIOCHIMICA ET BIOPHYSICA ACTA
BBA
www.bba-direct.com

Preface

This special issue comprises the texts of most of the invited lectures, in many instances largely of a review nature, presented at the 8th International Symposium on "Molecular Aspects of Chemotherapy" (8th IS-MAC), held in the historic city of Gdańsk, on the Polish Baltic coast, September 5-9, 2001. It is fitting that the Editors of BBA considered it appropriate for these proceedings to appear in the series on "Molecular Basis of Disease".

While serendipity and random screening continue to play a substantial role in the search for new drugs, particularly as regards identification of lead compounds (but to an ever increasing extent by high through-put screening of large compound libraries), current remarkable advances in molecular and structural biology, genomics and proteomics now dominate, to an ever increasing extent, the application of so-called rational approaches to drug design and development, in many instances relying on the molecular basis of a given disease. It has become standard practice to investigate both the mechanisms of action of drugs, and the sources of undesirable side-effects, at the molecular level, with the aid of broad interdisciplinary approaches, both theoretical and experimental, to improve existing drugs and to develop more effective ones.

It is with the foregoing in mind that the Gdańsk International Symposia have been organized biannually since 1984 by Professor E. Borowski of the Technical University of Gdansk, with the support of the Committee on Drug Research of the Polish Academy of Sciences, initially under the auspices of the International Society of Chemotherapy and, currently, also of the European Federation of Medicinal Chemistry, and the International Union Against Cancer.

As in the past, invited lectures, and a number of poster sessions, covered up-to-date achievements, and future perspectives, on molecular mechanisms of inhibition of cellular functions and metabolism, with emphasis on the design and mechanisms of action of chemotherapeutic agents for treatment of bacterial, neoplastic, parasitic and viral diseases. The range of disciplines represented was very broad, including theoretical and experimental chemists and physicists, molecular biologists, biochemists, virologists, clinicians, etc. from both academia and nonprofit research centers, as well as the pharmaceutical and biotechnology sectors.

Plans are already under way for the 9th International Symposium, to be held again in Gdańsk, in early September, 2003. Proposals of prospective participants for review lectures will be welcomed and will receive due consideration by the Organizing Committee during preparation of the scientific program.

We are indebted to Professor E. Borowski and Dr. Maria Bontemps-Gracz, to all those who helped out with review of manuscripts, and to Pat Crowley of the BBA Editorial Secretariat, for their unstinted assistance in the preparation of this special number.

David Shugar

ELSEVIER

Biochimica et Biophysica Acta 1587 (2002) 107–117

BIOCHIMICA ET BIOPHYSICA ACTA
BBA
www.bba-direct.com

Review

Development of transition state analogues of purine nucleoside phosphorylase as anti-T-cell agents

Vern L. Schramm*

Department of Biochemistry, Albert Einstein College of Medicine, 1300 Morris Park Avenue, Forch. 308, Bronx, NY 10461, USA

Received 24 January 2002; accepted 24 January 2002

Abstract

Newborns with a genetic deficiency of purine nucleoside phosphorylase (PNP) are normal, but exhibit a specific T-cell immunodeficiency during the first years of development. All other cell and organ systems remain functional. The biological significance of human PNP is degradation of deoxyguanosine, and apoptosis of T-cells occurs as a consequence of the accumulation of deoxyguanosine in the circulation, and dGTP in the cells. Control of T-cell proliferation is desirable in T-cell cancers, autoimmune diseases, and tissue transplant rejection. The search for powerful inhibitors of PNP as anti-T-cell agents has culminated in the immucillins. These inhibitors have been developed from knowledge of the transition state structure for the reactions catalyzed by PNP, and inhibit with picomolar dissociation constants. Immucillin-H (Imm-H) causes deoxyguanosine-dependent apoptosis of rapidly dividing human T-cells, but not other cell types. Human T-cell leukemia cells, and stimulated normal T-cells are both highly sensitive to the combination of Imm-H to block PNP and deoxyguanosine. Deoxyguanosine is the cytotoxin, and Imm-H alone has low toxicity. Single doses of Imm-H to mice cause accumulation of deoxyguanosine in the blood, and its administration prolongs the life of immunodeficient mice in a human T-cell tissue xenograft model. Immucillins are capable of providing complete control of in vivo PNP levels and hold promise for treatment of proliferative T-cell disorders. © 2002 Elsevier Science B.V. All rights reserved.

Keywords: Immucillin; Purine nucleoside phosphorylase; T-cell leukemia; Autoimmunity; Transition state; Apoptosis; Deoxyguanosine toxicity

1. Introduction

Purine nucleoside phosphorylase (PNP) catalyzes the reversible reactions [1]:

$$\begin{array}{l}\text{(deoxy)guanosine} \qquad\qquad \text{guanine}\\ \text{(deoxy)inosine} + PO_4 \leftrightarrow \text{hypoxanthine} + \alpha - D\\ \quad - \text{(deoxy)ribose } 1 - PO_4\end{array}$$

Prepared by her earlier discovery of severe combined immunodeficiency in adenosine deaminase deficiency, Eloise Giblett discovered that infants with a rare T-cell immunodeficiency lacked PNP [2]. Subsequent studies indicated that T-cell deficiency resulted from altered pathways of purine metabolism. Deoxyguanosine accumulates in the blood as a result of PNP deficiency, and is transported and phosphorylated by T-cell deoxynucleoside kinases to form pathologically elevated levels of dGTP specifically in these cells [3–6]. Inhibition of PNP was soon identified as a target for the regulation of undesirable T-cell proliferation, a campaign was launched for the discovery of powerful inhibitors [7]. Thirty-three patents for PNP inhibitors were listed by 1998, but clinical trials with the best of these inhibitors failed to show adequate inhibition to cause regulation of activated T-cells [8]. Type IV autoimmune disorders are a primary disease target for PNP inhibitors, and are caused by inappropriate activation of T-cells by self-antigens [9]. These disorders include rheumatoid arthritis, psoriasis, inflammatory bowel disorders and multiple sclerosis. In addition, T-cell leukemias and lymphomas would be primary proliferative targets for PNP inhibitors.

Inhibitor design for patented PNP inhibitors have used structure–activity relationships and structure-based design,

---

Abbreviations: PNP, purine nucleoside phosphorylase; Imm-H, Immucillin-H [(1*S*)-1-(9-deazahypoxanthin-9-yl)-1,4-dideoxy-1,4-imino-D-ribitol]; Imm-G, Immucillin-G [(1*S*)-1-(9-deazaguanin-9-yl)-1,4-dideoxy-1,4-imino-D-ribitol]; dNTP, 2′-deoxynucleoside 5′-triphosphates; K_i^*, the equilibrium dissociation constant between an enzyme and inhibitor that includes a slow onset step; IL-2, interleukin-2; SCID mice, a mouse strain with genetically derived severe combined immunodeficiency; BCX-1777 = Immucillin-H

* Tel.: +1-718-430-2813; fax: +1-718-430-8565.
E-mail address: vern@aecom.yu.edu (V.L. Schramm).

0925-4439/02/$ - see front matter © 2002 Elsevier Science B.V. All rights reserved.
PII: S0925-4439(02)00073-X

in which the catalytic site of PNP containing substrate or product analogues or weak inhibitors was sequentially filled with newly designed analogues followed by subsequent structural and kinetic characterization and refinement of catalytic site contacts [10,11]. The most powerful inhibitors obtained by these methods are in the low nanomolar range for inhibitory dissociation constants [8].

During this period, methods were also being developed for the experimental analysis of enzymatic transition states by kinetic isotope effect analysis [12–15]. Analogues that resemble enzymatic transition states capture the enzymatic forces used for catalysis and convert catalytic energy into binding energy, resulting in powerful inhibition [15–17]. The inversion of configuration at the anomeric carbon of PNP substrates suggested a nucleophilic displacement reaction, but compounds synthesized to resemble such transition states bound no better than substrates. The possibility of transition state inhibitor design for PNP became a reality in 1995, when the transition state structure was resolved from studies of the chemical mechanism and kinetic isotope effects [18–20]. This review provides a summary of the biology, enzymology and chemistry that led to the development of the immucillins, PNP inhibitors of sufficient specificity and affinity to cause deoxguanosine accumulation in mammals.

2. PNP in human nucleotide metabolism

The (deoxy)nucleoside substrates of PNP are normally absent from the blood as a result of robust PNP catalytic activity in the intestine, liver, erythrocytes, lymphocytes, spleen and kidney [21,22]. The activity of PNP in the blood alone causes injected nucleoside substrates to undergo phosphorolysis with a half-life of a few seconds. However, PNP substrates accumulate in the blood and urine of PNP-deficient patients, replacing uric acid, which is dramatically reduced in both blood and urine (summarized in Ref. [23]). This experiment of nature confirms that the pathway of purine nucleoside degradation requires PNP, and without it, nucleosides accumulate, purine bases for salvage pathways and degradation are depleted, and the rate of de novo purine synthesis increases [22]. Overproduction of purines is not accompanied by purine precipitation disorders in PNP deficiency since the (deoxy)nucleosides are more soluble than uric acid. Blood levels of these metabolites are significant and the primary purine excretion products are urinary nucleosides. In addition, (deoxy)nucleoside salvage increases because of excess substrate availability. Dividing T-cells express an active deoxycytidine kinase, whose normal role is the salvage of deoxycytidine to form dCMP → → dCTP for DNA synthesis in activated T-cells [24]. When deoxyguanosine accumulates beyond normal levels, deoxycytidine kinase accepts deoxguanosine to form dGMP → → dGTP. The allosteric inhibition site for dGTP on ribonucleotide diphosphate reductate inhibits cellular formation of dCDP and dUDP [25], thereby preventing DNA synthesis (Fig. 1).

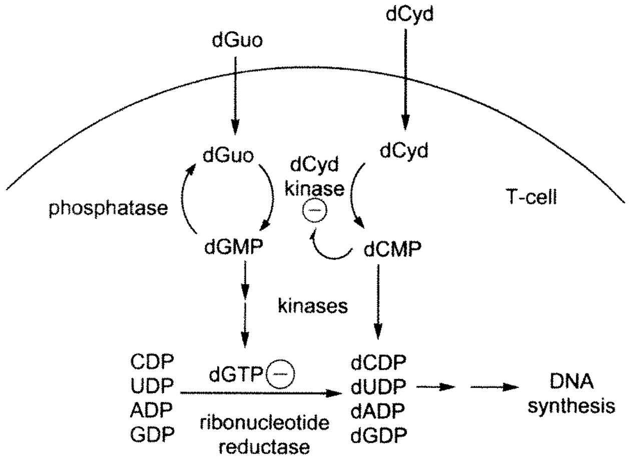

Fig. 1. Pathways of deoxyguanosine (dGuo) metabolism in human T-cells. The normal function of deoxycytidine (dCyd) kinase is salvage of dCyd arising from apoptosis of other T-cells. It is regulated by dCMP product inhibition. Excess dGuo is phosphorylated to dGMP by the same enzyme, but dGMP is not a good product inhibitor. Increased dGTP allosterically inhibits ribonucleotide reductase, preventing DNA synthesis and T-cell division.

Factors that have been proposed to make the disorder specific for T-cells include high capacity for deoxynucleoside transport, high expression levels of deoxycytidine kinase, and low levels of phosphatases for dGMP. The normal response to antigenic T-cell stimulation requires clonal expansion from a few cells with the appropriate receptors to the T-cell mass required for an activated T-cell response. This response requires rapid T-cell proliferation involving relatively large quantities of DNA synthesis. Activation of T-cells under conditions of unbalanced dNTPs induces apoptosis, and instead of T-cell proliferation, depletion of T-cells occurs [26]. T-cell populations are exquisitely poised for apoptotic responses, since ~ 99% of developing thymocytes do not receive an antigenic stimulatory response and undergo apoptosis under conditions of normal development [27].

Knowledge of human purine metabolism is required to understand PNP deficiency since the metabolism of deoxyguanosine differs between humans and mice. Mice made genetically deficient in PNP do not undergo T-cell depletion, and some of the cellular changes observed in the mice are attributed to the action of a mitochondrial deoxyguanosine kinase [28–30]. A useful outcome of this finding is that xenografts of human T-cells into mice allow analysis of the effects of PNP inhibitors with only modest effects on the host T-cell profile [31,32].

3. Catalytic properties of PNP

Mammalian PNPs catalyze the phosphorolysis of the natural 6-oxypurine (deoxy)nucleosides and are inactive against (deoxy)adenosine or the pyrimidine (deoxy)nucleosides [33]. The catalytic efficiency is high for the deoxyguanosine nucleoside that characterizes its biological function [1]. The homotrimer exhibits Michaelis–Menten initial rate kinetics and has no known physiologic regulatory sites. PNP is present at micromolar concentrations in blood cells and is coupled to a substrate trapping phenomenon known as catalytic commitment [14,19]. Every collision of a substrate (deoxy)nucleoside with the catalytic site leads to its trapping and conversion to product. With the high concentrations of enzyme, catalytic commitment, and low K_m value, cells containing high concentrations of PNP are assured of the virtual absence of free deoxyguanosine. Mitochondrial deoxyguanosine metabolism is exempt from this degree of deoxyguanosine removal since PNP is absent and a deoxyguanosine kinase is present [34]. Repair and recycling of mitochondrial DNA generates deoxguanosine that is proposed to remain in this compartment.

Under nonphysiological conditions, in the absence of phosphate, PNP catalyzes a slow hydrolysis of inosine in which the first catalytic site releases ribose, but binds tightly (1 pM) to the hypoxanthine product [18]. The enzyme stalls in a complex with hypoxanthine bound at one of the three catalytic sites, demonstrating sequential catalytic site action now made familiar from the action of F_1F_0 ATPase [35]. The relevance of sequential site catalytic action for cancer therapy is the prediction that inhibition of any single subunit of the PNP homotrimer will lead to full inactivation of catalytic activity. Immucillin-H (Imm-H) has been shown to act by this mechanism and one-third-the-sites inhibition is discussed in more detail in Section 5.

4. Transition state analysis and PNP

Chemical transition states occur within the lifetime of a single bond vibration, approximately 10^{-13} s, and direct observations have only been successful in gas-phase studies by laser spectroscopy [36]. Enzymatic transition states have similar lifetimes and can be established from intrinsic kinetic isotope effects by the experimental steps: (1) synthesis of substrates with specific atomic labels surrounding the bonds being made and broken in the transition state; (2) establish chemical or kinetic conditions where the catalytic step (transition state formation) is the first irreversible step in the catalytic cycle, or where intrinsic isotope effects can be obtained; (3) measure a family of kinetic isotope effects for the atoms whose bonding patterns are perturbed at the transition state; and (4) use bond vibrational analysis coupled to quantum chemistry predictions to match the kinetic isotope effects to the transition state structure. Geometric and electrostatic properties of the transition state can be used as an atomic blueprint to design stable analogues. Chemical synthesis of the transition state analogues provides the desired inhibitors for enzymatic and biological testing against the target. The experimental implementation of these steps has been outlined in reviews [14,37–39], and will be exemplified here with the example of PNP.

PNP demonstrated no kinetic isotope effects with inosine and phosphate as substrates, because of catalytic commitment, and bound products reforming substrates on the enzyme prior to product release [19]. Intrinsic isotope effects were established using the hydrolytic reaction, where catalysis is slow and no back-reaction occurs, and also with arsenate (AsO_4) as a phosphate analogue [20]. Arsenate reacts to form α-D-ribose 1-arsenate, an unstable intermediate that hydrolyzes rapidly and prevents the products of the reaction from reforming as substrates prior to release from the enzyme. The intrinsic isotope effects were used to establish the transition state features

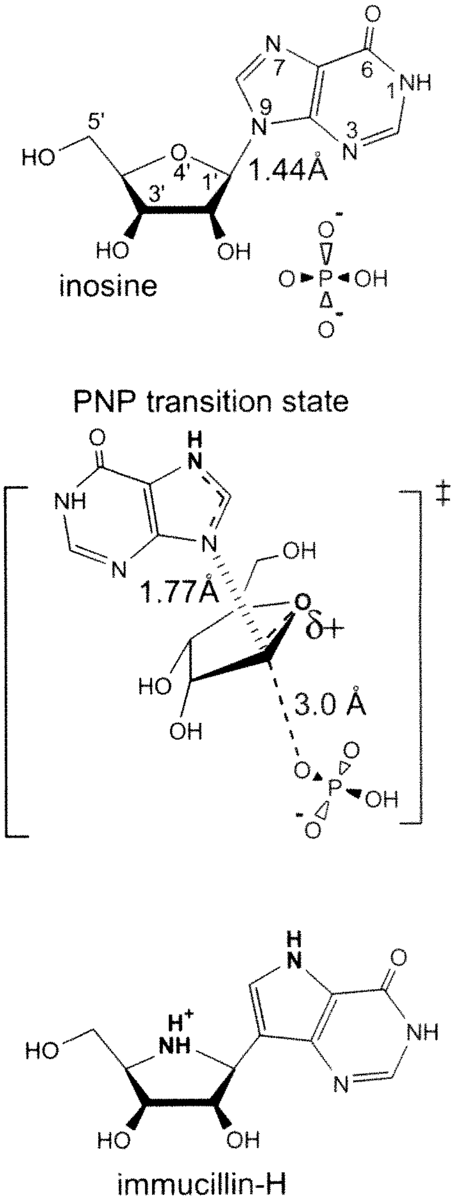

Fig. 2. Substrate (inosine), transition state and transition state inhibitor (Imm-H) for PNP. The geometry of the transition state is shown looking at C1′ of the ribosyl ring. Features of the transition state are highlighted in bold, and also appear in the inhibitor [51].

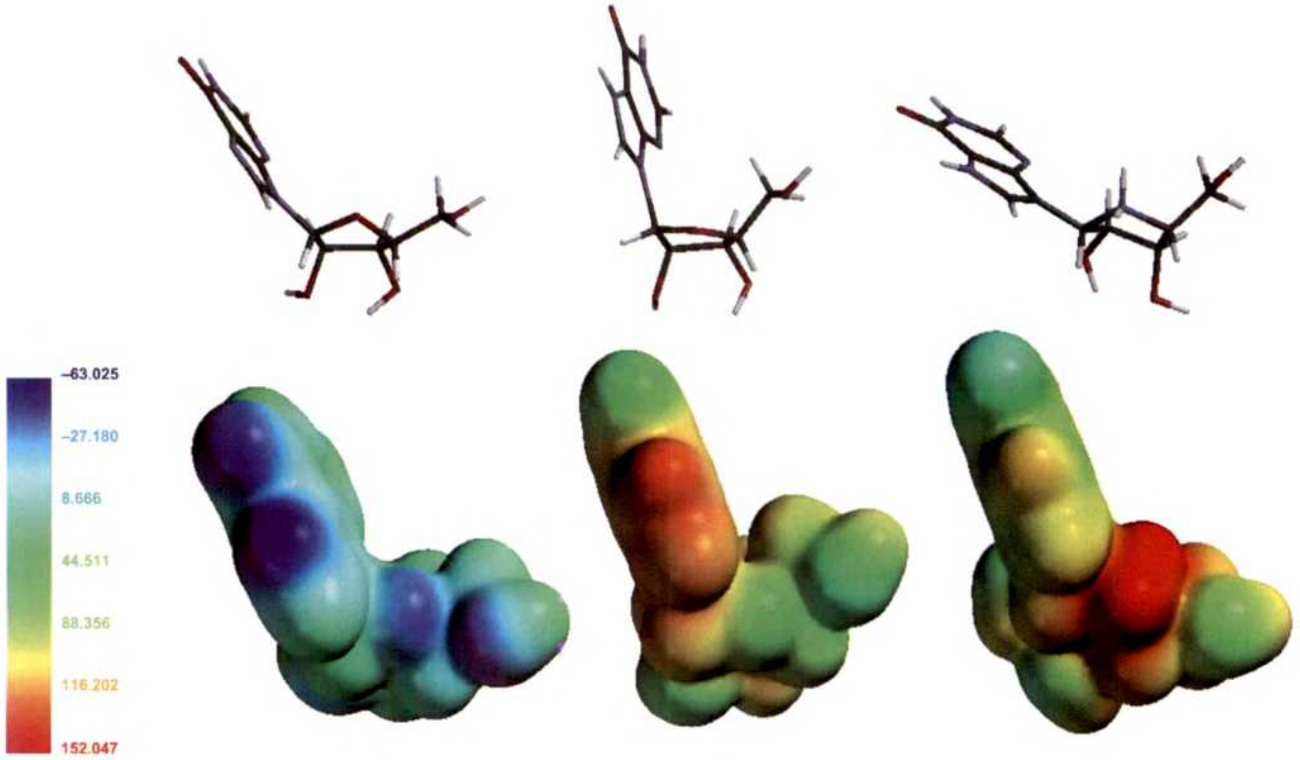

Fig. 3. Molecular electrostatic potential surfaces for inosine, the transition state of PNP and Imm-H. The geometry around the 5′-hydroxymethyl group and the ribosidic-base torsion angles were fixed at the values established from the X-ray crystallographic studies. In the transition state, N7 was protonated and the N9–C1′ bond was fixed at 1.8 Å. The electron distribution was calculated using Gaussian 98 with the STO-3G basis set.

of 0.38 Pauling bond order to the hypoxanthine leaving group, protonation or hydrogen-bond stabilization to N7 of the purine, van der Waals contact to the attacking phosphate nucleophile, and conversion of the ribosyl group to a partially charged ribooxacarbenium ion [20]. The results established that the chemical property of the transition state is dissociative, rather than the associative property expected for a symmetric nucleophilic displacement (Fig. 2). The results provided the first sufficiently complete structure of the transition state to permit the design of transition state inhibitors. These features were also consistent with the transition states established for other purine N-ribohydrolases [40,41], and with an earlier isotope effect measured for the PNP from *Escherichia coli* [42].

5. Imm-H design and synthesis

The features of the transition state structure for PNP were used to design a chemically stable isologue (same molecular shape and volume) to act as transition state analogue inhibitor (Fig. 2). Inosine was the substrate for transition state analysis, and the transition state inhibitor was designed to mimic this transition state. The ribosyl group at the transition state is a partially positively charged ribooxacarbenium ion, and was mimicked in Imm-H with an iminoribitol structure. In Imm-H, the imino group[1] is protonated with a pK_a of 6.5, providing a partial positive charge at physiological pH values. The bond to the leaving group purine is more than 60% dissociated at the transition state, causing the pK_a at N7 of the purine to increase. Immucillins were designed with a carbon–carbon ribosidic link to provide chemical stability relative to the carbon–nitrogen link in normal substrates. This carbon–ribosidic bond also changes the bond conjugation pattern of the inhibitor, increasing the pK_a of N7 from ~ 2 in inosine to ~ 9 in Imm-H. The pK_a of this group at the transition state has not been measured, but is elevated toward 7 or above as the ribosidic bond is broken. Nitrogen-7 is proposed to be a site of protonation or hydrogen bonding by the enzyme to form the transition state, since the bonding electrons must be accommodated in the leaving group and protonation at N7 or a favorable H-bond at this site assists in electron departure from the N-ribosidic bond. The elevated pK_a at this site constitutes one of the transition state features. The ability of N7-methyl substituted inosine and guanosine molecules to act as substrates of PNP [43] indicates that the Asn243 that H-bonds to this site is sufficiently flexible to accommodate an N7-methyl substituent. The methyl group provides a similar

---

[1] The IUPAC nomenclature for the ring nitrogen in sugar analogues accepts amino or imino. The original description of the deoxyiminoribitols [64] used the imino nomenclature, which we maintain here.

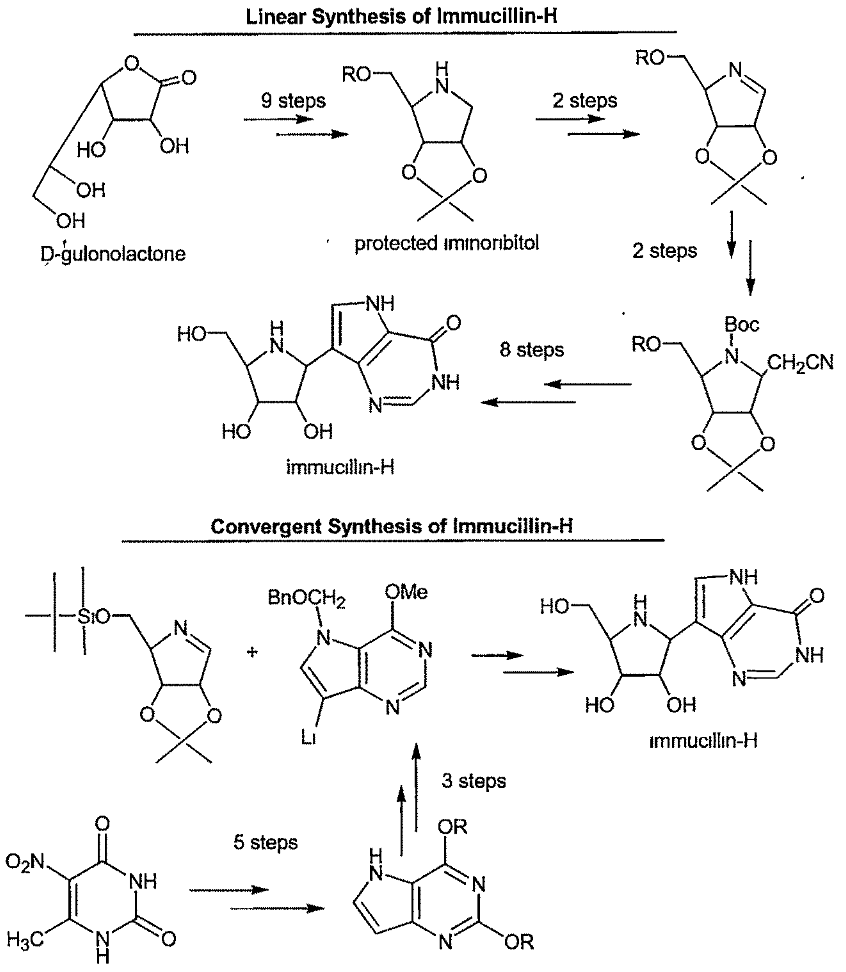

Fig. 4. Chemical synthesis of Imm-H by the linear and convergent pathways. These methods have been published and details of synthesis are provided in Refs. [48,50].

electronic effect in assisting the purine to accept bonding electrons.

The atomic replacements between inosine and Imm-H make an insignificant change in atomic size, but a dramatic change in the molecular electrostatic potential surface[2] (Fig. 3) [44]. Analysis of the molecular electrostatic potential surface similarity between transition state and transition state inhibitors for several enzymes have established that this and the atomic size correlate with the affinity between enzyme and inhibitor [45,46]. A departure from other inhibitor design programs was to eliminate features of the phosphate anion. Transition state analysis revealed that phosphate is not bonded at the transition state, but is in van der Waals contact, with less than 2% covalent bond order [20]. This finding established that the nucleoside contacts dominate transition state interactions, and that the phosphate binding site will fill with inorganic phosphate, an abundant component of cells.

Chemical synthesis of Imm-H was first accomplished in a linear sequence of over 20 steps, beginning with D-gulonolactone, and based on the precedents of aryl and alkyl 1-substituted iminoribitols [47,48] and for synthesis of 9-deazapurine nucleosides [49] (Fig. 4). This synthetic procedure builds the protected iminoribitol from D-gulonolactone, followed by the stepwise addition of the components of the 9-deazahypoxanthine and deprotection. The chemical stability of the compound is revealed in the final deprotection step, reflux in concentrated HCl. Although this route provided the first access to Imm-H and Imm-G (the 9-deazaguanine analogue), it was not suitable for large-scale synthesis. An improved synthetic route produced activated and protected iminoribitol and 9-deazahypoxanthine in separate procedures, followed by reaction of the two halves of the molecule [50] (Fig. 4).

6. Inhibition of PNPs by Imm-H

Imm-H and Imm-G inhibited both bovine and human PNP, and exhibited the characteristics of slow-onset tight-binding inhibitors [51]. Slow-onset inhibitors bind as reversible competitive ligands, followed by an isomerization of the enzyme that causes increased inhibitor binding affinity [52]. The initial binding phase for the bovine enzyme exhibits a K_i of 41 nM, followed by a time-dependent, slow onset ($k_5 = 0.06$ s^{-1}) increase of affinity by a factor of 2000, to give a K_i* of 23 pM (Fig. 5). For the human enzyme the initial binding phase is rapid, and the K_i* value is 72 pM (Table 1). The affinity of Imm-H is approximately one million times that for the inosine substrate. The size and molecular electrostatic potential properties of the inhibitor are similar to the transition state [51]. Binding affinity is dictated by on and off rates, in the case of tight-binding inhibitors, that for k_5 and k_6, the conformational changes that provide entry and departure from the tightly bound transition state analogue complex (Fig. 5). Release of Imm-

---

[2] The molecular electrostatic potential surface is the force observed by a point charge at every location on the van der Waals surface of the molecule [44].

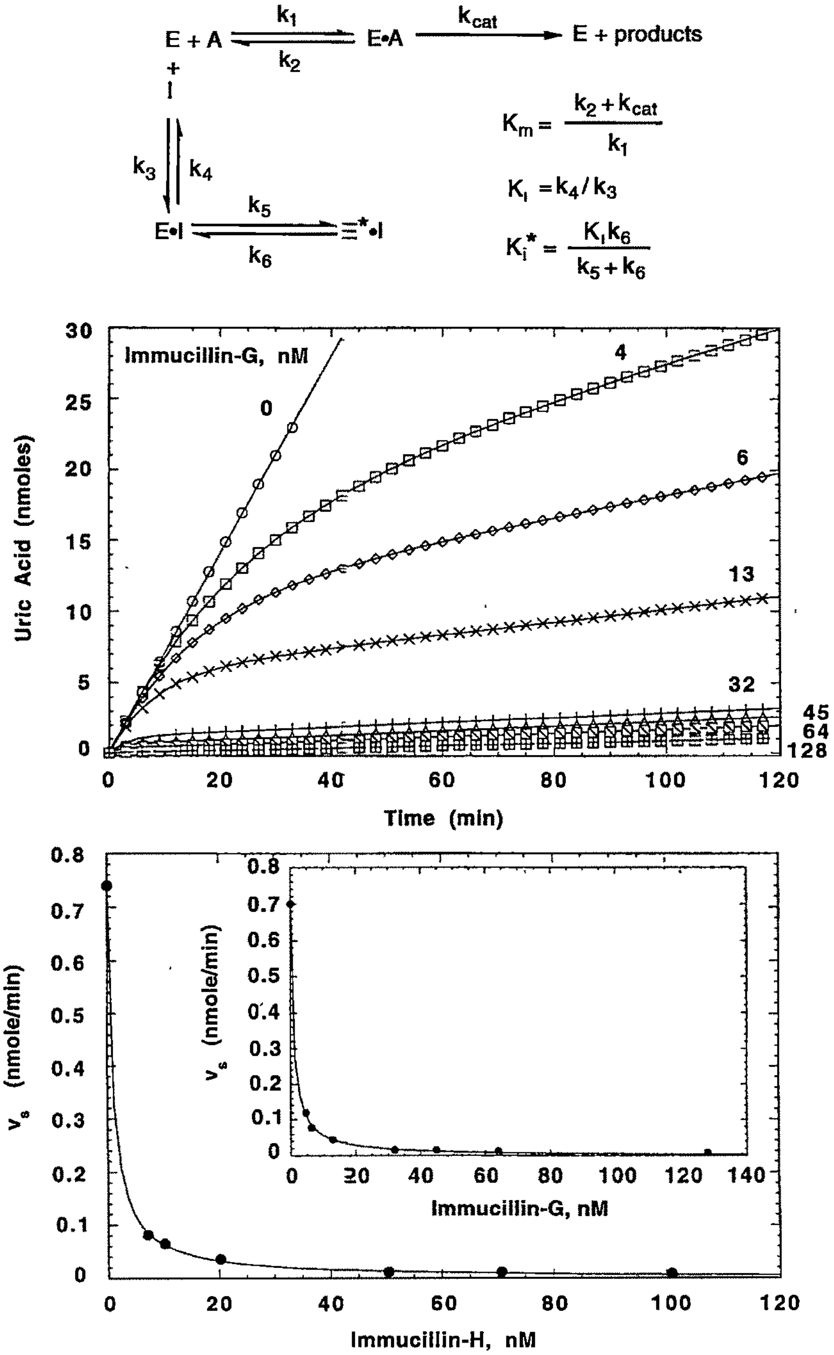

Fig. 5 The kinetics of PNP inhibition by Imm-G and Imm-H. E, A, P and I represent PNP, inosine, products and Imm-H or Imm-G, respectively. The rate constants k_5 and k_6 are the rate constants for formation of E*·I and its conversion to E·I. E·I is the rapidly reversible, weakly bound inhibitor and E*·I represents a conformational change that accompanies tight-binding of the inhibitor. The center panel demonstrates the slow-onset of inhibition, and the bottom panel demonstrates the post-slow onset rate (v_s) as a function of inhibitor concentration using inosine at a concentration of 200 times its K_m value. The reactions were coupled to xanthine oxidase to yield uric acid as product. Adapted from reference [51].

Table 1
Inhibition of PNPs by Imm-H

PNP source	K_i* (pM)	K_m (μM)	K_m/K_i
Human	73	40[a]	550,000
Bovine	23	17[a]	740,000
Mycobacterium tuberculosis	28	26[b]	930,000
Plasmodium falciparum	600	5[a]	8000

[a] The K_m values for inosine

[b] The K_m values for 6-thio-7-methylguanosine.

H from the bovine enzyme has a $t_{1/2}$ of 5 h, compared to that from the human enzyme of 8 min. Inhibition was correlated with moles of Imm-H bound per trimeric enzyme, and the results established that binding of one Imm-H molecule per trimer, with the affinity described above, is responsible for the inhibition [51]. These inhibitory and binding studies established that Imm-H was the most powerful PNP inhibitor yet described. It acts by complete inhibition of PNP catalytic activity by filling only one of the three catalytic sites of the trimer of PNP [51]. This result was unexpected based on earlier kinetic studies and the previous X-ray crystal structures of PNP, all of which indicated equivalent, noninteracting sites in a symmetric trimer with identical subunit occupancy with substrate and inhibitor analogues [53]. Binding studies of Imm-H to bovine PNP indicated that filling of the first subunit is responsible for the inhibition, and occurs with the highest affinity, followed by saturation of the second and third sites with affinity orders of magnitude lower than the first subunit [54]. However, at large Imm-H excess, all three sites can be occupied. The impact of the partial-sites inhibition for cancer therapy is that physiological inhibition of PNP activity can be achieved with only one molecule of inhibitor bound for every three PNP subunits.

Although other applications of PNP inhibitors are beyond the scope of this review, Imm-H is also a powerful inhibitor of PNP from *M. tuberculosis* and *P. falciparum* [55,56] (Table 1). The crystal structure of *M. tuberculosis* has been solved with Imm-H and phosphate binding, revealing that this enzyme is similar to the mammalism enzyme [57]. In contrast, the PNP from *P. falciparum* is more closely related to the hexameric *E. coli* PNP, and has a lower affinity for Imm-H. Despite the lowered affinity, the addition of Imm-H to cultures of human erythrocytes infected with *P. falciparum* causes purine-less death of the parasites under physiological culture conditions [58].

7. Structure of PNP·Imm-H·PO$_4$

Crystals of bovine PNP with Imm-H and phosphate at the catalytic sites were grown in the presence of large excesses of phosphate and of Imm-H to saturate the catalytic sites [59]. The crystals, demonstrated uniform catalytic site filling at all three sites, and permitted the collection of the highest resolution data (1.5 Å) obtained for a complex of the bovine enzyme. The structure was compared to structures of bovine PNP solved earlier [53], to reveal the structural changes as the enzyme progresses from the Michaelis complex to the transition state and product complexes. Imm-H is situated in the catalytic sites similar to the position of inosine, except that contacts to the enzyme are closer to most parts of the complex (Fig. 6). Comparison of substrate, Imm-H and product complexes to the actual transition state structure docked into the catalytic site permitted analysis of the atomic motion that occurs as substrates are converted to products, and the analysis of the similarity between Imm-H and the docked transition state.

One surprising result is that the reaction occurs by unprecedented atomic motion in the reaction coordinate. These steps include; (a) enzymatic immobilization of the purine ring and phosphate, (b) generation of the ribooxacarbenium ion transition state with the participation of neighboring group oxygens from phosphate and the 5′-hydroxyl to stabilize the ribooxacarbenium ion and (c) migration of the C1′ anomeric carbon over the relatively long distance of 1.7 Å between the enzymatically stabilized nucleophiles, while the 5′-region of the ribosyl group remains immobile. This mechanism is a departure from solution chemistry, and also occurs in other ribosyltransferases. This mechanism has been called a nucleophilic displacement by electrophilic migration, and reflects the ability of enzymes to accomplish atomic motion of reactive groups in the protected environment of the catalytic site, (exemplified here by the ribooxacarbenium ion) [59,60]. A second important lesson of the study was that the transition state analogue and the actual transition state occupy the same positions, except for the 0.4 Å difference in structures resulting from the C–C covalent bond in the transition state analogue [59]. A third surprise from the structure with Imm-H involves the nature of the enzymatic activation of the leaving group purine and the formation of the ribooxacarbenium ion. Enzyme-immobilized water oxygens form a proton transfer bridge to solvent and provide the protons required for a H-bond and a protonation of the leaving group hypoxanthine. Activation of the leaving group occurs by; (a) a hydrogen bond to N7 shared to the side-chain carbonyl oxygen of Asn243, where the H-bonded proton is provided by the water bridge, and (b) protonation of O6 by an immobilized water that is sandwiched between O6 and Glu201. Near-optimal contacts at every H-bond donor/acceptor pair on Imm-H and phosphate at the catalytic site indicated that improvement on the binding affinity by changing the structure of the immucillins might be difficult.

8. Effect of Imm-H on transformed and activated T-cells

Human T-cell immunodeficiency from PNP loss is completely dependent on the presence of deoxyguanosine and its conversion to dGTP [31,32]. Cultures of human T-cell leukemia lines were tested for growth in the presence of Imm-H with and without deoxyguanosine (Fig. 7). The selective inhibition of T-cells, only in the presence of deoxyguanosine, established that Imm-H is biologically available, and is dependent on deoxyguanosine. Analysis of treated cells established that Imm-H with deoxyguanosine caused the accumulation of dGTP [31]. Under conditions of 20 μM deoxyguanosine in the medium, the IC_{50} for Imm-H was 0.4 to 5 nM for reduction of thymidine incorporation in cells cultured for 3 days (Fig. 7). The toxicity of Imm-H and deoxyguanosine is rescued by deoxycytidine, a metabolite known to prevent dGTP accumulation by substrate competition for deoxycytidine kinase and by dCMP product inhibition of the enzyme [61] (Fig. 7C). Seventeen non-T-cell lines were unaffected by Imm-H at 10 μM, several thousand-fold above the effective dose for human leukemic T-cells [31]. T-cells isolated from normal human volunteers are not affected by Imm-H unless they are stimulated to divide, and show increasing sensitivity with increased stimulation [31,32] (Fig. 8). Peripheral human T-cells stimulated to rapid division by excess interleukin-2 (IL-2) and mononuclear cells were inhibited by Imm-H and deoxguanosine with an IC_{50} value of 5 nM. The results demonstrate that inhibition of PNP by

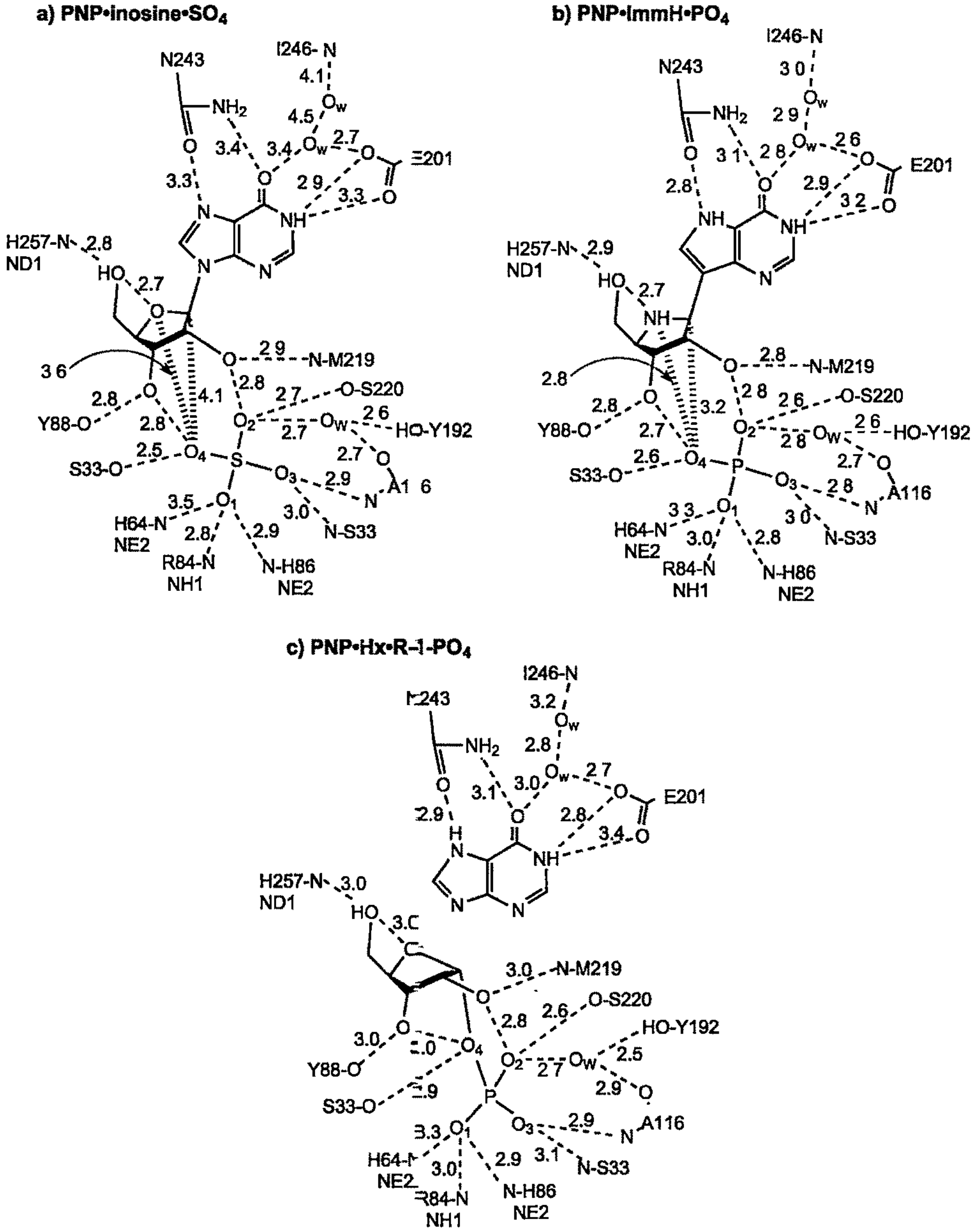

Fig 6. The structures of bovine PNP with substrate analogues (inosine + SO_4), transition-state complex (Imm-H + PO_4) and products (hypoxanthine + ribose 1-PO_4) bound at the catalytic sites. Substrate and product complexes are from Ref. [53], and this figure is reproduced from Ref. [59] Hydrogen bond distances are shown in angstroms. Red indicates bonds that shorten significantly and blue indicates bonds that lengthen significantly in the conversion of (a) to (b), and of (b) to (c).

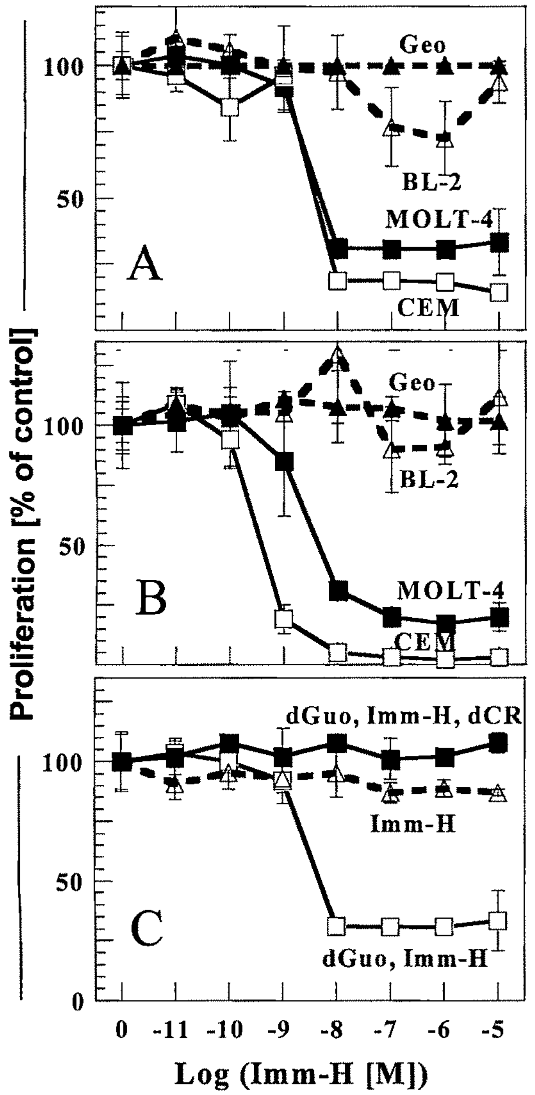

Fig 7 The inhibition of human T-cell leukemia lines by Imm-H and deoxyguanosine. MOLT-4 and CEM are human T-cell leukemia cell lines, while Geo is a human colon carcinoma cell line and BL-2 is a human B-cell leukemia cell line. Panel A demonstrates the response of cell lines to 20 μM deoxyguanosine and the indicated concentrations of Imm-H after 3 days of culture and analysis of cell activity by the viability dye WST-1 Panel B is the same experiment, but with cell viability tested by tritium–thymidine incorporation Panel C demonstrates that Imm-H alone has no effects on CEM cell viability, and that deoxycytidine (dCR) rescues against the effects of Imm-H and deoxyguanosine by the mechanism shown in Fig 1 This figure is reproduced from Ref [31]

Imm-H is sufficient to cause dGTP accumulation and to induce apoptosis specifically in rapidly dividing T-cells.

9. Imm-H in mice and effects on T-cell xenografts

Bioavailability of Imm-H was tested in mice by a comparison of oral and injected doses, and established that oral availability is high, at 63% of the injected dose [32]. A key test of the biological effectiveness of the inhibitor is the ability to increase the concentration of deoxyguanosine in blood. Both humans and mice have high concentrations of PNP in erythrocytes; therefore, deoxyguanosine is not present at detectable levels in the blood. A single oral dose of 10 mg/kg Imm-H to mice increased the plasma concen-

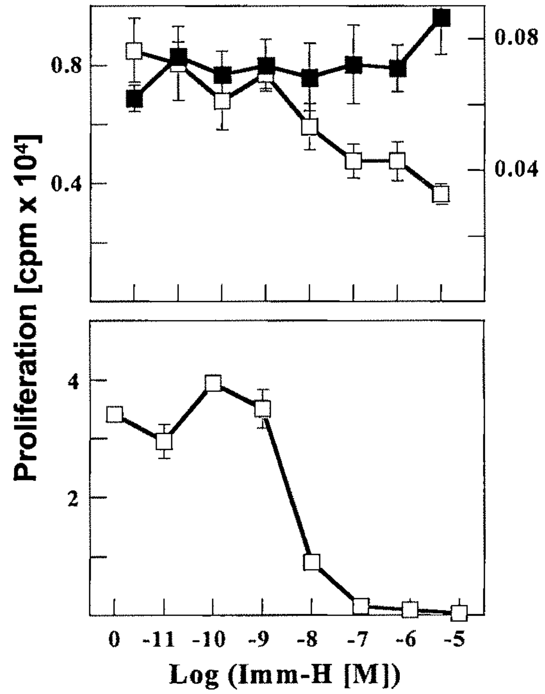

Fig 8 The effect of Imm-H on [^{3}H]thymidine incorporation by human T-lymphocytes Reproduced from Ref. [31] In the top panel, peripheral T-cells from four donors were incubated for 3 days with no stimulation (solid squares) or with physiological levels of IL-2 In the bottom panel, cells were treated with excess IL-2 and mitomycin-treated mononuclear cells, followed by 6-day incubation Error bars represent the results averaged for the T-cells of four donors.

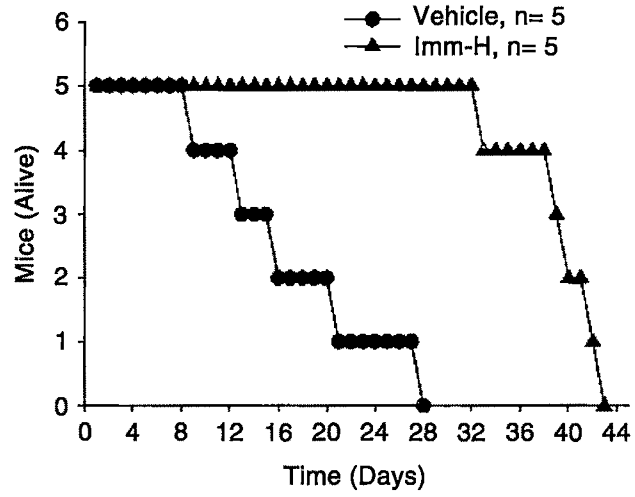

Fig 9. The effect of Imm-H on the human lymphocyte–mouse xenograft tissue rejection model. The results are reproduced from Ref [32] SCID (hu-PBL) mice were treated with 20 mg/kg Imm-H for 5 days, and the natural killer lymphocytes depleted with anti-ASGMI antibodies Mice were irradiated and human buffy coat cells were injected The group with Imm-H treatment (triangles) survived approximately twice as long as the control group

tration of deoxyguanosine to a peak concentration of 5 μM over a period of 3 h, establishing in vivo efficacy for whole-body PNP inhibition in the mouse [32]. Elevated deoxyguanosine also occurs in the human genetic deficiency of PNP, and plasma levels are reported to be in the range of 3 to 17 μM [23]. Thus, a single oral dose of Imm-H to mice can achieve a deoxyguanosine concentration that is adequate to cause T-cell deficiency in humans. These experiments were a prelude to the use of a mouse model of human immune transplantation rejection that has been developed and extended to SCID mice [62,63]. In this protocol, human peripheral blood lymphocytes (PBLs) are engrafted into SCID mice, and are stimulated to divide by the host antigens. Expansion of the human PBL cells causes the SCID mice to die from xenogenic graft vs host disease, approximately 4 weeks after engraftment. Death is caused by infiltration of human lymphocytes into the tissues of the host mouse. The effects of Imm-H were tested by pretreating mice with Imm-H to elevate the deoxyguanosine levels, followed by engraftment and continued treatment with Imm-H to determine effects on life span Control animals were treated in the same way, except that no Imm-H was given. The results demonstrated a two-fold increase in life span compared to control mice (Fig. 9) [32]. These results establish the ability of Imm-H to influence human T-cell proliferation in the mouse model of host vs. graft disease, and therefore the ability to obtain sufficient inhibition of whole body PNP to sustain elevated deoxyguanosine levels.

10. Prospectus for applications of Imm-H

Based on the enzymology, cell culture and animal model work published to date, the prospects for Imm-H to function as an in vivo anti-T-cell agent are the most encouraging yet obtained in the 26 years since Eloise Giblett discovered the genetic deficiency of PNP [2]. Recent studies on the mouse model of Imm-H immunosuppression of human T-cells concluded with the statement that this inhibitor is the first known example of a PNP inhibitor that elevates deoxyguanosine in mice similar to the levels observed in PNP-deficient patients [32]. Phase I/II clinical trials of Imm-H against human T-cell leukemia have been initiated under the trade name of BCX-1777.

Acknowledgements

Research in this laboratory is supported by research grants from the National Institutes of Health. Greg Kicska and Robert Miles have been instrumental in the research on PNP and Imm-H in this laboratory. Alexander Fedorov, Wuxian Shi and Steven Almo are responsible for the X-ray crystallography. Richard Furneaux and Peter Tyler of Industrial Research, New Zealand, pioneered the synthesis of Imm-H, and Shanta Bantia of BioCryst has had a central role in cellular and animal studies. The author thanks Brett Lewis for help in preparing figures.

References

[1] J.D. Stoeckler, C. Cambor, R.E. Parks Jr., Biochemistry 19 (1980) 102–107

[2] E.R. Giblett, A.J. Ammann, D.W. Wara, R. Sandman, L.K. Diamond, Lancet 1 (1975) 1010–1013

[3] T.A. Krenitsky, J.V. Tuttle, G.W. Koszalka, I.S. Chen, L.M. Beachman, J.L. Rideout, G.B. Elion, J. Biol. Chem. 251 (1976) 4055–4061.

[4] D.A. Carson, J. Kaye, J.E. Seegmiller, Proc. Natl. Acad. Sci. U. S. A. 74 (1977) 5677–5681

[5] B.S. Mitchell, E. Mejias, P.E. Daddona, W.N. Kelly, Proc. Natl. Acad. Sci. U. S. A. 75 (1978) 5011–5014.

[6] B. Ullman, L.J. Gudas, S.M. Clift, D.W. Martin Jr., Proc. Natl. Acad. Sci. U. S. A. (1979) 1074–1078.

[7] S.E. Ealick, Y.D. Babu, C.E. Bugg, M.D. Erion, W.C. Guida, J.A. Montgomery, J.A. Secrist III, Proc. Natl. Acad. Sci. U. S. A. 88 (1991) 11540–11544

[8] P.E. Morris, J.A. Montgomery, Expert Opin. Ther. Pat. 8 (1998) 283–299

[9] C.A. Janeway Jr., P. Travers, Immunobiology The Immune System in Health and Disease, 3rd edn., Current Biology/Garland Publishing, London and New York, 1997.

[10] M.D. Erion, S. Niwas, J.D. Rose, S. Ananthan, M. Allen, J.A. Secrist III, Y.S. Babu, et al., J. Med. Chem. 36 (1993) 3771–3783

[11] W.C. Guida, R.D. Elliott, H.J. Thomas, J.A. Secrist III, Y.S. Babu, C.E. Bugg, M.D. Erion, S.E. Ealick, J.A. Montgomery, J. Med. Chem. 37 (1994) 1109–1114

[12] J. Rodgers, D.A. Femec, R.J. Schowen, J. Am. Chem. Soc. 104 (1982) 3263–3268

[13] W.W. Cleland, Methods Enzymol. 87 (1982) 625–641.

[14] D.B. Northrop, Biochemistry 14 (1975) 2644–2651.

[15] V.L. Schramm, Ann. Rev. Biochem. 67 (1998) 693–720

[16] W.P. Jencks, Adv. Enzymol. 43 (1975) 219–410

[17] R. Wolfenden, Nature 223 (1969) 704–705.

[18] P.C. Kline, V.L. Schramm, Biochemistry 31 (1992) 5964–5973

[19] P.C. Kline, V.L. Schramm, Biochemistry 32 (1993) 13212–13219.

[20] P.C. Kline, V.L. Schramm, Biochemistry 34 (1995) 1153–1162.

[21] H.A. Simmonds, L.D. Fairbanks, G.S. Morris, G. Morgan, A.R. Watson, P. Timms, B. Singh, Arch. Dis. Child 62 (1987) 385–391

[22] A. Cohen, D. Doyle, D.W. Martin Jr., A.J. Ammann, N. Engl. J. Med. 295 (1976) 1449–1454

[23] M.S. Hershfield, B.S. Mitchell, in: C.R. Scriber, A.L. Beaudet, W.S. Sly, D. Valle (Eds.), The Metabolic Basis of Inherited Disease, 8th edn., McGraw-Hill, NY, 2001, pp. 2585–2624, Chapter 109

[24] N.S. Datta, D.S. Shewach, B.S. Mitchell, I.H. Fox, J. Biol. Chem. 264 (1989) 9359–9364

[25] L. Thelander, P. Reichard, Ann. Rev. Biochem. 48 (1979) 133–158

[26] M.L. Agarwal, A. Agarwal, W.R. Taylor, O. Chernova, Y. Sharma, G.R. Stark, Proc. Natl. Acad. Sci. U. S. A. 95 (1998) 14775–14780.

[27] C.D. Surh, J. Sprent, Nature 372 (1994) 100–103

[28] E.R. Mably, E. Fung, F.F. Snyder, Genome 32 (1989) 1026–1032

[29] F.F. Synder, J.P. Jenuth, E.R. Mably, R.K. Mangat, Proc. Natl. Acad. Sci. U. S. A. 94 (1997) 2522–2527

[30] E. Arpaia, P. Benveniste, A. Di Cristofano, Y. Gu, I. Dalal, S. Kelly, M. Hershfield, et al., J. Exp. Med. 191 (2000) 2197–2208.

[31] G.A. Kicska, K. Long, H. Horig, C. Fairchild, P.C. Tyler, R.H. Furneaux, V.L. Schramm, H.L. Kaufman, Proc. Natl. Acad. Sci. U. S. A. 98 (2001) 4593–4598.

[32] S. Bantia, P.J. Miller, C.D. Parker, S.L. Ananth, L.L. Horn, J.M. Kilpatrick, P.E. Morris, T.L. Hutchison, J.A. Montgomery, J.S. Sandhu, Int. Immunopharmacol. 1 (2001) 1199–1210.

[33] B.K. Kim, S. Cha, R E Parks Jr., J. Biol. Chem. 243 (1968) 1763–1770.

[34] E. Arpaia, P Benveniste, A. Di Cristofano, Y. Gu, I. Dalal, S. Kelly, M. Hershfield, P.P. Pandolfi, C.M Roifman, A Cohen, J. Exp Med 191 (2000) 2197–2207

[35] P.D Boyer, Ann Rev. Biochem 66 (1997) 717–749.

[36] D. Zhong, S Ahmad, P Y Cheng, A H. Zewail, J. Am Chem. Soc. 119 (1997) 2305–2306

[37] V L Schramm, Methods Enzymol. 308 (1999) 301–355.

[38] P J Berti, Methods Enzymol. 308 (1999) 355–397.

[39] B.B. Braunheim, S D. Schwartz, Methods Enzymol. 308 (1999) 398–426

[40] B A. Horenstein, D W. Parkin, B Estupinan, V.L. Schramm, Biochemistry 30 (1991) 10788–10795

[41] F. Mentch, D.W. Parkin, V L Schramm, Biochemistry 26 (1987) 921–930

[42] R.L Stein, E.H. Cordes, J. Biol Chem. 256 (1981) 767–772.

[43] A Bzowaka, E. Kulikowska, E. Darzynkiewicz, D. Shugar, J Biol. Chem. 263 (1988) 9212–9217

[44] B A. Horenstein, V.L Schramm, Biochemistry 32 (1993) 9917–9925

[45] C K. Bagdassarian, V L Schramm, S D. Schwartz, J. Am. Chem Soc 118 (1996) 8825–8836

[46] B.B. Braunheim, R.W Miles, V.L Schramm, S D Schwartz, Biochemistry 38 (1999) 16076–16083.

[47] B A Horenstein, R F Zabinski, V.L Schramm, Tetrahedron Lett 34 (1993) 7213–7216.

[48] G.B Evans, R H. Furneaux, G.J Gainsford, V.L Schramm, P.C. Tyler, Tetrahedron 56 (2000) 3053–3062.

[49] M I Lin, W Y. Ren, B A. Otter, R S. Kline, J Org Chem 48 (1983) 780–788

[50] G.B. Evans, R.H. Furneaux, T.L. Hutchison, H S Kezar, P E Morris, V.L Schramm, P.C. Tyler, J Org Chem. 66 (2001) 5723–5730.

[51] R.W. Miles, P.C Tyler, R H. Furneaux, C.K. Bagdassarian, V.L. Schramm, Biochemistry 37 (1998) 8615–8621

[52] J.F Morrison, C.T Walsh, Adv Enzymol. Relat. Areas Mol. Biol 61 (1988) 201–301

[53] C. Mao, W.J Cook, M Zhou, A.A. Fedorov, S.C. Almo, S E Ealick, Biochemistry 37 (1998) 7135–7146

[54] F Wang, R W. Miles, G A. Kicska, E. Nieves, V L. Schramm, R.H. Angeletti, Protein Sci. 9 (2000) 1660–1668.

[55] L A. Basso, D S Santos, W Shi, R.H Furneaux, P.C. Tyler, V L Schramm, J.S Blanchard, Biochemistry 40 (2001) 8196–8203.

[56] G A Kicska, P C. Tyler, G B Evans, R H Furneaux, K. Kim, V L Schramm, J Biol Chem. 277 (2002) 3219–3225.

[57] W Shi, L A Basso, D.S. Santos, P C. Tyler, R.H. Furneaux, J.S. Blanchard, S C. Almo, V.L. Schramm, Biochemistry 40 (2001) 8204–8215.

[58] G A. Kicska, P C. Tyler, G B. Evans, R.H. Furneaux, V.L. Schramm, K. Kim, J Biol Chem 277 (2002) 3226–3231.

[59] A Fedorov, W. Shi, G A Kicska, E. Fedorov, P.C Tyler, R H. Furneaux, J.C Hanson, G J Gainsford, J.Z. Larese, V.L Schramm, S C. Almo, Biochemistry 40 (2001) 853–860

[60] V.L Schramm, W. Shi, Curr. Opin Struct. Biol 11 (2001) 657–665

[61] W R. Osborne, C R. Scott, Biochem. J. 214 (1983) 711–718.

[62] D E. Mosier, R J Guilizia, S M. Baird, D B. Wilson, Nature 335 (1988) 256–259

[63] J.S Sandhu, R Gorczynski, B. Shpitz, S. Gallinger, H Nguyen, N A. Hozumi, Transplantation 60 (1995) 179–184

[64] G.W J Fleet, J C. Son, Tetrahedron 44 (1988) 2637–2647

ELSEVIER

Biochimica et Biophysica Acta 1587 (2002) 118–125

BIOCHIMICA ET BIOPHYSICA ACTA
BBA
www.bba-direct.com

Review

A simple model to predict blood–brain barrier permeation from 3D molecular fields

Frédéric Ooms, Peter Weber, Pierre-Alain Carrupt, Bernard Testa*

Institut de Chimie Thérapeutique, Section de Pharmacie, BEP, Université de Lausanne, CH-1015 Lausanne, Switzerland

Received 6 September 2001; accepted 15 October 2001

Abstract

We report a four-component partial least squares discriminant analysis (PLS) model for the prediction of blood–brain barrier (BBB) permeation using descriptors derived from 3D molecular fields. The 3D fields were transformed by VolSurf into suitable 1D descriptors, which were correlated to the ratio of blood–brain partitioning measured at steady state in rats (log $C_{\mathrm{brain}}/C_{\mathrm{blood}}$). The model so obtained sheds light on molecular properties influencing BBB permeation. It can also be used in the virtual screening of new chemicals. © 2002 Elsevier Science B.V. All rights reserved.

Keywords: Blood–brain barrier; Brain penetration; QSAR

---

1. Introduction

The blood–brain barrier (BBB) has peculiar characteristics among the various physiological barriers. Diffusion of drugs across this endothelium separating the blood from the central nervous system (CNS) is in fact more restrictive than elsewhere. Endothelial cells provide a crucial interface between blood and tissues. The free diffusion of chemicals across endothelia is prevented by endothelial tight junctions, the permeability of which varies considerably depending on tissue and conditions. In peripheral tissues (intestine, kidney, salivary gland), these cell barriers have fenestrations enabling relatively facile exchange of water and solutes. In contrast, the endothelial barrier separating the blood from the CNS is characterized by tight junctions of severely limited permeability (excluding molecules with a diameter larger than 20 Å), no fenestrae and an attenuated pinocytosis [1,2].

As a common feature, both peripheral and blood–brain endothelial cells have significant metabolic activity [3]. Moreover, and in contrast to what was for long the common view, the special features of the BBB seem to be subject to endogenous regulation [1].

Thus, the BBB is far from being a simple barrier. Understanding its structure and functions, as well as the physicochemical and biological factors that control solute transfer, is a problem of great currency in pharmaceutical research. This is true not only for the design and development of CNS-active agents, but also for drugs that must be forbidden entry into the CNS to avoid unwanted side-effects, as exemplified by anti-histamines [4] and β-blockers [5]. Hence, in drug discovery, early assessment of BBB permeation is of great importance, and in vitro and in vivo techniques have been devised for this purpose [6].

Besides these experimental techniques, computational approaches have also been developed to predict the BBB permeation of new chemicals since the experimental determination of BBB penetration is laborious, expensive, time-consuming and requires a sufficient quantity of pure compound, often in radiolabeled form, to obtain good experimental data. Therefore, a fast and reliable computational method to predict BBB permeation at an early stage of discovery could help decrease the attrition curve since it would allow the virtual screening of many compounds, prior to synthesis. Over the years, various authors have attempted to predict BBB transport using lipophilicity (log *P*) [7–9], solvatochromic parameters [10], H-bonding capacity [11–14], topolog-

---

Abbreviations: BBB, blood–brain barrier; CNS, central nervous system; MIF, molecular interaction field; PCA, principal component analysis; PLS, partial least squares discriminant analysis; PSA, polar surface area

* Corresponding author. Tel.: +41-21-692-4521; fax: +41-21-692-4525.
E-mail address: Bernard.Testa@ict.unil.ch (B. Testa).

0925-4439/02/$ - see front matter © 2002 Elsevier Science B.V. All rights reserved.
PII: S0925-4439(02)00074-1

ical indices [15], polar surface area (PSA) [16–19] and Molsurf descriptors [20].

Recently, a new method named VolSurf has been developed by Cruciani et al. [21]. This method is able to convert 3D fields into new descriptors well suited for structure–pharmacokinetic relationships [22,23] and have proven its efficacy, simplicity of use and chemical interpretability (see Ref. [21] for a detailed description of the method). A previous semiquantitative model was able to classify correctly more than 90% of BBB+ and BBB − permeation data [23]. In the present work, a quantitative model is presented, which was derived from $\log(C_{\mathrm{brain}}/C_{\mathrm{blood}})$ steady-state (log BB) values of 83 compounds measured in rats.

2. Experimental procedures

2.1. Overview

The overall procedure consisted in the following four major steps:

1. Compilation of a homogenous set of literature BBB data for 83 compounds.
2. Calculation of their 3D structure.
3. Computation of their molecular interaction fields (MIFs) using GRID probes.
4. Generation of the VolSurf descriptors.

Table 1
Experimental and calculated log BB values for the compounds included in this study

Compound	Name	log BB_{exp}	log BB_{calc}	Reference	Compound	Name	log BB_{exp}	log BB_{calc}	Reference
1	cimetidine	−1.42	−1.188	[14]	**44**	valproic-acid	−0.22	0.598	[25]
2	clonidine	0.11	0.462	[14]	**45**	chlorambucil	−1.70	outlier	[15]
3		−0.04	−0.563	[14]	**46**		−1.3	−1.162	[11]
4	imipramine	0.83	0.923	[14]	**47**		−1.4	−0.918	[11]
5	mepyramine	0.49	0.521	[14]	**48**		−0.43	−0.397	[15]
6	ranitidine	−1.23	−0.605	[14]	**49**		0.25	0.193	[15]
7	tiotidine	−0.82	−1.144	[14]	**50**		−0.3	−0.244	[11]
8	icotidine	−2	−1.222	[14]	**51**		−0.06	0.468	[11]
9	SKF-93619	−1.3	−0.410	[14]	**52**		−0.42	−1.435	[11]
10	lupitidine	−1.06	−1.232	[14]	**53**		−0.16	0.222	[15]
11		−1.17	−0.707	[14]	**54**	thioridazine	0.24	0.781	[25]
12		−2.15	outlier	[14]	**55**	chlorpromazine	1.06	0.422	[25]
13		−0.67	−0.718	[14]	**56**	desipramine	1.2	0.420	[25]
14		−0.66	−0.680	[14]	**57**	alprazolam	0.044	−0.375	[25]
15		−0.12	−0.603	[14]	**58**	codeine	0.55	0.543	[25]
16		−0.18	−0.282	[14]	**59**	didanosine	−1.301	−1.296	[15]
17		−1.15	−0.669	[14]	**60**	oxazepam	0.61	−0.659	[25]
18		−1.57	−1.313	[14]	**61**	verapamil	−0.7	−0.960	[25]
19		−1.54	−1.252	[14]	**62**	trifluopromazine	1.44	outlier	[25]
20		−1.12	−0.739	[14]	**63**	theophylline	−0.29	−0.955	[25]
21		−0.73	−0.763	[14]	**64**	pentobarbital	0.12	−0.535	[25]
22		−0.27	−0.231	[14]	**65**	hyroxyzine	0.39	−0.881	[25]
23		−0.28	−0.492	[14]	**66**	midazolam	0.36	0.412	[25]
24		−0.46	0.158	[14]	**67**	promazine	1.23	0.651	[25]
25		−0.24	0.111	[14]	**68**	physostigmine	0.079	0.380	[15]
26		−0.02	−0.037	[14]	**69**	nevirapine	0	0.083	[15]
27		0.69	0.322	[14]	**70**	mianserin	0.99	0.906	[17]
28		0.44	−0.222	[14]	**71**	Org-4428	0.82	1.010	[17]
29	zolantidine	0.14	−0.277	[14]	**72**	Org-5222	1.03	0.614	[17]
30		0.22	0.186	[14]	**73**	Org-12962	1.64	outlier	[17]
31	amitriptyline	0.89	0.742	[10]	**74**	Org-32104	0.52	0.066	[17]
32	carbamazepine	0	0.313	[15]	**75**	Org-30526	0.39	0.036	[17]
33		−0.34	−0.153	[15]	**76**	mirtazapine	0.53	0.506	[17]
34	L-663581	−0.3	−0.089	[24]	**77**	tibolone	0.4	0.911	[17]
35	M1L-663581	−1.34	−0.882	[24]	**78**	domperidone	−0.78	−0.586	[17]
36	M2L-663581	−1.82	−1.568	[24]	**79**	Org-34167	0	0.240	[17]
37	antipyrine	−0.097	0.495	[25]	**80**	risperidone	−0.02	−0.479	[17]
38	caffeine	−0.055	−0.870	[25]	**81**	9-OH-risperidone	−0.67	−0.909	[17]
39	ibuprofen	−0.18	0.220	[25]	**82**	BCNU	−0.52	−0.191	[15]
40	indomethacin	−1.26	−1.146	[25]	**83**	phenserine	1	0.679	[15]
41	salicylic-acid	−1.1	−0.657	[25]					
42	temelastine	−1.88	−1.059	[26]					
43	aspirin	−0.5	−0.516	[25]					

5. Statistical analysis using principal component analysis (PCA) and partial least squares discriminant analysis (PLS).

Steps 3–5 were performed automatically by the VolSurf program.

2.2. Dataset

Log BB data for 83 radiolabeled compounds were compiled from the literature (Table 1) [10,11,14,15,17,24–26]. These values were blood/brain concentration ratios obtained in the rat at steady state:

$$\text{logBB} = \log(C_{\text{brain}}/C_{\text{blood}}) \qquad (1)$$

The values within this dataset ranged from −2.16 to 1.64. A basic assumption of the study was that BBB permeation was purely passive.

2.3. Modelling of 3D molecular structures

The 3D structure of the selected compounds (Fig. 1) were drawn starting from the Corina-built structures, and energy-optimized using the MMFF94s force field including MMFF94 partial atomic charges as implemented in Sybyl 6.4 [27]. Minimization was performed in vacuo ($\varepsilon = 1$) using BFGS and continued until the root-mean-square energy gradient was lower than 0.001 kcal/mol. All molecules were built in their neutral forms. Because it is impossible to model mixtures of stereoisomers in 3D and since VolSurf descriptors are achiral, only one of stereoisomer was modelled.

2.4. Calculation of VolSurf descriptors and statistical analysis

The MIFs were calculated using the water, DRY, and carbonyl probes available in the GRID program [28]. The GRID forcefield is indeed well suited to characterize putative polar and hydrophobic interaction sites around target molecules. The water probe was used to simulate hydration–dehydration processes, the hydrophobic (DRY) probe was used to simulate drug–membrane hydrophobic interactions, and the carbonyl probe was used to simulate drug–membrane H-bonding interactions [23]. Descriptors were then automatically generated by VolSurf. These descriptors refer to molecular size and shape, to size and shape of hydrophilic and hydrophobic regions, and to the balance between them. Hydrogen bonding, amphiphilic moments

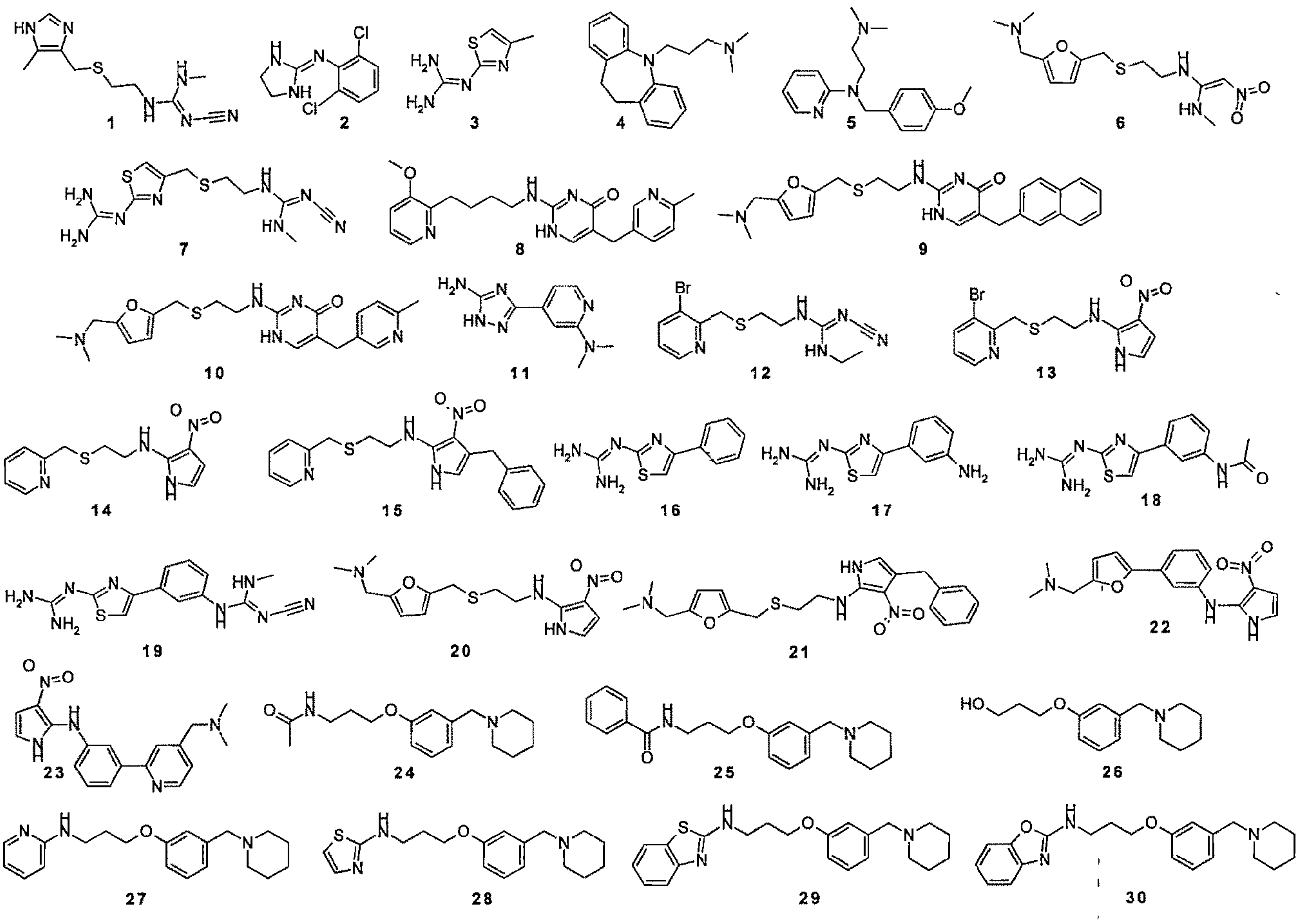

Fig 1. Chemical structure of the compounds in the dataset

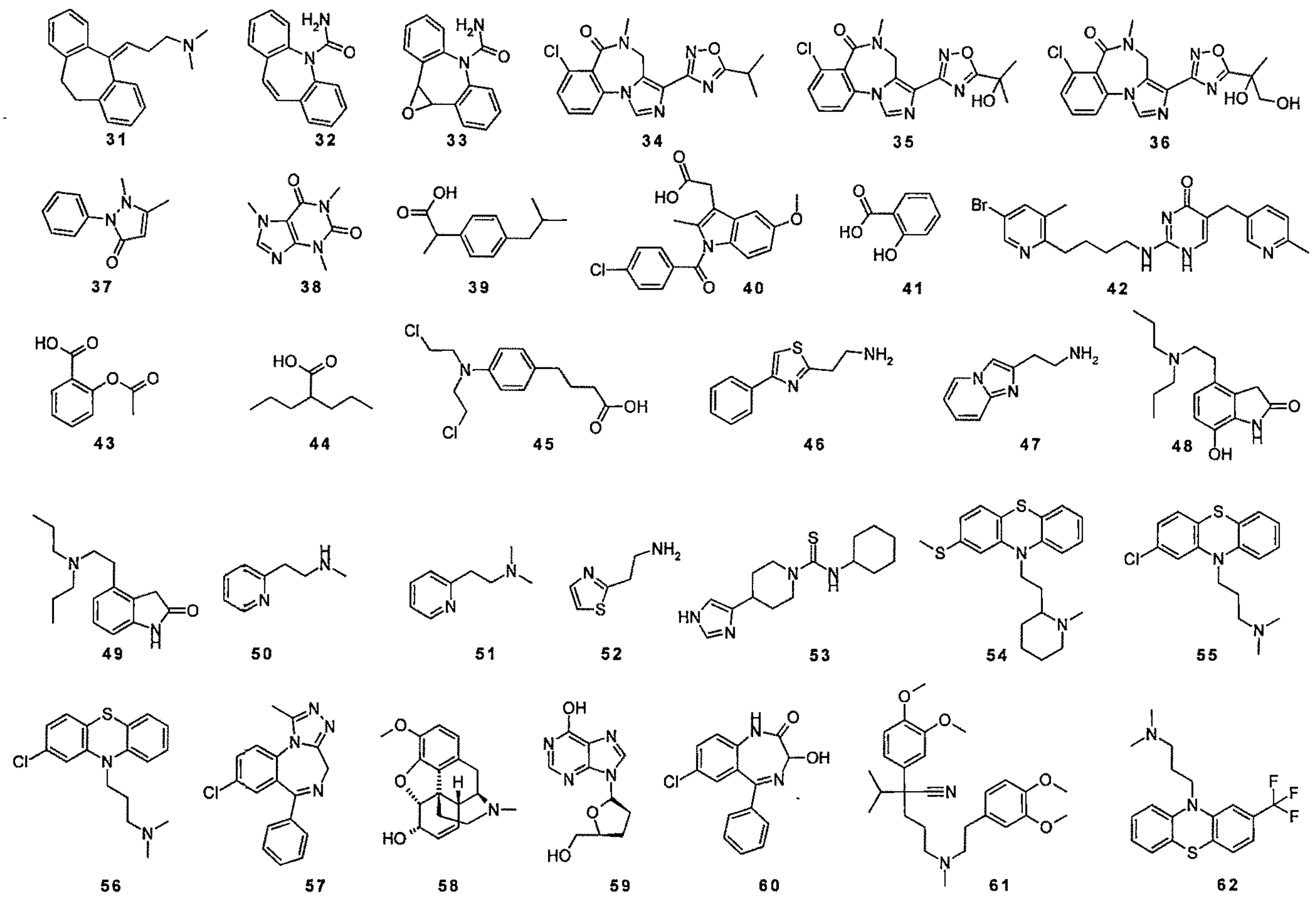

Fig. 1 (*continued*)

and critical packing parameters are other useful descriptors (for a more detailed description, see Ref. [21]).

PCA and PLS analyses were produced with the VolSurf program version 2.0.6. The number of significant latent variables and the quality of the models were determined using a leave-one-out cross-validation procedure (LOO-cv). In such a procedure, each compound is removed once from the dataset, and the remaining compounds are used to develop a new model, with which the left-out compound is then predicted.

3. Results and discussion

3.1. Preliminary BBB permeation model

In a first investigation, VolSurf molecular descriptors were computed for the 83 compounds included within the dataset using the water, DRY and carbonyl probes, yielding 72 descriptors. This led for the 83 compounds to a four-component PLS model (Table 2; model 1), which explained about 65% of the total variance of the matrix. The predictive ability of the model was assessed by means of cross-validation (leave-one-out). A detailed inspection of the predicted residual plots showed several strong outliers (eight compounds). Removing compounds **12** and **45** (the same outliers as in previous studies [10,15,26] and compounds **62** and **73** resulted for the 79 remaining compounds in an improved four-component PLS model (Table 2, model 1b). Compounds **62** and **73** were remove since a careful inspection of the MIFs obtained with the DRY probe showed that the trifluoromethyl group was not well described by this probe.

3.2. Final BBB permeation model and its interpretation

A systematic examination showed that it was possible to use only the three lowest energy levels calculated with the water and DRY probes, and canceling the carbonyl probe. Indeed, the correlation matrix revealed that several descriptors generated from the carbonyl probe correlated with those obtained with the water probe. This observation is not too surprising since the water probe already accounts for the polarity of the studied compounds.

As a result of these restrictions, the independent variables were reduced to 31 descriptors. The statistics of this new four-component PLS model (Table 2, model 2; Fig. 2) were similar to those of model 1b. The coefficient plot of this final model (Fig. 3) shows the contribution of the 31 VolSurf descriptors. The vertical bars represent the contri-

P. 25. 704

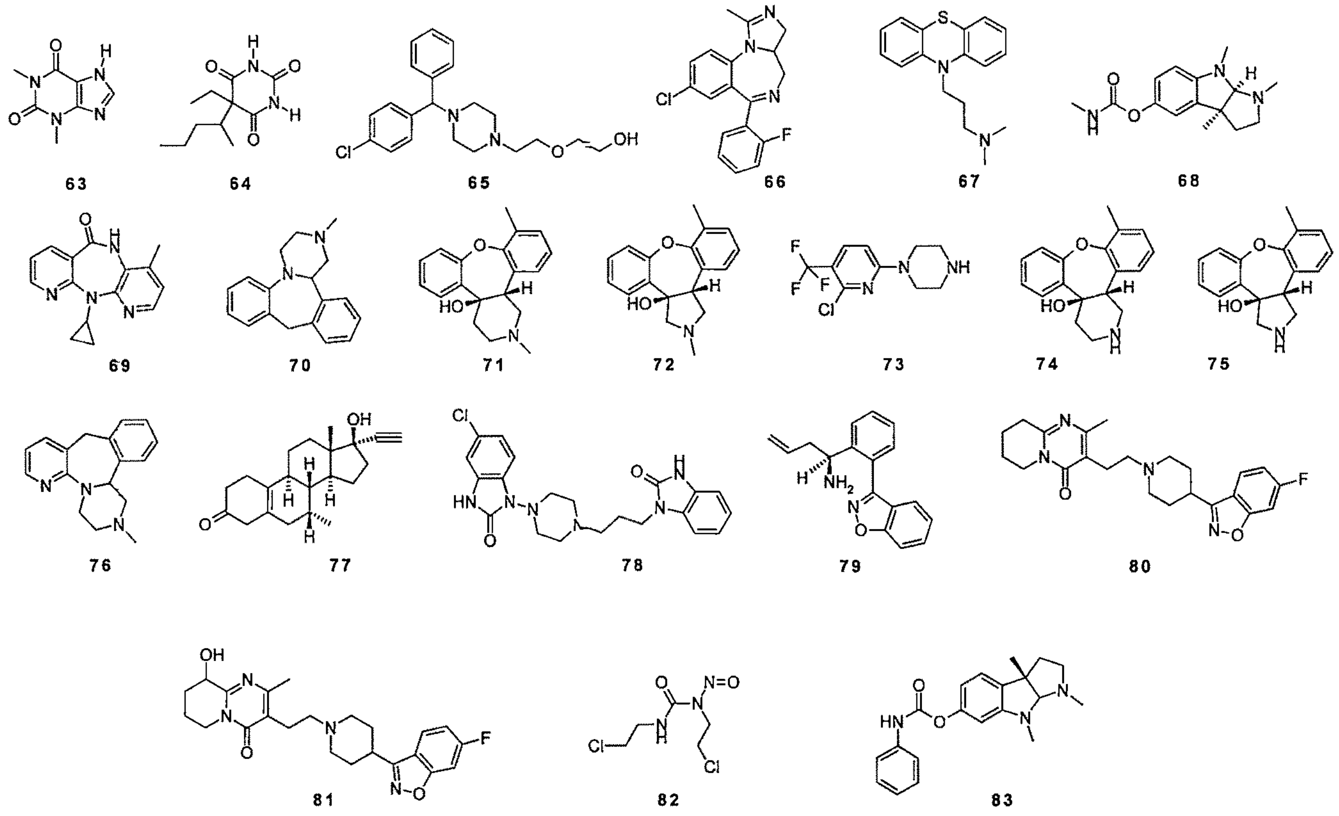

Fig 1 (*continued*)

bution of each single descriptor, a short bar denoting a minor contribution and a long bar a major one. The last bar on the right represents the dependent variable, i.e. log BB. The following conclusions can be drawn from this plot:

- Descriptors of polarity such as hydrophilic regions (W1–W3) and capacity factors (CW1–CW3) are inversely correlated with BBB permeability. Their negative coefficients are in line with the well-known fact that highly polar compounds have a very low BBB permeation.
- The descriptors of hydrophobic interactions (D1–D3) are directly correlated with BBB permeation, although their positive contribution appears somewhat smaller than the negative contribution of the polar descriptors. These positive contributions are in accordance with the fact that lipophilic compounds penetrate relatively easily into the brain.
- The size and shape descriptors have no marked impact on BBB permeation except for rugosity, which correlates positively with BBB permeation, and globularity, which correlates negatively. Rugosity is defined as the ratio of total volume (V_{tot}) over total surface (S_{tot}), and it is smaller the more the object differs from a sphere. Globularity is defined as the ratio between S_{tot} and the surface of a sphere of equivalent volume (V_{tot}), and it is larger the more the object differs from a sphere. In other words, both descriptors indicate that compounds having a high rugosity and a low globularity will have a spherical shape and will be better at crossing the BBB.

Table 2
Statistical properties of the models

Model	Training set	*N* descriptors	r^2 (four LVs)	q^2
1	83 compounds	72	0.68	0.50
1b	79 compounds	72	0.78	0.65
2	79 compounds	31	0.76	0.65

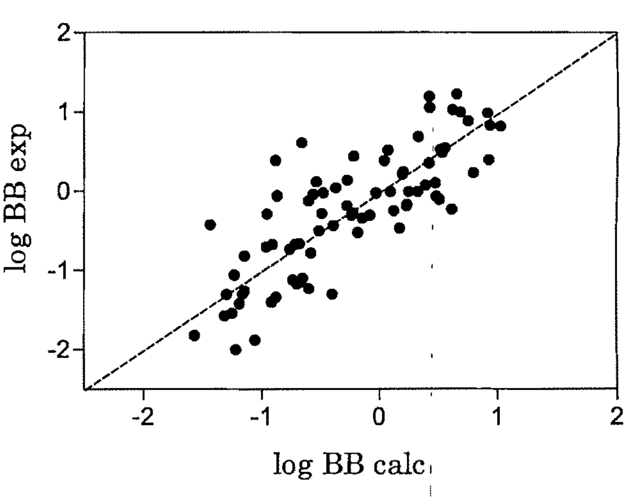

Fig. 2 Relationship between experimental and calculated BBB permeation using the four-component PLS model (Table 2, model 2)

3.3. Application to two compounds in the dataset

Here, we discuss in some detail two compounds to exemplify the interpretative value of the VolSurf model. These compounds are characterized by different BBB permeation properties: **70** easily crosses the BBB while **59** does not.

The scaled values of the descriptors (Fig. 4) show several trends:

- The hydrophilic descriptors (W1–W3, CW1–CW3) of **70** are lower than those of **59**.
- The hydrophobic descriptors (D1–D3) of **70** are larger than those of **59**.
- Relative to **59**, the rugosity of **70** is higher whereas the globularity is lower.

A visual comparison of the MIFs calculated around compounds **59** and **70** with the water and DRY probes also shows several differences (Fig. 5). The dark gray zones represent the hydrophilic regions in Fig. 5 left, and the hydrophobic regions in Fig. 5 right. As can be seen, the hydrophilic regions generated around **59** are larger than those around **70** while the reverse holds for the hydrophobic regions. These results are in agreement with our above analysis of the PLS coefficient plot (Fig. 3), namely that the size of the hydrophilic regions is inversely correlated with BBB permeation whereas the opposite is true for the hydrophobic regions. Furthermore, **70** indeed has a more spherical shape than **59**.

3.4. Interest of the model in virtual screening of BBB permeation

The four-component PLS model can also be used to perform a semiquantitative classification of compounds based on their permeation or nonpermeation of the BBB. Compounds having a log BB value >0 were classified has brain penetrators (BBB+) while those with a log BB value <0 were considered as not reaching the brain in sufficient concentrations (BBB –). It is important to note that this cutoff is arbitrary and would have to be defined with a specific pharmacology in mind. Indeed, the cutoff value will depend on which are more damaging to the classification, false positives or false negatives. Eighty-five percent of the BBB – compounds and 79% of BBB+ compounds were correctly classified with a cutoff of 0. If more restrictive cutoffs are chosen to define BBB – compounds (log BB < – 0.5) and BBB+ compounds (log BB>0.5), the model correctly assign more than 90% of the BBB – compounds and 65% of the BBB+ compounds.

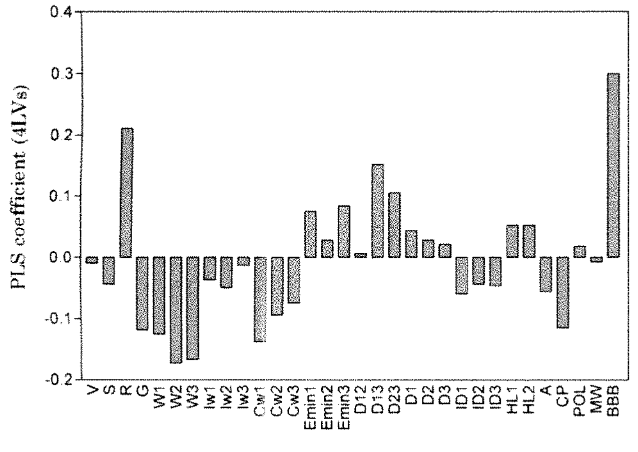

Fig. 3. PLS coefficient plot for the final model (Table 2, model 2) for the correlation of VolSurf descriptors with BBB permeation.

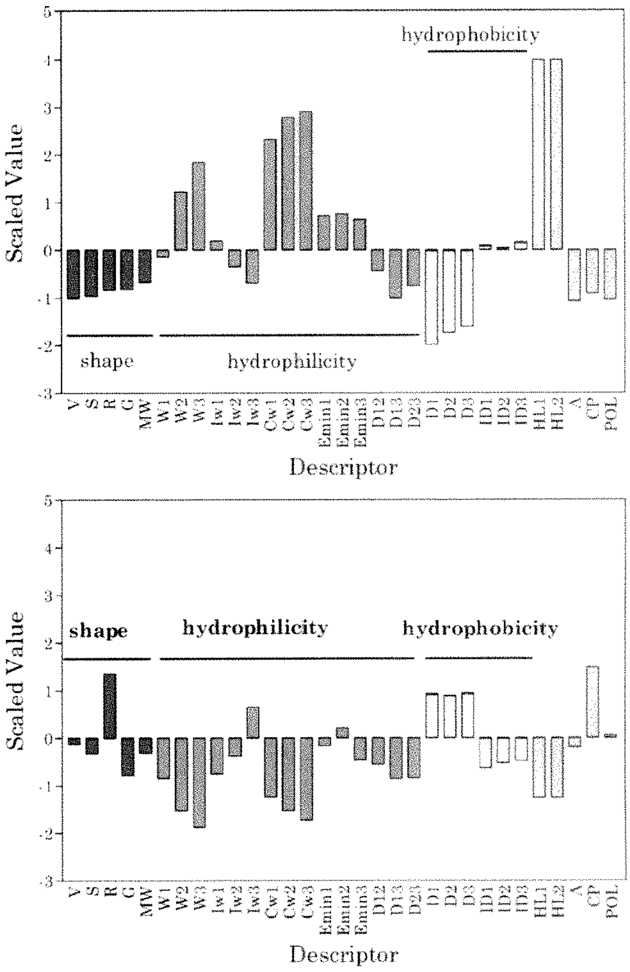

Fig. 4. Thirty-one VolSurf scaled descriptors calculated for compounds **59** (didanosine, upper part) and **70** (mianserine, lower part).

4. Conclusion

The model obtained in this study for the prediction of BBB permeation is relevant from a physiological point of view and is also in agreement with insights from other BBB permeation models. We show that VolSurf descriptors describing hydrophilic and hydrophobic properties are well

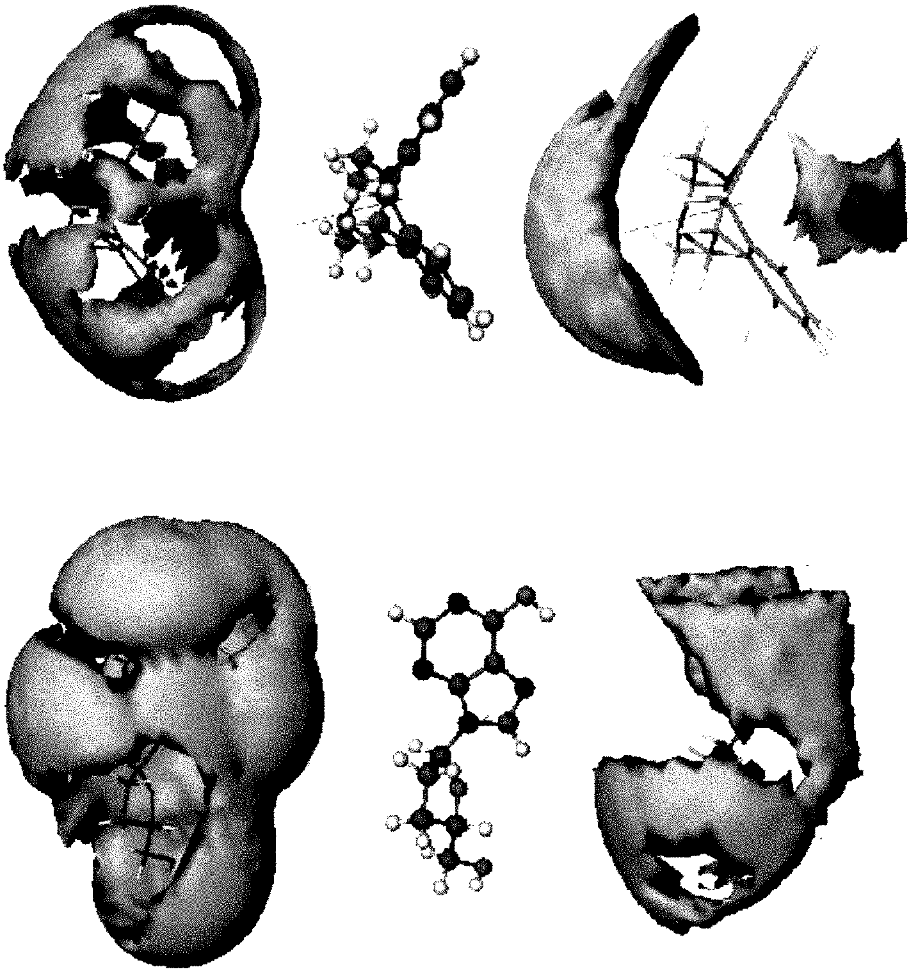

Fig. 5. GRID 3D molecular interaction fields of **70** (upper part) and **59** (lower part) calculated with the water (right) and the DRY (left) probes. The zones shown are contoured at − 1 kcal/mol.

suited to derive a PLS model able to discriminate good and poor BBB penetrators. Finally, we believe that a more robust model to predict log BB values could be obtained from BBB data measured by a single experimental protocol and for compounds permeating by a purely passive mechanism.

Acknowledgements

The authors are indebted to Dr. Gabriele Cruciani for his interest and support.

References

[1] J.B.M.M. van Bree, A.G. de Boer, M. Danhof, D.D. Breimer, Drug transport across the blood–brain barrier: I. Anatomical and physiological aspects, Pharm. Weekbl., Sci. Ed. 14 (1992) 305–310.

[2] T. Hirase, J.M. Staddon, M. Saitou, Y. Ando-Akatsuka, M. Itoh, M. Furuse, K. Fujimoto, S. Tsukita, L.L. Rubin, Occludin as a possible determinant of tight junction permeability in endothelial cells, J. Cell Sci. 110 (1997) 1603–1613.

[3] M.W. Brightman, The anatomic basis of the blood–brain barrier, in: E.A. Neuwelt (Ed.), Implications of the Blood–Brain Barrier and Its Manipulation: Volume 1. Basic Science Aspects, Plenum, New York, 1989, pp. 53–83.

[4] A.M. ter Laak, R.S. Tsai, G.M. Donné-op den Kelder, P.A. Carrupt, B. Testa, H. Timmerman, Lipophilicity and hydrogen-bonding capacity of H1-antihistaminic agents in relation to their central sedative side-effects, Eur. J. Pharm. Sci. 2 (1994) 373–384.

[5] P.B. Woods, M.L. Robinson, An investigation of the comparative liposolubilities of β-adrenoceptor blocking agents, J. Pharm. Pharmacol. 33 (1981) 172–173.

[6] A. Pagliara, M. Reist, S. Geinoz, P.A. Carrupt, B. Testa, Evaluation and prediction of drug permeation, J. Pharm. Pharmacol. 51 (1999) 1339–1357.

[7] C. Hansch, J.M. Clayton, Lipophilic character and biological activity of drugs: II. The parabolic case, J. Pharm. Sci. 62 (1973) 1–21.

[8] C. Hansch, J.P. Björkroth, A. Leo, Hydrophobicity and central nervous system agents: on the principle of minimal hydrophobicity in drug design, J. Pharm. Sci. 76 (1987) 663–687.

[9] D.D. Dischino, M.J. Welch, M.R. Kilbourn, M.E. Raichle, Relationship between lipophilicity and brain extraction of C-11-labeled radiopharmaceuticals, J. Nucl. Med. 24 (1983) 1030–1038.

[10] F. Lombardo, J.F. Blake, W.J. Curatolo, Computation of brain–blood partitioning of organic solutes via free energy calculations, J. Med. Chem. 39 (1996) 4750–4755.

[11] R.C. Young, C.R. Ganellin, R. Griffiths, R.C. Mitchell, M.E. Parsons, D. Saunders, N.E. Sore, An approach to the design of brain-penetrating histaminergic agonists, Eur. J. Med. Chem. 28 (1993) 201–211.

[12] E.G. Chikhale, K.Y. Ng, P.S Burton, R T. Borchardt, Hydrogen bonding potential as a determinant of the in vitro and in situ blood–brain barrier permeability of peptides, Pharm. Res. 11 (1994) 412–419.

[13] H. van de Waterbeemd, M. Kansy, Hydrogen-bonding capacity and brain penetration, Chimia 46 (1992) 299–303

[14] R C. Young, R.C Mitchell, T.H Brown, C R Ganellin, R Griffiths, M Jones, K.K. Rana, D Saunders, I.R Smith, N E. Sore, T.J. Wilks, Development of a new physicochemical model for brain penetration and its application to the design of centrally acting H2 receptor histamine antagonists, J. Med. Chem 31 (1988) 656–671.

[15] J.M Luco, Prediction of the blain–blood distribution of a large set of drugs from structurally derived descriptors using partial least-squares (PLS) modeling, J Chem Inf. Comput. Sci 39 (1999) 396–404.

[16] D.E. Clark, Rapid calculation of polar molecular surface area and its application to the prediction of transport phenomena: 2. Prediction of blood–brain barrier penetration, J Pharm Sci. 88 (1999) 815–921.

[17] J. Kelder, P D J Grootenhuis, D M Bayada, L P C Delbressine, J P Ploemen, Polar molecular surface as a dominating determinant for oral absorption and brain penetration of drugs, Pharm. Res 16 (1999) 1514–1519

[18] P. Ertl, B Rohde, P. Selzer, Fast contribution of molecular polar surface area as a sum of fragment-based contributions and its application to the prediction of drug transport, J Med Chem. 43 (2000) 3714–3717.

[19] M Feher, E Sourial, J M. Schmidt, A simple model for the prediction of blood–brain partitioning, Int. J. Pharm. 201 (2000) 239–247.

[20] U Norinder, P. Sjoberg, T Osterberg, Theoretical calculation and prediction of brain–blood partitioning of organic solutes using MolSurf parameterization and PLS statistics, J. Pharm. Sci 87 (1998) 952–959.

[21] G. Cruciani, P. Crivori, P A. Carrupt, B. Testa, Molecular fields in quantitative structure permeation relationships: the VolSurf approach, J Mol Struct, Theochem 503 (2000) 17–30.

[22] L.H Alifrangis, I.T. Christensen, A. Berglund, M. Sandberg, L Hovgaard, S Frokjaer, Structure–property model for membrane partitioning of oligopeptides, J. Med Chem 43 (2000) 103–113

[23] P Crivori, G Cruciani, P A Carrupt, B. Testa, Predicting blood–brain barrier permeation from three-dimensional molecular structure, J. Med Chem 43 (2000) 2204–2216

[24] J.H. Lin, I.W Chen, T.H Lin, Blood–brain barrier permeability and in vivo activity of partial agonists of benzodiazepine receptor: a study of L-663,581 and its metabolites in rats, J Pharmacol Exp Ther. 271 (1994) 1197–1202.

[25] T Salminen, A. Pulli, J Taskinen, Relationship between immobilised artificial membrane chromatographic retention and the brain penetration of structurally diverse drugs, J Pharm. Biomed Anal 15 (1997) 469–477

[26] M H Abraham, H.S. Chadha, R.C Mitchell, Hydrogen bonding: 33. Factors that influence the distribution of solutes between blood and brain, J. Pharm. Sci 83 (1994) 1257–1268.

[27] SYBYL 6 4, Tripos Associates, St Louis, MO, 1995.

[28] P.J Goodford, A computational procedure for determining energetically favorable binding sites on biologically important macromolecules, J Med Chem 28 (1985) 849–857.

ELSEVIER

Biochimica et Biophysica Acta 1587 (2002) 126–132

BIOCHIMICA ET BIOPHYSICA ACTA
BBA
www.bba-direct.com

Review

Control of alternative splicing by antisense oligonucleotides as a potential chemotherapy: effects on gene expression

Danielle R. Mercatante, Ryszard Kole*

Department of Pharmacology and Lineberger Comprehensive Cancer Center, University of North Carolina, Chapel Hill, NC, 27599 USA

Received 24 January 2002, accepted 24 January 2002

Abstract

Expression of alternatively spliced mRNA variants at specific stages of development or in specific cells and tissues contributes to the functional diversity of the human genome. Aberrations in alternative splicing were found as a cause or a contributing factor to the development, progression, or maintenance of various diseases including cancer. The use of antisense oligonucleotides to modify aberrant expression patterns of alternatively spliced mRNAs is a novel means of potentially controlling such diseases. However, to utilize antisense oligonucleotides as molecular chemotherapeutic agents, the global effects of these molecules need to be examined. The advent of gene expression array technology has now made it possible to simultaneously examine changes that occur in the expression levels of several thousand genes in response to antisense treatment. This analysis should help in the development of more specific and efficacious antisense oligonucleotides as molecular therapeutics. © 2002 Elsevier Science B.V. All rights reserved.

Keywords Alternative splicing; Antisense oligonucleotide; Apoptosis; Bcl-x; Cancer, Gene microarray

1. Introduction

Conservative estimates suggest that over 35% of all pre-mRNAs are spliced to yield alternative variants, the translated products of which may have very different functions. An unexpectedly small number of human genes contrasted with the complexity of the expressed gene products suggests that alternative splicing may be even more frequent. This review will present examples of the association between deregulation of the process of alternative splicing and genetic diseases and cancer. In addition, the potential use of antisense oligonucleotides to modify splicing pathways as a molecular chemotherapy will be discussed.

2. Aberrant splicing associated with disease

How the cell decides which alternative splice site to utilize is not fully understood. However, it is generally believed that splice site selection is determined by competition between splicing sequence elements for splicing factors during spliceosome assembly. See recent reviews for more detailed descriptions [1–4]. Aberrant splicing can result in deleterious consequences for the organism. In fact, approximately 15% of all mutations that cause genetic diseases result in defective splicing of pre-mRNA [5]. For example, aberrant pre-mRNA splicing occurs in genetic diseases such as β-thalassemia [6], cystic fibrosis [7], neurofibromatosis type 1 [8], ataxia-telangiectasia [9], and congenital lipoid adrenal hyperplasia [10]. Aberrant splicing events are also associated with neurological disorders [11] such as splicing of the IKBKAP pre-mRNA in familial dysautonomia [12].

Deregulated alternative splicing also results in the inappropriate expression levels of correct splice variants, which leads to altered cellular processes. A variety of cancers express an altered ratio of specific splice variants, suggesting that splice site selection is aberrantly regulated in cancer cells. For recent reviews, the reader is referred to Refs. [13,14]. Table 1 gives examples of some alternatively spliced pre-mRNAs and several cancers that are associated with specific splice variants. Many cancer-related alternatively spliced genes are associated with control of cellular signaling, proliferation, cell cycle, apoptosis, and DNA double-strand break repair. While the exact functions of many of the

---

Abbreviations. CFTR, cystic fibrosis transmembrane receptor; PARP, poly-ADP-ribose polymerase; RT-PCR, reverse transcription-polymerase chain reaction

* Corresponding author Tel.. +1-919-966-1143, fax. +1-919-966-3015.
E-mail address: kole@med.unc.edu (R. Kole)

0925-4439/02/$ - see front matter © 2002 Elsevier Science B.V. All rights reserved
PII S0925-4439(02)00075-3

Table 1
Alternatively spliced pre-mRNAs and examples of some cancers harboring specific splice variants

	pre-mRNA	Example of cancers harboring specific variants (refs.)
Proliferation/ signaling	FGFR1	glioblastoma [55–57]
	FGFR2	prostate [58–60]
	FGFR3	colorectal [61]
	FGFR4	gastric, colon, pancreatic [62]
	CD44	various [63–66]
	BDNF	neuroblastomas [67]
	HER2	various, including gastric [68], breast [69]
	Trx-1	various [70]
	PTPN6	acute myeloid leukemia [71]
Cell cycle/ apoptosis	Bcl-x	various, including prostate [72], ovarian [73], leukemia [74]
	Bax	various [75], including breast [76–78]
	FHIT	various [79], including renal cell [80], lung [81]
	p73	neuroblastomas [82], ovarian [83], breast [84]
	mdm2	astrocytoma [85], ovarian, bladder [86], breast [87]
	WT1	Wilms' tumor and leukemias [88–90]
DNA excision/ repair	BRCA1	breast, ovarian [91]
	BRCA2	breast [92]
	XPG	lung [93,94]

The pre-mRNAs are organized according to cellular function. Listed to the right of the pre-mRNA are some types of cancers that specific splice variants of the pre-mRNAs have been detected in (either in cell lines or in tissues from cancer patients).

cancer-related alternative splice variants are unknown, it seems likely that the shift in splicing results in variants that impart an increased survival capability on the cell. It therefore seems that manipulating the splicing pattern of those pre-mRNAs can be effective as a means to control a variety of diseases, including cancer.

3. Control of splice site selection by antisense oligonucleotides

To control pre-mRNA splicing patterns, antisense oligonucleotides must hybridize with specific splice sites and block spliceosome formation at the targeted splice site. This, because of the flexibility of splicing machinery, does not result in total inhibition of splicing, but in a shift of the spliceosome to another splice site. As a consequence, an alternative splicing pattern is established or a normally used alternative splice site is used with increased efficiency. It has been shown in this and other laboratories that antisense oligonucleotides modify the splicing patterns of pre-mRNAs that harbor aberrant splice sites or aberrant sequence elements involved in splicing. For example, antisense oligonucleotides have been used to restore correct pre-mRNA splicing patterns of β-globin in β-thalassemia [15–21] and cystic fibrosis transmembrane receptor (CFTR) in cystic fibrosis [22]. Antisense oligonucleotides have also been used to induce an alternative splicing pattern in a dystrophin pre-mRNA in Duchenne's muscular dystrophy [23,24] and affect the level of expression of Bcl-x splice variants in cancer cells [25,26].

In order to use antisense oligonucleotides to shift splicing patterns, the oligonucleotides must be stable in serum, produce high Tm and RNase H resistant oligonucleotide-RNA duplexes, and have the ability to enter the nucleus (the site of pre-mRNA splicing). This is accomplished by modification of the chemistries of oligonucleotide sugars, internucleotide linkages, and nucleotide bases. Examples include substitution of the 2′-hydroxyl with *O*-methyl, *O*-methoxyethyl, and *O*-aminopropyl residues or derivatives such as morpholino, N3′→P5′ phosphoroamidate, peptide nucleic acids, and methylphosphonate molecules. For a more detailed review, see Ref. [13]. In order to deliver the oligonucleotides to the nucleus, oligonucleotides have conventionally been complexed with cationic lipids. However, more recently, it has been found that several of the modified oligonucleotides have the ability to enter the nucleus without the aid of cationic lipids [17].

4. Modification of splicing in cancer-related pre-mRNAs

Many cancer-related pre-mRNAs that undergo alternative splicing are associated with apoptosis. Frequently, their splice variants have opposing functions in either promoting or preventing apoptosis. For reviews, see Refs. [13,14,27]. Thus, it appears that altered splicing patterns of many pre-mRNAs in neoplastic cells may impart an augmented capability of cellular survival. It then follows that modification of these splicing patterns may inhibit cancer cell growth and provide anticancer treatments. An antisense oligonucleotide-induced shift in splicing may be particularly effective because in this approach, lowering the level of an anti-apoptotic splice variant should simultaneously increase the levels of its pro-apoptotic counterpart. Recent results illustrating the effects of modification of splicing of a cancer-related gene, Bcl-x, are described below.

Bcl-x is an alternatively spliced member of the Bcl-2 family of apoptotic proteins. Use of the downstream alternative 5′ splice site within exon 2 results in Bcl-xL mRNA; the translated Bcl-xL protein has anti-apoptotic functions. Use of the upstream alternative 5′ splice site within exon 2 results in Bcl-xS protein, which promotes apoptosis. These two proteins appear to play critical roles during proper development. For example, Bcl-xL may contribute to the long-term survival of mature neural structures, while Bcl-xS may be important for the higher turnover rates of immature thymocytes undergoing selection [28]. In addition to contributing to the normal development of an organism, Bcl-xL is overexpressed in a number of human cancers such as multiple myeloma [29], small cell lung cancer [30], and breast cancer [31] and may render cells resistant to chemotherapeutics [32,33]. On the other hand, Bcl-xS inhibits pro-survival functions of Bcl-xL and Bcl-2 [28]. Two recent

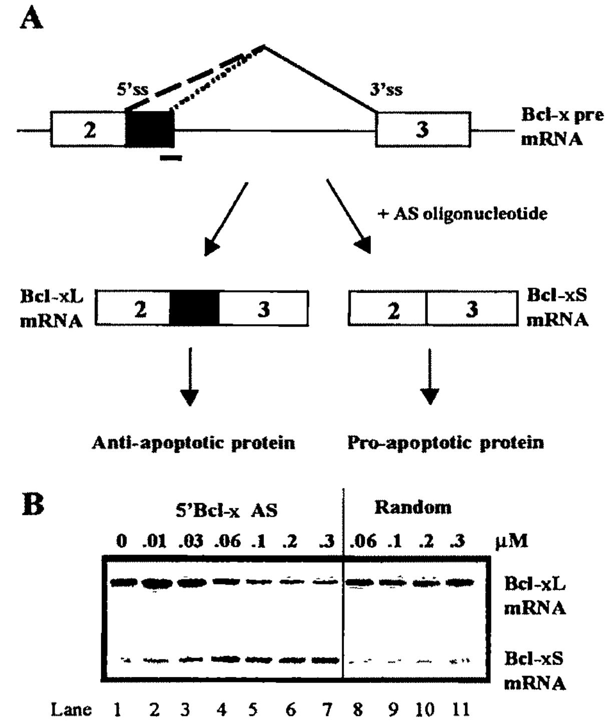

Fig 1 Bcl-x pre-mRNA is alternatively spliced to yield two products with opposing functions (A) Alternative splicing pathways for Bcl-xL (anti-apoptotic) and Bcl-xS (pro-apoptotic) Dashed line, Bcl-xS alternative splicing pathway, dotted line, Bcl-xL alternative splicing pathway; boxes, exons; line, introns; short bar below 5′ splice site, antisense oligonucleotide designed to shift the splicing pathway from Bcl-xL to Bcl-xS. (B) RT-PCR results RNA isolated from PC3 cells transfected with 5′ Bcl-x AS exhibited a dose dependent shift in splicing from Bcl-xL to Bcl-xS RNA isolated from PC3 cells treated with random oligonucleotide (negative control) did not show this shift in splicing (figure was modified from Ref [26])

papers report the use of antisense oligonucleotides in modification of splicing of Bcl-x pre-mRNA (Fig. 1A) [25,26].

Taylor et al. [25] targeted a 2′-*O*-methoxyethyl phosphorothioate oligoribonucleotide to a sequence adjacent to the alternative 5′ splice site of Bcl-xL pre-mRNA expressed in a human lung cancer epithelial cell line, A549. Transfection of the cells with the oligonucleotide in a complex with a cationic lipid delivery agent resulted in an increase of the pro-apoptotic Bcl-xS and a decrease in the anti-apoptotic Bcl-xL splice variants. However, in spite of the changed ratio of pro- and anti-apoptotic proteins, the treatment did not induce apoptosis in the cells. The increase in Bcl-xS and decrease in Bcl-xL did sensitize the cells to two different apoptosis inducers, cisplatin, and irradiation.

We have reported the use of 2′-*O*-methyl phosphorothioate oligonucleotide (5′Bcl-x AS) targeted to the alternative 5′ splice site of Bcl-xL in prostate (PC3) and breast (MCF7) cancer cell lines [26]. The shift in splicing (Fig. 1B) resulted in a marked decrease in cell viability and increased apoptosis in both cell lines as determined by colony formation and poly-ADP-ribose polymerase (PARP) assays. Interestingly, the extent and time course of induction of apoptosis, as determined by PARP cleavage, was lower and slower in the MCF7 compared with PC3 cells (Fig. 2A). In addition, the extent of overall cell death, as determined by colony formation, was lower in MCF7 cells than in PC3 cells (Fig. 2B).

The differences observed in the cellular responses to 5′Bcl-x AS treatment were also seen in their sensitization to chemotherapeutic agents. 5′Bcl-x AS treatment was less effective in sensitizing MCF7 cells to various chemotherapeutic agents than it was in PC3 cells. For example, PC3 cells treated with 5′Bcl-x AS were approximately three times more sensitive to 5-fluorouracil than cells treated with a negative control, randomized oligonucleotide. The same treatment of MCF7 cells resulted in 1.5 fold sensitization. A similar relationship held true for the sensitization of PC3 and MCF7 cells to several other chemotherapeutic reagents (Mercatante and Kole, unpublished data).

The above results show that altering splicing patterns has different effects depending upon the cellular milieu. We hypothesized that Bcl-2 could be a likely candidate to modulate cellular responses to 5′Bcl-x AS. This anti-apoptotic gene is up-regulated in many cancers and provides resistance to various chemotherapeutic agents. Furthermore, it is highly expressed in MCF7 cells. However, culturing MCF7 cells in media with charcoal stripped serum to downregulate Bcl-2 to

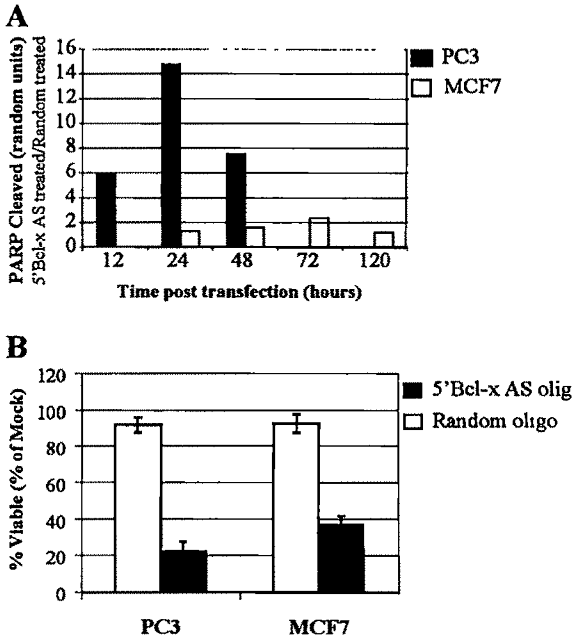

Fig. 2 Shifting splicing from Bcl-xL to Bcl-xS induced apoptosis. PC3 and MCF7 cells were transfected with 5′Bcl-x AS at concentrations that yielded approximately 55% shift in splicing (0.08 μM for PC3 and 0 4 μM for MCF7). (A) Examination of the amount of PARP cleaved (an indicator of apoptosis) showed that 5′Bcl-x AS induced apoptosis faster and to a greater extent in PC3 cells than in MCF7 cells (figure was modified from Ref [26]) (B) Treatment with 5′Bcl-x AS also decreased cell viability (measured by colony formation as a percentage of mock treated cells) to a greater extent in PC3 cells versus MCF7 cells

levels below those in PC3 cells did not increase apoptosis and/or cell death of 5′Bcl-x AS treated MCF7 cells [26]. Similar analysis of several other genes suggested that the endogenous levels of Bcl-x itself may be a more significant indicator of the effectiveness of 5′Bcl-x AS on inducing apoptosis (Mercatante and Kole, unpublished data).

The above analysis was limited to a several probable candidates and was carried out with one gene at the time. Recent developments in gene array technology allow simultaneous analysis of vast numbers of genes and identification of the important ones, which may have not been predicted by the existing data. For example, Cho et al. [34] found that antisense oligonucleotides designed to affect one gene also affected the expression of several other genes. Targeting these genes may enhance the biological effects of the original treatment and provide new insights into the development of combinations of antisense chemotherapeutics based on the molecular actions of the drugs. Furthermore, it may be possible to determine whether the antisense oligonucleotide treatment is clinically appropriate (i.e., does the treatment alter other genes in a way that enhances the desired effect while minimizing unwanted side effects).

5. Gene expression changes in response to antisense treatment

In the field of cancer research, gene arrays have been recently used to gain insight to the molecular basis of the disease [35,36]. Examples of this include determination of genetic changes associated with the progression of cancer [37,38] and with under- or over-expression of key proteins in cancer cells [39–41]. Identification of key genes that are up-regulated in more advanced cancers may indicate good targets for downregulation by antisense oligonucleotides. Gene expression array-based analyses have also identified changes that occur in response to various cancer treatments [42] and those responsible for resistance to therapeutics [43–45]. The data from experiments such as these may be used to tailor specific treatments to individuals that exhibit certain expression profiles.

Microarray analysis of gene expression showed that antisense oligonucleotides targeted to the RIα subunit of PKA not only induced downregulation of the targeted mRNA, but also induced changes in various other genes [34]. These changes were similar in two different cell lines, indicating that the treatment affected similar genomic pathways. This was expected since RIα antisense treatment in various other cancer cells resulted in similar anti-proliferative effects [46]. Since PC3 and MCF7 cells responded to 5′Bcl-x AS 2′-*O*-methyl phosphorothioate oligonucleotide treatment differently [26], we have recently carried out cDNA microarray experiments to examine gene expression patterns induced in both cell lines in response to the treatment.

PC3 and MCF7 cells were transfected with 5′Bcl-x AS, complexed with transfection reagent, at concentrations that yielded approximately 55% shift in splicing from Bcl-xL to Bcl-xS, (i.e. 0.08 μM for PC3 and 0.4 μM for MCF7). As a negative control, cells were treated in parallel with the same respective concentrations of random oligonucleotides (see Ref. [26] for a more detailed description of the treatment). At 36 h post transfection, total RNA was isolated from 5′Bcl-x AS and random oligonucleotide treated cells then labeled with Cy3 or Cy5, respectively. The labeled probes were co-hybridized to gene microarrays containing approximately 10,000 cDNAs fixed to a glass slide (University of North Carolina at Chapel Hill Genomics Core Facility). The

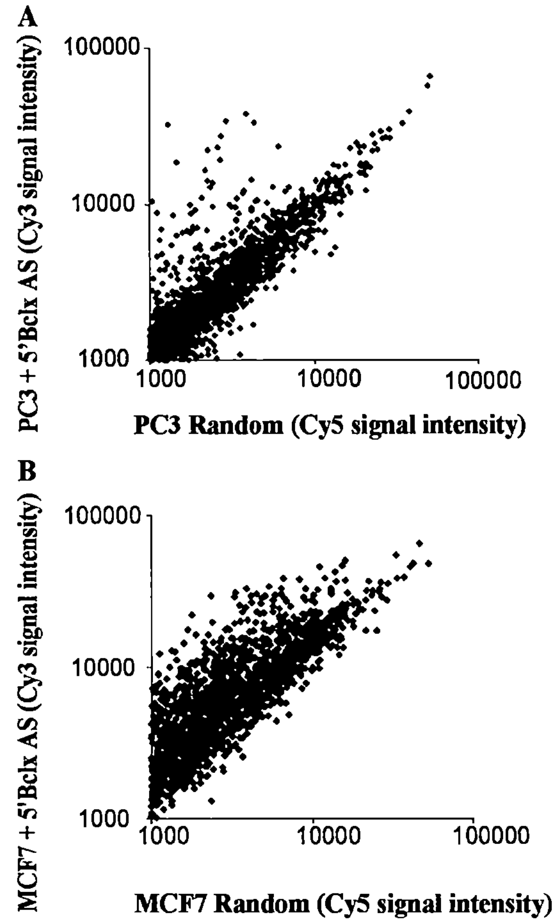

Fig. 3. Expression profiles of genes in MCF7 and PC3 cells treated with 5′Bcl-x AS. Cells were treated with 5′Bcl-x AS at concentrations that yielded approximately 55% shift in splicing (0.08 μM for PC3 and 0.4 μM for MCF7) or random oligonucleotide (0.08 μM for PC3 and 0.4 μM for MCF7). RNA was isolated 36 h post transfection, labeled with Cy3 or Cy5 dyes, and hybridized to human cDNA microarrays harboring approximately 10,000 cDNAs (both random oligonucleotide and 5′Bcl-x AS treated RNA from the same cell line were hybridized together). After sorting through the resulting data to discard any poor quality spots using Gene Pix Pro software, the intensity of the Cy3 (5′Bcl-x AS treated cells) and Cy5 (random oligonucleotide treated cells) signals were plotted against each other for each cDNA spot (approximately 7000 cDNAs are plotted for each cell line). Scatter plots show that the expression profiles are different for PC3 (A) and MCF7 (B) 5′Bcl-x AS treated cells.

analysis indicated that expression levels of approximately 308 genes in PC3 cells and 518 in MCF7 cells were altered more than 2.5-fold in antisense treated versus random oligonucleotide treated cells. Scatter plots of the results (Fig. 3) indicate that gene up-regulation was more pronounced in MCF7 cells. The significance of this observation is as yet not clear.

While it appears that many genes were differentially regulated in the two cell lines, we identified several genes that displayed similar expression patterns. For example, cDNA microarray analysis showed that the apoptosis-related genes *Mcl-*1, *Bak*, and *Bax* remained unaltered in response to 5′Bcl-x AS treatment in both MCF7 and PC3 cells. This is in agreement with the results obtained by RNAse protection assays that showed no significant changes in expression of these mRNAs in response to 5′Bcl-x AS in either cell line (Mercatante and Kole, unpublished data).

Further examination of genes with altered expression levels in response to 5′Bcl-x AS treatment showed changes specific to each cell line. The list of a few selected genes (Table 2) indicates that they are involved in apoptosis, cell signaling, nucleic acid and protein synthesis, cell structure, and ion transport. One gene, *Daxx* (death associated protein 6), which codes for a protein with pro-apoptotic functions and transcriptional repressor functions [47–50], was upregulated in PC3 cells but downregulated in MCF7 cells. It is possible that upregulation of *Daxx* in PC3 cells stimulates pro-death pathways that lead to a more rapid and effective means of 5′Bcl-x AS-induced apoptosis. Another candidate gene, *c-met* proto-oncogene, is involved in rendering cancer cells resistant to apoptotic stimuli [51,52]. Higher expression levels of *c-met* correlate with decreased rates of remission in oropharyngeal cancer [51]. Expression levels of *c-met* were downregulated in PC3 but not in MCF7 cells treated with 5′Bcl-x AS. Thus, it is possible that downregulation of this gene in 5′Bcl-x AS treated PC3 cells helps to activate apoptotic pathways.

Table 2
Differentially regulated genes in PC3 and MCF7 cells after treatment with 5′Bcl-x AS

	Gene	MCF7	PC3
Apoptosis	Daxx	–	+
Signaling/ proliferation/ structural	Met proto-oncogene	0	–
	TNFRSF8	+	–
	S100-calcium binding protein A10	+	0
	DUSP6	+	–
	Dynein	–	0
	Fibrinogen-like 1	+	0
	Tubulin, beta 5	0	–
Ion transport	Solute carrier family 25	+	0
	Solute carrier family 18	0	–
	Potassium voltage-gated channel	+	–
	Calcium channel, voltage dependent beta	+	0
Protein/nucleic acid synthesis	Transcription factor 4	+	0
	RNA polymerase II	+	–
	Eukaryotic translation initiation factor, eIF2	+	–

Gene microarray analysis uncovered several differentially regulated genes in MCF7 and PC3 cells post 5′Bcl-x AS treatment After sorting out poor-quality spots, the remaining cDNA spots were analyzed for differential expression patterns The table lists some genes that were altered greater than 2.5-fold after 5′Bcl-x AS treatment Genes are organized in classes of function. Upregulation of genes after treatment with 5′Bcl-x AS, (+), downregulation, (–), unchanged, (0).

Other differentially expressed genes were involved in nucleic acid and protein synthesis. For example, *RNA polymerase II, transcription factor 4* was upregulated in MCF7 cells but unchanged in PC3 cells. *RNA polymerase II* and *eukaryotic translation initiation factor, eIF2*, were upregulated in MCF7 cells but downregulated in PC3 cells treated with 5′Bcl-x AS. One interpretation of these results is that the MCF7 cells are compensating for the insult caused by the shift in splicing from Bcl-xL to Bcl-xS by increasing the synthesis of new nucleic acids and proteins. On the other hand, PC3 cells are turning off synthesis of new nucleic acids and protein as they halt the cell cycle and prepare to commit cell suicide.

The differentially expressed genes discussed above are examples of how an antisense oligonucleotide can cause changes in many genes. It will be important for the future of antisense technology to be able to identify changes in gene expression and identify those that are essential for producing desired antisense effects versus undesirable ones. Microarray technology will enable researchers to examine these changes in gene expression on a global scale.

6. Conclusion

Although to date, there are no clinical trials with antisense oligonucleotides being used to shift splicing, there are several clinical trials in progress that examine the therapeutic potential of antisense oligonucleotides to downregulate cancer-related genes [53,54]. Preliminary results suggest that oligonucleotides will be valuable molecular chemotherapeutics. Particularly interesting, however, is the use of antisense oligonucleotides to modify splicing patterns since it is estimated that a great majority of pre-mRNAs undergo alternative splicing, frequently resulting in products with antagonistic functions.

Changing the expression of a target gene is very likely to affect the expression of other genes thereby resulting in an altered cellular response. Examination of the gene expression profiles of antisense oligonucleotide treated cells will provide insight to the genetic mechanisms involved in eliciting the desired effect. Those results may be used in many aspects of drug development, including but not limited to the development of new combinations of chemotherapeutics, identification and development of safer chemotherapeutics, and identification of novel gene targets.

References

[1] A. Herbert, A Rich, Nat Genet 21 (1999) 265–269.

[2] A J. Lopez, Annu Rev. Genet. 32 (1998) 279–305

[3] J. Wang, J.L Manley, Curr Opin Genet. Dev 7 (1997) 205–211.

[4] Y C Wang, M. Selvakumar, D. Helfman, in. A.R. Kramer (Ed), Eukaryotic mRNA Processing, Oxford Univ. Press, New York, 1997, pp 242–279.

[5] M. Krawczak, J. Reiss, D N. Cooper, Hum Genet 90 (1992) 41–54

[6] E Schwartz, E Benz, Thalassemia Syndromes, Churchill Livingston, New York, 1995.

[7] D. Abeliovich, I P. Lavon, I Lerer, T Cohen, C Springer, A. Avital, G.R. Cutting, Am. J. Hum Genet. 51 (1992) 951–956

[8] G. Perrin, M A Morris, S E Antonarakis, E. Boltshauser, P Hutter, Hum. Mutat 7 (1996) 172–175

[9] C.M. McConville, T. Stankovic, P J Byrd, G M. McGuire, Q Y Yao, G.G Lennox, M.R. Taylor, Am. J Hum. Genet. 59 (1996) 320–330.

[10] E Okuyama, N. Nishi, S. Onishi, S Itoh, Y Ishii, H Miyanaka, K Fujita, Y. Ichikawa, J. Clin Endocrinol. Metab. 82 (1997) 2337–2342.

[11] B.K. Dredge, A D. Polydorides, R B. Darnell, Nat. Rev. Neurosci. 2 (2001) 43–50.

[12] S.A Slaugenhaupt, A. Blumenfeld, S.P Gill, M Leyne, J. Mull, M P Cuajungco, C.B Liebert, B Chadwick, M. Idelson, L. Reznik, C Robbins, I. Makalowska, M Brownstein, D. Krappmann, C Scheidereit, C. Maayan, F.B Axelrod, J.F Gusella, Am J. Hum Genet 68 (2001) 598–605.

[13] D Mercatante, P. Sazani, R Kole, Current Cancer Drug Targets 1 (2001) 211–230.

[14] D Mercatante, R. Kole, Pharmacol Ther. 85 (2000) 237–243.

[15] R Kole, Modification of alternative splicing of pre-mRNA by antisense oligonucleotides, Wiley, New York, 1998.

[16] G. Lacerra, H. Sierakowska, C. Carestia, S Fucharoen, J. Summerton, D Weller, R Kole, Proc. Natl. Acad. Sci U S A 97 (2000) 9591–9596

[17] G. Schmajuk, H. Sierakowska, R Kole, J. Biol Chem 274 (1999) 21783–21789.

[18] H. Sierakowska, M J. Sambade, S. Agrawal, R. Kole, Proc. Natl Acad Sci U S. A 93 (1996) 12840–12844

[19] H Sierakowska, M. Montague, S. Agrawal, R. Kole, Nucleosides Nucleotides 16 (1997) 1173–1182.

[20] H. Sierakowska, M J Sambade, D Schumperli, R. Kole, RNA 5 (1999) 369–377.

[21] H Sierakowska, L. Gorman, S H. Kang, R. Kole, Methods Enzymol. 313 (2000) 506–521

[22] K.J. Friedman, J. Kole, J A. Cohn, M.R Knowles, L M Silverman, R Kole, J. Biol Chem 274 (1999) 36193–36199.

[23] S D. Wilton, F Lloyd, K Carville, S Fletcher, K. Honeyman, S. Agrawal, R. Kole, Neuromuscular Disord. 9 (1999) 330–338

[24] C.J. Mann, K Honeyman, A.J. Cheng, T. Ly, F Lloyd, S Fletcher, J E Morgan, T.A Partridge, S.D. Wilton, Proc. Natl Acad Sci U S A 98 (2001) 42–47

[25] J K. Taylor, Q Q Zhang, J.R. Wyatt, N.M. Dean, Nat. Biotechnol. 17 (1999) 1097–1100.

[26] D.R Mercatante, C D Bortner, J.A Cidlowski, R Kole, J Biol. Chem. 276 (2001) 16411–16417

[27] Z H Jiang, J Y Wu, Proc Soc. Exp Biol Med 220 (1999) 64–72

[28] L.H Boise, M Gonzalez-Garcia, C E Postema, L Ding, T. Lindsten, L.A. Turka, X. Mao, G. Nunez, C.B Thompson, Cell 74 (1993) 597–608.

[29] Y. Tu, S Renner, F. Xu, A. Fleishman, J Taylor, J. Weisz, R Vescio, M. Rettig, J Berenson, S. Krajewski, J C Reed, A. Lichtenstein, Cancer Res 58 (1998) 256–262.

[30] J.G Reeve, J. Xiong, J Morgan, N.M Bleehen, Br J. Cancer 73 (1996) 1193–1200.

[31] O.I. Olopade, M.O. Adeyanju, A.R Safa, F. Hagos, R Mick, C B Thompson, W M. Recant, Cancer J Sci. Am. 3 (1997) 230–237

[32] R. Liu, C. Page, D R Beidler, M S Wicha, G. Nunez, Am. J Pathol. 155 (1999) 1861–1867

[33] E Schmitt, G. Cimoli, A Steyaert, R Bertrand, Exp Cell Res 240 (1998) 107–121

[34] Y S. Cho, M.K Kim, C. Cheadle, C. Neary, K G Becker, Y S Cho-Chung, Proc Natl. Acad Sci U. S. A. 98 (2001) 9819–9823.

[35] L Liotta, E Petricoin, Nat. Rev Genet 1 (2000) 48–56

[36] C S. Cooper, Breast Cancer Res 3 (2001) 158–175.

[37] G. Dong, E. Loukinova, Z. Chen, L. Gangi, T I Chanturita, E T Liu, C Van Waes, Cancer Res. 61 (2001) 4797–4808.

[38] C Khanna, J Khan, P Nguyen, J. Prehn, J Caylor, C Yeung, J Trepel, P Meltzer, L Helman, Cancer Res 61 (2001) 3750–3759

[39] Z. Li, A Khaletskiy, J Wang, J Y. Wong, L W. Oberley, J J Li, Free Radical Biol Med. 30 (2001) 260–267.

[40] R Reeves, D.D Edberg, Y Li, Mol Cell Biol 21 (2001) 575–594

[41] F. Verrecchia, J. Rossert, A Mauviel, J Invest Dermatol. 116 (2001) 755–763.

[42] Z Li, J J Li, Radiat Res 155 (2001) 543–553

[43] S Amundson, T Myers, D Scudiero, S Kitada, J Reed, A. Fornace, Cancer Res 60 (2000) 6101–6110.

[44] V V Levenson, I A. Davidovich, I B. Roninson, Cancer Res 60 (2000) 5027–5030.

[45] W. Wang, S Marsh, J. Cassidy, H L. McLeod, Cancer Res. 61 (2001) 5505–5510.

[46] Y S Cho-Chung, M. Nesterova, S. Pepe, G.R Lee, K. Noguchi, R.K Srivastava, A R Srivastava. O Alper, Y G Park, Y.N Lee, Front Biosci 4 (1999) D898–D907.

[47] Y. Ko, Y. Kang, H Park, W. Seol, J Kim, T. Kim, H Park, E. Choi, S. Kim, J. Biol Chem. 276 (2001) 23028–23033.

[48] R Gongora, R Stephan, Z. Zhang, M Cooper, Immunity 14 (2001) 727–737

[49] H. Li, C. Leo, J. Zhu, X Wu, J. O'Neil, E Park, J. Chen, Mol Cell Biol 20 (2000) 1784–1796

[50] S. Torii, D. Egan, R. Evans, J. Reed, EMBO 18 (1999) 6037–6049.

[51] D. Aebersold, A. Kollar, K. Beer, J Laissue, R Greiner, V Djonov, Int J Cancer 96 (2001) 41–54

[52] S. Kitamura, S Konda, Y. Shinomura, S Kanayama, Y. Miyazaki, T Kiyohara, S. Hiraoka, Y. Matsuzawa, Br. J Cancer 83 (2000) 668–673

[53] I. Tamm, B Dorken, G Hartmann, Lancet 358 (2001) 489–497

[54] A.R. Yuen, B.I. Sikic, Front Biosci 5 (2000) D588–D593

[55] W. Jin, I E. McCutcheon, G.N. Fuller, E S. Huang, G J. Cote, Cancer Res 60 (2000) 1221–1224

[56] R.S Morrison, F Yamaguchi, H Saya, J.M. Bruner, A M Yahanda, L.A. Donehower, M Berger, J. Neurooncol. 18 (1994) 207–216.

[57] F Yamaguchi, H Saya, J M. Bruner, R.S. Morrison, Proc Natl Acad Sci U. S A. 91 (1994) 484–488

[58] R.P Carstens, J.V Eaton, H.R. Krigman, P J. Walther, M A Garcia-Blanco, Oncogene 15 (1997) 3059–3065

[59] B Kwabi-Addo, F. Ropiquet, D. Giri, M. Ittmann, Prostate 46 (2001) 163–172

[60] R P. Carstens, E J Wagner, M.A. Garcia-Blanco, Mol Cell Biol 20 (2000) 7388–7400.

[61] J H. Jang, K.H. Shin, Y J Park, R J Lee, W L McKeehan, J G. Park, Cancer Res. 60 (2000) 4049–4052

[62] S Takaishi, M. Sawada, Y Morita, H. Seno, H Fukuzawa, T Chiba, Biochem Biophys Res. Commun. 267 (2000) 658–662.

[63] R J. Sneath, D.C Mangham, Mol. Pathol 51 (1998) 191–200

[64] A Herrera-Gayol, S. Jothy, Exp Mol. Pathol 66 (1999) 149–156.

[65] S B Wallach, A Friedmann, D. Naor, Cancer Detect. Prev. 24 (2000) 33–45.

[66] B M Wittig, R Goebel, S Weg-Remers, G. Pistorius, G Feifel, M Zeitz, A Stallmach, Exp Mol Pathol. 70 (2001) 96–102

[67] M. Aoyama, K Asai, T. Shishikura, T Kawamoto, T Miyachi, T Yokoi, H. Togari, Y. Wada, T. Kato, A. Nakagawara, Cancer Lett. 164 (2001) 51–60

[68] A. Aigner, H. Juhl, C. Malerczyk, A. Tkybusch, C C Benz, F Czubayko, Oncogene 20 (2001) 2101–2111

[69] K Y Kwong, M.C Hung, Mol. Carcinog. 23 (1998) 62–68.

[70] M.M Berggren, G. Powis, Arch Biochem Biophys 389 (2001) 144–149

[71] A. Beghini, C.B Ripamonti, P. Peterlongo, G. Roversi, R Cairoli, E Morra, L. Larizza, Hum Mol. Genet 9 (2000) 2297–2304

[72] M. Krajewska, S. Krajewski, J I Epstein, A Shabaik, J. Sauvageot, K Song, S Kitada, J C. Reed, Am J Pathol 148 (1996) 1567–1576.

[73] M Marone, G Scambia, S Mozzetti, G Ferrandina, S Iacovella, A. De Pasqua, P Benedetti-Panici, S Mancuso, Clin. Cancer Res 4 (1998) 517–524

[74] V Nuessler, O Stotzer, E Gullis, R Pelka-Fleischer, A Pogrebniak, F. Gieseler, W. Wilmanns, Leukemia 13 (1999) 1864–1872

[75] E Schmitt, C. Paquet, M Beauchemin, J. Dever-Bertrand, E Bertrand, Biochem Biophys Res. Commun. 270 (2000) 868–873.

[76] C Sakakura, E.A. Sweeney, T Shirahama, Y. Igarashi, S. Hakomori, H. Tsujimoto, T. Imanishi, M. Ohgaki, J. Yamazaki, A. Hagiwara, K. Sawai, T Yamaguchi, T Takahashi, Surg. Today 27 (1997) 90–93

[77] R.C. Bargou, C. Wagener, K. Bommert, M.Y Mapara, P T Daniel, W Arnold, M Dietel, H Guski, A. Feller, H D Royer, B Dorken, J. Clin. Invest 97 (1996) 2651–2659

[78] R C Bargou, P T. Daniel, M Y Mapara, K Bommert, C Wagener, B Kallinich, H D Royer, B Dorken, Int J Cancer 60 (1995) 858–859.

[79] S.A Gayther, P. Barski, S J Batley, L Li, K.A de Foy, S.N Cohen, B.A. Ponder, C Caldas, Oncogene 15 (1997) 2119–2126

[80] X. Luan, G. Shi, M Zohouri, W Paradee, D.I. Smith, H J Becker, L.A. Cannizzaro, Oncogene 15 (1997) 79–86

[81] H. Sato, K Hiyama, S Ishioka, H. Maeda, M. Yamakido, Int J Oncol. 15 (1999) 81–88

[82] I Fillippovich, N Sorokina, M Gatei, Y Haupt, K. Hobson, E. Moallem, K. Spring, M. Mould, M.A. McGuckin, M.F. Lavin, K K Khanna, Oncogene 20 (2001) 514–522.

[83] D Zwahlen, M.P. Tschan, T J Grob, U.R. Peters, D Fink, W Haenggi, H.J. Altermatt, J F Cajot, A Tobler, M F. Fey, S Aebi, Int J. Cancer 88 (2000) 66–70.

[84] A I Zaika, S. Kovalev, N D Marchenko, U.M. Moll, Cancer Res. 59 (1999) 3257–3263.

[85] R Matsumoto, M. Tada, M. Nozaki, C.L Zhang, Y. Sawamura, H. Abe, Cancer Res 58 (1998) 609–613

[86] I Sigalas, A H Calvert, J.J. Anderson, D E Neal, J. Lunec, Nat Med. 2 (1996) 912–917

[87] J. Lukas, D.Q. Gao, M. Keshmeshian, W H. Wen, D Tsao-Wei, S. Rosenberg, M.F Press, Cancer Res. 61 (2001) 3212–3219

[88] K Pritchard-Jones, L King-Underwood, Leuk. Lymphoma 27 (1997) 207–220.

[89] J. Renshaw, L. King-Underwood, K. Pritchard-Jones, Genes Chromosomes Cancer 19 (1997) 256–266.

[90] S. Iben, B Royer-Pokora, Oncogene 18 (1999) 2533–2536.

[91] T I Orban, E Olah, Biochem. Biophys Res Commun. 280 (2001) 32–38

[92] I. Bieche, R Lidereau, Cancer Res 59 (1999) 2546–2550.

[93] L Cheng, M.R. Spitz, W.K Hong, Q Wei, Carcinogenesis 21 (2000) 1527–1530.

[94] S Emmert, T.D Schneider, S.G Khan, K.H Kraemer, Nucleic Acids Res. 29 (2001) 1443–1452

ELSEVIER

Biochimica et Biophysica Acta 1587 (2002) 133–144

BIOCHIMICA ET BIOPHYSICA ACTA
BBA
www.bba-direct.com

Review

Homeostatic control of uridine and the role of uridine phosphorylase: a biological and clinical update

Giuseppe Pizzorno*, Deliang Cao, Janine J. Leffert, Rosalind L. Russell, Dekai Zhang, Robert E. Handschumacher

Departments of Internal Medicine and Pharmacology (Oncology), Yale University School of Medicine, 333 Cedar Street, New Haven, CT 06520, USA

Received 24 January 2002; accepted 24 January 2002

Abstract

Uridine, a pyrimidine nucleoside essential for the synthesis of RNA and bio-membranes, is a crucial element in the regulation of normal physiological processes as well as pathological states. The biological effects of uridine have been associated with the regulation of the cardio-circulatory system, at the reproduction level, with both peripheral and central nervous system modulation and with the functionality of the respiratory system. Furthermore, uridine plays a role at the clinical level in modulating the cytotoxic effects of fluoropyrimidines in both normal and neoplastic tissues. The concentration of uridine in plasma and tissues is tightly regulated by cellular transport mechanisms and by the activity of uridine phosphorylase (UPase), responsible for the reversible phosphorolysis of uridine to uracil. We have recently completed several studies designed to define the mechanisms regulating UPase expression and better characterize the multiple biological effects of uridine. Immunohistochemical analysis and co-purification studies have revealed the association of UPase with the cytoskeleton and the cellular membrane The characterization of the promoter region of UPase has indicated a direct regulation of its expression by the tumor suppressor gene p53. The evaluation of human surgical specimens has shown elevated UPase activity in tumor tissue compared to paired normal tissue © 2002 Elsevier Science B.V. All rights reserved.

Keywords. Uridine, Uridine phosphorylase; Pyrimidine; 5-Fluorouracil; p53; Cytoskeleton

1. Introduction: physiological and biological role of uridine

Pyrimidines are synthesized de novo in mammalian cells through a multistep process starting from glutamine and carbon dioxide to form, the pyrimidine ring in the second to last intermediate, orotic acid, which is then converted to its nucleotide form in the presence of PRPP. From the degradation of the nucleic acids and nucleotides a large portion of the pyrimidines are salvaged. The relative contribution of de novo synthesis and salvage pathway to the maintenance of the nucleotide pools varies in different cells and tissues [1]. A crucial difference between purine and pyrimidine metabolism is that purines are recycled from their bases while pyrimidines are salvaged from their nucleosides, particularly uridine. In fact, in patients with deficient pyrimidine biosynthesis, only uridine is able to overcome this pathological manifestation but uracil is not [2].

The concentration of circulating plasma uridine of approximately 3–5 μM is tightly regulated throughout different species and individuals [3–5]. The liver appears to have this homeostatic control on uridine degradation and formation [6]. Uridine is essentially cleared in a single pass through the liver and it is replaced in a highly regulated manner by "new uridine" formed by de novo synthesis [6]. We have previously reported the cellular basis for the catabolic component of this apparent paradox by the dissociation of the liver into two cell fractions, hepatocytes and a nonparenchymal cell population. Suspensions of the nonparenchymal cells were shown to rapidly cleave uridine to uracil, while in hepatocytes, this activity was barely detectable. Conversely, hepatocytes caused extensive degradation of uracil to β-alanine. These differences correlated with the

---

Abbreviations PRPP, 5-Phosphorylribose 1-pyrophosphate, BAU, Benzylacyclouridine, UDPG, Uridine 5′-diphosphoglucose, UPase, Uridine phosphorylase, TNF-α, Tumor necrosis factor-α, IL-1α, Interleukin-1α, IFN α and γ, Interferon α and γ; TPase, Thymidine phosphorylase; 5-FU, 5-Fluorouracil; PALA, *N*-(phosphonacetyl)-L-aspartate, MTD, Maximum tolerated dose, TAU, 2′,3′,5′-tri-*O*-acetyluridine; NBMPR, nitrobenzylthioinosine, PD-ECGF, platelet-derived endothelial cell growth factor; GAPDH, glyceraldehyde-3-phosphate dehydrogenase, NDPK, nucleoside diphosphate kinase; NTP, nucleotide triphosphates

* Corresponding author. Tel +1-203-785-4549; fax· +1-203-785-7670.
E-mail address Giuseppe.Pizzorno@yale.edu (G. Pizzorno).

0925-4439/02/$ - see front matter © 2002 Elsevier Science B V All rights reserved
PII. S0925-4439(02)00076-5

uridine phosphorylase (UPase) and dihydrouracil dehydrogenase activity present in each cell type [7].

Besides the critical role of uridine in the synthesis of RNA and bio-membranes, through the formation of pyrimidine-lipid and pyrimidine-sugar conjugates, experimental and clinical evidence suggests a role for uridine in regulating a series of biological functions [8].

Uridine and its nucleosides have shown a complex effect in the regulation of vascular resistance, producing opposing effects in some tissues, either by acting directly on the smooth muscle cells or by stimulating the surrounding endothelial cells [9].

Uridine is present in the seminal fluid at millimolar concentrations, a level that is approximately three orders of magnitude higher compared to other body fluids or tissues [10]. The presence of such a high uridine concentration and its correlation with sperm motility suggests a role of uridine in spermatogenesis [11]. Furthermore, a low level of uridine in prostatic secretions of patients with prostatitis also indicates a possible role of this nucleoside in the etiology of this disease [11].

In the area of the peripheral nervous system, uridine appears to have a modulatory role. It has been shown to hyperpolarize amphibian ganglia and rat superior cervical ganglia at submillimolar concentrations, possibly resulting in an inhibitory activity [12]. Several clinical observations indicate the crucial function of pyrimidine nucleoside salvage in the maintenance of normal CNS activity [13,14]. In the treatment of a form of autism with seizures, oral uridine administration has led to improvement in speech, behavior and decreased frequency in seizures [15]. Deficiencies in the catabolism of pyrimidines due to impaired activity of one of the steps in the catabolic pathway, such as dihydropyrimidine dehydrogenase or β-ureidopropionase, have resulted in autism, convulsions, mental retardation and decreased motor coordination [14].

In animal models, uridine has been shown to potentiate dopaminergic transmission and reduce anxiety [16]. Uridine has been documented as a sleep-inducing factor in rats and shown to increase the activity of barbiturates [17,18]. In mice and rats, high doses of uridine cause a dramatic reduction in body temperature [19]; whereas uridine induces fever in human and rabbits [20,21]. The co-administration of an inhibitor of UPase, benzylacyclouridine (BAU), almost completely prevented the effect on thermoregulation, suggesting that a pyrimidine catabolite, possibly β-alanine, could alter the control of the body temperature [21].

Aside from the 'physiological' effects that we have just briefly outlined, uridine appears to have remarkable functions in tissues under stress or pathological situations and in the clinical setting. In hearts subjected to ischemia, perfusion with uridine rapidly restored myocardial ATP levels, glycogen and UDPG [22]. Similarly, uridine perfusion resulted in the maintenance of brain metabolism during ischemia or severe hypoglycemia [23,24]. Furthermore, uridine induced recovery from neuronal degeneration produced by diabetic neuropathy [25]. Uridine has been used as a 'rescue' agent in cancer therapy to decrease bone marrow and gastrointestinal toxicity, following 5-fluorouracil-based drug regimens [4,26–31]. In combination with BAU, uridine has shown some activity in reducing neurotoxicity and the effects on the bone marrow of AZT during treatment for HIV infections [32].

1.1. Role of UPase on the pharmacological activity of uridine

Plasma and intracellular concentrations of uridine are regulated by the catabolic activity of UPase and by two transport mechanisms, facilitated diffusion and Na^+-dependent active transport. UPase catalyzes the reversible phosphorolysis of uridine and to a lesser degree of thymidine. It also cleaves pyrimidine 2′- and 5′-deoxyribosides at a much lower rate [33–37]. UPase is present in most tissues and in tumors, where its activity is generally elevated [33,35,38]. The mammalian enzyme appears to be a tetrameric protein with subunits of approximately 33,000 molecular weight. Initial velocity and product inhibition studies suggest an ordered bi–bi mechanism where Pi binds first before uridine and ribose-1-phosphate is released after uracil [39]. UPase plays an important role in the homeostatic regulation of uridine concentration in plasma and tissues [22–25] as well as affects activation and catabolism of fluoropyrimidines influencing their therapeutic capacity [40–43]. The expression of UPase has been shown to be induced in different tumor cell lines, such as Colon 26 and HCT-116, when in the presence of cytokines: TNF-α, IL-1α and IFN-α and γ, and vitamin D_3 [44–46]. A similar response to cytokines has been observed for thymidine phosphorylase (TPase) [47]. Induction of UPase expression has also been reported in c-H-ras transformed NIH 3T3 cells [48]. In a murine model, hepatic UPase has been found to follow a circadian rhythm which was the inverse of that for plasma uridine concentration, re-emphasizing its role in the regulation of blood uridine level and suggesting its possible involvement in the humoral control of sleep [49].

A misconception surrounds the role of UPase and TPase. Some literature reports UPase as the pyrimidine nucleoside phosphorylase in murine tissues and TPase the main phosphorolytic enzyme in human tissues [50]. UPase, however, has been shown to be present in all human tissues and tumors, whereas TPase activity has been found reduced or absent in many human tumors [4,17,26,27,33,35,40,51–54].

1 2. "Rescue" of 5-fluorouracil toxicity

As previously mentioned, UPase has a critical role in regulating the concentration of uridine in plasma and tissues. A number of clinical studies have demonstrated the ability of uridine to reduce 5-FU toxicity, without affecting its antitumor activity, if properly administered 18–24 h following the cytotoxic agent [26–29].

The combination 'rescue regimens' of 5-FU plus uridine were initially proposed to evaluate the hypothesis that the antitumor effect of 5-FU is primarily due to the inhibition of thymidylate synthase and the host toxicity caused by the incorporation of the fluoropyrimidine into RNA [55]. In vivo studies in a murine model [56] and in vitro data [57] have clearly indicated that the incorporation of 5-FU into RNA appears to be the major cause of gastrointestinal toxicity. Results show that uridine inhibited the incorporation and avoided the cytotoxic effect, whereas thymidine did not prevent 5-FU toxicity. Furthermore, a recent study has indicated that the p53-dependent apoptosis induced by 5-FU in intestinal cells was reduced by uridine administration but not by thymidine [58].

Because of its low oral bioavailability and a rapid half-life, large doses of uridine are necessary to achieve clinically relevant concentrations in plasma causing moderate to severe toxicity including severe diarrhea as dose-limiting toxicity [4,20]. On the other hand, infusion of uridine has resulted in fevers, phlebitis, cellulitis, superior vena cava syndrome, torpor and confusion, and precluded an extensive clinical use [20,59]. Nevertheless, clinical studies of 5-FU in combination with methotrexate and PALA, have shown that patients tolerated combination therapy with delayed uridine (infused over a 72-h period starting 2 h after 5-FU administration, 3 h on and 3 h off) up to a weekly dose of 750 mg/m^2 of 5-FU, with 25% experiencing moderate mucositis (grade II). In a previous clinical trial without uridine, four out of six patients could not tolerate a 600 mg/m^2 dose of 5-FU because of mucositis, diarrhea and a decrease in performance status. In another study, 5-FU treatment could be continued with delayed administration of uridine at a weekly dose of 5-FU, which alone caused dose-limiting myelosuppression. In most of the patients who had previously developed leukopenia, the WBC increased markedly despite continued 5-FU administration [59]. In a more recent study of high-dose 5-FU with doxorubicin, high-dose methotrexate and leucovorin, oral uridine administration allowed for dose intensification of 5-FU with a 33% increase in the MTD of 5-FU in the presence of doxorubicin and a 45% increase in 5-FU MTD without doxorubicin [60]. No responses were obtained in patients with gastric cancer (0/11) when uridine was administered 2 h after 5-FU, however 2/3 patients responded with the 24-h uridine delay. This last regimen, with a 24-h interval between the administration of 5-FU and uridine, ensured rescue from 5-FU-induced hematologic toxicity without adverse impact on tumor response [60]. As indicated in pre-clinical studies, properly delayed uridine rescue results in a faster clearance of 5-FU from RNA of bone marrow and tumors and enhancement of the rate of recovery of DNA synthesis only in the bone marrow [37].

Our laboratory has shown that the problem of a rapid disposition of uridine and the administration of large doses of the nucleoside could be overcome by utilizing inhibitors of UPase, such as BAU, to conserve endogenous uridine with consequent elevation of its concentration in plasma and tissues. This approach has resulted in the reduction in animal models of host toxicity, while maintaining the antineoplastic effect of 5-FU [34]. A phase I clinical trial of oral BAU administered as a single agent has shown the ability of this inhibitor to elevate 2–3-fold the plasma uridine concentration with no significant host toxicity in patients [3].

1.3. *Tri-O-acetyluridine (TAU)*

A new agent 2′,3′,5′-tri-*O*-acetyluridine (TAU; PN 401) has been tested recently in a clinical trial to rescue 5-FU toxicity. TAU is a uridine pro-drug, the presence of the acetyl groups increases the hydrophobicity, therefore enhancing the gastrointestinal transport and bioavailability, and protecting this agent from the catabolism by UPase. Uridine is then progressively released by plasma esterases resulting in sustained delivery over time without most of the side effects of uridine administration. The sustained elevated level of uridine, up to 50 μM in plasma, has allowed a dose escalation of 5-FU, administered as a rapid intravenous bolus weekly for 6 weeks, from 600 to 1000 mg/m^2. Still, an oral dose of 6 g of TAU at 6-h intervals was necessary to produce significant uridine levels [61].

2. Regulation of uridine homeostasis: transport mechanisms

Besides catabolism by nucleoside phosphorylase activity, the intracellular concentration of uridine is regulated by its transport through the cell membranes. A facilitated-diffusion mechanism, which equilibrates intracellular and extracellular uridine, has been considered for many years to be responsible for intracellular uridine concentration. This non-energy dependent process displays broad substrate specificity toward synthetic and naturally occurring pyrimidine nucleosides [62–65]. In addition to competition between functional substrates, the facilitated diffusion of nucleosides present in most cell lines can be reversibly inhibited by compounds such as dipyridamole and nitrobenzylthioinosine [66]. Studies by Belt [67,68] have revealed that the facilitated diffusion mechanism in cell lines can be distinguished by the sensitivity to inhibition by NBMPR or dipyridamole. Recently, both transporters, NBMPR-sensitive (es) and NBMPR-insensitive (ei) have been cloned and characterized [69,70].

In addition to the non-concentrative facilitated diffusion mechanism, renal and gut epithelial cells were shown to possess a Na$^+$-dependent transporter for nucleosides [71–77]. Our laboratory revealed the potential physiological significance of this Na$^+$-dependent transport system by the finding that concentrations of uridine in a variety of freeze-clamped normal murine tissues far exceeded the concentration of uridine in the plasma. We were able to demonstrate that BAU generated concentrations of uridine in selected tissues that were as much as 50–100 times that in control plasma [34]. The concentrative system in liver, kidney and gut appears to have different substrate specificity than in lymphoid cells (spleen or thymus). In addition, we have demonstrated the generality of the expression of a concentrative, active transport mechanism for uridine in a variety of normal murine tissues [53]. These observations changed the perception of the Na$^+$-dependent uridine transport process from a rate phenomenon observed in isolated cells to a major physiological effect that afforded therapeutic opportunities considering that the intracellular concentrations of uridine in a wide variety of neoplastic cell lines did not exceed those in the media. It has been shown that some lines express the concentrative mechanism to a very limited degree [78] but that it is overwhelmed by the equilibration of nucleoside achieved by an active facilitated diffusion mechanism. At this moment, five major Na$^+$-dependent active transport systems have been isolated: (1) the purine selective N1 system, or cif, shown to be present in rat intestinal epithelium, mouse enterocytes and lately in human kidney [79–82]; (2) the pyrimidine selective N2 system or cit described by Jarvis and Griffith [83], present in rabbit small intestine with selectivity for pyrimidine nucleosides and adenosine; (3) the N3 transport system (cib) isolated in rat jejunum sensitive to inhibition by both purine and pyrimidines [84]; (4) the N4 transport system, expressed in human kidneys, which is identical to the N2 system in substrate specificity [85]; and the N5, a cs transport system, found in freshly isolated human leukemia cells [86].

3. UPase: clinical, biological and regulation update

Over the past few years, we have focused on the role of UPase in regulating uridine metabolism and its intracellular levels in normal and neoplastic tissues and on the mechanisms controlling the expression and localization of UPase. We have determined that the activity of UPase is elevated in tumors as compared to their normal tissue counterpart and discovered variant uridine phosphorolytic activity in selected human tumors [54]. We have also defined the genomic structure of the UPase gene, characterized its promoter region, the p53-dependent control of its expression [87,88] and established its intracellular localization and association with cytoskeletal elements [89].

3.1. Expression and detection of UPase and identification of variant phosphorolytic activity in human tumors

TPase catalyzes the reversible phosphorolysis of thymidine to thymine and with less efficiency also contributes to the initial degradation of uridine. Since TPase has been shown to be identical to platelet-derived endothelial cell growth factor (PD-ECGF) and its angiogenic activity demonstrated [90,91], several studies have investigated the role of this protein in tumor progression and clinical outcome. Increased expression has been found in some solid tumors compared to the adjacent normal tissues [92] and TPase has been shown to be a negative prognostic indicator in bladder [93], colo-rectal [94,95], ovarian [92], pancreatic [96] and renal [97] cancers but its role is still controversial in breast carcinoma [98,99]. PD-ECGF/TPase has been shown to promote angiogenesis only when enzymatically active and in the presence of thymidine [100].

The intense investigation of the role of TPase on cancer invasiveness and malignancy has not translated to a similar interest for a potential involvement of UPase, despite its complementary phosphorolytic activity.

We have evaluated the activity of UPase in fresh tumor specimens and adjacent normal tissues of patients undergoing surgical resection of their malignancy. The enzymatic activity was variable among the different tissue specimens, but overall it was 2–3-fold higher in tumors compared with the paired normal tissue (Fig. 1). In the tissues that we were able to collect the most clinical specimens, breast ($n = 28$) and colon ($n = 9$) carcinomas, the difference in activity between tumor and normal tissues was statistically significant with P values of 0.012 and 0.021, respectively [54]. These results have been confirmed in a recent study in 35 human colo-rectal carcinomas also indicating higher UPase mRNA gene expression in tumor compared to paired normal tissue [101]. The same study concluded that higher UPase gene expression was a negative prognostic factor for the patient [101]. In all normal tissues and most tumor specimens evaluated in our investigation [54], UPase activity was completely inhibited by the UPase inhibitor BAU at 10 μM concentration. However, breast, head-neck, and ovarian tumors showed partial sensitivity to the inhibitor with ~ 40% of residual phosphorolytic activity still present after the addition of 100 μM BAU. Using the TPase inhibitor 5-bromo-6-aminouracil [102], we were able to establish that TPase does not significantly contribute to the BAU insensitive phosphorolytic activity present in breast tumor tissue.

The evaluation of the clinical specimens has clearly indicated that normal tissues like gastrointestinal tract and bone marrow, that are the most sensitive to fluoropyrimidine toxicity, possess UPase activity completely inhibitable by BAU. However, human breast tumors possess distinct phosphorolytic activity that is partially insensitive to the classical UPase inhibitors, therefore resulting in a more rapid degradation of uridine. This differential catabolism of the pyrimidine nucleoside could be exploited to create, in the presence of BAU, a selective rescue effect for normal tissues without affecting the antineoplastic activity in breast neoplastic tissues therefore enhancing the therapeutic index of the fluoropyrimidine.

Our study, on human clinical specimens revealing the presence of higher UPase enzymatic activity in tumor tissues as compared to paired normal tissue is in contrast with a previous report from Maehara et al. [48] indicating no difference in UPase activity between tumor and normal

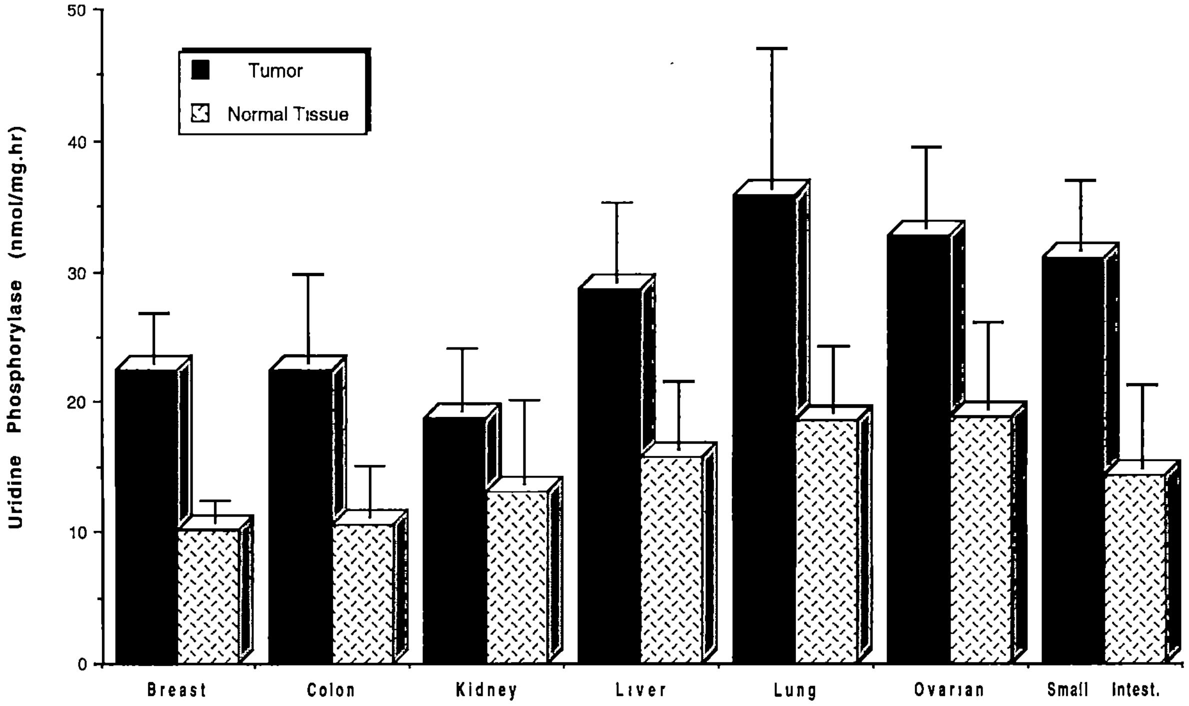

Fig 1 UPase activity in matched pairs of human breast tumor and normal tissues following surgical excision of the malignancy

tissues. We also disagree with another finding from the same group indicating that the main pyrimidine nucleoside phosphorylase in human is TPase with activity 20-fold higher than UPase [48]. In our evaluation, we have observed a degree of variation in the ratio of TPase to UPase activity in human tissues with an overall ratio of 2. However, in many tissues including breast tumors, the ratio was actually in favor of UPase. Our investigation has also indicated that both bone marrow and gut mucosa specimens possess low phosphorolytic activity compared to tumor tissues, suggesting that uridine rescue could specifically benefit these tissues representing the primary targets of 5-fluorouracil toxicity, as reported by Pritchard et al. [58] in a study on its effect on the intestinal mucosa.

A recent article from Kanzaki et al. [103] has examined the mRNA expression of UPase and TPase in surgical specimens of 43 patients with breast carcinoma and examined the correlation with clinical pathological factors. The investigators have found a large variation in the expression level of both genes with the highest level measured as more than 1000-fold higher than that in samples expressing the lowest level. There was a significant correlation between TPase expression and microvessel density but no correlation with UPase expression suggesting that UPase does not have any angiogenic activity in human breast carcinoma. In addition, no correlation was found between UPase gene expression and TPase expression level in those breast tumor samples. However, UPase gene expression was higher in patients who relapsed than in patients that did not and patients with high UPase mRNA levels had a significantly poorer overall survival than patients with lower levels. TPase gene expression did not correlate with either relapse or overall survival in these breast cancer patients [103]. This critical study confirms a previous study from the same group indicating a lack of correlation between clinical outcome and TPase mRNA expression in breast cancer [98]. However, it suggests that UPase could be an independent prognostic factor in breast cancer patients [103].

3.2. UPase genomic structure, characterization of its promoter region and p53-dependent control of its expression

We have recently isolated from a murine BAC library a genomic DNA fragment which included the entire murine UPase gene, whose full length approximates 18.0 kb. The UPase gene has been mapped by FISH to the murine chromosome 11A1–2. A series of oligonucleotide primers based on the cDNA sequence of murine UPase have been utilized to elucidate the intron–exon boundaries [87]. Our results indicate that the murine UPase gene consists of nine exons, ranging in length from 66 to 210 bp, and eight introns varying in size from 240 to 6.0 kb, with typical donor and acceptor sites (GT-AG rule). Exon 1, 2 and the 5′ end part of exon 3 do not encode amino acids, the first in-frame ATG codon is located in exon 3. Exon 8 encodes the C-terminus of murine UPase protein and contains a translation stop codon TGA. It also contains the first 70 bp of the 3′-untranslated region. A polyadenylation signal, AATAAA, is present at 45 bp downstream of the TGA codon [87]. We have now also concluded the characterization of the human UPase gene that presents the same basic structure with nine exons and eight introns. Chromosomal mapping of human UPase identified its location at 7p12, a position where frequent LOH has been found in human breast cancers [104].

The sequence of the 3′-untranslated flanking region of the murine UPase gene shows a GT-rich region present 22 bp downstream of the AATAAA polyadenylation signal. A TGGGG tandem repeat, TGGGGG(TGGGG)$_4$, is present at 154 bp downstream of AATAAA polyadenylation signal, which represents a putative recombination consensus sequence found in the immunoglobulin switch region (S region), in the α-globin gene cluster, in the putative arrest sites for polymerase α, and in the deletion hot spot (exon 8) of the survival motor-neuron (SMN) gene [105–107].

The 5′ flanking region of the murine UPase gene, the immediate full-length sequence (1703 bp) that has shown promoter activity in our studies, doesn't contain canonical CAAT box although a TATA-like sequence, CAATAAAA, is present from −41 to −49 bp upstream of the transcription start point at +1 bp. The lack of both canonical TATA and CAAT consensus sequences is a feature present in a group of genes, many of which have a housekeeping function, such as *N*-ras and transforming growth factor α [108]. At the 5′ end of UPase promoter (from −1619 to −1110) we identified a series of microsatellite and minisatellite repeat bases. In addition, an abundance of promoter regulatory elements are seen in the murine UPase promoter region including the presence of the consensus motifs for GATA-1 and two transcription factors. These factors mainly function as regulatory elements in the control of cellular differentiation of hematopoietic cells [109,110]. An IRF-1-like consensus element present just upstream (from −21 to −33) of the putative transcription start site of the UPase gene represents an important transcription factor in the regulation of the interferon response system for infection, cell growth and apoptosis [111,112]. Finally, two potential proto-oncogene binding sites for C-Myb and V-Myb [113–115], and a tumor suppressor gene, p53 putative regulatory element [116–118], located in the sequence −303 bp to −294 bp, have been found in the UPase promoter region.

To explore the possible effect of p53 on UPase expression, we have analyzed the effects of p53 on the murine UPase promoter activity [88]. We found that the deletion from −1619 to −445 of the UPase promoter had no effect on the ability of p53 to inhibit gene expression, however, the inhibitory activity was altered when the promoter region between −445 and −274 bp was deleted. Using transient-expression assays in EMT6 and NIH 3T3 cells, co-transfection with the wild-type p53 construct resulted in significantly less luciferase activity in the constructs from −1619 to −445 bp, whereas down to −274 bp and more, the promoter activity was not affected. These data indicate that the region between −445 and −274 bp is susceptible to regulation by p53 in the UPase promoter. This phenomenon was further confirmed in p53 nullified cells [88]. Sequencing analysis of this region found a putative p53-binding motif AGcCTTGTCC located at −303 to −294. This binding motif differs in one base (small case base) from the consensus binding element of p53 [119]. The gel mobility shift assay and DNase I footprinting have indicated that this putative regulatory motif exhibited specific binding with the p53 protein [88].

p53 has been shown, by Linke et al. [120], to be activated by ribonucleotide depletion caused by antimetabolite drugs such as PALA even in the absence of DNA damage. As previously mentioned, the phosphorolytic activity of UPase regulating intracellular uridine levels reveals the critical role of this enzyme in modulating the pyrimidine salvage pathway. The suppressive regulation of p53 on UPase gene indicates the presence of a negative control of the pyrimidine salvage pathway by p53 through UPase, probably as a cellular self-protection mechanism in case of ribonucleotide depletion. p53 has previously been shown to: (a) activate genes that initiate apoptosis to eliminate damaged cells and protect an organism from more severe damage and (b) cause cell-cycle arrest following DNA damage to prevent the replication of altered DNA. However, so far, any indication of the contribution of p53 to damage repair is quite limited. A recent report by Tanaka et al. [121] has described a p53-induced gene, p53R2 that encodes for a protein similar to one of the two subunits of ribonucleotide reductase, the rate-limiting step in the conversion of ribonucleotides to deoxyribonucleotides. The p53 regulated R2 subunit is found in the nucleus and its expression is induced by cellular damage (γ-radiation and doxorubicin treatment) suggesting that when repair is needed, the nuclear precursors have to be concentrated near the site of damage.

Somehow, the p53-regulated suppression of UPase expression exerts similar functions to the control that p53 has on p53R2. A cellular damage causing loss or imbalance in the ribonucleotide pools could cause activation of p53 leading to suppression of UPase expression and activation of the pyrimidine salvage pathway to replenish the affected pyrimidine nucleotide pools (Fig. 2). These two p53-regu-

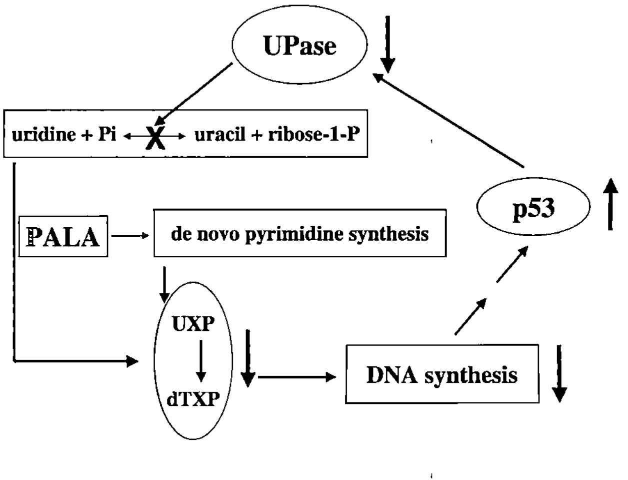
UPase
uridine + Pi ⟷ uracil + ribose-1-P
PALA
de novo pyrimidine synthesis
p53
UXP
dTXP
DNA synthesis

Fig 2 p53-dependent control of UPase expression and regulation of pyrimidine salvage pathway following PALA inhibition of de novo pyrimidine biosynthesis.

lated mechanisms provide a new level of control on ribo- and deoxy-ribonucleotide pools. Under normal replication conditions, the regulating mechanisms that control the appropriate balance of nucleotides are mostly based on the direct feedback regulation of the biosynthetic enzymes by some of the precursors or final products. However, the p53R2 study and our data on UPase possibly indicate that in case of cellular damage with depletion of nucleotide pools a more sophisticated level of regulation is triggered to more rapidly provide precursors for nuclear repair [88,121].

The elucidation of the negative control regulation of p53 on the UPase gene promoter and UPase expression could also have considerable implication at the clinical level since the human UPase DNA promoter presents, as we have shown for the murine gene, a p53 regulatory element [88]. It is conceivable that mutations and loss of functionality of the p53 gene product, which is a common event in many forms of cancer [122], could alter the suppressive regulatory control on UPase resulting in higher UPase mRNA expression and elevated UPase activity seen in many tumors as compared to paired normal tissues [54].

3.3. Intracellular distribution, localization and association with vimentin

We have established that UPase is associated with the intermediate filament vimentin in NIH 3T3 fibroblasts and Colon 26 cells through co-purification studies using a 5′-amino benzylacyclouridine affinity matrix. The separation of cytosolic proteins using gel filtration chromatography yields a high molecular weight complex containing UPase and vimentin in a 1:1 stoichiometry. Immunofluorescent techniques have confirmed that UPase is associated with vimentin and that the depolymerization of the microtubule system using nocodazole results in UPase remaining associated with the collapsed intermediate filament, vimentin [89].

UPase is associated with both the soluble pool of vimentin and also with its insoluble pool, with approximately 50–70% of the total UPase present in the cytosol as a soluble protein. However, sequential cell extraction liberates an additional 15–25% UPase activity associated with a Triton-X-100 soluble fraction and a remaining 10–20% UPase activity associated with a Triton-X-100 insoluble pool [89].

The role of UPase in the salvage pathway of pyrimidine nucleoside biosynthesis does not readily translate into a role for this enzyme in association with the cytoskeleton and more specifically with the intermediate filament vimentin. While a number of theories have been proposed for the function of this network, the data are not yet conclusive. Cellular processes as diverse as differentiation, motility, signal transduction, cell division, cytoskeletal stability and vesicular trafficking have been associated with alterations in the dynamics of the intermediate filaments [123–127].

A number of proteins have been shown to be associated with the vimentin intermediate filament scaffold including p53 [128], protein kinase C [129], Yes and cGMP kinase [130,131], glycolytic enzymes creatine phosphokinase and GAPDH [132–134] and nucleoside diphosphate kinase [132,135] as well as the cross-linking proteins plectin, IFAP-300 and filamin that link intermediate filaments to other cytoskeletal elements and membranes [136–139]. It is particularly interesting to note the number of proteins involved in signal transduction and energy metabolism that have been associated with vimentin. The proposed role for NDPK in nucleotide channeling [135], its co-purification with vimentin and enzymes involved in ATP formation/regeneration [132] together with our observation of UPase co-localization with this same cellular machinery, is making it more likely that such observations are biologically relevant. UPase, a nucleoside phosphorylase and NDPK, an enzyme that provides the majority of cellular non-ATP nucleoside triphosphates have both been co-localized to the intermediate filament vimentin. Since a number of biological responses have been associated with UTP and UDP [140] through the activation of pyrimidine receptors, it is possible that vimentin may play a role in the coordination of these signaling events.

In vitro enzymatic analyses of the detergent-resistant pool of UPase demonstrated that this source of enzyme retains enzymatic activity. The UPase found in association with the polymeric vimentin network may represent a mobilizable pool of enzyme that is only active when liberated from its three-dimensional network. It is also possible that UPase, in association with the insoluble vimentin network, represents a way of localizing enzymatic activity to a particular area within the cell. Vimentin has been proposed as a network that might target mRNA to areas of active protein synthesis [124]. This function for vimentin might explain the necessity of having machinery for pyrimidine synthesis/degradation in close proximity to areas of mRNA translation.

The interdependence of the dynein and kinesin motor proteins, microtubule and intermediate filament systems and the need to furnish this cellular machinery with high quantities of nucleotide triphosphates provides a basis for investigating the mechanisms responsible for the local delivery of high quantities of NTPs to the areas of active energy utilization. The question of what role UPase may play in close proximity to such machinery is at this moment cause for speculation.

4. Conclusions

Many factors have contributed to the limited attention uridine and UPase have received despite their physiologic and pharmacological role in comparison to the interest reserved over the years to adenosine and TPase.

Adenosine has been shown to have a general inhibitory effect on neuronal activity including regulation of sleep, neuroprotection and seizure control [141]. Furthermore, this purine nucleoside appears to have cardioprotective and immunomodulatory functions [142]. These regulatory and modulatory activities of adenosine are mediated by four subtypes of G-protein-coupled receptors [143]. As we have indicated in our introduction, uridine exerts very similar modulatory and regulatory functions to adenosine, however, no clear mechanism has been identified modulating these physiological activities. Receptors for uridine nucleotides have been mentioned and also the possible existence of a specific receptor for uridine itself has been postulated. A very recent report suggests the presence of a new receptor identified as "uridine receptor" regulating the hypnotic activity of uridine derivatives in rat brain [144]. More studies are needed to confirm this finding, to elucidate the biological and structural characteristic of the receptor, and the interactions with other receptors and substrates. It is critical to extend these studies to other organs to determine the presence of "uridine receptor(s)" not only in the central nervous system but also in the cardio-circulatory system and at the reproduction level. These studies will lead to the discovery of a new interacting molecules and the development of new class of therapeutic agents for various human diseases.

Similarly, the attention dedicated to TPase is associated to its angiogenic properties [144] and more recently, to its link to a human genetic disease, MNGIE [145], and it could be matched by UPase only after we have better defined its physiological function and its possible role in human diseases. Our discoveries of an elevated expression of UPase in human tumors [54], its altered pattern of inhibition in breast cancers [54] and the intracellular association with the cytoskeleton [89] only represent starting points to gain new insight in its biological functions and define its clinical–pathological role.

Acknowledgements

Supported in part by a grant from the National Cancer Institute CA67035, the United Army Medical Research Breast Cancer Research Program and the Anna Fuller Foundation.

References

[1] J D Moyer, J.T. Oliver, R E Handschumacher, Salvage of circulating pyrimidine nucleosides in the rat, Cancer Res 41 (1981) 3010–3017

[2] D M Becroft, L I Phillips, A Simmonds, Hereditary orotic aciduria long-term therapy with uridine and a trial of uracil, J Pediatr. 75 (1969) 885–891

[3] G Pizzorno, L. Yee, B A Burtness, J C Marsh, J W Darnowski, M Y Chu, S H Chu, J J Leffert, R.E Handschumacher, P. Calabresi, Clinical and pharmacological studies of Benzylacyclouridine, a uridine phosphorylase inhibitor, Clin Cancer Res 4 (1998) 1165–1175

[4] C J. Van Groeningen, A Leyva, I Kraal, G J Peters, H M Pinedo, Clinical and pharmacokinetic studies of prolonged administration of high-dose uridine intended for rescue from 5-FU toxicity, Cancer Treat Rep 70 (1986) 745–750

[5] T.W Traut, Physiological concentrations of purines and pyrimidines, Mol Cell Biochem. 140 (1994) 1–22.

[6] T Gasser, J D Moyer, R.E Handschumacher, Novel single pass exchange of circulating uridine in rat liver, Science 213 (1981) 777–778.

[7] M P Liu, E. Levy, R E Handschumacher, G Pizzorno, Discrete roles of hepatocytes and nonparenchymal cells in uridine catabolism as a component of its homeostasis, Am J. Physiol. 274 (1998) G1018–G1023

[8] G.P. Connolly, J.A Duley, Uridine and its nucleotides. biological actions, therapeutic potentials, Trends Pharmacol Sci. 20 (1999) 218–225

[9] R Seifert, G Schultz, Involvement of pyrimidinoceptors in the regulation of cell functions by uridine and by uracil nucleotides, Trends Pharmacol. Sci. 10 (1989) 365–369

[10] G Ronquist, F Niklasson, Uridine, xanthine, and urate contents in human seminal plasma, Arch Androl 13 (1984) 63–70

[11] G Ronquist, B Stegmayr, F Niklasson, Sperm motility and interactions among seminal uridine, xanthine, urate, and ATPase in fertile and infertile men, Arch Androl. 15 (1985) 21–27.

[12] G Siggins, D Gruol, A Padjen, D Forman, in. R.W. Ryall, J S Kelly (Eds), Iontophoresis and Transmitter Mechanisms Mammalian Central Nervous System, Elsevier, New York, 1978, pp 453–455

[13] F J Gonzalez, P Fernandez-Salguero, Diagnostic analysis, clinical importance and molecular basis of dihydropyrimidine dehydrogenase deficiency, Trends Pharmacol Sci 16 (1995) 325–327

[14] G P Connolly, H A. Simmonds, J.A Duley, Pyrimidines and CNS regulation, Trends Pharmacol Sci 17 (1996) 106–107

[15] T Page, A Yu, J Fontanesi, W L Nyhan, Developmental disorder associated with increased cellular nucleotidase activity, Proc Natl Acad Sci 94 (1997) 11601–11606

[16] N.N. Karkishchenko, I.S. Makliakov, B.V. Stradomskii, Pyrimidine derivatives their psychotropic properties and the molecular mechanisms of their central action, Farmakol Toksikol 53 (1990) 67–72

[17] A Leyva, C.J Van Groeningen, I Kraal, G J Peters, J Lankelma, H.M. Pinedo, Phase I and pharmacokinetic studies of high-dose uridine intended for rescue from 5-fluorouracil toxicity, Cancer Res 44 (1984) 5928–5933.

[18] T Kimura, J. Kuze, K Watanabe, S Kondo, I K. Ho, I Yamamoto, N3-phenacyluridine, a novel hypnotic compound, interacts with the benzodiazepine receptor, Eur J Pharmacol. 311 (1996) 265–269

[19] G J Peters, C J Van Groeningen, E.J Laurensse, J. Lankelma, A Leyva, H M Pinedo, Uridine-induced hypothermia in mice and rats in relation to plasma and tissue levels of uridine and its metabolites, Cancer Chem Pharm 20 (1987) 101–108.

[20] C.J. Van Groeningen, A Leyva, I. Kraal, G J Peters, H.M Pinedo, Clinical and pharmacokinetic studies of prolonged administration of high-dose uridine intended for rescue from 5-FU toxicity, Cancer Treat Rep 70 (1986) 745–750.

[21] G.J Peters, C.J. Van Groeningen, E Laurensse, I. Kraal, A Leyva, J. Lankelma, H.M Pinedo, Effect of pyrimidine nucleosides on body temperatures of man and rabbit in relation to pharmacokinetic data, Pharm Res. 4 (1987) 113–119.

[22] J Aussedat, Effect of uridine supply on glycogen resynthesis after ischaemia in the isolated perfused rat heart, Cardiovasc Res. 17 (1983) 145–151

[23] A Geiger, S. Yamasaki, Cytidine and uridine requirement of the brain, J Neurochem 1 (1956) 93–100.

[24] G Benzi, R F Villa, M Dossena, L Vercesi, A. Gorini, O. Pastoris, Cerebral endogenous substrate utilization during the recovery period after profound hypoglycemia, J Neurosci Res. 11 (1984) 437–450

[25] V Gallai, G Mazzotta, S Montesi, P. Sarchielli, F. Del Gatto, Effects of uridine in the treatment of diabetic neuropathy: an electrophysiological study, Acta Neurol Scand 86 (1992) 3–7.

[26] T A Krenisky, M. Barclay, J A Jacquez, Specificity of mouse uridine phosphorylase Chromatography, purification and properties, J Biol Chem 239 (1964) 805–812

[27] T A Krenisky, J W Mellors, R K Barclay, Pyrimidine nucleosidases,

their classification and relationship to uric acid ribonucleoside phosphorylase, J Biol Chem 240 (1965) 1281–1286.

[28] J.G. Niedzwicki, M.H. El Kouni, S.H Chu, S Cha, Pyrimidine acyclonucleosides inhibitors of uridine phosphorylase, Biochem. Pharmacol 30 (1981) 2097–2101

[29] J.G Niedzwicki, S.H. Chu, M.H. El Kouni, E.C Rowe, S. Cha, 5-Benzylacyclouridine and 5-benzyloxybenzylacyclorurdine, potent inhibitors of uridine posphorylase, Biochem Pharmacol 31 (1982) 1857–1861.

[30] H Pontis, G. Degerstedt, P. Reichard, Uridine and deoxyuridine phosphorylase from Ehrlich ascites tumor, Biochim. Biophys Acta 51 (1961) 138–147.

[31] M.P. Liu, S. Srimatkandada, R E. Handschumacher, G Pizzorno, Variant uridine phosphorolytic activity in human breast and head-neck tumors. a potential target for improving 5-FU therapy, Proc Am Assoc Cancer Res 37 (1996) 2786.

[32] P Calabresi, A. Falcone, M.H. St Clair, M C. Wiemann, S.H Chu, J W Darnowski, Benzylacyclouridine reverses azidothymidine-induced marrow suppression without impairment of anti-human immunodeficiency virus activity, Blood 76 (1990) 2210–2215.

[33] R Bose, E W. Yamada, Uridine phosphorylase molecular properties and mechanism of catalysis, Biochemistry 13 (1974) 2051–2056.

[34] J W Darnowski, R E Handschumacher, Tissue-specific enhancement of uridine utilization and 5-fluorouracil therapy in mice by benzylacyclouridine, Cancer Res 45 (1985) 5364–5368

[35] S.H. Chu, Z Y Weng, Z.H. Chen, E C Rowe, E Chu, F N M Naguib, M.H. El Kouni, S Cha, M Y. Chu, Synthesis of 5-benzyl and 5-benzyloxybenzyl 2,2′-anhydrouridines and related nucleoside analogs as inhibitors of uridine phosphorylase, Nucleosides Nucleotides 7 (1988) 91–102.

[36] A. Monks, O. Ayers, R.L. Cysyk, Effect of 5-benzylacyclouridine, a potent inhibitor of uridine phosphorylase, on the metabolism of circulating uridine by the isolated rat liver, Biochem. Pharmacol 32 (1983) 2003–2009.

[37] D.S. Martin, R.L. Stolfi, R.C Sawyer, Use of oral uridine as a substitute for parenteral uridine rescue of 5-fluorouracil therapy, with and without the uridine phosphorylase inhibitor 5-benzylacyclouridine, Cancer Chemother Pharmacol 24 (1989) 9–14

[38] G D Birnie, H. Kroeger, C Heidelberger, Studies of fluorinated pyrimidines: XVIII. The degradation of 5-fluoro-2′-deoxyuridine and related compounds by nucleoside phosphorylase, Biochemistry 2 (1963) 566–572

[39] P.W Woodman, A M. Sarrif, C Heidelberger, Specificity of pyrimidine nucleoside phosphorylases and the phosphorolysis of 5-fluoro-2′-deoxyuridine, Cancer Res 40 (1980) 507–511

[40] H Ishitsuka, M. Miwa, K Takemoto, K. Fukuoka, A Itoga, H.B Maruyama, Role of uridine phosphorylase for antitumor activity in 5′-deoxy-5-fluorouridine, Gann 71 (1980) 112–123.

[41] M Y Chu, F.N.M. Naguib, M H. Iltzsch, M H. El Kouni, S.H. Chu, S Cha, P Calabresi, Potentiation of 5-fluoro-2′ -deoxyuridine antineoplastic activity by the uridine phosphorylase inhibitors benzylacyclouridine and benzyloxybenzylacyclouridine, Cancer Res. 44 (1984) 1852–1856

[42] H Eda, K. Fujimoto, S Watanabe, T Ishikawa, T Ohiwa, K. Tatsuno, Y. Tanaka, H. Ishitsuka, Cytokines induce uridine phosphorylase in mouse colon 26 carcinoma cells and make the cells more susceptible to 5-deoxy-5-fluorouridine, Jpn. J Cancer Res 84 (1993) 341–347.

[43] S. Watanabe, A. Hino, K Wada, J F. Eliason, T. Uchida, Purification, cloning, and expression of murine uridine phosphorylase, J. Biol Chem. 270 (1995) 12191–12196.

[44] S Watanabe, T. Uchida, Cloning and expression of human uridine phosphorylase, Biochem. Biophys. Res Commun. 216 (1995) 265–272

[45] E L. Schwartz, E Wan, F. Wang, N Baptiste, Regulation of expression of thymidine phosphorylase/platelet-derived endothelial cell growth factor in human colon carcinoma cells, Cancer Res 58 (1998) 1551–1557

[46] Y. Geng, E Gheuens, E.A. De Bruijn, Activation and cytotoxicity of 5′-deoxy-5-fluorouridine in c-H-ras transformed NIH 3T3 cells, Biochem. Pharmacol. 41 (1991) 301–303

[47] M.H. El Kouni, F.N M. Naguib, K S Park, S Cha, J W. Darnowski, S.J Soong, Circadian rhythm of hepatic uridine phosphorylase activity and plasma concentration of uridine in mice, Biochem Pharmacol. 40 (1990) 2479–2485

[48] Y. Maehara, Y. Sakaguchi, T Kusumoto, H Kusumoto, K Sugimachi, Species differences in substrate specificity of pyrimidine nucleoside phosphorylase, J. Surg. Oncol. 42 (1989) 184–186.

[49] F N M. Naguib, J G Niedzwicki, M H Iltzsh, M C. Wiemann, M.H. El Kouni, S. Cha, Effects of N,*N*-dimethylformamide and sodium butyrate on enzymes of pyrimidine metabolism in cultures human tumor cells, Leuk. Res 11 (1987) 855–861

[50] D S Martin, R.L Stolfi, R C. Sawyer, S Spiegelman, C W Young, High dose 5-fluorouracil with delayed uridine "rescue" in mice, Cancer Res 42 (1982) 3964–3970.

[51] J.G. Niedzwicki, M.H El Kouni, S H Chu, S Cha, Structure–activity relationship of ligands of the pyrimidine nucleoside phosphorylases, Biochem Pharmacol. 32 (1983) 399–415.

[52] M.Y Chu, F N M. Naguib, M H. Itzsch, M.H El Kouni, S H Chu, P Calabresi, Potentiation of 5-fluoro-2′-deoxyuridine antineoplastic activity by the uridine phosphorylase inhibitors benzylacyclouridine and benzyloxybenzylacyclouridine, Cancer Res 44 (1984) 1852–1856

[53] J.W Darnowski, R E Handschumacher, Tissue uridine pools evidence in vivo of a concentrative mechanism for uridine uptake, Cancer Res 46 (1986) 3490–3494.

[54] M P Liu, D L Cao, R.L. Russell, R.E. Handschumacher, G Pizzorno, Expression, characterization and detection of human uridine phosphorylase and identification of variant uridine phosphorolytic activity in selected human tumors, Cancer Res. 58 (1998) 5418–5424.

[55] H M Pinedo, G J Peters, Fluorouracil: biochemistry and pharmacology, J Clin. Oncol 6 (1988) 1653–1654

[56] J.A. Houghton, P J Houghton, R S Wooten, Mechanism of induction of gastrointestinal toxicity in the mouse by 5-fluorouracil, 5-fluorouridine, and 5-fluoro-2′-deoxyuridine, Cancer Res 39 (1979) 2406–2413.

[57] F J Geoffroy, C.J. Allegra, B Sinha, J L. Grem, Enhanced cytotoxicity with interleukin-1 alpha and 5-fluorouracil in HCT116 colon cancer cells, Oncol. Res 6 (1994) 581–591

[58] M D. Pritchard, A.J M. Watson, C S Potten, A L Jackman, J.A Hickman, Inhibition by uridine but not thymidine of p53-dependent intestinal apoptosis initiated by 5-fluorouracil· evidence for the involvement of RNA perturbation, Proc. Natl Acad. Sci U. S. A. 94 (1997) 1795–1799.

[59] K Seiter, N. Kemeny, D Martin, A Schneider, L Williams, J Colofiore, R. Sawyer, Uridine allows dose escalation of 5-fluorouracil when given with *N*-phosphonacetyl-L-aspartate, methotrexate, and leucovorin, Cancer 71 (1993) 1875–1881

[60] G K. Schwartz, K. Christman, L Saltz, E. Casper, V Ouan, J. Bertino, D S. Martin, J. Colofiore, D Kelsen, A phase I trial of a modified, dose intensive FAMTX regimen (high dose 5-fluorouracil + doxorubicin + high dose methotrexate + leucovorin) with oral uridine rescue, Cancer 78 (1996) 1988–1995

[61] D.P. Kelsen, D S. Martin, J O'Neil, G Schwartz, L. Saltz, M T Sung, R. von Borstel, J.R. Bertino, Phase I clinical trial of PN401, an oral prodrug of uridine, to prevent toxicity from fluorouracil in patients with advanced cancer, J Clin. Oncol. 15 (1997) 1511–1517

[62] C E. Cass, A R.P. Paterson, Mediated transport of nucleosides in human erythrocytes Accelerative exchange diffusion of uridine and thymidine and specificity toward pyrimidine nucleosides as permeants, J Biol Chem. 247 (1972) 3314–3320

[63] C E Cass, A R P. Paterson, Mediated transport of nucleosides by human erythrocytes. Specificity toward purine nucleosides as permeants, Biochim. Biophys Acta 291 (1973) 734–746

[64] S M. Jarvis, J D Young, Nucleoside translocation in sheep reticulocytes and fetal erythrocytes. a proposed model for the nucleoside transporter, J. Physiol. 324 (1982) 47–66

[65] R M Wohlhueter, R Marz, P.G W. Plagemann, Thymidine transport in cultured mammalian cells. Kinetic analysis, temperature dependence and specificity of the transport system, Biochim Biophys Acta 553 (1979) 262–283

[66] A R P. Paterson, E S. Jakobs, E R Harley, C E. Cass, M.J. Robins, Inhibitors of nucleoside transport as probes and drugs, in: Y.C Cheng (Ed), Development of Target Oriented Anticancer Drugs, Raven Press, New York, 1983, pp 41–55.

[67] J A. Belt, Nitrobenzylthioinosine-insensitive uridine transport in human lymphoblastoid and murine leukemia cells, Biochem. Biophys Res. Commun. 110 (1983) 417–423

[68] J.A. Belt, Heterogeneity of nucleoside transport in mammalian cells. Two types of transport activity in L1210 and other cultured neoplastic cells, Mol Pharmacol 24 (1983) 479–484.

[69] S.Y. Yao, A.M Ng, W.R Muzyka, M. Griffiths, C E. Cass, S A Baldwin, J.D Young, Molecular cloning and functional characterization of nitrobenzylthioinosine (NBMPR)-sensitive (es) and NBMPR-insensitive (ei) equilibrative nucleoside transporter proteins (rent1 and rent2) from rat tissues, J Biol Chem 272 (1997) 28423–28430

[70] C R Crawford, D.H. Patel, C Naeve, J A Belt, Cloning of the human equilibrative, nitrobenzylmercaptopurine riboside (NBMPR)-insensitive nucleoside transporter ei by functional expression in a transport-deficient cell line, J Biol Chem 273 (1998) 5288–5293.

[71] J.F Kuttesch, J A Nelson, Renal handling of 2′-deoxyadenosine and adenosine in humans and mice, Chemother Pharmacol 8 (1982) 221–229

[72] J F. Kuttesch, M J Robins, J.A Nelson, Renal transport of 2′-deoxytubercidin in mice, Biochem. Pharmacol 31 (1982) 3387–3394.

[73] M. LeHir, U C. Dubach, Uphill transport of pyrimidine nucleosides in renal brush border vesicles, Pfluegers Arch 404 (1985) 238–243.

[74] C W. Lee, C.I Cheeseman, S M Jarvis, Na^+- and K^+-dependent uridine transport in rat renal brush border membrane vesicles, Biochim Biophys Acta 942 (1988) 139–149

[75] M E. Trimble, R. Coulson, Adenosine transport in perfused rat kidney and renal cortical membrane vesicles, Am. J Physiol. 246 (1984) F794–F803.

[76] S M. Jarvis, T C. Williams, C.W Lee, C I. Cheeseman, Active transport of nucleosides and nucleoside drugs, Biochem. Soc Trans. 17 (1989) 448–449

[77] M Schwenk, E. Hegazy, V Lopez del Pino, Uridine uptake by isolated intestinal epithelial cells of guinea pig, Biochim. Biophys Acta 805 (1984) 370–374.

[78] L. Dagnino, L L. Bennett, A R.P Paterson, Sodium-dependent nucleoside transport in mouse leukemia L1210 cells, J. Biol. Chem 266 (1991) 6308–6311.

[79] M. Roden, A.R P. Paterson, K. Turnhein, Sodium-dependent nucleoside transport in rabbit intestinal epithelium, Gastroenterology 100 (1991) 1553–1562

[80] S.L Betcher, J.N Forrest, R.G Knickelbein, J W. Dobbins, Sodium-dependent nucleoside co-transport in brush-border membranes from rabbit ileum, Am J Physiol 259 (1990) 504–510.

[81] D Vijayalakshmi, J.A. Belt, Sodium-dependent nucleoside transport in mouse epithelial cells Two transport systems with differing substrate specificities, J Biol Chem. 263 (1988) 19419–19423.

[82] M W.L Ritzel, S.Y.M Yao, M Y. Huang, J F Elliott, C.E Cass, J D Young, Molecular cloning and functional expression of cDNAs encoding a human Na^+-nucleoside co-transporter (hCNT1), Am J Physiol. 341 (1997) C707–C714.

[83] S M. Jarvis, D A. Griffith, Expression of the rabbit intestinal N2 Na^+-nucleoside transporter in *Xenopus laevis* oocytes, Biochem J. 278 (1991) 605–607

[84] Q Q Huang, C.M Harvey, A R P Paterson, C.E Cass, J.D. Young, Functional expression of Na^+-dependent nucleoside transport systems of rat intestine in isolated oocytes of *Xenopus laevis* Demonstration that rat jejunum expresses the purine-selective system N1 (cif) and a second, novel system N3 having broad specificity for purine and pyrimidine nucleosides, J. Biol Chem 268 (1993) 20613–20619

[85] M M. Gutierrez, C.M Brett, R.J. Ott, A C Hui, K M Giacomini, Nucleoside transport in brush border membrane vesicles from human kidney, Biochim Biophys Acta 1105 (1992) 1–9

[86] A.R P Patterson, W.P Gati, D Vijajalakshmi, C E. Cass, M J Mant, J D Young, A.R. Belch, Inhibitor-sensitive, sodium-linked transport of nucleoside analogs in leukemia cells from patients, Proc Am. Assoc Cancer Res. 34 (1993) 14

[87] D Cao, M A Nimmakayalu, F Wang, R E Handschumacher, P Bray-Ward, G Pizzorno, Genomic structure, chromosomal mapping and promoter region sequence of murine Uridine Phosphorylase Gene, Cancer Res 59 (1999) 4997–5001

[88] D Zhang, D Cao, R L Russell, G. Pizzorno, p53-dependent suppression of uridine phosphorylase gene expression through direct promoter interaction, Cancer Res 61 (2001) 6899–6905

[89] R L Russell, D Cao, D Zhang, R E Handschumacher, G Pizzorno, Uridine phosphorylase association with vimentin: intracellular distribution and localization, J. Biol Chem. 276 (2001) 13302–13307

[90] T. Furukawa, A Yoshimura, T Sumizawa, M. Haraguchi, S I. Akiyama, K. Fukui, M Ishizawa, Y. Yamada, Angiogenic factor, Nature 356 (1992) 668

[91] A. Moghaddam, H T Zhang, T.P D Fan, D E Hu, V C Lees, H Turley, S.B Fox, K.C Gatter, A.L Harris, R. Bicknell, Thymidine phosphorylase is angiogenic and promotes tumor growth, Proc. Natl. Acad Sci U S. A. 92 (1995) 998–1002

[92] K. Reynolds, F. Farnaneh, W.P. Collins, S Campbell, T H. Bourne, F. Lawton, A. Moghaddam, A L Harris, R Bicknell, Association of ovarian malignancy with expression of platelet-derived endothelial cell growth factor, J Natl Cancer Inst. 86 (1994) 1234–1237

[93] T S O'Brien, S.B Fox, A J Dickinson, H Turley, M Westwood, A Moghaddam, K C Gatter, R Bicknell, A.L Harris, Expression of the angiogenic factor thymidine phosphorylase/platelet-derived endothelial cell growth factor in primary bladder cancers, Cancer Res 56 (1996) 4799–4802

[94] C Luccioni, J. Beaumartin, V Bardot, D Lefrancois, Pyrimidine nucleotide metabolism in human colon carcinomas. comparison of normal tissues, primary tumors and xenografts, Int J Cancer 58 (1994) 571–575

[95] Y Takebayashi, S. Akiyama, S. Akiba, K Yamada, K Miyadera, T Sumizawa, Y Yamada, F. Murata, T Aikou, Clinicopathologic and prognostic significance of an angiogenic factor, thymidine phosphorylase, in human colorectal carcinoma, J Natl Cancer Inst. 88 (1996) 1110–1114

[96] K Fujimoto, R Hosotani, M Wada, J.U Lee, T Koshiba, Y. Miyamoto, S Tsuji, S Nakajima, R Doi, M. Imamura, Expression of two angiogenic factors, vascular endothelial growth factor and platelet-derived endothelial cell growth factor in human pancreatic cancer, and its relationship to angiogenesis, Eur J Cancer 34 (1998) 1439–1443.

[97] Y. Imazono, Y Takebayashi, K. Nishiyama, S Akiba, K Miyadera, Y Yamada, S Akiyama, Y Ohi, Correlation between thymidine phosphorylase expression and prognosis in human renal cell carcinoma, J. Clin Oncol 15 (1997) 2570–2573

[98] M. Toi, S Hoshina, T Taniguci, Y Yamamoto, H Ishitsuka, T. Tominaga, Expression of platelet-derived endothelial cell growth factor/thymidine phosphorylase in human breast cancer, Int J. Cancer 64 (1995) 79–82

[99] S B. Fox, M. Westwood, A Moghaddam, M. Comley, H Turley, R M Whitehouse, R Bicknell, K.C Gatter, A.L Harris, The angiogenic factor platelet-derived endothelial cell growth factor/thymidine phosphorylase is up regulated in breast cancer epithelium and endothelium, Br J Cancer 73 (1996) 275–278

[100] M. Haraguchi, K Miyadera, K. Uemura, T Sumizawa, T Furukawa,

K. Yamada, S.I Akiyama, Y. Yamada, Angiogenic activity of enzymes, Nature 368 (1998) 198.

[101] H. Uetake, W. Ichikawa, M Kirihara, M. Tajima, Z. Nihei, K Sugihara, Relationship between gene expression level of phosphorylating enzymes for 5-FU and chemosensitivity by drug response assay in human colorectal carcinoma, Proc Am Assoc Cancer Res 42 (2001) 3327.

[102] P. Langen, G Etzold, B. Barwolff, B Preussel, Inhibition of thymidine phosphorylase by 6-amino-thymine and derivatives of 6-aminouracil, Biochem. Pharmacol. 16 (1987) 1833–1837.

[103] A Kanzaki, Y Takebayashi, H. Bando, J.F. Eliason, S. Watanabe, H. Miyashita, M. Fukumoto, M Toi, T Uchida, Expression of uridine and thymidine phosphorylase genes in human breast carcinoma, Int J. Cancer 97 (2002) 631–635.

[104] R J. Osborne, M.G Hamshere, A genome-wide map showing common regions of loss of heterozygosity/allelic imbalance in breast cancer, Cancer Res. 60 (2000) 3706–3712.

[105] C.A Gritzmacher, Molecular aspects of heavy-chain class switching, Crit. Rev. Immunol. 9 (1989) 173–200.

[106] R D Nicholls, N. Fischel-Ghodsian, D.R Higgs, Recombination at the human alpha-globulin gene cluster· sequence features and topological constraints, Cell 49 (1987) 369–378.

[107] E. Hahnen, J Schonling, S Rudnik-Schoneborn, K. Zerres, B Wirth, Hybrid survival motor neuron genes in patients with autosomal recessive spinal muscular atrophy: new insights into molecular mechanisms responsible for the disease, Am. J. Hum. Genet. 59 (1996) 1057–1065.

[108] K Hagiwara, G. Stenman, H Honda, P Sahlin, A. Andersson, K Miyazono, C H. Heldin, F. Ishikawa, F Takaku, Organization and chromosomal localization of the human platelet-derived endothelial cell growth factor gene, Mol. Cell Biol. 11 (1991) 2125–2132

[109] S.H Orkin, GATA-binding transcription factors in hematopoietic cells, Blood 80 (1992) 575–581

[110] M. Maeda, K. Kubo, T Nishi, M Futai, Roles of gastric GATA DNA-binding proteins, J. Exp Biol. 199 (1996) 513–520

[111] C.R. Escalante, J Yie, D. Thanos, A K. Aggarwal, Structure of IRF-1 with bound DNA reveals determinants of interferon regulation, Nature 391 (1998) 103–106

[112] Y.C. Henderson, M Chou, A B. Deisseroth, Interferon regulatory factor-1 induces the expression of the interferon-stimulated genes, Br J. Haematol. 96 (1997) 566–575.

[113] C Grandori, R.N. Eisenman, Myc target genes, Trends Biochem 22 (1997) 177–181.

[114] S Ishida, S. Takada, K Koike, Isolation and analysis of cellular DNA fragments directly binding to c-Myc protein, Leukemia 3 (1997) 399–401.

[115] C. Rudolph, J P Halle, G Adam, Accelerated proliferative senescence of rat embryo fibroblasts after stable transfection of multiple copies of the c-Myc DNA-binding sequence, Exp Cell. Res. 239 (1998) 361–369.

[116] M.E. Anderson, B Woelker, M. Reed, P Wang, P. Tegtmeyer, Reciprocal interference between the sequence-specific core and nonspecific C-terminal DNA binding domains of p53: implications for regulation, Mol. Cell. Biol. 17 (1997) 6255–6264

[117] B.F. Muller-Tiemann, T.D. Halazonetis, J J Elting, Identification of an additional negative regulatory region for p53 sequence-specific DNA binding, Proc. Natl Acad. Sci U S. A. 95 (1998) 6079–6084

[118] G.W. Verhaegh, M.O. Parat, M J Richard, P. Hainaut, Modulation of p53 protein conformation and DNA-binding activity by intracellular chelation of zinc, Mol. Carcinog 21 (1998) 205–214.

[119] W.S. el-Deiry, S E - Kern, J A Pietenpol, K.W. Kinzler, B. Vogelstein, Definition of a consensus binding site for p53, Nat. Genet 1 (1992) 45–49.

[120] S P Linke, K.C. Clarkin, A. Di Leonardo, A Tsou, G.M. Wahl, A reversible, p53-dependent G0/G1 cell cycle arrest induced by ribonucleotide depletion in the absence of detectable DNA damage, Genes Dev. 10 (1996) 934–947

[121] H. Tanaka, H. Arakawa, T Yamaguchi, K. Shiraishi, S. Fukuda, K. Matsui, Y. Takei, Y. Nakamura, A ribonucleotide reductase gene involved in a p53-dependent cell-cycle checkpoint for DNA damage, Nature 404 (2000) 42–49

[122] D E Fisher, The p53 tumor suppressor: critical regulator of life and death in cancer, Apoptosis 6 (2001) 7–15.

[123] Y.H. Chou, O. Skalli, R.D. Goldman, Intermediate filaments and cytoplasmic networking· new connections and more functions, Curr Opin Cell Biol 9 (1997) 49–53

[124] O Skalli, R.D. Goldman, Recent insights into the assembly, dynamics, and function of intermediate filament networks, Cell Motil. Cytoskeleton 19 (1991) 67–79.

[125] J.E Eriksson, P Opal, R D Goldman, Intermediate filament dynamics, Curr Opin Cell Biol. 4 (1992) 99–104.

[126] R M Evans, Vimentin: the conundrum of the intermediate filament gene family, BioEssays 20 (1998) 79–86

[127] R.D. Goldman, S Khoun, Y.H. Chou, P. Opal, P.M. Steinert, The function of intermediate filaments in cell shape and cytoskeletal integrity, J. Cell Biol 134 (1996) 971–983.

[128] O. Klotzsche, D. Etzrodt, H Hohenberg, W. Bohn, W. Deppert, Cytoplasmic retention of mutant tsp53 is dependent on an intermediate filament protein (vimentin) scaffold, Oncogene 16 (1998) 3423–3431

[129] A. Spudich, T Meyer, L Stryer, Association of the beta isoform of protein kinase C with vimentin filaments, Cell Motil. Cytoskeleton 22 (1992) 250–256

[130] K.B Pryzwansky, T.A. Wyatt, T.M. Lincoln, Cyclic guanosine monophosphate-dependent protein kinase is targeted to intermediate filaments and phosphorylates vimentin in A23187-stimulated human neutrophils, Blood 85 (1995) 222–230

[131] J. Ciesielski-Treska, G Ulrich, S. Chasserot-Golaz, D. Aunis, Immunocytochemical localization of protein kinases Yes and Src in amoeboid microglia in culture. association of Yes kinase with vimentin intermediate filaments, Eur. J Cell Biol. 68 (1995) 369–376.

[132] A de S Otero, Copurification of Vimentin, energy metabolism enzymes, and a MER5 homolog with nucleoside diphosphate kinase, J. Biol Chem 272 (1997) 14690–14694.

[133] F.J. Doherty, J.A. Wassell, R.J. Mayer, A putative protein-sequestration site involving intermediate filaments for protein degradation by autophagy. Studies with microinjected purified glycolytic enzymes in 3T3-L1 cells, Biochem J 241 (1987) 793–800

[134] B S. Eckert, S.J Koons, A W. Schantz, C.R. Zobel, Association of creatine phosphokinase with the cytoskeleton of cultured mammalian cells, J. Cell Biol. 86 (1980) 1–5

[135] V.P. Pinon, G Millot, A Munier, J. Vassy, G. Linares-Cruz, J. Capeau, F Calvo, M.L. Lacombe, Cytoskeletal association of the A and B nucleoside diphosphate kinases of interphasic but not mitotic human carcinoma cell lines: specific nuclear localization of the B subunit, Exp. Cell Res. 246 (1999) 355–367.

[136] T.M. Svitkina, A B. Verkhovsky, G.B Borisy, Plectin sidearms mediate interaction of intermediate filaments with microtubules and other components of the cytoskeleton, J Cell Biol. 135 (1996) 991–1007

[137] R Foisner, W Bohn, K Mannweiler, G. Wiche, Distribution and ultrastructure of plectin arrays in subclones of rat glioma C6 cells differing in intermediate filament protein (vimentin) expression, J. Struct Biol 115 (1995) 304–317.

[138] H.Y. Yang, N. Lieska, A E Goldman, R.D. Goldman, A 300,000-mol-wt intermediate filament-associated protein in baby hamster kidney (BHK-21) cells, J. Cell Biol 100 (1985) 620–631

[139] K.D. Brown, L I Binder, Identification of the intermediate filament-associated protein gyronemin as filamin. Implications for a novel mechanism of cytoskeletal interaction, J. Cell Sci 102 (1992) 19–30

[140] C.M. Anderson, F E. Parkinson, Potential signalling roles for UTP and UDP: sources, regulation and release of uracil nucleotides, Trends Pharmacol. Sci 18 (1997) 387–392

[141] T.V Dunwiddie, S A Masino, The role and regulation of adenosine in the central nervous system, Annu. Rev. Neurosci. 24 (2001) 31–55

[142] H.T. Sommerschild, K A Kirkeboen, Adenosine and cardioprotection during ischaemia and reperfusion. an overview, Acta Anaesthesiol. Scand 44 (2000) 1038–1055.

[143] K N Klotz, Adenosine receptors and their ligands, Naunyn-Schmiedeberg's Arch Pharmacol 362 (2000) 382–391.

[144] T. Kimura, I.K. Ho, I Yamamoto, Uridine receptor discovery and its involvement in sleep mechanism, Sleep, (2001) 251–260

[145] I Nishino, A Spinazzola, M Hirano, Thymidine phosphorylase gene mutations in MNGIE, a human mitochondrial disorder, Science 283 (1999) 689–692

ELSEVIER

Biochimica et Biophysica Acta 1587 (2002) 145–154

BIOCHIMICA ET BIOPHYSICA ACTA

BBA

www.bba-direct.com

Review

Sequence-specific interactions of drugs interfering with the topoisomerase–DNA cleavage complex

Manlio Palumbo [*], Barbara Gatto, Stefano Moro, Claudia Sissi, Giuseppe Zagotto

Department of Pharmaceutical Sciences, University of Padova, Via Marzolo 5, 35131 Padua, Italy

Received 24 January 2002; accepted 24 January 2002

Abstract

DNA-processing enzymes, such as the topoisomerases (tops), represent major targets for potent anticancer (and antibacterial) agents. The drugs kill cells by poisoning the enzymes' catalytic cycle. Understanding the molecular details of top poisoning is a fundamental requisite for the rational development of novel, more effective antineoplastic drugs. In this connection, sequence-specific recognition of the top–DNA complex is a key step to preferentially direct the action of the drugs onto selected genomic sequences. In fact, the (reversible) interference of drugs with the top–DNA complex exhibits well-defined preferences for DNA bases in the proximity of the cleavage site, each drug showing peculiarities connected to its structural features. A second level of selectivity can be observed when chemically reactive groups are present in the structure of the top-directed drug. In this case, the enzyme recognizes or generates a unique site for covalent drug–DNA binding. This will further subtly modulate the drug's efficiency in stimulating DNA damage at selected sites. Finally, drugs can discriminate not only among different types of tops, but also among different isoenzymes, providing an additional level of specific selection. Once the molecular basis for DNA sequence-dependent recognition has been established, the above-mentioned modes to generate selectivity in drug poisoning can be rationally exploited, alone or in combination, to develop tailor-made drugs targeted at defined loci in cancer cells. © 2002 Elsevier Science B.V. All rights reserved.

Keywords: Topoisomerase; Antitumor drug; Poisoning; Sequence specificity; Isozyme selectivity

1. Introduction

DNA topoisomerases (tops) are essential enzymes present in all organisms [1,2]. They modify DNA topology in connection with a number of nuclear processes, such as replication, transcription, chromatin remodeling, chromatin condensation/decondensation, recombination and repair [3]. All tops can introduce breaks into DNA segments: type II tops transport a double helical portion of DNA through a cut involving both strands of another double-helical region; type I enzymes produce single-stranded breaks, and then either transport a DNA segment through the break (type I-A) or allow rotation of the broken strand around the intact strand (type I-B) [4,5]. In the human genome, five DNA tops are presently known: two type II tops (top2α and top2β), a type I-B enzyme (top1) and two type I-A enzymes (top3α and top3β) [1].

Top1 and top2 have been shown to represent the principal targets of effective antitumor drugs and, hence, have deserved investigation to understand the biochemical and pharmacological basis of drug action [6]. Indeed, topoisomerase poisons, such as antitumor drugs, transform these essential enzymes into lethal DNA-damaging agents. Circumstantial evidence indicates that top2 (and top1) can initiate cellular processes that eventually lead to chromosomal translocations and cell transformation [7,8]. Thus, a full understanding of molecular mechanisms of DNA topoisomerase functions leading to cell death and/or genome alterations may reveal unique opportunities to successfully treat human cancers.

2. The catalytic process and its poisoning

The enzymatic cycle of top1 [2], largely shared by top2 [9], can be divided into four steps: (1) binding of the enzyme to DNA, (2) DNA cleavage, (3) strand passage and (4) DNA

Abbreviations: top, topoisomerase; DNA, deoxyribonucleic acid; ATP, adenosine triphosphate; CPT, camptothecin; AmC, cytosine arabinoside; *m*-AMSA, amsacrine; ET, ecteinascidin 743; CL, clerocidin; XK469, 2-{4-[(7-chloro-2-quinoxalinyl)oxy]phenoxy}propionic acid; VM-26, teniposide; dh-EPI, 4-demethoxy-3′-deamino-3′-hydroxy-4′-epi-doxorubicin; da-IDA, 4-demethoxy-3′-deamino-4-deoxy-4′-epiaminodaunorubicin

[*] Corresponding author. Tel./fax: +39-49-8275-711.

E-mail address: manlio.palumbo@unipd.it (M. Palumbo).

0925-4439/02/$ - see front matter © 2002 Elsevier Science B.V. All rights reserved.
PII: S0925-4439(02)00077-7

religation. Once the protein and the nucleic acid are bound to each other, the phenolic OH of a tyrosine residue in the catalytic pocket reacts with a DNA phosphodiester bond by a transesterification process, producing a covalent enzyme–DNA intermediate linked through a phosphotyrosine bond (cleavage complex), while the DNA strand is cleaved. Cleavage may occur simultaneously on both strands in the presence of top2 enzymes, whereas it involves only one strand in the presence of top1 enzymes. In type I-A and type II topoisomerases, the enzyme becomes linked to the 5′-end of the cleaved phosphodiester bond, whereas in type I-B enzymes, it is bound to the 3′-end. The third step consists in the strand passing process, which involves a conformational rearrangement of the enzyme to allow one or both strands of DNA to pass through the gap generated by the cleavage step. The final religation process corresponds to the attack of the free 5′- or 3′-hydroxyl terminus of the cleaved bond onto the phosphotyrosine linkage to reseal the original phosphodiester bond. Then, enzyme release occurs (Fig. 1). Given the energy requirements of the enzyme, ATP binding and hydrolysis has to be included in the catalytic cycle of top2.

In the presence of a drug which is able to affect the DNA cleavage-religation process by increasing the DNA cleavage rate or by reducing the DNA religation rate, the cleavage complex has a longer life and DNA breaks persist [10,11]. This action converts top2 into an endogenous toxin that stabilizes damage in the genome and triggers a series of apoptotic events that finally lead to cell death. There are several modes for a drug to affect the cleavage complex, but it is generally believed that a ternary complex is formed, in which the drug is bound to the DNA and the enzyme simultaneously [2,9]. Hence, there will be normally two pharmacophoric regions in a poison molecule, one facing (and interacting with) the enzyme and the other the nucleic acid.

3. Structures of topoisomerase poisons

A large number of compounds have been shown to interfere with top (principally top2) activity, and they exhibit a variety of structural features [2,9,12,13]. The structures of selected compounds are shown in Fig. 2.

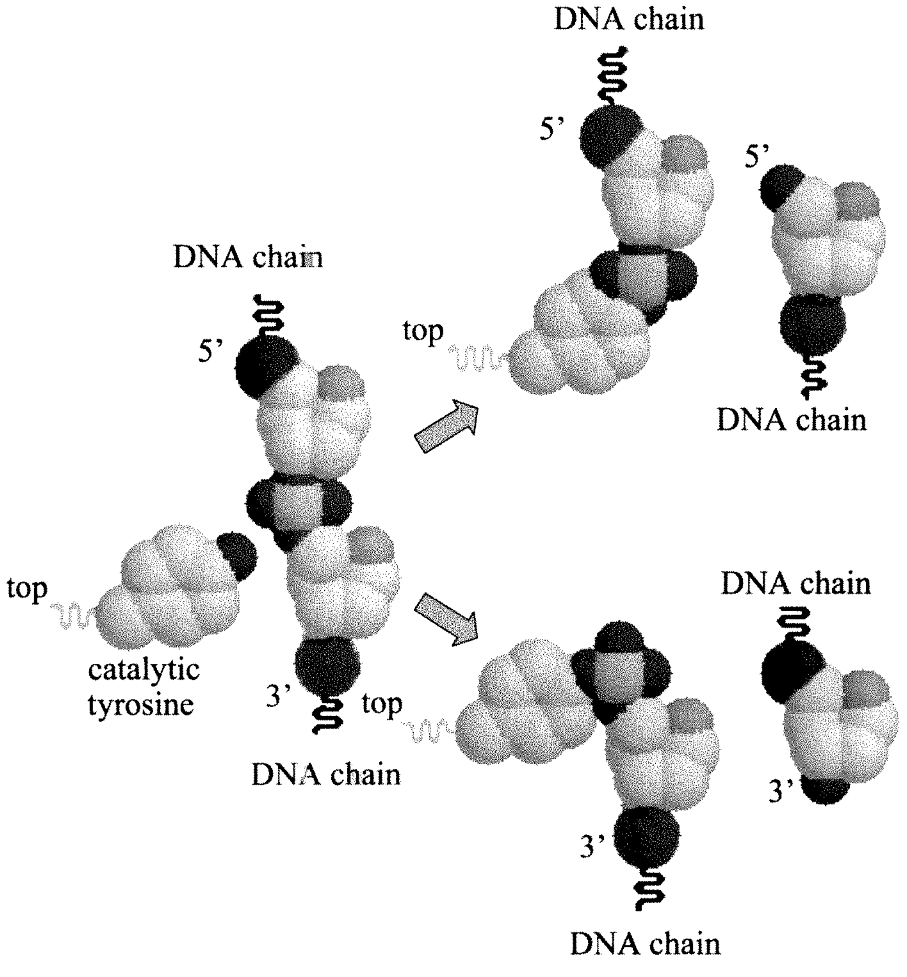

Fig. 1. Schematic representation of the chemical processes occurring in the topoisomerase catalytic cycle. The tyrosine residue at the active site (left) can attack a phosphodiester bond of DNA, giving a phosphotyrosine adduct linked either at the 3′ (upper reaction scheme) or at the 5′ (lower reaction scheme) position. This will produce a cut in the DNA chain leaving a free 5′ or 3′ hydroxyl group.

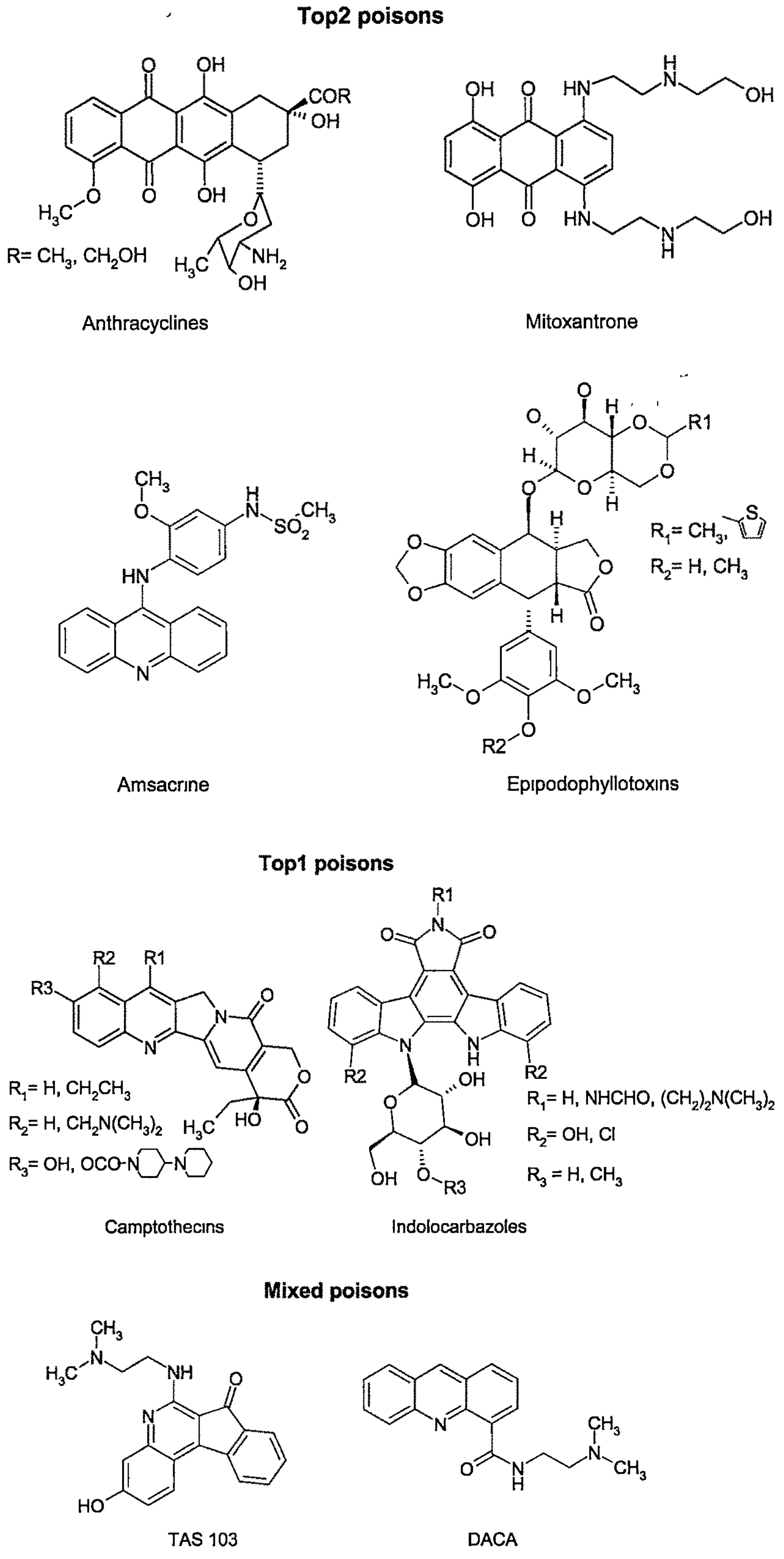

Fig. 2 Selected chemical structures of topoisomerases I and II poisons

Clinically useful top1 poisons include the natural compound camptothecin (CPT) and its synthetic analogues topotecan and irinotecan. In addition, minor groove binders, such as the bisbenzimidazoles Hoechst 33258 and Hoechst 33342, and the indolocarbazoles derived from rebeccamycin, were found to be top1 inhibitors.

Top2 poisons include drugs from different families, such as epipodophyllotoxins, anthracyclines, acridines, anthraquinones, ellipticines, bisantrene, actinomycin D, terpenoids, quinolones and flavonoids. It is difficult to envisage common structural features among them. In fact, some of the compounds do not bind to DNA, while others exhibit a high affinity for the nucleic acid. In particular, very effective are the intercalators (anthracyclines, anthracenediones, acridines, bisantrene, actinomycin). They are characterized by a planar polycyclic DNA-intercalating region, to which polar side chain groups are eventually attached. The planar region is supposed to be able to slip between DNA bases and generate efficient stacking interactions with them. This is likely to represent the DNA-binding domain in the cleavage complex. In addition, to further stabilize contacts with the nucleic acid, the side-chains are likely to interact with the enzyme, thus, acting as enzyme-recognition elements. Indeed, in addition to their chemical structure, the relative position of the (planar ring/side chain) pharmacophores plays a major role in modulating nucleic acid binding and enzyme poisoning effects [14–16]. Non-DNA-binders, like epipodophillotoxins, can also stabilize the cleavage complex. In this case, perhaps, stronger contacts are formed with the enzyme to compensate for poor interaction with the nucleic acid. Indeed, recent studies show that both the recombinant N-terminal ATPase domain and the B′A′ core domain of human top2α bind etoposide specifically, even in the absence of DNA. [17].

Dual top1 and top2 inhibitors have finally been described. Among others, they include saintopin, intoplicine, aclarubicin [18], acridine-4-carboxamide derivatives [19], bis(phenazine-1-carboxamides) [20], indeno-quinolines, [21] acetyl-boswellic acids [22] and fluorinated lipophylic epipodophylloids [23]. As with top2 poisons, different structural types are found, including intercalating and nonintercalating agents.

4. DNA sequence specificity of topoisomerase poisoning

4 1 Classical drugs

It has become evident that poisoning of the top–DNA cleavage complex by anticancer drugs does not occur at random along the DNA chain, but follows well defined rules, as demonstrated by the sequence analysis of the DNA regions where cutting had been stimulated by the top poison [24–26]. Top activity on the genome exhibits per se a certain degree of specificity. Indeed, significant nucleotide preferences were found in the regions flanking the cleavage site, often corresponding to alternating purine–pyrimidine tracts [27,28]. However, site selectivity exhibited by the poisons is more efficient and dependent on the poison's nature. Compounds of different chemical classes stimulate specific cleavage patterns in DNA fragments, which do not comprise all of the sites recognized by the enzyme. Moreover, the effects of specificity are principally due to the base immediately preceding (− 1) or following (+1) the cleavage site [29]. These findings confirm that the drugs are localized at (or very close to) the enzyme active site, and possibly contact both components of the cleavage complex. Localization of amsacrine at the active site has been demonstrated, using a covalently binding azido derivative, which was found to localize the drug molecule at the − 1 and +1 positions in the presence of top2 [30]. Another similar example is a reactive CPT derivative bound to top1 [31].

A peculiar case seems to be that of nogalomycin [32], which has been proposed to bind to an upstream site (from position − 6 to − 3) to provide a DNA structural bend that stimulates highly specific top1-mediated DNA cleavage. In this case, the drug would act at a distance from the catalytic site, like an allosteric effector.

An interesting mechanism is exhibited by the antimetabolite cytosine arabinoside (AraC) [33]. Lesions generated when the drug is incorporated into chromosomal DNA behave as position-specific top2 poisons and stimulate DNA cleavage mediated by the human type II enzymes. Moreover, additive or synergistic increases in DNA cleavage were observed in the presence of AraC lesions and etoposide, pointing to the possibility that the sequence-specific lesions might result from a combination of processes.

A question which arises when considering drug sequence specificity in producing protein-mediated DNA damage is related to possible species-related effects. This issue was recently addressed by Strumberg et al. [34], who performed a molecular analysis of drug interactions in yeast and human type II tops. Similarities and differences in DNA cleavage patterns and nucleic acid sequence preferences were observed between the human, yeast and *E. coli* top2 enzymes in the presence of the nonintercalators fluoroquinolone (CP-115,953), etoposide and azatoxin and the intercalators amsacrine and mitoxantrone. Additional base preferences were generally observed for the yeast, when compared with the human top2α, enzyme. Preferences in the immediate flanks of the top2-mediated DNA cleavage sites were, however, consistent with the drug-stacking model for both enzymes. Homologous mutations in yeast and human top2 decreased the reversibility of the drug-stabilized cleavage sites and produced consistent base sequence preference changes. These data indicate that the structure of the enzyme/DNA interface plays a key role in determining the specificity of top2 poisons and cleavage sites for both the intercalating and nonintercalating drugs. These effects must be borne in mind when comparing results obtained with topoisomerase enzymes of different origin. The principal base preferences exhibited by the drugs, thus, far investigated are summarized in Table 1.

Confirming the above-mentioned location of the drug at the enzyme active site, the principal preferences for DNA cutting correspond to the bases located at positions − 1/+1.

Table 1
Base preferences of selected topoisomerase poisons

-1[a]		$+1$[a]	
Poison	Base preference	Poison	Base preference
Doxorubicin[b]	A	Amsacrine[b]	A
Etoposide[b]	C(T)	Bisantrene[b]	A
Mitoxantrone[b]	C/T	Camptothecin[c]	G
Ellipticine[b]	T	Indolocarbazole[c]	G
Amonafide[b]	C	Saintopin[d]	G
Genistein[b]	T		

[a] Position from the cleavage site.
[b] top2 poisons.
[c] top1 poisons
[d] Dual poison

Generally, drugs having a strong -1 preference do not exhibit a strong $+1$ preference. This represents an indication that effective recognition of DNA by a drug is carried out either on one side or on the other of the cleavage complex, the drug molecule being principally located either upstream or downstream the cleaved phosphodiester bond.

A closer examination of individual specificities shows that a purine residue is invariantly found to be preferred at $+1$, both by top1 and top2 poisons. Considering the large planar portions of these drugs, this could indicate that DNA–drug stacking effects are operating in the ternary complex with the enzyme. Instead, the majority of -1 specific agents accept both pyrimidines and purines in the cut strand. Although the list of -1 specific agents includes nonintercalating agents, the majority of the compounds in this list are also intercalators, which prefer stacking interactions, so that the presence of pyrimidine preferences are not easily explainable at first glance. However, if we consider that all -1 specific agents are top2 poisons, and that the -1 base remains essentially paired to the complementary base located in the intact strand, the poison at -1 would always have a complete base pair to make contacts with, irrespective of the presence of a purine or a pyrimidine at the scissile strand.

It is very difficult to rationalize coupling of drug structures with corresponding specificities. The task could be made much easier, having tridimensional structures of the cleavage complex or, even better, of the ternary complex containing the drug.

Combining the biochemical and structural evidence, two models of the receptor site of CPT on the covalent complex of human top1 and DNA have been proposed [35,36]. Both attempt to explain the results of numerous CPT structure activity studies, and of investigations on drug-resistant top1 mutants. One model [35], schematically shown in Fig. 3A, uses the crystal structure of the human top1–DNA covalent complex and places the CPT molecule into the DNA duplex in a position that partially overlaps with the $+1$ guanine of the scissile strand; this placement requires the guanine base to flip out of the duplex and stack on the planar CPT. A second model [36] foresees intercalation of CPT into a B-form DNA duplex and models the positions of the phosphotyrosine723 and Asn722 residues as well (Fig. 3B). CPT occupies very different positions in the two models, neither of which can fully explain the experimental findings. In particular, no indication emerges for the requirement for a guanine at the $+1$ position of the scissile strand, as established by early investigations [25,26]. A theoretical structural model has been obtained very recently [37] by docking CPT into the top1–DNA cleavage complex obtained from X-ray data. The model of the lowest energy complex (Fig. 3C) is consistent with intercalation of the drug at the cleavage site, with the A-ring directed toward the major groove and the E-ring pointing into the minor groove. As shown in Fig. 3, the drug's orientation differs remarkably in the previous intercalation model [36], while it is similar in the guanine-flipping model [35]. Perhaps, publication of the X-ray structure of the ternary cleavage complex with topotecan, announced by Stewart et al. [38] at the 2001 AACR meeting will settle the question.

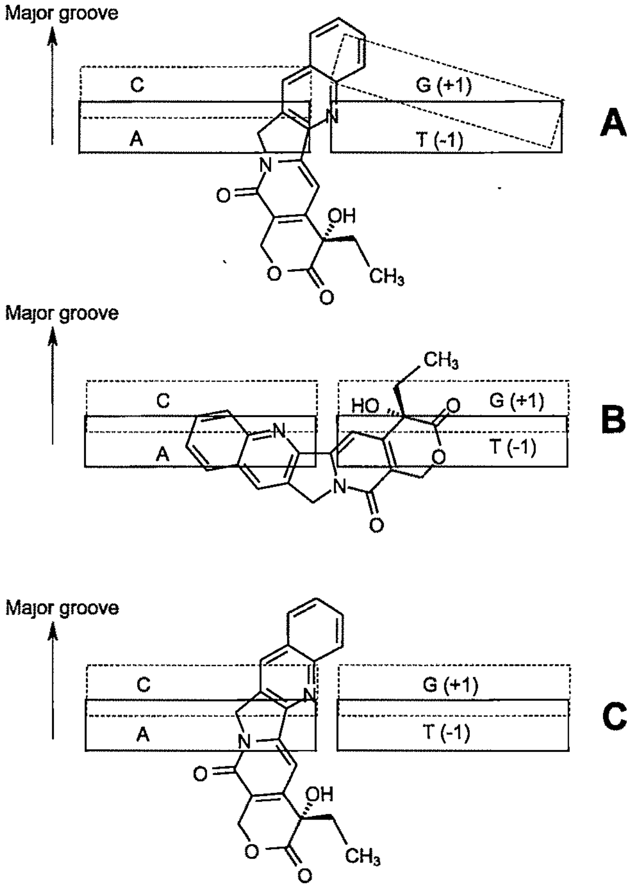

Fig. 3 Proposed orientations of CPT bound to DNA in the ternary CPT–DNA–top1 cleavage complex DNA bases are viewed from the helix axis and schematically drawn as rectangles Solid lines correspond to the pair at the -1 position (see text), while dashed lines correspond to the pair at $+1$ CPT is located between the -1 and $+1$ bases (A) Flipping guanine model from Ref. [35] (B) Intercalation model from Ref [36] (C) Intercalation model from Ref. [37]

An example of modulation of cleavage specificity is represented by homocamptothecin, containing a seven-membered β-hydroxylactone ring in place of the conventional six-membered α-hydroxylactone ring found in CPT [39]. Besides stimulating cleavage by top1 at preferred T.G sites, the homo derivative stabilizes cleavage at specific AAC.G sequences as well. Hence, notwithstanding the conserved primary G + 1 requirement, the ring homologation procedure generates a ternary complex structure which can discriminate up to three bases upstream the cleavage site. Clearly, further studies are required to fully elucidate the molecular interactions leading to specific DNA damage stimulation by the CPT family.

The presence of common pharmacophores for similar specificities of cleavage stimulation, and the importance of the relative positions of the planar ring system and of the side-chain groups, has been recently addressed by preparing amsacrine (*m*-AMSA)/bisantrene hybrids and bisantrene isomers [14]. The new compounds were able to poison DNA top2 with an activity intermediate between those of bisantrene and *m*-AMSA. Moving the side-chain from the central to a lateral ring (from C-9 to C-1/C-4) only slightly modified the drug DNA affinity, whereas it dramatically affected local base preferences of poison-stimulated DNA cleavage. In contrast, switching the planar aromatic systems of bisantrene and *m*-AMSA did not substantially alter the sequence specificity of drug action. A computer-assisted steric and electrostatic alignment analysis of the test compounds suggested that bisantrene, *m*-AMSA and 9-substituted analogs share a common pharmacophore, whereas the 1-substituted isomer showed a radically changed pharmacophoric structure.

A further question arising from this investigation, approached using the same set of compounds, is a possible relationship between sequence specificity for DNA in the presence and in the absence of the enzyme. We should remember that most of the known top2 poisons are also good DNA binders. The bisantrene analogues exhibited different DNA sequence preferences, depending on the locations of the side-chain groups, which suggests a major role for the side-chain position in generating specific contacts with the nucleic acid, even in the absence of enzyme [40]. More interestingly, the observed preferences compare well with the alteration of base specificity found for the top2-mediated DNA cleavage stimulated by the isomeric drugs. This confirms that not only DNA affinity, but also DNA-binding specificity, represents per se an important determinant for the recognition of the topoisomerase–DNA cleavable complex by the drug, at least for poisons belonging to the amsacrine–bisantrene family.

Thus, it has been concluded that the relative space occupancy and electron distribution of putative DNA binding (aromatic rings) and enzyme binding (side-chains) moieties are fundamental in directing the specific action of top2 poisons and in determining the poison pharmacophore.

4.2. Drug conjugates containing DNA-recognition elements

A useful approach to confer a desired sequence specificity is to synthesize drug conjugates with structural elements known to recognize well-defined features of DNA. Since the target for topoisomerase is a double-stranded helix, the following targeting elements can be used in combination with normal drugs: groove-binding AT specific structures, such as the antibiotics netropsin and distamycin [41–43], hairpin pyrrole–imidazole polyamides [44] and triplex-forming oligonucleotides [45,46]. In the first two, the conjugates are tethered to the minor groove; in the third, major groove binding occurs. The success of the above approaches rests on the ability to target the nucleic acid without impairing binding of the topoisomerase. The AT-binder conjugates with CPT proved to be poorly effective, due to their limited sequence-recognition properties [43].

Other top1 poisons were covalently attached to triple helix-forming oligonucleotides. Besides increasing the drug affinity for DNA, the conjugates were shown to stimulate top1-mediated DNA cleavage in a triplex-directed sequence-specific manner [46]. In addition, the results obtained with drug–polyamide conjugates showed that they were able to recruit top1 to produce DNA cleavage in high yield [44]. Hence, the new compounds could be considered as new artificial nucleases. It will be now interesting to verify whether conjugates targeted to the coding regions of selected genes will be able to regulate transcription elongation through a top1-dependent mechanism.

5. Drugs producing covalent adducts in the cleavage complex

Poisoning of the cleavage complex by the presently used drugs is a reversible process, and normal processing of the DNA by the enzyme is restored once the drug is removed [47]. Since triggering of the cell death events is initiated by the presence of the cleavage complex, the extent of this process will depend upon the drug's in and off kinetics. The longer the drug is bound to the cleavage intermediate, the more effective will be induction of apoptosis. Hence, if the drug becomes permanently linked to the DNA–enzyme complex, apoptosis signaling should be most prominent.

Compounds bearing DNA-reactive groups, such as the alkylators [48], usually produce generalized damage to the nucleic acid and to other cellular structures. Although the toxicity generated by these compounds is being used for the treatment of cancer, nonetheless the related side effects are quite marked. In addition, sequence selectivity is in general poor, as a large number of reactive group(s) in the DNA chain are available for targeting at the same time. It would be much more specific if the drug were to react with the nucleic acid only when topoisomerase is present. An enhancement in top activity at specific DNA alkylation sites has been found using *N*-methyl-*N′* -nitro-*N*-nitrosoguanidine [49]. This suggested a role for top1 poisoning by alkylated bases in the antiproliferative activity of alkylating agents, as well as in the DNA lesions resulting from endogenous and carcinogenic DNA modifications.

Other interesting examples are represented by the drugs psorospermin, ecteinascidin and some analogues [50–53]. These are weak DNA alkylators in the absence of top2 in the first case and top1 in the second. Significantly, the alkylation reactivity of psorospermin at specific sites on DNA increased 25-fold in the presence of top2 [50]. In addition, psorospermin trapped the top2-cleaved complex at the same sites. These results imply that the efficacy of psorospermin is related to its interaction with the top2–DNA complex. The site of alkylation of psorospermin is within the top2 gate site, as for other derivatized intercalators used to pinpoint the site of drug action in the cleavage complex.

Ecteinascidin 743 (ET), a potent antitumor agent from the Caribbean tunicate *Ecteinascidia turbinata*, can alkylate selectively guanine N2 in the DNA minor groove, a process reversed by DNA denaturation. However, it differs remarkably from other DNA alkylating agents presently in the clinic by both its biochemical activities and its profile of antitumor activity in preclinical models [52]. A 100-kDa protein was found to bind to DNA alkylated by ET and was identified as top1 [52]. DNA alkylation was essential for the formation of top1-mediated cleavage complexes by ET, and the distribution of the drug-induced top1 sites was different for ET and camptothecin, although they still share a G+1 preference. These data indicate that DNA minor groove alkylation by ET is required to produce top1-mediated protein-linked DNA breaks. Other studies, however, question the relevance of top1 poisoning by ET (and its synthetic analogue phthalascidin) as they show that in vivo top1 cross-linking is poor and that ET can be cytotoxic independently of top1 expression [53,54].

A more striking example is represented by clerocidin (CL) [55–58], reported to produce top2-mediated irreversible cleavage compatible with G-1 preference [57], a process unusual for topoisomerase poisoning. Since CL contains chemically reactive epoxy and carbonyl groups, studies were made to detect possible reaction with DNA. Indeed, the drug was able to nick negative supercoiled plasmids per se [58]. Covalent adducts with guanines at N7 position were formed in topoisomerase-free media, which were able to trigger phosphodiester bond cleavage at the modified site. Only single-stranded or distorted double-helical regions of DNA underwent CL alkylation. The guanine-alkylating ability of CL suggests an unprecedented mechanism of top2 sequence-specific poisoning, according to which the enzyme renders the drug reactive toward DNA by changing the local structure of the nucleic acid and by bringing drug and DNA reactive moieties in close proximity.

In conclusion, the combination of reversible (the drug must recognize the cleavage complex) and irreversible (drug covalent binding occurs only when the drug is appropriately located at the cleavage site in close contact with the target reactive group in DNA) effects will contribute to subtly modulate the drug's efficiency in stimulating DNA damage at selected sites.

6. Topoisomerase II isoform specificity

It has recently become evident that top2 is not a single enzyme in eukaryotic cells, but is present as two isoforms: a 170-kDa one, referred to as α, and a 180-kDa one, referred to as β. They differ in subcellular localisation and biochemical properties [59], suggesting that each isozyme has a distinct cellular function. Hence, studies aimed at evaluating the differential susceptibility to inhibition by anticancer drugs and site selectivity are of great help to better understand the role and actions of the various drugs. In addition, the relative level of expression of the α and β isoforms may contribute to the degree of tumor responsiveness to different chemotherapeutic agents.

The relationship between expression of top2 isoforms and established prognostic factors and pathological variables was examined in over 50 primary breast tumor samples [60]. The expression of the two top2 genes was apparently not coordinately regulated in these tissue samples. Immunohistochemical analysis revealed that top2β was widely distributed (>90% positive tumor cells), but that top2α expression was less widely expressed. This suggested that top2α, but not tp2β, expression is dependent upon cellular proliferation status, but that the more widely expressed top2β protein may play a significant role as a target for antitumor therapy. An immunofluorescence technique was also devised to visualize and quantify isoform-specific cleavable complexes in situ [61].

A number of studies have been performed on the major classes of anticancer drugs, including acridines, anthracyclines, anthraquinones, epipodophyllotoxins, 9-OH-ellipticine [62–70]. The methodological approaches include the use of human cancer cell lines having defined profiles of expression of the two enzymes (breast cancer, acute lymphoblastic leukemias, sensitive and resistant leukemia HL-60), viz. noncycling cells, where the α isoform is down-regulated, transgenic cells lacking one isoform, or resistant cells transfected with a plasmid carrying one of the two isoforms. In addition, biochemical studies were carried out with the human recombinant enzymes overexpressed and purified from yeast. All drugs were able to affect both the α and the β isoform, although to different extents, indicating that both enzymes are good targets. Hence, the observed differences are quantitative, not qualitative, and the drugs presently in use exhibit a low level of discrimination. However, it appears that the anthracyclines prefer the α enzyme, and amsacrine and mitoxantrone the β enzyme.

While no very selective top2α poison has been found as yet, an almost pure top2β poison has been recently identified [71]. Indeed, the synthetic quinoxaline phenoxypropionic acid derivative XK469 possesses unusual solid tumor selectivity and activity against multidrug-resistant cancer cells. In band depletion assays, XK469 caused little or no depletion of top2α and a significant dose-dependent reduction of top2β. In addition, exposure of subconfluent MCF-7 human breast cancer cells to the drug resulted in substantial cross-linking of top2β, but not top2α. Inhibition of superhelical DNA relaxation was also very effective in the presence of top2β. These findings indicate that the primary target of XK469 is top2β. Preferential targeting of this enzyme may explain the solid tumor selectivity of XK469 and its analogs because solid tumors, unlike leukemias, often have large populations of cells in the G(1)/G(0) phases of the cell cycle in which top2β is highly expressed whereas top2α is not.

It will be very important to define the molecular determinants for preferential top2βtargeting by XK469, in order to define structure–activity relationships for quinoxaline phenoxypropionic acid derivatives, and to design new classes of anticancer agents, perhaps endowed with prominent solid tumor cell killing potency.

The sequence selectivity of isoenzyme-mediated DNA cleavage for amsacrine, teniposide (VM-26) and an anthracycline derivative were determined using the human recombinant enzymes [72,73]. Local base preferences for DNA cleavage exhibited by the above drugs were essentially the same for both isozymes and corresponded to those determined using the murine enzyme. The identical drug sequence specificities suggest that molecular interactions of the tested drugs in the ternary complex are likely similar in the two isozymes. Evidently, the contacts formed between the tested drugs and the enzyme concern residues conserved in both isoforms. The high degree of sequence homology found at the top2 active site [74] justifies the above results. Drugs which stimulate α and β cleavage at different sites could possibly be designed by exploiting differential interactions with the nonconserved residue(s) of the protein's active site. To do so, the structure of the cleavage complex must be appropriately modeled.

7. In vivo specificity of topoisomerase poisoning

A final issue that deserves to be addressed deals with in vivo sequence-specific stimulation of top-mediated DNA cleavage and its relationship to in vitro findings. In vitro experiments are performed with the purified enzyme and a double helical DNA fragment. The situation in vivo is much more complicated, as a crowding of different enzymes and proteins occurs in chromatin, so that topoisomerase has to find its way by competing with other biological macromolecules. In addition, the structure and topology of DNA in vivo is greatly affected by specific interactions with histones and DNA-processing enzymes, which could greatly affect cleavable complex formation and drug interference both quantitatively and qualitatively. Hence, studies aimed at defining the exact location of drug-stimulated damage in living cells are very useful for a proper assessment of the biological significance of cell-free topoisomerase poisoning experiments. In addition, specific (different) cleavage locations generated by each drug along the eukaryotic genome might substantially contribute to differentiate the anticancer potential of the drug.

Recent in vivo studies are described by Borgnetto et al. [75] who investigated DNA cleavage sites stimulated by three poisons with diverse sequence specificity, CL, VM-26 and the anthracycline dh-EPI in two genomic regions of *Drosophila melanogaster* Kc cells. CL-stimulated DNA cleavage sites were rarer than those of VM-26 at the satellite locus. In the histone H2A–H2B intergenic region, CL and dh-EPI stimulated cleavage, whereas VM-26 was only weakly effective. As observed in vitro, some CL cleavage sites did not undergo spontaneous reversion, indicating that this agent can stimulate irreversible cleavage in vivo. Direct genomic sequencing showed that many CL and dh-EPI sites, although distinct, mapped to the transcription start and to the proximal promoter of the H2A gene. Hence, the in vivo specificity of topoisomerase poisoning is likely to arise from a combination of chromatin accessibility and local drug-related preferences.

DNA cleavage sites stimulated by the two anthracyclines dh-EPI and da-IDA were investigated at the histone gene cluster of cultured Drosophila Kc cells [76]. The two agents produced closely related patterns of double-stranded DNA cleavage in Kc cell chromatin. Analyses of numerous base sequences of dh-EPI and (fewer) of da-IDA sites showed that both compounds largely followed the in vitro requirement of (5)′ TA at 3′ ends of cleaved strands. Nonetheless, a modulation in DNA cleavage was found when using human top2 isoforms in vitro. Human top2α promoted cleavage patterns that were much more similar to those of Drosophila top2 than human top2β. Moreover, da-IDA showed a marked site-dependent preference for human top2 β, suggesting that, notwithstanding the similarities found comparing the in vivo and in vitro data, differential effects on the two isozymes might influence drug activity in human cells.

8. Conclusions

Specificity is a fundamental feature of effective drugs, to prevent simultaneous recognition of multiple targets and, hence, the onset of undesired side effects. Although the treatment of cancer often requires the use of potent cytotoxic compounds, poorly selective between normal and cancer cells, important knowledge is being acquired on the mechanisms of recognition of biological targets by effective drugs. In this context, topoisomerases are useful targets to be exploited for specificity. Available results indicate that the biologically relevant specific DNA-binding properties of topoisomerase poisons occur through a protein-mediated process. Hence, the cleavage complex interface represents a unique structural feature, differing from DNA-sequence to

DNA-sequence. Small molecules are able to fit into this intermediate and generate site-selective contacts with the enzyme–DNA adduct. By properly exploiting the drug's ability to recognize more specifically its target, it should be possible to rationally design compounds able to transform the topoisomerase into an endonuclease that cleaves DNA at very few selected sites along the genome, thus, triggering the apoptotic process in malignant cells only. This will hopefully yield new powerful anticancer agents, able to distinguish between mutated and normal DNA, hence, to spare healthy cells from death. Although we are still far from being able to do so, the combined information on reversible, irreversible, type and isoform specificities exhibited by the topoisomerase poisons is rapidly yielding the seminal knowledge to successfully proceed in that direction.

References

[1] J C Wang, Annu Rev. Biochem 65 (1996) 635–692.

[2] Y. Pommier, P Pourquier, Y Fan, D Strumberg, Biochim Biophys Acta 1400 (1998) 83–105

[3] R.P. Bakshi, S. Galande, K. Muniyappa, Crit. Rev Biochem. Mol Biol 36 (2001) 1–37.

[4] Z. Li, A. Mondragon, R J. DiGate, Mol. Cell 7 (2001) 301–307

[5] B O. Krogh, S Shuman, Mol Cell 5 (2000) 1035–1041

[6] P D'Arpa, L F. Liu, Biochim. Biophys Acta 989 (1989) 163–177

[7] M Stanulla, J. Wang, D S Chervinsky, S. Thandla, P D Aplan, Mol Cell Biol 17 (1997) 4070–4079

[8] R Strick, P.L Strissel, S. Borgers, S.L Smith, J.-D Rowley, Proc Natl Acad Sci. U. S A 97 (2000) 4790–4795

[9] D.A. Burden, N. Osheroff, Biochim Biophys. Acta 1400 (1998) 139–154

[10] L F Liu, T.C. Rowe, L. Yang, K.M Tewey, G.L Chen, J. Biol. Chem (1983) 15365–15370.

[11] M. Sander, T Hsieh, J Biol. Chem 258 (1983) 8421–8428

[12] B. Gatto, G. Capranico, M Palumbo, Curr. Pharm Des 5 (1999) 195–215.

[13] C Bailly, Curr Med. Chem. 7 (2000) 39–58

[14] G. Capranico, F Guano, S. Moro, G Zagotto, C. Sissi, B Gatto, F. Zunino, E. Menta, M. Palumbo, J Biol. Chem 273 (1998) 12732–12739

[15] C Sissi, S Moro, G Zagotto, M Ellis, A P. Krapcho, E Menta, M. Palumbo, Anticancer Drug Des. 14 (1999) 265–274

[16] C. Bailly, L Dassonneville, P. Colson, C. Houssier, K. Fukasawa, S Nishimura-S, T Yoshinari, Cancer Res. 59 (1999) 2853–2860

[17] D. Leroy, A.V Kajava, C. Frei, S M Gasser, Biochemistry 40 (2001) 1624–1634.

[18] D J.A Bridewell, G J. Finlay, B C Baguley, Oncol Res. 9 (1997) 535–542

[19] D J A. Bridewell, G.J Finlay, B C. Baguley, Cancer Chemother Pharmacol. 43 (1999) 302–308

[20] J A. Spicer, S.A. Gamage, G.W. Rewcastle, G.J. Finlay, D J A. Bridewell, B.C Baguley, W.A Denny, J Med Chem 43 (2000) 1350–1358

[21] T Ohyama, Y Li, T. Utsugi, S Irie, Y Yamada, T. Sato, Jpn. J Cancer Res 90 (1999) 669–691.

[22] T. Syrovets, B Buchele, E Gedig, J R Slupsky, T. Simmet, Mol. Pharmacol 58 (2000) 71–81.

[23] D Perrin, B van-Hille, J.M. Barret, A Kruczynski, C Etievant, T. Imber, B T. Hill, Biochem Pharmacol. 59 (2000) 807–819

[24] Y. Pommier, G. Capranico, A. Orr, K.W. Kohn, J. Mol. Biol. 222 (1991) 909–924.

[25] C. Jaxel, G. Capranico, D Kerrigan, K.W. Kohn, Y. Pommier, J Biol Chem 226 (1991) 20418–20423

[26] G Capranico, M. Binaschi, Biochim. Biophys Acta 1400 (1998) 185–194

[27] J.R Spitzner, I K Chung, M T. Muller, Nucleic Acids Res 18 (1990) 1–11

[28] J.Q Svejstrup, K. Christiansen, A H Andersen, K Lund, O Westergaard, J Biol. Chem 265 (1990) 12529–12535

[29] G. Capranico, M Binaschi, M.E Borgnetto, F. Zunino, M Palumbo, Trends Pharmacol. Sci 18 (1997) 323–329.

[30] C K Freudenreich, K N Kreuzer, Proc. Natl. Acad Sci U S A 91 (1994) 11007–11011

[31] Y Pommier, G Kohlhagen, K W. Kohn, F. Leteurtre, M C. Wani, M.E Wall, Proc Natl. Acad. Sci. U. S. A. 92 (1995) 8861–8865

[32] S P. Sim, D S. Pilch, L.F. Liu, Biochemistry 39 (2000) 9928–9934.

[33] S.D. Cline, N. Osheroff, J. Biol Chem 274 (1999) 29740–29743

[34] D Strumberg, J.L Nitiss, J. Dong, K.W Kohn, Y Pommier, J Biol Chem. 274 (1999) 28246–28255

[35] M R Redinbo, L. Stewart, P Kuhn, J J. Champoux, W G. Hol, Science 279 (1998) 1504–1513

[36] Y Fan, J N. Weinstein, K.W Kohn, L.M. Shi, Y Pommier, J Med Chem 41 (1998) 2216–2226

[37] J.E Kerrigan, D.S Pilch, Biochemistry 40 (2001) 9792–9798

[38] L Stewart, B Staker, K. Hjerrild, A J Burgin, H Kim, in. Proc. AACR 92nd Annual Meeting vol. 42, Cadmus, Linthicum, MD, 2001, p LB43

[39] C. Bailly, A Lansiaux, L Dassonneville, D. Demarquay, H Coulomb, M. Huchet, O. Lavergne, D C. Bigg, Biochemistry 38 (1999) 15556–15563

[40] C Sissi, L. Bolgan, S Moro, G. Zagotto, C Bailly, E Menta, G Capranico, M. Palumbo, Mol. Pharmacol 54 (1998) 1036–1045

[41] G. Xie, R. Gupta, K Atchison, J W Lown, J Med. Chem 39 (1996) 1049–1055

[42] R. Zhao, N H. al-Said, D L Sternbach, J W. Lown, J Med Chem 40 (1997) 216–225

[43] C Bailly, J B Chaires, Bioconjugate Chem. 9 (1998) 513–538

[44] C C Wang, P B Dervan, J Am Chem Soc. 123 (2001) 8657–8661

[45] P.B Arimondo, C Bailly, A.S Boutorine, P. Moreau, M. Prudhomme, J S. Sun, T. Garestier, C Helene, Bioconjugate Chem 12 (2001) 501–509.

[46] P.B Arimondo, C. Bailly, A.S Boutorine, V A Ryabinin, A.N. Syniakov, J S. Sun, T Garestier, C Hélène, Angew. Chem 113 (2001) 3135–3138.

[47] J L Nitiss, J C. Wang, Mol Pharmacol 50 (1996) 1095–1102

[48] D J Taatjes, D.J Fenick, G. Gaudiano, T.H Koch, Curr. Pharm Des 4 (1998) 203–221

[49] P. Pourquier, J L. Waltman, Y Urasaki, N.A Loktionova, A E Pegg, J L. Nitiss, Y Pommier, Cancer Res 61 (2001) 53–58

[50] Y Kwok, Q. Zeng, L.H Hurley, Proc Natl Acad Sci U S. A 95 (1998) 13531–13536

[51] Y. Kwok, L H. Hurley, J Biol Chem. 273 (1998) 33020–33026

[52] Y Takebayashi, P Pourquier, A. Yoshida, G Kohlhagen, Y. Pommier, Proc. Natl Acad Sci U S. A. 96 (1999) 7196–7201

[53] E.J. Martinez, T. Owa, S L. Schreiber, E.J Corey, Proc Natl Acad Sci U S. A. 96 (1999) 3496–3501

[54] Y Takebayashi, F. Goldwasser, Y Urasaki, G Kohlhagen, Y Pommier, Clin Cancer Res. 7 (2001) 185–191

[55] S Kawada, Y. Yamashita, N. Fujii, H Nakano, Cancer Res. 51 (1991) 2922–2925

[56] C Jamora, M.A. Theodoraki, V. Malhotra, E A Theodorakis, Bioorg. Med Chem 9 (2001) 1365–1370.

[57] M. Binaschi, G. Zagotto, M Palumbo, F Zunino, R. Farinosi, G. Capranico, Cancer Res. 9 (1997) 1710–1716.

[58] B Gatto, S. Richter, S Moro, G. Capranico, M. Palumbo, Nucleic Acids Res. 29 (2001) 4224–4230.

[59] H Turley, M Comley, S Houlbrook, N. Nozaki, A Kikuchi, I.D. Hickson, K Gatter, A.L. Harris, Br. J Cancer 75 (1997) 1340–1346.

[60] M.I Sandri, D Hochhauser, P. Ayton, R.C. Camplejohn, R. Whitehouse, H. Turley, K. Gatter, I D. Hickson, A L Harris, Br. J Cancer 73 (1996) 1518–1524

[61] E. Willmore, A J Frank, K. Padget, M J Tilby, C.A. Austin, Mol Pharmacol. 54 (1998) 78–85.

[62] D J Fernandes, J Qiu, C.V. Catapano, Adv. Enzyme Regul. 35 (1995) 265–281

[63] S Houlbrook, C.M. Addison, S.L Davies, J. Carmichael, I.J. Stratford, A L. Harris, I.D. Hickson, Br. J. Cancer 72 (1995) 1454–1461

[64] J M Fortune, N J. Osheroff, J. Biol. Chem. 273 (1998) 17643–17650

[65] G A Brown, J.P McPherson, L Gu, D W Hedley, R Toso, K.L. Deuchars, M H Freedman, G J Goldenberg, Cancer Res. 55 (1995) 78–82

[66] S Dereuddre, C. Delaporte, A Jacquemin-Sablon, Cancer Res. 19 (1997) 4301–4308.

[67] R.M Turnbull, E.L. Meczes, M Perenna-Rogers, R.B Lock, D.M. Sullivan, G.J Finlay, B.C Baguley, C A Austin, Cancer Chemother Pharmacol 44 (1999) 275–282.

[68] D R Grabowski, K A Holmes, M. Aoyama, Y. Ye, L.A. Rybicki, R M Bukowski, M K Ganapathi, I.D Hickson, R. Ganapathi, Mol. Pharmacol. 56 (1999) 1340–1345.

[69] F. Guano, P Pourquier, S. Tinelli, M. Binaschi, M. Bigioni, F. Animati, S Manzini, F Zunino, G. Kohlhagen, Y. Pommier, G Capranico, Mol. Pharmacol 56 (1999) 77–84

[70] F Errington, E. Willmore, M.J. Tilby, L. Li, G. Li, W. Li, B C Baguley, C A Austin, Mol. Pharmacol. 56 (1999) 1309–1316

[71] H. Gao, K.C Huang, E F Yamasaki, K.K Chan, L Chohan, R M. Snapka, Proc. Natl Acad. Sci U S A 96 (1999) 12168–12173

[72] K L. Marsh, E. Willmore, S. Tinelli, M Cornarotti, E.L. Meczes, G. Capranico, L M. Fisher, C A. Austin, Biochem. Pharmacol 52 (1996) 1675–1685

[73] M. Cornarotti, S. Tinelli, E. Willmore, F Zunino, L M. Fisher, C A Austin, G. Capranico, Mol. Pharmacol 50 (1996) 1463–1471

[74] C.A. Austin, J H Sng, S Patel, L M Fisher, Biochim Biophys Acta 1172 (1993) 283–291

[75] M.E. Borgnetto, S. Tinelli, L Carminati, G. Capranico, J Mol Biol. 285 (1999) 545–554

[76] M Binaschi, R. Farinosi, M E. Borgnetto, G. Capranico, Cancer Res 60 (2000) 3770–3776

ELSEVIER

Biochimica et Biophysica Acta 1587 (2002) 155–163

BIOCHIMICA ET BIOPHYSICA ACTA

BBA

www.bba-direct.com

Review

Self-association and unique DNA binding properties of the anti-cancer agent TAS-103, a dual inhibitor of topoisomerases I and II

Keisuke Ishida, Tetsuji Asao*

Chemistry Laboratory, Taiho Pharmaceutical Co., Ltd, 1-27 Misugidai, Hanno, Saitama 357-8527 Japan

Received 24 January 2002; accepted 24 January 2002

Abstract

The objective of our study was to investigate the self-association and DNA-binding properties of the DNA topoisomerases I (Topo I) and II (Topo II) dual inhibitor. 6-[[2-(dimethylamino)ethyl]amino]-3-hydroxy-7*H*-indeno[2,1-*c*]quinoline-7-one dihydrochloride (TAS-103), by means of ^{1}H-NMR and ^{31}P-NMR spectroscopy, structure computation techniques, thermal melting study, and UV–Visible spectroscopy. In aqueous solution, all chemical shifts of TAS-103 underwent upfield shifts depending with an increase in concentration. The two-dimensional (2D)-NMR spectra and structure computations indicated that TAS-103 self-associated through $\pi-\pi$ stacking and hydrophobic interactions of the aromatic chromophores. Thermal melting indicated that the binding of TAS-103 to DNA with a potency equal to that of ethidium bromide (EtBr). The UV–Visible spectra of TAS-103 titrated by several DNA exhibited hypochromic and hypsochromic effects. The ^{31}P-NMR spectrum of the 6:1 TAS-103/d(CGCGAATTCGCG)$_2$ complex showed two broadening signals. 2D-NMR spectra of the 1:1 TAS-103/d(CGCGAATTCGCG)$_2$ complex indicated that the chemical shift differences of the DNA are very small. However, those of the terminal region are relatively large. The chemical shift differences of TAS-103 showed that the proton resonances except H2 underwent downfield shifts. From these observations, we conclude that TAS-103 binds to DNA by two modes. The major binding mode is on the surface (outside binding) and the minor binding mode by intercalation. © 2002 Elsevier Science B.V. All rights reserved.

Keywords: TAS-103, Self-association, DNA binder; Topoisomerase; Dual inhibitor

1. Introduction

Topoisomerases are enzymes that relieve the secondary twist on the DNA strands in the process of DNA synthesis and transcription via breakage, passage and reunion of the DNA strands. Two types enzymes, topoisomerase I (Topo I) and II (Topo II), are known and they have been recognized as significant targets of anticancer agents. During our research for a novel DNA topoisomerase I and II dual inhibitor, one of some indenoquinorine derivatives (6-[[2-(dimethylamino) ethyl]amino]-3-hydroxy-7*H*-indeno[2,1-*c*]quinolin-7-one dihydrochloride (TAS-103); Fig. 1) was found to be such a dual inhibitor of Topo I and II and exhibited highly potent and broad anticancer activities in animal models [1–3]. The mechanism of TAS-103 at the molecular basis has not been clarified, but we considered that the major target would be DNA because of its strong binding affinity to DNA. We describe here the self-association and DNA-binding properties of TAS-103 determined with the aid of ^{1}H-NMR and ^{1}H-NMR spectroscopies, structure computation techniques, UV–Visible spectroscopy, and thermal melting study.

2. Experimental procedure

2.1. Sample preparation

Calf thymus DNA (CT-DNA), poly[d(A-T)$_2$], and poly [d(G-C)$_2$] were purchased from Pharmacia LKB Biotechnology. The synthetic oligonucleotide, d(CGCGAATTCGCG), was purchased from Sawady Technology (Tokyo, Japan). Stock solutions of these oligonucleotides for thermal melt-

---

Abbreviations: TAS-103, 6-[[2-(dimethylamino)ethyl]amino]-3-hydroxy-7*H*-indeno[2,1-*c*]quinoline-7-one dihydrochloride, Topo I, DNA topoisomerase I, Topo II, DNA topoisomerase II; 2D, two dimensional, CT-DNA, calf thymus DNA, EtBr, ethidium bromide; NOE, nuclear Overhauser effect; NOESY, NOE spectroscopy, DQF-COSY, double quantum filtered correlated spectroscopy, TOCSY, total correlated spectroscopy, T_m, melting temperature; RMSD, root mean square deviation

* Corresponding author.

E-mail address: asao@taiho.co.jp (T. Asao)

0925-4439/02/$ - see front matter © 2002 Elsevier Science B.V. All rights reserved
PII: S0925-4439(02)00078-9

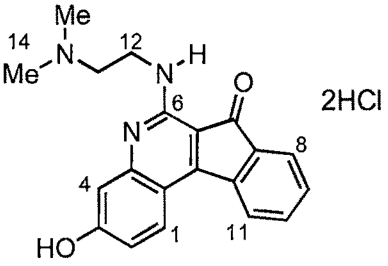

Fig. 1 Chemical structure of TAS-103

ing studies and UV–Visible spectroscopy (1 mM in nucleotide base) were prepared in buffer (10 mM Tris–HCl, 50 mM NaCl, 10 μM EDTA, pH 7.4). A stock solution of d(CGCGAATTCGCG)$_2$ for NMR spectroscopy (1.54 mM in double strand) was prepared in phosphate buffer (10 mM sodium phosphate, 50 mM NaCl, pH 7.0). The DNA duplex was annealed by heating at 80 °C for 1 h and cooling to 25 °C over 6 h. Concentrations of these oligomers (per nucleotide base) were determined from their absorbances at 260 nm after melting, using the following extinction coefficients: ε_{260}, of oligonucleotides: 9225 M^{-1} cm^{-1} for d(CGCGAATTCGCG) [4], 6600 M^{-1} cm^{-1} for CT-DNA [5], 6500 M^{-1} cm^{-1} for poly[d(A-T)$_2$] [6], 8400 M^{-1} cm^{-1} (255 nm) for poly[d(G-C)$_2$] [7]. TAS-103 was synthesized in our laboratory. Ethidium bromide (EtBr) was purchased from Nacalai Tesque (Kyoto, Japan), acti-nomycin D from Fluka, netropsin–HCl from SERVA. Stock solutions of these compounds were prepared by weighing and dissolving in D_2O, and pH was adjusted by adding small amounts of dilute HCl or NaOH solution.

For NMR experiments in H_2O, the DNA solution was lyophilized and then redissolved in 0.7 ml of 9:1 H_2O/D_2O. For NMR experiments in D_2O, the DNA solution was lyophilized three times from 99.9% D_2O and finally redissolved in 99.996% D_2O. TAS-103/DNA complexes were prepared by adding appropriate amounts of the stock solution of TAS-103 to the DNA solution. Sodium 3-trimethylsilylpropionate-2, 2, 3, 3-d_4 (TSP) and H_3PO_4 were used as an internal references for ^{1}H- and ^{31}P-NMR spectroscopy, respectively.

2.2. NMR spectroscopy

NMR experiments were carried out on a Varian UNITY*plus* 500 spectrometer operating at a proton resonance frequency of 499.85 MHz and equipped with a Sun SPARCstation 20 host computer running VNMR (Varian) system software.

The nuclear Overhauser effect spectroscopy (NOESY) [8], double quantum filtered correlated spectroscopy (DQF-COSY) [9], and total correlated spectroscopy (TOCSY) [10,11] spectra were acquired using the method of States et. al [12]. The NOESY spectra in H_2O were acquired by replacing the last 90° pulse by a 1–1 spin-echo pulse sequence to suppress the large water resonance [13]. All two-dimensional (2D) data sets were acquired non-spinning to reduce t_1 noise and other artifacts.

NMR data were processed with NMRPipe software (Molecular Simulations) on a Silicon Graphics Indigo^2 Extreme workstation. The 2D-NMR data sets were zero-filled to 2048 points in both dimensions and processed using 90°-shifted sinebell window function in t_1 and t_2.

NOE cross peak volumes of a NOESY spectrum were obtained by cross peak integration using NMRCompass software (Molecular Simulations). These peak volumes were converted into distances by the two-spin approximation [14]. The cross peak volumes were classified semi-quantitatively into three categories: strong (between 1.9 and 2.5 Å), medium (between 2.5 and 3.5 Å), or weak (between 3.5 and 5.0 Å).

2.3. Structure computations

All computations were executed on a Silicon Graphics Indigo^2 Extreme workstation. Model building and molecular dynamics were done with the programs QUANTA, CHARMm, and X-PLOR [15] (Molecular Simulations). The standard protocols were as follows: (a) high temperature dynamics in 2500 steps with a time step of 0.005 ps at 1000 K, (b) cooling dynamics in 3000 steps to a final temperature of 300 K, and (c) refine dynamics in 5000 steps with a time steps of 0.001 ps from an initial temperature of 300 K. During all computations, a square-well potential function was used for the NOE restraints, and the restraints scale factor for the NOE energy term was set to 100 kcal mol^{-1} Å^{-2}.

2.4. Determination of association constant for self-association of TAS-103

Association constant for TAS-103 was obtained from the simple dimerization model, which gives K_a=[A_2]/[A]^2 M^{-1} where [A_2] and [A] are the molar equilibrium concentrations for the dimer and monomer, respectively. K_a is the association constant [16]. Observed chemical shifts were given by $\delta_{obs}=f_A\delta_A+f_{A_2}\delta_{A_2}$, where δ_A and δ_{A_2} were the chemical shifts, f_A and f_{A_2} were the equilibrium mole fractions of the monomer and dimer forms. K_a, δ_A, and δ_{A_2} values were obtained by fitting to the observed δ-concentration curves using a commercial data analysis program (Kaleidagraph).

2.5. Thermal melting studies

Thermal melting experiments were performed on a HITACHI U-3210 spectrophotometer connected with a HITACHI SPR-10 temperature controller. A 40-μl portion of DNA (1 mM in nucleotide base) was added to the sample cell containing 1960 μl of binding buffer in the absence or presence (5 μM) of the compound (concentration of DNA in nucleotide base is 20 μM). The absorption at 260 nm was measured at 30-s intervals from 10 to 90 °C. The cell temperature was monitored and increased approximately 2.0 °C/min. Melting temperature (T_m) values were determined from first-derivative plots [17].

2.6 *UV–Visible spectroscopy*

UV–Visible absorption spectra were measured on a HITACHI U-3210 spectrophotometer linked with a HITACHI SPR-10 temperature controller. Spectral titrations were carried out at 18 °C. After a careful determination of the baseline of the spectrometer, an absorbance of 2.0 ml of the compound solution (4 μM) in binding buffer was measured from 420 to 650 nm, and then absorbance at 480 nm was measured. An 8 or 16 μl of DNA (1 mM in nucleotide base) was added to the sample and the reference cells, and the spectrum and absorbance at 480 nm were measured. This procedure was repeated until the spectrum remained unaltered.

Absorbance changes at 480 nm were used to obtain Scatchard plots [18]. The binding data expressed as Scatchard plots were analyzed by the excluded site model of McGhee and von Hippel [19]. The absorbance of the compound completely bound with DNA was obtained by extrapolation of the absorbance against compound-to-DNA molar ratio. The fraction of compound bound to DNA (c) after each addition during the titration was calculated from the equation $c=(A_f-A)/(A_f-A_b)$, where A_f is the absorbance of free compound, A_b is the absorbance of the bound compound and A is the observed absorbance. From the value of c, the variables C_f (molar concentration of free compound) and R, the binding ratio (compound bound per base pair) were calculated. The binding parameters were estimated using the model of McGhee and von Hippel [16]. The data were fitted to the equation

$$R/C_f = K(1-nR)\{(1-nR)/[1-(n-1)R]\}^{(n-1)}$$

where K is the intrinsic association constant and n is the number of nucleotide bases occluded by one bound compound. Only binding data in the fraction bound range between 0.2 and 0.8 were used. Binding data outside this range were subject to large errors as a result of experimental error in determining the free and bound absorbance.

3. Results

3.1. *Self-association of TAS-103*

The ^{1}H-NMR spectra of TAS-103 in D_2O at 20 °C (pH 1.5 or 7.5) were measured at several concentrations. A representative result is shown in Fig. 2. In acidic (pH 1.5) and neutral (pH 7.5) conditions, the chemical shifts of all proton resonances, particularly aromatic protons underwent upfield shifts in a concentration dependent manner. However, upfield shifts at pH 7.5 between 5.5 and 94 mM were relatively small and line-broadening of the signals were observed. Any significant signals at pH 7.5 were not detected over 100 mM because of the poor solubility.

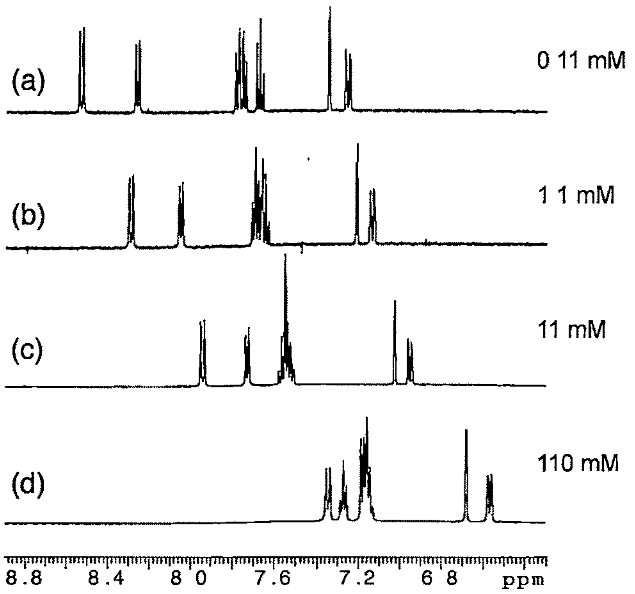

Fig. 2 ^{1}H-NMR of aromatic region of TAS-103 in D_2O at 20 °C, pH 1 5 The concentrations of TAS-103 are (a) 0.11 mM, (b) 1 1 mM, (c) 11 mM, (d) 110 mM

Self-association constants of TAS-103 were determined by comparing the chemical shift-concentration data of H4 at pH 1.5 and 7.5 with theoretical δ-concentration curves (Fig. 3), where the simple dimerization model was used. The calculated association constant (K_a), limiting chemical shift of monomer (δ_A), and that of dimer (δ_{A_2}) were 0.10×10^3 M^{-1}, 7.33 ppm, and 6.39 ppm at pH 1.5 and 8.87×10^3 M^{-1}, 6.83 ppm, and 5.91 ppm at pH 7.5, respectively. Similar values were obtained upon calculation based on the chemical shift changes of the other aromatic protons (the data are not shown).

Assignments of the proton resonances of TAS-103 were performed by several 2D-NMR spectra (DQF-COSY, TOCSY, NOESY) (Table 1).

Interproton distance constraints were estimated from the cross peak volume of the NOESY spectrum. Linearity of the NOE peak volume was checked at $\tau_m = 60-360$ ms to avoid spin diffusion contribution and there was little effect in this mixing time range. Therefore, the data for $\tau_m = 300$ ms were used to get the peak volumes that were converted into the interproton distance by a two-spin approximation based on an H1–H2 distance of 2.4 Å as a reference. Ambiguous distance constraints between intra- and intermolecular and all of the intramolecular distance constraints were rejected. Finally, 24 intermolecular distance constraints were obtained.

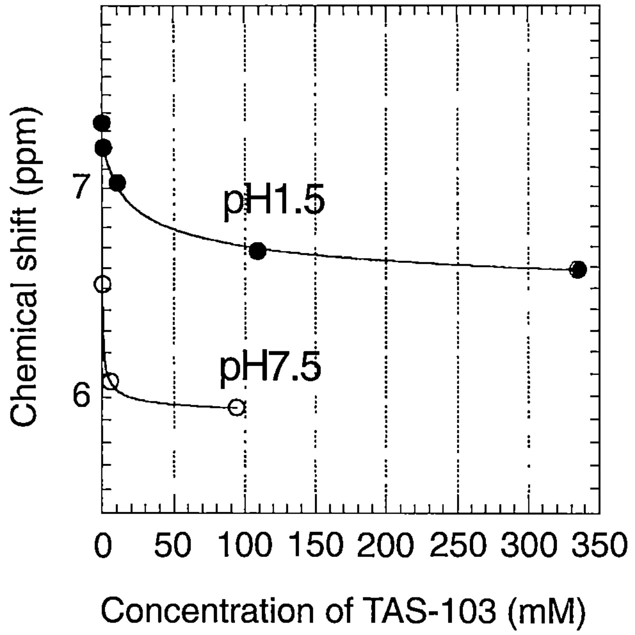

Fig 3 Concentration dependence of H4 of TAS-103 at 20 °C, pH 1 5 and 7 5. Solid curves give the best-fit theoretical curves

3.2. Thermal melting studies

The ΔT_m ($\Delta T_m = T_m$ of complex − T_m of free nucleic acid) values of DNA gives a qualitative comparison of the relative binding strengths of a compound with DNA. The ΔT_m of typical DNA-binding compounds, EtBr, actinomycin D, and netropsin were measured, together with that of TAS-103, in order to compare their relative binding affinities. The results are shown in Table 2.

3.3. UV–Visible spectroscopy

The UV–Visible spectra of TAS-103 titrated with d(CGCGAATTCGCG)$_2$ at 18 °C are shown in Fig. 5. The same experiments were executed poly[d(A-T)$_2$], poly[d(G-C)$_2$], and CT-DNA, respectively. The titration curves were nearly identical with each oligomer producing hypochromic and hypsochromic effects. The Scatchard plots at 480 nm are shown in Fig. 6. The solid lines drawn through the data are nonlinear least-squares best fit values with the cooperative model of McGhee and von Hippel [19]. The intrinsic association constant, *K*, and the number of nucleotide bases occluded by one bound compound, *n*, for each oligomer are provided in Table 3.

Table 1
Proton chemical shift assignments (ppm) of 5 5 mM TAS-103 in D_2O at 11 °C, pH 9 9

H1	6 68
H2	6 03
H4	5 64
H8	6.48
H9	6.77
H10	6.72
H11	6.58
H12	2 97
H13	2.67
H14	2 52

Table 2
Thermal melting studies[a]

Compound	Calf thymus DNA ΔT_m (°C)[b]	Poly[d(A-T)$_2$] ΔT_m (°C)[b]	d(CGCGAATTCGCG)$_2$ ΔT_m (°C)[b]
TAS-103	6 0	12 5	3 0
EtBr	6 0	10.0	4.0
Actinomycin D	7 5	0.0	14.5
Netropsin	10 5	27 5	–[c]

[a] Polymer T_ms are 77 5 °C for calf thymus DNA, 56.5 °C for poly[d(A-T)$_2$] and 45 0 °C for d(CGCGAATTCGCG)$_2$

[b] ΔT_m is the [(T_m of bound) − (T_m of native polymer)]

[c] Not detected

3.4. ^{31}P-NMR spectroscopy

Fig. 7 shows the ^{31}P-NMR spectra of d(CGCGAATTCGCG)$_2$ in the presence and the absence of TAS-103. Six resonance signals in the region between −3.0 and −2.4 ppm were observed. Addition of TAS-103 to the d(CGCGAATTCGCG)$_2$ solution caused two broadening signals in the region between −3.3 and −1.0 ppm, the main signal at −2.5 ppm and the minor signal at −1.7 ppm. By contrast, all resonances of d(CGCGAATTCGCG)$_2$ were upfield-shifted upon addition of a typical intercalator EtBr.

3.5. ^{1}H-NMR spectroscopy

3.5.1. Titration of d(CGCGAATTCGCG)$_2$ with TAS-103

^{1}H-NMR spectra of the imino proton region of d(CGCGAATTCGCG)$_2$ upon titrating with TAS-103 in H_2O are shown in Fig. 8. The ^{1}H-NMR spectrum of the free DNA shows five imino proton resonances at 12.6–13.9 ppm. The terminal imino proton of the duplex was not observed by rapid exchange with solvent protons. However, a broad resonance of the imino proton of the terminal base pairs was detected at 3 °C. These results indicate that this symmetrical oligonucleotide is present in double stranded form in this condition.

Table 3
Binding parameters of TAS-103 to various oligonucleotides

Oligonucleotide	K (M^{-1})[a]	n[b]
d(CGCGAATTCGCG)$_2$	2 2 × 10^5	4.7
Poly[d(A-T)$_2$]	4 6 × 10^5	3.3
Poly[d(G-C)$_2$]	5 5 × 10^5	5 5
Calf thymus DNA	4 8 × 10^5	3.0

[a] The intrinsic association constant.

[b] The number of nucleotide bases occluded by one bound compound

When the duplex was titrated with TAS-103, all imino proton resonances were broad, particularly over the DNA/TAS-103 ratio 1:2. With DNA/TAS-103 ratio of 1:1, only one broadening was observed at 13.0 ppm. Therefore, the 1:1 TAS-103/d(CGCGAATTCGC)$_2$ complex was used for further NMR experiments.

3.5.2. *Proton resonance assignments*

The nonexchangeable proton resonances of the free DNA were assigned using the DQF-COSY, TOCSY, and NOESY spectra recorded in D$_2$O buffer in a sequential manner according to the reported procedures [20–23]. Sequential assignment of the base protons (purine H8 and pyrimidine H6) and sugar H1′ protons have been performed by NOESY (200 ms mixing time) spectrum. Spin connectivity between deoxyribose and cytosine (H5–H6) or thymine (Me H6) was identified by TOCSY spectrum.

The exchangeable proton resonances of the free DNA were assigned using the NOESY (200-ms mixing time) spectrum recorded in H$_2$O buffer [24]. The amino proton resonances of the cytosines were assigned by the correlation of the guanine imino proton with hydrogen-bonded and exposed cytosine amino protons within a GC base pair. Adenine H2 resonances were identified by NOESY cross-peaks from base-paired thymine H3 imino protons (Table 4).

Similarly, the nonexchangeable and exchangeable proton resonances of the 1:1 complex of the DNA with TAS-103 were assigned. The nonexchangeable proton resonances of TAS-103 in the TAS-103/DNA complex were identified by TOCSY and NOESY spectra (Table 5).

The chemical shift differences between the free and the complex forms are shown in Fig. 9. The proton resonances of the DNA except G12–H2′ underwent upfield shifts and the proton resonances of TAS-103 except H2 underwent downfield shifts.

Table 4
Proton chemical shifts (ppm) of free DNA, d(CGCGAATTCGCG)$_2$[a]

Residue	H1/3	H2	H4(1)[b]/ 4(2)[c]	H8/ H6	H5/ Me	H1′	H2′ /2″	H3′	H4′
C1				7.65	5.92	5.76	1.98/2.42	4.72	4.08
G2	13.10			7.96		5.89	2.66/2.72	4.98	4.35
C3			6.47/8.41	7.28	5.38	5.57	1.86/2.28	4.81	4.14
G4	12.70			7.87		5.46	2.67/2.77	5.01	4.33
A5		7.21		8.12		6.00	2.71/2.96	5.07	4.48
A6		7.63		8.13		6.17	2.58/2.96	5.03	4.48
T7	13.70			7.15	1.28	5.93	2.03/2.60	4.85	4.23
T8	13.84			7.39	1.54	6.12	2.19/2.57	4.92	4.23
C9			6.85/8.43	7.47	5.63	5.70	2.08/2.44	4.90	4.17
G10	12.92			7.92		5.85	2.67/2.69	5.00	4.38
C11			6.64/8.49	7.35	5.45	5.75	1.91/2.34	4.82	4.16
G12				7.96		6.17	2.63/2.38	4.69	4.19

[a] Nonexchangeable and exchangeable hydrogen resonances were assigned from data recorded at 20 °C. The spectra were collected in buffer (50 mM NaCl, 10 mM sodium phosphate, pH 7.5). Chemical shifts were relative to the methyl singlet of TSP at 0 ppm.

[b] The non-hydrogen-bonded amino proton.

[c] The hydrogen-bonded amino proton.

Table 5
Proton chemical shifts (ppm) of the 1:1 TAS-103/d(CGCGAATTCGCG)$_2$ complex[a]

Residue	H1/3	H2	H4(1)[b]/ 4(2)[c]	H8/ H6	H5/ Me	H1′	H2′ /2″	H3′	H4′
C1				7.60	5.83	5.69	1.95/2.38	4.70	4.07
G2	13.00			7.93		5.84	2.64/2.66	4.96	4.33
C3			6.42/8.35	7.26	5.35	5.56	1.84/2.25	4.74	4.12
G4	12.67			7.85		5.43	2.65/2.74	4.95	4.30
A5		7.19		8.11		5.98	2.69/2.94	5.04	4.45
A6		7.59		8.12		6.15	2.57/2.93	5.02	4.46
T7	13.68			7.14	1.26	5.91	2.01/2.58	–	4.20
T8	13.82			7.37	1.52	6.10	2.17/2.55	4.90	–
C9			6.81/8.40	7.46	5.60	5.69	2.05/2.41	–	4.16
G10	12.87			7.90		5.82	2.64/2.67	5.00	4.36
C11			6.55/8.40	7.30	5.38	5.71	1.86/2.29	4.79	4.12
G12				7.90		6.06	2.63/2.38	4.67	4.17

[a] Nonexchangeable and exchangeable hydrogen resonances were assigned from data recorded at 20 °C. The spectra were collected in buffer (50 mM NaCl, 10 mM sodium phosphate, pH 7.7). Chemical shifts were relative to the methyl singlet of TSP at 0 ppm.

[b] The non-hydrogen-bonded amino proton.

[c] The hydrogen-bonded amino proton.

4. Discussion

4.1. *Self-association of TAS-103*

The chemical shifts of all proton resonances of TAS-103 in D$_2$O underwent upfield shifts depending upon the increase of concentration. The upfield shifts of aromatic protons are explained by intermolecular stacking interaction of the aromatic chromophores as observed in a wide variety of molecules containing delocalized π-ring system such as purine derivatives, acridines, and actinomycin [25–27]. It is interesting that the self-stacking of TAS-103 was pH dependent as well as concentration dependent. The association constant at pH 7.5 was $8.87 \times 10^3\ M^{-1}$ and it was about 90 times greater than that at pH 1.5 of $0.10 \times 10^3\ M^{-1}$.

A model of self-associated TAS-103 was prepared based on the intermolecular distance constraints obtained by the NOESY spectrum and subjected to molecular dynamics calculations. One hundred conformers of the dimer were generated. Ten structures having lower potential energy were selected and the resulting RMSDs of these structures were within 2.0 Å. The aromatic chromophores of TAS-103 were stacked with each other as shown in the 10 superimposed structures (Fig. 4). The amino side chains were located in the opposite side. This conformation would be reasonable in aqueous solution since the hydrophobic chromophores interact through π–π stacking and hydrophobic interactions. The positive-charged hydrophilic side chains located outside of the

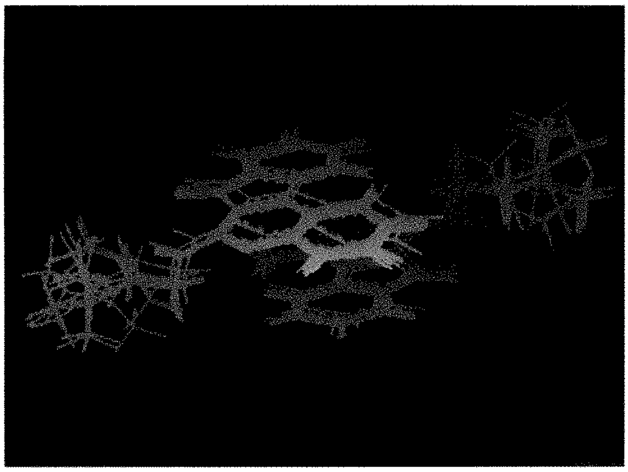

Fig. 4. Ten superimposed structures of the TAS-103 dimer.

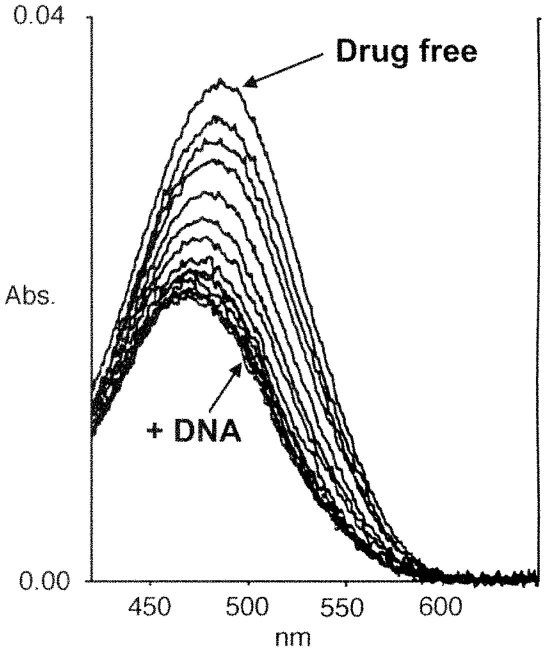

Fig. 5. UV–Visible spectra of TAS-103 titrated by d(CGCGAATTCGCG)$_2$ at 18 °C. The concentration of the compound is 4.0 μM. The ratios of nucleotide bases per compound of spectra are 0, 1, 2, 3, 5, 7, 9, 11, 13, 15, 17, 19, 21, 23, and 25 from top to bottom respectively.

dimer and face to water that stabilizes by hydrogen bonding and solvation effects. Less association constant at lower pH could be explained by the repulsion of the positive charges on the ring nitrogen against a hydrophilic aromatic chromophore.

4.2. DNA-binding of TAS-103

The melting temperatures of CT-DNA, poly[d(A-T)$_2$], and d(CGCGAATTCGCG)$_2$ were increased by approximately 6.0, 12.5, and 3 °C, respectively, when TAS-103 bound to DNA. Increase of the melting temperature (ΔT_m) of a typical intercalator EtBr was 6.0 °C for CT-DNA, 10.0 °C for poly[d(A-T)$_2$], and 4.0 °C for d(CGCGAATT CGCG)$_2$, respectively. These results indicate that the relative binding strength of TAS-103 for the double-stranded form of DNA is equal to that of EtBr.

Titration of TAS-103 with DNA was monitored by UV–Visible spectra to determine the binding constant. When TAS-103 was titrated with d(CGCGAATTCGCG)$_2$, hypochromic and hypsochromic effects were observed without any isosbestic point (Fig. 5). A similar change of spectra was also exhibited on titrations with poly[d(A-T)$_2$], poly[d(G-C)$_2$], and CT-DNA, respectively. On the other hand, titration of a typical intercalator such as EtBr or actinomycin D with DNA caused a bathochromic effect with isosbestic point. These results suggest that TAS-103 bound to DNA by multiple modes and not intercalation. The Scatchard plots of TAS-103 with oligonucleotide showed an intrinsic binding constant and number of nucleotide bases occluded by one bound TAS-103 (Fig. 6 and Table 2). TAS-103 bound to Poly[d(A-T)$_2$], poly[d(G-C)$_2$], and CT-DNA with high affinities, $K = 4.6 \times 10^5$, 5.5×10^5, and 4.8×10^5 M^{-1}, respectively. However, d(CGCGAATTCGCG)$_2$ exhibited about half binding constant of 2.2×10^5 M^{-1}.

Next, we analyzed the ^{31}P-NMR spectroscopy of the complex of TAS-103 with the double-stranded form of DNA. The ^{31}P-NMR spectrum of d(CGCGAATTCGCG)$_2$ showed six sharp resonance signals at −3.0 to −2.4 ppm (Fig. 7a), indicating a single conformer. When TAS-103 was added to the DNA solution, two broadening signals in the

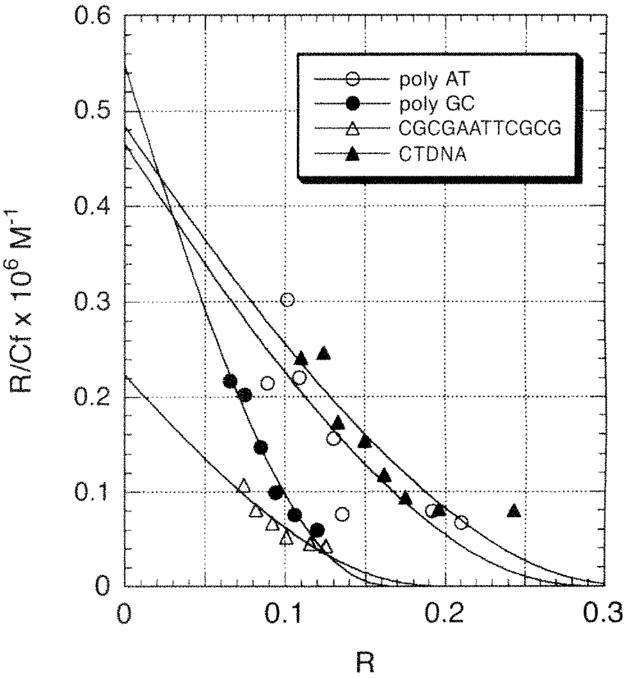

Fig. 6. Scatchard plots for titrations of TAS-103 with poly[d(A-T)$_2$] (open circles), poly[d(G-C)$_2$] (solid circles), d(CGCGAATTCGCG)$_2$ (open triangles) and calf thymus DNA(CTDNA) (solid triangles) at 18 °C. The points are experimental binding data in the fraction bound range between 0.2 and 0.9. The solid lines are the nonlinear least-squares best fits to the McGhee and von Hippel model.

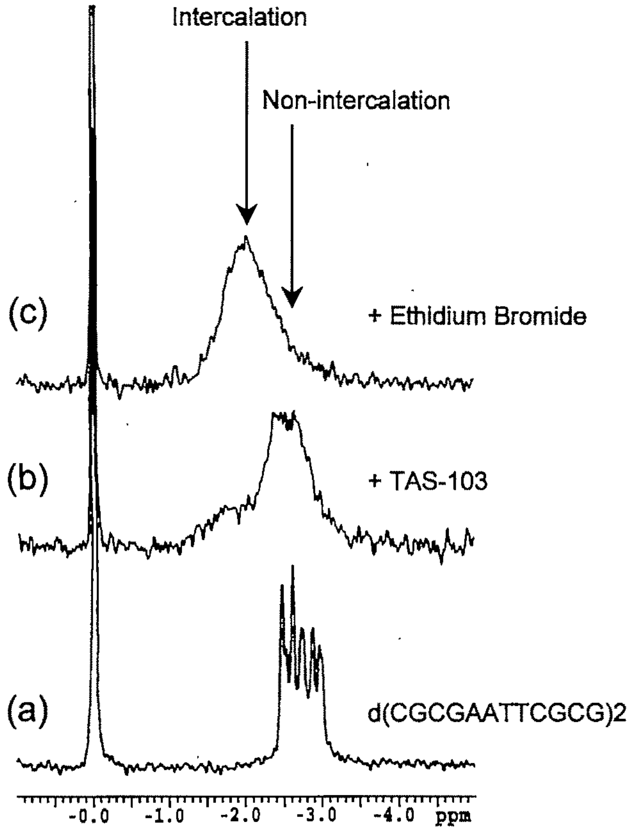

Fig. 7. ^{31}P-NMR spectra of (a) d(CGCGAATTCGCG)$_2$, (b) the 6:1 TAS-103/d(CGCGAATTCGCG)$_2$ complex, and (c) the 6:1 EtBr/d(CGCGAAT TCGCG)$_2$ complex in H_2O buffer at 20 °C, pH 7.0.

region between −3.3 and −1.0 ppm appeared (Fig. 7b) (main signal at −2.5 ppm and minor signal at −1.7 ppm). On the other hand, upon addition of EtBr to the DNA solution, one new broadening signal at −1.9 ppm was observed (Fig. 7c). These downfield shifts of the ^{31}P resonances of DNA backbone have been reported in previous studies on DNA–intercalator complexes [28,29]. From these results, the new minor downfield-shifted signal at −1.7 ppm observed in TAS-103 would be attributed to intercalation. However, the another main signal at −2.5 ppm could not be explained by intercalation.

The imino proton resonances of DNA are good probes for identifying binding mode of a DNA-binding compound. It is able to distinguish three modes of drug binding based on the spectral changes [30]. Intercalators show upfield shifts of both the AT and GC resonances, often accompanied by some broadening of the resonance. Minor groove binders show downfield shifts of the AT resonances. Little or no spectral changes in the imino proton resonances occur in outside binders that are caused by electrostatic interactions between the phosphate backbone of DNA and positive charge of the compound with an unspecified manner. Therefore, change of imino proton resonances of DNA titrated by TAS-103 was analyzed by ^{1}H-NMR spectroscopy in order to identify the two binding modes of TAS-103 to DNA assumed by ^{31}P-NMR spectroscopy. When d(CGCGA-ATTCGCG)$_2$ was titrated with TAS-103, all imino proton resonances were gradually broadening and the chemical shift changes were small, as shown in Fig. 8. However, minor upfield-shifted signals were detected in the region from 11.6 to 12.3 ppm and from 13.0 to 13.4 ppm. These data indicate that TAS-103 has mainly two binding modes as observed in the study of ^{31}P-NMR spectroscopy. Minor binding mode was confirmed to be an intercalation, which was assumed by ^{31}P-NMR spectrum, and major binding mode would be an outside binding. Similar binding models have been proposed in intoplicine derivatives by surface-enhanced Raman scattering (SERS) and CD spectroscopy [31]. They concluded that the poisoning ability of dual Topo I and Topo II of intoplicine would due to its ability simultaneously to form two types of DNA complexes: a 'deep intercalation mode' responsible for Topo I-mediated cleavages and an 'outside binding mode' responsible for Topo II-mediated cleavage.

Finally, 2D-NMR experiments were executed using the 1:1 TAS-103/d(CGCGAATTCGCG)$_2$ complex. The chemical shift differences of the central residues (G4–C9) of the DNA were very small (<0.04 ppm), as shown in Fig. 9, but those of the terminal region were relatively large. These

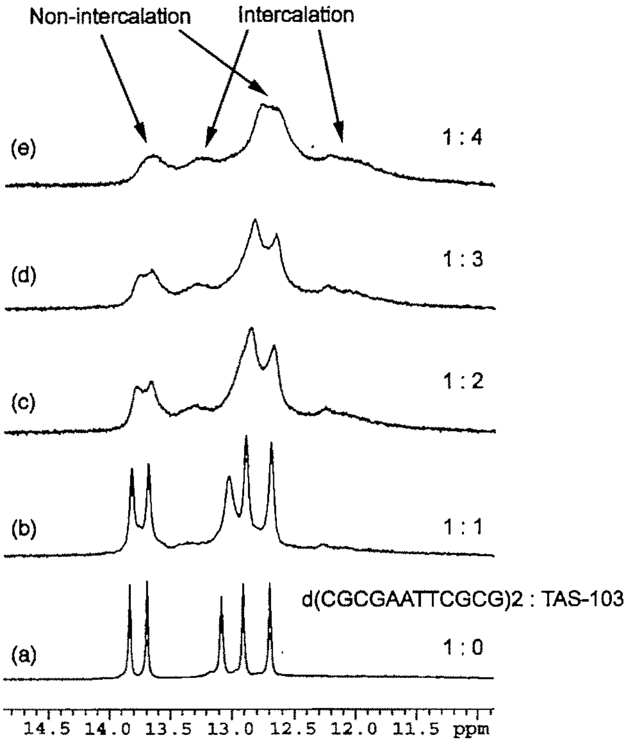

Fig. 8. Imino region of ^{1}H-NMR spectra of (a) d(CGCGAATTCGCG)$_2$, (b) 1:1, (c) 2:1, (d) 3:1, (e) 4:1 TAS-103/d(CGCGAATTCGCG)$_2$ complex in H_2O buffer at 20 °C, pH 7.6.

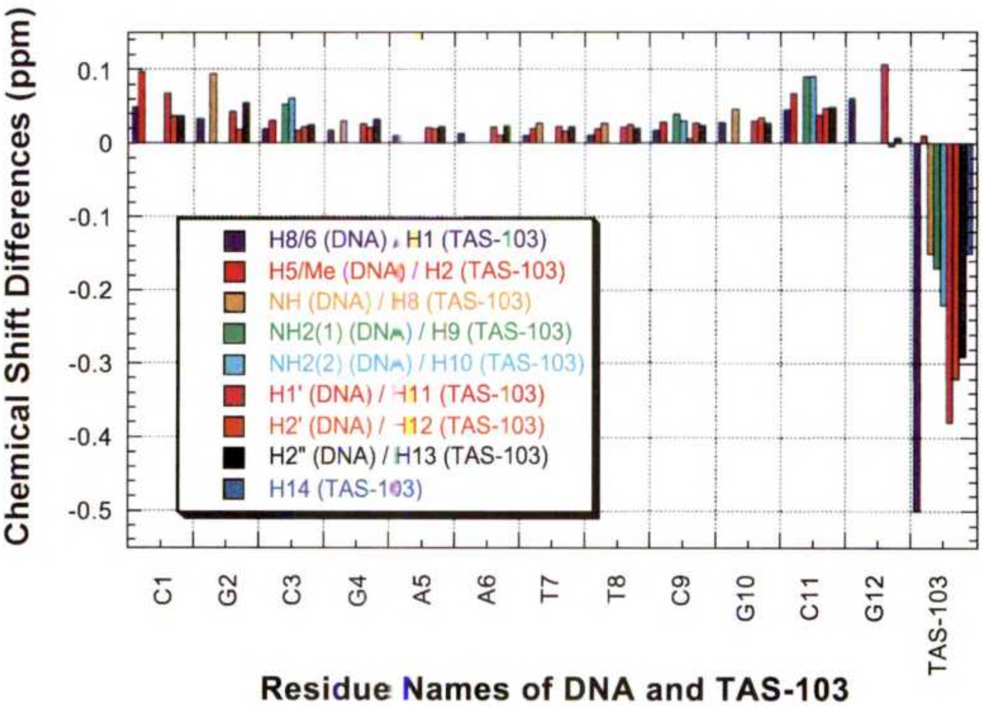

Fig. 9. Chemical shift differences of DNA and TAS-103 proton resonances between the free and complex form. The values indicate the chemical shift difference (ppm) obtained from (chemical shift of free form) − (chemical shift of complex form). The positive and the negative values indicate the upfield and the downfield shift of resonance, respectively.

small chemical shift changes indicated that conformational change of the DNA was small and the binding mode of TAS-103 was an outside binding. Upfield-shifted protons (> 0.05 ppm) were located in the DNA major groove where C1–H5, G2–NH, C3–NH2(1,2), C11–H5, C11–NH2(1,2), and G12–H8 are located. TAS-103 would interact with the terminal region of DNA by outside binding from the major groove followed by with the central region on concentration dependent manner of TAS-103.

In conclusion, TAS-103 was self-associated in aqueous solution through π–π stacking and hydrophobic interactions. TAS-103 showed a strong binding affinity for DNA and it interacts with DNA by mainly two binding modes. Major binding mode is an outside binding from major-groove and minor binding mode is an intercalation. Interacting with DNA would cause simultaneous destabilization of the self-association property of TAS-103. The schematic representation of the self-association and DNA-binding of TAS-103 is shown in Fig. 10. We recently have found that the mode of DNA binding of TAS-103 was greatly dependent upon the pH. Its detail analyses are ongoing.

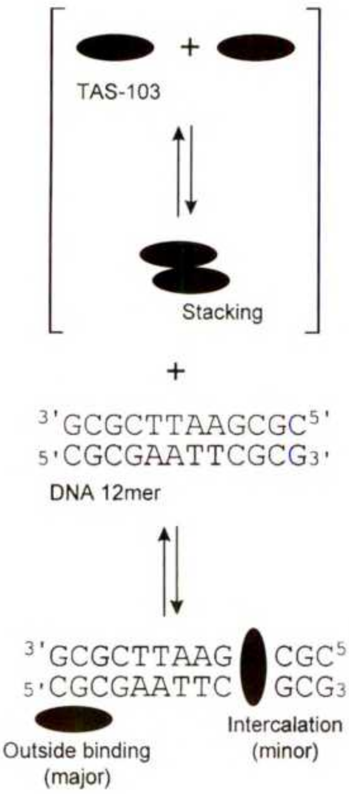

Fig. 10. Schematic representation of the self-association and DNA-binding of TAS-103.

Acknowledgements

We thank Professor Luigi G. Marzilli (Emory University) for helpful discussion.

References

[1] T Utsugi, K Aoyagi, Y. Furune, M Sano, K Wierzba, S. Okazaki, T Asao, Y. Yamada, Proc Am Assoc Cancer Res. 37 (1996) 427 (Abstract 2915).

[2] T Ishida, K Nishio, H Arioka, H. Kurokawa, H Fukumoto, K. Furuoka, T. Nomoto, A Tomonari, H Yokote, Y Iwamoto, T Suzuki, J Usuda, N Saijo, Proc. Am Assoc Cancer Res. 38 (1997) 21 (Abstract 137)

[3] T. Ishida, K. Nishio, H. Arioka, H. Kurokawa, H Fukumoto, K Fukuoka, T Nomoto, H Yokote, N Saijo, Proc Am Assoc Cancer Res 37 (1996) 428 (Abstract 2922)

[4] G.D. Fasman (Ed), CRC Handbook of Biochemistry and Molecular Biology, 3rd edn , vol I, The Chemical Rubber Publishing Co , Cleveland, OH, 1975, p. 589

[5] R.M. Wadkins, T M Jovin, Biochemistry 30 (1991) 9469–9478.

[6] W Chu, M Shinomiya, K Y Kamitori, S. Kamitori, R G. Carlson, R.F. Weaver, F Takusagawa, J Am Chem Soc 116 (1994) 7971–7982

[7] F.-M. Chen, Biochemistry 27 (1988) 1843–1848.

[8] A. Kumar, R R Ernst, K. Wuthrich, Biochem. Biophys Res. Commun 95 (1980) 1–6

[9] U Piantini, O.W Sorensen, R R. Ernst, J. Am Chem Soc 104 (1982) 6800–6801.

[10] L. Braunschweiler, R.R Ernst, J. Magn Reson 53 (1983) 521–528

[11] A Bax, D G Davis, J. Magn. Reson 65 (1985) 355–360.

[12] D J. States, R A. Haberkorn, D.J Ruben, J Magn. Reson. 48 (1982) 286–292

[13] V. Sklenar, A. Bax, J. Magn Reson. 74 (1987) 469–479

[14] B R. Reid, K Banks, P Flynn, W. Nerdal, Biochemistry 28 (1989) 10001–10007

[15] A.T. Brunger, X-PLOR Version 3.1 A System for X-ray Crystallography and NMR, Yale University Press, New Heaven, CT, 1992.

[16] N S Angerman, T A Victor, C.L Bell, S.S Danyluk, Biochemistry 11 (1972) 2402–2411

[17] W.D Wilson, L Ratmeyer, M. Zhao, L. Strekowski, D. Boykin, Biochemistry 32 (1993) 4098–4104

[18] G. Scatchard, Ann N Y Acad Sci 51 (1949) 660–672.

[19] J.D McGhee, P H von Hippel, J Mol Biol 86 (1974) 469–489

[20] D.R Hare, D.E Wemmer, S.H. Chou, G Drobny, B R. Reid, J Mol. Biol. 171 (1983) 319–336

[21] R M Scheek, N Russo, R Boelens, R Kaptein, J.H van Boom, J Am Chem Soc 105 (1983) 2914–2916

[22] R M. Scheek, R. Boelens, N Russo, J.H van Boom, R Kaptein, Biochemistry 23 (1984) 1371–1376.

[23] K. Wüthrich, NMR of Proteins and Nucleic Acids, Wiley, New York, 1986

[24] R. Boelens, R M Scheek, K Dijkstra, R Kaptein, J Magn Reson 62 (1985) 378–386

[25] S.I Chan, M.P. Schweizer, P O.P Ts'o, G K. Helmkamp, J Am Chem Soc. 86 (1964) 4182–4188.

[26] D J. Blears, S S. Danyluk, J. Am. Chem Soc 89 (1967) 21–26.

[27] A D Broom, M P Schweizer, P O P Ts'o, J Am Chem Soc 89 (1967) 3612–3622

[28] L G Marzilli, D.L Banville, G. Zon, W.D. Wilson, J Am. Chem Soc 108 (1986) 4188–4192

[29] J -Y. Fan, D Sun, H Yu, S M Kerwin, L.H Hurley, J Med Chem 38 (1995) 408–424.

[30] J Feigon, W A Denny, W Leupin, D R Kearns, J. Med Chem 27 (1984) 450–465

[31] I Nabiev, I. Chourpa, J -F. Riou, C.H. Nguyen, F Lavelle, M. Manfait, Biochemistry 33 (1994) 9013–9023

ELSEVIER
Biochimica et Biophysica Acta 1587 (2002) 164–173
BIOCHIMICA ET BIOPHYSICA ACTA
BBA
www.bba-direct.com

Review

Novel aspects of resistance to drugs targeted to dihydrofolate reductase and thymidylate synthase

Debabrata Banerjee[a,*,1], Philipp Mayer-Kuckuk[a], Gina Capiaux[a,b], Tulin Budak-Alpdogan[a], Richard Gorlick[c], Joseph R. Bertino[a,d]

[a]*Program of Molecular Pharmacology and Experimental Therapeutics, Memorial Sloan Kettering Cancer Center, 1275 York Avenue, New York, NY 10021, USA*
[b]*Graduate Program, Department of Pharmacology, Weill-Cornell University School of Medicine, Memorial Sloan Kettering Cancer Center, 1275 York Avenue, New York, NY 10021, USA*
[c]*Department of Pediatrics, Memorial Sloan Kettering Cancer Center, 1275 York Avenue, New York, NY 10021, USA*
[d]*Department of Pharmacology, Weill-Cornell University School of Medicine, Memorial Sloan Kettering Cancer Center, 1275 York Avenue, New York, NY 10021, USA*

Received 24 January 2002, accepted 24 January 2002

Abstract

Drug resistance is often a limiting factor in successful chemotherapy. Our laboratory has been interested in studying mechanisms of resistance to drugs that are targeted to the thymidylate biosynthesis pathway especially those that target thymidylate synthase (TS) and dihydrofolate reductase (DHFR). We have used leukemia as a model system to study resistance to methotrexate (MTX) and colorectal cancer as the model system to study 5-fluorouracil (5-FU) resistance. In leukemias, we and others have shown that transport, efflux, polyglutamylation and hydrolase activities are major determinants of MTX resistance. We have further reported that some leukemic cells have an increase in DHFR gene copy number possibly contributing to the resistant phenotype. Recently, we have begun to study in detail the molecular mechanisms that govern translational regulation of DHFR in response to MTX as an additional resistance mechanism. Studies thus far involving colorectal tumors obtained from patients have focused predominantly on the predictive value of levels of TS expression and *p53* mutations in determining response to 5-FU. Although the predictive value of these two measures appears to be significant, given the variety of resistance to 5-FU observed in cell lines, it is not likely that these are the only measures predictive of response or responsible for acquired resistance to this drug. The enzyme uridine–cytidine monophosphate kinase (UMPK) is an essential and rate-limiting enzyme in 5-FU activation while dihydropyrimidine dehydrogenase (DPD) is a catabolic enzyme that inactivates 5-FU. Alterations in UMPK and DPD may therefore explain failure of 5-FU response in the absence of alterations in TS or *p53*. Transcription factors that regulate TS may also influence drug sensitivity. We have found that mRNA levels of the E2F family of transcription factors correlates with TS message levels and are higher in lung metastases than in liver metastases of colorectal cancers. Moreover, gene copy number of the E2F-1 gene appears to be increased in a significant number of samples obtained from metastases of colorectal cancer. We have also generated mutants of both DHFR and TS that confer resistance to MTX as well as 5-FU by random as well as site-directed mutagenesis. These mutants used alone or as fusion cDNAs of the mutants have proven to be useful in transplant studies where transfer of these mutant cDNAs to bone marrow cells have been shown to confer drug resistance to recipients. The fusion cDNAs of DHFR such as the DHFR–herpes simplex virus type 1 thymidine kinase (HSVTK) are also useful for regulation of gene expression in vivo using MTX as the small molecule regulator that can be monitored by positron

---

Abbreviations: AML, acute myeloid leukemia, ALL, acute lymphoblastic leukemia, AICAR, aminoimidazole carboxamide ribonucleotide transformylase; DHFR, dihydrofolate reductase, DPD, dihydropyrimidine dehydrogenase, 5-FU, 5-fluorouracil, FAB, Franco American British classification, FUDR, fluordeoxyuridine, FPGS, folylpolyglutamate synthase, GGH, gamma glutamyl hydrolase; GARFT, 5′ phosphoribosyl glycinamide transformylase; GLUT1, glucose transporter 1; HSVTK, herpes simplex virus type 1 thymidine kinase, IRES, internal ribosome entry site; MTX, methotrexate, OPRTase, orotic acid phosphoribosyl transferase, PET, positron emission tomography, PCR, polymerase chain reaction, RFC, reduced folate carrier, pRb, retinoblastoma susceptibility gene product, TK, thymidine kinase, TP, thymidine phosphorylase; TS, thymidylate synthase; UMPK, uridine–cytidine monophosphate kinase

[*] Corresponding author. Tel +1-732-235-6458, fax. +1-732-235-8181

E-mail address banerjed@umdnj.edu (D Banerjee)

[1] Present address: The Cancer Institute of New Jersey and Departments of Medicine and Pharmacology, University of Medicine and Dentistry of New Jersey, New Brunswick, NJ 08901, USA.

0925-4439/02/$ - see front matter © 2002 Elsevier Science B V All rights reserved
PII S0925-4439(02)00079-0

emission tomography (PET) scanning or by optical imaging using a fusion construct such as DHFR–EGFP. © 2002 Elsevier Science B V. All rights reserved.

Keywords: Drug resistance; Antifolate; Fluoropyrimidine, Myeloprotection; In vivo imaging

1. Introduction

A major problem in chemotherapy is resistance to the chemotherapeutic agents. There are generally two major forms of resistance encountered in the clinic. One is intrinsic resistance, which is an innate property of the tumor cells and is not triggered by drug exposure. The other is known as acquired resistance, which occurs following exposure to the drug(s). Antifolates such as methotrexate (MTX) and fluoropyrimidines such as 5-fluorouracil (5-FU) have been used in the clinic for the management of childhood acute lymphoblastic leukemias (ALL) and colorectal cancer, respectively, with modest success. Laboratory studies carried out over the years, on cell culture models as well tumor samples from blood and biopsy materials, have revealed a wealth of information regarding mechanisms of resistance to both these drugs.

MTX, in combination with other chemotherapeutic agents, has been used for treatment of malignancies including ALL, non-Hodgkin's lymphoma, osteogenic sarcoma, choriocarcinoma and carcinomas of breast, head and neck. In addition to the use of MTX for treatment of malignancies, it is also used for treatment of nonmalignant conditions such as rheumatoid arthritis, psoriasis and in the prevention of graft versus host disease [1]. Although response to treatment is observed in patients, many of them relapse due to development of resistance. The underlying mechanisms responsible for resistance to MTX have been the subject of intense investigation for the past decade.

The primary cellular target of MTX, and other antifolates, is the enzyme dihydrofolate reductase (DHFR), which catalyzes the reduction of folate and 7,8 dihydrofolate to 5,6,7,8 tetrahydrofolate [2]. To act on this intracellular target, MTX enters the cell primarily by an active carrier transport mechanism also shared by the reduced folates and mediated by the reduced folate carrier (RFC) [3]. Once inside the cell, MTX is modified so that it is retained in the cell. This is accomplished by addition of glutamate residues (up to five) catalyzed by the enzyme folylpolyglutamate synthetase (FPGS) [4,5]. MTX and polyglutamylated forms of MTX are tight binding inhibitors of DHFR and interfere with pyrimidine viz. thymidylate biosynthesis. MTX polyglutamates as well as dihydrofolate polyglutamates are also inhibitors of enzymes involved in purine biosynthesis including 5′-phosphoribosylglycinamide transformylase (GAR transformylase) and aminoimidazole carboxamide ribonucleotide transformylase (AICAR transformylase) [6–8]. Enzymatic removal of glutamyl groups from polyglutamylated forms of both folates and MTX is catalyzed by gamma glutamyl hydrolase (GGH). This enzyme maintains a balance between the various glutamylated forms in concert with FPGS [9–12].

2. Mechanisms of resistance

In experimental cell culture model systems, four common mechanisms of resistance to MTX have been identified; decreased uptake of the drug, decreased retention due to defective polyglutamylation or increased polyglutamate breakdown, increased DHFR activity as well as decreased binding of MTX to DHFR [13].

2.1. Transport

The most common mechanism of resistance to MTX is defective transport of the drug. This is true for cell culture model systems as well as leukemic blast cells from patients with ALL and osteogenic sarcoma at the time of relapse after MTX treatment. This is an example of acquired resistance to MTX after acute or chronic exposure to MTX [14–16]. With the recent cloning of the gene encoding the mouse as well as the human RFC, it is now possible to determine the molecular basis of resistance in cells that have impaired MTX uptake [16–19]. Using a complementation assay, a mouse cDNA clone has been identified that partially restores the transport defect in a human breast cancer cell line ZR75 [18]. This gene codes for a protein of 58 kDa and has structural similarity with the human glucose transporter GLUT1. Hydropathy analysis has revealed that it contains 12 transmembrane domains and belongs to the superfamily of transporter molecules collectively referred to as the major facilitator superfamily, members of which carry out sugar transport in mammalian cells [20]. The human cDNA clone that complement transport defect in a Chinese hamster ovary cell line encodes a putative RFC of 64 kDa with approximately 50% homology to the hamster and mouse RFCs at the amino acid level [19]. Yang et al. [21] have identified mutations in the human RFC protein as major determinants of MTX resistance in leukemia and osteogenic sarcoma patient samples.

2.2. Polyglutamylation

MTX, upon entry into the cell, is modified by the sequential addition of glutamate residues catalyzed by the enzyme FPGS. The ability to form long chain polyglutamates of MTX correlates well with the therapeutic outcome of several leukemias. Adult T and B lineage ALL have been found to accumulate lower amounts of long chain polyglutamates as compared to pediatric B lineage ALL and this correlates with poorer prognosis for the former [22–25]. Pediatric T lineage ALL was also seen to accumulate less long chain polyglutamates as compared to its B lineage counterpart [25]. Nonhyperdiploid B lineage blasts were also found to accumulate significantly less long chain polyglutamates once again correlating with outcome [24]. The ability to polyglutamylate has now been accepted to be an important determinant of outcome of leukemias, most likely through predicting response to MTX. It is of interest to note that the monoblastic subset of acute myeloid leukemia (AML) Franco American British (FAB) classification-M5 subtype was found to form polyglutamates of MTX as efficiently as childhood ALL blasts [26]. MTX may be an effective therapy for this subtype and may have been overlooked because other subtypes of AML are intrinsically resistant to MTX. Lack of accumulation of MTX polyglutamates may be due lack of formation of long chain polyglutamates due to impaired activity of FPGS or due to enhanced breakdown of the formed long chain polyglutamates due to increased activity of GGH [27]. The relative contribution of FPGS and GGH to overall MTX resistance remains an area of active investigation. Mammalian FPGS has molecular mass of 60 kDa and catalyzes the addition of glutamates to all naturally occurring folates as well some folate analogs such as MTX. Characterization of alterations in FPGS at the molecular level will now be possible with the recent cloning of the cDNA for human FPGS [28]. Using sequence information made available recently a quantitative polymerase chain reaction (PCR) method has been developed to measure FPGS mRNA levels in leukemic blasts. FPGS mRNA expression using this method correlated well with the enzyme activity levels [29]. Less is known about the enzyme GGH as compared to FPGS. The hydrolases can be classified broadly into two types; the lysosomal type with a pH optimum around 4.4 and a cytoplasmic type with an alkaline pH optimum with a restricted expression (small intestine, brain). It appears that the lysosomal hydrolase is more important in regulation of polyglutamate chain length. The bovine hepatic enzyme remains the most well-characterized lysosomal hydrolase to date. This enzyme has a molecular mass of 108 kDa and contains highly reactive sulfhydryl groups. Several laboratories including our own are engaged in the purification and further molecular characterization of GGH from tumor cells in an attempt to understand the role of GGH in intrinsic and acquired resistance to MTX [30,31]. Recently, Cole et al. [32] have reported that transfection and overexpression of GGH in HT-1080 human fibrosarcoma cells and MCF-7 human breast carcinoma cells, unexpectedly, did not result in MTX resistance. The clones overexpressing GGH were not resistant to short-term MTX exposure although these cells showed altered MTX accumulation and metabolism to long-chain polyglutamates. Moreover, changes in MTX metabolism were found to be balanced by alterations in accumulation and metabolism of folic acid, suggesting that ratio of MTX/folate accumulation may be a better predictor of MTX effect than accumulation of either alone.

2 3 DHFR gene amplification

As MTX is a tight-binding inhibitor of the enzyme DHFR, an increase in the level of intracellular DHFR would be expected to cause MTX resistance. Exposure of tumor cells to increasing doses of MTX results in amplification of the DHFR gene. Initially, four case reports were published, indicating that low-level gene amplification occurs in tumor cells from patients treated with MTX [33a–36]. In a recent study reported from this laboratory, approximately 30% of relapsed ALL patients (9 of 29) had low level DHFR gene amplification (two to four copies of the gene) as compared to only 10% (4 of 38) of newly diagnosed ALL patients. This study confirmed that low level DHFR gene amplification is a mechanism of acquired resistance to MTX [36]. Of interest, mutations in *p53* gene were seen in 7 of 9 ALL blast samples with DHFR amplification. In contrast, only 2 of 26 ALL blast samples without DHFR gene amplification had *p53* mutations [36]. In cell lines with mutated *p53*, a tumor suppressor gene, amplification of the target gene has been observed after antimetabolite exposure [37,38].

2.4. Mutations in DHFR

Mutant forms of DHFR with reduced affinity for MTX have been identified in cell lines that were exposed to increasing doses of the drug [39–44]. In order to examine whether mutations in DHFR occur in patient samples, we have tested blast samples from over 20 patients for decreased binding of MTX to DHFR; in addition, we have analyzed the complete DHFR cDNA sequence of eight patients; six ALL (four relapsed and two untreated) and two patients with untreated AML. No evidence for decreased binding at the enzymatic level or alterations in the coding region of the DHFR cDNA were found from these patient samples. It seems unlikely that mutations in DHFR are a major mechanism of acquired resistance in patients exposed to MTX [45a]. In contrast, mutations leading to a decreased affinity of DHFR for the antifolate pyrimethamine, used in the treatment of malaria, is the major cause of resistance to this drug [45b].

2.5. Translational autoregulation of DHFR

Previous studies have shown that administration of MTX to patients leads to an increase in the level of DHFR protein in both normal and leukemic leukocytes as well as in erythrocytes within hours to days [46]. Studies carried out in vitro using a lymphoblastoid cell line showed that an increase in DHFR protein is not transcriptionally mediated but was abrogated by cycloheximide treatment, suggesting that new protein synthesis was involved. The rapid increase in DHFR observed after MTX treatment could have been due to either protection of DHFR from degradation by bound MTX and/or dihydrofolate, or to an in increase in translation of this enzyme [47]. An increase in thymidylate synthase (TS) activity has been reported after 5-FU treatment, and it has been suggested that this increase may be due to regulation at the translational level [48]. Using a rabbit reticulocyte translation system, we have found that DHFR protein inhibited its own synthesis. The reversal of this inhibition by MTX or FH_2 may explain in part the observed induction of DHFR activity in normal and leukemic cells after MTX treatment [49a]. In order to locate the region of DHFR mRNA involved in binding to the DHFR protein, we used a system where ^{32}P-labelled in vitro transcribed RNA from different regions of the coding sequence of DHFR mRNA is UV cross-linked to DHFR protein and electrophoresed after RNAse treatment. Competition experiments with molar excess of cold RNA fragments revealed that a 100-base-long fragment in the coding region may be involved in the binding [49b].

2.6. Cell cycle genes and resistance to antifolates

Loss of the functional retinoblastoma protein (pRb) may also contribute to antimetabolite resistance as cells lacking pRb may have increased levels of enzymes associated with proliferation (e.g. DHFR, TS) as a consequence of increased levels of free E2F, a transcription factor(s) that is normally quenched by hypophosporylated pRb. When cells begin to move out of G1 and into S phase, pRb becomes hyperphosphorylated and releases bound E2F, which then enhances the transcription of genes involved in DNA synthesis [50]. We have observed that a human osteosarcoma cell line SaOs2 that lacks pRb is intrinsically resistant to MTX and fluoropyrimidines (FUDR) as compared to lines with pRb present. This cell line has a higher level of DHFR and TS and the increase in this activity is attributable to increased trancriptional activity of DHFR and TS genes. When the cDNA encoding pRb is reintroduced into this cell line, sensitivity to MTX is restored. There are other human sarcoma cell lines established in the laboratory that lack pRb and these cell lines also show a similar resistance to MTX and FUDR [51].

Since free or unbound E2F levels increase when pRb is hyperphosphorylated, we reasoned that activation of regulators of pRb phosphorylation like the cyclin dependent kinase system (the cyclin D1–Cdk4) may also result in an increase in DHFR levels and hence MTX resistance. Transfection of cyclin D1 into HT-1080 human sarcoma cell line resulted in an increase in MTX resistance in clones that expressed high levels but not in clones that expressed low levels of the gene, suggesting a direct relationship between the level of cyclin D1 expression and DHFR transcription [52]. Since certain tumors have been shown to express high levels of cyclin D1, it will be interesting to examine the relationship between overexpression of cyclin D1, DHFR transcription and MTX sensitivity in these tumors. It is becoming increasingly clear that deregulation of cell cycle genes has a profound effect on antimetabolite resistance.

3. Resistance to fluorpyrimidines

3.1. Increased levels of TS

The levels of TS, the target enzyme of the fluoropyrimidines, and antifolate inhibitors of TS, frequently correlates with and may predict response to inhibitors of this enzyme. Although fluoropyrimidines such as 5-FU have been used in the clinic for colorectal cancer, drug resistance is still a major hurdle to successful therapy. Studies have therefore been undertaken to determine both intrinsic and acquired resistance to 5-FU. Intrinsic resistance has mostly been attributed to high levels of TS in tumors that occur as a result of increased copy number or increased transcription/translation of the message and protein. Determination of factors that result in intrinsic resistance to fluoropyrimidines may allow the clinician to separate the predicted nonresponders from the group and provide them with more meaningful chemotherapeutic options.

High TS levels generally predict for lack of response while lower levels are correlated with response in colorectal cancers [53–55]. Several groups have reported that TS levels generally predict not only for response but also for overall survival in colorectal cancers. Generally, mRNA levels of TS have proven to be as good predictors of response as well as protein levels determined by immunohistochemistry [53–57]. We have shown that lung metastases, which are less responsive to fluoropyrimidine based therapies, have a higher mean TS gene expression level than hepatic metastases [58a,b]. It has been reported that abdominal metastasis had a higher level of TS gene expression than hepatic metastasis, and this correlated well with response; the hepatic metastasis being more responsive than the abdominal metastasis group [59], suggesting that TS levels vary among metastatic sites.

In a few cases, the increase in TS was attributable to increased copy number while in others, the increase has been suggested to be a result of increased E2F-1 levels [58a,b]. Increased levels of TS as a result of translational upregulation or increased stability in the presence of fluoropyrimidines has been shown to occur in cell culture model systems [60,61]. The resultant increase in TS levels may also contribute to the resistant phenotype, although the importance of these mechanisms in human cancers is yet to be established.

Polymorphisms in the TS promoter have also been reported to be correlated with response. Patients who are homozygous for a triple tandem repeat of a 28-bp sequence within the TS promoter had a higher level of TS gene expression than patients who were homozygous for a double tandem repeat of the same 28-bp sequence while an intermediate response pattern was observed for heterozygous patients [62]. Cell culture models have identified several mutations in TS being responsible for drug resistance; however, no examples of mutant forms of TS have been reported in tumor samples from patients resistant to fluoropyrimidines [63–65].

3.2. E2F levels

TS and other proteins involved in DNA synthesis such as DHFR, thymidine kinase (TK), ribonucleotide reductase (RR), and DNA Pol α are transcribed in the late G1 and S-phase of the cell cycle. Regulation of cell cycle progression at the Gl checkpoint appears to be largely dependent upon the ability of pRb and related proteins to sequester and inhibit the activity of the E2F family of transcription factors, which results in transcription of these enzymes. Disruption of the pRb–E2F complex by phosphorylation of pRb by Cdks or p16 dysfunction leads to "free" E2F, which can then transactivate target genes such as TS. Studies on forced overexpression of E2F-1 in cell culture by us and others have indicated that increased expression of E2F-1 in these cells is associated with an increase in TS levels and to a lesser extent DHFR and TK levels [66–69]. In order to understand the biochemical basis for the differential response of hepatic metastases and pulmonary metastases to fluoropyrimidine-based therapies, we have measured TS mRNA and protein levels as well as levels of E2F-1 in colorectal tumor samples. High TS mRNA levels were found in lung metastasis as compared to liver metastasis and correspondingly the E2F-1 levels were also higher in lung metastasis compared to liver metastasis [58a,b]. Kasahara et al. [70] have also reported a close correlation between TS and E2F-1 levels in colon cancer.

Although E2F-1 overexpression is associated with cell proliferation, high levels of E2F-1 have also been shown to be apoptotic in many cell systems. Recent evidence suggests that tumor cells, which express high levels of E2F-1, are protected from apoptosis by deletion or mutation in genes that could result in apoptotic cell death, including *p53*, $p14^{ARF}$ and *bax*. Alterations in *p53*, $p14^{ARF}$ or *mdm2* interfere with the cell's ability to conduct the proapoptotic signal allowing the high levels of E2F-1 to stimulate cell proliferation [66,67]. Mutations in *p53*, *p16*, *bax* and $p14^{ARF}$ occur frequently in colon cancer, and coupled with high levels of E2F-1 point to a more aggressive phenotype of the tumor. Along with the loss in the apoptotic signaling pathway, overexpression of E2F-1 may also activate genes whose products confer a more invasive phenotype. Interestingly, recent reports indicate that forced over expression of E2F-1 results in activation of the invasive phenotype [71]. Several studies using comparative genomic hybridization (CGH), have shown that 20q is a region of frequent gain in colorectal cancers and more specifically regions from 20q11.2 to 20q13 showed frequent gains. The chromosomal location of E2F-1 is 20q11.2 and, therefore, based on preliminary measurements of E2F-1 gene copy number in metastatic tumors, we have reason to believe that gains in this chromosomal region leads to an increase in copy number of E2F-1 in these tumors. We have analyzed the available tumors for E2F-1 gene copy number by quantitative DNA PCR and further confirmed that the copy number of E2F-1 gene is increased in colorectal cancers (Iwamoto et al., in preparation). Correlation of either TS levels or response with other E2Fs is not clear at present.

3.3. Decreased UMPK as a mechanism of resistance to 5-FU

We had previously shown that decreased expression of UMPK was a mechanism of resistance to pulse (4 h) Fura exposure in a 5-FU resistant HCT8 cell line [72]. Using the human UMPK as a positive control, we have performed real-time fluorescent quantitative RT-PCR on 31 patient-derived colon adenocarcinoma tumor samples. Of the 31, 8 patients had not received any prior chemotherapy and had detectable UMPK levels. In contrast, 10 of 23 previously treated patients had no detectable expression of UMPK. This strongly suggests that decreased UMPK expression is a mechanism of 5-FU resistance (Banerjee et al., in preparation).

This is the first evidence for a correlation between lack of UMPK expression and acquired resistance to 5-FU in patients with colorectal cancer. As cytogenetic abnormalities are common in the chromosomal region believed to contain UMPK, we have begun to determine if this marked decrease in UMPK expression is secondary to a genetic deletion or mutation.

Decreased levels of the Fura-activating enzyme orotic acid phosphoribosyl transferase (OPRTase) have also been reported to be a cause of resistance to Fura in experimental systems [73] although decreased activity of this enzyme has not been found in tumors from patients resistant to 5-FU.

3.4. Thymidine phosphorylase (TP)

TP, also known as platelet-derived endothelial growth factor, is an enzyme that catalyzes the phosphorolysis of thymidine to 2-deoxy-D-ribose and thymine intracellularly. Capecitabine, a new orally available fluoropyrimidine carbamate, is converted to 5-FU by the action of enzymes including TP in the final step in tumors. Lack of TP would then be associated with less intratumoral 5-FU generation and therefore would be predicted to be less effective. The angiogenic property of TP due to its endothelial growth factor activity has been shown to be important in several human cancers. Studies on expression levels of TP at different stages of tumor development have suggested that TP is important in early neovascularization although its role in colon cancer progression remains to be determined [74].

3.5. Dihydropyrimidine dehydrogenase (DPD) levels

DPD catalyzes the major catabolic step in pyrimidine metabolism. Lack of DPD expression correlates with 5-FU toxicity in patients and sometimes can even be fatal. However, low levels of DPD in colorectal tumors have been shown to add to the predictive of low TS and to correlate with response to 5-FU-based chemotherapy [75]. This correlation holds true for mRNA levels as well as protein levels. As further evidence for the involvement of DPD in 5-FU resistance, we have recently demonstrated that overexpression of human DPD in NIH 3T3 cells leads to increased resistance to 5-FU. Murine bone marrow stem cells transduced with a retroviral construct containing DPD cDNA and expressing higher levels of the protein show increased number of drug resistant colonies as measured by the CFU-GM assay. Similar increase in 5-FU resistant CFU-GM colonies were obtained when human peripheral blood stem cells were transduced with the retroviral construct bearing DPD cDNA [76].

Of the various enzymatic steps depicted above, reactions catalyzed by enzymes OPRTase, UMPK, TS, TP, and DPD appear to have greater impact on fluoropyrimidine response than DHFR and TK. Levels of OPRTase, UMPK, TS, TP, and DPD have all now been shown to be correlated with clinical response to the fluoropyrimidine therapy. Accordingly, determinations of levels of this panel of enzyme prior to chemotherapy may allow one to predict response.

4. Strategies to overcome or exploit antifolate resistance

The observation that defective transport was a common mechanism of resistance to MTX in ALL has prompted the use of lipophilic antifolates such as trimetrexate (TMTX), which do not use the RFC to enter cells. TMTX has now been approved for use against *Pneumocystis carinii* infections in acquired immunodeficiency syndrome (AIDS) patients without severe side effects because of the simultaneous administration of 5-formyltetrahydrofolate (leucovorin: LV). The combination of TMTX and LV rescues the host cells from TMTX toxicity but is toxic to the parasite cells as they have no RFC and hence cannot take up LV. This selectivity has encouraged use of TMTX to target transport-deficient MTX-resistant cells with the TMTX–LV combination. Initial in vitro studies with CCRF–CEM cells have shown that transport-deficient MTX-resistant cells are sensitive to TMTX while the MTX-sensitive cells can be protected by LV. In order to test this concept in an animal model, SCID mice bearing tumors from transport-deficient MTX-resistant CCRF–CEM ALL cells were treated with the TMTX–LV combination, which led to tumor regression without any significant toxicity [77].

4.1. Myeloprotection using drug resistance genes

Introduction and efficient expression of drug-resistant genes such as mutant DHFR cDNAs into bone marrow progenitor cells should allow further dose intensification and has the potential to increase the cure rate for drug sensitive tumors. Using retroviral constructs containing a mutant human DHFR cDNA (the Ser^{31} mutant), we have infected mouse marrow progenitor cells and have transplanted irradiated mice with these transduced cells. Mice receiving transduced marrow progenitor cells were protected from the lethal effects of MTX while the controls died [78,79]. Human CD34+ peripheral blood stem cells transduced with the Ser^{31} DHFR cDNA were less sensitive to MTX than mock transduced controls [80]. We have initiated studies using the Ser^{31}/Phe^{22} double mutant of DHFR cDNA (dmDHFR) as the double mutant form of the enzyme has been shown to impart greater resistance to MTX than the single mutants [81]. Our results indicate that CD34+ stem cells transduced with the dmDHFR are less sensitive to MTX than mock transduced cells. We plan to exploit this system for cotransduction and ultimate in vivo selection of nonselectable genes [82]. We are currently evaluating myeloprotection in animal model systems using both mutant human TS genes (mhTS) as well fusion mDHFR–mhTS genes. (Capiaux et al., in preparation). We have recently shown that transplantation of bone marrow progenitor cells retrovirally transduced and expressing two drug-resistance genes in a construct SFG–dmDHFR–CD and SFG–dmDHFR–IRES–ALDH can protect against a combination of chemotherapeutic agents using either MTX and Ara-C or MTX and cyclophosphamide, respectively [83,84]. This suggests that the fusion genes may be very useful for protection against a combination of drugs that are often used in cancer chemotherapy.

4.2. Exploiting translational regulation of DHFR for monitoring in vivo gene expression

The “induction” of wild-type DHFR protein in cancer cells exposed to antifolates has been reported by this laboratory [49a,b]. Such translational upregulation after antifolate treatment may also occur for fusion proteins, e.g. comprising DHFR and herpes simplex virus type 1 thymidine kinase (HSVTK). Since a high intracellular level of the DHFRF/S fusion protein may improve the therapeutic use of the HSVTK/GCV therapy, we generated a retroviral construct containing this fusion cDNA and investigated the possibility of induction of the fusion protein by antifolates. The retroviral vectors generated contain a double mutant (Phe^{22}–Ser^{31} referred to as F/S), single mutant Ser^{31} or wild-type DHFR gene, fused to the HSV1Tk gene.

HCT-8 cells were transduced and selected in 100 nM TMTX and then exposed to ganciclovir (GCV). The TMTX selected cells were over two logs more sensitive to GCV than the untransduced or transduced but unselected cells, correlating with the expression of the fusion protein [85].

4.2.1 In vivo imaging of DHFR–HSVTK gene expression using ^{124}I-FIAU

An animal model using RNU (nude) rats and tumors generated from untransduced HCT-8 cells and HCT-8 transduced with the DHFR–HSVTK fusion gene was set up in the following manner. Animals were injected with 10^5 cells in the left flank with HCT-8 untransduced cells and in the right flank with DHFR–HSVTK transduced HCT-8 cells, respectively. At 12 days postinjection, palpable tumors were observed in both flanks. The animals were then treated with a previously established maximum tolerated dose of TMTX. A control group of animals was treated with the same volume of vehicle. The immobilized animals (six at a time) were positioned on a specially designed animal holder and placed within the positron emission tomography (PET) scanner (GE Advanced Scanner). The excitation scan was of 20-min duration and the transmission scan was of 7-min duration. At the end of the imaging session, a digital image of the animal showing the flank tumors was also recorded in order to superimpose the position of the PET scanning image with the tumor location. To quantitate radioactivity retained in the tumor versus background radioactivity in tissues, the animals were sacrificed and counts in tumors, plasma and muscle tissue were determined by scintillation counting. Results of the PET imaging and the scintillation counting indicate that treatment of tumor-bearing animals with TMTX resulted in increased expression of the fusion gene expressing both DHFR and HSVTK (Mayer-Kuckuk et al., submitted for publication, 2001).

4.2.2. Imaging DHFR gene expression using DHFR–EGFP

In order to circumvent the use of isotopes for imaging, we have initiated work with other fusion genes such as DHFR–EGFP to monitor gene expression in vivo using fluorescence microscopy. We have established in an AM12 (transduced with a SFG–DHFR–EGFP retroviral construct) cell culture model that the induction of the DHFR–EGFP fusion protein is comparable to the induction of the native DHFR protein in response to antifolate treatment. Moreover, this induction is not prevented by addition of ActD but can be inhibited by cycloheximide treatment. The induction in DHFR–EGFP protein levels is specific to the antifolate treatment of cells and is not observed when other drugs such as fluoropyrimidines, etoposide or doxorubicin are used.

5. Conclusions and perspectives

Study of resistance to drugs such as MTX and 5-FU continue to reveal interesting and often novel mechanisms, both intrinsic and acquired. With available molecular techniques, it is now possible to examine which of the resistance mechanisms studied in cell culture models are operative in tumor samples from cancer patients treated with the drugs. These studies, on tumor biopsies prior to chemotherapy, may help predict tumor response to the chemotherapy.

Myeloprotection strategies based on use of mutant forms of DHFR and TS are poised to enter clinical trials and will test the hypothesis that higher doses of drugs can be used in a posttransplant situation without the risk of myelosuppression.

Translational regulation of DHFR is being exploited for noninvasive in vivo imaging of tumors. We have developed fusion proteins of DHFR and HSVTK for PET imaging as well as DHFR and EGFP for optical imaging. We also plan to explore the possibility of using fusion genes of DHFR to increase intracellular levels of gene products that may be of therapeutic benefit.

Acknowledgements

Supported by USPHS grants CA-08010; CA-61586 and P50-CA-86438.

References

[1] J.R Bertino, Karnofsky Memorial Lecture ode to methotrexate, J Clin Oncol 11 (1993) 5–14

[2] R L Blakley, Dihydrofolate reductase in folates and pterins, in. R L. Blakley, S.J Benkovic (Eds), Vol 1 Chemistry and Biochemistry of Folates· Dihydrofolate Reductase, Wiley, New York, 1984, pp 191–251

[3] I.D. Goldman, L.H Matherly, The cellular pharmacology of methotrexate, in: I D Goldman (Ed), Membrane Transport of Antineoplastic Agents (International Encyclopedia of Pharmacology and Therapeutics, Section 118), Pergamon, Oxford, UK, 1986, p. 283.

[4] J J. McGuire, P Hsieh, J K Coward, J R Bertino, Enzymatic synthesis of folylpolyglutamates characterization of the reaction and its products, J. Biol. Chem 255 (1980) 5776–5788

[5] V.M. Whitehead, D. Rosenblatt, M J Vuchich, J.J. Shuster, A Witte, D. Beaulieu, Methotrexate and methotrexate polyglutamates in lymphoblasts at diagnosis of childhood ALL· a pilot prognostic factor analysis, Blood 76 (1990) 44–50.

[6] C J. Allegra, B A Chabner, J C Drake, R. Lutz, D. Rodbard, J Jolivet, Enhanced inhibition of thymidylate synthase by methotrexate polyglutamates, J. Biol Chem. 260 (1985) 9720–9726.

[7] C J Allegra, J.C Drake, J. Jolivet, B.A Chabner, Inhibition of phosphoribosyl-aminoimidazolecarboxamide transformylase by methotrexate and dihydrofolic acid polyglutamate, Proc. Natl Acad Sci U S. A 82 (1985) 4881–4885.

[8] J Jolivet, K H. Cowan, G A Curt, B.A. Chabner, The pharmacology and clinical use of methotrexate, N Engl J Med 309 (1983) 1094–1103

[9] M Silnik, R Reddel, M Bethel, P B Rowe, Gamma-glutamyl hydrolase (conjugase) purification and properties of the bovine hepatic enzyme, J. Biol. Chem 250 (1975) 5982–5994

[10] B. Elsenhans, O Ahmad, I. Rosenberg, Isolation and characterization of pteroylglutamate hydrolase from rat intestinal mucosa, J. Biol. Chem 259 (1984) 6364–6368.

[11] C Chandler, T Wang, C Halsted, Pteroylglutamate hydrolase from human jejunal brush borders: purification and characterization, J. Biol. Chem 261 (1986) 928–933

[12] T Wang, C Chandler, C Halsted, Intracellular pteroylglutamate hydrolase from human jejunal mucosa· isolation and characterization, J Biol. Chem 261 (1986) 13551–13555

[13] B.I. Schweitzer, A P Dicker, J.R. Bertino, Dihydrofolate reductase as a therapeutic target, FASEB J. 4 (1990) 2441–2452.

[14] T Trippett, S. Schlemmer, Y Elisseyeff, E Goker, M Wachter, P. Steinherz, C Tan, E Berman, J S. Wright, A Rosowsky, B I Schweitzer, J R Bertino, Defective transport as a mechanism of acquired resistance to methotrexate in patients with acute leukemia, Blood 80 (1992) 1158–1162

[15] L.H Matherly, S M Angeles, C A Czajkowski, Characterization of

transport mediated methotrexate resistance in human tumor cells with antibodies to the membrane carrier for methotrexate and tetrahydrofolate cofactors, J Biol Chem. 267 (1992) 23253–23260

[16] L H. Matherly, J W Taub, Y Ravindranath, S. Proefke, S C Wong, P. Gimotty, S Buck, J.S Wright, A Rosowsky, Elevated dihydrofolate reductase and impaired methotrexate transport as elements in methotrexate resistance in childhood acute lymphoblastic leukemia, Blood 85 (1995) 500–509

[17] F M. Williams, R C. Murray, T M Underhill, W F Flintoff, Isolation of a hamster cDNA clone coding for a function involved in methotrexate uptake, J Biol Chem 269 (1994) 5810–5816

[18] K H Dixon, B.C Lanpher, J Chiu, K Kelley, K H Cowan, A novel cDNA restores reduced folate carrier activity and methotrexate sensitivity to transport deficient cells, J Biol Chem 269 (1994) 17–20

[19] F M Williams, W F Flintoff, Isolation of a human cDNA that complements a mutant hamster cell defective in methotrexate uptake, J Biol Chem 270 (1995) 2987–2992

[20] M D Marger, M H. Saier Jr, A major superfamily of transmembrane facilitators that catalyze uniport, symport and antiport, Trends Biochem. Sci. 18 (1993) 13–20

[21] R Yang, B Mazza, R Sowers, J Healey, A Huvos, J.R Bertino, P Meyers, R Gorlick, Mutations/polymorphisms in the reduced folate carrier(RFC) are observed frequently in osteosarcoma tumor samples, Proc AACR Abstract #4942 92nd Annual Meeting, New Orleans, LA, 2001

[22] E Goker, J T Lin, T Trippett, Y Elisseyeff, W P. Tong, D. Niedzwiecki, C Tan, P Steinherz, B.I Schweitzer, J.R Bertino, Decreased polyglutamylation of methotrexate in acute lymphoblastic leukemia blasts in adults compared to children with this disease, Leukemia 7 (1993) 1000–1004

[23] J.T. Lin, W.P Tong, T Trippett, D Niedzwiecki, Y Tao, C Tan, P Steinherz, B.I Schweitzer, J R Bertino, Basis for natural resistance to methotrexate in human acute non-lymphocytic leukemia, Leuk Res 15 (1991) 1191–1196.

[24] T.W. Synold, M V. Relling, J M Boyett, G K Rivera, J T Sandlund, H Mahmoud, W M. Crist, C.H Pui, W.E Evans, Blast cell methotrexate polyglutamate accumulation in vivo differs by lineage, ploidy, and methotrexate dose in acute lymphoblastic leukemia, J Clin Invest. 94 (1994) 1996–2001.

[25] J C. Barredo, T W. Synold, J Laver, M.V Relling, C H. Pui, D G Priest, W E Evans, Differences in constitutive and post-methotrexate folylpolyglutamate synthetase activity in B-lineage and T-lineage leukemia, Blood 84 (1994) 564–569

[26] E Goker, A. Kheradpour, M C Waltham, D Banerjee, W.P. Tong, Y Elisseyeff, J.R Bertino, Acute monocytic leukemia a myeloid subset that may be sensitive to methotrexate, Leukemia 9 (1995) 274–276

[27] J Galivan, T Johnson, M Rhee, J J McGuire, D G Priest, V Kesevan, The role of folylpolyglutamate synthetase and gamma-glutamylhydrolase in altering cellular folyl- and antifolyl-polyglutamates, Adv Enzyme Regul 26 (1987) 147–155

[28] T A. Garrow, A Admon, B Shane, Expression cloning of a human cDNA encoding folylpoly(-glutamate) synthetase and determination of its primary structure, Proc Natl Acad. Sci. U S. A 89 (1992) 9151–9155

[29] H J Lenz, K Danenberg, B Schnieders, E Goker, G J Peters, T Garrow, B. Shane, J R Bertino, P V Danenberg, Quantitative analysis of folylpolyglutamate synthetase gene expression in tumor tissues by the polymerase chain reaction. marked variation of expression among leukemia patients, Oncol. Res. 6 (1994) 329–335

[30] L L. Samuels, L J Goutas, D.G Priest, J R Piper, F M. Sirotnak, Hydrolytic cleavage of methotrexate-polyglutamates by folylpolyglutamyl hydrolase derived from various tumors and normal tissues of the mouse, Cancer Res. 46 (1986) 2230–2235

[31] M S Rhee, Y Wang, M. Gopal Nair, J Galivan, Acquisition of resistance to antifolates caused by enhanced gamma-glutamyl hydrolase activity, Cancer Res 53 (1993) 2227–2230.

[32] P.D Cole, B A Kamen, R. Gorlick, D Banerjee, A K. Smith, E Magill, J R Bertino, Effects of overexpression of gamma-glutamyl hydrolase on methotrexate metabolism and resistance, Cancer Res 61 (2001) 4599–4604

[33] (a) M D Carman, J H Schornagel, R S Rivest, S Srimatkandada, C S Portlock, T Duffy, F J R. Bertino, Resistance to methotrexate due to gene amplification in a patient with acute leukemia, J Clin Oncol 2 (1984) 16–20
(b) R C Horns, W J Dower, R.T Schimke, Gene amplification in a leukemia patient treated with methotrexate, J Clin Oncol 2 (1984) 2–5.

[34] J M Trent, R N Buick, S. Olson, R.C. Horns, R T Schimke, Cytologic evidence for gene amplification in methotrexate resistant cells obtained from a patient with ovarian adenocarcinoma, J Clin Oncol 2 (1984) 8–12

[35] G A Curt, D.N Carney, K H Cowan, J Jolivet, B D Bailey, J C Drake, C.S Kao-Shan, J Minna, B A. Chabner, Unstable methotrexate resistance in human small cell lung cancer associated with double minute chromosomes, N Engl J Med 308 (1983) 99–104

[36] E. Goker, M C Waltham, A. Kheradpour, T Trippett, M Majumdar, Y Elisseyeff, B Schnieders, P Steinherz, C. Tan, E Berman, J R Bertino, Amplification of the dihydrofolate reductase gene is a mechanism of acquired resistance to methotrexate in patients with acute lymphoblastic leukemia and is correlated with *p53* gene mutations, Blood 86 (1995) 677–684

[37] L R Livingstone, A. White, J Sprouse, E Livanos, T. Jacks, T Tlsty, Altered cell cycle arrest and gene amplification potential accompany loss of wild type *p53*, Cell 70 (1992) 923–930

[38] Y Yin, M A. Tainsky, F Z Bischoff, L C Strong, G.M Wahl, Wild-type *p53* restores cell cycle control and inhibits gene amplification in cells with mutant *p53* alleles, Cell 70 (1992) 937–944

[39] C C Simonsen, A D. Levinson, Isolation and expression of an altered dihydrofolate reductase cDNA, Proc Natl Acad Sci. U S A 80 (1983) 2495–2499

[40] D A Haber, S M Beverly, M.L Kiely, R T Schimke, Properties of an altered dihydrofolate reductase encoded by amplified genes in cultured mouse fibroblasts, J Biol Chem 256 (1981) 9501–9510

[41] S Srimatkandada, B I Schweitzer, B.A Moroson, S Dube, J R Bertino, Amplification of a polymorphic dihydrofolate reductase gene expressing an enzyme with a decreased binding to MTX in a human colon carcinoma cell line, HCT-8R4 resistant to this drug, J Biol Chem 264 (1989) 3524–3528

[42] P W Melera, J P. Davide, C A. Hession, K W Scotto, Phenotypic expression in *Escherichia coli* and sequence of two Chinese hamster lung cDNA encoding different dihydrofolate reductase, Mol Cell. Biol. 4 (1984) 38–48

[43] A.P Dicker, M V Volkenandt, B I Schweitzer, D Banerjee, J.R Bertino, Identification and characterization of a mutation in the dihydrofolate reductase gene from methotrexate resistant CHO cell line Pro-3 MTX RIII, J Biol Chem 265 (1990) 8317–8321

[44] R S McIvor, C C. Simonsen, Isolation and characterization of a variant dihydrofolate reductase cDNA from the methotrexate resistant murine L5178Y cells, Nucleic Acids Res 18 (1990) 7025–7032

[45] (a) H T Spencer, B P Sorrentino, C H Pui, S K Chunduru, S E Sleep, R L Blakley, Mutations in the gene for human dihydrofolate reductase an unlikely cause of clinical relapse in pediatric leukemia after therapy with methotrexate, Leukemia 10 (3) (1996) 439–446
(b) J E Hyde, The dihydrofolate reductase-thymidylate synthase gene in the drug resistance of malaria parasites, Pharmacol Ther 48 (1990) 45–59

[46] J.R Bertino, D M Donohue, B Simmons, B W Gabrio, R. Silber, F.M Huennekens, The induction of dihydrofolate reductase in leukocytes and erythrocytes of patients treated with methotrexate, J Clin. Invest. 423 (1963) 466–475

[47] B L Hillcoat, V Swett, J R. Bertino, Increase of dihydrofolate reductase activity in cultured mammalian cells after exposure to methotrexate, Proc. Natl. Acad Sci. U S A 58 (1967) 1632–1637

[48] E Chu, D M Koeller, J L Casey, J.C Drake, B.A Chabner, P C

Elwood, S Zinn, C.A. Allegra, Autoregulation of human thymidylate synthase messenger RNA translation by thymidylate, Proc Natl. Acad. Sci. U. S. A 88 (1991) 8977–8981

[49] (a) E Ercikan, D. Banerjee, M C. Waltham, B Schnieders, K W Scotto, J.R Bertino, Translational regulation of the synthesis of dihydrofolate reductase, in· J E. Ayling (Ed), Chemistry and Biology of Pteridines and Folates, Plenum, New York, 1993, pp 537–540
(b) E A. Ercikan-Abali, D Banerjee, M.C Waltham, N Skacel, K W Scotto, J R Bertino, Dihydrofolate reductase protein inhibits its own translation by binding to dihydrofolate reductase mRNA sequences within the coding region, Biochemistry 36 (1997) 12317–12322

[50] J R. Nevins, E2F, a link between the Rb tumor suppressor protein and viral oncoproteins, Science 258 (1992) 424–427.

[51] W W Li, J. Fan, D. Hochhauser, D Banerjee, Z. Zielinski, A Almasan, Y Yin, R. Kelly, G M. Wahl, J R. Bertino, Lack of functional retinoblastoma protein mediates increased resistance to antimetabolites in human sarcoma cell lines, Proc. Natl. Acad. Sci U S A 92 (1995) 10436–10440

[52] D. Hochhauser, B Schnieders, E A. Ercikan-Abali, R. Gorlick, R Muise-Helmericks, W.W Li, J Fan, D Banerjee, J.R. Bertino, Effect of cyclin D1 over expression on drug sensitivity in a human fibrosacoma cell line, JNCI 88 (1996) 1269–1275.

[53] H J Lenz, C G Leichman, K.D Danenberg, P V Danenberg, S. Groshen, H Cohen, L Laine, P Crookes, H Silberman, J. Baranda, Y. Garcia, J. Li, L. Leichman, Thymidylate synthase m RNA level in adenocarcinoma of the stomach: a predictor of primary tumor response and overall survival, J. Clin Oncol. 14 (1996) 176–182

[54] L Leichman, H J Lenz, C.G. Leichman, K.D. Danenberg, J Baranda, S. Groshen, W. Boswell, R Metzger, M. Tan, P V Danenberg, Quantitation of intratumoral thymidylate synthase expression predicts for disseminated colorectal response and resistance to protracted infusion of fluorouracil and weekly leucovorin, J. Clin Oncol 15 (1997) 3223–3229.

[55] P G. Johnston, H.J. Lenz, C.G Leichman, K D Danenberg, C J Allegra, P V Danenberg, L. Leichman, Thymidylate synthase gene and protein expression correlate and are associated with response to 5-fluorouracil in human colorectal and gastric tumors, Cancer Res 55 (1995) 1407–1412.

[56] H.J. Lenz, K. Hayashi, D. Salonga, K D Danenberg, P.V. Danenberg, J R Bertino, S. Groshen, L. Leichman, C G Leichman, *p53* point mutations and thymidylate synthase messenger RNA levels in disseminated colorectal cancer· an analysis of response and survival, Clin. Cancer Res 4 (1998) 1243–1250

[57] C Aschele, D Debernardis, S Casazza, G Antonelli, C. Baldo, R Lionetto, F Maley, A Sobrero, Immunohistochemical quantitation of thymidylate synthase expression in colorectal cancer metastases predicts for clinical outcome to fluorouracil-based chemotherapy, J Clin. Oncol 17 (1999) 1760–1767

[58] (a) R Gorlick, R. Metzger, K.D. Danenberg, D Salonga, J S. Miles, G S A Longo, J. Fu, D Banerjee, D. Klimstra, S C Jhanwar, P V. Danenberg, N. Kemeny, J R. Bertino, Higher levels of thymidylate synthase gene expression are observed in pulmonary as compared with hepatic metastases of colorectal adenocarcinoma, J Clin Oncol 16 (1998) 1465–1469
(b) D Banerjee, R Gorlick, A Liefshitz, K Danenberg, P.C Danenberg, P V Danenberg, D Klimstra, S C. Jhanwar, C Cardon-Cardo, Y. Fong, N Kemeny, J R. Bertino, Levels of E2F-1 expression are higher in lung metastasis of colon cancer as compared with hepatic metastasis and correlate with levels of thymidylate synthase, Cancer Res. 60 (2000) 2365–2367.

[59] S. Cascinu, C. Aschele, S Barni, D. Debernadis, C. Baldo, G Tunesi, V Catalano, M P. Staccioli, A. Brenna, P Muretto, G Catalano, Thymidylate synthase protein expression in advanced colon cancer correlation with the sites of metastasis and the clinical response to leucovorin-modulated bolus 5-fluorouracil, Clin. Cancer Res 5 (1999) 1996–1999.

[60] E Chu, D Voeller, D.M. Koeller, J C. Drake, C H Takimoto, G.F Maley, F. Maley, C J Allegra, Identification of an RNA binding site for human thymidylate synthase, Proc. Natl Acad Sci. U. S. A 90 (1993) 517–521

[61] M E Kitchens, A M. Forsthoefel, Z. Rafique, H.T Spencer, F G. Berger, Ligand-mediated induction of thymidylate synthase occurs by enzyme stabilization. Implications for autoregulation of translation, J Biol Chem 274 (1999) 12544–12547.

[62] T S Pullarkat, V Ghaderi, S A Ingles, Y.-P. Xiong, P Chen, J Stoehlmacher, M. Gupta, D Tsao-Wei, S. Groshen, H J Lenz, Human thymidylate synthase gene polymorphism determines response to 5-FU, ASCO Annual Meeting 2000 Abstract #942. Proc ASCO, vol 19, 2000

[63] K W Barbour, S H. Berger, F.G. Berger, Single amino acid substitution defines a naturally occurring genetic variant of human thymidylate synthase, Mol Pharmacol 37 (1990) 515–518.

[64] Y Tong, X Liu-Chen, E.A. Ercikan-Abali, G.M. Capiaux, S C. Zhao, D Banerjee, J R. Bertino, Isolation and characterization of Thymitaq (AG 337) and 5-Fluoro-2-deoxyuridylate–resistant mutants of human thymidylate synthase from ethyl methanesulfonate–exposed human sarcoma HT-1080 cells, J Biol Chem 273 (1998) 11611–11618.

[65] D M. Landis, L A Loeb, Random sequence mutagenesis and resistance to 5-fluoruridine in human thymidylate synthases, J Biol Chem 273 (1998) 25809–25817

[66] N Dyson, The regulation of E2F by pRB-family proteins, Genes Dev 12 (1998) 2245–2262

[67] H. Muller, K Helin, The E2F transcription factors key regulators of cell proliferation, Biochim Biophys Acta 1470 (2000) M1–M12 (Review)

[68] J DeGregori, U Kowalik, J.R Nevins, Cellular targets for activation by the E2F1 transcription factor include DNA synthesis- and G1S-regulatory genes, Mol Cell Biol. 15 (1995) 4215–4224

[69] D Banerjee, B. Schnieders, J.Z Fu, D Adhikari, S -C Zhao, J.R Bertino, Role of E2F-1 in chemosensitivity, Cancer Res. 58 (1998) 4292–4296.

[70] M Kasahara, Y Takahashi, U. Nagata, S Asai, T Eguchi, Y Ishii, M Fujii, K Ishikawa, Thymidylate synthase expression correlates closely with E2F1 expression in colon cancer, Clin Cancer Res. 6 (2000) 2707–2711.

[71] S Y. Zhang, S -C Shao, D G Johnson, A.J.P. Klein-Szanto, E2F-1 gene transfer enhances invasiveness of human head and neck carcinoma cell lines, Cancer Res 60 (2000) 5972–5976

[72] C Aschele, A Sobrero, M. Faderan, J.R. Bertino, Novel mechanism(s) of resistance to 5-fluorouracil in human colon cancer (HCT 8) sublines following exposure to two different clinically relevant dose schedules, Cancer Res. 52 (1992) 1855–1864

[73] M A Mulkins, C Heidelberger, Biochemical characterization of fluoropyrimidine resistant murine leukemic cell lines, Cancer Res 42 (1982) 965–973

[74] R Metzger, K Danenberg, C.G. Leichman, D. Salonga, E.L Schwartz, S Wadler, H J Lenz, S. Groshen, L. Leichman, P.V. Danenberg, High basal level gene expression of thymidine phosphorylase (platelet derived endothelial growth factor) in colorectal tumors is associated with non-response to 5 fluorouracil, Clin Cancer Res 4 (1998) 2371–2376

[75] R.B Diasio, Z. Lu, Dihydropyrimidine dehydrogenase activity and fluorouracil chemotherapy, J Clin Oncol. 12 (1994) 2239–2242.

[76] N Takebe, S.-C. Zhao, A Ural, M Johnson, D Banerjee, R.B Diasio, J R Bertino, Retroviral transduction of human dihydropyrimidine dehydrogenase cDNA confers resistance to 5 fluorouracil in murine hematopoietic progenitor cells and human CD34+ enriched peripheral blood progenitor cells, Cancer Gene Ther 8 (2001) 966–973.

[77] J F Lacerda, E Goker, A Kheradpour, D Dennig, Y Elisseyeff, C Jagiello, R J. O'Reilly, J R Bertino, Selective treatment of SCID mice bearing methotrexate transport resistant human ALL tumors with trimetrexate and leucovorin, Blood 85 (1995) 2675–2679

[78] M -X. Li, D Banerjee, S -C Zhao, B.I Schweitzer, S. Mineishi, E Gilboa, J R Bertino, Development of a retroviral construct containing

a human mutated dhfr cDNA for hematopoietic stem cell transduction, Blood 33 (1994) 3403–3408.

[79] D Banerjee, S-C. Zhao, S Mineishi, J.R Bertino, Post-transplant methotrexate administration leads to improved curability of mice bearing a mammary tumor transplanted with marrow transduced with a mutant human dihydrofolate reductase cDNA, Hum. Gene Ther 8 (1997) 903–909

[80] M Flasshove, D. Banerjee, S Mineishi, M.-X. Li, J.R. Bertino, M A.S. Moore, Ex vivo expansion and selection of human CD34+ peripheral blood progenitor cells after introduction of a mutated dihydrofolate reductase cDNA via retroviral gene transfer, Blood 85 (1995) 566–574.

[81] E.A. Ercikan-Abali, S. Mineishi, Y Tong, S Nakahara, M.C. Waltham, D Banerjee, W Chen, M. Sadelain, J.R Bertino, Active site directed double mutants of dihydrofolate reductase, Cancer Res 56 (1996) 4142–4145.

[82] D. Banerjee, S C. Zhao, M.-X Li, B I Schweitzer, S. Mineishi, J.R Bertino, Gene therapy utilizing drug resistance genes: a review, Stem Cells 12 (1994) 378–385

[83] A. Sauerbrey, J P McPherson, S-C Zhao, D. Banerjee, J R Bertino, Expression of a novel double mutant dihydrofolate reductase cytidine deaminase fusion gene confers resistance to both methotrexate and cytosine arabinoside, Hum. Gene Ther. 10 (1999) 2495–2504

[84] N Takebe, S.-C. Zhao, D Adhikari, S. Mineshi, M Sadelain, J. Hilton, M. Colvin, D Banerjee, J.R. Bertino, Generation of dual resistance to 4 hydroperoxycyclophosphamide and methotrexate by retroviral transfer of the human aldehyde dehydrogenase class 1 gene and a mutated dihydrofolate reductase gene, Mol Ther 3 (2001) 88–96

[85] P Mayer-Kuckuk, D Banerjee, S. Malhotra, M. Doubrovin, M Iwamoto, T. Akhurst, J Balatoni, W Bornmann, R Finn, S Larson, Y. Fong, J Gelovani Tjuvajev, R Blasberg, J.R. Bertino, Cells exposed to antifolates show increased cellular levels of proteins fused to dihydrofolate reductase· A method to modulate gene expression, Proc. Natl. Acad Sci U S. A 99 (2002) 3400–3405

ELSEVIER

Biochimica et Biophysica Acta 1587 (2002) 174–182

BIOCHIMICA ET BIOPHYSICA ACTA
BBA
www bba-direct com

Review

Thymidylate synthase as a translational regulator of cellular gene expression

Jun Liu, John C. Schmitz, Xiukun Lin, Ningwen Tai, Wu Yan, Michael Farrell, Michelle Bailly, Tian-min Chen, Edward Chu*

Department of Medicine and Pharmacology, Yale Cancer Center, Yale University School of Medicine, USA
VA CT Cancer Center, VA CT Healthcare System, West Haven, CT 06516, USA

Received 24 January 2002; accepted 24 January 2002

Abstract

Studies from our laboratory have shown that the folate-dependent enzyme, thymidylate synthase (TS), functions as an RNA binding protein. There is evidence that TS, in addition to interacting with its own TS mRNA, forms a ribonucleoprotein complex with a number of other cellular mRNAs, including those corresponding to the p53 tumor suppressor gene and the *myc* family of transcription factors. Using both in vitro and in vivo model systems, we have demonstrated that the functional consequence of binding of TS protein to its own cognate mRNA, as well as binding of TS to the p53 mRNA, is translational repression. Herein, we review current work on the translational autoregulatory control of TS expression and discuss the molecular elements that are required for the TS protein–TS mRNA interaction. TS may play a critical role in regulating the cell cycle and the process of apoptosis through its regulatory effects on expression of p53 and perhaps other cell cycle related proteins Finally, the ability of TS to function as a translational regulator may have important consequences with regard to the development of cellular resistance to various anticancer drugs © 2002 Elsevier Science B.V. All rights reserved.

Keywords Thymidylate synthase, Translational regulation: RNA binding protein; Gene regulation; Cancer chemotherapy

1. Introduction

Control of eukaryotic gene expression is regulated at several levels, including gene amplification, transcription, splicing, nucleocytoplasmic transport, mRNA stability, translation, and post-translational modification and/or protein processing. During the last several years, it has become increasingly clear that translational control represents an important process for regulating protein synthesis [1–4]. This mechanism is based on the central concept that cellular gene expression is controlled by the efficiency of translation of a given mRNA, in the absence of a corresponding change in steady-state mRNA levels.

The ability to control protein synthesis by regulating the translational efficiency of a given mRNA provides several advantages to an organism. Translational control is an energy-efficient process to control the expression of a given protein. Using this mechanism, a given cell can respond rapidly to exposure to various genotoxic and/or cytotoxic stresses as well as to changes in the extracellular environment. It serves as a fine-tuning mechanism to ensure the precise and desired level of a given cellular protein. To do so, it works in close concert with other regulatory mechanisms including transcription, post-transcription, and post-translation. Moreover, a significant lag-time, which is normally required for signaling of various processes within the nucleus including gene amplification, activation of transcription, RNA processing, and nucleocytoplasmic transport of RNA, is effectively bypassed, thereby allowing for rapid changes in protein synthesis to be effected. As this process represents the last step in protein synthesis, the overall metabolic and energy requirements are minimized to a significant extent. One further advantage of this control pathway is that it is readily reversible. Once the cellular requirements have been sufficiently met, protein synthesis can be quickly restored to basal levels.

Abbreviations TS, thymidylate synthase; 5-FU, 5-fluorouracil, FdUMP, 5-fluorodeoxyuridine monophosphate; UTR, untranslated region; DHFR, dihydrofolate reductase; LV, leucovorin; rPCR, random polymerase chain reaction, IRF, iron-responsive factor, RNP, ribonucleoprotein

* Corresponding author VA CT Healthcare System, Cancer Center 111D, 950 Campbell Ave , West Haven, CT 06516, USA Tel +1-203-937-3421; fax. +1-203-937-3803

E-mail address chueyale@yahoo.com (E. Chu)

0925-4439/02/$ - see front matter © 2002 Elsevier Science B V All rights reserved
PII S0925-4439(02)00080-7

Control of the cell cycle is a highly ordered process, and it is regulated by the expression of certain critical checkpoint proteins. Translational control of these proteins ensures and maintains the ordered nature of the cell cycle that is necessary for normal cell division to occur. It is, therefore, not surprising that several cell cycle-related mRNAs have been identified whose expressions are specifically regulated at the translation level [4].

The present review focuses on translational control of the folate-dependent enzyme thymidylate synthase (TS). We provide an overview on the role of TS as a chemotherapeutic target, the mechanism of TS translational autoregulation, and the potential role of TS as a translational regulator of other cellular genes with specific focus on p53. In its role as an RNA binding protein, TS may act to coordinately regulate the cellular expression of several genes, and in so doing, may function as a critical regulator of several key aspects of cell cycle control, apoptosis, and chemosensitivity.

2. Thymidylate synthase

TS plays an essential role in catalyzing the reductive methylation of deoxyuridylate (dUMP) to thymidylate (dTMP), which provides the sole intracellular de novo source of dTMP (Fig. 1) [5]. Once synthesized, dTMP is then metabolized intracellularly to the dTTP triphosphate form, an essential precursor for DNA biosynthesis. This reaction is critical as it maintains the essential metabolic requirements for cellular proliferation and growth. As a result, TS represents a key target of cancer chemotherapeutic drugs, including the fluoropyrimidines and various antifolate analogs [6,7].

There are several lines of evidence which provide further support to the concept that TS is an important chemotherapeutic target. The first comes from in vitro, in vivo, and clinical studies, which document a strong correlation between the level of TS enzyme activity and/or TS protein expression and response to fluoropyrimidines [8–10]. It has been well-established that cancer cell lines and malignant tumors expressing higher levels of TS are relatively more resistant to the cytotoxic and antitumor effects of the fluoropyrimidines and antifolate analogs targeting TS. Second, there is a strong correlation between the level of TS enzyme inhibition within patient tumor samples following 5-FU therapy and eventual clinical response [11,12]. Third, the higher response rates observed with the combination of 5-FU and the reduced folate leucovorin (LV) when compared to single-agent 5-FU provides support for the cell-free experimental data which demonstrated that inhibition of the TS enzyme was maximal in the presence of increasing concentrations of the reduced folate 5,10-methylenetetrahydrofolate [13–17]. Finally, clinical trials with the antifolate analog ZD1694, a specific inhibitor of TS, have revealed surprisingly good activity as a single-agent against advanced colorectal cancer with response rates of 25–30%. These response rates compare favorably with the combination of 5-FU and LV. Based on these clinical results, this agent was approved as first-line therapy for advanced, metastatic colorectal cancer in several countries in Europe, Asia, Australia, and Canada [18–20].

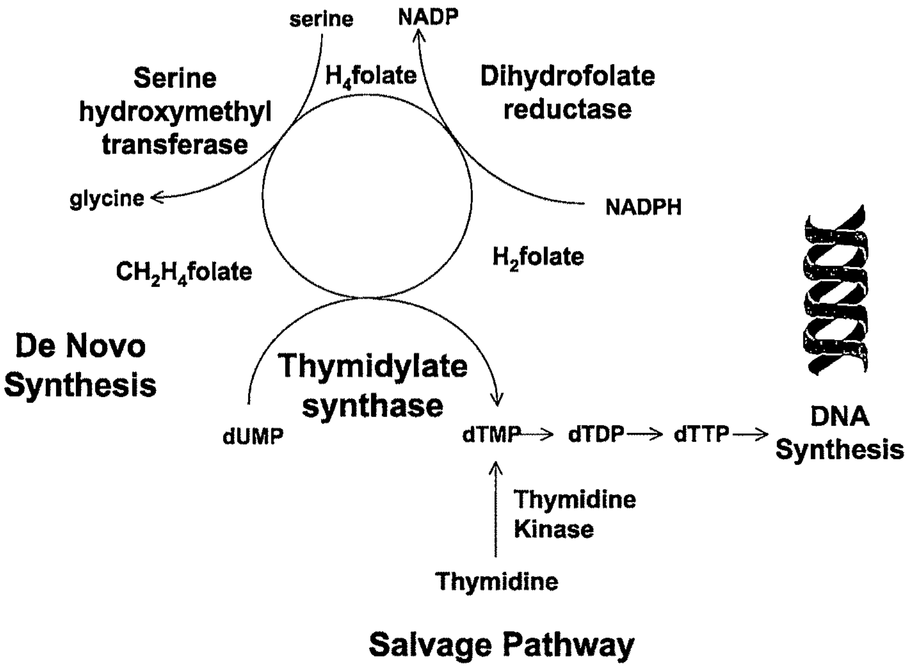

Fig 1 Enzyme reaction catalyzed by TS

It is now well-established that regulatory events at the level of gene amplification, transcription, post-transcription, translation, and post-translation are all involved in controlling TS expression as it relates to cell cycle-directed events, growth proliferation, and in response to various cytotoxic agents (Fig. 2) [21–31]. There is growing evidence that the precise control of TS may require multiple mechanisms acting in close coordination with one another. Moreover, there are several factors that must be taken into account, including the specific cellular and/or genotoxic stress, the timing and scheduling of exposure of a given cytotoxic agent, the dose, and the specific cellular environment and model system under investigation (Fig. 3).

The possibility for translational control of TS was postulated by Belfort et al. [32] upon initial analysis of the structural features of the *E coli* TS *thyA* gene. In their cloning and characterization of the human TS cDNA sequence, Takeishi et al. [33] identified three tandem repeat sequences in the 5′-untranslated region (UTR). Secondary structure analysis predicted for the presence of a series of three secondary stem-loop structures that might directly influence TS mRNA translation. Further studies by Kaneda et al. [34] confirmed that deletion of any one of these tandem repeat sequences significantly altered the translational efficiency of TS mRNA in vivo. These initial findings suggested that these tandem sequences might regulate TS mRNA translation, either directly or through their interaction with other cellular proteins and/or cofactors.

Rapid increases in TS enzyme activity have been described in various in vitro, in vivo, and clinical model systems following short-term exposure to the fluoropyrimidines [11,12,35–40]. While the precise mechanism(s) for the 5-FU-induced expression of TS in response to 5-FU was not well-characterized in these initial studies, increased transcription, enhanced stability of TS mRNA, increased efficiency of TS mRNA translation, and enhanced stability of TS protein were all proposed as potential mechanisms. Significant efforts have subsequently focused on defining the molecular events that control this induction of TS.

Investigations by Keyomarsi et al. [41] using synchronized normal human epithelial cells and human breast cancer MCF-7 cells revealed a 40-fold increase in TS enzyme level during the S phase with no apparent change in the level of TS mRNA expression. They also showed that treatment of MCF-7 cells with the antifolate analog ZD1694 gave rise to a 10- to 40-fold increase in TS enzyme levels, as determined by the FdUMP radioenzymatic binding assay, with no associated alteration in TS mRNA levels [41]. Work from our own lab showed that short-term, 24-h treatment of a human colon cancer H630 cell line with 5-FU resulted in a 5.5- to 6-fold elevation in TS protein expression with no corresponding change in TS mRNA expression [42]. Subsequent work revealed that the increased expression in TS protein was the direct result of newly synthesized protein, thereby providing the first direct evidence in vivo for the role of translational regulation in controlling TS expression. Taken together, the ability to regulate TS expression at the translational level may provide (1) an important mechanism by which normal cellular synthetic function can be precisely and tightly regulated, and (2) a critical protective mechanism for the rapid development of cellular resistance in response to exposure to a cytotoxic stress such as 5-FU and/or ZD1694 in order to maintain cellular synthetic function.

Molecular Mechanisms Regulating the Expression of Thymidylate Synthase

- Gene amplification
- Transcription
- Post-transcription
- Translation
- Post-translation

Fig 2 Molecular mechanisms regulating the expression of TS

Determinants of Cellular Gene Expression

- Specific cytotoxic/genotoxic stress
- Dose
- Timing and duration
- Model system and cellular environment

Fig 3 Determinants of cellular gene expression

3. TS translational autoregulation

Since the regulation of TS expression during the cell cycle and in response to exposure to various cytotoxic stresses appears, in part, to be regulated by translational control, our lab has focused on elucidating, in more detail, the regulation of TS mRNA translation. Our current working model for TS translational autoregulation and the interaction between TS protein and its own TS mRNA is presented in Fig. 4. This regulatory process is well-established as a critically important mechanism controlling the expression of bacteriophage and prokaryotic systems [43–47]. However, TS represents the first eukaryotic gene whose expression is controlled in such a fashion. The expression of three other eukaryotic genes, including dihydrofolate reductase (DHFR) [48–50], serine hydroxymethyl transferase [51], and p53 [52,53] have now been shown to be controlled by a similar autoregulatory feedback process.

Using a well-established RNA gel shift assay, we observed that human recombinant TS was able to directly bind to its own mRNA [54,55]. Subsequent work using the rabbit reticulocyte lysate in vitro translation system revealed that

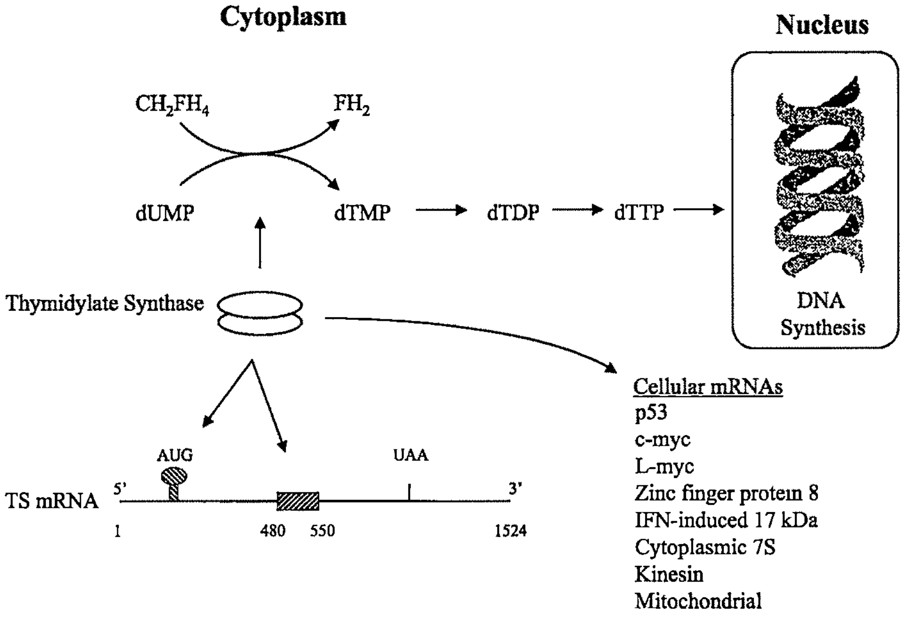

Fig. 4 Model for TS as a translational regulator of cellular gene expression

this TS protein–TS mRNA interaction resulted in translational suppression. Two cis-acting elements have been identified on TS mRNA, which interact with high affinity, on the order of 1–3 nM, to TS protein [55]. The first site is a 30-nt sequence residing in the 5′-UTR and includes the AUG start site in the loop aspect of a stable stem-loop structure. The secondary structure appears to be critical for protein recognition as a series of mutations that abolished the stem-loop resulted in RNA sequences that were unable to interact with TS protein. The second site has recently been localized to a 70-nt sequence within the coding region corresponding to nt 480–550 [56]. In vivo studies using a luciferase reporter system have confirmed the translational regulatory activities of each element. While both sequences require the presence of an intact TS protein and can function independently of one another in vivo, both elements are required for complete translational autoregulatory effect [56]. At present, it remains somewhat unclear as to how binding of TS protein to the sequence in the coding region leads to translational suppression. It is conceivable that some type of interactive cross-talk occurs between the elements in the coding region and the 5′-upstream region. A similar scenario has been observed with sequences residing in the protein-coding region and the 3′-UTR as playing a key role in controlling translational initiation [57–60]. Detailed molecular modeling studies will need to be performed to more precisely define the molecular events controlling this very complex process.

In order to more fully characterize the molecular elements underlying the TS protein–TS mRNA interaction, our lab has attempted to identify the specific domain(s) on the TS protein that are required for RNA recognition. We have shown that the RNA binding activity of human TS is exquisitely sensitive to the presence of reducing agents and requires the presence of at least one free sulfhydryl group [61]. In the presence of increasing concentrations of either 2-mercaptoethanol or dithiothreitol, the RNA binding activity of TS was markedly increased. In contrast, treatment with the oxiding agent diamide or *N*-ethylmaleimide blocked RNA binding in a dose-dependent manner. Recent preliminary work has shown that a cysteine → alanine mutation at cysteine residue 180 completely eliminated RNA binding. In contrast, mutations at cysteine residues 43, 195, and 210 did not adversely impact on RNA binding activity. The precise mechanism(s) by which the cysteine sulfhydryl residue at position 180 on the TS protein mediates RNA binding remains to be more accurately defined. However, several possibilities exist to explain its potential central role. They include: (1) direct formation of a covalent Michael adduct between the active sulfhydryl residue and the C-6 position of a uracil ring on TS mRNA, (2) occupation of the cysteine alters RNA binding via a steric hindrance mechanism, and/or (3) the cysteine residue maintains the protein in a certain conformation that then allows for the true RNA binding domain to be accessible. Studies are currently in progress to determine which of these mechanism(s) is involved.

In addition to the redox state of the protein, the state of ligand occupancy of TS appears to play a key role as a determinant of RNA binding [61]. For example, we have shown that when TS is ligand-free, maximal RNA binding activity is maintained, thereby resulting in complete translational repression of TS mRNA. In contrast, when TS is bound by either its physiologic substrates, dUMP or 5,10-methylentetrahydrofolate, or bound by the 5-FU metabolite FdUMP or by an antifolate analog such as ZD1694, the RNA binding activity of TS is dramatically decreased. The net effect of reduced RNA binding activity is relief of translational repression, a process that leads to increased synthesis of new TS protein. Such a scenario would exist in cells exposed to direct inhibitor compounds of TS, whether they should be nucleotide analogs such as 5-FU or antifolate analogs such as the Astra-Zeneca compound ZD1694 or the Eli Lilly compound LY231514. Thus, this model provides a rational mechanism for the acute induction of TS that arises in response to exposure to TS inhibitor compounds. Moreover, it offers a novel mechanism for the development of acute cellular drug resistance to compounds that directly target TS.

4. TS as a translational regulator of cellular gene expression

There are growing examples in the literature documenting that a given RNA binding protein has the potential to interact with more than one cellular mRNA species [62,63]. Perhaps the best example is the iron-responsive factor (IRF), which binds to its target iron-responsive element located within the 5′-UTRs of ferritin and erythroid 5-aminolevulinate synthase mRNAs, and within the 3′-UTR of the transferrin receptor mRNA [64,65]. The ability of the IRF to coordinately regulate these different mRNAs allows for exquisite control of iron metabolism within the cell. Based on this elegant work, studies were undertaken in our lab to determine whether TS, in its role as an RNA binding protein, might be able to interact with other cellular RNAs. For these studies, we developed a novel immunoprecipitation-RNA: random polymerase chain reaction (rPCR) method to isolate TS ribonucleoprotein (RNP) complexes from intact human colon cancer H630 cells [66]. This technique was based on the immunoprecipitation procedure of Steitz [67], and was modified by incorporating the RNA:rPCR method of Froussard [68]. Using this approach, we isolated eight different cellular RNAs that formed a ribonucleoprotein (RNP) complex with TS [66]. While TS was one of the RNAs identified in this RNP complex, p53 and two members of the *myc* family of transcription factors, c- and L-*myc*, were also isolated. These specific mRNAs were of particular interest as they play a critical role in cell cycle progression, DNA synthesis, and apoptosis. Careful analysis of the eight RNA sequences has, to date, failed to identify a consensus nucleotide sequence. However, one potential drawback of such an approach is that most of the RNA binding proteins, characterized to date, appear to recognize a sequence contained within the context of a stable secondary structure as opposed to a simple sequence. In fact, there is preliminary evidence to suggest the presence of such a consensus secondary structure amongst these cellular mRNAs.

The critical role of p53 in tumor suppression, cell cycle regulation, cell cycle arrest, and the cellular response to DNA damage has been extensively reviewed [69–71]. The mechanisms controlling the expression of p53, in response to genotoxic and/or cytotoxic stress, are complex. Much of the work performed to date has shown that the induction of p53 following exposure to DNA-damaging agents is controlled at the post-translational level, mainly through enhanced stability of the protein [69,70,72]. It has been well-established that post-translational modifications including phosphorylation and acetylation at both the amino- and carboxy-terminus are critical for activation of DNA binding activity [73–75]. However, there is growing evidence that translational control may play an important role in the induction and activation of p53 in response to exposure to cytotoxic agents [76]. For example, when murine fibroblast Swiss 3T3 cells were exposed to γ-irradiation, the expression of p53 protein increased significantly while the corresponding p53 mRNA levels were unchanged [52]. Treatment with the transcriptional inhibitor actinomycin D did not alter the induced levels of p53 protein, in contrast to treatment with cycloheximide which completely repressed the induced synthesis of p53. Subsequent investigations have confirmed that the expression of p53 is controlled, in part, at the translational level through an autoregulatory feedback loop identical to what has been described for TS and DHFR [52,53]. One element in the 5′-UTR of murine p53 mRNA has been identified as a cis-acting target sequence for p53 protein, while the essential cis-acting element for the human p53 mRNA has been localized to the 3′-UTR [77].

Because translational control appears to be at least one mechanism governing p53 expression, and given our observation that a TS RNP complex composed of TS protein and a sequence corresponding to the human p53 mRNA was isolated from human colon cancer cells, further investigations were performed to confirm the interaction between TS protein and p53 mRNA and to elucidate the potential biological consequences of such an interaction. Using a combination of RNA gel shift and in vitro translation assay systems, we have shown that TS directly binds to a sequence within the protein-coding region of p53 mRNA at the C-terminal region [78,79]. The functional consequence of this RNA–protein interaction is translational repression. These studies have been extended to the in vivo setting to document the biologic relevance of the TS protein–p53 mRNA interaction. As part of these studies, human colon cancer RKO cells were transfected with the human TS cDNA under the control of a tetracycline-inducible expression system. Treatment of TS-transfected RKO cells with doxycycline (1 μg/ml), a tetracycline analog, resulted in a 15-fold induction of TS protein, which was accompanied by a dramatic decrease in the expression of p53 protein. Of note, no corresponding change in p53 mRNA levels was observed. Immunoprecipitation studies to isolate TS RNP complexes revealed a significantly greater level of p53 mRNA bound to TS protein in doxycycline-treated cells when compared to uninduced cells. As a second model system, we transfected TS-deficient, parent HCT-C18 cells expressing a functionally inactive TS with a human His-Tag TS cDNA under the control of a constitutive CMV promoter. We have shown that p53 expression in these TS-transfected cells (HCT-C18:His-TS+) was markedly decreased, and that this decreased p53 expression was directly controlled at the translational level. These TS-overexpressing cells were significantly impaired in the their ability to arrest at either the G_1/S or G_2/M boundaries, in response to γ-irradiation and/or treatment with various anticancer drugs including doxorubicin and 5-FU, when compared to their corresponding parent HCT-C18 cells [79]. In addition, the apoptotic response to drug exposure was dramatically reduced in TS-overexpressing cells, as evidenced by decreased activation of caspase-3 following treatment with 5-FU. More recently, we have shown that TS-overexpressing, HCT-C18:His-TS + cells are significantly more resistant to TS inhibitor compounds such as 5-FU and ZD1694, as well as to non-TS-related anticancer agents such as doxorubicin and cisplatin by up to 4 -to 7-fold [80]. These observations lend support for the biological relevance of the interaction between TS and p53 mRNA and suggest that loss of p53 function through translational repression results in an altered cell cycle checkpoint, in an altered apoptotic response, and in the development of pleiotropic drug resistance.

Taken together, these studies show that TS, in its capacity as an RNA-binding protein, interacts with high affinity with its own mRNA as well as with the mRNAs of the p53 tumor suppressor gene. Thus, TS may be involved in the coordinate regulation of expression and/or function of other genes. Given the importance of p53 in the cell cycle and in maintaining the requirements for cellular growth and proliferation, it is conceivable that TS may play an essential role as a regulator of cell cycle-directed events. This may be especially relevant given the essential role of TS in providing the requisite nucleotide substrates for DNA biosynthesis. Studies in our lab are currently focused on more precisely defining the molecular elements mediating the interaction between TS protein and the p53 mRNA, with emphasis on defining the cis-acting elements on each of these mRNAs. In addition, studies are in progress to determine whether the same domain(s) is involved in binding of TS to its own cognate TS mRNA as well as to other cellular mRNAs. Finally, extensive efforts are being directed at elucidating the downstream biological consequences of TS-mediated suppression of p53 mRNA translation with specific emphasis on cell cycle progression, cell cycle arrest, apoptosis, and chemosensitivity.

5. Discussion

In this review, we have highlighted the role of translational regulation as a mechanism for controlling the expression of TS. Moreover, we show that in addition to its critical catalytic function, TS serves an important role as an RNA binding protein. In this capacity, TS binds with high affinity to its own mRNA and directly regulates its own biosynthesis through a translational autoregulatory feedback mechanism. Through its role as an RNA binding protein, it interacts with several other cellular mRNAs including those corresponding to the p53 tumor suppressor gene and the *myc* family of transcription factors. In each of these cases, TS functions as a translational repressor to coordinately regulate the expression and/or function of these important genes. Our studies have shown that TS is able to serve as an effective translational regulator of cell cycle arrest, apoptosis, and chemosensitivity.

6. Conclusions and perspectives

There are several issues that remain to be addressed regarding the molecular basis for the interaction between TS and its own TS mRNA, as well as with other cellular mRNAs. It is clear that a more thorough understanding of the optimal nucleotide sequences and/or secondary structures required for protein recognition is needed. In addition, further work will focus on more precisely defining the critical amino acids and binding domain(s) on the TS protein that is needed for RNA recognition. For sure, definitive characterization of both the critical RNA binding domain(s) as well as the essential nucleotide sequences and/or secondary structures awaits the results of X-ray crystallography and/or NMR analysis of the TS protein–TS mRNA complex. While these structural studies have been limited, to date, by the availability of only small amounts of pure TS mRNA and human TS protein, these technical limitations should be resolved in the very near future.

One important issue to address relates to the intracellular localization of the TS protein–TS mRNA complex as well as the cellular localization of the other TS RNP complexes. For this work, our lab is developing an in vivo fluorescence immunohistochemistry approach. As a first step, we have generated a series of deletional TS cDNA constructs with a His-Tag placed at either the 5′ or 3′ terminus, and these respective constructs have been transfected into human colon cancer RKO cells. The intracellular localization of these deletion proteins was compared with that of the wild-type, full-length human TS protein [81]. Our studies, thus far, have revealed that deletion of the first 10 amino acids at the amino-terminus and deletion of 9 amino acids at the carboxy terminus significantly altered cellular localization. Wild-type, human TS protein was distributed uniformly throughout the cell in both the nucleus and cytoplasm. In contrast, the deleted TS proteins localized exclusively to the cytoplasm with absolutely no nuclear localization. Studies are in progress to isolate the cellular location of TS mRNA using in situ hybridization methods. Once these initial series of experiments are performed, co-localization studies are planned to determine the actual cellular location of the TS RNP complex.

These molecular-based studies will expand our current understanding of TS as an RNA binding protein and should provide new insights into the role of TS as an important regulator of certain critical aspects of cellular metabolism. Moreover, such a detailed characterization of the interaction

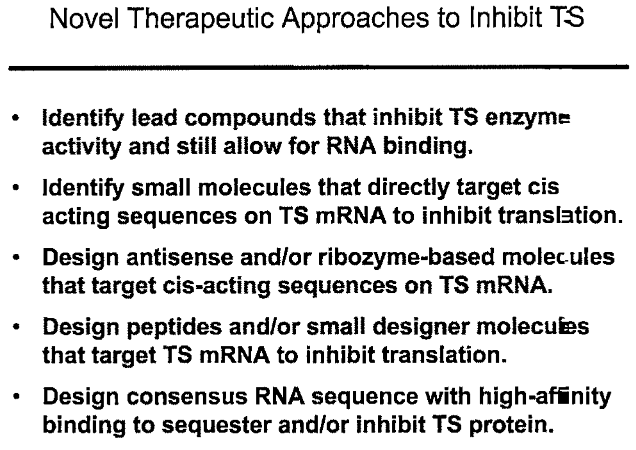

Novel Therapeutic Approaches to Inhibit TS

- **Identify lead compounds that inhibit TS enzyme activity and still allow for RNA binding.**
- **Identify small molecules that directly target cis acting sequences on TS mRNA to inhibit translation.**
- **Design antisense and/or ribozyme-based molecules that target cis-acting sequences on TS mRNA.**
- **Design peptides and/or small designer molecules that target TS mRNA to inhibit translation.**
- **Design consensus RNA sequence with high-affinity binding to sequester and/or inhibit TS protein.**

Fig. 5 Development of novel therapeutic approaches to inhibit TS

between TS and its own TS mRNA as well as with other cellular RNAs may also serve as the rational basis for the future development of novel therapeutic approaches

There are several potential strategies that may arise from such molecular-based studies as outlined in Fig. 5. For example, identification of the specific RNA binding domain may result in the development of novel inhibitors of TS enzymatic activity that would still allow for formation of the TS mRNA–TS protein complex in vivo. A stable ternary complex composed of inhibitor, TS protein, and TS mRNA might then result in marked suppression of new TS protein synthesis. As an alternative approach, identification of the putative RNA binding domain may lead to the development of a small peptide that would then be used to target TS mRNA and repress new TS protein synthesis. The use of innovative modeling programs may identify small "designer" molecules that mimic the structural features of the binding peptide. Certainly, the potential advantage of such an approach would be that novel organic molecules with enhanced spatial and biophysical and biochemical properties could be designed. Currently, this strategy is being taken in anti-HIV drug development where small basic Rev and Tat peptides that mimic the function of their corresponding native proteins are being to tested for their ability to inhibit HIV viral replication.

Identification of the consensus nucleotide sequence and/or secondary structure containing the high affinity protein binding site may lead to the design of an RNA oligonucleotide that can be used to sequester and/or repress TS enzymatic function. An alternative strategy would be to design a consensus nucleotide sequence/structure that might serve as the target for either antisense- or ribozyme-based strategies with resultant inhibition of TS protein synthesis. With this in mind, our lab has recently showed that an 18-nt RNA antisense molecule directed against the 5′-upstream cis-acting element of TS mRNA can specifically inhibit TS expression in human colon cancer RKO cells [82]. This antisense oligoribonucleotide exerts its effects by inhibiting TS mRNA translation, and in so doing, is able to inhibit growth of the RKO cells with an IC_{50} concentration of 200 nM. However, one significant drawback to the use of nucleic acids, whether it be RNA or DNA, is the inherent difficulty in efficiently and specifically delivering them into their target cells. The use of molecular modeling programs to design small organic molecules that closely resemble the consensus RNA sequence and/or structure may help to circumvent this problem. Such compounds should then be delivered with much greater efficiency and at relatively higher concentrations into malignant cells than their nucleic acid counterparts. Several of these therapeutic approaches are now under development in our lab in an attempt to bring more specific and effective therapies into the clinic for the treatment of human malignancies.

Acknowledgements

This work was supported by grants from the National Cancer Institute (CA16359 and CA75712 to E.C.) and from the Department of Veteran Affairs (VA Merit Review Award to E.C.).

References

[1] M B Mathews, N Sonenberg, J W B Hershey, Origin and targets of translational control, in: M.B Mathews, N Sonenberg, J W B Hershey (Eds), Translational Control, Cold Spring Harbor Press, Cold Spring Harbor, NY, 1996, pp. 1–27

[2] E J. Brown, S L Schreiber, A signalling pathway to translational control, Cell 86 (1996) 517–520

[3] V M Pain, Initiation of protein synthesis in eukaryotic cells, Eur J Biochem 236 (1996) 747–771

[4] M J. Clemens, U A Bommer, Translational control: the cancer connection, Int J Biochem Cell Biol 31 (1999) 1–23

[5] C. Carreras, D V. Santi, The catalytic mechanism and structure of thymidylate synthase, Annu Rev. Biochem 64 (1995) 721–762.

[6] P V Danenberg, Thymidylate synthase: a target enzyme in cancer chemotherapy, Biochim Biophys Acta 473 (1977) 73–79

[7] L W Hardy, J.S Finer-Moore, W.R. Montfort, M O Jones, D.V. Santi, R M Stroud, Atomic structure of thymidylate synthase: target for rational drug design, Science 235 (1987) 448–455.

[8] P.G Johnston, C.M. Liang, S. Henry, B A Chabner, C.J Allegra, Production and characterization of monoclonal antibodies that localize thymidylate synthase in the cytoplasm of human cells and tissue, Cancer Res. 51 (1991) 6668–6676

[9] L. Leichman, K Danenberg, J. Baranda, S Groshen, W. Boswell, R. Metzger, M Tan, P V. Danenberg, Quantitation of intratumoral thymidylate synthase expression predicts for disseminated colorectal cancer response and resistance to protracted-infusion fluorouracil and weekly leucovorin, J Clin Oncol. 10 (1997) 3223–3230

[10] H J Lenz, K. Hayashi, D Salonga, K D Danenberg, P.V Danenberg, R. Metzger, D. Banerjee, J R Bertino, S Groshen, L P Leichman, C.G. Leichman, p53 mutations and thymidylate synthase messenger RNA levels in disseminated colorectal cancer: an analysis of response and survival, Clin. Cancer Res. 4 (1998) 1243–1250

[11] S M. Swain, M C. Lippman, E.F. Egan, J C. Drake, S M Steinberg, C J. Allegra, 5-Fluorouracil and high-dose leucovorin in previously treated patients with metastatic breast cancer, J. Clin Oncol 7 (1989) 890–899

[12] C.L. Van der Wilt, H.M. Pinedo, K Smit, G J Peters, Elevation of thymidylate synthase following 5-fluorouracil treatment is prevented by the addition of leucovorin in murine colon tumors, J. Clin. Oncol. 12 (1994) 2035–2042.

[13] D V. Santi, C S McHenry, H. Sommer, Mechanism of interaction of thymidylate synthetase with 5-fluorodeoxyuridylate, Biochemistry 13 (1974) 471–480

[14] K Keyomarsi, R.G. Moran, Folinic acid augmentation of the effects of fluoropyrimidines on murine and human leukemic cells, Cancer Res. 46 (1988) 5229–5235

[15] C Erlichman, S Fine, A. Wong, T Elhakim, A randomized trial of fluorouracil and foloiic acid in patients with metastatic colorectal carcinoma, J. Clin. Oncol. 6 (1988) 469–475.

[16] M A Poon, M J O'Conell, C G Moertel, H S. Wieand, S A Cullinan, L.K Everson, J E Krook, J A Mailliard, J.A. Laurie, L.K Tschetter, Biochemical modulation of fluorouracil: evidence of a significant improvement of survival and quality of life in patients with advanced colorectal carcinoma, J. Clin. Oncol 10 (1989) 1407–1418

[17] Advanced colorectal cancer meta-analysis project Modulation of fluorouracil by leucovorin in patients with advanced colorectal cancer: evidence in terms of response rate, J Clin Oncol. 10 (1992) 896–903.

[18] D Cunningham, J.R. Zalcberg, U. Rath, I Oliver, E. van Cutsem, C. Svensson, J.F Seitz, P Harper, D Kerr Tomudex Colorectal Cancer Study Group, Tomudex (ZD1694): results of a randomized trial in advanced colorectal cancer demonstrate efficacy and reduced mucositis and leucopenia, Eur J Cancer 12 (1995) 1945–1954

[19] J R. Zalcberg, D. Cunningham, E. van Cutsem, E Francois, J. Schomagel, A. Adenis, M. Green, A. Iveson, M Azab, I Seymour, ZD1694: a novel thymidylate synthase inhibitor with substantial activity in the treatment of patients with advanced colorectal cancer, J. Clin. Oncol 14 (1996) 716–721

[20] G Cocconi, D. Cunningham, E van Cutsem, E. Francois, B. Gustavsson, G. van Hazel, D. Kerr, K. Possinger, S.M. Hietschold, Open, randomized, multicenter trial of raltitrexed versus fluorouracil plus high-dose leucovorin in patients with advanced colorectal cancer, J. Clin Oncol 16 (1998) 2943–2953

[21] S H. Berger, C.H Jenh, L.F Johnson, F.G Berger, Thymidylate synthase overproduction and gene amplification in fluorodeoxyuridine-resistant human cells, Mol. Pharmacol. 28 (1985) 461–467.

[22] M.S Copur, K Aiba, J.C. Drake, C.J. Allegra, E. Chu, Thymidylate synthase gene amplification in human colon cancer cells resistant to 5-fluorouracil, Biochem. Pharmacol 49 (1995) 1419–1426

[23] L G. Navalgund, C. Rossana, A.L Muench, L F. Johnson, Cell cycle regulation of thymidylate synthase gene expression in cultured mouse fibroblasts, J. Biol. Chem. 255 (1980) 7386–7390.

[24] C.H. Jenh, L G Rao, L F Johnson, Regulation of thymidylate synthase enzyme synthesis in 5-fluorodeoxyuridine-resistant mouse fibroblasts during the transition from the resting to growing state, J Cell Physiol 122 (1985) 149–154.

[25] C.H. Jenh, P.K Geyer, L F Johnson, Control of thymidylate synthase mRNA content and gene transcription in an overproducing mouse cell line, Mol Cell. Biol. 5 (1985) 2527–2532.

[26] D Ayusawa, K Shimizu, H Koyama, S Kaneda, K Takeishi, T. Seno, Cell-cycle-directed regulation of thymidylate synthase messenger RNA in human diploid fibroblasts stimulated to proliferate, J. Mol Biol 190 (1986) 559–567

[27] Y. Geng, L F Johnson, Lack of an initiator element is responsible for multiple transcriptional initiation sites of the TATA-less mouse thymidylate synthase promoter, Mol Cell. Biol. 13 (1993) 4894–4903

[28] S Dong, L Lester, L.F. Johnson, Transcriptional control elements and complex initiation pattern of the TATA-less bidirectional human thymidylate synthase promoter, J Cell. Biochem. 77 (2000) 50–64.

[29] Y. Ke, J. Ash, L.F Johnson, Splicing signals are required for S-phase regulation of the mouse thymidylate synthase gene, Mol. Cell Biol 16 (1996) 376–383.

[30] E. Chu, J C Drake, D M. Koeller, S. Zinn, C.A Jamis-Dow, G.C Yeh, C J Allegra, Induction of thymidylate synthase associated with multidrug resistance in human breast and colon cancer cell lines, Mol Pharmacol 39 (1991) 136–143

[31] M.E Kitchens, A.M. Forshoefel, Z. Rafique, H.T Spencer, F G. Berger, Ligand-mediated induction of thymidylate synthase occurs by enzyme stabilization, J Biol. Chem. 274 (1999) 12544–12547

[32] M. Belfort, G. Maley, J. Pederson-Lane, F Maley, Primary structure of the *Escherichia coli* thyA gene and its thymidylate synthase product, Proc. Natl. Acad. Sci. U S. A 80 (1983) 4914–4918.

[33] K. Takeishi, S Kaneda, D Ayusawa, K. Shimizu, O. Gotoh, T Seno, Nucleotide sequence of a functional cDNA for human thymidylate synthase, Nucleic Acids Res 13 (1985) 2035–2043.

[34] S Kaneda, K. Takeishi, D. Ayusawa, K Shimizu, T. Seno, S Altman, Role in translation of a triple tandemly repeated sequence in the 5′ untranslated region of human thymidylate synthase mRNA, Nucleic Acids Res. 15 (1987) 1259–1270.

[35] R. Labow, G.F. Maley, F Maley, The effect of methotrexate on TS-enzyme induced following partial hepatectomy, Cancer Res 29 (1969) 366–372

[36] R J Bonney, F. Maley, Effect of methotrexate on thymidylate synthetase in cultured parenchymal cells isolated from regenerating rat liver, Cancer Res 25 (1975) 1950–1956

[37] C.P. Spears, A.H. Shahinian, R.G Moran, et al., In vivo kinetics of thymidylate synthase inhibition in 5-fluorouracil-sensitive and -resistant murine colon adenocarcinoma, Cancer Res. 42 (1982) 450–456

[38] W L Washtien, Increased levels of thymidylate synthase in cells exposed to 5-fluorouracil, Mol Pharmacol 25 (1984) 171–177

[39] E Chu, S Zinn, D Boarman, C J Allegra, Interaction of gamma-interferon and 5-fluorouracil in the H630 human colon carcinoma cell line, Cancer Res. 50 (1990) 5834–5840.

[40] S J. Welsh, L Titley, L Brunton, M Valenti, P Monaghan, A L Jackman, G W Aherne, Comparison of thymidylate synthase (TS) protein up-regulation after exposure to TS inhibitors in normal and tumor cell lines and tissues, Clin. Cancer Res. 6 (2000) 2538–2546

[41] K. Keyomarsi, J Samet, G Molnar, A.B. Pardee, The thymidylate synthase inhibitor, ICI D1694, overcomes translational detainment of the enzyme, J Biol. Chem 268 (1993) 15142–15149.

[42] E Chu, D.M. Koeller, P G Johnston, S Zinn, C J Allegra, Regulation of thymidylate synthase in human colon cancer cells treated with 5-fluorouracil and interferon-gamma, Mol Pharmacol. 43 (1993) 527–533

[43] A. Bernardi, P F Spahr, Nucleotide sequence at the binding site for coat protein on RNA of bacteriophage R17, Proc Natl Acad. Sci U S A 69 (1972) 3033–3037

[44] J Carey, V Cameron, P L de Haseth, O C Uhlenbeck, Sequence-specific interaction of R17 coat protein with its ribonucleic acid binding site, Biochemistry 22 (1983) 2601.

[45] M. Andrake, N Guild, T Hsu, L Gold, C Tuerk, J. Karam, DNA polymerase of bacteriophage T4 is an autogenous translational repressor, Proc. Natl Acad Sci U S A 85 (1988) 7942–7946

[46] L. Gold, Posttranscriptional regulatory mechanisms in *Escherichia coli*, Annu Rev Biochem 57 (1988) 199–203

[47] G Spedding, D E Draper, Allosteric mechanism for translational repression in the *Escherichia coli* alpha operon, Proc. Natl. Acad. Sci U S. A. 90 (1993) 4399–4403.

[48] E Chu, C.H Takimoto, D M Voeller, J L Grem, C J Allegra, Specific binding of human dihydrofolate reductase protein to dihydrofolate reductase messenger RNA in vitro, Biochemistry 32 (1993) 4756–4760

[49] E Ercikan, D. Banerjee, M Waltham, B Schnieders, K W Scotto, J.R. Bertino, Translational regulation of the synthesis of dihydrofolate reductase, Adv Exp Med. Biol 338 (1993) 537–540.

[50] E.A Ercikan-Abali, D Banerjee, M.C. Waltham, N Skacel, K W Scotto, J.R. Bertino, Dihydrofolate reductase protein inhibits its own translation by binding to dihydrofolate reductase mRNA sequences within the coding region, Biochemistry 36 (1997) 12317–12322.

[51] X. Liu, B. Reig, I M. Nasrallah, P J Stover, Human cytoplasmic serine

hydroxymethyltransferase is an mRNA binding protein, Biochemistry 39 (2000) 11523–11531

[52] J Mosner, T Mummenbrauer, C. Bauer, G. Sczakiel, F Grosse, W Deppert, Negative feedback regulation of wild-type p53 biosynthesis, EMBO J. 14 (1995) 4442–4449

[53] L. Fu, M.D Minden, S Benchimol, Translational regulation of human p53 regulation, EMBO J 15 (1996) 4392–4401

[54] E Chu, D Voeller, J L Casey, J.C Drake, B.A. Chabner, P C Elwood, S Zinn, C J. Allegra, Autoregulation of human thymidylate synthase messenger RNA translation by thymidylate synthase, Proc. Natl Acad. Sci U. S A 88 (1991) 8977–8981

[55] E Chu, D M Voeller, J.C Drake, C.H Takimoto, G.F. Maley, C J Allegra, Identification of an RNA binding site for human thymidylate synthase, Proc Natl Acad Sci. U. S A 90 (1993) 517–521

[56] X Lin, L.A Parsels, D M Voeller, C.J Allegra, G F Maley, F Maley, E Chu, Characterization of a cis-acting regulatory element in the protein coding region of thymidylate synthase mRNA, Nucleic Acids Res. 28 (2000) 1381–1389

[57] D R Gallie, The cap and poly (A) tail function synergistically to regulate mRNA translation efficiency, Genes Dev 5 (1991) 2108–2116

[58] R J Jackson, Cytoplasmic regulation of mRNA function: the importance of the 3′ untranslated region, Cell 74 (1993) 9–14

[59] V Leathers, R Tanguay, M. Koyayashi, D R Gallie, A phylogenetically conserved sequence within viral 3′ untranslated RNA pseudoknots regulates translation, Mol Cell Biol 13 (1993) 5331–5347

[60] A D. Ostareck-Lederer, D.H. Ostareck, N Standard, B J Thiele, Translation of 15-lipoxygenase mRNA is inhibited by a protein that binds to a repeated sequence in the 3′ untranslated region, EMBO J 13 (1994) 1476–1481

[61] E Chu, D.M Voeller, P F Morrison, K.L Jones, T. Takechi, G F. Maley, F. Maley, C J Allegra, The effect of reducing reagents on binding of thymidylate synthase protein to thymidylate synthase messenger RNA, J Biol Chem 269 (1994) 20289–20293.

[62] O C. Uhlenbeck, H N Wu, J R Sampson, Recognition of RNA by proteins, Molecular Biology of RNA, Academic Press, New York, 1987, pp 285–294.

[63] O. Melefors, M W Hentze, Translational regulation by mRNA/protein interactions in eukaryotic cells: ferritin and beyond, BioEssays 15 (1993) 85–90.

[64] R D Klausner, T A. Rouault, J.B Harford, Regulating the fate of mRNA. the control of cellular iron metabolism, Cell 72 (1993) 19–28

[65] B.R. Henderson, E Menotti, C Bonnard, L C. Kuhn, Optimal sequence and structure of iron-responsive element, J Biol. Chem 269 (1994) 17481–17489

[66] E Chu, T Cogliati, S M. Copur, A. Borre, D M. Voeller, C J Allegra, S Segal, Identification of in vivo target RNA sequences bound by thymidylate synthase, Nucleic Acids Res 24 (1996) 3222–3228

[67] J Steitz, Immunoprecipitation of ribonucleoproteins using autoantibodies, Methods Enzymol 180 (1989) 468–481.

[68] P Froussard, rPCR· a powerful tool for random amplification of whole RNA sequences, PCR Methods Appl. 2 (1992) 185–190

[69] L J Ko, C Prives, p53. puzzle and paradigm, Genes Dev 10 (1996) 1054–1072

[70] A J Levine, p53, the cellular gatekeeper for growth and division, Cell 88 (1997) 323–331

[71] M R.A Mowat, p53 in tumor progression life, death and everything, Adv. Cancer Res 74 (1998) 25–48

[72] W Maltzman, L Czyzyk, UV irradiation stimulates levels of p53 cellular tumor antigen in nontransformed mouse cells, Mol Cell Biol 4 (1984) 1689–1694

[73] S Y Shieh, M Ikeda, Y. Taya, C Prives, DNA damage-induced phosphorylation of p53 alleviates inhibition by MDM2, Cell 91 (1997) 325–334

[74] W. Gu, R G Roeder, Activation of p53 sequence-specific DNA binding by acetylation of the p53 C-terminal domain, Cell 90 (1997) 595–606

[75] K Sakaguchi, J E Herrera, W Saito, et al , DNA damage activates p53 through a phosphorylation–acetylation cascade, Genes Dev 12 (1998) 2831–2841

[76] M B. Kastan, O. Onyekwere, D Sidransky, B Vogelstein, R.W Craig, Participation of p53 protein in the cellular response to DNA damage, Cancer Res. 51 (1991) 6304–6311

[77] L. Fu, S. Benchimol, Participation of the human p53 3′-UTR in translational repression and activation following gamma-irradiation, EMBO J 16 (1997) 4117–4125

[78] E Chu, S. Copur, J Ju, T.M Chen, S Khleif, D.M Voeller, N. Mizunuma, M. Patel, G F Maley, F Maley, C J. Allegra, Thymidylate synthase protein and p53 mRNA form an in vivo ribonucleoprotein complex, Mol Cell Biol 19 (1999) 1582–1594.

[79] J.F Ju, J. Pederson-Lane, F Maley, E. Chu, Regulation of p53 expression by thymidylate synthase, Proc Natl Acad. Sci U. S A 96 (1999) 3769–3774

[80] J. Ju, E Chu, Translational regulation of 5-FU-induced p53 expression in human cancer RKO cell, Proc Am. Assoc Cancer Res 41 (2000) 854, 5422a

[81] J Liu, X K Lin, F Gorelick, F. Maley, E Chu, Sequence requirements for the intracellular localization of human thymidylate synthase, Proc. Am Assoc Cancer Res 43 (2002) 100, 502a

[82] J C Schmitz, D. Yu, S. Agrawal, E Chu, Effect of 2′-*O*-methyl antisense ORNs on expression of thymidylate synthase in human colon cancer RKO cells, Nucleic Acids Res 29 (2000) 415–422.

ELSEVIER

Biochimica et Biophysica Acta 1587 (2002) 183–193

BIOCHIMICA ET BIOPHYSICA ACTA
BBA
www.bba-direct.com

Review

Natural antisense (rTSα) RNA induces site-specific cleavage of thymidylate synthase mRNA

Jianxiong Chu, Bruce J. Dolnick*

Department of Pharmacology and Therapeutics, Roswell Park Cancer Institute, Elm and Carlton Streets, Buffalo, NY 14263, USA

Received 24 January 2002, accepted 24 January 2002

Abstract

The 3′ untranslated region (UTR) of rTSα RNA is complementary (i.e., antisense) to human thymidylate synthase (TS) RNA. When HEp2 cells (human epidermoid carcinoma) progressed from late-log to plateau phase growth, ribonuclease protection assay (RPA) revealed an inverse correlation between the levels of rTSα RNA and TS mRNA, suggesting a possible effect of rTSα RNA on TS mRNA levels. HEp2 cells expressing a Tet-On transactivator were transiently co-transfected with pHook-1 and a construct containing rTSα (protein and antisense RNA), rTSαΔ3′ (rTSα protein only), rTSα-3′ (antisense RNA–luciferase) or luciferase. Transfected cells were selected and evaluated for the effects of induced transgene expression on TS mRNA. Induced expression of transfected rTSα or rTSα-3′, but not rTSαΔ3′ or luciferase, resulted in decreased TS mRNA levels as measured by RPA. These results demonstrated that the antisense region of rTSα RNA is necessary and sufficient for this down-regulation of TS mRNA. RPA for TS mRNA also showed the enhanced appearance of two partial-length protected fragments in rTSα or rTSα-3′ transfected cells. RPA stringency evaluations and primer extension assays indicated that TS mRNA is cleaved in vivo in a site-specific manner. These data demonstrate that rTS gene expression likely plays a role in down-regulating TS through a natural RNA-based antisense mechanism. © 2002 Elsevier Science B.V. All rights reserved.

Keywords: Chemotherapy; Thymidylate synthase; RNA editing; Antisense RNA

---

1. Introduction

Thymidylate synthase (TS, EC 2.1.1.45) is the enzyme that catalyzes the methylation of deoxyuridylate to deoxythymidylate (dTMP). This enzymatic reaction provides the sole de novo intracellular source of dTMP, an essential nucleotide precursor for DNA replication and repair. As a result, TS has been a major target in cancer chemotherapy for over 30 years [1]. Since some tumor cell lines resistant to TS inhibitors overproduce the enzyme [2,3], a better understanding of mechanisms underlying the regulation of TS levels is important for the development of cancer therapies involving TS inhibition.

The TS gene is expressed at a much higher level in rapidly proliferating cells than in nondividing cells [4–10]. However, nuclear run-on assays showed that the rate of the TS gene transcription is relatively invariant as cells are activated from a resting to a cycling state [5,11]. Therefore, TS gene expression appears to be controlled mainly at the posttranscriptional level in growth-stimulated cells [12]. Since growing cells are comprised of a large percentage of cells in S phase, which generally parallels changes in TS levels, TS appears to be an S-phase enzyme. This is supported by the evidence that elevated expression of E2F results in increased TS protein levels [13]. However, studies on exponentially growing asynchronous cells have indicated that the levels of TS mRNA [4], TS protein and TS activity [6,10] fluctuate only within a narrow range throughout the cell cycle, with the largest increase occurring during the G_0/G_1 transition [6,10].

In 1993, our laboratory reported the discovery of a naturally occurring antisense RNA to TS (now referred as rTSα EMBL accession #X67098) [14]. The 3′ untranslated region (UTR) of rTSα mRNA is complementary (antisense) to both TS pre-mRNA and TS mRNA (Fig. 1). Natural antisense RNA was first discovered in prokaryotes and has been demonstrated to exert negative control of

---

Abbreviations. BSA, bovine serum albumin; Cyc, cyclophilin; Dox, doxycycline; RPA, ribonuclease protection assay; TS, thymidylate synthase; UTR, untranslated region

* Corresponding author. Tel. +1-716-845-5828; fax: +1-716-845-8857.
E-mail address: bruce.dolnick@roswellpark.org (B.J. Dolnick).

0925-4439/02/$ - see front matter © 2002 Elsevier Science B.V. All rights reserved
PII: S0925-4439(02)00081-9

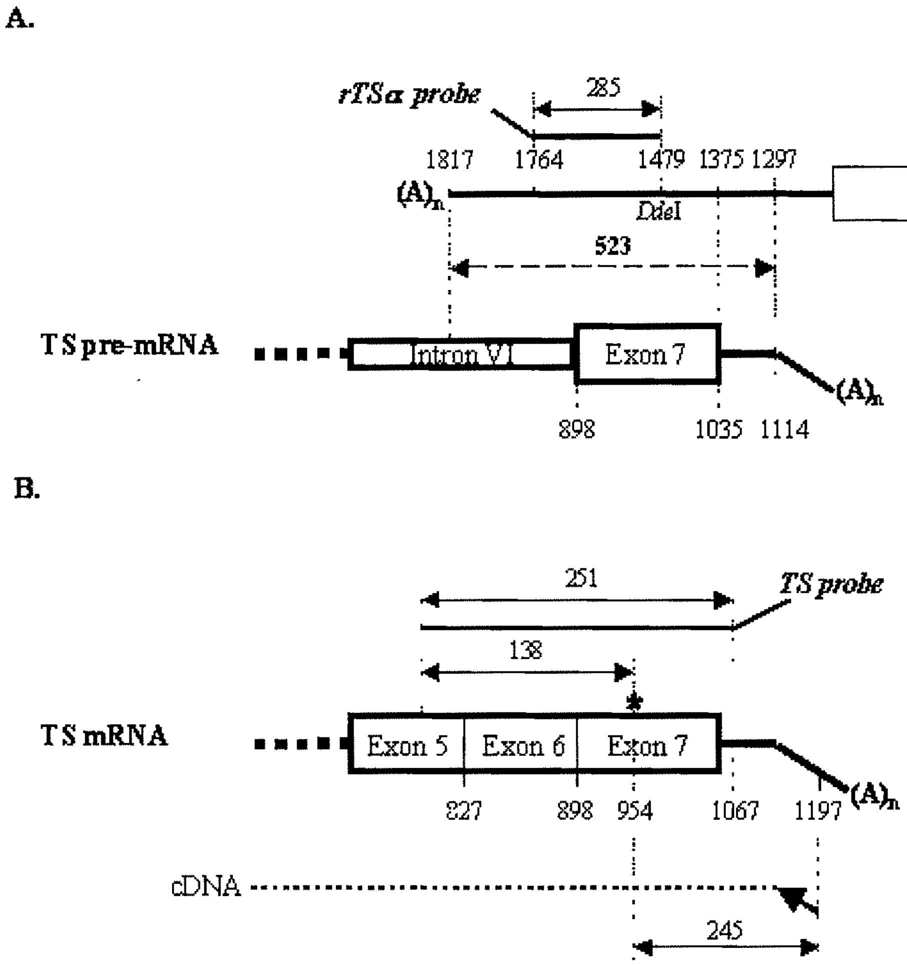

Fig. 1. (A) The relationship between the rTSα mRNA and the TS gene/pre-mRNA. The protein coding region and 3′ UTR of rTSα are indicated by an open box and a solid line, respectively. The two boxes in the TS pre-mRNA represent a portion of intron VI and the protein coding region of exon 7 as indicated. The 3′ UTR of exon 7 is indicated by a solid line. The rest of TS pre-mRNA is represented by a dotted line. Numbers represent nucleotide distance either from the 5′ end of the rTSα RNA or over the spans indicated by double arrows. rTSα mRNA is complementary to TS pre-mRNA over a span of 523 nt, including the first A of the rTSα poly (A) tail. The targeted region (285 nt) of the rTSα riboprobe is also indicated at the top. (B) Targeted region of the TS riboprobe and the expected cDNA products from primer extension assay. Open boxes represent exons 5, 6 and 7 of TS mRNA with the solid line representing the 3′ UTR. The rest of the TS mRNA is represented by a dotted line. The TS probe is represented by a solid line at the top. The full-length protected fragment would be 251 nt as indicated at the top. The primer used in primer extension assays is represented by the left-facing arrow. A TS RNA editing site that generates a mismatch in the TS probe.mRNA duplex is indicated by an asterisk (see Results and Discussion). The protected fragment in RPA resulting from cleavage at the editing site is 138 nt. The predicted length of cDNA produced by primer extension from the TS mRNA cleaved at the editing site is 245 nt.

gene expression at multiple levels, such as transcriptional attenuation, interference with RNA processing, RNA destabilization and translational inhibition [15]. Increasing numbers of naturally occurring antisense RNAs have been identified in eukaryotes, raising the possibility that they might play a role in the regulation of eukaryotic gene expression [16,17]. However, in mammalian cells, the functions of natural antisense RNAs in regulating the expression of their counterpart (sense) genes have not been established.

In the present study, we show that rTSα RNA and TS mRNA levels vary inversely when cell growth transits from late-log to plateau phase. We demonstrate that the antisense portion of rTSα mRNA alone can down-regulate TS mRNA levels in transiently transfected cells. Our data also show that this down-regulation is associated with increased site-specific cleavage of TS mRNA.

2. Experimental procedures

2.1. Plasmids and probes

The plasmids for the Tet-On gene expression system (pUHD 172-1 neo, pUHD 10-3 and pUHC13-3) were obtained from Dr. Hermann Bujard [18]. To construct the expression vector for rTSα, we cloned the *Eco*RI–*Hin*dIII fragment of rTSα containing the full-length cDNA into the *Eco*RI and *Xba*I sites of pUHD10-3. The *Hin*dIII site of the rTSα insert and *Xba*I site of pUHD10-3 were partially filled in by Klenow enzyme (Life Technologies) to generate cohesive ends. The expression vector for rTSα protein without antisense RNA (rTSαΔ3′) was constructed by cloning the *Eco*RI–*Blp*I (blunt-ended) fragment of the rTSα cDNA into the *Eco*RI and *Xba*I sites (blunt-ended) of pUHD 10-3. The 3′ UTR was generated by PCR using primers containing the *Sty*I recognition sequence (boldface type) (5′-primer: CGTGACC**CCAAGG**AAGTGCTCAGCCCCA-ACAACT, 3′-primer: GCGTGCT**CCTTGG**TGACTGTGTTCCTGTCTTTAA). The vector for expressing rTSα antisense RNA without rTSα protein (rTSα-3′) was constructed by cloning the PCR generated fragment into the *Sty*I site of pUHC13-3. The sequences of all cloned cDNAs were confirmed by sequencing at the RPCI Biopolymer Facility.

The template for in vitro transcription used to generate the TS riboprobe was *Sma*I linearized plasmid pTS-PCRmut1 [19]. The targeted region of this TS probe includes part of exon 5 (10 nt), exon 6 (72 nt) and part of exon 7 (169 nt) (Fig. 1B). The template for the rTSα riboprobe was *Dde*I linearized plasmid pTOPO/G4, produced by inserting a PCR fragment from H630 cell genomic DNA corresponding to rTSα mRNA nt 1326–1764 (Fig. 1A) into pCR2.1-TOPO (Invitrogen). The template for making the cyclophilin (Cyc) riboprobe was pTRI–Cyc–Human (Ambion). The lengths of TS, rTSα and Cyc probes (and protected fragments) were 265 (251), 354 (285) and 165 (103) nt, respectively. All ^{32}P-RNA probes were produced by in vitro transcription using MaxiScript/T7 polymerase kits (Ambion) as recommended by the manufacturer using [α-^{32}P]CTP (800 Ci/mmol, 10 mCi/ml, NEN Life Science Products). DNA templates were removed by DNaseI digestion. All ^{32}P-labelled riboprobes were purified by 5% polyacrylamide/8 M urea gel electrophoresis. Specific radioactivities of the TS, rTSα and Cyc probes used were 1.8×10^9, 1.5×10^9 and 8×10^7 cpm/μg, respectively.

2.2. Cell culture and transfections

The HEp2 cell line (human epidermoid carcinoma, ATCC CCL 23) was maintained in RPMI 1640 supplemented with 10% fetal bovine serum (Life Technologies) at 37 °C in a 5% CO_2 humidified atmosphere. The HEp2 cell line was chosen for study because of its low level of endogenous rTSα expression and because of a robust response to doxycycline (Dox) induction in preliminary co-transient transfection assays using pUHD172-1 neo and pUHC 13 3 (data not shown).

For the cell growth experiment (Fig. 2A), HEp2 cells were seeded on multiple plates (8.0×10^5 cells/10 cm plate) and allowed to grow for different periods of time. Cells were extracted to obtain both RNA and protein using TRIZOL reagent (Life Technologies) as recommended by the manufacturer. For each time point, the cell number in a duplicate plate was determined using a Coulter counter.

For transfections to establish the Tet-On gene expression system, pUHD 172-1 neo was first stably transfected into HEp2 cells using lipofectin (Life Technologies) as recommended by the manufacturer. Clones were selected in the presence of G418 (500 μg/ml) and were screened for their ability to be induced for luciferase expression by transient-transfection assays. Clone P9E was Dox-inducible for luciferase expression (100-fold), and was used in subsequent experiments. For each co-transient transfection with pHook-1 (Invitrogen) [20] and one of the four constructs (rTSα, rTSαΔ3′ rTSα-3′ and luciferase, Fig. 3A), cells at about 50% confluence were harvested and washed with ice-cold PBS. The cell pellet was resuspended in ice-cold PBS at a density of $\sim 5.7\times10^7$ cells/ml, and 2.1 ml of cell suspension was mixed with 150 μg plasmid DNA (molar ratio of pHook1/experimental construct = 10:1) and incubated on ice for 10 min. The cells plus DNA mixture was evenly transferred into three prechilled cuvettes (BTX, 4 mm gap). Electroporation was performed using a BTX ECM 600 electroporator (400 V, 800 μF, 48 Ω). After the pulse, the cuvettes were returned to ice for 10 min. The electroporated cells were pooled and resuspended with RPMI 1640 medium containing 10% fetal bovine serum and 300 μg/ml G418, and plated on 25 15-cm plates. After 20 h, transfected cells were selected with Capture-Tec™ Beads (200 μl bead slurry, Invitrogen) as recommended by the manufacturer. The selected cells (~ 20% of total viable cells) were plated at $\sim 1.0\times10^6$ cells/10 cm plate and returned to culture in the presence or absence of Dox (1.0 μg/ml).

2.3. Western blot

Protein concentrations were determined using a BCA™ Protein Assay Kit with bovine serum albumin (BSA) as a standard as described by the manufacturer (Pierce). Proteins (35 μg) were resolved by 10% SDS polyacrylamide gel electrophoresis and immunoblotting was performed as previously described [21].

2.4. RNase protection assay (RPA)

RPA to measure TS mRNA or rTSα RNA was carried out using the HybSpeed RPA kit (Ambion) essentially as described by the manufacturer. The amount of each probe needed to achieve a molar excess over its target RNA was determined by pilot experiments that established the linearity of the assay. Cyc mRNA was also measured to serve as an internal standard for quantitating protected fragments [22]. Briefly, 5 μg of RNA, 6×10^4 cpm of TS or rTSα riboprobe and 3×10^4 cpm of Cyc riboprobe were mixed and co-ethanol-precipitated with yeast RNA (45 μg) as carrier. The RNA pellet was dissolved in 10 μl of hybridization buffer by heating at 95 °C with vortexing. Hybridization was performed at 68 °C for 18 h, and RNase digestions were carried out at 37 °C for 40 min with RNase A/T1 (1:100),

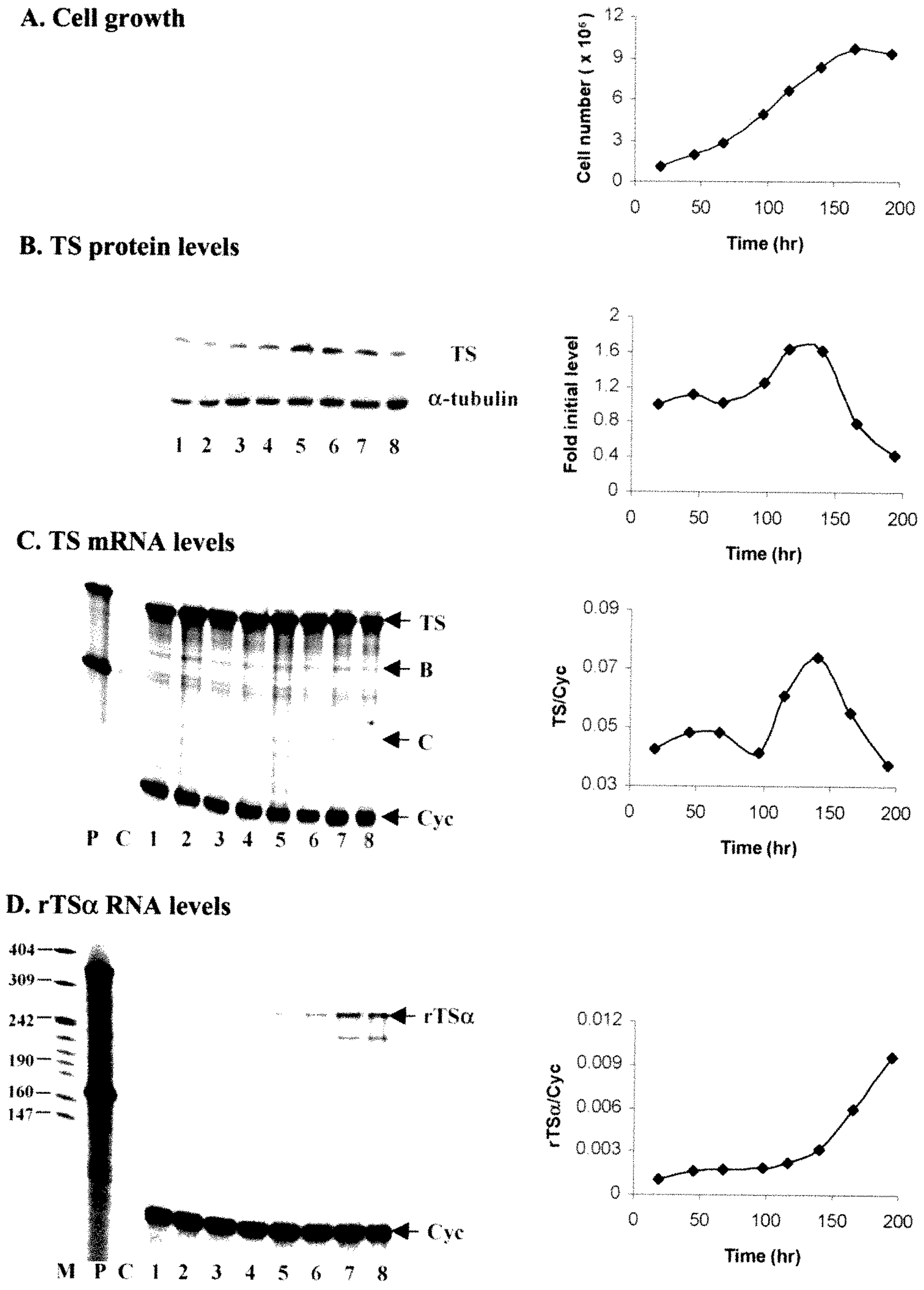

Fig. 2. Variation of TS protein, TS mRNA and rTSα RNA levels during asynchronous cell growth. (A) HEp2 cell growth. Cells were seeded at time 0 h (8×10^5 cells/10 cm plate) and extracted at 19, 45, 67, 97, 116, 140, 166 and 194 h after seeding as described in Experimental procedures. The doubling time of this cell line is 40 h. (B) Lanes 1–8: Proteins obtained from different time points of cell growth (19–194 h) were subjected to Western blot analysis for TS and α-tubulin as described in Experimental procedures (left). The change of TS protein levels with cell growth normalized to α-tubulin is shown on the right. Panels (C) and (D) are the results of RPA for TS mRNA and rTSα RNA, respectively. For all RPA experiments, Cyc mRNA was used as an internal standard. Left panels show the phosphorimages of electrophoretic gels and positions of relevant protected fragments are indicated to the right of the images (TS, 251 nt TS fragment; B, 195 nt TS fragment; C, 138 nt TS fragment; Cyc, 103 nt Cyc fragment; rTSα 285 nt rTSα fragment). Lanes 1–8: Cellular RNAs from different time points of cell growth (19–194 h) were hybridized with TS and Cyc probes. M: pBR322/*Msp*I molecular weight marker. Lanes P and C: The TS or rTSα and Cyc probes were hybridized with yeast RNA either with (C) or without (P) RNase digestion. In lane P, discrete bands can be seen at the predicted lengths of 265 (TS), 354 (rTSα) and 165 nt (Cyc), whereas lane C shows complete digestion of unprotected probes. The graphs on the right show the molar ratios of TS mRNA (B) or rTSα RNA (D) to Cyc mRNA at each time point of cell growth (calculated according to the formula given in Experimental procedures).

unless otherwise indicated. Protected fragments were resolved by 5% polyacrylamide/8 M urea gel electrophoresis and quantitated by phosphor screen imaging (Molecular Dynamics Storm 860 with a setting of 750 V, 200 μm). The lower specific activity of the Cyc probe allowed simultaneous quantitation of TS mRNA and rTSα RNA.

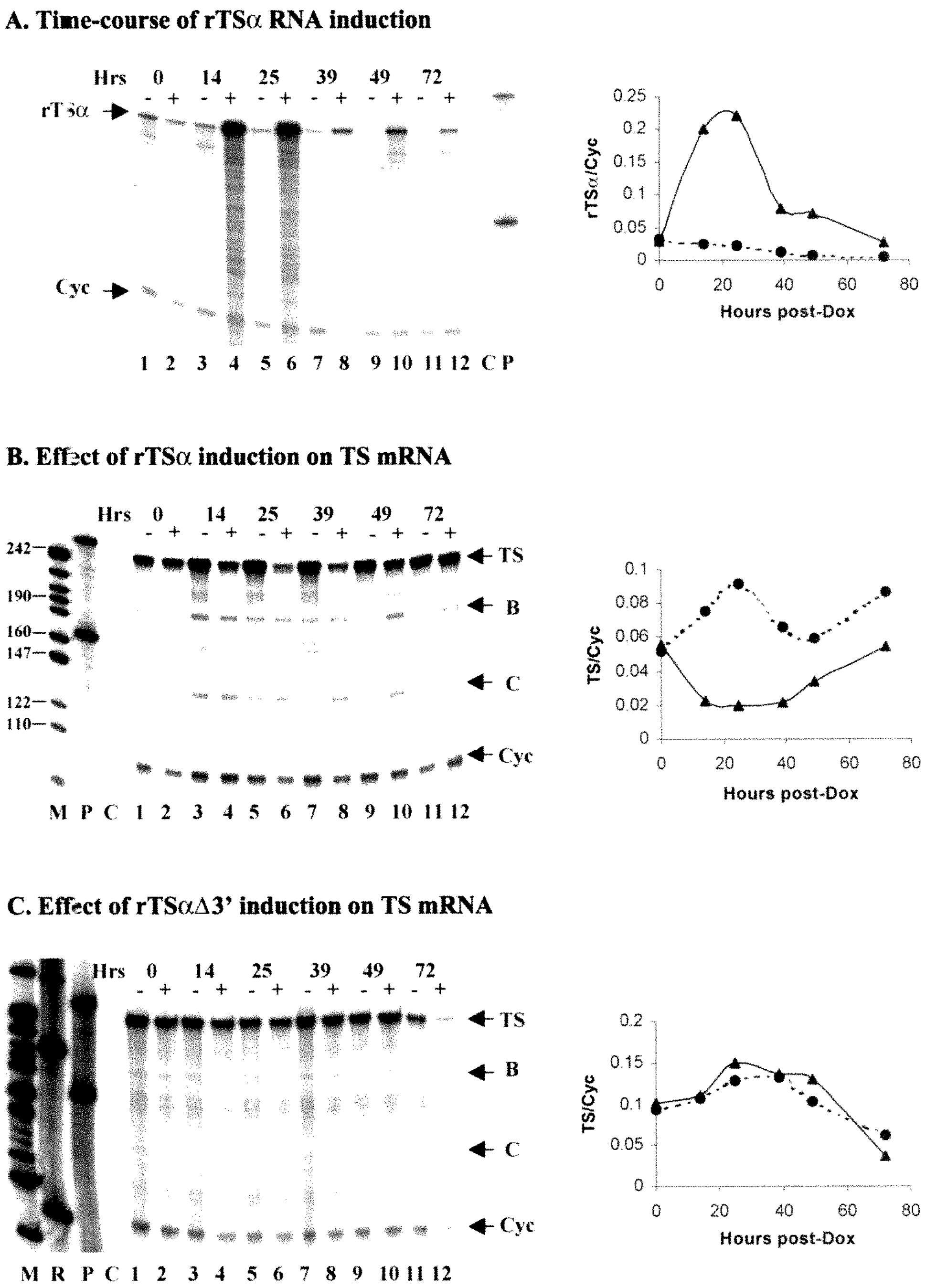

A. Time-course of rTSα RNA induction

B. Effect of rTSα induction on TS mRNA

C. Effect of rTSαΔ3' induction on TS mRNA

Fig. 3. RPA results for rTSα and rTSαΔ3′ transiently transfected cells. (A) Time course analysis of rTSα RNA induction in rTSα transfected cells. (B,C) Time-course analyses of TS mRNA levels in rTSα and rTSαΔ3′ transfected cells, respectively. Panels are labeled as in the legend to Fig. 2. Lanes 1–12: RNA samples obtained at 0–72 h after adding Dox (0 and 1.0 μg/ml as indicated by " – " and " + ", respectively) were subjected to RPA as described in Experimental procedures. R:RNA marker (Ambion's century marker). For each graph on the right, the solid line with triangles represents induced cells (+ Dox) and the dotted line with circles uninduced cells (– Dox).

2.5. Primer extension assay

Cellular RNA (20 μg) was mixed with 0.1 μmol primer (ACATTTGCCAGT-GGCAACAT, Fig. 1) and incubated at 70 °C for 5 min. The reverse transcription reaction (60 μl) contained sample RNA, the primer, 10 mM DTT, 500 μM each of dATP, dGTP, dTTP, 20 μM dCTP, 17 μM [α-^{32}P]dCTP (3000 Ci/mmol, 10 mCi/ml, NEN Life Science Products), 1 × first strand buffer (Life Technologies) and 400 units of Superscript II reverse transcriptase (Life Technologies). The reaction was carried out by incubation at room temperature for 15 min followed by heating at 37 °C for 1 h. The reaction was terminated and RNA hydrolyzed by adding EDTA (40 mM) and NaOH (400 mM) and heating at 68 °C for 30 min. The DNA products were ethanol-precipitated, washed with 70% ethanol, and dissolved in water. An excess amount of biotinylated TS transcript generated from the *Hin*dIII linearized pTOPO/G4 by T7 polymerase was added and the nucleic acid mixture ethanol-precipitated. The pellet was dissolved in 10 μl of hybridization buffer (Ambion's HybSpeed RPA kit) by heating at 95 °C for 5 min with vortexing. Hybridization was performed by incubation at 56 °C for 18 h. Streptavidin superparamagnetic beads suspension (40 μl, Sigma) was washed twice with 1.0 ml of TNE 300 (50 mM Tris–HCl, pH 7.5, 1 mM EDTA, 0.1% SDS and 300 mM NaCl) and resuspended in 100 μl TNE 300. Forty micrograms of yeast RNA was added to the suspension and incubated at 37 °C for 30 min with mixing by rotation. The pretreated streptavidin beads in 100 μl of TNE 300 were added to the hybridization reaction followed by incubation at 37 °C for 30 min with mixing by rotation. One milliliter of TNE 300 was then added and mixed well by vortexing. The supernatant was removed after placing the tube in a magnetic stand. This washing procedure was repeated five times at which time the ^{32}P-cpm in the supernatant decreased to

A. Time-course of rTSα-3' RNA induction

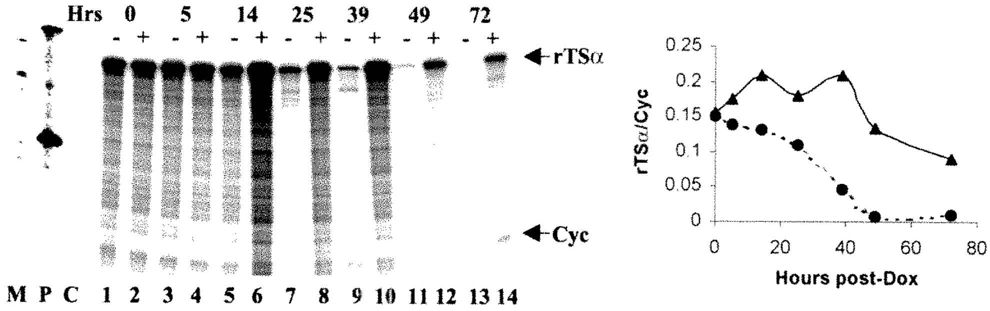

B. Effect of rTSα-3' induction on TS mRNA

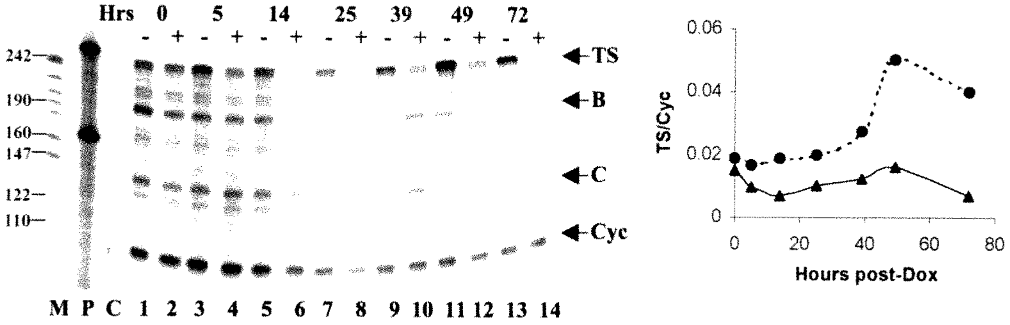

C. Effect of luciferase induction on TS mRNA

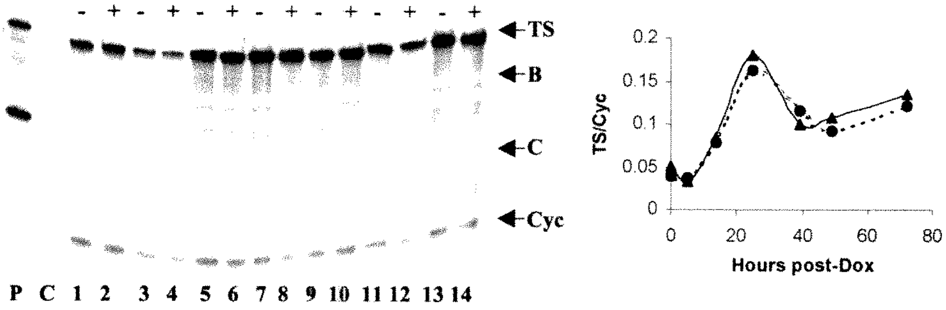

Fig. 4. Results for rTSα-3′ and luciferase transiently transfected cells. (A) Time course analysis of rTSα RNA induction in rTSα-3′ transfected cells. (B,C) Time-course analyses of TS mRNA levels in rTSα-3′ and luciferase transfected cells, respectively. Panels are labeled as in the legends to Figs. 2 and 3.

background level. The bound ^{32}P-cDNAs were then recovered by heating the beads in 40 μl of gel loading buffer (95% formamide, 18 mM EDTA, 0.025% SDS, xylene cyanol and bromophenol blue) at 100 °C for 5 min and resolved by 5% polyacrylamide/8 M urea gel electrophoresis.

3. Results

3.1. TS mRNA levels decrease while rTSα RNA levels increase as cell growth progresses from late-log to plateau phase

It has previously been demonstrated that TS activity and protein levels do not change much during the log-phase of asynchronous cultured cell growth but decrease when cells reach plateau phase growth [6,10]. To investigate whether changes in TS mRNA levels behave this way in HEp2 cells, and how rTSα RNA levels vary in relation to TS mRNA, the levels of both TS mRNA and rTSα RNA during asynchronous cell growth were determined by RPA. HEp2 cells were seeded and extracted at the indicated time points to measure the levels of TS and rTS gene expression (Fig. 2). As shown in Fig. 2A, cell growth began to reach plateau phase at 166 h after seeding. Consistent with previous findings [6,10], the levels of TS protein fluctuated within a narrow range (1.6-fold) during log-phase growth (45 to 116 h, Fig. 2B) but decreased 4-fold when cells transited from late-log to plateau phase growth (140 to 194 h, Fig. 2B). In agreement with the decline in TS protein during the transition to plateau phase, TS mRNA levels decreased 2-fold (140 to 194 h, Fig. 2C). In contrast to TS mRNA, rTSα RNA levels increased more than 3-fold when cells progressed from late-log to plateau phase (140 to 194 h, Fig. 2D). The inverse variation between the levels of TS mRNA and rTSα RNA during the late-log and plateau stages of cell growth (140 to 194 h, Fig. 2C,D) suggested a possible role of rTSα RNA in the down-regulation of TS mRNA levels. RPA for TS mRNA also showed the appearance of other fragments smaller than the full-length protected probe (Fig. 2C). Two of these fragments (B, 195 nt and C, 138 nt) were later found to correspond to in vivo TS mRNA cleavage products.

3.2. TS mRNA levels can be down-regulated by rTSα antisense RNA

To investigate the possibility that rTSα RNA can mediate a decline in TS mRNA levels, cell transfections were performed. Since we were unable to obtain a permanent stably transfected cell line expressing rTSα [23], rTSα transient co-transfections of HEp2 cells containing the Tet-On transactivator [18] with pHook-1 and rTSα or rTSαΔ3′ were carried out. Co-transfection with pHook-1 allows specific selection of transfected cells for evaluation [20]. After selection, cells were seeded in the presence or absence of Dox and extracted at different time intervals to obtain both RNA and protein. RPA clearly showed that increased expression of rTSα RNA led to decreased TS mRNA levels

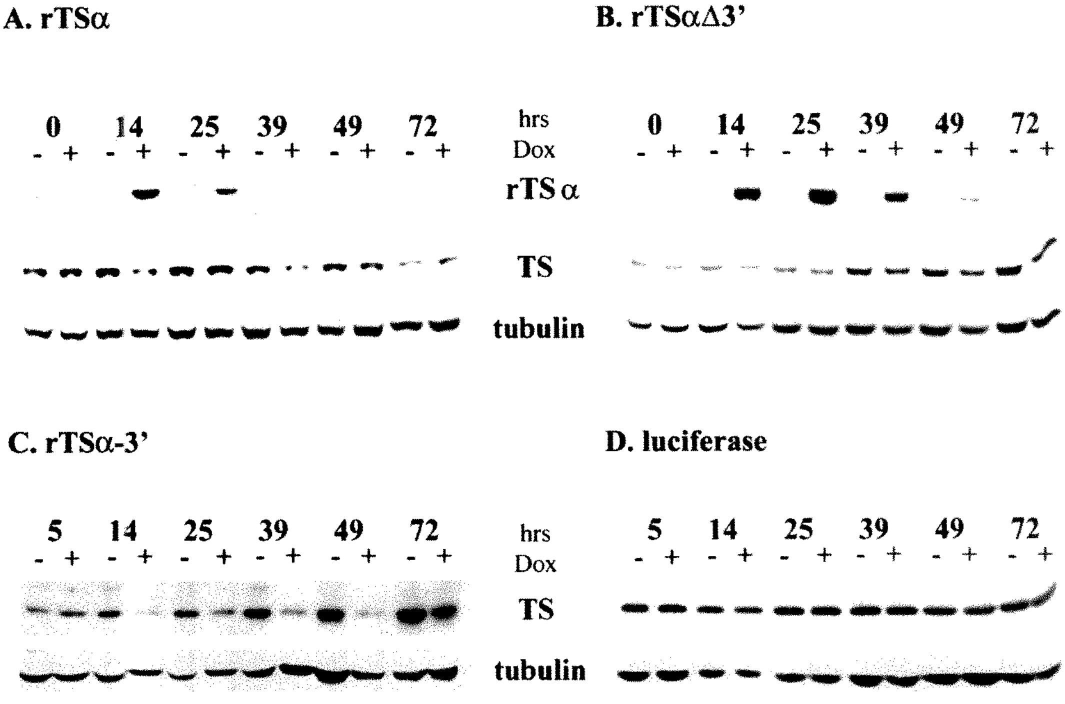

Fig. 5. Western blots showing rTSα and TS protein expression after transient transfections with rTSα (A), rTSαΔ3′ (B), rTSα-3′ (C) and luciferase (D). Each blot was sequentially probed for rTSα, TS and α-tubulin as described in Experimental procedures. rTSα was not visible in the blots shown in panels C and D.

(Fig. 3A,B). At 25 h post-Dox, the TS mRNA level decreased by 80%. TS protein levels were also down regulated by the increased expression of rTSα (Fig. 5A). After 39 h post-Dox, rTSα RNA was still inducible with Dox (Fig. 3A) but rTSα protein was no longer detected (Fig. 5A). This suggested that the down-regulation of TS mRNA levels by the induced expression of rTSα was most likely mediated by rTSα RNA rather than by rTSα protein. This conclusion is supported by data obtained from transfections performed with rTSαΔ3′, which contains the rTSα protein coding region but does not have a region of RNA antisense to TS RNA (Figs. 3C and 5B). Higher levels of rTSα protein have been induced for a longer duration in comparison with the rTSα mRNA transfected cells (Fig. 5B). The effects of rTSα protein (rTSαΔ3′) induction differed from those of rTSα mRNA. The rTSαΔ3′ transfected cells did not display significant changes in TS mRNA (Fig. 3C) but did show alterations in TS protein levels after 39 h (Fig. 5, compare B with C).

Down-regulation of TS by rTSα mRNA but not by rTSα protein suggested that the 3′-antisense portion of rTSα RNA might be sufficient for the observed negative regulation of TS mRNA. To investigate this further, transient transfections with rTSα-3′ or luciferase were performed. While increased expression of luciferase had no effect on the levels of either TS mRNA (Fig. 4C) or protein (Fig. 5D), induced expression of rTSα-3′ resulted in decreased levels of both TS mRNA (Fig. 4A,B) and protein (Fig. 5C).

3.3. *rTSα RNA induces site-specific cleavage of TS mRNA at physiologic cleavage sites*

As shown in Fig. 2C, RPA of TS mRNA in non-transfected HEp2 cells showed numerous smaller protected fragments in addition to the full-length protected fragment (251 nt). Interestingly, the intensity of two of these fragments (B, 195 nt and C, 138 nt) were increased in rTSα antisense RNA transfected cells in comparison with non-transfected cells and rTSαΔ3′ or luciferase transfected cells (Figs. 3B and 4B compared with Figs. 2C, 3C and 4C). The levels of the 195 (B) and 138 nt (C) bands were found to correlate with the levels of rTSα antisense RNA in rTSα antisense RNA transfected cells. When rTSα or rTSα-3′ transfected cells were induced to express higher levels of the antisense RNA (Figs. 3A and 4A), the levels of these two smaller fragments relative to TS mRNA levels also increased(Fig. 6). With the decline of rTSα antisense RNA in uninduced cells during 72 h after seeding rTSα or rTSα-3′ transfectants (Figs. 3A and 4A), the intensity of these two fragments also declined (Fig. 6). During the first 39 h, rTSα-3′ transfected cells displayed higher, uninduced levels of the antisense RNA compared with rTSα transfected cells (Fig. 6, compare A and B). Correspondingly, rTSα-3′ transfected cells in the absence of Dox had an increased relative abundance of these two bands (Fig. 6, compare A and B).

A. Effect of rTSα induction on levels of (B+C)

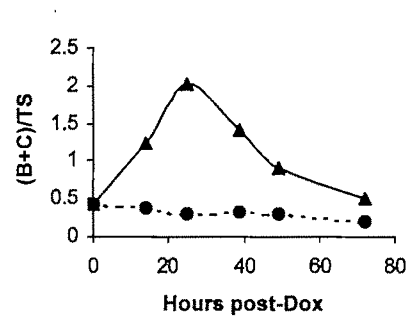

B. Effect of rTSα-3′ induction on levels of (B+C)

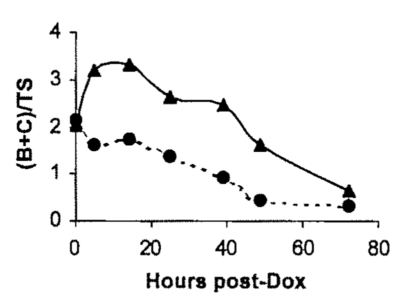

Fig. 6. Levels of two protected fragments (i.e., B and C) relative to TS mRNA from the time-course study of rTSα (A) and rTSα-3′ (B) transfected cells. The values in panels A and B are based on quantitations of the relevant protected fragments as shown in the gel images of Figs. 3B and 4B, respectively. The (B + C)/TS molar ratio is calculated as the sum of these two fragments (i.e., (B + C)/Cyc) divided by the amount of TS mRNA (i.e., TS/Cyc).

The origin of the 195 (B) and 138 (C) nt protected fragments could be cleavage of TS probe:mRNA hybrids due to mismatches or transient destabilization (i.e., breathing) during RPA or they could represent in vivo cleaved TS mRNA molecules. Resolving these possibilities is important because the complementarity of rTSα and TS RNAs suggests that rTSα:TS RNA hybrids could form in vivo and serve as substrates for adenosine deaminases that act on RNA (ADAR) [16,24,25]. Our laboratory has identified five editing sites (adenosine to inosine) in TS pre-mRNA in the region of TS RNA complementary to rTSα RNA (unpublished data). One editing site is predicted to generate a mismatch with the ^{32}P-labeled probe that would produce a 138 (C) nt protected fragment in the RPA (Fig. 1). The abundance of this protected fragment along with the 195 (B) nt fragment increased in response to elevated levels of rTSα antisense RNA in rTSα and rTSα-3′ transfected cells (Fig. 7), suggesting that the 138 (C) nt fragment could arise by cleavage at an RNA editing site.

To verify that these two species (B and C) are not cleavage products resulting from RNA duplex breathing during RPA, RNase digestions were performed at different

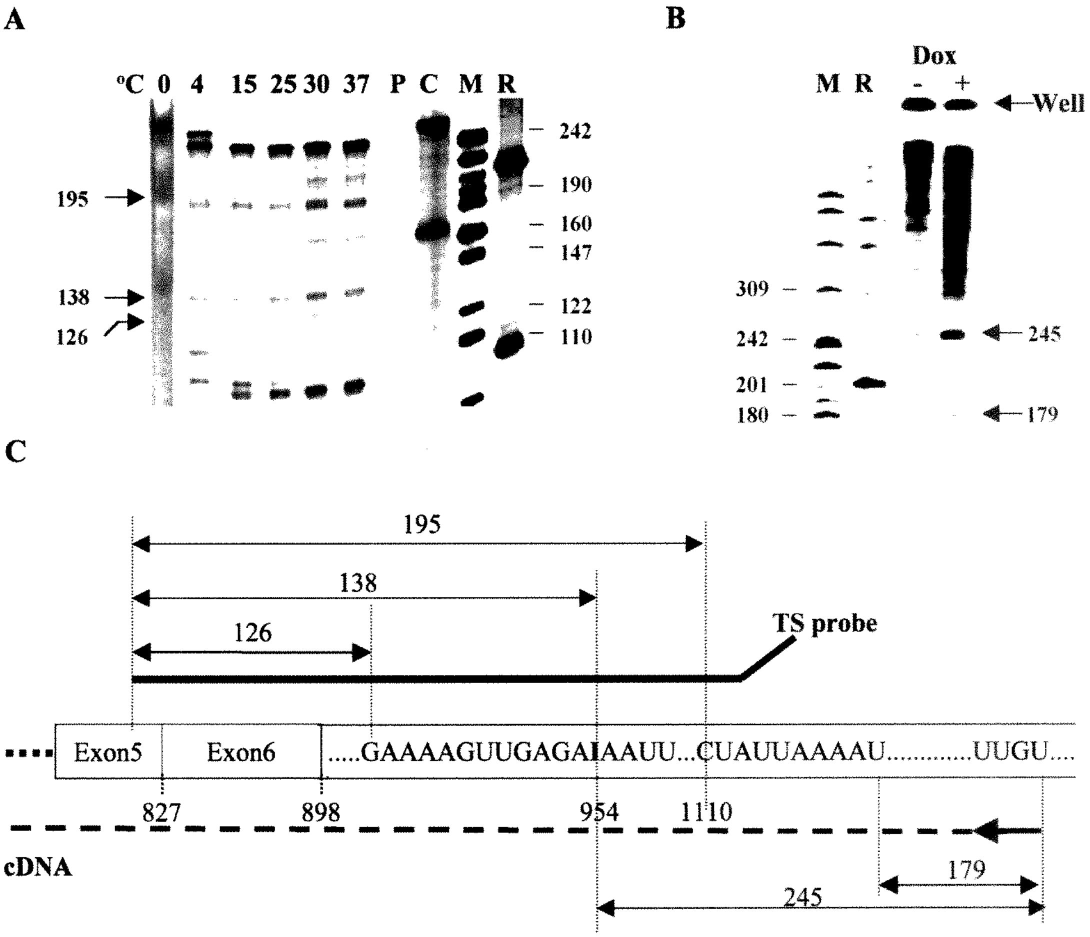

Fig. 7. (A) Results of RPA for TS mRNA performed with varying stringency of RNase digestion. Cellular RNA from rTSα-3′ transfected cells was subjected to RPA as described in Experimental procedures except that the RNase digestion step was performed over a range of temperatures (0–37 °C) as indicated. (B) Results of primer extension assays. Assays were performed as described in Experimental procedures to detect in vivo generated TS mRNA fragments from rTSα-3′transfected cells (with or without Dox). (C) Schema showing the protected fragments (195 and 138 nt) of RPA and their corresponding ^{32}P-cDNA products (179 and 245 nt) produced by the primer extension.

stringencies by altering the temperature (0 to 37 °C). As shown in Fig. 7A, the amounts of these two fragments relative to TS mRNA remained unchanged over a wide range of temperatures. The levels were relatively unchanged even at 4 °C where the unprotected 3′-overhang of the TS probe:TS mRNA duplex was not digested, leaving the entire probe intact. This result suggests that the protected fragments detected by our RPA are less likely to have been produced in vitro by RNase digestions of unstable duplexed regions of the TS probe:mRNA hybrids.

The likelihood that TS mRNAs are cleaved in vivo in response to increased levels of rTSα antisense RNA was investigated further using a primer extension assay. Cellular RNA extracted from rTSα-3′ transfected cells (39 h post-Dox) were reverse transcribed using a TS gene specific primer (Fig. 1) in the presence of [α-^{32}P]dCTP. The ^{32}P-cDNA products are expected to have lengths reflecting TS in vivo cleavage sites. If TS mRNA is cleaved in vivo, a limited number of discrete ^{32}P-cDNA fragments should be detectable provided that the cleaved RNA molecules are relatively stable during the time course of study. To minimize the background generated from nonspecific priming, TS ^{32}P-cDNAs were selected by hybridization to biotinylated TS RNA prepared by in vitro transcription. Hybridized TS ^{32}P-cDNAs were then purified by affinity chromatography with immobilized streptavidin. As shown in Fig. 7B, increased amounts of TS ^{32}P-cDNAs of 245 and 179 nt are observed for primer extension performed with RNA from transfected cells induced to express rTSα antisense RNA. The size of the ^{32}P-cDNA (245 nt) is that for a cDNA produced from TS mRNA cleaved at one of the two editing sites identified in exon 7 of TS pre-mRNA (unpublished data) (Fig. 7C). This ^{32}P-cDNA corresponds to the 138 (C) nt RPA protected fragment (B and C in Fig. 4B). Therefore, TS mRNA was cleaved in vivo at an editing site in response to rTSα antisense RNA. The 179 nt ^{32}P-cDNA was the result of extension to an adenosine site in an AU rich region of TS mRNA as shown in Fig. 7C. This ^{32}P-cDNA corresponds to an in vivo cleaved TS mRNA molecule with a cleavage site 9 nt downstream from the site that would generate the 195 nt protected fragment (B) observed in the RPA. This difference probably reflects the AU-rich nature of the intervening region between these two sites (Fig. 7C) that likely gets degraded during the RPA (see Discussion).

4. Discussion

The rTS gene was originally identified by sequencing a cDNA clone for a naturally occurring antisense RNA to human TS mRNA [14]. These two genes are located at the same locus of chromosome 18 [26]. The rTS gene overlaps the 3′ end of the TS gene [27], and is transcribed convergently with TS. Through alternative splicing, the rTS gene transcript produces two mRNAs, rTSα and rTSβ [28,29]. The 3′ UTR of rTSα RNA is complementary to TS RNA near its 3′ end including exon 7 and part of the last intron (Fig. 1). As an initial investigation into the possible role of rTSα RNA in the growth regulation of TS gene expression, we first evaluated rTSα RNA and TS mRNA levels during cell growth to determine their relationship. An inverse relationship was found as cells progressed from late-log to plateau phase (140 to 194 h in Fig. 2: C vs. D). In agreement with the decline of TS mRNA levels, TS protein levels also decreased (Fig. 3B). Although rTSα RNA levels increased as cell growth progressed from late-log to plateau phase, rTSα protein remained undetectable (data not shown). The low-level expression of rTSα protein in HEp2 cells is consistent with our previous observations for other human tumor cell lines [21]. Because of the complementarity between these two RNAs, the association between increased rTSα RNA levels and decreased TS mRNA levels suggests that rTSα RNA might be involved in the down-regulation of TS gene expression.

The possibility that rTSα RNA down-regulates TS mRNA was further investigated through transient transfections. Transient transfection experiments performed with rTSα mRNA, rTSαΔ3′, rTSα-3′ and luciferase as the inducible genes demonstrate that rTSα antisense RNA can down-regulate the levels of TS mRNA. Increased expression of rTSα mRNA or rTSα-3′ but not rTSαΔ3′ or luciferase (Figs. 3 and 4) resulted in decreased TS mRNA levels. These results indicate that the antisense RNA portion of rTSα RNA is both necessary and sufficient for the observed down-regulation of TS mRNA levels.

In addition to the expected protected fragment (251 nt) corresponding to a perfect hybrid of the ^{32}P-probe with TS mRNA, RPA of TS mRNA displayed other smaller fragments. Among these smaller fragments, two discrete bands (B, 195 nt and C, 138 nt) are of particular interest because their intensities increased in the rTSα antisense RNA transfected cells (Figs. 3B and 4B compared with Figs. 2C, 3C and 4C). Further investigations into the nature of these two fragments shed some light on the mechanism for rTSα antisense RNA mediated down-regulation of TS mRNA levels in transiently transfected cells and nontransfected cells as well. There are three possible sources for the appearance of these two bands. First, they might result from the cleavage at some transiently destabilized regions of the TS probe:mRNA duplex during RNase digestion. If this is the case, the levels of these two bands relative to TS mRNA should be identical among all the samples since they were subjected to the same RPA procedure. Since their relative abundance increased in response to the increased levels of rTSα antisense RNA in transfected cells (Fig. 7) and were not affected by altering the stringency of the RNase digestion step of the RPA (Fig. 7A), this possibility can be ruled out. Secondly, some mismatches in the TS probe:mRNA duplex might be susceptible to RNase digestion thus leading to the production of partial-length protected probes. In rTSα antisense RNA transfected cells, the correlation between the increased intensity of these two fragments and the elevated levels of rTSα antisense RNA suggests that the antisense RNA might induce TS mRNA modifications leading to mismatches in the TS probe:mRNA hybrid. This possibility is supported by the finding that TS pre-mRNA is edited (adenosine to inosine) at five sites across the intron 6–exon 7 junction [30]. One editing site in the region targeted by the ^{32}P-labeled TS probe (Fig. 1B) is predicted to generate a mismatch that would produce a 138 nt protected fragment upon cleavage in the RPA (Fig. 1B). Finally, it is also possible that these two fragments might result from in vivo cleaved TS mRNA molecules. This possibility is more likely because the relative intensity of these two bands remained at a similar level even when RNase digestions were performed at temperatures when the mismatched duplexes should be stabilized (Fig. 7A). The detection of elevated levels of a 245 nt ^{32}P-cDNA as a result of primer extension of TS mRNA (Fig. 7B), corresponding to the 138 nt protected fragment in RPA (Fig. 7C), demonstrated that TS mRNA was indeed cleaved in vivo and that cleavage occurred predominantly at this editing site. Another ^{32}P-cDNA of 179 nt corresponds to an adenosine site of an AU-rich region in TS mRNA (Fig. 7B,C). The RNA fragment upstream of this in vivo cleavage site was detected by RPA as the protected 195 nt fragment either because the AU-rich end of the probe:mRNA duplex was susceptible to RNase digestion or because the AU-rich region was degraded in vivo subsequent to cleavage. The 126 nt fragment observed in RPA may be derived from the 138 nt fragment due to RNase-susceptibility of the AU-rich region (AAAAGUUGA) at the end of the duplex formed between the TS probe and mRNA (Fig. 7C). This appears to be likely since the 126 nt fragment diminished in abundance with decreasing temperatures during RNase digestion (Fig. 7A). Consistent with the RPA data, increased expression of rTSα antisense RNA led to increased levels of both ^{32}P-cDNA fragments of 245 and 179 nt, indicating that more TS mRNA molecules were cleaved in vivo in response to the elevated antisense RNA levels.

The 195 nt (B) and 138 nt (C) protected fragments in RPA of TS mRNA were also observed in the nontransfected

HEp2 cells (Fig. 2C). This suggests that the cleavage of TS mRNA induced by rTSα antisense RNA in the transient transfection assays also occurs in the more physiological environment of nontransfected cells. One possible mechanism for the demonstrated down-regulation of TS mRNA levels by rTSα RNA is through duplex formation between their complementary regions. In vivo hybrids have been reported between antisense n-cym RNA and a subset of sense n-myc RNA [31] and in the case of mbp sense and antisense transcripts [32]. The current study provides the evidence for one possible consequence of such duplex formation, site-specific cleavage of TS mRNA. Antisense (PSV-A) RNA-mediated RNA hybrid degradation resulting in down-regulation of the sense RNA has also been implicated in *Dictyostelium* [33]. It was thought that dsRNA-specific RNases might exist in vivo and are responsible for the rapid degradation of duplex RNAs. Indeed, enzymes with this specificity have been described and partially purified [34–36] but their physiological functions remain to be established.

In summary, expression of rTSα RNA down-regulates TS mRNA through an antisense-mediated mechanism. The levels of rTSα antisense RNA and TS mRNA vary inversely when cell growth progresses from late-log to saturation phase (Fig. 2C,D). Additionally, increased expression of the antisense RNA portion of rTSα but not rTSα protein leads to decreased levels of TS mRNA (Figs. 3 and 4). One of the contributors for this decline of TS mRNA is increased site-specific cleavage, particularly at a TS RNA editing site (Fig. 7), which also occurs in nontransfected cells. Therefore, the negative regulation of TS mRNA levels by rTSα RNA is likely mediated by increased TS RNA editing followed by cleavage.

5. Conclusions and perspectives

Based upon the data presented here and the previous observation that most rTSα RNA is nuclear, we suggest that rTSα RNA could play a role in the down-regulation of TS RNA in vivo. While induction of transfected rTSα antisense RNA can cause the down-regulation of TS mRNA, we suspect that the rTSα RNA acts to cause RNA editing with either simultaneous or subsequent cleavage of the TS pre-mRNAs at the editing site(s) in vivo. The implications for chemotherapy will depend upon the mechanism used for the activation of this pathway. For example, if the antisense RNA is constantly in excess to the TS pre-mRNA in the nucleus, then activation of this pathway by some signaling mechanism suggests that this could be exploited in combination with small molecule inhibitors of TS to help prevent new synthesis of TS protein (dependent upon turnover of the TS mRNA). Our laboratory is actively pursuing this possibility.

Acknowledgements

This work was supported by PHS grants CA 57634, CA80684, CA86876 awarded to BJD and core grant CA 16056 from the National Cancer Institute.

References

[1] P.V. Danenberg, Biochim. Biophys Acta 473 (1977) 73–79
[2] W.L Washtien, Mol. Pharmacol 25 (1984) 171–177
[3] P.G Johnston, J.C Drake, J Trepel, C.J Allegra, Cancer Res 52 (1992) 4306–4312
[4] A.M Ali Imam, P.H Crossley, A.L Jackman, P.F.R Little, J Biol Chem 262 (1987) 7368–7373
[5] D Ayusawa, K. Shimizu, H. Koyama, S. Kaneda, K. Takeishi, T Seno, J Mol Biol 190 (1986) 559–567
[6] E Cadman, R. Heimer, Cancer Res 46 (1986) 1195–1198
[7] A.H Conrad, J Biol Chem 246 (1971) 1318–1323.
[8] A.H. Conrad, F.H. Ruddle, J Cell Sci 10 (1972) 471–486
[9] L.G Navalgund, C Rossana, A.J Muench, L.F Johnson, J Biol Chem 255 (1980) 7386–7390
[10] B.C Pestalozzi, C.J McGinn, T.J Kinsella, J.C Drake, M.C Allegra, C.J Allegra, P.G Johnston, Br J. Cancer 71 (1995) 1151–1157
[11] C.-H Jenh, P.K Geyer, L.F Johnson, Mol. Cell Biol 5 (1985) 2527–2532
[12] L.F Johnson, J Cell Biochem 54 (1994) 387–392
[13] J. DeGregori, T Kowalik, J.R Nevins, Mol Cell Biol 15 (1995) 4215–4224.
[14] B.J Dolnick, Nucleic Acids Res 21 (1993) 1747–1752
[15] E.G Wagner, R.W. Simons, Annu Rev Microbiol. 48 (1994) 713–742
[16] B.J Dolnick, Pharmacol Ther 75 (1997) 179–184
[17] C Vanhee-Brossollet, C Vaquero, Gene 211 (1994) 1–9
[18] M. Gossen, S Freundlieb, G Bender, G Muller, W Hillen, H Bujard, Science 268 (1995) 1766–1769
[19] B.J Dolnick, Z.G Zhang, J.D Hines, Y.M Rustum, Oncol Res 4 (1992) 65–72.
[20] J.D. Chesnut, A.R Baytan, M Russell, M.P Chang, A Bernard, I.H Maxwell, J.P. Hoeffler, J Immunol Methods 193 (1996) 17–27
[21] B.J Dolnick, K Lu, M.B Yin, Y.M Rustum, Adv Enzyme Regul. 37 (1997) 95–109
[22] B Haendler, E. Hofer, Eur J Biochem 190 (1990) 477–482
[23] J. Chu, B.J Dolnick, in Proc AACR, vol 39, 1998, Cadmus, New Orleans, p 257.
[24] B.L Bass, Trends Biochem Sci 22 (1997) 157–162
[25] B.L Bass, K Nishikura, W Keller, P.H. Seeburg, R.B Emeson, M.A O'Connell, C.E. Samuel, A Herbert, RNA 3 (1997) 947–949
[26] B.J Dolnick, A.R. Black, P.M Winkler, K. Schindler, C.T Hsueh, Adv. Enzyme Regul 36 (1996) 165–180
[27] B Dolnick, J Su, GenBank X89602, 2000
[28] B.J Dolnick, A.R Black, Cancer Res 56 (1996) 3207–3210
[29] A.R. Black, B.J Dolnick, Cancer Res 56 (1996) 700–705
[30] B.J Dolnick, in Proc AACR, vol 41, 2000, Cadmus, San Francisco, p 945
[31] G. Krystal, B Armstrong, J Battey, Mol Cell Biol 10 (1990) 4180–4191
[32] H Okano, J Aruga, T Nakagawa, K Mikoshiba, J Neurochem 56 (1991) 560–567
[33] M. Hildebrandt, W Nellen, Cell 69 (1992) 197–204.
[34] S.H Hall, R.J Crouch, J Biol Chem 252 (1977) 4092–4097
[35] J.M Meegan, P.I. Marcus, Science 244 (1989) 1089–1091
[36] J Rech, G Cathala, P Jeanteur, Nucleic Acids Res 3 (1978) 2055–2065

ELSEVIER

Biochimica et Biophysica Acta 1587 (2002) 194–205

BIOCHIMICA ET BIOPHYSICA ACTA
BBA
www.bba-direct.com

Review

Induction of thymidylate synthase as a 5-fluorouracil resistance mechanism

G.J. Peters [a,*], H.H.J. Backus [a], S. Freemantle [b], B. van Triest [a], G. Codacci-Pisanelli [a], C.L. van der Wilt [a], K. Smid [a], J. Lunec [b], A.H. Calvert [b], S. Marsh [c], H.L. McLeod [c], E. Bloemena [d], S. Meijer [e], G. Jansen [f], C.J. van Groeningen [a], H.M. Pinedo [a]

[a]Department of Medical Oncology, VU University Medical Center, P.O. Box 7057, 1007 MB Amsterdam, The Netherlands
[b]Cancer Research Unit, The Medical School, University of Newcastle upon Tyne, NE2 4HH Newcastle upon Tyne, UK
[c]Division of Molecular Oncology, Washington University School of Medicine, CSRBNT 1021,
Campus Box 8069, 660 S Euclid Ave, St Louis, MO 63110, USA
[d]Department of Pathology, VU University Medical Center, P.O. Box 7057, 1007 MB Amsterdam, The Netherlands
[e]Department of Surgery, VU University Medical Center, P.O. Box 7057, 1007 MB Amsterdam, The Netherlands
[f]Department of Rheumatology, VU University Medical Center, P.O. Box 7057, 1007 MB Amsterdam, The Netherlands

Received 24 January 2002, accepted 24 January 2002

Abstract

Thymidylate synthase (TS) is a key enzyme in the de novo synthesis of 2′-deoxythymidine-5′-monophosphate (dTMP) from 2′-deoxyuridine-5′-monophosphate (dUMP), for which 5,10-methylene-tetrahydrofolate (CH_2-THF) is the methyl donor. TS is an important target for chemotherapy; it is inhibited by folate and nucleotide analogs, such as by 5-fluoro-dUMP (FdUMP), the active metabolite of 5-fluorouracil (5FU). FdUMP forms a relatively stable ternary complex with TS and CH_2THF, which is further stabilized by leucovorin (LV). 5FU treatment can induce TS expression, which might bypass dTMP depletion. An improved efficacy of 5FU might be achieved by increasing and prolonging TS inhibition, a prevention of dissociation of the ternary complex, and prevention of TS induction. In a panel of 17 colon cancer cells, including several variants with acquired resistance to 5FU, sensitivity was related to TS levels, but exclusion of the resistant variants abolished this relation. For antifolates, polyglutamylation was more important than the intrinsic TS level. Cells with low p53 levels were more sensitive to 5FU and the antifolate raltitrexed (RTX) than cells with high, mutated p53. Free TS protein down-regulates its own translation, but its transcription is regulated by E2F, a cell cycle checkpoint regulator. Together, this results in low TS levels in stationary phase cells. Although cells with a low TS might theoretically be more sensitive to 5FU, the low proliferation rate prevents induction of DNA damage and 5FU toxicity. TS levels were not related to polymorphisms of the TS promoter. Treatment with 5FU or RTX rapidly induced TS levels two- to five-fold. In animal models, 5FU treatment resulted in TS inhibition followed by a two- to three-fold TS induction. Both LV and a high dose of 5FU not only enhanced TS inhibition, but also prevented TS induction and increased the antitumor effect. In patients, TS levels as determined by enzyme activity assays, immunohistochemistry and mRNA expression, were related to a response to 5FU. 5FU treatment initially decreased TS levels, but this was followed by an induction, as seen with an increased ratio of TS protein over TS-mRNA. The clear retrospective relation between TS levels and response now forms the basis for a prospective study, in which TS levels are measured before treatment in order to determine the treatment protocol. © 2002 Elsevier Science B.V. All rights reserved.

Keywords Thymidylate synthase; p53, E2F; 5-fluorouracil; Antifolate

---

Abbreviations: 5FU, 5-fluorouracil; FUdR, 5-fluoro-2′-deoxyuridine, TS, thymidylate synthase; TSER, TS enhancer regions, FPGS, folylpolyglutamate synthetase, dUMP, 2′-deoxyuridine-5′-monophosphate, FdUMP, 5-fluoro-dUMP; dTMP, 2′-deoxythymidine-5′-monophosphate; CH_2-H_4-folate, N^5,N^{10}-methylene-5,6,7,8-tetrahydrofolate, LV, leucovorin; RTX, raltitrexed, *N*-[5-(*N*-(3,4-dihydro-2-methyl-4-oxoquinazolin-6-yl-methyl)-amino)-2-thenyl)]-L-glutamic acid (Tomudex, ZD1694); ALIMTA, multitargeted antifolate, *N*-(4-(2-(2-amino-4,7-dihydro-4-oxo-3*H*-pyrrolo[2,3-D]pyrimidin-5-yl)-ethyl)-benzoyl]-L-glutamic acid (LY231514), GW1843U89, (*S*)-2-(5-(((1,2-dihydro-3-methyl-1-oxobenzo(f)quinazolin-9-yl)-methyl)-amino)-1-oxo-2-isoindolinyl)-glutaric acid, AG337, nolatrexed, 3,4-dihydro-2-amino-6-methyl-4-oxo-5-(4-pyridylthio)-quinazoline (Thymitaq), SRB, sulforhodamine B, MTT, 3-[4,5-dimethylthiazol-2-yl]-2,5-diphenyl tetrazolium bromide, CDK, cyclin-dependent kinase, DPD, dihydropyrimidine dehydrogenase; wt-p53, wild type p53; mt-p53, mutant p53

[*] Corresponding author. Tel +31-20-4442633; fax: +31-20-4443844

E-mail address gj.peters@vumc.nl (G.J. Peters)

0925-4439/02/$ - see front matter © 2002 Elsevier Science B.V. All rights reserved
PII: S0925-4439(02)00082-0

1. Introduction

Thymidylate synthase (TS) is a key enzyme in the de novo synthesis of 2′-deoxythymidine-5′-monophosphate (dTMP). TS catalyzes the methylation of 2′-deoxyuridine-5′-monophosphate (dUMP) to dTMP for which 5,10-methylene-tetrahydrofolate (CH_2-THF) is the methyl donor. Detailed characteristics of the TS enzyme have been described by others [1,2]. TS is an important target for chemotherapy. It is inhibited by analogs of the folate cofactor, such as raltitrexed (RTX) and ALIMTA, and the nucleotide co-factor, such as 5-fluoro-dUMP (FdUMP), which is the active metabolite of 5-fluorouracil (5FU). FdUMP is a competitive inhibitor with a K_i in the low nanomolar range. Inhibition of TS by FdUMP is considered to be the main mechanism for the action of 5FU (Fig. 1). The inhibition by FdUMP is mediated by the formation of a covalent ternary complex between FdUMP, TS and CH_2-THF, while the retention of inhibition is also dependent on the ratio between free dUMP and FdUMP levels [3,4]. A low sensitivity to 5FU has been related to a rapid disappearance of FdUMP. A high dUMP concentration or a limited FdUMP binding to TS may reduce retention of TS inhibition.

Several mechanisms of resistance to 5FU have been attributed to TS (Table 1) [5]. The stability of the ternary complex is highly dependent on the availability of CH_2-THF or one of its polyglutamates [4]. LV can increase the availability of CH_2-THF (Fig. 1). After transfer across the membrane, mediated by the reduced folate carrier [6], LV will be metabolized to CH_2-THF [7], which will be polyglutamylated leading to enhanced inhibition of TS [8]. A decreased activity of folylpolyglutamate synthetase (FPGS) [9] and altered binding of FdUMP to TS [10–12] have been associated with acquired 5FU resistance. In the absence of CH_2-THF or one of its polyglutamates [5,12–14], FdUMP forms an unstable binary complex, which results in poor inhibition. Disturbed folate pools [14] (usually decreased) and a high level of enzyme before treatment lead to intrinsic resistance [5,11,12]. Gene amplification of TS and mutations in the gene lead to acquired resistance [12,13,15]. This paper focuses on the role of intrinsic TS levels and that of TS induction in 5FU resistance and on their regulation in various systems.

Table 1
Mechanisms of resistance to 5FU

(A) Decreased accumulation of activated metabolites
(a) Decreased activation
(b) Increased inactivation
(c) Increased inactivation of 5FU nucleotides
(B) Target-associated resistance
(a) Decreased RNA effect
(b) Altered effect on thymidylate synthase
• Aberrant enzyme kinetics
• Increased dUMP levels
• Decreased FdUMP accumulation
• Decreased stability of ternary complex
• Depletion of intracellular folates
• Decreased polyglutamylation of folates
• Recovery and enhanced enzyme synthesis
• Gene amplification
• Enzyme induction
(C) Pharmacokinetic resistance
(a) The drug does not reach the tumor
(b) Disease state affects drug distribution
(c) Increased elimination

Modified from Ref [5]

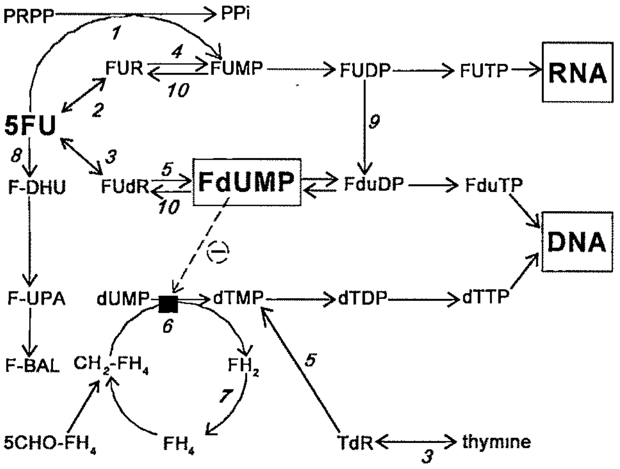

Fig 1. Metabolic conversions of 5FU The enzymes involved in these reactions are: (1) orotate phosphoribosyltransferase (OPRT), (2) uridine phosphorylase (UP), (3) thymidine phosphorylase (TP), (4) uridine kinase (UK), (5) thymidine kinase 1 (TK1), (6) thymidylate synthase (TS), (7) dihydrofolate reductase, (8) dihydropyrimidine dehydrogenase (DPD); (9) ribonucleotide reductase; (10) 5′-nucleotidases and phosphatases Metabolic pathways are depicted as solid lines The inhibition of TS by FdUMP is depicted as a broken line with a minus sign.

2. Experimental procedures

2.1. Cell lines and tissues

The sources of the cell lines have been described previously [16,17]. Sensitivity to 5FU and antifolates was determined in 96-wells plates using either the sulforhodamine B (SRB) or 3-[4,5-yl]-2,5-diphenyl tetrazolium bromide (MTT) assays as described previously [16,18,19]. In some cell lines, antifolates cause swelling of the cells leading to an increased protein content, which interferes with the protein-based SRB assay. In case this swelling was observed, we used the MTT assay for antifolates. 5FU did not cause swelling. For all cell lines, we added drugs 24 h after plating of the cells. Cells were exposed for 72 h and linearity of growth was assured for untreated cells during this 72-h period.

For enzyme assays, immunoblotting, RNA and DNA extraction, all cell lines were cultured in 75-cm^2 flasks and harvested in the logarithmic growth phase by trypsinization, then washed and counted. Thereafter, the cell pellets were frozen in liquid nitrogen.

Tumors from animals were removed before and at different time points after drug treatment and immediately frozen in liquid nitrogen. Tumors (primary tumors and liver metastases) from patients were removed during surgery (after administration of 5FU) and immediately frozen in liquid nitrogen as described previously [20]. Frozen tissues were pulverized [21] and the still frozen powder was further processed in appropriate buffer either for enzyme assays or RNA/DNA extraction.

2.2. *TS enzyme assays*

TS assays in cell lines were performed as described previously [16]. We used two assays. One assay measured the number of free FdUMP binding sites of TS by estimation of the binding capacity of ^{3}H-FdUMP. The other determined the catalytic activity of TS by means of [^{3}H]-H_2O-release during the TS catalyzed conversion of ^{3}H-dUMP into dTMP. Measurement of TS levels in tissues was slightly different from that in cell lines, which has been previously described [20,22,23]. In tissues from 5FU-treated patients and animals, we measured TS levels in the extracts containing the non-dissociated ternary complex, which enabled TS inhibition to be expressed as the residual TS catalytic activity (TS-residual), and as the number of free binding sites for FdUMP (TS-free). We also dissociated the ternary complex, which enabled the measurement of total catalytic activity (TS-total) and all available FdUMP binding sites (TS-tot). The ratios between TS-residual/TS-total and TS-free/TS-tot (× 100%) was considered as the percentage inhibition.

2 3. *TS immunoblotting*

Protein expression was estimated using Western blotting as described earlier [24,25]. Proteins were separated by size through a 10% SDS-polyacrylamide gel and were electrophoretically transferred to a nitrocellulose membrane, on which they were detected using horseradish peroxidase (HRP)-conjugated secondary antibodies directed against primary antibodies. The HRP reaction was visualized by means of chemiluminescence and autoradiography.

2.4. *TS immunohistochemistry*

Sources of primary and secondary antibodies, staining procedures and evaluation of staining have been described previously [26,27]. A pathologist and two investigators investigated all slides. Statistical evaluation was performed using the nonparametric Kruskal–Wallis and Mann–Whitney *U* ranking test. All values were based on two-tailed statistical analysis. Survival was evaluated using Kaplan–Meier curves. All statistical procedures were carried out with SPSS 9.0 (SPSS, Chicago, IL, USA).

2.5. *TS-mRNA expression*

Total RNA was isolated from pulverized tissues using the RNAzole method and purity was checked by UV absorbance and electrophoresis of 1 μg RNA on a neutral 1.2% agarose gel. cDNA was synthesized from 5 μg of total RNA with 6 μg of random primers using M-MLV reverse transcriptase as described previously [28]. PCR amplifications were carried out in a Perkin/Elmer/Cetus DNA thermal cycler. A total of 25 cycles was used, in which each cycle consisted of 1 min primer denaturation at 94 °C, 1 min of primer annealing at 55 °C, and 1 min of primer extension at 72 °C. The cDNA samples were diluted depending on transcript abundance, while three cDNA dilutions were used for each primer in order to verify that measurements were taken in the linear phase of the reaction A detailed description of the procedure as well as the sequences of the primers for the target gene TS and the reference genes β-actin and 18S are described previously [28].

2 6 *TS enhancer region (TSER)*

TSER was amplified [29,30] from genomic DNA with the sense primer (5′-GTGGCTCCTGCGTTTCCCCC-3′ and the antisense primer: 5′-GCTCCGAGCCGGCCACAGGCATGGCGCGG-3′). PCR was carried out in 1 × PCR buffer (50 mM KCl, 10 mM Tris pH 9, 0.1% Triton X-100), containing 1.25 mM magnesium chloride, 10% DMSO, 0.2 mM dNTPs, 0.2 ng each primer, 50–100 ng genomic DNA and 2.5 units of Taq in a 50 μl reaction. Samples were overlaid with mineral oil and amplified in a thermal cycler for 30 cycles. Each cycle was 1 min at 94 °C, 1 min at 60 °C and 2 min at 72 °C, and the final cycle was maintained at 72 °C for 5 min. PCR products were separated by electrophoresis on a 4% agarose gel and visualized with ethidium bromide.

3. TS and p53 levels in relation to sensitivity to 5FU and antifolates

3.1. *Physiological regulation of TS levels*

Expression of TS under physiological conditions is related to the cell cycle, and has a high activity during the S-phase [31], but decreases when the cells do not proliferate [32]. Various transcription factors and cell cycle-dependent kinases (CDK) control the increase in TS levels in the cell cycle. Cell cycle progress through the G1/S checkpoint is tightly regulated by cyclin/CDK complexes, which are activated by phosphorylation. Phosphorylation of various cyclins-CDKs can subsequently hyperphosphorylate the Rb and E2F complex, which results in the release of E2F from phosphorylated Rb. The free transcription factor E2F can subsequently activate the transcription of several DNA synthesis-dependent proteins such as TS.

TS levels are also controlled at the level of translation. The translation of the TS-mRNA appears to be controlled by its end product, the TS protein, in an autoregulatory manner. This phenomenon possibly contributes to the large variation of TS levels not only in normal tissues, but also between tumors and within tumors. TS protein cannot only regulate its own translation but also that of other proteins, such as p53 [33]. In addition, wild-type p53 (wt-p53) protein can also inhibit TS promoter activity [34]. Thus, regulation of TS expression is a very complicated process, which may even be more disrupted (more induction) in cells with mutated p53 (mt-p53) than with wt-p53 (low induction). Although many nucleotide synthesizing enzymes are increased in tumors compared to their normal counterparts [35], the increase of TS levels in, e.g. colon tumors compared to normal colon mucosa, varies from negligible to many fold higher [36,37], and is even higher in metastases compared to primary colon tumors [38,39]. This increase was associated with an increase in p53 and cell cycle genes. Consequently, in colon cancer cell lines and tumors, a large variation in TS levels has been observed [4,12,16–18,24,25,39–41].

3.2. Intrinsic and amplified TS levels in relation to sensitivity to 5FU and antifolates

Since TS is the target for 5FU, it was hypothesized that the large variation in TS levels would be related to 5FU sensitivity. Indeed, in a small panel of cell lines consisting of several 5FU-resistant cells and some nonselected cells, Johnston et al. [17] found a relation between TS levels and 5FU sensitivity, but omission of the resistant lines weakened this relation considerably. In a limited number of cell lines with a different histological origin, Beck et al. [40] found a weak correlation ($r^2=0.22$, $P=0.042$) between 5FU sensitivity and TS levels, but in the subpanel of colon cancer cells this relation was not present.

Recently, we reported TS levels in a panel of 13 unselected colon cancer cell lines, not including cells with induced resistance. The TS catalytic activity varied from 62 to 777 pmol/h/10^6 cells, while the number of FdUMP binding sites varied from 203 to 2758 fmol/mg protein [16]. This panel has now been extended with several cell lines with intrinsic TS levels in the same range and with cell lines with induced resistance to 5FU described by Johnston et al. [17]. In this panel, levels of the TS catalytic activity were in a range up to 51,000 pmol/h/10^6 cells, and the number of FdUMP binding sites in a range up to 6800 fmol/mg protein (Fig. 2). In this extended panel including the resistant cells, the number of FdUMP binding sites correlated positively with the sensitivity to 5FU ($r=0.864$; $P<0.0001$). However, when the resistant cell lines were excluded (FdUMP binding sites varying from 203–2758 fmol/mg protein; 15 cell lines), no relation between TS levels and 5FU sensitivity could be found. As shown in our previous results, sensitivity to the antifolates RTX, ALIMTA, AG337 and GW1843 was not related to the TS levels [16]. However, the activity of FPGS was still positively correlated to sensitivity to both RTX and ALIMTA. TS catalytic activity was significantly correlated to both FdUMP binding (Fig. 2) and TS protein measured by Western blotting as described previously [16,17]. TS levels were also related to TS-mRNA expression. Recently, Grem et al. [41] also observed a lack of correlation between 5FU sensitivity and TS levels in the National Cancer Institute 60-cell line panel, either evaluated as TS protein or TS-mRNA expression. This lack of correlation might have several reasons, such as the relatively short drug exposure time (48 h), after which growth inhibition was determined. This continuous presence of 5FU possibly leads to a complete inhibition of TS independently of the endogenous TS levels as was observed in cells with induced TS [32]. Thus, growth inhibition might be dependent on additional parameters, such as the extent of induction of DNA damage [42]. Alternatively, sensitivity to 5FU might also be dependent on other parameters in addition to TS levels, such as toxicity mediated by incorporation of 5FU into RNA. Recently, Scherf et al. [43] investigated a large panel of mechanistically different drugs using cluster analysis after running microarrays. 5FU clustered with drugs with an RNA-directed effect, rather than with other TS inhibitors.

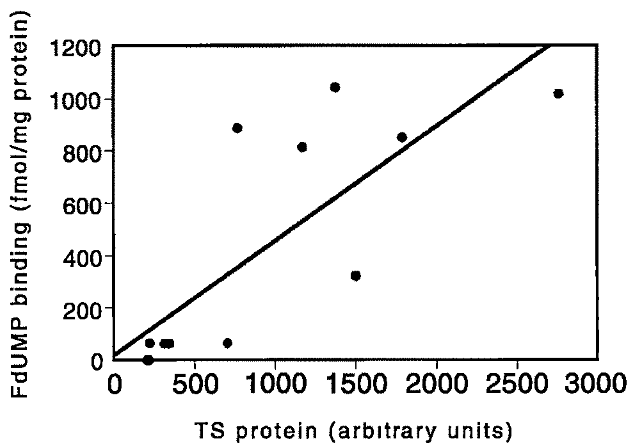

Fig. 2. Relationship between FdUMP binding (fmol/mg protein) and relative TS protein content as determined by Western blotting (Pearson correlation 0.786, $P=0.002$). TS protein was quantified using purified TS as a standard. Updated from Ref. [16]. FdUMP binding was also correlated with TS catalytic activity (expressed as pmol/h/10^6 cells) measured at saturating substrate concentrations ($r=0.810$, $P=0.0001$) and at half-maximal substrate concentration ($r=0.732$, $P=0.003$). TS catalytic activity correlated with TS-mRNA expression ($r=0.733$, $P=0.04$).

It seems that very high amplified TS levels as found in cells with acquired resistance to 5FU are only related to 5FU sensitivity. In other cells, the mechanism of 5FU might not be TS directed (e.g. RNA-mediated). Alternatively, the continuous exposure to 5FU (varying from 48 to 96 h) may produce sufficient FdUMP to inhibit TS intracellularly to undetectable levels even in cells with a 10-fold difference in TS levels. In an in situ TS assay, 5FU at IC_{50} levels inhibited intracellular TS more than 50% within only 4 h in cells with varying levels of TS [18]. With RTX, we observed using in situ TS inhibition that a partial inhibition after 4 h exposure increased to a complete inhibition after 24 h exposure [32]. Therefore, it seems that the usual in vitro cell culture conditions (continuous exposure) are not representative for evaluation of a relation between TS levels and 5FU sensitivity, and certainly not for an evaluation of antifolate sensitivity [43]. The latter is due to the fact that intracellular folate homeostasis will rescue cells from antifolate toxicity [44,45], especially when FPGS levels are high, since this would enable trapping of normal folates as polyglutamates in the cell.

3.3. Sensitivity to 5FU and RTX in relation to p53 expression

Besides the well-known and reasonably well-characterized resistance mechanisms of 5FU (Table 1), recently more evidence for other potential mechanisms has been provided. Ample evidence is now available that cytotoxic drug treatment of cells will result in an induction of p53 in cells with wt-p53 (reviewed in Ref. [42]). This will lead to an increase of p21, which can inhibit cell cycle progress by inhibition of CDK2, resulting in a cell cycle arrest and enabling the cells to repair drug-induced DNA damage. Alternatively, p53 induction can also transactivate bax levels, which promotes cell death. However, in cells with mt-p53, the expression of bax also increased [24,25], and cells died, but without the appearance of apoptotic features. In contrast, cells became necrotic. The difference in p53 status indeed led to a significantly different sensitivity for 5FU and RTX sensitivity in wt-p53 and mt-p53 cells (Fig. 3). For 5FU, these results are comparable to the increased 5FU sensitivity in wt-p53 cells from the National Cancer Institute 60-cell line panel compared to the cells with a mt-p53 expression [41,46]. This might be related to higher susceptibility of wt-p53 cells to enter apoptosis.

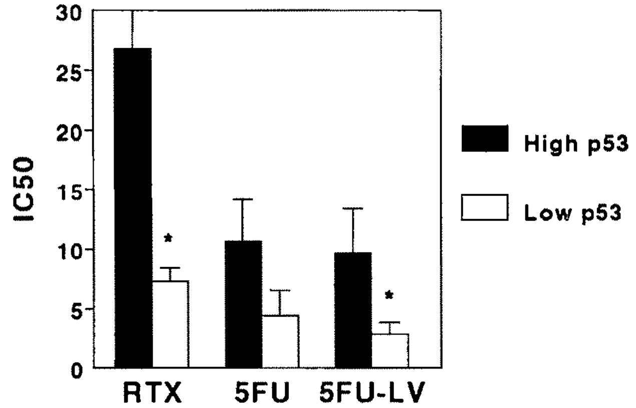

Fig. 3. Relation between p53 expression and sensitivity to 5FU and RTX. Sensitivity was determined by means of a 72-h exposure to the drugs, values are means ± S.E. of IC_{50} values (nM for RTX, μM for 5FU and 5FU-LV, LV was added at 10 μM). IC_{50} values for RTX and LV-5FU were significantly lower (*) in cells with a wt-p53 (4 cell lines with a low p53; $P = 0.042$ and 0.019, respectively) than in cells with a mt-p53 phenotype (10 cell lines with high p53). For 5FU, this difference tended to be significant ($P = 0.060$). From Refs. [16,24].

Table 2
Expression of TSER and p53 in colon cancer cells

Cell line	p53		TSER
SW620	mut	7.29	2/2
SNU-C4	wild	0.27	2/2
SW1116	mut	8.31	2/2
WiDr	mut	7.86	2/2
WiDr/F	mut	5.06	2/2
Colo320	mut	6.99	2/2
SNU-C1	wild	0.37	3/3
Lovo	wild	0.09	2/2
LS174T	wild	0.11	2/3
SW948	mut	0.08	2/2
HT29	mut	6.07	2/2
SW1398	mut	7.24	2/2
Colo205	mut	7.31	2/2
Colo201	mut	5.3	2/3
H630	mut	n.d.	3/3

Blots were scanned for p53, actin was used to control blots for loading of protein. The p53 status was based on mutation analysis reported; p53 expression were normalized on a reference amount of p53 protein. TSER 2/2 means that the cells were homogenous for the double repeat, 2/3 that they were heterogeneous for the double and triple repeat, and 3/3 that they were homogenous for the triple repeat. n.d., not done.

3.4. TS levels in relation to TS gene promoter polymorphisms

Evidence has been provided by Marsh et al. [29], that polymorphism of TS gene promoter regions may be related to TS-mRNA and protein expression. Tandem repeat sequences near the initiation start site in the 5′-untranslated region (5′ UTR) of the human TS promoter act as a *cis*-acting enhancer element in the TS gene and have been shown to influence TS expression. These TSERs are polymorphic and contain either two or three 28-bp tandem repeats. In vitro the triple tandem repeat (TSER*3) increased the TS expression compared to the double tandem repeat (TSER*2). Therefore, we also analyzed the tandem repeats in our panel of cell lines (Table 2). Only two cell lines (H630 and SNU-C1) showed a homogenous TSER*3, and two other cell lines a heterogeneous double/triple repeat. Interestingly, SNU-C1 and SNU-C4, which are cell lines derived from the same patients, showed a different TSER genotype. When the TS levels (activity, protein, mRNA) in these lines (TSER*3 and TSER*2/3) were compared with the other cell lines (all TSER*2), no significant differences were found. In addition, the 5FU resistant variants H630-R1 and H630-R10 also showed a homogenous TSER*3, although their TS levels were markedly increased compared to H630 cells. Apparently, in this cell line panel, the tandem repeats do not influence TS levels, or the number of cell lines was too small to draw such conclusions.

Also in patients, the occurrence of tandem repeats has been investigated. In DNA from 121 patients with colorectal cancer, 29% of the patients were homogenous for TSER*3, 16% were homogenous for TSER*2 and 55% were heterogeneous [29]. In 44/45 paired samples, the TSER was similar in colon tumors and normal mucosa. Patients homogenous for TSER*2 had a longer survival than those with a homogenous TSER*3. Also, Villafranca et al. [47] observed that patients with homogenous TSER*2 and heterogeneous TSER*2/3 tended to have a longer survival than patients with a homogenous TSER*3 (81% vs. 41%, $P=0.17$). Iacopetta et al. [48] observed that from 221 patients with Dukes' C colon cancer, 26% were homogenous for TSER*3 and did not benefit from 5FU-based chemotherapy. However, those patients with a heterogeneous TSER*2/3 or homogenous TSER*2 genotype showed significant gain in survival ($P=0.005$) from treatment. The value of the genomic polymorphisms in the TS gene promoter region should be investigated prospectively.

4. TS induction in cell lines

The regulation of TS levels in the cell cycle can be disrupted by various TS inhibitors [49]. When FdUMP is bound to TS in the ternary complex, the protein can no longer autoregulate its own synthesis, leading to a derepression and increase in TS protein. Thus, inhibition of TS in vitro either by the formation of the ternary complex between FdUMP, the enzyme and 5,10-CH_2-THF [50,51], or by specific TS inhibitors such as RTX [49], disrupt the regulation of enzyme synthesis. This is shown as an increase in TS protein expression, which is not accompanied by an increase in TS-mRNA. The increase in TS protein, however, may also be due to stabilization of the protein due to decreased degradation of the ternary complex [52]. The 5FU induced increase could be prevented by interferon-γ [53]. Increase in TS levels in cell lines after exposure to 5FU or antifolate TS inhibitors seems to be a universal finding, but it is not clear from the in vitro studies whether this increase is related to sensitivity to 5FU or antifolate TS inhibitors. The increase is usually between two- and five-fold, but is concentration and time-dependent [24,25,54]. Exposure to 5FU leads to an initial decrease in free TS and an increase in the ternary complex (Fig. 4); however, the total amount of TS protein exceeded that of untreated cells [24,25,55]. In cells treated with RTX and other antifolate TS inhibitors, free TS protein accumulated in time [24,25,32,54]. In a panel of six colon cancer cell lines, the extent of TS protein induction was not related to sensitivity to 5FU or RTX [24]. Actually, in WiDr cells, induction of TS protein by RTX was not sufficient to prevent complete inhibition of TS in the in situ TS inhibition assay [32]. Apparently, the continuous presence of the inhibitor will lead to TS protein induction, but will also be sufficient to allow complete inhibition of TS catalytic activity. As mentioned above, this possibly also explains the lack of correlation between TS protein levels and 5FU and antifolate sensitivity.

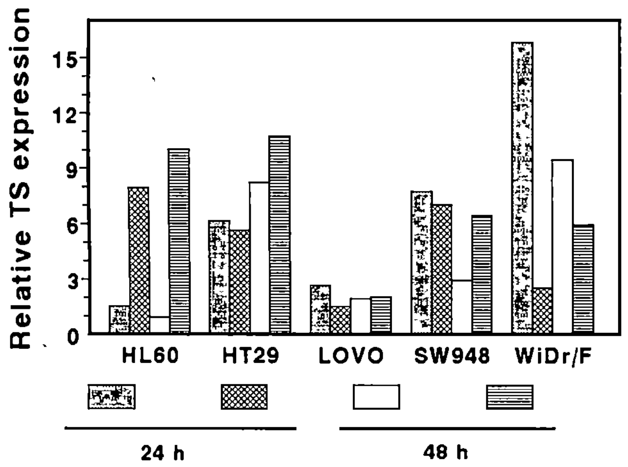

Fig 4 Effect of 24- and 48-h treatment with 50 μM 5FU on TS levels in the colon cancer cell lines, HT29, SW948, WiDr/F (all mt-p53) and LoVo (wt-p53) and the p53 null myeloid leukemia cell line HL60. Data were expressed as the ratio of $(OD \times mm^2)_{treated}/(OD \times mm^2)_{control}$ Specific protein levels in drug-treated cells were expressed relatively to the specific protein levels in the untreated control cells (at similar total protein loads; set at 1) Data are from one representative experiment as described previously [24]. ▨, ☐ free TS (36-kDa band) after 24 and 48 h, respectively; ▩, ▤ ternary complex (38-kDa band) after 24 and 48 h, respectively

5. TS levels and induction in solid experimental tumors

Evidence for a lack of relation (or at most a poor relation) between TS levels and in vitro sensitivity patterns for 5FU and antifolates is accumulating. However, this does not mean that such a relationship would not exist in vivo. Spears et al. [56] have already observed that experimental colon tumors with a high TS activity were less sensitive to 5FU. Although the reported panels are not as large as for the in vitro studies, all together there seems to be a reasonably good relationship between TS levels and 5FU sensitivity, despite the fact that in vivo pharmacokinetics determine 5FU concentrations. Actually, the similarity of 5FU plasma pharmacokinetics between humans and mice might be in favor for extrapolation of murine data to humans [21]. Also, in our panel of tumors, we found that 5FU-sensitive tumors had a lower TS activity than 5FU-resistant tumors [22,23,57]. Treatment with a therapeutic dose of 5FU resulted in a more pronounced inhibition in the sensitive tumors compared to the resistant tumors. In addition, 5FU treatment resulted in a two- to three-fold induction of TS in the resistant tumors, which already had a high activity [22,23,57]. This TS induction was already found 7 days after treatment with 5FU at 100 mg/kg and was more pronounced after three treatment cycles (Fig. 5). However, in the sensitive tumors, this induction was not observed, and TS levels were further reduced following the second and third injection. In the resistant tumors, the induction could also be prevented by repeated administration, but only by the use of a higher dose of 5FU (150 mg/kg) (Fig. 6). The latter is only possible when toxicity of

5FU to mice is selectively protected by uridine (or a uridine prodrug) administration [58]. Uridine administration enabled a 1.5-fold increase in the 5FU dose, which was also associated with an increased antitumor activity. Also, treatment with 5-fluorodeoxyuridine (FUdR) resulted in a two-fold induction of TS; however, for FUdR the onset of TS induction was later (10 days) than for 5FU (7 days). FUdR, when given as a bolus, was a more effective treatment than 5FU and is thought to be entirely TS directed [57].

The most relevant clinically important finding was the observation that the enhanced antitumor activity of the 5FU/LV combination compared to 5FU alone, was associated with the prevention of TS induction by LV (Fig. 5) The combination of 5FU with LV and uridine provided a double modulation: LV increased the antitumor effect of 5FU, while uridine enabled to use a higher 5FU dose by protection of gastrointestinal and myeloid toxicity. Uridine selectively protects normal tissues since the toxicity is mediated by incorporation into RNA [59,60], which is protected by uridine. Uridine also protected 5FU-induced apoptosis in the gut [61]. The double modulation resulted in the best therapeutic efficacy compared to 5FU alone, since both LV and an increased 5FU dose apparently provide an enhanced and prolonged TS inhibition in tumors.

TS induction was not only observed in tumors, but also in normal tissues. Local administration either by hepatic artery infusion or isolated liver perfusion of 5FU are more effective treatments than systemic administration, but may result in local hepatotoxicity. Local administration of 5FU not only exposes the liver metastases but also the normal liver tissue to the high concentrations of 5FU. Local administration of 5FU resulted in a pronounced inhibition of TS in liver metastases (> 70%) [62]. In contrast, local 5FU administration resulted in a six- to seven-fold TS induction in normal liver. Since no liver toxicity was seen with local 5FU administration, the induction of TS apparently provides an additional protection of the normal tissues. Interestingly, TS was also induced in normal gastrointestinal mucosa, adding to a selective effect. Similarly, Welsh et al. [54] observed a larger induction of TS in normal tissues compared to tumor tissues, although this was after treatment with an analog of RTX, ZD9331.

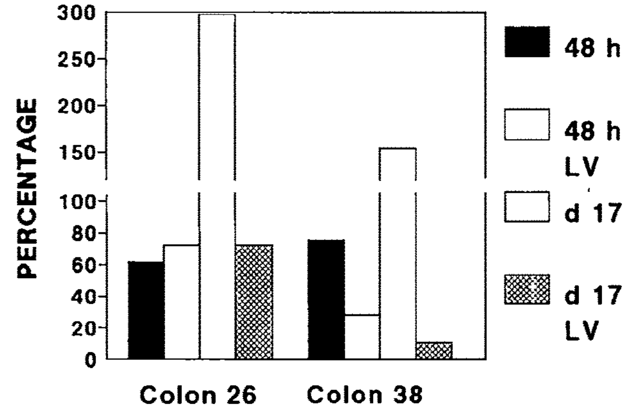

Fig. 5 Effect of 5FU treatment on TS levels (TS inhibition and induction) in experimental tumors Mice bearing Colon 26 (5FU resistant) or Colon 38 (5FU sensitive with complete remissions) were treated weekly (days 0, 7, 14) at the therapeutic dose of 5FU (100 mg/kg) LV was given as a double dose of each 50 mg/kg, the first dose at 1 h before 5FU and one dose together with 5FU [22] TS catalytic activity in untreated tumors was 2.32 ± 0.72 and 0.80 ± 0.23 nmol/h/mg protein, respectively (means ± S.D.), and was set at 100% Values are means, S.D were less than 15%

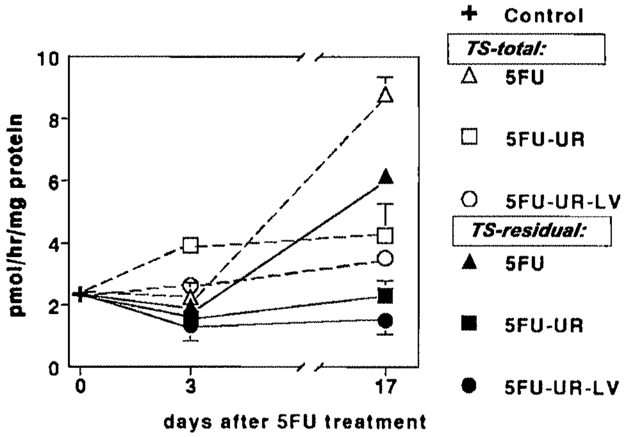

Fig 6 Effect of uridine (UR) and LV on 5FU-induced TS inhibition and induction in Colon 26 tumors. Mice were treated weekly (days 0, 7, 14) with 5FU alone at 100 mg/kg and in combination with uridine (3500 mg/kg, 2 and 18 h after each 5FU dose) at 150 mg/kg. LV was given as described in the legend to Fig 5 This 5FU dose was well tolerated because normal tissue toxicity could be protected by providing uridine as a salvage treatment Values are means ± S D After 17 days, TS-total and TS-residual were significantly higher after 5FU treatment compared to 5FU-UR and 5FU-UR-LV ($P<0.02$); after 3 days, TS-total, and after 17 days, TS-residual were significantly higher after 5FU-UR compared to 5FU-UR-LV ($P<0.05$) From Ref [58]

6. TS inhibition and induction in human disease

6.1. TS levels and inhibition in relation to response and survival

Although one of the most widely used drugs, 5FU is only moderately active in patients. Since modulation of 5FU with LV enhanced in vitro cytotoxicity of 5FU and the in vivo antitumor effect of 5FU (reviewed in Refs. [63,64]), the combination was entered into the clinic and proved to give a better therapeutic efficacy than 5FU alone [65], both in terms of survival and response. In order to determine whether tumoral TS levels and 5FU-induced inhibition would be related to the response to 5FU, we gave patients a 500 mg/m^2 i.v. dose before surgery and removed the tumors between 1 and 72 h after drug administration. Most patients were subsequently entered in a clinical study in which they were treated with a hepatic artery infusion of 5FU at a dose of 1000 mg/m^2/day for 6 days. The study aimed to determine what extent of TS inhibition in primary human colon tumors and in liver metastases would be sufficient to result in a response to 5FU. TS inhibition in tumors is retained for at least 48–72 h after a bolus injection of 500 mg/m^2 5FU [20,66]. In those patients in whom the TS activity in tumors remained low after 45 h, we observed a significantly higher response compared to patients, in which the activity was high. In 19 patients responding to 5FU hepatic artery infusion, TS levels in the tumor were significantly lower than in the tumors from 21 non-responding patients (Fig. 7). In breast cancer patients, the number of FdUMP binding sites increased and the effect of CH_2-THF decreased during development of resistance [67].

TS levels were also evaluated using immunohistochemistry, which essentially resulted in a similar pattern [26,27]; untreated patients had a relatively high TS expression in the tumor, while 5FU administration decreased this level. After 45 h, most patients displayed a normal level of TS expression. In addition, patients with a low TS expression had a longer survival than patients with a high TS staining (Fig. 8).

This study also evaluated the effect of LV on TS levels. The TS assays not only enabled us to evaluate TS inhibition, but by dissociation of the ternary complex also to evaluate total TS levels. 5FU administration increased total TS levels two-fold at 24 h (Table 3); LV not only increased TS inhibition, but also reduced the TS induction. These clinical data support the biochemical basis for LV modulation and also demonstrate the validity of the translation of preclinical data to the clinic.

6.2. Regulation of TS induction

Although immunohistochemistry gives a good insight in the morphological distribution of TS, its discriminative potential is rather poor, while the cytosolic staining of TS is more difficult to quantify than an enzyme assay and mRNA expression. Since TS-mRNA expression in colon tumors is relatively low, Northern blots could not be used and TS expression was quantified using RT-PCR with β-actin and 18S as the reference genes. TS-mRNA expression varied 17.7-fold relative to β-actin-mRNA and 41.7-fold relative to 18S-rRNA (Fig. 9). TS-mRNA was correlated with TS catalytic activity in these samples; both when expressed as TS/β-actin ($P=0.8243$, $P=<0.0001$) and TS/18S ($r=0.6226$, $P=0.0034$); also for FdUMP binding capacity, a good correlation was found with TS-mRNA

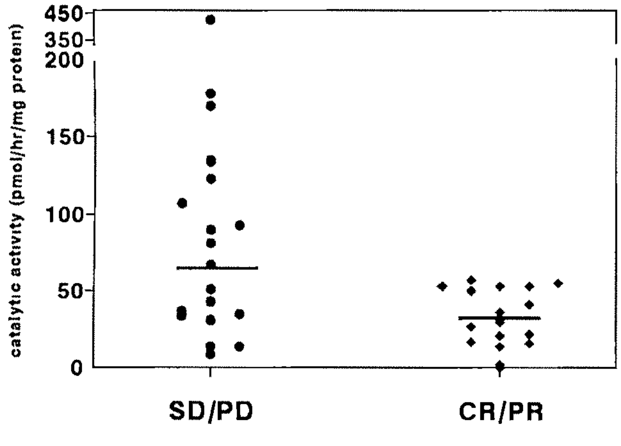

Fig. 7 Relation between TS levels and response to 5FU treatment Tumors were removed from the patients at the indicated time points and immediately stored in liquid nitrogen TS-total levels (measured at 1 μM dUMP) are given The difference in TS levels between both groups is significant at the level $P<0$ 01 Modified from Refs [20,66]

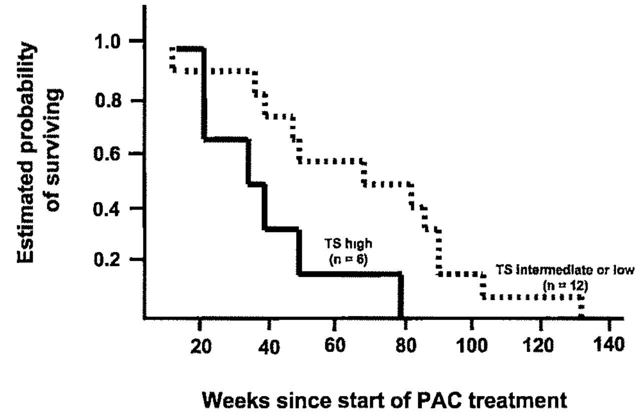

Fig 8 Relation between TS expression as determined by immunohistochemistry and survival after 5FU treatment via hepatic artery infusion given with a Porth-a-Cath (PAC) The Kaplan–Meier curves show the probability of survival of 18 patients with liver metastases Patients with a low expression had a significantly better survival than those with a high expression ($P=0$ 025, log-rank test) From Ref [27]

Table 3
TS levels in patients after 5FU administration

TS assay	Drug/time			
	5FU (2 h)	5FU (23 h)	5FU (45 h)	5FU/LV (45 h)
TS catalytic activity (pmol/h/mg protein)				
TS-total	21	53*	37	31
TS-residual	11	32*	30	13
FdUMP binding (fmol/mg protein)				
TS-tot	58	128**	72	92
TS-free	0	22**	23	22
TS-mRNA expression				
TS/β-actin ($\times 10^{-3}$)	4 2 ± 1 1	8 0 ± 1 5*	3 2 ± 1 0	n a
TS/18S ($\times 10^{-6}$)	1 5 ± 3 1	15 2 ± 5 0**	5 7 ± 1 5	n a

Values for TS catalytic activity and FdUMP binding are medians of 11–15 patients. TS-total is the total catalytic activity, and TS-tot the total number of FdUMP binding sites, as measured after dissociation of the ternary complex TS inhibition is given as TS-residual, which is the catalytic activity of TS, and TS-free, which is the number of free FdUMP binding sites, as measured before the dissociation of the ternary complex was performed [20] The TS-mRNA expression (means ± SD) is a relative TS-mRNA expression calculated as the ratio between TS-mRNA expression and that of either β-actin or 18S [28]. Significantly different from the 2-h values at the level *, $P<0$ 05 or **, $P<0$ 02 using either Mann–Whitney test (TS activity) or a Student's t-test (TS-mRNA) Time points indicate medians of the sample times There was no significant difference in the β-actin/18S expression ratio between the various time points

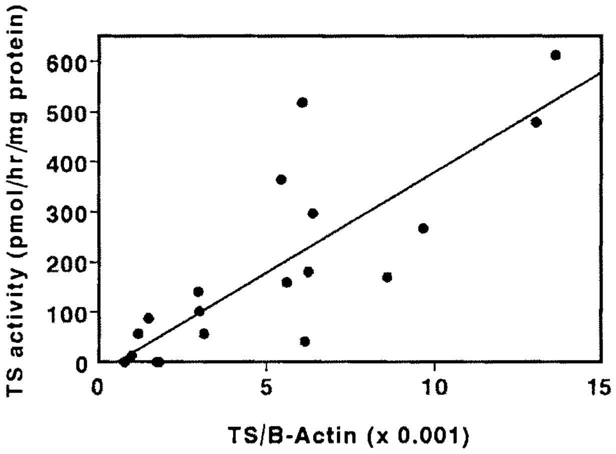

Fig. 9. Relation between TS-mRNA expression (normalized to β-actin) and TS catalytic activity (pmol/h/mg protein measured at 10 μM dUMP) in colon tumors. The linear regression coefficient was 0.8243 with a $P<0.001$.

expression. Following 5FU treatment, the TS/β-actin ratio significantly ($P=0.0493$) increased two-fold from the 2 h samples to the 23 h samples followed by a significant ($P=0.0212$) decrease from the 23 to 45 h samples (Table 3). Induction of TS was also found when comparing enzyme activities at these time points.

In order to determine whether the amount of TS enzyme per expression unit of TS-mRNA changed, we calculated the ratio of enzyme levels relative to TS/β-actin. Interestingly, the ratio catalytic activity compared to either TS/βactin or TS/18S gradually increased (Fig. 10). However, the ratio FdUMP binding compared to TS/β-actin or TS/18S was induced at 23 h compared to 4 h, but decreased again at 45 h. For TS/18S, these data were significant. These data indicate a greater induction of TS protein (as seen for the FdUMP binding) relative to TS-mRNA. This is in line with a TS autoregulation as proposed by Chu et al. [33,53]. According to this model, TS protein binds to TS-mRNA inhibiting its own translation, TS bound by FdUMP will not be not able to inhibit its translation, and the translation is derepressed, leading to more enzyme synthesis. Since in 2-h samples, the major part of TS is bound by FdUMP, the autoregulation is disrupted and TS protein is synthesized more compared to TS-mRNA. The TS protein then reaches a plateau at 23 h when evaluated as the ratio TS protein/TS-mRNA (measured as FdUMP binding capacity), but when expressed as TS catalytic activity/TS-mRNA the ratio increased. This indicates that more functional protein is present after 45 h.

Altogether, the pattern of changes in TS-mRNA and TS protein is quite complicated, and possibly due to a dual or even triple effect in these tumors. Initially, TS bound by FdUMP derepresses the autoregulation of TS-mRNA translation, leading to more synthesis of TS protein. Subsequently, the amount of E2F [26] increases, which induces transcription leading to more TS-mRNA, encoding for even more TS protein. Next to these effects, formation of the ternary complex also leads to a stabilization of TS, with as an ultimate effect an increase in total TS protein. Fortunately, although TS protein is induced, FdUMP at sufficiently high concentrations can still almost completely inhibit TS. This was associated with a better response to 5FU therapy when the residual TS and free TS were below certain thresholds [20].

7. Conclusions and perspectives

The expression of TS is controlled at several levels, which may all affect the final enzyme catalytic activity in the cell and the ability of drugs to inhibit the functional activity of the enzyme. Since TS is the target for 5FU and several folate-based TS inhibitors, it was expected that TS expression would be related to the sensitivity to 5FU and the antifolates. Acquired resistance to 5FU or antifolates has indeed been associated with an increased TS expression (both at the mRNA and protein level) [5,11,15]. When such cell lines are included in panels to evaluate a potential

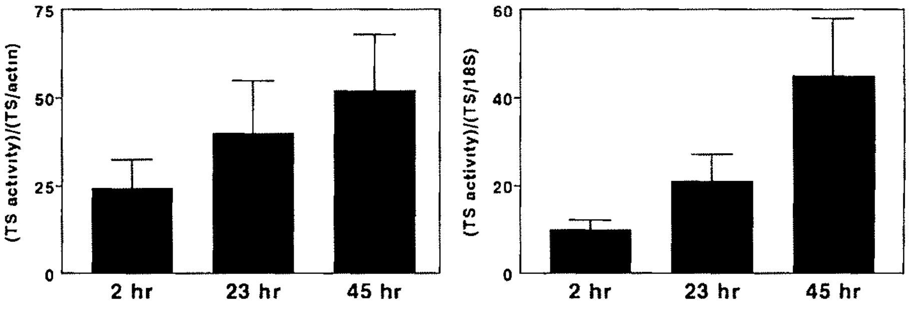

Fig. 10. Effect of 5FU treatment on TS enzyme levels in relation to TS-mRNA expression. The ratio TS catalytic activity divided by the relative TS-mRNA expression was calculated for each patient. Values are means ± S.D. The increase was significant ($P<0.05$) at 45 h for the TS/β-actin data and at 23 and 45 h for the TS/18S data. Interestingly, for the ratio FdUMP binding/TS-mRNA, a peak (3-fold for TS/β-actin $P=0.0136$; and 4.5-fold for TS/18S, $P=0.0115$) was observed at 23 h, while after 45 h, the ratio was back to that observed at 2 h.

relationship between TS levels and 5FU sensitivity, a significant correlation has been found repeatedly [5,16,17]. When including resistant cell lines in our cell line panel, 5FU sensitivity was related to TS levels. Although we previously reported a poor relation between TS levels and 5FU sensitivity [16], this relation did not exist when we extended the cell line panel with more unselected cells. Statistically, this unexpected finding might be explained by inclusion of more data, which will correct for an intrinsically poor relationship. Mechanistically, the lack of correlation may be explained by the fact that the cell lines are exposed continuously to 5FU. This leads to a continuing synthesis of FdUMP, which enables an almost complete inhibition of TS. This has been seen in the in situ TS inhibition assay with intact cells, in which TS activity was still inhibited although TS protein was induced [32]. In addition, a more pronounced effect may be found in rapidly proliferating cells that tend to have a higher TS activity [41]. The continuous exposure does not reflect most commonly used schedules to treat either animals or patients [5,21,65]. Currently, most treatment protocols consist of bolus injections or short infusion up to 24 or 48 h, which will result in high drug levels for a relatively short period followed by a rapid plasma clearance. Although the drug is retained longer in tissues [21], continuous exposure in vitro in cell lines does not reflect the in vivo conditions in animals and patients. In cell lines, the effect is quantified at the end of the exposure, while in animals and patients, the response is evaluated after a period of at least several weeks. Therefore, extrapolation of experiments with cell lines should be done carefully, taking into account these variations. In contrast, cell lines can very well be used to study single parameters, such as the potential mechanism of TS induction and the mechanisms by which 5FU and antifolates can cause cell death. In cell lines, it has also been shown that phosphorylation of the protein [68,69] may affect TS activity, which might explain some of the discrepancies between TS catalytic activity and FdUMP binding. In addition, the presence of antisense TS-mRNA [70] may affect expression of the normal TS-mRNA.

Protein expression (either with immunohistochemistry or Western blots) and TS-mRNA expression may reflect the catalytic activity of TS in the cell. However, when cells are treated, TS protein can be induced without a corresponding increase in TS-mRNA levels. Several studies now report a consistent relationship between intrinsic TS levels and response and survival to 5FU-based chemotherapy (reviewed in Ref. [71]). This relationship was found for various types of cancer, when TS levels were evaluated either by classical TS activity assays (e.g. Refs. [20,67]), TS immunohistochemistry (e.g. Refs. [27,72]) or TS-mRNA expression [73,74]. However, when the role of TS expression in adjuvant treatment of primary disease is evaluated, the role of TS expression is less clear. For example, Johnston et al. [72] reported that patients with a high TS expression had a longer survival when treated with adjuvant chemotherapy than patients with a low TS expression. Apparently in primary disease other factors, such as proliferation markers and repair enzymes may play another important role [73,75]. Before using TS expression to select patients for a specific type of adjuvant therapy, these factors should be characterized in large patient populations. However, in advanced disease, the correlation between TS levels and effect of 5FU is consistent throughout a variety of studies [71]. Therefore, the type of treatment of advanced colorectal cancer can be based on the TS expression in a prospective manner. Patients with low TS enzyme levels (TS activity, immunohistochemistry or mRNA) are expected to respond better to a 5FU-based therapy than patients with a high TS expression. When TS expression was combined with that of dihydropyrimidine dehydrogenase (DPD), none of the patients with high TS and DPD expression responded to 5FU-based therapy [76]. These patients should be selected for a non-5FU-based therapy such as with the topoisomerase I inhibitor irinotecan or the platinum analog oxaliplatin.

Acknowledgements

This research was supported by various grants from the Dutch Cancer Society (IKA 92-88, VU 93-627, VU 96-1240). We also thank M. Koudijs, M. Van der Ent and P. Noordhuis for technical assistance. Drs. G.W. Aherne and S. Welsh (Institute for Cancer Research, Sutton, Surrey, England) are acknowledged for critical reading of the paper.

References

[1] P.V Danenberg, Biochim Biophys Acta 473 (1977) 73–92
[2] C W Carreras, D V. Santi, Ann Rev Biochem 64 (1995) 721–762.
[3] S H Berger, M T Hakala, Mol Pharmacol 25 (1984) 303–309
[4] J.A. Houghton, P J Houghton, Eur J Cancer Clin Oncol 19 (1983) 807–815
[5] G.J Peters, G. Jansen, in R L. Schilsky, G A Milano, M J Ratain (Eds), Principles of Antineoplastic Drug Development and Pharmacology, Marcel Dekker, New York, 1996, pp 543–585
[6] G Jansen, in A L Jackman (Ed), Antifolate Drugs in Cancer Therapy, Humana Press, Totowa, NJ, 1999, pp 293–321.
[7] C L Van der Wilt, H M Pinedo, M De Jong, G J Peters, Biochem Pharmacol. 45 (1993) 1177–1179
[8] S Radparvar, P.J Houghton, J A Houghton, Biochem Pharmacol 38 (1989) 335–342
[9] F S Wang, C Aschele, A. Sobrero, Y M Chang, J R Bertino, Cancer Res. 53 (1993) 3677–3680
[10] A.R Bapat, C Zarov, P V Danenberg, J Biol Chem 258 (1983) 4130–4136
[11] D G Priest, S.E Ledford, M T Doig, Biochem Pharmacol 29 (1980) 1549–1553
[12] S.H Berger, K W. Barbour, F G Berger, Mol Pharmacol. 34 (1988) 480–484
[13] C P Spears, B G Gustavsson, M Berne, R. Frosing, L. Bernstein, A A Hayes, Cancer Res 48 (1988) 5894–5900

[14] M.B Yin, S F Zakrzewski, M.T. Hakala, Mol Pharmacol 23 (1983) 190–197.

[15] C H Jenh, PK Geyer, F Baskin, L.F. Johnson, Mol Pharmacol 28 (1985) 80–84.

[16] B Van Triest, H M. Pinedo, Y Van Hensbergen, K. Smid, F Telleman, C.L. Van der Wilt, J A M Van Laar, P Noordhuis, G Jansen, G J. Peters, Clin. Cancer Res 5 (1999) 645–655

[17] PG Johnston, J C. Drake, J Trepel, C J Allegra, Cancer Res 52 (1992) 4306–4312.

[18] C.L Van der Wilt, C M Kuiper, G J Peters, Oncol Res. 11 (1999) 383–391

[19] Y.P. Keepers, P.E Pizao, G J Peters, J Van Ark-Otte, B Winograd, H.M Pinedo, Eur. J. Cancer 27 (1991) 897–900

[20] G J Peters, C L. Van der Wilt, C J. Van Groeningen, S Meijer, K. Smid, H.M. Pinedo, J Clin Oncol. 12 (1994) 2035–2042

[21] G J Peters, J Lankelma, R M Kok, P Noordhuis, C.J. Van Groeningen, C L. Van der Wilt, S. Meijer, H M. Pinedo, Cancer Chemother Pharmacol. 31 (1993) 269–276

[22] C.L Van der Wilt, H M. Pinedo, K Smid, G J Peters, Cancer Res 52 (1992) 4922–4928

[23] G Codacci-Pisanelli, C.L. Van der Wilt, H M Pinedo, F Franchi, P Noordhuis, J A.M Van Laar, B J.M Braakhuis, G J Peters, Eur J. Cancer 31A (1995) 1517–1525

[24] G J Peters, B Van Triest, H.H.J Backus, C M Kuiper, C L Van der Wilt, H M. Pinedo, Eur. J Cancer 36 (2000) 916–924.

[25] H H J. Backus, H M Pinedo, D Wouters, C M Kuiper, G. Jansen, C J. Van Groeningen, G J Peters, Oncol Res 12 (2000) 231–239

[26] H H J Backus, D F. Dukers, C J Van Groeningen, W Vos, E Bloemena, D Wouters, J M G H. Van Riel, K Smid, H M Pinedo, G J Peters, Ann Oncol 12 (2001) 209–216

[27] H H J. Backus, J M G.H Van Riel, C.J Van Groeningen, W Vos, D.F Dukers, E Bloemena, D. Wouters, H M Pinedo, G J. Peters, Ann. Oncol. 12 (2001) 779–785.

[28] S J Freemantle, A.L. Jackman, L R Kelland, A H Clavert, J Lunec, Br J Cancer 71 (1995) 925–930.

[29] S. Marsh, J.A. McKay, J Cassidy, H.L McLeod, Int J. Oncol 19 (2001) 383–386.

[30] S Marsh, E S R Collie-Duguid, T. Li, X. Liu, H L McLeod, Genomics 58 (1998) 310–312

[31] L.G. Navelgund, C Rossana, A.J. Muench, L F Johnson, J. Biol Chem 255 (1980) 7386–7390.

[32] G J Peters, E Smitskamp-Wilms, K Smid, H.M Pinedo, G Jansen, Cancer Res. 59 (1999) 5529–5535.

[33] E. Chu, C.J. Allegra, Bioassays 18 (1996) 191–198.

[34] Y Lee, L F Johnson, L S Chang, Y Chen, Exp Cell Res 234 (1997) 270–276

[35] G Weber, Cancer Res 43 (1983) 3466–3492

[36] G.J. Peters, C J Van Groeningen, E J. Laurensse, H M Pinedo, Eur J Cancer 27 (1991) 263–267

[37] M C. Etienne, X Pivot, J.L Formento, R J Bensadoun, P Formento, O Dassonville, M Francoual, G Poissonnet, X Fontana, M. Schneider, F Demard, G. Milano, Br J Cancer 79 (1999) 1864–1869

[38] D. Banerjee, R Gorlick, A. Liefshitz, K Danenberg, P.V. Danenberg, D Klimstra, S Jhanwar, C Cordon-Cardo, Y. Fong, N. Kemeny, J R Bertino, Cancer Res 60 (2000) 2365–2367

[39] H H J Backus, C J Van Groeningen, D.F. Dukers, E Bloemena, D. Wouters, H M Pinedo, G J Peters, J Clin Pathol 55 (2002) 206–211

[40] A Beck, M C. Etienne, S Chéradame, J L. Fischel, P Formento, N Renée, G Milano, Eur J Cancer 30A (1994) 1517–1522

[41] J.L Grem, K.D. Danenberg, K Behan, A Parr, L Young, P.V Danenberg, D. Nguyen, J Drake, A Monks, C J Allegra, Clin Cancer Res 7 (2001) 999–1009

[42] B Van Triest, H M Pinedo, G Giaccone, G J Peters, Ann Oncol 11 (2000) 385–391.

[43] U Scherf, D T Ross, M Waltham, L H Smith, J.K Lee, L Tanabe, K W Kohn, W.C Reinhold, T.G. Myers, D.T. Andrews, D.A. Scudiero, M B Eisen, E A. Sausville, Y. Pommier, D. Botstein, P.O. Brown, J.N Weinstein, Nat Genet 24 (2000) 236–244.

[44] H.H J. Backus, H M Pinedo, D. Wouters, J M Padron, N Molders, C.L Van der Wilt, C.J. Van Groeningen, G Jansen, G J. Peters, Int J. Cancer 87 (2000) 771–778

[45] G J Peters, G Jansen, Nutrition 17 (2001) 737–738

[46] PM O'Connor, J Jackman, I. Bae, TG. Myers, F Fan, M. Mutoh, D A. Scudiero, A Monks, E A Sausville, J N. Weinstein, S Friend, A.J. Fornace, K W Kohn, Cancer Res 57 (1997) 4285–4300

[47] E. Villafranca, Y. Okruzhnov, M A Dominguez, J Garcia-Foncillas, I Azinovic, E Martinez, J J Illarramendi, F Arias, R Martinez, E. Monge Salgado, S Angeletti, A. Brugarolas, J Clin Oncol 19 (2001) 1779–1786

[48] B Iacopetta, F Grieu, D Joseph, H. Elsaleh, Br J Cancer 85 (2001) 827–831

[49] K Keyomarsi, J. Samet, G. Molnar, A B Pardee, J Biol Chem 268 (1993) 15142–15149

[50] E Chu, D Voeller, J Casey, J Drake, B Chabner, P Elwood, S Zinn, C. Allegra, Proc Natl. Acad Sci U. S A. 88 (1991) 8977–8981

[51] E. Chu, D M Voeller, K L Jones, T Takechi, G.F Maley, F Maley, S Segal, C J Allegra, Mol. Cell. Biol 14 (1993) 207–213

[52] M E Kitchens, A M Forsthoefel, K W Barbour, Z Rafique, H T Spencer, F G. Berger, J Biol Chem 274 (1999) 12544–12547

[53] E. Chu, D M. Voeller, PG Johnston, S. Zinn, C J Allegra, Mol Pharmacol 43 (1993) 527–533

[54] S.J Welsh, J Titley, L Brunton, M. Valenti, P Monaghan, A.L Jackman, G W. Aherne, Clin Cancer Res 6 (2000) 2538–2546

[55] A L Parr, J C Drake, R.E Gress, G. Schwartz, S M. Steinberg, C J. Allegra, Biochem Pharmacol. 56 (1998) 231–235.

[56] C P Spears, A H. Shahinian, R.G. Moran, C Heidelberg, T.H Corbett, Cancer Res. 42 (1982) 450–456.

[57] J A M Van Laar, C.L Van der Wilt, Y.M Rustum, P. Noordhuis, K Smid, H M Pinedo, G J Peters, Clin. Cancer Res 2 (1996) 1327–1333

[58] G Codacci-Pisanelli, C L Van der Wilt, K Smid, P Noordhuis, D. Voorn, H M Pinedo, G J Peters, Oncology 64 (2002)

[59] G J Peters, J. Van Dijk, E. Laurensse, C J Van Groeningen, J Lankelma, A. Leyva, J. Nadal, H M. Pinedo, Br. J. Cancer 57 (1988) 259–265.

[60] D S Martin, R L Stolfi, R C Sawyer, S Spiegelman, C W Young, Cancer Res 42 (1982) 3964–3970

[61] D M Pritchard, A J M Watson, C.S. Potten, A.L Jackman, J.A Hickman, Proc. Natl Acad Sci U S A. 94 (1997) 1795–1799.

[62] C L Van der Wilt, A Marinelli, H.M Pinedo, J Cloos, K Smid, C J H. Van de Velde, G J Peters, Eur J Cancer 31A (1995) 754–760.

[63] C L Van der Wilt, G.J. Peters, Pharm. World Sci 16 (1994) 84–103

[64] G J Peters, C L Van der Wilt, C J Van Groeningen, Eur J Cancer 30A (1994) 1408–1411

[65] P Piedbois, M. Buyse, Y Rustum, D Machover, C Erlichman, R.W. Carlson, F Valone, R. Labianca, J H Doroshow, N Petrelli, J. Clin. Oncol 10 (1992) 896–903

[66] G.J Peters, C L. Van der Wilt, C J Van Groeningen, D G Priest, J. Schmitz, K Smid, S. Meijer, P. Noordhuis, K Hoekman, H M Pinedo, in. W Pfleiderer, H Rokos (Eds), Chemistry and Biology of Pteridines and Folates (Proc 11th International Symposium), Blackwell, Berlin, 1997, pp 145–150.

[67] S.M Swain, M.E Lippman, E F Egan, J C Drake, S M. Steinberg, C.J Allegra, J Clin Oncol 7 (1989) 890–899

[68] B J. Dolnick, A R. Black, Cancer Res 56 (1996) 3207–3210

[69] B J Dolnick, K. Lu, M B. Yin, Y M. Rustum, Adv Enzyme Regul. 37 (1997) 95–109

[70] W A Samsonoff, J. Reston, M McKee, B O'Connor, J Galivan, G Maley, F Maley, J. Biol Chem 272 (1997) 13281–13285

[71] B Van Triest, G.J Peters, Oncology 57 (1999) 179–194

[72] P.G. Johnston, E.R. Fisher, H.E Rockette, B Fisher, N. Wolmark, J C. Drake, B.A. Chabner, C.J Allegra, J Clin Oncol 12 (1994) 2640–2647

[73] R Metzger, C G Leichman, K D Danenberg, H -J Lenz, K. Hayashi, S. Groshen, D Salonga, H Cohen, L Laine, P Crookes, H Silberman, J Baranda, B. Konda, L Leichman, J Clin Oncol 16 (1998) 309–316

[74] H J. Lenz, K Hayashi, D Salonga, K D Danenberg, P V. Danenberg, R. Metzger, D Banerjee, J R Bertino, S Groshen, L P Leichman, C G Leichman, Clin Cancer Res 4 (1998) 1243–1250

[75] T. Watanabe, T -T Wu, P J. Catalano, T Ueki, R. Satriano, D G Haller, A B Benson, S R Hamilton, N Eng J Med 344 (2001) 1196–1206.

[76] D Salonga, K D Danenberg, M Johnson, R Metzger, S Groshen, D D Tsao-Wei, H J Lenz, C.G. Leichman, L Leichman, R.D Diasio, P V Danenberg, Clin Cancer Res. 6 (2000) 1322–1327

ELSEVIER

Biochimica et Biophysica Acta 1587 (2002) 206–214

BIOCHIMICA ET BIOPHYSICA ACTA

BBA

www.bba-direct.com

Review

Structure-based studies on species-specific inhibition of thymidylate synthase

M. Paola Costi[a,*], Donatella Tondi[a], Marcella Rinaldi[a], Daniela Barlocco[b], Piergiorgio Pecorari[a], Fabrizia Soragni[a], Alberto Venturelli[a], Robert M. Stroud[c]

[a]*Dipartimento di Scienze Farmaceutiche, Università di Modena e Reggio Emilia, Via G Campi n 183, 41100 Modena, Italy*

[b]*Istituto Chimico Farmaceutico, Università di Milano, Milan, Italy*

[c]*Department of Biochemistry and Biophysics, University of California San Francisco, San Francisco, CA, USA*

Received 24 January 2002; accepted 24 January 2002

Abstract

Thymidylate synthase (TS) is a well-recognized target for anticancer chemotherapy. Due to its key role in the sole de novo pathway for thymidylate synthesis and, hence, DNA synthesis, it is an essential enzyme in all life forms. As such, it has been recently recognized as a valuable new target against infectious diseases. There is also a pressing need for new antimicrobial agents that are able to target strains that are drug resistant toward currently used drugs. In this context, species specificity is of crucial importance to distinguish between the invading microorganism and the human host, yet thymidylate synthase is among the most highly conserved enzymes. We combine structure-based drug design with rapid synthetic techniques and mutagenesis, in an iterative fashion, to develop novel antifolates that are not derived from the substrate and cofactor, and to understand the molecular basis for the observed species specificity. The role of structural and computational studies in the discovery of nonanalog antifolate inhibitors of bacterial TS, naphthalein and dansyl derivatives, and in the understanding of their biological activity profile, are discussed. © 2002 Elsevier Science B.V. All rights reserved.

Keywords. Enzyme inhibition, Thymidylate synthase, Structure-based drug design, Specificity

---

1. Introduction

Folate-dependent enzymes have always been considered as attractive targets for hyperproliferative diseases, including cancer and infectious diseases [1,2]. Since they are usually involved in processes related to nucleic acid synthesis, their inhibitors act as antimetabolites, inhibiting cell division [3]. A problem with the current antimetabolite drugs is the development of resistance in human and pathogenic cells. Such resistance has arisen under intense and continuous chemotherapy, and can diminish or abrogate the therapeutic responses to these drugs [4]. The mechanisms of drug resistance can be seen both in multidrug resistant proteins that pump drug molecules out of the cell, and in mutations in the structural gene for the target itself that directly diminishes the affinity of the drug for the target enzyme. In recent years, with the advent of modern technologies in drug discovery, better understanding of the molecular basis of drug–target interactions have been reached and suggest new strategies to solve the abovementioned problems [5].

Because of its essential role in DNA synthesis, thymidylate synthase (TS) is among the most studied of folate-dependent enzymes. We report the development of two novel classes of inhibitors of TS that were discovered through structural insights, and that have no roots in the initial substrate or cofactor. We show how a 100-fold species selectivity was developed into an antipathogenic inhibitor by structure-based elaboration.

Thymidylate synthase has a dual function, acting both as an enzyme and as a regulator of its own expression by binding and inactivating its own RNA. As a catalytic protein, it catalyzes the reductive methylation of 2′-deoxyuridine-5′-monophosphate (dUMP) to 2′-deoxythymidine-5′-mono-

---

Abbreviations hTS, human thymidylate synthase, LcTS, *L casei* TS, EcTS, *E coli* TS, dUMP, 2′-deoxyuridine-5′-monophosphate; FdUMP, 5-fluoro-2′-deoxyuridine-5′-monophosphate; RFC, reduced folate factor, DDT, didansyltyrosine; FPGS, folylpolyglutamyl synthetase, PTH, phenolphthalein

* Corresponding author Tel +39-59-205-5125; fax. +39-59-205-5131

E-mail address. costimp@unimo.it (M.P Costi)

0925-4439/02/$ - see front matter © 2002 Elsevier Science B V All rights reserved

PII S0925-4439(02)00083-2

phosphate (dTMP) [6]. As a regulatory protein, TS may also be involved in the synthesis of proteins that regulate the apoptotic process [7,8].

The sequences of the TS enzymes from more than 30 organisms have been determined. Among them, many are from pathogenic microorganisms that include the fungi *Cryptococcus neoformans* and *Pneumocistis carinii*; parasites, *Trichinella spiralis*, *Leishmania major*, *Tripanosoma cruzi*, *Plasmodium malariae*; and bacteria, *Escherichia coli* and *Staphylococcus aureus*. Sequence alignment and comparisons show that, of 26 residues involved in substrates binding, 16 are completely conserved, so that TS is one of the most conserved enzyme known [6]. Therefore, inhibitors against one species can be used as a starting point for development of species specific inhibitors, by taking advantage of the unique features of the active sites of each pathogenic species.

The inhibition of TS can be accomplished through the design of molecules that interfere with substrate binding. After 5-fluorouracil (the active form of which is 5-fluoro-2′-deoxyuridine-5′-monophosphate, FdUMP) the first mechanism-based inhibitor of TS introduced in anticancer chemotherapy, ZD1694 (Fig. 1), a folate-related compound, is effective in clinical therapy against colorectal cancer. Other molecules with folate-related structures have been synthesized, including CB3717, GW1843, AG337, ZD9331, LY21514 (Alimta) [9] (Fig. 1). These molecules have different metabolism according to how well they can be transported into the cells through the RFC system, or other transporter mechanisms. They can be polyglutamylated by folylpolyglutamyl synthetase (FPGS), which increases their intracellular concentration, and their affinity for the enzyme. Drug resistance mechanisms include changes in FPGS or in TS itself.

One strategy to sidestep these problems is to design compounds that avoid the metabolic steps, do not need activation and bypass the FPGS transporter mechanisms. In fact, one of the most important mechanisms of resistance is overproduction of TS due to failure of the feedback regulation of TSmRNA transcription mediated by TS [10].

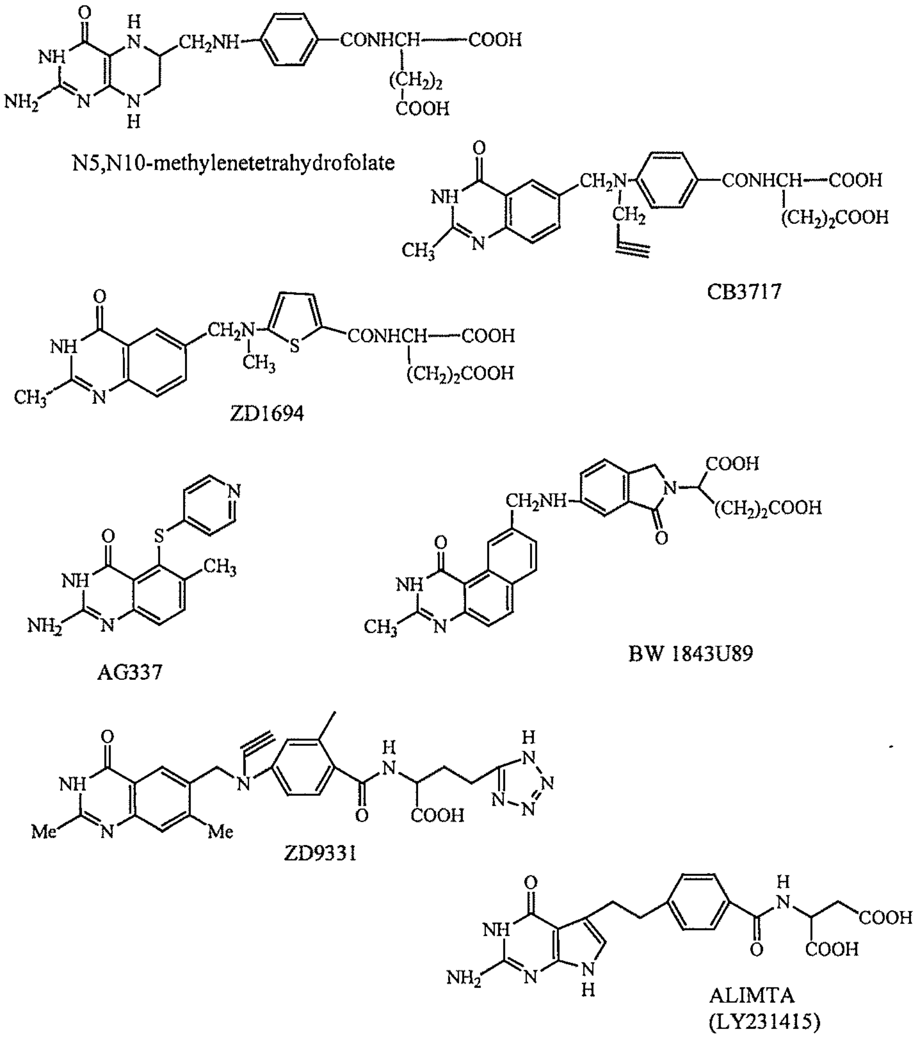

Fig. 1 Known folate analogs acting as TS inhibitors

2. Experimental procedures

Docking calculations were performed with the computer program DOCK 3.5 using rigid body energy minimization (500 steps) [11]. Electrostatic and van der Waals interaction energies were calculated using a potential map calculated by CHEMGRID. For van der Waals terms, no upper maximum was set on the interaction energy (i.e., high-energy contacts were not truncated). For electrostatic terms, a distance-dependent dielectric constant of 4R was adopted. The standard AMBER-based parameter set was used [12]. Docking calculations used crystallographically determined structures of LcTS in complex with phenolphthalein [13], compounds a156 and MR20 (Fig. 2). The atoms of these inhibitors were used as "sphere centers" in these calculations [14].

Ligand structures were built using SYBYL (Tripos Associates, St. Louis) without minimization. Partial atomic charges were calculated using the method of Marsili and Gasteiger [15].

The hTS model used here was derived from the structure of *E. coli* TS [16]. The humanized *E. coli* TS crystal structure has been used very successfully as a model of the human enzyme in previous inhibitor design studies [17–19].

3. Structure-based design of non analog antifolate inhibitors

Thymidylate synthase remains a good target for structure-based drug design [20,21]. Over 90 X-ray crystal structures have been solved since 1987, when the first X-ray structure of the apoenzyme from *Lactobacillus casei* was determined in Stroud's laboratory at UCSF in San Francisco. It was not until 1996 that the first structure of human TS was determined, initially for the apoenzyme [22,23]. Unfortunately, it was not suitable for typical antifolate drug design because the catalytic loop is twisted relative to the liganded structure [24,25]. In former years, to overcome the problem of not having the liganded hTS structure, scientists used a so-called humanized *E.coli* TS. This structure was a modification of the native EcTS in which some residues involved in ligand binding were substituted with the corresponding residues from hTS (i.e., Glu82 was truncated to alanine, Trp83 was modified to asparagine and Ile264 was modified to valine, according to EcTS numbering). Such a structure was suggested to have the correct sequence/folding for modelling hTS and it was used to design anticancer compounds [17]. Many leads and one drug have been discovered so far, using the humanized EcTS structure, such as the compounds developed at Agouron. Only recently have the ternary complex of hTS with dUMP and ZD1694 [24], and the complex with dUMP and LY21514, been obtained [25]. In principle, it is possible to rationally design compounds directed to a pathogenic TS whose X-ray structure is known, e.g., that for *P. carinii* [26], taking advantage of the sequence/structure differences with respect to human TS.

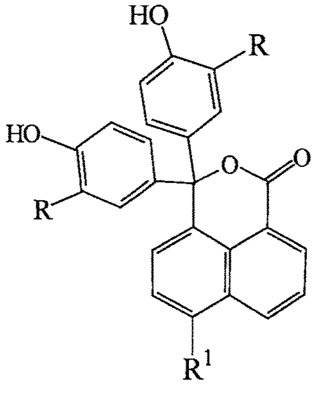

a156 R=Cl, R^1=H

MR20 R=H, R^1=NO_2

Fig 2 Naphthalein derivatives acting as nonanalog antifolate inhibitors (NAAI)

Efforts to discover species-specific inhibitors of TS often led to folate related compounds with classical nonspecific biological activity profiles. These molecules, structurally related to the folate cofactor, inhibit at the same level hTS and bacterial/fungal TS [27,28].

3.1. Phthalein derivatives discovery

In 1993, Shoichet et al. [13] published a pioneering structure-based inhibitor search based on application of docking algorithms to *L. casei* TS, and searching the available chemical database using the computational program DOCK [14]. For the X-ray ternary complex of LcTS–dUMP–CB3717, DOCK screened the FCD (Fine Chemical Directory) database, but notably excluding analogs of the substrates, i.e., dUMP analogs and folate-related compounds. This led to discovery of phenolphthalein (PTH) as a low-micromolar inhibitor of LcTS. The biological activity profile of this molecule was nonspecific: K_i vs. LcTS was 4.7 μM and K_i vs. hTS was 1.3 μM. PTH is a dye and a well-known laxative agent, so it could not be considered a lead, but a hit. Nevertheless, it is an interesting molecule because it suggested that nonfolate related molecules could bind to the TS binding site with good affinity. The X-ray crystal structure revealed that this molecule binds competitively, close to the area where CB 3717 binds in the ligand binding cavity.

Starting from PTH, the design of novel inhibitors of TS was further developed through a combination of X-ray structure analysis, database exploration and combinatorial studies. This led to new candidates that underwent synthetic optimization and biological evaluation in our hands. In such a structure-based approach, the knowledge of the 3D structure of the target in complex with the evolving compounds is key to improving the quality and reliability of successive iterations, as is the feedback from biochemical and biological screening. Applying these techniques, it was possible to develop a series of nonfolate analog TS inhibitors that included naphthalein and dansyl derivatives, as described in the following sections.

3.2. Naphthalein derivatives

Starting from the X-ray structure of the binary complex of LcTS with PTH [13], the structure of the ligand was further modified with other substituents. Small substituents on the phenolic ring, such as halogens, were introduced and their biological activity evaluated [29,30]. This led to the 2,3-naphthalein and the 1,8-naphthalein derivatives. With the latter, the results were most interesting: since introduction of the substituents on the naphthalene ring and, in particular, on the phenolic rings, influenced the biological activity profile, and the 'affinity fingerprint' [29]. Applications of docking algorithms using DOCK suggest that the naphthalein derivatives bind in the same site as PTH, with two families of orientations, both close to the classical folate recognition site. When the compounds were tested, a156 (Fig. 2) inhibited LcTS and EcTS with the same affinity ($K_i = 0.5$ μM) while it bound to hTS 40-fold less. This is, to our knowledge, the first species-specific TS inhibitor. By contrast, MR20 (Fig. 2) shows the same affinity for bacterial TS and hTS ($K_i = 1$ μM) [30]. The structural basis for the specificity of a156 was investigated by means of X-ray crystallography, mutagenesis and computation.

The X-ray crystal structure of the binary complex LcTS–a156 was determined [30]. Surprisingly, this molecule binds in a different binding site than the parent compound (PTH). It is shifted 5 Å towards the entrance of the active site with respect to the folate site. In Fig. 3, CB3717 is represented bound to its crystallographic binding site to show its relative position with respect to a156.

The X-ray structure of the LcTS–a156 complex differed from the DOCK prediction, in that the crystallographic binding mode placed the molecule close to the small domain, while DOCK placed the same molecule close to the folate recognition domain. It is well known that DOCK has such limitations, emphasizing the need for successive crystal structure determinations as the series progresses. Nevertheless, this case was not a simple one, since some experimental results suggested that these molecules could bind to more than one binding site. Mutagenesis studies were designed to better understand the mode of action of these compounds [30]. Residues that represented key interactions with the ligands involved were mutated: V316A, W82Y and E60D. The three residues are directly or indirectly involved in ligand interactions and direct or long range effects could be expected. The apparent K_i values were measured and it was observed that some substitutions diminished the extent of inhibitor binding from 3- to 20-fold (V316A and E60D with a156). Several substitutions improved the extent of inhibitor binding up to 2.5-fold (E60D with PTH and MR20). These results were ascribed to multiple binding modes in which these molecules can bind to more than one binding site with different K_i values. The crystallographic structure seems most definitive. The X-ray crystal structure was difficult to obtain and the occupancy (in terms of electron density of the ligand) of the crystallographic configuration was not complete, suggesting some disorder or multiple binding configurations [30]. Also,

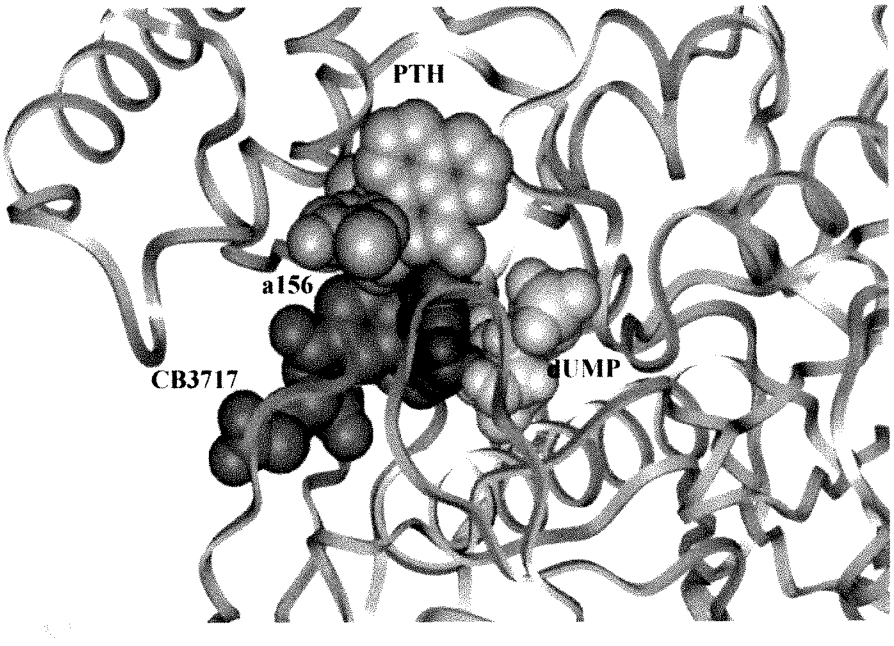

Fig. 3. Superimposition of the folate analog CB3717 and the nonfolate analogs PTH and a156 in their crystallographic binding configuration in *L. casei* TS. The X-ray crystal structures of the three compounds with LcTS have been superimposed to show the different binding configurations.

the kinetics were difficult to interpret: since some compounds were almost competitive inhibitors with respect to the folate cofactor, some were 'mixed' type inhibitors, while others were noncompetitive [29].

4. Docking analysis of naphthalein binding

Computational analysis, based on the three X-ray structures of PTH, a156, MR20 with LcTS, were applied to define the basis of species specificity. Rigid-body energy minimization and molecular docking calculations were performed to investigate how well the compounds fit into each others' binding sites, and the analogous sites in a humanized (see Section 2) *E. coli* EcTS structure [33]. The results derived from a comparison with the humanized EcTS showed how the small domain is especially important in terms of specificity, since this region is much shorter in the human enzyme.

4.1. Binding analysis of phthalein derivatives to hTS

When compound a156 is fitted into the human TS structure, in the same binding site as that of LcTS, it appears to be poorly accommodated, physically intersecting several residues. In this orientation in hTS, a156 has a high energy of interaction due to these steric conflicts. On rigid-body minimization, which allows the ligand to move as a rigid body but keeps the receptor rigid, the ligand moved by 4.2 Å from its analogous position in hTS, achieving a final energy that was higher (worse) than when minimized from its LcTS orientation (Tables 1 and 2). Molecular docking, which typically allows for further relaxation, could not fit compound a156 into hTS in a similar orientation as it adopts in LcTS (data not shown).

Although the complex between LcTS and MR20 involved several residues that differed between the human and *L. casei* enzymes, MR20 lacked the steric conflicts with the humanized *E. coli* model that compound a156 had (Table 1). Moreover, compound MR20 had few interactions with the "small domain" of LcTS. Both observations are consistent with the low specificity of compound MR20 for the bacterial vs. the human enzyme. Similar conclusions can be drawn for PTH, which can be well accommodated in the humanized EcTS binding site (Table 1).

Table 1
Energies of inhibitors in three different binding modes in the "humanized" *E. coli* TS structure after rigid body minimization

Ligand	Energy in *E. coli* site (kcal/mol)[a]	RMS (Å)[b]
PTH	−17	2.4
a156	−7.6	4.2
MR20	−17	2.2

[a] The structures of the LcTS complexes were RMS-fit on the "humanized" *E. coli* structure to orient compounds PTH, a156 and MR20 in the humanized *E. coli* structure. The positions of the inhibitors were then allowed to relax as rigid bodies to minimize their interaction energies with the protein.

[b] The RMS distance from the initial fit positions to the final energy miminized positions.

Table 2
Rigid body minimized energies of inhibitors in three different binding modes

Ligands	Score in the three binding sites (kcal/mol)					
	Site of PTH	RMS (Å)[a]	Site of a156	RMS (Å)[a]	Site of MR20	RMS (Å)[a]
PTH	−25.4	0.93	−20.9	0.25	−18.4	1.98
a156	−4.6	1.33	−26.7	0.13	−14.1	1.68
MR20	−18.3	0.9	−17.2	1.95	−17.4	1.60

[a] RMS deviation from X-ray crystallographic configuration, or best fit onto that configuration using common atoms.

4.2. Binding of inhibitors to other inhibitors site

In the calculations for LcTS, the question was whether compounds for which enzyme complex structures were available could fit well into the binding modes defined by the other two inhibitors. For instance, how well does PTH fit into the sites occupied by compounds a156 and MR20, and how well does compound a156 fit into the site occupied by compound MR20. The compounds were fitted into the three different orientations to match equivalent atoms. High-energy contacts were relaxed through rigid-body minimization keeping the conformation of the enzyme constant.

PTH and a156 fitted best in their own crystal structures of TS, while MR20 fitted equally well in all three sites (Table 2). Compound a156 showed the highest specificity for its site, both energetically and in terms of displacement on rigid body minimization, and compound MR20 showed the lowest specificity.

4.3. Molecular docking

To investigate the problem more thoroughly, we docked the individual molecules into crystal structures of LcTS using the molecular docking program DOCK 3.5 (Table 3) [11]. DOCK considers multiple orientations of a ligand in a site and is able to explore possibilities that might be missed by rigid-body energy minimizations. Docking led to orientations whose geometry corresponded more closely to the crystallographic result than did the rigid-body minimization calculations, but did not find geometries that were energetically more favorable unless we allowed for large deviations from the canonical binding modes. Considering both energy and RMS deviation, PTH and compound MR20 showed little specificity for their own binding sites, whereas compound a156 could only be fitted into its own binding sites; it could not be fitted into the PTH or compound MR20 sites unless substantial deviation was allowed.

In conclusion, modeling suggests that the crystallographic structure of each molecule represents a unique

Table 3
Molecular docking energies of inhibitors in three different binding modes

Ligands	Score in the three binding sites (kcal/mol)					
	Site of PTH	RMS (Å)[a]	Site of a156	RMS (Å)[a]	Site of MR20	RMS (Å)[a]
PTH	−21.2	0.27	−20.6	0.23	−20.0	1.55
a156	2.5	1.00	−26.7	0.10	−18.7	1.39
MR20	−20.3	0.79	−7.0	1.35	−11.5	0.85

[a] RMS deviation from X-ray crystallographic configuration, or best fit onto that configuration using common atoms.

low energy binding orientation. Alternatively this family of molecules might bind to LcTS in several low energy modes, of which the primary ones are represented by the three crystal structures. The theory of multiple binding modes is complex and cannot yet be completely interpreted by energy calculations, since the inherent errors are large. Therefore modeling studies have to be considered in light of mutagenesis and enzymology.

5. Dansyl derivatives discovery

In 1999, a new series of nonfolate analog inhibitors of LcTS were discovered through a combined approach of structure-based drug design and in parallel synthetic chemistry [31,32]. This approach has the potential to discover new hits and new scaffolds rapidly for further chemical elaboration toward a specific biological profile [32]. DOCK 3.5 was applied to screen the ACD (Available Chemicals Database) database for compounds that might bind to the binding site from the ternary complex LcTS–dUMP–CB3717. The aim was to identify nonfolate chemical structures, and particularly those suitable for further rapid elaboration by parallel synthetic chemistry and solid phase methods [33].

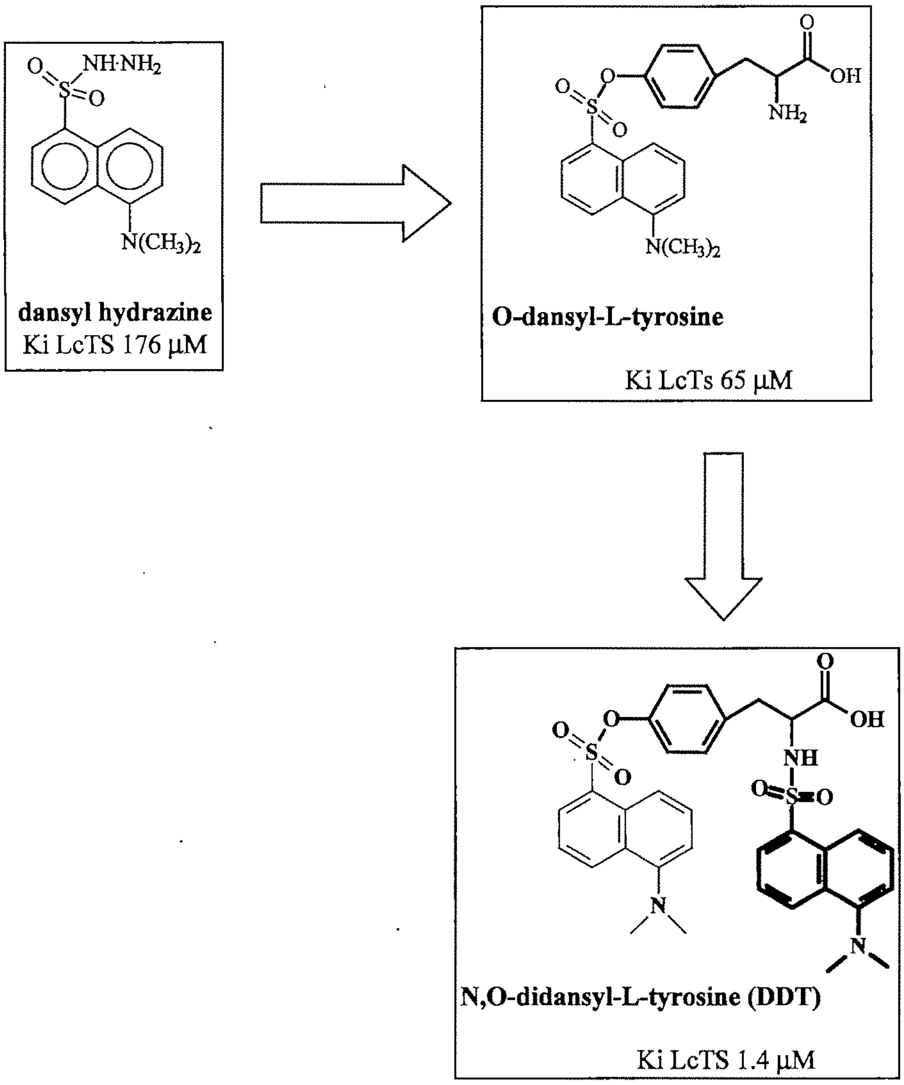

Fig. 4. Evolution of the molecular structure of the dansyl derivatives. The fragments in black show the increasing molecular complexity that is related to the improved affinity for bacterial TS and improved specificity with respect to human TS.

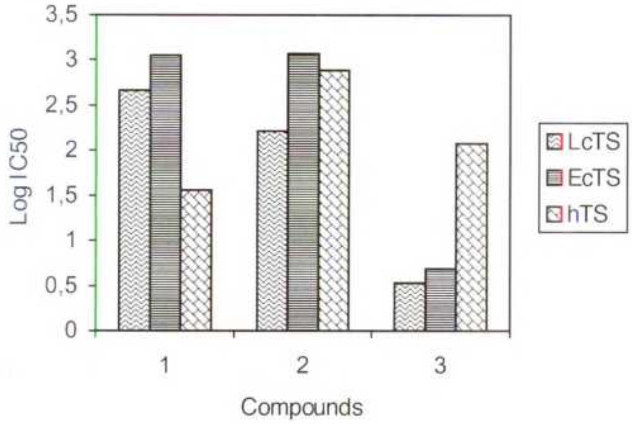

Table 4
Inhibitory activity data of dansyl derivatives towards LcTS, EcTS and hTS

Compounds	IC_{50} vs. LcTS	IC_{50} vs. EcTS	IC_{50} vs. hTS
(1) Dansyl hydrazine	458	1114	36
(2) Dansyl tyrosine	163	1170	771
(3) Didansyl tyrosine	3.4	5.0	119

Their specificity profile is represented in the plot, the log IC_{50} is reported instead of the IC_{50}, for clarity.

Four hundred molecules with the highest score were gleaned by this method and scored on the basis of the electrostatic and van der Waals (VdW) interaction energy with the enzyme, after correcting for ligand solvation [12,34]. On the basis of the DOCK score, and the number of specific interactions with the protein, five hits (IC_{50} between 300 μM and 2 mM) were tested for their ability to inhibit LcTS. Among the selected molecules, dansyl hydrazine (IC_{50} 439 μM; $K_i = 176$ μM) (Fig. 4) was a good starting point for synthetic elaboration.

The predicted binding mode for dansyl hydrazine suggested that bulkier fragments attached to the dansyl scaffold could be accommodated in the enzyme pocket. Among the more interesting was dansyl tyrosine, with a somewhat better K_i (= 65 μM) than dansyl hydrazine (Fig. 4). The molecule bears both an 'anchor site,' a functional group for linking the scaffold to the resin, and a diversity-derivatizable group (the carboxyl group and the amino group, respectively). Molecular diversity was introduced in the dansyl tyrosine molecule by synthesizing a series of analogs that carry different substituents on the amino group. A library of 34 molecules was created using in-parallel solid phase synthesis. The best of the synthesized analogs, DDT, had a K_i of 1.4 μM towards LcTS, while several others had K_i values below 10 μM. These analogs (Fig. 4) are structurally dissimilar to either of the substrates but bind competitively with them.

5.1. Docking of didansyltyrosine to L. casei TS

Further calculations were performed to understand the molecular basis for DDT affinity: 500 multiple conformations were generated by rotating all single, nonterminal bonds in increments of 120° [35]. Each conformer was independently docked and scored into the LcTS binding

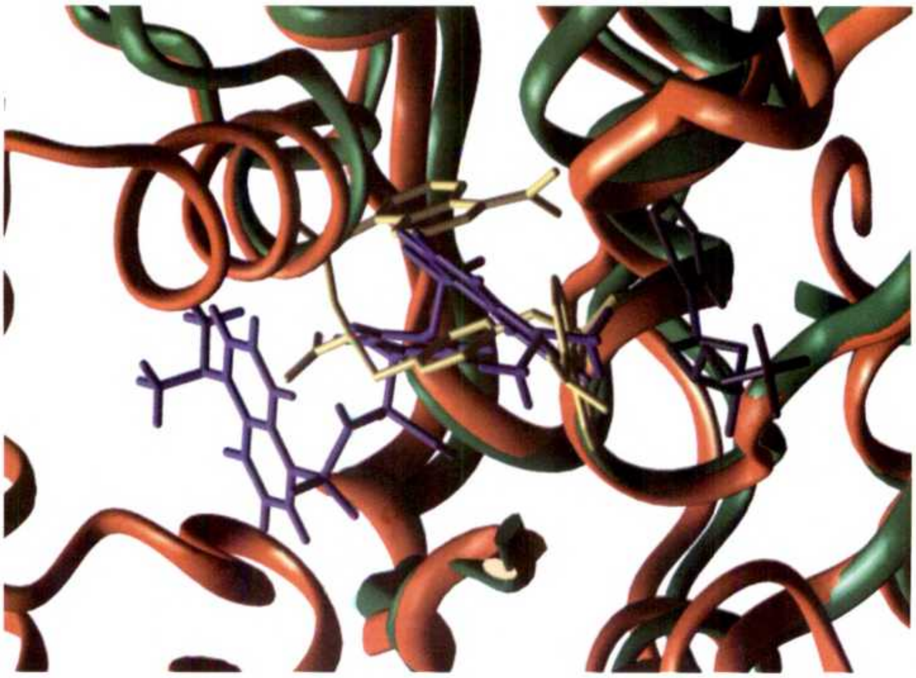

Fig. 5. Superimposition of the X-ray ternary complex EcTS–dUMP–DDT (green yellow) and the DOCK model of DDT (brown blue) with LcTS. The two molecules are reported in the same frame of reference to show the difference in the respective binding modes: DDT from the X-ray crystal structure is in the folded conformation and DDT from the DOCK model is oriented towards the entrance to the active site.

site. In the best scoring orientation, the anchor dansyl ring forms nonpolar charge transfer interactions with the pyrimidine ring of dUMP.

Increasing the molecular complexity of the dansyl derivatives, the predicted binding mode is conserved, demonstrating the value of the incremental approach to design new hits. By adding fragments under computational control, a sensible gain in binding energy can be observed (from dansyl hydrazine to DDT, the K_i is improved by 500-fold). The biological activity profile of the dansyl derivatives shows the same trend observed in the computational studies in that increasing the molecular diversity led to rapid improvement of selectivity (Table 4).

5.2. X-ray crystal structure of EcTS–DDT–dUMP

The crystal structure of the ternary complex DDT–dUMP–EcTS was subsequently solved at 2.0 Å resolution [36] (Fig. 5). The *O*-dansyl ring of DDT binds also to the site normally occupied by the quinazoline group of folate analogues, as predicted by our model for LcTS, though in a different orientation. It interacts more deeply in the binding site due to specific protein rearrangements (i.e., Arg23, Ala315, dUMP). These deep rearrangements avoid bad clashes with the inhibitor DDT and could not be predicted in our present calculations since the receptor was kept rigid. This underlines the failure of the rigid receptor hypothesis in drug design.

In the EcTS X-ray structure, the tyrosine ring is oriented close to Phe228 and Leu224, in the area normally occupied by the PABA moiety. However, this region is now occupied by the combination of the phenyl ring and *N*-dansyl group of DDT. The phenyl ring and the *N*-dansyl group form favourable aromatic stacking interactions with each other and are sandwiched between the hydrophobic residues Leu172 and Ile79. Consequently, we encounter several protein rearrangements in this site, so that the enzyme could accommodate such a complex moiety (Leu224, Phe228, Ile81, Leu56, Lys259 are the residues most involved in protein rearrangements).

The X-ray structure shows that DDT binds to EcTS in a conformation not predicted by molecular docking studies and one substantially different from other TS inhibitors. Binding of DDT is accompanied by large rearrangements of the protein that involve areas both near and far from the active site. Not surprisingly, the predicted model for DDT in LcTS and the crystallographic orientation of DDT in EcTS differ considerably from each other (Fig. 5). Moreover, the protein plasticity results in novel interactions of DDT with residues conserved in bacterial TS but not humanTS and which are hypothesized to account for DDT's species specificity.

The comparison between the binding mode that DDT displays with the two enzymes, LcTS and EcTS, underlies the fact that binding of a ligand by a protein is highly specific, often relying on subtle changes between the structures of even closely related species of a protein, and in this case, closely related species of one of the most conserved of all enzymes, TS.

6. Conclusions

Structure-based drug design is a powerful technique, especially when combined with mutagenesis and species specific competition assays. Starting from early hits, it is possible to discover new scaffolds placing the immediate computational products alongside the structural analysis of the crystal/model of the complexes. In the present cases, two series of compounds were discovered and elaborated to develop a ~ 100-fold selective inhibitor for bacterial TSs vs. human TS. The naphthalein derivatives, after two cycles of design, synthesis and evaluation, have reached an advanced stage. The dansyl derivatives are being attractive probes for structural/functional studies and more efforts are directed to improve their biological activity profiles.

Acknowledgements

The Authors kindly acknowledge Dr. Daniel V. Santi for providing the TS plasmids, Dr. Brian Shoichet for computational support, Dr. Renata Battini for molecular biology facilities. Dr. Stroud is supported by a grant from the National Institutes of Health (R01 CA 63081), Dr. Costi is supported by MURST, ex 60%.

References

[1] G.H Hitchings Jr., Selective inhibitors of dihydrofolate reductase, Angew Chem., Int Ed Engl 28 (1989) 879–889.

[2] M.P. Costi, S Ferrari, Update on antifolate drugs targets, Curr Drug Targets 2 (2001) 135–166.

[3] N Anand, Metabolite antagonism, in W.O. Foye, T L Lemke, D.A. Williams (Eds.), Principles of Medical Chemistry, 4th edn , pp. 830–835

[4] T.D. Read, S R Gill, H. Tettelin, B.A. Dougherty, Finding drug targets in microbial genomes, Discovery Today 6 (2001) 887–892.

[5] H.J Bohm, M Stahl, Structure-based library design molecular modelling merges with combinatorial chemistry, Curr Opin Chem Biol. 4 (2000) 283–286.

[6] C.W Carreras, D V Santi, The catalytic mechanism and structure of thymidylate synthase, Annu Rev Biochem 64 (1995) 721–762

[7] J C Schmitz, D. Yu, S Agrawal, E Chu, Effect of 2′-*O*-methyl antisense ORNs on expression of thymidylate synthase in human colon cancer RKO cells, Nucleic Acids Res 29 (2001) 415–422

[8] E Chu, C.J. Allegra, The role of thymidylate synthase as an RNA binding protein, BioEssay 18 (1996) 191–198

[9] A L. Jackman, Antifolate Drugs in Cancer Therapy, Humana Press, Totowa, NJ, 1999 (references therein).

[10] J Phan, D J. Steadman, S Koli, W.C. Ding, W Minor, R B Dunlap, S.H Berger, L Lebioda, Structure of human thymidylate synthase suggests advantages of chemotherapy with noncompetitive inhibitors, J Biol Chem 276 (2001) 14170–14177

[11] E.C Meng, D A Gschwend, J.M Blaney, I.D Kuntz, Orientational

sampling and rigid-body minimization in molecular docking, Proteins 17 (1993) 266–278.

[12] E.C. Meng, B. Shoichet, I.D Kuntz, Automated docking with grid-based energy evaluation, J Comp. Chem 13 (1992) 505–524

[13] B.K. Shoichet, K.M. Perry, D.V Santi, R.M. Stroud, I.D. Kuntz, Structure-based discovery of inhibitors of thymidylate synthase, Science 259 (1993) 1445–1450

[14] B. Shoichet, D.L. Bodian, I.D Kuntz, Molecular docking using shape descriptors, J. Comp. Chem. 13 (1992) 380–397.

[15] M Marsili, J Gasteiger, Fast calculation of atomic charges from molecular topology and orbital electronegativities, Stud. Phys Theor Chem. 16 (1981) 56–67

[16] W.R. Montfort, K.M Perry, E.B. Fauman, J.S. Finer-Moore, G.F Maley, L Hardy, R.M. Stroud, Structure, multiple site binding, and segmental accommodation in thymidylate synthase on binding dUMP and an anti-folate, Biochemistry 29 (1990) 6964–6976

[17] K. Appelt, R.J. Bacquet, C.A. Bartlett, C.L. Booth, S T Freer, M A Fuhry, M R. Gehring, S M. Herrmann, E F Howland, C.A. Janson, et al., Design of enzyme inhibitors using iterative protein crystallographic analysis, J Med. Chem. 34 (1991) 1925–1934

[18] T.R. Jones, M.D. Varney, S E. Webber, K.K Lewis, G.P. Marzoni, C.L. Palmer, V. Kathardekar, K.M. Welsh, S Webber, D.A Matthews, K Appelt, W.W. Smith, C.A Janson, J.E. Villafranca, R.J. Bacquet, E F Howland, C.L Booth, S M Herrmann, R.W Ward, J. White, E.W. Moomaw, C A. Bartlett, C.A. Morse, Structure-based design of lipophilic quinazoline inhibitors of thymidylate synthase, J. Med. Chem 39 (1996) 904–917.

[19] S.H. Reich, M.A Fuhry, D. Nguyen, M.J. Pino, K.M. Welsh, S. Webber, C A. Janson, S.R. Jordan, D A. Matthews, W.W. Smith, J. White, et al., Design and synthesis of novel 6,7-imidazotetrahydroquinoline inhibitors of thymidylate synthase using iterative protein crystal structure analysis, J. Med. Chem. 35 (1992) 847–858

[20] T.R. Jones, S E. Webber, M D Varney, M.R. Reddy, K K. Lewis, V Kathardekar, H. Mazdiyasni, J. Deal, D. Nguyen, K M. Welsh, S. Webber, A. Johnston, D A Matthews, W W. Smith, C.A. Janson, R J Bacquet, E F Howland, C.L. Booth, S.M. Herrmann, R W. Ward, J. White, C A Bartlett, C A Morse, Structure-based design of substituted diphenyl sulfones and sulfoxides as lipophilic inhibitors of thymidylate synthase, J Med Chem. 40 (1997) 677–683.

[21] M P. Costi, Thymidylate synthase inhibition: a structure-based rationale for drug design, Med. Res Rev. 1 (1998) 21–42

[22] C A Schiffer, V.J. Davisson, D.V. Santi, R M. Stroud, Crystal structure of human thymidylate synthase: a structural mechanism for guiding substrates into the active site, J. Mol. Biol 219 (1991) 161–163.

[23] C.A. Schiffer, I J Clifton, V.J. Davisson, D.V. Santi, R.M. Stroud, Crystallization of human thymidylate synthase, Biochemistry 34 (1995) 16279–16287.

[24] J Phan, S. Koli, W. Minor, R.B Dunlap, S H. Berger, L Lebioda, Human thymidylate synthase is in the closed conformation when complexed with dUMP and raltitrexed, an antifolate drug, Biochemistry 40 (2001) 1897–1902

[25] P.H Sayre, J.S Finer-Moore, T A. Fritz, D. Biermann, S B Gates, W C. MacKellar, V F Patel, R.M. Stroud, Multi-targeted antifolates aimed at avoiding drug resistance form covalent closed inhibitory complexes with human and *Escherichia coli* thymidylate synthases, J. Mol Biol 313 (2001) 813–819.

[26] A C Andersen, R M. O'Neil, T.S Surti, R.M. Stroud, Approaches to solving the rigid receptor problem by identifying a minimal set of flexible residues during ligand docking, Chem. Biol. 8 (2001) 445–447.

[27] A. Gangjee, A Vidwans, E Elzein, J J. McGuire, S.F. Qeener, R.L Kisliuk, Synthesis, antifolate, and antitumor activities of classical and nonclassical 2-amino-4-oxo-5-substituted-pyrrolo[2,3-d]pyrimidines, J. Med Chem. 44 (2001) 1993–2003.

[28] M.D Varney, C.L Palmer, J.G. Deal, Agouron Pharmaceuticals, USA, PCT Int Appl W096 02, 502 (CL C07D209762), 1 Feb 1996, U S. Appl. 276,929, 19 July 1994, 44 pp.

[29] M P Costi, M Rinaldi, D. Tondi, P. Pecorari, D Barlocco, S. Ghelli, R.M. Stroud, D.V. Santi, T.J. Stout, C. Musiu, E.M. Marangiu, A. Pani, D. Congiu, G.A. Loi, P. La Colla, Phthalein derivatives as a new tool for selectivity in thymidylate synthase inhibition, J. Med Chem. 42 (1999) 2112–2124

[30] T J Stout, D. Tondi, M Rinaldi, D Barlocco, P. Pecorari, D.V. Santi, I.D. Kuntz, R.M Stroud, B.K Shoichet, M P. Costi, Structure-based design of inhibitors specific for bacterial thymidylate synthase, Biochemistry 38 (1999) 1607–1617

[31] D. Tondi, Structure-based drug design, synthesis and biological evaluation of novel thymidylate synthase inhibitors, PhD thesis, University of Modena, 1997

[32] D. Tondi, U Slomczynska, S. Ghelli, D.M. Watterson, M.P. Costi, B. Shoichet, Structure-based discovery and in-parallel optimization of novel competitive inhibitors of thymidylate synthase, Chem Biol 6 (1999) 319–331.

[33] D Tondi, M.P. Costi, Enhancement of the drug discovery process by integration of structure-based drug design and combinatorial chemistry, in A.K. Ghose, V.N. Viswanadhan (Eds), Combinatorial Library Design and Evaluation. Principles, Methods, Software Tools and Applications for Drug Discovery, Marcel Dekker, New York-Basel, June 2001, pp 563–603.

[34] I D Kuntz, E C Meng, B.K. Shoichet, Structure-based molecular design, Acc Chem. Res 27 (1994) 117–123

[35] D M. Lorber, B K Shoichet, Flexible ligand docking using conformational ensembles, Prot. Sci. 7 (1998) 151–158

[36] T.A. Fritz, D. Tondi, J S. Finer-Moore, M.P. Costi, R.M. Stroud, Predicting and harnessing protein flexibility in the design of species-specific inhibitors of thymidylate synthase, Chem. Biol. 8 (2001) 981–995

ELSEVIER

Biochimica et Biophysica Acta 1587 (2002) 215–223

BIOCHIMICA ET BIOPHYSICA ACTA
BBA
www.bba-direct.com

Review

A rationale for the clinical development of the thymidylate synthase inhibitor ZD9331 in ovarian and other solid tumours[☆]

Ann L. Jackman[a,*], Camille J. Melin[b], Rosemary Kimbell[b], Lisa Brunton[b], G. Wynne Aherne[b], Davinder S. Theti[a], Mike Walton[b]

[a]*The Section of Medicine, Institute of Cancer Research, 15 Cotswold Road, Belmont, Sutton, Surrey, SM2 5NG, UK*
[b]*CRC Centre for Cancer Therapeutics, Institute of Cancer Research, Block E, 15 Cotswold Road, Belmont, Sutton, Surrey, SM2 5NG, UK*

Received 24 January 2002, accepted 24 January 2002

Abstract

ZD9331 is an antifolate drug that potently and specifically inhibits thymidylate synthase (TS). In contrast with TS inhibitors such as raltitrexed, it cannot be polyglutamated, leading to antitumour activity independent of folylpolyglutamyl synthetase (FPGS) activity. The growth inhibition IC_{50} values for ZD9331 and raltitrexed were determined for a panel of 18 human tumour cell lines, that included six colon and six ovarian. The colon lines largely displayed overlapping sensitivities to both drugs with only one of the six lines being drug resistant. In contrast, the ovarian cell lines displayed non-overlapping sensitivities with four being highly resistant to raltitrexed and only one was cross-resistant to ZD9331. Studies were undertaken to explain these results. The colon and ovarian cell lines were characterised for TS activity, and TS and FPGS mRNA expression. TS activity correlated with sensitivity to ZD9331 ($r=0.50, p=0.097$) and raltitrexed ($r=0.74; p=0.0063$). Provided the data from the highly drug-resistant cell lines (BE and 41 M) were omitted, TS mRNA expression levels also correlated with ZD9331 ($r=0.77$, $p=0.013$) and raltitrexed IC_{50} ($r=0.84$; $p=0.0031$). FPGS mRNA expression correlated with higher sensitivity to raltitrexed relative to ZD9331 (higher ZD9331/raltitrexed IC_{50} ratios) ($r=0.62$; $p=0.048$). Similarly, cell lines with IC_{50} ratios > median expressed a 1.8-fold higher median level of FPGS mRNA ($p=0.0087$) compared with those with ratios ≤ median. The four ovarian and one colon cell line that were relatively more sensitive to ZD9331 expressed FPGS mRNA ≤ median ($p=0.061$). Thus, ZD9331 overcomes resistance to raltitrexed in ovarian tumour cell lines expressing low levels of FPGS. These data, and others demonstrating a lack of cross-resistance between cisplatin and ZD9331, support the clinical evaluation of ZD9331 in platinum-refractory ovarian cancer. © 2002 Published by Elsevier Science B.V.

Keywords: ZD9331; Raltitrexed; Thymidylate synthase; Folylpolyglutamyl synthetase; Ovarian cancer

1. Introduction

Thymidylate synthase (TS) is the rate-limiting enzyme in a key pathway leading to the synthesis of thymidine nucleotides and consequently is one of several enzymes expressed early in S-phase that regulate DNA synthesis, cell cycle progression and proliferation. Recent evidence suggests that TS is an RNA binding protein, putatively binding and regulating the translation of itself, p53, c-myc and other mRNAs of growth regulatory proteins [1]. The emerging importance of TS as part of a coordinated S-phase driving machinery may explain why drugs that have direct or indirect inhibition of this enzyme, as at least part of their mechanism of action, remain widely used in cancer medicine. These include the antifolate, methotrexate and the fluoropyrimidines (5-fluorouracil and its prodrugs). More recently, the highly specific antifolate inhibitor of TS, raltitrexed, a polyglutamatable drug has become clinically available for the treatment of advanced colorectal cancer [2,3]. Predictably, the differences in metabolism, target specificity and TS binding site interactions of these drugs leads to them possessing incompletely overlapping spectra of antitumour activity and toxic side effects. An understanding of these differences led to the design and discovery

---

Abbreviations: CRC, Cancer Research Campaign; TS, thymidylate synthase; FPGS, folylpolyglutamyl synthetase; RFC, reduced-folate carrier; dUMP, 2′ deoxyuridylate; NCI, National Cancer Institute; 5-FU, 5-fluorouracil; FdUMP, 5-fluorodeoxyuridine-2′-monophosphate

[☆] This work was sponsored by the Cancer Research Campaign, UK and AstraZeneca, PLC.

[*] Corresponding author. Tel.: +44-81-643-8901; fax: +44-81-770-7885.
E-mail address: annj@icr.ac.uk (A.L. Jackman).

0925-4439/02/$ - see front matter © 2002 Published by Elsevier Science B.V.
PII: S0925-4439(02)00084-4

of the folate-based TS inhibitor, ZD9331 (TS $K_i = 0.4$ nM) [4,5]. In many respects, it shares properties with raltitrexed in that it is transported into cells via the reduced-folate carrier (RFC), binds to the folate-binding site of TS and does not inhibit other metabolic pathways. However, ZD9331 is not metabolised by folylpolyglutamyl synthetase (FPGS) and in contrast with raltitrexed (polyglutamates), ZD9331 freely effluxes across the plasma membrane. Thus, it was predicted that ZD9331 would need to be administered in a more frequent dosing schedule than the 3-weekly short infusion used for raltitrexed. However, clinical studies showed that TS inhibition recovered slowly after administration of ZD9331 and was attributed to a slow terminal phase of plasma clearance in humans. The schedule primarily being used for phase II evaluation is a short infusion on days 1 and 8 in a 3-weekly schedule [6].

Cell lines with increased TS expression through acquired resistance to TS inhibitors display cross-resistance to raltitrexed and ZD9331 [7]. However, those expressing low levels of FPGS are resistant to raltitrexed but not to ZD9331. This implies that TS and FPGS gene expressions will determine intrinsic sensitivity to these drugs in experimental and clinical settings. Indeed, in a small advanced colorectal cancer study, it was shown that low TS mRNA levels in metastatic tumour biopsies significantly predicts for increased response and survival to raltitrexed [8].

In this present study, we have used a panel of 18 human tumour cell lines (not previously exposed to antifolates) to evaluate the relative activity of ZD9331 and raltitrexed. Tumour types represented are ovarian, colon, lung, mesothelioma and vulvular. The study focuses on some molecular determinants of response to raltitrexed and ZD9331 in the six ovarian and six colon cell lines because they represent tumour types relatively clinically resistant and sensitive to raltitrexed, respectively. The response rate in platinum-refractory ovarian cancer was ~ 7% while first-line treatment in colorectal cancer patients was ~ 20% [9]. Across the whole cell line panel, these drugs displayed incompletely overlapping spectra of antitumour activity. Interestingly, ZD9331 overcame resistance to raltitrexed in ovarian cell lines expressing low FPGS mRNA. Taken together, these data predict that ZD9331 may have greater clinical activity than raltitrexed in this tumour type. Furthermore, we have demonstrated that ZD9331 and cisplatin, the commonly used first-line of treatment for ovarian cancer, are non-cross-resistant in the ovarian tumour cell lines.

2. Experimental procedures

2.1. Cell lines, media and drugs

Colon tumour cell lines HT29, SW620, SW480, Mawi, BE and LoVo were obtained from stocks held at the Institute of Cancer Research, UK. The biological details of the ovarian cell lines have been described previously [10,11]. Two of the ovarian cell lines had been obtained from patients previously treated with cytotoxic drugs: platinum-based drugs (CH1 and PXN94), thiotepa (SKOV-3). All cell lines were grown as adherent monolayers in DMEM medium (Gibco, Paisley, Scotland) plus 10% (v/v) dialysed foetal calf serum (ICN Flow, Thames, Oxfordshire, UK), 50 μg/ml gentamicin, 2.5 μg/ml amphotericin B, 2 mM glutamine (all from Gibco), 5.5 μg/ml insulin and 0.44 μg/ml hydrocortisone in a 10% CO_2, 90% air atmosphere. All cell lines were negative for mycoplasma as measured by the Strategen PCR kit (Cambridge, UK).

RTX and VDX were obtained from AstraZeneca, PLC and cisplatin (CDDP) was obtained from Sigma-Aldrich (Poole, Dorset, UK). The antifolates were dissolved in 0.15 M $NaHCO_3$ (stored at − 20 °C for up to 3 months) at 10 mM and CDDP in saline at 2 mM. Dilutions were in unsupplemented medium.

2.2. Growth inhibition assays

Single cells (harvested after trypsinisation of a ~ 70% confluent flask) were seeded at 1 to 3×10^3 cells/well (in 160 μl) into 96-well plates. After overnight incubation to allow attachment, drug dilutions (40 μl) were added at various concentrations in quadruplicate wells. After incubation for 96–120 h (three to four population doublings) growth inhibition was then assessed using an MTT assay as a surrogate end-point of viability as described previously [12,13]. The IC_{50} was defined as the concentration of compound required to inhibit cell growth/reduce absorbance at 540 nm by 50%.

2.3. TS activity measurements

The rate of $[^3H]_20$ release from 5-$[^3H]$dUMP was measured in freshly prepared supernatants from each cell line as described previously [7,14]. The results are expressed as nmol product formed/h/mg protein.

2.4. TS and FPGS mRNA expression by Northern blotting

RNA was extracted from exponentially growing cells using guinidinium isothiocyanate and separated through a cesium chloride gradient [15]. RNA concentrations were determined spectrophotometrically. RNA samples were separated on 1.2% formaldehyde gels and transferred to Hybond N nylon membranes by capillary transfer. The human FPGS probe was a full-length cDNA *Eco*R1 restriction of pTZ18U-hFPGS plasmid [16]. The TS probe was a 750-bp Pst1 fragment of the mouse TS cDNA from pMTS-3 plasmid [17]. The GAPDH probe was a 1.3-kb Pst1 restriction fragment of a rat cDNA. Probes were random prime labelled using a commercial kit (Amersham Pharmacia, UK). Hybridization, washing, visualisation and quantification were as previously described [18].

Two sets of RNA were prepared from each of the six ovarian cell line and each set subjected to Northern blotting four times. Each blot included all six ovarian cell lines and also a lane loaded with RNA from the HT29 colon cell line as a reference. Following phosphoimaging, the bands for TS, FPGS and GAPDH for each cell line were expressed as the percentage of the total sum above background (this allows for any differences in exposure times for one or more of the RNA species of interest between experiments). TS and FPGS for each cell line in each blot were then expressed relative to GAPDH (to accommodate any differences in loading). The results are expressed as the mean of each set of RNA which in turn is expressed relative to the mean value for HT29. This allowed the results to be compared with those for the colon tumour cell lines that were determined separately from the ovarian tumour cell lines. For the colon lines, each blot included RNA from all six cell lines. One set of RNA was subjected to Northern blotting four times and the second set three times. The mean of results of each set was expressed relative to HT29 as described above.

2.5. Statistical analyses

The non-parametric Spearman correlation was used to quantitate the degree of linear association between two variables (GraphPad Instat). Linear regression was used to fit a line to data not containing significant outliers (GraphPad Prism). The non-parametric Mann–Witney test was used to test whether variables differed between two subsets of a group.

In some cases the subsets were separated with respect to their position above or below the median for the group. Some data were anlysed by a 2 × 2 contingency table (Fischers exact test; GraphPad Prism).

3. Results

3.1. Sensitivity of 18 human tumour cell lines to ZD9331 and raltitrexed

The 18 human tumour cell lines displayed a wide range of sensitivities to raltitrexed and ZD9331. A correlation was observed between the IC_{50} for the two drugs ($r = 0.72$; $p = 0.0007$) although there were a significant number of outliers illustrated by a weak linear correlation ($r^2 = 0.27$; $p = 0.026$; data not shown). The log IC_{50}s for raltitrexed and ZD9331 were calculated for all cell lines and the medians generated for each drug. These medians were subtracted from the individual log IC_{50}s and presented as difference median plots for each drug in Fig. 1. This gives broad

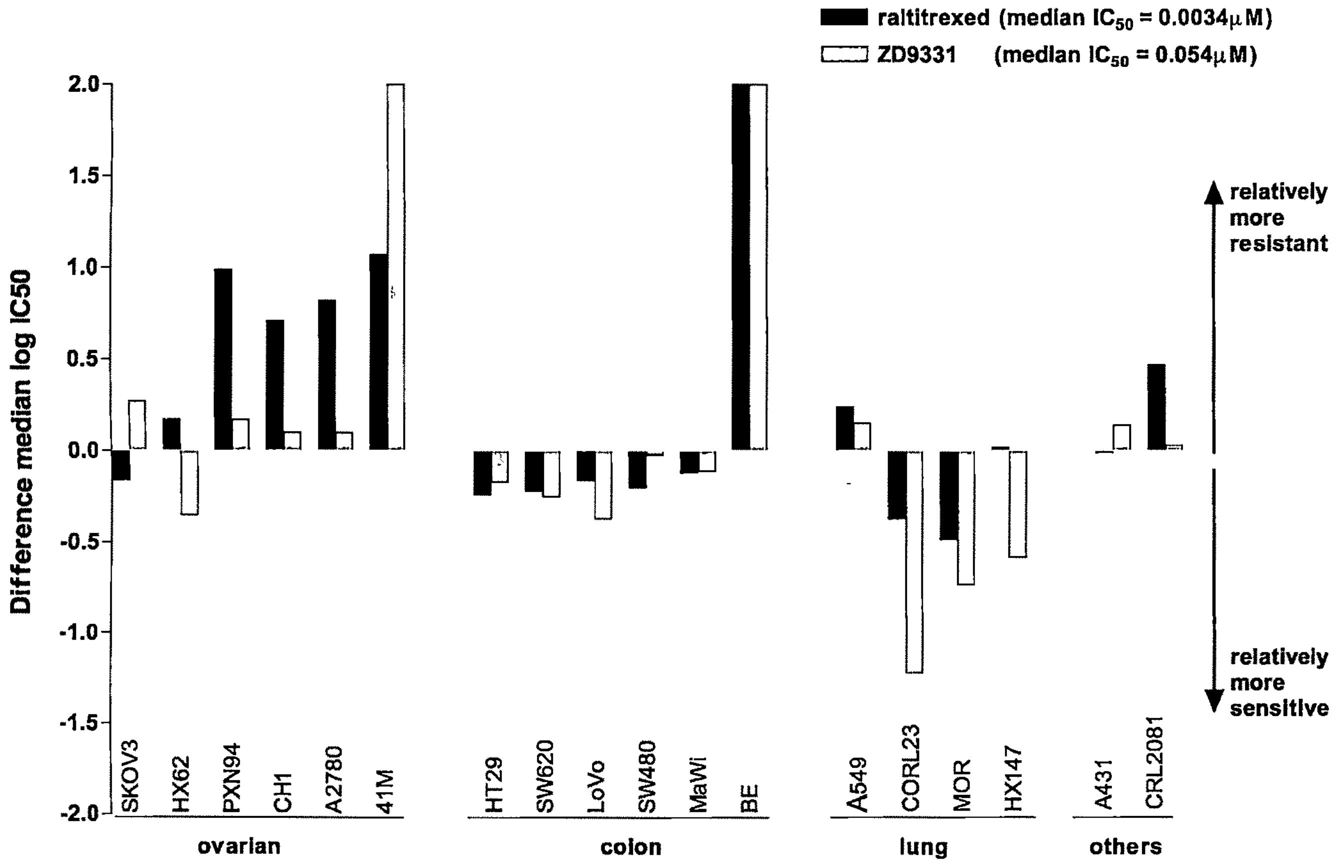

Fig. 1 Difference median plots for ZD9331 and raltitrexed in 18 human tumour cell lines The IC_{50} data for ZD9331 and raltitrexed were log-transformed and medians derived for each drug. The plot was generated by subtracting the medians from the individual IC_{50}s

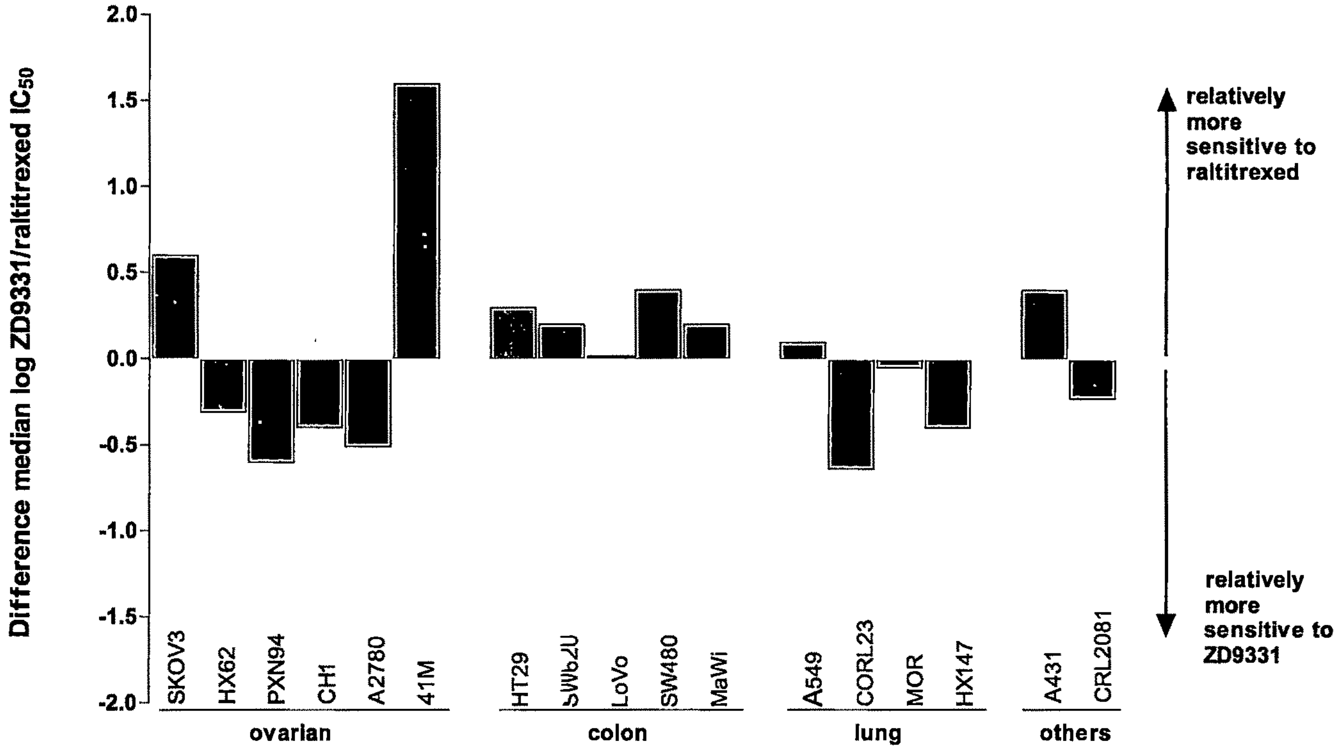

Fig. 2. Difference median plots for relative sensitivity to ZD9331 and raltitrexed in 18 human tumour cell lines The ratios of the IC$_{50}$ ZD9331/IC$_{50}$ raltitrexed were log-transformed and the median subtracted.

patterns of activity of the two drugs with positive values representing relative resistance and negative values representing relative sensitivity. The median is generated from a relatively low number of cell lines compared with the 60 lines in the National Cancer Institute (NCI) panel and therefore values falling slightly on either side of the median should not be over-interpreted in terms of relative sensitivities. The BE colon cell line was highly resistant to both

Table 1
Growth inhibition and target expression in human ovarian and colon tumour cell lines

	Histological tumour type	Growth inhibition IC$_{50}$ (μM)[a]		ZD9331 IC$_{50}$/ raltitrexed IC$_{50}$	TS activity (nmol/h/mg protein)[b]	mRNA relative to GAPDH (normalised to HT29)[c]	
		ZD9331	Raltitrexed			TS	FPGS
SKOV3	ovarian	0.098	0.0023	43	2.6	2.5	1.2
HX62	ovarian	0.024	0.0049	4.9	8	1.5	0.49
PXN94	ovarian	0.081	0.032	2.5	13	2.6	0.57
CH1	ovarian	0.068	0.017	4.0	19	2.6	0.71
A2780	ovarian	0.068	0.022	3.1	16	2.6	0.44
41M	ovarian	15	0.039	385	8	0.88	0.71
Median	ovarian	0.075	0.020	4.5	11	2.6	0.64
HT29	colon	0.036	0.0019	19	2.5	1.0	1.0
SW620	colon	0.031	0.0020	16	6.6	1.1	0.80
LoVo	colon	0.023	0.0023	10	2.3	0.8	0.44
SW480	colon	0.051	0.0021	24	7.1	1.2	0.64
MaWi	colon	0.042	0.0025	17	2.9	1.3	0.91
BE	colon	~ 10	~ 10	–	14	0.85	0.53
Median	colon	0.039	0.0022	17	4.8	1.1[d]	0.72
Median	colon + ovarian	0.06	0.0037	–	7.6	1.2	0.68
Median	– BE	0.051	0.0025	15	7.1	1.3	0.71

[a] Mean of 3 to 6 separate experiments.

[b] Mean of 5 to 10 separate experiments.

[c] TS/GAPDH or FPGS/GAPDH ratios for each cell line are expressed relative to the HT29/GAPDH ratio

[d] Significantly different from ovarian ($p < 0.05$).

Table 2
Relationship between growth inhibition and target expression in colon and ovarian human tumour cell lines

		TS activity	mRNA	
			TS	FPGS
ZD9331 IC_{50}	all cell lines	$r=0.50$	$r=0.17$	$r=0.17$
		$p=0.097$	$p=0.60$	$p=0.60$
	−BE	$r=0.46$	$r=0.41^{a}$	$r=0.26$
		$p=0.16$	$p=0.20$	$p=0.45$
Raltitrexed IC_{50}	all cell lines	**$r=0.74$**	$r=0.1$	$r=-0.45$
		$p=0.0063$	$p=0.63$	$p=0.14$
	−BE	**$r=0.72$**	$r=0.44^{b}$	$r=-0.43$
		$p=0.014$	$p=0.18$	$p=0.19$
ZD9331/ raltitrexed IC_{50}[c]	−BE	$r=-0.53$	$r=-0.61$	**$r=0.62$**
		$p=0.094$	$p=0.052$	**$p=0.048$**

The non-parametric Spearman correlation was used to quantitate the degree of linear association between two variables. TS mRNA vs FPGS mRNA: $r=0.042$, $p=0.90$.

[a] Removal of 41 M gives $r=0.77$, $p=0.013$.

[b] Removal of 41 M gives $r=0.84$; $p=0.0031$

[c] No ratio can be generated for the BE cell line

drugs while data for the other five colon lines clustered close to the median (Fig. 1). In contrast, four of the six ovarian lines (PXN94, CH1, A2780 and 41 M) were resistant to raltitrexed while only one (41 M) was resistant to ZD9331. The four lung cell lines in the panel generally displayed high sensitivity to raltitrexed and particularly to ZD9331.

More information regarding the mechanisms underlying the different patterns of drug activity is gained by presenting the data as the ratio of the IC_{50} of ZD9331 to the IC_{50} of raltitrexed for each cell line. These ratios were log-transformed and the median subtracted and are presented in Fig. 2. Four of the five colon cell lines were relatively more sensitive to raltitrexed, while two of the four lung and four of the six ovarian cell lines were relatively more sensitive to ZD9331. The ovarian panel displayed the largest range of relative sensitivities, with PXN94, A2780, CH1 and HX62 being markedly more sensitive to ZD9331 than raltitrexed. In contrast, the SKOV3 and 41 M cell lines were relatively more sensitive to raltitrexed than ZD9331.

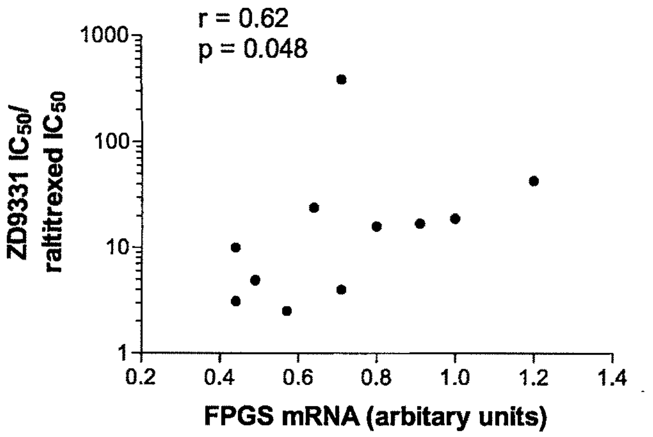

Fig. 3. Relationship between FPGS mRNA expression and relative sensitivity to raltitrexed compared with ZD9331 FPGS/GAPDH mRNA (relative to HT29) is plotted against the ratio of the ZD9331 IC_{50}/raltitrexed IC_{50} for each cell line. A ratio could not be generated for BE (IC_{50} for both cell lines >10 μM)

3.2. TS activity, TS mRNA and FPGS mRNA in 12 human ovarian and colon tumour cell lines

The 12 colon and ovarian cell lines displayed a 3.3-fold variation in TS mRNA levels and an 8-fold variation in TS activity (Table 1). A relationship was found between TS mRNA and TS activity that was not quite statistically significant ($r=0.45$, $p=0.072$; data not shown). This was largely because two cell lines, SKOV3 and BE had discordant values, with TS activity low relative to the mRNA level for SKOV3 and vice versa for BE. If these cell lines were excluded from the dataset, the correlation became significant ($r=0.80$; $p=0.0072$) (data not shown). FPGS mRNA expression varied 2.7-fold among the 12 colon and ovarian cell lines. There was no relationship between FPGS and TS mRNA expression.

The median TS activity level was 2.3-fold higher in the ovarian cell line panel compared with the colon cell line panel that was not quite statistically significant (11 and 4.8 pmol/h/mg protein, respectively; $p=0.093$). However, there was 2.4-fold higher median TS mRNA expression in the ovarian compared with the colon panel (median = 2.6 and 1.1, respectively; $p=0.026$) (Table 1). Median FPGS mRNA levels were lower in the ovarian panel than the colon panel (0.64 and 0.72, respectively) but this difference was not statistically different.

Table 3
Target expressions stratified for growth inhibition in colon and ovarian tumour cell lines

		Inhibition of cell growth (IC_{50})	TS activity	mRNA	
				TS	FPGS
ZD9331 $IC_{50}IC_{50}$	all cell lines	≤ median	**4.8**	1.2	0.72
		> median	**14**	2.6	0.64
			$p=0.026$	$p=0.24$	$p=0.82$
	−BE	≤ median	4.8	1.2	0.72
		> median	13	2.6	0.71
			$p=0.052$	$p=0.082^{a}$	$p=0.93$
Raltitrexed IC_{50}	all cell lines	≤ median	**2.8**	1.2	0.86
		> median	**14**	2.1	0.55
			$p=0.0022$	$p=0.31$	$p=0.093$
	−BE	≤ median	**2.8**	1.2	0.86
		> median	**13**	2.6	0.57
			$p=0.0043$	$p=0.13^{a}$	$p=0.13$
ZD9331/ RTX IC_{50}[b]	−BE	≤ median	13	2.6	**0.49**
		> median	4.8	1.2	**0.86**
			$p=0.13$	$p=0.18$	**$p=0.0087$**

The non-parametric Mann–Whitney test was used to test whether the variables differed between IC_{50} values above or below the median

[a] $p=0.032$ if 41 M cell line data omitted.

[b] Cannot be generated for the BE cell line.

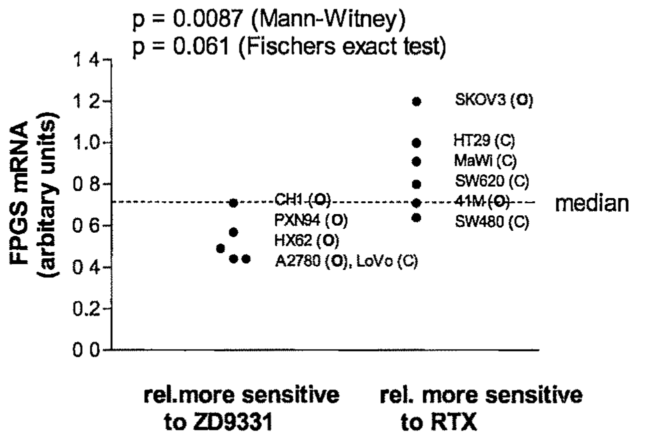

Fig 4 FPGS mRNA expression stratified for cell line relative drug sensitivity FPGS/GAPDH mRNA (relative to HT29) is stratified for cell lines with ZD9331 IC_{50}/raltitrexed IC_{50} ratios above and below the median. O = ovarian; C = colon No ratio could be generated for BE

3 3. Determinants of sensitivity—statistical analyses

The relationships between cell line sensitivity to the drugs and target expression profiles are given in Table 2. TS activity for all cell lines correlated with raltitrexed IC_{50}s ($r = 0.74$; $p = 0.0063$) but not quite significantly with ZD9331 IC_{50}s ($r = 0.50$; $p = 0.097$). TS mRNA expression did not correlate with sensitivity to either drug unless the data for the two highly drug resistant BE and 41 M cell lines were omitted (raltitrexed, $r = 0.84$, $p = 0.0031$; ZD9331, $r = 0.77, p = 0.013$).

There was an inverse relationship between FPGS mRNA expression and raltitrexed IC_{50}s but this was not statistically significant ($r = -0.45$; $p = 0.14$). However, a significant correlation ($r = 0.62$; $p = 0.048$) was found between FPGS mRNA expression and the relative ZD9331/raltitrexed IC_{50} ratios, i.e. increasingly high levels of FPGS expression are associated with increasing sensitivity to raltitrexed relative to ZD9331 (Fig. 3).

Table 3 stratifies drug sensitivities (IC_{50}s) above and below their respective medians and then compares the gene expressions/activity for each group. Cell lines with higher sensitivity to ZD9331 or raltitrexed ($IC_{50} \leq$ median) displayed a significantly lower ($p < 0.05$) median TS activity level (3- and 5-fold, respectively). Those with raltitrexed $IC_{50} \leq$ median expressed a 1.6-fold higher median FPGS mRNA level ($p = 0.093$). However, those with ZD9331/raltitrexed IC_{50} ratios $\leq$ median expressed a 1.8-fold lower median level of FPGS ($p = 0.0087$) compared with those with ratios>median. These data, which is shown graphically in Fig. 4, are consistent with FPGS mRNA expression being a determinant of cell line sensitivity to raltitrexed relative to ZD9331. The five cell lines relatively more sensitive to ZD9331, which included four ovarian, had FPGS mRNA levels $\leq$ to the median. Only two of the six cell lines relatively more sensitive to raltitrexed (one ovarian and one colon) had FPGS mRNA levels $\leq$ median ($p = 0.061$; Fischers exact test).

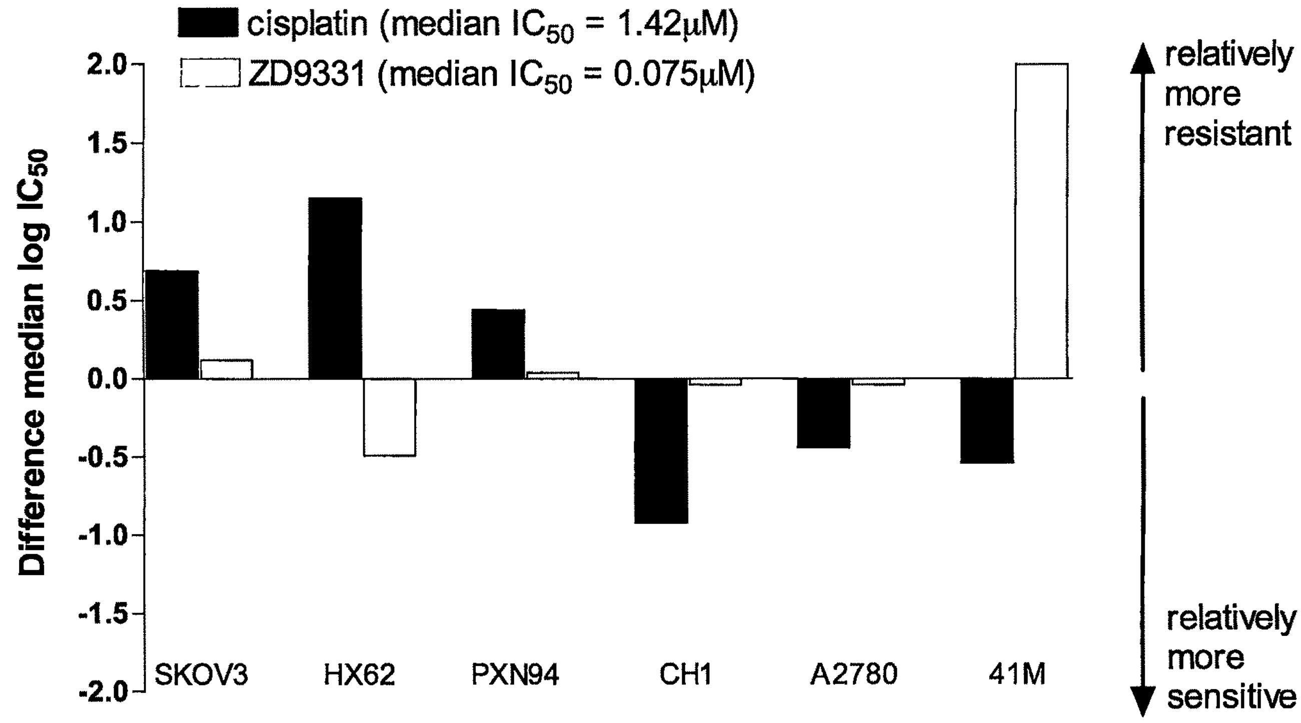

Fig. 5 Difference median plots for ZD9331 and cisplatin in six human ovarian tumour cell lines The IC_{50} data for ZD9331 and cisplatin were log-transformed and medians derived for each drug The plot was generated by subtracting the medians from the individual IC_{50}s.

3.4. Relative sensitivity of the ovarian cell line panel to ZD9331 and cis-platinum

The relative sensitivity of ZD9331 was compared with that of published data for cisplatin from these laboratories. Three cell lines (CH1, A2780 and 41 M) are platinum-sensitive (IC_{50}s 0.1–0.3 μM), and three (SKOV3, HX62 and PXN94) are relatively platinum-resistant (IC_{50}s 3–13 μM). In contrast, the 41 M cell line is highly resistant to ZD9331 and the others, particularly the HX62, are highly sensitive to ZD9331. Thus, no cross-resistance is observed between these two drugs (Fig. 5).

4. Conclusions and perspectives

4.1. Cell line sensitivity to raltitrexed and ZD9331

Different classes of TS inhibitors have been developed in recent years, each with different cellular pharmacology and specificity for the enzyme. Although drug-resistant cell lines (usually with high levels of in vitro acquired resistance) have been useful in describing the different patterns of activity of these drugs, they do not necessarily reflect patterns of resistance in vivo. Thus, it can be more relevant to use intrinsically resistant lines, or lines developed from patients resistant to chemotherapy, to evaluate tumour sensitivity. However, predicting clinical sensitivity to new agents by extrapolation from in vitro cell lines is difficult. The problem has been addressed, in part, by the use of panels of human tumour cell lines (such as the NCI in vitro cell line panel), with several representatives from each of a number of tumour types [19]. This allows the assessment of the relative sensitivity of tumour types to given agents, by expressing activity relative to a mean or median for all the cell lines, and the sensitivity of individual cell lines within that panel. This information can also be used in the context of gene expression patterns to tease out potential determinants of sensitivity and resistance to anticancer agents. This type of approach has been applied in this present study and has provided a rationale for the clinical development of ZD9331 in solid tumours such as ovarian cancer.

This study has focused primarily on colon and ovarian tumours although other cell lines have been included in order to derive a more representative median growth inhibition IC_{50} value. Five of the six colon tumour cell lines were uniformly sensitive to raltitrexed while only two of the six ovarian tumour cell lines displayed a similar level of sensitivity. Thus, the cell line panel broadly reflects the clinical sensitivity and resistance to raltitrexed in clinical colon and ovarian cancer [9]. Interestingly, ZD9331 was more broadly active than raltitrexed and overcame resistance to raltitrexed in three of four highly raltitrexed-resistant ovarian cell lines (PXN94, CH1 and A2780). A further cell line, HX62, was also relatively more sensitive to ZD9331 than raltitrexed. Although the number of cell lines evaluated was small, the data suggests that ZD9331 may have greater clinical activity than raltitrexed in ovarian cancer.

4.2. Molecular determinants of sensitivity to TS inhibitors

In order to explore the molecular basis for the differences observed in sensitivity to the raltitrexed and ZD9331, TS and FPGS gene expressions were measured in the colon and ovarian cell lines. Despite the small number of cell lines examined, a number of correlations were observed, some of which attained significance at the 95% confidence level. The activity of the target, TS, significantly correlated with sensitivity to raltitrexed in all of the 12 colon and ovarian cell lines ($p = 0.0063$), which is in contrast with reported data for 13 colon tumour cell lines [20]. TS activity correlated with ZD9331 sensitivity ($p = 0.097$). Our data are broadly consistent with a report that TS activity is related to Nolatrexed sensitivity in colon and leukaemia cell provided that the data for three cell lines were omitted [21]. A difference between these reports and our data may relate to the method of calculation of the activity measurements. We have normalised data to protein concentration rather than cell number. This may account for the very different ranking of cell lines common to this report and that of Estlin et al. [21]. Normalising to protein content may also explain our better relationship between TS activity and mRNA expression. However, the number of cell lines included in both of these studies is small, and consequently, outliers often markedly reduced the significance of the correlations. Recently, Grem et al. [19] performed a similar correlation across most of the NCI 60 human tumour cell line panel. They reported only a weak to moderate correlation between TS protein and TS mRNA ($r = 0.45$).

TS mRNA did not correlate with sensitivity to ZD9331 and raltitrexed. However, if the data for the highly resistant 41 M and BE cell lines were omitted, significance was attained. Those cell lines that displayed ZD9331 or raltitrexed IC_{50}s higher than the median had a 2-fold higher median TS mRNA level that was statistically significant if the data for the highly drug resistant 41 M and BE cell lines were omitted. These data are consistent with clinical reports that TSmRNA expression predicts for response and survival to 5-FU or raltitrexed [8,22].

Possible explanations for the failure of TS expression to correlate with sensitivity to 5-FU or 5-fluorodeoxyuridine (5-FdUrd) in the NCI human tumour panel are given by Grem et al. [19]. They include the short duration of the assay (48 h) relative to the median cell doubling time of 34 h (18–38 h) with the general failure to induce cytotoxicity. This may explain why the median 96 h IC_{50}s of 5-FdUrd in our panel of six colon tumour cell lines was 0.008 μM compared with a GI_{50} of 1.2 μM for the six colon cell lines in the NCI panel. Two cell line examples common to both panels are the SW620 and HT29 in which we reported IC_{50}

values of 0.007 and 0.0067 μM for 5-FdUrd [2], whereas the NCI reported GI_{50}s of 23 and 0.75 μM, respectively. Furthermore, we use MTT as a surrogate end-point of growth inhibition as we have found this a more reliable end-point for TS inhibitors than SRB (used by the NCI and others). TS inhibition induces megaloblastosis and leads to an increase in total protein content, that is detectable until lethality and cell loss has occurred. A consequence can be shallow dose–response curves and high IC_{50}s. Grem et al. [19] argued that the high dThd concentration in the medium did not contribute to the lack of correlation between fluoropyrimidine sensitivity and TS expression because the concentration is lower than that often reported to reverse TS inhibition. However, it is important to note that in vitro, dThd is high at the time of drug addition and then decreases largely as a function of proliferation rate as it becomes depleted through its incorporation into DNA [23]. Thus, plating density and the rate of DNA synthesis (related to cell doubling times) determine how rapidly dThd falls to a concentration that will not protect cells from TS inhibition. This may explain why, in contrast with 5-FdUrd, the median 5-FU GI_{50} in the NCI colon panel (6.3 μM) is very similar to our own IC_{50} value of 4.7 μM. The mechanism of action of 5-FU partly relates to its RNA-directed effects and would therefore be less affected by the dThd in the medium.

FPGS is the enzyme responsible for catalysing the formation of the active raltitrexed polyglutamates, and in this study, FPGS mRNA levels did not correlate with sensitivity to raltitrexed. This may be due, at least in part, to post-translational regulation of this enzyme [24]. However, Van Triest et al. [20] measured FPGS activity in a panel of 13 non-selected colon cell lines and did not find a positive correlation with sensitivity to raltitrexed. Nevertheless, FPGS activity is itself a fairly crude assay in that it only measures mono to diglutamate formation and does not necessarily predict for the formation of the important long chain-length polyglutamates of raltitrexed. Data not presented showed a significant correlation between FPGS mRNA and raltitrexed (polyglutamate) accumulation in 11 of the 12 cell lines after 24 h exposure to 0.1 μM [^{3}H]-raltitrexed ($r = 0.75$; $p = 0.0049$). Data from the HX62 was excluded from the analyses because of the discordantly high raltitrexed uptake relative to its FPGS mRNA expression. However, no correlation was seen between drug accumulation and raltitrexed sensitivity.

These data are consistent with other reports that suggest that the measurement of a single gene expression, activity or drug concentration in small numbers of cell lines do not provide highly significant statistical correlations with drug sensitivity. Furthermore, the fact that correlations are generally weak reinforces the belief that drug sensitivity is multifactorial and will rarely be attributable to expression of a single gene. Hence, expression of components of downstream pathways including the uracil–DNA misincorporation pathway and those driving survival and apoptosis may be significant. This is supported by data from experimental cell lines, including those transfected with dUTPase or bcl-2, that are less sensitive to raltitrexed and ZD9331 [25,26].

4 3 Rationale for the use of ZD9331 in ovarian cancer

The primary purpose of the gene expression measurements was to explain the relative sensitivity of the ovarian cell lines to ZD9331 compared with raltitrexed and therefore to provide a rationale for the clinical evaluation in this disease. We rationalised that downstream gene expressions that may impact on sensitivity would commonly affect both drugs, and therefore ZD9331/raltitrexed IC_{50} ratios may correlate with FPGS expression or raltitrexed polyglutamate formation. Indeed, a significant correlation with FPGS mRNA expression was observed. However, there was also a trend towards an inverse relationship between the IC_{50} ratio and TS activity or TS mRNA suggesting that cell lines with high TS were relatively more sensitive to ZD9331 than raltitrexed. Similar observations were made when relative drug sensitivity was stratified above and below the median and correlated with gene expressions. Furthermore, the four ovarian cell lines (HX62, PXN94, CH1 and A2780) and the one colon line (LoVo) that were relatively less sensitive to raltitrexed than ZD9331, expressed FPGS mRNA levels ≤ median ($p = 0.061$; Fischers exact test).

An important conclusion from the study is that ZD9331 largely overcomes resistance to raltitrexed in ovarian tumour cell lines expressing low FPGS mRNA, and may also overcome resistance due to small elevations in TS expression. Recently, we reported higher TS mRNA and lower FPGS mRNA (median = 9.4 and 6.2×10^3 relative to β-actin, respectively) in 42 ovarian tumours compared with 20 metastatic colon tumours (median = 5.6 and 26×10^3 relative to β-actin, respectively, $p < 0.05$) [8,27]. Taken together, these data may explain the low clinical response rate to raltitrexed in ovarian cancer, and predict for increased sensitivity to ZD9331. Furthermore, the lack of cross-resistance between cisplatin and ZD9331 in the ovarian cell line panel supports the further clinical evaluation of ZD9331 in platinum-refractory ovarian cancer. Finally, a relevant observation reported elsewhere by ourselves, is that ZD9331 can be alternatively transported into tumours via the α-folate receptor (α-FR) and has high activity in α-FR overexpressing cell lines [28]. However, this activity is not observed in cell lines grown in commercial media that contain supraphysiological concentrations of folic acid. Thus, the ZD9331 sensitivity described herein cannot be attributed to α-FR mediated uptake. Approximately, 90% of ovarian tumour specimens overexpress this receptor [29] and we predict that this will contribute to ZD9331 clinical activity in ovarian cancer.

In summary, experimental data supports the clinical evaluation of ZD9331 in platinum-refractory ovarian cancer. Potential molecular predictors of response are TS and α-FR and we recommend incorporation of these markers into further ovarian cancer clinical studies.

Acknowledgements

The authors would like to thank Dr. Tom Boyle and his colleagues at AstraZeneca for their valuable contributions to the work associated with ZD9331.

References

[1] E. Chu, J Ju, J C. Schmitz, Molecular regulation of expression of thymidylate synthase, in: A L. Jackman (Ed.), Anticancer Drug Development Guide: Antifolate Drugs in Cancer Therapy, Humana Press, Totowa, NJ, 1999, pp. 397–408

[2] A.L. Jackman, D Farrugia, W. Gibson, R. Kimbell, K.R Harrap, T C. Stephens, M. Azab, F T. Boyle, ZD1694 (Tomudex): a new thymidylate synthase inhibitor with activity in colorectal cancer, Eur J. Cancer 31A (1995) 1277–1282.

[3] A.J Matheson, S. Noble, Management of colorectal cancer: defining the role of raltitrexed, Dis Manag Health Outcomes 9 (2001) 269–287. Adis International, Ltd

[4] A L. Jackman, R Kimbell, G W. Aherne, L Brunton, G Jansen, T.C. Stephens, M Smith, J M Wardleworth, F T Boyle, The cellular pharmacology and in vivo activity of a new anticancer agent, ZD9331. a water-soluble, non-polyglutamatable quinazoline-based inhibitor of thymidylate synthase, Clin Cancer Res. 3 (1997) 911–921.

[5] F T Boyle, T.C Stephens, S D Averbuch, A.L Jackman, ZD9331· preclinical and clinical studies, in· A L. Jackman (Ed), Antifolate Drugs in Cancer Therapy, Humana Press, Totowa, NJ, USA, 1999, pp 243–260.

[6] R. Plummer, C Rees, I. Judson, H Calvert, M. Highly, J. Trigo, A Jackman, R Smith, M. Hutchison, M Smith, Phase I trial of ZD9331 in aduly patients with refractory solid malignancies adminsitered by 30-min infusion on days 1 and 8 with the cycle repeated every 3 weeks, Proc. Amer. Soc Clin Oncol. 18: Abstract number 861 (1999).

[7] A.L Jackman, L.R Kelland, R Kimbell, M Brown, W Gibson, G W Aherne, A Hardcastle, F.T. Boyle, Mechanisms of acquired resistance to the quinazoline thymidylate synthase inhibitor, ZD1694 (Tomudex) in one mouse and three human cell lines, Br J. Cancer 71 (1995) 914–924

[8] H E R. Ford, D Farrugia, D Cunningham, G W. Aherne, A Hardcastle, F. Mitchell, M. Hill, K. McCarthy, D. McVicar, P. Danenberg, K. Danenberg, A.L. Jackman, High thymidylate synthase may predict non-response in tumour and increased risk of toxicity in normal gastrointestinal mucosa following treatment with raltitrexed, Proc Am Soc. Clin. Oncol 19 (2000) 243

[9] P. Beale, S Clarke, Tomudex· Clinical Development, in· A L. Jackman (Ed.), Antifolate Drugs in Cancer Therapy, Humana Press, Totowa, NJ, USA, 1999, pp. 167–181.

[10] C.A Hills, L.R. Kelland, G Abel, J. Siracky, A.P Wilson, K.R Harrap, Biological properties of ten human ovarian carcinoma cell lines. calibration in vitro against four platinum complexes, Br J Cancer 59 (1989) 527–534

[11] B.C Behrens, T.C. Hamilton, H. Masuda, K.R Grotzinger, J Whag-Peng, K.G Louie, T Knutsen, W M McKoy, R C. Young, R.F. Ozols, Characterisation of a *cis*-diamminedichloroplatinum (II)-resistant human ovarian carcinoma cell line and its use in evaluation of platinum analogs, Cancer Res. 47 (1987) 414–418.

[12] L.A Skelton, M G Ormerod, J Titley, R. Kimbell, L.A. Brunton, A.L. Jackman, A novel class of lipophilic quinazoline-based folic acid analgues cytotoxic agents with a folate-independent locus, Br J Cancer 79 (1999) 1692–1701.

[13] P R Twentyman, M Luscombe, A study of some variables in a tetrazolium dye (MTT) based assay for cell growth and chemosensitivity, Br. J. Cancer 56 (1987) 279–285

[14] A.L. Jackman, D.I Alison, A.H Calvert, K R. Harrap, Increased thymidylate synthase in L1210 cells possessing acquired resistance to N^{10}-propargyl-5,8-dideazafolic acid (CB 3717): development, characterisation and cross-resistance studies, Cancer Res 46 (1986) 2810–2815.

[15] J.M Chirgwin, A E. Przybyla, R.J. MacDonald, W.J. Rutter, Isolation of biologically active ribonucleic acid from sources enriched in ribonuclease, Biochemistry 18 (1979) 5294–5299

[16] T A. Garrow, A. Admon, B Shane, Expression cloning of a human cDNA encoding folylpoly(γ-glutamate) synthetase and determination of its primary structure, Proc. Natl Acad. Sci. 89 (1992) 9151–9155.

[17] P K. Geyer, L.F. Johnson, Molecular cloning of DNA sequences complimentary to mouse thymidylate synthase messenger RNA, J Biol Chem 259 (1984) 7206–7211.

[18] K E Pestell, S.M Hobbs, J C Titley, L R. Kelland, M I Walton, Effects of p53 status on sensitivity to platinum complexes in a human ovarian cancer cell line, Mol. Pharmacol. 57 (2000) 503–511

[19] J.L Grem, K D Danenberg, K. Behan, A. Parr, L. Young, P.V. Danenberg, D. Nguyen, J. Drake, A. Monks, C.J. Allegra, Thymidine kinase, thymidylate synthase, and dohydropyrimidine dehydrogenase profiles of cell lines of the National Cancer Institute's anticancer drug screen, Clin. Cancer Res. 7 (2001) 999–1009.

[20] B Van Triest, H.M. Pinedo, Y.V Hensbergen, K. Smid, F Telleman, P S. Schenmakers, C L Van der Wilt, J.A.M van Laar, J A.M Noordhuis, G. Jansen, G.J. Peters, Thymidylate synthase level as the main predictive parameter for sensitivity to 5-fluorouracil, but not for folate-based thymidylate synthase inhibtors, in 13 nonselected colon cancer cell lines, Clin Cancer Res. 5 (1999) 643–654.

[21] E J. Estlin, K Balmanno, A H. Calvert, A G Hall, J Lunec, D.R Newell, A D.J. Pearson, G A. Taylor, The relationship between intrinsic thymidylate synthase expression and sensitivity to THYMITAQ™ in human leukaemia and colorectal carcinoma cell lines, Br. J. Cancer 76 (1997) 1579–1585

[22] D Salonga, K.D. Danenberg, M. Johnson, R. Metzger, S Groshen, D D Tsao-Wei, H J Lenz, C G. Leichman, L. Leichman, R B Diasio, P V Danenberg, Colorectal tumors responding to 5-fluorouracil have low gene expression levels of dihydropyrimidine dehydrogenase, thymidylate synthase, and thymidine phosphorylase, Clin Cancer Res. 6 (2000) 1322–1327.

[23] A.L Jackman, G.A Taylor, A.H Calvert, K.R. Harrap, Modulation of antimetabolite effects: effects of thymidine on the efficacy of the quinazoline-based thymidylate synthetase inhibitor, CB 3717, Biochem Pharmacol. 33 (1984) 3269–3275

[24] G J. Leclerc, J.C. Barredo, Folylpoly-γ-glutamate synthetase gene mRNA slice variants and protein expression in primary human leukemia cells, cell lines, and normal human tissues, Clin Cancer Res 7 (2001) 942–951.

[25] S.J Welsh, M. Ormerod, W. Aherne, Misincorporation of uracil into DNA may result in cell cycle progression and greater sensitivity to thymidylate synthase inhibitors, Proc Am Assoc. Cancer Res 42 (2001) 510

[26] T C. Fisher, A.E. Milner, C D Gregory, A.L Jackman, G W Aherne, J A Hartley, C Dive, J.A Hickman, BCL-2 modulation of apoptosis induced by anticancer drugs: resistance to thymidylate stress is independent of classical resistance pathways, Cancer Res 53 (1993) 3321–3327.

[27] T Benepal, M Gore, S. Johnston, H Ford, J. Brabender, K. Danenberg, P. Danenberg, A. Jackman, Folylpolyglutamyl synthetase mRNA expression in ovarian cancer, Proc. Am Soc Clin Oncol 20 (2001) 187b.

[28] D.S Theti, D Gibbs, A L Jackman, Pharmacodynamic and growth inhibition consequences of α-folate receptor (α-FR) mediated transport of ZD9331 in human tumor cell lines that co-express the α-FR and the reduced-folate carrier, Proc. AACR-NCI-EORTC (2001) p 91.

[29] P. Garin-Chesa, I. Campbell, P E. Saigo, J L Lewis, L J. Old, W.J Rittig, Trophoblast and ovarian cancer antigen LK26 sensitivity and specificity in immunopathology and molecular identification as a folate-binding protein, Am J Pathol 142 (1993) 557–567

ELSEVIER

Biochimica et Biophysica Acta 1587 (2002) 224–233

BIOCHIMICA ET BIOPHYSICA ACTA
BBA
www.bba-direct.com

Review

From natural products to clinically useful antifungals

David Barrett*

Medicinal Chemistry Research Laboratories, Fujisawa Pharmaceutical Co., Ltd., 2-1-6 Kashima, Yodogawa, Osaka 532-8514, Japan

Received 24 January 2002; accepted 24 January 2002

I would like to dedicate this paper to the memory of Dr. Kazuo Sakane, Director of these laboratories, who passed away on October 1st 2001. His caring, considerate nature, inspirational leadership and keen sense of responsibility contributed critically to the success of this project and he will be sorely missed

Abstract

In our search for natural products with a broad spectrum of antifungal activity as lead compounds for novel treatments for mycoses, we have isolated echinocandin-type lipopeptide FR901379 and lipopeptidolactone FR901469, as novel water-soluble antifungal agents that inhibit the synthesis of 1,3-β-glucan, a key component of the fungal cell wall. Since the cell wall is a feature unique to fungi and is not present in nonfungal eukaryotic cells, inhibitors of the synthesis of fungal cell wall components such as 1,3-β-glucan have potential for selective toxicity to fungi and not to the host. In this short review, we describe efforts directed at synthetic modification of FR901469 and FR901379 with the ultimate goal of identifying new entities with suitable profiles as development candidate compounds. The main thrust of our work to date has been replacement of the highly flexible lipophilic side chains of the natural products with a view to reducing the hemolytic potential associated with these compounds, and to enhance chemical stability and/or in vivo antifungal efficacy. As a result of these efforts, we recently discovered a novel analog, FK463 (micafungin). Micafungin is currently in phase III clinical trials worldwide as a parenteral agent for various mycoses, and a new drug application (NDA) was recently filed in Japan © 2002 Elsevier Science B.V. All rights reserved.

Keywords: Antifungals; Natural product; Micafungin; Drug discovery

1. Introduction

Fungal diseases in humans can be classified into (a) allergic reactions to fungal proteins, (b) toxic reactions to toxins present in certain fungi and (c) infections (mycoses). By far the most serious and difficult to diagnose and treat, mycoses come in many forms. Otherwise healthy individuals are susceptible to a host of superficial, cutaneous, subcutaneous, and in certain instances, systemic infections that cause a variety of conditions ranging from Athletes foot and nail infections to severe life-threatening disseminated disease (e.g. histoplasmosis). On the other hand, immunocompromised individuals are susceptible to a large number of opportunistic systemic mycoses, resulting from the inability of host immune response to fight off attack from normally benign environmental fungal pathogens. Indeed, the last 20 years has witnessed a remarkable increase in the incidence of deep-seated, disseminated mycoses [1]. The reasons are manifold; however, the advent of aggressive cancer chemotherapy, highly effective immunosuppressants for organ transplantation, widespread use of powerful broad spectrum antibacterial agents and the explosion in the number of cases of human immunodeficiency virus (HIV) infection have all contributed to the increase in life-threatening fungal disease [2]. Furthermore, ongoing demographic trends would tend to strongly suggest that the number of fungal infections will continue to increase due to the aging of the population in developed countries [3].

Whilst difficulty in diagnosis of fungal infections and delays in initiation of treatment are important factors, drugs

---

Abbreviations: MIC, minimum inhibitory concentration; IC$_{50}$, 50% inhibitory concentration; ED$_{50}$, 50% effective dose; NDA, new drug application; HIV, human immunodeficiency virus; MLC, minimum lytic concentration; BOC, *tert*-butoxycarbonyl; SCID Mouse, severe combined immunodeficient mouse; PCP, *Pneumocystis carinii*-associated pneumonia; Amp-B, amphotericin B; ITCZ, itraconazole; CFU, colony forming units; FLCZ, fluconazole; AcOH, acetic acid; MeOH, methanol; THF, tetrahydrofuran; EtOAc, ethyl acetate; DMF, *N,N*-dimethylformamide; TFA, trifluoroacetic Acid; HOBT, 1-hydroxybenzotriazole; WSCD·HCl, 1-ethyl-3-dimethylaminopropylcarbodiimide hydrochloride; EtN^{i}Pr$_2$, diisopropylethylamine; LiOH, lithium hydroxide; Z, benzyloxycarbonyl. MTPA, α-methoxy-α-(trifluoromethyl)phenylacetic acid

* Tel.: +81-6-6390-1285; fax: +81-6-6304-5435.

E-mail address: david_barrett@po.fujisawa.co.jp (D. Barrett).

0925-4439/02/$ - see front matter © 2002 Elsevier Science B.V. All rights reserved.
PII: S0925-4439(02)00085-6

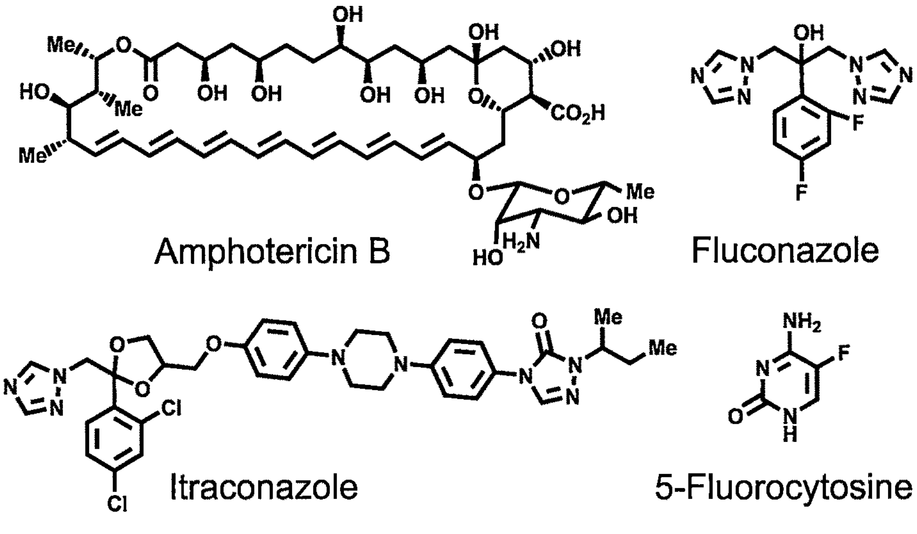

Fig 1 Major available drugs for systemic mycoses

for effective treatment of these emerging infections are in short supply, thereby contributing to a high mortality rate. Available drugs are essentially limited to the polyene natural product amphotericin B [4,5] and various newer lipid formulations [6], the azole compounds such as fluconazole and itraconazole, and flucytosine (5-fluorocytosine) (Fig. 1). These established agents suffer from a number of limitations that can render their use difficult; for example, dose-limiting nephrotoxicity associated with amphotericin B, rapid development of resistance with flucytosine, drug–drug interactions, fungistatic mode of action and resistance development with the azoles. There is thus an urgent need for new antifungals with a broad, fungicidal spectrum of action, and with fewer dose-limiting side effects [7,8]. Whilst a number of lipid-based formulations of amphotericin B have been shown to be effective in ameliorating the toxic liabilities associated with this agent, and a number of new azoles are in the final stages of clinical development, the fundamental problems described above remain. Accordingly, it is particularly imperative that we bring agents to the clinic that have new mechanisms of action and have good, broad-spectrum, cidal antifungal activity.

2. Natural product screening: novel antifungal agents

As a part of our efforts to discover new compounds with potential as lead compounds for optimization studies leading to novel antifungal candidates, we first must answer a simple key question: how do we identify and select a lead

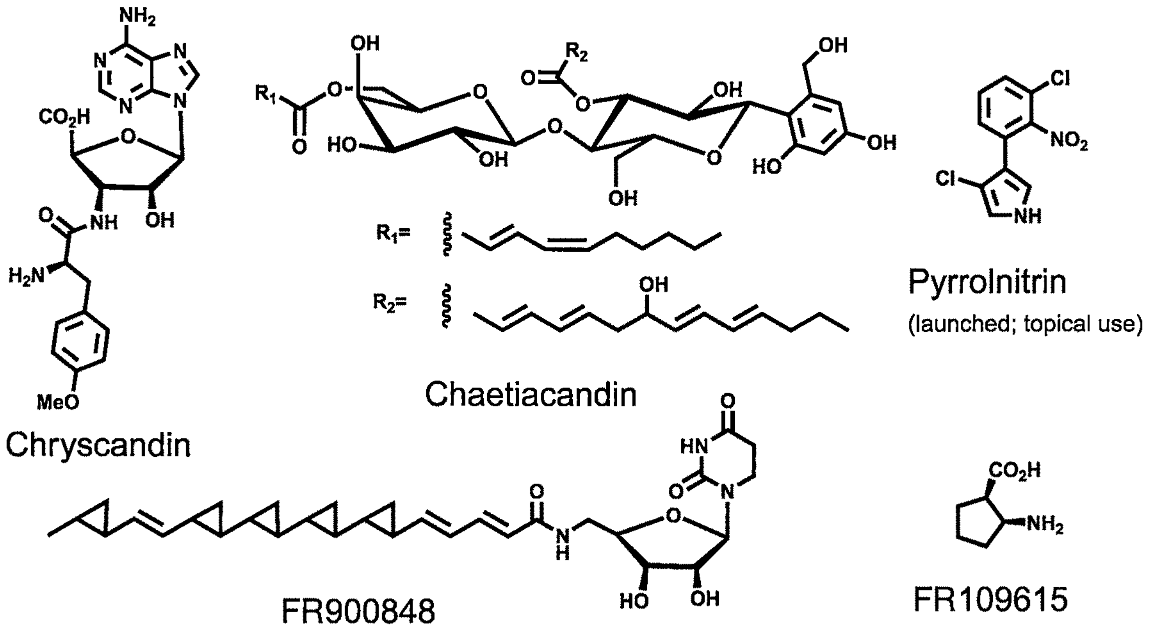

Fig 2 Antifungal natural products discovered at Fujisawa

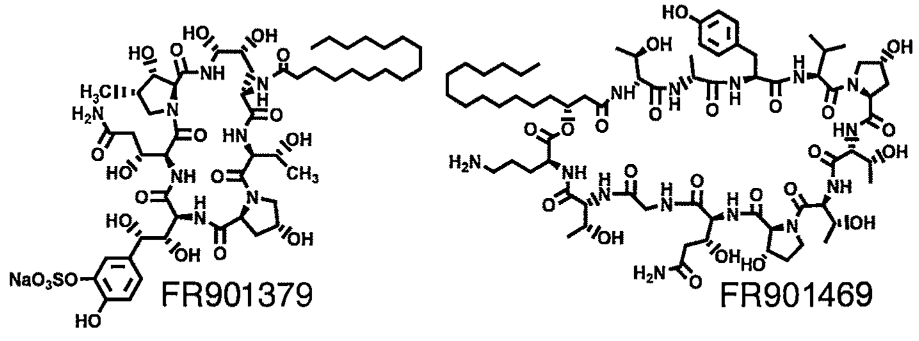

Fig. 3 Water-soluble antifungal natural products discovered at Fujisawa

compound for further study? This is an important question as it is clearly critical that any potential compound must meet a number of criteria, otherwise the chances of ultimate success will not be high. The questions that we ask when selecting compounds for further investigation are as follows: (1) Is the compound structurally novel? (2) Is the mechanism of action novel and/or potentially useful? (3) Is intrinsic biological activity good? (4) Is clinical proof of concept possible? (5) Is chemical modification/optimization of the structure possible? It has become clear over a number of years that all of these questions are critical and impact greatly upon the chances of final success.

Since natural products have been proven to be an excellent source of novel chemical entities, we have employed screening of microbial extracts in our search for compounds that match the criteria discussed above, and have disclosed a number of structurally unique biologically active materials. In the course of screening for novel antifungal antibiotics, Fujisawa scientists have previously described the isolation of antifungals such as chryscandin [9], chaetiacandin [10], pyrrolnitrin [11], FR900848 [12] and FR109615 [13,14] (Fig. 2). Whilst pyrrolnitrin is marketed in Japan for topical indications, the other natural products had various limitations in terms of spectrum of in vitro activity, in vivo activity, water-solubility, lack of success in the chemical modification studies, mechanism of action limitations and potential for resistance development.

More recently, we have been engaged in the search for water-soluble inhibitors of fungal 1,3-β-D-glucan synthase [15], an enzyme critical to the synthesis of 1,3-β-D-glucan, a major component of the cell wall of a number of key pathogenic fungii [16]. The fungal cell wall is an attractive target for the discovery of new antifungal agents [17], primarily because it is essential for the viability of fungal cells, and also because the fungal cell wall has no counterpart in mammalian cells. Accordingly, compounds that selectively target the biosynthesis of key components of the fungal cell wall have potential to be nontoxic to mammalian hosts.

As a result of our continuous screening of microbial extracts, we have discovered two unique, water-soluble antifungals that express their activity by inhibition of the synthesis of 1,3-β-D-glucan (Fig. 3). FR901379 is the first example of a naturally water-soluble echinocandin derivative [18,19]. This natural product displays excellent water-solubility by virtue of the presence of a sulfate moiety on the homotyrosine group. FR901469 is the first example of a new type of 1,3-β-glucan synthase inhibitor based upon a 40-membered cyclic lipopeptidolactone structure [20–22]. FR901469 also displays excellent water-solubility.

In this short review, we briefly describe some of our efforts directed at synthetic modification of FR901469 and FR901379. The main thrust of our work has been replacement of the highly flexible lipophilic side chains and/or chemical derivatization with a view to reducing the hemolytic potential associated with the natural products, and to enhance chemical stability and/or in vivo antifungal efficacy. As a result of these efforts, we have discovered a novel analog, FK463 (micafungin), which is currently in worldwide phase III clinical trials as a parenteral agent for various mycoses.

3. Discovery and biological activity of FR901469 and related derivatives

FR901469 was isolated as a hydrochloride salt from an unidentified fungus no. 11243 [20]. This compound displayed water solubility of > 50 mg/ml, which compares with

Table 1
FR901469, a water-soluble lipopeptidolactone

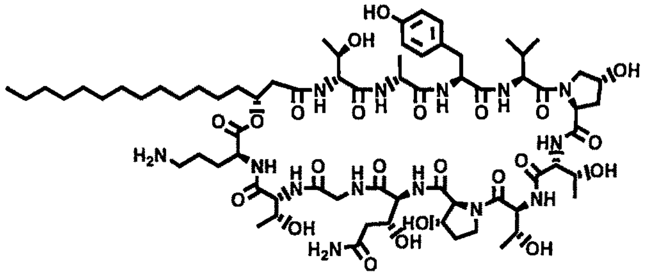

β-1,3-glucan synthase inhibition (from *C. albicans* 6406)

Compound	IC_{50} (μg/ml)
FR901469	0.05
FR901379	0.7
Echinocandin B	2.6
Cilofungin	2.9
Papulacandin B	2.5

Table 2
Biological properties of FR901469

Compound	Hemolysis	*C. albicans* FP633		*A. fumigatus* FP1305
	MLC (μg/ml)	MIC (μg/ml)	ED_{50} (mg/kg/day)	ED_{50} (mg/kg/day)
FR901469	250	0.1	0.4	0.42
Echinocandin B	125	2.5	>32	>100
Fluconazole	NT	>100	>20	>40
Amphotericin B	<50	0.39	0.13	0.13

0.008 mg/ml for echinocandin B, the prototype 1,3-β-glucan synthase inhibitor. Furthermore, inhibition of the enzyme from *Candida albicans* 6406 showed an IC_{50} of 0.05 μg/ml, significantly more potent than echinocandin B and papulacandin B (Table 1). The antifungal activity of FR901469 is also excellent (Table 2), however, hemolytic activity is high and comparable to echinocandin B, indicating the potential for drug–erythrocyte interactions and hemolysis under in vivo conditions, especially in the multiple dose regimens of usual drug treatment protocols. Early work on echinocandin B indicated that major toxic liabilities resulted from its high hemolytic potential [23,24]. Minimum lytic concentration (MLC) for FR901469 was 250 μg/ml, compared to 125 μg/ml for echinocandin B. Reduction of hemolysis was considered critical in order to improve the overall profile of this natural product, since echinocandin B was unsuitable as a development candidate due to its hemolysis and toxicity. An additional notable structural feature of FR901469 is the juxtaposition of an ornithine amino group adjacent to a lactone moiety. This feature leads to a pH-dependent ring opening process, which whilst not effecting in vivo antifungal potency significantly, presumably due to amino group protonation at physiological pH, is potentially a source of chemical instability in the drug isolation/development process (Fig. 4).

We have already reported some of our efforts on the site-specific chemical modification of FR901469. In particular, we have described selective direct modification of the ornithine residue by synthesis of acylated and amidine conjugates of the ornithine amino group [25,26], selective functionalization of the tyrosine moiety [27] and complete replacement of the ornithine by a novel substituted glutamic acid residue [28]. In the course of these studies, it became apparent that the hemolysis associated with the natural product could be reduced significantly by chemical modification whilst maintaining the potent in vitro and, especially, in vivo antifungal activity. After completion of this work, scientists at Nippon Roche described the discovery of aerothricins, a series of lipopeptides closely related to FR901469 [29]. A number of studies aimed at exploring modifications at the ornithine moiety with a view to improving the therapeutic index and antifungal potency have also appeared recently [30,31].

As a part of continuing studies on FR901469, in order to remove the propensity for ring opening leading to a biologically inactive linear peptide, we designed the amide analog of the natural product (Fig. 4). This design is a rational one since an amide bond is significantly more stable to hydrolysis compared to an ester, however, it was unclear how such a modification would effect biological activity. On the assumption of retention of activity, we were particularly interested in the possibility of development of new methodology that would be applicable to the synthesis of a variety of novel lipophilic side chain-modified analogs, since work in the echinocandin B area established the influence of lipophilicity of the acyl side chain on antifungal potency and hemolysis of lipopeptides [24].

We based our approach to the synthesis of the amide analog of FR901469 on deacylation of the lipophilic side chain of the natural product, introduction of a pre-formed amide-substituted side chain moiety, macrolactamization and ornithine amino group deprotection. The key linear peptide intermediate was produced in 35% yield by direct incubation of FR901469 with *Actinoplanes utahensis* IFO-13244 in 0.2 M phosphate at pH 7.8 and 60 °C (Fig. 5). This organism has been employed for deacylation of various lipopeptide compounds, including echinocandin B, and cleaves only the amide bond connecting the lipophilic side chain to the peptide skeleton [32]. In this work, we have demonstrated another feature of this organism, whereby simultaneous removal of a β-hydroxyacid side chain and an ornithine moiety is also possible [33].

For this synthesis, the appropriate side-chain fragment was prepared as shown (Fig. 6). Myristylaldehyde was converted over six synthetic steps to an activated ester

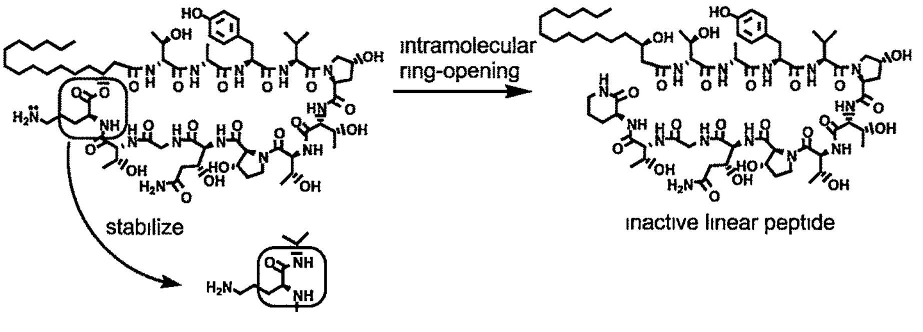

Fig. 4. Intramolecular ring-opening of FR901469.

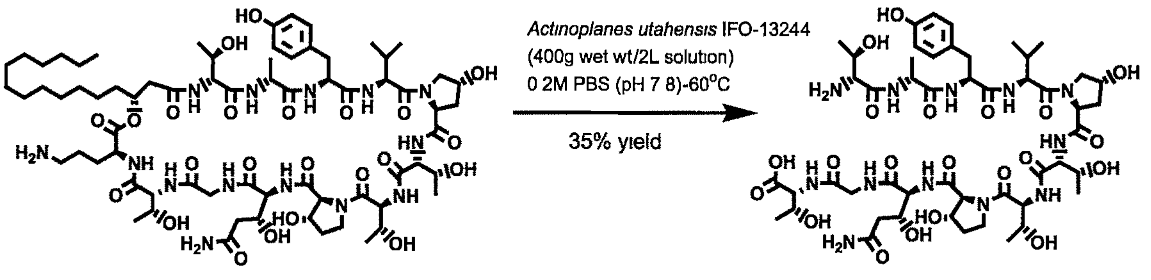

Fig 5 Microbial deacylation of FR901469

building block containing all required functionality. The β-amino acid portion of the fragment was prepared by adaptation of Davies methodology. The final steps in the synthesis of the amide analog of FR901469 are shown in Fig. 7. Acylation of the linear peptide produced by microbial biotransformation with the activated synthetic dipeptide, followed by protecting group manipulation, macrocyclization under high dilution conditions and removal of the *tert*-butoxycarbonyl (BOC) protecting group afforded the amide analog (FR207010) as the hydrochloride salt after ion-exchange chromatography and freeze-drying. In support of our original expectations, this compound was significantly more stable compared to FR901469 under high pH conditions, and the antifungal potency was comparable to the lactone natural product (Table 3).

Whilst FR207010 displayed comparable antifungal activity to FR901469, the presence of a linear unbranched lipophilic side chain meant that hemolysis was still high. This methodology is readily applicable to the synthesis of a variety of novel lipophilic side chain-modified analogs, and indeed, synthesis and biological activity of such analogs has revealed that nonhemolytic compounds with natural product-like levels of antifungal activity can be identified in this series (data not shown).

4. Discovery and biological activity of FR901379 and FK463, novel water-soluble echinocandin derivatives

The first example of a naturally occurring, water-soluble echinocandin-like lipopeptide, FR901379 (Table 4), was isolated from the culture broth of *Coleophoma empetri* F-11899 [18,19]. This compound was originally designated WF11899A and is one member of a family of three related cyclic hexapeptides (WF11899A, B, C) that differ only in the number of hydroxyl groups on the hexapeptide skeleton. FR901379 is a cyclic hexapeptide bearing a fatty acid acyl group on the N-terminal moiety and has excellent water-solubility by virtue of the presence of a sulfonate moiety on the homotyrosine residue. The water-solubility is greater than 50 mg/ml, which is much higher than the water-solubility of echinocandin B (0.008 mg/ml). FR901379

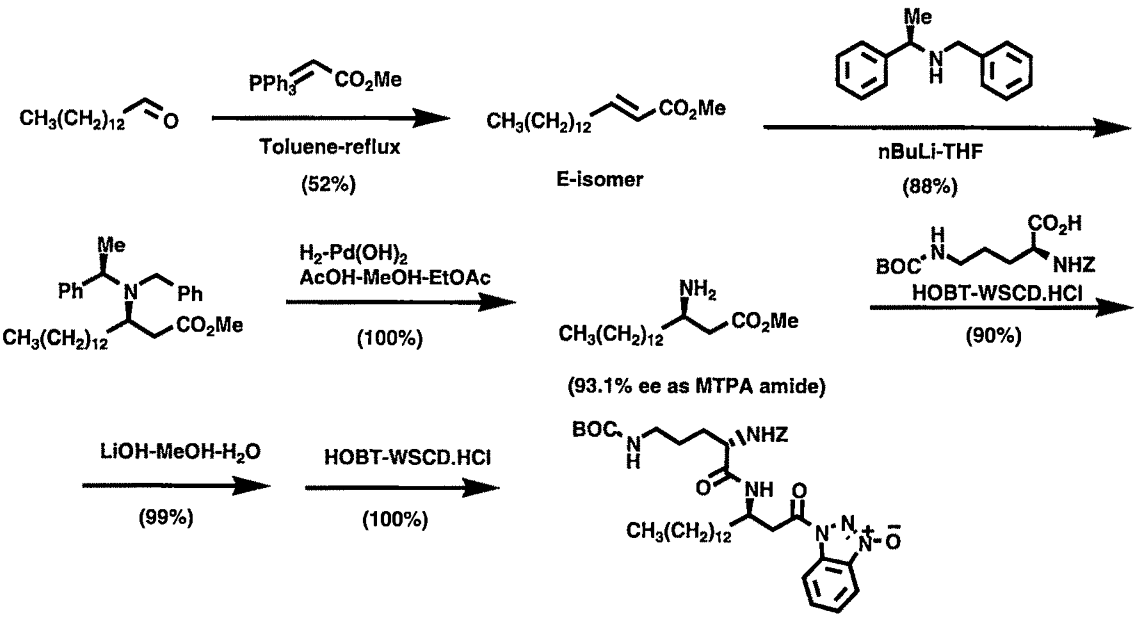

Fig 6 FR901469 amide analog: activated ester fragment.

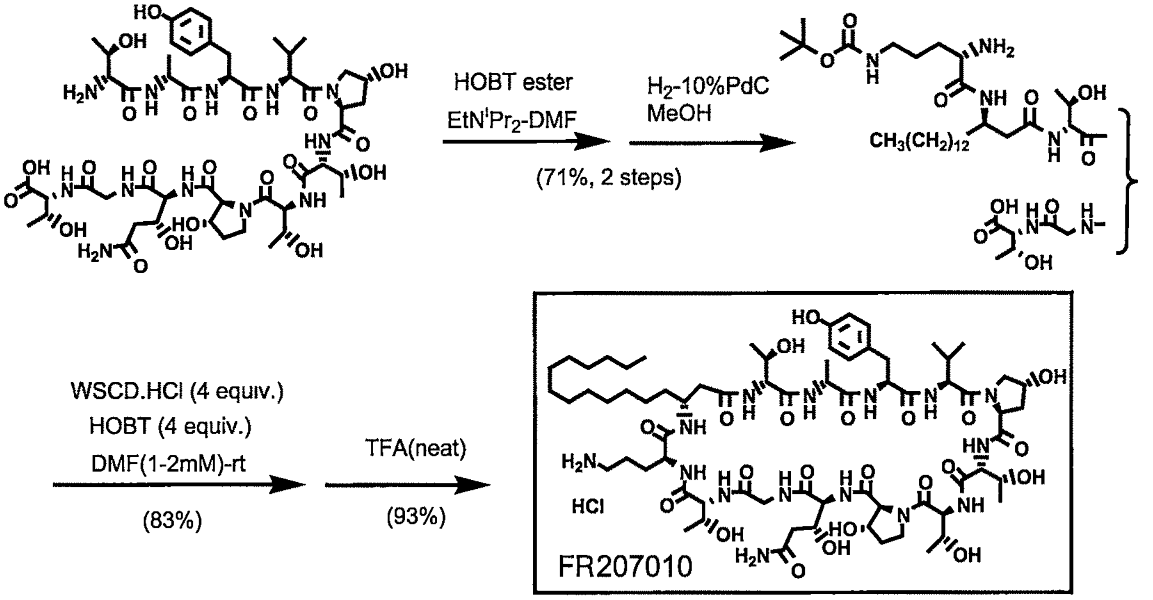

Fig 7 FR901469 amide analog. completion of synthesis.

displayed more potent inhibition of β-1,3-glucan synthase from *C albicans* 6406 (IC_{50} = 0.7 μg/ml) than echinocandin B (IC_{50} = 2.6 μg/ml), and in a *C albicans* murine infection model, displayed a superior protective effect relative to echinocandin B and fluconazole, but was weaker than amphotericin B (Table 5). However, this compound was not strongly effective in prolonging survival in a model of disseminated aspergillosis, and it had an MLC of 62 μg/ml, indicating that chemical modification would be required to improve antifungal potency and to reduce hemolysis.

Recently, scientists at Lilly reported that the in vivo, but not in vitro, activity of cilofungin, an echinocandin B derivative with a modified fatty acid side chain, against *Aspergillus fumigatus* correlated with inhibition of *A. fumigatus* glucan synthase [34], and that the hemolytic potential of echinocandin B could be reduced by incorporation of benzoyl-type side chains. In our studies, enyzmatic deacylation of FR901379 was readily achieved and reacylation of the resulting key skeleton, FR179642, afforded novel side chain-modified antifungal agents. FR131535 [35,36] was the first key compound prepared and displayed excellent antifungal activity, comparable to FR901379, but without the hemolysis associated with the natural product. Subsequent optimization studies were then initiated, leading ultimately to the discovery of a novel analog, FK463, with an excellent profile. The synthesis of FK463 is outlined in Fig. 8, and involves a straightforward reacylation of the hexapeptide skeleton FR179642 with a pre-formed novel isoxazole-containing benzoyl-like side-chain [37]. In com-

Table 3
Antifungal activity of FR207010, the amide analog of FR901469

Fungal Species	MIC (μg/ml)			
	FR207010	FR901469	Amp-B	Fluconazole
C. albicans ATCC90028	1	0.5	0.5	0.5
C tropicalis TIMM0313	2	1	0.5	4
C krusei ATCC6258	1	0.5	1	32
C. guilliermondii ATCC9390	1	0.5	0.5	4
C parapsilosis ATCC22019	4	2	0.5	2
A fumigatus TIMM0063	1	0.5	0.5	>64
A. niger ATCC6275	0.5	0.25	0.25	>64

Table 4
FR901379: a water-soluble echinocandin lipopeptide

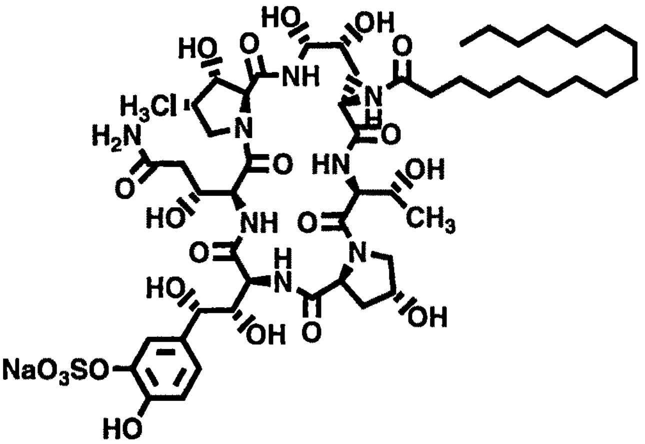

β-1,3-glucan synthase inhibition (from *C albicans* 6406)

Compound	IC_{50} (μg/ml)
FR901379	0.7
FR901469	0.05
Echinocandin B	2.6
Cilofungin	2.9
Papulacandin B	2.5

Table 5
Biological properties of FR901379

Compound	Hemolysis	C. albicans FP633		A. fumigatus FP1305
	MLC (μg/ml)	MIC (μg/ml)	ED_{50} (mg/kg/day)	ED_{50} (mg/kg/day)
FR901379	62	0.2	1.8	70
Echinocandin B	125	2.5	>32	>100
Fluconazole	NT	>100	>20	>40
Amphotericin B	<50	0.39	0.13	0.13

mon with FR901379 and FR131535, FK463 displays excellent water-solubility.

Biological evaluation of FK463 has revealed that it possesses potent in vitro antifungal activity [38–41]. In comparison to the established agents, amphotericin B, itraconazole and fluconazole, FK463 displayed excellent activity against *Candida* species (Table 6) and *Aspergillus* species (Table 7). In common with other 1,3-β-D-glucan synthase inhibitors, FK463 was not active against *Cryptococcus neoformans* strains. [37]. FK463 was shown to be fungicidal to *C. albicans* FP633 by examination of the relationship between change in viable cell counts and drug concentration after exposure for 24 h in comparison to other drugs. A 99% or greater reduction in viability was observed after 24 h of exposure to >0.0156 μg/ml of FK463 (Fig. 9). As can be seen from the data in Fig. 9, FK463 exhibited fungicidal activity at concentrations lower than those at which amphotericin B was fungicidal, and was clearly superior to itraconazole and fluconazole, which displayed fungistatic effects.

Table 6
Antifungal spectrum of FK463 (1)

Organism	MIC (μg/ml)			
	FK463	Amp-B	ITCZ	FLCZ
Candida albicans ATCC90028	0.0156	0.5	0.0313	0.5
Candida tropicalis TIMM0313	0.0313	0.5	0.125	4
Candida glabrata ATCC90030	0.0156	0.5	1	16
Candida kefyr ATCC28838	0.125	0.5	0.0625	0.5
Candida krusei ATCC6258	0.125	1	0.25	32
Candida guilliermondii ATCC9390	0.125	0.5	0.25	4
Candida parapsilosis ATCC22019	2	0.5	0.25	2
Candida stellatoidea IFM5491	0.0313	0.0625	0.0078	0.125
Saccharomyces cerevisiae ATCC9763	0.125	0.5	0.25	2

The in vivo antifungal efficacy of FK463 is also good when drug is administered as an intravenous injection (Table 8). In murine models of disseminated candidiasis and aspergillosis, FK463 displayed comparable efficacy to amphotericin B, and superior efficacy compared to fluconazole [42]. In particular, in the candidiasis model, FK463 significantly prolonged the survival of intravenously infected mice at doses of 0.125 mg/kg of body weight or higher. In the disseminated aspergillosis model, FK463 given at doses of 0.5 mg/kg or higher significantly prolonged the survival of mice infected intravenously with *A. fumigatus* conidia. This result indicates that the efficacy of FK463 was about two times inferior to that of amphotericin B. Furthermore, FK463 has demonstrated good in vivo activity in mouse models of pulmonary aspergillosis [43]. Pulmonary aspergillosis in mice was induced by intranasal inoculation and administration was by the intravenous route.

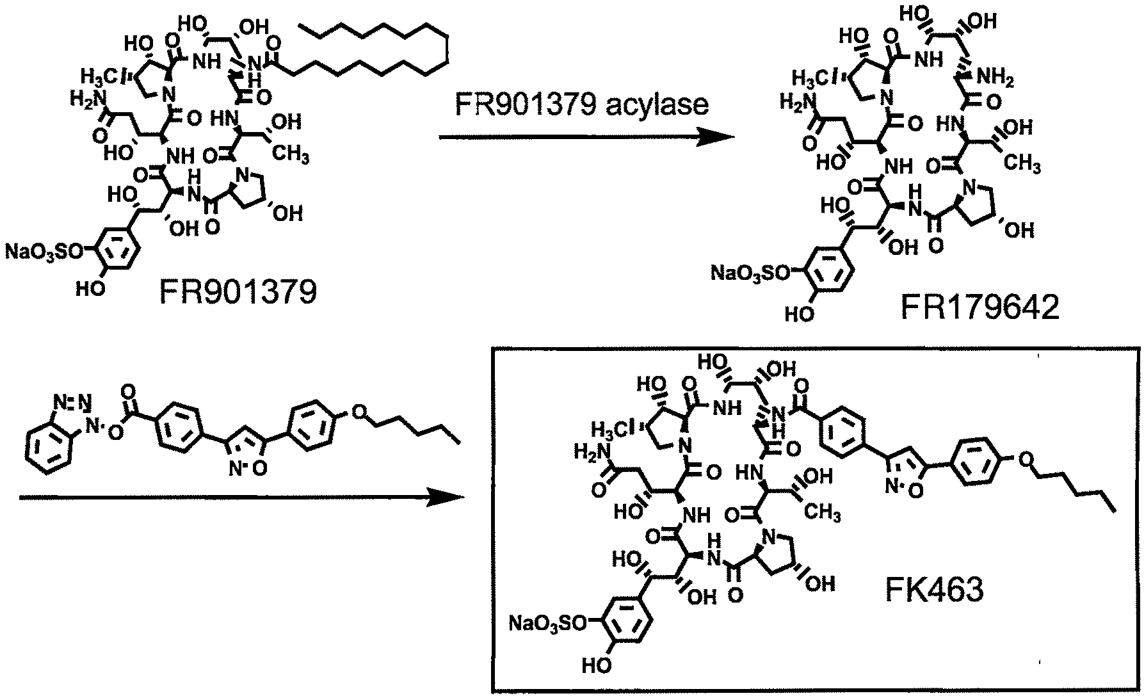

Fig. 8. Deacylation of FR901379 and synthesis of FK463.

Table 7
Antifungal spectrum of FK463 (2)

Organism	MIC (μg/ml)			
	FK463	Amp-B	ITCZ	FLCZ
Cryptococcus neoformans TIMM0354	>64	0.25	0.0313	0.5
Trichosporon cutaneum IFM4-1-4	>64	2	0.5	8
Trichosporon asahii TIMM3144	>64	0.25	0.25	2
Aspergillus fumigatus TIMM0063	0.0078	0.5	0.5	>64
Aspergillus niger ATCC6275	0.0078	0.25	0.5	>64
Aspergillus nidulans IFM5369	0.0078	1	0.0625	32
Aspergillus flavus ATCC9643	0.0156	1	0.25	64
Aspergillus terreus IFM5369	0.0156	1	0.125	>64
Aspergillus versicolor IFM41406	0.0156	0.5	0.0625	32
Fusarium solani IFM41532	>64	0.25	>8	>64

The 50% effective dose was in the range 0.26–0.51 mg/kg of body weight, which was comparable to amphotericin B. The minimum effective plasma FK463 concentration in murine pulmonary aspergillosis was determined to be 0.55–0.80 μg/ml by a viable-cell reduction assay in the target organs [43]. Good protection against infection due to azole-resistant *C. albicans* has also been described [44]. The prophylactic effect of FK463 against *Pneumocystis carinii* infection in the severe combined immunodeficient (SCID) mouse model has also been described [45]. *P. carinii* is an opportunistic pathogen that causes *P. carinii*-associated pneumonia (PCP), a cause of morbidity and mortality in immunocompromised patients. A recent summary article describes all available biological and clinical evaluation data, including pharmacokinetic data, for FK463 (micafungin) [46]. FK463 is currently in late-stage phase III clinical development.

Table 8
In vivo efficacy of FK463: disseminated candidiasis and aspergillosis

Organism	ED_{50} (mg/kg/day)		
	FK463	FLCZ	Amp-B
C. albicans FP633	0.14	2.15	0.08
C. glabrata 13002	0.30	6.27	0.11
C. tropicalis 16009	0.28	3.71	0.09
C. krusei FP1866	0.77	9.52	0.26
C. parapsilosis FP1946	1.00	10.9	0.06
A. fumigatus IFM41209	0.50	>20	0.29

Once-daily treatment for 4 days starting 1 h after infection by intravenous administration to mice.

5. Conclusions

The recent FDA approval of the Merck compound caspofungin as a therapy for refractory invasive aspergillosis has opened up the first chapter in a new era for antifungal therapy [47]. The confirmation that 1,3-β-D-glucan synthase inhibition can provide compounds with significant clinical utility bodes well for the future of treatment of severe systemic fungal infections. Our efforts in this area have culminated in the identification of FK463 (micafungin). This compound is in phase III clinical trials worldwide, and a new drug application (NDA) has been filed recently in

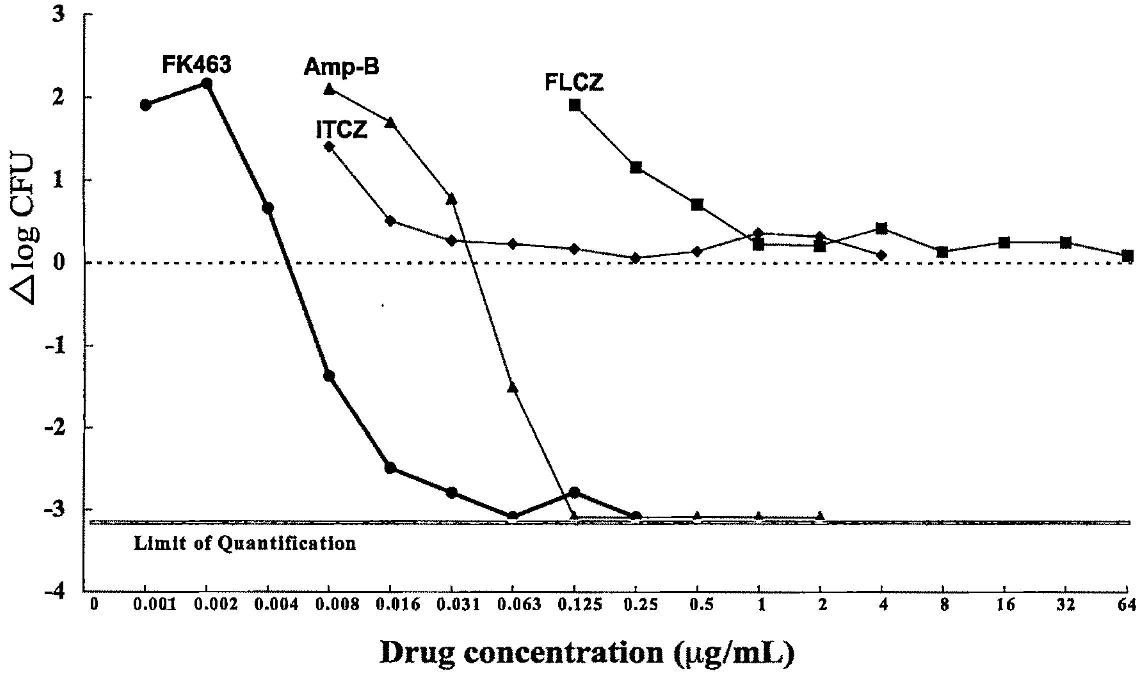

Fig. 9. Fungicidal activity against *C. albicans* FP633 after 24-h exposure

Japan. These developments clearly show that a rational approach to antifungal drug discovery, focussing on compounds that interfere selectively with elements essential to the survival of fungal cells, can lead to new agents with the potential to become key components in the arsenal of weapons directed at serious systemic fungal disease.

References

[1] C M. Beck-Cague, W R Jarvis, Secular trends in the epidemiology of nosocomial fungal infections in the United States, 1980–1990, J. Infect Dis 167 (1993) 1247–1251

[2] E. Anaissie, Opportunistic mycoses in the immunocompromised host: experience at a Cancer Center and review, Clin Infect Dis. 14 (Suppl. 1) (1992) S43–S53.

[3] C A Kauffman, Fungal infections in older adults, Clin Infect. Dis. 33 (2001) 550–555

[4] H A Gallis, R.H. Drew, W W. Pickard, Amphotericin B: 30 years of clinical experience, Rev Infect Dis 12 (1990) 308–329

[5] J R Wingard, P Kubilis, L Lee, G. Yee, M White, L Walshe, R. Bowden, E. Anaissie, J Hiemenz, J Lister, Clinical significance of nephrotoxicity in patients treated with amphotericin B for suspected or proven aspergillosis, Clin Infect Dis 29 (1999) 1402–1407

[6] J W Hiemenz, T.J Walsh, Lipid formulations of amphotericin B recent progress and future directions, Clin Infect Dis 22 (Suppl 2) (1996) S133–S144

[7] J R Graybill, The future of antifungal therapy, Clin. Infect Dis 22 (Suppl 2) (1996) S166–S178

[8] J A Maertens, M A Boogaerts, Fungal cell wall inhibitors emphasis on clinical aspects, Curr. Pharm. Des 6 (2000) 225–239.

[9] M. Yamashita, Y. Tsurumi, J Hosoda, T Komori, M Kohsaka, H Imanaka, Chryscandin, a novel peptidyl nucleoside antibiotic I Taxonomy, fermentation, isolation and characterization, J Antibiot 38 (1984) 1279–1283.

[10] T Komori, M Yamashita, Y Tsurumi, M Kohsaka, Chaetiacandin, a novel papulacandin I Fermentation, isolation and characterization, J Antibiot 38 (1985) 455–459

[11] M Nishida, T. Matsubara, N Watanabe, Pyrrolnitrin, a new antifungal antibiotic, J Antibiot 18 (1965) 211–219.

[12] M Yoshida, M Ezaki, M Hashimoto, M Yamashita, N Shigematsu, M. Okuhara, M Kohsaka, K. Horikoshi, A novel antifungal antibiotic, FR-900848: I. Production, isolation, physicochemical and biological properties, J. Antibiot 43 (1990) 748–754.

[13] T Iwamoto, E Tsujii, M. Ezaki, A Fujie, S Hashimoto, M. Okuhara, M Kohsaka, H. Imanaka, K Kawabata, Y Inamoto, K Sakane, FR109615, a new antifungal antibiotic from streptomyces setonii taxonomy, fermentation, isolation, physicochemical properties and biological activity, J. Antibiot. 43 (1990) 1–7

[14] K Kawabata, Y. Inamoto, K. Sakane, T Iwamoto, S. Hashimoto, Synthesis and structure determination of FR109615, a new antifungal antibiotic, J Antibiot 43 (1990) 513–518

[15] N H. Georgopapadakou, Update on antifungals targeted to the cell wall focus on β-1,3-glucan synthase inhibitors, Expert Opin Invest Drugs 10 (2001) 269–280

[16] Y. Hori, Current status of β-1,3-glucan synthase inhibitors from microbial products as systemic antifungal agents, Kagaku to Seibutsu 39 (2001) 154–164 (In Japanese).

[17] N H Georgopapadakou, J S Tkacz, The fungal cell wall as a drug target, Trends Microbiol 3 (1995) 98–104

[18] T. Iwamoto, A Fujie, K Sakamoto, Y Tsurumi, N Shigematsu, M Yamashita, S Hashimoto, M Okuhara, M Kohsaka, WF11899A, B and C, novel antifungal lipopeptides I Taxonomy, fermentation, isolation and physicochemical properties, J Antibiot 47 (1994) 1084–1091

[19] T Iwamoto, A Fujie, K Nitta, S. Hashimoto, M Okuhara, M. Kohsaka, WF11899A, B and C, novel antifungal lipopeptides: II Biological properties, J Antibiot 47 (1994) 1092–1097.

[20] A Fujie, T Iwamoto, H. Muramatsu, T. Okudaira, K Nitta, T. Nakanishi, K. Sakamoto, Y. Hori, M Hino, S. Hashimoto, M. Okuhara, FR901469, a novel antifungal antibiotic from an unidentified fungus no 11243· I. Taxonomy, fermentation, isolation, physicochemical properties and biological properties, J Antibiot. 53 (2000) 912–919

[21] A Fujie, T Iwamoto, H Muramatsu, T. Okudaira, I Sato, T. Furuta, Y Tsurumi, Y. Hori, M. Hino, S Hashimoto, M. Okuhara, FR901469, a novel antifungal antibiotic from an unidentified fungus No 11243. II In vitro and in vivo activities, J Antibiot. 53 (2000) 920–927

[22] A Fujie, H Muramatsu, S Yoshimura, M Hashimoto, N. Shigematsu, S Takase, FR901469, a novel antifungal antibiotic from an unidentified fungus No 11243· III Structure determination, J. Antibiot 54 (2001) 588–594

[23] L C Howard, M D Gunnoe, M Debono, B.J. Abbott, J R Turner, Utilization of in vitro erythrocyte fragility to predict toxicity of a group of antifungal echinocandin B analogs, Toxicologist 2 (1982) 184

[24] M. Debono, B J. Abbott, J.R Turner, L C Howard, R S Gordee, A.S Hunt, M Barnhart, R.M Molloy, K E. Willard, D Fukuda, T F Butler, D.J Zeckner, Synthesis and evaluation of LY121019, a member of a series of semisynthetic analogues of the antifungal lipopeptide echinocandin B, Ann. N Y. Acad Sci 544 (1988) 152–167

[25] D. Barrett, A Tanaka, K Harada, H Ohki, E Watabe, K Maki, F. Ikeda, Synthesis and biological activity of novel macrocyclic antifungals· acylated conjugates of the ornithine moiety of the lipopeptidolactone FR901469, Bioorg Med Chem. Lett 11 (2001) 479–482.

[26] D. Barrett, A Tanaka, E Watabe, K Maki, F Ikeda, Novel amidine conjugates of the ornithine moiety of the macrocyclic lipopeptidolactone FR901469, J. Antibiotics 54 (2001) 844–867

[27] D Barrett, A. Tanaka, K. Harada, E. Watabe, K. Maki, F. Ikeda, Synthesis and biological activity of novel macrocyclic antifungals· modification of the tyrosine moiety of the lipopeptidolactone FR901469, Bioorg. Med Chem Lett 11 (2001) 1843–1849

[28] A Tanaka, D Barrett, A Fujie, N Shigematsu, M Hashimoto, S Hashimoto, F. Ikeda, Site-specific transformation of the novel antifungal cyclic depsipeptide FR901469· synthesis and biological activity of FR203903, J Antibiotics 54 (2001) 193–197.

[29] M. Aoki, M Kohchi, K Masubuchi, E Mizuguchi, T Murata, H Ohkuma, T. Okada, M Sakaitani, N Shimma, T. Watanabe, M Yanagisawa, Y. Yasuda, PCT patent application, WO 0005251 (Feb 3, 2000)

[30] K Masubuchi, T Okada, M Kohchi, M. Sakaitani, E. Mizuguchi, H. Shirai, M Aoki, T Watanabe, O. Kondoh, T Yamazaki, Y Satoh, K. Kobayashi, T Inoue, I Horii, N. Shimma, Synthesis and antifungal activity of novel 1,3-β-D-glucan synthase inhibitors Part 1, Bioorg Med Chem Lett 11 (2001) 395–398

[31] K Masubuchi, T Okada, M. Kohchi, T Murata, M Tsukazaki, O Kondoh, T Yamazaki, Y. Satoh, Y Ono, T. Tsukaguchi, K Kobayashi, N. Ono, T Inoue, I. Horii, N. Shimma, Synthesis and antifungal activity of novel 1,3-β-D-glucan synthase inhibitors Part 2, Bioorg. Med. Chem Lett. 11 (2001) 1273–1276.

[32] L D Boeck, D S. Fukuda, B J Abbott, M. Debono, Deacylation of echinocandin B by *Actinoplanes utahensis*, J Antibiotics 52 (1989) 382–388

[33] D. Barrett, A Tanaka, A. Fujie, N Shigematsu, M Hashimoto, S Hashimoto, An expedient synthesis of the amide analog of the potent antifungal lipopeptidolactone FR901469, Tetrahedron Lett 42 (2001) 703–705

[34] D. Beaulieu, J Tang, D J Zeckner, T.R. Parr, Correlation of cilofungin in vivo efficacy with its activity against *Aspergillus fumigatus* (1,3)-β-D-glucan synthase, FEMS Microbiol Lett 108 (1993) 133–138

[35] A Fujie, T Iwamoto, B. Sato, H Muramatsu, C Kasahara, T. Furuta, Y Hori, M. Hino, S Hashimoto, FR131535, a novel water-soluble

echinocandin-like lipopeptide: synthesis and biological properties, Bioorg Med. Chem. Lett. 11 (2001) 399–402

[36] T. Furuta, H. Muramatsu, A. Fujie, S. Fujihira, N R Abdullah, S. Kojima, Therapeutic effects of water-soluble echinocandin compounds on Pneumocystis pneumonia in mice, Antimicrob Ag Chemother. 42 (1998) 37–39.

[37] M. Tomishima, H. Ohki, A Yamada, H Takasugi, K. Maki, S. Tawara, H Tanaka, FK463, a novel water-soluble echinocandin lipopeptide: synthesis and antifungal activity, J. Antibiotics 52 (1999) 674–676

[38] K. Uchida, Y. Nishiyama, N. Yokota, H. Yamaguchi, In vitro antifungal activity of a novel antifungal agent. FK463, against various fungal pathogens, J. Antibiotics 53 (2000) 1175–1181

[39] S. Tawara, F. Ikeda, K. Maki, Y. Morishita, K Otomo, N. Teratani, T. Goto, M. Tomishima, H. Ohki, A. Yamada, K. Kawabata, H Takasugi, K Sakane, H Tanaka, F Matsumoto, S. Kuwahara, In vitro activities of a new lipopeptide antifungal agent, FK463, against a variety of clinically important fungi, Antimicrob. Ag. Chemother. 44 (2000) 57–62

[40] H. Mikamo, Y. Sato, T. Tamaya, In vitro antifungal activity of FK463, a new water-soluble echinocandin-like lipopeptide, J. Antimicrob Chemoth 46 (2000) 485–487.

[41] I Bekersky, D Buell, M Tomishima, K Maki, I Lawrence, R.M. Fielding, New approaches to systemic antifungal therapy: case studies of Ambisome and FK463, Recent Res. Devel. Antimicrob. Ag. Chemother. 3 (1999) 407–413.

[42] F. Ikeda, Y. Wakai, S. Matsumoto, K Maki, E. Watabe, S. Tawara, T Goto, Y. Watanabe, F Matsumoto, S. Kuwahara, Efficacy of FK463, a new lipopeptide antifungal agent, in mouse models of disseminated candidiasis and aspergillosis, Antimicrob. Ag. Chemother. 44 (2000) 614–618

[43] S Matsumoto, Y. Wakai, T. Nakai, K Hatano, T Ushitani, F Ikeda, S. Tawara, T. Goto, F. Matsumoto, S Kuwahara, Efficacy of FK463, a new lipopeptide antifungal agent, in mouse models of pulmonary aspergillosis, Antimicrob Ag Chemother. 44 (2000) 619–621.

[44] S. Maesaki, M.A. Hossain, Y. Miyazaki, K Tomono, T. Tashiro, S. Kohno, Efficacy of FK463, a (1,3)-β-D-glucan synthase inhibitor, in disseminated azole-resistant *Candida albicans* infection in mice, Antimicrob. Ag. Chemother. 44 (2000) 1728–1730.

[45] M Ito, R. Nozu, T. Kuramochi, N. Eguchi, S Suzuki, K Hioki, T Itoh, F Ikeda, Prophylactic effect of FK463, a new antifungal lipopeptide, against *Pneumocystis carinii* infection in mice, Antimicrob. Ag. Chemother 44 (2000) 2259–2262.

[46] A H. Groll, T.J Walsh, FK-463, Curr Opin Anti-infective Invest Drugs 2 (2000) 405–412.

[47] B M Lomaestro, Caspofungin, an echinocandin antifungal for the treatment of invasive aspergillosis, Formulary 36 (2001) 427–436

ELSEVIER

Biochimica et Biophysica Acta 1587 (2002) 234–239

BIOCHIMICA ET BIOPHYSICA ACTA
BBA
www.bba-direct.com

Review

Trypanosome alternative oxidase as a target of chemotherapy☆

Coichi Nihei, Yoshihisa Fukai, Kiyoshi Kita*

Department of Biomedical Chemistry, Graduate School of Medicine, University of Tokyo, 7-3-1 Hongo, Bunkyo-ku, Tokyo 113-0033, Japan

Received 24 January 2002; accepted 24 January 2002

Abstract

Parasites have developed a variety of physiological functions necessary for their survival within the specialized environment of the host. Using metabolic systems that are very different from those of the host, they can adapt to low oxygen tension present within the host animals. Most parasites do not use the oxygen available within the host to generate ATP, but rather employ systems anaerobic metabolic pathways. The enzymes in these parasite-specific pathways are potential targets for chemotherapy. Cyanide-insensitive trypanosome alternative oxidase (TAO) is the terminal oxidase of the respiratory chain of long slender bloodstream forms of the African trypanosome, which causes sleeping sickness in human and nagana in cattle. TAO has been targeted for the development of anti-trypanosomal drugs because it does not exist in the host Recently, we found the most potent inhibitor of TAO to date, ascofuranone, a compound isolated from the phytopathogenic fungus, *Ascochyta visiae*. © 2002 Elsevier Science B.V. All rights reserved

Keywords *Trypanosoma brucei brucei*, Trypanosome alternative oxidase, Alternative oxidase; Parasite mitochondria, Ascofuranone, Quinol oxidase

1. Introduction

The survival of parasites is dependent on that of the host. It is thought that parasites originated from non-parasitic ancestors and adapted to the environment in the host, evolving host and organ specificities. Parasites adapt to a low oxygen tension environment in the host using metabolic pathways that are very different from those of the host animals. In such systems, parasite mitochondria undergo significant changes in their morphology and composition during development and environmental adaptation [1]. These unique aspects of parasite mitochondria may be promising targets for chemotherapy.

Recently, we isolated a novel compound, nafuredin, from *Aspergillus niger* [2]. Nafuredin inhibits NADH-fumarate reductase (complexes I+II) activity, a unique anaerobic electron transport system in helminth mitochondria. This compound is active at nanomolar concentrations. It competes for the quinone-binding site in complex I and shows high selective toxicity for the helminth enzyme. Moreover, nafuredin exerts anti-helminthic activity against *Haemonchus contortus* in in vivo trials in sheep. These findings show that the parasite mitochondrial respiratory chain is a worthwhile target for chemotherapy.

In this review, we describe an additional novel inhibitor of parasite mitochondrial function, ascofuranone. This compound blocks the cyanide-insensitive terminal oxidase of *Trypanosoma brucei brucei* mitochondria, an enzyme also known as trypanosome alternative oxidase (TAO) [3]. In addition, this compound inhibits trypanosomal growth in heavily infected mice, and is, therefore a good lead for the development of new treatments for African trypanosomiasis [4]. Also, this validates TAO as a good target for the development of anti-trypanosomal chemotherapeutic agents.

2. African trypanosome

2.1. African trypanosomiasis

African trypanosomes are protozoan parasites responsible for sleeping sickness and nagana, diseases mediated by tsetse flies. Trypanosome infections are not only a problem in humans, but they are also a major issue for animals, livestock in particular, and are a principle issue in the

---

Abbreviations AF, ascofuranone; AOX, alternative oxidase; DFMO, α-difluoromethylornithine, LS, long slender form; SHAM, salicylhydroxamic acid, TAO, trypanosome alternative oxidase, VSG, variant surface glycoprotein

☆ Nucleotide sequence data reported in this review is available in the DDBJ, EMBL and NCBI data bases under the accession number AB070617

* Corresponding author Tel · +81-3-5841-3526; fax +81-3-5841-3444
E-mail address: kitak@m.u-tokyo.ac.jp (K Kita).

0925-4439/02/$ - see front matter © 2002 Elsevier Science B V All rights reserved.
PII S0925-4439(02)00086-8

Table 1
Change of energy metabolism during life cycle in *T b brucei*

Host stage	Tsetse procyclic	Human trypomastigote	
		LS	SS
Mitochondria	active	inactive	active
TCA cycle	+	–	+
Cytochromes	+	–	+
Alternative oxidase	–	+	–
ATP synthesis	mitochondria	glycosome	mitochondria

LS long slender form, SS. short stumpy form.

African food supply problem. Trypanosomes escape elimination by the host immune system by varying their cell surface antigens, including repeated changes of the variant surface glycoprotein (VSG), a glycolipid-anchored glycoprotein [5]. Therefore, it is quite difficult to produce effective vaccines against them, and anti-trypanosomal chemotherapy is a major strategy against this African trypanosomiasis [6].

The two most commonly used chemotherapeutic compounds against trypanosomiasis are suramin and pentamidine. These compounds are effective during the hematological stage of the disease. Melarsoprol and α-difluoromethylornithine (DFMO), on the other hand, are used in late-stage disease. However, the first two agents are ineffective at eradicating the parasite if it already has surmounted the blood–brain barrier, and the latter two frequently have fatal side effects [7]. Clearly, research and development of new drugs for the treatment of African trypanosomiasis is urgently needed.

2.2. Mitochondria of T b. brucei

T. b. brucei, the causative agent of nagana in cattle, is closely related to *T. b. rhodesiense* and *T. b. gambiense*, which cause sleeping sickness in humans. We have been studying mitochondria of *T. b brucei* as a target for chemotherapy because of its unique metabolic properties. Flagellates generally have one mitochondrion per cell, which contains RNA-editing kinetoplast DNA. Also, previous studies have shown that the structure and function of *T b brucei* mitochondria change markedly during their life cycle (Table 1) [8].

In the procyclic forms of *T. b brucei* found in the tsetse fly vector, ATP is synthesized by oxidative phosphorylation, and the mitochondria possess developed cristae containing

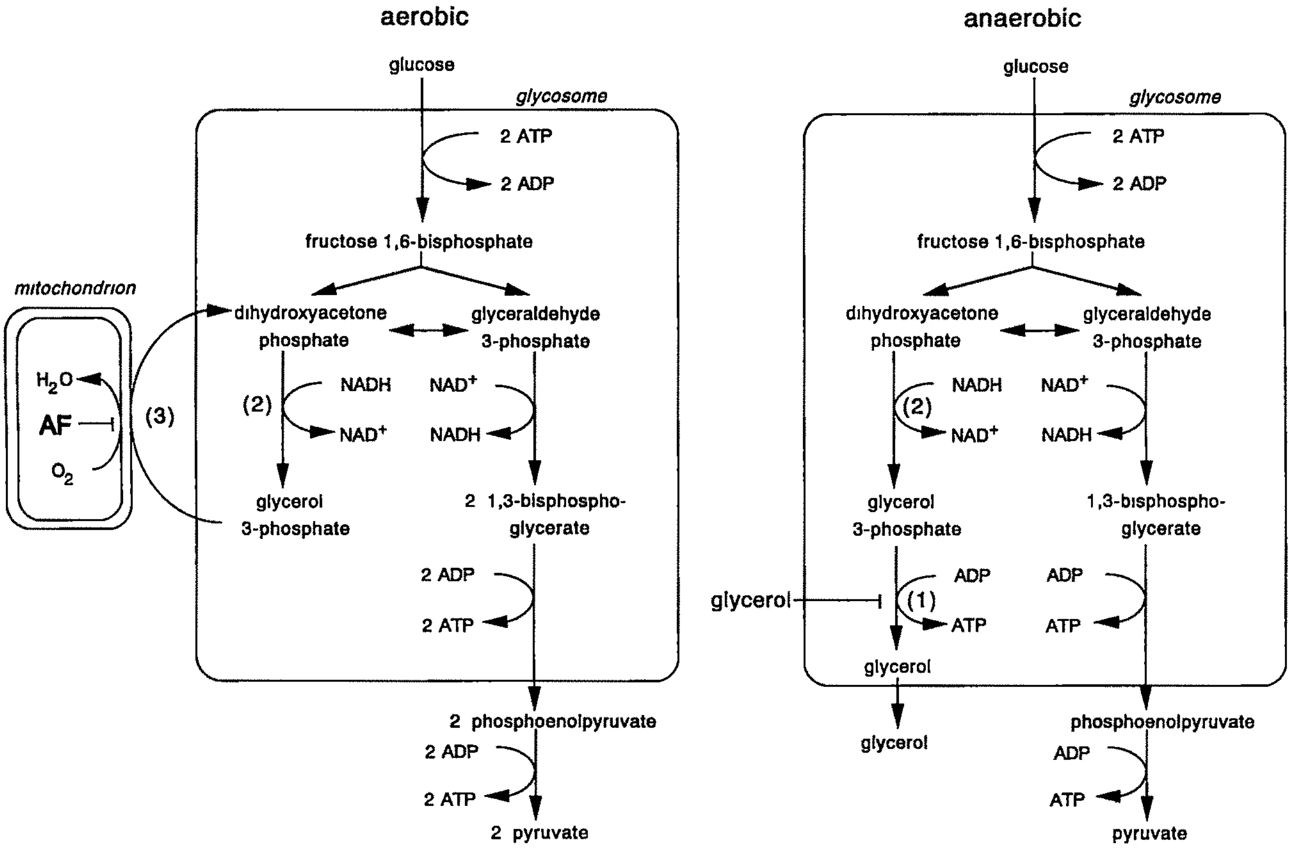

Fig 1. Glucose metabolism in bloodstream form of *T. b brucei* under aerobic and anaerobic conditions. (1) Glycerol kinase, (2) glycerol-3-phosphate dehydrogenase, (3) cyanide-insensitive quinol ozidase (TAO). AF and glycerol inhibit TAO and glycerol kinase, respectively. Modified from Ref. [26]

the respiratory chain and ATP synthetase systems. In contrast, in the long slender (LS) bloodstream form, which lives in the host mammal's blood, energy metabolism occurs mostly by the glycolytic pathway in a specific organelle called the glycosome (Fig. 1) [9]. Glycosomes contain a 100-fold higher concentration of glycolytic enzymes than the cytoplasm of typical cells, and the glycolytic reaction proceeds at a high efficiency. Further, mitochondria of the LS form contain no cytochrome systems and do not synthesize ATP by oxidative phosphorylation. Rather, the mitochondrial cyanide-insensitive glycerol-3-phosphate oxidase system is used to re-oxidize of NADH produced in the glycolytic pathway (Fig. 2). Specifically, this system oxidizes glycerol-3-phosphate produced in the glycosomes using an electron transport system in the inner mitochondrial membrane consisting of glycerol-3-phosphate dehydrogenase, ubiquinone, and TAO [10]. Because the trypanosome glycerol-3-phosphate oxidase system does not exist in the host, it has attracted attention as a target for trypanocides. Indeed, suramin may act by inhibiting the glycerol-3-phosphate oxidation system, although the mechanism is not certain at this time [11].

Under anaerobic conditions, or in the presence of a respiratory inhibitor such as salicylhydroxamic acid (SHAM), glycerol-3-phosphate accumulates inside the glycosome, and this is converted to glycerol by a reverse action of glycerol kinase [9]. In other animals, this enzyme functions almost exclusively in the forward direction, producing glycerol-3-phosphate from ATP and glycerol. This new anaerobic glycolytic pathway leads to the synthesis of 1 mol of ATP and 1 mol of glycerol. In this way, 1 mol of glucose is dismutated into equimolar amounts of pyruvate and glycerol, with a net synthesis of 1 mol of ATP, even under anaerobic conditions or in the presence of respiratory inhibitors (Fig. 1). Therefore, inhibition of cyanide-insensitive respiration alone is not sufficient to kill the parasite, and the trypanosome can survive as long as glycerol does not accumulate in the medium. However, once the concentration of glycerol in the medium becomes several millimolar, mass action causes the enzyme to reverse and produce glycerol-3-phosphate from glycerol and anaerobic glycolysis in the glycosome stops. In fact, simultaneous administration of SHAM and glycerol leads to an immediate lysis and disappearance of the parasite from the blood [12].

3. Effect of ascofuranone

3.1. Effect of ascofuranone on cultured *T. b. brucei*

Because ubiquinone is an essential component of the glycerol-3-phosphate oxidase system, we searched for compounds with a structure similar to ubiquinone that might inhibit the respiratory chain of the LS trypanosome. We found ascofuranone, a potent and specific inhibitor of glucose-dependent respiration in cultured cells and of the glycerol-3-phosphate oxidase from isolated mitochondria (Fig. 3) [3].

Ascofuranone is isolated from phytopathogenic fungus, *Ascochyta visiae* [13]. This compound possesses host-mediated anti-tumor activity because it activates macrophages [14]. This appears to be due to the respiratory inhibition of macrophages via the quinone site [15]. Therefore, we examined the effect of ascofuranone on the respiration of cultured trypanosomes to determine if it might inhibit the glycerol-3-phosphate oxidase system. Surprisingly, we found that nanomolar concentrations of ascofuranone inhibit mitochondrial glycerol-3-phosphate dependent oxidase activity as well as glucose-dependent respiration of cultured cells [3]. In contrast, micromolar concentrations of ascofuranone are required for inhibition of mitochondria from other organisms. At least, one of the targets of this compound seems to be TAO because it potently inhibited mitochondrial quinol oxidase activity ($K_i = 2.38$ nM). This value is three orders of magnitude lower than that of suramin ($K_i = 4.1$ μM) and *n*-propyl gallate ($K_i = 6.3$ μM) [11,16], suggesting that ascofuranone is a specific inhibitor of the oxidase system. Because 4-*O*-methoxycarbonylmethyl and 4-*O*-carboxymethyl-substitutions (Fig. 3) decrease its effect dramatically, the 4-OH group of the compound likely plays an important role in the inhibitory mechanism [3]. Finally, in vitro growth of the LS form of the trypanosome is also inhibited by ascofuranone.

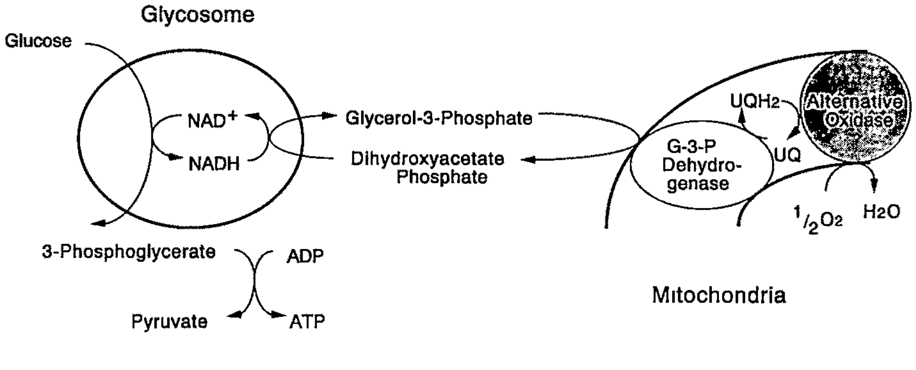

Fig. 2. Glycerol-3-phosphate oxidase system in *T. b. brucei* mitochondria. This system oxidizes glycerol-3-phosphate produced in the glycosomes using the electron transport system consisting of glycerol-3-phosphate dehydrogenase, ubiquinone, and cyanide-insensitive alternative oxidase (TAO) localized in the mitochondrial inner membrane.

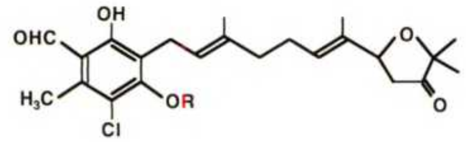

R = H : Ascofuranone
R = CH_2COOH : 4-*O*-Carboxymethyl ascofuranone
R = CH_2COOCH_3 : 4-*O*-Methoxycarbonylmethyl ascofuranone

Fig. 3. Ascofuranone and its derivatives.

3.2. Effect of ascofuranone on mice infected with T. b. brucei

Ascofuranone is not only a potent inhibitor in vitro, but it also is an effective chemotherapeutic agent for the treatment of African trypanosomiasis in mice with a high level of parasitemia [4]. Combination of 3 g/kg glycerol with either oral (100 mg/kg) or intraperitoneal (25 mg/kg) ascofuranone provided dramatic antitrypanosomal activity in infected mice. In fact, all trypanosomes disappeared within 30 min of intraperitoneal treatment and within 180 min after oral administration.

The efficacy of oral treatment is an extremely important factor for practical use of ascofuranone because a simple mode of administration is essential in rural conditions. Presently, all drugs available for human and animal trypanosomiasis are administered intramuscularly (pentamidine, diminazene aceturate and isometamidium chloride) or intravenously (suramin, melarsoprol and DFMO) [7]. In addition, our recent studies in rat and human cell lines show that ascofuranone has desirable pharmacokinetic properties, is safe, and is without any side effect (Hosokawa, unpublished observation).

4. TAO as a target of ascofuranone

4.1. Alternative oxidase (AOX)

As described in the previous section, TAO appears to be at least one of the sites of inhibition in the glycerol-3-phosphate oxidase system of LS form mitochondria. This

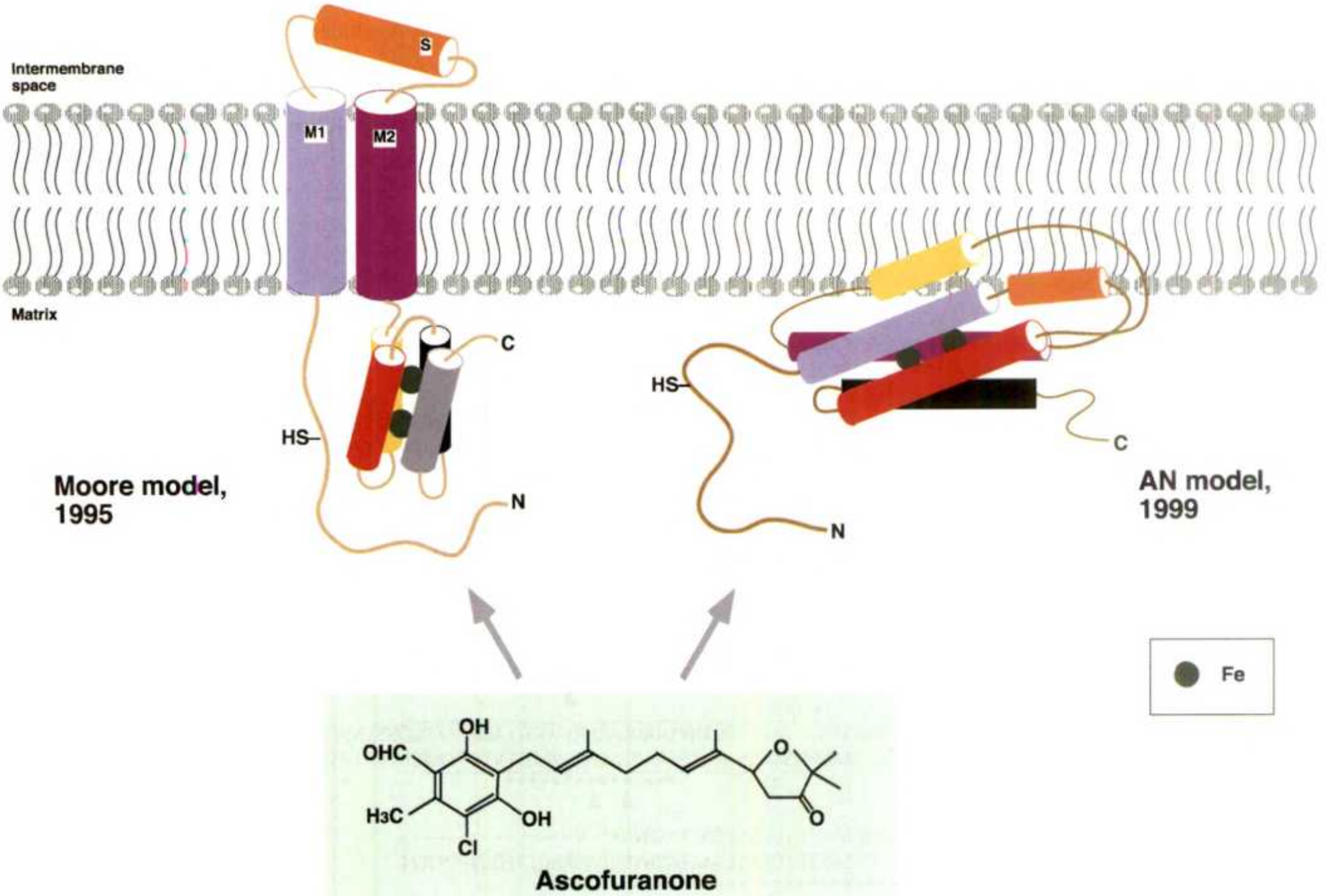

Fig. 4. Two proposed models of AOX and inhibition by ascofuranone. (left) Transmembrane model proposed by Siedow et al. [27], (right) interfacial membrane model proposed by Andersson and Nordlund [28].

terminal oxidase is completely different in structure than the cyanide-sensitive mammalian type cytochrome *c* oxidase found in the mitochondria of the procyclic trypanosome forms. Like other forms of AOX, TAO is thought to contain iron rather than heme as the prosthetic group. Chaudhuri et al. [17] showed by cDNA analysis that TAO belongs to the AOX family of mitochondrial oxidase of higher plants, algae, yeast, slim molds, and free-living amoebae. TAO and AOX have many characteristics in common, including: (1) they possess a cyanide-insensitive ubiquinol oxidase activity; (2) both enzymes are specifically inhibited by SHAM and *n*-propyl gallate; (3) they are mitochondrial inner membrane proteins containing four α-helices and with a mass of 30–38 kDa (Fig. 4); (4) like ribonucleotide reductase R2 and methane monooxygenase, they have a catalytic site containing a putative binuclear iron center coordinated by two helices that include a Glu–X–X–His motif as well as two helices with a conserved Glu or Asp residue; (5) TAO cross-reacts with an anti-plant AOX monoclonal antibody recognizing the region (RADEXXHXXXNH), which contains the C-terminal iron-bound motif [18].

In plant AOX, there is a conserved Cys residue close to the N-terminus, and the disulfhydryl-bound dimer has low activity. The activity increases when an α-keto acid is bound to the sulfhydryl group of the reduced monomer by a thiohemiacetal linkage [19]. In contrast, in amoebae, algae, and yeast, AOX is activated by purine nucleotides such as AMP and GMP [20]. However, these studies were performed using intact cells or mitochondria, because the purified enzyme is very labile. The same problem has limited the study of TAO from trypanosomes.

4.2. TAO

Because TAO is a unique enzyme in trypanosome LS form, and may be a good target for anti-trypanosome chemotherapy, many studies have examined the effects of TAO electron transport inhibitors. SHAM and *n*-propyl gallate, inhibitors of plant AOX with a benzene ring-like ubiquinone, inhibit TAO [16,21]. Structure–function relationships of *p*-alkyloxybenzhydroxaminc acid and of 3,4-dihydroxybenzoic acid, have been studied in detail [16,22]. Alkyl esters of 3,4-dihydroxybenzoic acid inhibit the glycerol-3-phosphate oxidase system at concentration 400-fold lower than that needed for inhibition by SHAM. However, no drug has been developed from these compounds because of their low solubility and selectivity.

Clearly, understanding the function of TAO is essential for developing new inhibitors. Chaudhuri et al. [23] partially purified TAO from NP-40-solubilized mitochondria. The specific activity of TAO increased 10-fold by gel filtration, and a 33-kDa peptide was identified as TAO, but no further information could be obtained due to its low stability and recovery. To solve this problem, TAO has been expressed in an *E. coli* heme synthesis mutant lacking a functional terminal oxidase such as cytochrome *bo* and *bd* complexes. In this system, TAO restores respiration, but the amount of recombinant enzyme produced is not enough for biochemical analyses.

Recently, we have established a system for over-expressing TAO in *E. coli* using pET expression vector [24]. TAO-expressing *E. coli* are easily identified because they are resistant to cyanide. Further, the respiratory activity of their cell membranes is also cyanide-insensitive. In addition, the

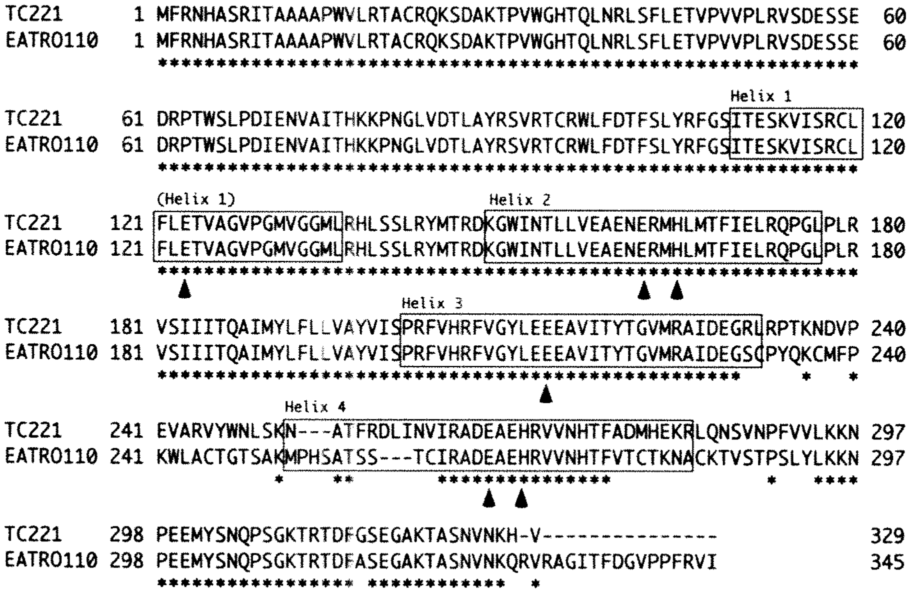

```
TC221      1 MFRNHASRITAAAAPWVLRTACRQKSDAKTPVWGHTQLNRLSFLETVPVVPLRVSDESSE  60
EATRO110   1 MFRNHASRITAAAAPWVLRTACRQKSDAKTPVWGHTQLNRLSFLETVPVVPLRVSDESSE  60
             ************************************************************

                                                              Helix 1
TC221     61 DRPTWSLPDIENVAITHKKPNGLVDTLAYRSVRTCRWLFDTFSLYRFGSITESKVISRCL 120
EATRO110  61 DRPTWSLPDIENVAITHKKPNGLVDTLAYRSVRTCRWLFDTFSLYRFGSITESKVISRCL 120
             ************************************************************

             (Helix 1)                   Helix 2
TC221    121 FLETVAGVPGMVGGMLRHLSSLRYMTRDKGWINTLLVEAENERMHLMTFIELRQPGLPLR 180
EATRO110 121 FLETVAGVPGMVGGMLRHLSSLRYMTRDKGWINTLLVEAENERMHLMTFIELRQPGLPLR 180
             ************************************************************
               ▲                                      ▲  ▲
                                  Helix 3
TC221    181 VSIIITQAIMYLFLLVAYVISPRFVHRFVGYLEEEAVITYTGVMRAIDEGRLRPTKNDVP 240
EATRO110 181 VSIIITQAIMYLFLLVAYVISPRFVHRFVGYLEEEAVITYTGVMRAIDEGSCPYQKCMFP 240
             **************************************************    *    *
                                              ▲
                        Helix 4
TC221    241 EVARVYWNLSKN---ATFRDLINVIRADEAEHRVVNHTFADMHEKRLQNSVNPFVVLKKN 297
EATRO110 241 KWLACTGTSAKMPHSATSS---TCIRADEAEHRVVNHTFVTCTKNACKTVSTPSLYLKKN 297
                       *    **       ***************             *   ****
                                         ▲  ▲

TC221    298 PEEMYSNQPSGKTRTDFGSEGAKTASNVNKH-V---------------             329
EATRO110 298 PEEMYSNQPSGKTRTDFASEGAKTASNVNKQRVRAGITFDGVPPFRVI             345
             ***************** ************  *
```

Fig. 5. Amino acid sequences of cDNA for TAO from two strains of *T. b. brucei*. Amino acid sequences of TAO from *T. b. brucei* strain TC221 (present study, the accession number AB070617 in DDBJ) and EATRO110 [25] are compared. (*) Identical amino acid; (arrows) conserved di-iron coordination motif (–E– and –EXXH–).

respiratory activity is sensitive to ascofuranone, which does not inhibit *E. coli* terminal oxidases. This system, therefore, allows detailed analysis of TAO. Indeed, enzymological analysis using the recombinant TAO revealed that the inhibitory effect of ascofuranone is due to competitive inhibition for ubiquinone, suggesting that the quinone ring structure is closely involved in the inhibition mechanism (Fukai et al., unpublished results).

During the establishment of the *E. coli* expression system for TAO, we found strain-specific differences in TAO's amino acid sequence (Fig. 5). The C-terminal part of TAO from the strain that we are using, *T. b. brucei* TC221, is considerably different than that cloned by Hill's group from the EATRO110 strain [25]. Further, the amino acid sequence of TC221 TAO is much more closer than EATRO110 TAO to other forms of AOX. Both forms of TAO contained the conserved diiron-coordination motif, consistent with the ability of both TAO cDNAs to restore of respiration of an *E. coli* heme synthesis mutant. Comparative analysis of these two enzymes, including sensitivity to ascofuranone, may reveal structure–function relationship of TAO and provide insight into its mechanism of inhibition.

5. Conclusions and perspectives

As described in this review, the parasite metabolic system is an attractive target for chemotherapy because it is different than the host metabolic system and because it is essential for parasite survival. TAO in trypanosome mitochondria and its specific inhibitor, ascofuranone are excellent examples in this regard. As pointed out by Opperdoes [9], ascofuranone is the most potent TAO inhibitor to date. Because of its high selectivity and low toxicity, ascofuranone is a potential candidate for the next generation of anti-trypanosomal agents. Indeed, current studies are examining the molecular mechanism of ascofuranone and ways of improving its efficacy in vivo.

One problem that must be solved is that glycerol must be administered along with ascofuranone, to inhibit the reverse reaction of glycerol kinase (see Fig. 1). Although glycerol is not toxic, it is not practical to give the large dose (3 g/kg) required, and an inhibitor of the reverse reaction of glycerol kinase is expected to be more useful. Fortunately, glycerol kinase has been cloned and the recombinant enzyme can be over-expressed [26]. In addition, studies on glycerol kinase from trypanosomastids that lack or have a limited capacity to produce glycerol, such as *T. vivax* and *T. congolense*, will provide useful information on the glycerol kinase enzyme.

Acknowledgements

We would like to acknowledge Dr. K. Nagai, Dr. Y. Yabu, Dr. N. Minagawa and Dr. T. Hosokawa for their helpful discussions. This study was supported by a grant-in-aid for scientific research on priority areas from the Ministry of Education, Science, Culture and Sports, Japan (13226015 and 13854011) and for research on emerging and re-emerging infectious diseases from the Ministry of Health and Welfare.

References

[1] K. Kita, H. Hirawake, H. Miyadera, H. Amino, S. Takeo, Biochim. Biophys. Acta, in press.
[2] S. Omura, H. Miyadera, H. Ui, K. Shiomi, Y. Yamaguchi, R. Masuma, T. Nagamitsu, D. Takano, T. Sunazuka, A. Harder, H. Kölbl, M. Namikoshi, H. Miyoshi, K. Sakamoto, K. Kita, Proc. Natl. Acad. Sci. U. S. A. 98 (2001) 60–62.
[3] N. Minagawa, Y. Yabu, K. Kita, N. Ohta, K. Meguro, S. Sakajo, A. Yoshimoto, Mol. Biochem. Parasitol. 81 (1996) 127–136.
[4] Y. Yabu, N. Minagawa, K. Kita, K. Nagai, M. Honma, S. Sakajo, T. Koide, N. Ohta, A. Yoshimoto, Parasitol. Int. 47 (1998) 131–137.
[5] E. Pays, in: M. Dumas, B. Bouteille, A. Buguet (Eds.), Progress in Human African Trypanosomiasis, Sleeping Sickness, Springer, Paris, 1999, pp. 31–52.
[6] J. Keiser, A. Stich, C. Burri, Trend. Parasitol. 17 (2001) 42–49.
[7] S.V. Nieuwenhove, in: M. Dumas, B. Bouteille, A. Buguet (Eds.), Progress in Human African Trypanosomiasis, Sleeping Sickness, Springer, Paris, 1999, pp. 253–280.
[8] K. Vickerman, Br. Med. Bull. 41 (1985) 105–114.
[9] F.R. Opperdoes, in: M. Dumas, B. Bouteille, A. Buguet (Eds.), Progress in Human African Trypanosomiasis, Sleeping Sickness, Springer, Paris, 1999, pp. 53–80.
[10] A.B. Clarkson Jr., E.J. Bienen, G. Pollakis, R.W. Grady, J. Biol. Chem. 264 (1989) 17770–17776.
[11] A.H. Fairlamb, I.B.R. Bowman, Exp. Parasitol. 43 (1977) 353–361.
[12] A.B. Clarkson Jr., F.H. Brohn, Science 194 (1976) 204–206.
[13] J. Magae, T. Hosokawa, K. Ando, K. Nagai, G. Tamura, J. Antibiot. 35 (1982) 1547–1552.
[14] J. Magae, J. Hayasaki, Y. Matsuda, M. Hotta, T. Hosokawa, S. Suzuki, K. Nagai, K. Ando, G. Tamura, J. Antibiot. 41 (1988) 959–996.
[15] J. Magae, K. Nagai, K. Ando, G. Tamura, Agric. Biol. Chem. 52 (1988) 3143–3147.
[16] R.W. Grady, E.J. Bienen , A.B. Clarkson Jr., Mol. Biochem. Parasitol. 21 (1986) 55–63.
[17] M. Chaudhuri, W. Ajayi, G.C. Hill, Mol. Biochem. Parasitol. 95 (1998) 53–68.
[18] D.A. Berthold, M.E. Andersson, P. Nordlund, Biochim. Biophys. Acta 1460 (2000) 241–254.
[19] T. Joseph-Horne, J. Babij, P.M. Wood, D. Hollomon, R.B. Sessions, FEBS Lett. 481 (2000) 141–146.
[20] F.E. Sluse, W. Jarmuszkiewicz, Braz. J. Biol. Res. 31 (1998) 733–747.
[21] A.B. Clarkson Jr., R.W. Grady, S.A. Grossman, R.J. McCallum, F.H. Brohn, Mol. Biochem. Parasitol. 3 (1981) 271–291.
[22] R.W. Grady, E.J. Bienen , A.B. Clarkson Jr., Mol. Biochem. Parasitol. 19 (1986) 231–240.
[23] M. Chaudhuri, W. Ajayi, S. Temple, G.C. Hill, J. Eukaryotic Microbiol. 42 (1995) 467–472.
[24] Y. Fukai, H. Amino, H. Hirawake, Y. Yabu, N. Ohta, N. Minagawa, S. Sakajo, A. Yoshimoto, K. Nagai, S. Takamiya, S. Kojima, K. Kita, Comp. Biochem. Physiol. 124 (1999) 141–148.
[25] M. Chaudhuri, G.C. Hill, Mol. Biochem. Parasitol. 83 (1996) 125–129.
[26] I. Kralova, D.J. Rigden, F.R. Opperdoes, P.A.M. Michels, Eur. J. Biochem. 267 (2000) 2323–2333.
[27] J.N. Siedow, A.L. Umbach, A.L. Moore, FEBS Lett. 362 (1995) 10–14.
[28] M.E. Andersson, P. Nordlund, FEBS Lett. 449 (1999) 17–22.

ELSEVIER

Biochimica et Biophysica Acta 1587 (2002) 240–248

BIOCHIMICA ET BIOPHYSICA ACTA
BBA
www.bba-direct.com

Review

The genetic basis of fluconazole resistance development in *Candida albicans*

Joachim Morschhäuser*

Institut für Molekulare Infektionsbiologie, Universität Würzburg, Röntgenring 11, D-97070 Würzburg, Germany

Received 24 January 2002; accepted 24 January 2002

Abstract

Infections by the opportunistic fungal pathogen *Candida albicans* are widely treated with the antifungal agent fluconazole that inhibits the biosynthesis of ergosterol, the major sterol in the fungal plasma membrane. The emergence of fluconazole-resistant *C. albicans* strains is a significant problem after long-term treatment of recurrent oropharyngeal candidiasis (OPC) in acquired immunodeficiency syndrome (AIDS) patients. Resistance can be caused by alterations in sterol biosynthesis, by mutations in the drug target enzyme, sterol 14α-demethylase (14DM), which lower its affinity for fluconazole, by increased expression of the *ERG11* gene encoding 14DM, or by overexpression of genes coding for membrane transport proteins of the ABC transporter (*CDR1*/*CDR2*) or the major facilitator (*MDR1*) superfamilies. Different mechanisms are frequently combined to result in a stepwise development of fluconazole resistance over time. The *MDR1* gene is not or barely transcribed during growth in vitro in fluconazole-susceptible *C. albicans* strains, but overexpressed in many fluconazole-resistant clinical isolates, resulting in reduced intracellular fluconazole accumulation. The activation of the gene in resistant isolates is caused by mutations in as yet unknown trans-regulatory factors, and the resulting constitutive high level of *MDR1* expression causes resistance to other toxic compounds in addition to fluconazole. Disruption of both alleles of the *MDR1* gene in resistant *C. albicans* isolates abolishes their resistance to these drugs, providing genetic evidence that *MDR1* mediates multidrug resistance in *C. albicans*. © 2002 Elsevier Science B.V. All rights reserved.

Keywords: *Candida albicans*; Drug resistance; Efflux pump; Fluconazole; Major facilitator

1. Introduction

The yeast *Candida albicans* is a harmless colonizer of mucosal surfaces in many healthy persons, but it can cause superficial as well as life-threatening systemic infections in immunocompromised patients. Especially people infected with the human immunodeficiency virus (HIV) and acquired immunodeficiency syndrome (AIDS) patients frequently suffer from oropharyngeal candidiasis (OPC). Few classes of antifungal drugs are available to treat *Candida* infections. The azoles affect the biosynthesis of ergosterol, the major sterol in the fungal plasma membrane, by inhibiting the enzyme sterol 14α-demethylase (14DM), a cytochrome P-450 enzyme. This key enzyme in the ergosterol biosynthesis pathway catalyzes the oxidative removal of the 14α-methyl group from lanosterol. Azoles bind to the heme in the active site of 14DM, competing with substrate binding [1]. The triazole fluconazole is the most widely used drug to treat *Candida* infections, due to its favourable bioavailability and safety profile. The clinical response to fluconazole in patients with OPC is usually good but because of incomplete eradication of the fungi due to the fungistatic rather than fungicidal effect of azoles, relapses occur frequently [2]. The prolonged and repeated treatment of OPC in AIDS patients has resulted in an increasing frequency of therapy failures caused by the emergence of fluconazole-resistant *C. albicans* strains [3].

2. The development of fluconazole resistance in *C. albicans*

Especially in AIDS patients receiving long-term fluconazole therapy, clinical resistance is usually correlated with

---

Abbreviations: ABC, ATP-binding cassette; AIDS, acquired immunodeficiency syndrome; ATP, adenosine triphosphate; 14DM, sterol 14α-demethylase; GFP, green fluorescent protein; HIV, human immunodeficiency virus; 4-NQO, 4-nitroquinoline-*N*-oxide; OPC, oropharyngeal candidiasis

* Tel.: +49-931-31-2152; fax: +49-931-31-2578.
E-mail address: joachim.morschhaeuser@mail.uni-wuerzburg.de (J. Morschhäuser).

0925-4439/02/$ - see front matter © 2002 Elsevier Science B.V. All rights reserved.
PII: S0925-4439(02)00087-X

the isolation of *C. albicans* strains displaying decreased in vitro susceptibility to fluconazole [3,4]. To determine whether fluconazole resistance is due to the aquisition of a new, resistant strain that replaces a previously infecting, susceptible strain, or if resistance has developed in a previously susceptible strain that colonized the patient before, it is necessary to discriminate genetically unrelated *C. albicans* strains from each other. Many molecular typing methods are available for *C. albicans*, but Southern hybridization of genomic DNA with moderately repetitive DNA elements has been shown to have the highest reproducibility and discriminatory power (see Fig. 1). Molecular typing has demonstrated that colonizing populations of *C. albicans* are usually clonal, i.e. a single strain is in most cases the cause of recurrent infections in a patient, but the strain may evolve into subtypes [5]. However, it has also been shown that a patient can be colonized by several different *C. albicans* strains at the same time [6–8]. In many studies, only a single isolate is characterized from each infection episode. Therefore, a strain that was present as a minor constituent of the colonizing population in the patient may be isolated for the first time after it has acquired resistance and overgrown a previously dominating other strain, thereby giving the appearance of resistance being due to strain replacement. Although transmission of a resistant strain, for example from the sexual partner, may occur [9], the analysis of many *C. albicans* isolates from patients with recurrent infections has demonstrated that fluconazole resistance usually developed in a previously susceptible strain from the same patient [10,11]. Such series of matched isolates, i.e. isolates representing the same *C. albicans* strain but differing in their susceptibility to fluconazole, are an excellent tool to study the mechanisms of drug resistance, since genetic alterations in a resistant isolate as compared to a matched susceptible isolate are likely to be related to the resistant phenotype [4].

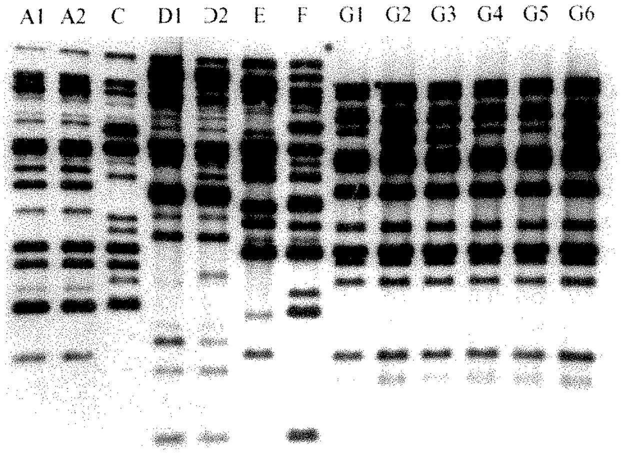

Fig. 1. DNA fingerprint pattern obtained after Southern hybridization of *Eco*RI-digested genomic DNA of *C. albicans* isolates with the *C. albicans*-specific repetitive DNA element *CARE-2* [64]. Isolates obtained from different patients (letters A–G) exhibit different fingerprints. The two isolates from patient A have an identical fingerprint, the two isolates from patient D are highly similar and represent subtypes of the same strain. Patient G harboured three subtypes of the same strain: Isolates G2, G3 and G6 are identical, isolates G4 and G5 are also identical and differ from the former by the absence of one band, and isolate G1 exhibits an additional weak band as compared to G4 and G5.

3. The molecular mechanisms of fluconazole resistance in *C. albicans*

Several different mechanisms may be responsible for the development of fluconazole resistance in *C. albicans*. These include alterations in the sterol biosynthesis pathway, overexpression of the *ERG11* gene encoding the drug target enzyme 14DM, mutations in the *ERG11* gene which result in reduced affinity of 14DM to fluconazole, and reduced intracellular drug accumulation, which is correlated with the overexpression of membrane transport proteins. In contrast, inactivation of the drug, a frequent cause of resistance to antibiotics in bacteria, has not been described as a resistance mechanism in *C. albicans*. The following sections summarize the genetic evidence that is available for the involvement of the various mechanisms in fluconazole resistance.

3.1. Alterations in the sterol biosynthesis pathway

Inhibition of 14DM by fluconazole not only results in ergosterol depletion but also in the accumulation of the methylated sterol 14α-methylergosta-8,24(28)-dien-3β,6α-diol, which inhibits cell growth [12]. Alterations in the sterol biosynthesis pathway that avoid the accumulation of this growth inhibiting sterol in the presence of fluconazole can cause fluconazole resistance. Inactivation of $\Delta^{5,6}$ desaturase (ERG3), an enzyme that acts at an earlier step than 14DM in the ergosterol biosynthesis pathway, results in altered sterole composition of the membrane (high fecosterol content) and fluconazole resistance, possibly by accumulation of 14α-methylfecosterol, which allows growth [12–14]. Recently it was shown that deletion of the *ERG3* gene in *C. albicans* resulted in reduced susceptibility of the mutants to fluconazole, providing direct genetic evidence that alteration of the sterol biosynthesis pathway can cause fluconazole resistance [15].

3.2. Mutations in the ERG11 gene encoding the drug target enzyme, 14DM

A frequent cause of drug resistance are mutations in the target structure that reduce its binding to the drug without preventing function. To identify alterations in 14DM that might cause fluconazole resistance, several investigators compared the sequence of the *ERG11* gene of fluconazole-resistant *C. albicans* strains with the published *ERG11* sequence and that of fluconazole-susceptible strains. As compared with the published *ERG11* sequence, the amino acid exchanges F105L, E266D, K287R, G448E, G450E, G464S and V488I were found only in fluconazole-resistant isolates, but not in sensitive isolates in one study [16]. However, such sequence differences may simply reflect allelic variation and by themselves do not prove a causal relationship with resistance. Similarly, the amino acid exchanges K128T and K147R were found in sensitive isolates and were therefore suggested not to cause resistance, but such a conclusion would require a comparison of the fluconazole susceptibilities of the mutated and an otherwise identical enzyme. Alterations in the *ERG11* sequence in comparison with the published sequence in fluconazole-resistant isolates were also found by other investigators [17–19]. In these latter studies it was shown that the enzymes from the resistant isolates exhibited reduced sensitivity to inhibition by fluconazole, but the enzymes exhibited several different amino acid exchanges and it was not established which were responsible for the resistant phenotype.

Stronger evidence for mutations in the *ERG11* gene conferring fluconazole resistance was provided by comparing the sequence of the *ERG11* alleles of matched pairs of fluconazole-susceptible and resistant isolates obtained at different infection episodes from the same patient. An R467K mutation was detected in both *ERG11* alleles of a fluconazole-resistant *C. albicans* isolate as compared with matched isolates from the same patient with higher sensitivity [20]. Similarly, a G464S mutation was found in the *ERG11* alleles of an isolate displaying enhanced fluconazole resistance from another series of clinical *C. albicans* isolates [21]. Both amino acids are located near the heme binding site, and the mutations probably result in structural or functional alterations associated with the heme. The relationship of these mutations to the enhanced drug resistance of the strains was confirmed by the demonstration that higher fluconazole concentrations were needed to inhibit enzyme activity in cell free extracts of isolates containing the mutation as compared with isolates without the mutation [20,21].

A successful approach to demonstrate the involvement of *ERG11* mutations in fluconazole resistance has been the heterologous expression of different *ERG11* alleles in *S. cerevisiae* and comparing the susceptibility of the strains to fluconazole [22]. Since all the variant enzymes were expressed equally well in the heterologous host, an increased resistance should be due to differences in the amino acid sequence of the protein. The amino acid exchanges G129A, Y132H, S405F, G464S and R467K were shown to cause fluconazole resistance by this approach [22]. Using a similar strategy, an I471T exchange in *ERG11* was also shown to result in reduced fluconazole susceptibility [23], and recently an involvement in fluconazole resistance was demonstrated for additional amino acid exchanges, F126L, T229A, G307S and F449S [24]. Other mutated *ERG11* genes also conferred increased resistance on *S. cerevisiae* transformants, but these genes encoded enzymes with multiple amino acid exchanges and it could not be deduced which of them was responsible for the resistant phenotype [19,24].

Direct evidence for certain mutations resulting in decreased affinity to the drug was provided by biochemical analysis of heterologously expressed enzymes. The affinity for fluconazole of 14DM containing the mutations Y132H, G464S or R467K was reduced as compared with the wild-type enzyme, confirming that these naturally occurring mutations indeed caused drug resistance in clinical *C. albicans* isolates [25–27]. Mutations that should affect substrate or inhibitor binding can also be inferred from knowledge of the three-dimensional structure of the enzyme. Molecular modeling predicted a hydrogen bond between sterol C3-OH and the threonine at position 315 in the active center of 14DM. A T315A mutation that was introduced by design into the *C. albicans* enzyme indeed reduced its affinity to fluconazole [28]. The T315A mutation has, however, so far not been found in clinical *C. albicans* isolates.

A change from heterozygosity to homozygosity for a mutated *ERG11* gene seems to confer increased resistance. Such a change was found for clinical isolates with the G464S or the R467K mutations [20,21]. Genetic evidence suggests that a cell with two copies of R467K is significantly more resistant than a cell in which only one allele has the mutation [4]. The selection pressure exerted by the presence of fluconazole seems to favour the conversion to homozygosity once a mutation conferring enhanced fluconazole resistance has been introduced into one of the *ERG11* alleles.

Mutations in the drug target enzyme clearly are an important mechanism resulting in the emergence of fluconazole-resistant *C. albicans* strains. Table 1 provides a list of

Table 1
ERG11 mutations causing fluconazole resistance in clinical *C. albicans* strains

Mutation	Evidence for contribution to fluconazole resistance				Reference
	A	B	C	D	
F126L			+		[24]
G129A	+		+[a]		[22]
T229A	+		+		[24]
Y132H	+		+	+	[22,23,25]
G307S	+		+		[24]
S405F	+		+		[22]
F449S			+		[24]
G464S	+	+	+	+	[21,22,24,26]
R467K	+	+	+	+	[20,22,27]
I471T			+		[23]

A: Mutation found in a fluconazole-resistant isolate but not in a matched susceptible isolate from the same patient.

B: Increased fluconazole resistance of enzyme activity in cell-free extracts of isolates containing the mutation as compared with extracts from matched isolates without the mutation.

C: Expression of mutated *ERG11* gene in *S. cerevisiae* conferred higher resistance than otherwise identical gene without the mutation.

D: Biochemical analysis showed reduced affinity of the mutated 14DM for fluconazole as compared with wild-type enzyme.

[a] Conferred increased resistance only in combination with the G464S mutation, but not alone.

ERG11 mutations that have been found in clinical *C. albicans* isolates and whose contribution to fluconazole resistance has been confirmed by various experimental approaches. As stated above, more sequence variations have been found in resistant isolates, but a definite proof for their involvement in resistance remains to be established. It is also important to note that the contribution of a mutation to a resistance phenotype depends on the sequence context of the particular *ERG11* allele in which it occurs, and the effects of some mutations can be additive [22–24].

3.3. Overexpression of the ERG11 gene

In the presence of fluconazole, *C. albicans* upregulates the *ERG11* gene, presumably as a feedback mechanism to make up for ergosterol depletion [21,29]. Franz et al. [21] reported that even in the absence of fluconazole some fluconazole-resistant isolates express *ERG11* mRNA at higher levels than matched susceptible isolates in the presence of the drug. This constitutive *ERG11* overexpression seemed to contribute to fluconazole resistance, although to a lesser degree than *ERG11* mutations, since twice as much fluconazole was needed to inhibit 14DM activity in a cell free extract of such a resistant isolate to the same level as in the extract of a matched susceptible isolate [21]. *ERG11* overexpression has been found in many other fluconazole-resistant *C. albicans* isolates compared with matched susceptible isolates [24,30]. Enhanced gene expression is expected to result in higher enzyme levels and, consequently, a need for higher intracellular fluconazole concentrations to inhibit enzyme activity. There is experimental evidence that such overexpression confers fluconazole-resistance. Overexpression of *ERG11* from *C. albicans* conferred a five-fold enhanced resistance to fluconazole on *S. cerevisiae* as compared to transformants carrying the vector control [28]. When the *ERG11* gene was expressed from doxycyclin-repressible promoters in *C. glabrata*, increased levels of *ERG11* mRNA correlated with reduced fluconazole susceptibility [31]. Therefore, constitutive *ERG11* overexpression may contribute to fluconazole resistance in clinical *C. albicans* strains.

3.4. Overexpression of genes encoding efflux pumps

An important mechanism of fluconazole resistance is reduced intracellular accumulation of the drug. In recent years, it became evident that fluconazole is actively transported out of the cells in an energy-dependent manner and that an enhanced drug efflux is caused by the overexpression of genes encoding membrane transport proteins. The highly homologous genes *CDR1* and *CDR2* (*Candida* drug resistance) encode ATP-binding cassette (ABC) transporters, which use adenosine triphosphate (ATP) as the energy source, whereas the *MDR1* (multidrug resistance) and *FLU1* (fluconazole resistance) genes encode major facilitators, which use the proton gradient across the membrane as the driving force for transport. The *MDR1* gene (originally termed *BEN*^{r}) had been cloned by its ability to confer resistance to benomyl and methotrexate upon *S. cerevisiae* transformants [32], and its overexpression in *S. cerevisiae* was later shown to mediate resistance to a variety of other drugs [33]. The *CDR1* gene is a homolog of the *S. cerevisiae* pleiotropic drug resistance gene *PDR5* and was cloned by complementation of the cycloheximide hypersensitivity of an *S. cerevisiae pdr5* mutant [34]. Transformants carrying the *CDR1* gene displayed increased resistance to many other drugs, suggesting that *CDR1* also is a multidrug resistance gene. Sanglard et al. [35] demonstrated that many fluconazole-resistant, clinical *C. albicans* isolates displayed strongly increased mRNA levels of *CDR1* or *MDR1* in comparison with matched susceptible isolates and accumulated less intracellular fluconazole. They also showed that *S. cerevisiae pdr5* mutants are hypersusceptible to fluconazole and other azoles and that overexpression of *CDR1* from *C. albicans* complemented this phenotype, whereas overexpression of *MDR1* restored increased resistance to fluconazole, but not other azoles. Inactivation of *CDR1* in *C albicans* itself resulted in enhanced intracellular fluconazole levels and increased susceptibility of the mutant to fluconazole and many other drugs, providing genetic evidence that *CDR1* is a multidrug resistance gene in *C. albicans* [36]. In contrast, disruption of *MDR1* had no effect on intracellular fluconazole accumulation and did not influence the susceptibility of the mutants to fluconazole [36,37]. However, the latter result is probably related to the fact that the strains in which *MDR1* had been inactivated, like most fluconazole-susceptible *C. albicans* isolates, did not or barely express *MDR1* under the test conditions used [11,21,29].

The *CDR2* gene, which is highly similar to *CDR1*, was identified in a screen for *C. albicans* genes that complement the hypersusceptibility of *S. cerevisiae pdr5* mutants to azoles [38]. Inactivation of *CDR2* in *C. albicans* had no effect on intracellular fluconazole accumulation and did not influence the susceptibility of the mutants to fluconazole, but this result was probably caused by the absence of *CDR2* expression in azole-susceptible *C. albicans* strains, similar to what is observed for *MDR1* (see above). However, disruption of *CDR2* in a *cdr1* mutant background further increased the susceptibility to fluconazole and other drugs. Interestingly, derivatives of a *cdr1* mutant that regained wild-type levels of fluconazole-susceptibility expressed the *CDR2* gene, and *CDR2* overexpression was also observed in fluconazole-resistant clinical *C. albicans* isolates [38]. Therefore, *CDR2* encodes a multidrug resistance gene that can mediate resistance to fluconazole and other drugs in *C. albicans*.

The *CDR* gene family in *C. albicans* comprises many more genes, but apart from *CDR1* and *CDR2* no evidence for the involvement of other members of the gene family in fluconazole resistance has been obtained so far [39,40]. Recently, a gene that is homologous to *MDR1*, *FLU1*, has been isolated by its ability to confer fluconazole resistance on hypersusceptible *S. cerevisiae* transformants [41]. Inactivation of *FLU1* in a *C. albicans* strain in which several other multidrug resistance genes had been deleted resulted in increased susceptibility to fluconazole, demonstrating that *FLU1* can mediate fluconazole resistance in *C. albicans*. However, overexpression of *FLU1* has not yet been found as a cause of fluconazole resistance in clinical *C. albicans* isolates.

Overexpression of efflux pumps encoded by the *CDR1*, *CDR2* and *MDR1* genes has been shown to be one of the most frequent mechanisms of fluconazole resistance [8,11,21,24,30,35,38,42,43], but the exact mechanism how resistance is mediated has not been resolved, nor is the physiological function of these membrane transport proteins known. Recent studies suggested that Cdr1p transports phospholipids from the inner to the outer leaflet of the cytoplasmic membrane, thereby changing the membrane structure [44]. Earlier studies had demonstrated that reduced intracellular fluconazole accumulation was associated with an altered membrane structure, presumably resulting in reduced drug uptake [45]. The resistance phenotype associated with overexpression of membrane transport proteins may therefore not only be caused by enhanced efflux, but could in part also be due to membrane alterations resulting in reduced drug uptake, a possibility that has not been investigated so far and should be kept in mind.

3.5. Multiple mechanisms contribute to a stepwise development of fluconazole resistance in C. albicans

Each of the mechanisms described above can cause reduced susceptibility of *C. albicans* to fluconazole. Several studies have shown that multiple mechanisms may be combined to result in a stepwise development of fluconazole resistance, which ultimately becomes clinically relevant and causes therapy failure. For example, White [30] described gradual increases in fluconazole resistance in serial isolates of a *C. albicans* strain by overexpression of *MDR1*, *ERG11*, and one or more of the *CDR* genes, combined with the aquisition of the R467K mutation in *ERG11*. Sanglard et al. [22] found different combinations of *ERG11* mutations with overexpression of *MDR1*, *CDR1* or *CDR2*, in other series of *C. albicans* isolates, and Franz et al. [21] reported two series of clinical *C. albicans* isolates in which *MDR1* overexpression was combined with either the G464S mutation or *ERG11* overexpression. Combinations of different resistance mechanisms have recently been reported to be responsible for fluconazole resistance in the majority of clinical *C albicans* strains studied [24]. It is therefore evident that the generation of a highly resistant strain from a highly susceptible strain is the result of multiple mechanisms, each of which contributes only partially to the resistant phenotype. Whether a particular alteration creates a clinically resistant *C. albicans* strain therefore depends on the genetic background in which this alteration occured, i.e. if the strain already exhibited other mutations resulting in decreased susceptibility, even when the previous changes did not cause a clinically relevant resistance level. For example, some *ERG11* mutations which have been shown experimentally to cause fluconazole resistance have also been found in isolates with MICs in the susceptible range [24], and the overexpression of genes encoding efflux pumps is not necessarily sufficient to result in clinically relevant resistance.

4. The regulation and role of the *MDR1* gene in *C. albicans* fluconazole resistance

In the presence of fluconazole, *C albicans* induces expression of the *ERG11* gene above its normal level, presumably in response to ergosterol limitation [21,29]. In contrast, the genes encoding efflux pumps, *MDR1*, *CDR1* and *CDR2*, are not activated under same conditions [21,29]. However, in many fluconazole-resistant clinical *C. albicans* isolates, these genes are constitutively overexpressed, indicating that mutations must have occurred in these strains that abolish the normal regulation of the genes. Such mutations could either occur in the promoter region of the genes themselves or involve trans-regulatory factors. The comparison of the promoter sequences of both *MDR1* alleles of two matched pairs of clinical *C. albicans* isolates in which fluconazole resistance correlated with constitutitve *MDR1* expression did not reveal promoter mutations that might be responsible for *MDR1* activation in the resistant isolates [46]. Direct evidence for the involvement of an altered regulatory factor was obtained by integrating a green fluorescent protein (*GFP*) reporter gene under the control of

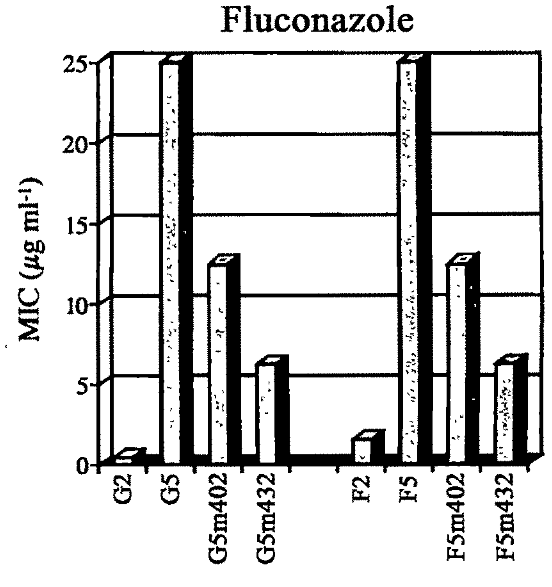

Fig. 2 Minimal inhibitory concentration of fluconazole for the fluconazole-susceptible *C albicans* isolates F2 and G2, the matched resistant isolates F5 and G5, and the heterozygous (F5M402 and G5M402) and homozygous (F5M432 and G5M432) *mdr1* mutants derived from the resistant isolates.

the *MDR1* promoter from a fluconazole-susceptible *C. albicans* strain at an ectopic site into the genome of the two matched pairs of clinical isolates. Although the *MDR1* promoter controlling *GFP* expression was identical in all four reporter strains, only the fluconazole-resistant isolates, but not the matched susceptible isolates, expressed the GFP [46]. Therefore, the activation of the *MDR1* gene in these fluconazole-resistant isolates must have been caused by mutations in regulatory factors, and this is likely to be true also for other fluconazole-resistant *C. albicans* isolates and other genes encoding efflux pumps. Several *C. albicans* genes encoding regulatory factors that influence the expression of efflux pumps have been identified, for example the *CAP1* gene, which is homologous to *YAP1* from *S. cerevisiae*, or the *FCR1*, *FCR2* and *FCR3* genes [47–49]. However, there is no evidence so far for these transcriptional regulators being the cause of the constitutive overexpression of efflux pumps in clinical *C. albicans* strains.

The involvement of regulatory factors in *MDR1* overexpression pointed to the possibility of a simultaneous activation of additional genes, including genes encoding yet unknown efflux pumps. Therefore, the activation of other genes than *MDR1* might be the cause of fluconazole resistance. In fact, *MDR1* disruption in *C. albicans* laboratory strains did not enhance the susceptibility of the mutants to fluconazole [36,37]. However, these strains did not detectably express the *MDR1* in vitro and, as noted above, fluconazole also does not induce *MDR1* expression in *C. albicans*. To assess the contribution of *MDR1* overexpression to fluconazole resistance, it was therefore necessary to inactivate the gene in fluconazole-resistant, clinical *C. albicans* isolates. Until recently, the gene disruption

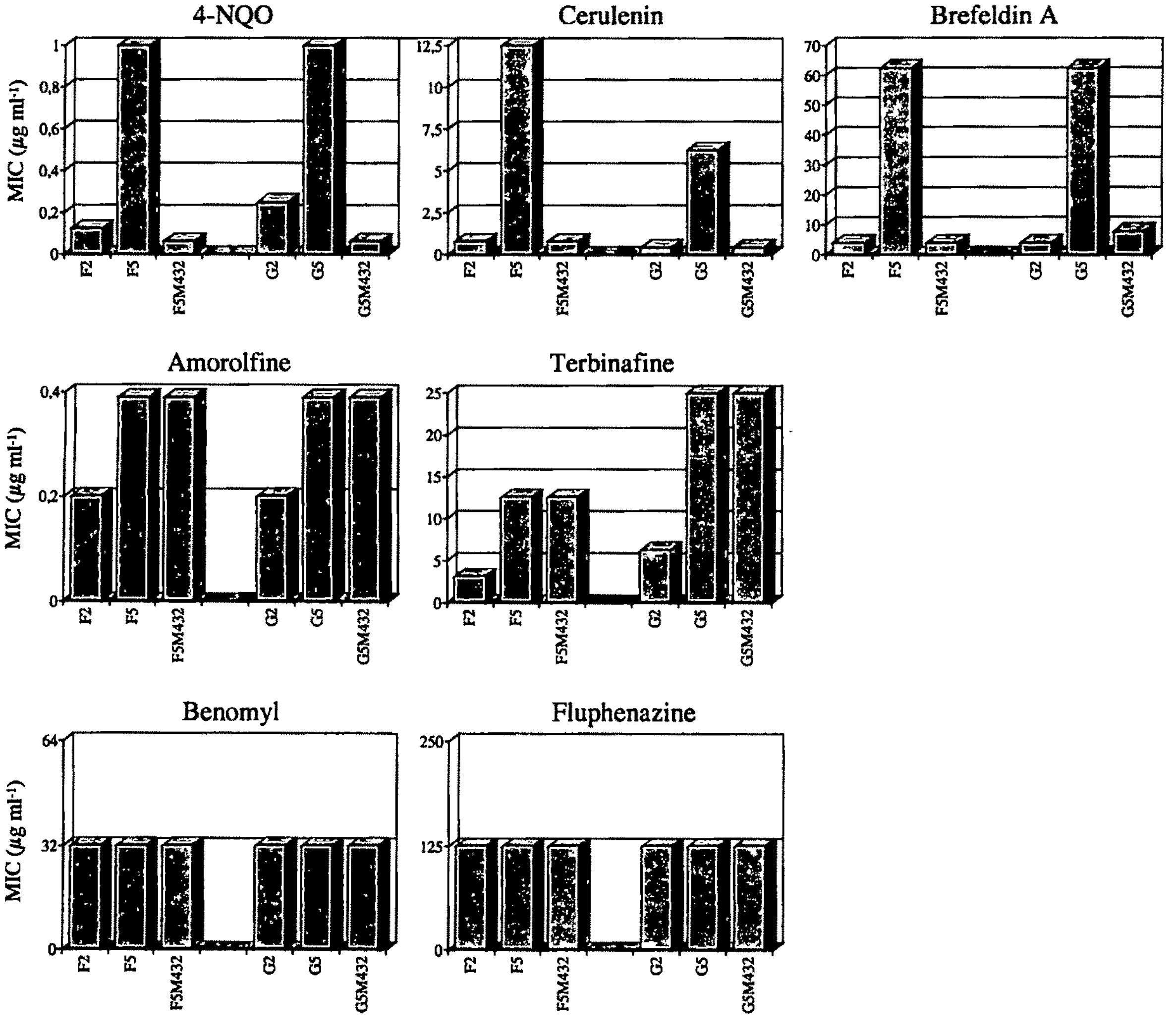

Fig. 3 Susceptibility of the matched fluconazole-susceptible and resistant clinical *C albicans* isolate pairs (F2/F5 and G2/G5) and the *mdr1* null mutants F5M432 and G5M432 derived from the resistant isolates F5 and G5, respectively, to other drugs The enhanced resistance of isolates F5 and G5, as compared with F2 and G2, to 4-NQO, cerulenin, and brefeldin A is due to *MDR1* overexpression, because it is abolished by deletion of the *MDR1* gene The slightly increased resistance of F5 and G5 to amorolfine and terbinafine was not affected by *MDR1* deletion, and therefore, must have been caused by other genomic alterations than *MDR1* overexpression The susceptibilities of the strains to fluphenazine and benomyl remained unchanged by either *MDR1* overexpression or deletion of the gene in the *MDR1* overexpressing isolates.

approach in *C. albicans* was confined to auxotrophic *ura3* mutants, but could not conveniently be performed in wild-type strains [50]. The development of a mutagenesis procedure that is based on the use of a recyclable, dominant selection marker allowed targeted gene inactivation also in clinical *C albicans* isolates [51]. Disruption of the *MDR1* gene in two different, *MDR1* overexpressing *C. albicans* isolates resulted in enhanced susceptibility of the mutants to fluconazole, providing direct genetic evidence that *MDR1* overexpression contributes to fluconazole resistance in clinical *C. albicans* isolates [51] (Fig. 2).

5. *MDR1* overexpression mediates multidrug resistance in *C. albicans*

The results of experiments in which *MDR1* overexpression in hypersusceptible *S. cerevisiae* strains conferred resistance to a variety of structurally unrelated drugs in addition to fluconazole suggested that Mdr1p transports many different toxic substances. Consequently, deletion of the *MDR1* gene in a *C. albicans* strain that expressed high *MDR1* mRNA levels resulted in an enhanced susceptibility of the mutant to several of these drugs [52]. Interestingly, however, *mdr1* deletion in this strain had no effect on the susceptibility to benomyl, a drug that was thought to be an Mdr1p substrate from the heterologous expression studies. This result was interpreted as *C. albicans* having other resistance mechanisms, presumably efflux systems that compensate for the loss of the *MDR1* gene. Clinical *C. albicans* isolates which overexpressed *MDR1* were also more resistant to other drugs in addition to fluconazole, e.g. 4-nitroquinoline-*N*-oxide (4-NQO), cerulenin, and brefeldin A, as compared with matched isolates that did not detectably express *MDR1* in vitro [53] (Fig. 3) The increased resistance was abolished when the *MDR1* gene was deleted from the genome of these isolates, providing genetic evidence that *MDR1* overexpression in clinical *C. albicans* isolates indeed confers resistance to various, structurally unrelated drugs [53]. However, *MDR1* overexpression in such clinical isolates did not enhance resistance to some other drugs that were thought to be Mdr1p substrates, e.g. amorolfine, terbinafine, fluphenazine and benomyl, and *MDR1* deletion did not influence the susceptibility of the strains to these drugs (Fig. 3). Even if *C. albicans* possesses other mechanisms of resistance to these toxic compounds one would expect that, if Mdr1p can transport these substances out of the cell, a strong overexpression of *MDR1* should further increase resistance, similar to its contribution to fluconazole resistance, which is often mediated by several additive mechanisms. These findings, together with the absence of an effect of *MDR1* deletion, suggests that heterologous expression studies may in some cases give misleading results about the substrate spectrum of the efflux pumps in *C. albicans*. The expression of *C. albicans* membrane proteins in *S cerevisiae* host strains may alter the structure of the cell membrane, especially in strains in which one or several of their own genes encoding membrane proteins were deleted, and these alterations might indirectly influence the susceptibility of the cells to toxic compounds. As mentioned above, such alterations in membrane structure have been observed after overexpression of the *CDR1* gene in *S cerevisiae* [44]. It should also be noted that no direct proof has yet been provided that the *C. albicans* efflux pumps bind and transport antifungal drugs. Whatever the mechanism is, there is now convincing evidence that the overexpression of *MDR1*, and also the *CDR1* and *CDR2* genes, contributes to the fluconazole-resistant phenotype of clinical *C. albicans* isolates.

6. Conclusions and perspectives

Considerable efforts have been undertaken in the past years to unravel the molecular mechanisms of fluconazole resistance in *C. albicans*, and this knowledge should help to devise strategies to overcome the resistance problem. Mutations resulting in reduced affinity of the target enzyme 14DM to fluconazole have been uncovered, but the precise way how the amino acid exchanges influence the binding of the drug can only be fully understood when more structural information on wild-type and mutated enzymes becomes available. This information may allow the design of drug derivatives whose binding is not affected by the resistance mutations.

The development of efflux pump inhibitors that could be used in combination with fluconazole is a promising strategy to abolish resistance of strains overexpressing these transporters [54]. Interestingly, *S. cerevisiae* transformants expressing *CDR1* from *C. albicans* exhibited increased sensitivity to peptidic antifungals and other drugs [34,55]. Although similar findings have not been reported for *CDR1* overexpressing *C albicans*, these observations suggest that the development of drug resistance may also create new vulnerable sites which may be exploited to preferentially attack fluconazole-resistant strains. The mutations responsible for overexpression of the genes encoding efflux pumps in fluconazole-resistant clinical *C albicans* isolates are still unknown, but presumably involve alterations in regulatory proteins [46]. The elucidation of the regulatory pathways controlling expression of these genes may provide a rationale basis for approaches to interfere with their activation and thus overcome resistance.

Mutations resulting in drug resistance provide a selective advantage in the presence of the drug. However, some of the described alterations might reduce the fitness of the resistant strains under non-selective conditions, for example *ERG11* mutations that also lower 14DM activity [26,27] or the unregulated expression of genes encoding efflux pumps, which is tightly controlled in the parental strains [46]. Some fluconazole-resistant isolates in fact exhibit reduced virulence, but virulence may also remain unaltered or even be increased [56,57]. Fluconazole-resistant strains can loose the resistant phenotype during propagation in drug-free medium, arguing for a selective disadvantage of some resistance mutations [42]. On the other hand, it was recently also demonstrated that the costs of resistance can be overcome during further evolution of in vitro generated fluconazole-resistant *C. albicans* strains [58]. It will be interesting to test whether clinical *C. albicans* having different resistance mutations may display a reduced fitness as compared with their drug-sensitive parents within the complex environment of the host. Adequate treatment strategies might reduce the frequency of resistant strains [59]. An important research area also is the intrinsic resistance of *C. albicans* to fluconazole when the organism grows as a biofilm [60–62]. The basis of biofilm resistance, which seems to be independent of the expression of efflux pumps [63], and its implications for the treatment of *Candida* infections remain to be elucidated.

Acknowledgements

The author's work is supported by grants from the Deutsche Forschungsgemeinschaft (DFG grants MO846/2 and MO846/3).

References

[1] S.L Kelly, A. Arnoldi, D.E Kelly, Biochem Soc Trans. 21 (1993) 1034–1038

[2] J H Rex, M G Rinaldi, M.A. Pfaller, Antimicrob. Agents Chemother. 39 (1995) 1–8.

[3] M. Ruhnke, A Eigler, I. Tennagen, B Geiseler, E. Engelmann, M Trautmann, J Clin. Microbiol 32 (1994) 2092–2098

[4] T C. White, K A. Marr, R.A. Bowden, Clin. Microbiol. Rev. 11 (1998) 382–402

[5] S R Lockhart, J J. Fritch, A.A. Meier, K Schröppel, T Srikantha, R Galask, D.R. Soll, J. Clin. Microbiol. 33 (1995) 1501–1509

[6] A. Schoofs, F C. Odds, R. Colebunders, M. Ieven, L. Wouters, H. Goossens, Antimicrob. Agents Chemother. 41 (1997) 1625–1635

[7] F. Barchiesi, D Arzeni, M S Del Prete, A. Sinicco, L Falconi Di Francesco, M.B Pasticci, L Lamura, M M. Nuzzo, F Burzacchini, S Coppola, F Chiodo, G Scalise, J Antimicrob Chemother 41 (1998) 541–548.

[8] J.L. Lopez-Ribot, R.K McAtee, S. Perea, W.R. Kirkpatrick, M G Rinaldi, T F Patterson, Antimicrob Agents Chemother. 43 (1999) 1621–1630.

[9] K Schröppel, M. Rotman, R. Galask, K Mac, D R. Soll, J Clin. Microbiol 32 (1994) 2646–2654

[10] L Millon, A. Manteaux, G Reboux, C Drobacheff, M Monod, T. Barale, Y Michel-Briand, J Clin. Microbiol 32 (1994) 1115–1118.

[11] R. Franz, M. Ruhnke, J Morschhauser, Mycoses 42 (1999) 453–458.

[12] S L. Kelly, D.C Lamb, D.E. Kelly, N.J Manning, J Loeffler, H Hebart, U. Schumacher, H. Einsele, FEBS Lett. 400 (1997) 80–82.

[13] S.L. Kelly, D.C. Lamb, D E. Kelly, J. Löffler, H Einsele, Lancet 348 (1996) 1523–1524

[14] F S. Nolte, T Parkinson, D J. Falconer, S Dix, J Williams, C. Gilmore, R Geller, J R Wingard, Antimicrob Agents Chemother. 41 (1997) 196–199.

[15] T. Miyazaki, Y Miyazaki, H Kakeya, H Miyazaki, K. Nakamura, S Kohno, Abstracts to the 41st Interscience Conference on Antimicrobial Agents and Chemotherapy, Abstract J-1840. Chicago, IL (2001)

[16] J. Loffler, S.L Kelly, H. Hebart, U. Schumacher, C. Lass-Florl, H. Einsele, FEMS Microbiol. Lett. 151 (1997) 263–268

[17] K Asai, N Tsuchimori, K. Okonogi, J.R. Perfect, O. Gotoh, Y Yoshida, Antimicrob. Agents Chemother. 43 (1999) 1163–1169

[18] P. Marichal, L Koymans, S. Willemsens, D. Bellens, P Verhasselt, W Luyten, M. Borgers, F C Ramaekers, F C. Odds, H.V. Bossche, Microbiology 145 (1999) 2701–2713

[19] B Favre, M Didmon, N.S Ryder, Microbiology 145 (1999) 2715–2725.

[20] T C. White, Antimicrob. Agents Chemother 41 (1997) 1488–1494.

[21] R. Franz, S L. Kelly, D C. Lamb, D E Kelly, M Ruhnke, J. Morschhauser, Antimicrob. Agents Chemother 42 (1998) 3065–3072.

[22] D Sanglard, F Ischer, L Koymans, J Bille, Antimicrob. Agents Chemother. 42 (1998) 241–253.

[23] H Kakeya, Y. Miyazaki, H. Miyazaki, K. Nyswaner, B. Grimberg, J.E. Bennett, Antimicrob Agents Chemother 44 (2000) 2985–2990.

[24] S. Perea, J.L. Lopez-Ribot, W.R. Kirkpatrick, R.K. McAtee, R.A. Santillan, M Martinez, D Calabrese, D. Sanglard, T F. Patterson, Antimicrob Agents Chemother 45 (2001) 2676–2684

[25] S L. Kelly, D C. Lamb, D.E. Kelly, FEMS Microbiol Lett. 180 (1999) 171–175.

[26] S.L Kelly, D.C. Lamb, J Loeffler, H. Einsele, D E. Kelly, Biochem Biophys Res. Commun 262 (1999) 174–179

[27] D C. Lamb, D.E. Kelly, T C. White, S L. Kelly, Antimicrob. Agents Chemother 44 (2000) 63–67.

[28] D.C Lamb, D E. Kelly, W.H. Schunck, A Z Shyadehi, M. Akhtar, D.J. Lowe, B C Baldwin, S L Kelly, J. Biol Chem. 272 (1997) 5682–5688.

[29] G.D. Albertson, M. Niimi, R.D. Cannon, H F. Jenkinson, Antimicrob. Agents Chemother. 40 (1996) 2835–2841

[30] T C White, Antimicrob Agents Chemother 41 (1997) 1482–1487

[31] H Nakayama, N. Nakayama, M Arisawa, Y. Aoki, Antimicrob. Agents Chemother 45 (2001) 3037–3045

[32] M E Fling, J. Kopf, A Tamarkin, J A Gorman, H.A. Smith, Y Koltin, Mol. Gen Genet 227 (1991) 318–329

[33] R. Ben-Yaacov, S. Knoller, G.A Caldwell, J M. Becker, Y Koltin, Antimicrob. Agents Chemother 38 (1994) 648–652

[34] R. Prasad, P De Wergifosse, A. Goffeau, E. Balzi, Curr Genet. 27 (1995) 320–329

[35] D. Sanglard, K Kuchler, F Ischer, J L Pagani, M. Monod, J Bille, Antimicrob. Agents Chemother. 39 (1995) 2378–2386.

[36] D Sanglard, F. Ischer, M Monod, J Bille, Antimicrob. Agents Chemother 40 (1996) 2300–2305.

[37] J Morschhäuser, S. Michel, P. Staib, Mol. Microbiol 32 (1999) 547–556

[38] D. Sanglard, F. Ischer, M. Monod, J Bille, Microbiology 143 (1997) 405–416

[39] I Balan, A M Alarco, M. Raymond, J. Bacteriol. 179 (1997) 7210–7218

[40] R. Franz, S. Michel, J Morschhauser, Gene 220 (1998) 91–98

[41] D. Calabrese, J. Bille, D Sanglard, Microbiology 146 (2000) 2743–2754

[42] K.A Marr, C.N. Lyons, K Ha, T.R Rustad, T.C. White, Antimicrob. Agents Chemother. 45 (2001) 52–59

[43] J.L. Lopez-Ribot, R.K McAtee, L.N. Lee, W R. Kirkpatrick, T C White, D. Sanglard, T F Patterson, Antimicrob. Agents Chemother 42 (1998) 2932–2937.

[44] S Dogra, S. Krishnamurthy, V Gupta, B L Dixit, C M. Gupta, D Sanglard, R. Prasad, Yeast 15 (1999) 111–121.

[45] C.A. Hitchcock, K.J. Barrett-Bee, N.J. Russell, J. Gen Microbiol. 132 (1986) 2421–2431.

[46] S. Wirsching, S. Michel, G Köhler, J. Morschhauser, J Bacteriol 182 (2000) 400–404

[47] A M Alarco, I Balan, D. Talibi, N Mainville, M Raymond, J Biol. Chem. 272 (1997) 19304–19313.

[48] A.M. Alarco, M Raymond, J. Bacteriol 181 (1999) 700–708

[49] D Talibi, M Raymond, J Bacteriol 181 (1999) 231–240

[50] W A Fonzi, M Y. Irwin, Genetics 134 (1993) 717–728

[51] S Wirsching, S. Michel, J Morschhäuser, Mol. Microbiol. 36 (2000) 856–865

[52] M Goldway, D. Teff, R Schmidt, A.B Oppenheim, Y. Koltin, Antimicrob Agents Chemother 39 (1995) 422–426.

[53] S Wirsching, G P Moran, D J. Sullivan, D.C Coleman, J Morschhäuser, Antimicrob Agents Chemother. 45 (2001) 3416–3421

[54] M D Lee, J L. Galazzo, A L Staley, J C. Lee, M.S Warren, H Fuernkranz, S Chamberland, O. Lomovskaya, G H Miller, Farmaco 56 (2001) 81–85.

[55] S Milewski, F Mignini, R Prasad, E Borowski, Antimicrob Agents Chemother 45 (2001) 223–228

[56] J R Graybill, E. Montalbo, W.R Kirkpatrick, M F. Luther, S G Revankar, T F Patterson, Antimicrob Agents Chemother 42 (1998) 2938–2942.

[57] K Fekete-Forgacs, L Gyure, B Lenkey, Mycoses 43 (2000) 273–279.

[58] L.E Cowen, L.M. Kohn, J.B Anderson, J Bacteriol. 183 (2001) 2971–2978.

[59] J. Lopez, C. Pernot, S Aho, D. Caillot, O Vagner, F Dalle, M.J Durnet-Archeray, P Chavanet, A. Bonnin, J. Hosp Infect 48 (2001) 122–128

[60] S P. Hawser, L J Douglas, Antimicrob. Agents Chemother 39 (1995) 2128–2131.

[61] G. Ramage, K Vande Walle, B.L. Wickes, J.L. Lopez-Ribot, Antimicrob. Agents Chemother 45 (2001) 2475–2479

[62] J Chandra, D M. Kuhn, P.K Mukherjee, L L Hoyer, T. McCormick, M A. Ghannoum, J Bacteriol 183 (2001) 5385–5394

[63] S.P Bachmann, T F Patterson, B L Wickes, J L Lopez-Ribot, Abstracts to the 41st Interscience Conference on Antimicrobial Agents and Chemotherapy, Abstract J-119, p. 362 Chicago, IL (2001).

[64] B A Lasker, L S. Page, T J Lott, G.S Kobayashi, Gene 116 (1992) 51–57

ELSEVIER

Biochimica et Biophysica Acta 1587 (2002) 249–257

BIOCHIMICA ET BIOPHYSICA ACTA
BBA
www.bba-direct.com

Review

Inhibitors of dihydrofolate reductase in leishmania and trypanosomes

Ian H. Gilbert*

Welsh School of Pharmacy, Cardiff University, Redwood Building, King Edward VII Avenue, Cardiff, CF10 3XF, UK

Received 24 January 2002, accepted 24 January 2002

Abstract

The protozoan diseases leishmaniasis, Chagas' disease and African trypanosomiasis are major health problems in many countries, particularly developing countries, and there are few drugs available to treat these diseases. Dihydrofolate reductase (DHFR) inhibitors have been used successfully in the treatment of a number of other diseases such as cancer, malaria and bacterial infections; however they have not been used for the treatment of these diseases. This article summarises studies on leishmanial and trypanosomal DHFR inhibitor development and evaluation. Possible mechanisms of resistance to DHFR inhibitors are also discussed. © 2002 Elsevier Science B.V. All rights reserved.

Keywords Dihydrofolate reductase; *Trypanosoma cruzi*, *Trypanosoma brucei*; *Leishmania*

1. Introduction

Leishmaniasis, African trypanosomiasis (sleeping sickness) and Chagas' disease are major causes of mortality and cause much economic hardship, particularly in the developing world. The World Health Organisation estimates that millions of people are infected, or are at risk, from these diseases [1]. In addition, leishmaniasis is increasingly a complication with AIDS patients. Unfortunately, there are few drugs available to treat these diseases and most of these suffer from poor clinical efficacy, unwanted effects, and require parenteral administration, which is not appropriate in rural areas. The situation is made more serious by reports of treatment failures of the existing drugs, for example, melarsoprol for the treatment of African trypanosomiasis.

Dihydrofolate reductase (DHFR) is a key enzyme in folate metabolism and, therefore, in the production of thymidine [2,3]. Its role in thymidine biosynthesis is the reduction of dihydrofolate to tetrahydrofolate using the cofactor NADPH (Fig. 1). Following this reduction, tetrahydrofolate is methenylated to form methylene-tetrahydrofolate, which then methylates deoxyuridine monophosphate (dUMP) to give TMP in a reaction catalysed by thymidylate synthase (TS) (Fig. 1). During this reaction, methylene-tetrahydrofolate is converted back to dihydrofolate, completing the cycle. Therefore, inhibition of DHFR prevents biosynthesis of thymidine, and as a consequence, DNA biosynthesis. In addition, inhibition of DHFR probably leads to a buildup in levels of dUMP and hence to a biosynthetic precursor, deoxyuridine triphosphate [4]. High levels of deoxyuridine triphosphate lead to incorporation of uracil into DNA to levels beyond which the DNA repair enzymes (uracil-DNA-glycosylase) can cope, leading to cell death.

2. Background to the diseases

The parasites that cause leishmaniasis, African trypanosomiasis and Chagas' disease are protozoan parasites of the order kinetoplastida [5,6]. They are all transmitted to the human host by various vectors (see below) and have complex life cycles; each stage of which has different morphologies and different metabolic properties. The parasites are phylogenetically related and share many similarities, but there are also significant differences between them.

Leishmaniasis is caused by various species and subspecies of *Leishmania*, of which the most important include subspecies of *Leishmania donovani*, *Leishmania tropica*, *Leishmania mexicana* and *Leishmania braziliensis*. These cause a variety of diseases in humans. The diseases found

---

Abbreviations DHFR, dihydrofolate reductase, DHFR-TS, dihydrofolate reductase-thymidylate synthase; dUMP, deoxyuridine monophosphate, EC_{50}, the effective concentration of a compound to produce a therapeutic effect in 50% of the sample, IC_{50}, the concentration of compound which gives 50% inhibition of an enzyme, QSAR, quantitative structure activity relationship; TMP, thymidine monophosphate; TD_{50}, the effective concentration of a compound to kill 50% of the host cells, TS, thymidylate synthase

* Tel.: +44-29-2087-5800, fax: +44-29-2087-4149

E-mail address gilbertih@cf.ac.uk (I.H. Gilbert).

0925-4439/02/$ - see front matter © 2002 Elsevier Science B.V All rights reserved
PII: S0925-4439(02)00088-1

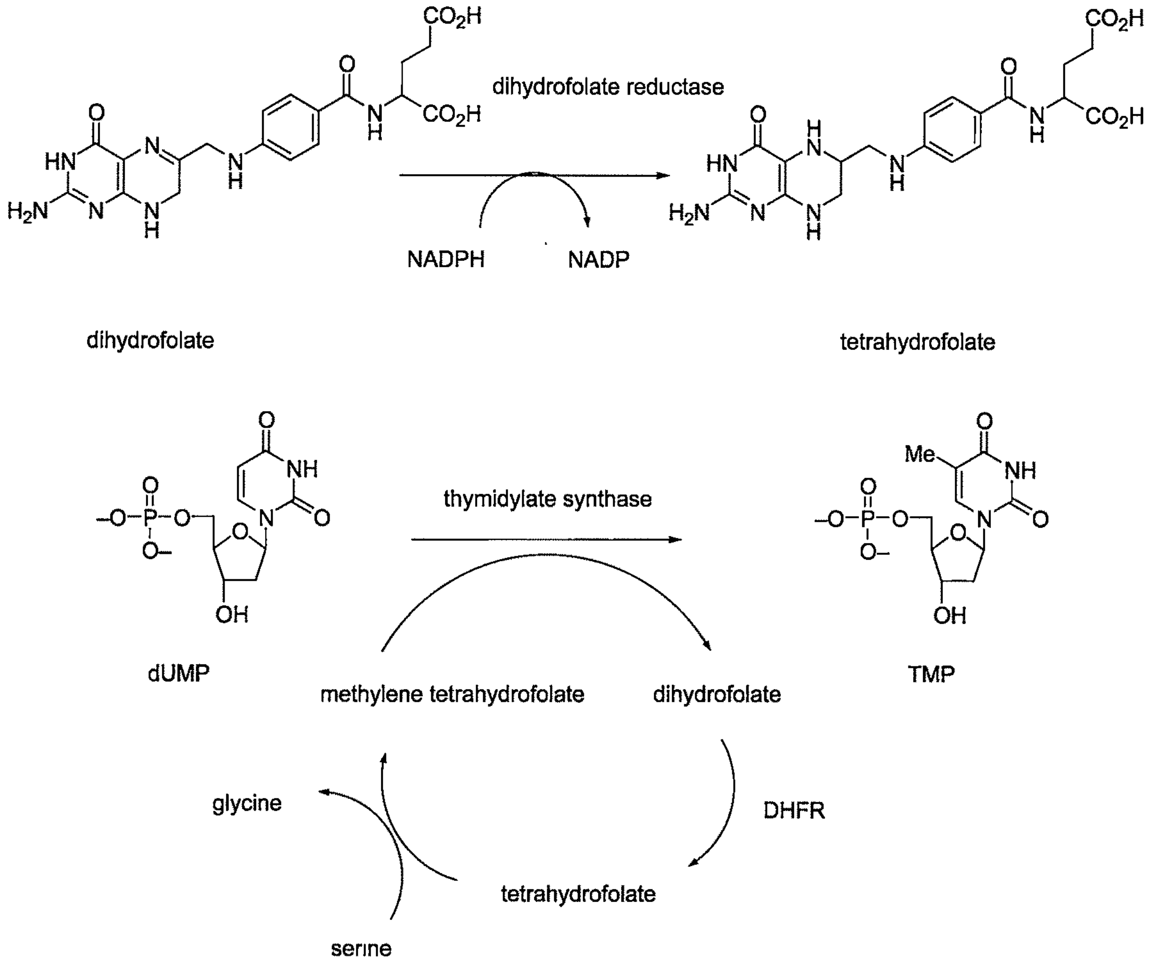

Fig 1. The reaction carried out by DHFR the reduction of dihydrofolate to tetrahydrofolate (shown in the box); and the role of this reaction in the folate-mediated production of TMP from dUMP

are: cutaneous leishmaniasis, which can vary from small self-healing skin lesions to a more widespread and disfiguring condition; mucocutaneous leishmaniasis, which leads to highly disfiguring lesions of the mouth, nose and throat; and visceral leishmaniasis, which is a systemic infection that is usually fatal if not treated, with the parasites multiplying within macrophages, giving rise to damage of the liver, spleen, bone marrow and lymph nodes. The parasite is found in the vector stage (the sandfly) as the promastigote and in the human host as an amastigote in acidic phagolysomes within macrophages.

African trypanosomiasis in humans is caused by two subspecies of *Trypanosoma brucei*: *T. b. rhodesiense* and *T. b. gambiense*. The parasites live in the bloodstream and invade the central nervous system giving rise to the neurological symptoms of African trypanosomiasis and eventually to death unless the disease is treated. The human form of the life cycle is the trypomastigote and the vector stage (tsetse fly) is the epimastigote.

Chagas' disease is caused by the parasite *Trypanosoma cruzi*. The parasite is found in the vector (reduviid bug) as an epimastigote and in the human host as an intracellular amastigote. The disease causes a chronic infection in humans, with particular effects on the heart, colon, oesophagus and peripheral nervous system. There is a high death rate amongst children.

3. The parasite enzyme

3.1. Characterisation

DHFR has been cloned and over-expressed from *Leishmania major*, [7,8] *T. cruzi* [9] and *T. brucei* [10]. These enzymes show high sequence identity, especially the *T. brucei* and *T cruzi* enzymes (Table 1). The enzyme is actually a bi-functional dimeric enzyme linked to TS (Fig. 2). This is a common occurrence amongst protozoa, in contrast to the situation in mammalian and bacterial cells where the enzyme is a monomer [11]. Gene knockout experiments have shown the enzyme to be essential in *Leishmania*, at least in the promastigote stage of the life cycle [12].

Table 1
Sequence alignment (percentage identity) of DHFR from different organisms

	L major	*T cruzi*	*T brucei*	*E coli*
Human	26	27	26	27
L major		50	46	24
T cruzi			58	26
T. brucei				23

Modified from Ref. [14] with permission

3.2. Structural data

The enzyme from *L. major* has been crystallised by Knighton et al. [13] and homology models have been produced of the *T. brucei* and *T. cruzi* enzymes [14]. Detailed analysis [14] and comparison of the structures of the *L. major*, human and bacterial enzymes, and the homology models of the *T. brucei* and *T. cruzi* enzymes, suggests the following:

- The *L. major*, *T. brucei* and *T. cruzi* enzymes show high structural similarity.
- The three protozoan enzymes show structural differences from the human and bacterial enzymes.
- The three-dimensional shapes of the parasite enzyme folate binding sites are slightly different to the corresponding human active sites. Points of particular difference are: a slightly larger binding pocket in the region where the benzamide moiety of the substrate binds in the case of the trypanosomal and leishmanial enzymes; and a small tunnel under the pteridine ring in the case of the trypanosomal enzymes.
- Differences in residues in the active sites (Table 2, Fig. 3).

It may be possible to exploit these differences between the parasite and human enzymes to design selective inhibitors.

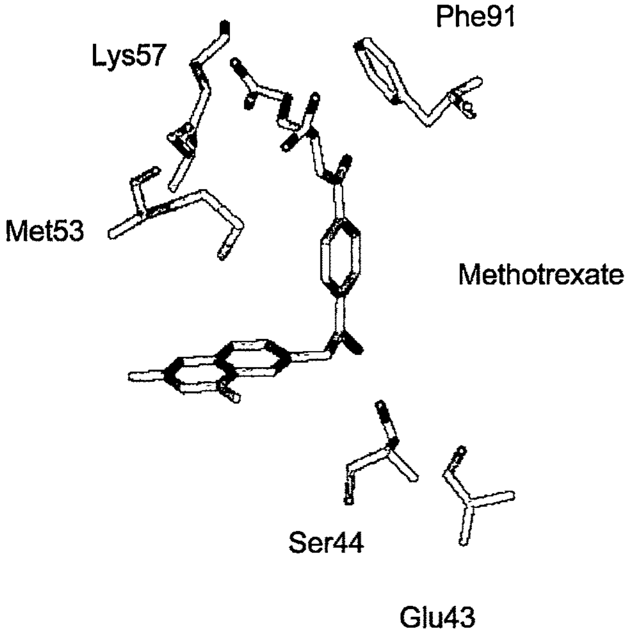

Fig 3 Part of the active site of the *L major* DHFR. This figure shows the location of methotrexate and those residues in the active site of *L. major* DHFR which are not homologous to the corresponding residues in human DHFR (Glu43, Ser44, Met53, Lys57, Phe91)

Knighton et al. [13] studied the crystal structure of the bifunctional DHFR-TS enzyme and concluded that there is substrate channelling between the DHFR and TS domains of the enzyme, by a positively charged electrostatic channel on the protein surface, which interacts with the negatively charged substrate. Liang and Anderson [15] have done detailed kinetic analysis, which supports this model and, in addition, they suggest that there may be interaction between the DHFR and TS domains.

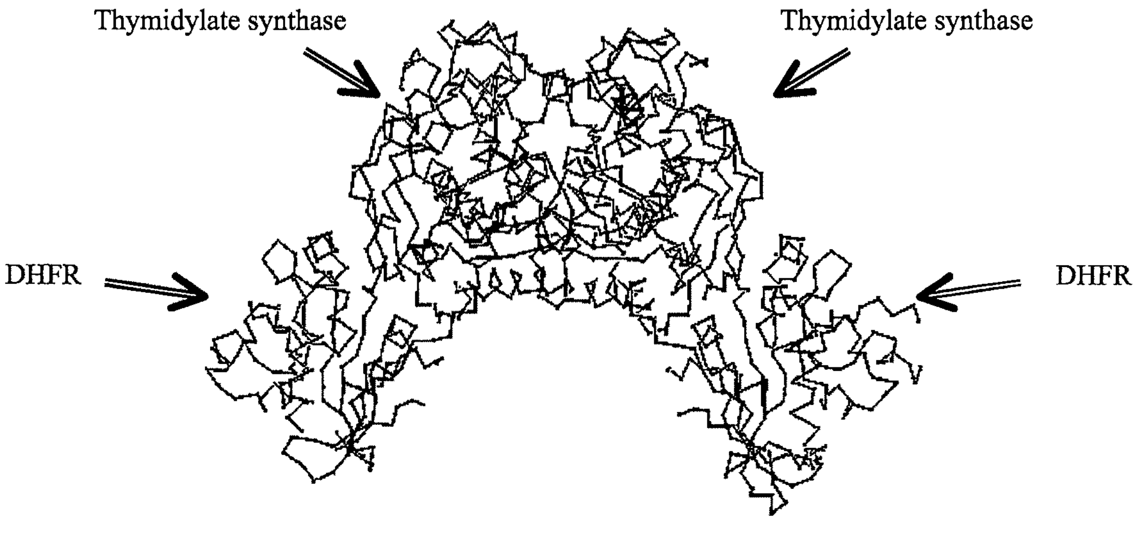

Fig. 2. A representation of the crystal structure of *L. major* DHFR-TS prepared by Web-lab Viewer The enzyme is a symmetrical dimer of TS and DHFR.

4. Inhibitors of parasite DHFR

4.1. *Trimethoprim, cycloguanil, pyrimethamine and methotrexate: known DHFR inhibitors*

Classical anti-microbial DHFR inhibitors, such as pyrimethamine and trimethoprim (Fig. 4) are, in general, not very selective for the analogous leishmanial and trypanosomal enzymes. Thus, trimethoprim ($K_i = 0.12$ μM), pyrimethamine ($K_i = 0.25$ μM) and cycloguanil ($K_i = 5.8$ μM) are only weakly active against *L. major* DHFR. Pyrimethamine is weakly selective for the human, relative to the parasite enzyme (1- to 2-fold). Trimethoprim has been reported as weakly selective for either the *L. major* or human enzyme. There is weak inhibition and selectivity of trimethoprim ($K_i = 1$ μM, selectivity 1- to 30-fold) and pyrimethamine ($K_i = 0.1$ μM, no selectivity) for the *T. cruzi* enzyme. In the case of *T. brucei*, trimethoprim ($K_i = 0.01$ μM, selectivity 134- to 600-fold) and pyrimethamine ($K_i = 0.01$ μM, selectivity 10-fold) were more selective for the parasite enzyme [10,16–18].

Trimethoprim, pyrimethamine and cycloguanil are weakly active against *L major* promastigotes ($EC_{50} = 175$, 32, >500 μM, respectively) and *L. donovani* amastigotes ($EC_{50} = 160$, 34, >100 μM, respectively) [16,19]. In rodent models of leishmaniasis, Peters et al. [20] reported that activity was species-specific; trimethoprim exhibited some activity against infection by *L. major*, cycloguanil had some activity against infection by *Leishmania infantum*, while pyrimethamine exhibited poor activity.

Methotrexate, a potent inhibitor of DHFR, is 8-fold selective for the *L. major* DHFR, and also showed activity against *L. major* promastigotes ($EC_{50} = 0.3$ μM) [12]. Scott et al. [21] investigated the activity of methotrexate against promastigotes from various species of *Leishmania* (*L. major*, *L. donovani*, *L. m mexicana*) and found *L. major* most susceptible. Methotrexate has been reported as a potent inhibitor of the *T. cruzi* enzyme ($K_i = 0.038$ nM), but it is poorly active against the amastigotes ($EC_{50} = 9.2$ μM) [18,22].

4.2. *Novel DHFR inhibitors*

Relatively little has been reported on the development of specific inhibitors of leishmanial and trypanosome DHFR.

Coombs' group [21,23] investigated some 5-substituted 2,4-diaminopyrimidines that were good inhibitors of *L. m. mexicana* DHFR in crude extracts of the enzyme ($IC_{50} = 0.2–2$ μM) and showed activity against the promastigotes ($EC_{50} = 12–24$ μM) (Fig. 5). One of the compounds was studied further in amastigotes, where it showed some activity at concentrations below that at which it killed the host macrophages. However, in a mouse study, the compound was too toxic to warrant further study.

Quantitative structure activity relationship (QSAR) analysis was carried out on the inhibition of *L. major* [24] and human [25] DHFR for a series of triazines of the general structures shown in Fig. 6(a),(b). Compounds with lipophilic substituents (X) showed greater activity than compounds with polar substituents. However, few compounds

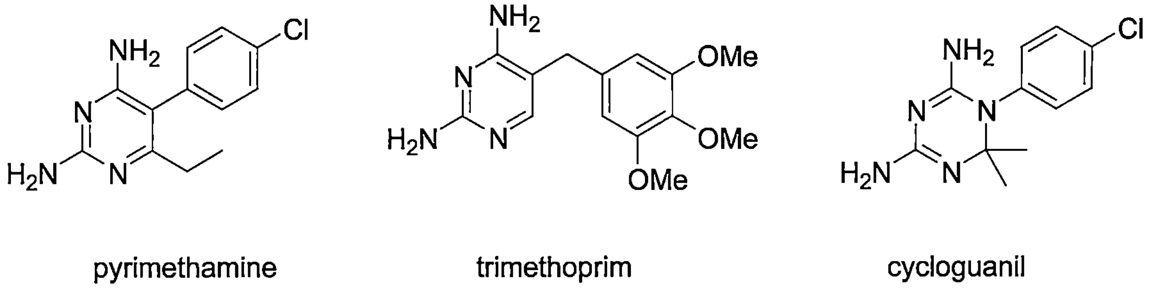

pyrimethamine trimethoprim cycloguanil

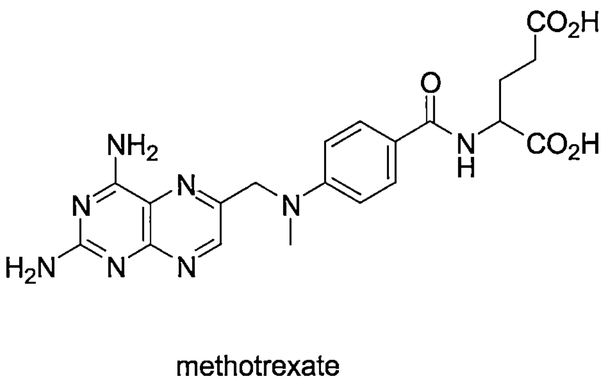

methotrexate

Fig 4 Some clinically used DHFR inhibitors pyrimethamine and cycloguanil as anti-malarials, trimethoprim as anti-bacterial; and methotrexate as anti-cancer

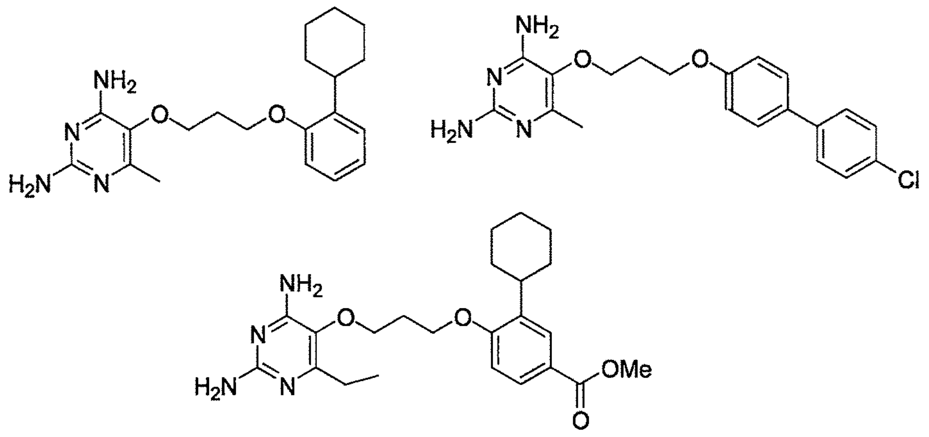

Fig 5. A series of 2,4-diaminopyrimidines showing activity against *Leishmania* DHFR [21,23]

showed selectivity for the *Leishmania* enzyme over the human enzyme, notable exceptions being when X = nonyl, dodecyl and CH_2O-1-napthyl. Some of the compounds were assayed for activity against *L. major* promastigotes and showed activities varying from 1 to 500 μM.

Sirawarapom et al. [16] studied a series of substituted 5-benzyl-2,4-diaminopyrimidines, some of which showed selectivity for the *L. major* DHFR in enzyme assays and moderate activity against *L. major* promastigotes and *L. donovani* amastigotes. The most active and selective compound in the enzyme assay experiments was the 8-octyloxy derivative ($n = 8$, Fig. 6(c)), with a selectivity of 130-fold for the *L. major* DHFR and EC_{50} against *L. major* promastigotes of 5.6 μM and *L. donovani* amastigotes of 4.6 μM.

A detailed structure-activity study on these alkyl-substituted 5-benzyl-2,4-diaminopyrimidines (Fig. 6(c)) was undertaken by Chowdhury et al. [17]. They varied the length of the substituent chain from hydrogen to decyl ($n = 0$ to $n = 10$) and also extended the study to include both *T. cruzi* and *T. brucei*. Optimum activity and selectivity against *L. major*, *T. cruzi* and *T. brucei* DHFR was found for compounds with a chain length of 2–6 carbon atoms. The maximum selectivities of these compounds, compared to the human enzyme, were 20-, 5- and 250-fold, respectively, and inhibition constants were 0.13, 0.22 and 0.01 μM, respectively. These compounds were modelled in the active sites of the *L. major* and human enzymes. In the *L. major* enzyme, the alkyl chain of the substituent appears to interact with a phenylalanine residue in the enzyme active site. This interaction appears to be optimal for a chain length of 4–6 carbon atoms. As the alkyl chain length increases further, the alkyl substituent appears to move away from the Phe residue, decreasing the interaction and offering a possible explanation for the optimal activity. This model can also explain the selectivity of the compounds. In the human enzyme, the phenylalanine is replaced by asparagine (Table 2) [14], which does not interact with the alkyl chain.

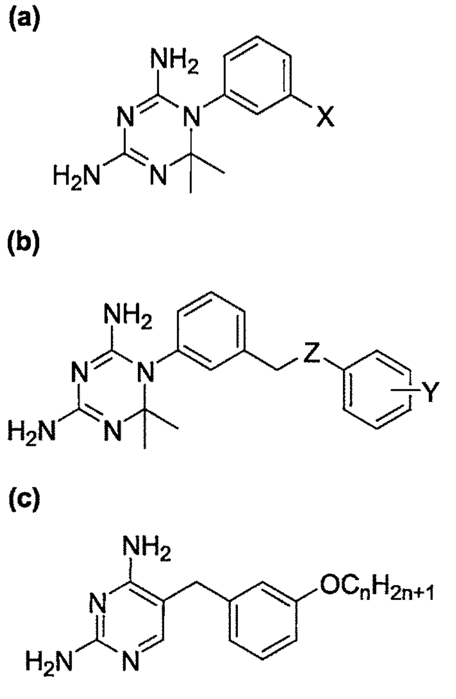

Fig. 6. Compounds (a) and (b) are the basic structures used for QSAR analysis by Booth et al. [24] and Hathaway et al. [25] Compound (c) is the basic structure studied by Sirawarapom et al [16] and Chowdhury et al. [17]

Table 2

Differences in residues in the folate binding sites of human and trypanosomal and leishmanial DHFR

Human Residue	*L major* residue	*T cruzi* residue	*T brucei* residue	Interaction with folate
Gly20	Glu43	Arg39	Gly45	pteridine/NADPH
Asp21	Ser44	Ser40	Thr46	pteridine/NADPH
Phe31	Met53	Met49	Met55	pteridine/benzamidine/ glutamate
Gln35	Lys57	Arg53	Arg59	glutamate
Asn64	Phe91	Phe88	Phe94	glutamate

The portion of the substrate with which residues interact is indicated as pteridine, benzamidine, and glutamate Modified from Ref. [14] with permission.

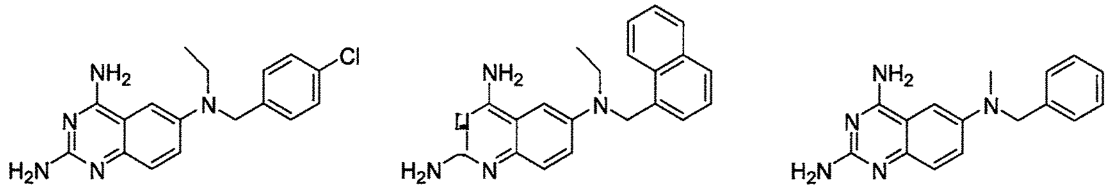

DHFR: 45% inhibition at 0.23μM
EC_{50} (amastigotes): 0.04nM
TD_{50}: 15.2μM

DHFR: 41% inhibition at 0.22μM
EC_{50} (amastigotes): 0.26nM
TD_{50}: 3.6μM

DHFR: 48% inhibition at 0.27μM
EC_{50} (amastigotes): 25nM
TD_{50}: 17.9μM

Fig 7. Examples of 2,4-diaminoquinazolines tested by Berman et al. [26] The activities against the enzyme, *L major* amastigotes cultured in macrophages and cellular toxicity values (against macrophages) are given for the most active compounds

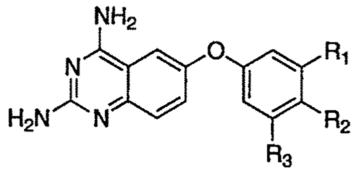

R_1	R_2	R_3	
R_1 = H	R_2 = Cl	R_3 = H	15 fold selectivity, EC_{50} (promastigotes) 0.5μM
R_1 = Cl	R_2 = Cl	R_3 = H	9 fold selectivity, EC_{50} (promastigotes) 0.4μM
R_1 = Cl	R_2 = H	R_3 = Cl	7 fold selectivity, EC_{50} (promastigotes) 0.2μM

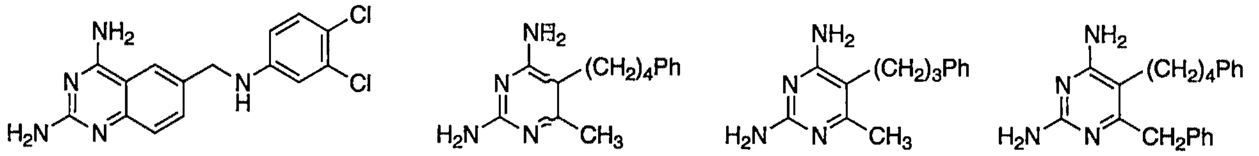

1.6-fold selectivity
EC_{50} (promast.) 0.6μM

0.7-fold selectivity
EC_{50} (promast.) 0.2μM

1.7-fold selectivity
EC_{50} (promast.) 0.5μM

41-fold selectivity
EC_{50} (promast.) 0.3μM

Fig. 8. Quinazolines and 2,4-diamino-pyrimidines showing activity against *L. major* DHFR [12]

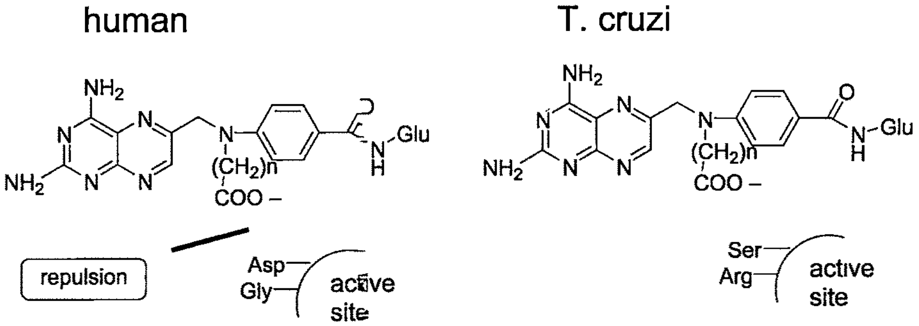

Fig 9 Differences in the active site between the human and *T cruzi* enzymes used by Zuccotto et al. [22] to design novel inhibitors

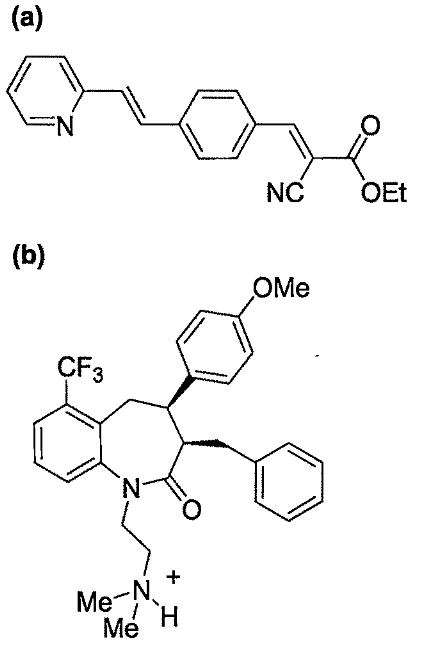

Fig. 10. Examples of novel inhibitors of *L major* (a) and *T cruzi* (b) DHFR identified by database mining using DOCK 3.5 [30,31]

These substituted 5-benzyl-2,4-diaminopyrimidines showed in vitro activity against *T. cruzi* amastigotes and *T. brucei* trypomastigotes, with the best activity being found for chain lengths of 6–10 carbon atoms (Fig. 6(c)). The most active compounds gave 100% inhibition of growth of *T. cruzi* amastigotes at 3 μM and an EC_{50} of 1 μM against *T brucei* trypomastigotes. The chain length for optimum activity against the intact parasites (6–10 carbon atoms) does not correspond to that for optimum activity against the enzyme (2–6 carbon atoms). This suggests that inhibition of DHFR is not the only factor for activity against the parasite. The compounds were generally inactive against *L. infantum* amastigotes. In rodent models of African trypanosomiasis, several of the 5-benzyl-2,4-diaminopyrimidines showed a marginal effect, while against a rodent model of Chagas' disease, the compounds were inactive.

Some 2,4-diaminoquinazolines investigated by Berman et al. [26] showed reasonable inhibition of DHFR isolated from *L. mexicana* promastigotes (Fig. 7). The compounds also showed very potent activity against *L. major* amastigotes cultured in human macrophages (ED_{50} = 0.04–25 nM), and a large therapeutic index compared to uninfected macrophages. However, there was little correlation between inhibition of DHFR and activity against the *L. major* amastigotes, suggesting an alternate mode(s) of action, other than or in addition to inhibition of DHFR, may be operating with these compounds. In the case of *T. cruzi*, some 2,4-diaminoquinazolines showed good activity against the amastigote form [27,28] and were able to prolong the life of infected mice, but not to give a radical cure [29].

Hardy et al. [12] screened a set of pteridines, quinazolines and pyrimidines against *L. major* and human DHFR and against *L. major* promastigotes (for representative structures see Fig. 8). Generally, compounds that showed good inhibition of DHFR were active against the *L. major* promastigotes and conversely those which showed poor activity against the DHFR were also poorly active against the promastigotes. Some of the compounds also showed reasonable levels of selectivity for the *L. major* enzyme over the human enzyme; the most potent and selective compounds were some quinazolines and a pyrimidine (Fig. 8). However, some of these compounds were also active in *L major* promastigotes that lacked the enzyme DHFR-TS suggesting that they might have (an) additional enzymatic targets within the cell.

Zuccotto et al. [22] used differences in the structures of the *T. cruzi* and human DHFRs to design a series of selective inhibitors of the *T. cruzi* enzyme. In the human enzyme, the channel linking the folate to the NADPH binding sites contains the sequence Gly20–Asp21, which is overall negatively charged. In contrast, the *T. cruzi* enzyme contains the sequence Arg39–Ser40, which is overall positively charged (Table 2). Modelling suggested substitution of a negatively charged substituent on methotrexate should lead to repulsion with Asp21 in the case of the human enzyme and possibly attraction in the case of the *T. cruzi* enzyme (Fig. 9). The compounds did appear to have increased selectivity for the parasite enzyme but unfortunately showed weak in vitro activity against *T. cruzi* amastigotes.

An approach to discover novel parasite DHFR inhibitors using database mining has been reported by Chowdhury et al. [30] and Zuccotto et al. [31] who used the programme DOCK 3.5 [32] to search the Cambridge Structural Database. The goal of their research was to find DHFR inhibitors that were not based on the 2,4-diaminopyrimidine motif. Chowdhury et al. [30] used the *L. major* active site for docking and identified compounds with weak activity against both the enzyme and parasite (EC_{50} = 20–60 μM).

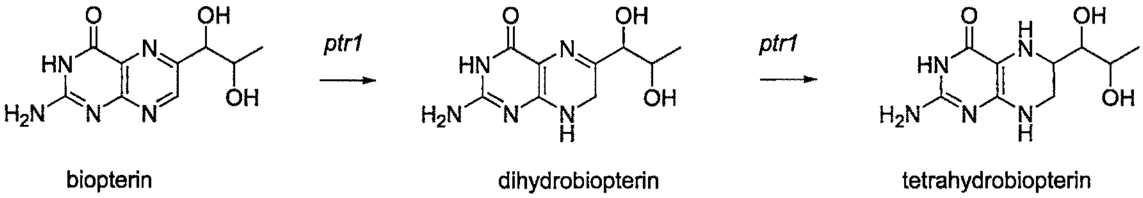

Fig. 11. Reduction of biopterin by *ptr1*

It is not known whether this anti-parasitic activity is due to inhibition of DHFR (Fig. 10(a)). Zuccotto et al. [31] found one particular compound that had activity against *T cruzi* DHFR (Fig. 10(b)) and also showed good activity against *T. brucei* trypomastigotes ($EC_{50} = 3.6$ μM).

5. Resistance

There are a number of possible mechanisms of resistance to DHFR inhibitors in *Leishmania* which include over-expression of the enzyme DHFR-TS and over-expression of the enzyme *ptr1*.

ptr1 is an enzyme involved in the reduction of biopterin to dihydrobiopterin and terahydrobiopterin (Fig. 11) [33,34]. It has been shown that this enzyme can also reduce dihydrofolate to tetrahydrofolate, although the enzyme is structurally unrelated to DHFR. Under normal conditions, the majority of reduction of dihydrofolate to tetrahydrofolate is carried out by DHFR. However, should *ptr1* be over-expressed (which has been demonstrated in laboratory models of resistance [35]), then this enzyme could substitute, albeit much less efficiently, for DHFR [36]. It has been shown that while it is probable that *ptr1* could not fully replace the role of DHFR, it is important in reducing the sensitivity of *Leishmania* to antifolates [37]. Compounds that inhibit both DHFR and *ptr1* may make prospects as drug candidates [12]. While there are differences in substrate specificity between DHFR and *ptr1*, some compounds inhibit both well. The presence of *ptr1* has been shown in *L. major* promastigotes and more recently in *L mexicana* amastigotes [38]. This contrasts to the situation in *T. cruzi* where levels of *ptr1* are not detectable in the amastigote stage, although the enzyme is expressed in the epimastigote (vector) form [39].

A recent publication by Beverley's group [40] showed that *ptr1* knockouts are in fact more virulent against mouse models of leishmaniasis than the wild-type, and they suggest that targeting of *ptr1* on its own is not a suitable drug target.

6. Conclusions

DHFR is a drug target that has not been fully investigated in the protozoan parasites *Leishmania* and *Trypanosoma*. The structure of the enzyme and the enzyme specificity is significantly different from that of the human enzyme suggesting the possibility of selective drug design. However, clinical DHFR inhibitors in current use are not suitable for treatment of the diseases caused by *Leishmania* and *Trypanosoma*. Hence, there is need for development of new, selective inhibitors, which are active in vivo. Several potential mechanisms of resistance have been discovered, including the enzyme *ptr1*. In order to avoid this mechanism of resistance, it may be necessary to inhibit *ptr1* in addition to DHFR.

Acknowledgements

I would like to acknowledge the following people who have worked on design and synthesis of inhibitors of DHFR in my research group (Shafinaz F. Chowdhury, Raffaella Di Lucrezia, Didier Pez, Richard Weaver, Fabio Zuccotto) and my collaborators (Victor Bernier Villamor, Reto Brun, Simon L. Croft, Dolores Gonzalez Pacanowska, Jonathan Goodman, Ramon Hurtardo Guerrero, Isabel Leal, Louis Maes, Luis M. Ruiz Perez). I would also like to acknowledge the following organisations who have contributed funding: The British Council/Overseas Development Agency, Acciones Integradas, the Welsh School of Pharmacy, the Welsh Scheme for the Development of Health and Social Research, the World Health Organisation Special Programme for Research and Training in Tropical Diseases. I would also like to acknowledge Dr. Suzanne Duce and Dr. Claire Simons for reading this manuscript.

References

[1] http.//www.who int
[2] J.M Blaney, C Hansch, C. Silipo, A Vittoria, Chem Rev 84 (1984) 333–407
[3] C.D. Selassie, T E Klein, Comparative QSAR, Taylor & Francis, London, 1997
[4] E M. McIntosh, R H Haynes, Acta Biochim. Pol 44 (1997) 159–172
[5] D M James, H.M Gilles (Eds), Human Antiparasitic Drugs Pharmacology and Usage, Wiley, Chichester, 1985.
[6] http //www who int/tdr
[7] T D Meek, E P Garvey, D V. Santi, Biochemistry 24 (1985) 678–686
[8] R. Grumont, W Sirawarapom, D V Santi, Biochemistry 27 (1988) 3776–3784
[9] P. Reche, R Arrebola, A Olmo, D V Santi, D Gonzalez Pacanowska, L M Ruiz Perez, Mol. Biochem. Parasitol 65 (1994) 247–258.
[10] F Gamarro, P L Yu, J. Zhao, U Edman, P.J Greene, D Santi, Mol Biochem Parasitol. 72 (1995) 11–22
[11] K.M Ivanetich, D V Santi, Exp. Parasitol. 70 (1990) 367–371
[12] L W Hardy, W Matthews, B. Nare, S.M Beverley, Exp Parasitol 87 (1997) 157–169
[13] D.R. Knighton, C C Kan, E. Howland, C A Janson, Z Hostomska, K M Welsch, D A Matthews, Nat Struct Biol 1 (1994) 186–194
[14] F Zuccotto, A C R. Martin, R A. Laskowski, J.M Thornton, I H. Gilbert, J Comput -Aided Mol. Des 12 (1998) 241–257
[15] P H Liang, K.S Anderson, Biochemistry 37 (1998) 12195–12205
[16] W. Sirawarapom, R Sertsrivanich, R G. Booth, C Hansch, R.A Neal, D V Santi, Mol. Biochem Parasitol 31 (1988) 79
[17] S F Chowdhury, V.B Villamor, R H Guerrero, I Leal, R. Brun, S L. Croft, J M. Goodman, L. Maes, L.M Ruiz-Perez, D G Pacanowska, I H Gilbert, J Med Chem. 42 (1999) 4300–4312
[18] J J Jaffe, J J. McCormack, W.E Gutteridge, Exp Parasitol 25 (1969) 311–318
[19] R A Neal, S L Croft, J Antimicrob Chemother. 14 (1984) 463–475
[20] W Peters, E R. Trotter, B.L Robinson, Ann Trop. Med. Parasitol 74 (1980) 321–335
[21] D A Scott, G H Coombs, B E Sanderson, Biochem Pharmacol. 36 (1987) 2043–2045
[22] F. Zuccotto, R Brun, D.G Pacanowska, L M.R. Perez, I.H Gilbert, Bioorg. Med. Chem Lett 9 (1999) 1463–1468.
[23] C A Hunter, G H Coombs, Med Sci Res 15 (1987) 1233–1234

[24] R.G. Booth, C D Selassie, C Hansch, D.V. Santi, J Med Chem. 30 (1987) 1218–1224.

[25] B A Hathaway, Z. Guo, C Hansch, T J Delcamp, S.S Susten, J.H. Freisheim, J Med Chem 27 (1984) 144–149.

[26] J D. Berman, M. King, N. Edwards, Antimicrob Agents Chemother. 33 (1989) 1860–1863

[27] J. Davoll, A.M. Johnson, H J Davis, O D. Bird, J. Clarke, E.F. Elslager, J. Med Chem. 15 (1972) 812–826.

[28] E.F Elslager, O D Bird, J Clarke, S.C. Perricone, D.F. Worth, J Med Chem. 15 (1972) 1138–1146

[29] P.E. Thompson, A. Bayles, B Olszewski, Exp. Parasitol. 25 (1969) 32–49

[30] S.F. Chowdhury, R. Di Lucrezia, R H Guerrero, R. Brun, J Goodman, L.M. Ruiz-Perez, D.G Pacanowska, I.H. Gilbert, Bioorg Med Chem Lett. 11 (2001) 977–980.

[31] F. Zuccotto, M Zvelebil, R. Brun, S F Chowdhury, R. Di Lucrezia, I. Leal, L Maes, L M. Ruiz-Perez, D. Gonzalez Pacanowska, I.H. Gilbert, Bioorg Med Chem Lett 36 (2001) 395–405

[32] I.D. Kuntz, Science 257 (1992) 1078–1082

[33] A R Bello, B Nare, D. Freedman, L Hardy, S.M Beverley, Proc. Natl Acad Sci U. S. A. 91 (1994) 11442–11446

[34] J.Y. Wang, E Leblanc, C F Chang, B. Papadopoulou, T Bray, J M. Whiteley, S.X Lin, M Ouellette, Arch. Biochem. Biophys 342 (1997) 197–202.

[35] B Papadopoulou, G Roy, M Ouellette, EMBO J 11 (1992) 3601–3608

[36] B. Nare, L.W. Hardy, S M Beverley, J Biol. Chem. 272 (1997) 13883–13891.

[37] M P. Barrett, J C. Mottram, G.H Coombs, Trends Microbiol. 7 (1999) 82–88

[38] M.L Cunningham, S.M. Beverley, Mol Biochem Parasitol 113 (2001) 199–213.

[39] C Robello, P. Navarro, S Castanys, F. Gamarro, Mol Biochem. Parasitol 90 (1997) 525–535.

[40] M.L Cunningham, R.G. Titus, S J Turco, S.M Beverley, Science 292 (2001) 285–287

ELSEVIER

Biochimica et Biophysica Acta 1587 (2002) 258–275

BIOCHIMICA ET BIOPHYSICA ACTA
BBA
www.bba-direct.com

Review

New developments in anti-HIV chemotherapy ☆

Erik De Clercq*

Rega Institute for Medical Research, Katholieke Universiteit Leuven, Minderbroedersstraat 10, B-3000 Leuven, Belgium

Received 24 January 2002; accepted 24 January 2002

Abstract

Virtually all the compounds that are currently used, or are subject of advanced clinical trials, for the treatment of human immunodeficiency virus (HIV) infections, belong to one of the following classes: (i) nucleoside/nucleotide reverse transcriptase inhibitors (NRTIs): i.e. zidovudine (AZT), didanosine (ddI), zalcitabine (ddC), stavudine (d4T), lamivudine (3TC), abacavir (ABC), emtricitabine [(−)FTC], tenofovir disoproxil fumarate; (ii) non-nucleoside reverse transcriptase inhibitors (NNRTIs): i.e. nevirapine, delavirdine, efavirenz, emivirine, and (iii) protease inhibitors (PIs): i.e. saquinavir, ritonavir, indinavir, nelfinavir, amprenavir and lopinavir. In addition to the reverse transcriptase (RT) and protease reaction, various other events in the HIV replicative cycle can be considered as potential targets for chemotherapeutic intervention: (i) viral adsorption, through binding to the viral envelope glycoprotein gp120 (polysulfates, polysulfonates, polycarboxylates, polyoxometalates, polynucleotides, and negatively charged albumins); (ii) viral entry, through blockade of the viral coreceptors CXCR4 [bicyclam (AMD3100) derivatives] and CCR5 (TAK-779 derivatives); (iii) virus–cell fusion, through binding to the viral envelope glycoprotein gp41 (T-20, T-1249); (iv) viral assembly and disassembly, through NCp7 zinc finger-targeted agents [2,2′-dithiobisbenzamides (DIBAs), azadicarbonamide (ADA)]; (v) proviral DNA integration, through integrase inhibitors such as 4-aryl-2,4-dioxobutanoic acid derivatives; (vi) viral mRNA transcription, through inhibitors of the transcription (transactivation) process (flavopiridol, fluoroquinolones). Also, various new NRTIs, NNRTIs and PIs have been developed that possess, respectively: (i) improved metabolic characteristics (i.e. phosphoramidate and *cyclo*saligenyl pronucleotides by-passing the first phosphorylation step of the NRTIs), (ii) increased activity ["second" or "third" generation NNRTIs (i.e. TMC-125, DPC-083)] against those HIV strains that are resistant to the "first" generation NNRTIs, or (iii) as in the case of PIs, a different, nonpeptidic scaffold [i.e. cyclic urea (mozenavir), 4-hydroxy-2-pyrone (tipranavir)]. Nonpeptidic PIs may be expected to inhibit HIV mutant strains that have become resistant to peptidomimetic PIs. Given the multitude of molecular targets with which anti-HIV agents can interact, one should be cautious in extrapolating the mode of action of these agents from cell-free enzymatic assays to intact cells. Two examples in point are L-chicoric acid and the nonapeptoid CGP64222, which were initially described as an integrase inhibitor or Tat antagonist, respectively, but later shown to primarily act as virus adsorption/entry inhibitors, the latter through blockade of CXCR4.
© 2002 Elsevier Science B.V. All rights reserved.

Keywords: Human immunodeficiency virus (HIV); Reverse transcriptase (HIV); Protease (HIV); CXCR4 (HIV); CCR5 (HIV); Integrase (HIV); Fusion (HIV); Transcription (HIV)

Abbreviations: HIV, human immunodeficiency virus; NRTIs, nucleoside/nucleotide reverse transcriptase inhibitors; NNRTIs, non-nucleoside reverse transcriptase inhibitors; PIs, protease inhibitors; DIBA, 2,2′-dithiobisbenzamide; ADA, azadicarbonamide; AIDS, acquired immune deficiency syndrome; HSV, herpes simplex virus; STD, sexually transmitted disease; MIP-1α and -1β, macrophage inflammatory proteins; SDF-1, stromal-cell derived factor; PBMCs, peripheral blood mononuclear cells; TM4, transmembrane segment; SI, syncytium-inducing; NSI, non-syncytium-inducing; NOBA, 3-nitrosobenzamide; AZT, zidovudine; ddI, didanosine; ddC, zalcitabine; d4T, stavudine; 3TC, lamivudine; ABC, abacavir; bis(POM)-PMEA, bis(pivaloyloxymethyl)-9-(2-phosphonylmethoxyethyl)adenine, adefovir dipivoxyl; bis(POC)-PMPA, bis(isopropyloxycarbonyloxymethyl)-(*R*)-9-(2-phosphonylmethoxypropyl)adenine, tenofovir disoproxil; dOTC, (±)2′-deoxy-3′-oxa-4-thiocytidine; (−)FTC, emtricitabine; DAPD, amdoxovir, (−)-β-D-2,6-diaminopurine dioxolane; bis(SATE)ddAMP, bis(*S*-acetyl-2-thioethyl)phosphotriester of ddA

☆ Proceedings of the 8th International Symposium on Molecular Aspects of Chemotherapy, Gdansk, Poland, 5–9 September 2001.

* Tel.: +32-16-337341; fax: +32-16-337340.

E-mail address: erik.declercq@rega.kuleuven.ac.be (E. De Clercq).

0925-4439/02/$ - see front matter © 2002 Elsevier Science B.V. All rights reserved.
PII: S0925-4439(02)00089-3

1. Introduction

Combination therapy, comprising at least three anti-human immunodeficiency virus (HIV) drugs, has become the standard treatment of acquired immune deficiency syndrome (AIDS) or HIV-infected patients. Virtually all drugs that have been licensed for clinical use (or made available through expanded access programmes) for the treatment of HIV infections fall into one of the following three categories: (i) nucleoside/nucleotide reverse transcriptase inhibitors (NRTIs), that, following two phosphorylation steps (tenofovir) or three phosphorylation steps [zidovudine (AZT), didanosine (ddI), zalcitabine (ddC), stavudine (d4T), lamivudine (3TC), abacavir (ABC)], act, as chain terminators, at the substrate binding site of the reverse transcriptase (RT); (ii) non-nucleoside reverse transcriptase inhibitors (NNRTIs) that interact with the RT at an allosteric, non-substrate binding site (nevirapine, delavirdine, efavirenz); and (iii) protease inhibitors (PIs) that specifically inhibit, as peptidomimetics, the virus-associated protease (saquinavir, ritonavir, indinavir, nelfinavir, amprenavir, lopinavir). Guidelines to the major clinical trials with these compounds have been recently published [1].

Although the long-term goal of eradicating the virus from latently and chronically infected cells remains forbidding [2], the advent of so many new compounds other than those that have been formally approved, for the treatment of HIV infections, will undoubtedly improve the prognosis of patients with AIDS and AIDS-associated diseases. Here, I will primarily address those new anti-HIV compounds that (i) have emerged as promising anti-HIV drug candidates during the last few years, that (ii) are in preclinical or early-clinical development, and that (iii) are targeted at well-defined steps in the HIV replicative cycle.

2. Virus adsorption (gp120) inhibitors

A great variety of polyanionic compounds have been described to block HIV replication through interference with virus adsorption (or binding) to the cell surface: i.e. polysulfates, polysulfonates, polycarboxylates, polyphosphates, polyphosphonates, polyoxometalates, etc. This class of compounds also comprises the cosalane analogues (**1**) containing the polycarboxylate pharmacophore [3], as well as the sulfated polysaccharides extracted from sea algae [4]. All these compounds, whether synthetic or of natural origin, are assumed to exert their anti-HIV activity by shielding off the positively charged sites in the V3 loop of the viral envelope glycoprotein (gp120) [5,6], which is necessary for virus attachment to the cell surface heparan sulfate, a primary binding site, before a more specific binding occurs

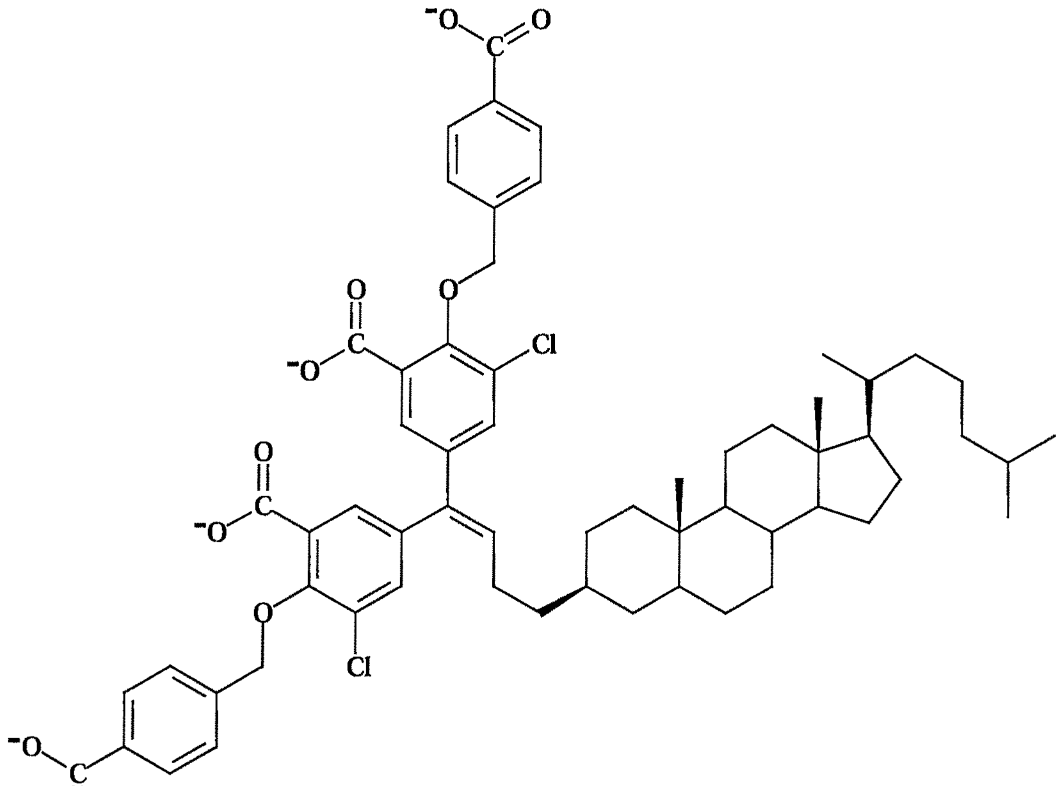

Compound 1
Cosalane analogue

to the CD4 receptor of the CD4$^+$ cells, and to the CXCR4 coreceptor of the CXCR4$^+$ cells (the latter in the case of X4 and dual tropic X4/R5 HIV strains). Heparan sulfate is widely expressed on animal cells and, as it is involved in the virus-cell binding of a broad spectrum of enveloped viruses, including herpes simplex virus (HSV) [7], dengue virus [8] and other flaviviruses (i.e. Japanese encephalitis virus) [9], it also explains why polysulfates have a broad-spectrum antiviral activity against HIV, HSV and various other enveloped viruses [10].

ligand, namely SDF-1 ("stromal-cell derived factor") has been identified. Of these chemokines, the LD78β isoform of MIP-1α has emerged as the most potent chemokine for inhibiting HIV-1 infection in peripheral blood mononuclear cells (PBMCs) [14,15] as well as monocytes/macrophages [16].

TAK-779, a quaternary ammonium derivative (2) is the first nonpeptidic molecule that has been described to block the replication of M-tropic R5 HIV-1 strains at the CCR5 level [17].

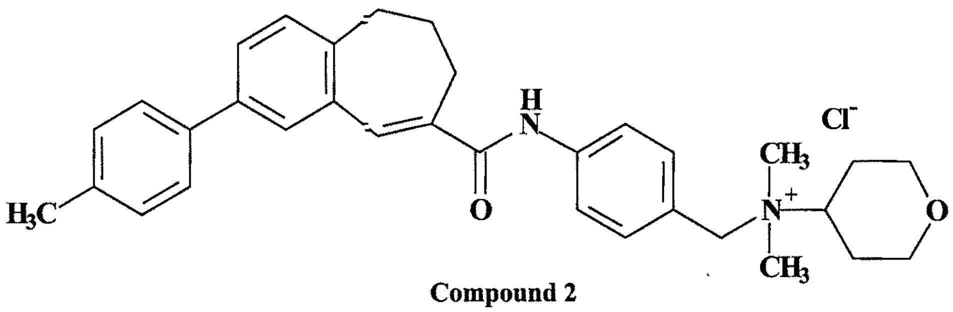

Compound 2
TAK-779

The major role of polysulfates or polyanionic substances in general in the management of HIV infections may reside in the prevention of sexual transmission of HIV infection, as these compounds, if applied as a vaginal formulation, may successfully block HIV infection through both virus-to-cell and cell-to-cell contact. These compounds therefore merit being pursued as vaginal microbicides. The fact that in addition to their anti-HIV activity, these polyanionic substances, as demonstrated, for example, for poly(sodium(4-styrene)sulfonate), also inhibit other sexually transmitted disease (STD) pathogens, i.e. HSV, *Neisseria gonorrheae* and *Chlamydia trachomatis* [11], further adds to their potential therapeutic and preventive value.

3. Viral coreceptor antagonists

To enter cells, following binding with the CD4 receptor, the HIV-1 particles must interact, again through the viral envelope glycoprotein gp120, with the CXCR4 coreceptor [12] or CCR5 coreceptor [13]. CXCR4 is the coreceptor for HIV-1 strains that infect T-cells (T-tropic or X4 strains), and CCR5 is the coreceptor for HIV-1 strains that infect macrophages (M-tropic or R5 strains). CXCR4 and CCR5 have not evolved simply to act as coreceptors for HIV entry; they normally act as receptors for chemokines (chemoattractant cytokines). The normal ligands for CCR5 are RANTES ("regulated upon activation, normal T-cell expressed and secreted") and MIP-1α and -1β ("macrophage inflammatory proteins"), whereas for CXCR4, only one natural

A binding site for TAK-779 has been identified within the transmembrane helices 1, 2, 3 and 7 of CCR5 [18]. TAK-779 has been found to inhibit R5 HIV-1 strains in the nanomolar concentration range, while not affecting X4 HIV-1 strains at 10,000-fold higher concentrations [17]. TAK-779 is not a "pure" CCR5 antagonist, as it also demonstrates some antagonism towards CCR2b. Unlike RANTES, TAK-779 does not induce internalization of CCR5. The clinical potential of TAK-779 and its congeners [19] in the therapy and/or prophylaxis of HIV-1 infections remains to be further explored. Meanwhile, several new CCR5 antagonists have been reported [20,21], and a lead clinical candidate (SCH C) for further development has been identified.

Almost simultaneously [22–24], three compounds, i.e. the bicyclam AMD3100 [22], [Tyr-5,12,Lys-7]polyphemusin or T22 [23] and the nonapeptide (D-Arg)$_9$ or ALX40-4C [24] were announced as CXCR4 antagonists, blocking the replication of T-tropic X4, but not M-tropic R5, HIV-1 strains through selective antagonism of CXCR4. The bicyclams are the most specific and most potent CXCR4 antagonists that have been described to date [25,26]. The bicyclams had been known as potent and selective HIV inhibitors for a number of years [27,28], before their target of action was identified as the CXCR4 coreceptor [22,29,30]. The bicyclam AMD3100 (3) inhibits the replication of X4 HIV-1 strains within the nanomolar concentration range [28]. As it is not toxic to the host cells at concentrations up to 500 μM, its selectivity index, or ratio of 50% cytotoxic concentration (CC$_{50}$) to 50%

antivirally effective concentration (EC_{50}) can be estimated at > 100,000.

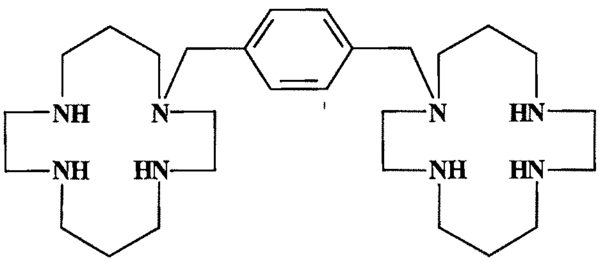

Compound 3
AMD3100

A close correlation has been found, over a concentration range of 0.1–1000 ng/ml, between the AMD3100 concentrations required to inhibit (i) HIV-1 NL4-3 replication, (ii) monoclonal antibody (mAb 12G5) binding to the CXCR4 coreceptor, and (iii) SDF-1-induced signal transduction (Ca^{2+} flux), suggesting an intimate relationship between these three parameters [29,30]. The inhibitory effects of AMD3100 on the T-tropic HIV-1 NL4-3 strain have been demonstrated in a wide variety of cells expressing CXCR4, including PBMCs; and, vice versa, various T-tropic and dual-tropic, but not M-tropic, HIV-1 strains have proven sensitive to AMD3100 in PBMC.

Negatively charged amino acid (i.e. aspartic acid) residues in the extracellular regions of CXCR4 must be involved in its interaction with both AMD3100 and SDF-1, and the V3 loop of X4 HIV gp120, which are all three highly basic. Substitutions of a neutral amino acid residue for aspartic acid in the second extracellular loop generated resistance to AMD3100 [31]. In particular, the aspartate residues at positions 171 and 262, located close to the extracellular sides of the transmembrane segments TM4 and TM6, may represent crucial sites of interaction with the bicyclam AMD3100 [32].

When the bicyclam AMD3100 was added to PBMC infected with clinical HIV isolates displaying the syncytium-inducing (SI) phenotype, these strains reverted to the non-syncytium-inducing (NSI) phenotype, and, concomitantly, these strains switched from CXCR4 to CCR5 coreceptor use [33]. These findings indicate that selective blockade of CXCR4 by AMD3100 may prevent the switch from the less pathogenic M-tropic R5 to the more pathogenic T-tropic X4 strains of HIV, which in vivo heralds the progression to AIDS. AMD3100 has proved efficacious, alone and in combination with other anti-HIV drugs, in achieving a marked reduction in viral load in the SCID-hu Thy/Liv mouse model [34]. Following a phase I clinical trial for safety in normal healthy volunteers [35], AMD3100 recently entered phase II clinical trials in HIV-infected individuals.

Given their high potency and selectivity as CXCR4 antagonists, bicyclams, such as AMD3100, may not only have great potential for the therapy and/or prophylaxis of X4 HIV infections, but also other pathologic processes, such as breast cancer metastasis, which are at least partially dependent of, or mediated by, signaling through CXCR4 [36].

4. Viral fusion (gp41) inhibitors

The interaction of the X4 or R5 HIV-1 envelope glycoprotein gp120 with the coreceptor CXCR4 or CCR5, respectively, is followed by a spring-loaded action of the viral glycoprotein gp41 (normally covered by the bulkier gp120), which then anchors through its amino terminus (the "fusion peptides") into the target cell membrane. This initiates the fusion of the two lipid bilayers, that of the

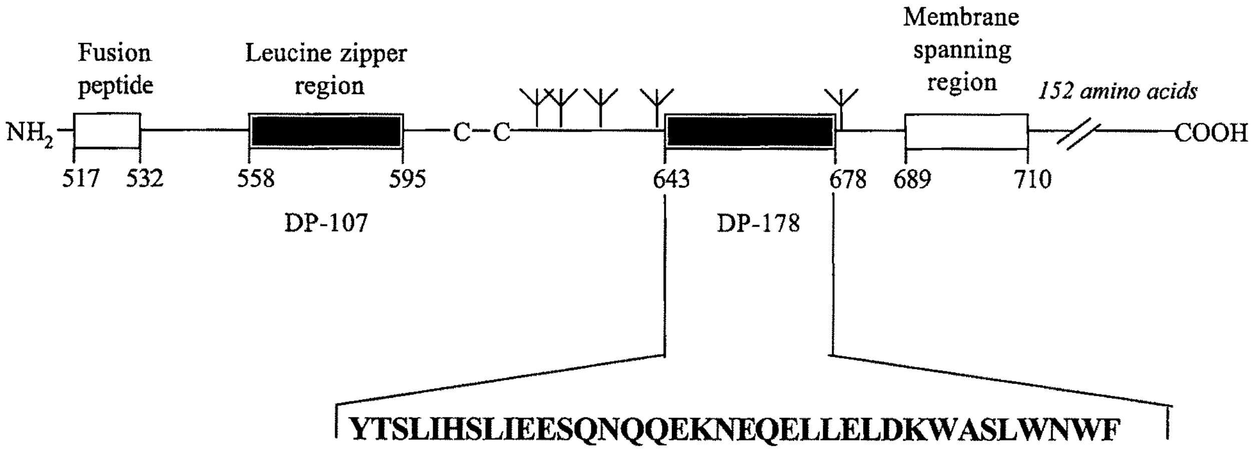

Compound 4
T-20 (pentafuside)

viral envelope with that of the cellular plasma membrane [37]. At the onset of the fusion process, the hydrophobic grooves on the surface of the N36 coiled coil in the gp41 ectodomain become available for binding with extraneous inhibitors, such as DP-178 (T-20), a 36-residue peptide, that binds to the hydrophobic groove of N36 [37].

T-20 (pentafuside) (4) is a synthetic, 36-amino acid peptide corresponding to residues 127–162 of the ectodomain of gp41 (or residues 643–678 in the gp160 precursor). T-20, previously called DP-178, was modeled after a specific domain (within gp41) predictive of α-helical secondary structure: DP-178 consistently afforded 100% blockade of virus-mediated cell–cell fusion (syncytium formation) at concentrations ranging from 1 to 10 ng/ml, i.e. 10^4- to 10^5-fold lower than the cytotoxic concentration [38]. An initial clinical trial has been carried out with T-20 at four doses (3, 10, 30 and 100 mg twice daily, intravenously, for 14 days) in 16 HIV-infected adults: at the highest dose (100 mg, twice daily), T-20 achieved by the 15th day a 1.5- to 2.0-fold reduction in plasma HIV RNA [39]. These data provide proof-of-concept that HIV fusion inhibitors are able to reduce virus replication in vivo.

The betulinic acid derivative RPR 103611 (**5**) is the only nonpeptidic low-molecular-weight compound that has been reported to block HIV-1 infection through interaction with gp41: this triterpene derivative has been found to inhibit the infectivity of a number of HIV-1 strains in the 10 nM concentration range [41], apparently through interference with a post-binding, envelope-dependent step involved in the fusion of the virus with the cell plasma membrane.

The exact mode of action of RPR 103611 remains to be elucidated. Sequence analysis of RPR103611-resistant mutants indicated that a single amino acid change, I84S, in HIV-1 gp41 is sufficient to confer drug resistance [42]. However, this I84S mutation did not occur in some of the naturally RPR103611-resistant HIV-1 strains such as NDK. More recently, the action of RPR103611 has been thought to depend on the accessibility of gp41 [43], and for the isomeric betulinic acid derivative IC 9564, HIV-1 gp120, rather than gp41, has been proposed as the prime target (based on the mutations G237R and R252K emerging in gp120 of drug-resistant mutants) [44]. YK-FH312, a betulinic acid derivative unrelated to RPR103611 or IC 9564, was reported to block the assembly and/or budding of HIV particles [45].

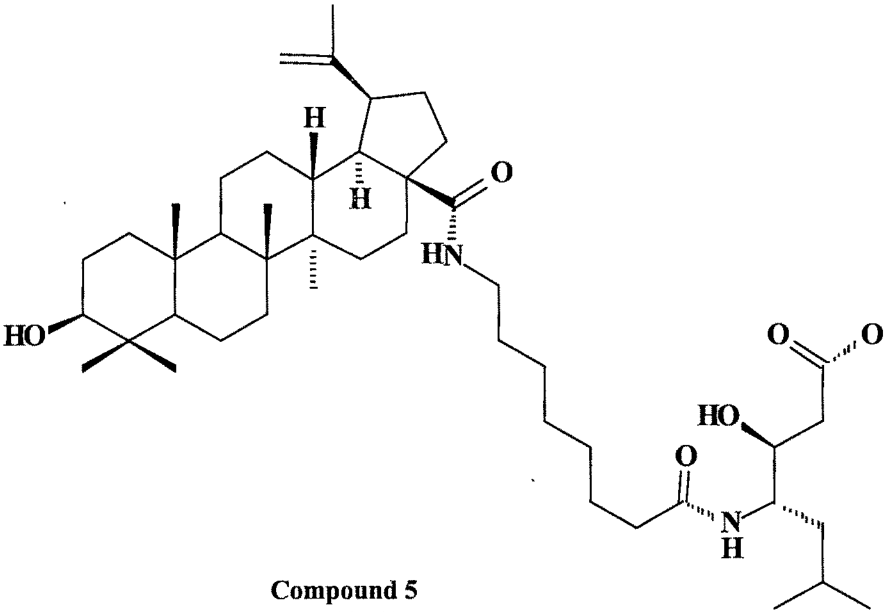

Compound 5
RPR 103611

Meanwhile, T-20 has proceeded to phase II/III clinical trials, and phase I clinical trials have been initiated with T-1249, a 39-amino acid peptide derived from DP-107 (which is a 38-amino acid peptide corresponding to residues 558–595 of gp160); T-1249 would be 10-fold more potent than T-20 when evaluated in vitro against HIV under the same conditions [40].

5. Nucleocapsid protein (NCp7) Zn finger-targeted agents

The two zinc fingers [Cys-X_2-Cys-X_4-His-X_4-Cys (CCHC), whereby X = any amino acid] in the nucleocapsid (NCp7) protein [46] comprise the proposed molecular target for zinc-ejecting compounds such as 3-nitrosobenzamide

(NOBA), 2,2′-dithiobisbenzamide (DIBA), SRR-SB3 (cyclic DIBA) [47], 1,2-dithiane-4,5-diol,1,1-dioxide (dithiane) [48] and azadicarbonamide (ADA) [49,50]. These compounds should be able to interfere with both early (uncoating, disassembly) and late phases (packaging, assembly) of retrovirus replication. Their effect at the early phase (disassembly) may also be ascribed to cross-linkage among adjacent zinc fingers. The DIBAs are able to enter intact virions and the cross-linkage of NCp7 in virions correlates with loss of infectivity and decreased proviral DNA synthesis during acute infection [51]. Electron microscopically, the effect bestowed by DIBAs on virus morphology could be described as "core-freezing" [52].

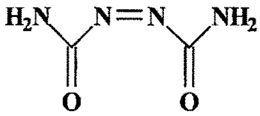

Compound 6
ADA (azodicarbonamide)

Although NOBA, DIBA, dithiane and ADA have been shown to dock nicely on the NCp7 Zn finger domains [53] and are believed to selectively target these Zn fingers without affecting the cellular Zn finger proteins, their selectivity indexes [ratio of CC_{50} (50% cytotoxic concentration) over EC_{50} (50% effective concentration)] are not that impressive [53]. Of the NCp7-targeted compounds, ADA (**6**) has been the first to proceed to phase I/II clinical trials in advanced AIDS patients. Some preliminary evidence of efficacy was witnessed with add-on ADA in patients failing current antiretroviral therapy [54]; these studies should be further extended. Although ADA is an HIV NCp7 Zn-finger inhibitor, its action in vivo is likely to be multipronged. ADA may well interact with a variety of targets and, certainly, its inhibitory effects on T-cell responses in vitro and in vivo [55] can hardly be attributed to an action targeted at the HIV NCp7 Zn fingers.

6. RT inhibitors targeted at the substrate binding site

The substrate (dNTP) binding site of the HIV-1 RT is the target for a large variety of NRTI analogues, which have for several years [56] been recognized as efficacious drugs for the treatment of HIV infections: i.e. AZT, ddI, ddC, d4T, 3TC, ABC, and the yet experimental drug emtricitabine [(−)FTC]. Fozivudine tidoxil is a thioether lipid AZT conjugate that has recently passed phase II clinical trials [57] and should be as effective as, and potentially better tolerated than, AZT. As a rule, all these compounds must be phosphorylated to their 5′-triphosphate form, before they can act as competitive inhibitors/substrate analogues/chain terminators at the RT level. In contrast to the nucleoside analogues, the nucleotide analogues PMEA and PMPA are already equipped with a phosphonate group, and therefore only need two phosphorylation steps to be converted to the active metabolite [58]. From PMEA and PMPA, the oral prodrug forms [bis(pivaloyloxymethyl)-9-(2-phosphonylmethoxyethyl)adenine (bis(POM)-PMEA) or adefovir dipivoxyl (**7**), and bis(isopropyloxycarbonyloxymethyl)-(***R***)-9-(2-phosphonylmethoxypropyl)adenine (bis(POC)-PMPA) or tenofovir disoproxil (**8**) fumarate, respectively] have been prepared. The former is in advanced phase III clinical trials for the treatment of hepatitis B virus (HBV) infections, whereas the latter has completed phase III clinical trials for the treatment of HIV infections. A new drug application (NDA) and market authorization application (MAA) has been recently filed for tenofovir disoproxil fumarate with the FDA (US) and EMEA (EU), respectively. In rhesus macaques infected with the highly pathogenic chimeric virus SHIV, tenofovir treatment initiated 1 week post-infection, at a time when disseminated infection and extensive viral replication had already been established and CD4$^+$ T-cell loss had begun, led to prompt, virtually complete suppression of viral replication and long-term stabilization of CD4$^+$ T-cell levels, which were sustained, even after withdrawal of tenofovir (after 12 weeks of treatment) [59].

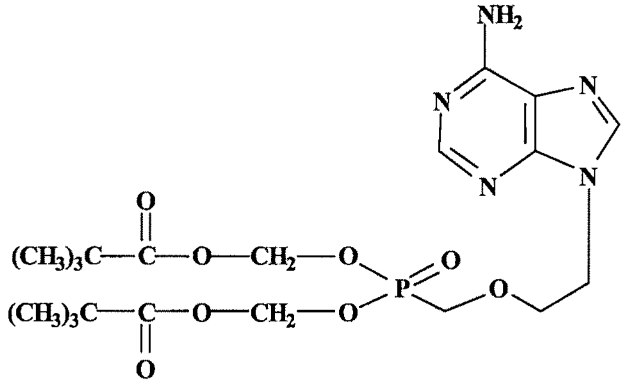

Compound 7
bis(POM)-PMEA
Adefovir dipivoxyl

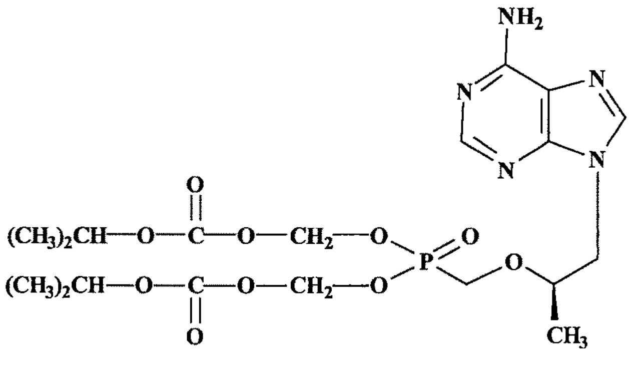

Compound 8
bis(POC)-PMPA
Tenofovir disoproxil

In addition to 3TC and (−)FTC, the structurally related (±)2′-deoxy-3′-oxa-4′-thiocytidine (BCH-10652,dOTC) [60], the dioxolane purine nucleoside analogues [61], the methylenecyclopropane nucleoside analogues (and their phosphoro-L-alaninate diesters) [62,63] and the 4′-ethynyl nucleoside analogues [64] have recently been described as new anti-HIV agents. [(−)FTC] (**9**) is in phase III trials for HIV and phase I/II trials for HBV; it is considered for use in the multidrug combination therapy of HIV-1 and HBV infections. Amdoxovir [DAPD, (−)-β-D-2,6-diaminopurine dioxolane] (**10**), which is converted by adenosine deaminase to dioxolane guanine (DXG), has proven active against AZT- and 3TC-resistant HIV-1 strains and has proceeded to phase I/II clinical studies [65,66]. BCH-10652 (dOTC) (**11**) has demonstrated activity against HIV-1 in the SCID-hu Thy/Liv model. Despite its structural similarity to 3TC, dOTC proved also active against 3TC-resistant HIV-1 (M184V), albeit at a relatively high dosage level (400 mg/kg/day) [67]. Also in vitro, dOTC and its (+) and (−) enantiomers still retained, albeit reduced, activity against 3TC-resistant M184V and M184I HIV-1 mutants [68].

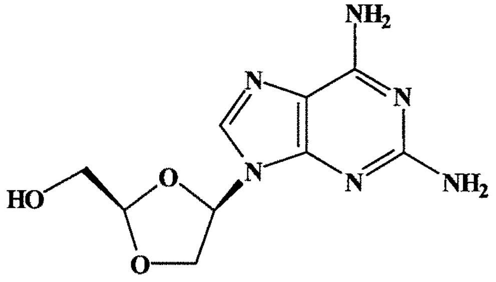

Compound 10
Amdoxovir
[DAPD, (-)-β-D-2,6-diaminopurine dioxolane]

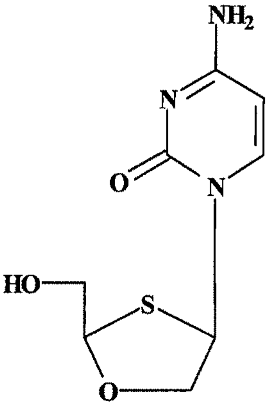

Compound 11
(±)2'-deoxy-3'-oxa-4'-thiocytidine (dOTC)

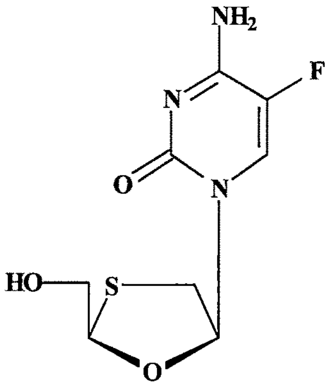

Compound 9
Emtricitabine [(-)FTC]

The bottleneck in the metabolic pathway leading from AZT and the other 2′,3′-dideoxynucleoside (ddN) analogues to their active 5′-triphosphate form is the first phosphorylation step. Therefore, attempts have been made at constructing 2′,3′-dideoxynucleotide (ddNMP) prodrugs that, once they have been taken up by the cells, deliver the nucleotide (ddNMP) form. This approach has proven particularly successful for a number of NRTIs such as 2′,3′-dideoxyadenosine (ddA) and d4T. Thus, the bis(*S*-acetyl-2-thioethyl)phosphotriester of ddA [bis(SATE]d-dAMP] (**12**) was synthesized and found to be 1000-fold more potent against HIV than the parent compound ddA [69]. Similarly, aryloxyphosphoramidate derivatives of d4T [i.e. So324, a d4T-MP prodrug containing at the phosphate moiety a phenyl group and the methylester of alanine linked to the phosphate group through a phosphoramidate linkage] have been constructed [70–72]. After the d4T aryloxyphosphoramidate (**13**) has been taken up by the cells, d4TMP is released intracellularly and then processed onto its active metabolite d4TTP [73]. This "thymidine kinase bypass" explains the high anti-HIV activity of d4T aryloxyphosphoramidate derivatives in thymidine kinase deficient cells and resting monocytes/macrophages [74]. The thymidine kinase (in the case of d4T) and the adenosine deaminase (in the case of ddA) can also be bypassed by using the cyclic saligenyl approach [75,76]. *Cyclo*saligenyl pronucleotides of d4T and ddA deliver exclusively the nucleotides d4TMP and ddAMP, not only under chemical-simulated hydrolysis conditions but also under intracellular conditions [77,78]. This has been convincingly shown for the *cyclo*-saligenyl derivative of d4TMP (**14**) in a number of cell lines [79].

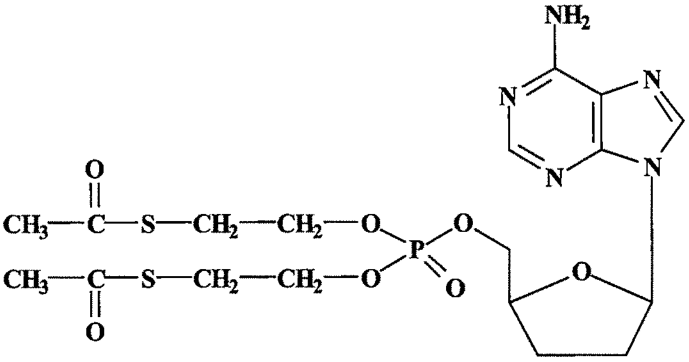

Compound 12
bis(S-acetyl-2-thioethyl)phosphotriester of ddA [bis(SATE)ddAMP]

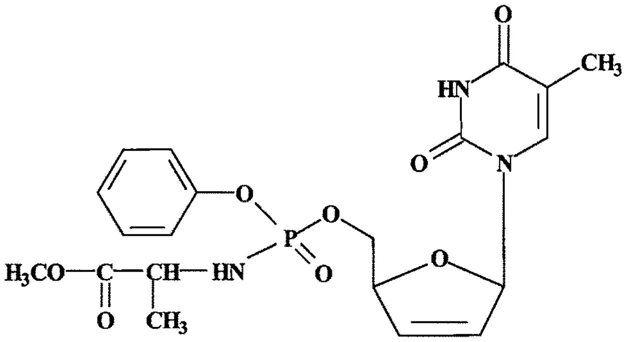

Compound 13
d4T aryloxyphosphoramidate

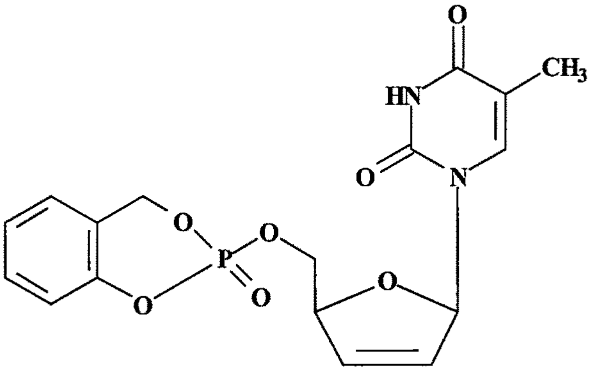

Compound 14
***cyclo*saligenyl d4TMP**

7. RT inhibitors targeted at the allosteric, nonsubstrate binding site

More than 30 structurally different classes of compounds have been identified as NNRTIs, viz. compounds that are specifically inhibitory to HIV-1 replication and targeted at a nonsubstrate binding site of the RT [80]. Three NNRTIs (nevirapine, delavirdine and efavirenz) have so far been formally licensed for clinical use in the treatment of HIV-1 infections, emivirine (MKC-442) (**15**) is in advanced (phase III) clinical trials, and others are in preclinical or early clinical development. The NNRTIs interact with a specific "pocket" site of the HIV-1 RT [81], which is closely associated with, but distinct from, the substrate binding site. NNRTIs are notorious for rapidly eliciting resistance [82], resulting from mutations at the amino acid residues that surround the NNRTI-binding site of HIV-1 RT. However, emergence of NNRTI-resistant HIV strains can be prevented if the NNRTIs are combined with NRTIs and used from the beginning at sufficiently high concentrations [80].

The thiocarboxanilide UC-781 (**16**) is an exceptionally potent inhibitor of HIV-1 replication [80]. It has been found to restore the antiviral activity of AZT against AZT-resistant HIV-1 [83]. UC-781 has been recognized as a (retro)virucidal agent, capable of reducing the infectivity of HIV-1 virions, and, therefore, yielding considerable promise for the use in (retro)virucidal formulations to prevent the transmission of HIV from infected to noninfected individuals [84]. UC-781 would seem an ideal candidate for application as a vaginal microbicide (virucide), i.e. when formulated in replens gel [85].

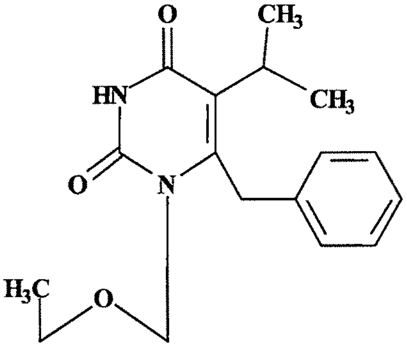

Compound 15
Emivirine (MKC-442)

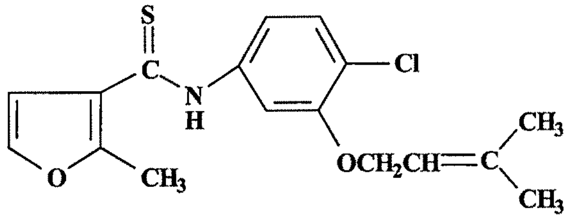

Compound 16
Thiocarboxanilide UC-781

To the new classes of NNRTIs that offer potent anti-HIV-1 activity belong the thieno[3,4][1,2,4]thiadiazine derivative QM96521 [86], the quinoxaline GW420867X [87], the imidazole derivative S-1153 (AG1549, capravirine) [88–90], (−)-6-chloro-2-[(1-furo[2,3-c]pyridin-5-yl-ethyl)thio]-4-pyrimidinamine (PNU-142721) [91], *N*-[2-(2,5-dimethoxyphenylethyl]-*N'*-[2-(5-bromopyridyl]-thiourea (HI-236) [92], the pyrido[1,2*a*]indole derivative BCH-1 [93], the 4-cyclopropylalkynyl-4-trifluoromethyl-3,4-dihydro-2(1*H*) quinazolinones DPC 961 and DPC 963, the 4-cyclopropylalkenyl-4-trifluoromethyl-3,4-dihydro-2(1*H*)quinazolinones DPC 082 and DPC 083 [94], the thiophene-ethylthiourea (TET) derivative HI-443 [95], the cyclohexenylethylthiourea derivatives HI-346 and HI-445 [96], the *cis*-cyclopropyl urea-PETT derivatives [97], the alkenyldiarylmethane (ADAM) series of compounds [98], the pyrrolobenzoxazepinone (PBO) derivatives [99], the quinoxalinylethylpyridyl thioureas (QXPTs) [100], the emivirine (MKC-442) derivative SJ-3366 [101] and R165335(TMC125) [102]. As a rule, the "new" ("second" or "third" generation) NNRTIs exhibit higher potency than the "old" ("first" generation) NNRTIs against wild-type and NNRTI-resistant HIV-1 [91,94–96,99,102]. This is particularly prominent for DPC 083 (**17**) and R165335 (TMC125) (**18**) that showed activity against L100I, K103N, Y181C, Y188L, K103N+L100I and K103N+Y181C RT mutant strains in the nanomolar concentration range [102]. This makes R165335 (TMC125) an excellent candidate for further clinical development.

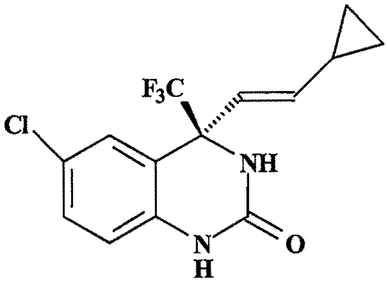

Compound 17
DPC 083

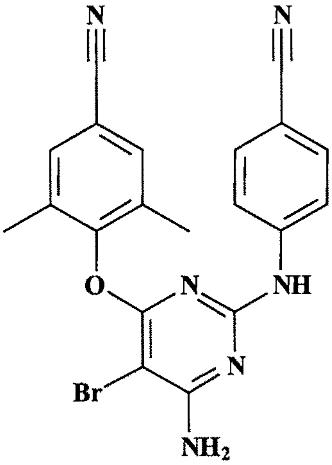

Compound 18
R165335 (TMC125)

Some of the new NNRTIs, such as SJ-3366 (**19**), possess remarkable features. This compound was reported to inhibit HIV-1 replication at a concentration below 1 nM with a therapeutic index greater than 4,000,000, and to inhibit HIV-2 replication (albeit at higher concentrations than those required for inhibition of HIV-1) at the viral entry stage [101].

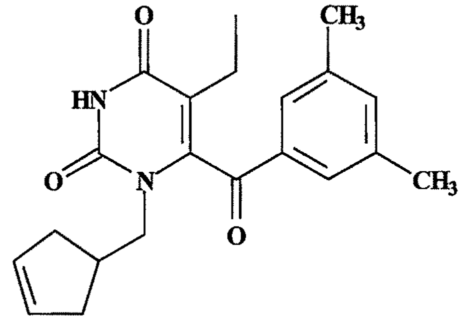

Compound 19
SJ-3366

Capravirine (AG1549) (**20**) has a favorable profile of resilience to many drug resistance mutations, which has been attributed to extensive main chain hydrogen bonding involving the main chain of residues 101, 103, and 236 of the p66 RT subunit [89]. Capravirine has proceeded to phase II/III clinical trials [90].

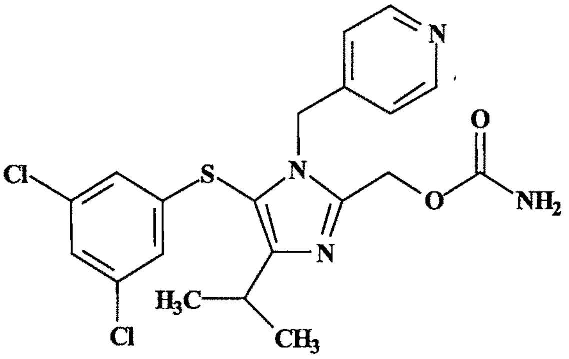

Compound 20
Capravirine (AG1549)

The NNRTIs *cis*-cyclopropylurea-PETT [97] and PBO derivatives [99] are orally bioavailable and penetrate well into the brain. The broad, potent antiviral activity, and favorable pharmacokinetic profile, have led to the selection of PNU-142721 (**21**) for clinical studies [91]; and DPC 961, DPC 963, DPC 082 and DPC 083 for clinical development [94].

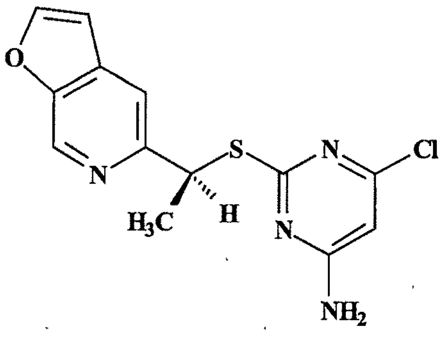

Compound 21
PNU-142721

(+)-Calanolide A (**22**) is the only naturally occurring NNRTI: it was first isolated from a tropical tree (*Calophyllum lanigerum*) and has already been the subject of a phase I clinical study in healthy, HIV-negative individuals [103].

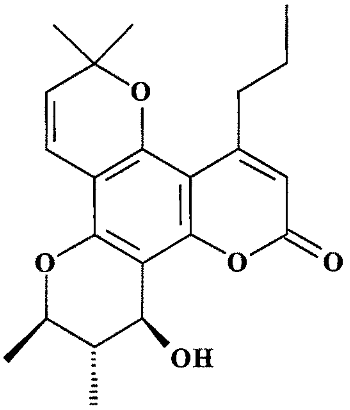

Compound 22
(+)-Calanolide A

Recently, an unexpected effect of NNRTIs on HIV-1 RT dimerization was documented [104]: several NNRTIs, including efavirenz, were found to enhance the association between the RT subunits p66 and p51, apparently due to a conformational change in the p66 subunit that resulted in enhanced binding to the p51 subunit. It remains to be established if this enhanced dimerization has any bearing on the anti-HIV-1 potency of the NNRTIs.

8. HIV integrase inhibitors

Retrovirus integration requires at least two viral components, the retroviral enzyme integrase, and *cis*-acting sequences at the retroviral DNA termini U3 and U5 ends of the long terminal repeats (LTRs). Since HIV, like other retroviruses, cannot replicate without integration into a host chromosome, integrase has been considered as an attractive therapeutic target. Numerous compounds have been described as inhibitors of HIV-1 integrase (for a recent review, see Ref. [105]): for example, polyamides, bisdistamycins and lexitropsins [106], polyhydroxylated aromatic type of compounds, including ellagic acid, purpurogallin, 4,8,12-trioxatricornan and hypericin [107] and a series of thiazolothiazepine derivatives, preferably possessing the pentatomic moiety SC(O)CNC(O) with two carbonyl groups [108]. The problem with integrase inhibitors is that while they might be effective in an enzyme-based assay, their anti-HIV activity in cell culture may be masked by cytotoxicity, and if they do exhibit anti-HIV activity, this could, at least in some cases, be attributed to antiviral actions targeted at other steps in the HIV replicative cycle.

L-chicoric acid [109–111] is such a case. L-chicoric acid is structurally reminiscent of curcumin [112], 3,5-dicaffeoylquinic acid [113], rosmarinic acid [114] and dicaffeoyltartaric acids (DCTAs) [115], and all these compounds have been reported to inhibit HIV-1 integrase. Integrase was identified as the molecular target for the action of L-chicoric acid (**23**) since a single amino acid substitution (G140S) in the integrase rendered the corresponding HIV-1 mutant resistant to L-chicoric acid [111]. We have recently demonstrated [116], however, that L-chicoric acid owes its anti-HIV activity in cell-culture to an interaction with the viral envelope gp120. Upon repeated passages of the virus in the presence of the compound, mutations were found in the V2, V3 and V4 loop of gp120, while no mutations were seen in the integrase. We did confirm that in an enzymatic assay L-chicoric acid inhibited HIV integrase activity, but integrase carrying the G140S mutation appeared to be as sensitive to the inhibitory effect of L-chicoric acid as the wild-type integrase. Furthermore, L-chicoric acid proved inactive against HIV strains that were resistant to polyanionic compounds known to interact at the virus adsorption level, and time-of-addition experiments further corroborated an interaction of L-chicoric acid at the virus adsorption stage [116].

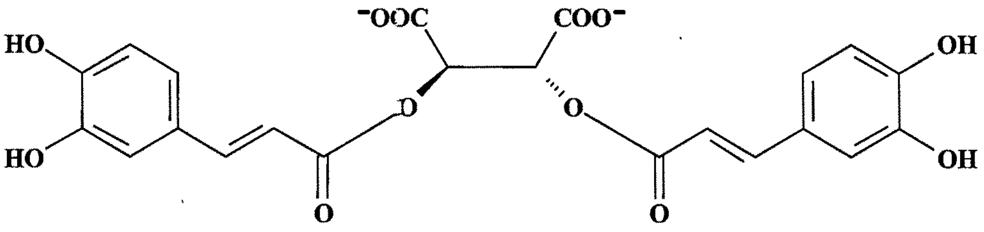

Compound 23
L-chicoric acid

Recently, the structure of the HIV-1 integrase core domain complexed with an inhibitor [1-(5-chloroindol-3-yl)-3-hydroxy-3-(2*H*-tetrazol-5-yl)-propenone] has been described as a platform for structure-based design of novel HIV-1 integrase inhibitors [117]. This was followed by the description of a number of diketo acids (such as L-731,988 and L-708,906) as inhibitors of the integrase-mediated strand transfer reaction that leads to the covalent linkage of the viral DNA 3′ends to the cellular (target) DNA [107]. These compounds were also found to inhibit HIV-1 replication in cell culture. Furthermore, mutations in the HIV-1 integrase conferred resistance to the inhibitory effects of the compounds on both strand transfer and HIV-1 infectivity [118]. Thus, it was surmised that these diketo acids owe their antiviral activity exclusively to inhibition of one of the two catalytic functions of integrase, namely strand transfer [the other catalytic function being endonucleolytic processing of the (pro)viral DNA to remove the terminal dinucleotide (GT) from the 3′ end]. Starting from L-731, 988 (**24**), additional 4-aryl-2,4-dioxobutanoic acid derivatives have been reported as inhibitors of HIV-1 integrase [119].

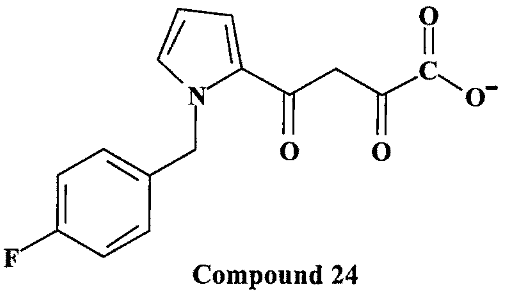

Compound 24
L-731,988

9. Transcription (transactivation) inhibitors

At the transcription level, HIV gene expression may be inhibited by compounds that interact with cellular factors that bind to the LTR promoter and that are needed for basal level transcription, such as the NF-κB inhibitors [120]. Greater specificity, however, can be expected from those compounds that specifically inhibit the transactivation of the HIV LTR promoter by the viral Tat (*trans*-activating) protein [120]. Tat has pleiotropic effects: it not only activates the transcription of HIV-1 RNA, but also binds to a number of receptors, i.e. on smooth muscle and skeletal muscle cells [121]: the basic domain of Tat may be important, not only for translocation but also for nuclear localisation and *trans*-activation, and thus targeting of the Tat basic domain may provide great scope for therapeutic intervention in HIV-1 infection [121].

A number of compounds have been reported to inhibit HIV-1 replication in both acutely and chronically infected cells through interference with the transcription process: i.e. fluoroquinoline derivatives [122]. The inhibitory effects of the fluoroquinolines (K-12) [8-difluoromethoxy-1-ethyl-6-fluoro-1,4-dihydro-7-[4-(2-methoxyphe-nyl)-1-piperazinyl]-4-oxoquinoline-3-carboxylic acid] and (K-37) [7-(3,4-dehydro-4-phenyl-1-piperidinyl)-1,4-dihydro-6-fluoro-1-methyl-8-trifluoromethyl-4-oxoquinoline-3-carboxylic acid] (**25**) on the HIV-1 LTR-driven gene expression may at least in part be attributed to inhibition of Tat [123] or other RNA-dependent transactivators [124].

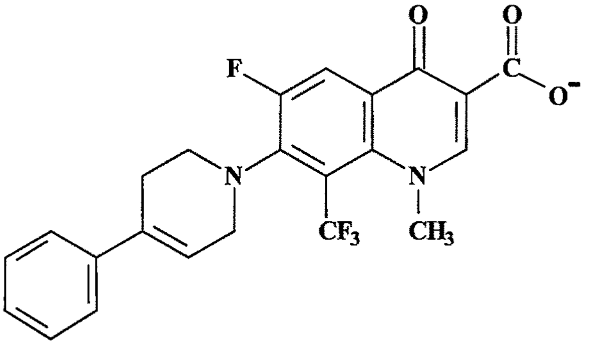

Compound 25
Fluoroquinoline K-37

The bistriazoloacridone temacrazine [1,4-bis(3-(6-oxo-6H-v-triazolo[4,5,1]acridin-5-yl-aminopropyl)piperazine] (**26**) was found to block HIV-1 RNA transcription from the HIV proviral DNA without interfering with the transcription of any cellular genes [125]: the compound inhibited HIV-1 replication in both acutely and chronically infected cells. Resistance was generated upon serial passage of the virus in the presence of temacrazine and was associated with several unique nucleotide changes in HIV-1 LTR at positions − 1, − 2 and + 111 relative to the start of transcription [126].

Tat peptide analogs, encompassing the Tat core domain (amino acid residues 36–50) [127], or the basic domain (amino acids 48–56: RKKRRQRRR) [128] have been reported to inhibit HIV-1 replication, and, as expected, these peptide analogs were able to effectively block the Tat transactivation process. The 9-mer peptoid CGP64222 (**27**), which is structurally reminiscent of the amino acid 48–56 sequence RKKRRQRRR of Tat, was also reported, on the one hand, to block the Tat/TAR interaction, and, on the other hand, to suppress HIV-1 replication [129]. We have demonstrated, however, that the peptoid CGP64222 owes its anti-HIV activity in cell culture primarily to an interaction with CXCR4, the coreceptor for X4 HIV strains [130], which is, perhaps, not surprising given the structural similarity of CGP64222 to the other, polypeptidic, CXCR4

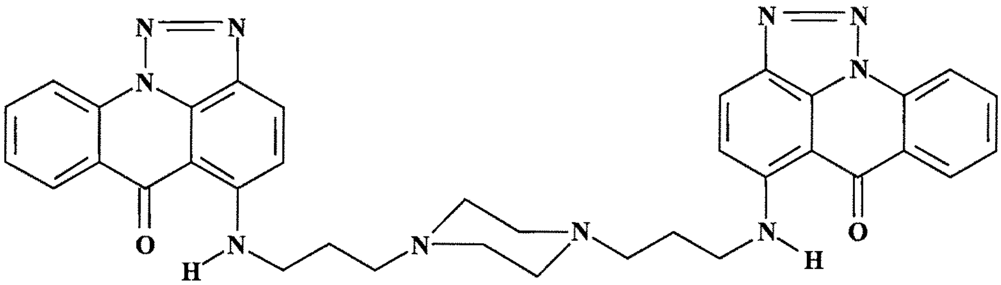

Compound 26
Temacrazine

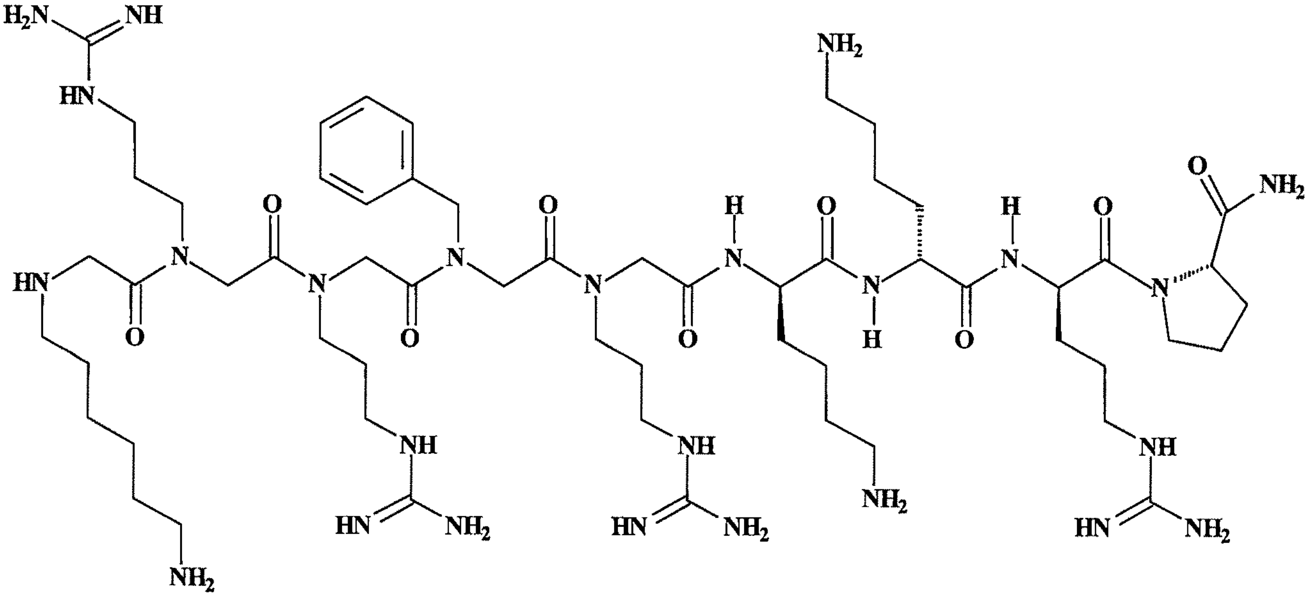

Compound 27
CGP64222

antagonists such as T22 [23] and nona-arginine (ALX40-4C) [24]. In fact, Tat itself (following its extracellular release) has recently been shown to block CXCR4-dependent HIV-1 infection [131], presumably through blockade of CXCR4 by the above-mentioned 48–56 amino acid portion (RKKRRQRRR) of the molecule.

Flavopiridol (L86-8275, HMR1275) is a cyclin-dependent kinase (Cdk) and P-TEFb inhibitor, which is in clinical trials for the treatment of cancer because of its antiproliferative properties. P-TEFb is a protein kinase composed of Cdk9 and cyclin T1 and secures the elongation phase of transcription by RNA polymerase II (through phosphorylation of the carboxyl-terminal domain). Tat forms a triple complex with P-TEFb (composed of Cdk9 and cyclin T1) and the nascent transcript from the HIV-1 LTR promoter. Consistent with its ability to block P-TEFb, flavopiridol (**28**) was found to block Tat transactivation, and, concomitantly, also inhibited HIV replication [132].

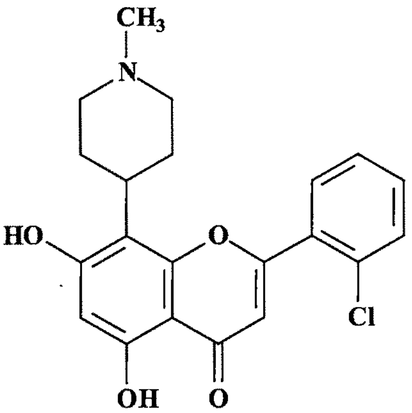

Compound 28
Flavopiridol

10. HIV PIs

HIV PIs prevent the cleavage of the gag and gag-pol precursor polyproteins to the structural proteins (p17, p24, p7, p6, p2, p1) and functional proteins (protease, RT/RNase H, integrase), thus arresting maturation and thereby blocking infectivity of the nascent virions [133]. The HIV PIs have been tailored after the target peptidic linkage in the gag and gag-pol polyproteins that are cleaved by the protease, viz. the phenylalanine–proline sequence at positions 167 and 168 of the gag-pol polyprotein. All PIs that are currently licensed for the treatment of HIV infection, namely saquinavir, ritonavir, indinavir, nelfinavir, amprenavir and lopinavir, share the same structural determinant, i.e. an hydroxyethylene (instead of the normal peptidic) bond, which makes them nonscissile substrate analogues for the HIV protease. All six licensed PIs follow the same principle; that is, they act as peptidomimetic inhibitors of HIV protease [134]. Lopinavir is co-dosed with ritonavir at 400/100 mg twice daily. The reason for this combination is that ritonavir strongly inhibits the metabolism of lopinavir and allows lopinavir to reach much higher plasma drug levels upon oral administration [135]. In phase III clinical trials is atazanavir (BMS-232632) (**29**), which has been accredited with a favorable resistance profile that does not parallel any of the other PIs currently in clinical use, as well as a favorable pharmacokinetic profile that would allow once-daily dosing [136].

Resistance mutations have been reported for most, if not all, peptidomimetic inhibitors of HIV protease. This has prompted the search for new, nonpeptidic inhibitors of HIV protease, which, in addition to a broader anti-HIV activity spectrum, might also offer increased oral bioavailability and/or pharmacokinetic properties. Examples of nonpeptidic PIs of HIV protease include 4-hydroxycoumarins and 4-

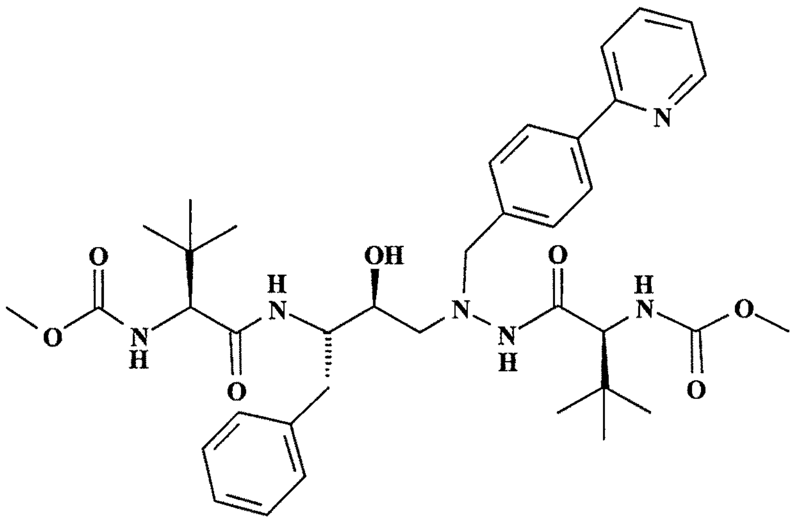

Compound 29
Atazanavir (BMS-232632)

hydroxy-2-pyrones [137], sulfonamide-substituted derivatives [138], cyclic ureas (i.e. DMP-323 and DMP-450) [139,140], cyclic cyanoguanidines [141], aza-dipeptide analogues [142], and tipranavir (PNU-140690), a sulfonamide-containing 5,6-dihydro-4-hydroxy-2-pyrone [143–145]. The major advantage of the cyclic urea mozenavir (DMP-450) (**30**) is its substantial oral bioavailability observed in all species examined, including man [140]. DMP-450 has been the subject of phase I/II dose-escalating clinical studies and appears to have good antiviral activity and tolerability at all doses tested [146]. The new aza-dipeptide analogues combine excellent anti-HIV potency with high blood drug levels after oral administration, and, furthermore, they show no cross-resistance with saquinavir-resistant HIV strains [142]. Tipranavir (**31**) showed low cross-resistance to HIV strains that were resistant to the established (peptidomimetic) inhibitors of HIV protease [145]. Also, tipranavir retained marked activity against HIV-1 isolates derived from patients with multidrug resistance to other PIs [147].

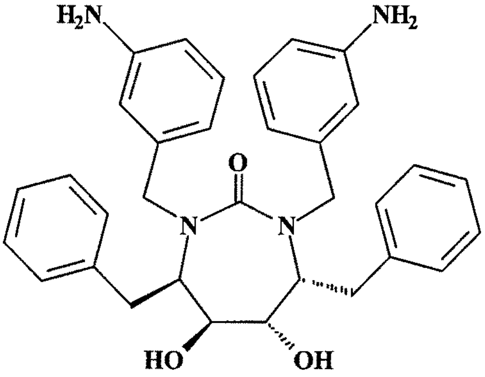

Compound 30
Mozenavir (DMP-450)

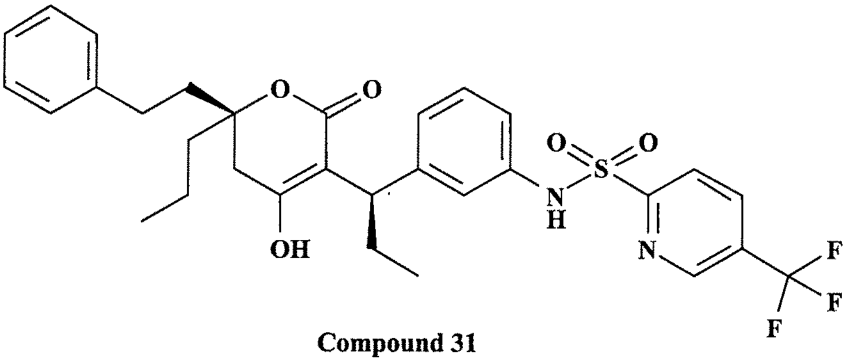

Compound 31
Tipranavir (PNU-140690)

Independently of the HIV protease itself, proteasomes play a role in the processing of the gag polyprotein, and proteasome inhibitors, such as epoxomicin, have been shown to inhibit gag polyprotein processing as well as HIV maturation and release [148]. While a potentially interesting approach, it remains to be seen whether inhibitors of the proteasome/ubiquitin system display sufficient specificity in their anti-HIV action so as to suppress virus replication without (overt) cytotoxicity.

11. Conclusions

In recent years, an ever increasing number of compounds have been uncovered as anti-HIV agents targeted at virtually any step of the virus replicative cycle: adsorption, entry, fusion, uncoating, reverse transcription, integration, transcription (transactivation) and maturation. In addition to the "newer" NRTIs, NNRTIs and PIs, various other compounds, i.e. those that are targeted at viral entry (i.e. CXCR4 and CCR5 antagonists) and virus-cell adsorption/fusion (i.e. compounds interacting with either gp120 or gp41), offer great potential for the treatment of HIV infections. Quite a number of compounds are capable of interacting with more than one target. Two examples in point are the DCTA L-chicoric acid, and the nonapeptoid CGP 64222. L-chicoric acid was originally identified as an integrase inhibitor, and the nonapeptoid as a transactivation (Tat) antagonist, and their anti-HIV activity in acutely infected cells was ascribed to interference with the integration and transactivation process, respectively. As it now appears, L-chicoric acid primarily interacts as a virus adsorption inhibitor, and the nonapeptoid as a CXCR4 antagonist, and thus these compounds owe their anti-HIV activity mainly to interference with an early event (adsorption, entry) of the HIV replicative cycle.

Acknowledgements

Prof. Erik De Clercq holds the Professor P. De Somer Chair of Microbiology at the Katholieke Universiteit Leuven School of Medicine and thanks Christiane Callebaut for her invaluable editorial assistance.

References

[1] J A Tavel, K D. Miller, H Masur, Clin Infect Dis. 28 (1999) 643–676.

[2] Z Zhang, T. Schuler, M. Zupancic, S Wietgrefe, K.A Staskus, K A Reimann, T A Reinhart, M. Rogan, W Cavert, C J Miller, E S Veazey, D Notermans, S. Little, S A Danner, D D Richman, D Havlir, J Wong, H.L. Jordan, T.W Schacker, P Racz, K. Tenner-Racz, N.L. Letvin, S. Wolinsky, A.T Haase, Science 286 (1999) 1353–1357

[3] K.C. Santhosh, G.C Paul, E. De Clercq, C Pannecouque, M Witvrouw, T L Loftus, J A Turpin, R.W Buckheit Jr, M Cushman, J Med Chem 44 (2001) 703–714

[4] M. Witvrouw, E De Clercq, Gen Pharmacol 29 (1997) 497–511

[5] W R Gallaher, J.M. Ball, R.F. Garry, A M. Martin-Amedee, R C Montelaro, AIDS Res Hum Retroviruses 11 (1995) 191–202

[6] M. Moulard, H Lortat-Jacob, I Mondor, G. Roca, R Wyatt, J Sodroski, L. Zhao, W. Olson, P.D Kwong, Q.J Sattentau, J Virol 74 (2000) 1948–1960.

[7] D Shukla, J Liu, P Blaiklock, N.W Shworak, X Bai, J D Esko, G H Cohen, R J Eisenberg, R D Rosenberg, P G. Spear, Cell 99 (1999) 13–22

[8] Y Chen, T Maguire, R E Hileman, J.R Fromm, J D. Esko, R J Linhardt, R M. Marks, Nat. Med 3 (1997) 866–871

[9] C.-M. Su, C -L Liao, Y-L Lee, Y-L Lin, Virology 286 (2001) 206–215

[10] M Luscher-Mattli, Antiviral Chem. Chemother 11 (2000) 249–259

[11] B C Herold, N Bourne, D Marcellino, R Kirkpatrick, D.M Strauss, L.J. Zaneveld, D P. Waller, R A Anderson, C.J. Chany, B.J Barham, L R Stanberry, M.D. Cooper, J. Infect Dis 181 (2000) 770–773

[12] J.F Berson, D. Long, B J Doranz, J Rucker, F.R Jirik, R W Doms, J. Virol 70 (1996) 6288–6295

[13] B J. Doranz, Z.H. Lu, J. Rucker, T Y. Zhang, M Sharron, Y.H Cen, Z.X. Wang, H.H Guo, J.G. Du, M A Accavitti, R W. Doms, S.C Peiper, J. Virol. 71 (1997) 6305–6314.

[14] P Menten, S Struyf, E Schutyser, A. Wuyts, E De Clercq, D. Schols, P Proost, J. Van Damme, J Clin Invest 104 (1999) R1–R5

[15] R J Nibbs, J Yang, N R Landau, J.H. Mao, G J. Graham, J Biol. Chem 274 (1999) 17478–17483

[16] S Aquaro, P Menten, S. Struyf, P Proost, J. Van Damme, E De Clercq, D. Schols, J Virol 75 (2001) 4402–4406

[17] M. Baba, O Nishimura, N Kanzaki, M Okamoto, H Sawada, Y Iizawa, M Shiraishi, Y. Aramaki, K Okonogi, Y Ogawa, K Meguro, M. Fujino, Proc. Natl Acad Sci U S. A. 96 (1999) 5698–5703.

[18] T Dragic, A Trkola, D.A Thompson, E G. Cormier, F A Kajumo, E. Maxwell, S W Lin, W. Ying, S.O Smith, T P. Sakmar, J P Moore, Proc. Natl Acad. Sci U. S A 97 (2000) 5639–5644

[19] M Shiraishi, Y Aramaki, M Seto, H. Imoto, Y Nishikawa, N Kanzaki, M Okamoto, H Sawada, O Nishimura, M. Baba, M. Fujino, J. Med Chem 43 (2000) 2049–2063.

[20] M Baroudy, Abstracts of the 7th Conference on Retroviruses and Opportunistic Infections, San Francisco, California, USA, 30 January–2 February 2000, no S17

[21] G Reyes, Abstracts of the 8th Conference on Retroviruses and Opportunistic Infections, Chicago, Illinois, USA, 4–8 February 2001, no L11

[22] D Schols, S. Struyf, J. Van Damme, J A Esté, G. Henson, E De Clercq, J Exp Med 186 (1997) 1383–1388.

[23] T Murakami, T Nakajima, Y Koyanagi, K Tachibana, N. Fujii, H. Tamamura, N Yoshida, M Waki, A Matsumoto, O Yoshie, T Kishimoto, N. Yamamoto, T Nagasawa, J Exp Med 186 (1997) 1389–1393

[24] B.J Doranz, K. Grovit-Ferbas, M P Sharron, S.H. Mao, M B. Goetz, E S. Daar, R.W. Doms, W A O'Brien, J Exp Med 186 (1997) 1395–1400.

[25] E De Clercq, Mol. Pharmacol 57 (2000) 833–839

[26] G J Bridger, R T. Skerlj, S Padmanabhan, S.A Martellucci, G W Henson, S Struyf, M Witvrouw, D Schols, E. De Clercq, J. Med Chem 42 (1999) 3971–3981

[27] E De Clercq, N Yamamoto, R Pauwels, M. Baba, D Schols, H. Nakashima, J. Balzarini, Z. Debyser, B A Murrer, D Schwartz, D Thornton, G. Bridger, S. Fricker, G Henson, M. Abrams, D Picker, Proc Natl. Acad Sci U S A 89 (1992) 5286–5290

[28] E. De Clercq, N. Yamamoto, R. Pauwels, J. Balzarini, M Witvrouw, K. De Vreese, Z. Debyser, B Rosenwirth, P. Peichl, R. Datema, D Thornton, R. Skerlj, F. Gaul, S Padmanabhan, G Bridger, G Henson, M Abrams, Antimicrob. Agents Chemother. 38 (1994) 668–674.

[29] D Schols, J A Esté, G Henson, E De Clercq, Antiviral Res 35 (1997) 147–156.

[30] G A Donzella, D Schols, S.W Lin, J A Esté, K.A. Nagashima, P J Maddon, G.P. Allaway, T.P Sakmar, G. Henson, E De Clercq, J.P Moore, Nat Med 4 (1998) 72–77

[31] B Labrosse, A. Brelot, N. Heveker, N. Sol, D Schols, E De Clercq, M Alizon, J Virol. 72 (1998) 6381–6388.

[32] S Hatse, K. Princen, L.O Gerlach, G. Bridger, G. Henson, E. De Clercq, T.W Schwartz, D Schols, Mol. Pharmacol. 60 (2001) 164–173

[33] J.A. Esté, C Cabrera, J. Blanco, A Gutierrez, G Bridger, G. Henson, B. Clotet, D Schols, E. De Clercq, J Virol 73 (1999) 5577–5585.

[34] R Datema, L Rabin, M. Hincenbergs, M.B. Moreno, S. Warren, V Linquist, B Rosenwirth, J Seifert, J.M McCune, Antimicrob Agents Chemother. 40 (1996) 750–754

[35] C W. Hendrix, C. Flexner, R T MacFarland, C Giandomenico, E.J. Fuchs, E Redpath, G Bridger, G W. Henson, Antimicrob Agents Chemother. 44 (2000) 1667–1673.

[36] A. Müller, B Homey, H Soto, N. Ge, D Catron, M.E Buchanan, T. McClanahan, E Murphy, W. Yuang, S.N. Wagner, J L Barrera, A Mohar, E. Verastegui, A Zlotnik, Nature 410 (2001) 50–56.

[37] J G Sodroski, Cell 99 (1999) 243–246

[38] C T Wild, D.C Shugars, T.K. Greenwell, C B McDanal, T J Matthews, Proc. Natl. Acad. Sci. U. S A 91 (1994) 9770–9774

[39] J M Kilby, S. Hopkins, T.M Venetta, B DiMassimo, G A Cloud, J.Y Lee, L. Alldredge, E Hunter, D. Lambert, D. Bolognesi, T. Matthews, M.R Johnson, M.A. Nowak, G M Shaw, M S. Saag, Nat. Med 4 (1998) 1302–1307

[40] B Conway, Curr Opin Anti-Infect. Invest Drugs 2 (2000) 317–322.

[41] J F Mayaux, A Bousseau, R Pauwels, T Huet, Y. Henin, N Dereu, M Evers, F. Soler, C Poujade, E De Clercq, J B Le Pecq, Proc. Natl. Acad. Sci U. S. A 91 (1994) 3564–3568.

[42] B. Labrosse, O Pleskoff, N. Sol, C Jones, Y Henin, M Alizon, J. Virol 71 (1997) 8230–8236

[43] B. Labrosse, C. Treboute, M Alizon, J. Virol. 74 (2000) 2142–2150

[44] S.L Holz-Smith, I C Sun, L. Jin, T J. Matthews, K.H Lee, C H Chen, Antimicrob. Agents Chemother 45 (2001) 60–66

[45] T Kanamoto, Y. Kashiwada, K. Kanbara, K. Gotoh, M Yoshimori, T Goto, K Sano, H. Nakashima, Antimicrob Agents Chemother. 45 (2001) 1225–1230.

[46] W.G. Rice, J A. Turpin, L O Arthur, L.E. Henderson, Int Antiviral News 3 (1995) 87–89.

[47] M. Witvrouw, J. Balzarini, C Pannecouque, S. Jhaumeer-Laulloo, J.A Esté, D. Schols, P Cherepanov, J.-C. Schmit, Z. Debyser, A -M Vandamme, J Desmyter, S.R Ramadas, E. De Clercq, Antimicrob Agents Chemother 41 (1997) 262–268.

[48] W.G Rice, D.C Baker, C A Schaeffer, L. Graham, M. Bu, S Terpening, D. Clanton, R Schultz, J.P. Bader, R W. Buckheit Jr., L Field, P K Singh, J A. Turpin, Antimicrob Agents Chemother 41 (1997) 419–426

[49] M. Vandevelde, M. Witvrouw, J -C. Schmit, S. Sprecher, E. De Clercq, J.P. Tassignon, AIDS Res Hum. Retroviruses 12 (1996) 567–568.

[50] W G. Rice, J.A. Turpin, M. Huang, D. Clanton, R W. Buckheit Jr., D.G. Covell, A. Wallqvist, N.B. McDonnell, R.N DeGuzman, M F Summers, L. Zalkow, J P Bader, R D Haugwitz, E.A. Sausville, Nat Med 3 (1997) 341–345.

[51] J.A Turpin, C.A. Schaeffer, S J Terpening, L. Graham, M. Bu, W.G Rice, Antiviral Chem. Chemother 8 (1997) 60–69.

[52] L Berthoux, C. Péchoux, J.-L Darlix, J Virol. 73 (1999) 10000–10009

[53] M. Huang, A. Maynard, J.A Turpin, L. Graham, G M. Janini, D.G. Covell, W G Rice, J. Med. Chem 41 (1998) 1371–1381.

[54] F.-D. Goebel, R Hemmer, J.-C. Schmit, J R. Bogner, E. De Clercq, M. Witvrouw, C. Pannecouque, R. Valeyev, M. Vandevelde, H Margery, J -P Tassignon, AIDS 15 (2001) 33–45.

[55] J. Tassignon, J. Ismaili, A Le Moine, F Van Laethem, O. Leo, M. Vandevelde, M. Goldman, Nat Med 5 (1999) 947–950

[56] E. De Clercq, J. Med. Chem. 38 (1995) 2491–2517.

[57] P.-M. Girard, P.S. Pegram, B. Diquet, R. Anderson, F Raffi, R Tubiana, D. Sereni, D Boerner, J Acquired Immune Defic Syndr 23 (2000) 227–235

[58] L Naesens, R Snoeck, G Andrei, J. Balzarini, J. Neyts, E De Clercq, Antiviral Chem. Chemother 8 (1997) 1–23.

[59] M S Smith, L Foresman, G.J. Lopez, J. Tsay, D Wodarz, J.D. Lifson, A. Page, C. Wang, Z. Li, I Adany, S Buch, N. Bischofberger, O Narayan, Virology 277 (2000) 306–315.

[60] J.-M de Muys, H Gourdeau, N. Nguyen-Ba, D.L. Taylor, P.S Ahmed, T. Mansour, C. Locas, N. Richard, M.A Wainberg, R F Rando, Antimicrob Agents Chemother 43 (1999) 1835–1844.

[61] Z. Gu, M A Wainberg, N. Nguyen-Ba, L L'Heureux, J.-M de Muys, T.L. Bowlin, R.F. Rando, Antimicrob Agents Chemother. 43 (1999) 2376–2382.

[62] H Uchida, E.N. Kodama, K. Yoshimura, Y Maeda, P Kosalaraksa, V Maroun, Y.L Qiu, J Zemlicka, H Mitsuya, Antimicrob. Agents Chemother. 43 (1999) 1487–1490.

[63] K Yoshimura, R. Feldman, E. Kodama, M.F. Kavlick, Y.L Qiu, J. Zemlicka, H Mitsuya, Antimicrob Agents Chemother 43 (1999) 2479–2483

[64] E.I. Kodama, S. Kohgo, K. Kitano, H. Machida, H. Gatanaga, S Shigeta, M. Matsuoka, H. Ohrui, H. Mitsuya, Antimicrob. Agents Chemother. 45 (2001) 1539–1546

[65] P.A. Furman, J. Jeffrey, L.L Kiefer, J.Y. Feng, K.S. Anderson, K. Borroto-Esoda, E. Hill, W.C. Copeland, C K Chu, J -P. Sommadossi, I. Liberman, R F. Schinazi, G R Painter, Antimicrob. Agents Chemother. 45 (2001) 158–165

[66] A.H. Corbett, J C Rublein, Curr. Opin. Invest Drugs 2 (2001) 348–353

[67] C A Stoddart, M E Moreno, VD Linquist-Stepps, C Bare, M.R Bogan, A. Gobbi, R W Buckheit Jr, J. Bedard, R F. Rando, J.M McCune, Antimicrob Agents Chemother 44 (2000) 783–786

[68] D.L Taylor, P.S. Ahmed, A S Tyms, L J. Wood, L A Kelly, P Chambers, J Clarke, J Bedard, T L Bowlin, R F. Rando, Antiviral Chem Chemother. 11 (2000) 291–301.

[69] C. Perigaud, A M Aubertin, S. Benzaria, H. Pelicano, J L. Girardet, G Maury, G. Gosselin, A Kirn, J -L Imbach, Biochem Pharmacol 48 (1994) 11–14

[70] C McGuigan, H.W Tsang, D Cahard, K Turner, S. Velazquez, A Salgado, L. Bidois, L. Naesens, E De Clercq, J. Balzarini, Antiviral Res. 35 (1997) 195–204.

[71] A Q Siddiqui, C Ballatore, C McGuigan, E De Clercq, J Balzarini, J Med Chem. 42 (1999) 393–399.

[72] A Q. Siddiqui, C McGuigan, C. Ballatore, F Zuccotto, I.H De Clercq, E. De Clercq, J Balzarini, J Med. Chem 42 (1999) 4122–4128

[73] D Saboulard, L Naesens, D Cahard, A. Salgado, R. Pathirana, S Velazquez, C. McGuigan, E De Clercq, J Balzarini, Mol. Pharmacol 56 (1999) 693–704

[74] S. Aquaro, O. Wedgwood, C. Yarnold, D Cahard, R. Pathirana, C. McGuigan, R. Calio, E. De Clercq, J. Balzarini, C -F Perno, Antimicrob. Agents Chemother. 44 (2000) 173–177

[75] C Meier, M Lorey, E De Clercq, J. Balzarini, Bioorg Med Chem Lett 7 (1997) 99–104

[76] C Meier, T Knispel, E. De Clercq, J. Balzarini, Bioorg Med Chem Lett. 7 (1997) 1577–1582.

[77] C. Meier, M. Lorey, E De Clercq, J. Balzarini, J Med. Chem. 41 (1998) 1417–1427

[78] C Meier, T Knispel, E De Clercq, J Balzarini, J. Med Chem 42 (1999) 1604–1614

[79] J. Balzarini, S Aquaro, T Knispel, C Rampazzo, V. Bianchi, C.-F Perno, E De Clercq, C. Meier, Mol Pharmacol. 58 (2000) 928–935

[80] E. De Clercq, Antiviral Res 38 (1998) 153–179

[81] J Ren, R M. Esnouf, A.L Hopkins, J Warren, J Balzarini, D.I. Stuart, D K Stammers, Biochemistry 37 (1998) 14394–14403

[82] S G Deeks, J. Acquired Immune Defic Syndr 26 (2001) S25–S33

[83] G Borkow, D Arion, M A. Wainberg, M A Parniak, Antimicrob. Agents Chemother 43 (1999) 259–263

[84] G Borkow, J. Barnard, T.M Nguyen, A Belmonte, M A. Wainberg, M.A. Parniak, J. Virol 71 (1997) 3023–3030

[85] J. Balzarini, L Naesens, E Verbeken, M Laga, L Van Damme, M. Parniak, L. Van Mellaert, J Anné, E De Clercq, AIDS 12 (1998) 1129–1138.

[86] M Witvrouw, M E. Arranz, C Pannecouque, R Declercq, H Jonckheeree, J.-C. Schmit, A.-M Vandamme, J.A. Diaz, S.T. Ingate, J. Desmyter, R. Esnouf, L Van Meervelt, S Vega, J Balzarini, E De Clercq, Antimicrob Agents Chemother 42 (1998) 618–623

[87] W Prince, K. Moore, L Cass, N Dallow, A Jones, J -P Kleim, P Mutch, M St. Clair, Abstracts of the 12th International Conference on Antiviral Research, Jerusalem, Israel, 21–25 March 1999, Antiviral Res 41 (1999) A48

[88] T. Fujiwara, A. Sato, M el-Farrash, S. Miki, K. Abe, Y Isaka, M Kodama, Y Wu, L B. Chen, H. Harada, H. Sugimoto, M. Hatanaka, Y Hinuma, Antimicrob Agents Chemother. 42 (1998) 1340–1345

[89] J Ren, C Nichols, L E Bird, T. Fujiwara, H Sugimoto, D I Stuart, D K Stammers, J. Biol Chem 275 (2000) 14316–14320

[90] W M Brown, Curr Opin Anti-Infect Invest. Drugs 2 (2000) 286–294.

[91] D G. Wishka, D R Graber, L A Kopta, R A Olmsted, J.M. Friis, J.D. Hosley, W J. Adams, E.P. Seest, T M. Castle, L A. Dolak, B J Keiser, Y Yagi, A. Jeganathan, S T Schlachter, M.J Murphy, G J. Cleek, R A. Nugent, S M. Poppe, S.M Swaney, F Han, W. Watt, W.L White, T -J Poel, R C Thomas, R L Voorman, K J Stefanski, R.G. Stehle, W G Tarpley, J Morris, J Med. Chem. 41 (1998) 1357–1360

[92] C Mao, E A. Sudbeck, T.K. Venkatachalam, F M. Uckun, Bioorg Med Chem Lett 9 (1999) 1593–1598

[93] D.L Taylor, P.S. Ahmed, P Chambers, A S Tyms, J Bedard, J

Duchaine, G Falardeau, J F Lavallee, W Brown, R.F Rando, T Bowlin, Antiviral Chem Chemother. 10 (1999) 79–86.

[94] J W Corbett, S S. Ko, J D Rodgers, S Jeffrey, L T. Bacheler, R.M. Klabe, S. Diamond, C.M Lai, S.R. Rabel, J A. Saye, S.P Adams, G L Trainor, P S. Anderson, S K Erickson-Viitanen, Antimicrob. Agents Chemother. 43 (1999) 2893–2897

[95] F.M. Uckun, S. Pendergrass, D Maher, D Zhu, L Tuel-Ahlgren, C. Mao, T.K Venkatachalam, Bioorg. Med. Chem Lett. 9 (1999) 3411–3416

[96] F M Uckun, C Mao, S Pendergrass, D. Maher, D Zhu, L. Tuel-Ahlgren, T.K Venkatachalam, Bioorg Med Chem. Lett. 9 (1999) 2721–2726.

[97] M. Hogberg, C. Sahlberg, P. Engelhardt, R Noreen, J Kangasmetsa, N.G Johansson, B. Öberg, L. Vrang, H. Zhang, B L. Sahlberg, T Unge, S Lövgren, K Fridborg, K Backbro, J Med. Chem 42 (1999) 4150–4160

[98] A Casimiro-Garcia, M Micklatcher, J A Turpin, T L. Stup, K Watson, R.W. Buckheit, M. Cushman, J Med Chem. 42 (1999) 4861–4874

[99] G. Campiani, E Morelli, M. Fabbrini, V Nacci, G. Greco, E. Novellino, A. Ramunno, G. Maga, S. Spadari, G Caliendo, A. Bergamini, E Faggioli, I. Uccella, F Bolacchi, S. Marini, M Coletta, A Nacca, S Caccia, J Med Chem 42 (1999) 4462–4470

[100] G. Campiani, F. Aiello, M. Fabbrini, E Morelli, A Ramunno, S Armaroli, V Nacci, A Garofalo, G. Greco, E Novellino, G. Maga, S Spadari, A Bergamini, L Ventura, B Bongiovanni, M. Capozzi, F. Bolacchi, S. Marini, M Coletta, G. Guiso, C Caccia, J. Med Chem 44 (2001) 305–315

[101] R W Buckheit Jr., K Watson, V. Fliakas-Boltz, J. Russell, T L. Loftus, M C. Osterlin, J.A. Turpin, L A Pallansch, E L White, J W. Lee, S.H. Lee, J W. Oh, H.S. Kwon, S G Chung, E H Cho, Antimicrob Agents Chemother 45 (2001) 393–400.

[102] K Andries, M -P. de Béthune, M.J. Kukla, H. Azijn, P.J. Lewi, P A J. Janssen, R Pauwels, Abstracts of the 40th Interscience Conference on Antimicrobial Agents and Chemotherapy, Toronto, Canada, 17–20 September 2000, no. 1840

[103] T. Creagh, J.L. Ruckle, D.T Tolbert, J Giltner, D A. Eiznhamer, B Dutta, M T. Flavin, Z Q. Xu, Antimicrob Agents Chemother 45 (2001) 1379–1386

[104] G. Tachedjian, M Orlova, S G Sarafianos, E Arnold, S P Goff, Proc Natl Acad Sci. U S A. 98 (2001) 7188–7193

[105] Y Pommier, C Marchand, N Neamati, Antiviral Res. 47 (2000) 139–148

[106] N. Neamati, A. Mazumder, S. Sunder, J M. Owen, M. Tandon, J W. Lown, Y. Pommier, Mol Pharmacol. 54 (1998) 280–290

[107] C M Farnet, B Wang, M Hansen, J R Lipford, L Zalkow, W E Robinson Jr, J. Siegel, F Bushman, Antimicrob. Agents Chemother. 42 (1998) 2245–2253.

[108] N Neamati, J A Turpin, H E Winslow, J L. Christensen, K Williamson, A Orr, W G Rice, Y Pommier, A Garofalo, A. Brizzi, G Campiani, I Fiorini, V Nacci, J. Med. Chem. 42 (1999) 3334–3341.

[109] W E Robinson Jr, M G Reinecke, S. Abdel-Malek, Q Jia, S.A Chow, Proc Natl. Acad. Sci U S. A. 93 (1996) 6326–6331

[110] W E Robinson Jr., Antiviral Res 39 (1998) 101–111

[111] P.J King, W.E Robinson Jr, J. Virol. 72 (1998) 8420–8424

[112] A Mazumder, K Raghavan, J Weinstein, K.W Kohn, Y. Pommier, Biochem. Pharmacol 49 (1995) 1165–1170

[113] W.E Robinson Jr, M Cordeiro, S Abdel-Malek, Q Jia, S.A. Chow, M.G. Reinecke, W M. Mitchell, Mol Pharmacol 50 (1996) 846–855

[114] A Mazumder, N. Neamati, S Sunder, J. Schulz, H. Pertz, E Eich, Y Pommier, J Med Chem 40 (1997) 3057–3063

[115] B McDougall, P J. King, B.W Wu, Z Hostomsky, M.G. Reinecke, W E Robinson Jr., Antimicrob. Agents Chemother 42 (1998) 140–146

[116] W Pluymers, N. Neamati, C Pannecouque, V Fikkert, C. Marchand T R. Burke Jr., Y Pommier, D. Schols, E. De Clercq, Z. Debyser, M. Witvrouw, Mol Pharmacol. 58 (2000) 641–648

[117] Y Goldgur, R. Craigie, G.H. Cohen, T. Fujiwara, T Yoshinaga, T Fujishita, H Sugimoto, T Endo, H Murai, D.R. Davies, Proc. Natl. Acad. Sci U S A. 96 (1999) 13040–13043.

[118] D.J. Hazuda, P Felock, M. Witmer, A. Wolfe, K. Stillmock, J A Grobler, A. Espeseth, L. Gabryelski, W Schleif, C. Blau, M D. Miller, Science 287 (2000) 646–650

[119] J S Wai, M.S Egbertson, L.S. Payne, T E. Fischer, M W Embrey, L.O. Tran, J.Y. Melamed, H.M. Langford, J.P. Guare Jr, L. Zhuang, V.E Grey, J P Vacca, M.K. Holloway, A.M Naylor-Olsen, D J. Hazuda, P J. Felock, A.L. Wolfe, K.A Stillmock, W A Schleif, L J. Gabryelski, S.D Young, J. Med. Chem. 43 (2000) 4923–4926

[120] D. Daelemans, A -M. Vandamme, E De Clercq, Antiviral Chem Chemother. 10 (1999) 1–14.

[121] K Watson, R J Edwards, Biochem. Pharmacol 58 (1999) 1521–1528

[122] M. Baba, M. Okamoto, M. Makino, Y. Kimura, T Ikeuchi, T Sakaguchi, T. Okamoto, Antimicrob. Agents Chemother. 41 (1997) 1250–1255

[123] M. Baba, M Okamoto, M. Kawamura, M. Makino, T Higashida, T. Takashi, Y Kimura, T Ikeuchi, T Tetsuka, T Okamoto, Mol Pharmacol. 53 (1998) 1097–1103

[124] H Okamoto, T.P Cujec, M. Okamoto, B.M. Peterlin, M. Baba, T Okamoto, Virology 272 (2000) 402–408

[125] J.A Turpin, R W Buckheit Jr., D Derse, M. Hollingshead, K Williamson, C. Palamone, M.C. Osterling, S A. Hill, L Graham, C A. Schaeffer, M. Bu, M Huang, W M Cholody, C J Michejda, W.G Rice, Antimicrob Agents Chemother 42 (1998) 487–494

[126] J A. Turpin, M Kearney, R G Ptak, V Fliakas-Boltz, L Pallansch, C. Michejda, W C. Cholody, R.W. Buckheit Jr., Abstracts of the 4th International Workshop on Drug Resistance and Treatment Strategies, Sitges, Spain, 12–16 June 2000, Antiviral Ther. 5 (Suppl 3) (2000) 37, no 50

[127] F. Kashanchi, M R. Sadaie, J N. Brady, Virology 227 (1997) 431–438.

[128] I Choudhury, J Wang, A.B Rabson, S. Stein, S. Pooyan, S Stein, M.J. Leibowitz, J. Acquired Immune Defic. Syndr Hum Retrovirol 17 (1998) 104–111

[129] F Hamy, E.R Felder, G. Heizmann, J Lazdins, F. Aboul-ela, G Varani, J. Karn, T Klimkait, Proc Natl Acad Sci U S. A 94 (1997) 3548–3553

[130] D. Daelemans, D. Schols, M. Witvrouw, C. Pannecouque, S Hatse, S Van Dooren, F Hamy, T Klimkait, E. De Clercq, A.-M Vandamme, Mol. Pharmacol. 57 (2000) 116–124

[131] S Ghezzi, D.M Noonan, M G Aluigi, G Vallanti, M. Cota, R. Benelli, M Morini, J.D Reeves, E Vicenzi, G. Poli, A Albini, Biochem. Biophys Res Commun. 270 (2000) 992–996.

[132] S -H Chao, K. Fujinaga, J E. Marion, R. Taube, E A Sausville, A.M. Senderowicz, B M. Peterlin, D H. Price, J Biol Chem. 275 (2000) 28345–28348

[133] C. Flexner, N Engl J Med 338 (1998) 1281–1292

[134] A Molla, G R Granneman, E Sun, D J Kempf, Antiviral Res 39 (1998) 1–23

[135] H.L. Sham, D.J. Kempf, A Molla, K.C Marsh, G N Kumar, C M. Chen, W. Kati, K Stewart, R. Lal, A Hsu, D Betebenner, M Korneyeva, S Vasavanonda, E McDonald, A Saldivar, N. Wildeburg, X Chen, P. Niu, C. Park, V. Jayanti, B Grabowski, G R. Granneman, E Sun, A J. Japour, J M Leonard, J J Plattner, D.W. Norbeck, Antimicrob Agents Chemother 42 (1998) 3218–3224.

[136] R.J. Colonno, K. Hertogs, B.A. Larder, K Limoli, G. Heilek-Snyder, N Parkin, Abstracts of the 4th International Workshop on Drug Resistance and Treatment Strategies, Sitges, Spain, 12–16 June 2000, Antiviral Ther 5 (Suppl. 3) (2000) 7 no 8

[137] S. Thaisrivongs, P.K. Tomich, K.D Watenpaugh, K -T. Chong, W J. Howe, C -P. Yang, J W Strohbach, S.R. Turner, J.P McGrath, M.J. Bohanon, J.C Lynn, A M. Mulichak, P A Spinelli, R R Hinshaw,

P.J Pagano, J B Moon, M.J Ruwart, K F. Wilkinson, B.D Rush, G.L. Zipp, R J. Dalga, F.J. Schwende, G.M Howard, G E. Padbury, L N Toth, Z Zhao, K.A. Koeplinger, T J. Kakuk, S.L. Cole, R.M Zaya, R C. Piper, P. Jeffrey, J. Med. Chem. 37 (1994) 3200–3204

[138] H.I. Skulnick, P.D Johnson, W J Howe, P K Tomich, K -T Chong, K.D. Watenpaugh, M N Janakiraman, L A. Dolak, J P McGrath, J.C. Lynn, M.-M. Horng, R.R Hinshaw, G.L. Zipp, M J Ruwart, F J. Schwende, W.-Z. Zhong, G.E. Padbury, R J Dalga, L. Shiou, P L Possert, B D Rush, K.F Wilkinson, G M. Howard, L.N. Toth, M.G. Williams, T J. Kakuk, S L. Cole, R.M Zaya, K.D Lovasz, J.K Morris, K.R. Romines, S. Thaisrivongs, P.A. Aristoff, J Med Chem 38 (1995) 4968–4971.

[139] P.Y Lam, Y. Ru, P.K Jadvah, P E. Aldrich, G V DeLucca, C.J Eyermann, C.-H. Chang, G. Emmett, E R. Holler, W F Daneker, L. Li, P.N. Confalone, R.J. McHugh, Q. Han, R. Li, J.A. Markwalder, S.P. Seitz, T.R. Sharpe, L T Bacheler, M M Rayner, R.M. Klabe, L. Shum, D L. Winslow, D.M. Kornhauser, D.A. Jackson, S. Erickson-Viitanen, C N. Hodge, J Med. Chem. 39 (1996) 3514–3525

[140] C N Hodge, P.E Aldrich, L T Bacheler, C H Chang, C.J Eyermann, S. Garber, M. Grubb, D A. Jackson, P.K Jadhav, B. Korant, P Y. Lam, M B. Maurin, J.L. Meek, M J Otto, M.M. Rayner, C Reid, T.R Sharpe, L Shum, D L Winslow, S. Erickson-Viitanen, Chem Biol 3 (1996) 301–314.

[141] P.K. Jadhav, F J. Woerner, P.Y Lam, C.N. Hodge, C J Eyermann, H W. Man, W F Daneker, L T Bacheler, M M. Rayner, J L Meek, S. Erickson-Viitanen, D.A. Jackson, J C. Calabrese, M. Schadt, C.H. Chang, J. Med. Chem 41 (1998) 1446–1455.

[142] G Bold, A Fassler, H.G. Capraro, R Cozens, T. Klimkait, J Mestan, J Mestan, B. Poncioni, J. Rosel, D. Stover, M. Tintelnot-Blomley, F. Acemoglu, W. Beck, E. Boss, M Eschbach, T Hurlimann, E. Masso, S. Roussel, K. Ucci-Stoll, D Wyss, M. Lang, J. Med Chem. 41 (1998) 3387–3401

[143] K.S. Fors, J.R Gage, R.F Heier, R C Kelly, W R Perrault, N Wicnienski, J Org. Chem. 63 (1998) 7348–7356.

[144] S.R Turner, J.W Strohbach, R A Tommassi, P A. Aristoff, P D Johnson, H.I Skulnick, L A Dolak, E P Seest, P.K. Tomich, M J Bohanon, M.M Horng, J C. Lynn, K.T. Chong, R.R. Hinshaw, K D Watenpaugh, M.N. Janakiraman, S. Thaisrivongs, J Med Chem. 41 (1998) 3467–3476.

[145] S M. Poppe, D.E. Slade, K T Chong, R.R Hinshaw, P.J Pagano, M. Markowitz, D D. Ho, H. Mo, R R. Gorman III, T.J. Dueweke, S Thaisrivongs, W G. Tarpley, Antimicrob. Agents Chemother 41 (1997) 1058–1063

[146] J. Sierra, S. Nino, P Volkow, D. Sereni, P Yeni, S Staszewski, J Gatell, L Wang, N McMillan, F Rousseau, G D Miralles, Abstracts of the 4th International Workshop on Drug Resistance and Treatment Strategies, Sitges, Spain, 12–16 June 2000, Antiviral Ther. 5 (Suppl. 3) (2000) 6, no. 6.

[147] S. Rusconi, S. La Seta Catamancio, P. Citterio, S. Kurtagic, M. Violin, C Balotta, M Moroni, M. Galli, A d'Arminio-Monforte, Antimicrob. Agents Chemother 44 (2000) 1328–1332

[148] U. Schubert, D.E Ott, E.N Chertova, R. Welker, U. Tessmer, M.F Princiotta, J R. Bennink, H.-G. Kräusslich, J W. Yewdell, Proc Natl Acad Sci. U. S A. 97 (2000) 13057–13062

ELSEVIER

Biochimica et Biophysica Acta 1587 (2002) 276–286

BIOCHIMICA ET BIOPHYSICA ACTA
BBA
www.bba-direct.com

Review

Lipophilic phosphoramidates as antiviral pronucleotides

Jiri Zemlicka*

Department of Chemistry, Developmental Therapeutics Program, Barbara Ann Karmanos Cancer Institute, Wayne State University School of Medicine, 110 E. Warren Ave., Detroit, MI 48201-1379, USA

Received 24 January 2002; accepted 24 January 2002

Abstract

In order to overcome restrictions imposed by activation (phosphorylation) mechanism of antiviral and antitumor nucleoside analogues several prodrug approaches have been designed. Lipophilic pronucleotides are capable of intracellular delivery of monophosphates of nucleoside analogues, thus circumventing the limitations of enzymic phosphorylation. One of the successful approaches employs lipophilic amino acid ester (alanine) phenyl phosphoramidates as pronucleotides. This approach was applied to AIDS drugs such as AZT, d4T and related analogues but also to nonclassical nucleoside analogues based on allenic and methylenecyclopropane structure. Antiviral effects of the parent analogues were in many cases increased by conversion to phenyl phosphoralaninate (PPA) pronucleotides. Although cytotoxicity increase frequently accompanies antiviral effects of these pronucleotides, a favorable selectivity index can be obtained by manipulation of the parent structure as shown, e.g., for 2,6-diaminopurine methylenecyclopropane pronucleotide **15c**. A lack of in vivo toxicity was demonstrated for 2-amino-6-methoxypurine methylenecyclopropane pronucleotide **15e** in mice. The PPA pronucleotides can overcome deficiency of phosphorylating enzymes and offer favorable cross-resistance patterns when compared with other antiviral drugs. © 2002 Elsevier Science B.V. All rights reserved.

Keywords: Prodrug; Pronucleotide, Antiviral; Phosphoramidate; Phenyl phosphoralaninate, Esterase, Phosphoamidase; Reverse transcriptase

1. Introduction

Nucleoside analogues have been a subject of numerous studies as antiviral and anticancer agents [1]. In order to be active they must be transformed to nucleotide metabolites by viral and/or cellular enzymes. This activation process follows the pathway utilized by natural nucleosides (Scheme 1). In the first step, catalyzed by nucleoside kinases or phosphorylases, nucleosides or their analogues **1** are phosphorylated to give monophosphates **2**. The latter are converted to diphosphates **3** by the action of nucleotide kinases. In the next step, they are further processed to triphosphates **4** with the aid of nucleotide diphosphate kinases. Triphosphates of nucleoside analogues **4** then compete with their natural counterparts for DNA or RNA polymerases. They either act as terminators of growing polynucleotide chain or get incorporated into the chain modifying thus the properties of the polymer. Selectivity of the antiviral effect is then achieved by a differential inhibition of viral and cellular polymerases by the corresponding nucleoside triphosphates. In this respect, the latter analogues are the actual therapeutic agents whereas parent nucleosides can be considered as prodrugs of triphosphates.

It is then clear that intracellular introduction of nucleoside analogues as phosphorylated metabolites could circumvent difficulties associated with the use of nonphosphorylated analogues and even activate inactive or less active compounds. Such an approach obviates the crucial [2] first phosphorylation step (Scheme 1) and delivers the mono-

---

Abbreviations: araA, 9-β-(D-arabinofuranosyl)adenine; ACV, acyclovir; AIDS, acquired immunodeficiency syndrome; AZT, 3′-azido-3′-deoxythymidine, zidovudine; CC$_{50}$, cytotoxic concentration required to inhibit cellular growth by 50%; cycloSal, cyclosaligenyl; d4A, 2′,3′-didehydro-2′,3′-dideoxyadenosine; dCK, deoxycytidine kinase; ddA, 2′,3′-dideoxyadenosine; ddC, 2′,3′-dideoxycytidine, zalcitabine; ddI, 2′,3′-dideoxyinosine, didanosine; d4T, 2′,3′-didehydro-3′-deoxythymidine, stavudine; EBV, Epstein–Barr virus; EC$_{50}$, effective concentration required to inhibit virus replication by 50%; ELISA, enzyme-linked immunosorbent assay; HBV, hepatitis B virus; HCMV, human cytomegalovirus; HIV, human immunodeficiency virus; HSV-1 and -2, herpes simplex virus 1 and 2; MCMV, murine cytomegalovirus; NNRTI, non-nucleoside reverse transcriptase inhibitor; NRTI, nucleoside reverse transcriptase inhibitor; PLE, pig (porcine) liver esterase; PMEA, 9-(2-phosphonomethoxyethyl)adenine, adefovir; PMPA, 9-(2-phosphonomethoxypropyl)adenine, tenofovir; PPA, phenyl phosphoralaninate; RT, reverse transcriptase; SATE, S-acylthioethyl; SI, selectivity index (CC$_{50}$: EC$_{50}$); 3TC, L-3′-thia-2′,3′-dideoxycytidine, lamivudine; THF, tetrahydrofuran; TK, thymidine kinase; VZV, varicella zoster virus

* Tel.: +1-313-833-0715; fax: +1-313-832-7294.
E-mail address: zemlicka@kci.wayne.edu (J. Zemlicka).

0925-4439/02/$ - see front matter © 2002 Elsevier Science B.V. All rights reserved
PII: S0925-4439(02)00090-X

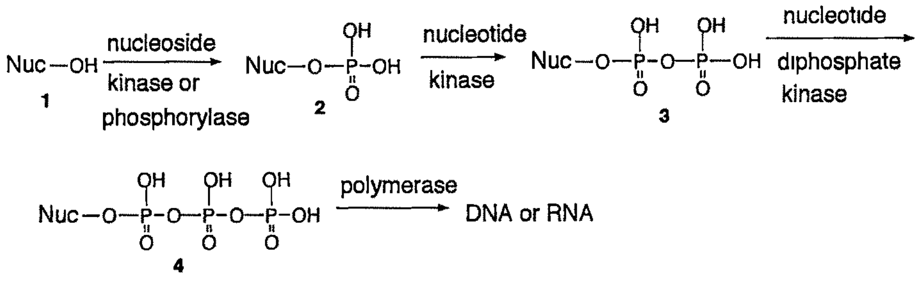

Scheme 1 Activation of nucleoside analogues

phosphate **2** into the cells. However, polarity (hydrophilicity) and a ready degradation with phosphatases makes the use of free nucleotide analogues **2** impractical. Therefore, much of the recent effort has been focussed on finding suitable prodrugs of monophosphates of nucleoside analogues (pronucleotides). It is clear that requirements for such pronucleotides include (i) resistance to degradation by phosphatases, (ii) capability of penetrating the cellular membrane and (iii) generation of the requisite nucleotide analogues **2** inside the cell.

Three groups of pronucleotides, each with a different mechanism of action, have gained prominence as antiviral agents effective primarily against HIV (Scheme 2). The S-acylthioethylphosphate (SATE) pronucleotides **5** elaborated by Perigaud et al. [3], the phosphoramidates derived from amino acids introduced by McGuigan et al. [4] and, finally, cyclosaligenyl (cycloSal) pronucleotides **6** designed and studied by Meier [5]. In the case of amino acid phosphoramidates, the studies have been largely focussed on phenyl phosphoralaninates (PPA) **7** of anti-HIV agents zidovudine (AZT) and stavudine (d4T). Extensive structure–activity relationship studies [4,6–9] indicated that a combination of alanine ester amidate and phenyl phosphate provides for the most effective agents. Consequently, PPA triesters have been used by several groups of investigators as antiviral pronucleotides [10–15] and potential antitumor agents [16,17]. In stereochemical terms, only SATE pronucleotides do not contain a chiral phosphorus atom but both cycloSal and amidate prodrugs **6** and **7** (alanine ester has an L-configuration) derived from natural (D) nucleosides are mixtures of two diastereoisomers.

The pronucleotide approach has been a subject of several excellent reviews [3,5,18]. Therefore, this contribution will focus on subjects not discussed in detail therein and, in particular, PPA pronucleotides.

2. Synthesis

The synthesis of PPA triesters is shown for stavudine (d4T) pronucleotide **8** [4,19] in Scheme 3. d4T (**9**) is phosphorylated by reagent **10** in the presence of *N*-methylimidazole as a base to give directly pronucleotide **8**. Tetrahydrofuran (THF) is a suitable solvent. For less soluble nucleoside analogues pyridine can be used [13]. Alternately, *tert*-butylmagnesium chloride was also employed as a base [20,21]. Starting analogues containing thymine (like AZT), uracil or adenine moiety are phosphorylated without forma-

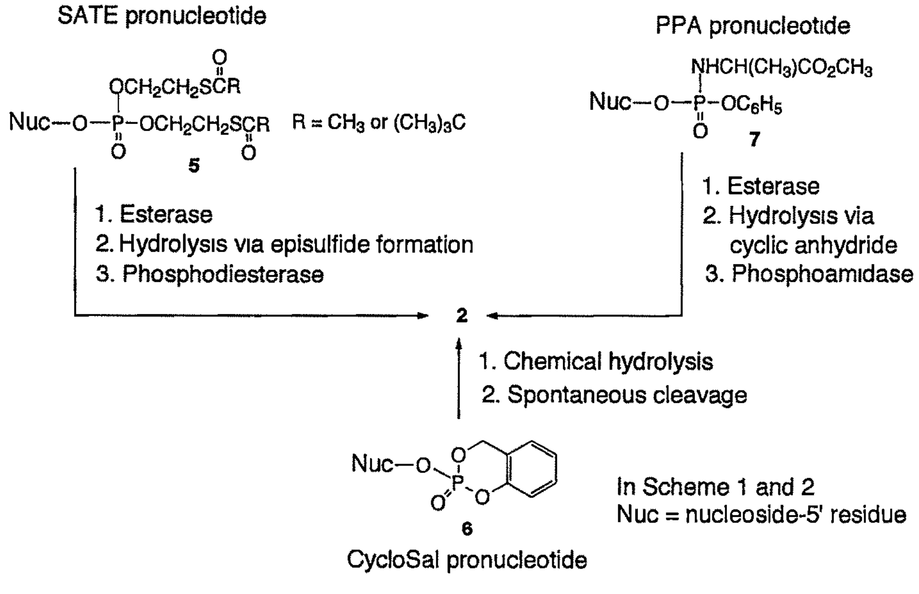

Scheme 2 Pronucleotide approach.

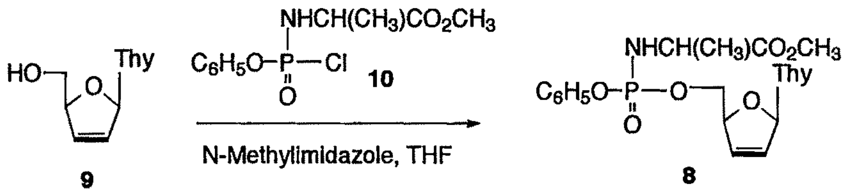

Scheme 3. Synthesis of PPA pronucleotides

tion of a significant amounts of side-products (phosphorylation of the heterocyclic portion). For more reactive bases (hypoxanthine, guanine, 2,6-diaminopurine), a prolonged treatment of the crude product with acid (80% acetic acid) is mandatory to remove products of concommitant phosphorylation of the nucleic acid base [11–13]. Alternately, and this could be of advantage for nucleoside analogues with limited acid stability, the guanine moiety was protected before phosphorylation with an N^2-dimethylaminomethylene group, which was then removed by treatment with propanol [22]. Also, no phosphorylation of the cytosine ring using *tert*-butylmagnesium chloride as a base was reported [20].

3. Antiviral activity of PPA triesters with an intact or modified furanose ring

These studies have been focussed on PPA pronucleotides of AIDS drugs zidovudine (AZT), stavudine (d4T) and lamivudine (3TC), anti-HIV agents ddA and d4A as well as attempts at introducing anti-HIV activity into some less potent or inactive nucleoside analogues (Table 1). The PPA pronucleotides of d4T [23], ddA [24] and d4A [21,24] have an improved potency over the parent analogues against both HIV-1 and HIV-2. However, this was not the case of AZT [23]. Both AZT-PPA and d4T-PPA [23] were more active in thymidine kinase-deficient cells (CEM/TK$^-$) than AZT or d4T but the efficacy of pronucleotide d4TPPA surpassed that of AZT-PPA. The results have indicated that the respective monophosphates were successfully delivered into the host cells. It then appears that the rate limiting step for AZT is conversion of monophosphate **2** to diphosphate **3** (Scheme 1) whereas the first phosphorylation may be decisive for d4T [23]. By contrast, 3TC-PPA lost most of anti-HIV potency associated with 3TC but activity (EC_{50} ~ 0.02 μM) against hepatitis B virus (HBV) in Hep G2 2.2.15 cells was preserved [20]. As expected, in CEM-TK$^-$ cells the anti-HIV activity pattern remained the same but in cells deficient in deoxycytidine kinase (dCK), an enzyme crucial for phosphorylation of 3TC, 3TC-PPA had no effect. These data were interpreted in terms of differences in monophosphate delivery in CEM vs. 2.2.15 cells. An inactive analogue ddisoA was successfully activated by conversion into PPA pronucleotide [10] but this approach failed with araA [25].

Table 1
Comparison of Anti-HIV Activity of PPA pronucleotides and parent nucleoside analogues

Compound	EC_{50}/CC_{50} (μM)		
	HIV-1/CEM	HIV-2/CEM[a]	HIV-2/CEM-TK$^-$
AZT-PPA[23]	0 055/> 172	0 07	12
AZT[23]	0 005/>100	0 008	>100
d4T-PPA[23]	0.085/>100	0 102	0 075
d4T[23]	0.16/≥ 100	0 27	25
ddA-PPA[24]	0 016/2 57	0.35	–
ddA[24]	4/>100	8	–
d4A-PPA[21]	0.006/3 8	0 018	–
d4A[21]	20/91	20	–
3TC-PPA[20]	2.5/–	3.0	5.5 (65)[b]
3TC[20]	0 01/–	0 02	0 07 (30)[b]
ddisoA-PPA[10,c]	0.06/2.9	0.04	–
ddisoA[10,c]	>425/>425	>425	–
araA-PPA[25]	>250/225	>250	–
araA[25]	>10/20	>10	–

[a] For cytotoxicity see HIV-1/CEM

[b] HIV-2/CEM-dCK$^-$

[c] MT-4 cells

The PPA pronucleotides were only rarely investigated with viruses other than HIV or HBV. Recently, acyclovir derivative, acyclovir phenyl phosphoralaninate (ACV-PPA), was tested [22] against human cytomegalovirus (HCMV), herpes simplex virus 2 (HSV-2) and varicella zoster virus (VZV) with disappointing results. The potency against HSV-2 was significantly inferior to ACV indicating possibly a poor delivery into the infected host cells. The efficacy against HCMV and VZV corresponded roughly to that of ACV.

More interesting results were obtained with phosphonate analogues of PPA triesters of antiviral agents adefovir (PMEA) and tenofovir (PMPA, Chart 1) [26]. In this case, the parent phosphonates are already surrogates of monophosphates capable of penetrating cellular membrane, and the effect of more lipophilic “prophosphonate” is on delivery of the phosphonate rather than obviating the first phosphorylation step (Scheme 1). Both prophosphonates surpass the potency of PMEA and PMPA (Table 2). This is most likely due to an increased penetration of cellular membrane relative to negatively charged parent phosphonates [27]. Nevertheless, a significantly increased efficacy of prodrug **11b** relative to its lower homologue **11a** is probably indicative of some other important factors. A large-scale separation [28] of both diastereoisomeric isopropyl alaninates **11c** by chiral chroma-

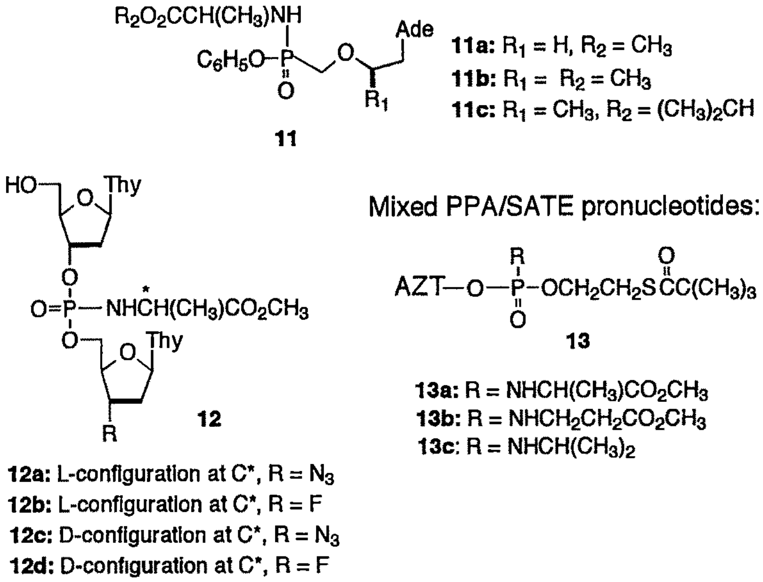
R2O2CCH(CH3)NH
C6H5O
Ade
R1
11
11a: R1 = H, R2 = CH3
11b: R1 = R2 = CH3
11c: R1 = CH3, R2 = (CH3)2CH
HO
Thy
NHCH(CH3)CO2CH3
12
R
12a: L-configuration at C*, R = N3
12b: L-configuration at C*, R = F
12c: D-configuration at C*, R = N3
12d: D-configuration at C*, R = F
Mixed PPA/SATE pronucleotides:
AZT—O—P—OCH2CH2SCC(CH3)3
13
13a: R = NHCH(CH3)CO2CH3
13b: R = NHCH2CH2CO2CH3
13c: R = NHCH(CH3)2

Chart 1. Miscellaneous prodrugs based on PPA concept

tography has made possible for the first time to investigate anti-HIV potency of pure diastereoisomers differing by configuration at the phosphorus atom [28,29]. The S_p diastereoisomer was about 10 times more potent than the R_p counterpart. Similar differences in antiviral activity between R_p and S_p diastereoisomers were noted in the case of cycloSal pronucleotides [30,31]. One factor that was not previously considered for explanation of these results is a different behavior of stereoisomers in passage through chiral membrane channels. In contrast, earlier experiments with partially separated R_p and S_p diastereoisomers of moderately effective hexyl phosphorovalinate isopropyl ester of AZT did not indicate significant differences in anti-HIV activity [6].

An attempted activation of dinucleoside phosphates derived from AZT and 3′-fluoro-3′-deoxythymidine (compounds **12a–12d**) by introducing a methyl alaninate function was not successful [32]. This is not surprising because the rationale was based on a no longer tenable concept that HIV protease might assist in hydrolysis of the PPA prodrugs [6]. The AZT "pronucleotides" **12a** and **12c** were about 30 to 40 times less potent against HIV-1 than AZT alone. There was no significant difference between D- and L-alanine derivatives in both pairs of analogues **12a**, **12c** and **12b**, **12d** indicating a similar type of cleavage of the phosphodiester bond accompanied by release of some AZT.

Table 2
Anti-HIV activity of phenyl phosphonic alaninates **11a** and **11b** derived from PMEA and PMPA

Compound	HIV-1/MT-4[a] (SI)	HIV-2/M-T4[a] (SI)	MT-4[b]
Phosphonate **11a**	0.23 (22)	0.15 (34)	5.1
PMEA	7.0 (21)	7.5 (19)	144
Phosphonate **11b**	0.029 (2462)	0.026 (2746)	71.4
PMPA	2.3 (86)	1.4 (141)	197

Selected data from Ref [26].
[a] EC_{50} (μM).
[b] CC_{50} (μM).

Combining SATE and PPA structures has led to mixed PPA/SATE pronucleotides **13a** that can be activated [33] by two different mechanisms (Scheme 3). A comparison of anti-HIV effects has shown that potency of **13a** is slightly higher than that of AZT-PPA. Interestingly, both α- and β-alaninates **13a** and **13b** were almost equipotent (EC_{50} 2.9 and 2.5 μM) whereas the corresponding phenyl phosphoro-β-alaninate triester was inactive (see also Ref. [14]). This indicates differences in mechanisms of phosphoramidate cleavage of both types of pronucleotides although the SATE function is preferentially attacked by esterase and the delivery of monophosphate occurs via phosphoro-β-alaninate (see Section 5). Replacement of amino acid moiety with simple amines led also to active pronucleotides [34]. The isopropylamidate **13c** was the most potent (EC_{50} 0.63 μM).

4. Antiviral activity of PPA triesters of "nonclassical" nucleoside analogues

4.1. Allenes and methylenecyclopropanes

It is clear from the results discussed above (Table 1) that the most extensively studied PPA pronucleotides have been derived from nucleoside mimics with a five-membered ring (mostly furanose), e.g., AZT, d4T and 3TC. Acyclic analogues were investigated only rarely [22]. In this chapter, an application of the PPA pronucleotide approach to nucleoside analogues, which do not possess a furanose moiety or an acyclic portion thereof, will be summarized. The list of investigated structures is given in Chart 2. Three groups of PPA pronucleotides are readily discerned. The first group (compounds **14a** and **14b**) is derived from allenic analogues [35,36] **14c** and **14d**; adenallene (**14c**) is an anti-HIV agent. For comparison, SATE pronucleotide **14e** was also included. The second group (compounds **15a**–**15e**) is related to (*Z*)-methylenecyclopropane analogues [37] (**15f**–**15j**), which have a broad antiviral selectivity. The structures of the third group of PPA pronucleotides are more diversified and include (*E*)-methylenecyclopropane pronucleotide **16a** (parent analogue **16b**) as well as unsaturated derivatives **17a**–**19a** (parent analogues **17b**–**19b**). A common feature of parent analogues in this group is a lack of significant antiviral potency. Finally, spiropentane pronucleotide **20a** derived from a moderately active anti-HCMV agent **20b** was also examined.

Conversion of racemic or (*R*)-adenallene—**14c** or (***R***)-**14c**—to PPA pronucleotides **14a** and (“***R***”)-**14a** did indeed increase the anti-HIV-1 activity [11] in ATH-8 cells but at an expense of increased cytotoxicity and overall selectivity index (SI) was lower than that of adenallene **14c** or (***R***)-**14c** (Table 3). This is probably caused by an elevated intracellular level of adenallene phosphates which could then interact with cellular DNA polymerases. Comparison of anti-HIV-1 potency of PPA and SATE pronucleotides **14a** and **14e** in three different assays [38] has indicated that the former prodrugs are more potent and they exhibit a more favorable SI (Table 4). It is possible that intracellular phosphodiesterase, which is necessary in the process of activation [3] of SATE pronucleotides, is unable to efficiently cleave phosphodiester intermediate arising during activation of allenic pronucleotide **14e**. Although anti-HIV activity of adenallene (**14c**) parallells that of ddA and ddI

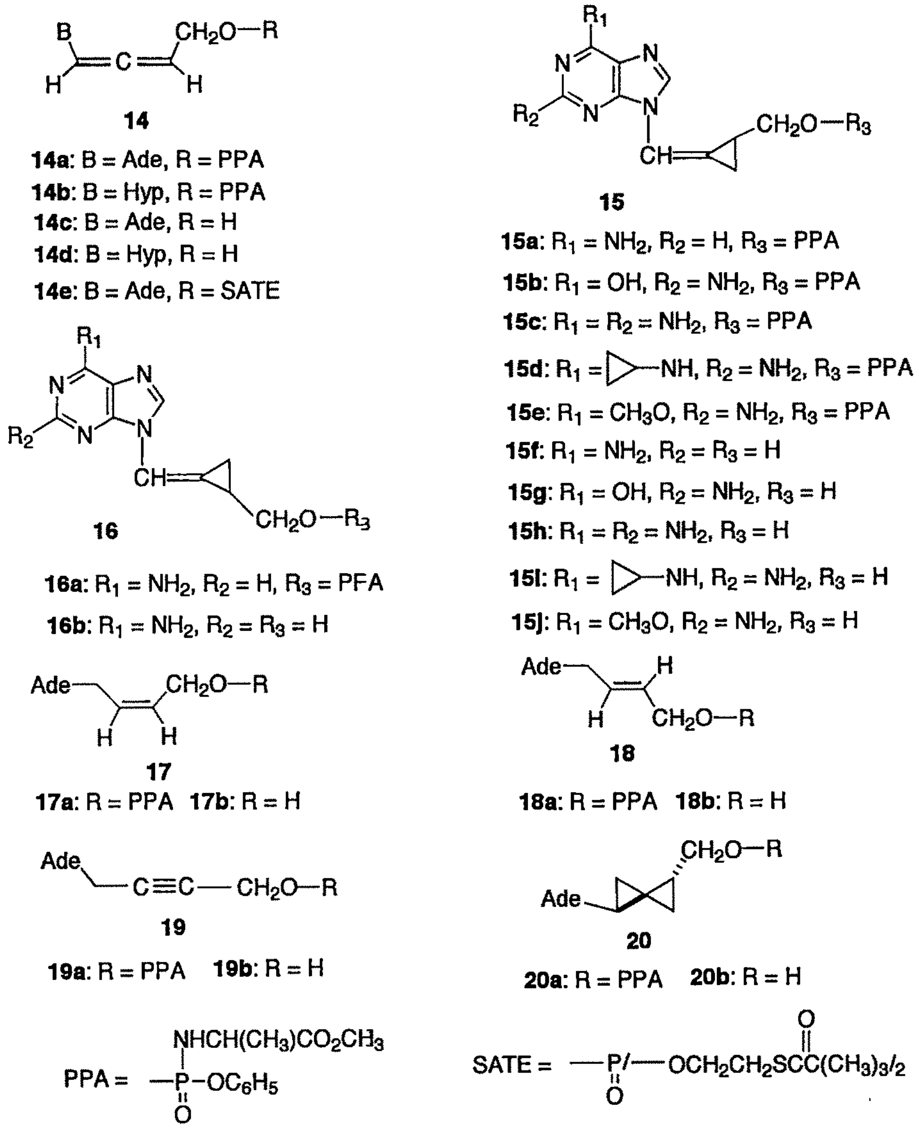

14

14a: B = Ade, R = PPA
14b: B = Hyp, R = PPA
14c: B = Ade, R = H
14d: B = Hyp, R = H
14e: B = Ade, R = SATE

15

15a: $R_1 = NH_2$, $R_2 = H$, $R_3 = PPA$
15b: $R_1 = OH$, $R_2 = NH_2$, $R_3 = PPA$
15c: $R_1 = R_2 = NH_2$, $R_3 = PPA$
15d: $R_1 =$ ▷—NH, $R_2 = NH_2$, $R_3 = PPA$
15e: $R_1 = CH_3O$, $R_2 = NH_2$, $R_3 = PPA$
15f: $R_1 = NH_2$, $R_2 = R_3 = H$
15g: $R_1 = OH$, $R_2 = NH_2$, $R_3 = H$
15h: $R_1 = R_2 = NH_2$, $R_3 = H$
15i: $R_1 =$ ▷—NH, $R_2 = NH_2$, $R_3 = H$
15j: $R_1 = CH_3O$, $R_2 = NH_2$, $R_3 = H$

16

16a: $R_1 = NH_2$, $R_2 = H$, $R_3 = PFA$
16b: $R_1 = NH_2$, $R_2 = R_3 = H$

17

17a: R = PPA **17b**: R = H

18

18a: R = PPA **18b**: R = H

19

19a: R = PPA **19b**: R = H

20

20a: R = PPA **20b**: R = H

$\text{PPA} = -\overset{\displaystyle NHCH(CH_3)CO_2CH_3}{\underset{\displaystyle O}{\overset{|}{\underset{\|}{P}}}}-OC_6H_5$

$\text{SATE} = -\underset{\displaystyle O}{\underset{\|}{P}}/-OCH_2CH_2S\overset{\displaystyle O}{\overset{\|}{C}}C(CH_3)_3/_2$

Chart 2 Pronucleotides of “nonclassical” antiviral nucleotide analogues.

Table 3
Anti-HIV activity of PPA pronucleotides of adenallene[a] **14a**

Compound	EC$_{50}$/CC$_{50}$ (µM)	SI
14a	0.88/2.1	2.4
Adenallene (**14c**)	14/>100	>7 1
(“*R*”)-**14a**	0.21/3	14
(*R*)-Adenallene [**(R)-14c**]	5 8/>200	>35

Selected data from Ref. [11].

[a] HIV-1/ATH8

Table 5
Inhibition of HIV-1 replication by phosphoralaninate prodrugs of *Z*- and *E*-methylenecyclopropane analogues **15a**, **15b**, **15c**, **16a** and parent analogues **15f**, **15g**, **15h**, **16b**

Compound	EC$_{50}$/CC$_{50}$ (µM)[a]		
	HIV$_{\mathrm{IIIB}}$ RT[b]	HIV$_{\mathrm{LAI}}$	
	CEM-SS	MT-2[c]	MT-2[d]
15a	0 05/1 1 (22)	0.0026/0 24 (92)	0 0022
15f	20/>100 (>5)	0.75/32 (43)	0.54
15b	>100/>100	>76/76	–
15g	>100/>100	>70/70	–
15c	0.2/38 (190)	0 034/21 (618)	0 0038
15h	>100/>100	12/>100 (>8)	4.1
16a	1 3/66 (51)	0.66/24 (6)	0 51
16b	>100/>100	>100/>100	not tested

Selected data from Refs. [13,40]

[a] The SI values are in parentheses

[b] Reverse transcriptase (RT) activity assay.

[c] Cytopathic effect (CPE) assay

[d] Inhibition of p24 Gag protein production

[35], the corresponding hypoxallene analogue **14d** and PPA prodrug **14b** had little anti-HIV activity [11]. The activation mechanism, initiated by phosphorylation [39] which is available to ddI (conversion to ddA monophosphate) is then inoperative in the case of hypoxallene (**14d**) or the corresponding monophosphate generated from **14b**.

Investigation of PPA pronucleotides of methylenecyclopropane analogues was performed in several viral assays and permitted to draw some conclusions about the structure–activity relationships. From prodrugs **15a**–**15e** listed in Chart 1, adenine and 2,6-diaminopurine pronucleotides [13,40] **15a** and **15c** were the most potent against HIV-1 in three assays (Table 5). Although they were more toxic, their SI values surpassed that of parent compounds **15f** and **15h**. Especially effective was the 2,6-diaminopurine analogue **15c**. Interestingly, active PPA prodrug **16a** was also obtained from inactive *E*-analogue **16b**. Both pronucleotides **15a** and **15c** were also active [40] against a clinical HIV-1 isolate in PHA–PBM cells. They were about 10 times less active against HIV-2 than HIV-1 [40] (Table 6). Because most of the non-nucleoside reverse transcriptase inhibitors (NNRTIs) are effective only against HIV-1 (see Ref. [41] for an exception), this result has indicated that **15a** and **15c** act as nucleoside reverse transcriptase inhibitors (NRTIs) or their phosphorylated metabolites. Pronucleotides **15a** and **15c** derived from racemic analogues **15f** and **15h** are mixtures of four diastereoisomers. Anti-HIV activity of diastereoisomers **15c** obtained from enantiomers of **15h** (2 diastereoisomers from each enantiomer) indicated that both are effective against HIV-1 albeit the **(“*R*”)-15c** was about six times more potent than **(“*S*”)-15c** [42]. Guanine pronucleotide **15b** and the parent analogue **15g** were inactive.

Sensitivity of pronucleotides **15a** and **15c** toward HIV-1 strains resistant to AZT, ddI and multiple NRTIs was also investigated [40]. No cross-resistance of **15a** and **15c** with any of these strains was observed (Table 7) as judged from the EC$_{50}$ values compared with a wild type of HIV-1. As a continuation of these studies, an HIV-1$_{\mathrm{P16}}$ variant resistant to most effective pronucleotide **15c** was selected [43]. The variant exhibited cross-resistance to 3TC but not AZT or ddI (Table 8). It was also less sensitive to pronucleotide **15a**. Nevertheless, initial mutation M184 from Met to Ileu persisted after 16 passages and it did not change to Val as observed with 3TC. Further investigation has indicated that HIV-1M$_{148\mathrm{I}}$ and HIV$_{148\mathrm{V}}$ variants [43] resistant to 3TC are sensitive to AZT and ddI. Resistance to pronucleotides **15a** and **15c** is approximately 50–70 times lower than to 3TC (Table 9). There is little structural similarity between 3TC and pronucleotide **15c** except the diaminopyrimidine portion of the base which resembles the cytosine ring of 3TC. Molecular modeling studies of a “stalled” complex of 3TC triphosphate with reverse transcriptase (RT) indicate that oxathiolane portion interacts with Ileu or Val [44] of mutated enzyme. Such interaction may be sterically less demanding in a more compact methylenecyclopropane triphosphate generated from **15c**. At any rate, studies of diastereoisomers **(“*R*”)-15c** and **(“*S*”)-15c** are necessary to clarify the mechanism of resistance.

Pronucleotides **15a**, **15c** and **16a** were significantly more effective against HBV in vitro [13] than parent analogues **15f**, **15h** and **16b** (Table 10). The activity pattern followed that found in HIV assays (Table 5). Again, the

Table 4
Comparison of anti-HIV activity of PPA and SATE pronucleotides of adenallene **14a** and **14e** [38]

Compound	EC$_{50}$/CC$_{50}$ (µM)[a]		
	HIV-1/IIIB	HIV-1/LAI	
	CEM-SS	MT-4	MT-2
14a	0.35/44 (126)	0.4/7 5 (19)	0 41/5 (12)
14e	1 2/>10 (>8.3)	8.9/>10 (>1 1)	6.4/28 (4 4)

[a] The SI values are in parentheses

Table 6
Comparison of activity of PPA pronucleotides **15a** and **15c** against HIV-2 and HIV-1

Compound	EC$_{50}$ (µM)	
	HIV-2$_{\mathrm{ROD}}$/MT-2	HIV-1$_{\mathrm{LAI}}$/MT-2
15a	0 03	0 002
15c	0 38	0 038

Data from Ref [40]

Table 7
Activity of PPA pronucleotides **15a** and **15c** against wild-type and drug-resistant infectious HIV-1

Compound	EC$_{50}$ (μM)^a			
	HIV-1_{wt}	HIV-1_{215}	HIV-1_{74}	HIV-$1_{62/75/77/116/151}$
15a	0.029	0 03	0.013	0.037
15c	0.36	0 30	0 39	0.39
AZT	0.017	0 14	0 013	11
ddI	3.7	4.2	25.4	47

HIV-1_{wt} = wild-type, HIV-1_{215} = AZT-resistant, HIV$_{74}$ = ddI-resistant, HIV-$1_{62/75/77/116/151}$ = multiple ddN-resistant strain of HIV-1
Adapted from Ref [40]

[a] MT-2 cells, p24 Gag protein was determined by radioimmunoassay

Table 9
Sensitivity of infectious HIV-1 reverse transcriptase mutants to PPA pronucleotides **15a** and **15c** and other anti-HIV agents

Compound	EC$_{50}$ (μM)			CC$_{50}$ (μM)
	HIV-1_{wt}	HIV-1_{M141I}	HIV-1_{M184V}	
15a	0 026	0 24 (9 ×)	0 3 (12 ×)	0 52
15c	0.29	2.6 (9 ×)	3.1 (11 ×)	23
AZT	0.04	0.008 (0 2 ×)	0.006 (0 15 ×)	>100
ddI	3.0	2 3 (0 8 ×)	4.5 (2 ×)	61
3TC	1 7	>1000 (>590 ×)	>1000 (>590 ×)	>1000

The fold differences relative to HIV-1_{wt} are given in parentheses.
Adapted from Ref. [43]

2,6-diaminopurine pronucleotide **15c** has the most favorable SI. Importantly, it has also little long-term toxicity measured as inhibition of mitochondrial DNA synthesis. Anti-HBV activity of diastereoisomers **15c** obtained from enantiomers of **15h** exhibited a trend reversed from that found in HIV assays; the **("*S*")-15c** was about twice as potent as **("*R*")-15c** [42]. A strong anti-HIV and anti-HBV potency of PPA pronucleotides **15a** and **15c** (Tables 5 and 10) was not duplicated in prodrugs **15d** and **15e,** which were equally or more active but also cytotoxic. Only guanine pronucleotide **15b** was five times more effective than the parent analogue **15g** and noncytotoxic. Consequently, circumvention of the first phosphorylation step (Scheme 1) provided little benefit.

Against HCMV and murine cytomegalovirus (MCMV), all parent analogues **15f–15j** were active [45,46] and, therefore, it was of interest to study the respective PPA pronucleotides **15a–15e** (Table 11). The antiviral potency of pronucleotides remained roughly the same [13] and any increases were accompanied by an elevated cytotoxicity (see **15a** and **15e**). Interestingly, a slightly improved activity without cytotoxic effect was noted with 2,6-diamino pronucleotide **15c** but guanine analogue **15b** was less potent than the parent compound **15g.** Potency of 2,6-diaminopurine pronucleotide **15c**, which was effective against HIV and HBV (Tables 5 and 10), was increased only two to six times over that of **15h** and it decreased in MCMV assay. Interestingly, the cytotoxicity effects observed in human (HFF) culture were absent in murine (MEF) cells throughout this series of pronucleotides. The diastereoselectivity—**("*S*")-15c** was more potent than **("*R*")-15c**—[42] followed *S* enantioselectivity pattern observed in purine methylenecyclopropane nucleoside analogues **15f–15j.**

The results with other herpesviruses followed a similar trend. Parent analogues **15f–15j** are only poor inhibitors of replication of HSV-1 and HSV-2 [45,46]. The antiviral activity was increased in all tested pronucleotides [13] except guanine PPA prodrug **15b** (Table 12), which was inactive and noncytotoxic. Cytotoxicity increases were apparent with other pronucleotides.

The activity of parent analogues **15f–15j** against Epstein–Barr virus (EBV) (Table 13) is similar to that of observed in anti-HCMV assays (Table 11) [45,46]. A comparison of pronucleotide effects is then of interest. Introduction of PPA grouping into parent analogues increased significantly the anti-EBV potency in both H-1 and Daudi cells only in a single case of pronucleotide **15e.** This effect was accompanied by cytotoxicity. Overall, the

Table 8
Sensitivity of the strain HIV-1_{P16} resistant to PPA pronucleotide **15c** toward anti-HIV agents

Compound	EC$_{50}$ (μM)		CC$_{50}$ (μM)
	HIV-1_{LAI}	HIV-1_{P16}	MT-2
15a	0.012	>0 49 (>41 ×)	0.49
15c	0.047	4.9 (104 ×)	28
AZT	0.028	0 02 (1 ×)	>100
ddI	3.9	5.7 (2 ×)	59
3TC	0 91	>1000 (>1100 ×)	–

The fold differences relative to HIV-1_{LAI} are given in parentheses
Adapted from Ref. [43].

Table 10
Inhibition of replication of HBV by PPA pronucleotides **15a, 15b, 15c, 15d, 15e, 16a** and parent analogues **15f, 15g, 15h, 15i, 15j, 16b**

Compound	EC$_{50}$/CC$_{50}$ (μM)	
	HBV/2.2.15	mtDNA^a
15a	0 01/0 3 (30)^b	–
15f	2/>100^c	–
15b	2/>100^c	
15g	10/>100^c	
15c	0 08/45 (564)^b	>50
15h	10/>100^c	–
15d	2/9^c	–
15i	2/>100^c	–
15e	2/2.2^c	–
15j	>10/>100^c	–
16a	1 2/4 5	–
16b	>10/>100^c	–
ddC	1.4	0 07

Selected data from Ref [13]

[a] IC$_{50}$ (μM) of inhibition of mitochondrial (mt) DNA synthesis in CEM cells

[b] Selectivity index (SI)

[c] Cytotoxicity was determined in CEM cells.

Table 11
Inhibition of HCMV and MCMV replication by PPA pronucleotides and parent methylenecyclopropane analogues

Compound	EC_{50}/CC_{50} (μM)		
	HCMV/HFF		MCMV/MEF
	Towne[a]	AD 169[b]	
15a	0.14/2.5	not tested	not tested
15f	2.1/>100	–	–
15b	4.2/>100	25/>206	3.3/>206
15g	2.1//>100	1.2/>429	0.3/>429
15c	4/>100	7.8/121	3.2/211
15h	24/>100	16/266	0.6/293
15d	0.25/10	6.2/126	0.94/101
15i	0.4/>100	2.4/327	0.37/220
15e	0.16/3.7	4.5/34	0.24/126
15j	3.1/>100	5.3/>404	0.4/261

Selected data from Ref [13].

[a] Visual cytotoxicity.

[b] Cytotoxicity by neutral red dye uptake

effect of PPA pronucleotides seems to be less pronounced than in HCMV assays. Stronger assay variations (H-1 vs. Daudi) are also typical. For example, pronucleotide **15a** was cytotoxic only in H-1 cells. The "*R*" and "*S*" diastereoisomers of **15c** exhibited a varying assay-dependent stereoselectivity against EBV as observed with the enantiomers of parent analogue **15h** [42].

Anti-VZV activity can be, to some extent, compared to HSV-1 and HSV-2 results (Table 12). Parent analogues **15f**–**15j** lack, with the exception of **15f**, any significant potency against VZV in HFF cells (Table 13). Adenine analogue **15f** was the only one whose activity was not substantially increased after transformation to pronucleotide **15a**. In other cases, quite substantial increases of activity were observed pointing to importance of the first phosphorylation step (Scheme 1). The SI of **15c**, **15d** and **15e** was significantly increased over the parent analogues, a trend not seen in other herpesvirus assays (Tables 11–13). The diastereoisomer "*S*"-**15c** was three times more active than "*R*"-**15c** [42].

Table 12
Inhibition of HSV-1 and HSV-2 replication by PPA pronucleotides and parent methylenecyclopropane analogues

B	EC_{50}/CC_{50} (μM)			CC_{50} (μM)
	HSV-1		HSV-2	KB
	BSC-1[a]	Vero[b]		
15a	2.5	>1/1	>1/1	0.5
15f	26	28/>100	59/>100	78
15b	>100	>100/>100	>100/>100	>100
15g	>100	>100/>100	>100/>100	>100
15c	50	30/35	15/35	40
15h	>100	>100/>100	>100/>100	>100
15d	5	0.9/9	1.8/9	65
15i	15	31/>100	41/>100	>100
15e	2	0.6/2.2	0.6/2.2	80
15j	33	>50/>100	>50/>100	>100

Selected data from Ref. [13].

[a] ELISA (enzyme-linked immunosorption assay). For cytotoxicity see KB cells.

[b] Plaque reduction assay. Cytotoxicity was determined in CEM cells.

Table 13
Inhibition of EBV and VZV replication by PPA pronucleotides and parent methylenecyclopropane analogues

Compound	EC_{50}/CC_{50} (μM)		
	EBV/H-1	EBV/Daudi	VZV/HFF
15a	0.1/1[a]	1.0/>108	7.6/4.3
15f	0.2/>50	3.2/368	2.5/>429
15b	>10/>50	0.31/>103	8.1/>206
15g	0.3/>50	5.6/>214	61/279
15c	5.5/35[a]	3.8/26	1.0/121
15h	1.5/>50	6.9/>215	93/266
15d	10/23	2.3/19	0.64/126
15i	4/>100[a]	12/>184	13/327
15e	0.4/4.6	0.75/4.4	0.12/34
15j	1.6/>50	18/>202	24/404

Selected data from Ref [13]

[a] Cytotoxicity was determined in CEM cells

Parent analogues **15h**–**15j** can be considered as potential precursors of guanine derivative **15g** [13]. Nevertheless, guanine pronucleotide **15b** showed lesser activity than 2,6-diaminopurine prodrug **15c** in almost all assays and, most notably, against HIV (Table 5). This supports a hypothesis that antiviral potency of **15c** is not dependent on intracellular conversion to phosphorylated intermediates resultant from guanine analogue **15g**. It is possible that 2,6-diaminopurine pronucleotide **15c** is an analogue of adenine prodrug **15a**. Although the results with pronucleotides **15d** and **15e** are less clear-cut, evidence from several assays suggests that their antiviral effects do not require transformation to phosphorylated metabolites of **15g**. Alternately, guanine pronucleotide **15b** may not penetrate the cellular membrane as easily as the more lipophilic prodrugs **15a** and **15c**–**15e**, which are then converted to phosphates of **15g**. In addition, a weak substrate efficiency of phosphoramidate intermediates for phosphoamidase, an enzyme important for metabolism of PPA pronucleotides (see Section 5), may also hamper the antiviral potency of **15b**. Interestingly, ACV-PPA, a guanine derivative, is likewise a poor antiviral agent [22]. Further studies are clearly needed to clarify all these aspects.

Although PPA pronucleotides of nucleoside analogues, particularly of AZT and d4T, were subjects of many studies (see Section 3) data on in vivo activity have been scarce [18]. In one instance [47], mice infected with MCMV were treated orally with 2-amino-6-methoxypurine pronucleotide **15e** (Table 14). The results were almost identical with those obtained for a ganciclovir control at both tested levels (40 and 10 mg/kg) and no toxicity was observed. Equally, cytotoxicity was absent in in vitro assay of pronucleotide **15e** against MCMV as contrasted with HCMV (Table 11). Therefore, prodrug **15e** may not be a drug candidate of choice against HCMV but the results indicate that PPA pronucleotides can be effective in vivo without adverse toxicity. The results with **15e** also indicate that phenol [18] released from PPA pronucleotides in the process of activation (see Section 5) does not cause toxicity, at least in mice.

4.2. *Other nucleoside analogues lacking the carbohydrate moiety*

It was of interest to extend the PPA pronucleotide concept to other analogues whose structures are distant from a "classic" ribofuranose form of nucleosides. Four types of such prodrugs (**17a**–**20a**), which were all derived from inactive or moderately active parent compounds (**17b**–**20b**, Chart 2) were investigated. The focus of pronucleotides **17a**–**19a** was on anti-HIV activity [11,12] whereas a more comprehensive antiviral study was performed [48] with spiropentane prodrug **20a**. Pronucleotide of *cis*-butenol analogue **17a** was effective against HIV-1 in ATH-8 cell submicromolar level with a low cytotoxicity (EC_{50}/CC_{50} 0.5/100 μM). By contrast, the *trans* isomer **18a** was inactive but it was cytotoxic (CC_{50} 1 μM) [12]. Acetylenic compound **19a** was inactive and noncytotoxic [11]. Pronucleotide **20a** whose parent analogue **20b** is only moderately effective against HCMV was active [48] against HCMV in HFF cells (Table 15) without cytotoxicity. Inhibition of replication of EBV, HIV-1 and HBV in micromolar range was also noted although accompanied by a varying degree of cytotoxicity. Prodrug **20a** was only moderately effective against HSV-1 and HSV-2.

The results with **17a** and **20a** along with the results obtained with allenic and methylenecyclopropane pronucleotides (Section 4.B) show that a wide range of nucleoside analogues can be activated by a PPA pronucleotide approach.

Table 14
Effect of oral treatment with pronucleotide **15e** on the mortality of Balb/c mice inoculated with MCMV

Treatment	Mortality				
	Number	Percent	*P*-value	MDD[a]	*P*-value
Pronucleotide **15e**					
Placebo–0.4% CMC[b]	13/15	87	–	6	–
40 mg/kg	1/15	7	<0.0001	6	NS[c]
40 mg/kg-toxicity[d]	0/10	0	–	–	–
10 mg/kg	8/15	53	NS	5	NS[c]
10 mg/kg-toxicity[d]	0/10	0	–	–	–
Ganciclovir					
Placebo–water	14/15	93	–	6	–
40 mg/kg	2/15	13	<0.0001	10	NS[c]
10 mg/kg	7/15	47	<0.05	7	NS[c]

Animals were treated twice daily for 5 days beginning 24 h after viral inoculation.
Adapted from Ref. [47].
[a] MDD, mean day of death.
[b] CMC, carboxymethyl cellulose.
[c] NS, not statistically significant when compared to placebo control.
[d] Uninfected animals.

Table 15
Antiviral activity of phosphoralaninate prodrug of *medial-syn* spiropentane analogue of 2′-deoxyadenosine **20a** and parent analogue **20b**

Compound[a]	HCMV	HSV-1		HSV-2
	HFF[b]	BSC-1[c]	Vero[b,d]	Vero[b,d]
20a	0.38/100	7.0/70	20/27	31/27
20b	20/100	70/>100	>50/>100	>50/>100

Compound[a]	EBV	HIV-1[e]	HBV
	Daudi	CEM-SS	2.2.15
20a	2.8/7.6	3.5/32	3.1/27[d]
20b	22/202	>100/>100	>10/>100[d]

Selected data from Ref. [48].
[a] EC_{50}/CC_{50} (μM).
[b] Plaque reduction.
[c] ELISA.
[d] Cytotoxicity was determined in CEM cells.
[e] Reverse transcriptase assay.

5. Mechanism of action of PPA pronucleotides

The mode of action of PPA pronucleotides is shown in Scheme 4. The matter is a subject of current intense investigation and more refinements of this mechanism are to be expected. As in the case of SATE pronucleotides [3], the alanine ester group of PPA pronucleotide is first hydrolyzed by an intracellular esterase to give intermediate **21**. Pig liver esterase (PLE) has been widely used as a model of intracellular enzyme(s) [11,12,48,49,50] but, recently, esterase(s) capable of hydrolyzing PPA pronucleotides were detected in cellular extracts and serum [51]. It was suggested that PLE-catalyzed hydrolysis can be used as a predictor for anti-HIV activity of PPA pronucleotides and related analogues [8]. Nevertheless, other studies have indicated that this activity is just one of several factors determining the antiviral efficacy of PPA prodrugs [11,12, 51–53].

The esterase step is followed by an intramolecular displacement of the phenoxy group by the carboxylate anion of intermediate **21** to form a five-membered ring mixed anhydride **22**. The ease of cyclization depends on the structure of the analogue. Thus, cyclization of intermediate **21** derived from AZT is more difficult than that of d4T [51]. In case of β-alaninate pronucleotide, the esterase-catalyzed hydrolysis stops after the first step and no cyclic anhydride with a six-membered ring is formed [33,51].

In the next step, anhydride **22** suffers a hydrolysis which is not enzyme-assisted to give phosphoralaninate **23**. Because possibility of a P–N bond cleavage was ruled out [50], hydrolysis can only proceed by an attack A at the carbonyl group of **22** or attack B at the phosphate portion. Usually, hydrolysis or methanolysis of mixed

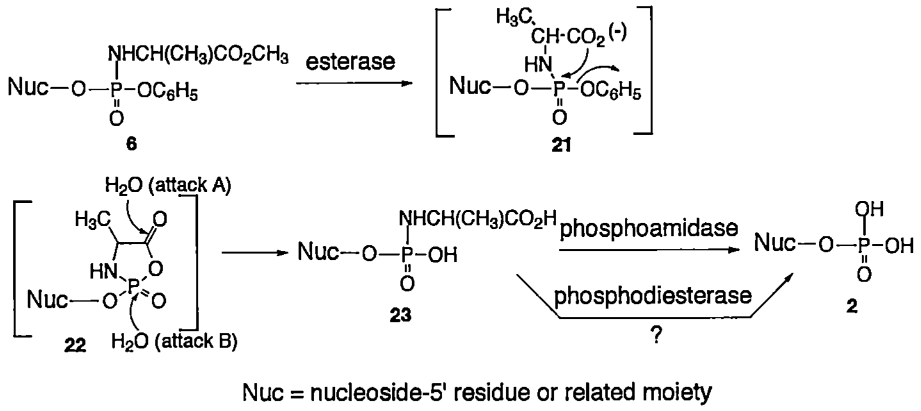

Scheme 4. Mechanism of action of PPA pronucleotides

carboxylic and phosphoric anhydrides [54] proceeds by attack A, but in the case of five-membered ring anhydrides attack B can prevail [55,56]. The mode of hydrolysis of intermediate **22** then remains to be established.

Phosphoralaninate **23** was the final product of PLE-catalyzed hydrolysis of a number of PPA pronucleotides of different structure [11,12,48–50]. It was shown that product **23** can be accumulated inside the cells and serve as a depository form of the respective monophosphate [49]. Interestingly, d4T phosphoralaninate **23** exhibited anti-HIV effect comparable to d4T [49] but a similar derivative of adenallene (**14c**) was inactive [12]. The latter more polar analogue may be less penetrable through the cellular membrane. Adenallene phosphoralaninate **23** also did not inhibit HIV-RT.

Although it was suggested earlier that the last activation step, conversion of phosphoralaninate **23** to monophosphate **2**, is catalyzed by intracellular phosphoamidase [11,49], a direct evidence has been missing. More recently, a purified enzyme obtained from rat liver was capable of converting intermediates **23** derived from AZT-PPA and d4T-PPA to the corresponding monophosphates **2** [51]. The substrate efficiency can vary substantially. Thus, AZT phosphoralaninate **23** is less readily hydrolyzed than the d4T derivative [51]. However, phosphoamidase is apparently capable of hydrolyzing substrates of a wide range of structures, e.g., phosphoralaninates **23** of isoddA [10], allenic [11], spiropentane [48], methylenecyclopropane [13] and other unsaturated analogues [12], as judged from antiviral activity of the corresponding PPA pronucleotides. It was suggested earlier [50] that intermediates **23** can also be converted to monophosphates by the action of phosphodiesterase. Such a proposal seemed at variance with a report [57] that phenylalanyl analogue of intermediate **23** derived from thymidine was a product of cleavage of the corresponding oligonucleotide by snake venom phosphodiesterase. This indicated that P–N bond in **23** was resistant to the action of latter enzyme. Also, phosphoramidate **23** resultant from adenallene PPA (**14a**) was not cleaved by snake venom phosphodiesterase [11]. However, according to more recent findings, phosphoralaninates **23** derived from AZT and d4T were degraded [51]. At any rate, it is not clear whether a mammalian phosphodiesterase (5′-exonuclease) can effectively cleave intermediates of type **23**.

Acknowledgements

This study was supported by research grant CA32779 (National Cancer Institute) and program project AI46390 (National Institute of Allergy and Infectious Diseases), NIH, Bethesda, MD, USA.

References

[1] C.K. Chu, D.C. Baker (Eds.), Nucleosides and Nucleotides as Antitumor and Antiviral Agents, Plenum, New York, 1993.

[2] Y-C. Liaw, Y.-G. Gao, V.E. Marquez, A.H.-J. Wang, Nucleic Acids Res. 20 (1992) 459–465.

[3] C Pengaud, G Gosselin, J-L Imbach, Curr. Top. Med Chem 2 (1997) 15–29.

[4] C. McGuigan, D Cahard, H M. Sheeka, E De Clercq, J. Balzarini, J. Med Chem 39 (1996) 1748–1753

[5] C. Meier, Synlett (1998) 233–242.

[6] C. McGuigan, K G. Devine, T.J. O'Connor, S A. Galpin, D.J Jeffries, D. Kinchington, Antiviral Chem Chemother 1 (1990) 107–113

[7] C McGuigan, R N Pathirana, J Balzarini, E. De Clercq, J. Med Chem 36 (1993) 1048–1052.

[8] C. McGuigan, H-W Tsang, P W. Sutton, E. De Clercq, J. Balzarini, Antiviral Chem Chemother 9 (1998) 109–115.

[9] C. McGuigan, L. Bidois, A Hiouni, C Ballatore, E. De Clercq, J. Balzarini, Antiviral Chem Chemother. 11 (2000) 111–116

[10] P. Franchetti, L Cappellacci, M Grifantini, L Messini, G.A. Sheikha, A G. Loi, E Tramontano, A De Montis, M G Spiga, P La Colla, J Med. Chem. 37 (1994) 3534–3541.

[11] H Winter, Y. Maeda, H Mitsuya, J. Zemlicka, J Med Chem. 39 (1996) 3300–3306

[12] H Winter, Y. Maeda, H Uchida, H Mitsuya, J. Zemlicka, J Med Chem. 40 (1997) 2191–2195.

[13] Y-L. Qiu, R G Ptak, J M. Breitenbach, J.-S Lin, Y-C. Cheng, J C Drach, E R Kern, J Zemlicka, Antiviral Res 43 (1999) 37–53

[14] D. Egron, I Lefebvre, C. Pengaud, T. Beltran, A. Pompon, G Gosselin, A-M. Aubertin, J-L Imbach, Bioorg. Med Chem. Lett. 8 (1998) 1045–1050

[15] T.K. Venkatachalam, H.-L. Tai, R Vig, C -L. Chen, S -T Jan, F.M Uckun, Bioorg Med Chem. Lett 8 (1998) 3121–3126

[16] S Manfredini, P.G Baraldi, E. Durini, S. Vertuani, J. Balzarini, E. De Clercq, A. Karlsson, V Buzzoni, L. Thelander, J. Med Chem 42 (1999) 3243–3250.

[17] D Kimar, B Kanz, B.M Mamiya, J T Kern, S M Kerwin, Tetrahedron Lett 42 (2001) 565–567

[18] C R Wagner, V V Iyer, E.J McIntee, Med Res Rev 20 (2000) 417–451

[19] C McGuigan, H -W. Tsang, D Cahard, K Turner, S Velazquez, A Salgado, L. Bidois, L. Naesens, E De Clercq, J. Balzarini, Antiviral Res. 35 (1997) 195–204

[20] J Balzarini, O Wedgwood, J Kruining, H. Pelemans, R. Heijtink, E De Clercq, C McGuigan, Biochem. Biophys. Res Commun 225 (1996) 363–369

[21] C McGuigan, O.M Wedgwood, E De Clercq, J Balzarini, Bioorg Med Chem Lett 6 (1996) 2359–2362

[22] C McGuigan, M.J Slater, N R Parry, A Perry, S Harris, Bioorg Med Chem. Lett 10 (2000) 645–647

[23] A Q Siddiqui, C McGuigan, C Ballatore, O Wedgwood, E. De Clercq, J Balzarini, Bioorg Med Chem Lett 9 (1999) 2555–2560

[24] C McGuigan, D. Cahard, H M Sheeka, E De Clercq, J Balzarini, Bioorg Med. Chem Lett. 6 (1996) 1183–1186

[25] C Ballatore, C. McGuigan, E. De Clercq, J. Balzarini, Antiviral Res 46 (2000) A63; 13th International Conference on Antiviral Research, April 16–21, 2000, Baltimore, Maryland, USA, Poster #92, Poster and Slide Reproductions, Compro, Inc , Bayport, New York, USA.

[26] C Ballatore, C. McGuigan, E. De Clercq, J Balzarini, Bioorg Med Chem Lett 11 (2001) 1053–1056.

[27] E J Eisenberg, G.-X He, W.A. Lee, Nucleosides, Nucleotides Nucleic Acids 20 (2001) 1091–1098.

[28] H. Chapman, M Kernan, E. Prisbe, J Rohloff, M Sparacino, T Terhorst, R. Yu, Nucleosides, Nucleotides Nucleic Acids 20 (2001) 621–628

[29] H Chapman, M. Kernan, J. Rohloff, M Sparacino, T Terhorst, Nucleosides, Nucleotides Nucleic Acids 20 (2001) 1085–1090

[30] C Meier, M Lorey, E. De Clercq, J. Balzarini, J Med Chem 41 (1998) 1417–1427.

[31] C. Meier, T. Knispel, E. De Clercq, J. Balzarini, J Med Chem. (1999) 1604–1614

[32] G H Hakimelahi, A.A Moosavi-Mohavedi, M.M. Sadeghi, S -C Tsay, J.R Hwu, J Med. Chem. 38 (1995) 4648–4659.

[33] T Beltran, D Egron, I. Lefebvre, C Perigaud, A Pompon, G. Gosselin, A.-M Aubertin, J -L. Imbach, Nucleosides Nucleotides 18 (1999) 973–975.

[34] T Beltran, D. Egron, A Pompon, I Lefebvre, C. Perigaud, G. Gosselin, A -M Aubertin, J -L Imbach, Bioorg Med Chem. Lett. 11 (2001) 1775–1777.

[35] J Zemlicka, in: C K Chu, D.C. Baker (Eds), Nucleosides and Nucleotides as Antitumor and Antiviral Agents, Plenum, New York, 1993, pp 73–100.

[36] J Zemlicka, Nucleosides Nucleotides 16 (1997) 1003–1012.

[37] J. Zemlicka, in: C.K. Chu (Ed.), Recent Advances in Nucleosides· Chemistry and Chemotherapy, Elsevier, Amsterdam, The Netherlands (2002) in press

[38] D Egron, C Perigaud, G Gosselin, A -M Aubertin, H Gatanaga, H. Mitsuya, J. Zemlicka, J -L. Imbach, Bioorg. Med Chem. Lett. 12 (2002) 265–266.

[39] M.A Johnson, G. Ahluwalia, M.C. Connelly, D A Cooney, S Broder, D G Johns, A. Fridland, J. Biol Chem 263 (1988) 15354–15357.

[40] H. Uchida, E N Kodama, K Yoshimura, Y Maeda, P. Kosalaraksa, V Maroun, Y.-L Qiu, J. Zemlicka, H. Mitsuya, Antimicrob Agents Chemother 43 (1999) 1487–1490

[41] R W. Buckheit, J A Turpin, Antiviral Res 51 (2001) 2–3

[42] Y -L Qiu, F Geiser, T Kira, E Gullen, Y.-C Cheng, R.G. Ptak, J M. Breitenbach, J.C. Drach, C.B. Hartline, E.R Kern, J Zemlicka, Antiviral Chem. Chemother. 11 (2000) 191–202.

[43] K Yoshimura, R Feldman, E Kodama, M F. Kavlick, Y -L. Qiu, J Zemlicka, H Mitsuya, Antimicrob. Agents Chemother 43 (1999) 1483–2479

[44] H Huang, R Chopra, G L. Verdine, S C. Harrison, Science 282 (1998) 1669–1675.

[45] Y -L Qiu, M B Ksebati, R G Ptak, B Y Fan, J M. Breitenbach, J -S. Lin, Y -C Cheng, E R Kern, J C Drach, J. Zemlicka, J. Med. Chem. 41 (1998) 10–23

[46] Y -L. Qiu, R G Ptak, J M Breitenbach, J -S. Lin, Y.-C Cheng, E R Kern, J.C. Drach, J. Zemlicka, Antiviral Chem Chemother 9 (1998) 341–352

[47] R J Rybak, J. Zemlicka, Y -L Qiu, C B Hartline, E R Kern, Antiviral Res 43 (1999) 175–188

[48] H -P Guan, M Ksebati, Y -C Cheng, J C. Drach, E R. Kern, J. Zemlicka, J. Org Chem 65 (2000) 1280–1290.

[49] J Balzarini, A. Karlsson, S Aquaro, C.-F. Perno, D Cahard, L. Naesens, E De Clercq, C McGuigan, Proc Natl. Acad Sci U S A 93 (1996) 7295–7299

[50] G. Valette, A Pompon, J -L Girardet, L. Cappelacci, P Franchetti, M Grifantini, P. La Colla, A G. Loi, C. Perigaud, G Gosselin, J -L Imbach, J Med. Chem 39 (1996) 1981–1990.

[51] D Saboulard, L Naesens, D Cahard, A Salgado, R Pathirana, S. Velasquez, C McGuigan, E. De Clercq, J Balzarini, Mol Pharmacol 56 (1999) 693–704

[52] C. McGuigan, D. Cahard, C Ballatore, A. Siddiqui, E De Clercq, J. Balzarini, Bioorg Med Chem Lett 8 (1998) 2949–2954.

[53] C McGuigan, P W. Sutton, D Cahard, K Turner, G. O'Leary, Y. Wang, M Gumbleton, E De Clercq, J Balzarini, Antiviral Chem Chemother. 9 (1998) 473–479

[54] G DiSabato, W.P Jencks, J. Am Chem. Soc. 83 (1961) 4400–4405.

[55] V M. Clark, A J. Kirby, J. Am Chem Soc 85 (1963) 3705–3706.

[56] V.S Tsivunin, N.I. D'yakonova, J. Gen. Chem. USSR (Engl Transl) 40 (1970) 1983–1987

[57] B Yuodka, V. Kirviliene, L Liorancaite, J Carbohydr , Nucleosides, Nucleotides 6 (1979) 337–357

ELSEVIER

Biochimica et Biophysica Acta 1587 (2002) 287–295

BIOCHIMICA ET BIOPHYSICA ACTA

BBA

www.bba-direct.com

Review

Chemotherapy of varicella-zoster virus by a novel class of highly specific anti-VZV bicyclic pyrimidine nucleosides

J. Balzarini[a,*], C. McGuigan[b]

[a]*Rega Institute for Medical Research, Katholieke Universiteit Leuven, Minderbroedersstraat 10, B-3000 Leuven, Belgium*
[b]*Welsh School of Pharmacy, University of Wales Cardiff, Cardiff CF10 3XF, UK*

Received 24 January 2002, accepted 24 January 2002

Abstract

(*E*)-5-(2-bromovinyl)-2′-deoxyuridine (BVDU) is a potent inhibitor of herpes simplex virus type 1 (HSV-1) and varicella-zoster virus (VZV). Its mechanism of action is based on a specific conversion to its 5′-mono- and 5′-diphosphate derivative by HSV-1- and VZV-encoded thymidine kinase, and after further conversion to its 5′-triphosphate derivative, inhibition of the viral DNA polymerase and eventual incorporation into the viral DNA. Recently, a new structural class of bicyclic pyrimidine nucleoside analogues (designated BCNAs) with highly specific and selective anti-VZV activity in cell culture has been discovered. The compounds need a long alkyl or alkylaryl side-chain at the base moiety for pronounced biological activity. This property makes these compounds highly lipophilic. They are also endowed with fluorescent properties when exposed to light with short UV wavelength. In striking contrast to BVDU, the members of this class of compounds are active only against VZV, but not against any other virus, including the closely related HSV-1, HSV-2 and cytomegalovirus. The most active compounds inhibit VZV replication at subnanomolar concentrations and are not toxic at high micromolar concentrations. The compounds lose their antiviral activity against thymidine kinase (TK)-deficient VZV strains, pointing to a pivotal role of the viral TK in their activation (phosphorylation). Kinetic studies with purified enzymes revealed that the compounds were recognized by VZV TK as a substrate, but not by HSV-1 TK, nor by cytosolic or mitochondrial TK. VZV TK is able to phosphorylate the test compounds not only to their corresponding 5′-mono- but also to their 5′-diphosphate derivatives. These data may readily explain and rationalize the anti-VZV selectivity of the BCNAs. There is no clear-cut correlation between the antiviral potency of the compounds and their affinity for VZV TK, pointing to a different structure/activity relationship of the eventual antiviral target of these compounds. The compounds are stable in solution and, in contrast to BVDU, not susceptible to degradation by thymidine phosphorylase. The bicyclic pyrimidine nucleoside analogues represent an entirely new class of highly specific anti-VZV compounds that should be further pursued for clinical development. © 2002 Elsevier Science B.V. All rights reserved.

Keywords: Varicella-zoster virus; Bicyclic nucleoside analogues; Thymidine kinase; Antiviral activity; Chemotherapy

1. Introduction

Nucleoside analogues are well known as antiviral agents of biological interest and clinical utility, dominating the current treatment protocols for human viral infections. In particular, many nucleoside analogues with interesting biological properties have arisen by substitution at the 5-position of the uracil base in the 2′-deoxyuridine series [1]. The 5-(2-substituted-vinyl)-2′-deoxyuridines, in particular ((*E*)-5-(2-bromovinyl)-2′-deoxyuridine, BVDU, Brivudin®), have emerged as potent and selective inhibitors of herpes virus replication, particularly against HSV-1 (herpes simplex virus type 1) [2–4]. 5-Alkynyl-2′-deoxyuridines have also been studied as potential antiviral agents, the parent 5-ethynyl derivative being a potent inhibitor of HSV-1, HSV-2 (herpes simplex virus type 2) and VV (vaccinia virus) [4]. However, this compound is also rather cytotoxic and its antiviral selectivity is low [4,5].

Herpes virus-encoded thymidine kinases (TK) often appear to be able to phosphorylate 5-substituted 2′-deoxy-

---

Abbreviations: BVU, (*E*)-5-(2-bromovinyl)uracil; BVaraU, arabinosyl derivative of BVDU; BVDU, (*E*)-5-(2-bromovinyl)-2′-deoxyuridine; BVriboU, ribosyl derivative of BVDU; ACV, acyclovir; HSV-1, herpes simplex virus type 1; HSV-2, herpes simplex virus type 2; CMV, cytomegalovirus; EC_{50}, 50% effective concentration; CC_{50}, 50% cytostatic concentration; TK, thymidine kinase; VZV, varicella-zoster virus; BCNA, bicyclic nucleoside analogue; TPase, thymidine phosphorylase; DPD, dihydropyrimidine dehydrogenase; $C_{\log}P$, calculated logarithm of the partition coefficient

[*] Corresponding author. Tel.: +32-16337-352/341; fax: +32-16337-340.

E-mail address: jan.balzarini@rega.kuleuven.ac.be (J. Balzarini).

0925-4439/02/$ - see front matter © 2002 Elsevier Science B.V. All rights reserved.
PII: S0925-4439(02)00091-1

uridines to their 5′-monophosphate derivatives [6], and HSV-1 and VZV TK can even further convert the 5′-monophosphates to their 5′-diphosphate counterparts [7–9]. Most nucleoside analogues are further phosphorylated to the triphosphate derivatives by cellular enzymes, acting as inhibitors of virus-encoded DNA polymerase and/or as substrate analogues of these enzymes. Subsequent incorporation into viral DNA often represents the molecular basis of their antiviral action, although other targets such as virus-specified ribonucleotide reductase or even thymidylate synthase [10,11] can be considered as a potential antiviral target for the phosphorylated nucleoside analogues as well. So far, all anti-VZV drugs and the majority of antiherpes agents are specifically activated (phosphorylated) by the virus-encoded thymidine kinase (TK) [2,12].

The structure of HSV-1 thymidine kinase was initially solved as a complex with gancyclovir [13] and with the natural substrate [14,15]. More recently, complexes of HSV-1 TK with the antiherpes drug, acyclovir, [16] and a non-substrate inhibitor, to high resolution, have been published [17], but VZV TK has not been crystallized and its three-dimensional structure is unknown. However, the numerous detailed coordinate sets of HSV-1 TK should be of value in determining the structure of the VZV TK, as these two enzymes share 29% amino acid sequence identity [18]. Knowledge of the sites of binding of many ligands of interest should provide a framework for understanding the different substrate specificities of a range of TKs, including those from other herpes viruses.

The chemical synthesis of 5-alkynyl-2′-deoxyuridines involves the Pd-catalysed coupling of a terminal alkyne with a 5-substituted (usually 5-iodo) 2′-deoxyuridine [19,20]. Whilst these methods give reasonable yields of the desired 5-alkynyl product, they always give variable quantities of a fluorescent by-product, characterized as the cyclised furano system [19–21]. Such by-products apparently arise from the Pd (or Cu) catalysed cyclisation of the desired product and, indeed, can be prepared directly from the 5-alkynyl product upon copper treatment [19]. Previously, the only well-characterized examples of these furano nucleosides have been the parent compound (arising from cyclisation of 5-ethynyl-2′-deoxyuridine) [22–24] and the *n*-butyl analogue [19]. Biological evaluation of these furano nucleosides has not been extensive to date but the parent compound was noted to be inactive against HSV-1, HSV-2, CMV and VZV [24]. Conventional wisdom would be that longer chain homologues would be similarly inactive.

We have recently discovered that certain long-chain substituted fluorescent furano *bic*yclic *n*ucleoside *a*nalogues (designated BCNAs) are in fact potent and selective inhibitors of VZV replication in cell culture [25–28]. This novel discovery has great potential for further exploration with the distinct possibility of new and improved drug discovery. The lead compound Cf1368 has—in cell culture—an anti-VZV activity, which is 100-fold more potent (EC_{50}: 0.008 μM) than the current anti-VZV drug of choice (acyclovir: prodrug Valtrex) [25]. Moreover, we could not detect pronounced toxicity in cell culture. Surprisingly, this drug is active only against VZV, being completely inactive against any other virus, including the closely related HSV-1, HSV-2 and CMV. This pronounced antiviral selectivity is unprecedented.

This review describes the antiviral activities of the novel anti-VZV compounds, their structure–antiviral activity relationships and initial studies on their metabolic/enzymatic activation/inactivation pathways and the possible mechanism of antiviral action.

2. Structure–antiviral activity relationship of BCNAs against VZV replication in cell culture

All BCNAs were evaluated for their inhibitory activity against VZV replication in human embryonic lung (HEL) cell cultures. Confluent HEL cells were grown in 96-well microtiter plates and innoculated with two wild-type (OKA and YS) and two thymidine kinase-deficient (07/1 and YS/R) VZV strains at 100 plaque-forming units (PFU)/well. Antiviral activity of the test compounds was expressed as their 50% effective concentration (EC_{50}) or compound concentration required to reduce viral plaque formation by 50% compared with untreated controls. The 50% cytostatic concentration (CC_{50}) of the BCNAs was determined as the compound concentration required to inhibit exponentially growing HEL cell cultures by 50% (after counting the cell number using semiautomated Coulter counting).

2.1. *BCNAs with a simple n-alkyl side-chain*

Among those BCNAs that contain a simple alkyl side-chain on the bicyclic base ring, the optimal carbon chain length to display the most potent anti-VZV activity ranked between 8 and 10 (Table 1). Indeed, the anti-VZV activity (EC_{50}) of these BCNAs was between 0.008 and 0.02 μM. At shorter or longer side-chain lengths, the antiviral activity markedly decreased by at least 1–2 orders of magnitude. When compared with BVDU and acyclovir (ACV), the most active anti-VZV BCNAs with a simple alkyl side-chain were virtually equally effective as the antiherpes virus drug BVDU (EC_{50}: 0.005 μM) but at least 200-fold more active than ACV, the current drug of choice for the clinical treatment of VZV (Table 1). As for ACV and BVDU, the BCNAs fully lose antiviral activity against thymidine kinase-deficient VZV strains, pointing to a crucial role of the VZV-encoded TK in the activation (phosphorylation) of the BCNAs (Table 1). Interestingly, none of the BCNAs listed in Table 1 were toxic to HEL cell proliferation at concentrations as high as 50–200 μM. As a result, the selectivity index (ratio CC_{50}/EC_{50}) of the prototype compounds Cf1368, Cf1369 and Cf1676 is at least as high as 5000–20,000.

Table 1
Anti-VZV activity of BCNAs containing an alkyl side-chain of the furanyl ring

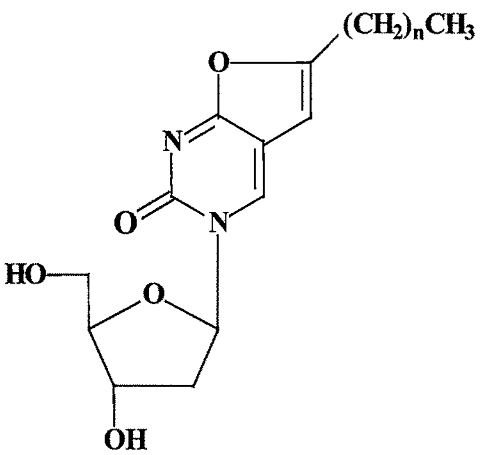

Compound	Total carbons in alkyl side-chain	EC$_{50}$ (µM)[a]				CC$_{50}$ (µM)[a]
		VZV		VZV TK$^-$		
		OKA	YS	07	YS-R	
Cf1382	6 (hexyl)	1.3	2.8	>50	>50	>200
Cf1398	7 (heptyl)	0.12	0.33	>50	>50	>50
Cf1368	8 (octyl)	0.008	0.02	>50	>50	>50
Cf1676	9 (nonyl)	0.02	0.02	>200	>200	>200
Cf1369	10 (decyl)	0.02	0.008	>50	>50	>50
Cf1717	11 (undecyl)	0.4	0.37	>50	>50	>200
Cf1449	12 (dodecyl)	0.8	1.2	>50	>50	>200
BVDU	–	0.005	0.005	>50	>50	>400
ACV	–	1.9	2.1	>50	>50	>200

[a] Data from Ref [25]

2.2. BCNAs with terminal alkyl unsaturation

A variety of BCNAs were synthesized containing a terminal alkyl unsaturation in the side-chain on the furanyl ring of the bicyclic base (Table 2). Although a significant antiviral activity was recorded for the ω-alkenyl- and ω-alkynyl-BCNA derivatives, there is clearly a decreased antiviral efficiency of the ω-alkenyl-, and even more of the ω-alkynyl-BCNAs. Compared with the *n*-octyl-BCNA derivative (Cf1368), the ω-octenyl-BCNAs lost ~ 10-fold antiviral activity, and the ω-octynyl-BCNAs lost approximately 300-fold anti-VZV activity relative to the corresponding parental *n*-octyl-BCNA (Table 2). As found for the simple *n*-alkyl-substituted BCNAs, the terminally unsaturated *n*-alkenyl- and *n*-alkynyl-BCNAs completely lost antiviral activity against VZV TK$^-$ strains (data not shown).

2.3. BCNAs with a terminal halogen substitution in the n-alkyl side-chain

When the terminal methyl group of the alkyl side-chain of the *n*-decyl-BCNA was replaced by a halogen, ω-fluoro substitution virtually retained full antiviral efficacy, and the ω-chloro-, ω-bromo- and ω-iodoalkyl-substituted BCNAs marginally lost antiviral efficacy (up to 2–4-fold) (Table 3). There was no significant difference for the anti-VZV activities of the different ω-halo-substituted alkyl-BCNAs.

2.4. BCNAs with an n-alkylaryl side-chain

In an attempt to restrict the conformational freedom of the alkyl side-chain of the prototype BCNAs Cf1368 and Cf1369, an aromatic ring system (phenyl) was introduced in the side-chain. In particular, a variety of *p*-alkylphenyl-BCNAs have been synthesized and evaluated for anti-VZV activity. As is clear from the antiviral data depicted in Table 4, several members of the alkylaryl-BCNAs were exquisitely inhibitory against VZV replication In particular, the *n*-pentylphenyl- and *n*-hexylphenyl-BCNAs were antivirally active at a concentration as low as 0.0001–0.0005 µM, being endowed with a 10–50-fold higher antiviral potency than the original prototype alkyl-BCNAs Cf1368 and Cf1369. Interestingly, longer and shorter alkyl groups at the para position on the phenyl group of the BCNAs led to lower antiviral activities (Table 4). In fact, shortening or lengthening the optimal pentylphenyl by only two to three carbons lead to a more than 100-fold lowering of the antiviral activity of the test compounds. The existence of an optimal chain length and the close dependence of the anti-VZV activity on the alkylaryl chain length have been also observed for the simple *n*-alkyl-substituted BCNAs. There appeared a strong correlation between the size

Table 2
Anti-VZV activity of BCNAs containing a terminal alkyl unsaturation in the side-chain of the furanyl ring

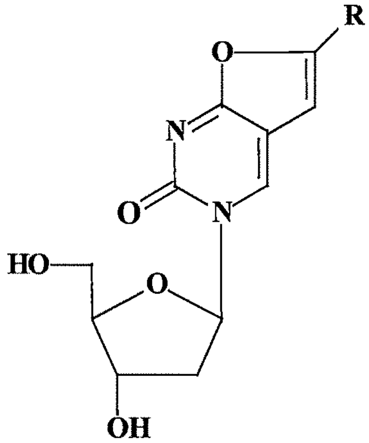

Compound	Side-chain R	EC$_{50}$ (µM) (VZV)[a]		CC$_{50}$ (µM)[a]
		OKA	YS	
Cf1382	$(CH_2)_4CH_2{-}CH_3$	1.3	2.8	>200
Cf1657	$(CH_2)_4CH{=}CH_2$	14	13	>200
Cf1625	$(CH_2)_4C{\equiv}CH$	25	33	>200
Cf1368	$(CH_2)_6CH_2{-}CH_3$	0.008	0.02	>50
Cf1658	$(CH_2)_6CH{=}CH_2$	0.27	0.06	>200
Cf1662	$(CH_2)_6C{\equiv}CH$	5.0	4.0	>200

[a] Data from Ref [29]

Table 3
Anti-VZV activity of BCNAs containing a terminal halogen substitution in the alkyl side-chain of the furanyl ring

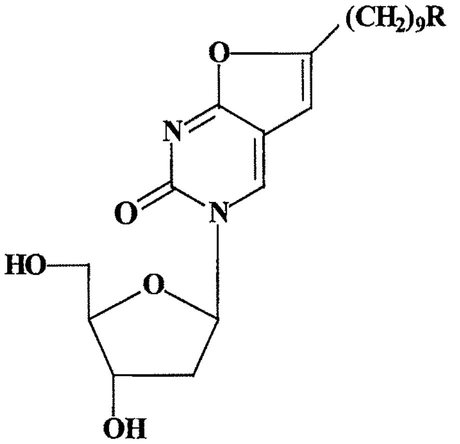

Compound	R	EC$_{50}$ (μM) (VZV)[a]		CC$_{50}$ (μM)[a]
		OKA	YS	
Cf1656	F	0.022	0 014	>200
Cf1770	Cl	0.04	0.02	>200
Cf1558	Br	0.03	0 03	≥50
Cf1649	I	0 06	0 03	>200
Cf1369	CH$_3$	0 02	0.008	≥50

[a] Data from Ref. [30]

(length) of the *n*-alkyl and *n*-alkylaryl moiety of the BCNAs on the one hand, and their optimal antiviral activity on the other (Fig. 1). In fact, if the size of the phenyl group in the alkylaryl-BCNAs is considered as equivalent to ~ 4 methylene groups, the butylaryl-, pentylaryl- and hexylaryl-BCNAs and the octyl-, nonyl- and decyl-BCNAs represent members within each series of BCNAs with the highest antiviral potency (Tables 1 and 4; Fig. 1). It is striking, however, that the alkylaryl-BCNAs are invariably more potent than the *n*-alkyl-BCNAs. This may likely be related to the reduced conformational freedom of the alkylaryl side-chain relative to the long alkyl side-chain and, therefore, the alkylaryl-BCNAs may more optimally fit to their target enzyme than the more flexible *n*-alkyl-BCNAs. The pentylphenyl-BCNA represents the most potent anti-VZV compound hitherto reported. Due to lack of measurable cellular toxicity at 200 μM, its antiviral selectivity (ratio of CC$_{50}$/EC$_{50}$) amounts to ~ 1,000,000, and its anti-VZV potency is 10–30-fold more pronounced than BVDU, and ~ 10,000-fold more pronounced than ACV.

2.5. BCNAs with other heteroatoms in the bicyclic ring

The parent furano nucleus in the BCNAs has also been changed to a pyrro or thieno ring system, and the antiviral activities of these analogues compared for a series of *n*-alkyl-substituted BCNAs (Table 5). Whereas substitution of the oxygen in the furano moiety by a nitrogen generally reduced the antiviral activity by 10–50-fold, the replacement of the oxygen by a sulfur atom resulted in most cases in a further 5–10-fold increased anti-VZV activity. It is unclear whether the increased potency of

Table 4
Anti-VZV activity of BCNAs containing a *p*-alkyl-substituted phenyl group as the side-chain of the furanyl ring

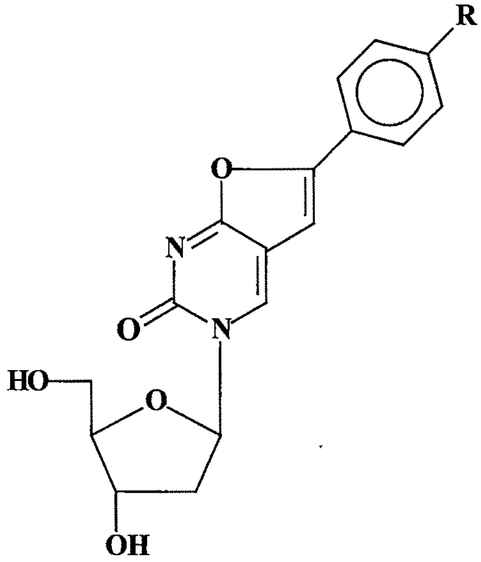

Compound	R	EC$_{50}$ (μM) (VZV)[a]		CC$_{50}$ (μM)[a]
		OKA	YS	
Cf1837	H	0.28	0.16	>200
Cf1835	Methyl	0.06	0 06	>200
Cf1836	Ethyl	0.09	0.07	123
Cf1698	*n*-Propyl	0 01	0.008	188
Cf1744	*n*-Butyl	0.002	0 0005	>200
Cf1743	*n*-Pentyl	0.0003	0.0001	>200
Cf1742	*n*-Hexyl	0.0005	0.0001	18
Cf1712	*n*-Heptyl	0 005	0.003	18
Cf1711	*n*-Octyl	0 04	0.03	>200

[a] Data from Ref. [26].

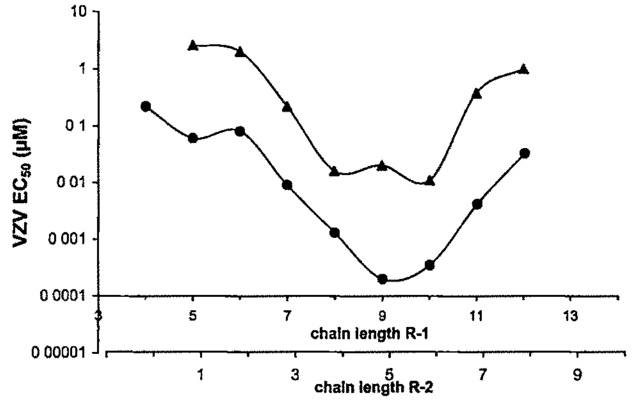

Fig. 1 Correlation between the anti-VZV activity of the simple *n*-alkyl- (▲) (alkyl chain length R-1) and alkylphenyl-BCNAs (●) (alkyl chain length R-2) and the carbon side-chain length of the molecules. Assuming that the phenyl group in the alkylaryl-BCNA series accounts for four-carbon chain lengths, the correlation of optimal anti-VZV activity between both series of compounds fits very well.

Table 5
Anti-VZV activity of BCNAs containing different hetero atoms in the five-membered ring of the base

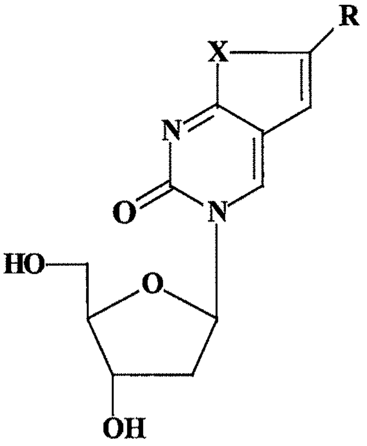

Compound	Nature of the X hetero atom	Carbon length in *n*-alkyl (R) side-chain	EC_{50} (μM) (VZV)[a]		CC_{50} (μM)[a]
			OKA	YS	
Cf1382	O	6	1.3	2.8	>200
Cf1368	O	8	0.008	0.02	>50
Cf1369	O	10	0.02	0.008	>50
Cf1449	O	12	0.8	1.2	>200
Cf2011	S	6	0.08	0.08	>200
Cf2012	S	8	0.001	0.001	53
Cf1603	S	10	0.03	0.06	54
Cf2013	S	12	0.20	0.20	49
Cf1395	NH	6	>50	>50	>50
Cf1397	NH	8	0.15	0.48	>50
Cf1681	NH	10	~ 10[b]	~ 2[b]	>200
Cf1450	NH	12	2.4	14	>200

[a] Data from Refs. [25,31,32].

[b] An accurate EC_{50} value could not be calculated due to incomplete inhibition of VZV replication at higher drug concentrations and lack of a consistent dose–response curve

most thieno-BCNAs compared with the furano-BCNA is of benefit due to the higher cellular toxicity of the thieno-BCNAs.

2.6. BCNAs with a different sugar moiety

Since the arabinosyl derivative of BVDU (designated BVaraU or Sorivudine®) is at least as potent an antiherpetic agent as the deoxyriboside derivative [33], and since it has also been reported that BVriboU is endowed with antiherpetic activity [34], the sugar-modified arabinosyl and ribofuranosyl derivatives of the prototype *n*-octyl-BCNA (Cf1368) were synthesized and evaluated for their antiviral (VZV) potencies (Table 6). In marked contrast with BVaraU, the arabinosyl-BCNA was 300-fold less potent as an anti-VZV agent than its 2′-deoxy derivative, and the BCNA riboside was 3000-fold less potent in its anti-VZV activity. The free *n*-octyl-bicyclic base was devoid of any measurable anti-VZV activity (as also observed for BVU, the free base of BVDU).

3. Lipophilicity and water solubility of BCNAs

There is a stringent requirement of a relatively long alkyl or alkylphenyl side-chain at C-6 of the bicyclic furano or thieno pyrimidine ring of the BCNAs to display optimal anti-VZV activity. This property results in a relatively high lipophilicity of the compounds (represented by their calculated log *P* values ($C_{\log}P$) that range between 2.5 and 3.5). This striking observation has been noticed for the different series of BCNAs, including the *n*-alkylfurano (series 1), alkylphenylfurano (series 2), terminally unsaturated *n*-alkylfurano (series 3), *n*-alkylthieno (series 4) and *n*-alkylpyrro (series 5) BCNAs (Fig. 2). The fact that a higher lipophilicity of BCNAs more or less corresponds with higher bulkiness of the side-chain, it is conceivable that an optimal $C_{\log}P$ value for optimal anti-VZV activity reflects an optimal lipophilic interaction in the active site of the enzymes, or an optimal size of the side-chain that must fit in a lipophilic pocket of the particular enzymes. In an attempt to enhance the water solubility of the lead BCNAs, replacement of one of the methylene units in the *n*-decyl-BCNA chain by an oxygen (resulting in glycol/ether derivatives of the *n*-decyl-BCNA) resulted in a dramatically decreased $C_{\log}P$ value of ~ 1.1 and a concomittantly decreased antiviral activity by 100- to >1000-fold [35]. Also, the terminally unsaturated *n*-alkyl-BCNAs have a low (alkene) to dramatically lower (alkyne) $C_{\log}P$, and also a concomittant 50–500-fold lower antiviral activity [29]. However, in both glycol/ether and terminal unsaturated *n*-alkyl-BCNA series, the overall size of the side-chain is virtually constant. Therefore, these observations suggest that the overall lipophilicity, rather than the size of the side-chain, is a predominant property

Table 6
Anti-VZV activity of BCNAs as a free base, or with modifications in the sugar moiety

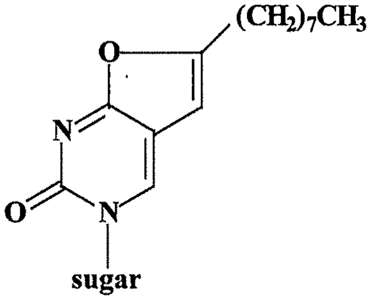

Compound	Sugar configuration	EC_{50} (μM) (VZV)[a]		CC_{50} (μM)[a]
		OKA	YS	
Cf1368	2′-deoxyribose	0.008	0.024	>50
Cf1400	ribose	23	21	50
Cf1433	arabinose	3.6	3.3	>20
Cf1381[b]	–	>20	>20	>20
Cf2200[c]	–	>20	>20	>20

[a] Data from Refs [27,28].

[b] Free base of Cf1368.

[c] Free base of Cf1743.

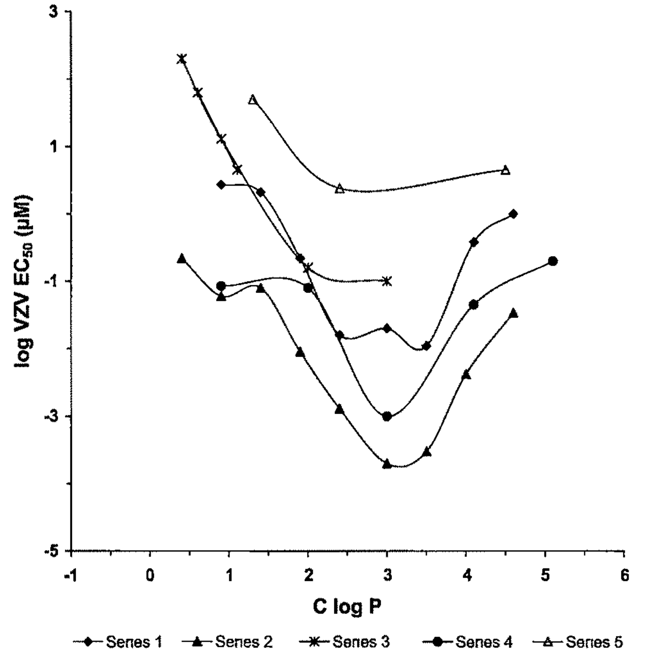

Fig 2 Correlation between calculated log$P$ ($C_{\log}P$) of BCNAs and their anti-VZV activity The data of five series of BCNAs are shown Series 1. *n*-alkyl-BCNAs (Table 1) Series 2: *n*-alkylphenyl-BCNAs (Table 4) Series 3· terminal unsaturated *n*-alkyl-BCNAs (Table 2) Series 4 thienopyrimidine BCNAs (Table 5) Series 5: pyrrolopyrimidine BCNAs (Table 5)

that eventually determines the antiviral potency of the test compounds. It may be somewhat surprising that a presumed lipophilic pocket to accommodate the rather bulky side-chain on the bicyclic pyrimidine ring of the BCNAs must be able to optimally adapt in at least two different enzymes (the activating (phosphorylating) VZV TK and the eventual antiviral target enzyme).

Although the high lipophilicity of the BCNAs results in a low to very low water solubility (< 1 mg/l of the *n*-decyl-BCNA at room temperature), it is expected to lead to an efficient penetration of the BCNAs through cellular membranes and biological barriers such as the blood/brain barrier and the skin. This property may be advantageous for this novel class of anti-VZV compounds because uptake of the lipophilic BCNAs into cells and into biological compartments that may harvest the virus, may be facilitated by the higher lipophilicity of these drugs.

4. Anabolic conversion of BCNAs to their phosphorylated derivatives

Since the BCNAs listed in Tables 1–6 markedly lose antiviral activity against VZV strains that are deficient in the virus-encoded thymidine kinase, it can be anticipated that the compounds need to be activated (phosphorylated) by the viral TK before they inhibit their antiviral targets.

A variety of BCNAs, in particular the series of *n*-alkylphenyl-BCNAs, were evaluated for their inhibitory effect against 1 µM [^{3}H]dThd phosphorylation by VZV TK, HSV-1 TK, HSV-2 TK, TK-1 and TK-2 (Table 7). Only VZV TK-catalysed [^{3}H]dThd phosphorylation was inhibited by the BCNAs, reflecting their affinity for VZV TK, likely a competitive inhibition of the enzyme reaction with the natural substrate. It also became obvious from these data that there was no close correlation between affinity for VZV TK and the eventual anti-VZV activity of the BCNAs. These observations make it clear that the SARs of the activating (phosphorylating) enzyme are different from those of the (antiviral) target enzyme.

Cf1368 and Cf1369 were directly investigated as substrates for purified VZV TK, and also for purified HSV-1 and HSV-2 TK [36]. Interestingly, only VZV TK measurably converted the compounds to their 5′-monophosphate derivatives. By contrast, BVDU was easily converted to its 5′-monophosphate derivative by VZV TK, and also by HSV-1 TK, and HSV-2 TK (and mitochondrial TK) [6]. BVDU is not measurably phosphorylated by cytosolic TK-

Table 7
Inhibitory effect of *n*-alkylphenyl-BCNAs against [^{3}H]dThd phosphorylation by cytosolic TK-1, mitochondrial TK-2, HSV-1 TK, HSV-2 TK and VZV TK

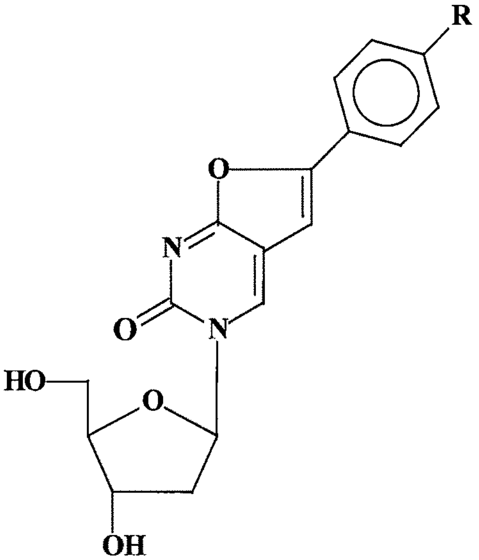

Compound	R	IC$_{50}$ (µM)[a]				
		TK-1	TK-2	HSV-1 TK	HSV-2 TK	VZV TK
Cf1837	H		>500	>500	≥500	0.37
Cf1835	Methyl		>500	>500	>500	3.1
Cf1836	Ethyl	>500	>500	>500	>500	13
Cf1698	Propyl	>500	>500	>500	>500	25
Cf1744	Butyl	>500	>500	>500	>500	4.7
Cf1743	Pentyl	>500	>500	>500	>500	3.9
Cf1742	Hexyl	>500	>500	>500	>500	4.5
Cf1712	Heptyl		>500	>500	>500	3540
Cf1711	Octyl		>500	>500	>500	>5000
Cf1368		>500	>500	>5000	>5000	37
BVDU		>1000	0.34	2.9	5.6	1.5

[a] 50% Inhibitory concentration or compound concentration required to inhibit nucleoside kinase-catalysed phosphorylation of 1 µM [CH_3-^{3}H]dThd by 50%

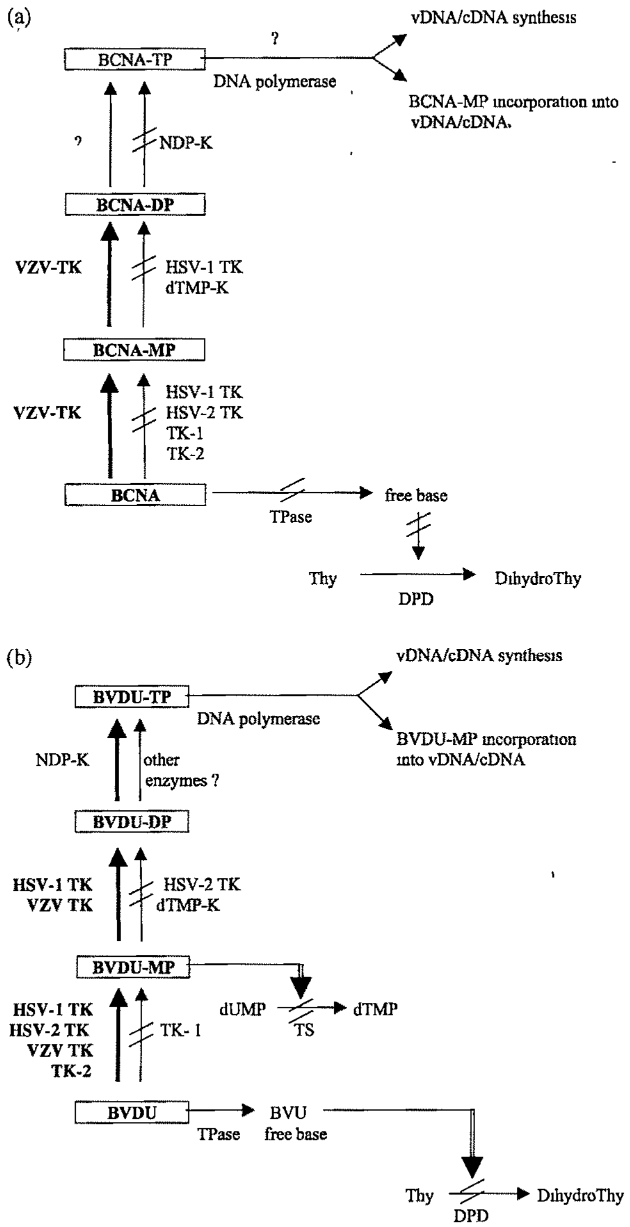

Fig 3. (a) Metabolic fate of BCNAs BCNA is converted to its 5′-mono- (BCNA-MP) and 5′-diphosphate (BCNA-DP) by TK encoded by VZV, but not by HSV-1 TK, HSV-2 T, mitochondrial TK-2 or cytosolic TK-1 BCNA-DP is not a substrate for *E coli* or human erythrocyte nucleoside diphosphate kinase (NDP-K) It is not known whether other cellular enzymes may recognize BCNA-DP as a substrate to be converted to BCNA-TP BCNA is not measurably hydrolysed by *E coli* or human erythrocyte TPase to its free base [39] The free bicyclic base does not inhibit dihydropyrimidine dehydrogenase (DPD) [39] (b) Metabolic fate of BVDU. BVDU is converted to its 5′-monophosphate derivative by the TKs encoded by HSV-1, HSV-2 and VZV, and by mitochondrial TK-2, but not by cytosolic TK-1 BVDU-MP inhibits thymidylate synthase (TS) BVDU-MP is converted to its 5′-diphosphate derivative by the TKs encoded by HSV-1 and VZV TK, but not by HSV-2 TK or cytosolic dTMP kinase (dTMP-K). BVDU-DP is converted by NDP kinase (NDP-K) to BVDU-TP. The latter metabolite is recognized by cellular and herpetic DNA polymerases, and incorporated into viral and cellular DNA BVDU is hydrolysed by thymidine phosphorylase (TPase) to its free base BVU, which in turn is a potent inhibitor of dihydropyrimidine dehydrogenase (DPD).

1. Compared with BVDU, the BCNAs had a much higher V_{max} but also a much higher K_m, for VZV TK. The exact V_{max} values for the BCNAs could not be measured due to limited solubility of the compounds, in the millimolar concentration range.

We also evaluated the 5′-monophosphate derivatives of Cf1368 (Cf1928) and Cf1369 (Cf1602) as substrates for the dTMP kinase activity associated with VZV TK and HSV-1 TK [36]. Again, both enzymes displayed a striking discrimination between BVDU-MP and the BCNA-MPs. Whereas BVDU-MP was efficiently converted by both enzymes to its 5′-diphosphate derivative (BVDU-DP), only VZV TK, but not HSV-1 TK, was able to recognize the BCNA-MPs as efficient substrates for phosphorylation. Cellular dTMP kinase was also unable to recognise the BCNA-monophosphates. Thus, it became clear that the BCNAs are selectively phosphorylated to their 5′-diphosphates by the two successive enzyme activities of VZV TK (thymidine kinase and dTMP kinase), while they are not recognized by the TK/dTMP kinase activity of HSV-1 or the cytosol under similar experimental conditions (Fig. 3a). In this respect, the BCNAs strikingly differ from BVDU (Fig. 3b) and our observations provide an explanation for the unprecedented inhibitory specificity of the BCNAs for VZV.

Interestingly, when human erythrocyte NDP kinase was added to a reaction mixture containing BVDU or BCNAs and VZV TK, a considerable amount of BVDU-TP was formed, whereas no trace of BCNA-TP could be detected [36]. Although it cannot be excluded that the BCNA-DPs can be recognized by other NDP kinase isoenzymes or by other (less obvious) cellular enzymes, our observations may indicate that the mechanism of anti-VZV activity of the novel class of BCNAs may be entirely different from that of BVDU (being a competitive inhibitor of viral DNA polymerase and incorporated into viral DNA upon conversion to the 5′-triphosphate derivative). This is being further studied in our laboratories.

5. Catabolic conversion of BCNAs by cellular enzymes

Nucleoside analogues may be prone to catabolic hydrolysis by several enzymes (i.e., purine nucleoside phosphorylase (PNPase), thymidine phosphorylase (TPase), uridine phosphorylase (UPase)). In particular, 2′-deoxyribonucleoside analogues such as BVDU are good substrates for thymidine phosphorylase, which efficiently converts BVDU to its free (antivirally inactive) base BVU [37]. Crystals of *E. coli* TPase complexed with the natural substrate dThd [38] demonstrate that the hydrogen at the N(3) position of the pyrimidine ring forms a hydrogen bridge with amino acid Ser-186 of TPase, and the carbonyl group at position 4 of the pyrimidine ring forms a close interaction with amino acid Arg-171. Interestingly, the BCNAs have no free carbonyl at the same position in the pyrimidine ring, but more importantly, due to the fused ring system, the bicyclic base of the BCNAs has no hydrogen available on the original N(3) position of the pyrimidine ring. Therefore, it could be anticipated that TPase would not efficiently recognize the BCNAs as substrates for cleavage to the free base. Indeed, when the BCNAs were exposed to both *E coli* or human TPase, no hydrolysis to the free base could be detected under conditions where BVDU and dThd were markedly converted to their free bases BVU and Thy, respectively [39]. It follows that—in contrast to BVDU—the BCNAs do not act as substrates for the catabolic TPase and thus, should be rather stable in biological systems (i.e., plasma). Indeed, preliminary experiments in which Cf1368 was administered both intravenously or perorally, no indication of release of the free base was obtained, and a pronounced appearance of unaltered drug in plasma upon oral administration was found (unpublished data).

6. Conclusions

The novel class of BCNAs represents the most potent and selective anti-VZV compounds hitherto described. The selectivity is at least partially based on a specific ability of VZV TK to convert the compounds to their 5′-mono- and 5′-diphosphate derivatives. Although the BCNAs have a number of interesting properties that make them prime candidates for further development to the clinic, their molecular mechanism of action remains to be resolved and is currently the subject of further investigations.

Acknowledgements

The auhors are grateful to R. Alvarez, H. Barucki, O. Bidet, S. Blewett, A. Brancale, A. Carrangio, C. Jarvis, G. Jones, A. Jukes, G. Luoni, R. Pathirana, G. Srinivasan, S. Velázquez and C.-J. Yarnold for chemical synthesis, and G. Andrei, A. Camps, S. Carmans, L. Naesens, R. Sienaert, R. Snoeck and L. Vandenheurck for their contributions to the biological evaluations. We thank also Christiane Callebaut for dedicated editorial assistance.

References

[1] E De Clercq, Targets for the antiviral activity of pyrimidine and purine nucleoside analogues, Nucleosides Nucleotides 6 (1987) 197–207

[2] E De Clercq, Biochemical aspects of the selective antiherpes activity of nucleoside analogues, Biochem Pharmacol 33 (1984) 2159–2169

[3] E De Clercq, J Descamps, P De Somer, P.J. Barr, A.S. Jones, R T Walker, *E*-5-(2-bromovinyl)-2′-deoxyuridine: a potent and selective antiherpes agent, Proc Natl. Acad. Sci U S. A 76 (1979) 2947–2951

[4] E De Clercq, J. Descamps, G. Verhelst, R T Walker, A S Jones, P F Torrence, D Shugar, Comparative efficacy of different antiherpes drugs against different strains of herpes simplex virus, J Infect. Dis 141 (1980) 563–574.

[5] E De Clercq, J Balzarini, P F Torrence, M.P Mertes, C L. Schmidt, D. Shugar, P J. Barr, A S Jones, G Verhelst, R T Walker, Thymidylate synthetase as target enzyme for the inhibitory activity of 5-substituted 2′-deoxyuridines on mouse leukemia L-1210 cell growth, Mol Pharmacol 19 (1981) 321–330

[6] Y-C Cheng, G. Dutschman, E De Clercq, A S Jones, S G. Rahim, G Verhelst, R.T Walker, Differential affinities of 5-(2-halogenovinyl)-2′-deoxyuridines for deoxythymidine kinases of various origins, Mol. Pharmacol 20 (1981) 230–233

[7] Y-C Cheng, W P. Summers, J Walker, W C. Summers, W H. Prusoff, Characterization of pyrimidine deoxyribonucleoside kinase (thymidine kinase) and thymidylate kinase as a multifunctional enzyme in cells transformed by herpes simplex virus type 1 and in cells infected with mutant strains of herpes simplex virus, J Virol 30 (1979) 942–945

[8] M S Chen, W.H Prusoff, Association of thymidylate kinase activity with pyrimidine deoxyribonucleoside kinase induced by herpes simplex virus, J Biol Chem 253 (1978) 1325–1327

[9] J A Fyfe, Differential phosphorylation of (*E*)-5-(2-bromovinyl)-2′-deoxyuridine monophosphate by thymidylate kinases from herpes simplex virus type 1 and 2 and varicella-zoster virus, Mol Pharmacol 21 (1981) 432–437

[10] P J Barr, P.A. Nolan, D V Santi, M J Robins, Inhibition of thymidylate synthetase by 5-alkynyl-2′-deoxyuridylates, J Med Chem 24 (1981) 1385–1388.

[11] J Balzarini, E De Clercq, M P Mertes, D Shugar, P F Torrence, 5-substituted 2′-deoxyuridines· correlation between inhibition of tumor cell growth and inhibition of thymidine kinase and thymidylate synthetase, Biochem Pharmacol. 31 (1982) 3673–3682

[12] Y C Cheng, G. Dutschman, E De Clercq, A S Jones, S G Rahim, G Verhelst, R.T. Walker, Differential affinities of 5-(halogenovinyl)-2′-deoxyuridines for deoxythymidine kinases of various origins, Mol Pharmacol 20 (1981) 230–233.

[13] D G Brown, R Visse, G. Sandhu, A Davies, P.J Rizkallah, C. Melitz, W C. Summers, M R Sanderson, Crystal structures of the thymidine kinase from herpes simplex virus type-1 in complex with deoxythymidine and ganciclovir, Nat Struct Biol 2 (1995) 876–881.

[14] K Wild, T Bohner, A Aubry, G Folkers, G E. Schulz, Three-dimensional structure of thymidine kinase from herpes simplex virus type 1, FEBS Lett. 368 (1995) 289–292

[15] K Wild, T Bohner, G. Folkers, G E. Schulz, The structures of thymidine kinase from herpes simplex virus type 1 in complex with substrates and a substrate analogue, Protein Sci 6 (1997) 2097–2106

[16] J N. Champness, M S Bennett, F Wien, R Visse, W C Summers, P. Herdewijn, E De Clercq, T Ostrowski, R L Jarvest, M.R. Sanderson, Exploring the active site of herpes simplex virus type-1 thymidine kinase by X-ray crystallography of complexes with aciclovir and other ligands, Proteins 32 (1998) 350–361

[17] M S Bennett, F Wien, J N Champness, T Batuwangala, T Rutherford, W C. Summers, H Sun, G Wright, M R Sanderson, Structure to 1 9 Å resolution of a complex with herpes simplex virus type-1 thymidine kinase of a novel, non-substrate inhibitor: X-ray crystallographic comparison with binding of aciclovir, FEBS Lett. 443 (1999) 121–125.

[18] P T Harrison, R Thompson, A J Davison, Evolution of herpesvirus thymidine kinases from cellular deoxycytidine kinase, J Gen Virol 72 (1991) 2583–2586.

[19] M J Robins, P J Barr, Nucleic acid related compounds 39 Efficient conversion of 5-iodo to 5-alkynyl and derived 5-substituted uracil bases and nucleosides, J Org. Chem 48 (1983) 1854–1862

[20] M J Robins, P J Barr, Nucleic acid related compounds 31 Smooth and efficient palladium-copper catalyzed coupling of terminal alkynes with 5-iodouracil nucleosides, Tetrahedron Lett. 22 (1981) 421–424

[21] G T Crisp, B L Flynn, Palladium-catalysed coupling of terminal alkynes with 5-(trifluoromethanesulfonyloxy)pyrimidine nucleosides, J. Org Chem 58 (1993) 6614–6619

[22] R Kumar, E E Knaus, L.I Wiebe, Synthesis and properties of 5-(1,2-

dihaloethyl)-2′-deoxyuridines and related analogs, J. Heterocycl. Chem. 28 (1991) 1917–1925

[23] K. Eger, M. Jalalian, M Schmidt, Steric fixation of bromovinyluracil—synthesis of furo[2,3-D]pyrimidine nucleosides, J. Heterocycl Chem. 32 (1995) 211–218.

[24] R Kumar, L.I. Wiebe, E E. Knaus, Synthesis of 5-(1-aridovinyl) and 5-[2-(1-azirinyl)] analogs of 2′-deoxyuridine, Can. J. Chem. 74 (1996) 1609–1615

[25] C McGuigan, C.J. Yarnold, G. Jones, S Velazquez, H. Barucki, A. Brancale, G Andrei, R Snoeck, E. De Clercq, J Balzarini, Potent and selective inhibition of varicella-zoster virus (VZV) by nucleoside analogues with an unusual bicyclic base, J. Med. Chem 42 (1999) 4479–4484.

[26] C. McGuigan, H. Barucki, S. Blewett, A Carangio, J T Erichsen, G. Andrei, R Snoeck, E De Clercq, J Balzarini, Highly potent and selective inhibition of varicella-zoster virus by bicyclic furopyrimidine nucleosides bearing an aryl side-chain, J. Med Chem. 43 (2000) 4993–4997.

[27] C McGuigan, A. Brancale, H. Barucki, S Srinivasan, G. Jones, R. Pathirana, S Blewett, R Alvarez, C J. Yarnold, A. Carangio, S. Velázquez, G. Andrei, R. Snoeck, E. De Clercq, J Balzarini, Fluorescent bicyclic furo pyrimidine deoxynucleoside analogs as potent and selective inhibitors of VZV and potential future drugs for the treatment of chickenpox and shingles, Drugs of the Future 25 (2000) 1151–1161.

[28] C McGuigan, A Brancale, H Barucki, S. Srinivasan, G Jones, R. Pathirana, A Carangio, S Blewett, G. Luoni, O. Bidet, A Jukes, C. Jarvis, G Andrei, R. Snoeck, E De Clercq, J. Balzarini, Furano pyrimidines as novel potent and selective anti-VZV agents, Antiviral Chem Chemother. 12 (2001) 77–89.

[29] S. Srinivasan, C. McGuigan, G Andrei, R. Snoeck, E De Clercq, J Balzarini, Bicyclic nucleoside inhibitors of varicella-zoster virus (VZV)· the effect of terminal unsaturation in the side chain, Bioorg Med. Chem Lett. 11 (2001) 391–393.

[30] A. Brancale, C. McGuigan, G. Andrei, R. Snoeck, E De Clercq, J. Balzarini, Bicyclic nucleoside inhibitors of varicella-zoster virus (VZV): the effect of a terminal halogen substitution in the side chain, Bioorg. Med Chem Lett. 10 (2000) 1215–1217

[31] C. McGuigan, R.N Pathirana, G. Jones, G Andrei, R. Snoeck, E De Clercq, J. Balzarini, Anti-varicella-zoster virus bicyclic nucleosides: replacement of furo by pyrro base reduces antiviral potency, Antiviral Chem Chemother. 11 (2000) 343–348

[32] A Brancale, C McGuigan, B. Algain, P. Savy, R Benhida, J -L. Fourrey, G. Andrei, R. Snoeck, E. De Clercq, J. Balzarini, Bicyclic anti-VZV nucleosides: thieno analogues retain full antiviral activity, Bioorg. Med Chem Lett 11 (2001) 2507–2510

[33] H Machida, A Kuninaka, H. Yoshino, K. Ikeda, Y. Mizuno, Antiherpesviral activity and inhibitory action on cell growth of 5-alkenyl derivatives of 1-β-D-arabinofuranosyluracil, Antimicrob. Agents Chemother. 17 (1980) 1030–1031

[34] R Bernaerts, C. Desgranges, E. De Clercq, (*E*)-5-(2-bromovinyl)uridine requires phosphorylation by the herpes simplex virus (type 1)-induced thymidine kinase to express its antiviral activity, Biochem Pharmacol 38 (1989) 1955–1961

[35] A. Brancale, S Srinivasan, C. McGuigan, G. Andrei, R. Snoeck, E De Clercq, J. Balzarini, Synthesis and anti-varicella-zoster virus activity of some novel bicyclic nucleoside inhibitors: effect of enhanced aqueous solubility, Antiviral Chem. Chemother 11 (2000) 383–393

[36] R. Sienaert, L. Naesens, A. Brancale, E. De Clercq, C McGuigan, J Balzarini, Specific recognition of the bicyclic pyrimidine nucleoside analogues, a new class of highly potent and selective inhibitors of varicella-zoster virus (VZV), by the VZV-encoded thymidine kinase, Mol. Pharmacol 61 (2002) 249–256

[37] C Desgranges, G. Razaka, M. Rabaud, H Bricaud, J Balzarini, E. De Clercq, Phosphorolysis of (*E*)-5-(2-bromovinyl)-2′-deoxyuridine (BVDU) and other 5-substituted 2′-deoxyuridines by purified human thymidine phosphorylase and intact blood platelets, Biochem Pharmacol 32 (1983) 3583–3590

[38] M.R. Walter, W.J. Cook, L.B. Cole, S.A. Short, G W. Koszalka, T.A Krenitsky, S.E Ealick, Three-dimensional structure of thymidine phosphorylase from Escherichia coli at 2.8 A resolution, J Biol Chem. 265 (1990) 14016–14022

[39] J Balzarini, R. Sienaert, S Liekens, A. Van Kuilemburg, A Carangio, R Esnouf, E. De Clercq, C. McGuigan, Lack of suspectibility of bicyclic nucleoside analogs, highly potent inhibitors of varicella-zoster virus, to the catabolic action of thymidine phosphorylase and dihydropyrimidine dehydrogenase, Mol Pharmacol 61 (2002) 1146–1153.

ELSEVIER

Biochimica et Biophysica Acta 1587 (2002) 296–299

BIOCHIMICA ET BIOPHYSICA ACTA

BBA

www.bba-direct.com

Review

Perspectives on the molecular mechanism of inhibition and toxicity of nucleoside analogs that target HIV-1 reverse transcriptase

Karen S. Anderson*

Department of Pharmacology, Yale University School of Medicine, 333 Cedar Street, New Haven, CT 06520, USA

Received 24 January 2002, accepted 24 January 2002

Abstract

Among the acquired immunodeficiency syndrome (AIDS) drugs approved by the FDA for clinical use, two are modified cytosine analogs, Zalcitabine (ddC) and Lamivudine [(−)3TC] (−)3TC is the only analog containing an unnatural L (−) nucleoside configuration. Similar to other dideoxy nucleosides, these analogs are metabolically activated to the triphosphate that is incorporated into DNA by human immunodeficiency virus type 1 (HIV-1) reverse transcriptase (RT) resulting in DNA chain termination and ultimately cessation of viral replication. The natural D (+) 3TC isomer also acts in a similar manner to inhibit HIV-1 RT. In cell culture, (−)3TC is less toxic than its D (+) isomer, (+)3TC, containing the natural nucleoside configuration, and both are considerably less toxic than 2′,3′-dideoxycytidine (ddC) The mechanistic basis for the stereochemical selectivity and differential toxicity of the isomeric 2′,3′-dideoxy-3′-thiacytidine (3TC) and ddC compounds is not completely understood although a number of factors may clearly come into play. We have previously investigated the mechanistic basis for the differential stereoselective inhibition and toxicity of these three cytosine analogs by comparing the effects of 2′,3′-deoxycytidine-5′-triphosphate (ddCTP), β-D-(+)-2′3′-dideoxy-3′-thiacytidine-5′-triphosphate [(+)3TC-TP] and β-L-(−)-2′3′-dideoxy-3′-thiacytidine-5′-triphosphate [(−)3TC-TP] on the HIV-1 RT as well as a recombinant form of the human mitochondrial DNA polymerase gamma (Pol γ), the holoenzyme polymerase responsible for mitochondrial DNA replication. In this review, we discuss studies which may provide insight into the molecular mechanism for the stereochemical selectivity and differential toxicity. © 2002 Published by Elsevier Science B.V.

Keywords HIV-1 RT; Cytosine analog, Mitochondrial DNA polymerase gamma; 3TC

---

1. Introduction

Virally encoded reverse transcriptase (RT) is required for replication of the human immunodeficiency virus (HIV), an etiological agent for acquired immunodeficiency syndrome (AIDS). RT is considered to be the molecular target of several therapeutic agents that interfere with HIV replication, including the 5′-*O*-triphosphates of 3′-azido-3′-deoxythymidine (AZT), 2′,3′-didehydro-2′,3′-dideoxythymidine (d4T), 2′,3′-dideoxycytidine (ddC) and the β-L-(−)-2′,3′-dideoxy-3′-thiacytidine [3TC, (−)SddC]. Among all of the nucleoside inhibitors currently used clinically, 2′,3′-dideoxy-3′-thiacytidine (3TC) is the only one with the unnatural L-configuration. Most interestingly, 3TC has been shown to be more potent and less toxic than the D-isomer [1–4]. The mechanistic basis for the stereochemical selectivity and differential toxicity of the isomeric 3TC and ddC compounds is not completely understood although a number of factors may clearly come into play. The differences in potency and toxicity may be a combination of factors including uptake, transport, metabolic activation, incorporation and degradation [1–3,5–9]. In addition, toxicity to the host may also be related to inhibition of human mitochondrial DNA polymerase gamma (Pol γ) [8–10].

The mechanism of inhibition of HIV type 1 (HIV-1) RT and Pol γ by dideoxy nucleoside analogs such as 3TC and

---

Abbreviations AIDS, acquired immunodeficiency syndrome, AZT, 3′-azido-3′-deoxythymidine, d4T, 2′,3′-didehydro-2′,3′-deoxythymidine, ddC, 2′,3′-dideoxycytidine; ddI, 2′,3′-dideoxyinosine, Pol γ, DNA polymerase gamma, dCMP, 2′-deoxycytidine-5′-monophosphate; ddCMP, 2′,3′-deoxycytidine-5′-monophosphate; dCTP, 2′-deoxycytidine-5′-triphosphate; ddCTP, 2′,3′-deoxycytidine-5′-triphosphate, HIV-1, human immunodeficiency virus type 1, RT, reverse transcriptase; (+)3TC-TP, β-D-(+)-2′3′-dideoxy-3′-thiacytidine-5′-triphosphate, (−)3TC-TP, β-L-(−)-2′3′-dideoxy-3′-thiacytidine-5′-triphosphate; 3TC, 2′,3′-dideoxy-3′-thiacytidine, 3TC-MP, 2′,3′-dideoxy-3′-thiacytidine-5′-monophosphate; 3TC-TP, 2′,3′-dideoxy-3′-thiacytidine-5′-triphosphate

* Corresponding author. Tel.: +1-203-785-4526, fax. +1-203-785-7670.

E-mail address: karen anderson@yale.edu (K S Anderson)

0925-4439/02/$ - see front matter © 2002 Published by Elsevier Science B.V.

PII: S0925-4439(02)00092-3

Table 1
Comparison of incorporation efficiencies for modified dNTPs by HIV-1 RT or Pol γ [15]

Polymerase	dCTP analogs	k_{pol} (s^{-1})	K_d (μM)	k_{pol}/K_d ($\mu M^{-1}\ s^{-1}$)	Selectivity[a]
HIV-1 RT	dCTP	1.88 ± 0.10	23.6 ± 5.0	0.080	
	ddCTP	0.35 ± 0.02	68.7 ± 11.4	0.0051	15.7
	(+)3TC-TP	0.036 ± 0.003	43.5 ± 8.9	0.0008	100
	(−)3TC-TP	0.019 ± 0.001	14.8 ± 2.8	0.0013	62
Pol γ	dCTP	44 ± 2	1.1 ± 0.1	40	
	ddCTP	0.66 ± 0.02	0.041 ± 0.007	16	2.5
	(+)3TC-TP	0.35 ± 0.01	1.5 ± 0.1	0.23	179
	(−)3TC-TP	0.125 ± 0.005	9.2 ± 0.9	0.014	2857

[a] Selectivity = (k_{pol}/K_d)natural substrate/(k_{pol}/K_d)analog taken from Refs. [14,15]

ddC [(−)SddC][1] involves in vivo phosphorylation to the triphosphate [2′,3′-dideoxy-3′-thiacytidine-5′-triphosphate (3TC-TP) and ddCTP] and subsequent incorporation into the DNA primer strand resulting in chain termination. Thus, in vitro studies have focused on evaluating the triphosphate form of the analogs primarily using a steady-state kinetic analysis to assess affinity and incorporation efficiency. These steady-state methods are important to provide an initial kinetic comparison; however, to obtain mechanistic and quantitative information, a more detailed transient kinetic analysis is required [11–13]. Our efforts to delineate the molecular mechanisms of nucleoside analog inhibition of HIV-1 RT and Pol γ are based upon a transient kinetic approach using rapid chemical quench and stopped-flow fluorescence methodologies. The important advantage of this approach is the ability to observe *directly* events occurring at the active site including binding events, protein conformational changes, and catalysis. The rate constants of individual steps can be measured directly and any enzyme intermediates including different conformational species that might be formed can be observed directly. Using transient kinetic methods, the rate of polymerization (k_{pol}), the dissociation constant for the ground state nucleotide binding (K_d) and incorporation efficiency or specificity constant (k_{pol}/K_d) for the natural substrate, 2′-deoxycytidine-5′-triphosphate (dCTP), as well as for 2′,3′-deoxycytidine-5′-triphosphate (ddCTP), β-D-(+)-2′3′-dideoxy-3′-thiacytidine-5′-triphosphate [(+)3TC-TP] and β-L-(−)-2′3′-dideoxy-3′-thiacytidine-5′-triphosphate [(−)3TC-TP] was assessed for HIV-1 RT and Pol γ [14,15], using a synthetic 23/45-mer DNA/DNA primer-template.

Our goal in this analysis is to develop an understanding of the structure activity relationship (SAR) that allows a correlation between the structural and stereochemical features of nucleoside analog drugs with their kinetic and mechanistic behavior toward relevant HIV-1 RT and host polymerase targets such as Pol γ. An in-depth understanding of the mechanisms of inhibition of these enzymes may be important in overcoming problems associated with toxicity. For example, if both the structural similarities and differences were understood, this might identify features important in selective interaction with HIV-1 RT over Pol γ.

HIV-1 RT and Pol γ both have the ability to carry out DNA-dependent as well as RNA-dependent DNA synthesis. In contrast to HIV-1 RT that has no proofreading activity, and similar to many of the DNA polymerases, Pol γ has 3′–5′ exonuclease activity, which is believed to perform a proofreading function [16,17]. It is possible that the failure of 3′–5′ exonuclease of Pol γ to efficiently remove chain terminators may play a role in mitochondrial toxicity of nucleoside analogs. However, discrepancies exist in the literature concerning the efficiency of the exonuclease in removal of these analogs and correlation to drug toxicity. It has been proposed that efficient removal of 3′ terminal (−)3TC-MP by the 3′–5′ exonuclease activity of Pol γ could be responsible for the low toxicity of (−)3TC [9]; however, similar rates of exonuclease removal were reported for the excision of 2′-deoxycytidine-5′-monophosphate (dCMP), 2′,3′-deoxycytidine-5′-monophosphate (ddCMP) and (−)3TC-MP from the 3′-terminus of a DNA primer, even though there are significant differences in mitochondrial toxicity [9]. We have also investigated the exonuclease cleavage of Pol γ by evaluating the excision of dCMP, ddCMP, (+)3TC-MP, (−)3TC-MP, and dTMP, from the 3′-terminus of the corresponding DNA 23- or 24-mer primer [15].

2. Results

2.1. A comparison of dNTP incorporation efficiency

A comparison of the k_{pol}, K_d, and k_{pol}/K_d values for each dCTP analog for HIV-1 RT and Pol γ is shown in Table 1. A comparison of these analogs reveals that the natural substrate, dCTP, serves as the best substrate for HIV-1 RT and the human mitochondrial DNA γ polymerase. In general, the incorporation efficiency (k_{pol}/K_d) for Pol γ is much higher than HIV-1 RT and thus a more proficient polymerase. The selectivity values in Table 1 indicate the ability of the polymerase to discriminate between the natural substrate and the substrate analog. It is interesting to note that while, in general, the Pol γ has an overall higher level of discrimination, the exception is ddCTP. In this case, Pol γ has a selectivity of 2.5 over dCTP while for HIV-1 RT, this value is 15.7. It is surprising that Pol γ incorporates ddCTP with such a high level of efficiency. A second important distinction between the two polymerases relates to the issue of stereochemistry and the selectivity for incorporating the natural analog versus the unnatural one with the L-(−) configuration. The HIV-1 RT incorporates the natural (+)3TC-TP analog with a selectivity of only 1.6 over (−)3TC-TP while Pol γ is much more highly discriminating on the basis of stereochemistry with a value of 16. The affinity of (−)3TC-TP for the enzyme–DNA complex is six- to eight-fold weaker than that of the analog of (+)3TC-TP, containing the natural nucleoside configuration. Accordingly, Pol γ incorporates the (−) isomer at least 16-fold less efficiently than the (+) isomer as defined by the specificity constants summarized in Table 2. This difference in incorporation efficiency is in good agreement with cell culture studies with the nucleoside form of the compounds where the (+)3TC isomer has been reported to be 25- and 12-fold more toxic than the (−)3TC in terms of inhibition of cell growth and mitochondrial DNA synthesis, respectively [5].

---

[1] The abbreviation 3TC is most commonly used to refer to the unnatural L or (−) isomer, (−)SddC while the natural D or (+)SddC. While we have used the common nomenclature in the literature, the most appropriate chemical nomenclature for 3TC is (−)-*cis*-1-[2-hydroxymethyl-1,3-oxathiolan-5-yl]cytosine.

2.2. Exonuclease activity

An in-depth analysis of Pol γ 3′–5′exonuclease removal of ddC, (+) and (−)3TC monophosphates (MP) from duplex DNA with highly purified Pol γ reconstituted holoenzyme complex was conducted [15]. Our analysis was carried out using DNA substrates that were 3′-terminated with ddCMP (D24-ddC), (+)3TC-MP [D24-(+)3TC] or (−)3TC-MP [D24-(+)3TC], along with the corresponding unmodified DNA 24-mers containing dCMP (D24-dC). A summary of the rates of exonuclease activity (k_{exo}) for the holoenzyme complex of Pol γ, using various D24-mer substrates is shown in Table 3. In spite of the slow excision rate, the exonuclease should still effectively remove the 3TC-chain terminators with a half-life of approximately 1 min. Although this will slow the rate of mitochondrial DNA replication, the low rate of 3TC incorporation will minimize the toxic effects.

Table 2
Understanding the molecular basis for differential toxicity of modified cytosine analogs [15]

dNTP	Relative incorporation[a]	Relative exonuclease[b]	Relative toxicity[c]
ddCTP	1140	<0.001	2300
(+)3TC-TP	16	1.2	12
(−)3TC-TP	1	1	1

[a] Calculated from $k_{\text{pol}}/K_{\text{d}}$ for each nucleotide from Table 1.

[b] Calculated from the observed exonuclease rate from Table 3.

[c] From Ref. [5] in which the nucleoside form of the analogs are assessed.

Table 3
Comparing the removal of DNA chain terminated substrates by Pol γ exonuclease activity [15]

DNA substrates primer[a]	Holoenzyme k_{exo} (s^{-1})
D24-dC	0.022 ± 0.001
D24-ddC	<0.00001[b]
D24-(+)3TC	0.012 ± 0.001
D24-(−)3TC	0.010 ± 0.001

[a] All of the templates used in this study were a DNA 45-mer.

[b] The minimum estimate of the rate of hydrolysis was calculated from the observation that less than 1% of the DNA was hydrolyzed after 12 h of incubation with the holoenzyme [15].

In contrast, little or *no* DNA cleavage was observed for D24-ddC, 12 h with the holoenzyme. The insusceptibility of the 3′-terminal ddCMP to base excision was also reported for a 3′–5′ exonuclease with porcine liver DNA polymerase γ [18]. Similar results have been reported in studies on yeast mitochondrial DNA polymerases, where the terminally incorporated ddTMP, AZTMP, and ddCMP were not removed by the 3′–5′exonuclease activity of Pol γ [19]. This striking observation may explain why inhibition of mitochondrial DNA synthesis by ddC is so profound.

3. Discussion

Our studies have shown that (−)3TC-TP is less efficiently incorporated than (+)3TC-TP into DNA by Pol γ and both are incorporated less efficiently than ddCTP. Moreover, the efficiency of incorporation by Pol γ is directly correlated with toxicity of each nucleoside analog. These observations point to incorporation by Pol γ into mitochondrial DNA as a major site of toxicity of nucleoside analogs. The availability of reliable preparations of Pol γ [20] now affords a rapid method to screen drugs for toxicity and opens the path toward further structure/function studies to aid in the design of less toxic analogs.

The unnatural L-(−) configuration of (−)3TC seems to play an important role in preserving the anti-viral activity while decreasing the inhibitory effect on the host Pol γ. This example suggests that other unnatural nucleoside analogs may show similar effectiveness combined with low toxicity.

In contrast, the effects of inhibition on mitochondrial DNA synthesis in vivo and in vitro by ddC are profound [21,22]. The IC_{50} value for ddC relative to the (+) and (−) isomers of 3TC, indicated that ddC is 180- and 2300-fold more toxic than the (+) and (−) isomers, respectively [3]. A number of factors may clearly come into play including uptake, transport, metabolic activation, degradation and removal from the system, but our studies have shown a lack of exonucleolytic removal of a 3′ ddC that may significantly contribute to drug toxicity. Conversely, analogs that activate the exonuclease removal by Pol γ may exhibit even lower toxicity; and this may provide a new avenue for exploration of less toxic drugs. Clearly, additional studies are required to identify the structural features of nucleoside analogs that may be utilized to obtain selectivity for HIV-1 RT over DNA Pol γ.

4. Conclusions and perspectives

In summary, our studies have demonstrated that the (+)3TC-TP is a more potent inhibitor for human mitochondrial DNA Pol γ than the (−) isomer, through tighter binding and faster incorporation rate into a DNA duplex, leading to greater toxicity [15,23]. Using highly purified Pol γ, there is no significant difference in the excision of the incorporated (+) and (−)3TC-MP by the 3′–5′ exonuclease activity of Pol γ from the 3′-terminus of a DNA primer, indicating this step likely does *not* contribute to the low toxicity of (−)3TC. Additionally, our studies have shown that a terminally incorporated ddCMP is not efficiently removed by the 3′–5′ exonuclease activity of Pol γ, suggesting this may play a role in the high level of inhibition of ddC on mitochondrial DNA synthesis observed in vitro and in vivo. The overall toxicity of a nucleoside analog towards replication will be a function of the frequency of incorporation of the chain terminator and the kinetics of excision by the proofreading exonuclease, relative to the rate of DNA replication required to sustain growth. We can now quantify these parameters and begin to assess the structural/functional determinants that govern nucleotide selectivity for Pol γ in each step.

An in-depth understanding of the mechanism of inhibition of DNA polymerase γ is important in defining the cytotoxicity of anti-HIV drugs towards mitochondrial replication. A knowledge of the mechanistic and structural similarities and differences between Pol γ and HIV-1 RT may identify key features important for selective drug incorporation by the viral HIV-1 RT but not by Pol γ and therefore facilitate the design of less toxic, viral-specific AIDS drugs.

Acknowledgements

This work is supported by NIH Grant GM49551 to K.S.A.

References

[1] N. Cammack, P. Rouse, C.L. Marr, P.J. Reid, R.E. Boehme, J A. Coates, C.R Penn, J M. Cameron, Biochem Pharmacol. 43 (1992) 2059–2064

[2] R.F. Schinazi, C.K Chu, A Peck, A. McMillan, R. Mathis, D Cannon, L.-S. Jeong, J.W. Beach, W.B Choi, S Yeola, D C. Liotta, Antimicrob. Agents Chemother. 36 (1992) 672–676

[3] C N Chang, S.L. Doong, J.H Zhou, J W Beach, L S Jeong, C K Chu, C H Tsai, Y C. Cheng, D Liotta, R. Schinazi, J Biol Chem 267 (1992) 13938–13942.

[4] P.A Furman, M Davis, D C. Liotta, M. Paff, L.W Frick, D J. Nelson, R E. Dornsife, J.A. Wurster, L J Wilson, J A. Fyfe, J.V. Tuttle, W H. Miller, L. Condreay, D.R Averett, R F Schinazi, G.R. Painter, Antimicrob Agents Chemother 36 (1992) 2686–2692.

[5] C.N Chang, V. Skalski, J H Zhou, Y.C. Cheng, J. Biol Chem 267 (1992) 22414–22420

[6] V. Skalski, C.N. Chang, G. Dutschman, Y.C Cheng, J Biol. Chem. 268 (1993) 23234–23238.

[7] G.J. Hart, D C. Orr, C.R. Penn, H.T Figueiredo, N.M. Gray, R E Boehme, J M. Cameron, Antimicrob. Agents Chemother 36 (1992) 1688–1694.

[8] W.B. Parker, Y.-C Cheng, J NIH Res. 6 (1994) 57–61.

[9] N.M Gray, C L. Marr, C.R. Penn, J.M Cameron, C Bethell, Biochem. Pharmacol 50 (1995) 1043–1051

[10] M. Kukhanova, S.-H. Liu, D. Mozzherin, T.-S Lin, C.K Chu, Y.-C. Cheng, J. Biol Chem 270 (1995) 23055–23059.

[11] K S Anderson, J A. Sikorski, K.A. Johnson, Biochemistry 27 (1988) 7395–7406.

[12] K.A. Johnson, Enzymes 20 (1992) 1–61

[13] K A Johnson, Annu. Rev. Biochem. 62 (1993) 685–713

[14] J Y. Feng, K S Anderson, Biochemistry 38 (1999) 55–63

[15] J.Y. Feng, A. Johnson, K.A. Johnson, K.S Anderson, J Biol. Chem 276 (2001) 23832–23837

[16] H Gray, T W Wong, J. Biol Chem 267 (1992) 5835–5841

[17] M W. Olson, L.S. Kaguni, J Biol Chem. 267 (1992) 23136–23142

[18] M J. Longley, D.W Mosbaugh, J Biol Chem 266 (1991) 24702–24711

[19] S Eriksson, B Xu, D.A. Clayton, J Biol Chem. 270 (1995) 18929–18934.

[20] A A. Johnson, Y Tsai, S W. Graves, K A. Johnson, Biochemistry 39 (2000) 1702–1708

[21] R M. Dubinsky, R Yarchoan, M. Dalakas, S Broder, Muscle Nerve 12 (1989) 856–860.

[22] C.H Chen, M. Vazquez-Padua, Y.C. Cheng, Mol Pharmacol. 39 (1991) 625–628.

[23] K.S. Anderson, Antiviral Chemistry + Chemotheraphy 12 (Suppl 1) (2001) 13–17.

ELSEVIER

Biochimica et Biophysica Acta 1587 (2002) 300–308

BIOCHIMICA ET BIOPHYSICA ACTA

BBA

www.bba-direct.com

Review

Targeting critical regions in genomic DNA with AT-specific anticancer drugs

Jan M. Woynarowski*

Cancer Therapy and Research Center, Institute for Drug Development, University of Texas Health Science Center at San Antonio, 14960 Omicron Drive, San Antonio, TX 78245, USA

Received 24 January 2002; accepted 24 January 2002

Abstract

Cellular DNA is not a uniform target for DNA-reactive drugs. At the nucleotide level, drugs recognize and bind short motifs of a few base pairs. The location of drug adducts at the genomic level depends on how these short motifs are distributed in larger domains. This aspect, referred to as region specificity, may be critical for the biological outcome of drug action. Recent studies demonstrated that certain minor groove binding (MGB) drugs, such as bizelesin, produce region-specific lesions in cellular DNA. Bizelesin binds mainly T(A/T)$_4$A sites, which are on average scarce, but occasionally cluster in distinct minisatellite regions (200–1000 bp of ~ 85–100% AT), herein referred to as AT islands. Bizelesin-targeted AT islands are likely to function as strong matrix attachment regions (MARs), domains that organize DNA loops on the nuclear matrix. Distortion of MAR-like AT islands may be a basis for the observed inhibition of new replicon initiation and the extreme lethality of bizelesin adducts (< 10 adducts/cell for cell growth inhibition). Hence, long AT-islands represent a novel class of critical targets for anticancer drugs. The AT island paradigm illustrates the potential of the concept of regional targeting as an essential component of the rational design of new sequence-specific DNA-reactive drugs. © 2002 Elsevier Science B.V. All rights reserved.

Keywords: Bizelesin; DNA damage; AT island; Mapping DNA binding site; Sequence specificity; Region specificity

1. Introduction: The concept of region-specific DNA damage

Recent developments of new anticancer therapeutic strategies emphasize specific cellular targets. Pointed interventions exploiting molecular differences between tumor and normal cells promise better treatment selectivity. Nonetheless, killing tumor cells, rather than just re-regulating their growth, remains the ultimate clinical objective. Damage to cellular DNA by nonspecific drugs is a clinically proven, although definitely not ideal, "lethal" strategy. This review discusses alternative lethal strategies based on targeting distinct critical regions of cellular DNA with small molecule, sequence-specific agents.

Cellular DNA is not a uniform target for DNA-reactive drugs. At the nucleotide level, drugs recognize and bind short motifs of a few base pairs (*sequence specificity*). The location of drug adducts at the genomic level depends on how these short motifs are distributed in larger domains (*region specificity*). Region-specific targeting signifies not only the ability to damage a desired critical target that may have distinct structural and/or functional properties, but also implies limited collateral damage elsewhere in the genome. DNA lesions in critical domains of cellular DNA are likely to have grave biological consequences. In contrast, damage to nonessential targets may contribute little to killing cancer cells, yet result in adverse effects in normal cells [1,2]. DNA-reactive drugs currently in the clinic, which bind to cellular DNA indiscriminately, cannot be region-specific [1]. Moreover, the profound majority of adducts formed by such drugs are with macromolecules other than DNA [1,3]. Increased treatment selectivity could be anticipated for the treatment strategies that: (i) eliminate, or at least limit, nonessential collateral damage and (ii) result in drug-induced damage localized to critical regions of the genome.

Abbreviations: bp, base pairs; CPI, cyclopropylpyrroloindole, MAR, matrix associated region

* Molecular Pharmacology, Cancer Therapy and Research Center, Institute for Drug Development, 14960 Omicron Drive, San Antonio, TX 78245-3217, USA. Tel.: +1-210-677-3832, fax: +1-210-677-0058

E-mail address: jmwl@saci.org (J.M. Woynarowski)

0925-4439/02/$ - see front matter © 2002 Elsevier Science B.V. All rights reserved

PII S0925-4439(02)00093-5

2. The potential of sequence-specific small molecules for region-specific DNA damage

Progress in the rational design of sequence-specific molecules [4–8], in particular the elucidation of base-pairing rules for pyrrole–imidazole polyamides [4,9–11], has allowed for the recognition of relatively long discrete motifs of several base pairs. In principle, agents of this level of sequence specificity should enable region-specific targeting of individual genes ("anti-gene" strategy), which necessitates the recognition of a single site in the genome. Thus far, "anti-gene" strategies have been pursued with triple-helix-forming oligonucleotides (TFO) or oligonucleotide-mimicking compounds [12–14]. These efforts, although intensive, were mainly limited to model systems and have not yet resulted in agents capable of in vivo activity in tumor-bearing animals.

Sequence-specific agents that do exhibit promising in vivo antitumor activities are found among minor groove binding (MGB) drugs. Studies by us and other researchers demonstrated that AT-specific anticancer drugs, such as tallimustine, the cyclopropylpyrroloindole (CPI) family (such as adozelesin and bizelesin, Fig. 1), and strand scission enediyne agents exhibit a remarkable sequence specificity with intracellular DNA [15–23]. Several of these AT-specific MGBs are in clinical trials [24–30].

The importance of determining which specific domains are damaged by DNA-reactive drugs has been recognized [31–33]. However, our investigations were the first that established a systematic approach that allows us to assess the potential of sequence-specific agents for localized damage in longer stretches of DNA (i.e., region specificity). Our approach combines molecular pharmacology and bioinformatics tools and comprises the following elements: (i) experimental determination of drug sequence specificity (binding motifs), (ii) in silico analysis of binding motif distribution at the genomic level to identify which genomic regions may be particularly vulnerable to a specific drug, and, (iii) the experimental verification of such predictions by mapping drug sites and quantitating drug-induced lesions in selected specific regions. Consistent results with drugs of divergent sequence specificities strongly suggest the utility of this approach [19,21,34–38].

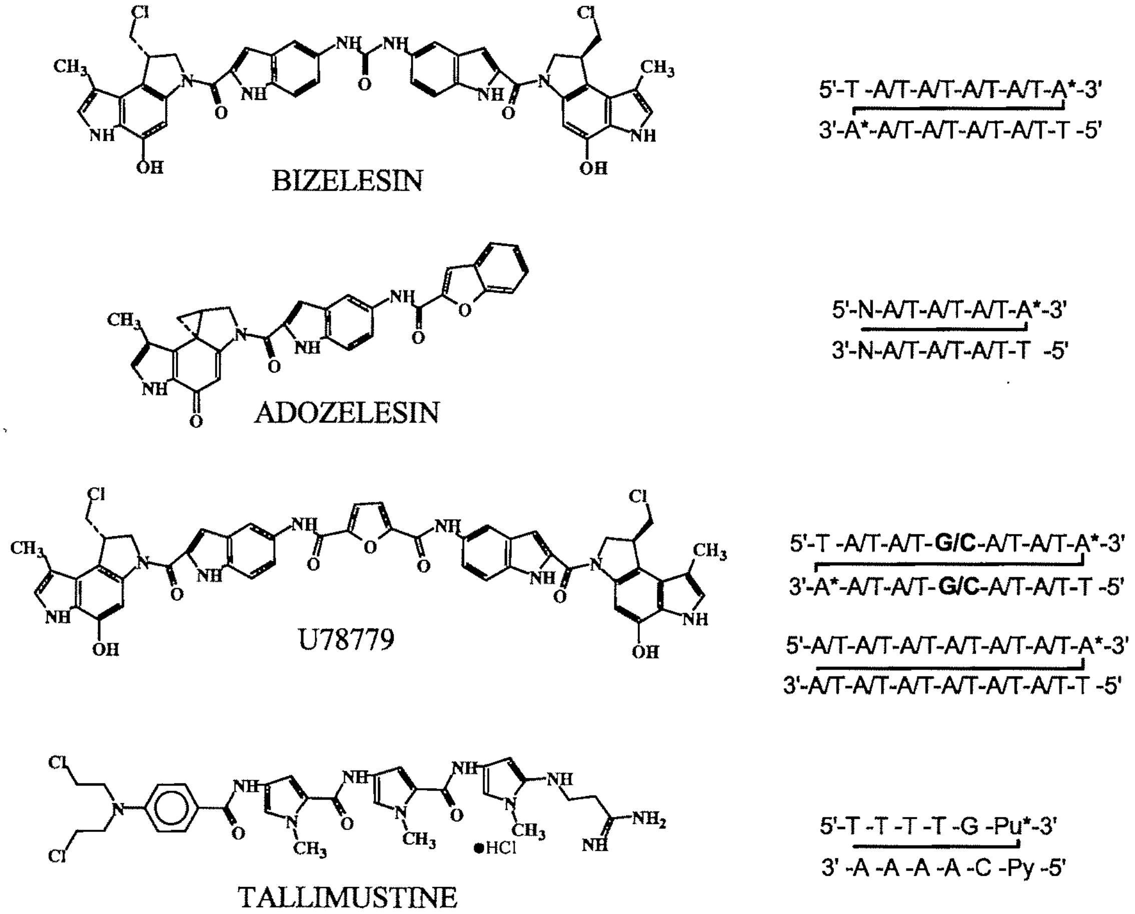
BIZELESIN
5'-T -A/T-A/T-A/T-A/T-A*-3'
3'-A*-A/T-A/T-A/T-A/T-T -5'
ADOZELESIN
5'-N-A/T-A/T-A/T-A*-3'
3'-N-A/T-A/T-A/T-T -5'
U78779
5'-T -A/T-A/T-G/C-A/T-A/T-A*-3'
3'-A*-A/T-A/T-G/C-A/T-A/T-T -5'
5'-A/T-A/T-A/T-A/T-A/T-A/T-A*-3'
3'-A/T-A/T-A/T-A/T-A/T-A/T-T -5'
TALLIMUSTINE
5'-T -T -T -T -G -Pu*-3'
3' -A -A -A -A -C -Py -5'

Fig. 1. AT-specific drugs of the CPI family (bizelesin, adozelesin and U78779), and tallimustine and their preferred binding motifs [18,19,21,35]. U78779 prefers mixed AT–GC motifs (top motif is an example), although the drug binds also pure AT motifs (bottom). Asterisks indicate covalently adducted bases.

2.1. Region-specific damage to AT islands by bizelesin: a proof of principle

Our studies demonstrated for the first time that sequence-specific small molecules can produce a nonrandom, region-specific damage to genomic DNA. Importantly, these findings have been made with bizelesin, a CPI drug with demonstrated antitumor activity in vivo [39] and indications of antitumor efficacy in patients in Phase I trials (Ref. [28] and Dr. E. Rowinsky, personal communication).

Bizelesin binds mainly to $T(A/T)_4A$ sites in cellular DNA, forming interstrand crosslinks (Fig. 1), although some mono-adducts are also possible [18]. Long-range in silico analysis shows that at the genomic level, the bizelesin binding motif $T(A/T)_4A$ is found on average 2.8 times/250 bp. However, approximately every 10^6 bp, a hot spot is found with high

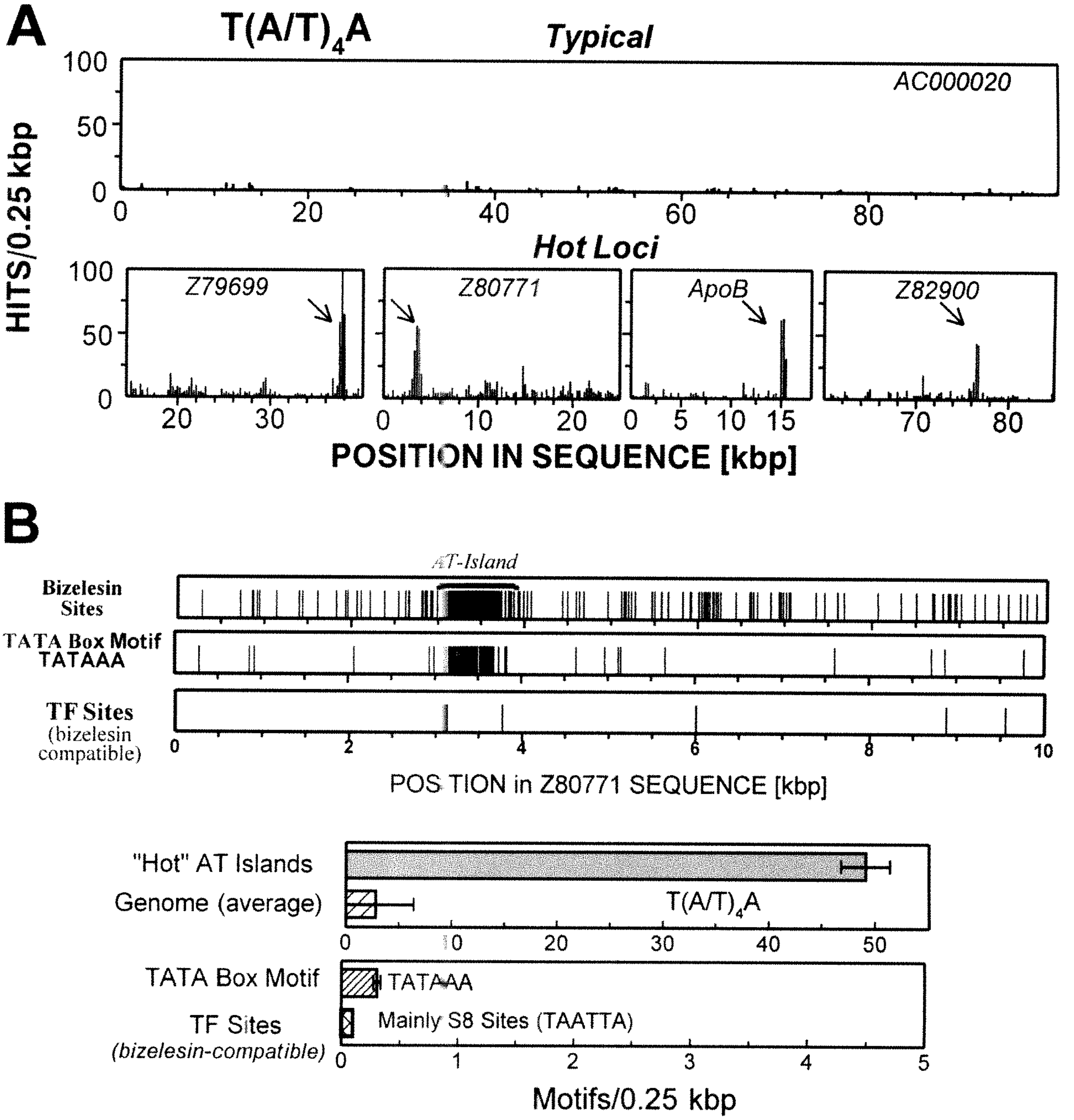

Fig. 2. (A) Bizelesin binding sites in genomic DNA are infrequent but clustered in long AT islands. Examples of in silico analysis of the distribution of bizelesin binding motif. The histograms depict the number of exact matches to the bizelesin motif in bins of 250 bp along the indicated GenBank sequences. (B) TATA boxes, transcription factor (TF) binding sites and other short AT tracts are insignificant as bizelesin targets. Top: The distribution of bizelesin binding sites and the consensus motifs for bizelesin-compatible AT elements around an AT island (in GenBank Z80771). Bottom: The density of bizelesin binding motif in long AT islands markedly exceeds genome average. TATA boxes and bizelesin-compatible TF binding sites are even less frequent than this low average. (Note the expanded scale for TATA boxes and TF. Adapted with permission from Ref. [38]).

clusters of potential binding sites (up to 99 sites/250 bp, Fig. 2A). These clusters of bizelesin motifs are in 200–1000 bp long islands of highly (up to 100%) AT-rich DNA. Notably, compared to these long AT islands, various short AT-tracts are unlikely to be significant as a target for bizelesin (Fig. 2B).

Actual bizelesin lesions show an excellent agreement with the in silico predictions based on the distribution of bizelesin binding motifs $T(A/T)_4A$ [21,38]. Fig. 3 illustrates the sites of predicted and actual drug lesions in the naked DNA of a model AT island. Bizelesin was ~ 100-fold more reactive with this AT island than with a model non-AT island DNA [21,38]. Consistent with the in silico predictions, the same preference for long AT islands is maintained in drug-treated cells. The examples of data illustrate a large differential in lesions in AT islands and lesions in non-AT islands and in bulk DNA, in particular for the lowest drug concentrations (Fig. 4A). The predictive power of the in silico analysis is underscored by an excellent correlation between the actual lesions and the densities of drug binding motifs (Fig. 4B). Bizelesin is the first anticancer drug for which such a differential, region-specific damage has been documented. These results provide a proof of principle that targeting distinct noncoding regions is feasible.

2.2. *Is region-specific damage to AT islands a common property of other AT-specific drugs?*

Our studies with other drugs, where computational predictions were also fully corroborated by experimental determinations of drug adducts, allow us to propose the general requirements for a region-specific DNA damage. High motif specificity, such as that of bizelesin, is essential for a significant preference for AT islands [21]. U78779, an analog that binds at $(A/T)_6A$, is also highly preferential for long AT islands, despite the fact that it prefers mixed A/T–G/C sequences [35,41]. The less sequence-specific adozelesin, which recognizes $N(A/T)_3A$ and $NN(A/T)_2A$ sites [21], retains some preference for AT-rich islands (Fig. 5). However, in contrast to bizelesin, adozelesin binding to AT tracts outside of the long AT islands is substantial, and adozelesin cannot be regarded as a region-specific agent.

Sequence specificity alone is insufficient for region specificity. Tallimustine has a strong preference for 5′-TTTTGPu-3′ [19]. Consistent with this stringent sequence, the tallimustine motif is approximately 10 and 100 times less frequent than motifs for bizelesin and adozelesin, respectively (Fig. 5) [19]. However, the infrequent tallimustine sites are distributed nearly randomly throughout the genome, which explains the experimentally determined lack of region specificity [19]. Drugs like tallimustine, which are devoid of any regional specificities, do not offer any significant advantages over typical non-sequence-specific DNA-reactive agents. As shown for cisplatin, the latter, nondiscriminating drugs cannot be region-specific due to their low specificity of DNA recognition and the ubiquitous distribution of the potential binding sites (mainly GG clusters). Still, even these marginal specific-

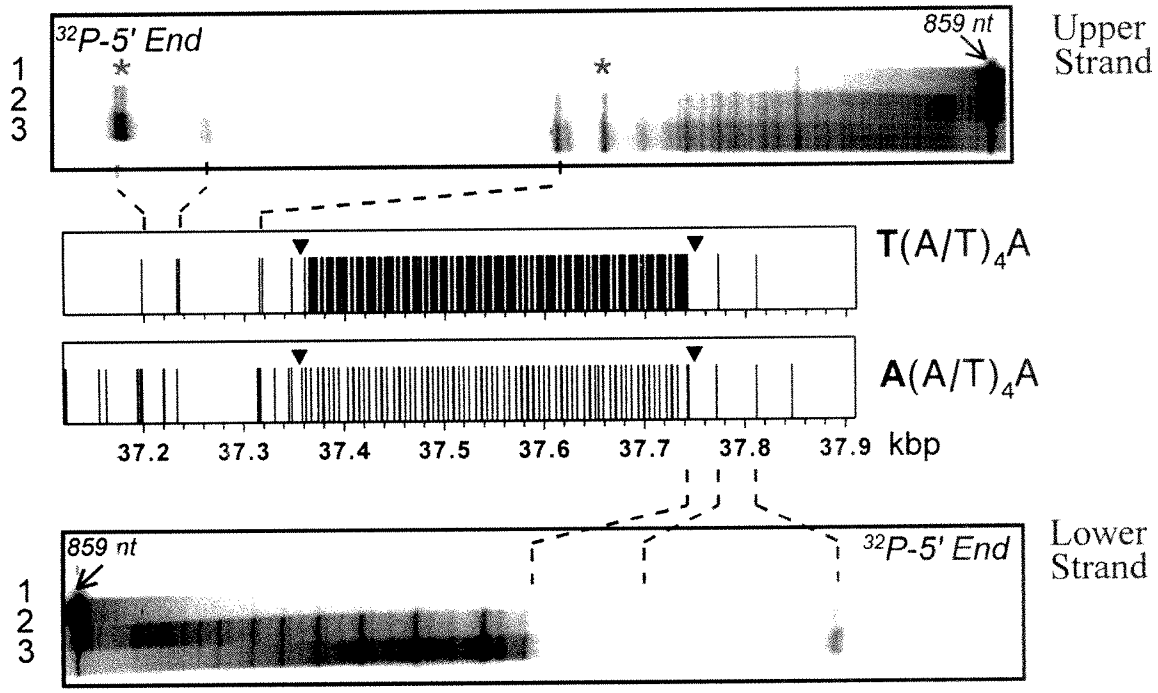

Fig. 3. Predicted (middle panel) and actual bizelesin-induced lesions in the naked DNA of a model AT island. The triangles in the middle panel indicate the positions of the G/C pairs that flank the 100% AT core of this AT island, while each vertical spike corresponds to an exact match of the sequence to drug binding motif. Experimental panels (top and bottom) show drug sites monitored as sub-bands with singly end-labeled DNA after the conversion of adducts to strand breaks (adapted with permission from Ref. [38]).

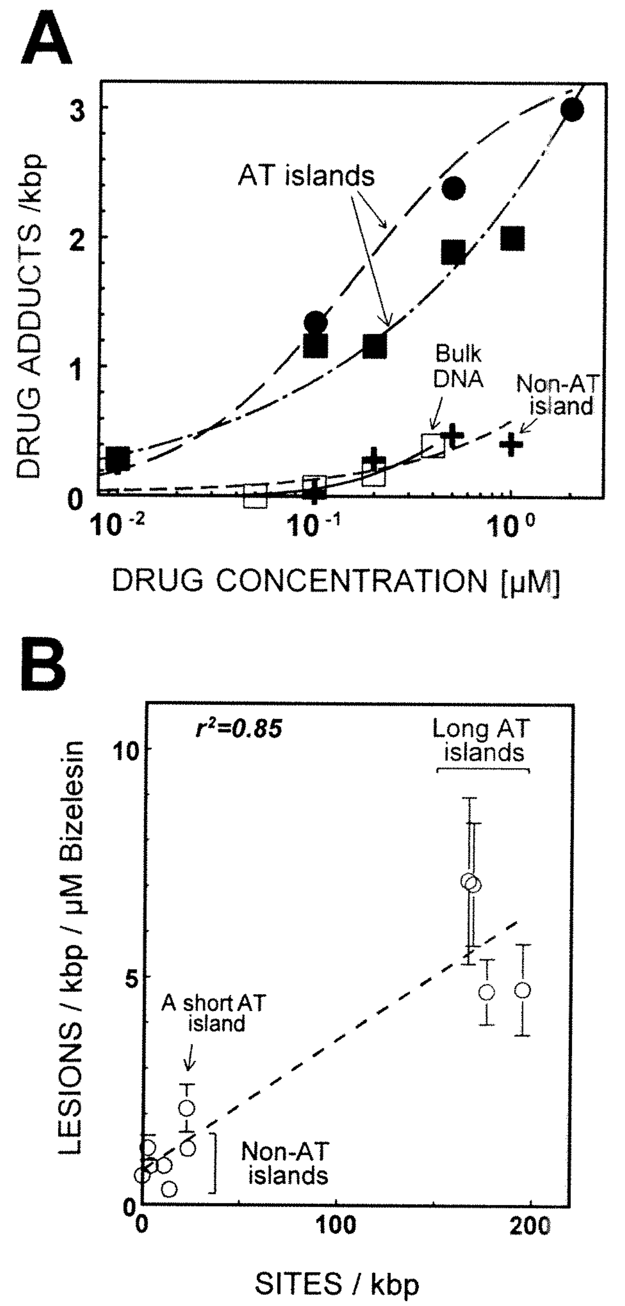

Fig. 4. Bizelesin preferentially damages MAR-like AT islands versus non-AT island regions in leukemic CEM cells (adapted with permission from Refs. [21,38] with additional unpublished data). (A) Examples of region-specific lesions monitored by quantitative polymerase chain reaction stop assay in DNA from drug-treated CEM cells in AT islands (ApoB MAR, ■; Fra16D, ●) in comparison to lesions a non-AT island (in β-globin, ✚) and in bulk DNA (□). (B) Correlation between the density of the predicted bizelesin binding sites and actual levels of region-specific adducts.

ities translate into more platinum adducts formed in GC-rich regions that contain large number of drug binding motifs. [37]. The ability to correctly predict such rather subtle effects points to the general utility of the in silico approach for drugs from both high- and low-ends of sequence specificities.

3. Long AT islands as critical regions

Targeting of AT islands is more lethal by several orders of magnitude than non-region-specific damage to DNA [18,19, 21,36,40,41]. Region-specific bizelesin and U78779, which also targets AT islands, need to form very few lesions (< 10 DNA adducts/cell) to block cell growth (Table 1). Adducts by AT-specific, but non-region-specific, tallimustine are markedly less lethal (~ 200 adducts/cell). In striking contrast to AT-specific drugs, non-sequence-specific classical drugs need to form several thousands of DNA lesions/cell to inhibit cell growth. It is clear that damage to AT islands by CPI drugs impedes functions that are crucial for the growth of cancer cells.

3.1. Matrix associated regions (MARs) and AT islands

Although specific functions of the individual AT-islands identified, as bizelesin targets remain mostly undefined, several lines of evidence suggest that these domains can function as MARs. MAR domains are specialized loci that anchor cellular DNA to the nuclear matrix, a proteinaceous scaffolding that organizes chromatin fibers into looped domains participating in the spatial organization of chromosome territories [42–45] and is the site of DNA replication and transcription [42,44–48]. A high MAR potential is a consistent attribute of AT island domains. In addition, evidence of actual MAR function is available for several loci [38]. The MAR attributes positively and significantly correlate with the number of bizelesin binding sites and actual levels of lesions in these AT islands [38].

3.2. Inhibition of DNA replication and damage to MAR-like AT islands

Bizelesin-induced damage to MAR-like AT islands may explain the observed specific inhibition of new replicon initiation [40,49]. Intriguingly, only one to two bizelesin adducts per ~ 10^6 bp (i.e., per several typical replicons) are needed for a genome-wide inhibition of replicon initiation [40]. Thus, bizelesin adducts seem to exert inhibitory effects on cellular DNA replication at a substantial distance from their actual location. By contrast, in a cell-free system, only modest inhibition, consistent with a local blockade to chain elongation, is observed [40].

This differential pattern of anti-replicative properties could be explained by the functional association of cellular replication, but not cell-free replication, with the nuclear matrix [42,50]. In the cell, strong MAR domains form the boundaries of replication factories. An unperturbed MAR structure seems essential for the near simultaneous firing of each replicon clustered in a given replication factory [50,51]. The blocked initiation of several replicons by a single bizelesin adduct spaced every 10^6 bp is consistent with (i) an average size of a replication factory (~ 10^6 bp) [50], (ii) the occurrence of strong MAR domains (~ $1/10^6$

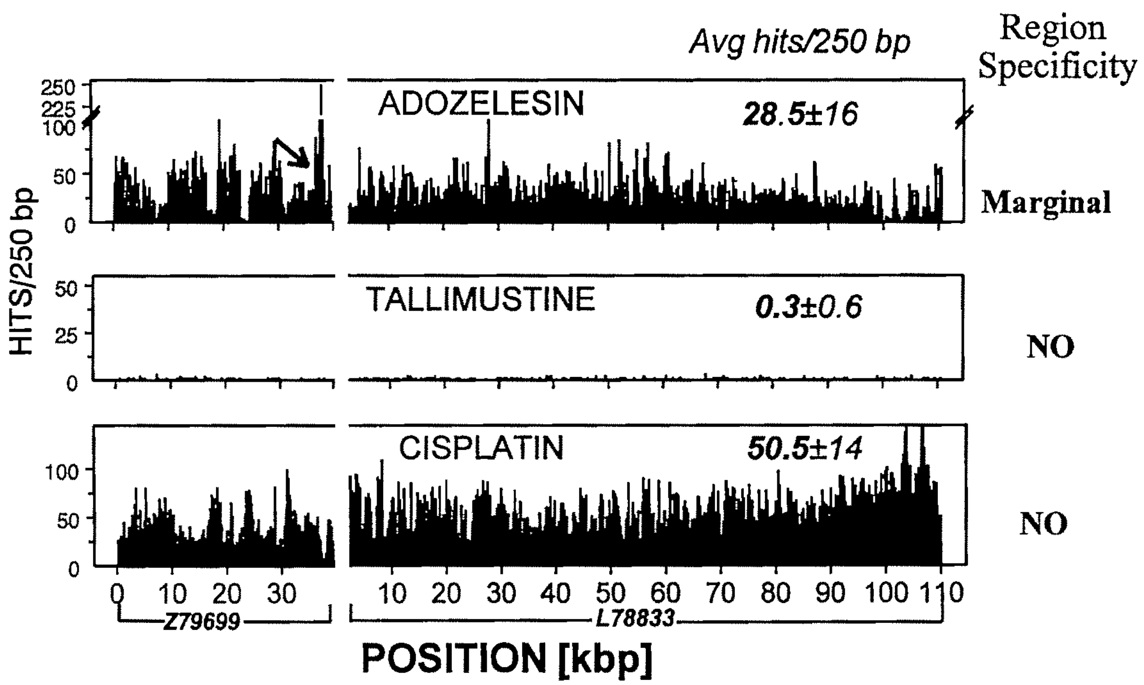

Fig. 5. Examples of the distribution of drug binding motifs at the genomic level (in silico analysis) for adozelesin, tallimustine and cisplatin. The histograms depict the number of exact matches to the bizelesin motif in bins of 250 bp along the indicated GenBank sequences. Average hits/250 bp in the genome are also given for each drug. The examples shown are for GenBank sequences Z79699 L78833 (data for tallimustine and cisplatin were adapted with permission from Ref. [19]). The arrow points to one of the long AT island, that is among bizelesin targets (c.f. Fig. 3).

bp)[50–54], and (iii) the occurrence of bizelesin hot spot AT-islands (also ~ $1/10^6$ bp) [38]. Further investigations are needed to test the possibility that lesions in MAR-like AT islands distort the integrity of replication factories.

3.3. Genetic instability of AT islands and drug targeting

Bizelesin-targeted MAR-like AT islands are minisatellites [38], which are, in general, known to be genetically unstable elements. Polymerase slippage on repetitive sequences and/or amplification may expand such domains by many kbp [55–57]. Well-known elements of genomic instability, the AT-rich fragile sites Fra16B and Fra16D, are among bizelesin targeted AT islands [38], and their vulnerability has been verified by recent experimental determinations (c.f., Fig. 4, [76] and Woynarowski et al., unpublished data). Importantly, repeat expansion of such inherently unstable domains and associated downstream rearrangements are thought to contribute to tumorigenic phenotype. AT-rich sites of genomic instability have been particularly implicated in leukemias and lymphomas [55,58–62], including acute lymphoblastic leukemia (ALL), the most frequent pediatric malignancy [63–66]. The inherent instability of AT islands may thus give rise to fundamental differences among various cancer and normal lines.

Our recent data prompted us to investigate the possibility that such differences in the abundance and/or function of AT islands might be associated with differential responses to AT-island targeting drugs. Whereas bizelesin is generally cytotoxic in picomolar concentrations, some tumor cell lines appear to be significantly ($P<0.05$) hypersensitive than some other tumor and normal cell lines examined ([76] and Woynarowski et al., unpublished data). For human leukemia CEM and normal WI-38 cells, we additionally demonstrated that the differential sensitivity to bizelesin is not due to any differences in drug reactivity with cellular DNA, or lesion repair ([76] and Woynarowski et al., unpublished data). Our recent data show also that Fra16B

Table 1
Cytotoxicity and lethality of DNA lesions induced in CEM cells by drugs of varying degree of sequence and region specificity

Drug	Type	Cytotoxicity[a], GI_{50} [M]	Lesions/ kbp/μM	Estimated lesions/ cell at GI_{50}[b]	References
Bizelesin	AT-specific and region-specific (AT islands)	0.6×10^{-12}	0.88	2	[21,41]
U78779	AT-specific and region-specific (AT islands)	3.3×10^{-12}	0.22	2	[34,35,41]
Tallimustine	AT-specific, non-region-specific	3.5×10^{-9}	0.022	220	[41]
Cisplatin	G/C preferring, non-region-specific	1.5×10^{-6}	0.032	14,000	[75]

[a] Drug concentration inhibiting net cell growth by 50% determined by the MTT assay.

[b] Estimated by linear extrapolation of lesion frequencies/kbp/μM to the GI_{50} concentration assuming 2.9×10^9 bp/cell (rounded values).

AT islands are more abundant in hypersensitive leukemic CEM cells, but not in non-hypersensitive normal WI-38 and several other cell lines. We speculate that expansion (increased abundance) of AT islands, such as these fragile sites, may sensitize certain tumors to bizelesin-type drugs by increasing the number of potential drug binding sites. Alternatively, while all the identified bizelesin-targeted AT islands are capable of MAR function, the actual association of such domains with the nuclear matrix may differ among various cell types [42,67]. For instance, the Fra16B and c-myc MAR domains co-localize mainly with matrix DNA in bizelesin-sensitive cancer CEM cells but not in normal WI-38 cells ([76] and Woynarowski et al., unpublished data). Loop localization of the c-myc was also found with other normal cells [68]. It seems plausible that damage to a given AT island may be more critical for those cell types, in which such sequences are associated with the nuclear matrix and function as MARs. Studies are underway to verify these possibilities.

4. Relevance of AT island targeting to anticancer therapies and perspectives for region-specific targeting of other repetitive sequences

There are several reasons why targeting AT islands may offer potential therapeutic benefits over non-region-specific classical DNA-reactive drugs used in the clinic. First, certain abnormal AT islands, such as expanded fragile sites Fra16B and Fra16D, are thought to contribute to tumorigenic phenotypes. Although this aspect still requires substantial investigation, AT-island targeting may offer increased selectivity for such tumors. Second, rapid cell proliferation is a hallmark of many tumors, especially these of pediatric origin. Rapidly replicating cells should be preferentially eliminated by highly localized lesions in replication-related regions, such as MAR-like AT islands. In contrast, typical DNA-reactive drugs extensively damage regions that are also crucial for functioning of nonreplicating cells. Finally, treatment with classical DNA-reactive drugs results in thousands (10^4–10^5) of low-lethality but mutagenic DNA lesions/cell in normal tissues [1]. Consequently, secondary, drug-induced tumors are a common and dramatic problem, pertinent in particular to children who typically live for many years after the eradication of their primary cancers [69]. In contrast to classical drugs, lesions in AT islands are extremely lethal [19,21] (see above). Lethal lesions, by definition, cannot lead to mutations. Hence, therapies based on AT island targeting should be associated with a reduced risk of secondary tumors.

Beyond the AT island paradigm, targeting of other repetitive and potentially critical domains may also offer significant benefits. One prominent example of a critical and highly abundant target is telomeric DNA with its $(TTAGGG)_n$ repeats. Telomeric sequences, both terminal and interstitial, may have a role in chromosomal aberrations and can be amplified in cancer cells in proportion to the invasive and metastatic potential [70,71]. Maintaining telomere length, usually by the specialized enzyme telomerase, gives a growth advantage to cancer cells by extending their life span [72–74]. Conversely, damage to telomeres should be detrimental to cancerous growth [72–74]. The modular structure of the telomeric repeats consisting of discrete A/T and G/C blocks should facilitate the design of small-molecule region-specific drugs with sufficiently high preferences for these motifs.

5. Conclusions: Significance of region specificity for rational drug design and targeting

Targeting specific domains in the genome should limit various adverse effects of current anticancer therapies, which use non-region-specific DNA-reactive drugs. In particular, further exploration of distinct repetitive sequences in noncoding regions as potentially critical targets should generate leads for better, more selective drugs. In contrast to targeting unique sites in specific genes, domains of repetitive sequences with clusters of drug binding sites constitute highly abundant targets that can be selectively targeted with agents of less than ideal specificity. Bizelesin is the first example of a drug that not only is region-specific in tumor cells but also exhibits antitumor activity in vivo and promising clinical properties. Region-specific damage to MAR-like AT islands by bizelesin provides a proof of principle that targeting repetitive sequences crucial for the survival of cancer cells is feasible.

The significance of sequence specificity at the nucleotide level is generally recognized, even if a given drug is not explicitly designed to target specific domains. The established prerequisites of drug regional preferences [19,21,37] point to the definite need for appreciable drug binding specificity. Equally important, however, is genomic composition. Tallimustine is not region-specific because its highly specific motif is distributed nearly randomly and infrequently throughout the genome. Bizelesin is region-specific because its binding motifs are nonrandomly distributed, with clusters in repetitive sequences of AT islands and infrequent sites elsewhere.

In contrast to drug sequence specificity, drug regional preferences at the genomic level are usually not addressed or are taken for granted. The reviewed studies emphasize that lesions distribution may critically depend on the genome itself, and how misleading it could be to rely on the seemingly intuitive opinions, such as "...the more sequence specificity the better..." or that "...AT-specific drugs equally target various AT elements". In contrast to such misleading or downright incorrect subjective judgments, the developed bioinformatics tools demonstrate the ability to accurately predict and verify which genomic elements are likely and which are unlikely to be targeted by specific drugs. This rigorous and objective analysis is generally applicable to any kind of DNA targeting. In a not too distant future, it should be possible to analyze the entire human genome in that way. Bioinformatics tools, such as those used in our studies, can accelerate the development of new region-specific molecules against various targets. The rapid optimization of drug binding motif by in silico analysis should limit the number of compounds that need to be synthesized, and eliminate many prototypes that would unlikely have any regional preferences. We feel that once the concept of regional targeting is systematically developed, it should become an essential component of the rational design of new sequence-specific drugs.

Acknowledgements

The reviewed research in the author's laboratory was supported in part by grants from the National Cancer Institute (CA71969) and the Children Cancer Center at the University of Texas Health Science Center, San Antonio, TX. I am grateful to all members of my laboratory, whose enthusiasm and contributions helped to define the emerging area of region-specific drug targeting. I also thank Drs. Barbara Woynarowska and Terence Herman for constant encouragement and numerous inspiring discussions.

References

[1] P.D. Lawley, D.H Phillips, Mutat Res 355 (1996) 13–40.

[2] B.J Sanderson, A.J Shield, Mutat Res. 355 (1996) 41–57

[3] L.F Povirk, D.E Shuker, Mutat Res 318 (1994) 205–226

[4] D.E Wemmer, Annu. Rev. Biophys. Biomol. Struct 29 (2000) 439–461

[5] S. Neidle, Biopolymers 44 (1997) 105–121.

[6] B.S. Reddy, S.K. Sharma, J.W. Lown, Curr Med Chem 8 (2001) 475–508

[7] P.G. Baraldi, B. Cacciari, A. Guiotto, R Romagnoli, A.N. Zaid, G. Spalluto, Curr Pharm. Des 4 (1998) 249–276.

[8] J.B Chaires, Curr. Opin. Struct Biol 8 (1998) 314–320

[9] S. White, E.E. Baird, P.B Dervan, Chem Biol 4 (1997) 569–578.

[10] S White, E.E. Baird, P.B. Dervan, Biochemistry 35 (1996) 12532–12537

[11] R.E Bremer, J.W Szewczyk, E.E Baird, P.B. Dervan, Bioorg Med Chem 8 (2000) 1947–1955.

[12] P.B. Dervan, Science 232 (1986) 464–471.

[13] D.M Gowers, K.R. Fox, Nucleic Acids Res. 27 (1999) 1569–1577

[14] K.R. Fox, Curr Med Chem. 7 (2000) 17–37.

[15] B.S. Reddy, S.M. Sondhi, J.W. Lown, Pharmacol Ther. 84 (1999) 1–111

[16] C.S Lee, G.P Pfeifer, N.W Gibson, Biochemistry 33 (1994) 6024–6030.

[17] M.M. McHugh, J.M. Woynarowski, L.S Gawron, T Otani, T.A. Beerman, Biochemistry 34 (1995) 1805–1814

[18] J.M Woynarowski, W.G. Chapman, C Napier, M.C.S Herzig, Biochim. Biophys Acta 1444 (1999) 201–217.

[19] M.C. Herzig, A.V Trevino, B. Arnett, J.M Woynarowski, Biochemistry 38 (1999) 14045–14055

[20] J.M. Woynarowski, M.M McHugh, L.S. Gawron, T.A Beerman, Biochemistry 34 (1995) 13042–13050.

[21] J.M Woynarowski, C. Napier, A.V. Trevino, B Arnett, Biochemistry 39 (2000) 9917–9927

[22] J Xu, J Wu, P.C. Dedon, Biochemistry 37 (1998) 1890–1897

[23] M. Broggini, H.M. Coley, N Mongelli, E. Pesenti, M.D Wyatt, J.A Hartley, M D'Incalci, Nucleic Acids Res 23 (1995) 81–87.

[24] G.R. Weiss, I. Poggesi, M. Rocchetti, D DeMaria, T. Mooneyham, D Reilly, L.V. Vitek, F. Whaley, E Patricia, D.D Von Hoff, P O'Dwyer, Clin. Cancer Res 4 (1998) 53–59.

[25] B.J. Foster, P.M. LoRusso, E Poplin, M. Zalupski, M Valdivieso, A. Wozniak, L. Flaherty, D.A Kasunic, R.H Earhart, L.H Baker, Invest. New Drugs 13 (1995) 321–326

[26] G.F Fleming, M.J Ratain, O.B SM, R.L. Schilsky, P.C Hoffman, J.M Richards, N.J Vogelzang, D.A. Kasunic, R.H. Earhart, J. Natl Cancer Inst 86 (1994) 368–372

[27] G.J. Shamdas, D.S. Alberts, M. Modiano, C. Wiggins, J. Power, D.A Kasunic, G.L Elfring, R.H Earhart, Anticancer Drugs 5 (1994) 10–14.

[28] G.H. Schwartz, C Aylesworth, J. Stephenson, T Johnson, E Campbell, L. Hammond, D.D Von Hoff, E.K. Rowinsky, Proc Am. Soc. Clin Oncol. 19 (2000) 235a

[29] N Pavlidis, S Aamdal, A Awada, H Calvert, P Fumoleau, R Sorio, C. Punt, J Verweij, A. Van Oosterom, R. Morant, J. Wanders, A.R Hanauske, Cancer Chemother Pharmacol. 46 (2000) 167–171

[30] C.J. Punt, Y. Humblet, E. Roca, L.Y. Dirix, R Wainstein, A Polli, I Corradino, Br. J Cancer 73 (1996) 803–804.

[31] J.A. Hartley, J.W. Lown, W.B Mattes, K.W. Kohn, Acta Oncol 27 (1998) 503–510.

[32] S. Neidle, M.S. Puvvada, D.E. Thurston, Eur J Cancer 4 (1994) 567–568.

[33] W.B. Mattes, J.A Hartley, K.W. Kohn, D.W Matheson, Carcinogenesis 9 (1988) 2065–2072

[34] M.C.S Herzig, J Dziegielewski, B Arnett, L. Hurley, J.M Woynarowski, Proc Am Assoc. Cancer Res 41 (2000) 97.

[35] K. Rodriguez, M.C.S Herzig, A.V. Trevino, L Hurley, J.M. Woynarowski, Proc Am Assoc Cancer Res 42 (2001) 202

[36] J.M Woynarowski, M. McHugh, L.S. Gawron, T.A Beerman, Biochemistry 3 (1995) 13042–13050

[37] J.M. Woynarowski, W.G. Chapman, C. Napier, M.C.S Herzig, P. Juniewicz, Mol. Pharmacol 54 (1998) 770–777

[38] J.M Woynarowski, A.V. Trevino, K.A Rodriguez, S.C Hardies, C.J Benham, J Biol Chem 276 (2001) 40555–40566.

[39] C.A. Carter, W.R Waud, L.H Li, T.F DeKoning, J.P McGovren, J Plowman, Clin Cancer Res 2 (1996) 1143–1149

[40] J.M. Woynarowski, T.A Beerman, Biochim Biophys. Acta 1353 (1997) 50–60

[41] M.C.S. Herzig, K. Rodriguez, A Trevino, B Arnett, J Dziegielewski, L Hurley, J.M. Woynarowski, Biochemistry 41 (2002) 1545–1555

[42] R Berezney, X.Y Wei, J Cell Biochem., Suppl 30–31 (1998) 238–242

[43] J. Tajbakhsh, H. Luz, H. Bornfleth, S Lampel, C. Cremer, P Lichter, Exp. Cell Res 255 (2000) 229–237.

[44] J.A Nickerson, J. Cell Sci 114 (2001) 463–474

[45] V.V Philimonenko, J.E Flechon, P Hozak, Exp Cell Res 264 (2001) 201–210.

[46] Y.S. Vassetzky, A. Hair, S.V Razin, J Cell Biochem 35 (2000) 54–60.

[47] B.K Kennedy, D.A Barbie, M Classon, N. Dyson, E Harlow, Genes Dev. 14 (2000) 2855–2868.

[48] J.R Davie, S.K Samuel, V.A Spencer, L.T. Holth, D.N. Chadee, C.P Peltier, J.M. Sun, H.Y. Chen, J.A. Wright, Biochem Cell Biol. 77 (1999) 265–275.

[49] M.M. McHugh, S.R Kuo, M.H. Walsh-O'Beirne, J.S. Liu, T Melendy, T.A Beerman, Biochemistry 38 (1999) 11508–11515.

[50] R Berezney, D.D Dubey, J.A Huberman, Chromosoma 108 (2000) 471–484

[51] M.L. DePamphilis, J Struct Biol 129 (2000) 186–197.

[52] N.N. Khodarev, I.A. Sokolova, A.T.M Vaughan, J Cell. Biochem 70 (1998) 604–615.

[53] Y.S. Vassetzky, A.N. Bogdanova, S.V Razin, J Cell. Biochem. 79 (2000) 1–14.

[54] PN Cockerill, WT Garrard, Cell 44 (1986) 273–282.

[55] R.I. Richards, Trends Genet 17 (2001) 339–345.

[56] O. Handt, GR Sutherland, RI Richards, Mol. Genet. Metab. 70 (2000) 99–105

[57] G.R Sutherland, E Baker, RI Richards, Trends Genet. 14 (1998) 501–506

[58] D.I Smith, H. Huang, L Wang, Int J. Oncol 12 (1998) 187–196

[59] NC. Popescu, Crit. Rev Oncog 5 (1994) 121–140.

[60] K Huebner, P.N Garrison, LD Barnes, CM Croce, Annu Rev Genet. 32 (1998) 7–31.

[61] M Mangelsdorf, K Ried, E Woollatt, S Dayan, H. Eyre, M. Finnis, L Hobson, J. Nancarrow, D. Venter, E Baker, RI. Richards, Cancer Res 60 (2000) 1683–1689

[62] K. Ried, M. Finnis, L Hobson, M Mangelsdorf, S Dayan, J.K Nancarrow, E Woollatt, G Kremmidiotis, A Gardner, D Venter, E. Baker, RI Richards, Hum Mol. Genet 9 (2000) 1651–1663

[63] R. Nishimura, Y Niida, Y Saikawa, Y. Goto, T Noguchi, T Ichihara, S Koizumi, Pediatr. Int 41 (1999) 346–352.

[64] Y.M Zhu, E.P. Das-Gupta, NH Russell, Blood 94 (1999) 733–740

[65] A Baccichet, N Benachenhou, F. Couture, JM. Leclerc, D. Sinnett, Leukemia 11 (1997) 797–802

[66] G Reato, G Basso, M.C Putti, A. Cignetti, A. Guarini, R Foa, Haematologica 83 (1998) 403–407

[67] AA Terent'ev, G.V Kostyuk, P.Y Boikov, Biochemistry (Moscow) 63 (1998) 533–536

[68] LP Djondjurov, MM Andreeva, DZ. Markova, RM Donev, Oncol Res. 6 (1994) 347–356.

[69] CA Felix, Biochim. Biophys. Acta 1400 (1998) 233–255.

[70] S.D Bouffler, Mutat Res. 404 (1998) 199–204.

[71] A.S Multani, M. Ozen, S. Sen, AK. Mandal, J.E Price, D Fan, R. Radinsky, F. Ali-Osman, AC Von Eschenbach, IJ Fidler, S. Pathak, Int. J Oncol 15 (1999) 423–429

[72] E Raymond, JC. Soria, E. Izbicka, F Boussin, L Hurley, DD. Von Hoff, Invest New Drugs 18 (2000) 123–137.

[73] L.H. Hurley, R.T Wheelhouse, D Sun, SM. Kerwin, M. Salazar, OY Fedoroff, FX Han, H. Han, E. Izbicka, DD. Von Hoff, Pharmacol. Ther. 85 (2000) 141–158

[74] AJ Davis, L.L Siu, Cancer Invest 18 (2000) 269–277.

[75] JM Woynarowski, S Faivre, MCS Herzig, B Arnett, W.G Chapman, AV Trevino, E. Raymond, S.G Chaney, A. Vaisman, M. Varchenko, PE Juniewicz, Mol Pharmacol. 58 (2000) 920–927

[76] J. Jackson, AV Trevino, M.CS Herzig, JM Woynarowski, Proc Amer Assoc Cancer Res 43 (2002) 1092

ELSEVIER

Biochimica et Biophysica Acta 1587 (2002) 309–317

BIOCHIMICA ET BIOPHYSICA ACTA

BBA

www.bba-direct.com

Review

Preferential targeting of apoptosis in tumor versus normal cells

Barbara A. Woynarowska [a,*], Jan M. Woynarowski [a,b]

[a] *Department of Radiation Oncology, The University of Texas Health Science Center, 14960 Omicron Drive, San Antonio, TX 78245, USA*
[b] *Cancer Therapy and Research Center, Institute for Drug Development, 14960 Omicron Drive, San Antonio, TX 78245, USA*

Received 24 January 2002; accepted 24 January 2002

Abstract

Elimination of cancer cells by early apoptosis is preferred over other forms of cell growth inhibition. Apoptosis directly leads to tumor regression and reduces risks of selecting more aggressive and/or drug-resistant phenotypes that are often responsible for tumor regrowth and treatment failure. Although DNA damage by anticancer drugs is commonly recognized as an apoptotic stimulus, there is enormous variability in the magnitude and timing of such effects. Especially potent and rapid apoptosis seems to be a hallmark of various alkylating anticancer drugs that are regarded as DNA-reactive agents but are observed to react mainly with cellular proteins. Our studies with such dual-action drugs (irofulven, oxaliplatin) suggest that not only DNA damage, but also protein damage, contributes to apoptosis induction. DNA damage is well known to initiate death-signaling pathways leading to mitochondrial dysfunction. Protein damage, in turn, can distort cell redox homeostasis, which facilitates apoptosis execution. Such dual effects can be particularly lethal to tumor cells, which tend to function under pro-oxidative conditions. In contrast to tumor cells that are highly susceptible, normal cells show marginal apoptotic responses to the dual action drugs. This protection of normal cells might reflect their greater ability to buffer pro-oxidative changes and quickly restore redox homeostasis, despite substantial drug uptake and macromolecular binding. Importantly, by targeting the death process at multiple points, DNA- and protein-damaging drugs can be less vulnerable to various bypass mechanisms possible with single targets. The reviewed studies provide a proof of concept that differential apoptosis targeting in cancer versus normal cells can be a basis for tumor selectivity of anticancer drugs. © 2002 Elsevier Science B.V. All rights reserved.

Keywords: DNA damage; Protein damage; Differential apoptosis; Irofulven; Oxaliplatin

1. Introduction: the need for apoptosis in anticancer strategies

Whereas the ultimate goal of all anticancer strategies is to eradicate tumor cells, early apoptosis is by far the pharmacologically preferred form of cell growth inhibition. A rapid death of cancer cells is not only needed to achieve tumor regression but also to reduce risks of selecting more aggressive and/or drug-resistant phenotypes that are often responsible for tumor regrowth and treatment failure (Fig. 1). Slowly growing but viable tumor cells, recovering from non-apoptotic damage, were proposed to be an overlooked factor in the therapeutic failure of various cancer treatments [1]. Unless such cells are physically eliminated, there is a remaining danger of clonal selection and tumor recurrence. Initiation of apoptosis irrevocably eliminates this threat since apoptotic cells cannot be clonogenic.

Conversely, dysregulation of normal apoptosis pathways extends the cell life span and can contribute to tumor expansion, even if the cell division rate remains normal [2]. Hence, targeting apoptosis is particularly relevant to those forms of cancer that have a significantly reduced rate of cell death and are relatively slowly proliferating tumors. For instance, slowly dividing prostate cancer cells are very difficult to eradicate with current anticancer drugs, which target rapidly proliferating cells [3]. Being a physiological process, apoptosis is associated with fewer side effects than non-apoptotic modes of cell death. Various anticancer drugs induce apoptosis but there is enormous variability in the magnitude and timing of such effects. Recent

---

Abbreviations: ASK 1, apoptosis signaling kinase 1; $\Delta\psi$, mitochondrial membrane potential; HMAF, hydroxymethylacylfulvene, irofulven; NF-κB, nuclear factor κB; AP-1, activator protein 1; Glu-SH, glutathione; TRX, thioredoxin; IC_{80}, drug concentration inhibiting cell growth by 80%; ROS, reactive oxygen species

[*] Corresponding author. Tel.: +1-210-677-3846; fax: +1-210-677-0058.
E-mail address: bwoynar@saci.org (B.A. Woynarowska).

0925-4439/02/$ - see front matter © 2002 Elsevier Science B.V. All rights reserved.
PII: S0925-4439(02)00094-7

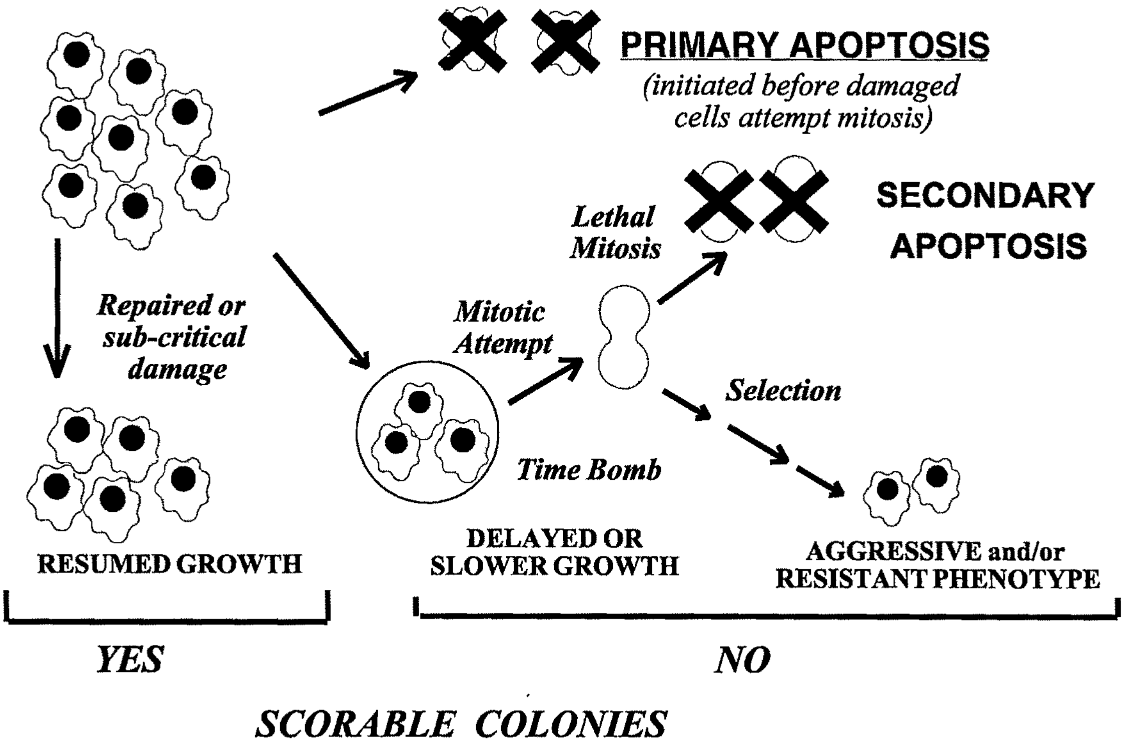

Fig. 1 The significance of apoptosis for antitumor drugs The elimination of affected cells by early, ideally premitotic apoptosis is the most desirable scenario. Postmitotic apoptosis can eliminate additional cancer cells However, each mitotic attempt poses a risk that genetic rearrangements may lead to the selection of cells with a more aggressive and/or resistant phenotype Viable cells that are not eliminated may not form scorable colonies under typical assay conditions but may resume growth and lead to tumor recurrence

years have brought an increased understanding of the complexity of cellular responses to drug interactions with a variety of cellular targets that ultimately result in cell death [4,5]. This review discusses the potential for selective targeting of apoptosis in cancer cells focusing on novel anticancer drugs that react with cellular DNA and proteins.

2. Central role of redox imbalance in apoptosis

Whereas various insults can initiate apoptosis (for a recent review, see Ref. [6]), a consistent picture that emerges from studies in various laboratories points to the pivotal role of redox homeostasis in apoptotic process. Oxidative stress and reactive oxygen species can be either the initiating stimulus or mediator of apoptosis [7,8]. Factors that regulate the levels and responses to oxidative stress [9–11] are believed to play a decisive role in determining the "point of no return" in cell death [12–14]. In that context, the mitochondria are now well established as critical for processing and integrating pro-apoptotic signals. Diverse apoptotic stimuli can cause mitochondrial dysfunction leading to pro-oxidative changes in redox homeostasis. Pro-oxidants per se cause the efflux of mitochondrial components, further increasing the oxidative stress [8,10,15,16].

The cross-talk between cellular signaling and the redox status of the cell is presently believed to dictate, more than any other factors, whether or not a cell will undergo apoptosis [10,11,13]. A balance of pro- and anti-apoptotic factors allows cells to survive despite various insults for prolonged times. However, apoptosis seems to proceed like a chain reaction and relatively small perturbations in the equilibrium may either rapidly amplify or successfully attenuate the process. The amplification or attenuation of pro-apoptotic responses is tightly coupled to the thiol redox status of the cell, with a critical role of protein sulfhydryls [10,17,18].

Whereas glutathione system provides redox buffering at the level of small molecule sulfhydryls, the thioredoxin (TRX) family of multifunction disulfide reductases is the key system responsible for maintaining the reduced form of protein sulfhydryls [17,19–21]. TRX participates directly in cellular death signaling pathways by inhibiting apoptosis signal-regulating kinase 1 (ASK 1) and the subsequent ASK 1-dependent apoptosis [18]. TRX also mediates the effects of redox-sensing transcription factors, which allow the cell to reprogram its gene expression in response to pro-oxidative insults [11,21,22]. The rapidly inducible increase in TRX expression can prevent apoptosis [9,16], consistent with the reports implicating TRX in the resistance of cancer cells to drug-induced apoptosis [23–26].

3. Is drug-induced DNA damage sufficient for apoptosis induction?

3.1. DNA damage as apoptotic stimulus

Lesions in DNA are generally considered as the primary apoptotic stimulus for DNA-damaging agents. DNA damage elicits complex responses which are mediated by various intracellular and extracellular factors such as p53, abl, c-myc, Rb, E2F, growth factors, and which often involve multiple and redundant pathways [27,28]. If these responses are not extinguished by anti-apoptotic signals (such as Bcl-2), Bax and related death proteins decrease mitochondrial membrane potential ($\Delta\Psi$) [29–31], which, in turn, leads to cytochrome *c* release and oxidative stress [16,32–36], followed by the activation of cysteine proteases of the caspase family and subsequent apoptotic DNA fragmentation [37]. This general route has been implicated in the action of various DNA-damaging agents [5,38–40] (Fig. 2). Beyond doubt, DNA damage can be a critical factor for the action of anticancer drugs. It is important to recognize, however, that it represents only one facet of the pleiotropic reactivities of nominally DNA-reactive drugs.

3.2. Protein damage as apoptotic stimulus

The profound ability of various alkylating drugs to bind cellular proteins seems to be particularly under-appreciated as a contributing factor in apoptotic responses. The normally functioning cell maintains reductive conditions. Numerous proteins require reduced sulfhydryl groups for their proper function. It is well established that compounds that form adducts only with proteins, such as diamide, distort the redox homeostasis of the cell in the pro-oxidative direction [10,41–46] (Fig. 2). Consequently, thiol-reactive compounds themselves can induce apoptosis without reacting with cellular DNA [10,42,44,46].

Importantly, the thiol–disulfide balance has also been implicated in redox-sensitive gene expression, which drives critical steps in signal transduction [22,47–49]. Drug binding to sulfhydryl-containing proteins, especially those involved in redox regulation, may have a profound effect on cellular responses determining apoptosis progression. If TRX and related systems can respond in a sufficient and timely manner, transcriptional reprogramming can increase the redox buffering capacity of the cell and annihilate the effects of potentially apoptotic insults. However, extensive protein damage is likely to compromise the cell capacity for such restorative responses and precipitate responses that accelerate rather than slow down cell self-deterioration. Given that tumor cells may have already a compromised capacity to buffer pro-oxidative changes, the "redox factor" resulting from drug-induced protein damage could be of profound importance for both the efficiency and selectivity of drug-induced apoptosis.

3.3. The puzzle of DNA- and protein-reactive antitumor drugs

Several lines of observations strongly suggest that DNA damage does not fully account for the pro-apoptotic effects of at least some nominally DNA-reactive drugs. New clinically

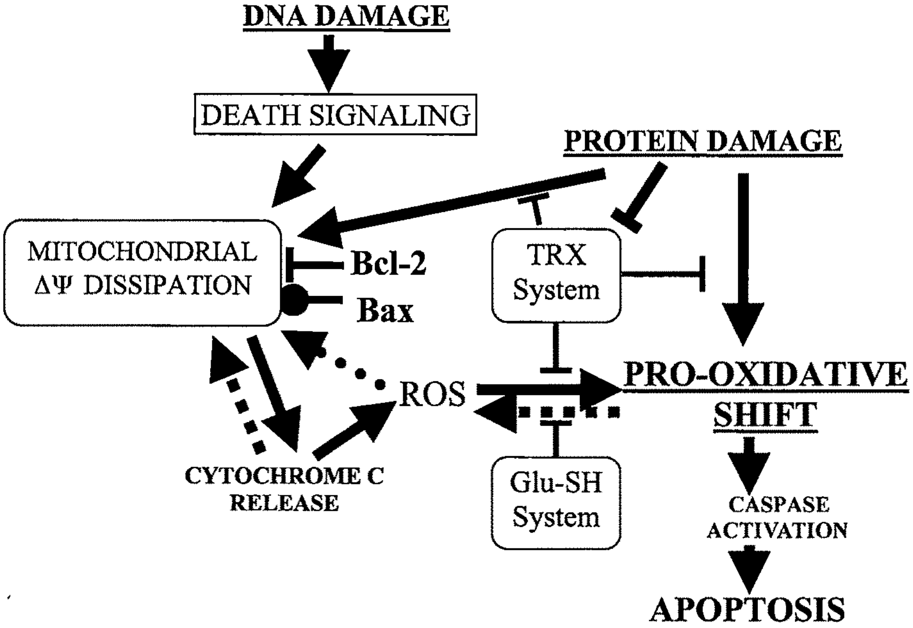

Fig 2 Model for processing of DNA and protein damage in apoptosis DNA damage elicits complex death signaling pathways that ultimately lead to mitochondrial dysfunction Mitochondria process and integrate pro-apoptotic signals triggered by other apoptotic stimuli, including protein damage and pro-oxidative changes Pro-oxidative distortion of redox homeostasis appears to be a common mediator of apoptosis by various stimuli Whereas the glutathione (Glu-SH) system can buffer redox changes at the level of small molecules, the thioredoxin (TRX) system is a key component controlling the redox status of the protein sulfhydryls. Downstream effects can provide positive feedback loops (dotted arrows) resulting in the self-amplifying nature of apoptosis

relevant anticancer drugs, irofulven and oxaliplatin, belong to the category of agents that bind to cellular DNA but mainly react with cellular proteins. Irofulven (HMAF, hydroxymethylacylfulvene, MGI 114, NSC 683863, Fig. 3) is a semisynthetic analog of the sesquiterpene Illudin S [50]. This drug is currently undergoing a Phase III clinical trial for gemcitabine-refractory pancreatic cancer and several Phase II trials for different tumor types [51–54]. Irofulven binds to cellular DNA but appears to form only monoadducts [55,56], usually not considered as lethal lesions. Yet, the drug is a potent apoptosis inducer [55,57] and produces tumor shrinkage and curative antitumor effects in several human xenograft models [58–62]. Not only does irofulven bind to multiple cellular proteins but also the magnitude of protein adducts (60% of total covalent adducts) exceeds nearly four-fold the levels of cellular DNA adducts [56].

Oxaliplatin, a third generation platinum antitumor analog in which 1,2 diaminocyclohexane ligand substitutes the amine groups of cisplatin, has demonstrated a broad spectrum of activity in a wide range of human tumors in vitro and in vivo [63] (Fig. 3). Our studies showed that oxaliplatin forms fewer DNA lesions than its parent drug cisplatin at equimolar concentrations [64,65]. In spite of reduced DNA damage, oxaliplatin is at least as cytotoxic and as potent inducer of apoptosis as cisplatin [64]. Moreover, oxaliplatin is clinically superior to cisplatin by being less toxic and retaining activity against cisplatin-resistant tumors [63,66,67]. Whereas protein reactivity of oxaliplatin has not been directly investigated, binding to cellular proteins of platinum drugs is, in general, an order of magnitude greater than DNA binding (~ 75–85 vs. ~ 10% of total cellular adducts, respectively, for cisplatin [68,69]). Moreover, the hydrophobic diaminocyclohexane moiety in oxaliplatin may facilitate drug interaction inside hydrophobic pockets of cellular proteins [65].

3.4 DNA and protein damage as apoptotic stimuli for irofulven and oxaliplatin?

An intriguing possibility is that functional protein damage (interference with enzymatic, receptor and/or structural functions) may markedly contribute to apoptosis induction by DNA- and protein-reactive drugs, such as irofulven and oxaliplatin. To address this possibility, we compared the levels of apoptosis induced by these dual-action drugs with apoptosis by diamide, which binds only proteins, and apoptosis by bizelesin, a drug that reacts only with DNA [70] (Fig. 3). The protein damaging agent, diamide, and dual action drugs, irofulven and oxaliplatin, were found to induce apoptosis at pharmacologically relevant levels. In contrast, the purely DNA-damaging drug bizelesin induced only marginal levels of apoptotic DNA fragmentation at supralethal concentrations. Since bizelesin, diamide, irofulven and oxaliplatin were all compared at equitoxic levels, our

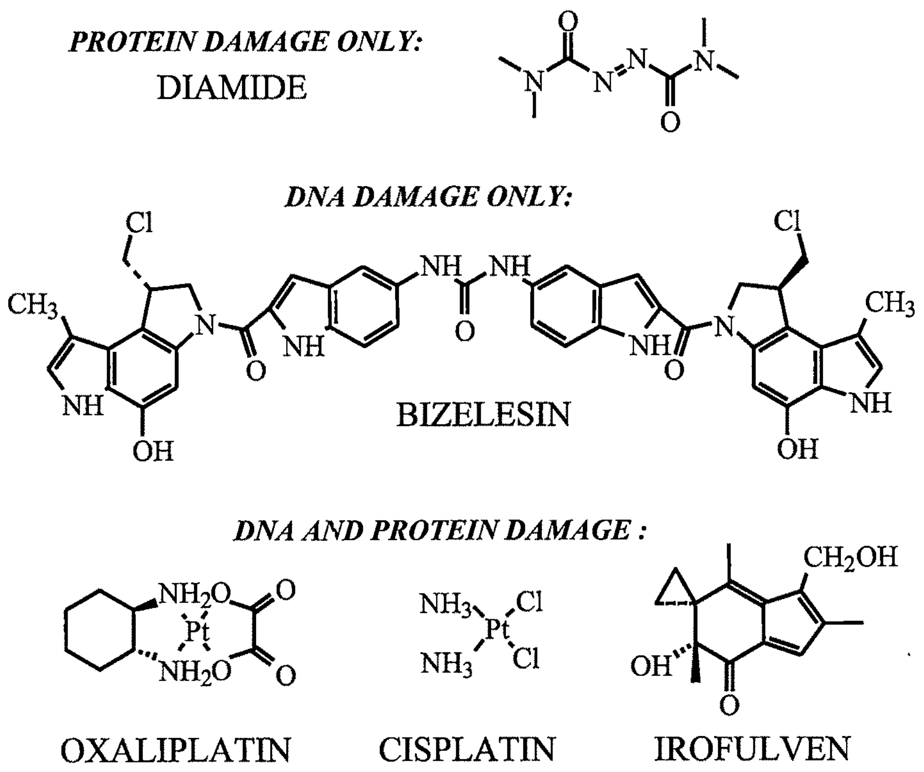

Fig. 3. Examples of pro-apoptotic DNA- and protein-damaging drugs (irofulven, oxaliplatin and cisplatin). Model single action drugs, diamide and bizelesin, represent compounds that react only with protein and DNA, respectively.

results illustrate the situation when protein damage alone may be sufficient, and DNA damage alone insufficient, for substantial apoptosis [57,71–73] (Fig. 4).

The effects of irofulven and oxaliplatin suggest that the most potent apoptosis induction occurs when both DNA- and protein reactivities are combined. Such a self-potentiating apoptosis can explain the potent pro-apoptotic and antiproliferative effects of irofulven and oxaliplatin [55,57,64,65,73]. DNA adducts by these drugs, like DNA damage, in general, are probably important in initiating death signaling. However, if DNA damage is accompanied by protein damage, apoptotic progression might accelerate. Although woefully understudied, protein damage is highly likely to contribute as well to the apoptotic effects of other dual-action drugs. Notably, a recent study by other authors linked apoptosis induction to protein damage by helenalin [74]. This antitumor agent, like irofulven, is a sesquiterpenoid capable of reacting with protein sulfhydryls, but possibly does not react with DNA [75]. Importantly, protein damage would push cell metabolism in the same pro-apoptotic direction as DNA lesions but acting in a nonoverlapping manner at the redox level, i.e., downstream from DNA damage-inducible death signaling. The idea that protein-damage may actively contribute to apoptosis induction by DNA-damaging agents challenges the common belief that binding of a DNA-reactive drug to proteins is merely a "detoxification" event. Collectively, the results with model compounds and known pro-apoptotic properties of other protein-damaging agents strongly suggest that DNA- and protein-reactive drugs may be particularly suitable for targeting apoptosis.

4. Preferential apoptosis induction in tumor cells by dual action drugs

A question of paramount importance for targeting apoptosis with dual-action drugs is whether they have the ability to selectively affect tumor cells. Our recent studies, discussed below, provide a proof of concept that differential apoptosis in cancer versus normal cells is feasible and can be considered as a potential basis for tumor selectivity with apoptosis targeting strategies.

4.1. Differential apoptotic responses in tumor versus normal cells

The potent induction of apoptosis is the most prominent feature of irofulven action in various tumor cell systems, including several human prostate, colon, breast and leukemia tumor cell lines [55–57,76,77]. In striking contrast to tumor cells, normal cells tend to be remarkably resistant to the induction of apoptosis by irofulven treatment. Marginal or very low levels of apoptosis, as measured by DNA fragmen-

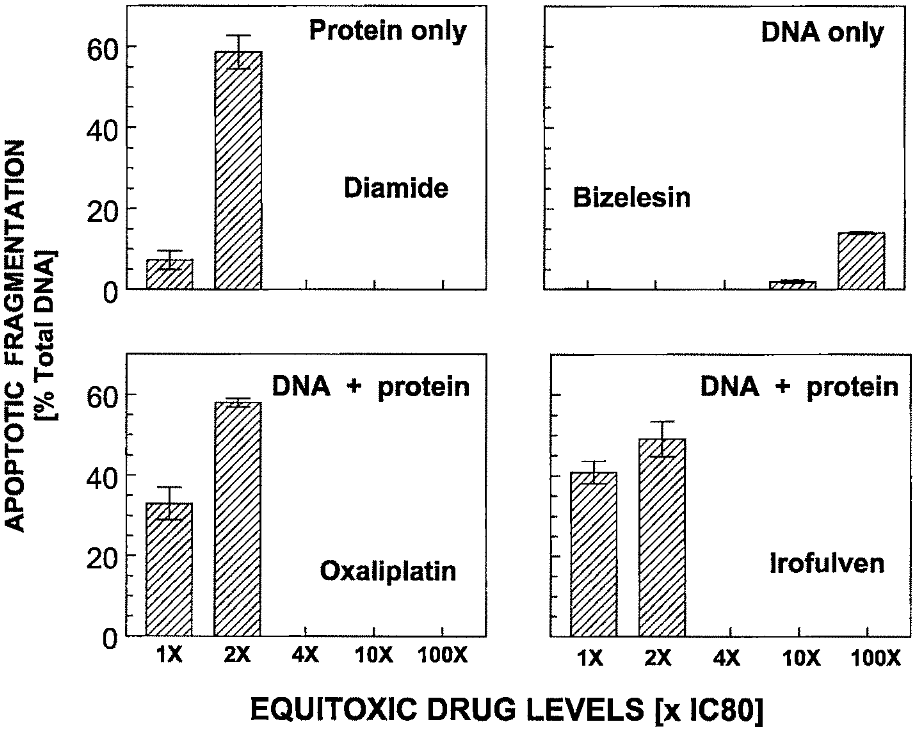

Fig. 4 Apoptotic potential of single and dual-action drugs [71,73] Human leukemia CEM cells were treated for 24 h with model drugs damaging only proteins (diamide), only DNA (bizelesin), and both DNA and protein (irofulven and oxaliplatin). To relate the effectiveness of these agents to the pharmacologically relevant levels, the abscissa indicates equitoxic concentrations expressed as the multiples of the IC_{80} values (drug concentrations inhibiting cell growth by 80%) The examples shown are for quantitative DNA fragmentation assay Analogous pattern of apoptotic potential was found based on changes in cell morphology and several other apoptotic assays

tation and other apoptotic assays, were detected in normal mucosa, fibroblasts, epithelial and endothelial cells. While cancer cells underwent apoptosis after relatively brief treatments, normal cells remained refractory even to prolonged incubations with irofulven at concentrations that exceeded up to hundred-fold the levels sufficient for growth inhibition and apoptosis in tumor cells (Fig. 5A,B and Fig. 6). Although data for oxaliplatin are less extensive, this drug also showed indications of preferential apoptosis in some tumor cells over normal cells (Fig. 5C,D) [64,73]. A profound apoptosis in tumor cells with marginal effect in normal peripheral blood cells was recently observed also for the protein-reactive helenalin [74].

4.2. Cytotoxic versus cytostatic effects of irofulven

Importantly, the resistance of normal cells to irofulven could not be accounted for by differences in drug accumulation or drug covalent binding to macromolecules [56,57,76]. Drug-induced growth inhibition paralleled the

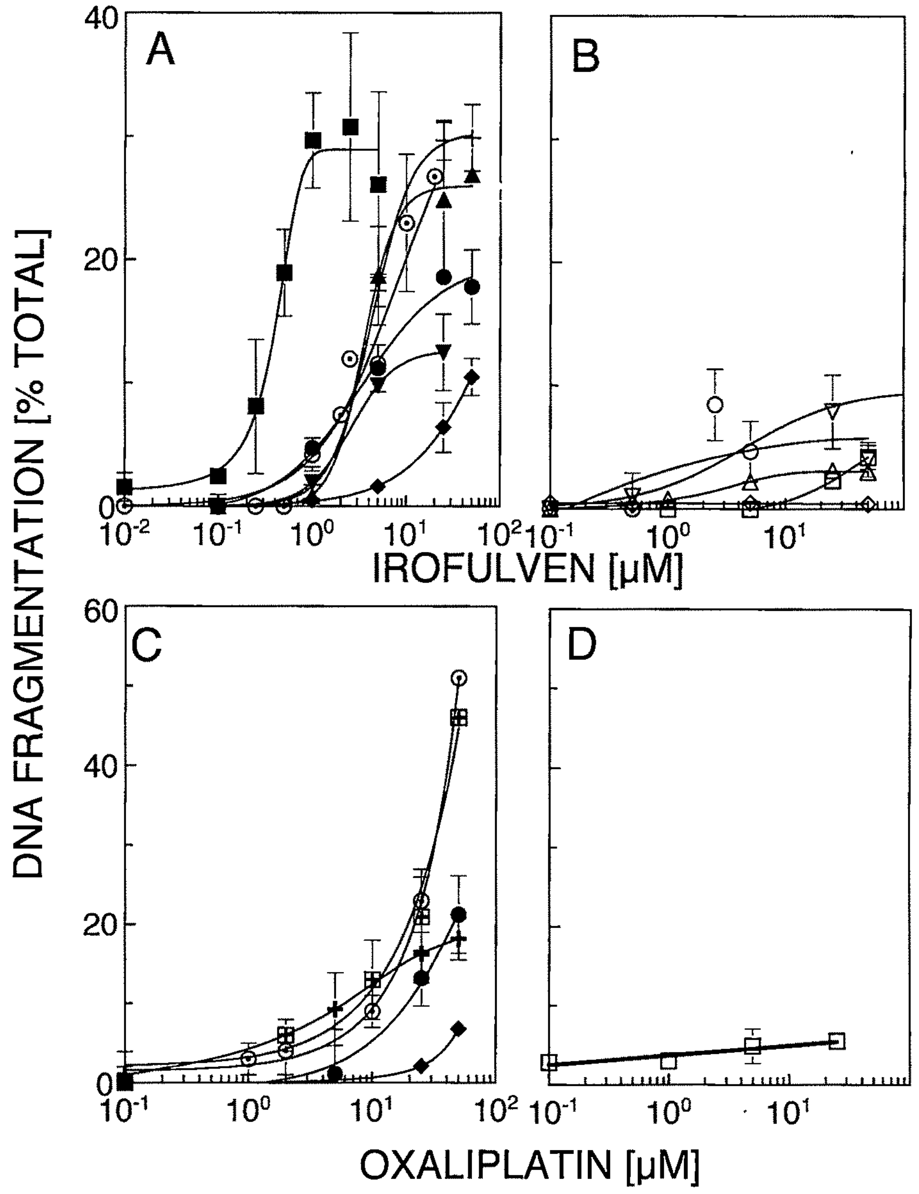

Fig. 5. Differential induction of apoptosis in tumor (A,C) and normal (B,D) cells by dual-action drugs. Cells were treated with various concentrations of irofulven for 4 h followed by 20 h post-incubation in drug-free medium (A,B) or with oxaliplatin for 24 h (C,D) before determination of apoptotic DNA fragmentation. Human tumor cell lines LNCaP-Pro5 (+); LNCaP (▲), LNCaP-LN3 (●), LNCaP-C4-2 (▼), PC-3 (♦), Colo 320DM (■); CEM (◎) and A2780 (⊞). Human normal cell lines. PrEC (□), NCM 460 (△); WI 38 (◇) RPTEC (▽) and HUVEC (○). The composite data in the figure are from the Refs. [57,64,73]. (Panels A and B reprinted from B.A. Woynarowska, et al., Differential cytotoxicity and induction of apoptosis in tumor and normal cells by hydroxymethylacylfulvene (HMAF), Biochem. Pharmacol 59 (2000) 1217–1226, 59 pp. Copyright 2000, with permission from Elsevier).

uptake of [^{14}C]irofulven, although normal cells were three- to four-fold more tolerant to the accumulated drug [57]. In both tumor and normal cells, approximately two-thirds of the internalized irofulven was bound covalently to macromolecules [57]. Notably, normal cells, even while growth inhibited, maintained their viability for long times and showed indications of continuation of growth after several days. In contrast, progressive apoptosis in tumor cells resulted in a profound decrease in viability paralleled by the net decrease of cell number below the initial values (Fig. 6) [57,76]. Thus, irofulven is cytotoxic and apoptotic in tumor cells but only cytostatic in normal cells. The qualitatively different responses of the tumor and normal cells demonstrate an inherently greater tolerance of normal cells to molecular lesions induced by irofulven. The possible connection between this tolerance and redox homeostasis is discussed below.

The potent and differential pro-apoptotic properties of irofulven in tumor but not in normal cells strongly suggests its potential utility as an apoptosis-enhancing agent in combination with other modalities. Indeed, the combination of irofulven with γ-radiation was at least additive with indications of supra-additivity in terms of apoptosis and survival of human prostate tumor cells [76]. Most importantly, irofulven did not sensitize normal cells to ionizing radiation [76].

4.3. Distortion of redox homeostasis in tumor cells

The pattern of apoptosis induction by irofulven is consistent with the distortion of the redox balance of the cancer cell (Table 1) [73,78,79]. Several findings implicate TRX, a key redox-controlling factor, in irofulven-induced apoptosis. The drug can bind covalently to purified TRX [56], adducting one of its sulfhydryl groups [79]. In cancer cells, irofulven causes an early and transient up-regulation of TRX, which is detected at both mRNA and protein levels. Consistently, TRX-dependent redox-sensing transcription factors, nuclear factor κB (NF-κB) and activator protein 1 (AP-1) are also activated (Table 1). Irofulven treatment results also in the early and profound translocation of pro-apoptotic Bax to mitochondria, dissipation of mitochondrial membrane potential, the release of cytochrome *c*, and activation of a caspase cascade [78]. At later times, there is a profound depletion in TRX protein levels (below the basal level), accompanied by massive pro-oxidative changes in cellular proteins, manifested as the increase in protein carbonyls and decrease in protein sulfhydryls (Table 1, Ref. [79]). The observed pattern suggests that irofulven induces a rapid and possibly self-amplifying cascade of pro-oxidative changes in cancer cells. Whereas further studies are needed for better understanding of these effects, the profound and irreversible collapse of the redox homeostasis supports the notion that drug-induced protein damage may contribute to apoptosis induction in cancer cells.

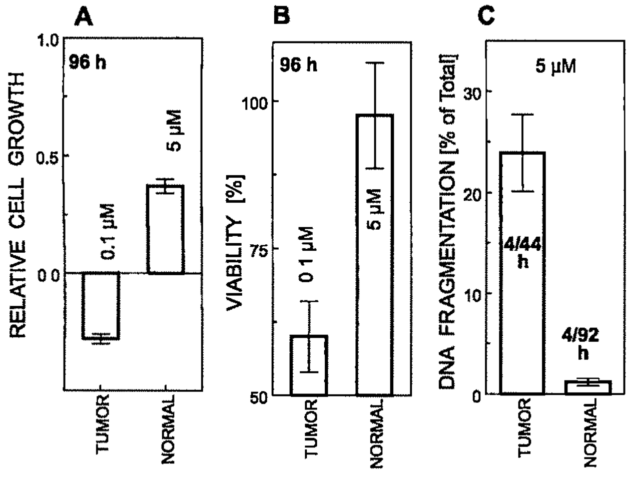

Fig. 6. Irofulven is cytotoxic for tumor but cytostatic for normal cells Tumor cells (prostate cancer LNCaP-Pro5) and normal cells (normal colon mucosa NCM-460) were incubated with irofulven for various times as indicated. Data for three endpoints are shown: cell growth inhibition (Panel A), cell viability (by trypan blue exclusion, Panel B) and quantitative apoptotic DNA fragmentation (Panel C). Note that normal cells were treated with the 50-fold higher concentration of irofulven than cancer cells (5 and 0.1 µM, respectively). Although normal cells are growth inhibited, they remain viable and do not undergo apoptotic DNA fragmentation. Data are the examples taken from Refs [57,76].

Table 1
Differential redox-related responses to irofulven in tumor and normal cells[a]

Cell line	Tumor[b]	Normal[b]
TRX protein basal level	+	+++
TRX upregulation (mRNA and protein)	++ (transient)	+++ (transient)
TRX protein depletion	yes	no
NF-κB binding activation	+++	± (transient)
AP-1 binding activation	+++	N D.[c]
Increase in protein carbonyls	+++	±
Decrease in protein sulfhydryls	+++	–
Transcriptional responses	+++	+++

[a] Based on Refs. [73,78,79] and Liang et al, in preparation

[b] Results obtained using prostate tumor LNCaP-Pro5 cells and normal colon mucosa NCM-460 cells

[c] N.D., not determined

4.4. Redox-related responses in normal cells

Normal cells, in general, are believed to be better protected from pro-oxidative insults than tumor cells [18,80]. The greater capacity of normal cells to maintain reducing conditions could explain their relative insensitivity to drugs such as irofulven and oxaliplatin. For instance, irofulven-resistant normal cells have markedly higher basal TRX levels than irofulven-sensitive tumor cells (Table 1). While irofulven also causes a transient stimulation of TRX expression in normal cells, the initial TRX levels are soon restored, and, in contrast to tumor cells, no TRX depletion is observed (Table 1). Hence, irofulven-treated normal cells do initiate redox-related responses, but their overall redox homeostasis remains stable, even after prolonged times. This pattern is consistent with the observed cytostatic effects of irofulven in normal cells, as opposed to cytotoxic effects seen in cancer cells (c.f., Fig. 6). These findings warrant further investigations to clarify the significance of TRX and other redox-buffering elements in apoptosis by dual action drugs, in particular in a broader range of cell lines with varying basal TRX levels.

4.5. Bypass of apoptosis-inhibiting mechanisms by dual-action drugs

Several studies showed that dual-action drugs may remain pro-apoptotic under various pharmacologically unfavorable conditions. Irofulven and oxaliplatin seem to induce apoptosis in cancer cells regardless of their p53 status [57]. Pro-apoptotic effects of irofulven are largely bcl-2-independent, as found in a system with forced bcl-2 overexpression [81]. Finally, irofulven apoptosis is apparently not mediated by caspase-3, a generally important apoptosis executioner. Consequently, irofulven retains its full pro-apoptotic activity in caspase-3 deficient cells [77]. Hence, differences in the levels of pro- and anti-apoptotic factors, which may, in principle, affect cellular responses to various drugs, should be less critical for agents that target the apoptotic process at multiple, nonoverlapping points.

5. Concluding remarks

Both DNA damage and protein damage can, in principle, promote apoptosis. While DNA damage initiates death signaling, protein damage is known to distort the cell redox homeostasis, which facilitates apoptosis execution. The reviewed findings with novel anticancer drugs that react with both DNA and proteins suggest that both reactivities may indeed contribute to their pro-apoptotic properties. This notion challenges the common belief that binding of such drugs to cellular proteins is merely a detoxification event. Clearly, further studies are needed to better understand whether and when DNA damage alone, or in conjunction with protein damage, determines the fate of cancer cells treated with dual-action anticancer drugs.

Importantly, the reviewed investigations provide a proof of principle that dual-action drugs can target apoptosis in tumor cells, but spare normal cells. The qualitatively different responses and profoundly greater tolerance of normal cells to molecular lesions that promote apoptosis in tumor cells point to fundamental differences that can be therapeutically exploited. In that context, it could be important that drugs, such as irofulven, affect multiple cellular molecules. Although damage to some specific targets might be particularly lethal, all the DNA- and protein-lesions may well act in concert (Fig. 2). Hence, DNA- and protein-damaging drugs can be perceived as agents targeting a process, rather than a specific single biological entity, or one specific pathway.

Acknowledgements

This review was made possible in part by NIH Grants CA78706 and CA71969, and a grant from the Children's Cancer Research Center University of Texas Health Science Center. We thank also Dr. S. Waters for the critical reading of this manuscript.

References

[1] C Schober, J F Gibbs, M B Yin, H.K Slocum, Y.M. Rustum, Biochem Pharmacol. 48 (1994) 997–1002.
[2] J C Reed, J Clin Oncol 17 (1999) 2941–2953
[3] S R Denmeade, X.S Lin, J.T. Isaacs, Prostate 28 (1996) 251–265
[4] S W Lowe, A.W Lin, Carcinogenesis 21 (2000) 485–495
[5] S H Kaufmann, W C Earnshaw, Exp Cell Res. 256 (2000) 42–49.
[6] A Strasser, L O'Connor, V.M. Dixit, Ann Rev. Biochem. 69 (2000) 217–245.
[7] R J. Carmody, T G Cotter, Redox Rep. 6 (2001) 77–90
[8] J. Chandra, A Samali, S. Orrenius, Free Radic. Biol. Med 29 (2000) 323–333.
[9] S Iwata, T Hori, N Sato, K. Hirota, T Sasada, A. Mitsui, T Hirakawa, J Yodoi, J Immunol. 158 (1997) 3108–3117.
[10] P Marchetti, D. Decaudin, A. Macho, N Zamzami, T Hirsch, S A. Susin, G Kroemer, Eur J Immunol 27 (1997) 289–296
[11] H Kamata, H. Hirata, Cell Signal 11 (1999) 1–14
[12] S Desagher, J C Martinou, Trends Cell Biol. 10 (2000) 369–377
[13] S A Susin, N Zamzami, G Kroemer, Biochim. Biophys Acta 1366 (1998) 151–165
[14] K.F Ferri, G. Kroemer, Bioessays 23 (2001) 111–115.
[15] R.J. Carmody, T.G Cotter, Cell Death Differ 7 (2000) 282–291.
[16] S.P. Kantrow, L G Tatro, C A Piantadosi, Free Radic Biol. Med 28 (2000) 251–260.
[17] G. Powis, W.R Montfort, Annu Rev Biophys. Biomol Struct 30 (2001) 421–455
[18] M Saitoh, H Nishitoh, M Fujii, K Takeda, K Tobiume, Y Sawada, M. Kawabata, K Miyazono, H Ichijo, EMBO J 17 (1998) 2596–2606
[19] H. Nakamura, K Nakamura, J. Yodoi, Annu Rev Immunol 15 (1997) 351–369
[20] E.S J Arner, A Holmgren, Eur J. Biochem. 267 (2000) 6102–6109
[21] C K Sen, Curr Top Cell Regul 36 (2000) 1–30.
[22] A P Arrigo, Free Radic. Biol Med 27 (1999) 936–944.
[23] J Wang, M Kobayashi, K. Sakurada, M Imamura, T. Moriuchi, M. Hosokawa, Blood 89 (1997) 2480–2487.
[24] T Sasada, S. Iwata, N Sato, Y Kitaoka, K Hirota, K. Nakamura, A Nishiyama, Y Taniguchi, A Takabayashi, J Yodoi, J Clin Invest. 97 (1996) 2268–2276.
[25] P A Thibodeau, S. Kocsis-Bedard, J Courteau, T Niyonsenga, B Paquette, Free Radic. Biol. Med. 30 (2001) 62–73.
[26] K Becker, S Gromer, R H Schirmer, S Muller, Eur J. Biochem 267 (2000) 6118–6125
[27] M.L Smith, A J. Fornace Jr, Mutat. Res 340 (1996) 109–124.
[28] J.L.M Gervais, P Seth, H Zhang, J Biol Chem. 273 (1998) 19207–19212
[29] S Shimizu, M Narita, Y Tsujimoto, Nature 399 (1999) 483–487.
[30] U M Moll, A. Zaika, FEBS Lett 493 (2001) 65–69
[31] J C Yang, G A Cortopassi, Free Radic Biol Med. 24 (1998) 624–631
[32] A Kowaltowski, A.E. Vercesi, G. Fiskum, Cell Death Differ 7 (2000) 903–910.
[33] B. Single, M Leist, P. Nicotera, Exp Cell Res 262 (2001) 8–16
[34] J S Armstrong, K K Steinauer, J French, P.L Killoran, J Walleczek, J Kochanski, S J. Knox, Exp Cell Res. 262 (2001) 170–179.

[35] K Kannan, S K Jain, Pathophysiology 7 (2000) 153–163

[36] W. Davis Jr., Z. Ronai, K.D. Tew, J. Pharmacol. Exp. Ther. 296 (2001) 1–6.

[37] S. Nagata, Exp. Cell Res. 256 (2000) 12–18

[38] J.A. Hickman, C.S. Potten, A.J. Merritt, T C. Fischer, Philos. Trans. R. Soc. Lond., B Biol. Sci. 345 (1994) 319–325.

[39] C. Bowen, S Spiegel, E.P. Gelmann, Cancer Res. 58 (1998) 3275–3281

[40] B Guan, P Yue, G.L Clayman, S Y. Sun, J. Cell Physiol. 188 (2001) 98–105.

[41] S Ueda, H Nakamura, H. Masutani, T. Sasada, S Yonehara, A. Takabayashi, Y. Yamaoka, J. Yodoi, J Immunol. 161 (1998) 6689–6695.

[42] N. Zamzami, I. Marzo, S.A Susin, C Brenner, N Larochette, P. Marchetti, J. Reed, R. Kofler, G Kroemer, Oncogene 16 (1998) 1055–1063

[43] H Iwase, K Sakurada, H. Ikegaya, K Hatanaka, H. Takeichi, M Kobayashi, K Yoshida, IUBMB Life 51 (2001) 39–43.

[44] R.N. Coffey, R.W. Watson, N.J. Hegarty, A O'Neill, N Gibbons, H.R. Brady, J.M. Fitzpatrick, Cancer 88 (2000) 2092–2104.

[45] Y.E. Kushnareva, P.M. Sokolove, Arch Biochem. Biophys. 376 (2000) 377–388

[46] M. Pallis, M Grundy, J. Turzanski, R Kofler, N Russell, Blood 98 (2001) 405–413

[47] D. Gius, A. Botero, S Shah, H.A. Curry, Toxicol Lett 106 (1999) 93–106

[48] L.K. Moran, J M. Gutteridge, G J Quinlan, Curr. Med Chem 8 (2001) 763–772

[49] M R Volkert, P Landini, Curr. Opin Microbiol. 4 (2001) 178–185.

[50] M Kelner, T.C McMorris, R. Taetle, J. Natl Cancer Inst 82 (1990) 1562–1565.

[51] S G. Eckhardt, S.D. Baker, C D Britten, M. Hidalgo, L. Siu, L A. Hammond, M.A. Villalona-Calero, S Felton, R Drengler, J.G. Kuhn, G.M. Clark, S L Smith, J.R MacDonald, C. Smith, J. Moczygemba, S. Weitman, D.D Von Hoff, E.K. Rowinsky, J Clin Oncol 18 (2000) 4086–4097

[52] J E Dowell, D H Johnson, J.S Rogers, Y Shyr, N McCullough, P. Krozely, R.F. DeVore, Invest. New Drugs 19 (2001) 85–88.

[53] J E Dowell, A.M. Garrett, Y Shyr, D.H. Johnson, K R Hande, Cancer 91 (2001) 592–597

[54] F Giles, J Cortes, G. Garcia-Manero, S Kornblau, E. Estey, M Kwari, A. Murgo, H. Kantarjian, Invest New Drugs 19 (2001) 13–20.

[55] J.M. Woynarowski, C. Napier, S K. Koester, S F Chen, D. Troyer, W. Chapman, J.R. MacDonald, Biochem Pharmacol 54 (1997) 1181–1193

[56] M.C.S. Herzig, B Arnett, J R. MacDonald, J.M Woynarowski, Biochem. Pharmacol 58 (1999) 217–225

[57] B A Woynarowska, J.M. Woynarowski, M.C. Herzig, K. Roberts, A.L Higdon, J R MacDonald, Biochem. Pharmacol 59 (2000) 1217–1226

[58] J.R. MacDonald, C.C. Muscoplat, D.L. Dexter, G L. Mangold, S F. Chen, M J. Kelner, T C McMorris, Cancer Res 57 (1997) 279–283.

[59] S Weitman, H. Barrera, R Moore, C Gonzalez, J Marty, S. Hilsenbeck, J.R MacDonald, S J. Waters, D Von Hoff, Pediatr Hematol. Oncol 22 (2000) 306–314

[60] L A. Hammond, S.G. Hilsenbeck, S G. Eckhardt, J Marty, G Mangold, J.R. MacDonald, E.K. Rowinsky, D.D. Von Hoff, S. Weitman, Eur. J. Cancer [A] 36 (2000) 2430–2436

[61] M J. Kelner, T.C McMorris, L A Estes, M Y Oval, R J Rojas, J R Lynn, K A. Lanham, K.M Samson, Anticancer Drugs 11 (2000) 217–224

[62] C D. Britten, S G Hilsenbeck, S G Eckhardt, J. Marty, G. Mangold, J.R. MacDonald, E.K. Rowinsky, D D Von Hoff, S Weitman, Cancer Res. 59 (1999) 1049–1053

[63] E. Raymond, S. Faivre, J Woynarowski, S Chaney, Semin Oncol 25 (1998) 4–12.

[64] S. Faivre, J.M. Woynarowski, Proc. Am Assoc Cancer Res 39 (1998) 158

[65] J.M Woynarowski, S Faivre, M.C S Herzig, B Arnett, W.G Chapman, A.V. Trevino, E Raymond, S G. Chaney, A Vaisman, M. Varchenko, P E. Juniewicz, Mol. Pharmacol 58 (2000) 920–927.

[66] O. Rixe, W Ortuzar, M. Alvarez, R. Parker, E. Reed, K Paull, T. Fojo, Biochem. Pharmacol 52 (1996) 1855–1865.

[67] H. Akaza, N. Saijo, K Aiba, S. Isonishi, Y Ohashi, K Kawai, T. Konishi, T Saeki, S. Sone, S Tsukagoshi, T Tsuruo, S. Noguchi, T Miki, O Mikami, M Smith, G Hoctin-Boes, D. Stribling, Gan To Kagaku Ryoho 28 (2001) 625–635.

[68] M. Akaboshi, K. Kawai, H Maki, K Akuta, Y Ujeno, T Miyahara, Jpn J Cancer Res 83 (1992) 522–526

[69] M. Akaboshi, K. Kawai, Y Ujeno, S. Takada, T Miyahara, Jpn. J. Cancer Res. 85 (1994) 106–111

[70] J.M Woynarowski, M McHugh, L.S Gawron, T.A Beerman, Biochemistry 34 (1995) 13042–13050

[71] J.M Woynarowski, S. Koester, B. Woynarowska, B. Arnett, A.V Trevino, D. Chan, A. Higdon, R Munoz, M.C S Herzig, S Faivre, Proc. Am. Assoc Cancer Res 40 (1999) 736

[72] J M. Woynarowski, T.A Beerman, Biochim Biophys Acta N, Gene Struct. Expr. 1353 (1997) 50–60

[73] B. Woynarowska, J.M. Woynarowski, A.L. Higdon, R. Munoz, Proc Am. Assoc. Cancer Res. 40 (1999) 488.

[74] V.M Dirsch, H. Stuppner, A M Vollmar, Cancer Res 61 (2001) 5817–5823.

[75] A A Grippo, I.H. Hall, H Kiyokawa, O Muraoka, Y C. Shen, K.H Lee, Drug Des. Discov. 8 (1992) 191–206.

[76] B A Woynarowska, K. Roberts, J.M. Woynarowski, J.R. MacDonald, T.S Herman, Radiat. Res. 154 (2000) 429–438

[77] M.C.S. Herzig, H Liang, A.E Johnson, B Woynarowska, J.M Woynarowski, Breast Cancer Res. Treat 71 (2002) 133–143.

[78] H Liang, R Munoz, A L. Hidgon, S.J Waters, B Woynarowska, Proc Am Assoc. Cancer Res. 42 (2001) 640

[79] H Liang, M.C. Herzig, R Salinas, S T. Weintraub, M P. Moyer, S J Waters, J M. Woynarowski, B. Woynarowska, 2001. AACR-NCI-EORTC International Conference on Molecular Targets, Cancer Therapeutics, Miami Beach

[80] K. Kinoshita, M. Kanai, M. Awane, K Furuke, Y. Shirakata, T Gomi, Y. Nakamura, I. Ikai, A. Yamauchi, T. Inamoto, K. Ohmori, Y Yamaoka, J. Hepatol 26 (1997) 103–110

[81] M.C S Herzig, B. Woynarowska, A V Trevino, J.M. Woynarowski, Proc. Am Assoc Cancer Res. 41 (2000) 283

ELSEVIER

Biochimica et Biophysica Acta 1587 (2002) 318–325

BIOCHIMICA ET BIOPHYSICA ACTA
BBA
www.bba-direct.com

Review

Interaction of tyrosine kinase inhibitors with the human multidrug transporter proteins, MDR1 and MRP1

Tamás Hegedűs [a], László Őrfi [b], Attila Seprődi [c], András Váradi [d], Balázs Sarkadi [a,*], György Kéri [c]

[a] *National Institute of Haematology and Immunology, Membrane Research Group of the Hungarian Academy of Sciences, H-1113 Budapest, Daróczi u 24, Hungary*
[b] *Department of Pharmaceutical Chemistry, Semmelweis University, Budapest, Hungary*
[c] *Peptide Biochemistry Research Group of the Hungarian Academy of Sciences, Department of Medical Chemistry, Semmelweis University, Budapest, Hungary*
[d] *Institute of Enzymology, Biological Research Center, Hungarian Academy of Sciences, Budapest, Hungary*

Received 24 January 2002, accepted 24 January 2002

Abstract

Specific tyrosine kinase inhibitors (TKIs) are rapidly developing clinical tools applied for the inhibition of malignant cell growth and metastasis formation. Most of these newly developed TKI molecules are hydrophobic, thus rapidly penetrate the cell membranes to reach intracellular targets. However, a large number of tumor cells overexpress multidrug transporter membrane proteins, which efficiently extrude hydrophobic drugs and thus may prevent the therapeutic action of TKIs In the present work, we demonstrate that the most abundant and effective cancer multidrug transporters, MDR1 and MRP1, directly interact with several TKIs under drug development or already in clinical trials. This interaction with the transporters does not directly correlate with the hydrophobicity or molecular structure of TKIs, and shows a large variability in transporter selectivity and affinity. We suggest that performing enzyme- and cell-based multidrug transporter interaction tests for TKIs may greatly facilitate drug development, and allow the prediction of clinical TKI resistance based on this mechanism Moreover, diagnostics for the expression of specific multidrug transporters in the malignant cells, combined with information on the interactions of the drug transporter proteins with TKIs, should allow a highly effective, individualized clinical treatment for cancer patients.

© 2002 Elsevier Science B.V. All rights reserved.

Keywords· Chemotherapy, Multidrug resistance; MDR1; MRP, Tyrosine kinase inhibitor

1. Introduction

Carcinogenesis in numerous cases is based on a pathological intracellular signal transduction, in which the activation of specific tyrosine kinases plays a major role. Tyrosine kinases modify highly diverse cellular responses, including proliferation, differentiation, cell–cell interactions, or cell motility, thus aberrant TK activity leads to various disease states. Many oncogenes found in cancers are derived from tyrosine kinase genes that have been deregulated, leading to constitutive activity. Overexpression or activation of wild-type tyrosine kinases can also lead to cancer (see reviews [1–3]).

Tyrosine kinase inhibitors (TKI) with increased specificity and selectivity have been developed against misregulated or unregulated receptor-dependent and intracellular tyrosine kinases, which play a major role in cancer development. Modification of both tumor growth and metastatic potential of cancer cells has been reported by such agents (see [Refs. 4,5]). Based on these results, development of specific inhibitors of selected tyrosine kinases became a major area of modern antitumor drug research.

A prominent recent example for a successful antitumor application of TKIs is the development of specific Abl TKIs. The permanent activation or overexpression of the Abl cytosolic tyrosine kinase has been associated with a variety of human tumors, especially leukemias. In chronic

---

Abbreviations ABC transporters, ATP-binding cassette transporters, AM, acetoxy methylester; CSF, cerebrospinal fluid; GSH, free gluthathione; MDR1, human multidrug transporter (P-glycoprotein); MRP1, human multidrug resistance protein 1, MRP2, human multidrug resistance protein 2, NEM, *N*-ethylmaleimide; Sf9 cells, *Spodoptera frugiperda* ovarian cells, TKI, tyrosine kinase inhibitor

[*] Corresponding author Tel.. +36-1-372-4316; fax: +36-1-372-4353.

E-mail address sarkadi@biomembrane hu (B Sarkadi)

0925-4439/02/$ - see front matter © 2002 Elsevier Science B V All rights reserved
PII. S0925-4439(02)00095-9

myeloid leukemia (CML), the most common form of leukemias, a 210-kDa form of the Bcr–Abl fusion protein, resulting from a (9:22)-chromosome translocation (Philadelphia chromosome), is present in 95% of these patients. The transforming function of the Bcr–Abl fusion protein depends on the constitutive and elevated tyrosine kinase activity of the enzyme, thus the Abl tyrosine kinase has become a validated target for antitumor drug research.

Several effective inhibitors of the Bcr–Abl kinase have been synthesized and introduced into preclinical trials. Data in the literature indicate that CGP57148B (STI-571, Gleevee), a 2-phenylamino-pyrimidine derivative, selectively inhibits the tyrosine kinase Abl and Bcr–Abl. It has also been documented that this compound selectively suppresses the growth of Bcr–Abl-positive cells over a wide dose range, with a maximal differential effect at about 1 μM. Inhibition of the Bcr–Abl kinase by STI-571 preferentially inhibits the growth of immature leukemic precursor cells, and efficiently reverts the antiapoptotic effects of Bcr–Abl by down-regulating BCL-X [6]. According to the first clinical trials, STI-571 treatment of CML produced haematological remission in 90% of patients [7]. Further clinical studies have ascertained a significant antitumor effectivity of STI-571 both in CML and other cancerous diseases (see [Ref. 8]), thus a wide range of clinical applications for these compounds is expected in the near future.

Untoward activation of EGF receptor tyrosine kinases is another well-documented phenomenon in a variety of malignancies, thus a number of EGFR-TKIs have also reached various phases of clinical trials (see [Ref. 9]). An important irreversible inhibitor of the EGF receptor tyrosine kinase (EKI-785), has been recently introduced into preclinical investigations [10]. TRX-13 [11], and tyrphostins, including AG-213, AG-1112 and AG-1393, are molecules which were reported to inhibit various receptor-coupled tyrosine kinases with relatively high specificity (see [Ref. 12]).

In our research group, we have developed a series of novel TKIs with the aim of modifying cellular responses and inhibiting cancer cell growth [13–17]. In the rational drug design program, the synthesized molecules, examined under proper quality control, were screened in several enzyme-, and cell-based assays, showing significant tyrosine kinase modulating effects. Several of these molecules, including OBF-1622, OBF-1822, OBF-1834, and OL-57 are currently introduced into preclinical trials.

The therapeutic potential of the TKIs, targeted against cytosolic enzymes, depends both on specific kinase inhibitory potential, as well as their access to their intracellular targets. Most of the effective TKIs are hydrophobic molecules, which are rapidly absorbed, distributed, and penetrate the cell membranes. However, the so-called multidrug transporters, present in the physiological barriers and in a large variety of tumor cells, may significantly alter the bioavailability of TKIs both at the systemic and the cellular levels.

The human multidrug transporters are plasma membrane glycoproteins which provide a major obstacle in the efficient chemotherapy of patients suoffering from cancer. These transporters belong to the family of ABC proteins, and work as ATP-dependent primary active transporters, efficiently extruding the clinically applied chemotherapeutic compounds. The two key proteins currently believed to be involved in cancer multidrug resistance are MDR1 (P-glycoprotein) and MRP1 (multidrug resistance protein 1). Both of these proteins can recognize and transport a large variety of hydrophobic drugs, and MRP1 can also extrude anionic drugs or drug conjugates.

The exact mechanism of action of the multidrug transporters is not known, although their membrane topology and basic functional characteristics have been explored in a variety of biochemical and cell biology studies (see [Refs. 18–20]). Multidrug transporters were first described in drug-resistant tumor cells, but they also provide important physiological functions: both MDR1 and MRP1 are key players in tissue barriers, e.g. in the blood–brain barrier, and participate in various transport and secretory functions in the gut, liver, kidney, and several other organs. Modulators of drug transporters are regarded as potential clinically applicable agents to inhibit cancer multidrug resistance and alter tissue distribution for various pharmacons [21,22].

Since anticancer action and general tissue distribution for hydrophobic drugs are both significantly affected by the multidrug transporters, by now it has been generally accepted that cancer drug development should increase the examination of the interaction of the lead compounds with the multidrug transporters. In the area of TKIs, this has not been explored as yet, although recent studies clearly indicated the occurrence of cellular STI-571-resistance, which may involve the function of multidrug transporters [8].

In the present work, we have analyzed the interactions of MDR1 and MRP1 with a variety of TKIs, including STI-571, by using both enzyme-, and cell-based test systems. We found that the multidrug transporters directly interacted with several TKIs. These interactions did not directly correlate with the hydrophobicity or molecular structure of TKIs, and showed significant variability in selectivity and affinity. We suggest that such studies, used in the early stages of drug development, may significantly improve both the selection of lead molecules and the clinical application of TKIs.

2. Experimental procedures

2.1. Expression of MDR1 and MRP1 in insect cells

Recombinant baculoviruses containing the MDR1 and MRP1 cDNA were prepared as described in Refs. [23,24]. Sf9 (*Spodoptera frugiperda*) cells were cultured and infected with a baculovirus as described in Ref. [23].

2.2. Membrane preparation and immunoblotting

Virus-infected Sf9 cells were harvested, their membranes isolated and stored, and the membrane protein concentrations determined, as described in Ref. [25]. Immunoblot detection was performed and protein–antibody interaction was determined using the enhanced chemoluminescence technique as described earlier [24].

2.3. Membrane ATPase measurements

ATPase activity was measured basically as described in Ref. [25] by determining the liberation of inorganic phosphate from ATP with a colorimetric reaction. The incubation media contained 10 mM MgCl2, 40 mM MOPS–Tris (pH 7.0), 50 mM KCl, 5 mM DTT, 0.1 mM EDTA, 4 mM Na-azide, 1 mM ouabain, and 4 mM ATP.

2.4. Multidrug transporter assays in mammalian cells

For the investigation of the function of MDR1 and MRP1 in mammalian cells, we applied both well-characterized transfected (NIH-3T3-MDR1, MDCKII-MDR1) and drug-selected (HL60-MDR1, KBV1(MDR1), HL60-MRP1 (ADR), S1-MRP1, MDCKII-MRP1) cell lines, as described in Ref. [26].

The Calcein assay, used for the quantitative determination of multidrug transporter activity, was performed as described earlier [27,28]. In brief, fluorescence intensities were determined in a fluorescence microplate reader after a short in vitro incubation. Cultured and well-characterized MDR1-Pgp expressing cells were incubated with the non-fluorescent Calcein AM, and with the respective concentrations of the compounds to be examined. The increase in cellular fluorescence, due to the liberation of free Calcein inside the cells, was determined. MDR1- and/or MRP-interactive compounds inhibited the outward transport of Calcein AM, thus significantly increase the rate of Calcein accumulation. In order to obtain the respective IC_{50} values for the TKIs, a computer-based evaluation protocol was applied.

2 5. TKIs investigated in the present study

The TKIs used in these experiments were synthesized and characterized in our laboratory as it was published earlier [5,13–16]. Fig. 1 shows the structural formulas for the TKIs examined in the present experiments.

2.6. Hydrophobicity parameters

Hydrophobicity parameters for the TKIs were obtained by two independent methods, widely used to estimate membrane permeation of lipophilic compounds. In brief, the logarithmic values of the octanol/water distribution for each compound were estimated by using the Pomona database and the methods named clogp http://www.daylight.com/daycgi/clogp, based on Ref. [29]) and Kowwin (KOWWIN v1.55; SRC-LOGKOW for Microsoft Windows, Copyright W. Meylan, 1993–1997), based on Ref. [30], respectively.

3. Results

3.1 MDR1 and MRP1 ATPase activity measurements in isolated insect cell membranes

In the first set of experiments we have examined the effects of TKIs on the transport-related ATPase activity of human MDR1 and MRP1 multidrug transporter proteins, expressed in isolated insect cell membranes. The vanadate-sensitive ATPase activity of the MDR1 multidrug transporter is significantly stimulated by hydrophobic substrate drugs [25], while the specific ATPase activity of the human MRP1 protein is stimulated by various glutathione-conjugates (GS-X), glucuronate-conjugates, and anionic drugs. In the case of MRP1, the ATPase activity is also stimulated by some of the hydrophobic compounds, e.g. vincristine, but this stimulation, in some cases, requires the presence of free glutathione [31]. It has been documented in detail, that the stimulation of the MDR1-, or MRP1-ATPase activity and its drug concentration dependence closely correlates with the respective transport activity of these proteins [24,25,32]. Therefore, this relatively simple assay can be used as an efficient screening for a large number of different compounds.

In order to explore all possible forms of direct TKI interactions with the multidrug transporters, in the current study we also examined the TKI inhibition of the MDR1 and MRP1 ATPase activities in the presence of maximum-stimulating agents. In the case of MDR1, ATPase inhibition by TKI was measured in the presence of 30–50 μM verapamil, while inhibition of MRP1 was studied in the presence of 5 mM NEM-GS. The combination of these assays allows to distinguish among transported substrates and inhibitors of the drug transporter proteins.

Fig. 2 documents the MDR1-ATPase measurements for some of the compounds examined, as compared to the effect of verapamil, as a reference compound (data for all compounds are summarized in Table 1). As shown, OBF-1834, AG-1393, OL-57, and STI-571 significantly stimulated the MDR1-ATPase activity in the low micromolar concentration range. TRX-13 stimulated this ATPase only in higher concentrations, while EKI-785 had no significant activation effect. The different maximum levels of ATPase stimulation, which were generally lower than that obtained with verapamil (set as 100% activation), suggested that most of the activating TKI compound may have an MDR1-ATPase inhibitory effect in higher concentrations.

Fig. 3 shows the effect of the same compounds on the MDR1-ATPase activity in the presence of maximally stim-

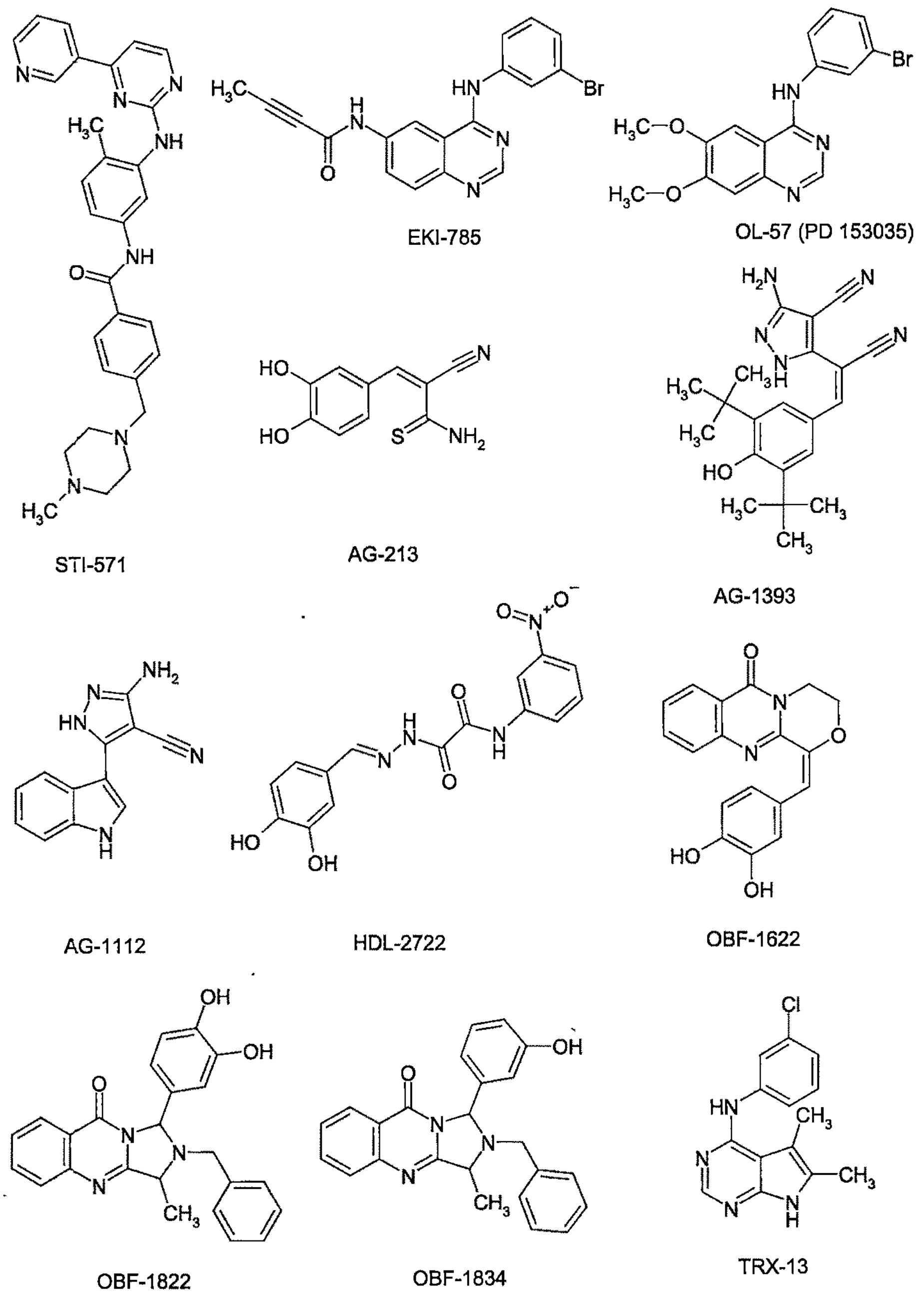

Fig. 1. Structures of the TKIs examined in the present experiments.

ulating verapamil concentrations (40 μM). In this case, we analyzed the possible inhibitory potential for the TKI compounds. As demonstrated, AG-1393 had the most pronounced MDR1-ATPase inhibitory effect in the low micromolar range, and STI-571 had a slightly lower inhibitory potential. OBF-1834 and OL-57 acted only at concentrations above 20 μM, while TRX-13 had no inhibitory effect at all. Interestingly, EKI-785 effectively inhibited the MDR1-ATPase activity at concentrations between 10 and 20 μM.

In the following experiments, we examined the effects of TKIs on the MRP1-ATPase activity in isolated Sf9 cell membranes. MRP1 has a much lower ATPase activity as compared to MDR1, and in this case we could not measure any significant activation of the basic MRP1-ATPase activity by any of the TKIs (not shown). Interestingly, when the MRP1-ATPase activity was maximally stimulated by 5 mM glutathione-conjugate, NEM-GS, we observed inhibitory actions for several compounds. As documented in Fig. 4, we found that EK-785 inhibited the MRP1-ATPase at the micromolar range (50% inhibition at about 10 μM), while STI-571 had a smaller effect and only at higher concentrations (50% inhibition at higher than 100 μM). AG-1393 and Ol-57 were effective inhibitors, while TRX-13 had only a partial inhibitory effect even at higher than 100 μM concentrations.

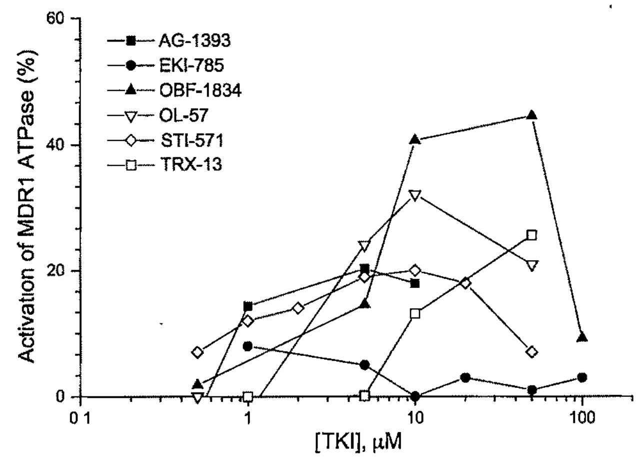

Fig 2 Activation of the human MDR1-ATPase activity by various concentrations of TKIs The data are presented as relative activation values, compared to 100% activation obtained with 40 μM verapamil (see Experimental procedures) Data compiled from at least four independent measurements for each compound.

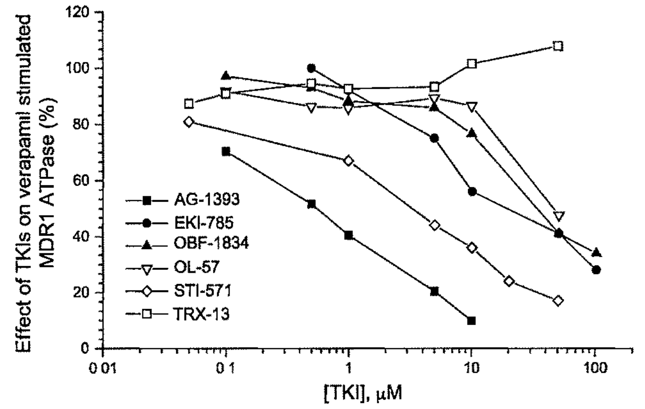

Fig 3 Inhibition of the verapamil-stimulated human MDR1-ATPase activity by various concentrations of TKIs Maximum activation (100%) was obtained with 40 μM verapamil Data compiled from at least four independent measurements for each compound

3.2. *Effects of TKIs in a cellular multidrug resistance activity (Calcein accumulation) assay*

In the following experiments, we applied a whole-cell screening system for studying the interactions of TKIs with the multidrug transporter proteins. When cells expressing the multidrug transporters are incubated with the non-fluorescent Calcein AM, due to an active dye extrusion, free Calcein accumulation is slow. MRP1 transports both Calcein AM and free Calcein, thus the assay can be used to study both drug transporters. Agents that interact with the multidrug resistance proteins inhibit dye extrusion and greatly accelerate fluorescent Calcein accumulation. The concentration dependence of this transport inhibition reflects the level of drug interaction with the drug pump proteins (see Experimental procedures). The relatively simple assay and the computer-based evaluation protocol allow the rapid in vitro screening of large numbers of agents selectively interacting with MDR1 or MRP1, although in this case competition or direct inhibition of the transporters cannot be distinguished.

Fig. 5 depicts some of the results obtained with the Calcein assay in a cell line expressing high levels of the human MDR1 protein (HL60-MDR1). All the data obtained for TKIs are summarized in Table 1. As shown in Fig. 5, Calcein AM extrusion by MDR1 was significantly inhibited by low concentrations of AG-1393, and at somewhat higher concentrations of STI-571, OL-57, or EKI-785. OBF-1834 had an incomplete inhibitory effect, and higher concentrations could not be examined, because of cellular toxicity. TRX-13 was quite ineffective in this whole-cell-based MDR1 assay.

Fig. 6 demonstrates a similar study for the inhibition by TKIs of the MRP1-dependent Calcein transport in HL60-MRP1 cells. As shown, MRP1-dependent transport was strongly inhibited by low micromolar concentrations of AG-1393, OBF-1834 and EKI-785, while OL-57 acted at somewhat higher concentrations. The MRP1-dependent transport was not significantly inhibited by TRX-13, and only at relatively high concentrations (above 20 μM) by STI-571.

Table 1
Summary of the parameters of the TKIs examined

TKI	Kowwin	clogP	K_{act} of MDR1-ATPase (μM)	K_{inh} of verpamil-stimulated MDR1-ATPase (μM)	K_{inh} of Calcein AM extrusion from HL60 MDR1 cells (μM)	K_{inh} of Calcein AM extrusion from HL60 MRP1 cells (μM)
AG-213	−0.73	0.048	>200	>200	>200	>200
OBF-1622	0.99	0.867	200	50	100	20
AG-1112	1.06	1.813	>200	>200	200	20
HDL-2722	1.29	0.439	100	>200	100	100
OBF-1822	2.19	3.551	50	100	10	10
OBF-1834	2.67	4.148	5	20	>30	4
STI-571	3.01	4.529	1	3	8	20–30
AG-1393	3.34	3.781	0.8	1	1	2
EKI-785	3.69	4.68	>200	20	20	4–5
OL-57	3.96	5.178	5	50	20	8
TRX-13	4.05	4.895	20	>200	>200	>200

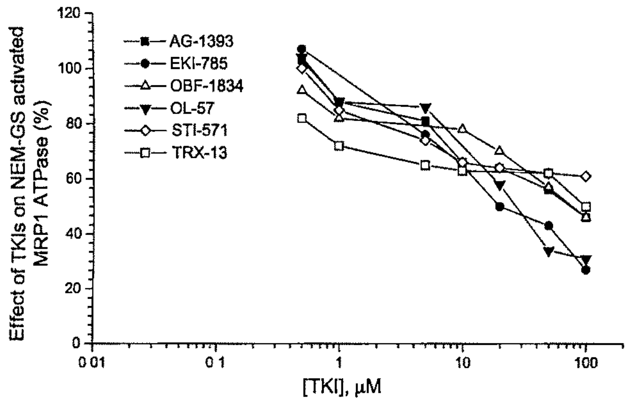

Fig. 4 Inhibition of the NEM-GS-stimulated human MRP1-ATPase activity by various concentrations of TKIs. Maximum activation (100%) was obtained with 5 mM NEM-GS. Data compiled from at least four independent measurements for each compound

3.3 *Comparison of hydrophobicity parameters and multidrug transporter interaction data*

When using the two widely accepted methods, Kowwin and clogp, respectively, to obtain hydrophobicity parameters (see Experimental procedures) for the TKIs examined, the values provided by the two independent methods were somewhat variable, but showed a very good correlation (see Table 1, rows 2 and 3). In order to examine the relationship between these values and the corresponding multidrug transporter interaction data, we compiled these values for all TKIs examined in this study. In Table 1, we present all these data by sorting according to the ascending Kowwin hydrophobicity values.

As documented in Table 1, while the two different estimations for the hydrophobicity values are in good correlation, the values obtained for the interaction of TKIs with either the MDR1 or the MRP1 protein show no apparent correlation with these parameters. The only appreciable information provided by this comparison is that no MDR1-interacting compounds were found with low hydrophobicity values (below Kowwin 1.29), while in the case of MRP1, even this relationship was absent.

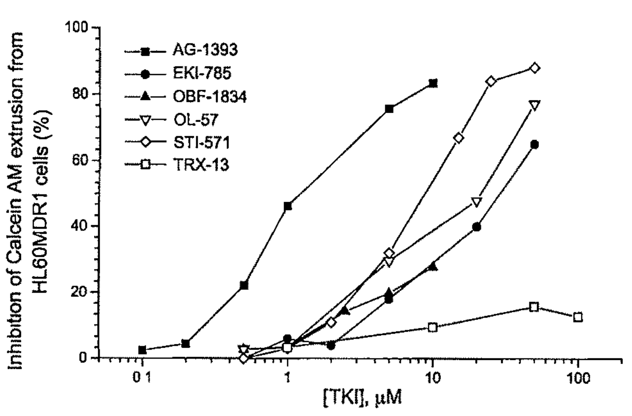

Fig 5. Inhibition of Calcein AM extrusion by the human MDR1 by various concentrations of TKIs. Calcein AM extrusion was measured in HL-60 MDR1 cells (see Experimental procedures). Data compiled from at least four independent measurements for each compound

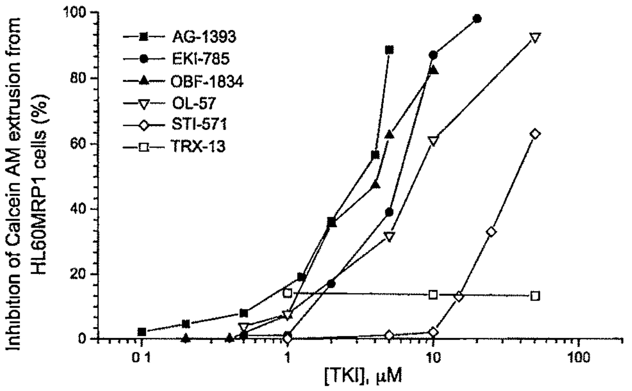

Fig. 6. Inhibition of Calcein AM and free Calcein extrusion by the human MRP1 by various concentrations of TKIs. Calcein AM extrusion was measured in HL-60 MRP1 cells Data compiled from at least four independent measurements for each compound

4. Discussion

TKIs are among the most important drug candidates in the area of signal transduction therapy, fighting cancer and other proliferative diseases [33–35]. Beside the success-story of STI-571 against chronic myelogenous leukemia, at present, there are several TKIs at various stages of clinical trials [4,5]. TKIs not only inhibit the proliferation of tumor cells, but also induce programmed cell death, which contribute to their therapeutic significance [36,37]. These inhibitors in most cases have to reach their intracellular targets, therefore membrane transport mechanisms significantly alter their effectiveness and inhibitory potential. Active transport mechanisms, mostly based on the functioning of multidrug transporter proteins, may be major players in modifying their cellular action.

The major multidrug transporters, MDR1 and MRP1, are involved in cancer drug resistance by extruding a large variety of hydrophobic compounds. In the case of MRP1, this is supplemented with the outward transport of already partially detoxified drugs (drug conjugates) from the tumor cells. In mammals, ABC transporters, like MDR1 and MRP1, have a key physiological role in the functioning of the blood–brain and blood–testis barriers, as well as the kidney, liver, lung, and intestinal epithelial cells. MDR1 is expressed normally on apical membranes of cells derived from excretory tissues, as well as on the luminal surface of cerebral capillary cells [38,39]. MDR1 and MRP1 are present in the epithelia of the choroid plexus (CP) and both transporters participate in the blood–CSF permeation barrier [38]. MDR1-Pgp contributes to the drug-permeation barrier in cerebral capillary endothelial cells and takes part in elimination of organic cations and xenobiotics from the central nervous system (CNS) [40,41]. MRP1 contributes to the basolateral broad-specificity drug-permeation barrier in CP, protects this epithelium from xenobiotics and extrudes organic anions and probably also some hydrophobic compounds from the CSF [42].

Drugs interacting with the multidrug transporter proteins may be useful for the reversal of cancer drug resistance, as well as for increasing the absorption, or the brain entry of various pharmacological agents (for review see [Ref. 43]). In the case of new anticancer agents, it is exceptionally important to obtain an estimate for their potential interaction with the multidrug transporter proteins, as such interactions will alter the anticancer activity and tissue distribution of the given drug.

In the present paper, we have shown that, by using relatively simple isolated membrane and whole-cel assays for analyzing the function of the multidrug transporters, it is possible to quantitatively examine the interactions of TKIs with these proteins. Here we applied the measurement of specific ATPase activity and Calcein extrusion function of the multidrug transporters for this analysis.

A few interesting examples of the TKIs examined here are worth discussing. One such molecule is STI-571, a specific inhibitor of the Bcr–Abl tyrosine kinase, which is already in wide-range clinical trials. Our data presented here indicate that STI-571 is an actively transported substrate of the human MDR1 P-glycoprotein, as STI-571 activates the MDR1-ATPase at low micromolar concentrations and interferes with MDR1-dependent active Calcein AM extrusion. The dual action of STI-571 on the MDR1-ATPase activity is similar to many drugs examined earlier, that is in higher concentration, a self-inhibition is observed. The exact significance of this phenomenon is not clear, but Cyclosporin A is a prototype compound with a similar MDR1-interaction [44]. In contrast to MDR1, STI-571 does not seem to be a good substrate or inhibitor of the human MRP1 protein. These data suggest that the clinical action of STI-571 may be significantly inhibited in MDR1-P glycoprotein expressing tumors, while no such interference should be expected in MRP1-expressing cancer tissues.

For another lead compound in preclinical and clinical trials, EKI-785, we found an opposite situation. This molecule does not seem to interact with MDR1 in the in vivo relevant micromolar concentration range. However, EKI-785 seems to specifically interact with the human MRP1 protein. This compound inhibits the MRP1-dependent Calcein transport and also inhibits the NEM-GS stimulated MRP1-ATPase activity. In order to explore the interaction of EKI-785 with MRP1, further transport and ATPase studies would be required. Especially, the interaction (ATPase activation) of this compound with MRP1 should be investigated in detail at various concentrations of free GSH, in order to establish if EKI-785 is a high-affinity actively transported substrate of MRP1.

When examining the data in Table 1, another few examples are also worth mentioning. It is quite obvious that TRX-13, a prospective clinically applicable compound has no apparent interaction with the multidrug transporters examined here, which may make this compound an important tool in the case of multidrug-resistant cancers. In contrast, when further developing AG-1393 or its derivatives, a major concern could be their high-affinity interactions with both MDR1 and MRP1. OL-57 or OBF-1822 are on the borderline of interacting with the multidrug transporters, thus each newly developed modifications of these lead compounds should be individually examined in this regard.

In numerous cases, the potential tissue distribution, blood–brain barrier penetration, or interaction with multidrug transporter proteins for a given lead compound is estimated based on molecular hydrophobicity parameters. An important message of the present study is that this estimation may be entirely misleading. As documented in Table 1, compounds with similar high hydrophobicity, like AG-1393 and TRX-13 may have an entirely different interaction pattern with both MDR1 and MRP1. Since these proteins are also major players in the blood–brain barrier, both penetration into the CNS and anticancer effects in multidrug-resistant tumors should be entirely different for these compounds.

We should emphasize in this discussion, that the current, relatively simple studies for the TKI molecules with the multidrug transporters provide only a basic information for these interaction patterns. When these measurements indicate a positive interaction, the evaluation of each lead compound should be extended to cellular drug-resistance and direct transport experiments, as we have done previously for the small hydrophobic peptide derivatives developed in our laboratory [32].

5. Conclusions

As a summary, in the present study, we found that several TKIs examined show a direct interaction with MDR1 and MRP1, although with a large variability in the transporter selectivity and specificity. This interaction does not directly correlate with the hydrophobicity or molecular structure of TKIs, thus the interactions cannot be correctly predicted on the basis of these parameters. We suggest that high-throughput enzyme- and cell-based interaction tests with the multidrug transporters should facilitate drug development, and allow the prediction of clinical TKI resistance based on this mechanism. We also suggest that pretreatment diagnostics for the expression of specific multidrug transporters in the malignant cells will allow a more effective, individualized clinical treatment for the cancer patients.

Acknowledgements

The technical help by Ilona Zombori, Zsuzsanna Andrasi, and Judit Kis is gratefully acknowledged. This work has been supported by grants from OTKA (T31952, T26388, T32415) and ETT, Hungary. B. Sarkadi is a recipient of a Howard Hughes International Scholarship.

References

[1] D Harari, Y Yarden, Oncogene 19 (2000) 6102–6114

[2] E Raymond, S. Faivre, J P. Armand, Drugs 60 (Suppl 1) (2000) 15–23.

[3] M J Mauro, B J Druker, Curr. Opin Oncol. 13 (2001) 3–7

[4] M.W Deininger, J.M. Goldman, N. Lydon, J.V. Melo, Blood 90 (1997) 3691–3698.

[5] J M Goldman, Lancet 355 (2000) 1031–1032

[6] M E O'Dwyer, B.J. Druker, J Intern. Med 250 (2001) 3–9.

[7] K J Garber, Natl Cancer Inst. 93 (2001) 970–973

[8] F X Mahon, M W. Deininger, B. Schultheis, J. Chabrol, J Reiffers, J.M. Goldman, J V. Melo, Blood 96 (2000) 1070–1079

[9] K J Garber, Natl. Cancer Inst 93 (2001) 970–973

[10] C.J. Torrance, P.E. Jackson, E Montgomery, K W Kinzler, B. Vogelstein, A. Wissner, M. Nunes, P. Frost, C M Discafani, Nat Med 6 (2000) 1024–1028.

[11] P.M. Traxler, P. Furet, H. Mett, E. Buchdunger, T. Meyer, N Lydon, J. Med Chem. 39 (1996) 2285–2292

[12] M. Anafi, A Gazit, A. Zehavi, Y Ben-Neriah, A Levitzki, Blood 82 (1993) 3524–3529.

[13] P.M. Traxler, P Furet, H. Mett, E Buchdunger, T. Meyer, N Lydon, J Med. Chem 39 (1996) 2285–2292.

[14] M. Idei, I. Mező, Zs Vadász, A. Horváth, J. Seprődi, J. Érchegyi, I Teplán, Gy. Kéri, Electrophoresis 17 (1996) 758–761

[15] Gy. Kéri, J. Érchegyi, A Horváth, I Mező, M. Idei, T. Vántus, É. Balogh, Zs. Vadász, Gy. Bökönyi, I. Teplán, O Csuka, M Tejeda, D. Gaál, Zs. Szegedi, B. Szende, C. Roze, H. Kalthoff, A Ullrich, Proc. Natl. Acad Sci U. S A. 93 (1996) 12513–12518

[16] L. Őrfi, F. Wáczek, I. Kovesdi, Gy Mészáros, M. Idei, A. Horváth, F Hollósy, M. Mák, Zs Szegedi, B Szende, Gy Kéri, Lett. Pept. Sci 6 (1999) 325–333.

[17] L M. Strawn, G. McMahon, H App, R Schreck, W R. Kuchler, M.P. Longhi, T H Hui, C. Tang, A. Levitzki, A Gazit, I. Chen, Gy Kéri, L. Őrfi, W. Risau, I Flamme, A. Ullrich, K.P. Hirth, L K Shawver, Cancer Res 56 (1996) 3540–3545.

[18] L.J. Goldstein, I. Pastan, M M. Gottesman, Crit Rev. Oncol /Hematol. 12 (1992) 243–253.

[19] S.P.C. Cole, G Bhardwaj, J.H Gerlach, J.E Mackie, K C Almquist, A J. Stewart, E U. Kurz, A M.V Duncan, R.G. Deeley, Science 258 (1992) 1650–1654.

[20] P Borst, R Evers, M Kool, J. Wijnholds, Biochim. Biophys. Acta 1461 (1999) 347–357.

[21] G A Fisher, B.L. Lum, J Hausforff, B I Sikic, Eur. J. Cancer 32 (1996) 1082–1088.

[22] É Bakos, R. Evers, E. Sinkó, A Váradi, P Borst, B Sarkadi, Mol Pharmacol. 57 (2000) 760–768

[23] M Müller, É Bakos, E Welker, A. Váradi, U A. Germann, M.M. Gottesman, B.S. Morse, I B Roninson, B. Sarkadi, J Biol Chem. 271 (1996) 1877–1883

[24] É Bakos, R. Evers, G. Szakács, G E. Tusnády, E. Welker, K Szabó, M. de Haas, L. van Deemter, P. Borst, A Váradi, B. Sarkadi, J Biol Chem 273 (1998) 32167–32175

[25] B Sarkadi, E.M. Price, R.C. Boucher, U.A Germann, G.A. Scarborough, J Biol. Chem. 267 (1992) 4854–4858

[26] Zs. Holló, L Homolya, T. Hegedűs, B. Sarkadi, FEBS Lett 383 (1996) 99–104.

[27] L. Homolya, Zs Holló, U A Germann, I. Pastan, M M Gottesman, B. Sarkadi, J. Biol Chem 268 (1993) 21493–21496.

[28] Zs Holló, L Homolya, C W Davis, B Sarkadi, Biochim Biophys Acta 1191 (1994) 384–388.

[29] C. Hansch, A Leo, Substituent Constants for Correlation Analysis in Chemistry and Biology, Wiley, New York, 1979.

[30] W.M. Meylan, P.H. Howard, J Pharm Sci. 84 (1995) 83–92

[31] D W. Loe, R.G. Deeley, S.P.C Cole, Cancer Res 58 (1998) 5130–5136

[32] F J. Sharom, X Yu, P. Lu, R. Liu, J.W Chu, K Szabó, M. Muller, C.D. Hose, A. Monks, A Váradi, J. Seprődi, B Sarkadi, Biochem Pharmacol. 58 (1999) 571–586

[33] A. Levitzki, Eur J Biochem 226 (1994) 1–13.

[34] A. Levitzki, Pharmacol. Ther 82 (1999) 231–239.

[35] K.S. Kolibaba, B J. Druker, Biochim Biophys. Acta/Reviews on Cancer 1333 (1997) F217–F248.

[36] B. Szende, Gy Kéri, Zs Szegedi, I Benedeczki, Cell Proliferation 28 (1995) 188.

[37] B. Szende, Gy. Kéri, Zs Szegedi, I. Benedeczky, A. Csikós, L Őrfi, A. Gazit, Cell Biol. Int 9 (1995) 903–911.

[38] M M. Gottesman, I. Pastan, Annu Rev Biochem. 62 (1993) 385–427.

[39] C. Cordon-Cardo, J.P. O'Brien, D. Casals, L Rittman-Grauer, J.L. Biedler, M.R Melamed, J.R. Bertino, Proc. Natl. Acad Sci. U. S A 86 (1989) 695–698.

[40] V V Rao, J.L Dahlheimer, M.E. Bardgett, A.Z. Snyder, R.A. Finch, A C. Sartorelli, D Piwnica-Worms, Proc Natl Acad Sci U S A 96 (1999) 3900–3905

[41] A.H. Schinkel, U Mayer, E. Wagenaar, C.A. Mol, L van Deemter, J.J. Smit, M.A. van der Valk, A.C Voordouw, H. Spits, O van Tellingen, J M Zijlmans, W E. Fibbe, P Borst, Proc. Natl Acad Sci. U. S A. 94 (1997) 4028–4033.

[42] J. Wijnholds, E C de Lange, G.L Scheffer, D J van Den Berg, C.A. Mol, M van Der Valk, A.H. Schinkel, R.J Scheper, D.D. Breimer, P Borst, J Clin. Invest 105 (2000) 279–285.

[43] P. Borst, Semin Cancer Biol 8 (1997) 3–8

[44] B. Sarkadi, M. Muller, L. Homolya, Zs Holló, J Seprődi, U.A. Germann, M.M. Gottesman, E. Price, R C Boucher, FASEB J 8 (1994) 766–770.

ELSEVIER

Biochimica et Biophysica Acta 1587 (2002) 326–337

BIOCHIMICA ET BIOPHYSICA ACTA
BBA
www.bba-direct.com

Review

Exemestane, a new steroidal aromatase inhibitor of clinical relevance☆

Paolo Lombardi

Biopharmascience, Executive Consultants in Research and Development, 20020 Cesate, Italy

Received 24 January 2002, accepted 24 January 2002

Abstract

Breast cancer is the leading cause of death among women and the contribution of circulating oestrogens to the growth of some mammary tumours has been recognized. Consequently, suppression of oestrogen action by inhibition of their biosynthesis at the androstenedione-oestrone aromatization step, by means of selective inhibitors of the enzyme aromatase, has become an effective therapeutic option for the treatment of hormone-dependent breast cancer. Exemestane (6-methylenandrosta-1,4-diene-3,17-dione) is a novel steroidal irreversible aromatase inhibitor recently approved and introduced into the global market under the name Aromasin®. The design, laboratory and viable syntheses of exemestane, starting from a variety of steroidal precursors, are presented and discussed. Data from biochemical and pharmacological studies as well as the clinical impact of the compound are briefly reviewed. The drug is an orally active and well-tolerated hormonal therapy for postmenopausal patients with advanced breast cancer that has become refractory to standard current hormonal therapies. © 2002 Elsevier Science B.V. All rights reserved.

Keywords Exemestane, 6-Methylenandrosta-1,4-diene-3,17-dione; Aromasin; Aromatase inhibitor; Steroid chemistry, Breast/hormone-dependent cancer

1. Introduction

Breast cancer is the leading cause of deaths among women with 1 million new cases in the world each year and with a rate of over 56 per 100,000 population in Western Europe [1]. One-third of human breast tumours are hormone-dependent [2] and epidemiological and experimental evidence strongly supported that oestrogens are the most important hormones involved in the growth of these tumours [3]. The observation that administration or subtraction of hormones could interfere with the growth of some tumours was first made over a century ago when regression of metastatic breast carcinoma was achieved successfully by ovariectomy [4], and significant advances in the endocrine ablative therapy for breast cancer were obtained with the introduction of bilateral adrenalectomy in the fifties, and of hypophysectomy in the sixties, as a mean of depleting oestrogens biosynthesis.

The development of hormone receptor measurements [5], by allowing the identification of patients likely to respond to hormonal therapy (60% of postmenopausal women), provided an impetus for the search and development of anti-oestrogens, progestins, LH-RH antagonists and inhibitors of oestrogen biosynthesis, in order to counteract oestrogen action.

The agents used to block oestrogen biosynthesis as a mean to deplete circulating oestrogen levels, highlighted the importance of the enzyme aromatase as a rational target for the effective and selective treatment for some postmenopausal patients with hormone-dependent breast cancer [6,7].

Aromatase, a *P*-450-dependent enzyme, catalyses the ultimate step in oestrogen biosynthesis (Scheme 1) that converts androgens to oestrogens both in pre- and postmenopausal women [8]. While the main source of oestrogen (primarily oestradiol) is the ovary in premenopausal women, the principal source of circulating oestrogens in postmenopausal women is from the aromatization of adrenal and ovarian androgens (androstenedione and testosterone) to oestrogens (oestrone and oestradiol) by the enzyme aromatase in peripheral tissues (muscle, body fat).

Abbreviations AcOH, acetic acid; *i*-AmOH, *iso*-amylic alcohol; DABCO, 1,4-diazabicyclo[2.2.2]octane, DDQ, dichlorodicyanobenzoquinone, DMBA, 7,12-dimethylbenzanthracene; DMF, *N*,*N*-dimethylformamide; ED$_{50}$, median effective dose, IC$_{50}$, median inhibiting concentration; K_i, inhibition constant; NADPH, reduced nicotinamide adenine dinucleotide phosphate; NaOAc, sodium acetate; PMSG, pregnant mares' serum gonadotropin; THF, tetrahydrofuran; *p*-TsOH, *para*-toluenesulfonic acid

☆ Text of oral presentation at the 8th International Symposium on Molecular Aspects of Chemotherapy, September, 2001, Gdansk, Poland

E-mail address: lombardi@maganet.net (P. Lombardi).

0925-4439/02/$ - see front matter © 2002 Elsevier Science B.V. All rights reserved.
PII S0925-4439(02)00096-0

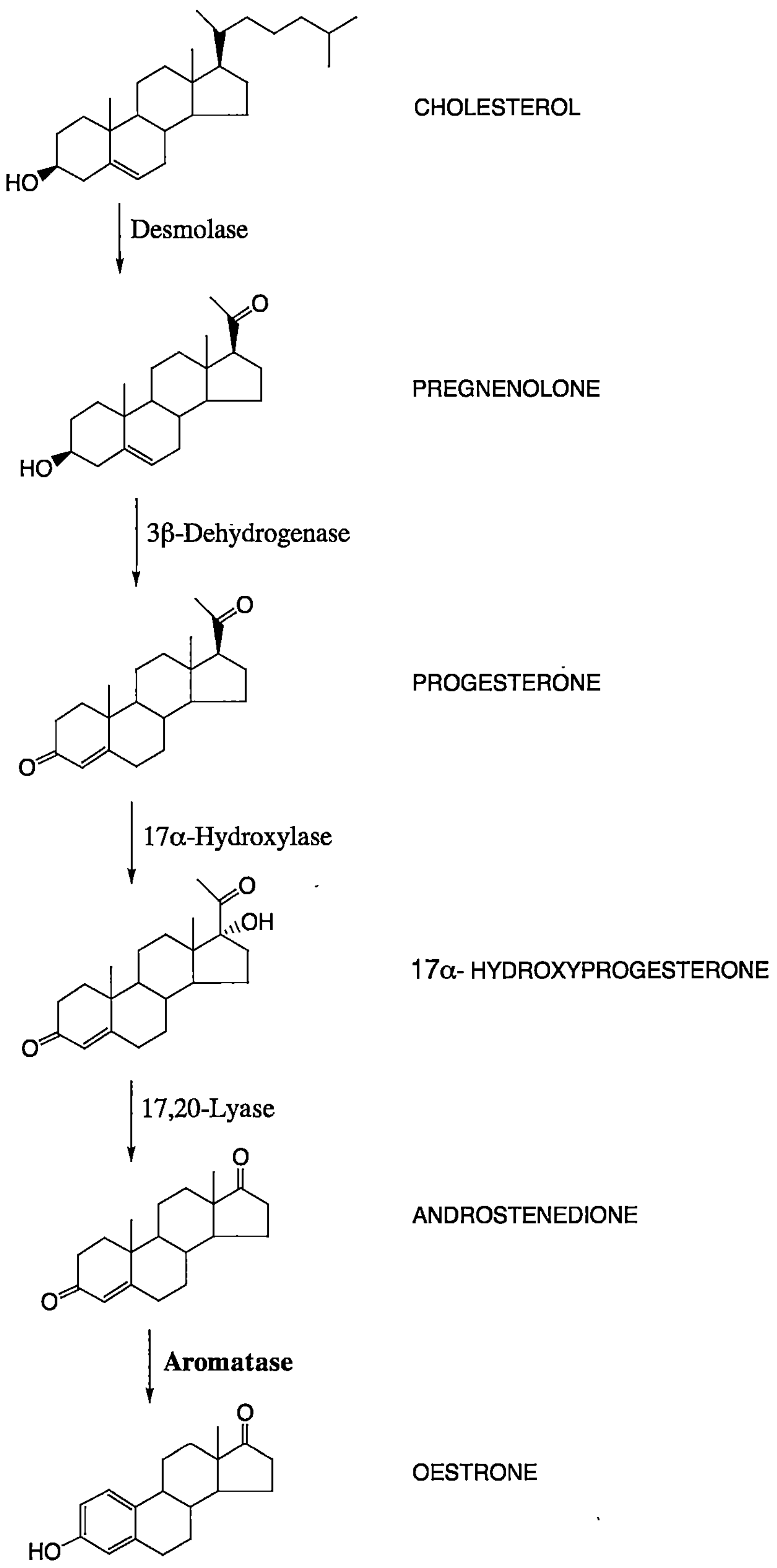

Scheme 1 Biosynthesis of oestrogens

Testololactone, marketed under the name TESLAC®, and aminoglutethimide, marketed under the name ORIMETEN®, may be regarded as the pioneer drugs of this type. The former has been used clinically in the treatment of postmenopausal breast cancer for 20 years with modest response rate, and later was discovered to be an irreversible aromatase inhibitor of very low potency [9]. The latter, a nonsteroidal, nonspecific, reversible and competitive inhibitor of aromatase, serendipitously showed its endocrine properties after years of clinical use as an anticonvulsant [10].

Since these drugs have been of some benefit in postmenopausal breast cancer but of moderate efficacy or tolerability, the search and development of new, more potent, specific and safer aromatase inhibitors became an attractive, shared and well-founded option in the early 1980s. Efforts from numerous research groups worldwide eventually produced a selection of aromatase inhibitors, which are now in clinical use or in advanced clinical trials [11–15] (Fig. 1), positioning today these new agents in the mainstay of endocrine therapy for breast cancer treatment [16–19,20a,b,21].

2. The enzyme aromatase and aromatase inhibitors

The aromatization of C19-steroids (androgens) to obtain C18-steroids (oestrogens) is performed by the enzyme complex aromatase (oestrogen synthetase). The complex

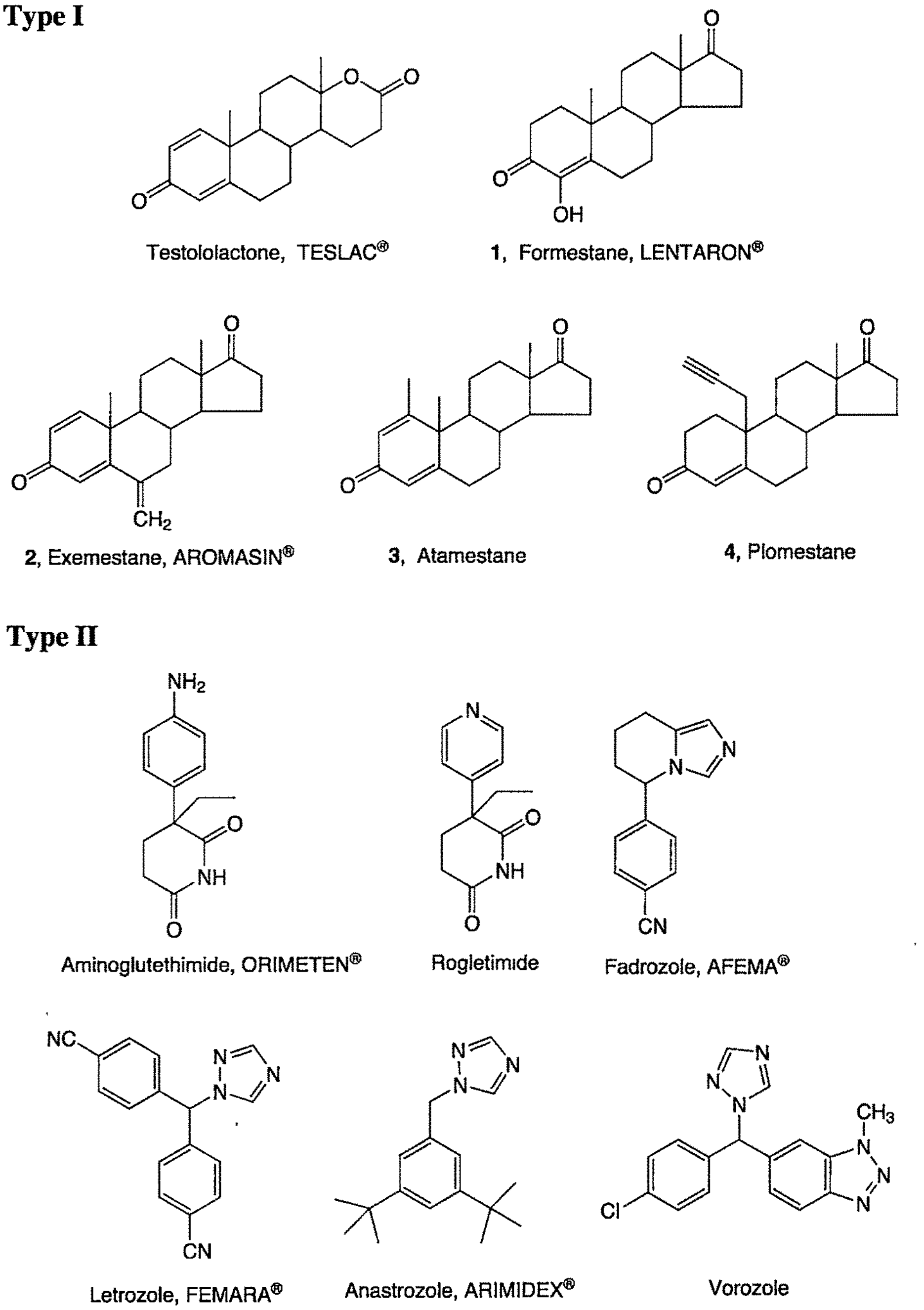

Fig 1. Structure and classification of aromatase inhibitors in the clinical practice or in the clinical testing

consists of a flavoprotein, reduced nicotinamide adenine dinucleotide phosphate (NADPH)–cytochrome *P*-450 reductase, that transfers electrons from NADPH to the terminal enzyme, and a specific form of the cytochrome *P*-450 enzyme system, known as aromatase cytochrome *P*-450, which is the protein involved in the specific recognition and binding of C19-steroid substrates. The protein catalyzes a three-step oxidative reaction sequence at C-19 culminating in the cleavage of the angular C-19 methyl group and in the aromatization of the ring A, releasing formic acid and water (Scheme 2) [22]. The process is allowed by the ability of the prosthetic group (haeme–iron porphyrin complex) of aromatase to activate dioxygen for insertion into C–H bonds. A number of postulated mechanisms have been considered over the years, and the rationalization of the third oxidative step as well as the stereochemical outcome of the elimination of the 1- and 2-hydrogens are still matters for debate. It is not a purpose of this paper to comment on various hypothesis, and authors active in this field are only referred [23–32].

Since aromatase has both an iron-containing and a steroid-binding site presenting two reasonable ways for inhibition, aromatase inhibitors have been traditionally divided into the two classes of Type I and Type II inhibitors.

2.1. Type II aromatase inhibitors

Type II aromatase inhibitors, such as aminoglutethimide, rogletimide, fadrozole, anastrozole, letrozole and vorozole, act by reversibly binding to the enzyme and by interfering with the haeme–iron group of the cytochrome *P*-450 moiety of the enzyme. A variety of enzymes possess cytochrome *P*-

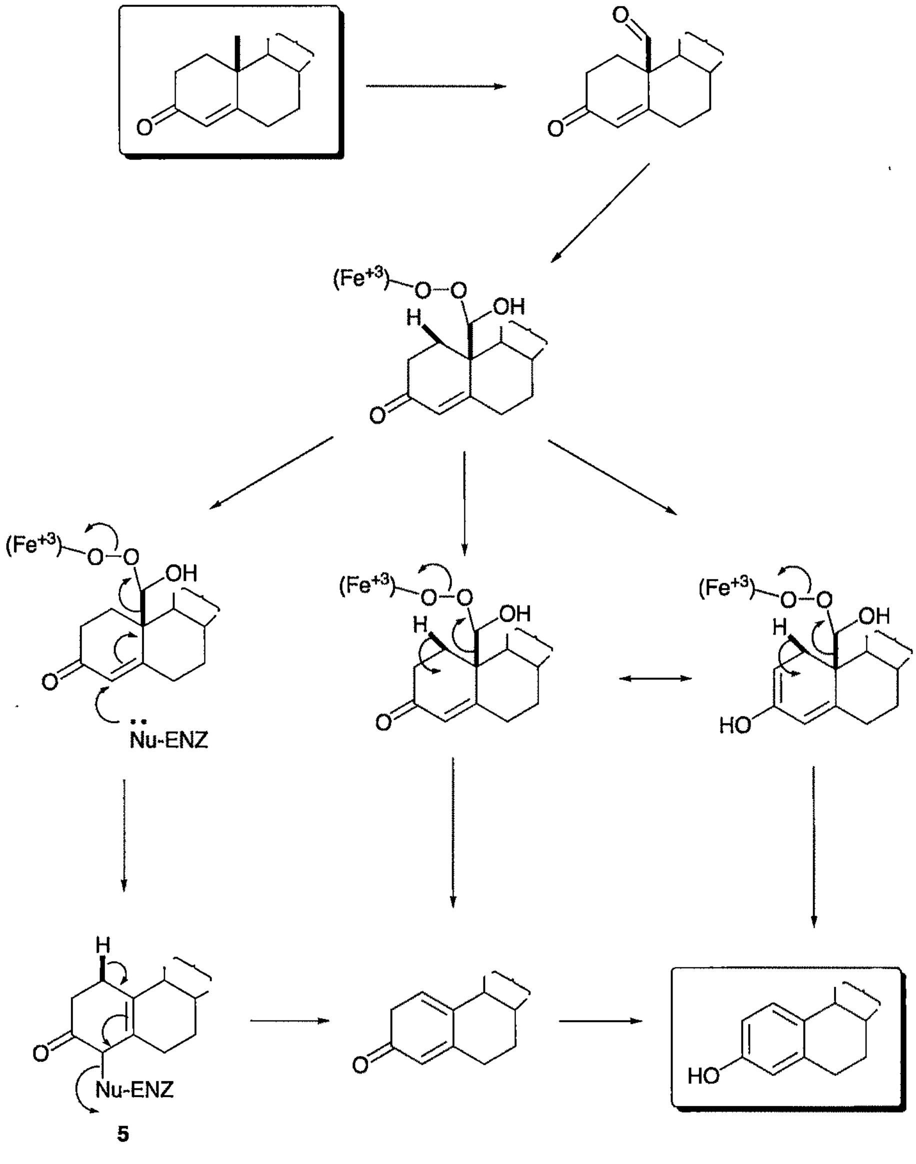

Scheme 2 Conversion of androgens into oestrogens. A number of postulated mechanisms about the last oxidative step have been considered over the years

450 prosthetic groups, therefore, candidate inhibitors should be carefully designed in order to be aromatase-specific. Because they are reversible, ongoing oestrogen deprivation depends upon the continued presence of the drug, thus posing potential toxicity issues [13–15].

2.2. *Type I aromatase inhibitors*

Type I, or irreversible inhibitors (also known as suicide or mechanism-based inactivators), such as testololactone, formestane (4-hydroxyandrost-4-ene-3,17-dione (**1**)), exemestane (6-methylenandrosta-1,4-diene-3,17-dione (**2**), FCE 24304, PNU 155971), atamestane (1-methylandrosta-1,4-diene-3,17-dione (**3**), SH 489) and plomestane (10β-(2-propynyl)estr-4-ene-3,17-dione (**4**), MDL 18692) interact with the substrate-binding site of the enzyme. They must have an androstenedione-like structure and should be designed in order to be transformed by the normal catalytic action of the target enzyme into reactive species. Covalent bond formation then occurs with a nucleophilic site of the enzyme, leading to the irreversible inactivation of the target enzyme by preventing enzyme catalysis from occurring [11]. Because the inhibition is irreversible, renewed oestrogen production requires biosynthesis of new enzyme aromatase [15]. This would result in reduced side effects when the inhibitor is used as a drug, since the inhibitor's effect can persist after its clearance from the system and the continuing presence of the drug to maintain inhibition is thus not necessary.

2.3. *Formestane*

As early as 1973, over 100 steroids were studied by the group led by H. Brodie and A. Brodie for potential anti-aromatase activity [33,34]. Candidate inhibitors were evaluated in vitro by comparing the extent of aromatization of [1β,2β-^{3}H]androstenedione to oestrogen in incubations of microsomes from aromatase-containing tissues (human placenta or ovaries of rats stimulated with pregnant mares' serum gonadotropin, PMSG). The inhibitors with greatest activity were 1,4,6-androstatriene-3,17-dione (**6**) [34,35], 4-androstene-3,6,17-trione (**7**) [33] (Fig. 2), and **1** [36a]. All showed Lineweaver–Burk plots typical of competitive inhibition, which occurs rapidly in the presence of both substrate (androstenedione) and inhibitor, and also caused slower time-dependent loss of enzyme activity which follows pseudo first-order kinetics in microsomes preincubated in the absence of substrate, but in presence of the cofactor NADPH [36a]. No loss of activity occurred in the absence of the cofactor. These findings suggested that all three compounds caused long-term inactivation or irreversible inhibition of aromatase, and that they can be regarded as mechanism-based or suicide inhibitors.

The most interesting compound resulted to be **1**, a potential anabolizing agent previously synthesized in the laboratories of Farmitalia [36b], which was evaluated clinically in the 1980s under the name formestane [37] and introduced into the market in 1993 under the name LENTARON® (Ciba-Geigy, now Novartis) with the indication for the treatment of advanced breast cancer in postmenopausal women. In clinical trials, weekly deep intramuscular injections with 500 mg of formestane to unselected breast cancer patients resulted in a 60% suppression of plasma oestradiol levels and an overall response rate of almost 30%. Similar responses, obtained with a daily oral administration of 500 mg, were however indicative of a poor bioavailability by this route. A rapid metabolization of formestane also occurs primarily as the glucoronide conjugate.

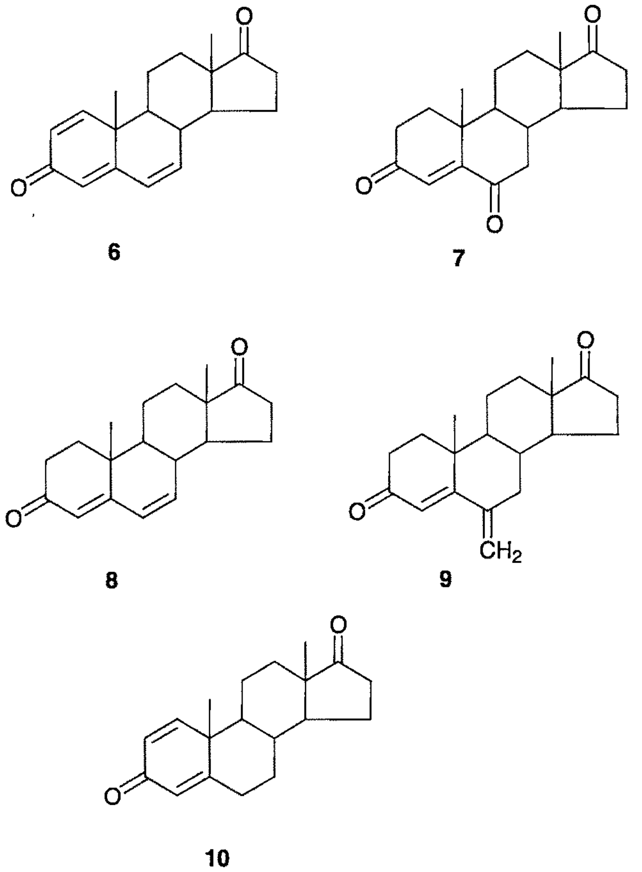

Fig. 2 Androstenedione-like structures tested as aromatase inhibitors.

3. Exemestane

In order to overcome the unfavourable metabolism and poor oral availability of 4-hydroxyandrostenedione, several groups were engaged in the synthesis and pharmacological evaluation of novel irreversible aromatase inhibitors with improved oral activity. The group led by E. di Salle and P. Lombardi at Farmitalia Carlo Erba (now Pharmacia) designed, synthesised and evaluated the novel steroid **2** (FCE 24304, exemestane). Despite impressive steroid chemistry conducted over the previous decades, the structure of exemestane resulted a new one. The design of the molecule was derived by early findings that effective aromatase inhibitors resemble the androst-4-ene-3,17-dione substrate sterically and electronically, and that better inhibition was found in derivatives containing the Δ^4-3,6-dione, $\Delta^{1,4,6}$-3-one or the $\Delta^{4,6}$-3-one moieties [33]. The 6-keto and Δ^6 groupings of these compounds extend linear conjugation of the parent Δ^4-3-one system and the enzyme system appeared to bind well to these longer, delocalised π bond systems. Exemestane was found to inhibit human placental aromatase with a potency similar to formestane (in comparative experiments, $IC_{50} = 42$ and 44 nM, respectively) and in preincubation studies exemestane caused time-dependent (irreversible) inactivation of the enzyme [38,39].

However, both androsta-4,6-diene-3,17-dione (**8**) [24] and 6-methylenandrost-4-ene-3,17-dione (**9**) [38] are not time-dependent inactivators, and irreversible aromatase inhibition exibited by exemestane as well as by ***6***, and 1,4-androstadiene-3,17-dione (**10**), may rely on the lack of the 1β-hydrogen. At the time these compounds were under characterization, a postulated mechanism for conversion of androgens into oestrogens hypothesised the formation of an enzyme-bound intermediate **5** [24]. This intermediate collapses to an aromatized product via elimination of the 1β-hydrogen and enolisation of the resulting keto-diene moiety, which releases the oestrogen and simultaneously regenerates the unaltered and active free enzyme (Scheme 2). In the presence of the 1,2-double bond, the enzyme-bound intermediate will aromatize without undergoing the final elimination reaction. Thus, the 1,2-unsaturation acts as a latent alkylating group (Scheme 3).

Exemestane entered preclinical development in 1986, and successfully performed clinical trials during the 1990s to receive FDA approval on October 21, 1999 for the treatment of advanced breast cancer in postmenopausal women whose disease has progressed following tamoxifen (antioestrogen) therapy. The compound, marketed under the name AROMASIN® (Pharmacia), is the first oral aromatase inactivator.

3.1. Chemistry

The direct introduction of a methylene group at 6-position of a 3-oxo-4-ene steroid is a known process. Therefore, the laboratory synthesis of exemestane, **2**, (Scheme 4) [40] exploited the 6-methylenation of androstenedione with formaldehyde acetal and $POCl_3$ to give **9**, according to the general method of Annen et al. [41]. The introduction of the required 1,2-double bond to obtain **2** was then per-

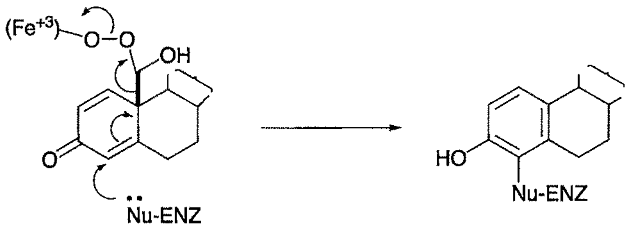

Scheme 3 Postulated aromatase inactivation mechanism by 1,4-androstadiene-like structures

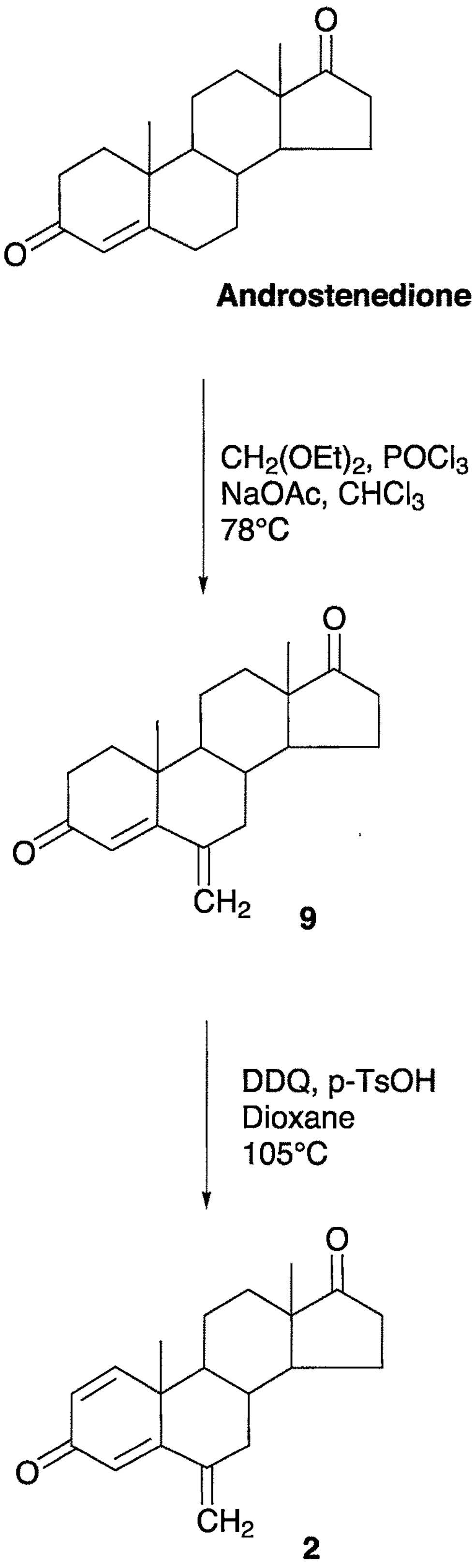

Scheme 4 Laboratory synthesis of exemestane (**2**).

formed by dichlorodicyanobenzoquinone (DDQ) dehydrogenation.

In order to overcome the disadvantages and drawbacks of these methods, represented by low yields, high price of DDQ and chromatographic purifications, other processes amenable to be scaled up were developed at Farmitalia Carlo Erba.

A more original and practical synthetic approach, starting from commercially available dehydrotestosterone, disclosed an unusual and unprecedented Mannich reaction on a cross-conjugated dienone moiety by fetching the direct introduction of the methylene group at the 6-position of a 3-oxo-1,4-diene steroid, performed with paraformaldehyde and dimethylamine in *iso*-amylic alcohol (*i*-AmOH) at 130 °C (Scheme 5) [42]. The hydroxyl function at C-17 of the ring D of the starting steroid must be initially present to avoid a competitive Mannich reaction occurring preferentially at C-16 if the 17-oxo analogue would have been the synthetic precursor. The 6-methylene intermediate (**11**), obtained by precipitation from the above reaction mixture in 35% yield, gave exemestane, **2**, in 28% overall yield, after crystallisation of the solid residue resulting from the work-up of the Jones oxidation to introduce the 17-keto group.

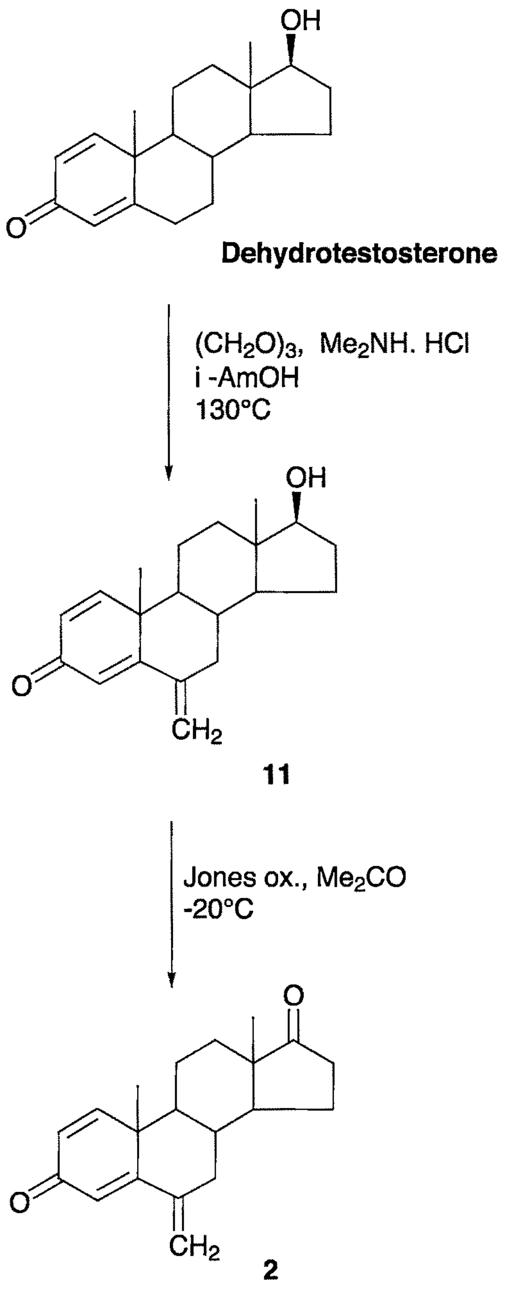

Scheme 5 Viable synthesis of exemestane (2) from dehydrotestosterone

An alternative synthetic viable route of exemestane was also set up after having performed a remarkably efficient 6-methylenation of the less expensive and more readily available androstenedione with a corporate know-how used in the industrial synthesis of Farmitalia's medroxyprogesterone acetate (Scheme 6) [43,44]. Accordingly, androstenedione was first reacted with triethylorthoformate in tetrahydrofuran (THF)–EtOH at 40 °C in the presence of *para*-toluenesulfonic acid (*p*-TsOH). The resulting ethyl 3,5-dienolether without isolation was subjected to Mannich reaction with *N*-methylaniline and aqueous formaldehyde. The adduct intermediate was decomposed with concentrated HCl and the resulting 6-methylene intermediate **9** was obtained in 73% yield after simple precipitation. The introduction of the double bond at 1,2-position of the 3-oxo steroid skeleton can be also easily carried out by bromination–dehyrobromination. However, in the present case, bromination of **9** with bromine in THF–AcOH at 0 °C and a catalytic amount of HBr afforded the expected tribromide (**12**) in 84% yield and in almost pure form after precipitation. Partial debromination with sodium iodide in refluxing acetone provided the crude 2-bromointermediate, which was dehydrohalogenated with LiCl and $LiCO_3$ in *N*,*N*-dimethylformamide (DMF) at 120 °C to give exemestane, **2**, by precipitation with water in 47% yield based on androstenedione.

A recent Pharmacia process entailed the enzymatic 1,2-dehydrogenation of **9** (Scheme 7) [45]. Accordingly, the intermediate **9** and whole cells of *Arthrobacter simplex* were mixed and agitated during some days in toluene and water in the presence of menadione, as a radical scavenger, and phosphate buffer. Exemestane, **2**, was collected from the toluene phase after concentration and precipitation with octane.

3.2. Biology

The properties of exemestane were compared in vitro and in vivo with the structurally related compounds **9** and **10** [38]. In initial co-incubation studies with the substrate, all three steroids were found to inhibit human placental aromatase, being exemestane the more potent (Table 1). However, this experiment gives only a preliminary indication of the compounds' inhibitory potency, since the values could be the result of both competitive and time-dependent

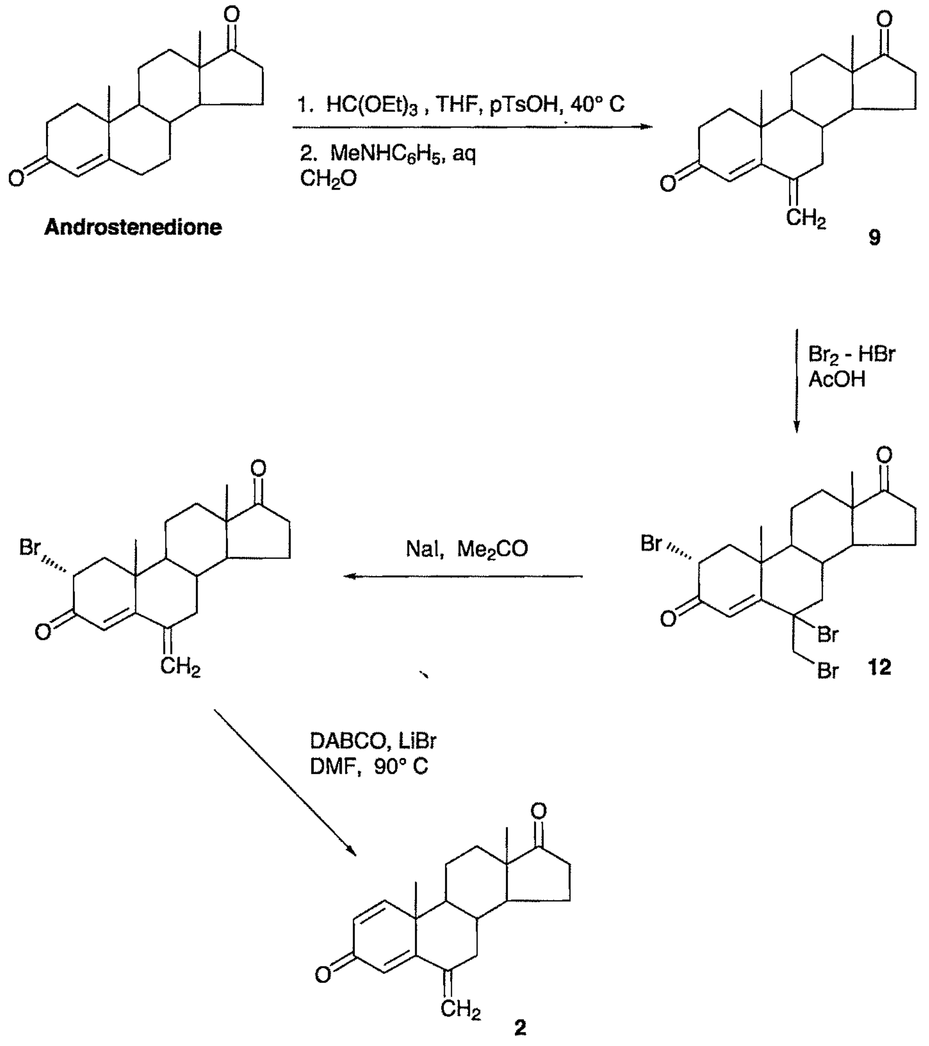

Scheme 6 Viable synthesis of exemestane (**2**) from androstenedione

enzyme inhibition. In pre-incubation studies (0–32 min with human placental aromatase and in the presence of NADPH) both exemestane, **2**, and **10** induced time-dependent enzyme inactivation, whereas no time-related decrease in aromatase activity was observed with the 6-methylene derivative **9** (Table 2). Exemestane showed a higher aromatase affinity than **10** ($K_i = 26$ and 92 nM, respectively) and a faster enzyme inactivation ($t_{1/2} = 13.9$ and 24.1 min, respectively).

For in vivo studies, female rats with PMSG-stimulated ovarian aromatase were used. Twenty-four hours after dosing (10 mg/kg subcutaneously), **9** was completely inactive, **10** lowered ovarian aromatase to 66% of the control value, whereas inhibition was far more pronounced with exemestane which reduced ovarian aromatase to 19% of control activity (Table 3). In further dose–response studies, exemestane was shown to reduce ovarian aromatase with an ED_{50} of 1.8 mg/kg (s.c.) and, much interestingly, the compound was also very potent when given orally, its ED_{50} being 3.7 mg/kg (p.o.) (Fig. 3).

The antitumour activity of exemestane was studied in rats with 7,12-dimethylbenzanthracene (DMBA)-induced tumours. Exemestane given s.c. induced 44% tumour regression at a dose of 3 mg/kg per day and, when the compound was given orally on the same treatment schedule, tumour regressions amounted to 50% at 100 mg/kg [46]. However, in the DMBA-induced mammary tumour in ovariectomized female rats treated with testosterone, a postmenopausal breast cancer model, exemestane was shown to be highly effective by both s.c. (88% and 96% tumour regression at 10 and 50 mg/kg daily, respectively), and oral routes (76% and 88% tumour regression at the same doses) [47].

The properties of exemestane were also compared with those of steroidal aromatase inhibitors developed by other research groups, namely formestane, **1**, atamestane, **3**, and plomestane, **4** [39]. In initial coincubation studies with the substrate, atamestane was found to be the most potent inhibitor, showing an IC_{50} of 20.3 nM, compared to 31.3 nM for plomestane, 42.5 nM for exemestane, and 43.7 nM

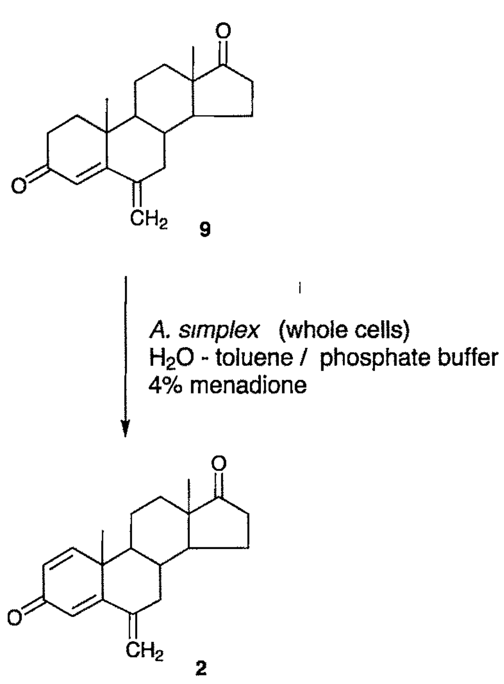

Scheme 7 Microbiological conversion of 6-methylenandrostenedione (**9**) to exemestane (*2*).

for formestane. In preincubation studies with the enzyme, formestane, atamestane and plomestane caused, like exemestane, time-dependent enzyme inhibition, and striking differences between them were observed. Formestane was the fastest aromatase inactivator, showing a $t_{1/2}$ of 2.1 min, whereas plomestane had a $t_{1/2}$ of 13.1 min, similar to exemesatne (13.9 min), and atamesatne was the slowest inactivator, with a $t_{1/2}$ of 45.3 min. Plomestane and atamestane showed very high affinity for the enzyme, having a K_i of 0.7 and 2.0 nM, respectively, compared to 26.0 nM for exemestane and 29.0 nM for formestane.

However, the most striking and significant differences were observed in vivo in the PMSG-pretreated rat experiment. Compared to formestane, plomestane and atamestane, exemestane was the most potent compound after both subcutaneous and oral administration, giving ED_{50} values of 1.8 and 3.7 mg/kg, respectively. Plomestane showed the same potency as exemestane only by the subcutaneous route (ED_{50} 1.4 mg/kg) and was less effective orally (ED_{50} 18 mg/kg). Formestane caused enzyme inactivation after subcutaneous dosing (ED_{50} 3.1 mg/kg), but had scant effect even at 100 mg/kg orally. Atamestane, despite its very high enzyme affinity, caused very low enzyme inactivation even subcutaneously (Table 4). In comparative DMBA-induced mammary tumour studies in rats, the antitumour efficacy of exemestane was much greater than that of atamestane, plomestane and formestane [48,49].

Table 1
In vitro inhibition of human placental aromatase

Compound	IC_{50} (nM)
Exemestane (**2**)	42.5
6-Methylenandrostenedione (**9**)	110.5
1,4-Androstadienedione (**10**)	81.1

The compounds were co-incubated for 15 min with substrate [1β,2β-^3H]androstenedione (50 nM).

Table 2
Time-dependent aromatase inhibition

Compound	K_i (nM)	$t_{1/2}$ (min)
Exemestane (**2**)	26	13.9
6-Methylenandrostenedione (**9**)	no time-dependent inhibition observed	
1,4-Androstadienedione (**10**)	92	24.1

The compounds were pre-incubated for 0–32 min with human placental aromatase in the presence of NADPH.

3.3. Clinical efficacy

In healthy postmenopausal volunteers, which were given single oral doses of exemestane ranging from 0.5 to 800 mg, the minimal effective dose in decreasing oestrogen levels was 5 mg and the minimal dose which produced the maximum suppression of plasma oestrogens, observed at day 3 and persisting on day 5, was 25 mg. The long-lasting inhibitory effect of exemestane on oestrogen synthesis is likely due to the irreversible nature of its enzyme inhibitory property, rather than to its pharmacokinetic properties. In fact, the drug was rapidly adsorbed and reached peak levels within 2 h after oral administration, rapidly disappearing thereafter [50, 51].

Exemestane was extensively metabolized in all species. The initial steps are the reduction of the 17-keto group to give the 17β-hydroxy steroid **11**, and the oxidation of the methylene group in position 6 with subsequent formation of many secondary metabolites, identified by comparison with synthetic reference compounds (Fig. 4) [52,53]. All metabolites were found to be either inactive in inhibiting aromatase or less potent than exemestane, thus excluding a possible contribution of any metabolite to the observed prolonged effect of the drug.

In earlier clinical studies with heavily pretreated, postmenopausal patients with advanced breast cancer failing multiple hormonal treatments, exemestane, at repeated daily oral doses ranging from 5 to 600 mg, caused a maximal

Table 3
Effect of subcutaneous dosing on ovarian aromatase activity in PMSG-stimulated rats

Compound	Dose (mg/kg, s.c.)	Ovarian aromatase (% controls)
Vehicle	–	100
Exemestane (**2**)	10	19
6-Methylenandrostenedione (**9**)	10	104
1,4-Androstadienedione (**10**)	10	66

Aromatase activity remaining was determined in the ovarian microsomal fraction obtained 24 h after inhibitor dosing.

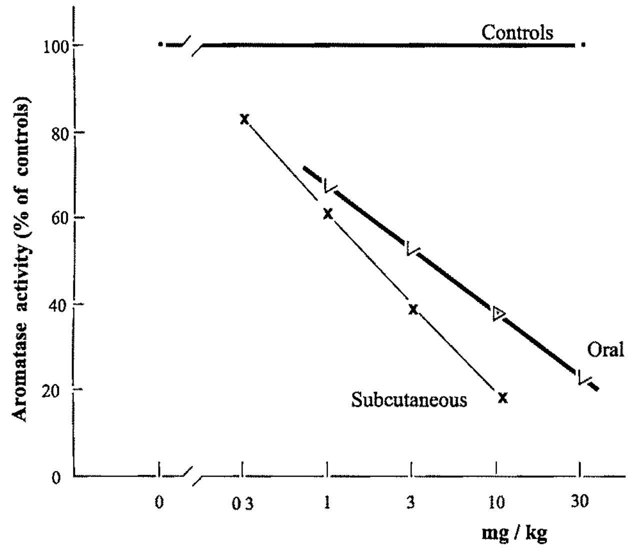

Fig 3. Effect of subcutaneous and oral dosing of exemestane (2) on ovarian aromatase activity in PMSG-stimulated rats Aromatase activity remaining was determined in the ovarian microsomal fraction obtained 24 h after inhibitor dosing and expressed as percentage (%) of controls

inhibition (>90%) of plasma oestrogens starting from the lower doses. An objective positive response was observed in up to 33% of evaluable patients, which was promising considering that exemestane was administered as third- or fourth-line hormonal treatment in most cases [54–57].

The minimal effective exemestane oral dose for endocrine activity in advanced breast cancer patients was assessed at 0.5 mg/day, achieving oestrogen suppression of about 25–30% versus baseline starting from day 7 of treatment [58]. The most favourable effects, as maximal suppression of oestrogens, tolerability and antitumour activity, were observed at 25 mg daily oral dose and a large, safe therapeutic window of up to 600 mg was defined [59,60].

Table 4
Effect of oral dosing on ovarian aromatase activity in PMSG-stimulated rats

Compound	Dose (mg/kg, orally)	Ovarian aromatase (% controls)	ED_{50} (mg/kg, orally)
Exemestane (2)	1	67.8	3 7
	3	53 6	
	10	34 8	
	30	23 6	
Formestane (1)	10	79 9	> 100
	30	75 7	
	100	71 6	
Plomestane (4)	3	71 6	18
	10	57.4	
	30	43 7	
Atamestane (3)	30	76 8	>100
	100	89.2	

Aromatase activity remaining was determined in the ovarian microsomal fraction obtained 24 h after inhibitor dosing

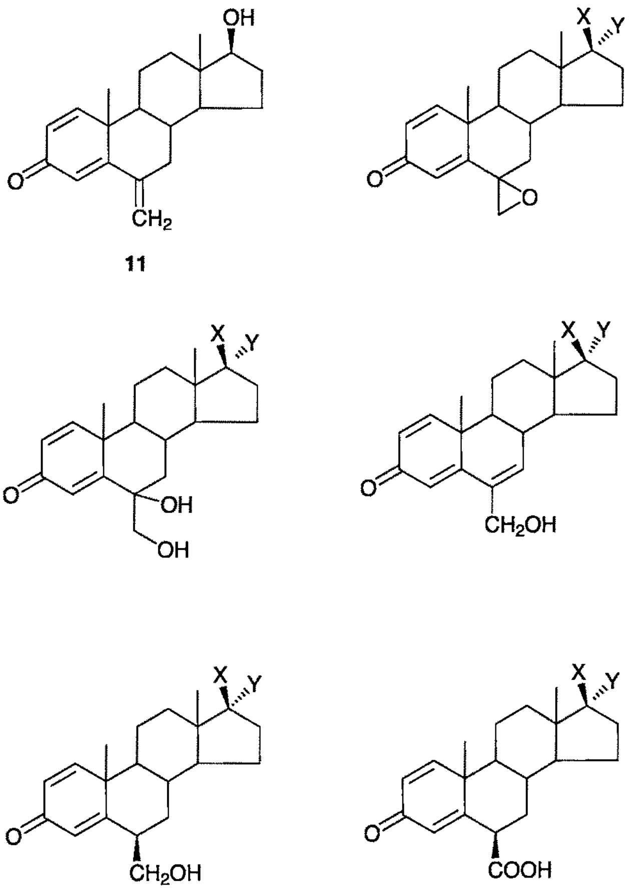

11

Fig 4 Metabolites of exemestane (2) Exemestane is extensively metabolized to the 17β-hydroxy derivative (11) and to other compounds following oxidation of the 6-exomethylene group (X=OH, Y=H; X,Y=O).

A study aimed at determining the effect of exemestane on in vivo aromatization in postmenopausal women with advanced breast cancer showed, that at 25 mg daily oral dose exemestane inactivated peripheral aromatase activity by approximately 98% and reduced basal plasma oestrone, oestradiol and oestrone sulfate levels by 85% to 95% after 6–8 weeks of therapy, with respect to values before treatment [61].

In later clinical trials, exemestane improved survival time in postmenopausal patients with either advanced breast cancer or metastatic breast cancer, who had previously failed on the antioestrogen agent tamoxifen or on non-steroidal aromatase inhibitors treatment [62–66]. Ongoing clinical studies, .aimed at comparing exemestane with tamoxifen as first-line therapy in metastatic breast cancer, already showed a preliminary, higher anti-tumour efficacy of 42–44% positive responses for exemestane versus 14–16% for tamoxifen [67,68].

4. Conclusions

Over the past decade, novel aromatase inhibitors have been discovered and introduced into the clinical practice, on the observation that the main mechanism of action of aminoglutethimide was via inhibition of the enzyme aromatase, thereby reducing levels of circulating oestrogens in postmenopausal breast cancer patients.

The second generation drug was **1** (formestane), introduced into the market in 1993 under the name LENTARON®. Although its use was limited by its need to be given parenterally, it was found to be a well-tolerated form of endocrine therapy.

Third-generation inhibitors include anastrozole, letrozole, vorozole and exemestane, the former three being nonsteroidal competitive inhibitors, the latter being a steroidal irreversible inhibitor. All are capable of inhibiting aromatase action by >90% compared to 80% in the case of formestane.

Exemestane (AROMASIN®), a rationally designed, selective, orally active, long-lasting and safe hormonal drug, has demonstrated impressive pharmacologic and clinical properties in improving the treatment of breast cancer patients. It has also showed a great potential to be more effective as first-line treatment than other current drugs, comprising antioestrogens and nonsteroidal aromatase inhibitors.

References

[1] K. McPherson, C.M Steel, J M. Dixon, Breast cancer: epidemiology, risk factors, and genetics, Br Med J. 321 (2000) 624–628

[2] I C Henderson, G P Canellos, Cancer of the breast the past decade (part 1), N Engl J Med 302 (1980) 17–30

[3] A Segaloff, Hormones and mammary carcinogens, in W L McGuire (Ed), Advances in Research and Treatment, Experimental Biology, Plenum, New York, 1978, pp 1–22

[4] G T Beatson, On the treatment of inoperable cases of carcinoma of the mamma: suggestion for a new method of treatment, with illustrative cases, Lancet 2 (1896) 104–107.

[5] E.V Jensen, G.L Greene, L.E Closs, E.R DeSombre, Receptors reconsidered. a 20-year perspective, Rec Prog Horm Res. 38 (1982) 1–40

[6] R J Santen, Potential clinical role of new aromatase inhibitors, Steroids 50 (1977) 575–593

[7] Various authors, Proceedings of the Conference Aromatase. New Perspectives for Breast Cancer, Cancer Res (1982) 42S

[8] E A Thompson Jr , P K Siiteri, The involvement of human placental microsomal cytochrome *P*-450 in aromatization, J Biol Chem 249 (1974) 5373–5378

[9] R M. Barone, I M Shamonki, P K Siiteri, H.L Judd, Inhibition of peripheral aromatization of androstenedione to estrone in postmenopausal women with breast cancer using Δ^1-testololactone, J Clin Endocrinol Metab 49 (1979) 672–676

[10] C T Griffiths, T.C Hall, Z Saba, J J. Barlow, H B. Nevinny, Preliminary trial of aminoglutethimide in breast cancer, Cancer 32 (1973) 31–37.

[11] P Lombardi, The irreversible inhibition of aromatase (oestrogen synthetase) by steroidal compounds, Curr Pharm Des 1 (1995) 23–50

[12] D W Combs, Recent developments in aromatase inhibitors, Expert Opin. Ther Pat. 5 (1995) 529–533

[13] A M.H. Brodie, V C O Njar, Aromatase inhibitors and breast cancer, Semin Oncol 23 (1996) 10–20

[14] H A Harvey, Aromatase inhibitors in clinical practice. current status and a look to the future, Semin Oncol 23 (1996) 33–38.

[15] W R Miller, Aromatase inhibitors, Endocr -Relat Cancer 3 (1996) 65–79

[16] A.U Buzdar, Role of aromatase inhibitors in advanced breast cancer, Endocr -Relat Cancer 6 (1999) 219–225

[17] P C de Jong, G H. Blijham, New aromatase inhibitors for the treatment of advanced breast cancer in postmenopausal women, Neth J. Med 55 (1999) 50–58

[18] R J Santen, H A Harvey, Use of aromatase inhibitors in breast carcinoma, Endocr -Relat Cancer 6 (1999) 75–92

[19] R.C Coombes, C Harper-Wynne, M Dowsett, Aromatase inhibitors and their use in the sequential setting, Endocr -Relat Cancer 6 (1999) 259–263.

[20] (a) A M Brodie, V C Njar, Aromatase inhibitors and their application in breast cancer treatment, Steroids 65 (2000) 171–179,
(b) S R Johnston, Irreversible aromatase inactivation treatment for breast cancer, Hosp Med 61 (2000) 650–655

[21] P E Goss, K Strasser, Aromatase inhibitors in the treatment and prevention of breast cancer, J Clin Oncol 19 (2001) 881–894

[22] S J M. Skinner, M Akhtar, The stereospecific removal of a C-19 hydrogen atom in oestrogen biosynthesis, Biochem J 114 (1969) 75–81

[23] J Fishman, Biochemical mechanism of aromatization, Cancer Res 42S (1982) 3277–3280

[24] D F Covey, W F Hood, A new hypothesis based on suicide substrate inhibitor studies for the mechanism of action of aromatase, Cancer Res. 42S (1982) 3327–3333.

[25] Y Watanabe, Y Ishimura, A model study on aromatase cytochrome *P*-450 reaction· trasformation of androstene-3,17,19-trione to 10β-hydroxyestr-4-ene-3,17-dione, J Am Chem Soc 111 (1989) 8047–8049.

[26] P A Cole, C H Robinson, Mechanistic studies on a placental aromatase model reaction, J Am Chem Soc 113 (1991) 8130–8137

[27] E Caspi, H.R W. Dharmaratne, E Roitman, C Shackleton, Estrogen biosynthesis. 2β-hydroxy-19-oxoandrost-4-ene-3,17-dione revisited, J. Chem. Soc , Perkin Trans , I (1993) 1191–1195

[28] M. Akhtar, V C O Njar, J.N Wright, Mechanistic studies on aromatase and related C–C bond cleaving *P*-450 enzymes, J Steroid Biochem. Mol Biol. 44 (1993) 375–387

[29] C.H Robinson, S S Oh, Mechanism of placental aromatase a new active site model, J Steroid Biochem Mol. Biol 44 (1993) 389–397

[30] S.S Oh, C.H Robinson, Synthesis and chemical model reaction studies with 3-deoxyandrogens evidence supporting a 2,3-enolization hypothesis in human placental aromatase catalysis, J Chem Soc , Perkin Trans , I (1994) 2237–2243

[31] S Ahmed, Review of the molecular modelling studies of the cytochrome *P*-450 estrogen synthetase enzyme, aromatase, Drug Des Discov. 15 (1998) 239–252

[32] Y C Kao, K R. Korzekwa, C A Laughton, S Chen, Evaluation of the mechanism of aromatase cytochrome *P*-450 a site-directed mutagenesis study, Eur J Biochem 268 (2001) 243–251

[33] W C Schwarzel, W G Kruggel, H J Brodie, Studies on the mechanism of estrogen biosynthesis. VIII The development of inhibitors of the enzyme system in human placenta, Endocrinology 92 (1973) 866–880.

[34] A M H. Brodie, W C Schwarzel, H.J. Brodie, Studies on the mechanism of estrogen biosynthesis in the rat ovary, J Steroid Biochem. 7 (1976) 787–793

[35] A.M.H Brodie, H.J Brodie, W M Garrett, J R Hendrickson, D H Marsh, C -H. Tsai-Morris, The effects of aromatase inhibitor 1,4,6-androstatrienedione (ATD) on DMBA-induced mammary tumors in the rat and its mechanim of action in vivo, Biochem Pharmacol 31 (1982) 2017–2023

[36] (a) A.M H. Brodie, W.C Schwarzel, A A Shaikh, H J Brodie, The effect of an aromatase inhibitor, 4-hydroxy-4-androstene-3,17-dione, on estrogen-dependent processes in reproduction and breast cancer, Endocrinology 100 (1977) 1684–1695,
(b) B Camerino, B Patelli, R Sciaky, Steroids methoxylated in the 3- and 4-positions, Gazz Chim Ital 92 (1962) 709–714

[37] A M H. Brodie, M. Dowsett, R.C Coombes, Basic and clinical studies with aromatase inhibitor 4-hydroxyandrostenedione, Prog Cancer Res Ther. 35 (1988) 318–325

[38] D. Giudici, G Ornati, G. Briatico, F Buzzetti, P. Lombardi, E. di Salle, 6-Methylenandrosta-1,4-diene-3,17-dione (FCE 24304). a new irreversible aromatase inhibitor, J. Steroid Biochem 30 (1988) 391–394

[39] E di Salle, D Giudici, G. Briatico, G. Ornati, Novel irreversible aromatase inhibitors, Ann N Y Acad. Sci 595 (1990) 357–367.

[40] F. Buzzetti, N Barbugian, P Lombardi, E. di Salle US Pat 4,808,616.

[41] K Annen, H. Hofmeister, H. Laurent, R Wiechert, Simple method for 6-methylenation of 3-oxo-Δ^4-steroids, Synthesis (1982) 34–40.

[42] A Longo, P Lombardi, US Pat 4,876,045

[43] A. Longo, P Lombardi, US Pat 4,990,635.

[44] A Longo, M Colombo, F. Orzi, P Lombardi, F Buzzetti, Synthesis of novel aromatase inhibitors from bromosteroidal intermediates, in. J.-R. Desmurs, B Gerard (Eds), Advance in Organobromine Chemistry I, Industrial Chemistry Library, vol. 3, Elsevier, Amsterdam, 1991, pp. 119–125

[45] M K Krook, B.D. Hewitt, PCT WO 01/04342.

[46] T Zaccheo, D Giudici, P Lombardi, E di Salle, A new irreversible aromatase inhibitor, 6-methylenandrosta-1,4-diene-3,17-dione (FCE 24304): antitumor activity and endocrine effects in rats with DMBA-induced mammary tumors, Cancer Chemother Pharmacol 23 (1989) 47–50

[47] T Zaccheo, E di Salle, Effect of the irreversible aromatase inhibitor FCE 24304 on DMBA-induced mammary tumors in ovariectomized rats treated with testosterone, Cancer Chemother. Pharmacol. 25 (1989) 95–98.

[48] E di Salle, G Briatico, D. Giudici, G Ornati, T Zaccheo, Aromatase inhibition and experimental antitumor activity of FCE 24304, MDL 18962 and SH 489, J. Steroid Biochem 34 (1989) 431–434

[49] T Zaccheo, D Giudici, G Ornati, A. Panzeri, E. di Salle, Comparison of the effects of the irreversible aromatase inhibitor exemestane with atamestane and MDL 18962 in rats with DMBA-induced mammary tumours, Eur. J. Cancer 27 (1991) 1145–1150

[50] E di Salle, G. Ornati, D Giudici, M. Lassus, T R J. Evans, R C. Coombes, Exemestane (FCE 24304), a new steroidal aromatase inhibitor, J Steroid Biochem Mol. Biol. 43 (1992) 137–143.

[51] T.R J Evans, E di Salle, G. Ornati, M. Lassus, M. Strolin Benedetti, E Pianezzola, R.C Coombes, Phase I and endocrine study of exemestane (FCE 24304), a new aromatase inhibitor, in postmenopausal women, Cancer Res 52 (1992) 5933–5939

[52] E. di Salle, G Ornati, R Paridaens, R C. Coombes, J P Lobelle, M.G. Zurlo, Preclinical and clinical pharmacology of the aromatase inhibitor exemestane (FCE 24304), in M Motta, M Serio (Eds), Sex Hormones and Antihormones in Endocrine Dependent Pathology: Basic and Clinical Aspects, Elsevier, Amsterdam, 1994, pp. 279–286

[53] G. Cocchiara, C Allievi, A Berardi, P Zugnoni, M. Strolin Benedetti, P. Dostert, Urinary metabolism of exemestane, a new aromatase inhibitor, in rat, dog, monkey and human volunteers, J. Endocrinol Invest. 17 (Suppl. 1 to no 3) (1994) 78.

[54] F Buzzetti, E. di Salle, A Longo, G. Briatico, Synthesis and aromatase inhibition by potential metabolites of exemestane (6-methylenandrosta-1,4-diene-3,17-dione), Steroids 58 (1993) 527–532.

[55] P E. Lonning, R Paridaens, B Thurliman, G. Piscitelli, E di Salle, Exemestane experience in breast cancer treatment, J. Steroid Biochem Mol Biol. 61 (1997) 151–155.

[56] D C. Johannessen, T Engan, E. di Salle, M.G. Zurlo, J Paolini, G. Piscitelli, G Piscitelli, S. Kvinnsland, P E Lonning, Endocrine and clinical effects of exemestane (PNU 155971), a novel steroidal aromatase inhibitor, in postmenopausal breast cancer patients a phase I study, Clin Cancer Res 3 (1997) 1101–1108

[57] B Thurlimann, R. Paridaens, D. Serin, J. Bonneterre, H Roche, R Murray, E di Salle, S Lanzalone, M G. Zurlo, G Piscitelli, Third-line hormonal treatment with exemestane in postmenopausal patients with advanced breast cancer progressing on aminoglutethimide a phase II multicentre multinational study, Eur J Cancer 33 (1997) 1767–1773.

[58] E Bajetta, N. Zilembo, C Noberasco, A. Martinetti, L Mariani, L Ferrari, R Buzzoni, M Greco, C Bartoli, I Spagnoli, G.M. Danesini, S. Artale, J Paolini, The minimal effective exemestane dose for endocrine activity in advanced breast cancer, Eur. J. Cancer 33 (1997) 587–591.

[59] N. Zilembo, C Noberasco, E Bajetta, A. Martinetti, L Mariani, S Orefice, R. Buzzoni, M Di Bartolomeo, A Di Leo, A Laffranchi, Endocrinological and clinical evaluation of exemestane, a new steroidal aromatase inhibitor, Br. J Cancer 72 (1995) 1007–1012.

[60] R Paridaens, J. Thomas, J Wildiers, P. Vermeiren, J.P. Lobelle, E. di Salle, G. Ornati, M G Zurlo, A Polli, S. Lanzalone, K de Belder, Safety, activity and estrogen inhibition by exemestane in postmenopausal women with advanced breast cancer a phase I study, Anticancer Drugs 9 (1998) 675–683

[61] J. Geisler, N King, G Anker, G Ornati, E di Salle, P.E Lonning, M Dowsett, In vivo inhibition of aromatization by exemestane, a novel irreversible aromatase inhibitor, in postmenopausal breast cancer patients, Clin Cancer Res. 4 (1998) 2089–2093.

[62] S Jones, C Vogel, A Arkhipov, L Fehrenbacher, P. Eisenberg, B. Cooper, S Honig, A Polli, F. Whaley, E di Salle, J Tiffany, A Consonni, L Miller, Multicenter, phase II trial of exemestane as third-line hormonal therapy of postmenopausal women with metastatic breast cancer, J Clin Oncol 17 (1999) 3418–3425

[63] M Kaufmann, E Bajetta, L Y Dirix, L E Fein, S E. Jones, N. Zilembo, J L Dugardyn, C. Nasurdi, R.G. Mennel, J Cervek, C Fowst, A. Polli, E di Salle, A. Arkhipov, G Piscitelli, L L. Miller, G Massimini, Exemestane is superior to megestrol acetate after tamoxifen failure in postmenopausal women with advanced breast cancer. results of a phase III randomized double-blind trial, J. Clin Oncol 18 (2000) 1399–1411

[64] P E. Lonning, E Bajetta, R. Murray, M. Tubiana-Hulin, P D Eisenberg, E Mickiewicz, L Celio, P Pitt, M Mita, N.K. Aaronson, C Fowst, A Arkhipov, E di Salle, A. Polli, G. Massimini, Activity of exemestane in metastatic breast cancer after failure of nonsteroidal aromatase inhibitors a phase II trial, J Clin. Oncol. 18 (2000) 2234–2244

[65] S. Kvinnsland, G Anker, L.Y Dirix, J Bonneterre, A M Prove, N. Wilking, J P Lobelle, O Mariani, E. di Salle, A Polli, G Massimini, High activity and tolerability demonstrated for exemestane in postmenopausal women with metastatic breast cancer who had previously failed on tamoxifen treatment, Eur. J Cancer 36 (2000) 976–982

[66] M. Kaufmann, E Bajetta, L Y Dirix, L E Fein, S E. Jones, J Cervek, C. Fowst, A Polli, E di Salle, G. Massimini, G Piscitelli, Exemestane improves survival compared with megoestrol acetate in postmenopausal patients with advanced brest cancer who have failed on tamoxifen. Results of a double-blind randomised phase III trial, Eur J Cancer 36 (Suppl 4) (2000) S86–S87

[67] R. Paridaens, L.Y Dirix, L Beex, M Nooij, T Cufer, C Lohrisch, L. Biganzoli, I Van Hoorebeeck, L Duchateau, J.-P. Lobelle, M Piccart, Exemestane (aromasin) is active and well tolerated as first-line hormonal therapy of metastatic breast cancer patients. results of a randomized phase II trial, 36th Annual Meeting of the American Society of Clinical Oncology, Abstract no. 316

[68] L Dirix, M.J. Piccart, C. Lohrisch, L Beex, M Nooij, D. Cameron, L. Biganzoli, T. Cufer, C Yague, L Duchateau, J.-P Lobelle, R Paridaens, Efficacy of and tolerance to exemestane versus tamoxifen in 1st line hormone therapy of postmenopausal metatstatic breast cancer patients. a European organisation for the research and treatment of cancer (EORTC breast group) phase II trial with pharmacia and upjohn, 37th Annual Meeting of the American Society of Clinical Oncology, Abstract no 114

ELSEVIER
Biochimica et Biophysica Acta 1587 (2002) 338–340
BIOCHIMICA ET BIOPHYSICA ACTA
BBA
www bba-direct com

Molecular Basis of Disease

Author Index

Aherne, G.W., see Jackman, A L. (1587) 215
Albano, E , see Vairetti, M. (1587) 83
Albers, J J., see Cheung, M C (1587) 53
Anderson, K.S.
Perspectives on the molecular mechanism of inhibition and toxicity of nucleoside analogs that target HIV-1 reverse transcriptase (1587) 296
Andrés, D., see Sanz, N. (1587) 12
Asao, T., see Ishida, K (1587) 155
Aukema, H.M , see Cuozzo, F.P. (1587) 99

Backus, H.H.J., see Peters, G.J. (1587) 194
Bailly, M., see Liu, J. (1587) 174
Balzarini, J. and McGuigan, C.
Chemotherapy of varicella-zoster virus by a novel class of highly specific anti-VZV bicyclic pyrimidine nucleosides (1587) 287
Banerjee, D , Mayer-Kuckuk, P , Capiaux, G., Budak-Alpdogan, T., Gorlick, R. and Bertino, J R.
Novel aspects of resistance to drugs targeted to dihydrofolate reductase and thymidylate synthase (1587) 164
Barlocco, D , see Costi, M.P. (1587) 206
Barrett, D.
From natural products to clinically useful antifungals (1587) 224
Ben-Shooshan, I., Kessel, A., Ben-Tal, N., Cohen-Luria, R and Parola, A.H
On the regulatory role of dipeptidyl peptidase IV (=CD26=adenosine deaminase complexing protein) on adenosine deaminase activity (1587) 21
Ben-Tal, N , see Ben-Shooshan, I. (1587) 21
Bernabeu, C., see Diez-Marques, L. (1587) 36
Bertè, F., see Vairetti, M. (1587) 83
Bertino, J.R., see Banerjee, D (1587) 164
Bertolini, S., see Pisciotta, L (1587) 7
Bloemena, E., see Peters, G.J (1587) 194
Brunton, L., see Jackman, A.L. (1587) 215
Budak-Alpdogan, T., see Banerjee, D (1587) 164

Calandra, S , see Pisciotta, L. (1587) 7
Calvert, A H., see Peters, G.J. (1587) 194
Cantafora, A., see Pisciotta, L. (1587) 7
Cao, D., see Pizzorno, G. (1587) 133
Capiaux, G , see Banerjee, D. (1587) 164
Carini, R , see Vairetti, M. (1587) 83
Carrupt, P.-A , see Ooms, F (1587) 118
Cascales, M., see Sanz, N. (1587) 12
Cerboni, B , see Micheli, V. (1587) 45
Chen, T -m., see Liu, J (1587) 174
Cheng, R , Lin, B. and Ortwerth, B.J.
Rate of formation of AGEs during ascorbate glycation and during aging in human lens tissue (1587) 65
Cheung, M.C , Knopp, R H., Retzlaff, B , Kennedy, H., Wolfbauer, G and Albers, J J.
Association of plasma phospholipid transfer protein activity with IDL and buoyant LDL impact of gender and adiposity (1587) 53
Chu, E , see Liu, J. (1587) 174
Chu, J. and Dolnick, B.J.
Natural antisense (rTSα) RNA induces site-specific cleavage of thymidylate synthase mRNA (1587) 183
Codacci-Pisanelli, G., see Peters, G J (1587) 194
Cohen-Luria, R , see Ben-Shooshan, I. (1587) 21
Costi, M.P., Tondi, D., Rinaldi, M., Barlocco, D., Pecorari, P., Soragni, F., Venturelli, A. and Stroud, R.M.
Structure-based studies on species-specific inhibition of thymidylate synthase (1587) 206
Cuozzo, F.P , Mishra, S , Jiang, J. and Aukema, H M.
Overexpression of kidney phosphatidylinositol 4-kinaseβ and phospholipase $C_{\gamma1}$ proteins in two rodent models of polycystic kidney disease (1587) 99

De Cesaris, M.G., see Vairetti, M. (1587) 83
De Clercq, E.
New developments in anti-HIV chemotherapy (1587) 258
De Stefano, F , see Pisciotta, L. (1587) 7
Dickson, G , see Graham, I.R (1587) 1
Díez-Fernández, C., see Sanz, N (1587) 12
Diez-Marques, L., Ortega-Velazquez, R., Langa, C., Rodriguez-Barbero, A., Lopez-Novoa, J.M., Lamas, S. and Bernabeu, C.
Expression of endoglin in human mesangial cells: modulation of extracellular matrix synthesis (1587) 36
Dolnick, B J., see Chu, J (1587) 183

Farrell, M., see Liu, J (1587) 174
Freemantle, S., see Peters, G J. (1587) 194
Fukai, Y., see Nihei, C. (1587) 234

Gathof, B S., see Micheli, V (1587) 45
Gatto, B., see Palumbo, M. (1587) 145
Gilbert, I H
Inhibitors of dihydrofolate reductase in leishmania and trypanosomes (1587) 249
Gorlick, R., see Banerjee, D (1587) 164
Graham, I.R and Dickson, G.
Gene repair and mutagenesis mediated by chimeric RNA–DNA oligonucleotides: chimeraplasty for gene therapy and conversion of single nucleotide polymorphisms (SNPs) (1587) 1

Handschumacher, R.E., see Pizzorno, G. (1587) 133
Harding, J J., see Shyadehi, A.Z. (1587) 31
Hayek, G , see Micheli, V. (1587) 45

PII S0925-4439(02)00150-3

Hazelrigg, S.R., see Husain, K. (1587) 75
Hegedűs, T., Őrfi, L., Seprődi, A , Váradi, A., Sarkadi, B. and Kéri, G
Interaction of tyrosine kinase inhibitors with the human multidrug transporter proteins, MDR1 and MRP1 (1587) 318
Ho Hong, S., Rhyne, J., Zeller, K. and Miller, M.
Novel *ABCA1* compound variant associated with HDL cholesterol deficiency (1587) 60
Husain, K. and Hazelrigg, S.R.
Oxidative injury due to chronic nitric oxide synthase inhibition in rat: effect of regular exercise on the heart (1587) 75

Ishida, K. and Asao, T.
Self-association and unique DNA binding properties of the anti-cancer agent TAS-103, a dual inhibitor of topoisomerases I and II (1587) 155

Jackman, A.L., Melin, C.J., Kimbell, R., Brunton, L., Aherne, G W , Theti, D S. and Walton, M
A rationale for the clinical development of the thymidylate synthase inhibitor ZD9331 in ovarian and other solid tumours (1587) 215
Jacomelli, G., see Micheli, V. (1587) 45
Jansen, G., see Peters, G J. (1587) 194
Jiang, J., see Cuozzo, F.P. (1587) 99

Kennedy, H., see Cheung, M.C. (1587) 53
Kéri, G., see Hegedűs, T. (1587) 318
Kessel, A , see Ben-Shooshan, I. (1587) 21
Kimbell, R., see Jackman, A.L. (1587) 215
Kita, K., see Nihei, C. (1587) 234
Knopp, R H., see Cheung, M.C. (1587) 53
Kole, R., see Mercatante, D R (1587) 126

Lamas, S., see Diez-Marques, L. (1587) 36
Langa, C., see Diez-Marques, L (1587) 36
Langheim, S., see Pisciotta, L. (1587) 7
Leffert, J.J , see Pizzorno, G (1587) 133
Lin, B., see Cheng, R. (1587) 65
Lin, X., see Liu, J. (1587) 174
Liu, J., Schmitz, J.C , Lin, X., Tai, N., Yan, W., Farrell, M., Bailly, M., Chen, T.-m. and Chu, E
Thymidylate synthase as a translational regulator of cellular gene expression (1587) 174
Lombardi, P
Exemestane, a new steroidal aromatase inhibitor of clinical relevance (1587) 326
Lopez-Novoa, J.M , see Diez-Marques, L (1587) 36
Lunec, J , see Peters, G J (1587) 194

Marsh, S., see Peters, G.J. (1587) 194
Mayer-Kuckuk, P., see Banerjee, D (1587) 164
McGuigan, C., see Balzarini, J. (1587) 287
McLeod, H.L., see Peters, G.J. (1587) 194
Meijer, S., see Peters, G J (1587) 194
Melin, C.J., see Jackman, A.L (1587) 215
Mercatante, D.R. and Kole, R
Control of alternative splicing by antisense oligonucleotides as a potential chemotherapy: effects on gene expression (1587) 126
Micheli, V , Gathof, B.S., Rocchigiani, M., Jacomelli, G , Sestini, S., Peruzzi, L., Notarantonio, L , Cerboni, B., Hayek, G. and Pompucci, G
Biochemical and molecular study of mentally retarded patient with partial deficiency of hypoxanthine-guanine phosphoribosyltransferase (1587) 45
Miller, M., see Ho Hong, S. (1587) 60
Mishra, S., see Cuozzo, F.P. (1587) 99
Moro, S , see Palumbo, M (1587) 145
Morsch, V.M., see Müller, T.C. (1587) 92
Morschhauser, J
The genetic basis of fluconazole resistance development in *Candida albicans* (1587) 240
Müller, T.C., Rocha, J B.T., Morsch, V.M., Neis, R.T. and Schetinger, M.R C.
Antidepressants inhibit human acetylcholinesterase and butyrylcholinesterase activity (1587) 92

Neis, R T., see Müller, T.C. (1587) 92
Nihei, C., Fukai, Y. and Kita, K.
Trypanosome alternative oxidase as a target of chemotherapy (1587) 234
Notarantonio, L , see Micheli, V (1587) 45

Ooms, F., Weber, P , Carrupt, P -A. and Testa, B.
A simple model to predict blood–brain barrier permeation from 3D molecular fields (1587) 118
Őrfi, L., see Hegedűs, T. (1587) 318
Ortega-Velazquez, R., see Diez-Marques, L. (1587) 36
Ortwerth, B J , see Cheng, R (1587) 65

Palumbo, M., Gatto, B., Moro, S., Sissi, C. and Zagotto, G.
Sequence-specific interactions of drugs interfering with the topoisomerase–DNA cleavage complex (1587) 145
Parola, A H., see Ben-Shooshan, I (1587) 21
Pecorari, P , see Costi, M.P. (1587) 206
Peruzzi, L., see Micheli, V (1587) 45
Peters, G.J., Backus, H.H J , Freemantle, S., Van Triest, B., Codacci-Pisanelli, G., Van der Wilt, C L., Smid, K , Lunec, J., Calvert, A H , Marsh, S., McLeod, H.L., Bloemena, E., Meijer, S., Jansen, G., Van Groeningen, C J. and Pinedo, H.M.
Induction of thymidylate synthase as a 5-fluorouracil resistance mechanism (1587) 194
Pinedo, H.M., see Peters, G J. (1587) 194
Pisciotta, L., Cantafora, A., De Stefano, F , Langheim, S., Calandra, S. and Bertolini, S.
A ade novob mutation of the LDL-receptor gene as the cause of familial hypercholesterolemia (1587) 7
Pizzorno, G., Cao, D., Leffert, J.J., Russell, R.L., Zhang, D. and Handschumacher, R.E.
Homeostatic control of uridine and the role of uridine phosphorylase· a biological and clinical update (1587) 133
Pompucci, G , see Micheli, V. (1587) 45

Retzlaff, B., see Cheung, M.C. (1587) 53
Rhyne, J., see Ho Hong, S. (1587) 60
Richelmi, P., see Vairetti, M (1587) 83
Rinaldi, M., see Costi, M.P. (1587) 206
Rocchigiani, M., see Micheli, V. (1587) 45
Rocha, J.B T , see Müller, T.C. (1587) 92
Rodriguez-Barbero, A., see Diez-Marques, L. (1587) 36
Russell, R.L., see Pizzorno, G (1587) 133

Sanz, N., Díez-Fernández, C., Andrés, D. and Cascales, M.
Hepatotoxicity and aging. endogenous antioxidant systems in hepatocytes from 2-, 6-, 12-, 18- and 30-month-old rats following a necrogenic dose of thioacetamide (1587) 12
Sarkadi, B., see Hegedűs, T. (1587) 318
Schetinger, M R.C., see Müller, T.C (1587) 92
Schmitz, J C., see Liu, J (1587) 174
Schramm, V.L.
Development of transition state analogues of purine nucleoside phosphorylase as anti-T-cell agents (1587) 107
Seprődi, A., see Hegedűs, T. (1587) 318
Sestini, S , see Micheli, V (1587) 45

Shyadehi, A.Z. and Harding, J J.
  Protective effects of ibuprofen and its major metabolites against in vitro inactivation of catalase and fumarase. relevance to cataract (1587) 31
Sissi, C , see Palumbo, M. (1587) 145
Smid, K., see Peters, G J. (1587) 194
Soragni, F., see Costi, M.P (1587) 206
Splendore, R., see Vairetti, M. (1587) 83
Stroud, R M , see Costi, M.P. (1587) 206

Tai, N., see Liu, J. (1587) 174
Testa, B., see Ooms, F (1587) 118
Theti, D S., see Jackman, A L. (1587) 215
Tondi, D., see Costi, M P (1587) 206

Vairetti, M., Carini, R., De Cesaris, M G , Splendore, R., Richelmi, P., Bertè, F. and Albano, E.
  Beta-alanine protection against hypoxic liver injury in the rat (1587) 83
Van der Wilt, C.L., see Peters, G J (1587) 194
Van Groeningen, C.J., see Peters, G J. (1587) 194
Van Triest, B., see Peters, G J (1587) 194

Váradi, A , see Hegedűs, T (1587) 318
Venturelli, A., see Costi, M.P. (1587) 206

Walton, M., see Jackman, A.L. (1587) 215
Weber, P., see Ooms, F. (1587) 118
Wolfbauer, G , see Cheung, M.C (1587) 53
Woynarowska, B A and Woynarowski, J.M.
  Preferential targeting of apoptosis in tumor versus normal cells (1587) 309
Woynarowski, J M
  Targeting critical regions in genomic DNA with AT-specific anticancer drugs (1587) 300
Woynarowski, J.M., see Woynarowska, B.A. (1587) 309

Yan, W., see Liu, J. (1587) 174

Zagotto, G., see Palumbo, M. (1587) 145
Zeller, K , see Ho Hong, S (1587) 60
Zemlicka, J.
  Lipophilic phosphoramidates as antiviral pronucleotides (1587) 276
Zhang, D., see Pizzorno, G. (1587) 133

ELSEVIER

Biochimica et Biophysica Acta 1587 (2002) 341–342

BIOCHIMICA ET BIOPHYSICA ACTA
BBA
www bba-direct.com

Molecular Basis of Disease
Cumulative Contents

Review

Gene repair and mutagenesis mediated by chimeric RNA–DNA oligonucleotides: chimeraplasty for gene therapy and conversion of single nucleotide polymorphisms (SNPs)
I.R. Graham and G. Dickson (UK) 1

Regular papers

A "de novo" mutation of the LDL-receptor gene as the cause of familial hypercholesterolemia
L. Pisciotta, A. Cantafora, F. De Stefano, S. Langheim, S. Calandra and S. Bertolini (Italy) 7

Hepatotoxicity and aging: endogenous antioxidant systems in hepatocytes from 2-, 6-, 12-, 18- and 30-month-old rats following a necrogenic dose of thioacetamide
N. Sanz, C. Díez-Fernández, D. Andrés and M. Cascales (Spain) 12

On the regulatory role of dipeptidyl peptidase IV (=CD26=adenosine deaminase complexing protein) on adenosine deaminase activity
I. Ben-Shooshan, A. Kessel, N. Ben-Tal, R. Cohen-Luria and A.H. Parola (Israel) 21

Protective effects of ibuprofen and its major metabolites against in vitro inactivation of catalase and fumarase: relevance to cataract
A.Z. Shyadehi and J.J. Harding (UK) 31

Expression of endoglin in human mesangial cells: modulation of extracellular matrix synthesis
L. Diez-Marques, R. Ortega-Velazquez, C. Langa, A. Rodriguez-Barbero, J.M. Lopez-Novoa, S. Lamas and C. Bernabeu (Spain) 36

Biochemical and molecular study of mentally retarded patient with partial deficiency of hypoxanthine-guanine phosphoribosyltransferase
V. Micheli, B.S. Gathof, M. Rocchigiani, G. Jacomelli, S. Sestini, L. Peruzzi, L. Notarantonio, B. Cerboni, G. Hayek and G. Pompucci (Italy, Germany) 45

Association of plasma phospholipid transfer protein activity with IDL and buoyant LDL: impact of gender and adiposity
M.C. Cheung, R.H. Knopp, B. Retzlaff, H. Kennedy, G. Wolfbauer and J.J. Albers (USA) 53

Novel *ABCA1* compound variant associated with HDL cholesterol deficiency
S. Ho Hong, J. Rhyne, K. Zeller and M. Miller (USA) 60

Rate of formation of AGEs during ascorbate glycation and during aging in human lens tissue
R. Cheng, B. Lin and B.J. Ortwerth (USA) 65

Oxidative injury due to chronic nitric oxide synthase inhibition in rat: effect of regular exercise on the heart
K. Husain and S.R. Hazelrigg (USA) 75

Beta-alanine protection against hypoxic liver injury in the rat
M. Vairetti, R. Carini, M.G. De Cesaris, R. Splendore, P. Richelmi, F. Bertè and E. Albano (Italy) 83

Antidepressants inhibit human acetylcholinesterase and butyrylcholinesterase activity
T.C. Müller, J.B.T. Rocha, V.M. Morsch, R.T. Neis and M.R.C. Schetinger (Brazil) 92

Overexpression of kidney phosphatidylinositol 4-kinaseβ and phospholipase $C_{\gamma 1}$ proteins in two rodent models of polycystic kidney disease
F.P. Cuozzo, S. Mishra, J. Jiang and H.M. Aukema (USA, Canada) 99

Reviews

Development of transition state analogues of purine nucleoside phosphorylase as anti-T-cell agents
V.L. Schramm (USA) 107

A simple model to predict blood–brain barrier permeation from 3D molecular fields
F. Ooms, P. Weber, P.-A. Carrupt and B. Testa (Switzerland) 118

Control of alternative splicing by antisense oligonucleotides as a potential chemotherapy: effects on gene expression
D.R. Mercatante and R. Kole (USA) 126

PII: S0925-4439(02)00151-5

Homeostatic control of uridine and the role of uridine phosphorylase: a biological and clinical update
G. Pizzorno, D. Cao, J.J. Leffert, R.L. Russell, D. Zhang and R.E. Handschumacher (USA) 133

Sequence-specific interactions of drugs interfering with the topoisomerase–DNA cleavage complex
M. Palumbo, B. Gatto, S. Moro, C. Sissi and G. Zagotto (Italy) 145

Self-association and unique DNA binding properties of the anti-cancer agent TAS-103, a dual inhibitor of topoisomerases I and II
K. Ishida and T. Asao (Japan) 155

Novel aspects of resistance to drugs targeted to dihydrofolate reductase and thymidylate synthase
D. Banerjee, P. Mayer-Kuckuk, G. Capiaux, T. Budak-Alpdogan, R. Gorlick and J.R. Bertino (USA) 164

Thymidylate synthase as a translational regulator of cellular gene expression
J. Liu, J.C. Schmitz, X. Lin, N. Tai, W. Yan, M. Farrell, M. Bailly, T.-m. Chen and E. Chu (USA) 174

Natural antisense (rTSα) RNA induces site-specific cleavage of thymidylate synthase mRNA
J. Chu and B.J. Dolnick (USA) 183

Induction of thymidylate synthase as a 5-fluorouracil resistance mechanism
G.J. Peters, H.H.J. Backus, S. Freemantle, B. van Triest, G. Codacci-Pisanelli, C.L. van der Wilt, K. Smid, J. Lunec, A.H. Calvert, S. Marsh, H.L. McLeod, E. Bloemena, S. Meijer, G. Jansen, C.J. van Groeningen and H.M. Pinedo (The Netherlands, UK, USA) 194

Structure-based studies on species-specific inhibition of thymidylate synthase
M.P. Costi, D. Tondi, M. Rinaldi, D. Barlocco, P. Pecorari, F. Soragni, A. Venturelli and R.M. Stroud (Italy, USA) 206

A rationale for the clinical development of the thymidylate synthase inhibitor ZD9331 in ovarian and other solid tumours
A.L. Jackman, C.J. Melin, R. Kimbell, L. Brunton, G.W. Aherne, D.S. Theti and M. Walton (UK) 215

From natural products to clinically useful antifungals
D. Barrett (Japan) 224

Trypanosome alternative oxidase as a target of chemotherapy
C. Nihei, Y. Fukai and K. Kita (Japan) 234

The genetic basis of fluconazole resistance development in *Candida albicans*
J. Morschhäuser (Germany) 240

Inhibitors of dihydrofolate reductase in leishmania and trypanosomes
I.H. Gilbert (UK) 249

New developments in anti-HIV chemotherapy
E. De Clercq (Belgium) 258

Lipophilic phosphoramidates as antiviral pronucleotides
J. Zemlicka (USA) 276

Chemotherapy of varicella-zoster virus by a novel class of highly specific anti-VZV bicyclic pyrimidine nucleosides
J. Balzarini and C. McGuigan (Belgium, UK) 287

Perspectives on the molecular mechanism of inhibition and toxicity of nucleoside analogs that target HIV-1 reverse transcriptase
K.S. Anderson (USA) 296

Targeting critical regions in genomic DNA with AT-specific anticancer drugs
J.M. Woynarowski (USA) 300

Preferential targeting of apoptosis in tumor versus normal cells
B.A. Woynarowska and J.M. Woynarowski (USA) 309

Interaction of tyrosine kinase inhibitors with the human multidrug transporter proteins, MDR1 and MRP1
T. Hegedűs, L. Őrfi, A. Seprődi, A. Váradi, B. Sarkadi and G. Kéri (Hungary) 318

Exemestane, a new steroidal aromatase inhibitor of clinical relevance
P. Lombardi (Italy) 326

Author Index 338

Cumulative Contents 341

CONTENTS
(continued from back cover)

The genetic basis of fluconazole resistance development in *Candida albicans*
J. Morschhäuser (Germany) 240

Inhibitors of dihydrofolate reductase in leishmania and trypanosomes
I.H. Gilbert (UK) 249

New developments in anti-HIV chemotherapy
E. De Clercq (Belgium) 258

Lipophilic phosphoramidates as antiviral pronucleotides
J. Zemlicka (USA) 276

Chemotherapy of varicella-zoster virus by a novel class of highly specific anti-VZV bicyclic pyrimidine nucleosides
J. Balzarini and C. McGuigan (Belgium, UK) 287

Perspectives on the molecular mechanism of inhibition and toxicity of nucleoside analogs that target HIV-1 reverse transcriptase
K.S. Anderson (USA) 296

Targeting critical regions in genomic DNA with AT-specific anticancer drugs
J.M. Woynarowski (USA) 300

Preferential targeting of apoptosis in tumor versus normal cells
B.A. Woynarowska and J.M. Woynarowski (USA) 309

Interaction of tyrosine kinase inhibitors with the human multidrug transporter proteins, MDR1 and MRP1
T. Hegedűs, L. Őrfi, A. Seprődi, A. Váradi, B. Sarkadi and G. Kéri (Hungary) 318

Exemestane, a new steroidal aromatase inhibitor of clinical relevance
P. Lombardi (Italy) 326

Author Index 338

Cumulative Contents 341

Information for Contributors can be found in http.//www bba-direct.com

This journal is in the *ADONIS Service*, whereby copies of individual articles can be printed out from CD-ROM on request. An explanatory leaflet can be obtained by writing to ADONIS B V., P O. Box 993, 1000 AZ Amsterdam, The Netherlands Or you can contact ADONIS by e-mail : info@adonis.nl or visit the website at www.adonis.nl

OASIS: **O**n-line **A**rticle **S**tatus **I**nformation **S**ystem **(http://www.elsevier.com/oasis)**
Authors of articles which are currently in production at Elsevier can obtain the following information on the status of their article·

- general production status (in preparation, in proof, in issue)
- date of publication and offprints dispatch date
- issue, volume and page numbers

This journal is a part of **ContentsDirect**, the ***free*** alerting service which sends tables of contents by e-mail for Elsevier Science books and journals. You can register for **ContentsDirect** online at: **www.elsevier.com/locate/contentsdirect**

BIOCHIMICA ET BIOPHYSICA ACTA
MOLECULAR BASIS OF DISEASE

VOL. 1587 NOS. 2–3 18 JULY 2002

(Abstracted/indexed in Biological Abstracts - Chemical Abstract - Current Contents / Life Sciences - EMBASE/Excerpta Medica - Index Chemicus - Index Medicus / MEDLINE - Science Citation Index)

CONTENTS

Reviews

Development of transition state analogues of purine nucleoside phosphorylase as anti-T-cell agents
V.L. Schramm (USA) 107

A simple model to predict blood–brain barrier permeation from 3D molecular fields
F. Ooms, P. Weber, P.-A. Carrupt and B. Testa (Switzerland) 118

Control of alternative splicing by antisense oligonucleotides as a potential chemotherapy: effects on gene expression
D.R. Mercatante and R. Kole (USA) 126

Homeostatic control of uridine and the role of uridine phosphorylase: a biological and clinical update
G. Pizzorno, D. Cao, J.J. Leffert, R.L. Russell, D. Zhang and R.E. Handschumacher (USA) 133

Sequence-specific interactions of drugs interfering with the topoisomerase–DNA cleavage complex
M. Palumbo, B. Gatto, S. Moro, C. Sissi and G. Zagotto (Italy) 145

Self-association and unique DNA binding properties of the anti-cancer agent TAS-103, a dual inhibitor of topoisomerases I and II
K. Ishida and T. Asao (Japan) 155

Novel aspects of resistance to drugs targeted to dihydrofolate reductase and thymidylate synthase
D. Banerjee, P. Mayer-Kuckuk, G. Capiaux, T. Budak-Alpdogan, R. Gorlick and J.R. Bertino (USA) 164

Thymidylate synthase as a translational regulator of cellular gene expression
J. Liu, J.C. Schmitz, X. Lin, N. Tai, W. Yan, M. Farrell, M. Bailly, T.-m. Chen and E. Chu (USA) 174

Natural antisense (rTSα) RNA induces site-specific cleavage of thymidylate synthase mRNA
J. Chu and B.J. Dolnick (USA) 183

Induction of thymidylate synthase as a 5-fluorouracil resistance mechanism
G.J. Peters, H.H.J. Backus, S. Freemantle, B. van Triest, G. Codacci-Pisanelli, C.L. van der Wilt, K. Smid, J. Lunec, A.H. Calvert, S. Marsh, H.L. McLeod, E. Bloemena, S. Meijer, G. Jansen, C.J. van Groeningen and H.M. Pinedo (The Netherlands, UK, USA) 194

Structure-based studies on species-specific inhibition of thymidylate synthase
M.P. Costi, D. Tondi, M. Rinaldi, D. Barlocco, P. Pecorari, F. Soragni, A. Venturelli and R.M. Stroud (Italy, USA) 206

A rationale for the clinical development of the thymidylate synthase inhibitor ZD9331 in ovarian and other solid tumours
A.L. Jackman, C.J. Melin, R. Kimbell, L. Brunton, G.W. Aherne, D.S. Theti and M. Walton (UK) 215

From natural products to clinically useful antifungals
D. Barrett (Japan) 224

Trypanosome alternative oxidase as a target of chemotherapy
C. Nihei, Y. Fukai and K. Kita (Japan) 234

(continued on inside back cover)

0925-4439(20020718)1587:2/3;1-P

ALSO AVAILABLE ONLINE:

http://www.bba-direct.com

BIOCHIMICA ET BIOPHYSICA ACTA

BBA

MOLECULAR BASIS OF DISEASE

ELSEVIER

BIOCHIMICA ET BIOPHYSICA ACTA

BBA

Founded in 1947 by H.G.K. Westenbrink
Managing Editor, 1947-1964

HONORARY EXECUTIVE EDITOR
E.C. Slater (Southampton, UK)

EDITOR-IN-CHIEF: Peter C. van der Vliet (Utrecht, The Netherlands)

EXECUTIVE EDITORS:

Bioenergetics (including *Reviews on Bioenergetics*): **P.R. Rich** (London, UK) and **M. Wikström** (Helsinki, Finland)
Biomembranes (including *Reviews on Biomembranes*): **A.G. Lee** (Southampton, UK) and **P.L. Yeagle** (Storrs, CT, USA)
Molecular and Cell Biology of Lipids: **D.E. Vance** (Edmonton, AB, Canada) and **F. Spener** (Münster, Germany)
Proteins and Proteomics: **A. Fink** (Santa Cruz, CA, USA), **Y. Lindqvist** (Stockholm, Sweden) and **F. Lottspeich** (Martinsried bei München, Germany)
Molecular Cell Research: **E.L.F. Holzbaur** (Philadelphia, PA, USA) and **N. Pfanner** (Freiburg, Germany)
Gene Structure and Expression: **C.L. Peterson** (Worcester, MA, USA) and **P.C. van der Vliet** (Utrecht, The Netherlands)
Molecular Basis of Disease: **P.E. Fraser** (Toronto, ON, Canada) and **J.R. Riordan** (Scottsdale, AZ, USA)
General Subjects: **M. Fukuda** (La Jolla, CA, USA) and **C.G. Gahmberg** (Helsinki, Finland)
Reviews on Cancer: **N.C. Jones** (Manchester, UK) and **G. Evan** (San Francisco, CA, USA)

Publication information: *Biochimica et Biophysica Acta* full subscription for 2002 consists of Volumes 1553-1603. Subscription prices are available upon reques from the Publisher or from the Regional Sales Office nearest you or from this journal's website (http://www.bba-direct.com) Further information is available on this journal and other Elsevier Science products through Elsevier's website (http //www.elsevier com). Subscription are accepted on a prepaid basis only and ar entered on a calendar year basis. Issues are sent by standard mail (surface within Europe, air delivery outside Europe). Priority rates are available upon request Claims for missing issues should be made within six months of the date of dispatch.

BBA – Publication schedule for 2002
BBA is published according to a volume-numbering scheme that embraces all section of the journal.
Full subscription: 51 volumes

BIO-ENERGETICS including Reviews on Bioenergetics 5 volumes:	BIO-MEMBRANES including Reviews on Biomembranes 10 volumes	GENE STRUCTURE AND EXPRESSION 6 volumes	GENERAL SUBJECTS 6 volumes	MOLECULAR AND CELL BIOLOGY OF LIPIDS 6 volumes:	MOLECULAR BASIS OF DISEASE 3 volumes:	MOLECULAR CELL RESEARCH 5 volumes:	PROTEINS AND PROTEOMICS 8 volumes:	REVIEWS ON CANCER 2 volumes:
1553–1557 (15 issues)	1558–1567 (20 issues)	1574–1579 (18 issues)	1568–1573 (18 issues)	1580–1585 (18 issues)	1586–1588 (9 issues)	1589–1593 (15 issues)	1594–1601 (16 issues)	1602–1603 (4 issues)

Submission
Authors should submit their manuscripts (four copies) to one of the appropriate Executive Editors at either of the following Editorial Offices:
BBA Editorial Secretariat, P.O. Box 1345, 1000 BH Amsterdam The Netherlands Tel.. (+31) 20 4853510, Fax: (+31) 20 4853506, E-mail: bba@elsevier cor
BBA Editorial Secretariat, 275 Washington Street, Newton, MA 02458, USA Tel (+1) (617) 630-2244; Fax: (+1) (617) 630-2245, E-mail: us_bba@elseviercon

Although most published *Review* articles are submitted on the invitation of the Executive Editor(s), authors of suitable (mini) reviews may also submit thei work unsolicited (four copies) by sending their paper(s) to one of the Executive Editors of the appropriate section.

For detailed instructions on the preparation of electronic artwork, consult the Author Gateway from Elsevier Science at http://authors elsevier com

Author enquiries
For enquiries relating to the submission of articles (including electronic submission where available) please visit the Author Gateway from Elsevier Science a http //www.authors.elsevier com. The Author Gateway also provides the facility to track accepted articles and set up e-mail alerts to inform you of when a article's status has changed, as well as detailed artwork guidelines, copyright information, frequently asked questions and more.

Contact details for questions arising after acceptance of an article, especially those relating to proofs, are provided after registration of an article for publication.

Authors in Japan please note: Upon request, Elsevier Science K.K. will provide authors with a list of people who can check and improve the English of thei paper (*before submission*). Please contact our Tokyo office Elsevier Science K K , 9-15 Higashi-Azabu 1-chome, Minato-ku, Tokyo 106-0044; Tel · (03)-5561 5032; Fax: (03)- 5561-5045.

Colour figures
Colour figures are published at the author's expense €340 for the first page and € 227 each subsequent page, excluding sales tax.

BBA has no page charges and 25 offprints are provided free to the corresponding author of each published paper.

ß. 10.03.03

BIOCHIMICA ET BIOPHYSICA ACTA

BBA

VOL. 1588
(2002)

BIOCHIMICA ET BIOPHYSICA ACTA

Founded in 1947 by H.G.K. Westenbrink, Managing Editor, 1947-1964

HONORARY EXECUTIVE EDITOR: E.C. Slater (Southampton, UK)

EDITOR-IN-CHIEF: Peter C. van der Vliet (Utrecht, The Netherlands)

EXECUTIVE EDITORS:

Bioenergetics (including *Reviews on Bioenergetics*): **P.R. Rich** (London, UK) and **M. Wikström** (Helsinki, Finland)
Biomembranes (including *Reviews on Biomembranes*): **A.G. Lee** (Southampton, UK) and **P.L. Yeagle** (Storrs, CT, USA)
Molecular and Cell Biology of Lipids: **D.E. Vance** (Edmonton, AB, Canada) and **F. Spener** (Münster, Germany)
Proteins and Proteomics: **A. Fink** (Santa Cruz, CA, USA), **Y. Lindqvist** (Stockholm, Sweden) and
F. Lottspeich (Martinsried bei München, Germany)
Molecular Cell Research: **E.L.F. Holzbaur** (Philadelphia, PA, USA) and **N. Pfanner** (Freiburg, Germany)
Gene Structure and Expression: **C.L. Peterson** (Worcester, MA, USA) and **P.C. van der Vliet** (Utrecht, The Netherlands)
Molecular Basis of Disease: **P.E. Fraser** (Toronto, ON, Canada) and **J.R. Riordan** (Scottsdale, AZ, USA)
General Subjects: **M. Fukuda** (La Jolla, CA, USA) and **C.G. Gahmberg** (Helsinki, Finland)
Reviews on Cancer: **N.C. Jones** (Manchester, UK) and **G. Evan** (San Francisco, CA, USA)

A.D. Albert (Storrs, CT, USA)
J.M. Allen (London, UK)
T.M. Allen (Edmonton, AB, Canada)
K. Altendorf (Osnabrück, Germany)
T. Arakawa (Thousand Oaks, CA, USA)
P.A. Baeuerle (Martinsried, Germany)
C. Balny (Montpellier, France)
R. Beckmann (Berlin, Germany)
U. Beisiegel (Hamburg, Germany)
D.J. Benos (Birmingham, AL, USA)
P. Bernardi (Padua, Italy)
R. Bernards (Amsterdam, The Netherlands)
A.J.M. Berns (Amsterdam, The Netherlands)
H. Beug (Vienna, Austria)
C.L. Bevins (Cleveland, OH, USA)
C. Birchmeier (Berlin, Germany)
T. Bisseling (Wageningen, The Netherlands)
C. Borner (Freiburg, Germany)
J.L. Bos (Utrecht, The Netherlands)
I. Braakman (Utrecht, The Netherlands)
U. Brandt (Frankfurt am Main, Germany)
R.J. Bridges (Pittsburgh, PA, USA)
C.L. Brooks, III (La Jolla, CA, USA)
D.D. Busath (Provo, UT, USA)
M. Busslinger (Vienna, Austria)
F. Carrière (Marseille, France)
J.E. Celis (Copenhagen, Denmark)
G. Cevc (München, Germany)
H. Chap (Toulouse, France)
A.H. Chishti (Boston, MA, USA)
R. Cogdell (Glasgow, UK)
N.H. Colburn (Frederick, MD, USA)
H.W. Cook (Halifax, NS, Canada)
P.F. Cook (Norman, OK, USA)
C. Cooper (Colchester, UK)
W.A. Cramer (West Lafayette, IN, USA)
B. de Crombrugghe (Houston, TX, USA)
R.D. Cummings (Oklahoma, OK, USA)
D.T. Curiel (Birmingham, AL, USA)
D.A. Day (Canberra, Australia)
J.P. Dekker (Amsterdam, The Netherlands)
B. De Strooper (Leuven, Belgium)
B. Desvergne (Lausanne, Switzerland)
G. Dickson (Egham, UK)
K.T. Douglas (Manchester, UK)
G.F. Draetta (Milan, Italy)
H.B. Dunford (Edmonton, AB, Canada)
D.H. Ellison (Portland, OR, USA)
T. Endo (Tokyo, Japan)
R.M. Epand (Hamilton, ON, Canada)
J. Fidy (Budapest, Hungary)
A. Fontana (Padua, Italy)
M. Fontecave (Grenoble, France)
J.-C. Fruchart (Lille, France)
J.T. Gallagher (Manchester, UK)
G. Geba (New Haven, CT, USA)
R. Geyer (Giessen, Germany)
T.E. Golde (Jacksonville, FL, USA)
F.M. Goñi (Bilbao, Spain)
Y. Goto (Osaka, Japan)
L.I. Grossman (Detroit, MI, USA)
A.P. Halestrap (Bristol, UK)
T.D. Heath (Madison, WI, USA)
J. Heberle (Jülich, Germany)
D. Hoekstra (Groningen, The Netherlands)
J. Horwitz (Los Angeles, CA, USA)
R.A. Houghten (San Diego, CA, USA)
G. Hübner (Halle/Saale, Germany)
R.C. Hughes (Mill Hill, UK)
S.W. Hui (Buffalo, NY, USA)
T. Hunter (La Jolla, CA, USA)
M. Ikeda-Saito (Cleveland, OH, USA)
A.N. Imbalzano (Worcester, MA, USA)
T. Iwatsubo (Tokyo, Japan)
R.L. Juliano (Chapel Hill, NC, USA)
W. Junge (Osnabrück, Germany)
C. Kaltschmidt (Witten, Germany)
S.E. Kearsey (Oxford, UK)
T. Kiefhaber (Basel, Switzerland)
J.A. Killian (Utrecht, The Netherlands)
K. Kimata (Aichi, Japan)
K.H. Kinne (Dortmund, Germany)
M. Kiso (Gifu, Japan)
W.N. Konings (Groningen, The Netherlands)
J.M. Kooter (Amsterdam, The Netherlands)
S.S. Krag (Baltimore, MD, USA)
I. Kudo (Tokyo, Japan)
K. Kuwajima (Tokyo, Japan)
W. Lamers (Amsterdam, The Netherlands)
T. Levade (Toulouse, France)
R. Luhrmann (Gottingen, Germany)
G.I. Makhatadze (Lubbock, TX, USA)
B. Mannervik (Uppsala, Sweden)
W. Mantele (Frankfurt am Main, Germany)
C.J. Marshall (London, UK)
W.F. Marzluff (Chapel Hill, NC, USA)
F. McCormick (San Francisco, CA, USA)
R.N. McElhaney (Edmonton, AB, Canada)
M.G. McNamee (Davis, CA, USA)
R. Mendelsohn (Newark, NJ, USA)
J. Moody (Plymouth, UK)
C.P. Moran Jr. (Atlanta, GA, USA)
O.G. Mouritsen (Odense, Denmark)
S. Nagata (Osaka, Japan)
P.E. Nielsen (Copenhagen, Denmark)
K.H. Nierhaus (Berlin, Germany)
E.A. Nigg (Martinsried bei München, Germany)
B. Nordén (Gothenburg, Sweden)
N. Oppenheimer (San Francisco, CA, USA)
J.F. Oram (Seattle, WA, USA)
N. Osheroff (Nashville, TN, USA)
R.P. Oude Elferink (Amsterdam, The Netherlands)
E. Padan (Jerusalem, Israel)
S. Parthasarathy (Atlanta, GA, USA)
M. Peters-Golden (Ann Arbor, MI, USA)
D.W. Pettigrew (College Station, TX, USA)
J. Philo (Thousand Oaks, CA, USA)
J.J.H.H.M. de Pont (Nijmegen, The Netherlands)
T. Pozzan (Padua, Italy)
N.C. Price (Glasgow, UK)
U.R. Rapp (Wurzburg, Germany)
N. Ridgway (Halifax, NS, Canada)
J.-L. Rigaud (Paris, France)
G.T. Robillard (Groningen, The Netherlands)
S. Rose-John (Kiel, Germany)
E. Rozengurt (Los Angeles, CA, USA)
F. Sachs (Buffalo, NY, USA)
M.S.P. Sansom (Oxford, UK)
S. Schuldiner (Jerusalem, Israel)
H.H. Schulz (New York, NY, USA)
K. Schulze-Osthoff (Münster, Germany)
J.M. Seddon (London, UK)
R. Serrano (Valencia, Spain)
D.L. Severson (Calgary, AB, Canada)
T. Shimizu (Tokyo, Japan)
H. Sjostrom (Copenhagen, Denmark)
S.T. Smale (Los Angeles, CA, USA)
S. Spiegel (Washington, DC, USA)
W.D. Stein (Jerusalem, Israel)
B. Svensson (Copenhagen, Denmark)
G. Tigyi (Memphis, TN, USA)
K.F. Tipton (Dublin, Ireland)
J. Travis (Athens, GA, USA)
L.-C. Tsui (Toronto, ON, Canada)
B. Tummler (Hannover, Germany)
G. van Meer (Amsterdam, The Netherlands)
M.H. Vos (Palaiseau, France)
K.H. Vousden (Frederick, MD, USA)
E. Wahle (Halle/Saale, Germany)
M.J. Waring (Cambridge, UK)
D. Wemmer (Berkeley, CA, USA)
R. Wetzel (Knoxville, TN, USA)
G.R. Willsky (Buffalo, NY, USA)
D.C. Wilton (Southampton, UK)
P. Workman (Sutton, UK)
R.F.A. Zwaal (Maastricht, The Netherlands)

BIOCHIMICA ET BIOPHYSICA ACTA

BBA

INTERNATIONAL JOURNAL OF BIOCHEMISTRY, BIOPHYSICS
AND MOLECULAR BIOLOGY

VOL. 1588 (1) (2002)

MOLECULAR BASIS OF DISEASE

Executive Editors: P.E. Fraser (Toronto, Canada) and
J.R. Riordan (Scottsdale, AZ, USA)

Section Editors:
C.L. Bevins
R.J. Bridges
B. De Strooper
G. Dickson
D.H. Ellison
G. Geba
T.E. Golde
R.A. Houghten
T. Iwatsubo
R.P. Oude Elferink
B. Tümmler

ELSEVIER
Amsterdam – London – New York – Oxford – Paris – Shannon – Tokyo

© 2002 Elsevier Science B V All rights reserved

This journal and the individual contributions contained in it are protected under copyright laws by Elsevier Science B.V, and the following terms and conditions apply to their use

Photocopying
Single photocopies of single articles may be made for personal use as allowed by national copyright laws Permission of the Publisher and the payment of a fee is required for all other photocopying, including multiple or systematic copying, copying for advertising or promotional purposes, resale, and all forms of document delivery. Special rates are available for educational institutions that wish to make photocopies for non-profit educational classroom use

Permissions may be sought directly from Elsevier Science via their homepage (http //www elsevier.com) by selecting "Customer support" and then "Permissions" Alternatively you can send an e-mail to permissions@elsevier co uk, or fax to· (+44) 1865 853333

In the USA, users may clear permissions and make payments through the Copyright Clearance Center, Inc , 222 Rosewood Drive, Danvers, MA 01923, USA, phone (+1) (978) 7508400, fax (+1) (978) 7504744, and in the UK through the Copyright Licensing Agency Rapid Clearance Service (CLARCS), 90 Tottenham Court Road, London W1P 0LP, UK, phone (+44) 20 7631 5555, fax (+44) 20 7631 5500 Other countries may have a local reprographic rights agency for payments.

Derivative Works
Subscribers may reproduce tables of contents of prepare lists of articles including abstracts for internal circulation within their institutions Permission of the Publisher is required for resale or distribution outside the institution.
Permission of the Publisher is required for all other derivative works, including compilation and translations

Electronic Storage or Usage
Permission of the Publisher is required to store or use electronically any material contained in this journal, including any article or part of an article

Except as outlined above, no part of this publication may be reproduced, stored in a retrieval system of transmitted in any form of by any means, electronic, mechanical, photocopying, recording or otherwise, without prior written permission of the Publisher

Address permission requests to Elsevier Science Global Rights Department, at the mail, fax and e-mail addresses noted above

Notice
No responsibility is assumed by the Publisher for any injury and/or damage to persons or property as a matter of products liability, negligence or otherwise, or from any use or operation of any methods, products, instructions or ideas contained in the material herein. Because of the rapid advances in the medical sciences, in particular, independent verification of diagnoses and drug dosages should be made

Although all advertising material is expected to conform to ethical (medical) standards, inclusion in this publication does not constitute a guarantee or endorsement of the quality or value of such product or of the claims made of it by its manufacturer.

Advertising Information
Advertising orders and enquiries can be sent to **USA, Canada and South America** Mr Tino DeCarlo, The Advertising Department, Elsevier Science Inc , 360 Park Avenue South, New York, NY 10010-1710, USA, phone (+1) (212) 633 3815, fax (+1) (212) 633 3820, e-mail t.decarlo@elsevier com **Japan** The Advertising Department, Elsevier Science K K , 9-15 Higashi-Azabu 1-chome, Minato-ku, Tokyo 106-0044, Japan, phone (+81) (3) 5561 5033, fax (+81) (3) 5561 5047 **Europe and ROW**. Commercial Sales Department, Elsevier Science Ltd , The Boulevard, Langford Lane, Kidlington, Oxford, OX5 1GB, UK, phone (+44) 1865 843016, fax (+44) 1865 843976, e-mail media@elsevier com

Orders, claims, and product enquiries: please contact the Customer Support Department at the Regional Sales Office nearest you
New York: Elsevier Science, PO Box 945, New York, NY 10159-0945, USA, phone (+1) (212) 633 3730 [toll free number for North American customers 1-888-4ES-INFO (437-4636)], fax (+1) (212) 633 3680, e-mail usinfo-f@elsevier com
Amsterdam: Elsevier Science, PO Box 211, 1000 AE Amsterdam. The Netherlands, phone (+31) 20 4853757, fax (+31) 20 4853432, e-mail. nlinfo-f@elsevier.com
Tokyo: Elsevier Science, 9-15 Higashi-Azabu 1-chome, Minato-ku, Tokyo 106-0044, Japan, phone (+81) (3) 5561 5033, fax (+81) (3) 5561 5047, e-mail info@elsevier co.jp
Singapore: Elsevier Science, 3 Killiney Road, #08-01 Winsland House I, Singapore 239519, phone (+65) 6349 0200, fax (+65) 6733 1510, e-mail asiainfo@elsevier com.sg
Rio de Janeiro: Elsevier Science, Rua Sete de Setembro 111/16 Andar, 20050-002 Centro, Rio de Janeiro-RJ, Brazil, phone· (+55) (21) 509 5340, fax (+55) (21) 507 1991, e-mail elsevier@campus com br [Note (Latin America) for orders, claims and help desk information, please contact the Regional Sales Office in New York as listed above]

USA mailing notice: *Biochimica et Biophysica Acta (Molecular Basis of Disease)* (ISSN 0925–4439) is published monthly except in February, May and September by Elsevier Science B V (PO Box 211, 1000 AE Amsterdam, The Netherlands)
Annual subscription price in the USA US$ 1165 00 (valid in North, Central and South America), including air speed delivery Second class Periodicals postage paid at Jamaica, NY 11431
USA POSTMASTER: Send address changes to *Biochimica et Biophysica Acta (Molecular Basis of Disease)*, Publications Expediting, Inc ,200 Meacham Avenue, Elmont, NY 11003
AIRFREIGHT AND MAILING in the USA by Publications Expediting, Inc , 200 Meacham Avenue, Elmont, NY 11003

Printed in The Netherlands
④ The paper used in this publication meets the requirements of ANSI/NISO Z39 48-1992 (Permanence of Paper)

ELSEVIER

Biochimica et Biophysica Acta 1588 (2002) 1–6

BIOCHIMICA ET BIOPHYSICA ACTA
BBA
www.bba-direct.com

Induction and expression of *βig-h3* in pancreatic cancer cells

Dominik Schneider[a], Jörg Kleeff[a,b], Pascal O. Berberat[a,b], Zhaowen Zhu[a],
Murray Korc[c], Helmut Friess[a,b,*], Markus W. Büchler[a,b]

[a]*Department of Visceral and Transplantation Surgery, University of Bern, Bern, Switzerland*
[b]*Department of General Surgery, University of Heidelberg, Heidelberg, Germany*
[c]*Departments of Medicine, Biological Chemistry and Pharmacology, University of California, Irvine, CA, USA*

Received 17 September 2001; received in revised form 4 February 2002; accepted 19 February 2002

Abstract

βig-h3 (TGFBI, keratoepithelin) was first identified as a transforming growth factor-β1 (TGF-β1)-inducible gene in a human lung adenocarcinoma cell line. It encodes for a secreted extracellular matrix (ECM) protein, which is thought to act on cell attachment and ECM composition. Mutations of the *βig-h3* gene are involved in several corneal dystrophies. Pancreatic cancers display multiple alterations in the TGF-β signaling pathway and in TGF-β response genes, such as overexpression of all three TGF-β isoforms and Smad4 mutations. In this report, we determined that *βig-h3* mRNA levels were induced by TGF-β1 in two out of five examined pancreatic cancer cell lines (CAPAN-1, PANC-1). In CAPAN-1 cells, which harbor a Smad4 mutation, *βig-h3* but not PAI-1 was induced by TGF-β1, whereas in PANC-1 cells that express wild-type Smad4, TGF-β1 induced both PAI-1 and *βig-h3*. In human pancreatic tissues, there was a 32.4-fold increase in *βig-h3* mRNA levels in pancreatic cancers in comparison to normal control tissues. In situ hybridization analysis revealed that *βig-h3* mRNA was expressed mainly in the cancer cells within the pancreatic tumor mass. These findings suggest that *βig-h3* is induced by TGF-βs in pancreatic cancer cells even in the presence of Smad4 mutations, which might explain, in part, the increased *βig-h3* mRNA levels observed in pancreatic cancer cells in vivo.

© 2002 Elsevier Science B.V. All rights reserved.

Keywords: *βig-h3*; TGF-β; SMAD4; Pancreatic cancer; PAI-1

1. Introduction

βig-h3 (TGFBI, keratoepithelin) is a gene that was first discovered by differential expression analysis of a transforming growth factor-β1 (TGF-β1)-treated human lung adenocarcinoma cell line [1]. It encodes a 68-kDa protein with an amino-terminal secretory sequence and a carboxy terminal sequence that can serve as a ligand recognition site for several integrins [1]. Subsequent analysis revealed that *βig-h3* is strongly induced by TGF-β1 in several cell lines, including human melanoma cells, human mammary epithelial cells, human keratinocytes, and human fibroblasts [2,3]. Expression of *βig-h3* has also been observed in corneal epithelial cells [4], skin fibroblasts [2], endothelial cells [5], in the juxtaglomerular apparatus and the pars recta of the proximal tubules in the kidney [6], in bladder smooth muscle cells, and in bladder urothelium [7].

Further functional analysis has revealed that *βig-h3* is secreted into the extracellular matrix (ECM), and that it may function as an extracellular attachment protein, thus influencing cell attachment and migration [2]. These initial results led to further investigations regarding the role of *βig-h3* in human diseases. For example, in coronary heart disease, restenotic coronary lesions showed high levels of *βig-h3* in areas of dense fibrous connective tissue. *βig-h3* was present in the cytoplasm of plaque macrophages as well as smooth muscle and endothelial cells. [5]. Most of the research has focused on the role of *βig-h3* in corneal dystrophy [8]. Thus, *βig-h3* mutations have been detected in six different autosomal dominant corneal dystrophies, such as Fuchs' dystrophy, Avellino corneal dystrophy,

---

Abbreviations: ECM, extracellular matrix; TGF-β, transforming growth factor-β; TβRI, TGF-β receptor type I; TβRII, TGF-β receptor type II; PBS, phosphate-buffered saline; CHO, Chinese hamster ovary

[*] Corresponding author. Department of General Surgery, University of Heidelberg, Im Neuenheimer Feld 110, 69120 Heidelberg, Germany. Tel.: +49-6221-56-6900; fax: +49-6221-56-6903.

E-mail address: helmut_friess@med.uni-heidelberg.de (H. Friess).

0925-4439/02/$ - see front matter © 2002 Elsevier Science B.V. All rights reserved
PII: S0925-4439(02)00052-2

Sardinian Reis Bucklers corneal dystrophy, and others, and the excessive *βig-h3* content in these corneas suggests that the mutated gene product is a fundamental constituent of the characteristic corneal accumulations [8–14].

Our current knowledge of the potential role of *βig-h3* in malignant processes is limited to data from cultured cell lines. For example, SV40-transformed human fibroblasts exhibit down-regulation of *βig-h3* expression in comparison to normal fibroblasts, suggesting that *βig-h3* expression is reduced during the malignant transformation of this cell type [15]. This is supported by experiments with Chinese hamster ovary (CHO) cells, in which transfection of a *βig-h3* expression plasmid led to a marked decrease in the ability of these cells to form tumors in nude mice [3].

In epithelial cells, TGF-βs usually exert strong growth inhibitory effects [16]. However, all three TGF-β ligands are overexpressed in pancreatic cancer, and that overexpression is associated with decreased patient survival following tumor resection [17]. Furthermore, expression analysis of the receptors has revealed that the type II and type I TGF-β signaling receptors are also present in pancreatic cancer [18,19], raising the possibility that TGF-βs may act in an autocrine manner in this malignancy to promote tumor growth. However, these cancer cells have lost their ability to respond to the growth suppressive effects of TGF-βs because of Smad4 mutations [20], decreased TGF-β receptor type I (TβRI) expression in a subgroup of patients [21,22] and overexpression of the TGF-β signaling inhibitors Smad6 and Smad7 [23,24]. Therefore, it has been difficult to demonstrate convincingly that TGF-βs act in an autocrine manner in pancreatic cancer. Since *βig-h3* is a downstream target of TGF-β1, in the present study, we examined the effects of TGF-β1 on *βig-h3* expression in cultured pancreatic cancer cells in relation to their Smad4 status, and determined whether *βig-h3* is present in human pancreatic tissues. We now show that TGF-β1 is able to induce *βig-h3* in pancreatic cancer cell lines, irrespective of whether Smad4 is mutated or not, and that *βig-h3* is overexpressed in pancreatic cancer cells in vivo.

2. Methods

2.1. Cell culture

Human pancreatic cancer cells were routinely grown in DMEM (PANC-1, MIA-PaCa-2) or RPMI (ASPC-1, CAPAN-1, T3M4) supplemented with 10% heat-inactivated FCS, 100 U/ml penicillin, 100 μg/ml streptomycin and 2 mM L-glutamine. Cells were maintained at 37 °C in a humid chamber with 5% CO_2 and 95% air atmosphere. For TGF-β1 experiments, subconfluent cells were incubated overnight in serum-free medium (containing 0.1% BSA, 5 μg/ml transferin, 5 ng/ml sodium selenite, and antibiotics), and subsequently incubated with 1 nM of TGF-β1 for the indicated time. Cells were then harvested for RNA extraction. ASPC-1, CAPAN-1, PANC-1, and MIA-PaCa-2 human pancreatic cell lines were obtained from ATCC (Rockville, MD, USA). T3M4 human pancreatic cell lines were a gift from Dr. R.S. Metzgar (Durham, NC, USA). TGF-β1 was a gift from Genentech, Inc. (South San Francisco, CA, USA).

2.2. Probe synthesis for Northern blot analysis

A fragment of human *βig-h3* cDNA was amplified by RT-PCR and subcloned into the pGEM-T Easy vector (Promega Biotechnology, Madison, WI, USA) according to the manufacturer's instructions. The identity of the cDNA fragments was confirmed by sequence analysis using the dye terminator method (ABI 373A, Perkin Elmer, Rot Kreuz, Switzerland). The mouse 7S cDNA probe that cross-hybridizes with human 7S and the human PAI-1 cDNA probe were generated as reported previously [24]. For Northern blot analysis, the probes were radiolabeled with ^{32}P-dCTP (Du Pont International, Regensdorf, Switzerland) using a random primer labeling system (Roche Diagnostic Ltd., Rotkreuz, Switzerland). For in situ hybridization, digoxigenin-labeled *βig-h3* cRNA sense and antisense probes were generated using the Ribomax System (Promega Biotechnology) and the appropriate polymerases [24].

2.3 Northern blot analysis

Following electrophoresis of total RNA in a 1.2% agarose/1.8 M formaldehyde gel, RNA was electrotransferred onto nylon membranes (Gene Screen, Du Pont, Boston, MA, USA) and cross-linked by UV irradiation. The filters were then prehybridized for 5 h at 42 °C and hybridized for 20 h at 42 °C in the presence of the radiolabeled cDNA probes for *βig-h3*. Blots were then rinsed twice with 2 × SSC at 50 °C and washed twice with 0.2 × SSC/2% SDS at 55 °C for 10 min. All blots were exposed

Table 1
Summary of TGF-β receptor expression, Smad4 mutations and effects of TGF-β1 on cell growth and PAI-1 and *βig-h3* expression in pancreatic cancer cell lines

	ASPC-1	CAPAN-1	MIA-PaCa-2	PANC-1	T3M4
TβRI [22]	+	++	+	++	+
TβRII [22]	+	++	–	+	+++
Smad4 [26]	mutated	mutated	wild type	wild type	wild type
Growth [22]	0	0	0	–	0
PAI-1 induction	0	0	0	+	0
βig-h3 induction	0	+	0	+	0

Expression of TβRI, TβRII as described previously [22] Symbols: low (+), moderate (++), high (+++) expression by Northern blotting Growth responsiveness to TGF-β1 as described previously [22] Symbols. no TGF-β1 responsiveness (0), weak to moderate (–) growth inhibition by TGF-β1. Induction of PAI-1 and *βig-h3* mRNA expression was determined by Northern blot analysis Symbols no induction (0), moderate to strong induction (+)

at − 80 °C to Kodak BioMax films with Kodak intensifying screens, and the intensity of the radiographic bands was quantified by video image analysis, using the Image-Pro plus software (Media Cybernetics, Silver Spring, MD, USA). To verify equivalent RNA loading on Northern blot membranes, filters were rehybridized with the 7S cDNA probe, as reported previously [24].

2.4. Patients and tissue collection

Normal pancreatic tissue samples were obtained through an organ donor program from 11 individuals who were free of any apparent disease. The median age of the organ donors was 34.8 years, with a range of 14 to 52 years. Pancreatic cancer tissue samples were obtained from 27 pancreatic cancer patients (9 female and 18 male, median age 69.6 years) undergoing pancreatic resection. Freshly removed tissue samples were fixed in paraformaldehyde solution for 12 to 24 h and paraffin-embedded for in situ hybridization. Tissue samples for RNA extraction were immediately snap frozen in liquid nitrogen upon surgical removal in the operating room and maintained at − 80 °C until use. All studies were approved by the Human Subjects Committee of the University of Bern.

2.5. In situ hybridization

The tissue sections (4 μm) were deparaffinized, dehydrated, and incubated in 0.2 M HCl for 20 min. The sections were treated with proteinase K (50 μg/ml) for 15 min at 37 °C. Following post-fixation with 4% paraformaldehyde in phosphate-buffered saline (PBS) for 5 min, the samples were prehybridized at 60 °C for 2 h in 50% formamide (v/v), 4 × SSC, 2 × Denhardt's solution and 250 μg/ml RNA. Hybridization was performed overnight at 60 °C in 50% (v/v) formamide, 4 × SSC, 2 × Denhardt's solution, 500 μg/ml RNA and 10% dextran sulfate (w/v). The final concentrations of the digoxigenin-labeled probes were approxi-

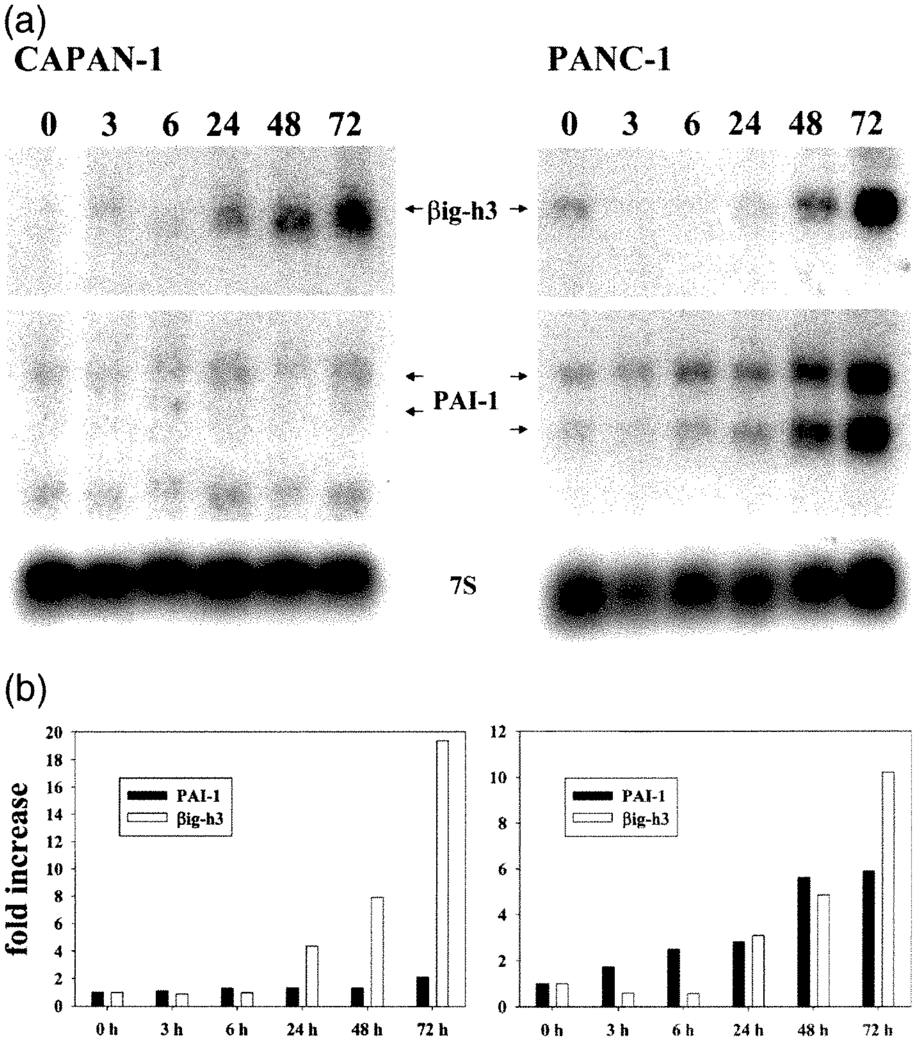

Fig. 1. (a) Effects of TGF-β1 on PAI-1 and *βig-h3* levels. Cells were serum-starved for 12 h and incubated in the absence (0 h) or presence of 1 nM TGF-β1 for the indicated time. Northern blot analysis of total RNA (20 μg/sample) was performed with ^{32}P-labeled PAI-1, *βig-h3* and 7S cDNA probes. (b) Bar graph of two experiments. The $OD_{\beta ig\text{-}h3}/OD_{7S}$ and $OD_{PAI\text{-}1}/OD_{7S}$ at 0 h were set to 1.

mately 0.5 ng/μl. After hybridization, the sections were washed and treated with RNase. The samples were then incubated with an anti-digoxigenin antibody conjugated with alkaline phosphatase (1:500). For color reaction, 5-bromo-4-chloro-3-indolyl phosphate and nitro-blue-tetrazolium (Sigma, Buchs, Switzerland) were used. For control experiments, the slides were incubated with RNase or with the corresponding sense probes. Pretreatment of the slides with RNase abolished the hybridization signals produced by the antisense probe. Furthermore, incubation with the sense probe failed to produce specific in situ hybridization signals.

3. Results and discussion

Cultured pancreatic cancer cell lines are usually resistant to the growth inhibitory effects mediated by TGF-β1 [22,25]. In the present study, we utilized five pancreatic cancer cell lines (ASPC-1, CAPAN-1, MIA-PaCa-2, PANC-1, and T3M4) to assess whether TGF-β1 induces *βig-h3* expression in these cells (Table 1). We have previously shown that of those five pancreatic cancer cell lines, only PANC-1 is growth inhibited by TGF-β1, and that this cell line expresses TβRI and TβRII and possesses a normal Smad4 gene [22,26]. ASPC-1 and CAPAN-1 cells are resistant towards the growth inhibitory effects of TGF-β1 due to Smad4 mutations [26], T3M4 cells are resistant because they underexpress TβRI [21], whereas MIA-PaCa-2 cells are resistant due to loss of TβRII expression [27]. In agreement with previous observations, we could demonstrate that TGF-β1 induced PAI-1 in a time-dependent manner in PANC-1 cells, but not in the other cell lines (Fig. 1). TGF-β1 also induced *βig-h3* mRNA expression in PANC-1 and CAPAN-1 cells in a time-dependent manner (Fig. 1). In contrast, TGF-β1 did not significantly alter *βig-h3* expression levels in the other three cell lines (data not shown).

The ability of TGF-β1 to induce *βig-h3* expression in CAPAN-1 cells that harbor Smad4 mutations [26] points to an Smad4-independent mechanism for this induction. Indeed, there is growing evidence that under some circumstances and in some cells, TGF-β signaling might be mediated in the absence of wild-type Smad4. Thus, in BxPc-3 pancreatic cancer cells, TGF-β1 exerts growth inhibitory effects despite the fact that this cell line has a deleted Smad4 gene [25]. In addition, in VACO-235 colon cells that harbor Smad4 mutations, TGF-β1 is still capable of exerting strong growth inhibitory effects [28]. These results collectively suggest that there is a non-Smad4-dependent pathway for TGF-β-mediated signaling.

In addition, our results that TGF-β1 induces *βig-h3* expression but not PAI-1 expression in CAPAN-1, whereas in PANC-1 TGF-β1 induces the expression of both genes, points to a dissociation of the TGF-β signaling pathway. This observation is in agreement with previous reports demonstrating that the expression of a truncated TβRII or a mutant TβRI does not attenuate TGF-β1-mediated induction of PAI-I, but does render Mv1Lu cells resistant to the antiproliferative effects of TGF-β1 [29]. In addition, transient overexpression of a mutated Smad3 protein blocks the antiproliferative effects of TGF-β1 in Mv1Lu cells, while still allowing for activation of PAI-I transcription [30]. Similarly, in pancreatic cancer cells, overexpression of Smad6 or Smad7 renders these cells insensitive to the growth inhibitory effects of TGF-β1, while still allowing for the induction of PAI-1 [23,24]. Collectively, these data suggest that there are divergent pathways of TGF-β signaling.

Since we observed TGF-β1-induced *βig-h3* expression in cultured pancreatic cancer cell lines, we next examined whether *βig-h3* is expressed in human pancreatic cancers in vivo. Therefore, 11 normal human pancreas samples and 27 human pancreatic cancer samples were investigated by Northern blot analysis. The *βig-h3* mRNA transcript was detected at moderate to strong levels in almost all pancreatic cancer samples, but was found at weak levels in normal pancreas samples. Densitometirc analysis indicated that there was a 32.4-fold increase in *βig-h3* mRNA levels in pancreatic cancer tissues in comparison to normal controls

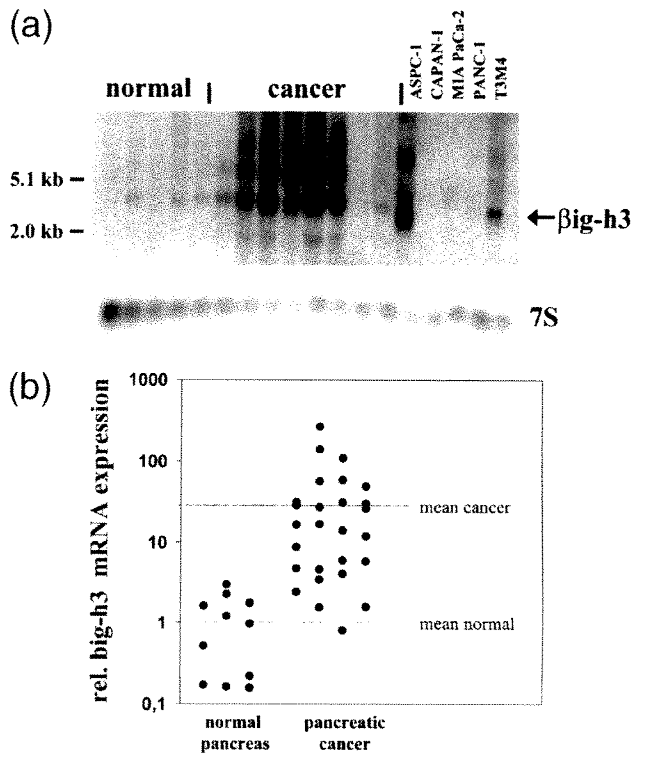

Fig. 2. Northern blot analysis of *βig-h3* mRNA in human pancreatic tissues. (a) Total RNA (20 μg) isolated from normal and cancerous pancreases and five pancreatic cancer cell lines was subjected to Northern blot analysis and probed with the ^{32}P labeled *βig-h3* cDNA. The blot was subsequently rehybridized with a 7S cDNA probe to verify equivalent RNA loading. (b) Densitometry of the Northern blots. Relative *βig-h3* mRNA expression was calculated as $OD_{\beta ig\text{-}h3}/OD_{7S}$ for each sample, and the fold increase over the mean in the normal pancreatic tissues was calculated. The mean in the normal samples was set to 1.

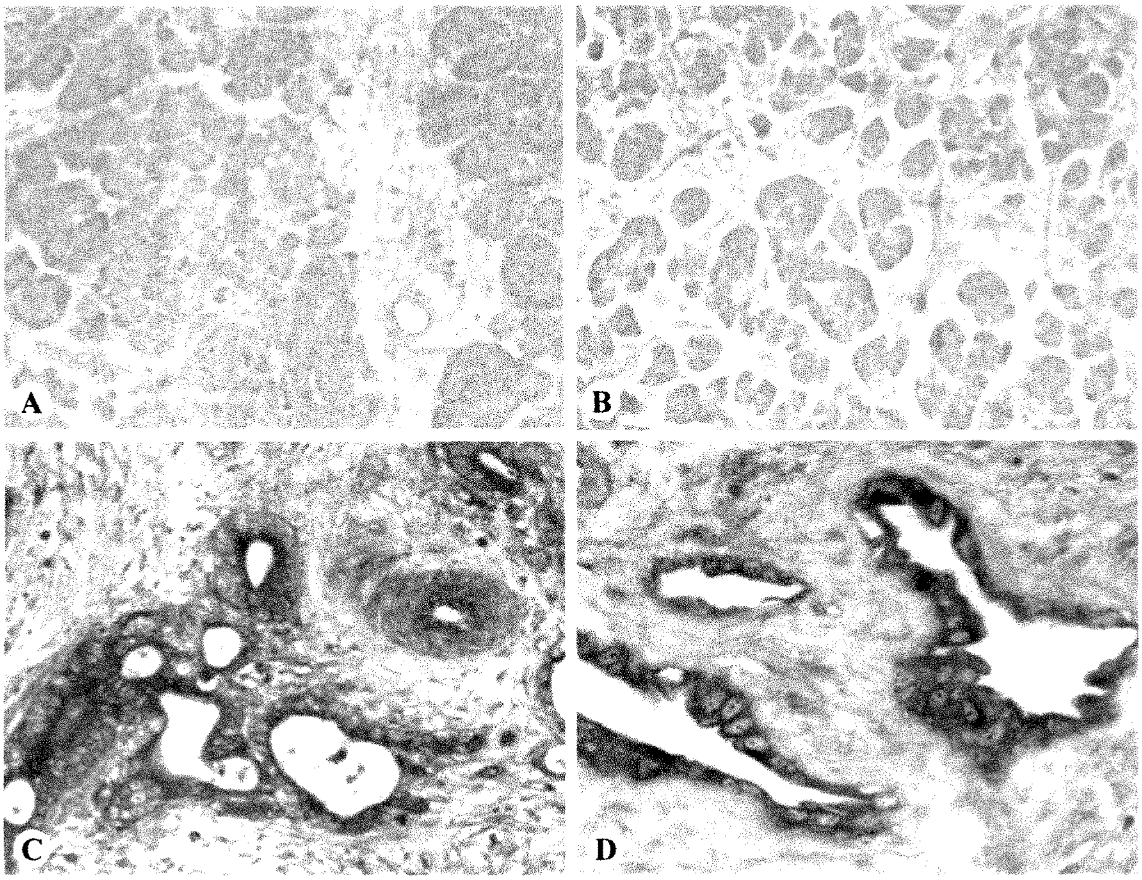

Fig. 3. In situ hybridization of *βig-h3* mRNA. (A) Normal pancreas: Weak signals were observed in some ductal and acinar cells. (B–D) Pancreatic cancer: Weak *βig-h3* mRNA signals were present in acinar cells that exhibited chronic pancreatitis-like alterations (B). *βig-h3* mRNA signals were predominantly observed in the cytoplasm of cancer cells.(C,D).

(Fig. 2b). Altogether, 26 of 27 pancreatic cancer samples expressed *βig-h3* levels that clearly exceeded the mean expression level in the normal samples.

To investigate the exact site of *βig-h3* mRNA expression in human pancreatic cancer samples, in situ hybridization was carried out next. The *βig-h3* mRNA in situ hybridization signal was intense in the cytoplasm of cancer cells (Fig. 3C,D). In contrast, in the normal pancreas, *βig-h3* mRNA signals were weakly present only in a few acinar and ductal cells (Fig. 3A,B). Previously, we have shown that human pancreatic cancers overexpress all three mammalian TGF-β isoforms [17]. Since our cell culture experiments indicate that TGF-β1 can up-regulate *βig-h3* even in the presence of Smad4 mutations, taken together, these observations suggest that up-regulation of *βig-h3* expression in vivo may be due, in part, to autocrine and paracrine effects of TGF-βs derived from the cancer cells.

The potential role of *βig-h3* in pancreatic cancer is not known. Since *βig-h3* is thought to be involved in cell attachment to the ECM, thereby influencing cell adhesion [2,31], it is possible that increased levels of *βig-h3* in pancreatic cancers influence cell adhesion and invasion of pancreatic cancer cells in vivo. Although further functional studies are required to address this question, the observation that *βig-h3* is strongly induced by TGF-β1 in some pancreatic cancer cells, irrespective of their Smad4 mutation status, and that *βig-h3* is overexpressed in pancreatic cancer cells, points to a potentially important autocrine loop that has the potential to contribute to the pathobiology of this disease.

References

[1] J. Skonier, M. Neubauer, L. Madisen, K. Bennett, G.D. Plowman, A.F. Purchio, DNA Cell Biol. 11 (1992) 511–522.

[2] R.G. LeBaron, K.I. Bezverkov, M.P. Zimber, R. Pavelec, J. Skonier, A.F. Purchio, J. Invest. Dermatol. 104 (1995) 844–849.

[3] J. Skonier, K. Bennett, V. Rothwell, S. Kosowski, G. Plowman, P. Wallace, S. Edelhoff, C. Disteche, M. Neubauer, H. Marquardt, et al., DNA Cell Biol. 13 (1994) 571–584.

[4] J. Escribano, N. Hernando, S. Ghosh, J. Crabb, M. Coca-Prados, J. Cell. Physiol. 160 (1994) 511–521.

[5] E.R. O'Brien, K.L. Bennett, M.R. Garvin, T.W. Zderic, T. Hinohara, J.B. Simpson, T. Kimura, M. Nobuyoshi, H. Mizgala, A. Purchio, S.M. Schwartz, Arterioscler. Thromb. Vasc. Biol. 16 (1996) 576–584.

[6] R.E. Gilbert, J.L. Wilkinson-Berka, D.W. Johnson, A. Cox, T. Soulis, L.L. Wu, D.J. Kelly, G. Jerums, C.A. Pollock, M.E. Cooper, Kidney Int. 54 (1998) 1052–1062.

[7] P.C. Billings, D.J. Herrick, U. Kucich, B.N. Engelsberg, W.R. Abrams, E.J. Macarak, J. Rosenbloom, P.S. Howard, J. Cell. Biochem. 79 (2000) 261–273.

[8] A.J. Bron, Cornea 19 (2000) 699–711.

[9] P. Dighiero, P. Ellies, S. Valleix, F. D'Hermies, M. Savoldelli, Y. Pouliquen, J.M. Legeais, G. Renard, J. Fr. Ophtalmol. 23 (2000) 735–737.

[10] P. Dighiero, S. Valleix, F. D'Hermies, S. Drunat, P. Ellies, M. Savoldelli, Y. Pouliquen, M. Delpech, J.M. Legeais, G. Renard, Ophthalmology 107 (2000) 1353–1357.

[11] N.T. Ha, K. Fujiki, Y. Hotta, K. Nakayasu, A. Kanai, Am. J. Ophthalmol. 130 (2000) 119–120.

[12] M. Konishi, M. Yamada, Y. Nakamura, Y. Mashima, Curr. Eye Res. 21 (2000) 891–896.

[13] Y. Mashima, S. Yamamoto, Y. Inoue, M. Yamada, M. Konishi, H. Watanabe, N. Maeda, Y. Shimomura, S. Kinoshita, Am. J. Ophthalmol. 130 (2000) 516–517.

[14] S. Yamamoto, M. Okada, M. Tsujikawa, H. Morimura, N. Maeda, H. Watanabe, Y. Inoue, Y. Shimomura, S. Kinoshita, Y. Tano, Cornea 19 (2000) S21–S23.

[15] T. Schenker, B. Trueb, Exp. Cell Res. 239 (1998) 161–168

[16] J. Massague, S.W. Blain, R.S. Lo, Cell 103 (2000) 295–309.

[17] H. Friess, Y. Yamanaka, M. Büchler, M. Ebert, H.G. Beger, L.I. Gold, M. Korc, Gastroenterology 105 (1993) 1846–1856.

[18] H. Friess, Y. Yamanaka, M. Büchler, H.G. Berger, M.S. Kobrin, R.L. Baldwin, M. Korc, Cancer Res. 53 (1993) 2704–2707.

[19] M. Wagner, J. Kleeff, H. Friess, M.W. Büchler, M. Korc, Pancreas 19 (1999) 370–376.

[20] S.A. Hahn, M. Schutte, A.T. Hoque, C.A. Moskaluk, L.T. da Costa, E. Rozenblum, C.L. Weinstein, A. Fischer, C.J. Yeo, R.H. Hruban, S.E. Kern, Science 271 (1996) 350–353.

[21] M. Wagner, J. Kleeff, M.E. Lopez, I. Bockman, J. Massaque, M. Korc, Int. J. Cancer 78 (1998) 255–260.

[22] R.L. Baldwin, H. Friess, M. Yokoyama, M.E. Lopez, M.S. Kobrin, M.W. Büchler, M. Korc, Int. J. Cancer 67 (1996) 283–288.

[23] J. Kleeff, H. Maruyama, H. Friess, M.W. Büchler, D. Falb, M. Korc, Biochem. Biophys. Res. Commun. 255 (1999) 268–273.

[24] J. Kleeff, T. Ishiwata, H. Maruyama, H. Friess, P. Truong, M.W. Büchler, D. Falb, M. Korc, Oncogene 18 (1999) 5363–5372.

[25] J. Kleeff, S. Wildi, H. Friess, M. Korc, Pancreas 18 (1999) 364–370.

[26] M. Schutte, R.H. Hruban, L. Hedrick, K.R. Cho, G.M. Nadasdy, C.L. Weinstein, G.S. Bova, W.B. Isaacs, P. Cairns, H. Nawroz, D. Sidransky, R.A. Casero Jr., P.S. Meltzer, S.A. Hahn, S.E. Kern, Cancer Res. 56 (1996) 2527–2530.

[27] J.W. Freeman, C.A. Mattingly, W.E. Strodel, J. Cell. Physiol. 165 (1995) 155–163.

[28] S.P. Fink, S.E. Swinler, J.D. Lutterbaugh, J. Massague, S. Thiagalingam, K.W. Kinzler, B. Vogelstein, J.K. Willson, S. Markowitz, Cancer Res. 61 (2001) 256–260.

[29] M. Saitoh, H. Nishitoh, T. Amagasa, K. Miyazono, M. Takagi, H. Ichijo, J. Biol. Chem. 271 (1996) 2769–2775.

[30] X. Liu, Y. Sun, S.N. Constantinescu, E. Karam, R.A. Weinberg, H.F. Lodish, Proc. Natl. Acad. Sci. U. S. A. 94 (1997) 10669–10674.

[31] J.E. Kim, S.J. Kim, B.H. Lee, R.W. Park, K.S. Kim, I.S. Kim, J. Biol. Chem. 275 (2000) 30907–30915.

ELSEVIER

Biochimica et Biophysica Acta 1588 (2002) 7–14

BIOCHIMICA ET BIOPHYSICA ACTA
BBA
www bba-direct com

Respiratory function in cybrid cell lines carrying European mtDNA haplogroups: implications for Leber's hereditary optic neuropathy

Valerio Carelli [a], Lodovica Vergani [b], Barbara Bernazzi [b], Claudia Zampieron [c], Laura Bucchi [a], Maria Lucia Valentino [a], Chiara Rengo [d,e], Antonio Torroni [d,f], Andrea Martinuzzi [c,*]

[a] *Istituto di Clinica Neurologica, Università di Bologna, Bologna, Italy*
[b] *Dipartimento di Scienze Neurologiche e Psichiatriche, Università di Padova, Padua, Italy*
[c] *IRCCS "E. Medea" Scientific Institute, Conegliano Research Centre, via Costa Alta 37, 31015, Conegliano (TV), Italy*
[d] *Dipartimento di Genetica e Biologia Molecolare, Università di Roma "La Sapienza", Rome, Italy*
[e] *Istituto di Medicina Legale, Università Cattolica del Sacro Cuore di Roma, Rome, Italy*
[f] *Dipartimento di Genetica e Microbiologia, Università di Pavia, Pavia, Italy*

Received 9 August 2001; received in revised form 8 January 2002; accepted 1 March 2002

Abstract

The possibility that some combinations of mtDNA polymorphisms, previously associated with Leber's hereditary optic neuropathy (LHON), may affect mitochondrial respiratory function was tested in osteosarcoma-derived transmitochondrial cytoplasmic hybrids (cybrids). In this cellular system, in the presence of the same nuclear background, different exogenous mtDNAs are used to repopulate a parental cell line previously devoid of its original mtDNA. No detectable differences in multiple parameters exploring respiratory function were observed when mtDNAs belonging to European haplogroups X, H, T and J were used. Different possible explanations for the previously established association between haplogroup J and LHON 11778/ND4 and 14484/ND6 pathogenic mutations are discussed, including the unconventional proposal that mtDNA haplogroup J may exert a protective rather than detrimental effect.

© 2002 Elsevier Science B.V. All rights reserved

Keywords. mtDNA, Mitochondrial haplogroup, Haplogroup J, LHON; Cybrid

1. Introduction

Analysis of human mtDNA variation has identified specific combinations of polymorphisms that have been used to systematically classify mtDNAs into haplogroups, and to study origin, dispersal and evolution of human populations [1,2]. Some authors have further suggested that certain mtDNA population polymorphisms may interact with environmental factors and/or mtDNA pathogenic mutations, and therefore that mtDNAs belonging to different haplogroups could result in mitochondria with differential functionality [2]. In this regard, the most debated case is the plethora of mtDNA nucleotide changes that have been associated with Leber's hereditary optic neuropathy (LHON) [2–10]. Three of these mutations, at positions 11778/ND4, 3460/ND1 and 14484/ND6, are now unanimously considered as pathogenic for most of the LHON cases worldwide [2,11]. At least five other transitions at positions 4216/ND1, 13708/ND5, 15257/*cytb*, 15812/*cytb* and 4917/ND2, defined as "secondary or intermediate mutations" [2], are polymorphisms of European populations [12]. Indeed, they occur in specific combinations within haplogroups J (4216/ND1, 13708/ND5, and in more recent sub-branches 15257/cytb and 15812/*cytb*) and T (4216/ND1 and 4917/ND2)[12]. Both haplogroups J and T have diverged from a more ancient mtDNA lineage defined by the 4216/ND1 change only [12]. These five polymorphisms were initially associated with LHON on the basis of their more frequent recurrence in LHON pedigrees compared to the general population [3–6]. Subsequently, a more rational investigation was performed to test their association with LHON and three laboratories published systematic haplotype and phylogenetic analyses of LHON patients from the USA [13], Italy [14] and Germany [15]. These independent studies showed a preferential association of the pathogenic mutations 11778/ND4 and 14484/ND6 with haplogroup J.

---

[*] Corresponding author. Tel . +39-438-4141; fax +39-438-410101
E-mail address andrea martinuzzi@cn inf it (A. Martinuzzi)

0925-4439/02/$ - see front matter © 2002 Elsevier Science B V. All rights reserved
PII. S0925-4439(02)00097-2

This association was particularly striking with the 14484/ND6 mutation. On the other hand, LHON pedigrees carrying the 3460/ND1 mutation seemed widely distributed among all haplogroups [13,14]. The currently favored interpretation is that the haplogroup J may lead to increased penetrance of the LHON pathogenic mutations 11778/ND4 and 14484/ND6 [13,14]. A more non-specific effect of the haplogroup J as a risk factor for neurodegenerative diseases in general, has also been suggested [9]. However, genetic and clinical investigations by other authors found no evidence for influence of the "secondary mutations", including those clustered in haplogroups J and T, on the pathogenesis and clinical expression of LHON [7,8,10,16]. Intriguingly, haplogroup J may also be associated with successful aging, as a recent study carried out on Italian centenarians has suggested [17]. Moreover, another recent report described the high prevalence of haplogroup T in individuals with reduced spermatozoa motility and of haplogroup H in those with normal motility and these associations correlated with significant differences in haplogroup-specific respiratory chain performance [18].

In the present study, we used the transmitochondrial cytoplasmic hybrid (cybrid) technology [19] to compare, in the nuclear background of the osteosarcoma 143B.TK-parental cell line, the respiratory chain function of mtDNA-less rho^0 cell lines (206) repopulated with mitochondria from control fibroblasts with different mtDNA haplogroups.

2. Materials and methods

2.1. Cells

Fibroblast cell lines have been obtained, after informed consent, from skin biopsies of normal subjects. Fibroblast cell lines were then enucleated and fused with the mtDNA-less 206 rho^0 cells following the described method [19]. Positive mtDNA re-population was identified by picking up growing clones (a minimum of four successful clones for each fusion) in selective medium: normal DMEM supplemented with 5% dialyzed fetal bovine serum (dFBS) (Seromed-Biochrom, Berlin), 0.1 mg/ml bromodeoxyuridine and no uridine. The re-population of the 206 rho^0 cells with the fibroblast mtDNA was confirmed by screening for the diagnostic mutations (Table 1) identified in the mtDNA of the fibroblast cell line. The human cell line 143B.TK- (obtained from G. Attardi as kind gift), from which the 206 rho^0 line was developed [19], was used as control. To ensure complete stabilization of mtDNA amount, functional assessment of selected clones was carried out only after at least 3 months of clone cycling.

2.2. High resolution RFLP analysis and haplogroup classification of mtDNAs

To determine high resolution RFLP haplotypes, the entire mtDNA from the fibroblast cell lines and the osteosarcoma 143B.TK-parental cell line was amplified in nine overlapping fragments by the use of PCR and the primer pairs previously described [14]. Each of the nine PCR segments was then digested with 14 restriction endonucleases (*Alu*I, *Ava*II, *Bam*HI, *Dde*I, *Hae*II, *Hae*III, *Hha*I, *Hinc*II, *Hinf*I, *Hpa*I, *Msp*I, *Mbo*I, *Rsa*I, *Taq*I) (Promega, Madison, WI, USA). In addition, mtDNAs were screened for the presence/absence of the *Bst*OI site at np 13704, the *Acc*I sites at nps 14465 and 15254, the *Bfa*I site at np 4914, the *Nla*III sites at nps 4216 and 4577, and the *Mse*I site at 14766. The A → G sequence polymorphism at np 12308 in the tRNA$^{\text{Leu}}$ gene was also tested by using a mismatched primer, which generates a *Hinf*I site when the A12308G mutation is present [14].

Table 1
Haplogroup classification of mtDNAs from the osteosarcoma 143B TK-parental cell line and control fibroblasts

Sample	Haplogroup	RFLP Haplotype[a,b]
143B TK-	X	*−1715c*; *+14465s*, +15397j, +16517e
PC	H	−6920c; *−7025a*, *−14766u*; −16303k
PS	T	*+4216q*, *+4914r*, +10727c; *+13366m*/*−13367b*/*+13367j*, *+15606a*; *−15925i*, +16517e
GA	J	*+4216q*; *+10394c*; *−13704t*, *−16065g*

[a] Sites are numbered from the first nucleotide of the recognition sequence A "+" indicates the presence of a restriction site, a "−" indicates the absence. The explicit indication of the presence/absence of a site implies the absence/presence in haplotypes not so designated The restriction enzymes used in the analysis are designated by the following single-letter codes: a, *Alu*I, b, *Ava*II, c *Dde*I, e, *Hae*III, g, *Hinf*I; i, *Msp*I, j, *Mbo*I, k, *Rsa*I; m, *Bam*HI, q, *Nla*III; r, *Bfa*I, s, *Acc*I, t, *Bst*OI; u, *Mse*I An oblique separating states indicates the simultaneous presence or absence of restriction sites that can be correlated with a single nucleotide substitution.

[b] Sites diagnostic of haplogroups are underlined

2.3. Oxygen consumption and rotenone sensitivity

Oxygen consumption was measured in intact cells (samples of 5 × 10^6 cells in 2 ml of DMEM lacking glucose, supplemented with 5% dialyzed FBS at 37 °C) with a YSI 5300 oxymeter (YSI Instruments, Yellow Springs, OH) [19,20]. Each clone was assessed in at least three independent experiments, and results are expressed as mean ± standard deviation. The sensitivity of the lines carrying the different haplogroups to the complex I inhibitor rotenone was assessed as described [21]. After testing the effects of a wide range of rotenone concentrations (5 nM–0.1 mM), we chose the concentration range of 5–500 nM for the subsequent experiments: the cells were treated with different concentrations (5, 10, 20, 40, 100 and 500 nM) of rotenone for 4 h, then were harvested and the endogenous cell respiration was measured in whole cells as detailed above. Results are expressed as percentage of remaining cell respiration.

2.4. Growth curves

Cell growth was assessed in glucose-free/galactose + medium (Gibco) [22]. Multiple series of 60 mm Petri dishes were seeded each with a constant number of cells (10^5) in glucose-free/galactose + medium: DMEM with L-glutamine without D-glucose, 0.9 mg/ml galactose, 10% dFBS. Duplicate dishes were trypsinized and counted daily for 7 days. Values obtained from fibroblast derived cybrid clones were compared to those for the parental 143B.TK-cell line. Measurements for each haplogroup were repeated at least in quadruplicate, and results are expressed for each time point as mean ± standard deviation.

2.5. Enzymatic activities

Cytochrome *c* oxidase (COX) and citrate synthase activities were assayed spectrophotometrically on freshly harvested and sonicated cells as described elsewhere [20]. COX activity was divided by the citrate synthase activity of that sample (citrate synthase ratio) to minimize the effects of variability in mitochondrial mass in the various cell culture samples.

2.6. Statistical analysis

One-way analysis of variance (ANOVA) was used to test for statistically significant differences ($P < 0.05$) between cybrid cell lines with different mtDNA haplogroups or between cybrids and the 143B.TK-parental cell line.

3. Results

On the basis of RFLP analysis (Table 1), we selected three fibroblast cell lines: one belonging to haplogroup J (HGA-haplo J), the second belonging to haplogroup T (HPS-haplo T), and the third belonging to haplogroup H

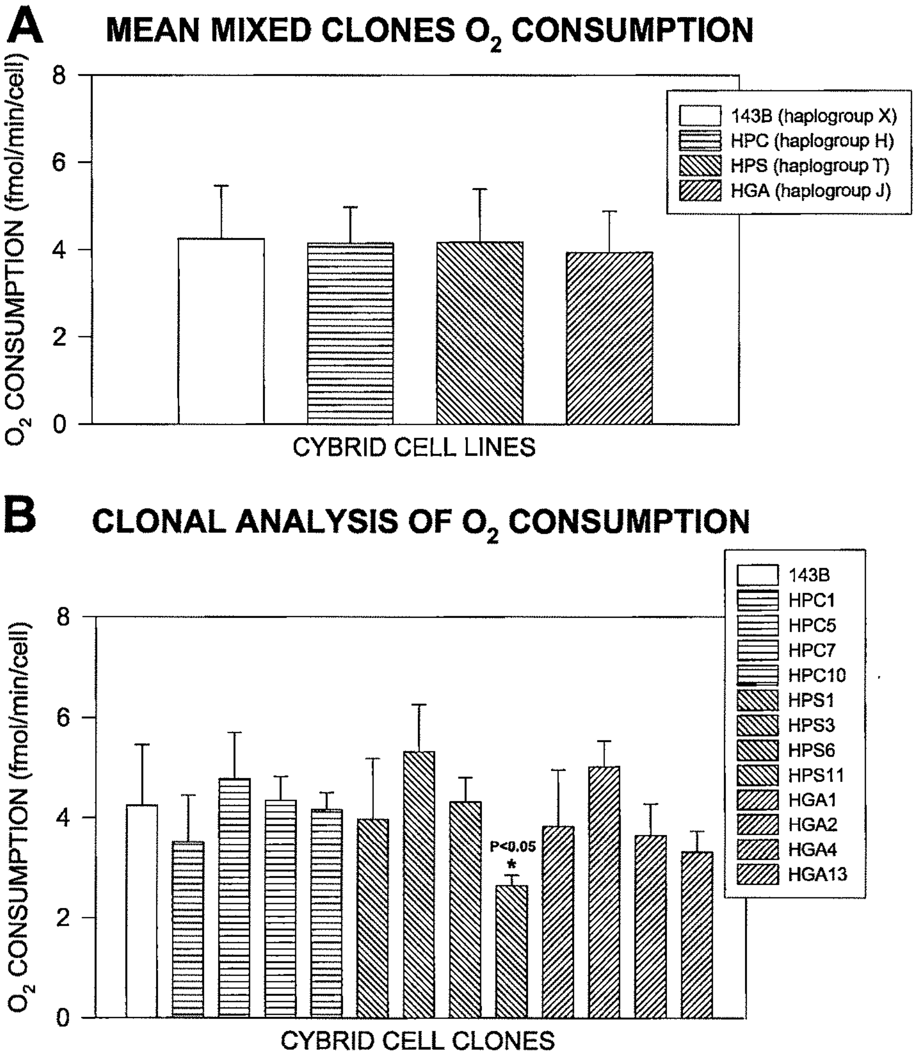

Fig 1 Oxygen consumption (A) The averaged oxygen consumption of all the clones derived from each of the fibroblast cell lines used as donors of mitochondria are compared No differences are observable among the four mtDNA haplogroups investigated (B) Clone by clone analysis reveals certain variability in oxygen consumption However, only the haplogroup T clone HPS11 tested significantly reduced at ANOVA

(HPC-haplo H), the most common (about 40%) haplogroup in Europe. The RFLP analysis showed that the 143B.TK-parental cell line harbored a mtDNA belonging to haplogroup X. All polymorphisms, including those putatively LHON-related, were found to be homoplasmic as expected. The three fibroblast-cell lines selected were then used to construct the cybrid cell lines. Four clones from each cybrid cell line were chosen for further investigations (HPC1, 5, 7, 10; HPS1, 3, 6, 11; HGA1, 2, 4, 13). Each of these clones was maintained for several months and haplogroup-specific RFLP markers were repeatedly checked to confirm that the mitochondrial re-population was with the expected mtDNAs.

The results of oxygen consumption studies are shown in Fig. 1. There were no significant differences in respiratory capacity among fibroblast-derived cybrid cell lines or between any of them and the parental 143B.TK-cell line (Fig. 1A). Although we observed some interclonal variability (Fig. 1B), we found no significant differences by clone-to-clone comparison, except for one single clone with haplogroup T (HPS11, Fig. 2B). The interclonal variability is a known phenomenon in cybrid studies even in control cell lines. It has been suggested that it probably relates to some nuclear variability of the recipient 206 rho^0 cell line, and it is not correlated to mtDNA content or growth rate, thus does not affect the general interpretation of the mean values obtained [22,23].

In order to explore even slight differences in complex I function that might not be reflected in its specific enzymatic activity, as happens for 11778/ND4 and 14484/ND6 LHON pathogenic mutations [24,25], we chose to test cybrid respiration sensitivity to the complex I specific inhibitor rotenone. Treatment of the cybrid cell lines with rotenone caused a dose-dependent inhibition of endogenous cell respiration in all tested lines (Fig. 2). The inhibition was slightly more marked in the parental 143B.TK-line (32.6% of baseline oxygen consumption with no inhibitor) compared to the fibroblast derived cybrids (40–46%). There was no difference in rotenone sensitivity amongst the fibroblast-derived lines carrying the three different haplogroups. These results suggest that complex I function was not significantly affected by the different sets of polymorphisms in ND subunits defining the three haplogroups here investigated.

Table 2
COX activity in cybrid clones

	143B TK-	HPC-haplo H	HPS-haplo T	HGA-haplo J
Cytochrome c oxidase	0.98 (0.25)	0.99 (0.37)	1.06 (0.46)	1.10 (0.47)

Enzyme activity is expressed as citrate synthase ratio. Values are mean of at least three separate experiments ± (S.D.).

There was also no difference in citrate synthase normalized COX activity among cybrid clones belonging to the various mtDNA haplogroups and between them and the parental line 143B.TK (Table 2). COX activity was the only respiratory complex previously reported to be clearly affected by haplogroup differences [18].

In order to disclose more subtle defects of respiratory function among the cybrid cell lines under investigation, growth experiments were carried out in a glucose-free/galactose + medium which is a reliable way of testing the respiratory chain-dependent metabolic capacity of cells [22]. Cybrid cell growth in glucose free/galactose + medium (Fig. 3) also failed to show any substantial difference among the clones investigated. However, the haplogroup T growth capacity was at the lower end of the range.

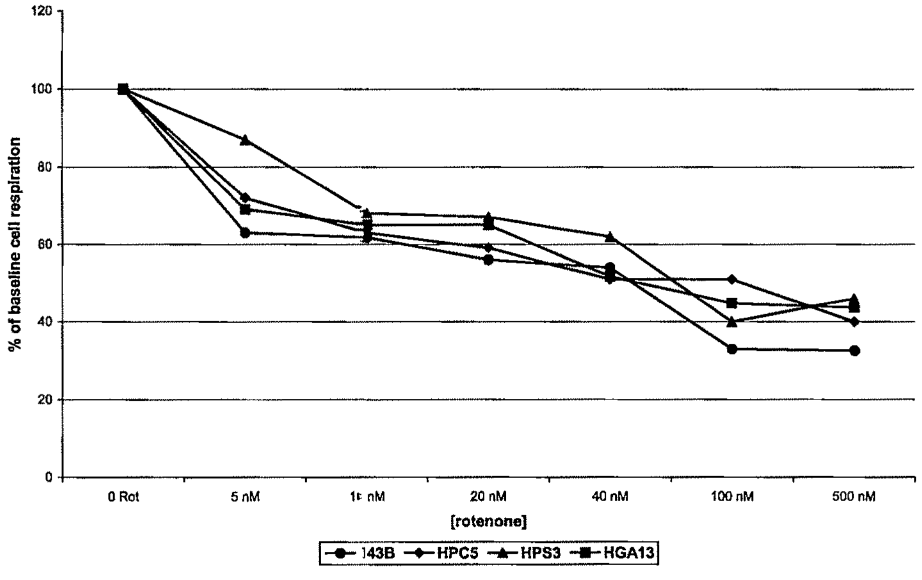

Fig. 2. Effect of complex I inhibition on endogenous cell respiration: values are expressed as percentage of baseline (no rotenone) cell O_2 consumption. The degree of endogenous cell respiration in presence of growing concentration of the complex I inhibitor rotenone is not different among the different lines

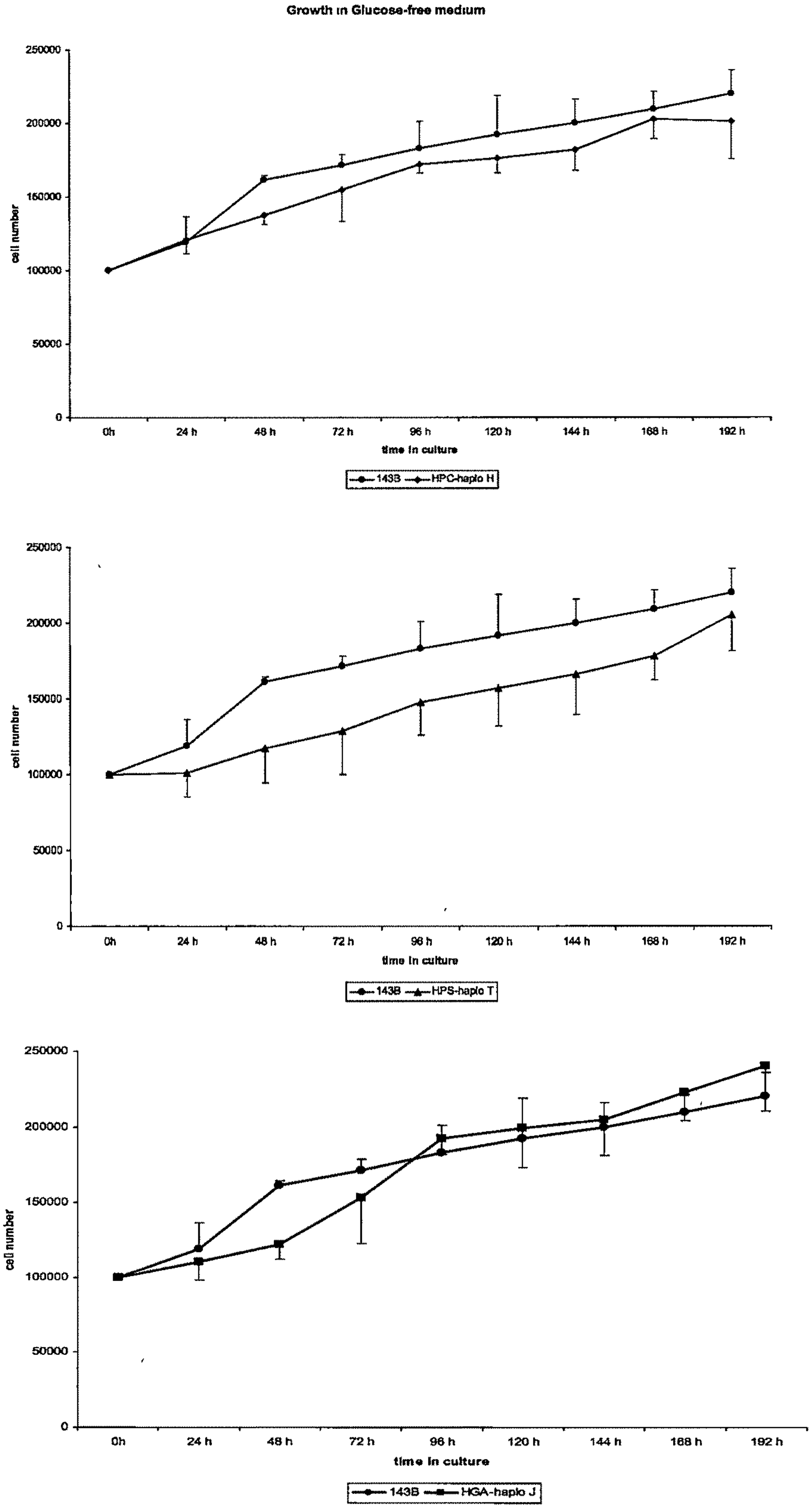

Fig 3 Cell growth in glucose-free/galactose+medium. In each graph, the parental 143B TK-line is compared with cybrids belonging to a different haplogroup Each point corresponds to the mean of cell counts ± S.D. at that time after seeding. All the cell lines were able to increment their number in this medium, with a pattern which did not significantly differ from the parental 143B.TK-line

4. Discussion

Our study, using a cybrid cellular model, does not reveal any significant overall respiratory defect in both haplogroups J and T cybrids. Few scenarios may be considered.

The first is that more subtle functional changes are induced by specific haplogroups, and these may in turn become relevant and observable only through the interaction with particular environmental conditions and/or nuclear background or tissue-specific nuclear expression. Wallace et al. [2] recently speculated that haplogroup J might induce a partially uncoupling effect on oxidative phosphorylation. This may be difficult to demonstrate using the experimental model of cybrid cells. However, others and we have been recently able to demonstrate a clear growth impairment, using the galactose medium, of cybrid cells harboring each of the LHON pathogenic mutations 11778/ND4, 3460/ND1 and 14484/ND6 [22] (Carelli V, Vergani L, Martinuzzi A, unpublished data). A defective oxidative phosphorylation has been difficult to demonstrate in LHON-derived cybrid cell lines, particularly for the 14484/ND6 mutation that showed only 10–15% reduction in respiration rate [26]. Thus, growth in galactose medium proved to be sensitive enough to unmask the defective phenotype induced by LHON pathogenic mutations.

A second scenario is that haplogroup J polymorphisms are functionally neutral unless the superimposition of a LHON pathogenic mutation occurs. In a previous study with LHON-derived cybrid cell lines, we showed that clones carrying the 11778-haplo J genotype had lower oxygen consumption and higher doubling time than those with the 11778-non J mtDNA [20]. Multiple cybrid cell clones, derived from a further individual with the same 11778-haplo J mitochondrial genome, are currently under investigation and they showed a milder defect, more similar to the defects observable in 11778-non J subjects (Carelli V, Vergani L, Martinuzzi A, unpublished data). To investigate the same issue, Lodi et al. [27] used ^{31}P MR spectroscopy to evaluate muscle and brain respiratory function “in vivo” in ten 11778-haplo J and ten 11778-non J individuals. This study failed to show any significant differences between the two groups, although both were clearly deficient compared to controls [27]. Thus, the co-occurrence of haplogroup J with the 11778 mutation does not seem to further worsen mitochondrial respiratory function in cybrid cell lines or “in vivo”. However, it must be kept in mind that LHON pathology is essentially limited to retinal ganglion cells [11] and cybrid cell studies nor ^{31}P MR spectroscopy studies of muscle and brain are truly indicative of the affected tissue. Thus, although unlikely, it cannot be formally excluded that haplogroup-specific differences in mitochondrial respiratory function might be observable only in the retinal ganglion cells.

Only one study of Finnish families systematically compared LHON sub-classified by haplogroups [28]. No major clinical differences were observed between 11778-haplo J and 11778-non J individuals, in agreement with other studies in different populations [7,16]. However, penetrance (males and females combined) was somewhat higher in the 11778-J families as well as, paradoxically, the frequency of visual recovery (see Table 3 in Ref. [28] and Table 7 in Ref. [29]). Furthermore, a case of remarkable visual recovery was reported in a single Italian patient carrying the 11778-haplo J [30]. A higher male penetrance in 11778-haplo J families was also reported for the Australian LHON families [31]. In our experience, the 11778-haplo J families were homoplasmic, larger and with higher penetrance compared to the 11778-non J (Carelli V. and Barboni P., unpublished data).

The association of the 14484/ND6 mutation with haplogroup J is even tighter than that of the 11778/ND4 mutation. To date, there are no comparative studies of 14484-haplo J versus 14484-non J families. However, the visual recovery frequently observed in Europeans with 14484/ND6 mutation does not seem to be associated with haplogroup J. Indeed, the occurrence of 14484/ND6 mutation in African and Japanese cases is still associated with a visual recovery [32,33]. Moreover, the biochemical phenotype induced by the 14484/ND6 mutation was not affected by differences in mtDNA background [25]. The European cases of LHON with 14484/ND6 mutation are frequently represented by large homoplasmic multigenerational pedigrees [11], and in some occasions the association with haplogroup J may relate to a common founder as for the Canadian families of French ancestry [34]. However, in other European populations, haplotype analysis has confirmed multiple independent origins of this mutation [13,14].

We believe there is need to investigate further the scenarios we outlined. A systematic comparative investigation of LHON pedigrees harboring 11778/ND4 and 14484/ND6 mutations associated or not to haplogroup J appears necessary to resolve the contradictory and anecdotal observations available so far. The comparison should consider penetrance and rate of spontaneous visual recovery, especially for the 11778-haplo J combination. Moreover, penetrance should be differentially evaluated between males and females, since the males are more frequently affected with LHON, but penetrance in females, who transmit their mtDNA, is the critical parameter for selective pressure and persistence of LHON pathogenic mutations in the population. Indeed, it would be important to investigate the persistence of LHON mutations in the population in relation to mtDNA haplogroups.

This last point is raised because of a third, unconventional scenario that may be suggested by the recently reported association of haplogroup J with successful aging [17], and high complex I activity found in spermatozoa with this haplogroup (see Fig. 5 in Ref. [18]). If haplogroup J exerts a protective rather than detrimental effect, this could lead to longer persistence of LHON mutations in the population. Interestingly, the highest male/female ratio (7–

8:1), an indirect indication of lower penetrance in females, was reported for the 14484/ND6 mutation [35–37]. This mutation may also be persistent in the population, as shown by the French-Canadian families with haplogroup J [34,37]. The recognition of the 11778/ND4 and 14484/ND6 LHON mutations in association with haplogroup J, according to this hypothesis, would be favored compared to the occurrence of these mutations in other background mtDNAs. As a consequence, the 11778/ND4-haplo J and 14484/ND6-haplo J LHON families should be more frequently large and homoplasmic rather than small, heteroplasmic pedigrees or sporadic cases. The unexpectedly high percentage of sporadic cases reported in some populations for the most frequent 11778/ND4 mutation provides a good opportunity to test this hypothesis [14,35,36,38]).

Acknowledgements

The financial support of Telethon-Italy (Grant #792 and E.0890) is gratefully acknowledged.

References

[1] R.L. Cann, M Stoneking, A.C. Wilson, Mitochondrial DNA and human evolution, Nature 325 (1987) 31–36

[2] D.C Wallace, M D Brown, M T. Lott, Mitochondrial DNA variation in human evolution and disease, Gene 238 (1999) 211–230.

[3] D R. Johns, J. Berman, Alternative, simultaneous complex I mitochondrial DNA mutations in Leber's hereditary optic neuropathy, Biochem. Biophys. Res. Commun 174 (1991) 1324–1330.

[4] D.R. Johns, M.J Neufeld, Cytochrome *b* mutations in Leber hereditary optic neuropathy, Biochem Biophys Res. Commun. 181 (1991) 1551–1557.

[5] M.D Brown, A S. Voljavec, M T Lott, I MacDonald, D.C. Wallace, Leber's hereditary optic neuropathy: a model for mitochondrial neurodegenerative diseases, FASEB J. 6 (1992) 2791–2799

[6] M D. Brown, A.S Voljavec, M.T. Lott, A Torroni, C C. Yang, D C Wallace, Mitochondrial DNA complex I and III mutations associated with Leber's hereditary optic neuropathy, Genetics 130 (1992) 163–173

[7] R J Oostra, P A Bolhuis, I Zorn-Ende, M.M. de Kok-Nazaruk, E M Bleeker-Wagemakers, Leber's hereditary optic neuropathy no significant evidence for primary or secondary pathogenicity of the 15257 mutation, Hum Genet. 94 (1994) 265–270

[8] D.A Mackey, R.J. Oostra, T Rosenberg, E Nikoskelainen, J. Bronte-Stewart, J Poulton, A.E. Harding, G. Govan, P.A. Bolhuis, S Norby, E M. Bleeker-Wagemakers, M.-L. Savontaus, C. Chan, N Howell, Primary pathogenic mtDNA mutations in multigeneration pedigrees with Leber hereditary optic neuropathy, Am J. Hum. Genet 59 (1996) 481–485.

[9] S. Hofmann, R. Bezold, M. Jaksch, P Kaufhold, B. Obermaier-Kusser, K -D. Gerbitz, Disease relevance of the so-called secondary Leber hereditary optic neuropathy mutations, Am. J Hum. Genet 60 (1997) 1539–1542.

[10] D.A Mackey, R.-J Oostra, T Rosenberg, E. Nikoskelainen, J Poulton, T. Barratt, P. Bolhuis, S Norby, M.-L. Savontaus, C Chan, N. Howell, Reply to Hofmann et al., Am J. Hum. Genet 62 (1998) 492–495.

[11] N Howell, Human mitochondrial diseases answering questions and questioning answers, Int. Rev Cytol. 186 (1999) 49–116.

[12] A. Finnila, M.S. Lehtonen, K Majamaa, Phylogenetic network for European mtDNA, Am. J. Hum. Genet. 68 (2001) 1475–1484.

[13] M D Brown, F Sun, D C Wallace, Clustering of Caucasian Leber hereditary optic neuropathy patients containing the 11778 or 14484 mutations on an mtDNA lineage, Am. J. Hum Genet 60 (1997) 381–387.

[14] A. Torroni, M Petrozzi, L D'Urbano, D. Sellitto, M Zeviani, F. Carrara, C. Carducci, V. Leuzzi, V. Carelli, P. Barboni, A. De Negri, R. Scozzari, Haplotype and phylogenetic analyses suggest that one European-specific mtDNA background plays a role in the expression of Leber hereditary optic neuropathy by increasing the penetrance of the primary mutations 11778 and 14484, Am J. Hum. Genet. 60 (1997) 1107–1121.

[15] S. Hofmann, M. Jaksch, R. Bezold, S. Mertens, S Aholt, A. Paprotta, K -D. Gerbitz, Population genetics and disease susceptibility: characterization of central European haplogroups by mtDNA gene mutations, correlation with D loop variants and association with disease, Hum. Mol. Genet 6 (1997) 1835–1846.

[16] R.-J. Oostra, P.A Bolhuis, F.A Wijburg, G Zorn-Ende, E M. Bleeker-Wagemakers, Leber's hereditary optic neuropathy correlations between mitochondria genotype and visual outcome, J. Med Genet. 31 (1994) 280–286.

[17] G. De Benedictis, G Rose, G. Carrieri, M. De Luca, E. Falcone, G Passarino, M Bonafe', D Monti, G. Baggio, S Bertolini, D. Mari, R Mattace, C. Franceschi, Mitochondrial DNA inherited variants are associated with successful aging and longevity in humans, FASEB J 13 (1999) 1532–1536.

[18] E. Ruiz-Pesini, A -C Lapena, C Diez-Sanchez, A. Perez-Martos, J. Montoya, E. Alvarez, M. Diaz, A. Urries, L Montoro, M J Lopez-Perez, J.A. Enriquez, Human mtDNA haplogroups associated with high or reduced spermatozoa motility, Am J. Hum Genet 67 (2000) 682–692

[19] M P. King, G Attardi, Human cells lacking mtDNA: repopulation with exogenous mitochondria by complementation, Science 246 (1989) 500–503

[20] L Vergani, A Martinuzzi, V Carelli, P Cortelli, P Montagna, G Schievano, R. Carrozzo, C Angelini, E Lugaresi, MtDNA mutations associated with Leber's hereditary optic neuropathy: studies on cytoplasmic hybrid (cybrid) cells, Biochem Biophys. Res. Commun. 210 (1995) 880–888.

[21] A Barrientos, C Moraes, Titrating the effects of mitochondrial complex I impairment in the cell physiology, J. Biol. Chem 274 (1999) 16188–16197.

[22] G Hofhaus, D R. Johns, O Hurko, G. Attardi, A Chomyn, Respiration and growth defects in transmitochondrial cell lines carrying the 11778 mutation associated with Leber's hereditary optic neuropathy, J. Biol. Chem 271 (1996) 13155–13161

[23] A. Chomyn, S T Lai, R Shakeley, N Bresolin, G Scarlato, G Attardi, Platelet-mediated transformation of mtDNA-less human cells analysis of phenotypic variability among clones from normal individuals—and complementation behcavior of the tRNALys mutation causing myoclonic epilepsy and Ragged Red Fibers, Am. J Hum Genet 54 (1994) 966–974.

[24] V Carelli, A. Ghelli, M Ratta, E Bacchilega, S. Sangiorgi, R Mancini, V Leuzzi, P. Cortelli, P. Montagna, E Lugaresi, M. Degli Esposti, Leber's hereditary optic neuropathy: biochemical effect of 11778/ND4 and 3460/ND1 mutations and correlation with the mitochondrial genotype, Neurology 48 (1997) 1623–1632.

[25] V. Carelli, A. Ghelli, L. Bucchi, P Montagna, A De Negri, V Leuzzi, C Carducci, G. Lenaz, E. Lugaresi, M. Degli Esposti, Biochemical features of mtDNA 14484 (ND6/M64V) point mutation associated with Leber's hereditary optic neuropathy, Ann. Neurol 45 (1999) 320–328

[26] M.D. Brown, I A Trounce, A.S. Jun, J C. Allen, D.C. Wallace, Functional analysis of lymphoblast and cybrid mitochondria containing the 3460, 11778 or 14484 Leber's Hereditary Optic Neuropathy mtDNA mutations, J Biol Chem 275 (2000) 39831–39836

[27] R Lodi, P. Montagna, P Cortelli, S. Iotti, S Cevoli, V. Carelli, B Barbiroli, Secondary 4216/ND1 and 13708/ND5 Leber's hereditary optic neuropathy mtDNA mutations do not further impair in vivo mitochondrial oxidative metabolism when associated with 11778/ND4 mtDNA mutation, Brain 123 (2000) 1896–1902

[28] T. Lamminen, K. Huoponen, P Sistonen, V Juvonen, P. Lahermo, P Aula, E Nikokelainen, M -L. Savontaus, mtDNA haplotype analysis in Finnish families with Leber hereditary optic neuroretinopathy, Eur. J. Hum Genet. 5 (1997) 271–279

[29] E.K Nikoskelainen, K Huoponen, V. Juvonen, T. Lamminen, K Nummelin, M.-L. Savontaus, Ophthalmologic findings in Leber hereditary optic neuropathy, with special reference to mtDNA mutations, Ophthalmology 103 (1996) 504–514

[30] A. Salmaggi, F. Carrara, M Zeviani, Remarkable recovery of visual function in a patient with Leber's optic neuropathy and multiple mutations of mitochondrial DNA, Int J. Neurosci. 77 (1994) 261–266.

[31] N Howell, I. Kubacka, S. Halvorson, Leber's hereditary optic neuropathy· the etiological role of a mution in the mitochondrial cytochrome *b* gene, Genetics 133 (1993) 133–136

[32] V. Carelli, P Barboni, A. Zacchini, R. Mancini, L. Monari, S Cevoli, R. Liguori, M Sensi, E Lugaresi, P Montagna, Leber's hereditary optic neuropathy (LHON) with 14484/ND6 mutation in a North African patient, J. Neurol. Sci 160 (1998) 183–188.

[33] K Yamada, Y Mashima, K. Kigasawa, K. Miyashita, M. Wakakura, Y Oguchi, High incidence of visual recovery among four Japanese patients with Leber's hereditary optic neuropathy with the 14484 mutation, J. Neuro-Ophthalmol 17 (1997) 103–107.

[34] C. Macmillan, T A Johns, K Fu, E A. Shoubridge, Predominance of the T14484C mutation in French-Canadian families with Leber hereditary optic neuropathy is due to a founder effect, Am J Hum. Genet. 66 (2000) 332–335.

[35] A E. Harding, M.G. Sweeney, G.G Govan, P. Riordan-Eva, Pedigree analysis in Leber hereditary optic neuropathy families with a pathogenic mtDNA mutation, Am J Hum. Genet 57 (1995) 77–86

[36] Y. Mashima, K Yamada, M. Wakakura, K. Kigasawa, J Kudoh, N Shimizu, Y Oguchi, Spectrum of pathogenic mitochondrial DNA mutations and clinical features in Japanese families with Leber's hereditary optic neuropathy, Curr. Eye Res 17 (1998) 403–408.

[37] C. Macmillan, T. Kirkham, K. Fu, V. Allison, E. Andermann, D Chitayat, D. Fortier, M Gans, H Hare, N. Quercia, D. Zackon, E A Shoubridge, Pedigree analysis of French Canadian families with T14484C Leber's herditary optic neuropathy, Neurology 50 (1998) 417–422

[38] N.J Newman, M.T Lott, D.C. Wallace, The clinical characteristics of pedigrees of Leber's hereditary oiptic neuropathy with the 11778 mutation, Am. J. Ohthalmol 111 (1991) 750–762

ELSEVIER

Biochimica et Biophysica Acta 1588 (2002) 15–25

BIOCHIMICA ET BIOPHYSICA ACTA
BBA
www.bba-direct.com

Cholesterol crystallite nucleation in supersaturated model biles from a thermodynamic standpoint

Chen-Lun Liu [a,*], William I. Higuchi [b]

[a] *Institute of Biotechnology, National Dong-Hwa University, Shou-Feng, Hualien Hsien 974, Taiwan, ROC*
[b] *Department of Pharmaceutics and Pharmaceutical Chemistry, College of Pharmacy, University of Utah, Salt Lake City, UT 84112, USA*

Received 2 April 2001, received in revised form 1 February 2002, accepted 20 March 2002

Abstract

A rapid, silicone polymer film uptake method was used to determine the cholesterol (Ch) thermodynamic activity (A_T) in taurocholate (TC)–lecithin (L) and taurochenodeoxycholate (TCDC)–L model biles supersaturated with Ch. Also, time-dependent quasielastic light scattering (QLS) measurements and microscopic observations were made to determine the nature of particle species and the Ch nucleation times. In all cases in which Ch–L vesicles were present, a linear relationship between the logarithm of Ch nucleation times and Ch A_T was found. These findings support that Ch A_T is the appropriate parameter that represents the Ch nucleation tendency and that vesicles are catalytic sites in the Ch nucleation process. When Ca^{2+}, a nucleation promoter ion, was present in the supersaturated model biles, the increased values of Ch A_T quantitatively correlated with shorter Ch nucleation times. These latter findings further demonstrate that Ch A_T is the dominant factor in explaining the Ch nucleation tendencies in supersaturated model biles.

© 2002 Elsevier Science B.V. All rights reserved.

Keywords: Cholesterol thermodynamic activity; Catalytic site

1. Introduction

Early studies have demonstrated that patients with cholesterol (Ch) gallstones have bile supersaturated with Ch and this led to the early viewpoint that the presence of Ch in bile in excess of the micellar solubilization capacity would lead to the formation of Ch gallstones [1,2]. Previously, the Ch saturation index (CSI), i.e., the ratio of the Ch concentration in a bile sample relative to its saturation solubility in that sample, was used to compare biles of gallstone patients with those of healthy humans [3]. Later, it was found that the Ch supersaturated bile was not uncommon in healthy humans who did not develop Ch gallstones [2]. This apparent discrepancy followed by evidence for the presence of Ch carriers other than micelles, i.e., Ch–phospholipid vesicles, led to the view that these carriers may help stabilize bile, which would otherwise be unstable with respect to Ch precipitation on the basis of micellar Ch solubilization alone. Subsequently, other factors such as the hypomotility of the gallbladder have also been thought to be possible triggers for gallstone formation [4–7].

Holan et al. [8,9] introduced the concept of the Ch nucleation time in human bile. They defined the Ch nucleation time as the time required for the first appearance of Ch crystals in crystal-free bile. They showed that vesicles in healthy biles were stable for many days without Ch nucleation but, in patients with Ch gallstones, vesicles were found to aggregate and nucleation occurred in a few days. Their findings suggested that vesicle aggregation is an important process in the Ch nucleation and gallstone formation. Nevertheless, recent findings have indicated that Ch may nucleate in supersaturated bile without prior aggregation and fusion of vesicles [10–12]. Therefore, it is important to further investigate the role of vesicles and other factors in the Ch nucleation process.

From a thermodynamic standpoint, the driving force for Ch nucleation and precipitation in supersaturated bile should be the thermodynamic activity (A_T) of Ch. Lee et al. [13,14] described a silicone polymer uptake method for determining Ch A_T as it pertains to Ch nucleation. This technique required equilibration of the silicone polymer with the bile solution for 12–24 h and is feasible for the measurement of Ch A_T of unsaturated biles. However, in the supersaturated bile, Halpern et al. [15,16] have shown that the Ch nucleation times could potentially be less than 12 h, especially in biles with a

---

[*] Corresponding author. Fax: +886-3-8661959.
E-mail address: cliu@mail.ndhu.edu.tw (C.-L. Liu).

0925-4439/02/$ - see front matter © 2002 Elsevier Science B.V. All rights reserved.
PII: S0925-4439(02)00098-4

high bile salt (BS)/lecithin (L) molar ratio. Because nucleation and crystal growth on the surface of the polymer may compromise both the Ch concentration determinations in the model bile and the Ch A_T measurements, it was considered necessary to improve the silicone polymer uptake method of Lee et al. [13,14] to substantially reduce equilibration times. Since the transfer of Ch into the silicone polymer was not diffusion-controlled in the silicone polymer itself but was interface-controlled, changing the thickness of the silicone film alone did not result in the desired reduction of equilibration times. Jain et al. [17] attempted to overcome the interfacial barrier by making the silicone polymer surface positively charged. This modified method was confirmed to be both satisfactory and useful in reducing the equilibration times to less than 1 h.

The modified rapid uptake method for Ch A_T determination was recently developed [18] to examine the possible correlation between the A_T for Ch in Ch-supersaturated BS–L solutions and the Ch nucleation times determined by quasielastic light scattering (QLS) measurements and by microscopic observations as a function of time in these solutions. QLS measurements have also provided information on the nature of the particulate species in the Ch supersaturated BS–L systems, i.e., whether micelles, vesicles and/or Ch crystallites are present. This previous investigation was limited to relatively few example experiments, which basically established that the approach for examining the relationship between Ch supersaturation, as represented by Ch A_T, and the Ch nucleation time was highly promising. In addition, the limited experiments indicated (1) that there was likely a strong correlation between Ch A_T and Ch nucleation times and (2) that Ch-L vesicles were likely catalytic sites of Ch nucleation.

The purpose of the present study was to provide a quantitative examination of the relationship between Ch A_T and Ch nucleation times over a wide range of conditions. The studies were to include both taurocholate (TC)–L and the taurochenodeoxycholate (TCDC)–L systems. As will be seen, results of the present studies together with our previous results validate the role of vesicles and the importance of the Ch A_T interpretation in the Ch nucleation process.

2. Materials and methods

2.1. Materials

The thin silicone polymer film (Silastic sheeting No. 500-3) was acquired from Dow Corning Company, Midland, MI. Prior to use, the thin film was washed with boiling 95% ethanol for 15 s, followed by a thorough rinse with boiling deionized water for a few seconds. Tetradecyldimethyl [3-(trimethoxysilyl)-propyl] ammonium chloride (TDTOP) was obtained as a 50% methanol solution from Petrarch Chemical Company, Bristol, PA. Sodium TC and sodium TCDC were purchased from Calbiochem Corporation, San Diego, CA. Their purities (>96%) were checked by a thin layer chromatography (TLC) procedure [19]. Egg yolk lecithin was purchased from Lipid Products (Surrey, UK) and its purity was also checked by TLC [20]. Ch was acquired from Sigma Chemical Company (St. Louis, MO) and was purified by recrystallization from 95% ethanol three times before use. Radioactive Ch monohydrate (ChM) crystals were prepared as described previously [21]. Other chemicals were analytical grade and were used as received.

2.2. Pretreatment of the silicone polymer

The silicone polymer film was pretreated with a cationic polymer solution as described earlier [17] so as to incorporate a positive charge on the silicone polymer surface. The thin silicone polymer film (20 × 1 × 0.0254 cm) was placed in a glass vial containing an aliquot of 0.6 ml 50% TDTOP diluted with 17.4 ml of methanol. The thin film was allowed to soak for 3 h with occasional shaking. At the end of 3 h, 2 ml of water was added to make the final TDTOP concentration equal to 1.5% and the thin film was left in this solution for another 12 h. Finally, the thin film was removed and dried overnight in a 37 °C incubator before cutting into 2 × 1 × 0.0254 cm sections and used in the uptake studies.

2.3. Ch A_T measurement

Basically, the procedures in the present study are quite similar to those that have been published [17,18]. The BS–L–Ch admixtures were heated at 80 or 90 °C until isotropically clear and were filtered while still hot. The hot filtrate (1.5 ml) and a section of the pretreated thin film were added to each sample vial. The thin film was placed in an arched position to ensure its complete immersion in the solution. After flushing with nitrogen, the vials were tightly capped and were shaken on a rotating shaker maintained at 37 °C. At predetermined time intervals (~ 1 h), vials were successively removed and duplicate samples (100 µl) of the model bile solution were taken and assayed for Ch concentration using a scintillation counter (Beckman Instruments, Irvine, CA). The thin polymer film was removed from the vial and quickly rinsed with three portions (10 ml each) of ethanol/water (1:4) mixture. The washed film was transferred to a scintillation vial and extracted for a minimum of three times with 3 ml portions of ethanol until no further radioactivity was observed in the final extract. The radioactivity from each extract was combined to determine the amount (and hence the concentration, C_{sp}) of Ch partitioned in the silicone polymer. The Ch A_T value was determined (± 10% error) based on the following equation [13,14,17,18,21,22]:

$$\text{Ch } A_T = C_{sp}/C^{\circ}_{sp} \qquad (1)$$

where C°_{sp} is the C_{sp} value at ChM saturation.

2.4. QLS measurement

Culture tubes (12 × 75 mm, American Scientific Products, McGaw Park, IL) were soaked in chromic acid overnight and then rinsed with distilled deionized water. The washed tubes were transferred into an 80 °C oven and dried. The procedure used in QLS sample preparation is similar to that described above for Ch A_T measurement except that after the clear solution was filtered at 80 °C, it was collected in the cleaned culture tubes and transferred into a 37 °C incubator without shaking.

The procedure used for QLS measurement is similar to that described earlier [27]. Briefly, the angle between the incident beam and the scattered beam was 90° to minimize stray light. A Cooper Laser Sonics (Model 95) argon ion laser operated at 514.5 nm wavelength and a temperature-controlled water bath maintained at 37 °C were part of the light-scattering apparatus. QLS measurements were performed with a Brookhaven BI-2030, extendable 72-channel, multi-bit correlator/computer. The scattered intensity from model bile solution was normalized by that from toluene (I_{sol}/I_{tol}). By analyzing the random fluctuations in scattered intensity, the autocorrelation function, i.e., the repetitive comparisons of the intensity of scattered light from different channels was calculated [23,24]. The mean hydrodynamic radius ($\bar{R}_h$) and polydispersity (V) of the different species, i.e., micelles and vesicles, were determined as described previously [18,25–27]. Briefly, three particle populations could be identified as follows: (a) those with an $\bar{R}_h$ value between 10 and 55 Å were categorized as micelles (including both simple and mixed micelles), (b) those with an $\bar{R}_h$ value from 150 to 700 Å were classified as vesicles, and (c) those with an $\bar{R}_h$ value >700 Å were characterized as aggregated vesicles, multilamellar vesicles or Ch crystallites.

2.5. Polarizing microscope nucleation time studies

Nucleation times (crystal observation times) were determined by experiments in which crystal (either needle or plate) appearance was observed microscopically. In general, several (5–10) 4-ml vials containing model bile solution at each supersaturation condition were maintained separately in an oven at 37 °C. They were successively removed at predetermined time intervals (every 3 h for the first day and once a day for the remaining days) and the model bile solution examined with a polarizing microscope (Nikon, Garden City, NY). The sample was placed on a clean flat microscope slide covered with a coverglass and observed immediately. Photographs were taken in complete extinction under crossed Nicols.

3. Results and discussion

3.1. Correlation between Ch A_T and Ch nucleation times

Previous studies [18] showed that nucleation of Ch crystallites in a supersaturated model bile may be catalyzed by Ch–L vesicles. In addition, QLS and microscopy studies suggested that, when vesicles were present, Ch nucleation times were an inverse function of Ch A_T; the higher the Ch A_T in the system, the shorter the Ch nucleation time [18]. In the present study, similar techniques were employed to determined A_T of Ch and Ch nucleation times over wide ranges of CSI, BS to L molar ratios, and total lipid concentrations in supersaturated TC–L and TCDC–L solutions. Eighteen systems (see Tables 1–4) in which vesicles were present were chosen in this study. Data examination revealed that the results from these 18 systems conform well ($R^2 = 0.972$) to the expression:

$$\text{Nucleation time (day)} = A' \times 10^{-B\,\text{Ch}A_T} \qquad (2)$$

where $A' = 1.56 \times 10^6$ day; $B = 4.06$.

When the scale of nucleation times is expressed logarithmically, the above equation can be rearranged as,

$$\text{Log (Nucleation Time)} = 6.193 - 4.06 \times \text{Ch}\ A_T \qquad (3)$$

Based on Eq. (3) and the experimental measurements of the Ch nucleation times and the Ch A_T, the relationship between the logarithm of the Ch nucleation times and the Ch A_T values can be seen in Fig. 1 as a straight line. The number adjacent to each data point in Fig. 1 is the sample number from Tables 1–4. Consistent with the R^2 value of 0.972, the experimental data are generally quite close to the

Table 1

Lipid particles present at the time of Ch A_T measurements and Ch nucleation times determined by QLS and microscopy in TCDC–L systems supersaturated with Ch

Phase region[a]	Sample number	Lipid composition (mM)			TCDC/L ratio	CSI	Ch A_T	Particles	Ch nucleation times
		TCDC	L	Ch					
I	1	44.0	22.0	9.65	2.0	1.82	1.08	Vesicles	79 days
I	2	72.9	21.2	10.56	3.4	1.82	1.36	Vesicles	3 days
I	3	72.9	21.2	11.35	3.4	1.95	1.39	Vesicles	3 days
I	4	111.9	22.0	12.22	5.1	1.94	1.67	Vesicles	6 h
I (near micellar zone)	5	72.9	21.2	7.66	3.4	1.32	1.12	Micelles only	>50 days
I	6	111.9	22.0	9.64	5.1	1.53	1.31	Micelles only	>9 days

[a] See text for definitions of I and II

Table 2
Lipid particles present at the time of Ch A_T measurements and Ch nucleation times determined by QLS and microscopy in TC–L systems supersaturated with Ch

Phase region[a]	Sample number	Lipid composition (mM)			TC/L ratio	CSI	Ch A_T	Particles	Ch nucleation times
		TC	L	Ch					
I (near micellar zone)	7	72.9	21.2	6.19	3.4	1.32	1.15	Micelles only	>50 days
I	8	111.9	22.0	7.97	5.1	1.63	1.35	Micelles only	>50 days
II	9	44.0	22.0	8.85	2.0	2.01	1.16	Vesicles	37 days
II (near I)	10	55.0	20.0	7.01	2.8	1.56	1.20	Vesicles	23 days
I	11	72.9	21.2	9.70	3.4	2.06	1.32	Vesicles	6 days
I	12	80.0	20.0	10.13	4.0	2.15	1.37	Vesicles	6 days
I	13	72.9	21.2	12.00	3.4	2.55	1.41	Vesicles	4 days
I	14	111.9	22.0	12.54	5.1	2.56	1.67	Vesicles	6 h

[a] See text for definitions of I and II

best straight line. It is noteworthy that Eq. (3) well represents the data over approximately a 1000-fold range of Ch nucleation times and that the experimental data are for both the TC–L and the TCDC–L systems. It is also noteworthy (see Tables 1–4) that wide ranges of BS–L ratios and total lipid concentrations were included in this study.

The influence of added calcium ions on both Ch A_T and Ch nucleation times are presented in Table 5 and Fig. 2. All four experiments of Table 5 yielded Ch A_T values and nucleation times that were in good agreement with Eq. (3). In Fig. 2, it is shown how the presence of Ca^{2+} changes both Ch A_T and the nucleation time; however, all of the data pairs remain close to the original correlation line.

3.2. Ch A_T versus CSI concept

Although it has been recognized for some time that CSI may not be a good predictor of Ch supersaturation [4–9,18], it is worthwhile to consider the possible correlation (or the lack thereof) between CSI and Ch nucleation times with the present data. The data of the 18 systems are presented in Fig. 3 in a manner similar to that of Fig. 1, i.e., data plotted as the logarithm of Ch nucleation time versus CSI. As can be seen, the correlation is quite poor. From a statistical analysis, the R^2 value is only 0.145 (compared to 0.972 in Fig. 1) if a linear relationship is assumed.

This poor correlation can be understood by an examination of Figs. 4 and 5 where plots of Ch A_T versus CSI are presented for the TC–L and the TCDC–L cases, respectively. First, it can be seen here that, for both the TC–L and the TCDC–L cases, Ch A_T and CSI are essentially equal for unsaturated and saturated solutions, i.e., when Ch $A_T \approx \mathrm{CSI} \leq 1.0$. However, for Ch-supersaturated solutions, CSI is no longer proportional to Ch A_T and no longer a single-valued function of Ch A_T; this is equivalent to Henry's law not being obeyed for Ch $A_T \geq 1.0$. In physiological bile, the BS/L molar ratio is in the range from 2.5 to 3.5 [21], which is well represented in Figs. 4 and 5. From this result, it is not surprising that CSI is often found to be a poor measure of the Ch nucleation tendency in supersaturated biles.

3.3. Role of vesicles as nucleation catalysts

Evidence from the present study and that from an earlier study [18] strongly support vesicles being catalysts for Ch nucleation: Ch nucleation times are much shorter when vesicles are present. Table 1 shows that, for sample 6, this solution without vesicles was stable for more than 9 days even though the Ch A_T value (1.31) was nearly the same as sample 2, which nucleated in 3 days. Also, it is seen from Table 2 that sample 8 (Ch A_T ~ 1.35), which did not contain vesicles was stable for more than 50 days, while sample 12 (Ch A_T ~ 1.37) nucleated in 6 days.

Another aspect of interest here is the evidence from a previous study [27] that vesicles may represent only a small proportion (~ 3%) of the total lipids, although they dominate scattered light because of their large sizes. In samples 1–3, the hydrodynamic radius of vesicles measured by QLS was ~ 200–500 Å, which is close to the size of vesicles formed in

Table 3
Lipid particles present at the time of Ch A_T measurements and Ch nucleation times determined by QLS and microscopy in supersaturated TC–L systems of the same TC/L molar ratio but different total lipid concentrations

Phase region[a]	Sample number	Lipid composition (mM)			TC/L ratio	CSI	Ch A_T	Total lipid (g/dl)	Particles	Ch nucleation times
		TC	L	Ch						
I or II	15	15	5	2.2	3.0	2.0	1.08	1.3	Vesicles	92 days
I or II	16	30	10	4.5	3.0	2.0	1.15	2.6	Vesicles	35 days
I or II	17	60	20	9.0	3.0	2.0	1.28	5.1	Vesicles	8 days
I or II	18	120	40	17.4	3.0	2.0	1.39	10.2	Vesicles	2 days

[a] See text for definitions of I and II

Table 4
Lipid particles present at the time of Ch A_T measurements and Ch nucleation times determined by QLS and microscopy in supersaturated TC–L (samples 19 and 20) and TCDC–L (samples 21 and 22) systems

Phase region[a]	Sample number	Lipid composition (mM)			BS/L ratio	CSI	Ch A_T	Total lipid (g/dl)	Particles	I_{sol}/I_{tol}	Ch nucleation times
		BS	L	Ch							
II (but near I)	19	91.0	31.8	13.5	2.9	1.9	1.28	7.9	Vesicles	289	12 days
I	20	63.4	10.6	4.8	6.0	2.0	1.51	4.4	Vesicles	135	1 day
I	21	91.0	31.8	17.0	2.9	2.0	1.55	7.9	Vesicles	346	12 h
I	22	68.7	10.6	6.1	6.5	2.1	1.83	4.6	Vesicles	105	3 h

[a] See text for definitions of I and II

80–32 mM tauroursodeoxycholate (TUDC)–L solutions with a Ch concentration of 6.5 mM [27]. Moreover, the total scattered light intensity of vesicles with respect to toluene (I_{sol}/I_{tol}) in samples 1–3 was close to that of the 80–32 mM TUDC–L system (300–350). These findings indicate that it is likely that vesicles also represent a small proportion of the total lipid content in model bile solutions of different total lipid concentrations, as reported previously [27].

3.4. Influence of lipid concentrations and the question of vesicle aggregation in Ch nucleation

Previous studies [21,28,35,36] have shown that, when the BS to L molar ratio of bile is mainly between 2.5 and 3.5, Ch crystallites nucleate from concentrated gallbladder bile (~ 10 g/dl) of gallstone patients much more rapidly than from more dilute hepatic bile (~ 3 g/dl). A possible explanation for this observation has been provided by Halpern et al. [9,15] and Strasberg et al. [28,29]: when the total lipid concentration increases, vesicles are in closer proximity; this promotes both vesicle aggregation and the onset of crystallite nucleation.

Another explanation can be gleaned from the data of Table 3. Here, it is seen that, at constant TC/L molar ratio (3:1) and constant CSI (~ 2.0), Ch A_T has increased significantly (from 1.08 to 1.39) with increasing total lipid concentration. This is accompanied by a decrease in Ch nucleation times from 92 to 2 days. Thus, it can be argued that the significant increase in Ch nucleation tendency with increasing total lipid concentration is only a result of increased Ch supersaturation (i.e., increased Ch A_T).

While in the foregoing, it has been argued that Ch A_T (and the nucleation tendency) may increase with increasing total lipids, an opposite outcome can be seen in the results shown in Table 4. As seen in Table 4, the experiments with the higher total lipid concentrations yielded longer Ch nucleation times; but here again, the correlation between Ch nucleation times and Ch A_T values was quite good (Fig. 1).

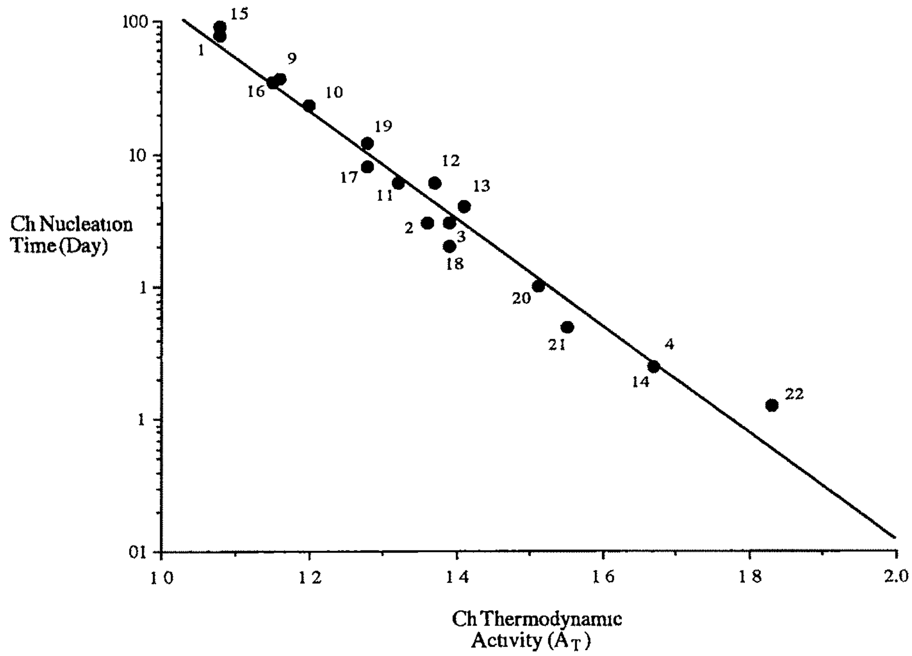

Fig. 1. Logarithm of Ch nucleation time (day) vs. Ch A_T when vesicles are present. Numbers adjacent to data points are sample numbers from Tables 1–4. Solid line indicates the best fit line.

Table 5
Lipid particles present at the time of Ch A_T measurements and Ch nucleation times determined by polarized microscope in supersaturated TC–L (sample 23) and TCDC–L (samples 24–26) systems

Sample number	Lipid composition (mM)			BS/L ratio	Ca^{2+} (mM)	Ch A_T	Particles	Ch nucleation times
	BS	L	Ch					
23	72.9	21.2	9.7	3.4	10.0	1.63	Vesicles	9 h
24	72.9	21.2	11.4	3.4	10.0	1.76	Vesicles	3 h
25	44.0	22.0	9.6	2.0	5.0	1.35	Vesicles	3 days
26	44.0	22.0	9.2	2.0	5.0	1.29	Vesicles	6 days

3.5. Effect of calcium ions on Ch A_T and Ch nucleation

Calcium has been considered among Ch nucleation pronucleating agents [29–34]. According to the vesicle aggregation/fusion hypothesis [37,38], it has been suggested that Ca^{2+} may help overcome the repulsion of the polar phospholipid head groups on the vesicles and thereby assist in promoting vesicle aggregation, vesicle fusion and Ch nucleation.

The results of the present study (Fig. 2) have clearly demonstrated a pronucleating effect of Ca^{2+} upon the Ch nucleation process. At 5 to 10 mM level of Ca^{2+}, the Ch nucleation times are reduced by a factor of 10 or more. It is quite interesting that the enhanced nucleation appears to be entirely associated with the increased thermodynamic activity of Ch; there is no evidence of Ca^{2+} influencing any "kinetic" factors involved. There is more discussion later on the Ca^{2+} effect.

3.6. A comparison of the present results with the work of Wang and Carey [39]

Wang and Carey, with the earlier work of Konikoff et al. [40] as a starting point, conducted a comprehensive study of crystallization pathways during Ch precipitation from model biles. These investigators observed the appearance of several Ch crystal forms and/or crystal habits in addition to the plate-like ChM crystals as functions of time and increasing lecithin concentration. The order of appearance of crystals, including ChM, varied depending upon the conditions of the supersaturated model bile solutions.

The basic aim and scope of our study have differed significantly from those of Wang and Carey and the results of their work were not available to us during the experimental phase of our study. Nonetheless, as there are important areas of overlap between the present work and that of Wang and Carey, a comparison of the results of the two studies should be of interest.

It is worthwhile to first point out that the aim of the present research, as was also our previous study [18], was to test the hypothesis that there should be a quantitative relationship between Ch nucleation time and Ch A_T. The Ch nucleation time was to be determined by both QLS and by microscopic observation. Ch A_T was to be determined at a time preceding the nucleation event so that no significant supersaturation relief would have occurred due to Ch precipitation [18]. Such data were to therefore provide unambiguous information for determining the relationship between Ch nucleation induction time and the driving force for Ch nucleation (i.e., Ch A_T). The experiments of Wang and Carey generally differed from

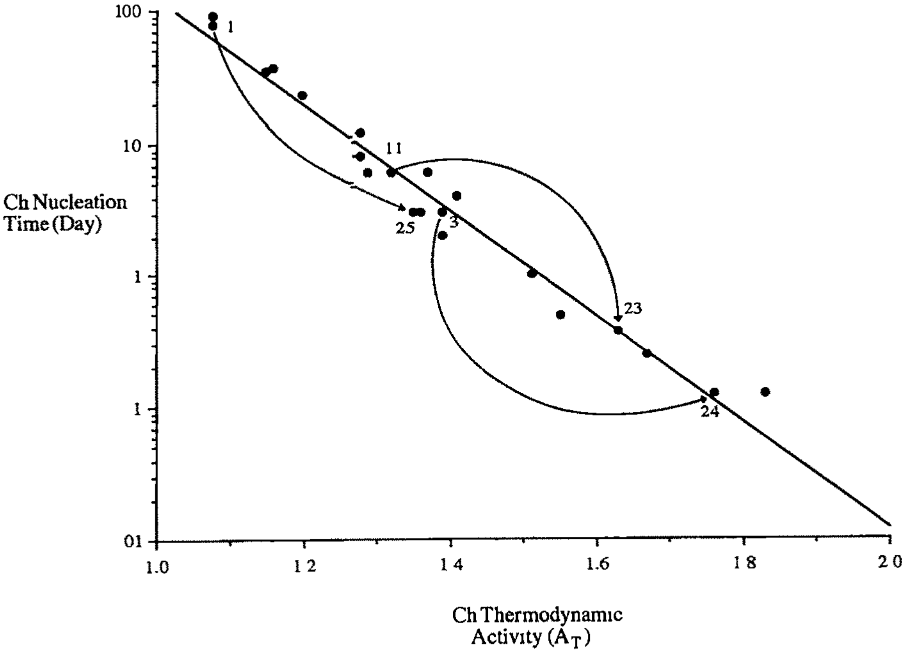

Fig. 2. Influence of Ca^{2+} on Ch A_T and Ch nucleation times when vesicles are present. Numbers adjacent to data points are sample numbers from Tables 1–5. Solid line indicates the best fit line from Fig. 1. Arrows indicate the movement of systems due to presence of Ca^{2+}

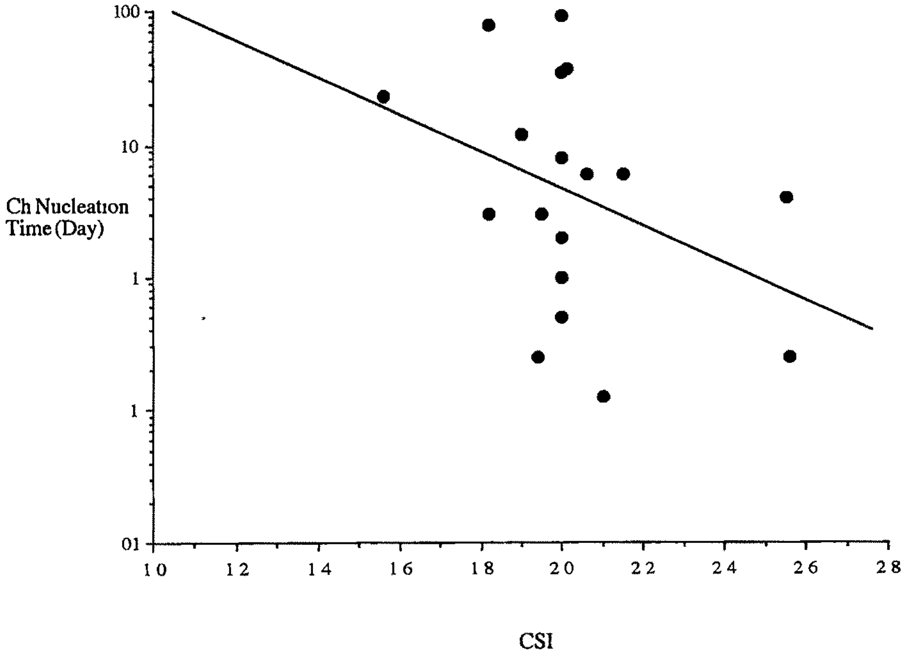

Fig. 3 Logarithm of Ch nucleation time (day) vs CSI when vesicles are present. Systems are from Tables 1–4. Solid line indicates the best fit line

ours in that their observations extended far into the crystallization/precipitation phase of the process, and Ch A_T would have been expected to decrease appreciably over the time period of the experiments. Another difference between our work and that of Wang and Carey is that the present work involves mainly Zone I of the equilibrium triangular phase diagram for the Ch–BS–L three component system, with a few experiments in or in the vicinity of Zone II (see Tables 1–4). Here, the zones are defined as follows. Zone I is the left two-phase zone of the phase diagram containing micelles and Ch crystals, Zone II is the central three-phase zone containing micelles, vesicles, and Ch crystals, and Zone III would be the right two-phase zone containing micelles and vesicles, but no crystals. The phase diagrams provided by Cabral and Small [41] were used to determine the appropriate zone for sample in Tables 1–4. We conducted no experiments in Zone

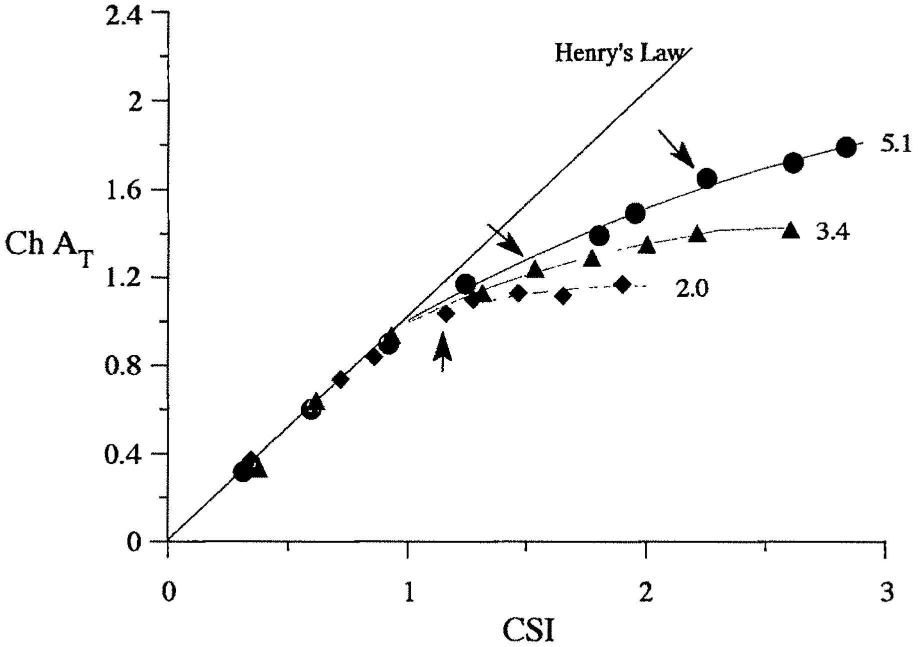

Fig. 4 The relationship between Ch A_T and CSI in TC–L system (●) indicates TC–L = 111.9–22 mM, TC/L = 5 1, (▲) indicates TC–L = 72 9–21.2 mM, TC/L = 3.4, (◆) indicates TC–L0 = 44–22 mM, TC/L = 2 0 Arrows indicate visual turbidity at 4 h from silicone polymer uptake study

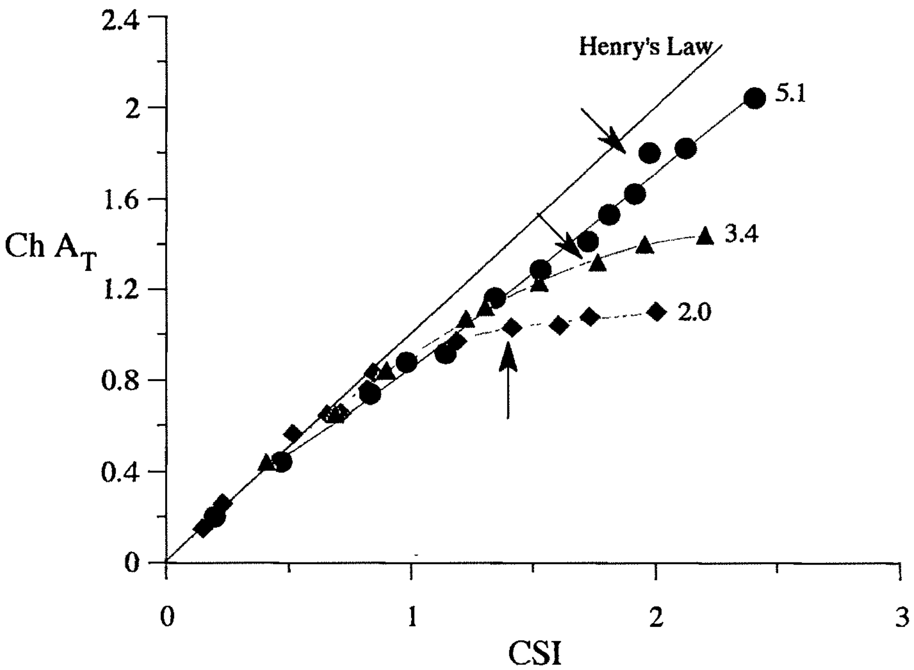

Fig. 5. The relationship between Ch A_T and CSI in TCDC–L system. (●) indicates TCDC–L=111.9–22 mM, TCDC/L=5.1, (▲) indicates TCDC–L=72.9–21.2 mM, TCDC/L=3.4; (◆) indicates TCDC–L=44–22 mM, TCDC/L=2.0. Arrows indicate visual turbidity at 4 h from silicone polymer uptake study.

III but Wang and Carey carried out representative studies in all three zones (I, II and III) of the equilibrium triangular phase diagrams.

3.6.1. *Crystal detection time as a function of the BS/L ratio*

An important result of the Wang and Carey study was the finding that the crystal detection time (same as our Ch nucleation time) increased with decreasing BS/L ratio over the entire range of their studies for both the TCDC–L–Ch and the TC–L–Ch systems. This finding is very consistent with the results of our present work. As a specific example, compare sample 3 and sample 4 of Table 1. Here the CSI values are essentially the same (1.95 and 1.94) while the TCDC/L ratios are 3.4 and 5.1 for sample 3 and sample 4, respectively. The nucleation times are 3 days for sample 3 and 6 h for sample 4. Another example: compare sample 13 and 14 of Table 2; again, the CSI values are essentially the same; the TC/L ratios are 3.4 and 5.1 while the nucleation times are 4 days and 6 h for samples 13 and 14, respectively. A generalization of these results can be found by considering Fig. 1 together with the results shown in Figs. 4 and 5 for the TC–L–Ch and the TCDC–L–Ch systems. In both Figs. 4 and 5, the L concentration was held relatively constant (~22 mM) while the BS concentration was varied. It can be clearly seen that as the BS/L ratio is increased, Ch A_T is increased in both systems. Thus, together with the plot of Fig. 1, one can see that the increase in Ch nucleation time with decreasing BS/L ratio may be correlated with the decrease in Ch A_T.

An important point that now deserves some discussion is that Wang and Carey determined crystal detection times for both ChM and anhydrous cholesterol (ACh).[1] In our studies, no distinction was made; however, the needle-shaped or the conventional plate-like ChM crystals were observed in different instances as the earliest microscopic detection of crystals in our experiments. Significantly, as mentioned earlier, the nucleation times determined by QLS and those determined by microscopic observation generally agreed quite well in our studies [18]. In the Wang and Carey study, while crystal detection times increased with decreasing BS/L ratio for both ACh and ChM crystals, there was a cross-over in the data plots for the two crystal forms: for the high BS/L ratio region [BS/L≳7.0], ACh appeared more rapidly (by around 1.5 ×) than ChM; for the low BS/L ratio region [BS/L≲7.0], ChM appeared more rapidly (by ~2 ×). It is noteworthy that in the Wang and Carey study the crystal detection times for ACh and ChM did not differ by more than about a factor of 2 over the entire range of study. Therefore, in the plot of Fig. 1, where the nucleation times are over about a 1000-fold range, the ACh and the ChM results could easily have fallen within the data scatter of both. Also, as discussed above (see also Figs. 4 and 5), Ch A_T would likely have been higher for model biles having higher BS/L ratios, it is possible this factor that may be the reason for the ACh crystals appearing earlier than the ChM crystals at the high BS/L ratio in the Wang and Carey study. We have anecdotally noted in a few limited instances (see, for example, Figs. 2 and 3 in Ref. [18]) that, at high Ch A_T, needle-shaped crystals appeared before the plate-like crystals and, at low Ch A_T, only the plate-like Ch could be seen during the entire time period of the experiment. We may speculate at this point that the kinetics of nucleation may favor the appearance of ACh at high A_T while both kinetics and/or the thermodynamics may favor ChM at low A_T values. Future systematic studies should provide clarification of this issue.

---

[1] Citing the work of Konikoff et al. [40], Wang and Carey offer a caveat that "the crystals were apparently ACh crystals as revealed by their habits, suggestive synchrotron X-ray spacings, and appropriate density. Nevertheless, more refined studies have yet to be carried out to conclusively prove that ACh and not a new ChM polymorph precipitates from bile under these circumstances."

3.6.2. Influence of calcium concentration

Wang and Carey reported that crystal detection times in the presence of added calcium ions were comparable to control biles without calcium; however, they systematically found that crystal numbers of both ACh and ChM increased with increased calcium concentration. Although it is unclear why crystal detection times did not correlate with increased crystal numbers, the latter suggests increased crystal nucleation rates with increased calcium concentration; this is in good agreement with our results (Fig. 2). The absence of a correlation between increased crystal numbers and the crystal detection times in the Wang and Carey study remains to be clarified.

3.7. Mechanistic and theoretical aspects of the present results

It should be instructive to first review from nucleation theory the viewpoint that the results presented in Fig. 1 are not consistent with homogeneous nucleation theory but are likely in agreement with heterogeneous nucleation (i.e., catalysis by vesicles). From classical homogeneous nucleation theory [42], one may write

$$\ln S^* = \left[\frac{32\sigma^3\upsilon^2}{3(kT)^3\ln A}\right]^{\frac{1}{2}} \tag{4}$$

Here S^* is the critical supersaturation below which crystal nucleation is very slow and above which nucleation is very fast. The critical supersaturation is usually chosen to correspond to the rate of production of one nucleus per second per unit volume of supersaturated solution. The other parameters in Eq. (4) are υ (molecular volume of Ch), σ (the Ch crystal solution interfacial tension), kT (the thermal energy), and A (the pre-exponential kinetic factor, which, for most purposes, is taken to equal $\sim 10^{25}\ \mathrm{s}^{-1}\ \mathrm{cm}^{-3}$). From Ch precipitation experiments in 63% ethanol–water systems, Walton [42] deduced an S^* value of $S^* \sim 15$ and a σ value of $\sigma \sim 15$ ergs/cm^3. In their studies on Ch solubilization and precipitation in model bile solutions, Mazer and Carey [43] concluded that S^* for homogeneous Ch nucleation in Ch supersaturated in TC (simple micelles only) solution was probably $S^*>6.8$, from which these investigators deduced σ for this system to be $\sigma>12.8$ ergs/cm^3 based on Eq. (4). Although the 6.8 value has involved some assumptions regarding Ch binding to simple TC micelles, these appear to be quite reasonable. Mazer and Carey point out the consistence of their result with Walton's result. Thus, it seems to be very likely Ch homogeneous nucleation conditions were being assessed in both instances. From this, it seems not unreasonable to believe that, for homogeneous nucleation of Ch in micellar bile salt only systems or in ethanol–water systems, a rather high S^* would be required (i.e., $S^* \geq 6.8$). It is evident that the modest supersaturation range (i.e., the Ch A_T range of 1.1 to 1.85) in Fig. 1 is far below the S^* values of Walton (for ethanol–water systems) and of Mazer and Carey (for TC only systems). The data of Fig. 1 would therefore not be consistent with homogeneous nucleation and may be best explained on the basis of heterogeneous nucleation, i.e., nucleation catalyzed by vesicles.

At this point, it is worthwhile to point out that the experimental nucleation time (crystal detection time in the Wang and Carey work) can be a function of both nucleation kinetics and crystal growth kinetics. When crystal growth rates are rapid, the nucleation time can be true measure of the inverse of the rate of nucleation. The exponential nature of the relationship between nucleation time and Ch A_T (see Eq. (2) and Fig. 1) would suggest a nucleation process and not simple diffusion-controlled crystal growth (which would be expected to follow a first-order dependence upon the concentration supersaturation, i.e., the differential between solution Ch concentration and Ch solubility). Significant contribution from a more complex crystal growth mechanism involving cooperativity of Ch molecules in the rate-determining step (e.g., two-dimensional nucleation controlled crystal growth), however, cannot be ruled out simply because of the exponential dependence. Perhaps the most persuasive evidence that crystal growth rates are likely not contributing significantly to Ch nucleation times comes from the fact that the QLS determined times for the "sudden" appearance of large particles (>700 Å) are of the same magnitude as nucleation times observed microscopically (the microscopically determined nucleation times are only 1.2 to 1.4 times greater [18]). Also, microscopically observed crystals are typically in the micron size range. Therefore, it seems reasonable to assume relatively rapid growth of crystals relative to the Ch nucleation rate for the results presented in Fig. 1.

We now come to the important question of what is the nature of the mechanism of Ch nucleation catalysis by vesicles. Here it is helpful to use a scenario presented by MacDonald [44] as a starting point. As $A_T \rightarrow 1.0$, Ch molecules in a phospholipid bilayer will begin to associate laterally. The propensity for lateral association and for Ch phase separation should increase with increasing A_T. Possibly, with increasing A_T, Ch may tend to form a relatively rigid two-dimensional patch at the bilayer surface. MacDonald suggests at this point that, as true nucleation would require growth in the third dimension, flat Ch surfaces on adjacent membranes may tend to adhere. Here, Ca^{2+} may assist to reduce the repulsive electrostatic effects in the adjacent regions of the bilayer. The highest probability of this process occurring would be in multilamellar liposomes or with aggregated vesicles as the interacting membrane surfaces have no chance of being far from each other. This scenario is plausible in light of, even at $A_T \sim 1.0$, the mole fraction of Ch in phospholipid bilayers can be as high as ~ 0.50. The catalytic effect of vesicles vis-a-vis the homogeneous nucleation barrier then likely arises from the favorable micro-environment provided by the bilayer(s) allowing the formation of an incipient crystal (i.e., the critical nucleus) with minimum free energy penalty. It would seem reasonable to speculate here that, perhaps, the presence of two membranes might not be necessary. This can arise if the free energy increment ingoing from the Ch monolayer patch (the embryo crystal in a single bilayer) to the Ch critical nucleus remains small; the need for the second membrane can then be circumvented. Unfortunately, both experimental and theoretical information is lacking on this issue.

The final point for discussion is that of the role of calcium in Ch nucleation. As mentioned earlier, it appears that the enhancement of Ch nucleation by calcium might be explained entirely on the basis of thermodynamics, i.e., on the basis that the presence of calcium simply moves the nucleation time downwards in the plot of Fig. 2, and three examples of this are shown. If one wishes to argue that it is *only* such a thermodynamic effect, one then must suggest that all kinetic factors must remain unchanged when calcium is added to the system. This would mean that the pre-exponential factor (not the same, but analogous to A in Eq. (4)) would remain unchanged. Here the pre-exponential factor is related to the local interfacial transport of Ch molecules. Additionally, it would require that calcium may not play a role assisting in overcoming the repulsion of polar phospholipid head groups at vesicle surfaces (and helping to promote vesicle aggregation, vesicle fusion and Ch nucleation). An alternate interpretation of the results of Fig. 2 would be that, while calcium increase A_T and the reduced Ch nucleation time does follow the straight line relationship obeyed by the 22 BS–L–Ch systems not containing calcium, this may be a coincidence arising from compensating cancellation of effects involving the above-mentioned kinetic factors

4. Conclusions

In the present investigation, a modified silicone polymer film uptake method has been used successfully to measure the true Ch supersaturation (Ch A_T) in model biles over a wide range of conditions. An important finding of this research has been that the Ch nucleation time in supersaturated model biles is a single-valued function of the Ch A_T over a wide range of conditions. Another important finding has been that Ch–L vesicles are catalytic sites for Ch nucleation.

Acknowledgements

This work was supported by National Science Council (NSC-87-2312-B-259-001), Taiwan, ROC and the National Institute of Health (DK 32472), USA.

References

[1] M.C. Carey, D.M. Small, The physical chemistry of cholesterol solubility in bile, J. Clin. Invest. 61 (1978) 998–1026
[2] M.C. Carey, Critical tables for calculating the cholesterol saturation of native bile, J. Lipid Res. 19 (1978) 945–955
[3] W.H. Admirand, D.M. Small, The physicochemical basis of cholesterol gallstone formation in man, J. Clin. Invest. 47 (1968) 1043–1052
[4] R.H. Dowling, G. Paumgartner, Summary discussion (Section III), Hepatology 12 (1990) 234S–244S.
[5] S. Gallinger, P.R.C. Harvey, C.N. Petrunka, R.G. Ilson, S.M. Strasberg, Biliary proteins and the nucleation defect in cholesterol cholelithiasis, Gastroenterology 92 (1987) 867–875
[6] S. Gallinger, R.D. Taylor, P.R.C. Harvey, S.M. Strasberg, Effect of mucous glycoprotein on nucleation time of human bile, Gastroenterology 89 (1985) 648–658
[7] A.K. Groen, Nonmucous glycoproteins as pronucleating agents, Hepatology 12 (1990) 189S–194S
[8] K.R. Holan, R.T. Holzbach, R.E. Hermann, A.M. Cooperman, W.J. Claffey, Nucleation time: a key factor in the pathogenesis of cholesterol gallstone disease, Gastroenterology 77 (1979) 611–617
[9] Z. Halpern, M.A. Dudley, A. Kibe, M.P. Lynn, A.C. Breuer, R.T. Holzbach, Rapid vesicle formation and aggregation in abnormal human biles: a time-lapse video-enhanced contrast microscopy study, Gastroenterology 90 (1986) 875–885
[10] S.A. Ahrendt, K. Fox-Talbot, H.S. Kaufman, K.D. Lillemore, H.A. Pitt, Cholesterol nucleates rapidly from mixed micelles in the prairie dog, Biochim. Biophys. Acta 1211 (1994) 7–13
[11] D.L. Gantz, D.Q.H. Wang, M.C. Carey, D.M. Small, Cryoelectron microscopy of a nucleating model bile in vitreous ice: formation of primordial vesicles, Biophys. J. 76 (1999) 1436–1451
[12] S. Tao, S. Tazuma, G. Kajiyama, Fatty acid composition of lecithin is a key factor in bile metastability in supersaturated model bile systems, Biochim. Biophys. Acta 1167 (1993) 142–146.
[13] P.H. Lee, D.C.H. Cheng, K. Takayama, W.I. Higuchi, Silicone polymer uptake method for determination of cholesterol thermodynamic activity in model bile systems, J. Pharm. Sci. 77 (1988) 610–614.
[14] W.I. Higuchi, P.H. Lee, K. Takayama, U.K. Jain, N.A. Mazer, Cholesterol monomer activity and its role in understanding cholesterol saturation and crystallization, Hepatology 12 (1990) 88S–93S
[15] Z. Halpern, M.A. Dudley, M.P. Lynn, J.M. Nader, A.C. Breuer, R.T. Holzbach, Vesicle aggregation in model systems of supersaturated bile: relation to crystal nucleation lipid composition of the vesicular phase, J. Lipid Res. 27 (1986) 295–306
[16] A. Kibe, M.A. Dudley, Z. Halpern, M.P. Lynn, A.C. Breuer, R.T. Holzbach, Factors affecting cholesterol monohydrate crystal nucleation time in model systems of supersaturated bile, J. Lipid Res. 26 (1985) 1102–1111
[17] U.K. Jain, W.I. Higuchi, P.H. Lee, C.L. Liu, A rapid method for the measurement of cholesterol thermodynamic activity in bile salt–lecithin–cholesterol solutions, J. Pharm. Sci. 82 (1993) 714–720
[18] C.L. Liu, U.K. Jain, P.H. Lee, N.A. Mazer, W.I. Higuchi, Cholesterol thermodynamic activity, quasielastic light scattering and polarizing microscopy studies in aqueous taurocholate–lecithin solutions supersaturated with cholesterol, J. Colloid Interface Sci. 165 (1994) 411–424
[19] M.T. Subbiah, A. Kuksis, Alkaline solvent systems for thin-layer chromatography of bile acids, J. Lipid Res. 9 (1968) 288–290.

[20] W.S. Singleton, M.S. Gray, M.L. Brown, J.L. White, Chromatographically homogeneous lecithin from egg phospholipids, J. Am. Oil Chem. Soc. 42 (1965) 53–56.

[21] U.K. Jain, W.I. Higuchi, C.L. Liu, P.H. Lee, N.A. Mazer, Cholesterol (thermodynamic) activity determination in bile salt–lecithin–cholesterol systems and cholesterol-rich liquid crystalline mesophase formation, Pharm. Res. 9 (1992) 792–799

[22] C.L. Liu, Cholesterol binding to simple micelles in aqueous bile salt–cholesterol solutions, J. Colloid Interface Sci. 190 (1997) 261–268

[23] D.E. Cohen, M.R. Fisch, M.C. Carey, Principles of laser light-scattering spectroscopy: applications to the physicochemical study of model and native biles, Hepatology 12 (1990) 113S–122S.

[24] N.A. Mazer, Quasielastic light scattering studies of aqueous biliary lipid systems and native bile, Hepatology 12 (1990) 39S–44S.

[25] D.E. Koppel, Analysis of macromolecular polydispersity in intensity correlation spectroscopy: the method of cumulants, J. Chem. Phys. 57 (1972) 4814–4820.

[26] P. Schurtenberger, N. Mazer, W. Kanzig, Micelle to vesicle transition in aqueous solutions of bile salt and lecithin, J. Phys. Chem. 89 (1985) 1042–1049.

[27] C.L. Liu, U.K. Jain, W.I. Higuchi, N.A. Mazer, Quasielastic light scattering and cholesterol thermodynamic activity studies of the micelle-to-vesicle transition in conjugated ursodeoxycholate–lecithin–cholesterol solutions, J. Colloid Interface Sci. 162 (1994) 437–453.

[28] S.M. Strasberg, J.L. Toth, S. Gallinger, P.R.C. Harvey, High protein and total lipid concentration are associated with reduced metastability of bile in an early stage of cholesterol gallstone formation, Gastroenterology 98 (1990) 1–8.

[29] S.M. Strasberg, P.R.C. Harvey, Biliary cholesterol transport and precipitation: introduction and overview of conference, Hepatology 12 (1990) 1S–5S

[30] P.R.C. Harvey, G.A. Upadhya, S.M. Strasberg, Immunoglobulins as nucleating proteins in the gallbladder bile of patients with cholesterol gallstones, J. Biol. Chem. 266 (1991) 13996–14003.

[31] L.J. Lis, W.T. Lis, V.A. Parsegian, R.P. Rand, Adsorption of divalent cations to a variety of phosphatidylcholine bilayers, Biochemistry 20 (1981) 1771–1777

[32] P.F. Levy, B.F. Smith, J.T. LaMont, Human gallbladder mucin accelerates nucleation of cholesterol in artificial bile, Gastroenterology 87 (1984) 270–275.

[33] A. Kibe, R.T. Holzbach, N.F. LaRusso, S.J.T. Mao, Inhibition of cholesterol crystal formation by apolipoproteins in supersaturated model bile, Science 225 (1984) 514–516

[34] T. Ohya, J. Schwarzendrube, N. Busch, S. Gresky, K. Chandler, A. Takabayashi, H. Igimi, K. Egami, R.T. Holzbach, Isolation of a human biliary glycoprotein inhibitor of cholesterol crystallization, Gastroenterology 104 (1993) 527–538

[35] P.R.C. Harvey, G. Somjen, M.S. Lichtenberg, C. Petrunka, T. Gilat, S.M. Strasberg, Nucleation of cholesterol from vesicles isolated from bile of patients with and without cholesterol gallstones, Biochim. Biophys. Acta 921 (1987) 198–204

[36] S.H. Gollish, M.J. Burnstein, R.G. Ilson, C.N. Petrunka, S.M. Strasberg, Nucleation of cholesterol monohydrate crystals from hepatic and gallbladder bile of patients with cholesterol gallstones, Gut 24 (1983) 836–844

[37] A.K. Groen, R. Ottenhoff, P.L.M. Jansen, J. van Marle, G.N.J. Tytgat, Effect of cholesterol nucleation-promoting activity on cholesterol solubilization in model bile, J. Lipid Res. 30 (1989) 51–58

[38] N. Duzgunes, Molecular control of vesicle aggregation and membrane fusion: hypotheses on bile vesicles, Hepatology 12 (1990) 67S–74S

[39] D.Q. Wang, M.C. Carey, Complete mapping of crystallization pathways during cholesterol precipitation from model bile: influence of physical–chemical variables of pathophysiologic relevance and identification of a stable liquid crystalline state in cold, dilute and hydrophilic bile salt-containing systems, J. Lipid Res. 37 (1996) 606–630.

[40] F.M. Konikoff, D.S. Chung, J.M. Donovan, D.M. Small, M.C. Carey, Filamentous, helical, and tubular microstructures during cholesterol crystallization from bile. evidence that cholesterol does not nucleate classic monohydrate plates, J. Clin. Invest. 90 (1992) 1155–1160

[41] D.J. Cabral, D.M. Small, Physical chemistry of bile, in: S.G. Schultz, et al. (Eds.), Handbook of Physiology, The Gastrointestinal System III, Section 6, American Physiological Society, Waverly Press, Baltimore, MD, 1989, pp. 621–662, Chapter 31

[42] A.G. Walton, The Formation and Properties of Precipitates, Interscience, New York, 1967.

[43] N.A. Mazer, M.C. Carey, Quasi-elastic light-scattering studies of aqueous biliary lipid systems: cholesterol solubilization and precipitation in model bile solutions, Biochemistry 22 (1983) 426–442.

[44] R.C. MacDonald, Surface chemistry of phospholipid vesicles relevant to their aggregation and fusion, Hepatology 12 (1990) 56S–60S.

ELSEVIER

Biochimica et Biophysica Acta 1588 (2002) 26–32

BIOCHIMICA ET BIOPHYSICA ACTA
BBA
www.bba-direct.com

3,4-Methylenedioxymethamphetamine ("Ecstasy") induces apoptosis of cultured rat liver cells

Cristina Montiel-Duarte [a], Marta Varela-Rey [a], Juan A. Osés-Prieto [a],
María Jesús López-Zabalza [a], Guadalupe Beitia [b], Edurne Cenarruzabeitia [b], María J. Iraburu [a,*]

[a] *Department of Biochemistry, University of Navarra, C/ Irunlarrea 1, 31008 Pamplona, Navarra, Spain*
[b] *Department of Pharmacology, University of Navarra, Pamplona, Spain*

Received 13 September 2001; received in revised form 23 January 2002; accepted 4 April 2002

Abstract

"Ecstasy" (3,4-methylenedioxymethamphetamine, MDMA) has been shown to be hepatotoxic for human users, but molecular mechanisms involved in this effect remained poorly understood. MDMA-induced cell damage is related to programmed cell death in serotonergic and dopaminergic neurons. However, until now there has been no evidence of apoptosis induced by MDMA in liver cells. Here we demonstrate that exposure to MDMA caused apoptosis of freshly isolated rat hepatocytes and of a cell line of hepatic stellate cells (HSC), as shown by chromatin condensation of the nuclei and accumulation of oligonucleosomal fragments in the cytoplasm. In both cell types, apoptosis correlated with decreased levels of bcl-x_L, release of cytochrome *c* from the mitochondria and activation of caspase 3. In HSC, but not in hepatocytes, MDMA induced poly(ADP-ribose)polymerase (PARP) proteolysis. These results suggest that apoptosis of liver cells could be involved in the hepatotoxicity of MDMA.

© 2002 Elsevier Science B.V. All rights reserved.

Keywords: MDMA; Hepatic stellate cell; Hepatocyte; bcl-2 family protein; Cytochrome *c*; Caspase 3

1. Introduction

3,4-Methylenedioxymethamphetamine (MDMA, "Ecstasy") is a derivative of amphetamine that has become extensively used as a recreational drug. Although MDMA has been popularly considered as a safe drug, there are increasing evidences of its toxicity. MDMA is neurotoxic for serotonergic and dopaminergic neurons and produces a decrease of 5-HT transporters [1,2]. Other side-effects of MDMA are hyperthermia, rhabdomyolysis and cardiac dysrhythmias [3,4]. Severe liver injury and hepatitis in the presence or absence of systemic features have also been described in MDMA users. MDMA hepatotoxicity is idiosyncratic and appears with different intensity, from mild hepatitis that resolves spontaneously, to fulminant liver failure requiring liver transplant. The latency is also variable, raging from days to weeks after the intake [5–9].

Programmed cell death is probably involved in the neurotoxic effects of MDMA, since MDMA induces apoptosis of serotonergic and neocortical neurons [10,11] and immortalized neuron cells [12] through regulation of proteins belonging to the bcl-2 family. However, the underlying mechanisms for the toxic effect of MDMA in liver cells are not fully established yet. MDMA has been shown to produce a decrease in the viability of freshly isolated hepatocytes [13] and to induce collagen production in hepatic stellate cells (HSC) [14]. To our knowledge, the possibility of MDMA exerting an apoptotic effect in liver cells as a mechanism involved in liver damage elicited by this drug, has not been studied until now.

In the present study, the ability of MDMA to induce programmed cell death of freshly isolated rat hepatocytes and a cell line of HSC has been examined. MDMA was found to exert a pro-apoptotic effect in both cell types, as demonstrated by biochemical and morphological parameters.

2. Materials and methods

2.1. Reagents

MDMA–HCl was a gift from the "Audiencia Provincial de Navarra". Tumor necrosis factor α (TNF-α) was from Boehringer Mannheim (Mannheim, Germany); Actinomycin

---

[*] Corresponding author. Tel. +34-48-425-600x6481; fax. +34-48-425-649.

E-mail address: miraburu@unav.es (M.J. Iraburu).

0925-4439/02/$ - see front matter © 2002 Elsevier Science B.V. All rights reserved.
PII: S0925-4439(02)00112-6

D (ActD) was purchased from Sigma (St. Louis, MO); Ac-DEVD-CHO, Hoechst 33342 and camptothecin were from Calbiochem (La Jolla, CA). Cell culture reagents were from Gibco BRL (Grand Island, NY). Poly(ADP-ribose)polymerase (PARP), bcl-x_L polyclonal rabbit and bax monoclonal mouse antibodies were from Santa Cruz Biotechnologies (Santa Cruz, CA). Cytochrome *c* monoclonal antibody was from BD PharMingen.

2.2. Cell culture and treatments

The HSC cell line CFSC-2G [15] was used for some experiments. Cells were cultured in minimum essential medium (MEM) supplemented with 10% fetal bovine serum (FBS) and nonessential amino acids for 36 h; after which the medium was replaced with a serum-free medium. Treatments were carried out 12 h later.

Freshly isolated hepatocytes were obtained by liver collagenase perfusion from male Wistar rats as described elsewhere [16]. Isolated hepatocytes were resuspended and plated in MEM supplemented with 10% FBS and nonessential amino acids. Four hours after platting the cells the medium was replaced by MEM supplemented with 1% FBS, and treatments were carried out 12 h later.

Cells were treated with the indicated concentrations of MDMA for 8 or 24 h. In some experiments hepatocytes were treated with camptothecin (10 μg/ml) or TNF-α (10 ng/ml) for 8 h. Prior to the addition of TNF-α, cells were sensitized by a 30-min pre-treatment with ActD (15 ng/ml).

2.3. Nuclear staining

Cell nuclei were visualized using the DNA-binding fluorochrome Hoechst 33342. Cells were fixed with methanol for 8 min at −20 °C. After washing with PBS, the cells were incubated at room temperature for 5 min with Hoechst 33342 (0.5 μg/ml), gently washed three times with PBS, embedded in glycerol/PBS (1:1) and examined under UV light on a fluorescence microscope Labophot-2 (Nikon).

2.4. Determination of oligonucleosomal (histone-associated) DNA fragments

The presence of soluble histone–DNA complexes, was measured by the Cell Death Detection Assay (Boehringer Mannheim). For this assay, HSC were seeded on 24-well plates at a density of 80,000 cells/well and hepatocytes in 35-mm culture dishes at a density of 3×10^6 cells/dish. In some cell cultures Ac-DEVD-CHO (0.1 mM) was added 3 h before treating hepatocytes and HSC with 1.0 and 5.0 mM MDMA, respectively. Cell death ELISA assays were performed according to the manufacturer's instructions. Specific enrichment of mono- and oligonucleosomes released into the cytoplasm (enrichment factor, EF) was calculated as the ratio between the absorbance values of the samples obtained from treated and control cells.

2.5. Western blot

After treatment with MDMA, cells were washed with PBS and whole-cell lysates were obtained. Equal amounts of protein were size-fractionated by 10% (PARP) or 12% (bcl-x and bax) sodium dodecylsulfate polyacrylamide gel electrophoresis (SDS-PAGE) and electrotransfered to nitrocellulose membranes. The membranes were incubated with anti-PARP, anti-bcl-x polyclonal rabbit or anti-bax monoclonal mouse antibodies, diluted 1:2000; and for 1 h with either anti-rabbit immunoglobulin horseradish peroxidase conjugate (Promega, Madison, WI) or anti-mouse immunoglobulin horseradish peroxidase conjugate (Amersham Pharmacia Biotech), diluted 1:4000. Bound antibodies were detected by enhanced chemiluminiscence autoradiography with ECL-Plus (Amersham Pharmacia Biotech). Equivalent loading was confirmed by Coomasie staining of an identical gel.

Cytochrome *c* was analyzed in cytosolic and mitochondrial fractions obtained by differential centrifugation in 250 mM sucrose buffer as described previously [17]. Five micrograms of protein were subjected to 15% SDS-PAGE. Membranes were exposed to mouse anti-cytochrome *c* monoclonal antibody at a 1:1000 dilution, followed by incubation with anti-mouse immunoglobulin horseradish peroxidase conjugate at a 1:2000 dilution.

2.6. Measurement of caspase 3 activity

Caspase 3 activity was measured using the Caspase-3/CPP32 Colorimetric Assay Kit (BioVision, Palo Alto, CA, USA). Cells (3×10^6 hepatocytes or 2×10^6 HSC) were scraped in culture medium, pelleted, resuspended in lysis buffer and caspase 3 activity was measured following manufacturer's instructions.

2.7. Statistical analysis

The data were analyzed using the Kruskal–Wallis test to determine differences between all independent groups. When significant differences were obtained ($P < 0.05$), differences between two groups were tested using the Mann–Withney *U* test.

3. Results

3.1. MDMA induces morphological changes and chromatin condensation in hepatocytes and HSC

The morphological effects of MDMA on hepatocytes and HSC were first evaluated by light microscopy. Hepatocytes exposed to 1.0 mM MDMA showed an

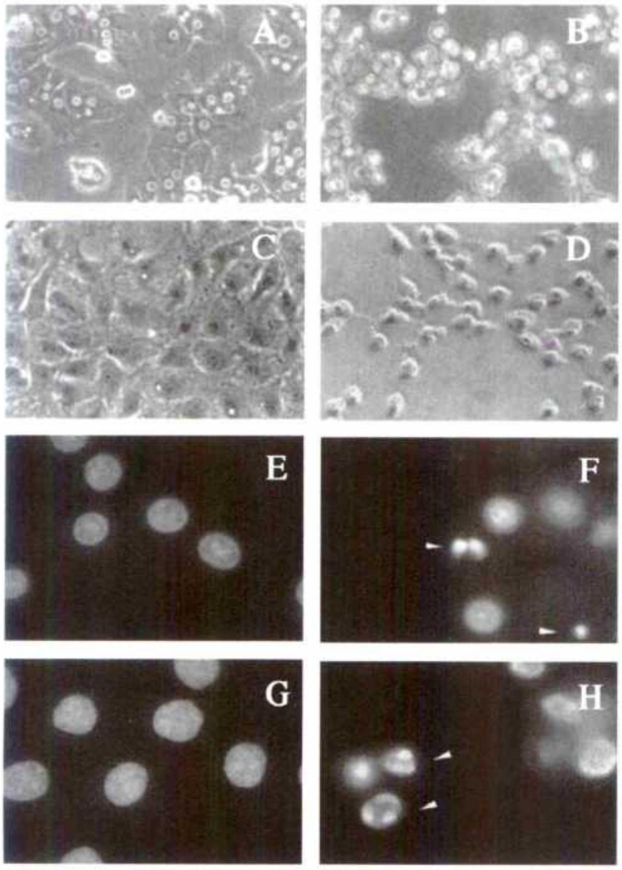

Fig. 1. Morphology of hepatocytes and HSC after treatment with MDMA. (A–D) Morphology by light microscopy of control and MDMA-treated hepatocytes and HSC. Original magnification × 200. (E–H) Nuclear staining of hepatocytes and HSC using Hoechst 33342. Arrowheads point to chromatin condensation and fragmented nuclei in MDMA-treated cells. Original magnification × 1000. (A, E) Control hepatocytes. (B, F) Hepatocytes incubated for 8 h with 1.0 mM MDMA. (C, G) Control HSC. (D, H) HSC incubated for 24 h with 5.0 mM MDMA.

altered morphology 8 h after treatment. As shown in Fig. 1B, MDMA-treated hepatocytes presented loss of membrane differentiations and were highly refringent, as compared to untreated cells. HSC required a longer treatment (24 h) and a higher dose of MDMA (5.0 mM) to show morphological modifications. HSC acquired a netlike disposition and cells became round-shaped and refringent in response to MDMA treatment (Fig. 1D). The concentrations of MDMA used were similar to those described in toxicity studies carried out either in neurons or hepatocytes [11,13].

In order to visualize the nuclei of the cells, preparations of hepatocytes and HSC were subjected to the same treatments as above and stained with Hoechst 33342. In both cell types, MDMA treatment resulted in chromatin condensation and nuclear fragmentation (Fig. 1F and H), alterations commonly associated with programmed cell death [18].

3.2. Accumulation of oligonucleosomal fragments in the cytoplasm of hepatocytes and HSC in response to MDMA treatment

The cytoplasmic levels of DNA (histone-associated) oligonucleosomal fragments in cells treated for 24 h with different concentrations of MDMA were determined. The presence of these fragments in the cytoplasm reflects the extent of DNA fragmentation and nuclear disruption that are characteristic of apoptosis [19].

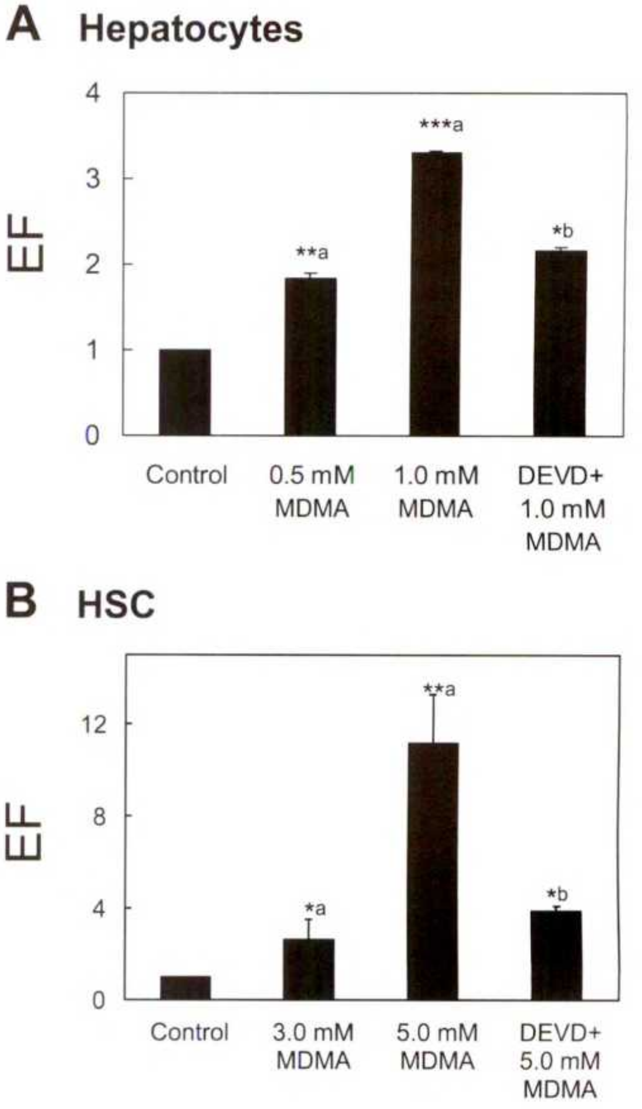

Fig. 2. Determination of oligonucleosomal fragments in cytoplasmic extracts from hepatocytes and HSC treated with MDMA. Hepatocytes and HSC were treated for 24 h with the indicated concentrations of MDMA. Oligonucleosomal fragments content was expressed as EF, as described in Materials and methods. In some cell cultures Ac-DEVD-CHO was added before treating hepatocytes and HSC with 1.0 and 5.0 mM MDMA, respectively. Each bar represents the mean ± S.D. of quadruplicate determinations from at least two independent experiments. (A) EF of hepatocytes treated with MDMA ($^{*}P<0.05$, $^{**}P<0.01$, $^{***}P<0.001$; a, vs. control; b, vs. 1.0 mM MDMA). (B) EF of HSC treated with MDMA ($^{*}P<0.05$, $^{**}P<0.01$; a, vs. control; b, vs. 5.0 mM MDMA).

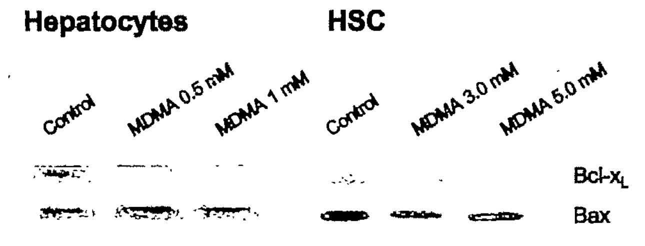

Fig. 3. Western Blot analysis of bcl-x$_L$ and bax in MDMA-treated hepatocytes and HSC. Hepatocytes and HSC were treated for 8 h with the indicated concentrations of MDMA.

As shown in Fig. 2, values of two- to threefold increase in the cytoplasmic content of oligonucleosomal fragments were obtained in hepatocytes treated with 0.5 and 1.0 mM MDMA, and three- to tenfold increase in HSC treated with 3.0 and 5.0 mM MDMA. In some experiments hepatocytes were exposed to higher concentrations of MDMA (3.0 and 5.0 mM), but despite the fact that chromatin condensation and nuclear fragmentation were observed, no significant accumulation of oligonucleosomal fragments was detected (data not shown). A post-apoptotic necrosis resulting in the degradation of the histone–DNA complexes could explain this finding.

The cytoplasmic accumulation of oligonucleosomal fragments was diminished in both cell types by pre-treatment with the inhibitor of the caspase 3 family Ac-DEVD-CHO (Fig. 2), suggesting the involvement of caspases in the cleavage of DNA associated with MDMA-induced apoptosis.

3.3. Bcl-x$_L$ and bax protein levels in hepatocytes and HSC treated with MDMA

Bcl-2 family members are proteins that modulate apoptosis mainly by controlling the release of pro-apoptotic factors from the mitochondrial intermembrane to the cytoplasm [20]. These proteins are regulated by different molecular mechanisms, including changes in protein levels through transcriptional and post-transcriptional alterations. Since MDMA has been shown to modify mRNA levels of bcl-x$_L$ and bax in neurons [11], we studied if these proteins were as well altered in liver cells exposed to the drug.

Protein levels of bcl-x$_L$ and bax were analyzed by Western blot after treating the cells for 8 h with MDMA at the previously tested concentrations (0.5 and 1.0 mM for hepatocytes, and 3.0 and 5.0 mM for HSC). The anti-apoptotic protein bcl-x$_L$ was decreased by MDMA treatment both in hepatocytes and HSC. However, protein levels of bax, a pro-apoptotic member of the bcl-2 protein family, remained unchanged in both cell types after treatment with MDMA (Fig. 3).

3.4. Cytochrome c release, caspase 3 activity and PARP proteolysis in hepatocytes and HSC treated with MDMA

Cytochrome *c* release from the mitochondria has been described as a central event in the stress-induced apoptotic pathway [21]. Cytochrome *c* release leads to the activation of downstream effector caspases, which cleave a number of cellular proteins facilitating DNA fragmentation and cell death [22]. We evaluated by Western blot the cytochrome *c* levels in cytoplasmic and mitochondrial extracts obtained from hepatocytes and HSC treated for 8 h with MDMA, at the concentrations previously indicated. MDMA treatment of both cell types resulted in increased cytosolic levels of cytochrome *c* that correlated with decreased levels of the protein in the mitochondria (Fig. 4). Since cytochrome *c* release has been related to caspase 3 activation [23], we also analyzed the activity of this enzyme in hepatocytes and HSC exposed to MDMA as above, to evaluate its involvement in MDMA-induced apoptosis. In both cell types, MDMA

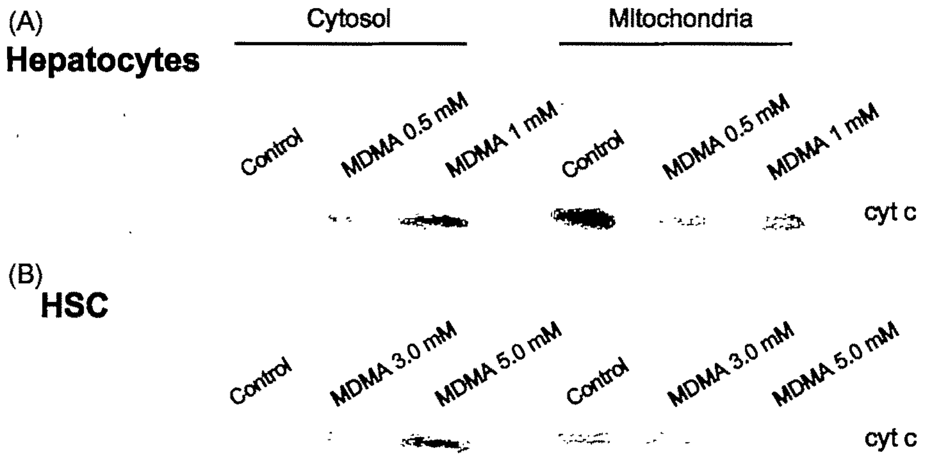

Fig. 4. Cytochrome *c* release from the mitochondria in MDMA-treated hepatocytes and HSC. Cells were treated for 8 h with the indicated concentrations of MDMA and cytosolic and mitochondrial extracts obtained. Western blot analysis using a monoclonal cytochrome c antibody was performed in extracts from hepatocytes (A) or HSC (B).

caused a moderate but significant increase in caspase 3 activity, which was assessed using a commercial colorimetric kit (Fig. 5).

PARP degradation by caspases is considered a biochemical marker for the execution phase of the apoptotic response [24]. PARP cleavage was evaluated in extracts from MDMA-treated cells by the appearance of the 85-kDa proteolytic fragment and the disappearance of the 116-kDa intact PARP, both of them recognized by the same antibody. As Fig. 6B shows, HSC presented an increased degradation of PARP in response to treatment with 3.0 and 5.0 mM MDMA for 8 h. On the contrary, MDMA treatment of primary hepatocytes for 8 h did not result in an increased degradation of PARP, as compared to samples obtained from untreated cells. Two widely used apoptotic inducers, such as camptothecin and ActD/TNF-α [25], also failed to enhance PARP proteolysis in this cell type (Fig. 6A).

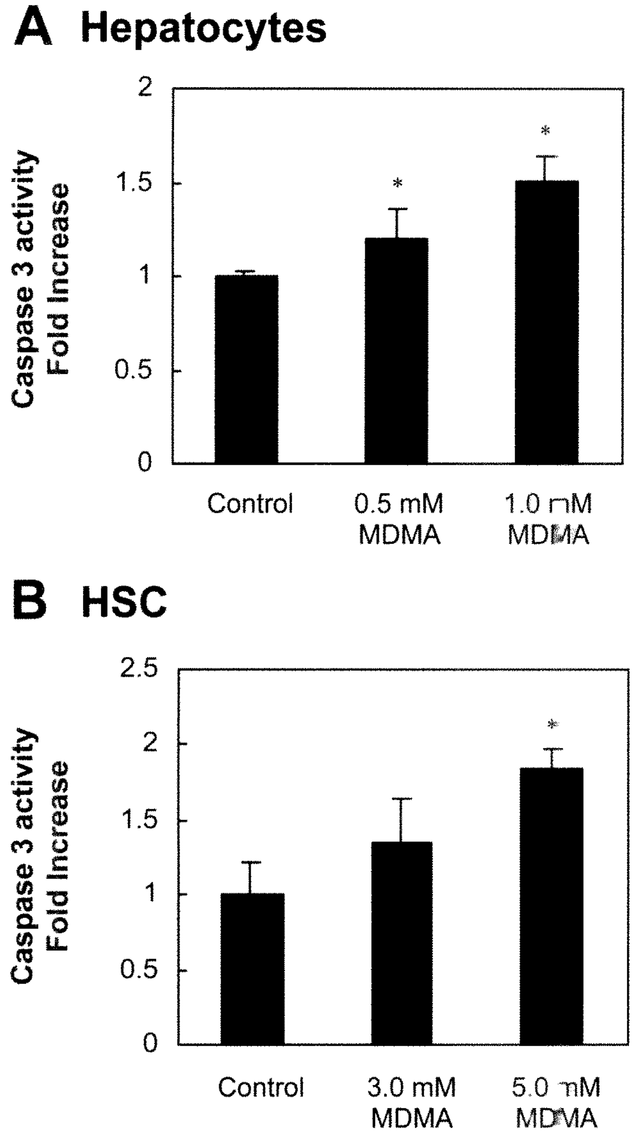

Fig. 5. Caspase 3 activity in hepatocytes and HSC treated with MDMA. Caspase 3 activity was assessed as described in Materials and methods, using 150 μg of protein extracts from hepatocytes (A) or HSC (B), treated with the indicated concentrations of MDMA for 8 h. Activity is referred to control, nontreated cells. Each bar represents the mean ± S.D. of quadruplicate determinations (* $P < 0.05$ vs. control).

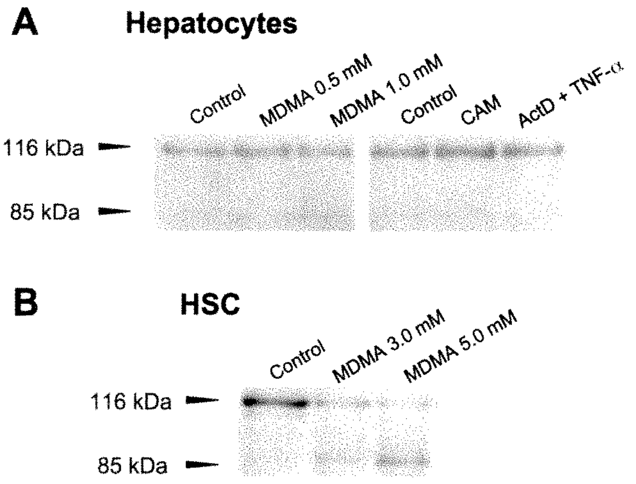

Fig. 6. Western Blot analysis of PARP in MDMA-treated hepatocytes and HSC. Hepatocytes and HSC were exposed for 8 h to treatment with the indicated concentrations of MDMA. Hepatocytes were also treated with camptothecin and ActD/TNF-α, as described in Materials and methods. Arrows indicate the 116-kDa band (intact PARP) and the 85-kDa band (PARP proteolytic fragment) from hepatocytes (A) or HSC (B), treated with the indicated apoptotic inducers.

4. Discussion

Apoptosis is a highly regulated process involved in an array of physiological and pathological responses, including cell damage associated with toxic substances. In the liver, apoptosis has been shown to be responsible for damage induced by endotoxic shock [26], copper accumulation in Wilson's disease [27] and hypoxia/reoxigenation injury [28]. Since MDMA had been described as a pro-apoptotic agent for neurons [10–12], we sought to investigate whether apoptosis of liver cells could contribute to the hepatotoxic effect of this drug, focussing on two of the cell types present in the liver, hepatocytes and HSC. MDMA was found to exert a pro-apoptotic effect in both cell types, as determined by morphological and biochemical alterations commonly associated with programmed cell death, such as chromatin condensation of the nuclei and accumulation of oligonucleosomal fragments in the cytoplasm. The involvement of caspases in the fragmentation of DNA induced by MDMA was demonstrated by pre-treatment of both cell types with the caspase 3 family inhibitor Ac-DEVD-CHO, which significantly prevented the cytoplasmic accumulation of oligonucleosomal fragments in both cell types. This inhibitory effect could be due to the participation of a caspase-activated DNase [29] in the apoptotic action of MDMA.

Previous data have shown that D-amphetamine, a drug structurally related to MDMA, can increase apoptosis in preneoplastic and neoplastic nodules in an animal model for hepatocellular carcinoma [30]. However, as the authors indicate, in these lesions liver cells are already undergoing high constitutive apoptosis as a result of treatment with a chemical agent, and are more sensitive to other substances. Our data show that MDMA is an apoptotic inducer for normal liver cells in the absence of other agents. This fact could be related to the increasing reports of severe liver damage caused by this particular derivative of amphetamine.

Proteins belonging to the bcl-2 family seem to play a key role in the apoptotic response triggered by derivatives of amphetamines. MDMA induces changes in the expression of the splice variants of the bcl-x gene in neurons [11], D-amphetamine increases basal apoptosis of neoplastic liver lesions through dysregulation of bcl-2 family genes [30], and an increased expression of bcl-2 can prevent apoptosis of immortalized neuron cells induced by methamphetamine [12]. Therefore, we sought to investigate whether alterations in the expression of members of the bcl-2 family could also be involved in the apoptotic effect of MDMA in normal liver cells. We found a similar pattern of alterations in the proteins obtained either from hepatocytes or HCS treated with MDMA. The anti-apoptotic member of the bcl-2 family, bcl-x_L, was diminished in MDMA-treated cells, while no changes were elicited by MDMA in the levels of the pro-apoptotic protein bax. Similar results have been described in neurons exposed to MDMA [11]. The fact that MDMA diminished bcl-x_L protein levels pointed out to mitochondria as a target for its pro-apoptotic effect, since bcl-2 family proteins have been shown to modulate the permeabilization of mitochondrial membranes and the subsequent liberation of pro-apoptotic factors such as cytochrome *c* [20]. MDMA treatment caused the release of cytochrome *c* in both cells types, as well as caspase 3 activation, thus suggesting the sequence of events already described for other apoptotic agents: alteration of mitochondrial membranes through changes in bcl-2-like proteins, release of cytochrome *c* and activation of effector caspases. The previously reported role of MDMA as an inductor of cellular oxidative stress [31], could explain these findings because apoptosis caused by redox disruption has been shown to happen in many instances through alterations in mitochondria [32]. PARP is a common substrate of caspases, mainly those belonging to caspase 3 family. In HSC, apoptosis induced by MDMA was accompanied by PARP proteolysis. On the contrary, in primary rat hepatocytes, neither MDMA nor other apoptotic agents such as camptothecin and ActD/TNF-α induced the proteolysis of PARP. In accordance with these findings, some authors find that caspase activation induced by several apoptotic stimuli does not result in proteolysis of PARP in hepatocytes [33,34].

We have previously described that exposure of HSC to MDMA produces a pro-fibrogenic effect, increasing the expression of α1(I) procollagen mRNA [14]. In the present study, higher concentrations of the drug that reduced viability of HSC by inducing programmed cell death were used. Therefore, we can deduce from our previous and present data that there is a double response of HSC to MDMA exposure: induction of either fibrogenesis or programmed cell death, depending on the dose of the drug. These responses could reflect differences between chronic hepatotoxicity or fibrosis and acute liver failure caused by MDMA. However, further investigation is required to determine the correlation between our results, either in hepatocytes or HSC, and the in vivo hepatotoxic action of MDMA. The doses of MDMA used in our cell culture experiments (0.5 to 5.0 mM) are significantly higher than peak plasma levels found in animal models for the neurotoxic effect of MDMA (15 μM) [35], but, to our knowledge, plasma levels of MDMA have not been determined in animal models for MDMA-induced liver damage, and therefore cannot be properly compared. Interestingly, in the aforementioned work MDMA levels in the brain have been found to be higher than plasma levels, reaching values of 0.1–0.25 mM [35]. A similar effect could happen in other target organs for MDMA like the liver. The study of the mechanisms of hepatotoxicity induced by MDMA, both in cellular and animal models, is particularly interesting due to the key role played by the liver as the organ responsible for detoxification.

Acknowledgements

The authors thank E.R. García-Trevijano, M.U. Latasa and M.V. Carretero for generously providing primary hepatocytes. Cristina Montiel-Duarte was supported by a pre-doctoral fellowship from *Gobierno de Navarra*. This work was supported by *Fondo de Investigaciones Sanitarias* (FIS) grant 00/0143.

References

[1] U.D. McCann, Z. Szabo, U. Scheffel, R.F. Dannals, G.A. Ricaurte, Positron emission tomographic evidence of toxic effect of MDMA ("Ecstasy") on brain serotonin neurons in human beings, Lancet 352 (1998) 1433–1437.

[2] T.D. Steele, U.D. McCann, G.A. Ricaurte, 3,4-Methylenedioxymethamphetamine (MDMA, "Ecstasy"): pharmacology and toxicology in animals and humans, Addiction 89 (1994) 539–551.

[3] C.M. Milroy, J.C. Clark, A.R. Forrest, Pathology of deaths associated with "ecstasy" and "eve" misuse, J. Clin. Pathol. 49 (1996) 149–153.

[4] R.T. Miller, S.S. Lau, T.J. Monks, Effects of intracerebroventricular administration of 5-(glutathion-*S*-yl)-alpha-methyldopamine on brain dopamine, serotonin, and norepinephrine concentrations in male Sprague–Dawley rats, Chem. Res. Toxicol. 9 (1996) 457–465.

[5] V. Andreu, A. Mas, M. Bruguera, J.M. Salmeron, V. Moreno, S. Nogue, J. Rodes, Ecstasy: a common cause of severe acute hepatotoxicity, J. Hepatol. 29 (1998) 394–397.

[6] R.S. Dykhuizen, P.W. Brunt, P. Atkinson, J.G. Simpson, C.C. Smith,

Ecstasy induced hepatitis mimicking viral hepatitis, Gut 36 (1995) 939–941.

[7] A.J. Ellis, J.A. Wendon, B. Portmann, R. Williams, Acute liver damage and ecstasy ingestion, Gut 38 (1996) 454–458.

[8] J.A. Henry, K.J. Jeffreys, S. Dawling, Toxicity and deaths from 3,4-methylenedioxymethamphetamine, Lancet 340 (1992) 384–387.

[9] S.I. Khakoo, C.J. Coles, J.S. Armstrong, R.E. Barry, Hepatotoxicity and accelerated fibrosis following 3,4-methylenedioxymetamphetamine ("ecstasy") usage, J. Clin. Gastroenterol. 20 (1995) 244–247.

[10] R. Simantov, M. Tauber, The abused drug MDMA (Ecstasy) induces programmed death of human serotonergic cells, FASEB J. 11 (1997) 141–146.

[11] G. Stumm, J. Schlegel, T. Schafer, C. Wurz, H.D. Mennel, J.C. Krieg, H. Vedder, Amphetamines induce apoptosis and regulation of bcl-x splice variants in neocortical neurons, FASEB J. 13 (1999) 1065–1072.

[12] J.L. Cadet, S.V. Ordoñez, J.V. Ordoñez, Methamphetamine induces apoptosis in immortalized neural cells: protection by the proto-oncogene, bcl-2, Synapse 25 (1997) 176–184.

[13] G. Beitia, A. Cobreros, L. Sainz, E. Cenarruzabeitia, 3,4-Methylenedioxymethamphetamine (ecstasy)-induced hepatotoxicity: effect on cytosolic calcium signals in isolated hepatocytes, Liver 19 (1999) 234–241.

[14] M. Varela-Rey, C. Montiel-Duarte, G. Beitia, E. Cenarruzabeitia, M.J. Iraburu, 3,4-Methylenedioxymethamphetamine ("Ecstasy") stimulates the expression of alpha1(I) procollagen mRNA in hepatic stellate cells, Biochem. Biophys. Res. Commun. 259 (1999) 678–682.

[15] P. Greenwel, J. Rubin, M. Schwartz, E.L. Hertzberg, M. Rojkind, Liver fat-storing cell clones obtained from a CCl_4-cirrhotic rat are heterogeneous with regard to proliferation, expression of extracellular matrix components, interleukin-6, and connexin 43, Lab. Invest. 69 (1993) 210–216.

[16] A.W. Wolkoff, A.C. Samuelson, K.L. Johansen, R. Nakata, D.M. Withers, A. Sosiak, Influence of Cl^- on organic anion transport in short-term cultured rat hepatocytes and isolated perfused rat liver, J. Clin. Invest. 79 (1987) 1259–1268.

[17] J. Yang, X. Liu, K. Bhalla, C.N. Kim, A.M. Ibrado, J. Cai, T.I. Peng, D.P. Jones, X. Wang, Prevention of apoptosis by Bcl-2: release of cytochrome *c* from mitochondria blocked, Science 275 (1997) 1129–1132.

[18] J.F. Kerr, G.C. Gobe, C.M. Winterford, B.V. Harmon, Anatomical methods in cell death, Methods Cell Biol. 46 (1995) 1–27.

[19] A.H. Wyllie, R.G. Morris, A.L. Smith, D. Dunlop, Chromatin cleavage in apoptosis: association with condensed chromatin morphology and dependence on macromolecular synthesis, J. Pathol. 142 (1984) 67–77.

[20] S. Shimizu, M. Narita, Y. Tsujimoto, Bcl-2 family proteins regulate the release of apoptogenic cytochrome *c* by the mitochondrial channel VDAC, Nature 399 (1999) 483–487.

[21] E. Bossy-Wetzel, D.D. Newmeyer, D.R. Green, Mitochondrial cytochrome *c* release in apoptosis occurs upstream of DEVD-specific caspase activation and independently of mitochondrial transmembrane depolarization, EMBO J. 17 (1994) 37–49.

[22] G. Kroemer, B. Dallaporta, M. Resche-Rigon, The mitochondrial death/life regulator in apoptosis and necrosis, Annu. Rev. Physiol. 60 (1998) 619–642.

[23] J. Cai, J. Yang, D.P. Jones, Mitochondrial control of apoptosis: the role of cytochrome *c*, Biochim. Biophys. Acta 1366 (1998) 139–149.

[24] Y.A. Lazebnik, S.H. Kaufmann, S. Desnoyers, G.G. Poirier, W.C. Earnshaw, Cleavage of poly(ADP-ribose) polymerase by a proteinase with properties like ICE, Nature 371 (1994) 346–347.

[25] Y. Xu, B.E. Jones, D.S. Neufeld, M.J. Czaja, Glutathione modulates rat and mouse hepatocyte sensitivity to tumor necrosis factor toxicity, Gastroenterology 115 (1998) 1229–1237.

[26] M. Leist, F. Gantner, I. Bohlinger, G. Tiegs, P.G. Germann, A. Wendel, Tumor necrosis factor-induced hepatocyte apoptosis precedes liver failure in experimental murine shock models, Am. J. Pathol. 146 (1995) 1220–1234.

[27] S. Strand, W.J. Hofmann, A. Grambihler, H. Hug, M. Volkmann, G. Otto, H. Wesch, S.M. Mariani, V. Hack, W. Stremmel, P.H. Krammer, P.R. Galle, Hepatic failure and liver cell damage in acute Wilson's disease involve CD95 (APO-1/Fas) mediated apoptosis, Nat. Med. 4 (1998) 588–593.

[28] S. Shimizu, Y. Eguchi, W. Kamiike, Y. Akao, H. Kosaka, J. Hasegawa, H. Matsuda, Y. Tsujimoto, Involvement of ICE family proteases in apoptosis induced by reoxygenation of hypoxic hepatocytes, Am. J. Physiol. 271 (1996) G949–G958.

[29] M. Enari, H. Sakahira, H. Yokoyama, K. Okawa, A. Iwamatsu, S. Nagata, A caspase-activated DNase that degrades DNA during apoptosis, and its inhibitor ICAD, Nature 391 (1998) 43–50.

[30] M.R. De Miglio, M.R. Muroni, M.M. Simile, D.F. Calvisi, P. Tolu, L. Deiana, A. Carru, G. Bonelli, F. Feo, R.M. Pascale, Implication of Bcl-2 family genes in basal and D-amphetamine-induced apoptosis in preneoplastic and neoplastic rat liver lesions, Hepatology 31 (2000) 956–965.

[31] J.L. Cadet, N. Thiriet, J. Subramanian, Involvement of free radicals in MDMA-induced neurotoxicity in mice, Ann. Med. Interne (Paris) 152 (2001) 57–59.

[32] J. Chandra, A. Samali, S. Orrenius, Triggering and modulation of apoptosis by oxidative stress, Free Radic. Biol. Med. 29 (2000) 323–333.

[33] R.A. Jones, V.L. Johnson, R.H. Hinton, G.G. Poirier, S.C. Chow, G.E. Kass, Liver poly(ADP-ribose)polymerase is resistant to cleavage by caspases, Biochem. Biophys. Res. Commun. 256 (1999) 436–441.

[34] R.A. Jones, V.L. Johnson, N.R. Buck, M. Dobrota, R.H. Hinton, S.C. Kass, G.E. Kass, Fas-mediated apoptosis in mouse hepatocytes involves the processing and activation of caspases, Hepatology 27 (1998) 1632–1642.

[35] T. Chu, Y. Kumagai, E.W. DiStefano, A.K. Cho, Disposition of methylenedioxymethamphetamine and three metabolites in the brains of different rat strains and their possible roles in acute serotonin depletion, Biochem. Pharmacol. 51 (1996) 789–796.

ELSEVIER

Biochimica et Biophysica Acta 1588 (2002) 33–40

BIOCHIMICA ET BIOPHYSICA ACTA
BBA
www.bba-direct.com

Telethonin protein expression in neuromuscular disorders

Mariz Vainzof[a,*], Eloisa S. Moreira[a], Oscar T. Suzuki[a], Georgine Faulkner[b], Georgio Valle[c], Alan H. Beggs[d], Olli Carpen[e], Alberto F. Ribeiro[a], Edmar Zanoteli[f], Juliana Gurgel-Giannetti[g], Ana Maria Tsanaclis[h], Helga C.A. Silva[h], Maria Rita Passos-Bueno[a], Mayana Zatz[a]

[a]*Center for the Study of the Human Genome, Department Biology, IBUSP, University of Sao Paulo, R. do Matão, 277, sala 220-Cidade Universitária, São Paulo, SP-CEP 05508-900, Brazil*
[b]*International Center for Genetic Engineering and Biotechnology, Tieste, Italy*
[c]*CRIBI Biotechnology Center, Universitá degli Studi de Padova, via Ugo Bassi 58b, I-35121, Padova, Italy*
[d]*Division of Genetics, Children's Hospital, Harvard Medical School, Boston, USA*
[e]*University of Helsinki, Helsinki, Finland*
[f]*Department of Neurology, UNIFESP, São Paulo, Brazil*
[g]*Department of Neurology, FMUSP, São Paulo, Brazil*
[h]*Department of Pathology, FMUSP, São Paulo, Brazil*

Received 30 October 2001; received in revised form 6 February 2002; accepted 4 April 2002

Abstract

Telethonin is a 19-kDa sarcomeric protein, localized to the Z-disc of skeletal and cardiac muscles. Mutations in the telethonin gene cause limb–girdle muscular dystrophy type 2G (LGMD2G). We investigated the sarcomeric integrity of muscle fibers in LGMD2G patients, through double immunofluorescence analysis for telethonin with three sarcomeric proteins: titin, α-actinin-2, and myotilin and observed the typical cross striation pattern, suggesting that the Z-line of the sarcomere is apparently preserved, despite the absence of telethonin. Ultrastructural analysis confirmed the integrity of the sarcomeric architecture. The possible interaction of telethonin with other proteins responsible for several forms of neuromuscular disorders was also analyzed. Telethonin was clearly present in the rods in nemaline myopathy (NM) muscle fibers, confirming its localization to the Z-line of the sarcomere. Muscle from patients with absent telethonin showed normal expression for the proteins dystrophin, sarcoglycans, dysferlin, and calpain-3. Additionally, telethonin showed normal localization in muscle biopsies from patients with LGMD2A, LGMD2B, sarcoglycanopathies, and Duchenne muscular dystrophy (DMD). Therefore, the primary deficiency of calpain-3, dysferlin, sarcoglycans, and dystrophin do not seem to alter telethonin expression.

© 2002 Elsevier Science B.V. All rights reserved.

Keywords: Telethonin; Limb–girdle muscular dystrophy; Limb–girdle muscular dystrophy type 2G; Neuromuscular disorder; Muscular dystrophy; Protein study

---

1. Introduction

The limb–girdle muscular dystrophies (LGMDs) include a heterogeneous group of progressive disorders mainly affecting the pelvic and shoulder girdle musculature. The inheritance may be autosomal dominant (LGMD1) or recessive (LGMD2). Clinically, it ranges from severe forms with onset in the first decade and rapid progression, to milder forms with later onset and slower progression [1,2].

Six autosomal dominant LGMD forms, designated LGMD1A to LGMD1F, were already mapped respectively at 5q22–q34 (myotilin) [3,4], 1q11–21 (lamin A/C [5]), 3p25 (caveolin-3 [6,7], 6q23, 5q31, and 7q (neuromuscular disorders—gene location, September 2001). At present, nine AR forms have been mapped and, with the exception of LGMD2H at 9q31–33 [8] and LGMD2I at 19q13.3 [9], all the others have had their protein products identified. Four of them, mapped at 17q21, 4q12, 13q12, and 5q33, encode respectively for α-sarcoglycan (α-SG), β-SG, γ-SG, and δ-SG, which are glycoproteins of the sarcoglycan sub-complex of the dystrophin–glycoprotein complex (DGC), which plays an important role in muscle fiber integrity [10,11]. Mutations in these genes cause, respectively, LGMD2C, 2D,

---

* Corresponding author. Tel.: +55-11-30917966x226; fax: +55-11-30917966x229.
E-mail address: mvainzof@usp.br (M. Vainzof).

0925-4439/02/$ - see front matter © 2002 Elsevier Science B.V. All rights reserved.
PII: S0925-4439(02)00113-8

2E, and 2F and constitute a distinct subgroup of LGMDs, the sarcoglycanopathies [12–23]. The three other identified forms are LGMD2B at 2p31, coding for dysferlin [24–26]; LGMD2A at 15q15.1, coding for calpain-3 [27–29] and LGMD2G at 17q11–12, coding for telethonin [22,23]. In addition to the mechanical and structural function of the DGC, it has been recently shown that this complex might play a role in cellular communication [30] as well as interact with the sarcomeric network, through the binding of dystrophin to F-actin [see revision in [31]].

Telethonin is a sarcomeric protein of 19 kDa possibly localized to the Z-disc of adult striated skeletal and cardiac muscles, where it interacts with the protein titin [32]. The sarcomere is the unit of skeletal and cardiac muscle contraction. In the past few years, there have been major advances in the elucidation of the role of skeletal and cardiac muscle proteins, and mutations in several sarcomeric proteins such as actin [33], tropomosin 3 and 2 [34,35], Troponin T1 [36], and myotilin [4] were shown to cause human muscle diseases.

Recently, we have shown that mutations in the telethonin gene cause LGMD2G, a relatively mild form of autosomal recessive LGMD, originally mapped in three Brazilian families. This was confirmed through immunohistochemistry and Western blot analysis using an anti-telethonin antibody in muscle of affected patients that presented no protein expression [22,23].

The protein α-actinin is localized in the Z-disk of the sarcomere [37], while the recently identified myotilin is a 57-kDa cytoskeletal protein, with two Ig-like domains homologous to titin, which co-localizes with α-actinin in the Z-line of the sarcomere [3].

Here, we are reporting the results from

(a) The analysis of the sarcomeric structure of muscle fibers in patients with LGMD2G, through double co-localization immunofluorescence for telethonin with the Z-band proteins α-actinin-2 and myotilin, as well as through electron microscopy (EM) analysis.
(b) The possible interaction of telethonin with other proteins associated with several forms of AR-LGMD (2A, 2B, SGpathies), Duchenne muscular dystrophy (DMD), nemaline myopathy (NM), and spinal muscular atrophy (SMA).

2. Patients and methods

2.1. Patients

A total of 42 myopathic patients with known mutations were included in this investigation: 6 LGMD2G (4 families), 9 LGMD2A, 14 LGMD2B, 2 LGMD2C, 3 LGMD2D, 2 LGMD2E, 1 LGMD2F, 3 DMD, and 2 NM. One of the LGMD2G patients was identified through telethonin analysis in a sample of 48 patients: 35 still unclassified LGMD patients and 13 with clinical diagnosis of Kugelberg–Welander SMA. Telethonin was also studied in 2 muscle samples from patients with known mutations in the SMA gene, for analysis of muscle under denervation.

The diagnosis of the patients was established through clinical examination and course of the disease, family history, serum creatine-kinase levels [3], DNA analysis (linkage or screening for mutations), and/or protein studies on muscle biopsies (dystrophin, the four sarcoglycans, calpain-3, dysferlin, and telethonin).

2.2. Muscle biopsies

Muscle samples were obtained from bicep biopsies (for diagnostic purposes or after informed consent) frozen in liquid nitrogen immediately after removal and stored at − 70 °C until use. Routine histological and histochemical procedures were done, with staining for HE, modified Gomori trichrome, NADH, ATPase 9.4, 4.3, and acid and alkaline phosphatase [38]. One female patient (Table 1, #2) underwent two muscle biopsies within a 10 year interval.

The fiber typing was determined by counting 300–500 fibers from each patient in ATPase 9.4 and 4.3 reactions, and by calculating the percentage of type I and type II fibers.

2.3. Protein analyses

Mouse anti-telethonin antibody was raised against a recombinant fragment of telethonin consisting of 128 C-terminus amino acids [39]. Additional antibodies used were: mouse anti-titin (Novacastra and Sigma), rabbit α-actinin-2 [37], rabbit myotilin antibody [4], rabbit polyclonal N-terminal 303-8 for dystrophin (kindly provided by J. Cham-

Table 1
Clinical and molecular data of the LGMD2G patients at time of biopsy

Patients (biopsy number)	Family	Age	CK (fold ↑)	Clinical stage (maximal motor ability)	Pattern of weakness (proximal/distal)	Mutation (telethonin gene)
1 (206)	1	male 17	13	walks, climbs stairs assisted	proximal	157C>T/157C>T
2A (207) (biopsy 1)	1	female 18	6	asymptomatic	–	157C>T/157C>T
2B (912) (biopsy 2)		female 28		walks, climbs stairs unassisted	proximal	
3 (913)	1	female 22		walks, climbs stairs unassisted	distal	157C>T/157C>T
4 (201)	2	female 30	15	walks, climbs stairs unassisted	proximal	157C>T/157C>T
5 (208)	3	male 21	3	walks, climbs stairs assisted	distal	157C>T/D637GGGG
6 (927)	4	male 27	20	walks, can not climb stairs	distal and proximal	157C>T/157C>T

Table 2
Histological and histochemical data in the 7 studied biopsies, from 6 LGMD2G patients

Patients	Histology							ATPase	
	Size variation	Connective tissue	Central nuclei	Spliting	Hyaline fibres	Macrophagic fibres	Rimmed vacuoles	Type I/II (%)	Atrophy
1	+++	+	+++	+++	0	2/500	1/500	55/45	type I
2A	++	0	+	+	0	2/200	0	52/48	type I
2B	++	+	+	+	0	2/200	0	62/38	type I
3	++	0	+	0	0	1/500	3/500	80/20	type I
4	+++	+	+++	+++	0	0	8/500	66/34	type I
5	+++	+	+++	+++	1/250	5/250	10/80	44/56	type I
6	++	0	++	++	1/300	3/500	0	12/88	type II

berlain) and C-terminal monoclonal Dy8/6C5 for dystrophin (kindly provided by L.V.B. Anderson), monoclonal antibodies for sarcoglycans (described in Ref. [40]), calpain-3 [41], and dysferlin [42].

Immunohistochemical staining of frozen sections was performed using double labeling reactions for α-actinin-2 and telethonin, titin or myotilin and analyzed by fluorescence or confocal microscopy (IBUSP), as described previously [43]. Secondary antibodies were FITC-labeled anti-rabbit and CY3-conjugated anti mouse (Sigma).

Western blot analysis was performed using 6% or 13% SDS-PAGE gels, and then proteins were transferred at 150 V for 1 h [44]. The blots were reacted with antibodies to telethonin or a mix of dystrophin, dysferlin, and calpain-3. The incubations with primary antibodies were done overnight, and the detection was done using alkaline phosphatase-conjugated second antibody.

3. Results

3.1. LGMD2G patients

The results of the clinical and histological analysis done in the six LGMD2G patients are described in Table 1. With exception of patient 5, who is a compound heterozygote (157C>T/Δ637GG), the others have the same homozygous 157C>T missense mutation, which creates a premature stop codon (Q53X) in the telethonin gene.

3.1.1. Histological analysis

Histological analysis showed a dystrophic pattern of muscle degeneration in all six patients, including fiber size variation, slight degree of connective tissue infiltration, presence of high number of internally localized nuclei, splitting, and a variable degree of rimmed vacuoles (Table 2 and Fig. 1). Only one patient (927) showed the presence of spread ghost fibers (see HE in Fig. 4).

Histochemical analysis revealed the presence of a mosaic pattern of type I/II fibers, with a type I predominance in two patients (#3 and 4) and type II predominance in patient 6. Small groups of fibers from the same type were observed in three patients (#1, 2, 5), a type I fiber atrophy in five patients (#1–5), while patient 6 showed type II atrophy (Table 2).

Patient #2, underwent a second muscle biopsy after 10 years, and the same anatomopathological alterations, with a very similar degree of muscle degeneration, were seen in both samples. The only observed difference was in type I/II fiber proportions, with an increase in type I predominance.

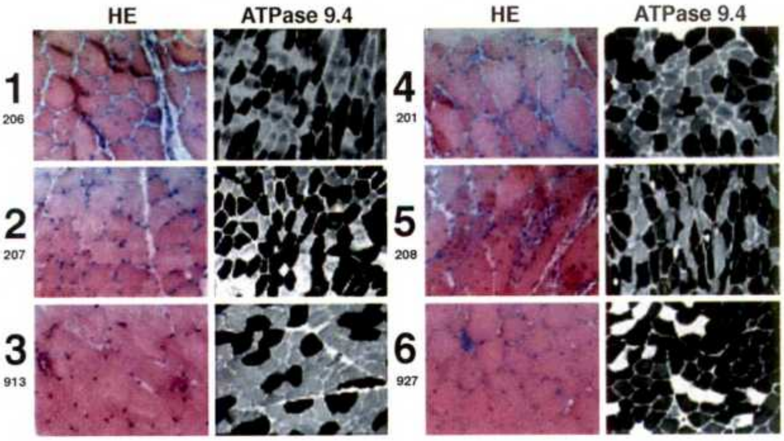

Fig. 1. Histological analysis (Hematoxilin & Eosin staining) and histochemical analysis (ATPase 9.4) in the 6 LGMD2G patients. Magnification: HE × 200, ATPase × 100.

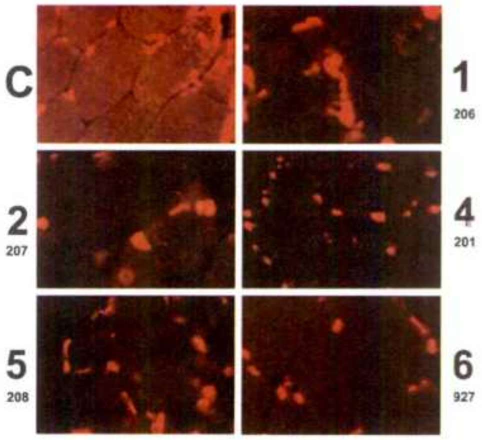

Fig. 2. Immunofluorescence analysis using anti-telethonin antibodies in LGMD2G patients, as compared to a normal control. Magnification: × 400.

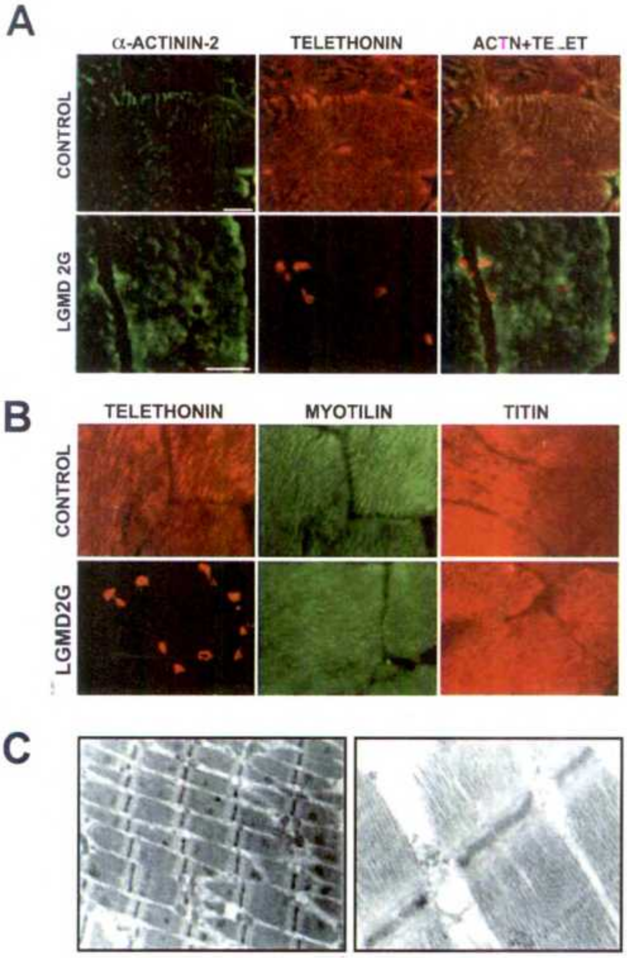

Fig. 3. (A) Double immunofluorescence for α-actinin-2 and telethonin in a normal control and in one LGMD2G patient (#2); (B) double IF for myotilin and telethonin, and the homogeneous reaction for titin (sigma antibody); (C) EM of the same sample of muscle, showing the maintenance of the sarcomeric structure (× 40,000).

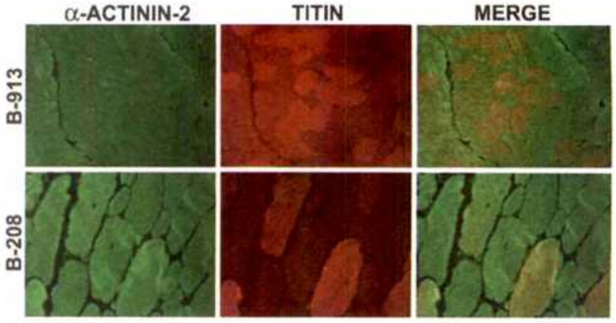

Fig. 4. Double immunofluorescence of α-actinin-2 and titin (Novacastra antibody) in two LGMD2G patients, showing the positive titin pattern with a mosaic of type II fibres with higher labeling for titin (magnification: × 200).

3.1.2. Immunohistochemical analysis

In normal controls, telethonin immunofluorescence analysis showed a strong sarcomeric labeling pattern, with the majority of myonuclei also positively labeled (Fig. 2). Both type I and type II fibers were equally labeled.

Muscle from all 6 LGMD2G patients showed a total absence of telethonin in the sarcomeric network, but some labeling in the nucleus (Fig. 2). Double immunofluorescence analysis for α-actinin 2 and telethonin showed a cross-striation pattern in muscle fibers with the first antibody but no labeling with the second one (Fig. 3A). Myotilin IF analysis also showed a sarcomeric pattern in their muscle fibers (Fig. 3B).

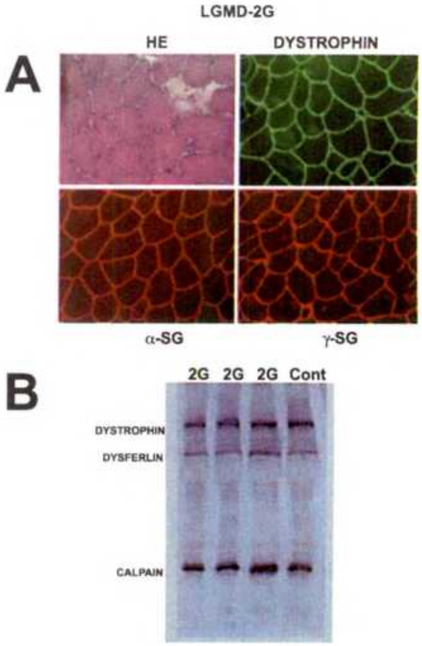

Fig. 5. Immunohistochemical analysis for dystrophin and two sarcoglycans, as well as multiplex western blot for dystrophin, dysferlin and calpain-3 in the LGMD2G patients, showing normal distribution and quantity of the proteins.

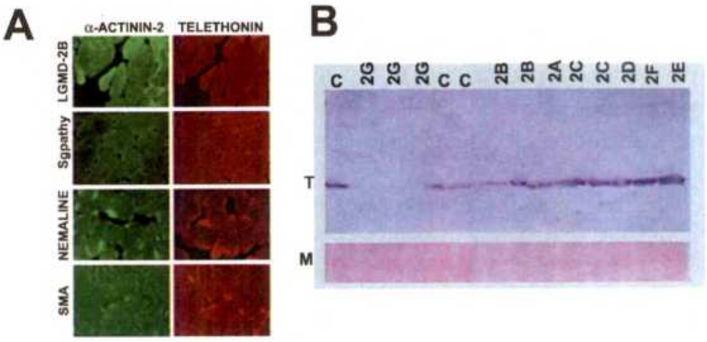

Fig. 6. (A) Double Telethonin and α-actinin-2 analysis in patients with other forms of MD (LGMD2B and sarcoglycanopathy 2D), in a patient with nemaline myopathy, showing the high concentration of telethonin in the rods, and the normal distribution of telethonin in a SMA patient. (B) Western blot analysis in some other forms of LGMD, as compared to control (C) and LGMD2G patients. T = Telethonin; M = myosin content in the ponceau pre-stained blot.

The analysis of titin through two antibodies showed a positive IF pattern with both in LGMD2G patients (Fig. 3), with a mosaic pattern of more positively labeled type II fibers through the antibody from Novacastra (Fig. 4).

Analysis for sarcolemmal proteins showed normal expression of dystrophin, sarcoglycans, dysferlin, and calpain-3 proteins in the LGMD2G patients (Fig. 5).

3.1.3. Ultrastructural analysis

Ultrastructural analysis confirmed the maintenance of the sarcomeric architecture integrity in the LGMD2G patients (Fig. 3C).

3.2. Other forms of neuromuscular disorders

The analysis of telethonin on muscle biopsies from patients with LGMD2A, LGMD2B, SGpathies, and DMD showed a positive sarcomeric pattern in all and a band of the expected MW by Western blot analysis (Fig. 6B). In addition, in muscle fibers from patients with NM, telethonin was clearly present in the rods while in SMA patients, also a normal telethonin IF pattern was observed (Fig. 6A).

4. Discussion

Mutations in the telethonin gene are apparently rare. As stated in our previous report, although the Brazilian population is highly miscigenated, an identical haplotype associated with the mutation 157C>T was found in three of the four families, suggesting a founder effect [23].

Telethonin, which is the 12th most abundant nuclear transcript in adult skeletal muscle [39], has been shown to be one of the substrates of titin, the giant 3–4 MDa sarcomeric protein. Titin acts as a molecular ruler for the assembly of the sarcomere by providing spatially defined binding sites for other sarcomeric proteins over the entire length of the half-sarcomere [45]. After its activation through phosphorylation and Ca^{2+}/calmodulin binding, titin was shown to phosphorylate the C-terminal domain of telethonin [46]. In addition, it was suggested that the N-terminal region of titin could adopt a closed conformation, which would block the telethonin binding site. In vivo, phosphorylation of the multiple serine–proline phosophorylation sites by developmentally controlled kinases could be the modulation factor controlling titin–telethonin interactions [32].

Telethonin also has putative phosphorylation sites in its C-terminal region [39], and the dual phosphorylation of both titin and telethonin might be important in controlling the interaction of both proteins. The mutations identified in our LGMD2G patients lead to the disruption of this functionally important region of telethonin [23], resulting in the absence of the telethonin protein in muscle fibers from all six studied LGMD2G patients. However, titin was clearly retained, as observed through the positive pattern on IF. Only one titin gene has been identified in the human genome. This gene has several isoforms produced by alternative splicing which are responsible for individual diversity of distribution in human muscles [47]. Therefore, the mosaic pattern of titin observed in our patient with a monoclonal titin antibody could reflect the recognition of an epitope in the C-terminal region, in a similar way to the one seen with myosin isoforms and fiber typing, although the possibility that the differential staining could be due to the accessibility of the epitopes rather than truly differentially expressed isoforms cannot be ruled out.

In cardiac myocytes, it has been shown that both the titin Z1–Z2 domains and telethonin (titin-cap) are required for the structural integrity of sarcomeres. A severe myofibril disruption is observed after over expression of either molecule, suggesting that their interaction is critical in titin filament-regulated sarcomeric assembly [32]. In our LGMD2G patients, immunofluorescence analysis for α-actinin-2 and myotilin, two proteins from the Z-disk of the sarcomere, showed a cross-striation pattern, suggesting that at least part of this myofibrilar structure is retained. Ultrastructural analysis confirmed the maintenance of the sarcomeric architecture in our telethonin deficient patients. These observations suggest that muscle degeneration and weakness in LGMD2G patients with null mutations in the telethonin gene are more likely to occur due to a functional defect than to an alteration in the sarcomeric structure. On the other hand, the presence of rimmed vacuoles in the muscle fibers from these patients might be due to focal regions of sarcomeric degeneration.

Mues et al. [45] demonstrated that telethonin localizes to the nascent Z-disk in cultured myocytes. Here, the analysis of muscle fibers from patients with NM demonstrated that telethonin was clearly present in the rods, which are formed by proteins from the Z-band of the sarcomere [48]. Therefore, the presence of telethonin in the rods as well as its co-localization with α-actinin and myotilin confirm the presence of telethonin in the Z-disk also in the mature muscle.

In our previous report, we have shown an identical haplotype associated with the mutation 157C>T in three of the four LGMD2G families. Families 1 and 2 (Table 2) are inbreed and of Negroid descent, while both parents in family 3, in which the mutation is in homozygosity, have Italian ancestry [23]. Therefore, although these three families apparently have distinct origin, our population is highly miscigenated and the finding of a common haplotype in them suggests a founder effect in Brazil.

4.1. Histological characterization of LGMD2G patients

In the first histopathological description of patients with LGMD2G, muscle biopsies showed the presence of a high number of rimmed vacuoles [49]. The analysis of four additional LGMD2G patients revealed that although present in the majority of muscle samples, the rimmed vacuoles were not the predominant histopathological marker of this disease. A high variability in the degree of muscle degeneration was observed among the six patients, which did not appear to be correlated to the clinical course.

Interestingly, the analysis of a new muscle biopsy sample of a female patient who was asymptomatic when the first biopsy was taken, but clearly affected 10 years later, showed very few pathological alterations, suggesting that no gross muscle degeneration occurs with time in telethonin-deficient patients.

Muscle fiber composition showed a variability of fiber typing. Five of the patients had a significant type I predominance, while in one patient, a very high type II predominance was observed, thus suggesting no direct correlation with the primary gene defect. As observed in the present patients, small areas of atrophy and fiber type predominance are characteristic of denervation. However, this can also be the result of the splitting of larger fibers, which is very common in the dystrophic process [38]. Therefore, caution should be taken in interpreting these type of results.

The analysis of the amount of the telethonin transcript in a number of mice muscles of different types, including slow-twitch postural (soleus) and fast-twitch (EDL) muscles, showed that there is no statistically different levels of expression between muscle of different fiber type composition [50]. In the present study, both type I and type II of human mature fibers expressed the same pattern of telethonin. Therefore, the apparent increase in proportion of type I fibers in five of the six patients (and also common in congenital myopathies [38]) appears not to be related to a preferential expression of telethonin in a specific type of fiber.

On the other hand, in one family, only proximal weakness occurred, while in three families, both distal and proximal involvement were observed. A mixed pattern of proximal and distal pattern of weakness may also be present in other forms of LGMD, such as the proximal LGMD2B and distal Miyoshi Myopathy, both associated with mutations in the dysferlin gene [25,26].

4.2. Denervation

Mason et al. [50] have shown that the mouse telethonin transcript is down-regulated in response to denervation. Short-term denervation (2 days) was sufficient to lead to a 50% fall in the level of telethonin in the muscle of the denervated animals, suggesting that innervation and/or muscular activity was necessary for the maintenance of telethonin expression. Our analysis of telethonin in muscle biopsies from SMA patients (genetically denervated) showed a sarcomeric pattern of labeling which did not differ from normal controls, suggesting no telethonin alteration in these cases.

4.3. Interactions

In our first studies, the observation of normal dystrophin and α-sarcoglycan staining in the muscle of LGMD2G patients [23] would indicate that the product of this gene apparently did not interact with the DGC. Here, we confirm that muscle from patients with LGMD2G showed normal expression of dystrophin, the four sarcoglycans, dysferlin and calpain-3. In addition, the analysis of telethonin on muscle biopsies from patients with LGMD2A, LGMD2B, SGpathies, and DMD showed normal localization, suggesting that the deficiencies of calpain-3, dysferlin, sarcoglycans, and dystrophin do not seem to alter telethonin expression.

4.4. Differential diagnosis

Since our LGMD2G patients showed a broad range of phenotypes, ranging from Kugelberg–Wellander-like to typical LGMD, we screened for telethonin deficiency in muscle biopsies from 48 patients with these phenotypes, in an attempt to identify additional cases of LGMD2G. One additional patient (#5), with a total deficiency of telethonin was detected. Complementary DNA studies detected homozygosity for the 157C>T/157C>T mutation in his telethonin gene.

In a recent report from our Center, we studied a total of 153 LGMD families (118 classified and 35 unclassified) by DNA and protein analysis [51]. Considering that in four of these families the patients are affected by LGMD2G, the frequency of telethonin deficiency is estimated as approximately 2.5% of all cases of LGMD in our population.

In conclusion, our data show that muscles from patients with LGMD2G have a normal expression for the proteins dystrophin, sarcoglycans, dysferlin, calpain-3, and titin, and the primary deficiencies of that proteins do not seem to alter telethonin expression. The observed maintenance of the sarcomeric architecture suggests that the primary absence of telethonin apparently has no effect on the formation and composition of the sarcomere in the LGMD2G patients.

Acknowledgements

We are very grateful to the following researchers for kindly supplying us with antibodies: Dr. L.V.B. Anderson, Dr. J. Chamberlain, Dr. L.M. Kunkel, Dr. C. Bonnemann, Dr. E.E. McNally, and V. Nigro. We also wish to thank Marta Canovas, for the excellent technical assistance. The collaboration of the following persons is also gratefully acknowledged: Dr. Rita C.M. Pavanello, Dr. Ivo Pavanello Filho, Flavia de Paula, Cleber S. Costa, Viviane P. Muniz, Antonia Cerqueira, Constância G. Urbani, and all the physicians who referred affected patients. G. Faulkner and G. Valle were supported by Fondazione Telethon (Italy), grant numbers 1278 and B.41, respectively. This work was supported by grants from Fundação de Amparo à Pesquisa do Estado de São Paulo (FAPESP-CEPID), Conselho Nacional de Desenvolvimento Científico e Tecnológico (CNPq), PRONEX, International Atomic Energy Agency (IAEA), and Associação Brasileira de Distrofia Muscular (ABDIM).

References

[1] R.W. Shields, Limb girdle syndromes, in: A.G. Engel, B.Q. Banker (Eds.), Myology, vol. II, Mc Graw-Hill, USA, 1986.

[2] K.M.D. Bushby, J.S. Beckmann, Diagnostic criteria for the limb–girdle muscular dystrophies: report of the ENMC workshop on limb–girdle muscular dystrophies, Neuromuscul. Disord. 5 (1995) 71–74.

[3] P. Salmikangas, O.M. Mykkanen, M. Gronholm, L. Heiska, J. Kere, O. Carpen, Myotilin, a novel sarcomeric protein with two Ig-like domains, is encoded by a candidate gene for limb–girdle muscular dystrophy, Hum. Mol. Genet. 8 (1999) 1329–1336.

[4] M.A. Hauser, S.K. Horrigan, P. Salmikangas, U.M. Torian, K.D. Viles, R. Dancel, R.W. Tim, A. Taivainen, L. Bartoloni, J.M. Gilchrist, J.M. Stajich, P.C. Gaskell, J.R. Gilbert, J.M. Vance, M.A. Pericak-Vance, O. Carpen, C.A. Westbrook, M.C. Speer, Myotilin is mutated in limb girdle dystrophy 1A, Hum. Mol. Genet. 9 (2000) 2141–2147.

[5] G. Bonne, E. Mercuri, A. Muchir, A. Urtizberea, H.M. Becane, D. Recan, L. Merlini, M. Wehnert, R. Boor, U. Reuner, M. Vorgerd, E.M. Wicklein, B. Eymard, D. Duboc, I. Penisson-Besnier, J.M. Cuisset, X. Ferrer, I. Desguerre, D. Lacombe, K. Bushby, C. Pollitt, D. Toniolo, M. Fardeau, K. Schwartz, F. Muntoni, Clinical and molecular genetic spectrum of autosomal dominant Emery–Dreifuss muscular dystrophy due to mutations of the lamin A/C gene, Ann. Neurol. 48 (2000) 170–180.

[6] C. Minetti, F. Sotgia, C. Bruno, P. Scartezzini, P. Broda, M. Bado, E. Masetti, M. Mazzocco, A. Egeo, M.A. Donati, D. Volonte, F. Galbiati, G. Cordone, F.D. Bricarelli, M.P. Lisanti, F. Zara, Mutations in the caveolin-3 gene cause autosomal dominant limb–girdle muscular dystrophy, Nat. Genet. 18 (1998) 365–368.

[7] E.M. McNally, E.S. Moreira, D. Duggan, C.G. Bonnemann, M.P. Lisanti, H.G. Lidov, M. Vainzof, M.R. Passos-Bueno, E.P. Hoffman, M. Zatz, L.M. Kunkel, Caveolin-3 in muscular dystrophy, Hum. Mol. Genet. 7 (1998) 871–878.

[8] T. Weiler, C.R. Greenberg, T. Zelinski, E. Nylen, G. Coghlan, M.J. Crumley, T.M. Fujiwara, K. Morgan, K. Wrogemann, A gene for autosomal recessive limb–girdle muscular dystrophy in Manitoba Hutterites maps to chromosome region 9q31–33: evidence for another limb–girdle muscular dystrophy locus, Am. J. Hum. Genet. 63 (1998) 140–147.

[9] A. Driss, R. Amouri, C. Ben Hamida, S. Souilem, N. Gouider-Khouja, M. Ben Hamida, F. Hentati, A new locus for autosomal recessive limb–girdle muscular dystrophy in a large consanguineous Tunisian family maps to chromosome 19q13.3, Neuromuscul. Disord. 10 (2000) 240–246.

[10] J.M. Ervasti, K. Ohlendieck, S.D. Kahl, M.G. Gaver, K.P. Campbell, Deficiency of a glycoprotein component of the dystrophin complex in dystrophic muscle, Nature 345 (1990) 315–319.

[11] M. Yoshida, E. Ozawa, Glycoprotein complex anchoring dystrophin to sarcolemma, J. Biochem. (Tokyo) 108 (1990) 748–752.

[12] K. Matsumura, F.M.S. Tomé, H. Collin, K. Azibi, M. Chaouch, J.C. Kaplan, M. Fardeau, K.P. Campbell, Deficiency of the 50 kDa dystrophin-associated glycoprotein in severe childhood autosomal recessive muscular dystrophy, Nature 359 (1992) 320–322.

[13] K. Azibi, L. Bachner, J.S. Beckmann, K. Matsumura, E. Hamouda, M. Chaouch, A. Chaouch, R. Ait-Ouarab, A. Vignal, J. Weissenbach, et al., Severe childhoood autosomal recessive muscular dystrophy with the deficiency of the 50 kDa dystrophin-associated glycoprotein maps to chromosome 13q12, Hum. Mol. Genet. 2 (1993) 1423–1428.

[14] S.L. Roberds, F. Leturcq, V. Allamand, F. Piccolo, M. Jeanpierre, R.D. Anderson, L.E. Lim, J.C. Lee, F.M. Tome, N.B. Romero, Missense mutations in the adhalin gene linked to autosomal recessive muscular dystrophy, Cell 78 (1994) 625–633.

[15] C.G. Bonnemann, R. Modi, S. Noguchi, Y. Mizuno, M. Yoshida, E. Gussoni, E.M. McNally, D.J. Duggan, C. Angelini, E.P. Hoffman, L.M. Kunkel, β-sarcoglycan (A3b) mutations cause autosomal recessive muscular dystrophy with loss of the sarcoglycan complex, Nat. Genet. 11 (1995) 266–273.

[16] L.E. Lim, F. Duclos, O. Broux, N. Bourg, Y. Sunada, V. Allamand, J. Meyer, I. Richard, C. Moomaw, C. Slaughter, et al., β-sarcoglycan (43 DAG): characterization and involvement in a recesive form of limb–girdle muscular dystrophy linked to chromosome 4q12, Nat. Genet. 11 (1995) 257–265.

[17] S. Noguchi, E.M. McNally, K. Ben Othmane, Y. Hagiwara, Y. Mizuno, M. Yoshida, H. Yamamoto, C.G. Bonnemann, E. Gussoni, P.H. Denton, Mutations in the dystrophin-associated protein γ-sarcoglycan in chromosome 13 muscular dystrophy, Science 270 (1995) 755–756.

[18] E.M. McNally, M.R. Passos-Bueno, C. Bonnemann, M. Vainzof, E.S. Moreira, H.G. Lidov, K.B. Othmane, P.H. Denton, J.M. Vance, M. Zatz, L.M. Kunkel, Mild and severe muscular dystrophy caused by a single gamma-sarcoglycan mutations, Am. J. Hum. Genet. 59 (1996) 1040–1047.

[19] M.R. Passos-Bueno, E.S. Moreira, M. Vainzof, S. Marie, M. Zatz, Linkage analysis in autosomal recessive limb–girdle muscular dystrophy (AR-LGMD) maps a sixth form to 5q33–34 (LGMD2F) and indicates that there is at least one more subtype of AR LGMD, Hum. Mol. Genet. 5 (1996) 815–820.

[20] V. Nigro, G. Piluso, A. Belsito, L. Politano, A.A. Puca, S. Papparella, E. Rossi, G. Viglietto, M.G. Esposito, C. Abbondanza, N. Medici, A.M. Molinari, G. Nigro, G.A. Puca, Identification of a novel sarcoglycan gene at 5q33 encoding a sarcolemmal 35 kDa glycoprotein, Hum. Mol. Genet. 5 (1996) 1179–1186.

[21] V. Nigro, E.S. Moreira, G. Piluso, M. Vainzof, A. Belsito, L. Politano, A.A. Puca, M.R. Passos-Bueno, M. Zatz, The 5q autosomal recessive limb–girdle muscular dystrophy, LGMD2F, is caused by a mutation in the δ-sarcoglycan gene, Nat. Genet. 14 (1996) 195–198.

[22] E.S. Moreira, M. Vainzof, A.L. Sertié, M. Zatz, The seventh form of autosomal recessive limb–girdle muscular dystrophy is mapped to 17q11–12, Am. J. Hum. Genet. 61 (1997) 151–159.

[23] E.S. Moreira, T.J. Wiltshire, G. Faulkner, A. Nilforoushan, M. Vainzof, O.T. Suzuki, G. Valle, R. Reeves, M. Zatz, M.R. Passos-Bueno, D. Jenne, Limb–girdle muscular dystrophy type 2G (LGMD2G) is caused by mutations in the gene encoding the sarcomeric protein telethonin, Nat. Genet. 24 (2000) 163–166.

[24] R. Bashir, T. Strachan, S. Keers, A. Stephenson, I. Mahjneh, G. Marconi, L. Nashef, K.M. Bushby, A gene for autosomal recessive limb–girdle muscular dystrophy maps to chromosome 2p, Hum. Mol. Genet. 3 (1994) 455–457.

[25] R. Bashir, S. Britton, T. Strachan, S. Keers, E. Vafiadaki, M. Lako, I. Richard, S. Marchand, N. Bourg, Z. Argov, M. Sadeh, I. Mahjneh, G. Marconi, M.R. Passos-Bueno, E.S. Moreira, M. Zatz, J.S. Beckmann, K. Bushby, A gene related to *Caenorhabditis elegans* spermatogenesis factor fer-1 is mutated in limb–girdle muscular dystrophy type 2B, Nat. Genet. 20 (1998) 37–42.

[26] J. Liu, M. Aoki, I. Illa, C. Wu, M. Fardeau, C. Angelini, C. Serrano, J.A. Urtizberea, F. Hentati, M.B. Hamida, S. Bohlega, E.J. Culper, A.A. Amato, K. Bossie, J. Oeltjen, K. Bejaoui, D. McKenna-Yasek, B.A. Hosler, E. Schurr, K. Arahata, P.J. de Jong , R.H. Brown Jr., Dysferlin, a novel skeletal muscle gene, is mutated in Miyoshi myopathy and limb–girdle muscular dystrophy, Nat. Genet. 20 (1998) 31–36.

[27] J. Beckmann, I. Richard, D. Hillaire, O. Broux, C. Antignac, E. Bois, H. Cann , R.W. Cottingham Jr., N. Feingold, J. Feingold, et al., A gene for limb–girdle muscular dystrophy maps to chromosome 15 by linkage, C. R. Acad. Sci., Ser. III 312 (1991) 141–148.

[28] I. Richards, O. Broux, V. Allamand, F. Fougerousse, N. Chiannilkulchai, N. Bourg, L. Brenguier, C. Devaud, P. Pasturaud, C. Roudaut, et al., Mutations in the proteolytic enzyme calpain-3 cause limb–girdle muscular dystrophy type 2a, Cell 81 (1995) 24–40.

[29] I. Richards, C. Roudaut, A. Saenz, R. Pogue, J.E. Grimbergen, L.V. Anderson, C. Beley, A.M. Cobo, C. Diego, B. Eymard, P. Gallano, H.B. Ginjaar, A. Lasa, C. Pollitt, H. Topaloglu, J.A. Urtizberea, M. de Visser, A. van der Kooi, K. Bushby, E. Bakker, A. Lopez de Munain, M. Fardeau, J.S. Beckmann, Calpainopathy—a survey of mutations and polymorphisms, Am. J. Hum. Genet. 64 (1999) 1524–1540.

[30] A.A. Hack, M.E. Groh, E.M. McNally, Sarcoglycans in muscular dystrophy, Microsc. Res. Tech. 48 (2000) 167–180.

[31] R.D. Cohn, K.P. Campbell, Molecular basis of muscular dystrophies, Muscle Nerve 23 (2000) 1456–1471.

[32] C.C. Gregorio, K. Trombitás, T. Centner, B. Kolmerer, G. Stier, K. Kunke, K. Suzuki, F. Obermayr, B. Herrmann, H. Granzier, H. Sorimachi, S. Labeit, The NH2 terminus of titin spans the Z-disc: its interaction with a novel 19 kda ligand (T-cap) is required for sarcomeric integrity, J. Cell Biol. 143 (1998) 1013–1027.

[33] K.J. Nowak, D. Wattanasirichaigoon, H.H. Goebel, M. Wilce, K. Pelin, K. Donner, R.L. Jacob, C. Hubner, K. Oexle, J.R. Anderson, C.M. Verity, K.N. North, S.T. Iannaccone, C.R. Muller, P. Nurnberg, F. Muntoni, C. Sewry, I. Hughes, R. Sutphen, A.G. Lacson, K.J. Swoboda, J. Vigneron, C. Wallgren-Pettersson, A.H. Beggs, N.G. Laing, Mutations in the skeletal muscle alpha actin gene in patients with actin myopathy and nemaline myopathy, Nat. Genet. 23 (1999) 208–212.

[34] N.G. Laing, S.D. Wilton, P.A. Akkari, S. Dorosz, K. Bound, C. Kneebone, P. Blumbergs, S. White, H. Watkins, D.R. Love, et al., A mutation in the alfa tropomyosin gene TPM3 associated with autosomal dominant nemaline myopathy, Nat. Genet. 9 (1995) 75–79.

[35] K. Donner, M. Ollikainen, M. Grönholm, O. Carpén, C. Wallgren-Pettersson, M. Ridanpää, Mutations in the beta-tropomyosin (TPM2) gene in rare cases of autosomal dominant nemaline myopathy, Neuromuscul. Disord. 10 (2000) 342–343.

[36] J.J. Johnston, R.I. Kelley, T.O. Crawford, D.H. Morton, R. Agarwala, T. Koch, A.A. Schäffer, C.A. Francomano, L.G. Biesecker, A novel nemaline myopathy in the Amish caused by mutation in troponin T1, Am. J. Hum. Genet. 67 (2000) 814–821.

[37] A.H. Beggs, T.J. Byers, J.H.M. Knoll, F.M. Boyce, G.A.P. Bruys, L.M. Kunkel, Cloning and characterization of two human skeletal muscle α-actinin genes located on chromosomes 1 and 11, J. Biol. Chem. 267 (1992) 9281–9288.

[38] V. Dubowitz, Muscle Disorders in Childhood, 2nd edn., Saunders, London, 1995, pp. 134–177.

[39] G. Valle, G. Faulkner, A. De antoni, B. Pacchioni, A. Pallavicini, D. Pandolfo, N. Tiso, S. Toppo, S. Trevisan, G. Lanfranchi, Telethonin, a novel sarcomeric protein of heart and skeletal muscle, FEBS Lett. 415 (1997) 163–168.

[40] M. Vainzof, M.R. Passos-Bueno, M. Canovas, E.S. Moreira, R.C. Pavanello, S. Marie, L.V.B. Anderson, C.G. Bonnemann, M.M. McNally, V. Nigro, L.M. Kunkel, M. Zatz, The sarcoglycan complex in the six autosomal recessive limb–girdle (AR-LGMD) muscular dystrophies, Hum. Mol. Genet. 5 (1996) 1963–1969.

[41] L.V.B. Anderson, K. Davison, J.A. Moss, I. Richard, M. Fardeau, F.M. Tome, C. Hubner, A. Lasa, J. Colomer, J.S. Beckmann, Characterization of monoclonal antibodies to calpain-3 and protein expression in muscle from patients with limb–girdle musclar dystrophy type 2A, Am. J. Pathol. 153 (1998) 1169–1179.

[42] L.V.B. Anderson, K. Davison, J.A. Moss, C. Young, M.J. Cullen, J. Walsh, M.A. Johnson, R. Bashir, S. Britton, S. Keers, Z. Argov, I. Mahjneh, F. Fougerousse, J.S. Beckmann, K.M. Bushby, Dysferlin is a plasma membrane protein and is expressed early in human development, Hum. Mol. Genet. 8 (1999) 855–861.

[43] M. Vainzof, E.E. Zubrzycka-Gaarn, D. Rapaport, M.R. Passos-Bueno, R.C. Pavanello, I. Pavanello-Filho, M. Zatz, Immunofluorescence dystrophin study in Duchenne dystrophy through the concomitant use of two antibodies directed against the carboxy-terminal and the amino-terminal region of the protein, J. Neurol. Sci. 101 (1991) 141–147.

[44] M.A. Ho-Kim, A. Bedard, M. Vincent, P.A. Rogers, Dystrophin: a sensitive and reliable immunochemical assay in tissue and cell culture homogenates, Biochem. Biophys. Res. Commun. 181 (1991) 1164–1172.

[45] A. Mues, P.F.M. Van der Vem, P. Young, D.O. Furst, M. Gautel, Two immunoglobulin-like domains of the Z-disc portion of titin interact in a conformation-dependent way with telethonin, FEBS Lett. 428 (1998) 111–114.

[46] O. Mayans, P.F.M. Van der Vem, M. Wilm, A. Mues, P. Young, D.O. Furst, M. Wilmanns, M. Gautel, Structural basis for activation of the titin kinase domain during myofibrillogenesis, Nature 395 (1998) 863–869.

[47] R. Bottinelli, C. Reggiani, Human skeletal muscle fibres: molecular and functional diversity, Prog. Biophys. Mol. Biol. 73 (2000) 195–262.

[48] H.H. Goebel, H.G. Lenard, Congenital myopathies, Handb. Clin. Neurol. 18 (1992) 331–359.

[49] M.R. Passos-Bueno, E.S. Moreira, S. Marie, R. Bashir, L. Vasquez, D.R. Love, M. Vainzof, P. Iughetti, J.R. Oliveira, E. Bakker, T. Strachan, K. Bushby, M. Zatz, Main clinical features for the three mapped autosomal recessive limb girdle muscular dystrophies and estimated proportion of each form in 13 brazilian families, J. Med. Genet. 33 (1996) 97–102.

[50] P. Mason, S. Bayol, P.T. Loughna, The novel sarecomeric protein telethonin exhibits developmental and functional regulation, Biochem. Biophys. Res. Commun. 257 (1999) 699–703.

[51] M. Zatz, M. Vainzof, M.R. Passos-Bueno, Limb–girdle muscular dystrophy: one gene, different phenotypes, one phenotype, different genes, Curr. Opin. Neurol. 13 (2000) 511–517.

ELSEVIER

Biochimica et Biophysica Acta 1588 (2002) 41–47

BIOCHIMICA ET BIOPHYSICA ACTA

BBA

www.bba-direct.com

The CD23b promoter is a target for NF-AT transcription factors in B-CLL cells

Christian Kneitz [a,*], Martin Goller [a], Hans-Peter Tony [a], Andreas Simon [a], Corinne Stibbe [b], Thomas König [b], Edgar Serfling [b], Andris Avots [b,c,*]

[a] *Medizinische Poliklinik, University of Wuerzburg, Klinikstrasse. 6-8, 97070 Wuerzburg, Germany*
[b] *Department of Molecular Pathology, Institute of Pathology, University of Wuerzburg, Klinikstrasse. 6-8, 97070 Wuerzburg, Germany*
[c] *Molecular Epigenetics Group, Institute of Medical Radiation and Cell Research (MSZ), University of Wuerzburg, Versbacher Str.5, 97070 Wuerzburg, Germany*

Received 6 November 2001; received in revised form 28 March 2002; accepted 4 April 2002

Abstract

CD23 is atypically highly expressed in various chronic diseases, including B-CLL, lupus erythematodes and rheumatoid arthritis. Its expression can be further enhanced by interleukin 4 (IL-4). We have shown before that in B-CLL cells *n*uclear *f*actor(s) of *a*ctivated *T* cells (NF-ATs) show permanent nuclear localization and therefore constitutive transcriptional activity. Here we identify CD23b promoter as a novel target for NF-AT factors in B-CLL cells. The CD23b promoter contains two NF-AT binding sites to which NF-ATp and NF-ATc factors bind with high affinity. Mutations introduced into these sites abolished NF-AT binding and impaired the promoter activity, as did cyclosporin A (CsA), an inhibitor of nuclear transport of NF-ATs. Furthermore, we show that IL-4-induced transcription factor STAT6 cooperates with NF-ATs in the induction of the CD23b promoter activity. These results show that the CD23b promoter is a target for NF-AT factors and suggest that the cooperation between NF-AT and STAT factors might be one of the molecular mechanisms responsible for high-level expression of CD23 on the surface of B-CLL cells.

© 2002 Elsevier Science B.V. All rights reserved.

Keywords: B-CLL; NF-AT factor; STAT6; CD23b promoter

1. Introduction

CD23 (also designated as FcεRII) is the low affinity receptor for IgE, which is expressed on numerous haematopoietic cells including B cells, T cells and monocytes [1]. In these cells CD23 mediates a variety of biological activities [2,3]. High CD23 expression is a typical property of various chronic diseases, such as B-CLL, rheumatoid arthritis and lupus erythematodes. It is assumed that signalling through CD23 contributes to the pathogenesis of these diseases [4,5].

CD23 is involved in regulation of IgE synthesis, IgE-dependent presentation of antigens to T cells and proliferation of myeloid precursors. Two isoforms, CD23a and CD23b, are described which differ only in a short amino acid sequence at the N-terminus. It was suggested that these differences are sufficient to propagate different signals after receptor ligation. CD23a is exclusively expressed on B cells, whereas CD23b is also expressed on a variety of cells of the myeloid lineage after stimulation. CD23a exhibits an endocytosis signal that renders it efficient in antigen uptake [6]. Ligation of CD23 was shown to trigger nitric oxide production and to induce the production of TNFα , cAMP and interleukin-10 (IL-10) [7,8]. The anti-apoptotic activity of nitric oxide has been discussed as a mechanism contributing to the prolonged viability of B-CLL cells [9].

The expression of the two isoforms is regulated by the use of two different promoters and alternative splicing events. The CD23b promoter is located between exon II and exon Ib (Fig 1A). So far, binding sites for STAT6, STAT1 and AP-1 family factors have been described to be

---

[*] Corresponding authors. C. Kneitz to be contacted at: Tel.: +49-931-201-70770; fax: +49-931-201-70680. A. Avots, Molecular Epigenetics Group, Institute of Medical Radiation and Cell Research (MSZ), University of Wuerzburg, Versbacher Str. 5, Wuerzburg, Germany; Tel.:+49-931-201-3851; fax:+49-931-201-3887.

E-mail addresses: c.kneitz@medizin.uni-wuerzburg.de (C. Kneitz), path061@mail.uni-wuerzburg.de (A. Avots).

0925-4439/02/$ - see front matter © 2002 Elsevier Science B.V. All rights reserved.
PII: S0925-4439(02)00114-X

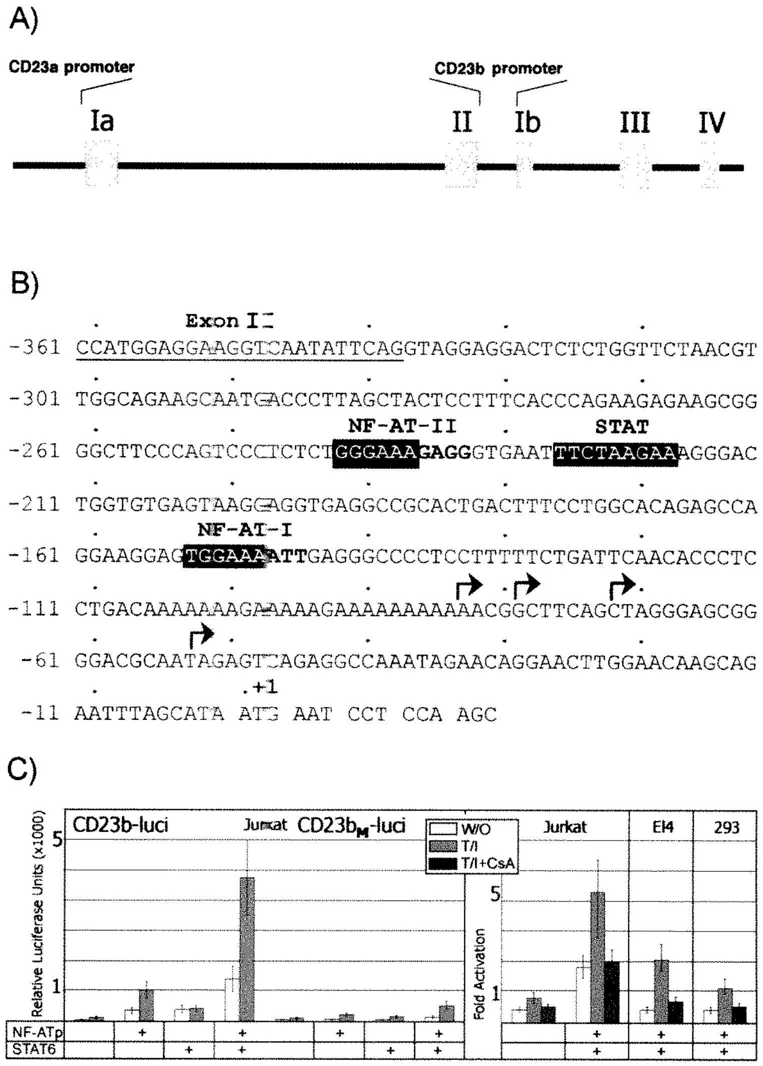
A)
CD23a promoter
Ia
CD23b promoter
II
Ib
III
IV
B)
Exon II
-361 CCATGGAGGAAGGTCAATATTCAGGTAGGAGGACTCTCTGGTTCTAACGT
-301 TGGCAGAAGCAATGACCCTTAGCTACTCCTTTCACCCAGAAGAGAAGCGG
NF-AT-II
STAT
-261 GGCTTCCCAGTCCCTCTCTGGGAAAGAGGGTGAATTTCTAAGAAAGGGAC
-211 TGGTGTGAGTAAGGAGGTGAGGCCGCACTGACTTTCCTGGCACAGAGCCA
NF-AT-I
-161 GGAAGGAGTGGAAAATTGAGGGCCCCTCCTTTTTCTGATTCAACACCCTC
-111 CTGACAAAAAAAGAAAAAGAAAAAAAAAAAACGGCTTCAGCTAGGGAGCGG
-61 GGACGCAATAGAGTCAGAGGCCAAATAGAACAGGAACTTGGAACAAGCAG
+1
-11 AATTTAGCATA ATG AAT CCT CCA AGC
C)
CD23b-luci
Jurkat
CD23b$_M$-luci
W/O
T/I
T/I+CsA
Jurkat
El4
293
Relative Luciferase Units (x1000)
5
1
Fold Activation
5
1
NF-ATp
STAT6
+

Fig. 1. NF-ATp and STAT6 collaborate in the induction of the CD23b promoter. (A) Schematic structure of the CD23 gene and localization of the CD23a and b promoters (adapted according to Ref. [1]). (B) Sequence of the CD23b promoter. The sequence motifs for the binding of NF-AT and STAT factors are indicated. The transcriptional start sites are marked by arrows. The translational start codon is indicated by +1; exon II sequences are underlined. (Note that the nucleotide positions are labelled according to Ref. [1] and refer to the translational start site). (C) NF-ATp and STAT6 enhance CD23 induction. Expression vectors encoding both factors were co-transfected as indicated into Jurkat T cells together with luciferase reporter gene constructs under the control of a wild-type (CD23b-luci) or a mutated (CD23b$_M$-luci, GG to CC mutations within the NF-AT-I site, positions −152/−151) CD23b promoter. Five hours later, the cells were left uninduced (W/O) or induced by TPA + Ionomycin (T/I) for 20 h (left part of the panel). The experiment with the wild-type CD23b-promoter (CD23b-luci) was also performed in Jurkat T cells, El-4 and 293 cells in the absence (T/I) or presence of CsA (100 ng/ml; T/I + CsA) (right part of the panel).

responsible for the transcriptional activity of the CD23b promoter [10,11].

IL-4 is the most potent inducer of CD23 expression [12]. IL-4 is mediating the translocation of the transcription factor STAT6 to the nucleus where STAT6 binds to the promoters of IL-4 responsive genes [13]. In addition to IL-4, mitogens such as phorbol-myristate acetate (PMA) also exert a strong stimulatory effect on CD23 expression in B-CLL, but only a weak one in normal B cells [14,15,16]. IFNγ reduces IL-4-mediated CD23 expression in normal B cells but augments CD23 expression in B-CLL cells, further emphasizing atypical regulation of CD23 expression in B-CLL. This also suggests that the IL-4-mediated activation of STAT6 is not the only signalling pathway activating the CD23 promoters in these cells. Moreover, B lymphocytes from STAT6-deficient mice were still found to express CD23 after stimulation with CD40 and IL-4 [17]. The analysis of numerous transcription factors, which are highly expressed in lymphoid cells, resulted in the detection of constitutive activity of several factors in B-CLL cells. Among them was NF-ATp, a member of the *n*uclear *f*actor(s) of *a*ctivated *T* cells (NF-AT) transcription factor family [18].

NF-AT proteins are characterized by a highly conserved DNA binding domain of approximately 300 amino acid residues and the control of their nuclear transport by calcineurin, a Ca^{+}/calmodulin-dependent protein phosphatase [19,20]. Among the four genuine NF-AT factors, NF-ATp and NF-ATc (also designated as NF-AT1 and 2, or NF-

ATc2 and c1, respectively) are highly expressed in peripheral lymphoid cells and known to bind to and control the promoters and enhancers of numerous genes. Most prominent targets for NF-AT factors in T cells are those of lymphokine genes IL-2, IL-3, IL-4, IL-5, TNFα and GM-CSF. Further targets are the promoters of FasL- and CD40L. Consensus sites for NF-AT (+AP-1) factors were detected in a large number of promoters/enhancers controlling the expression of genes, which regulate the cell cycle, Ca$^+$ metabolism and apoptosis of T cells [21]. Although NF-ATp and NF-ATc are also highly expressed and induced by Ca$^+$ signals in B cells, there are only a few published data concerning the role of NF-AT factors on particular gene expression in B cells and B cell-derived leukemias/lymphomas [18,22,23].

The constitutive nuclear localization (and supposedly transcriptional activity) of NF-ATp in B-CLL cells [18] prompted us to investigate whether the CD23 promoters are regulated by NF-AT factors in these cells. Inspection of the promoter DNA sequences revealed three putative NF-AT binding sites, one within the CD23a promoter and two within the CD23b promoter. Whereas DNA/protein binding studies specify the CD23a promoter site as a very weak one, those from the CD23b promoter are bound by NF-AT factors with high affinity. Moreover, we show that in transient transfection experiments using NF-ATp and STAT6 expression vectors, the induction of the CD23b promoter is strongly enhanced after TPA and ionomycin treatment of the cells. While NF-ATp or STAT6 expression alone resulted in a moderate 2–5-fold increase of CD23b promoter activity, co-expression of both factors led to a 15–30-fold increase. This increase was impaired by cyclosporin A (CsA), an inhibitor of nuclear translocation of NF-ATs, and by the site-specific mutation introduced into these two NF-AT sites. These results indicate that CD23b promoter (i) is a target for NF-AT factors; (ii) its induction is controlled by the concerted action of NF-ATp and STAT6 which both bind directly to this promoter with high affinity; and (iii) constitutive nuclear localization of NF-AT factors in B-CLL cells contributes to the malignant phenotype of B-CLL cells, which is characterized by atypically high level of CD23 expression.

2. Materials and methods

2.1. Preparation of B-CLL cells, cultivation and transfection of cell lines

B-CLL cells were isolated from peripheral blood of 10 different untreated patients who gave informed consent. Cell surface phenotyping revealed a staining pattern typical for B-CLL cells (i.e. CD5$^+$, CD19$^+$, CD23$^+$, CD40$^+$, HLA class II$^+$, CD10$^-$ and low level expression of light chain restricted surface IgM). B-CLL cells were purified by the centrifugation through a Ficoll–Hypaque gradient at 900 × *g*. T cells were removed by E-rosetting using AET-treated sheep erythrocytes. The final purity of B-CLL cells was estimated 99%. When necessary, B-CLL cells as well as human Jurkat T leukemia cell line were cultured in RPMI 1640 medium supplemented with 5 mM L-glutamin, 100 U/ml penicillin G, 100 µg/ml streptomycin and 5% fetal calf serum (FCS) (Gibco). HEK293 cell line was cultured in DMEM medium supplemented with 10% FCS. Both Jurkat and HEK293 cells were transfected using SuperFect reagent (Qiagen, Germany) according to the manufacturer's protocol. Five hours after transfection, the cells were treated with TPA (20 ng/ml) and ionomycin (0.5 mM) in the presence or absence of CsA (100 ng/ml). After 20 h of incubation cellular extracts were prepared and luciferase activities determined using a luminometer (Berthold).

2.2. Plasmids

The CD23b promoter–luciferase reporter construct (Fig. 1A and B) was created on the basis of plasmid pLuc+vector [24]. Point mutations abrogating the binding of NF-AT factors were introduced using QuikChange mutagenesis system (Stratagene) and following oligonucleotides NF-AT-I$_M$ (−160 to −135): 5′-GAAGGAGT**CCAA**AATT-GAGGGCCCCT-3′, and NF-AT-II$_M$ (−251 to −226): 5′-TCCCTCTCTG**CCAA**AGAGG GTGAATT-3′). Mutated positions within the underlined 'core' sequence are shown in bold letters. The sequence of all luciferase reporter constructs was confirmed by DNA sequencing. Expression vectors for NF-ATp, NF-ATc/A, STAT5 and a constitutive version of STAT5 (STAT5-CA) have been published previously [25,26]. The STAT6 expression vector was kindly provided by Dr. E. Pfitzner and contains a full size human STAT6 cDNA cloned in vector pXM.

2.3. Nuclear extracts and electrophoretic mobility shift assays (EMSAs)

Nuclear protein extracts from B-CLL cells were prepared as described [27] with slight modifications. NP40 was omitted and nuclei were released by passing the cells five times through an injection needle (26g3/8). In EMSAs, 5 µg of nuclear proteins was incubated with 40,000 cpm (equivalent to approximately 0.3 ng) of γ^{32}P-labelled double-stranded oligonucleotides as probes in the presence of 1 µg poly(dI–dC) as unspecific competitor and increasing amount (12.5–50 ng) of specific competitors, when indicated. After incubation on ice for 30 min, the samples were fractionated on nondenaturing 5% polyacrylamide gels at 15 V/cm at room temperature followed by autoradiography. In EMSA "super-shift" assays, 1 µg of polyclonal antibodies raised against STAT5 (Santa Cruz, sc-1656X), STAT6 (sc-981X), NF-ATp (sc-7295X) or NF-ATc (ABR) was added to binding reactions. The following double-stranded oligonucleotides were used as probes: the distal NF-AT site from the murine IL-2 promoter: (Pu-b$_d$-IL-2 5′-tcgaCAAAGAG-

GAAAATTT GTTTCATACAGAAG-3′); the NF-AT sites from the CD23b promoter: (NF-AT-I (− 160 to − 135): 5′-tcgaGAAGGAGT**GGAAA**AATTGAGGGCCCCT-3′, NF-AT-II (− 251 to − 226): 5′-tcgaTCCCTCTCTG**GGAAA**-GAGGGTGAATT-3′); and NF-AT-like site from the CD23a-promoter (− 28 to − 9): 5′-tcgaTTAGGTCTAT-**GAAA**ATAGAAGCTGTC-3′. Small letters indicate linker nucleotides; conserved ‘core’ nucleotides are shown in bold letters.

2.4. DNase I footprint protection assays

For DNase I footprinting assays, end-labeled DNA probes were prepared using [γ-^{32}P]ATP and T4 polynukleotide kinase; 10^4 cpm (ca. 0.2 ng) of labelled DNA fragments was used per binding reaction. Recombinant proteins from transformed *E. coli* BL21-DE bacteria were purified over Glutathione–Sepharose column (Amersham-Pharmacia) according to the specifications of manufacturer. In DNase I footprinting reactions, labeled DNA fragments were incubated for 1 h with increasing amounts (0.25–1.5 μg) of glutathione-S-transferase (GST) or GST–NF-ATp fusion protein [28] representing the DNA-binding domain of murine NF-ATp. After limited DNase I digestion, the samples were purified by organic extraction, DNA was precipitated and fractionated on 6% polyacrylamide/7 M urea DNA sequencing gels followed by autoradiography.

3. Results

The constitutive nuclear residence of NF-ATp in B-CLL cells [18] suggested that NF-AT transcription factors might exert an important role in the control of genes which are highly expressed in B-CLLs, such as CD23. To test this hypothesis, we co-transfected luciferase reporter genes controlled by the CD23a or CD23b promoter (Fig. 1C) with expression vectors encoding either NF-ATp or NF-ATc/A (the most abundant NF-ATc isoform in T effector cells [25,29]) into human Jurkat T cells or HEK 293 cells. In both cell types, expression of NF-ATp had a weak but reproducible stimulatory effect on the CD23b promoter-controlled increase of luciferase activity after treatment of cells with TPA and ionomycin (T + I) (Fig. 1C, left panel). No effect was observed on the CD23a promoter after transfection with the NF-ATc/A expression vector (results not shown). Since IL-4 is the most potent known inducer of CD23 expression and the IL-4-induced factor STAT6 binds to the CD23b promoter [16,11], we tested next whether STAT6 (or STAT5, also induced by IL-4: [30]) is able to collaborate with NF-ATp to enhance the induction of CD23b promoter. Indeed, a strong stimulatory effect on the T + I induction of the CD23b promoter was observed when NF-ATp was transfected along with vectors encoding either STAT6 (Fig. 1C, left panel) or STAT5 (data not shown). While transfection of vectors expressing either NF-ATp or STAT6 resulted in a 2–5-fold induction, co-transfection of NF-ATp expression vector together with one of the two STAT vectors resulted in a 20–50-fold increase of CD23b promoter activity in Jurkat (Fig. 1C) or HEK293 cells (data not shown). A strong repression of this induction was observed when Jurkat cells were induced by T + I in the presence of 100 ng/ml CsA, an inhibitor of calcineurin and therefore suppressor of nuclear translocation of NF-ATs. A similar CsA-mediated repression of NF-ATp + STAT6-mediated increase of CD23 activity was observed in HEK293 cells and murine EL-4 thymoma cells (Fig. 1C). This indicates that NF-ATp and STAT6 (or STAT5) can cooperate in the induction of the CD23b promoter.

Sequence inspection of the CD23b promoter revealed several putative NF-AT binding sites. As the first step in order to determine whether these sites might interact with NF-AT proteins, we tested the binding of bacterially expressed GST–NF-ATp fusion protein to the CD23b promoter in DNase I footprint protection assays, which identified several “would-be” regions of interaction (see Fig. 2). The most prominent one harboring the TGGAAAA core sequence spans the nucleotides from position − 160 to − 141 and was designated as NF-AT-I. A second motif (designated

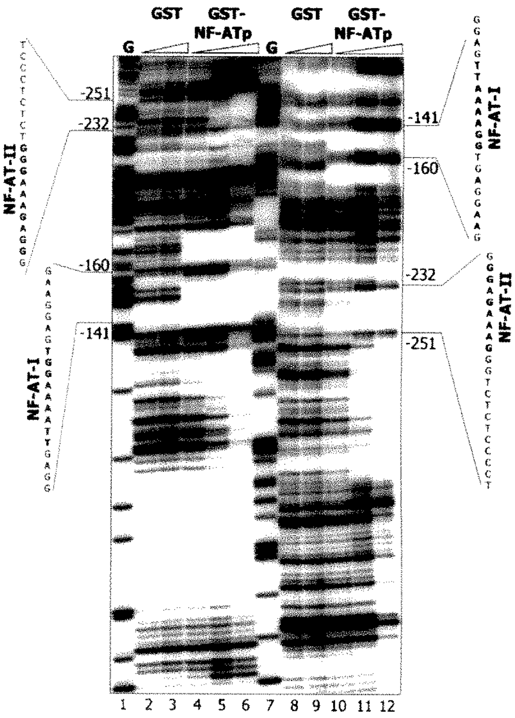

Fig. 2. NF-ATp binds to the CD23b promoter. DNase I footprint protection assay. A ^{32}P-labelled CD23b promoter probe was incubated with increasing amounts (0.25–1.5 μg) of GST protein (lanes 2 + 3 and 8 + 9) or GST–NFATp fusion protein (lanes 4–6 and 10–12). Samples were digested by DNase I and fractionated on a 6% polyacrylamide sequencing gel. G-specific DNA sequencing reactions of the CD23b promoter are shown in lanes 1 and 7. The sequences of the NF-ATp-specific footprints over the NF-AT-I and NF-AT-II sites are indicated; the NFAT core sequences are shown in boldface letters.

as NF-AT-II) bearing a slightly modified version of this sequence is located just 10 nucleotides 3′ from the known STAT 6 binding site. This is reminiscent to the configuration of composite NF-AT+AP-1 binding sites, which occur approximately 10 times more frequent in promoters of genes which are expressed upon T cell activation than in promoters active in other tissues [21]. Those have the general structure 5′-caxwGGAAAawxxxg/a TGAC/GTCAg/tc-3′ (where capital letters denote highly, lower case letters poorly, conserved nucleotides; w=A or T; x=any nucleotide), i.e. the AP-1 site is located about 10 nucleotides 3′ from the NF-AT ‘core’ motif as the STAT 6 site in the context of CD23b promoter NF-AT-II site (see Fig. 1B).

DNase I protection assays are performed at relatively high concentration of recombinant fusion protein, which may manifest significantly relaxed binding requirements in comparison to the native transcription factors. Therefore, we tested putative NF-AT binding sites in EMSA assays using nuclear extracts prepared from B-CLL cells (Fig. 3A). Oligonucleotides containing NF-AT-I or NF-AT-II sites (see Section 2) were included as competitors in EMSA using the high affinity distal NF-AT binding site (Pu-b_d-IL-2) from the murine IL-2 promoter [31] as a probe. A 10-fold molar excess of NF-AT-I or NF-AT II site was sufficient to suppress NF-AT complexes generated with nuclear proteins from B-CLL cells and the distal IL-2 NF-AT site (Fig. 3A, lanes 6–8 and 9–11, respectively). A similar effect was detected with a 10-fold molar excess of the unlabelled distal IL-2 site but not with a 10- or 100-fold excess of the NF-AT-like putative binding site from the CD23a promoter (Fig. 3A, lanes 3–5). This indicates that NF-AT-I and NF-AT-II sites from the CD23b promoter correspond to rather high affinity NF-AT binding sites.

In order to show which NF-AT proteins bind to the CD23b promoter in B-CLL cells, we performed EMSA supershift assays using the NF-AT sites I and II and nuclear proteins from nontreated and T+I-treated B-CLL cells. As shown in Fig. 3B (lanes 5–9), incubation of EMSAs with antibodies raised against NF-ATp or NF-ATc led to the generation of specific ‘supershift’ complexes. This indicates that in nuclear protein extracts from B-CLL cells, NF-ATp and NF-ATc are prominent proteins binding to the CD23b promoter. Next, we investigated whether the binding of NF-AT factors to the NF-AT-I and/or NF-AT-II sites contributes to the induction of CD23b promoter activity by NF-ATp and STAT6. Introduction of GG to CC mutations into the core

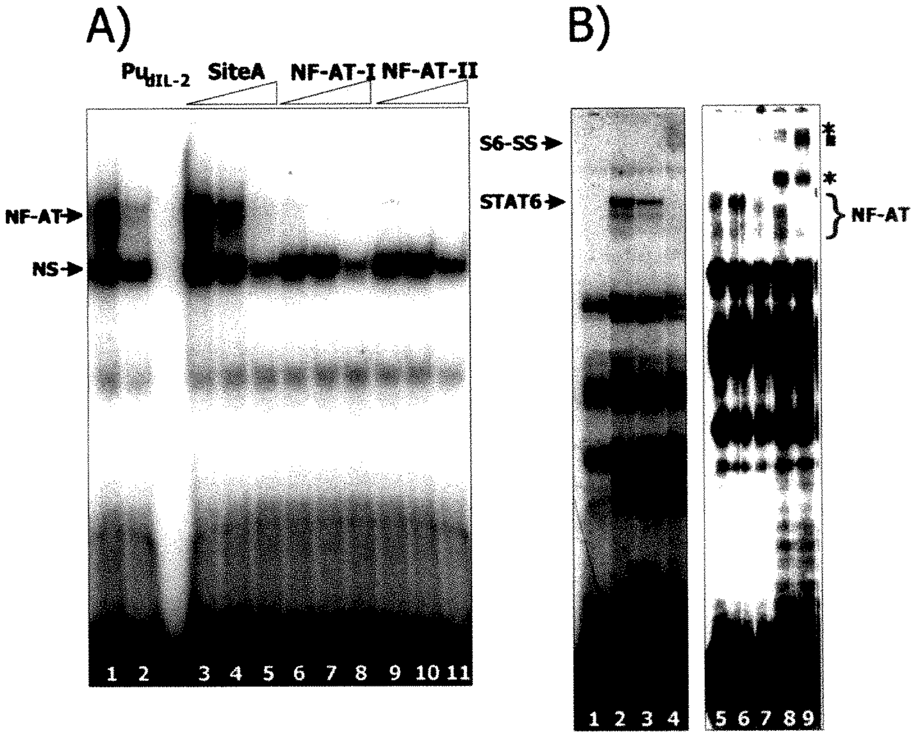

Fig. 3. NF-ATp and NF-ATc bind to the NF-AT-I site of the CD23b promoter in nuclear protein extracts from B-CLL cells. (A) EMSA competition assays. Five micrograms of nuclear proteins isolated from uninduced B-CLL cells was incubated with the high affinity distal NF-AT binding site (Pu-b_{dIL-2}) from the murine IL-2 promoter. For specific competition, a 10-fold molar excess of the cold probe (lane 2), a 10-, 100- or 1000-fold excess of the NF-AT-like site from the CD23a promoter (Site A) or of the NF-AT-I and NF-AT-II sites from the CD23b promoter were added. NS, nonspecific complex. (B) EMSA supershift assays. In lanes 1–4, nuclear proteins from uninduced (lane 1) or IL-4-induced B-CLLs (lanes 2–4) were incubated with a probe of the STAT6 site; in lanes 5–9, nuclear proteins from uinduced (lane 5) or T+I-induced B-CLLs (lanes 6–9) were incubated with a probe of NF-AT-I site from the CD23b promoter. In supershift assays, antibodies raised against STAT5 (lane 3), STAT6 (lane 4), NF-ATp (lane 7), NF-ATc (lane 8) or both NF-ATs (lane 9) were added. The STAT6-specific and the STAT6-supershift complex (S6-SS) are indicated by arrowheads. NF-AT complexes are indicated by a bracket. The filled square indicates the NF-ATp supershift complex; asterisks indicate NF-ATc-specific supershift complexes.

motifs of NF-AT-I (positions − 152/ − 151) or NF-AT-II sites (positions − 241/ − 240) completely abolished any NF-AT binding and competition with the NF-AT binding to Pu-b_d-IL-2 probe in EMSAs (data not shown). While the NF-AT-II mutation had only marginal effect on the activity of CD23b promoter (around 2-fold reduction, data not shown), the mutation of NF-AT-I site (positions − 152/ − 151, Fig. 1B) exerted deleterious effect on the induction of CD23b promoter activity (Fig. 1C, middle panel). In particular, the strong increase in constitutive and inducible activity of the CD23b promoter mediated through the collaboration between NF-ATp and STAT6 factors was abolished when a promoter bearing a defective NF-AT-I site was used in the transfection assays (Fig. 1C).

We also tested whether STAT5 or STAT6 is the most prominent STAT factor binding to the CD23b promoter in B-CLL cells following IL-4 induction. As shown in Fig. 3B (lanes 1–4), incubation with a STAT6, but not with a STAT5-specific antibody, led to the complete supershift of the STAT complex. This indicates that in agreement with our former published data, STAT6 is the most prominent STAT factor binding to the CD23b promoter after IL-4 treatment of B-CLL cells.

4. Discussion

There are several T/A GGAA sequence motifs within the CD23b promoter to which NF-AT factors appear to bind (Fig. 2). We have shown here that NF-AT factors bind to two sites of the promoter, i.e. to NF-AT-I and NF-AT-II, with high affinity (Fig. 3). Similar to the strong binding of NF-AT to composite NF-AT/AP-1 motifs [19], the binding of NF-ATs to the composite NF-AT/STAT binding site could facilitate NF-AT binding due to a collaboration between both factors. While no direct protein–protein interactions between NF-AT and AP-1 have been detected in solution, AP-1 facilitates the binding of NF-AT to DNA, and numerous contacts between both factors have been observed when they are bound to a composed NF-AT/AP-1 sequence motif [32]. In myocytes and cardiomyocytes, NF-AT factors were found to bind to and collaborate with MEF2 or GATA-2, respectively [33,34]. It is likely that in other cells, such as in B-lymphocytes where NF-AT factors are expressed, partners other than or in addition to AP-1, GATA-2 and MEF2 collaborate with NF-AT factors in gene activation.

We show here that STAT6 cooperates with NF-ATp in the activation of the CD23b promoter. Although binding to the composite NF-AT-II/STAT motif (− 242/− 218) was an attractive explanation for the cooperation between the NF-AT and STAT factors, mutations introduced into the NF-AT-II (positions − 241/− 240) site had only marginal effect on the activity of a reporter construct. Deleterious effect from the mutations at positions − 152/ − 151 indicates that in the case of CD23b promoter, the cooperation between the NF-AT and STAT factors is mainly going through the separate NF-AT-I (− 153/− 148) and STAT (− 226/− 218) binding sites (Fig. 1A,B).

Another promoter that harbors multiple NF-AT and STAT5/6 binding sites is the inducible NF-ATc promoter, which was found to be strongly enhanced by NF-AT and STAT6 in co-transfection experiments (Chuvpilo et al., in preparation). It remains to be shown how NF-ATp and STAT6, whose activities are controlled by different signalling pathways, collaborate in the control of these (and probably further) promoters, and whether this collaboration is going through the individual or/and composite NF-AT/STAT binding elements.

Our data indicate that the CD23b promoter is a target for NF-ATp and NF-ATc in B-CLL cells. We expect that this is important to understand the molecular basis of B-CLL since CD23 has been described to play a significant role in the control of B-CLL cell viability. It has been suggested that the CD23a and b promoters are differently regulated in B-CLL cells. Fournier et al. [15] reported the possibility of a selective up-regulation of CD23b isoform by IL-2 and IFNα, stimuli which are able to induce B-CLL growth. Furthermore, it was suggested that selective increase in the expression of the CD23b-isoform might provoke the entry of resting (G_o) B-CLL cells into the cell cycle [35]. While our recent data confirm differences in the regulation of CD23 expression between the B-CLL and normal B-cells [36], we do not find any evidence indicating differential regulation of two isoforms. The ratio between CD23a and CD23b stayed between 2:1 and 3:1, regardless of the stimuli used. Therefore, we expect that expression of CD23a and CD23b isoforms is regulated by different, but coordinated pathways.

In regard to the progression of B-CLL, stimulation of membrane-bound CD23 on B-CLL cells up-regulates functional iNOS enzyme, which is able to counteract the normal apoptotic process and, therefore, may contribute to the malignant phenotype [9,37]. We conclude that the constitutive nuclear expression of NFAT in B-CLL cells leads, in concert with STAT factors, to an enhanced activation of the CD23b-promoter, increased expression of CD23b isoform and therefore, to enhanced viability of these malignant cells.

Acknowledgements

We are indebted to Claudia Mehringer, Gloria Meister, Olga Reimer and Ilona Piotrowski for excellent technical assistance. For donations of materials we wish to thank Drs. J. Altschmied (Frankfurt/Main) and E. Pfitzner (Frankfurt/Main). Very special thanks to Dr. Anneliese Schimpl for suggestions and critical reading of our manuscript.

This work was supported by grants from the Interdisziplinäres Zentrum für Klinische Forschung (BMBF), the Wilhelm-Sander-Stiftung and the Deutsche Forschungsgemeinschaft (SFB 465).

References

[1] A. Yokota, H Kikutani, T. Tanaka, R. Sato, E.L Barsumian, M Suemura, T. Kishimoto, Cell 55 (1988) 611–618.

[2] J.Y. Bonnefoy, S. Lecoanet-Henchoz, J F Gauchat, P Graber, J.P. Aubry, P. Jeannin, C Plater-Zyberk, Int Rev Immunol. 16 (1997) 113–128

[3] M Sarfati, S. Fournier, C.Y. Wu, G. Delespesse, Immunol Res. 11 (1992) 260–272

[4] A. Bansal, T. Roberts, E.M Hay, R Kay, R.S Pumphrey, P.B. Wilson, Clin. Exp. Immunol. 89 (1992) 452–455

[5] A.S Bansal, A.J. MacGregor, R.S Pumphrey, A.J. Silman, W.E Ollier, P.B Wilson, Clin Exp Rheumatol. 12 (1994) 281–285

[6] A Yokota, K Yukawa, A. Yamamoto, K. Sugiyama, M. Suemura, Y. Tashiro, T Kishimoto, H Kikutani, Proc. Natl. Acad Sci U. S A 89 (1992) 5030–5034.

[7] N. Dugas, I. Vouldoukis, P Becherel, M. Arock, P. Debre, M Tardieu, D.M Mossalayi, J F. Delfraissy, J.P Kolb, B. Dugas, Eur. J Immunol 26 (1996) 1394–1398.

[8] J.P. Kolb, A. Abadie, N. Paul-Eugene, M. Capron, M. Sarfati, B Dugas, G. Delespesse, J. Immunol 150 (1993) 4798–4809.

[9] J.P. Kolb, V. Roman, F. Mentz, H Zhao, D. Rouillard, N. Dugas, B. Dugas, F. Sigaux, Leuk Lymphoma 40 (2001) 243–257.

[10] H.J. Park, E.Y So, C.E. Lee, Mol Immunol. 35 (1998) 239–247

[11] I Kohler, E P. Rieber, Eur. J. Immunol. 23 (1993) 3066–3071.

[12] T Defrance, J P Aubry, F. Rousset, B. Vanbervliet, J.Y Bonnefoy, N. Arai, Y Takebe, T. Yokota, F Lee, K Arai, et al , J Exp Med. 165 (1987) 1459–1467

[13] W.J. Leonard, J J O'Shea, Annu Rev Immunol. 16 (1998) 293–322.

[14] C.E. Lee, S.R. Yoon, K.H. Pyun, Cell Immunol 146 (1993) 171–185.

[15] S Fournier, L P Yang, G Delespesse, M. Rubio, G Biron, M. Sarfati, Br. J. Haematol 89 (1995) 373–379.

[16] C. Kneitz, M Goller, R. Seggewiss, A Yaman, E. Serfling, H.P. Tony, Leuk Res 24 (2000) 331–337

[17] S.B. Tinnell, S.M. Jacobs-Helber, E Sterneck, S.T. Sawyer, D H. Conrad, Int. Immunol 10 (1998) 1529–1538.

[18] K. Schuh, A. Avots, H.P. Tony, E Serfling, C. Kneitz, Leuk Lymphoma 23 (1996) 583–592.

[19] A. Rao, C Luo, P.G. Hogan, Annu. Rev. Immunol. 15 (1997) 707–747.

[20] E. Serfling, F Berberich-Siebelt, S. Chuvpilo, E Jankevics, S. Klein-Hessling, T Twardzik, A Avots, Biochim Biophys Acta 1498 (2000) 1–18

[21] A. Kel, O. Kel-Margoulis, V. Babenko, E Wingender, J. Mol. Biol. 288 (1999) 353–376

[22] M.S. Choi, R.D Brines, M J. Holman, G.G. Klaus, Immunity 1 (1994) 179–187

[23] L. Venkataraman, D A Francis, Z Wang, J Liu, T.L. Rothstein, R Sen, Immunity 1 (1994) 189–196.

[24] J. Altschmied, J Duschl, Biotechniques 23 (1997) 436–438.

[25] S. Chuvpilo, A Avots, F. Berberich-Siebelt, J Glockner, C. Fischer, A. Kerstan, C Escher, I. Inashkina, F Hlubek, E. Jankevics, T Brabletz, E. Serfling, J. Immunol. 162 (1999) 7294–7301.

[26] T. Nosaka, T Kawashima, K Misawa, K Ikuta, A.L. Mui, T. Kitamura, EMBO J. 18 (1999) 4754–4765.

[27] E. Schreiber, P. Matthias, M.M. Muller, W. Schaffner, Nucleic Acids Res 17 (1989) 6419.

[28] K. Schuh, T. Twardzik, B Kneitz, J. Heyer, A Schimpl, E. Serfling, J. Exp. Med 188 (1998) 1369–1373

[29] S. Chuvpilo, M Zimmer, A. Kerstan, J. Glockner, A. Avots, C Escher, C Fischer, I. Inashkina, E Jankevics, F. Berberich-Siebelt, E Schmitt, E. Serfling, Immunity 10 (1999) 261–269.

[30] A Lischke, R. Moriggl, S. Brandlein, S Berchtold, W. Kammer, W Sebald, B. Groner, X. Liu, L. Hennighausen, K Friedrich, J Biol. Chem. 273 (1998) 31222–31229.

[31] E. Serfling, A. Avots, M. Neumann, Biochim Biophys Acta 1263 (1995) 181–200

[32] L. Chen, J.N. Glover, P G. Hogan, A Rao, S.C. Harrison, Nature 392 (1998) 42–48.

[33] E.R. Chin, E.N. Olson, J.A. Richardson, Q Yang, C. Humphries, J M. Shelton, H Wu, W Zhu, R. Bassel-Duby, R S Williams, Genes Dev 12 (1998) 2499–2509

[34] J D Molkentin, J R. Lu, C L Antos, B Markham, J. Richardson, J. Robbins, S.R Grant, E.N. Olson, Cell 93 (1998) 215–228

[35] S. Fournier, M Rubio, G Delespesse, M. Sarfati, Blood 84 (1994) 1881–1886

[36] M. Goller, C Kneitz, C. Mehringer, K. Müller, D. Jelley-Gibbs, E Gosselin, M. Wilhelm, H.-P Tony, Leuk. Res , (2000) in press

[37] H. Zhao, N Dugas, C. Mathiot, A Delmer, B Dugas, F. Sigaux, J P Kolb, Blood 92 (1998) 1031–1043.

ELSEVIER

Biochimica et Biophysica Acta 1588 (2002) 48–55

BIOCHIMICA ET BIOPHYSICA ACTA
BBA
www.bba-direct.com

Functional interaction of lithocholic acid conjugates with M3 muscarinic receptors on a human colon cancer cell line

Kunrong Cheng [a], Ying Chen [a], Piotr Zimniak [a], Jean-Pierre Raufman [a,*], Yinghua Xiao [b], Harold Frucht [b]

[a] Division of Gastroenterology and Hepatology, Department of Internal Medicine, Central Arkansas Veterans Healthcare System and University of Arkansas for Medical Sciences, Slot 567, 4301 W. Markham Street, Little Rock, AR 72205-7199, USA
[b] Digestive and Liver Diseases, College of Physicians and Surgeons, Columbia University, New York, NY 10032, USA

Received 29 November 2001, received in revised form 25 March 2002, accepted 5 April 2002

Abstract

Lithocholic acid (LA) conjugates interact with M3 receptors, the muscarinic receptor subtype that modulates colon cancer cell proliferation This observation prompted us to examine the action of bile acids on two human colon cancer cell lines: H508, which expresses M3 receptors, and SNU-C4, which does not Cellular proliferation was determined using a colorimetric assay. Interaction with muscarinic receptors was determined by measuring inhibition of muscarinic radioligand binding and changes in cellular inositol phosphate (IP) formation. Lithocholyltaurine (LCT) caused a dose-dependent increase in H508 cell proliferation that was not observed in SNU-C4 cells. After a 6-day incubation with 300 μM LCT, H508 cell proliferation increased by 200% compared to control. Moreover, in H508 cells, LCT caused a dose-dependent inhibition of radioligand binding and an increase in IP formation. LCT did not alter the rate of apoptosis in H508 or SNU-C4 cells These data indicate that, at concentrations achievable in the gut, LA derivatives interact with M3 muscarinic receptors on H508 human colon cancer cells, thereby causing an increase in IP formation and cell proliferation. This suggests a mechanism whereby alterations in intestinal bile acids may affect the growth of colon cancer cells.

© 2002 Elsevier Science B.V. All rights reserved

Keywords Bile acid, Colon cancer; Cholinergic receptor, Proliferation, ^{3}H-NMS binding; Inositol phosphate formation

1. Introduction

In the United States, colorectal cancer is the second most common cause of cancer death [1]. Experimental data support the concept that most of these cancers arise as a consequence of progression from normal colonic mucosa to adenomatous polyp to cancer, associated with the accumulation of somatic genetic alterations [2]. These alterations include mutations of both oncogenes and suppressor genes [2]. Environmental factors, such as dietary components and fecal bile acid concentrations, may play an important promoting role in this process [3–6].

Epidemiological studies in humans have associated the development of colorectal cancer with elevations in fecal bile acid concentration, particularly lithocholic acid (LA) [3–5] (although the term *bile acid* refers to the protonated form and *bile salt* the ionized form of these molecules, in this paper, as is common in the literature, these terms will be used interchangeably, and bile salt nomenclature will conform to recommendations by Hofmann et al. [7]). It has been reported that the ratio of lithocholate to deoxycholate (LA/DCA ratio) is 2-fold greater in persons with colon cancer compared to controls [8]. There has been a suggestion that by altering the delivery of conjugated bile acids to the colon, particularly secondary bile acids to the cecum and ascending colon (increased LA/DCA ratio), cholecystectomy increases the incidence of colon cancer [9–11]. Animal data, particularly from rats treated with carcinogens, indicate that direct instillation, or other means of increasing fecal bile acids, augments the development of colon cancer [12–14], and that the timing of interventions is important to the outcome [15]. In some studies, mucosal toxicity was noted following intrarectal

---

Abbreviations ACh, acetylcholine; carbachol, carbamylcholine; FBS, fetal bovine serum; IP, inositol phosphate; LA, lithocholic acid, DCA, deoxycholic acid, LCG, lithocholylglycine; LCT, lithocholyltaurine; MAP kinase, mitogen-activated protein kinase; NMS, *N*-[methyl]scopolamine, S-LCT, 3-*O*-sulfate LCT, SRB, sulforhodamine B

* Corresponding author. Tel.: +1-501-686-6217, fax. +1-501-686-6248
E-mail address raufmanjeanpierre@uams edu (J -P Raufman).

0925-4439/02/$ - see front matter © 2002 Elsevier Science B V. All rights reserved.
PII S0925-4439(02)00115-1

instillation of bile acids. In rats fed LA, the risk of aberrant colonic epithelial growth is increased compared to those fed deoxycholic acid (DCA) [16]. The major beneficial effects of dietary elements like fiber and calcium are thought to result from binding of bile acids in the gut lumen, thereby inhibiting their damaging effects on epithelial cells and potentiating actions on experimental colon cancer [17–19]. Absent from this body of largely circumstantial evidence is a defined mechanism whereby bile acids promote the development or progression of colon cancer.

Recently, experimental findings in our laboratories suggested a possible mechanism that explains how bile acids might stimulate colon cancer cell proliferation. In the course of examining the actions of bile acids on pepsinogen secretion from gastric chief cells, Raufman et al. [20] reported that taurine conjugates of LA, but not other bile acids, bind to muscarinic receptors, increase cellular inositol phosphates (IP), and stimulate secretion by a cholinergic mechanism. Molecular cloning studies revealed the existence of five muscarinic receptor genes, designated M1–5 based on their order of cloning [21,22]. Because gastric chief cells express M3 muscarinic cholinergic receptors [23,24], we concluded that these actions were mediated by interaction of lithocholyltaurine (LCT) with that receptor subtype. These findings have been confirmed in preliminary studies using Chinese hamster ovary cells transfected with the gene for the M3 muscarinic receptor [25]. Frucht et al. [26,27] reported that several colon cancer cell lines express M3 receptors, and that activation of these receptors with cholinergic agonists stimulates an increase in IPs and cell proliferation. Together, these observations suggest the possibility that the proliferative effects of fecal bile acids, particularly LA conjugates, on colonic neoplasia are mediated by cholinergic actions.

In the present study, we tested the hypothesis that conjugated derivatives of LA interact with M3 muscarinic receptors on colon cancer cells, thereby stimulating proliferation. The specific aims of this study were to test the ability of LA conjugates to bind to M3 receptors on H508 colon cancer cells, to activate post-receptor signaling mechanisms, and to stimulate cell proliferation. These actions were compared to those of known cholinergic agents and to the actions of the LCT metabolite, 3-*O*-sulfate LCT (S-LCT). The SNU-C4 colon cancer cell line, which does not express muscarinic receptors [27], was used as a control. Our results support the hypothesis that chronic exposure of colon cancer cells to fecal bile acids may promote growth of neoplastic cells by a cholinergic mechanism.

2. Materials and methods

2.1. Cell lines and bile acids

Colon cancer cell lines (H508 and SNU-C4) were available in the investigator's laboratories. Cancer cells were grown in RPMI 1640 (ATCC) supplemented with 10% fetal bovine serum (FBS) (Biowhittaker). Adherent cultures were passaged weekly at subconfluence after trypsinization. Cultures were maintained in incubators at 37 °C in an atmosphere of 5% CO_2 and 95% air. LCT was from Sigma. Lithocholylglycine (LCG) was from Steraloids. Stock solutions of LCT and LCG (100 mM) were prepared using DMSO (100%). The highest DMSO concentration in solutions incubated with cells was 0.6%. Carbachol was from CalBiochem. All other chemicals were obtained from Sigma or Fisher.

2.2. Cytotoxicity assays

Potential cytotoxic actions of bile acids and other test agents on H508 and SNU-C4 cells were examined by trypan blue exclusion.

2.3. Cell proliferation assay

Cell proliferation was determined using the sulforhodamine B (SRB) colorimetric assay [28]. Cells were seeded in 96-well plates (Corning Glass Works, Corning, NY) at approximately 10% confluence and allowed to attach for 24 h. The growth medium was removed and fresh medium without FBS and containing the indicated concentration of test agent was added. Cells were incubated for the described period of time at 37 °C in an atmosphere of 5% CO_2 and 95% air. After incubation, cells were treated for 30 min with 0.4% (w/v) SRB dissolved in 1% acetic acid. Protein-bound dye was extracted with 10 mM unbuffered Tris base. Absorbance was measured at 560 nm using a computer-interfaced, 96-well microtiter plate reader.

2.4. Caspase-3 assay

Caspase-3 activation is a key step in the regulation of apoptosis [29,30]. H508 and SNU-C4 cellular caspase-3 activity was measured using a kit from Sigma. Cells ($2-4 \times 10^5$ cells/ml) were seeded in T75 flasks. Growth medium was removed after 24 h and cells were incubated with the indicated agent, containing no added FBS, for 3 or 6 days at 37 °C in an atmosphere of 5% CO_2 and 95% air. After incubation, cells were washed with PBS and lysed. Caspase-3 activity was examined with 96-well plates in duplicate for 90 min and absorbance was measured at 405 nm using a computer-interfaced 96-well microtiter plate reader. As a positive control, H508 and SNU-C4 cells were incubated with DCA (250 μM) for 1.5 h and 30 min, respectively.

2.5. Radioligand binding

Binding of radioligand to muscarinic receptors on test cell lines was examined using *N*-[^{3}H-methyl]scopolamine (^{3}H-NMS, 82 Ci/mmol) (New England Nuclear, Boston, MA). The ^{3}H-NMS binding assay was performed as described previously [20]. Cells (28 × 10^6 cells/ml) were incubated for 45 min at 22 °C with 0.6 nM ^{3}H-NMS alone or with unlabeled ligands in an incubation solution containing 50 mM Tris (pH 7.4), 5 mM $MgCl_2$, 130 mM NaCl, 7.7 mM KCl, 1 mM EGTA, 4 µg/ml leupeptin, 0.1% bacitracin and 0.1% BSA. Nonsaturable binding was determined in the presence of 10 µM unlabeled NMS and was <20% of total binding in all experiments. The reaction was terminated by centrifuging 500 µl of cell suspension (10,000 × *g*) for 7 min at room temperature. Supernatant (100 µl) was sampled for determination of free ligand concentration, and the remaining liquid was carefully decanted. The cell pellet was washed, drained, and dissolved in 100 µl Soluene 350. Ecoscint A was added, and the radioactivity in the tubes was measured in a liquid scintillation counter (1214 Rackbeta, LKB/Wallac, Gaithersburg, MD). Values shown represent binding with radioligand alone (total binding) minus nonsaturable binding. The concentration of agent that caused 50% inhibition of binding (IC_{50}) was determined by using a nonlinear, least-squares curve fitting program [31].

2.6 Inositol phosphates

Inositol phosphates were measured by previously described methods [32]. Cells were seeded onto 6-well plates at a density of 10^6 cells/well. After 18 h, growth medium was removed from subconfluent cell monolayers, and the cells were incubated with RPMI 1640 containing myo-[2-^{3}H(N)]-inositol (1 µCi/ml, New England Nuclear), 2% FBS at 37 °C for 24 h. Before the addition of agents to be tested, cells were treated with 20 mM LiCl in PBS for 30 min. Phosphoinositide hydrolysis was initiated with the addition of PI buffer (135 mM NaCl; 20 mM HEPES; 2 mM $CaCl_2$; 1.2 mM $MgSO_4$; 1.0 mM EGTA; 20 mM LiCl; 11.1 mM glucose and 0.05% BSA) containing various concentrations of test agents. The incubation was allowed to proceed at 37 °C for 30 min. The incubation was stopped by adding 2 ml MeOH/HCl to each well. Total IPs (inositol 1-phosphate, inositol 1,4-bisphosphate and inositol 1,4,5-trisphosphate) were purified by chromatography with AG1-X8 resin (BioRad) and eluted with 1 mM ammonium formate and 100 mM formic acid [33,34]. Hydrofluor was added and radioactivity determined in a liquid scintillation counter.

2.7. Statistical analysis

All data are reported as mean ± SE of at least three independent experiments. Statistical analysis was performed using unpaired Student's *t*-tests to determine significance between two means. Statistical significance was set at *P* values less than 0.05.

3. Results

3.1. Effects of bile acids on colon cancer cell proliferation

To determine whether, as observed with other cholinergic agonists [27], LCT would stimulate proliferation of H508 cells, the cell lines were incubated with increasing concentrations of the bile acid for 6 days. Over the course of a 6-day incubation, LCT caused a dose-dependent increase in H508 cell proliferation (Fig. 1). Fig. 1a shows the time-

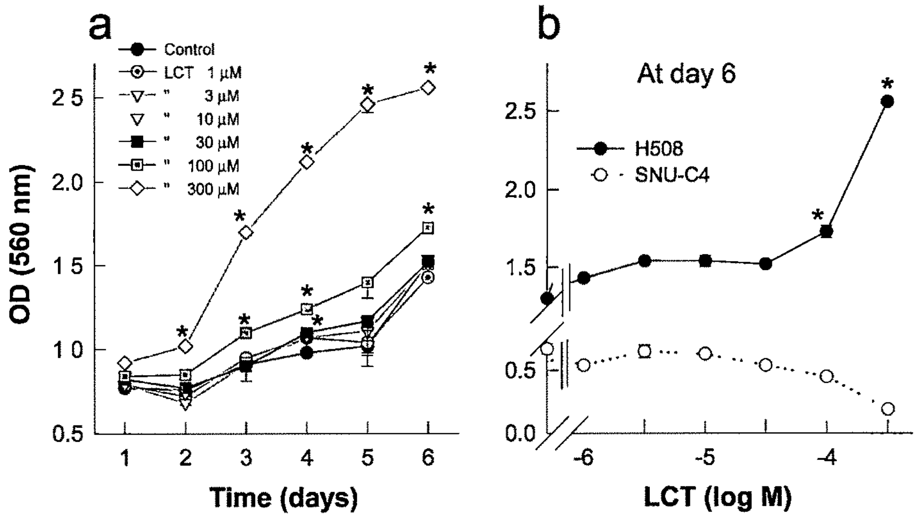

Fig 1 Actions of LCT on proliferation of H508 colon cancer cells. Cells were seeded on 96-well plates and incubated for 6 days with the indicated concentrations of LCT. Cellular proliferation was determined daily and expressed as optical density at 560 nm. Absorbance was determined after staining with SRB, as described in Materials and methods (a) Time-course for the effects of increasing concentrations of LCT on proliferation of H508 cells. (b) Dose–response curve for the effect of LCT on H508 and SNU-C4 cells at 6 days. In each experiment, values were determined in triplicate and results given are means from at least three separate experiments (*) Indicates values that are significantly greater ($P<0.05$) than those for control cells incubated without LCT Vertical bars, SE.

course for the effect on proliferation with increasing concentrations of the bile acid. With 100 and 300 μM LCT, a significant increase in cell proliferation was first detected at 3 and 2 days, respectively. With the highest concentration tested, 300 μM, the proliferative effects of LCT appeared to plateau after the 5th day of incubation, achieving an approximately 3-fold increase in proliferation. In the presence of 1 μM atropine (a concentration that did not significantly alter basal proliferation), after the 5th day of incubation, LCT (300 μM)-induced cell growth was inhibited to basal levels (data not shown). Fig. 1b shows the dose–response curve for LCT after 6 days of incubation. In the H508 cell line, significant stimulation was observed with LCT concentrations greater than 30 μM. In contrast, the SNU-C4 cells showed no significant change in cellular proliferation.

3.2. *Lack of cell toxicity with tested concentrations of bile acids*

To exclude cell damage as a reason for the differences in cell proliferation, we evaluated potential toxic effects of bile acid derivatives and DMSO, used as the solvent. We examined the actions of the bile acids and cholinergic agents on the exclusion of trypan blue from H508 and SNU-C4 cells. At concentrations used in the following experiments, none of these agents altered this measure of cell damage. Using conditions similar to those for cell proliferation and IP formation, no trypan blue staining was observed in 200 counted cells. Hence, there was no evidence of cell damage with these agents.

3.3. *Effect of bile acids on apoptosis in H508 and SNU-C4 cells*

To exclude apoptosis as a potential reason for the differences in cell proliferation, we evaluated the effects of bile acid derivatives and the other agents tested on caspase-3 activity in H508 and SNU-C4 cells. Caspase-3 plays a critical role in apoptosis [29] and caspase-3 activity has been used as an index of apoptosis by several investigators [30]. As shown in Fig. 2, after 3 and 6 days of incubation, in both colon cancer cell lines, DCA, used as a positive control [35], caused a 15- to 43-fold increase in apoptosis. This increase was abolished by addition of a caspase-3 inhibitor. In contrast, DMSO, carbachol and LCT had no effect on caspase-3 activity in H508 or SNU-C4 cells. S-LCT caused a small but significant increase in caspase-3 activation in H508, but not SNU-C4 cells. These results indicate that apoptosis is not the cause of the changes in cell proliferation observed with the LA derivatives.

3.4. *Effects of bile acids on binding of ^{3}H-NMS to H508 cells*

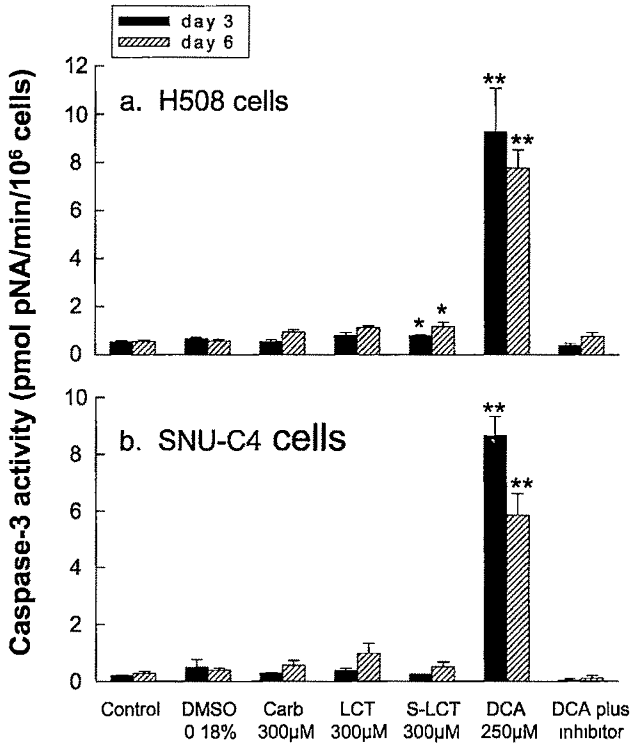

Fig 2. Actions of LCT, S-LCT, carbachol and solvents on caspase-3 activity in H508 and SNU-C4 cells (a) Caspase-3 activity in H508 cells following incubation with indicated concentrations of test agents for 3 and 6 days. (b) Caspase-3 activity in SNU-C4 cells following incubation with indicated concentrations of test agents for 3 and 6 days In each experiment, results given are means from at least three separate experiments Vertical bars, SE (*, **) Indicates values that are significantly greater ($P < 0.05$ and 0.001, respectively) than those for control cells

To determine the ability of LA conjugates to inhibit binding of a known muscarinic receptor ligand to M3 receptors, we used a radioligand binding assay. Binding of ^{3}H-NMS to H508 cells was examined alone, and in the presence of increasing concentrations of cholinergic agonists and conjugated derivatives of LA. Results of radioligand binding are not shown for SNU-C4 cells because, as published previously [26], ^{3}H-NMS does not bind to SNU-C4 cells. As shown in Fig. 3, acetylcholine (ACh), carbamylcholine (carbachol), LCT and LCG significantly inhibited binding of the cholinergic radioligand. In contrast, in the presence of S-LCT, the major human metabolite of LCT [36], binding of the radioligand was the same as the control. Inhibition of ^{3}H-NMS binding was detectable with 50 μM LCT or 120 μM LCG. Inhibition of binding observed with the maximal concentrations of LCT and LCG used, 250 and 600 μM, respectively, was approximately 25–30% of that observed with maximal concentrations of ACh or carbachol. Using a nonlinear, least-squares curve fitting program, LIGAND [31], the concentrations of ACh, carbachol, LCT and LCG that caused half-maximal inhibition of ^{3}H-NMS binding were 0.2, 0.3, 1.0 and 4.4 mM, respectively. These results indicate that, in terms of inhibition of ^{3}H-NMS binding, the bile acids are approximately 5 to 20 times less potent than ACh.

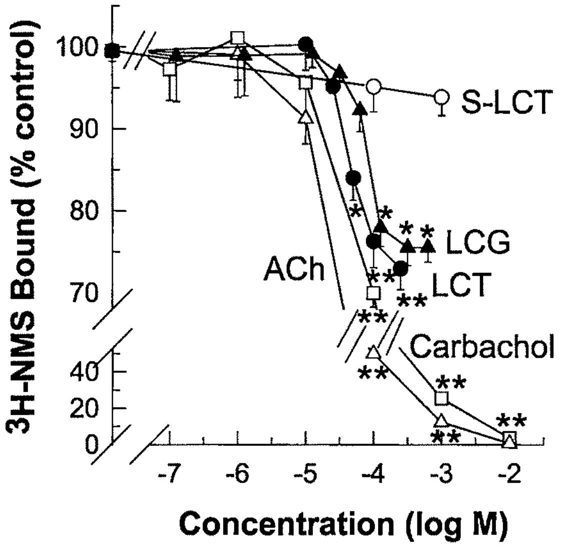

Fig 3. Actions of LCT on specific binding of ^{3}H-NMS to H508 colon cancer cells H508 cells (28 x 10^6 cells/ml) were incubated for 45 min at 22 °C with 0 6 nM ^{3}H-NMS and the indicated concentrations of ACh (open triangles), carbachol (open squares), LCT (closed circles), LCG (closed triangles) or 3-sul-LCT (S-LCT, open circles). Binding is expressed as the percentage of ^{3}H-NMS that was saturably bound in the absence of other agents. ^{3}H-NMS binding with the solvent for LCT, 0 6% DMSO, alone was 108 4 ± 5 4% control (not significantly different from control). In each experiment, results given are means from at least three separate experiments (*, **) Indicates values that are significantly less ($P<0$ 05 and 0 001, respectively) than ^{3}H-NMS binding in the absence of added agents. Vertical bars, SE

As shown in Fig. 4, although compared at different times, the pattern of interaction for 100 μM carbachol, LCT, and S-LCT was the same when comparing inhibition of ^{3}H-NMS binding to stimulation of cellular proliferation. That is, 100 μM carbachol and LCT caused similar inhibition of ^{3}H-NMS binding and stimulation of cellular proliferation, whereas the same concentration of S-LCT caused a significantly lesser effect on either parameter. This observation supports the hypothesis that LCT-induced stimulation of H508 cell proliferation is mediated by interaction with M3 muscarinic receptors. Neither LCT nor S-LCT (0.1–1000 μM) altered proliferation in the SNU-C4 cell line (data not shown).

3.5. Effects of bile acids on cellular formation of IPs

To confirm that interaction of bile acids with muscarinic receptors on H508 cells activates post-receptor signaling pathways, we examined the actions of these agents on cellular formation of IPs. Ligand interaction with M3 receptors stimulates activation of a guanine nucleotide binding (G) protein, $G_{q/11}$, with consequent activation of phospholipase C and an increase in cellular IPs and calcium [37]. As shown in Fig. 5a, in H508 cells, maximal concentrations of ACh and carbachol caused a robust, approximately 5-fold, increase in IP formation. LCT and LCG also caused a significant increase in cellular IP formation, but maximal stimulation was approximately 5% of that observed with ACh or carbachol (Fig. 5b). These results indicate that LA conjugates interact with M3 muscarinic receptors on H508 cells to stimulate the same post-receptor signaling cascade as ACh and carbachol. However, as expected, neither cholinergic agonists nor bile acids altered IP formation in SNU-C4 cells (Fig. 5a and b).

3.6. Effects of increasing concentrations of bile acids on carbachol- and ACh-induced increases in IPs

To test further the hypothesis that conjugates of LA interact with M3 muscarinic receptors on H508 cells, we examined the actions of increasing concentrations of LCT

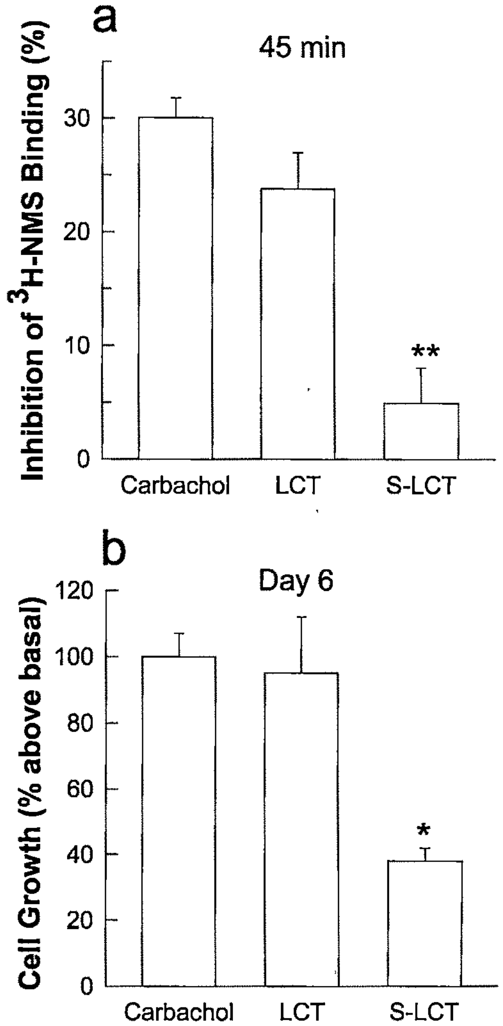

Fig 4 Comparison of the actions of LCT on inhibition of ^{3}H-NMS binding to H508 cells and cell proliferation (a) Actions of 100 μM carbachol, LCT and S-LCT on ^{3}H-NMS binding to H508 cells after 45 min incubation. (b) Actions of 100 μM carbachol, LCT and S-LCT on H508 cell proliferation after 6 days incubation. In each experiment, results given are means from at least three separate experiments. (*, **) Indicates that response with S-LCT is significantly less ($P<0$ 05 and 0 001, respectively) than that observed with carbachol or LCT Vertical bars, SE

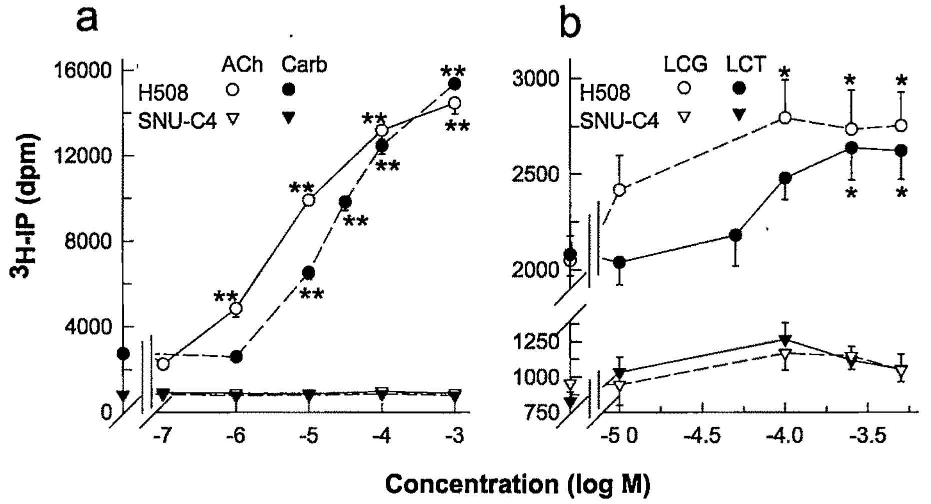

Fig. 5. Actions of ACh, carbachol, LCT, and LCG on H508 cellular IP formation in H508 and SNU-C4 cells. Cells (10^6 cells/well) were preincubated with myo-[2-^{3}H(N)]-inositol for 24 h at 37 °C, and the medium was replaced with a PBS solution containing 20 mM LiCl for 30 min. Cells were then incubated in PI buffer, alone or with test agents for 30 min at 37 °C Data are expressed as dpm in the IP fraction after separation by ion-exchange chromatography (a) Effect of increasing concentrations of ACh and carbachol on H508 and SNU-C4 cellular formation of IPs. (b) Effect of increasing concentrations of LCT and LCG on H508 and SNU-C4 cellular formation of IPs. Results given are means from 3 to 11 separate experiments. (*, **) Indicates values that are significantly greater ($P<0$ 05 and 0.001, respectively) than control. Vertical bars, SE

and LCG on ACh- and carbachol-induced increases in cellular IPs (Fig. 6). We hypothesized that if these agents were interacting with the same receptors, the less efficacious agents (LCT and LCG) would inhibit the actions of submaximal concentrations of the more efficacious agents (ACh and carbachol). As shown in Fig. 6a, increasing concentrations of LCT caused a progressive decrease in ACh- and carbachol-induced IP production. A similar effect was observed with LCG (Fig. 6b). In contrast, S-LCT did not alter carbachol-induced IP production (data not shown). These results support the hypothesis that the glycine and taurine conjugates of LA interact with the same receptors on H508 cells as ACh and carbachol.

4. Discussion

In animal models, increased concentrations of secondary bile acids are associated with increased proliferation of colorectal epithelium and the promotion of colon tumor growth [14]. Beneficial properties of agents like calcium and estrogens, that have been evaluated for chemopreven-

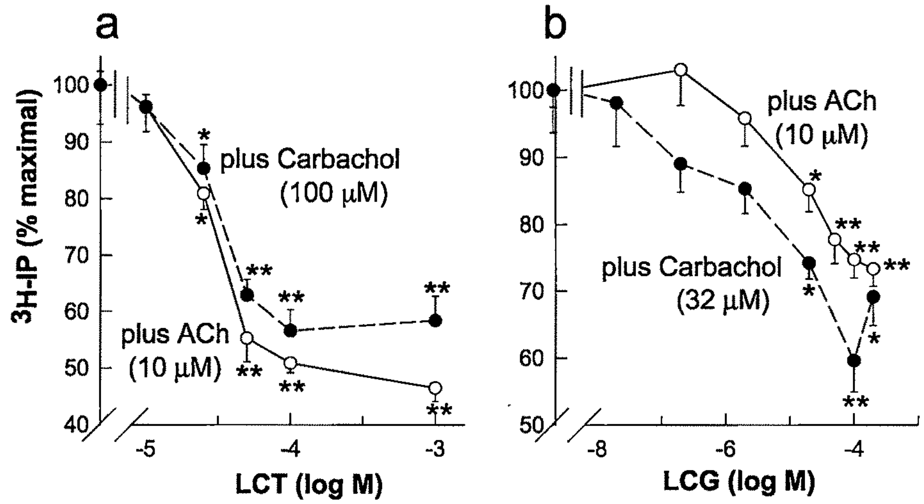

Fig. 6. Effects of LCT and LCG on the increase in IPs observed with submaximal concentrations of carbachol (closed circles) and ACh (open circles) (a) Effects of increasing concentrations of LCT on ACh- and carbachol-induced IP formation. (b) Effects of increasing concentrations of LCG on ACh- and carbachol-induced IP formation Results given are means from at least three separate experiments (*, **) Indicates values that are significantly less ($P<0$ 05 and 0 001, respectively) than control Vertical bars, SE.

tion of colon cancer in humans, result from the binding or reduced production of secondary bile acids [38]. Nevertheless, the mechanism whereby bile acids alter colonic epithelial-cell turnover has not been elucidated.

In the present study, we provide evidence that conjugates of LA stimulate colon cancer cell proliferation by muscarinic mechanisms. This includes the observations that LCT and LCG dose-dependently compete with a muscarinic radioligand for binding to M3 subtype receptors on cultured human colon cancer cells [27], and stimulate an increase in cellular formation of IPs. As predicted from the interaction at the same receptor, increasing concentrations of LCT or LCG inhibit IP formation by more efficacious cholinergic agonists (ACh or carbachol). More importantly, LCT at concentrations that inhibit ^{3}H-NMS binding and stimulate IP formation, increases proliferation of H508 cells and this increase can be inhibited by the muscarinic receptor inverse agonist atropine. Similar concentrations of LCT did not alter proliferation of colon cancer cells (SNU-C4) that do not express M3 receptors [27]. Moreover, LCT did not alter apoptosis in either cell line.

To draw conclusions regarding the physiological or pathophysiological implications of our observations, it is necessary to demonstrate in vivo in the organ of interest that LA derivatives achieve concentrations necessary for interaction with muscarinic receptors. In fact, concentrations of LA derivatives in proximal animal and human colon have been reported in the high micromolar to millimolar range [39–41], particularly if ileal damage prevents enterohepatic circulation. Hence, concentrations of LA conjugates that interact with muscarinic receptors on H508 colon cancer cells may be achieved in the normal colon. Moreover, although the effects of LA derivatives on muscarinic radioligand binding and stimulation of IP formation in H508 cells are less than those observed with ACh, several factors argue for a potential pathological role for the bile acids in vivo. This includes: (a) the likelihood that fecal bile acids that are normally found in stool will be in contact with colonic epithelial cells for many years (the average age for developing colon cancer is greater than 50 years [1]); (b) LA derivatives do not contain an ester linkage and, consequently, will not be subject to hydrolysis by tissue cholinesterases that rapidly inactivate ACh; and (c) lipophilic properties of monohydroxy LA derivatives allow these agents ready access to muscarinic receptors in the lipid bilayer of the colon cancer cell membrane.

Sulfation of LCT, a physiological detoxification mechanism [36], abolishes the molecule's ability to interact with muscarinic receptors. LCT is hepatotoxic in species that lack the enzyme necessary for sulfation [42]. The present study suggests the possibility that alterations in the ability to sulfate LA conjugates may alter initiation or progression of colon cancer. It is of interest to note that a colon cancer cell line has been reported to sulfate LA [43]. Hence, it may be of interest to study possible genotypic or phenotypic variation in expression of hepatic and colonic bile acid sulfatases in subjects with and without advanced colon cancer. Moreover, situations associated with decreased LA conjugate sulfation, like advanced liver disease, may result in augmented cholinergic actions of LA derivatives.

Although it is possible that chronic muscarinic receptor stimulation may lead to colonic epithelial cell proliferation and neoplastic transformation [3,44,45] the present studies do not address this. We did not examine the effect of LA derivatives on normal colonic epithelium. Nonetheless, because we show that LCT stimulates proliferation of already neoplastic cells, our data are compatible with the hypothesis that LA derivatives enhance the growth of existent cancer cells. Hence, once neoplastic transformation occurs as a consequence of genetic mutation or other causes, fecal bile acids may augment cancer cell proliferation and consequently tumor growth. Whether the use of selective anti-cholinergic agents or other approaches to blocking potential interactions of bile acids with neoplastic colonic epithelium is a useful adjunct to colon cancer prevention or treatment remains to be determined.

Acknowledgements

The authors thank Ms. Meshelle Helms for assistance in preparation of the manuscript. This work was supported by the Office of Research and Development, Medical Research Service, Department of Veterans Affairs (JPR) and NIH CA-70335 (HF).

References

[1] S.J. Winawer, R.H Fletcher, L Miller, F Godlee, M H Stolar, C D. Mulrow, S.H. Woolf, S N Glick, T.G. Ganiats, J H Bond, L. Rosen, J.G Zapka, S J Olsen, Gastroenterology 112 (1997) 594–642.

[2] D W Kinzler, B Vogelstein, Cell 87 (1996) 159–170.

[3] B.S Reddy, E L Wynder, Cancer 39 (1977) 2533–2539

[4] M.J Hill, B S. Drasar, R.E Williams, T W. Meade, A G Cox, J E. Simpson, B.C Morson, Lancet 1 (1975) 535–539.

[5] M J. Hill, Eur J Cancer Prev 1 (1991) 69–74

[6] P Lichtenstein, N V. Holm, P K Verkasalo, A Iliadou, J Kaprio, M Koskenvuo, E Pukkala, A Skytthe, K Hemminki, N Engl J Med 343 (2000) 78–85

[7] A F. Hofmann, J. Sjovall, G. Kurz, A Radominska, C D Schteingart, G S Tint, Z R Valacevic, D.R Setchell, J. Lipid Res 33 (1992) 599–604

[8] R W. Owen, P.J. Henly, M.H Thompson, M J. Hill, J Steroid Biochem 24 (1986) 391–394

[9] A Eckborn, J Yuen, H Adami, Gastroenterology 105 (1993) 142–147

[10] E. Giovannucci, G.A Colditz, M.J. Stampfer, Gastroenterology 105 (1993) 130–141

[11] E Zuccato, M. Venturi, G. Di Leo, L Colombo, C Bertolo, S.B Doldi, E. Mussini, Dig Dis Sci 38 (1993) 514–519

[12] T Narisawa, N.E. Magadia, J H Weisburger, E L. Wynder, J Natl Cancer Inst 53 (1974) 1093–1097.

[13] B.S. Reddy, T. Narasawa, J H. Weisburger, E L. Wynder, J Natl. Cancer Inst 56 (1976) 441–442

[14] F M. Nagengast, M J A L. Grubben, I P. van Munster, Eur J. Cancer 31A (1995) 1067–1070.

[15] PK Baijal, E P Clow, D W Fitzpatrick, R P. Bird, Can J. Physiol. Pharmacol 76 (1998) 1095–1102

[16] PK. Baijal, D.W Fitzpatrick, R P Bird, Nutr. Cancer 31 (1998) 81–89

[17] H.L Newmark, M J Wargovich, W.R. Bruce, J Natl Cancer Inst. 72 (1984) 1323–1325

[18] B.C Pence, Mutat Res. 290 (1993) 87–95

[19] B C Pence, F Buddingh, Carcinogenesis 9 (1988) 187–190.

[20] J P. Raufman, P. Zimniak, A. Bartoszko-Malik, Am J. Physiol 274 (1998) G997–G1004

[21] T Bonner, N Buckley, A Young, M Brann, Science 237 (1987) 527–532.

[22] M R. Brann, J Ellis, H Jorgensen, D Hill-Eubanks, S V Jones, Prog Brain Res 98 (1993) 121–127

[23] V.E Sutliff, S Rattan, J.D Gardner, R.T. Jensen, Am J Physiol. 257 (1989) G226–G234

[24] M Kajimura, M A. Reuben, G Sachs, Gastroenterology 103 (1992) 870–875.

[25] J -P Raufman, Y Chen, P. Zimniak, A Bartoszko-Malik, Gastroenterology 116 (1999) A638 (abstract)

[26] H Frucht, A F Gazdar, J -A Park, H Oie, R T Jensen, Cancer Res. 52 (1992) 1114–1122.

[27] H Frucht, R T Jensen, D. Dexter, W -L. Yang, Y Xiao, Clin. Cancer Res 5 (1999) 2532–2539.

[28] P Skekan, R. Storeng, D Scudier, A Monks, J McMahon, D. Vistica, J T Warren, H Bokesch, S. Kenney, M R Boyd, J Natl. Cancer Inst 82 (1990) 1107–1112.

[29] G.M Cohen, Biochem J. 326 (Pt. 1) (1997) 1–16.

[30] D. Mukhopadhyay, S Sundereshan, C. Rao, A.A. Karande, J. Biol Chem 276 (2001) 28268–28273.

[31] P J Munson, D Rodbard, Anal Biochem 107 (1980) 220–239

[32] C.M. Fraser, C Wang, D A Robinson, J.D Gocayne, J C. Venter, Mol Pharmacol 36 (1989) 840–847

[33] R V Benya, E Wada, J.F Battey, Z Fathi, L.H Wang, S A. Mantey, D.H. Coy, R.T Jensen, Mol Pharmacol. 42 (1992) 1058–1068

[34] R V. Benya, T. Kusui, F Shikado, J.F Battey, R T Jensen, J Biol. Chem 269 (1994) 11721–11728

[35] D Qiao, E D Stratagouleas, J D. Martinez, Carcinogenesis 22 (2001) 35–41.

[36] A E Cowen, M G Korman, A F. Hofmann, O W Cass, S B Coffin, Gastroenterology 69 (1975) 67–76.

[37] X Xu, W Zeng, S Muallem, J Biol. Chem. 271 (1996) 11737–11744

[38] P A Janne, R.J Mayer, N Engl J Med 342 (2000) 1960–1968

[39] C Klos, G Paumgartner, J Reichen, Am J Physiol 236 (1979) E434–E440.

[40] J M Pries, C A. Sherman, G C Williams, R F Hanson, Am J Physiol 236 (1979) E191–E197

[41] J.R Poley, A F. Hofmann, Gastroenterology 71 (1976) 38–44

[42] B.I Cohen, A F Hofmann, E.H. Mosbach, R J Stenger, M A Rothschild, L R. Hagey, Y B Yoon, Gastroenterology 91 (1986) 189–197

[43] B. Halvorsen, B.F Kase, K. Prydz, S Garagozlian, M S Andresen, S O Kolset, Biochem J 343 (1999) 533–539

[44] M Guizzetti, P Costa, J Peters, L.G Costa, Eur J Pharmacol. 297 (1996) 262–273.

[45] B Nicke, K Detjen, C D Logsdon, J Biol Chem. 274 (1999) 21701–21706

ELSEVIER

Biochimica et Biophysica Acta 1588 (2002) 56–64

BIOCHIMICA ET BIOPHYSICA ACTA
BBA
www.bba-direct.com

Molecular understanding of aluminum-induced topological changes in $(CCG)_{12}$ triplet repeats: relevance to neurological disorders

Kallur Siddaramaiah Latha [a], Suram Anitha [b], Kosagi Sharaf Jagannatha Rao [b,*], Mysore Ananthamurthy Viswamitra [a,†]

[a] *Centre for Human Genetics, Institute of Biotechnology, G-05, Discoverer, ITPL, Whitefield Road, Bangalore 560066, India*
[b] *Department of Biochemistry and Nutrition, Central Food Technological Research Institute, Mysore 570013, India*

Received 11 December 2001; received in revised form 23 April 2002, accepted 23 April 2002

Abstract

Recent studies have shown that gene mutations are involved in the pathology of neurological disorders. CCG repeats cause genetic instability and are localized at the 5′ end of the non-coding regions of the FMR1 gene in fragile X syndrome. Our studies for the first time showed that aluminum (Al) levels were elevated in the serum samples of fragile X syndrome and also provide evidence for the interaction of aluminum with $(CCG)_{12}$-repeats. Circular dichroism spectroscopic studies of $(CCG)_{12}$ indicated B-DNA conformation and in the presence of Al (10^{-5} M) CCG repeats attained Z-DNA conformation. Further spectroscopic studies, which included melting profiles, ethidium bromide binding patterns and interaction of Z-DNA specific polyclonal antibodies confirmed the Z-conformation in $(CCG)_{12}$-repeats in the presence of Al (10^{-5} M). It is interesting to mention that Al-induced Z-conformation is stable even after the total removal of Al from CCG by desferoximine, a chelating drug. This is the first report to proof the role of Al in modulating the DNA (CCG repeats) topology and this information provides a clue about the possible involvement of Al at a molecular level in neurological/neurodegenerative disorders.

© 2002 Elsevier Science B.V. All rights reserved.

Keywords: CCG-triplet repeat, Z-DNA; Fragile X syndrome; Aluminum; DNA topology

---

1. Introduction

DNA molecule is polymorphic in nature having many conformations [1–5] and these conformational changes are regulated by specific DNA sequences. Right-handed B-DNA conformation is the most predominant conformation in biological systems. Non-B-DNA conformations also occur in vivo like Z-DNA, triple helix and tetraplexes [6–8]. DNA topology has been proposed to have a crucial role in DNA transcription and susceptibility of DNA for oxidative damage [9]. The expansion of DNA-triplet repeats defines a new type of mutation in the human genome, namely "dynamic mutation" leading to genomic instability [10–14]. Mutation studies have revealed that abnormal expansion of CCG, CGG, CTG, CAG etc., were implicated in more than 12 neurological disorders [11]. GC*-rich triplet repeats CCG, CGG, GCC, GGC are predominantly involved in fragile X neurodisorder [11,15–19]. These repeats are localized both in coding and non-coding regions of genes [11,15,16]. Further, the expansion of these repeats differ, depending on the location of the repeat tract in the gene, and the consequences range from reduction of transcription initiation to protein toxicity [19].

Aluminum (Al) is one of the strong suspected etiological factors in neurodegenerative disorders like Alzheimer's, Parkinsonism and GuamParkinsonism/amyotrophic lateral sclerosis [20–23]. In the present study, we have reported for the first time elevated concentrations of Al in the serum samples of fragile X syndrome patients, thus providing a clue on possible role of Al in fragile X neurodisorder. Studies from our laboratory [24,25] and elsewhere [26] show that Al preferentially binds to DNA. However, our studies show for the first time that Al strongly binds to AT*-rich sequences with no conformational transition [25], where it causes a $Z \rightarrow A$ helical transition in GC*-rich oligomers [24]. From this perspective, it is important to know whether the topology of CCG repeats play a vital role in fragile X neurodisorders through the modulation of tran-

---

[*] Corresponding author. Fax +91-821-517233
E-mail address: kjr4n@yahoo.com (K.S.J. Rao)
[†] Recently deceased

0925-4439/02/$ - see front matter © 2002 Elsevier Science B.V. All rights reserved
PII S0925-4439(02)00133-3

scription of FMR1 gene. We hypothesize that DNA topology in these repeats plays an important role in the expression of FMR1 gene. Keeping the above complexity in view, the topology of $(CCG)_{12}$-long repeats and the role of Al in modulating CCG topology was studied. Further, the relevance of these topological changes to the expression of FMR1 gene was hypothesized.

2. Materials and methods

2.1. Aluminum levels in the serum of fragile X syndrome patients

Blood samples from 10 fragile X syndrome patients and 10 normal (no etiology of any neurological disorders) humans were collected from J.S.S. Medical College and Hospital, Mysore, India and the serum samples were separated. Al levels were estimated using Inductively coupled Plasma Atomic Emission Spectrometer (ICPAES) model JY 38 at wavelength 396.152 nm with detection limit at 0.002 ppm. The optimization of ICPAES was evaluated by line selection and detection limits and validation of analysis was tested by analyzing certified standard reference material (bovine liver 1577a) [27,28].

2.2. Ethical issue

Ethical approval for collecting blood samples from fragile X syndrome and normal humans was obtained from the Research Ethical Committee of J.S.S. Hospital. A written consent was obtained from the patients/carers prior to the collection of blood samples.

2.3. CCG repeats synthesis

The $(CCG)_{12}$ repeats were synthesized by phosphoramidite technique using a 380B ABI automated DNA synthesizer. Deprotection of the oligonucleotide bases were carried out in the presence of ammonia at 55 °C for 12 h. The samples were ethanol precipitated, FPLC purified and freeze-dried.

2.4. Aluminum maltolate synthesis

Aluminum maltolate was prepared in our laboratory from aluminum chloride hexahydrate and maltol (3-hydroxy-2-methyl-4H-pyran-4-one) following the method of Finneagen et al. [29].

2.5. Circular dichroism (CD) studies

CD spectra (210–330 nm) were recorded for $(CCG)_{12}$ (5×10^{-4} M) in 0.01 M HEPES buffer (pH 7.5). The effect of different concentrations of Al-maltolate (5×10^{-9} to 5×10^{-4} M) on the mean molar ellipticity values were studied. CD spectra were also recorded to understand the effect of the Al-chelating drug, desferoximine (5×10^{-5} M) on Al–$(CCG)_{12}$ (1:10 M) (the complex under Z-DNA conformation) complex spectra. The CD spectra were recorded on a JASCO-J500 Spectropolarimeter with 1 mm width and 1 mm cell length. The spectra at each concentration were averaged from four recordings. DNA conformations were characterized following the guidelines of Gray et al. [30].

2.6. C–C mismatch studies*

C–C* mismatch base pair formation in CCG repeats in the presence and absence of Al, was studied by monitoring the increase in the magnitude of long-wavelength positive CD band at 283 nm when pH was lowered from 7.0 to 5.0 in the presence of 0.1 and 0.5 M Na^+.

2.7. Melting temperature studies

The melting temperature curves for $(CCG)_{12}$ (5.0×10^{-4} M) were determined in the presence or absence of Al-maltolate (5.0×10^{-8} to 5.0×10^{-4} M) in 0.01 M HEPES buffer (pH 7.5). Absorbance at 260 nm was recorded at different temperatures (20–85 °C, 1 °C/min) using a Gilford Response II UV spectrophotometer. Tm values were determined graphically from the percent hyperchromicity vs. temperature plots. The temperature studies were also conducted in the presence and absence of Al-chelating drug desferoximine (5×10^{-5} M). The precision in Tm values estimated from the variance in three repeated experiments was +0.05 °C.

2.8. Fluorescence studies

Fluorescence emission studies were carried out using equimolar concentrations of CCG repeats and ethidium bromide (EtBr) (2.5×10^{-5}:2.5×10^{-5} M (1:1)) solutions. DNA/EtBr solutions were excited at 535 nm and emission was monitored at 600 nm using JASCO J77 spectrofluorimeter. The effect of different concentrations of Al (5×10^{-10} to 5×10^{-4} M) on the EtBr fluorescence was investigated and the percentage decrease in EtBr fluorescence was calculated. The effect of desferoximine on the EtBr fluorescence of DNA/EtBr complex in the presence of Al (5×10^{-10} to 5×10^{-4} M) was also investigated.

2.9. ELISA

$(CCG)_{12}$ (25 μg/ml) were mixed with different concentrations of Al-maltolate (5×10^{-10} to 5×10^{-4} M) and incubated for 30 min at room temperature. All solutions were in HEPES buffer (pH 7.5). Titer plates were pre-coated with 100 μl of protamine sulfate. After the incubation, the CCG/Al mixture was diluted to a CCG concentration of 2.5

μg/ml with no EDTA in the buffer. One hundred microliters of this mixture was added to micro titer plate and incubated overnight at 4 °C. Anti-Z-polyclone was used in this ELISA test. The absorbance was recorded at 410 nm.

2 10. Extra-helical alignment of CCG repeats

The possible alignment of CCG repeats were designed with reference to anti-parallel staggered, anti-parallel, and parallel and the bonding pattern with respect to Watson–Crick base pair, mismatch and protonated were derived theoretically using the Fresco and Alberts model [31]. The possible alignments were represented in Fig. 6.

3. Results

3.1. Aluminum levels in the serum of fragile X syndrome patients

Al levels were found to be 0.53 (± 0.06) × 10^{-4} M and 1.8 (± 0.2) × 10^{-4} M in normal and fragile X syndrome affected persons, respectively. This data indicates that Al level is high (+231%) in fragile X syndrome affected persons.

3.2 Al-maltolate

Understanding the toxicity of Al is governed by the speciation chemistry of Al over pH range. To overcome this hydrolytic chemistry problem in the present study, a highly soluble Al-maltolate is used. This Al complex is hydrolytically stable from pH 2.0 to 12.0 and possesses a neutral charge. It is highly soluble compound and enhances free Al existence by 100-fold at neutral pH compared to any other inorganic or organic Al complex and has been used as a model compound to be used for understanding molecular effects of Al in a biological system [32]. The application of this compound in DNA conformational studies will overcome Karlik et al.'s [26] complex explanation on Al speciation–DNA interactions. Most of the researchers have used inorganic salts of Al where the concentration of soluble free Al at pH 7.0 will be 50 μM in a 10 mM solution. This means free Al concentration is 10^{-12} M only and the rest of Al is in $Al(OH)_3$ precipitate form.

3.3. CD studies on DNA helicity

CD spectra of $(CCG)_{12}$ indicated classical B-DNA conformation with a characteristic positive peak at 275 nm and a negative peak at 245 nm (Fig. 1a). On addition of lower concentrations (10^{-8} to 10^{-6} M) of Al, there was a decrease in the magnitude of both the positive and negative peaks at 275 and 245 nm, respectively (Fig. 1b). But at higher Al concentrations (10^{-5} and 10^{-4} M), CCG attained Z-DNA conformation with characteristic two negative peaks at 245 and 290 nm, and a positive peak at 260 nm (Fig. 1c and d). The effect of Al-chelating drug, desferoximine (10^{-5}M) on Al–CCG complex (10^{-5} M of Al) indicated that the total removal of Al by the drug could not reverse the spectral characteristics back to B-conformation (free CCG) from Z-conformation (CCG–Al complex) (Fig. 1e). The total removal of Al from CCG complex was ensured by dialyzing desferoximine/Al–CCG (10^{-5}:10^{-5}:10^{-5} M) complex overnight in 0.001 M HEPES Buffer. The dialyzed CCG was digested in nitric acid and Al content in the CCG was estimated by ICPAES. We found no signal in the digested CCG solution indicating total removal of Al from CCG-oligomer by desferoximine.

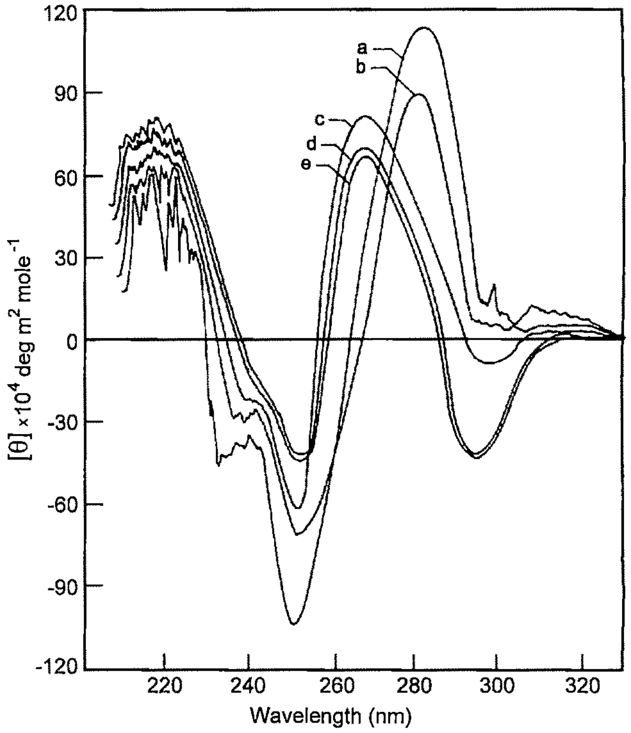

Fig. 1 Effect of Al on CD spectra of $(CCG)_{12}$ in 0 01 M HEPES buffer (pH 7 4). a=$(CCG)_{12}$, b=Al (5 × 10^{-7} M), c=Al (5 × 10^{-5} M), d=Al (5 × 10^{-4} M), e=Al (5 × 10^{-4} M)+desferoximine (5 × 10^{-4} M)

3.4. ELISA

Z-DNA conformation was further confirmed using left-handed Z-DNA-specific polyclonal antibody using ELISA reader. The data confirmed the presence of left-handed Z-DNA conformation in $(CCG)_{12}$ at Al concentrations above 10^{-5} M (Fig. 2). Immunochemical assay of Z-DNA using anti-Z–IgG polyclonal antibody at different Al concentrations (A=Al (5 × 10^{-9} M), B=Al (5 × 10^{-7} M), C=Al (5 × 10^{-6} M), D=Al (5 × 10^{-5} M) and E=Al (5 × 10^{-4} M)). Z-DNA conformation was observed in D and E columns, where Al concentration is 5 × 10^{-5} M and (5 × 10^{-4} M), respectively.

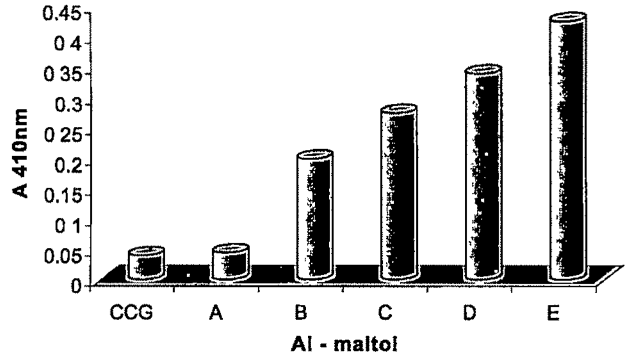

Fig. 2. Immunochemical assay of Z-DNA using anti-Z–IgG polyclonal antibody at different Al concentrations A=Al (5×10^{-9} M), B=Al (5×10^{-7} M), C=Al (5×10^{-6} M), D=Al (5×10^{-5} M), E=Al (5×10^{-4} M).

3.5. C–C* mismatch studies

C–C* mismatch base pairing was detected by monitoring CD changes at 283 nm with reference to pH 5.0 to 7.0 at 0.1 and 0.5 M Na^+ concentration. There was an increase in the magnitude of long-wavelength positive band at 283 nm when pH was lowered from 7.0 to 5.0 at 0.1 and 0.5 M Na, indicating the formation of C–C* mismatch base pairs. The lower concentration of Al (10^{-7} M) did not alter C–C* mismatch base pair formation (Fig. 3). But higher concentration of Al (10^{-4} M) caused a reduction in C–C* mismatch base pair formation, thus possibly favoring the stability of Z-DNA conformation.

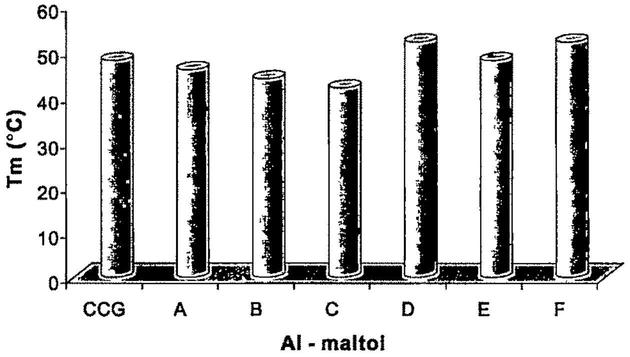

Fig. 4. Effect of Al on Tm (°C) values of $(CCG)_{12}$ oligomers in 0.01 M HEPES buffer (pH 7.4) CCG=$(CCG)_{12}$ oligomers alone, A=Al (5×10^{-8} M), B=Al (5×10^{-7} M), C=Al (5×10^{-6} M), D=Al (5×10^{-4} M), E=Al (5×10^{-7} M)+desferoximine (5×10^{-4} M), F=Al (5×10^{-4} M)+desferoximine (5×10^{-4} M).

3.6. Melting temperature studies

The Tm value for $(CCG)_{12}$ alone was found to be 48 °C. The lower concentrations of Al ($10^{-8}\times10^{-6}$ M) decreased the Tm to 42 °C. But higher concentrations of Al (10^{-4} M) increased the Tm to 52 °C. However, the addition of the drug desferoximine (10^{-4} M) on Al (10^{-4} M)/CCG complex did not alter Tm (52 °C) indicating the stable conformation of CCG complex even after Al is removed. However, desferoximine (10^{-4} M) could chelate Al ($10^{-8}\times10^{-6}$ M) from the CCG–Al complex and could reverse Tm from 42 to 48 °C (Fig. 4).

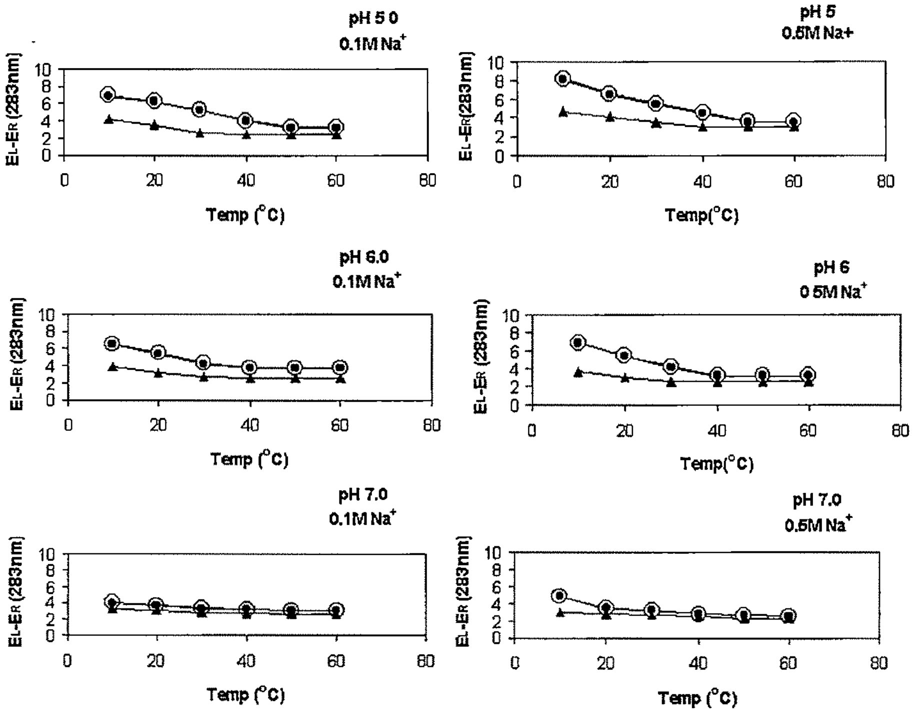

Fig. 3. Effect of Al on CD spectra of $(CCG)_{12}$ at 283 nm at different pH and Na^+ concentrations ○=$(CCG)_{12}$ (10^{-5} M), ●=$(CCG)_{12}$ (10^{-5} M)+Al (10^{-7} M), ▲=$(CCG)_{12}$ (10^{-5} M)+Al (10^{-4} M).

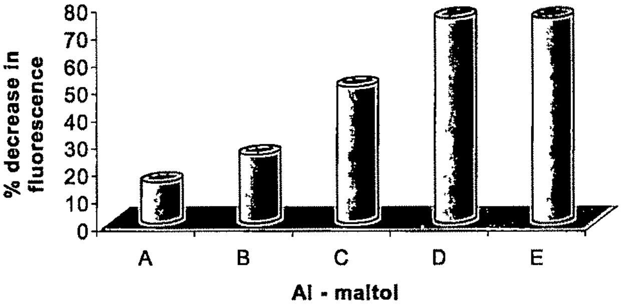

Fig 5. The effect of Al on percent change in EtBr fluorescence of $(CCG)_{12}$ oligomers in 0.01 M HEPES buffer (pH 7.4) A = Al (5×10^{-8} M), B = Al (5×10^{-7} M), C = Al (5×10^{-6} M), D = Al (5×10^{-4} M), E = Al (5×10^{-4} M) + desferoximine (5×10^{-4} M)

3.7. Fluorescence studies

Fluorescence emission spectra were monitored for equimolar concentrations of DNA/EtBr in the presence and absence of Al. On additions of different concentrations of Al to CCG/EtBr solutions, the fluorescence emission decreased in a concentration-dependent manner (Fig. 5). The concentrations of Al that caused 75%, 50%, and 25% reductions in EtBr fluorescence were 10^{-4}, 10^{-6}, and 10^{-7} M, respectively. The chelation of Al (10^{-4} M) by the chelating drug, desferoximine (10^{-4} M) did not alter the Al-induced EtBr fluorescence reduction (75%). This data clearly confirmed, once again, the formation of Z-DNA conformation in CCG repeats.

3.8. Extra-helical alignment of CCG repeats

Extra-helical alignment in CCG repeats showed the alignment with reference to anti-parallel staggered, anti-parallel, and parallel was designed. These alignments were similar to what was predicted for polynucleotides by Fresco and Alberts [31]. In the anti-parallel staggered conformation 5′-end, C– is unbound and free in nature in both the strands and the number of mismatches were 11 in $(CCG)_{12}$. The number of mismatches in anti-parallel, and parallel alignments were 12. The above alignments of $(CCG)_{12}$ triplet repeats were represented in Fig. 6.

4. Discussion

Our studies for the first time evidence that Al brought about helical transition from B- to Z-DNA conformation in $(CCG)_{12}$-repeats. The total removal of Al by chelating drugs, namely desferoximine, did not reverse the Z-DNA conformation to B-DNA, indicating the irreversible and stable conformation. The molar concentration of Al in the serum of fragile X syndrome is 1.8×10^{-4}M. In the

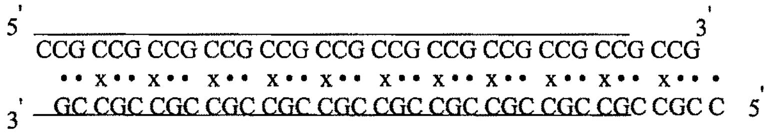
5'
3'
CCG CCG CCG CCG CCG CCG CCG CCG CCG CCG CCG CCG
• • x • • x • • x • • x • • x • • x • • x • • x • • x • • x • • x • • •
3'
GC CGC CGC CGC CGC CGC CGC CGC CGC CGC CGC CGC C
5'

Antiparallel Staggered. $(CCG)_{12}$ (11 mismatches)

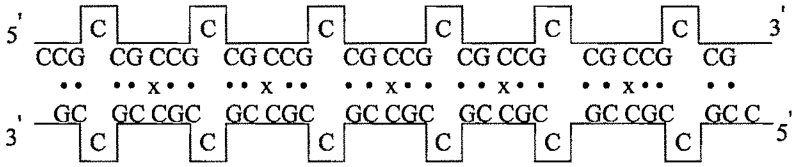
5'
3'
C
C
C
C
C
C
CCG CG CCG CG CCG CG CCG CG CCG CG CCG CG
GC GC CGC GC CGC GC CGC GC CGC GC CGC GC C
C
C
C
C
C
C
3'
5'

Detailed model of mismatches in Antiparallel Staggered of $(CCG)_{12}$ repeats.

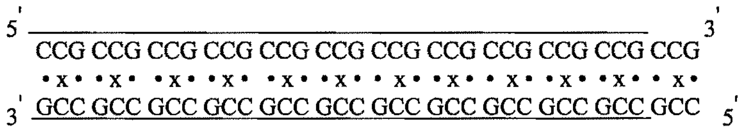
5'
3'
CCG CCG CCG CCG CCG CCG CCG CCG CCG CCG CCG CCG
•x• •x• •x• •x• •x• •x• •x• •x• •x• •x• •x• •x•
3'
GCC GCC GCC GCC GCC GCC GCC GCC GCC GCC GCC GCC
5'

Antiparallel pairing of $(CCG)_{12}$ repeats (12 mismatches)

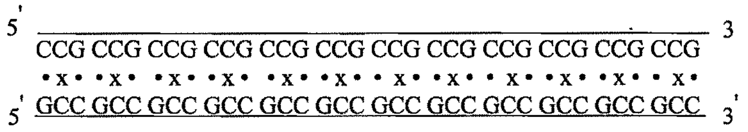
5'
3
CCG CCG CCG CCG CCG CCG CCG CCG CCG CCG CCG CCG
•x• •x• •x• •x• •x• •x• •x• •x• •x• •x• •x• •x•
5'
GCC GCC GCC GCC GCC GCC GCC GCC GCC GCC GCC GCC
3'

Parallel pairing of $(CCG)_{12}$ repeats (12 mismatches)

Fig 6. The possible alignments of $(CCG)_{12}$ triplet repeats.

present investigation, it was observed that 10^{-4} M and 10^{-5} M of Al could favor Z-conformation in CCG repeats. It is interesting to mention that Al concentration recorded (10^{-4} M) in serum could induce Z-DNA conformation in $(CCG)_{12}$ repeats and thus these findings have physiological significance. Further, Al-induced Z-DNA conformation is stable as evidenced by irreversibility of the conformation even after total removal of Al by desferoximine. Z-DNA conformation in CCG repeats could act physically to prevent the movement or the binding of RNA polymerase, thus modulating transcription. Therefore, in fragile X syndrome, the FMR1 gene might have been turned off due to the formation of Z-DNA by Al. We developed a hypothesis, which is explained in a later part of this discussion in strong support of the above concept. Thus, formation of Z-DNA topology in CCG long repeats may have a biological significance in molecular understanding of the role of FMR1 gene in fragile X syndrome and the relevance of Al in this neurological disorder.

The long CCG triplet repeats at the FRAXA site are involved in the pathology of fragile X syndrome [11]. The poor chromatin staining and the large expansions of the CCG repeats block at the FRAXA site suggested an altered chromatin structure and strong nucleosome exclusion [33]. It is hypothesized that Z-DNA conformation is also one of the likely factors which favor exclusion of nucleosome formation [34] and this will possibly explain the poor chromatin staining of the fragile site. The nucleosome formation depends on the bending and twisting elastic energy to transform the DNA intrinsic super structure into the nucleosome structure [35]. Z-DNA, being more rigid, cannot bend to favor the formation of nucleosome. Thus, DNA topology is very important for the histones protein binding, and this binding favors the formation of nucleosomes and also RNA polymerase binding during transcription [36,37]. It was previously shown that the Z-DNA conformation depends largely on the sequence and on the degree of negative super coiling [38].

4.1. Our hypothesis on how FMR1 gene regulation is modulated by Al-mediated CCG* topology

4.1.1. Al-mediated DNA topological changes from B- to Z-DNA

We hypothesize that the molecular involvement of Al in bringing about B- to Z-DNA conformation may be due to binding of Al to phosphate group and nitrogenous bases which may affect sugar puckering in dG leading to C2′ to

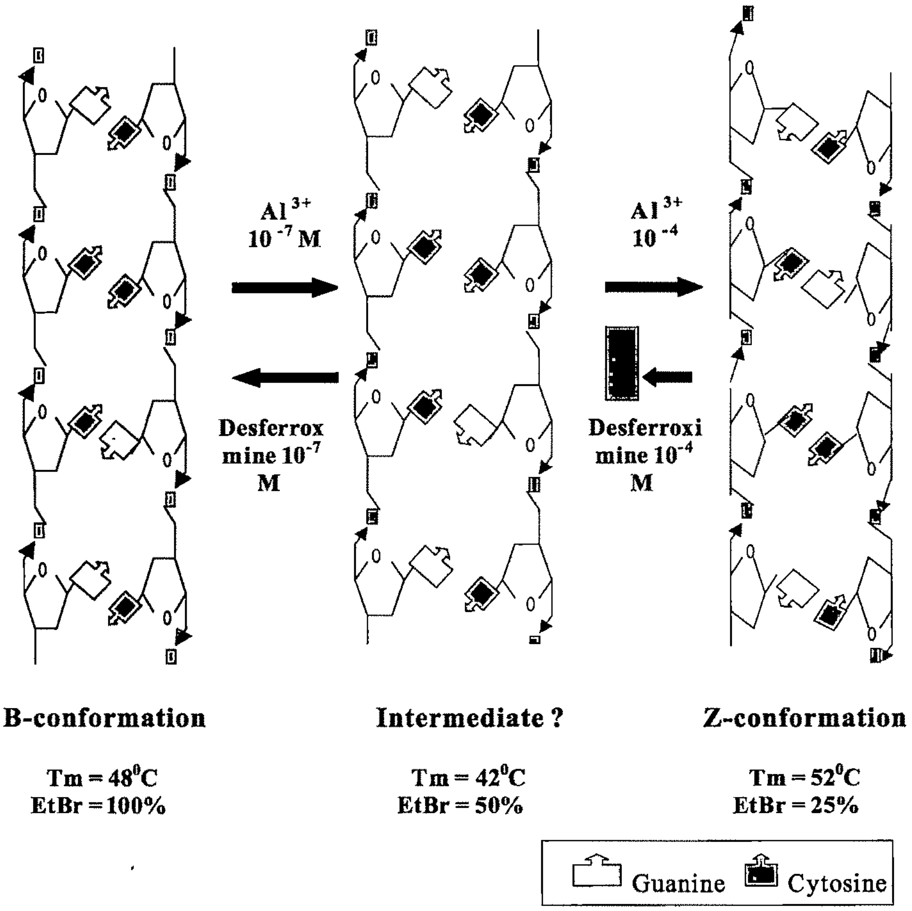

Fig 7 Theoretical Model representing the melting temperature and EtBr binding pattern in CCG repeats (GC* region) under Al-induced DNA conformation change

C3′ endo pucker and the configuration of glycosidic bond (torsion angle). Hence, negative super helical tension caused by Al binding may drive local transitions (B-DNA) to alternative DNA structures. This conformational change may affect the expression of FMR1 gene. The C−C* mismatches induce local flexibility to form non-B-DNA conformation. During B- to Z-DNA helical transitions, the intrastrand hydrogen bond distance between C−C* mismatches in B-DNA conformation should decrease due to Al binding (N4−N3, 4.38 Å B-DNA; O2−O2, 3.54 Å Z-DNA) in addition to change of torsion angle and sugar puckering in dG. This may be the reason for the reduction in C−C* mismatches at higher Al concentration leading to stable Z-DNA conformation. This may be the reason why total removal of Al by desferoximine could not reverse Z- to B-DNA.

4.1.2. *Z-DNA conformation stability pattern*

The duplex $(CCG)_{12}$ repeats with C−C* mismatch has Tm of 48 °C. Al (10^{-7} M) has decreased Tm to 42 °C. But at higher concentrations of Al (10^{-4} M), CCG has higher Tm of 52 °C. The reduced Tm by lower concentrations of Al may be due to the formation of intermediary and transition conformation from B-DNA. However, higher concentrations of Al increased the Tm due to stable conformation. The reason might be transition of nitrogen bases by 180 with respect to its B-conformation and change of deoxyribose molecule from perpendicular to parallel with respect to its helical axis. During this process, the hydrogen bonds may break due to favorable transition energy towards Z-conformation. Thus, the intermediary duplex needs less energy to melt (a hypothetical model: Fig. 7). Once the Z-conformation is attained, in addition to the usual three hydrogen bonds between guanine and cytosine, a hydrogen bond between N3 cytosine of one chain to NH2-C4-cytosine and other bond between O2 and N3 $(H)^+$ is observed. This is mainly because of Z-DNA conformation by bringing two cytosine molecules (which are in anti-conformation) nearer as compared to B-conformation and this explains the higher energy to melt in the Z-DNA duplex.

4.1.3 *How Al could modulate FMR gene expression (Fig. 8)*

Eukaryotic transcriptional control operates at three levels: (a) modulation of the levels and/or activities of activators and repressors, (b) change in chromatin structure

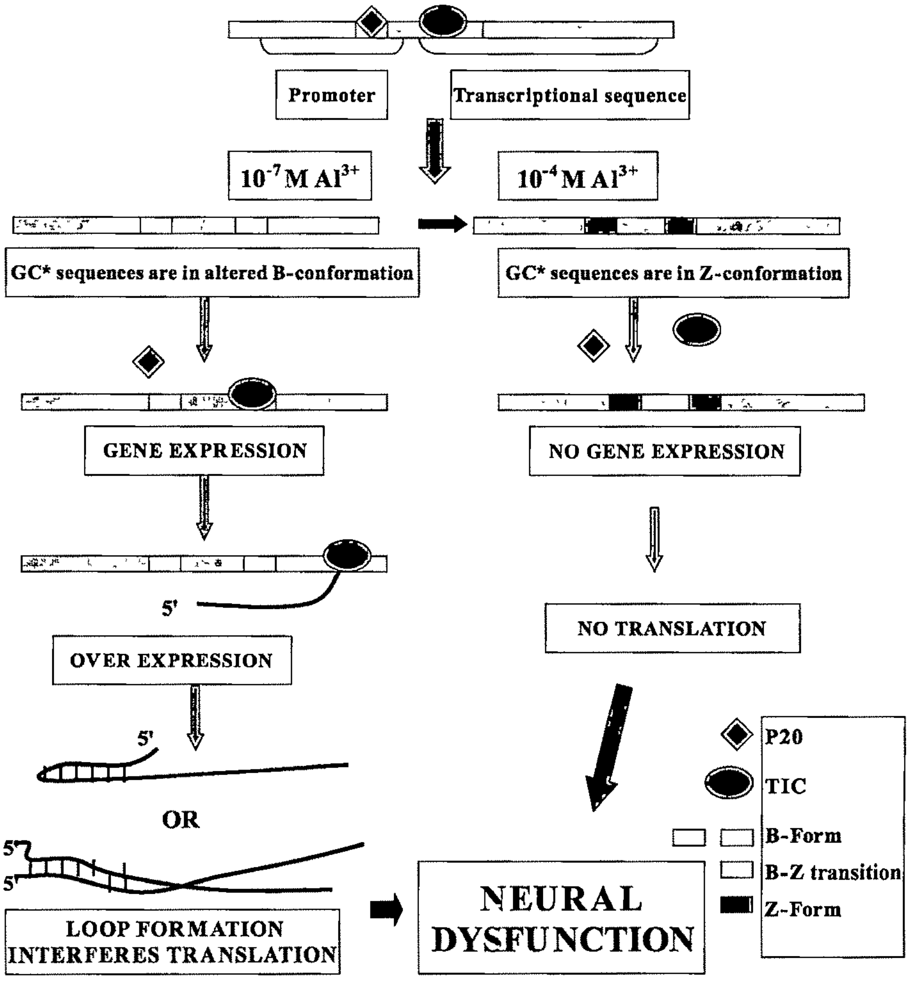

Fig. 8. Hypothesis model representing the switching off and on of FMR1 gene in fragile X syndrome as function of DNA structural dynamics.

directed by activators and repressors and (c) direct influence of activators and repressors on assembly of initiation complexes. Here, we hypothesize that Al-induced DNA topology is relevant to FMR1 gene regulation (Fig. 8). The promoter-proximal region at the 5′-end of FMR1 gene contains GC*-rich sequences and also CGG triplet repeats. This gene is hypothesized to be turned off when CCG/CGG repeats are longer than 200 with methylation [39–44]. In normal conditions, DNA is in B-conformation. The CCG repressor protein or p20 binds in the major groove of cognate site on B-DNA in a sequence-specific manner. This interferes with the general transcription factors (GTF's), which play a role in the formation of transcription–initiation complex and regulates gene repression. The binding and removal of the p20 from its cognate site is likely to control FMR1 gene expression. In conclusion, we provide for the first time, evidence that Al induces B- to Z-DNA conformation in CCG-rich repeats. In genetic neurodisorders, the trinucleotide repeats will be more than 200 with hypermethylation at FMR1 operon and this might be in Z-DNA conformation in the presence of Al. Under such conditions, both p20 and GTF's may not be able to assemble to form transcription–initiation complex at its cognate site, because there are no major grooves in Z-DNA″.

In our model, we concentrate on direct influence of Al on activators and repressors on assembly of transcription–initiation complex formation to explain the expression of FMR1 gene. Similar to other eukaryotic genes, these genes do have DNA regions coding for structural gene along with upstream promoter–proximal region where transcriptional factors (upstream transcriptional factors or UTF's) bind in a sequence-specific manner and stimulate/inhibit the formation of transcription–initiation complex formation (general transcription factors or GTF's). The FMR1 gene is known to contain GC*-rich sequence in the promoter–proximal region (5′-end), specific for UTF's [39–44]. The suppression/over-expression of FMR1 gene plays an important role in disease onset. Based on the gene expression during normal and disease condition, we have postulated that FMR1 gene is under repression control, since its expression is affected by 5′-(CCG)n-3′ binding protein [40,41].

Hence, these studies suggest that Al is likely to play a role in switching off the FMR1 gene by inducing helical transition from B- to Z-DNA, in addition to the factors involved in massive expansion of CCG triplet repeats and hypermethylation, imbalance in trace metal homeostasis, etc. (Fig. 9). This mechanism may provide a clue for the discovery of new drugs to convert Z-DNA back to B-DNA. It is hypothesized that through chelation of metal ions like aluminum, demethylation of the triplet repeats and acetylation of histones, it may be possible to switch on FMR 1 gene.

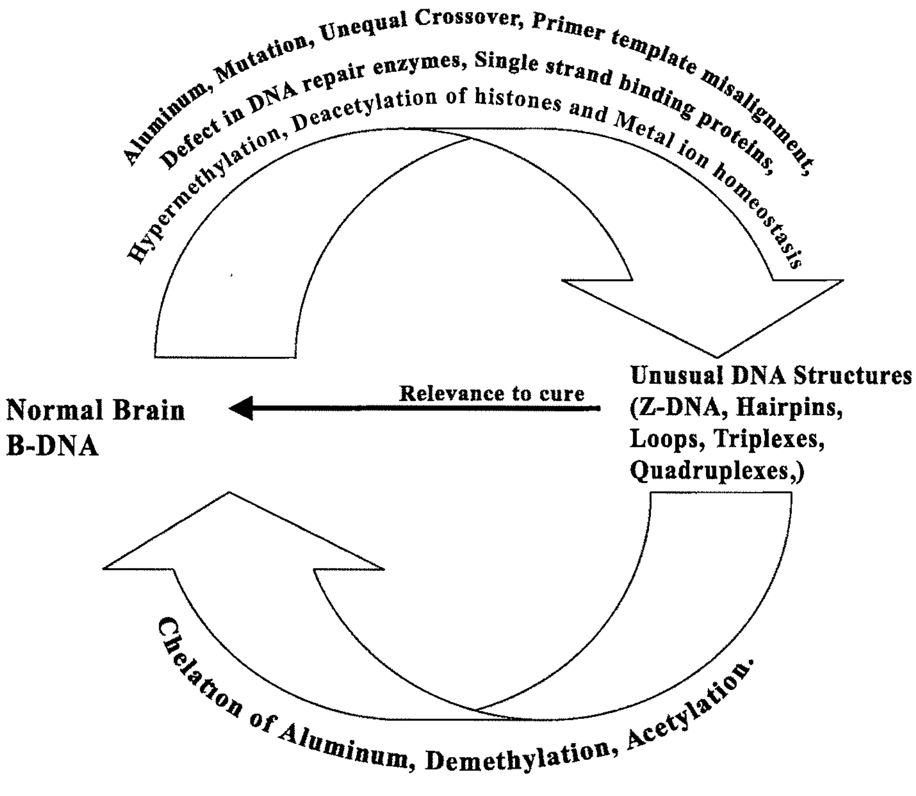
Aluminum, Mutation, Unequal Crossover, Primer template misalignment,
Defect in DNA repair enzymes, Single strand binding proteins,
Hypermethylation, Deacetylation of histones and Metal ion homeostasis
Normal Brain
B-DNA
Relevance to cure
Unusual DNA Structures
(Z-DNA, Hairpins,
Loops, Triplexes,
Quadruplexes,)
Chelation of Aluminum, Demethylation, Acetylation.

Fig 9. The complexity of DNA topology in fragile X disorder.

Acknowledgements

The authors profoundly thank Dr. V. Prakash, Director, CFTRI, Mysore, and Prof. Sharat Chandra, Director, Centre for Human Genetics, Bangalore, for their support and encouragement. The authors wish to thank the Department of Biotechnology, Government of India for providing finance under the Indo–Israel Joint Collaborative Project on Human Genome.

References

[1] W Saenger, Springer-Verlag, New York, 1983

[2] A Rich, Gene 135 (1993) 99–109.

[3] F.M Pohl, T M Jovin, J. Mol Biol 67 (1972) 375–396.

[4] A H Wang, G J Quigley, F J Kolpak, J L Crawford, J.H. van Boom, G van der Marel, A Rich, Nature 282 (1979) 680–686

[5] J Klysik, S M. Stirdivant, J E. Larson, P A Hart, R D. Wells, Nature 290 (1981) 672–677

[6] A Herbert, A Rich, J. Biol. Chem. 271 (1996) 11595–11598

[7] K. Usdin, Nucleic Acids Res 26 (1998) 4078–4085

[8] S.V. Mariappan, P. Catasti, L A Silks 3rd, E M. Bradbury, G Gupta, J. Mol. Biol 285 (1999) 2035–2052

[9] V. Michak, M S. Maurizot, M Charlier, J Biomol. Struct. Dyn 13 (1995) 565–575

[10] G R. Sutherland, R I Richards, Proc Natl Acad Sci U S A 92 (1995) 3636–3641

[11] S.V S Mariappan, X Chen, P Catasti, E M Bradbury, G Gupta, Chapter 41 (1998) 647–676.

[12] C T. Caskey, A. Pizzuti, Y H Fu, R G Fenwick, D.L. Nelson. Science 256 (1992) 784–789

[13] C.A. Ross, M.G McInnis, R L Margolis, S H Li, Trends Neurosci 16 (1993) 254–260

[14] C.E Pearson, R.R Sinden, Biochemistry 35 (1996) 5041–5053

[15] G Dover, Nat Genet. 10 (1995) 254–256.

[16] R D Wells, J. Biol Chem 271 (1996) 2875–2878

[17] M Mitas, A Yu, J Dill, T.J Kamp, E J Chambers, I S Haworth, Nucleic Acids Res 23 (1995) 1050–1059

[18] E E. Eichler, J.J.A Holden, B W Popovich, A L. Reiss, E Snow, S N Thibodeau, C S. Richards, P.A. Ward, D L Nelson, Nat Genet 8 (1994) 88–92.

[19] K. Usdin, E. Grabczy, Cell. Mol. Life Sci 57 (2000) 914–931

[20] D.P. Perl, D C Gajdusek, R M. Garruto, R.T. Yanagihara, C.J. Gibbs, Science 10 (1982) 1053–1055.

[21] R M Garruto, C Swyt, R. Yanagihara, C.E Fiori, D C Gajdusek, N Engl J. Med. 11 (1986) 711–712

[22] J. Savory, C Exley, W F Forbes, Y Huang, J.G Joshi, T Kruck, D.R. McLachlan, I. Wakayama, J Toxicol Environ Health 48 (1996) 615–635.

[23] K S.J. Rao, R.V Rao, P Shanmugavelu, R B. Menon, Alzheimer's Rep. 2 (1999) 4–9

[24] C S.D Champion, M.T Rajan, K S J Rao, M A. Viswamitra, Cell. Mol. Life Sci 54 (1998) 488–496

[25] M T. Rajan, C S.D. Champion, D Vishnuvardhan, K S J. Rao, M A Viswamitra, Mol. Biol Rep. 22 (1996) 47–52.

[26] S J Karlik, G.L Eichhorn, P.N. Lewis, D R. Crapper, Biochemistry 19 (1980) 5991–5998

[27] M.T. Rajan, K.S.J Rao, B M. Mamatha, R.V. Rao, P Shanmugavelu, R.B. Menon, M V Pavithran, J. Neurol Sci. 146 (1997) 153–166.

[28] K S. Jagannatha Rao, P. Shanmugavelu, S.K Shankar, R P Rukmini Devi, R V Rao, S Pande, R B. Menon, Alzheimer's Rep 2 (1999) 4–9

[29] M M. Finneagen, S.J. Rettig, C Orvig, J. Am. Chem. Soc 108 (1986) 5033–5035

[30] D.M Gray, R.L Ratlies, M.R Vaughan, Enzymology 211 (1992) 389–406

[31] J.R. Fresco, B.M Alberts, Proc Natl. Acad. Sci. U S. A 46 (1990) 311–321.

[32] K S J Rao, C D. Katsetos, M.M Hermann, J. Savory, Clin Lab. Med 18 (1998) 687–698.

[33] Y.-H. Wang, R. Gellibolian, M Shimizu, R.D. Wells, J. Griffith, J. Mol. Biol. 263 (1996) 511–516.

[34] M M. Garner, A. Felsenfeld, J Mol Biol 196 (1987) 581–590.

[35] C Anselmi, G Bocchinfuso, P.D. Santis, M Savino, A.A. Scipioni, Biophys J. 79 (2000) 601–613.

[36] R. Negri, G Costanzo, M. Buttinelli, S Venditti, E D. Mauro, Biophys Chemist 50 (1994) 169–181.

[37] W J Lukiw, H J. LeBlanc, L A. Carver, D.R McLachlan, N G. Bazan, J Mol. Neurosci. 11 (1998) 67–78

[38] P.S Ho, M J. Ellison, G J Quigley, A. Rich, EMBO J 5 (1986) 2737–2744.

[39] F Tassone, R J Hagerman, A.K Taylor, P J Hagerman, J. Med Genet 38 (2001) 453–456

[40] H.M. Hartmann, H. Deissler, F Naumann, B Schmitz, J Schroer, W. Doerfler, J Biol Chem 275 (2000) 6447–6452.

[41] A J Verkerk, E de Graaff, K De Boulle, E.E Eichler, D.S Konecki, E Reyniers, A. Manca, A Poustka, P.J. Willems, D L Nelson, et al., Hum Mol Genet 2 (1993) 1348

[42] J.S Sutcliffe, D.L Nelson, F. Zhang, M. Pieretti, C T Caskey, D Saxe, S.T Warren, Hum Mol Genet 1 (1992) 397–400.

[43] S D Fu, Y Shen, Y. Fan, Zhonghua Yixue Zazhi 74 (1994) 611–614

[44] S J. Knight, A V Flannery, M.C. Hirst, L Campbell, Z. Phelps, S R Phelps, J Pointon, H.R Middleton-Price, A. Barnicoat, M E. Pembrey, Cell 74 (1993) 127–134

ELSEVIER

Biochimica et Biophysica Acta 1588 (2002) 65–70

BIOCHIMICA ET BIOPHYSICA ACTA

BBA

www.bba-direct com

Frequency of duplications in the D-loop in patients with mitochondrial DNA deletions

Célia H. Tengan*, Claudia Ferreiro-Barros, Marina Cardeal, Moacir A.T. Fireman, Acary S.B. Oliveira, Beatriz H. Kiyomoto, Alberto A. Gabbai

Division of Neurology, Department of Neurology and Neurosurgery, Escola Paulista de Medicina, Universidade Federal de São Paulo, São Paulo, SP, Brazil

Received 7 March 2002; received in revised form 14 May 2002; accepted 16 May 2002

Abstract

Small duplications (miniduplications) of the D-loop of human mitochondrial DNA (mtDNA) have been described in patients with mtDNA deletions, mtDNA point mutations and in normal aged tissues. The origin of these miniduplications is still unknown but it is hypothesized that they could be formed after oxidative damage. The respiratory chain (RC) is the main source of free radicals in mitochondria and it is believed that a defect in RC increases free radical generation. If miniduplications are originated by oxidative damage, it is expected that they are more abundant in patients with a defect in the RC. We studied the frequency of miniduplications of D-loop in patients with a RC defect due to mtDNA deletions and in controls. We show that four types of miniduplications could be detected with a higher prevalence than in previous studies and that patients with mtDNA deletions did not have higher proportions or increased number of miniduplications, which is against the hypothesis that miniduplications are generated more abundantly in patients with RC defects. We also clearly demonstrate the age-related nature of these miniduplications by a carefully controlled study regarding the age of subjects, which was not considered in other studies on patients with a mitochondrial disease.

© 2002 Elsevier Science B.V. All rights reserved.

Keywords. Mitochondria, Mitochondrial DNA, Aging; Mitochondrial disease, mtDNA duplication, Free radical

1. Introduction

An approximate 260-bp tandem duplication in the D-loop region of human mitochondrial DNA (mtDNA) was first identified by Brockington et al. [1] and associated with mtDNA deletions in mitochondrial myopathy. The 260-bp duplication is a heteroplasmic length polymorphism found in low abundance and located in the region that controls replication and transcription of mtDNA (D-loop). Because of this location and the finding in 31% of patients with mtDNA deletions (18 out of 58) but not in normal subjects, it was suggested that this duplication could be relevant to deletions formation [1]. Since then, other studies did not confirm a high prevalence of this rearrangement in patients with mtDNA deletions, finding lower proportions that varied from 3% to 12% [2–4]. On the other hand, the 260-bp duplication and several other duplications in the D-loop (miniduplications) were also found in normal aged individuals [5,6], suggesting that these miniduplications in D-loop are early molecular events of the human aging process. More recently, Bouzidi et al. [7] described a 200-bp tandem duplication with high proportion associated with a cytochrome *b* mutation. It was suggested a relationship between miniduplication formation and respiratory chain (RC) deficiency, which was explained by a possible increase in free radical production from the defective RC whether the genetic origin of the deficiency be a deletion or a point mutation in the mtDNA [7].

In this study, we explore the idea that formation of miniduplications could be enhanced by a defective RC in patients with mtDNA deletions. We show that four types of miniduplications could be detected by polymerase chain reaction (PCR) with a higher prevalence than in previous studies and that patients with mtDNA deletions did not have higher proportions or increased number of miniduplications, which is against the hypothesis that miniduplications are generated more abundantly in patients with RC defects. We also clearly demonstrate the age-

---

* Corresponding author. Disciplina de Neurologia Clínica, Escola Paulista de Medicina, Universidade Federal de São Paulo, R. Pedro de Toledo, 781, setimo andar, 04039-032, São Paulo, SP, Brazil. Tel. +55-11-5579-9236, fax: +55-11-5081-5005

E-mail address chtengan@neuro epm br (C H Tengan)

0925-4439/02/$ - see front matter © 2002 Elsevier Science B.V. All rights reserved
PII S0925-4439(02)00140-0

related nature of this rearrangement by a carefully controlled study regarding the age of the subjects, which was not considered in other studies with patients with mtDNA deletions.

2. Materials and methods

2.1. DNA samples

DNA samples were obtained from autopsy material or muscle biopsies specimens performed exclusively for diagnostic purposes. Genomic DNA was isolated with SDS/proteinase K treatment followed by phenol/chloroform extraction. We studied samples divided in two groups: (1) *patients group*: patients with chronic external ophthalmoplegia and single mtDNA deletions (N=24); and (2) *control group*: individuals with no abnormalities on muscle histology (autopsy material or diagnostic muscle biopsies) (N=27). Quantification of total DNA was performed in the VersaFluor fluorometer (BioRad) using the Hoechst dye assay.

All patients had pathogenic deletions and not large-scale duplications as determined by a Southern blot study with different restriction enzymes and two probes according to Tengan et al. [8].

This study was approved by the Ethics Committee of Universidade Federal de São Paulo and is in accordance with the ethical standards of the Helsinki Declaration.

2.2. Detection of miniduplications

Miniduplications of the D-loop region were detected by PCR using 20 pmol of back-to-back primers located at positions 336–357 and 335–305 of mtDNA (5′→3′) [4], 10 ng of genomic DNA, 20 nmol of each deoxynucleotide triphosphate (dNTP), 10× PCR buffer, 2.5 units of Taq DNA polymerase (Amersham-Pharmacia Biotech). PCR conditions were: 94 °C for 5 min followed by 40 cycles with 94 °C for 30 s and 60 °C for 30 s. PCR products were separated by electrophoresis through an ethidium bromide stained agarose gel and then visualized under a UV source. A positive control of the reaction was performed using a DNA sample from cybrid cells containing 100% of the 260-bp miniduplication [9], kindly provided by Dr. C.T. Moraes. Positions in mtDNA were numbered according to the published mtDNA sequence [10].

2.3. DNA sequencing

PCR products encompassing miniduplications were gel purified according to GeneClean protocol (Bio101) and subcloned into vector pCRII (Invitrogen). Sequencing reaction was performed according to BigDye Sequencing kit instructions using M13 Universal primer and run in a ABI Prism 377 Automated Sequencer (Applied Biosystems).

2.4. Quantitative analyses

The quantitation of miniduplication was performed by the serial dilution method as previously described [11] with slight modifications in the PCR conditions. Briefly, 1 μl of serial 10-fold dilutions was submitted to a short cycle PCR (40 cycles consisted of 94 °C for 30 s and 60 °C for 30 s). Two parallel PCR reactions were performed using two pairs of primers. The first pair of primers flanked the miniduplication (primers as cited above). The second pair of primers (forward primer from mtDNA position 5472 to 5491 and reverse primer from mtDNA position 5982 to 5960) amplified a 510-bp fragment (control fragment) that is present both in normal and duplicated mtDNA. Ten microliters of the PCR amplification was submitted to electrophoresis through an ethidium bromide-stained agarose gel, visualized and photographed under a UV source. Optical densities (OD) of the bands were measured by scanning nonsaturated positive prints and quantifying the pixel density (freeware package NIH IMAGE 1.57). The OD obtained was plotted as a function of the template dilutions (the points corresponding to the saturation phase of the PCR amplification were excluded). A linear regression analysis was performed to identify the dilution corresponding to the disappearance of each specific template. The ratio between these dilutions (minidup ratio) was used to estimate the amount of miniduplications in each group (patient and control).

2.5. Phenotype–genotype correlation

The results on detection of miniduplications were correlated with clinical and molecular features of patients. The features analysed included age, type of clinical presentation, presence of endocrinopathy, molecular defect (deletion: size, location, proportion, direct repeats, presence of large duplication).

2.6. Statistical analyses

Statistical analyses were performed with Statview 5.01 (SAS Institute Inc.). Comparison of means was performed by the Student's t-test and statistical significance was set to a $P<0.05$.

3. Results and discussion

In order to determine the prevalence of miniduplications, we studied two groups (patients and controls), formed by individuals with similar distribution of age, from 11 to 70 years old in controls and from 11 to 66 years old in patients. PCR was performed with equal amounts of total DNA (10 ng) in both groups and miniduplications were detected in 17 (63%) controls and 14 (58%) patients. The higher frequency of miniduplications detected in our study could be explained by the use of different PCR conditions leading to a more efficient amplification. We detected four different bands that corresponded to duplications of approximately 150, 190, 260 and 650 bp (Fig. 1). The 190-bp duplication was the same duplication described by Lee et al. [5]. The other duplications had similar sizes to the ones described previously [1,2,4,5,7], but the exact breakpoints were slightly different. Although the 260-bp duplication was the first one to be described [1], it was not the most frequent, in fact it appeared in only two (9%) patients and six (20%) controls (Table 1). The 650-bp miniduplication was the most frequent in both groups, found in 48% of patients and 37% of controls. Some patients and controls presented two or three types of miniduplications at the same time. We detected only one band in seven patients and nine controls, and two or three bands in seven patients and eight controls. The number of bands obtained were not statistically different between both groups, but we observed that one band was obtained in individuals with age around 30 years and two or more bands around 50 years, suggesting an increase in the number of miniduplications with age (Fig. 2). A clear correlation between the presence of miniduplication and age could be observed when we analysed the age of the individuals with and without miniduplications. Miniduplications were detected mostly in patients and controls with higher ages (P<0.001), 40 years for patients (mean=40.4, S.E.=4.2) and controls (mean=40.1, S.E.=3.6). Samples without miniduplications had a mean age of 18.1 years (SE=2.6) for controls and 20.7 years (SE=2.7) for patients (Fig. 3). Previous studies on patients with mitochondrial diseases and miniduplications did not consider the age of the patients as a factor for the presence of miniduplications [1–4,7]. However, when the age of the subject is informed, we could observe that they were older than 35 years in those studies: 67 [1], 58 [4], 35 and 42 years [7].

The main proposed mechanism for the generation of duplications in the D-loop is by slipped strand mispairing during replication [12–14]. Analysis of nucleotide sequences at the breakpoint region demonstrated that duplications occurred in regions with polycytosine stretches and perfect direct repeats varying from 5 to 11 nucleotides (Fig. 1).

Table 1
Detection of four types of miniduplications in patients and controls

	150 bp (%)	190 bp (%)	260 bp (%)	650 bp (%)	Total (%)
Patient	5 (24)	4 (19)	2 (9)	10 (48)	21 (100)
Control	4 (13)	9 (30)	6 (20)	11 (37)	30 (100)
Total	9	13	8	21	49

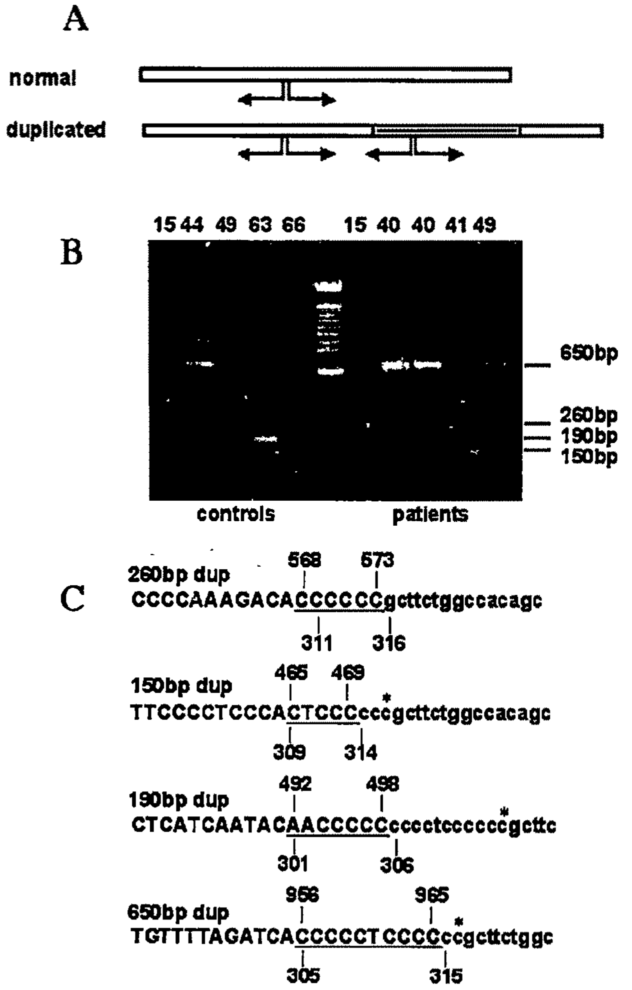

Fig 1 Detection of four types of miniduplications of the D-loop. PCR was performed with back-to-back primers located at positions 336–357 and 335–305 of mtDNA (5′→3′) This pair of primers can only amplify a fragment if there is a duplicated region (A) Miniduplications in the D-loop of mtDNA were observed in 17 (63%) controls and 14 (58%) patients Four different bands could be detected after electrophoresis through a 1% agarose gel: 150, 190, 260 and 650 bp (B) The ages of the individuals are showed at the top of the gel. Panel C shows the breakpoint region of each type of miniduplication Nucleotide positions are indicated above and below the sequence and direct repeats are underlined There was an insertion of a cytosine (*) just before the guanine at nucleotide position 316.

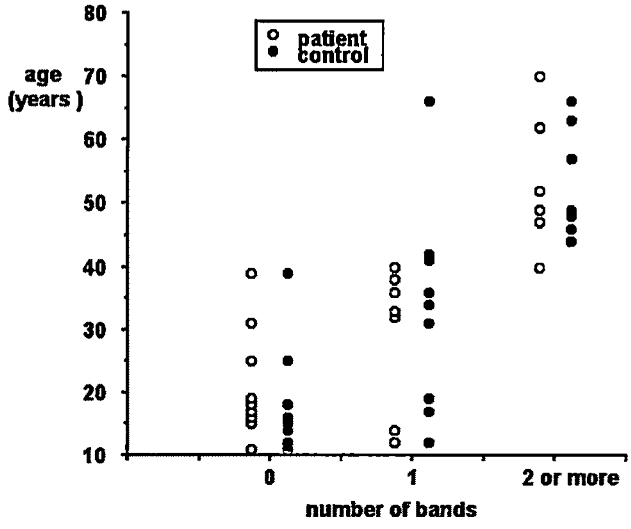

Fig 2. Number of bands detected in patient and control groups The primers used for the amplification of miniduplications amplified one, two or three bands in the same patient The graph demonstrates that the number of bands detected was not increased in the patients but two or more bands were detected in patients and controls with more than 40 years of age

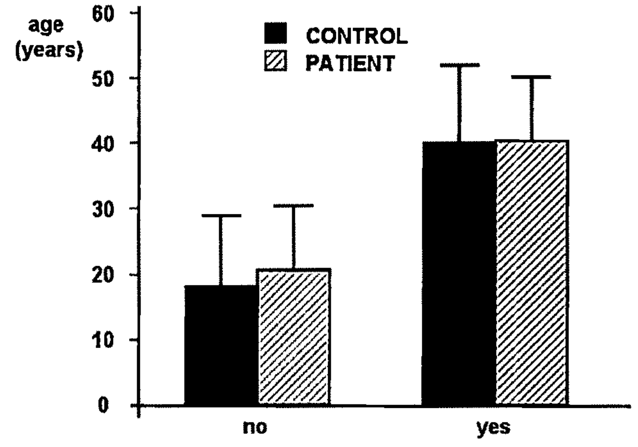

Fig. 3. Correlation of age and the presence of miniduplication. Miniduplications were detected mostly in patients and controls with higher ages (P<0.001), 40 years for patients (mean=40.4, S.E.=4.2) and controls (mean=40.1, S.E.=3.6). Samples without miniduplications had a mean age of 18.1 years (S.E.=2.6) for controls and 20.7 years (S.E.=2.7) for patients. No difference could be detected between patients and controls.

Another interesting feature was that one of the ends of the duplicated segment occurred in the same region in all four types, around nucleotide positions 306–316. This region corresponds to CSB2 (conserve sequence block II) and may represent a hot spot for this type of rearrangement.

Because of the hypothesis that these duplications could arise from oxidative damage favoured by a defective RC [7], we could expect that the appearance of miniduplications would be earlier in patients with mtDNA deletions. However, we did not confirm this expectation since the mean age of patients with duplications were the same in both groups. Furthermore, we could not find increased variety nor quantity of miniduplications detected in the patients group. Quantitation was performed in a total of eight patients and eight controls with similar ages. After obtaining the minidup ratio, the comparison between patients and controls showed a slight tendency of higher values for the patient group but this difference was not statistically significant (Fig. 4). Minidup ratio indicates the level of miniduplications in relation to a control amplification and was used to compare the amount of miniduplications in the patient and control groups. Miniduplications could not be detected by Southern blot (data not shown), demonstrating that they were present in very low levels in skeletal muscle, only detectable by PCR.

Brockington et al. [1] suggested that the presence of the duplication in the D-loop could increase the likelihood of slip replication and hence deletion. In that study, all the patients with miniduplications had deletions flanked by direct repeats and in one without flanking repeats the duplication was not present. The presence of miniduplication was not more frequent in patients and our results did not demonstrate an association between presence of direct repeats and presence of miniduplication. Among 12 patients with deletions flanked by direct repeats, 7 did not present miniduplications of the D-loop. There was also one patient with a miniduplication but no direct repeats. We could not find any other features of the mtDNA deletion that could be associated with the presence of miniduplications, such as location, proportion, presence of a large duplication and any correlation with other clinical features (Table 2).

Our study demonstrated that miniduplications of the D-loop of mtDNA are age-related rearrangements but are not increased in patients with a RC defect. The first age-related mtDNA mutation described and one of the most studied is the 4977 bp deletion of mtDNA [15]. This deletion can be present at high percentages in patients with mitochondrial myopathies [16], but it is also found in very low levels (less than 1%) in aged postmitotic tissues [11]. Other mtDNA deletions [17,18] and more recently several point mutations in D-loop [19] were also detected in aged tissues. The main mechanisms proposed for the appearance of these mutations are due to oxidative damage from free radicals generated in the RC [20]. This hypothesis is supported by the following evidences: increased production of 8-OH dG with age, increase in the levels of mtDNA mutations with age, in-

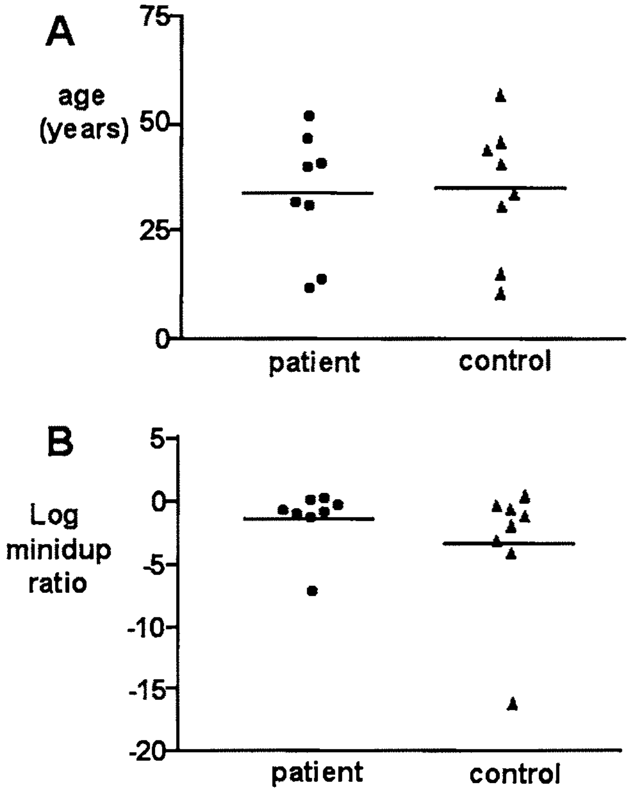

Fig. 4. Quantitative analysis of miniduplications in patients and controls. (A) The amount of miniduplications was estimated by the minidup ratio, as described in Materials and methods. We studied two groups, eight patients and eight age-matched controls with similar age distributions, ranging between 11 and 57 years. (B) Because minidup ratio is related to age in an exponential manner, the values were expressed as log minidup ratio to normalize the data and to better visualize the distribution of the results. The graph demonstrates that there was a slight tendency of increased values in the patient group but there was not statistical significant difference between both groups. Horizontal lines represent the mean values.

Table 2
Presence of miniduplications compared to features of the deletion and presence of a large-scale duplication of mtDNA

Patient	Presence of miniduplication	Location of the deletion	Direct repeats (number of bases)	Percentage of deleted mtDNA	Deletion size (bp)	Presence of a large duplication
1	no	6310–15611	4	60	9300	yes
2	yes	10951–15372	10	83	4420	no
3	yes	8482–13460	13	99	4977	no
4	no	8467–13444	6	82	4977	no
5	no	8482–13460	13	65	4977	no
6	no	7448–13475	no	53	6027	no
7	no	8468–13446	10	72	4978	no
8	no	8482–13460	13	68	4977	no
9	no	8817–15610	5	69	6792	no
10	no	12112–14422	10	89	2309	no
11	yes	9514–13052	no	54	3537	no
12	yes	8476–14812	7	81	6335	no
13	yes	6320–11272	6	19	4952	no
14	yes	8477–13592	10	25	5115	no

creased susceptibility of mtDNA compared to nuclear DNA, proximity of mtDNA to a continuous source of free radicals (RC), decrease of RC activity with age [21–24]. Bouzidi et al. [7] proposes that single-strand breaks, due to free radical damage combined with mispairing could explain the generation of miniduplications at the level of repeated sequences, which are relatively close to each other in the mtDNA D-loop. It is supposed that a defect of RC would increase the leakage of reactive oxygen species from the electron transfer chain. Free radicals induce secondary mtDNA mutations exacerbating mitochondrial respiratory defects, creating a vicious cycle [22]. Although, very attractive, the vicious cycle theory is an unproven hypothesis and it is still not determined whether age-related mtDNA mutations are generated by reactive oxygen species-mediated damage [25]. Based on this theory, we would expect an increase in age-related mtDNA mutations in patients with RC defects caused by high proportions of mtDNA deletions, specially considering that high production of lipid peroxides and 8-OHdG were found in cybrids harbouring high levels of deleted mtDNA [26]. Our results do not support this theory and are in agreement with our previous observation that mtDNA age-related deletions were not increased in patients with mitochondrial diseases caused by mtDNA point mutations [27]. Although it is clear that age-related mtDNA mutations accumulate during life, their contribution to the aging process is still not confirmed. Pathogenicity of miniduplications in the D-loop was not demonstrated in a study of cells homoplasmic for the 260-bp duplication [9]. Moreover, similar insertions in mtDNA control region were also found in other animals, such as rabbit [12] and monkey [28], suggesting that errors in mtDNA replication, leading to insertions, can occur during normal life.

Acknowledgements

This work was supported by a research grant from Fundação de Amparo à Pesquisa do Estado de São Paulo (FAPESP, Brazil) to Dr. CHT (97/06160-5). CHT and CCF-B were supported by FAPESP and MC by the Conselho Nacional de Desenvolvimento Científico e Tecnológico (CNPq, Ministry of Science and Technology, Brazil). We thank Dr. Carlos T. Moraes for revising the manuscript and Dr. Beny Schmidt for providing muscle biopsy specimens for the study.

References

[1] M. Brockington, M.G. Sweeney, S.R Hammans, J.A. Morgan-Hughes, A.E. Harding, A tandem duplication in the D-loop of human mitochondrial DNA is associated with deletions in mitochondrial myopathy, Nat. Genet. 4 (1993) 67–71.

[2] A. Torroni, M.T Lott, M.F. Cabell, Y-S. Chen, L. Lavergne, D G Wallace, mtDNA and the origin of Caucasians. identification of ancient Caucasian-specific haplogroups, one of which is prone to a recurrent somatic duplication in the D-loop region, Am J. Hum Genet. 55 (1994) 760–776

[3] J A Poulton, K.J. Morten, D Marchington, K Weber, G.K. Brown, A Rotig, L. Bindoff, Duplications of mitochondrial DNA in Kearns–Sayre syndrome, Muscle Nerve (Suppl 3) (1995) S154–S158.

[4] G Manfredi, S. Servidei, E. Bonilla, S. Shanske, E A Schon, S. DiMauro, C.T Moraes, High levels of mitochondrial DNA with an unstable 260-bp duplication in a patient with a mitochondrial myopathy, Neurology 45 (1995) 762–768

[5] H -C Lee, C.-Y. Pang, H -S Hsu, Y -H. Wei, Ageing-associated tandem duplications in the D-loop of mitochondrial DNA of human muscle, FEBS Lett. 354 (1994) 79–83.

[6] Y.-H. Wei, C.-Y Pang, B.-J. You, H -C. Lee, Tandem duplications and large-scale deletions of mitochondrial DNA are early molecular events of human aging process, Ann N Y. Acad. Sci. 789 (1996) 82–101

[7] M.F. Bouzidi, A Poyau, C. Godinot, Co-existence of high levels of a cytochrome b mutation and of a tandem 200pb duplication in the D-loop of muscle human mitochondrial DNA, Hum. Mol. Genet 7 (1998) 385–391

[8] C H. Tengan, B H. Kiyomoto, M.S. Rocha, V.L S. Tavares, A A Gabbai, C.T Moraes, Mitochondrial encephalomyopathy and hypoparathyroidism associated with a duplication and a deletion of mitochondrial deoxyribonucleic acid, J Clin. Endocrinol Metab. 83 (1998) 125–129.

[9] H. Hao, G. Manfredi, C T Moraes, Functional and structural features of a tandem duplication of the human mtDNA promoter region, Am. J. Hum Genet. (1997) 1363–1372

[10] S Anderson, A.T Bankier, B G Barrel, M H.L de Bruijin, A.R. Coulson, J Drouin, I C. Eperon, D.P. Nierlich, B A Roe, F Sanger, P H Schreier, A.J H. Smith, R Staden, I G Young, Sequence and organization of the human mitochondrial genome, Nature 290 (1981) 457–465

[11] M. Corral-Debrinski, G Stepien, J.M. Shoffner, M T. Lott, K. Kanter, D C Wallace, Hypoxemia is associated with mitochondrial DNA damage and gene induction. implications for cardiac disease, JAMA 266 (1991) 1812–1816

[12] F Mignotte, M Gueride, A -M Champagne, J -C Mounolou, Direct repeats in the non-coding region of rabbit mitochondrial DNA involvement in the generation of intra- and inter-individual heterogeneity, Eur J. Biochem 194 (1990) 561–571.

[13] S C. Guivizzani, S L D Mackay, C S Madsen, P.J. Laipis, W W Hauswirth, Transcribed heteroplasmic repeated sequences in the porcine mitochondrial DNA D-loop region, J Mol Evol. 37 (1993) 36–47

[14] P Savolainen, L. Arvestad, J. Lundeberg, mtDNA tandem repeats in domestic dogs and wolves· mutation mechanism studied by analysis of the sequence of imperfect repeats, Mol Biol. Evol 17 (2000) 474–488.

[15] G A. Cortopassi, N. Arnheim, Detection of a specific mitochondrial DNA deletion in tissues of older humans, Nucleic Acids Res 18 (1990) 6927–6933.

[16] C T. Moraes, S DiMauro, M Zeviani, A Lombes, S. Shanske, A F Miranda, H. Nakase Bonilla, E L C. Werneck Servidei, S.I Nonaka, Y. Koga, A Spiro, K.W. Brownell, B Schmidt, D L. Schotland, M D Zupanc, D.C. DeVivo, E A Schon, L.P Rowland, Mitochondrial DNA deletions in progressive external ophthalmoplegia and Kearns–Sayre syndrome, N Engl J Med. 320 (1989) 1293–1299.

[17] K Torii, S. Sugiyama, M. Tanaka, K Takagi, Y Hanaki, K. Iida, M Matsuyama, N Hirabayashi, Y. Uno, T Ozawa, Aging-associated deletions of human diaphragmatic mitochondrial DNA, Am J Respir. Cell Mol Biol. 6 (1992) 543–549

[18] S Melov, J.M. Shoffner, A Kaufman, D C Wallace, Marked increase in the number and variety of mitochondrial DNA rearrangement in aging human skeletal muscle, Nucleic Acids Res 23 (1995) 4122–4126.

[19] Y. Wang, Y Michikawa, C Mallidis, Y. Bai, L. Woodhouse, K E Yarasheski, C A Miller, V. Askanas, W.K Engel, S Bhasin, G Attardi, Muscle-specific mutations accumulate with aging in critical human mtDNA control sites for replication, Proc. Natl Acad Sci U S A 98 (2001) 4022–4027

[20] B Bandy, A J Davison, Mitochondrial mutations may increase oxidative stress implication for carcinogenesis and aging? Free Radic Biol Med 8 (1990) 523–539

[21] I Trounce, E Byrne, S. Marzuki, Decline in skeletal muscle mitochondrial respiratory chain function possible factor in aging, Lancet I (1989) 637–639.

[22] M Hayakawa, K Hattori, S. Sugiyama, T. Ozawa, Age-associated oxygen damage and mutations in mitochondrial DNA in human hearts, Biochem. Biophys Res. Commun 176 (1992) 87–93

[23] R S Sohal, Aging, cytochrome oxidase activity and hydrogen peroxide release by mitochondria, Free Radic Biol Med. 14 (1993) 583–588.

[24] P. Mecocci, U MacGarvey, A E Kaufman, D. Koontz, J M Shoffner, D.C. Wallace, M F. Beal, Oxidative damage to mitochondrial DNA shows marked age-dependent increases in human brain, Ann. Neurol. 34 (1993) 609–616

[25] I.G Kirkinezos, C T. Moraes, Reactive oxygen species and mitochondrial diseases, Semin. Cell Dev Biol. 12 (2001) 449–457

[26] Y.-H Wei, C -F. Lee, Y -S. Ma, C.-W Wang, C.-Y. Lu, C -Y. Pang, Increases of mitochondrial mass and mitochondrial genome in association with enhanced oxidative stress in human cells harboring 4,977bp-deleted mitochondrial DNA, Ann. N. Y Acad Sci. 928 (2001) 97–112.

[27] C H. Tengan, A A Gabbai, S. Shanske, M. Zeviani, C T. Moraes, Pathogenic point mutations in the mtDNA do no increase the rate of accumulation of age-related mtDNA deletions in skeletal muscle, Mutat Res 379 (1997) 1–11

[28] E M Karawya, R.G Martin, Monkey (CV-1) mitochondrial DNA contains a unique triplication of 108 bp in the origin region, Biochim. Biophys Acta 909 (1987) 30–34.

ELSEVIER

Biochimica et Biophysica Acta 1588 (2002) 71–78

BIOCHIMICA ET BIOPHYSICA ACTA
BBA
www.bba-direct.com

In vivo treatment with stobadine prevents lipid peroxidation, protein glycation and calcium overload but does not ameliorate Ca^{2+}-ATPase activity in heart and liver of streptozotocin-diabetic rats: comparison with vitamin E

The ADIC (Antioxidants in Diabetes-Induced Complications) Study Group
Bilgehan Pekiner[a], Nuray N. Ulusu[b], Net Das-Evcimen[a], Meral Sahilli[c], Fugen Aktan[a], Milan Stefek[d], Svorad Stolc[d], Çimen Karasu[e,*]

[a]*Department of Biochemistry, Faculty of Pharmacy, Ankara University, Ankara, Turkey*
[b]*Department of Biochemistry, Faculty of Medicine, Hacettepe University, Ankara, Turkey*
[c]*Department of Pharmacology, Faculty of Pharmacy, Ankara University, Tandoğan, Ankara, Turkey*
[d]*Institute of Experimental Pharmacology, Slovak Academy of Sciences, Bratislava, Slovak Republic*
[e]*Department of Pharmacology, Faculty of Medicine, Gari University, Besevler, Ankara, Turkey*

Received 11 December 2001; received in revised form 17 April 2002; accepted 23 May 2002

Abstract

Hyperglycemia leads to excess production of reactive oxygen species (ROS), lipid peroxidation and protein glycation that may impair cellular calcium homeostasis and results in calcium sequestration and dysfunction in diabetic tissues. Stobadine (ST) is a pyridoindole antioxidant has been postulated as a new cardio- and neuroprotectant. This study was undertaken to test the hypothesis that the treatment with ST inhibits calcium accumulation, reduces lipid peroxidation and protein glycation and can change Ca^{2+},Mg^{2+}-ATPase activity in diabetic animals. The effects of vitamin E treatment were also evaluated and compared with the effects of combined treatment with ST. Diabetes was induced by streptozotocin (STZ, 55 mg/kg i.p.). Some of diabetic rats and their age-matched controls were treated orally with a low dose of ST (24.7 mg/kg/day), vitamin E (400–500 IU/kg/day) or ST plus vitamin E for 10 weeks. ST and vitamin E separately produced, in a similar degree, reduction in diabetes-induced hyperglycemia. Each antioxidant alone significantly lowered the levels of plasma lipid peroxidation, cardiac and hepatic protein glycation in diabetic rats but vitamin E treatment was found to be more effective than ST treatment alone. Diabetes-induced increase in plasma triacylglycerol levels was not significantly altered by vitamin E treatment but markedly reduced by ST alone. The treatment with each antioxidant completely prevented calcium accumulation in diabetic heart and liver. Microsomal Ca^{2+},Mg^{2+}-ATPase activity significantly decreased in both tissues of untreated diabetic rats. ST alone significantly increased microsomal Ca^{2+},Mg^{2+}-ATPase activity in the heart of normal rats However, neither treatment with ST nor vitamin E alone, nor their combination did change cardiac Ca^{2+},Mg^{2+}-ATPase activity in diabetic heart. In normal rats, neither antioxidant had a significant effect on hepatic Ca^{2+},Mg^{2+}-ATPase activity. Hepatic Ca^{2+},Mg^{2+}-ATPase activity of diabetic rats was not changed by single treatment with ST, while vitamin E alone completely prevented diabetes-induced inhibition in microsomal Ca^{2+},Mg^{2+}-ATPase activity in liver Combined treatment with ST and vitamin E provided more benefits in the reduction of hyperglycemia and lipid peroxidation in diabetic animals. This study describes potential mechanisms on cellular effects of ST in the presence of diabetes-induced hyperglycemia that may delay or inhibit the development of diabetic complications The use of ST together with vitamin E can better control hyperglycemia-induced oxidative stress.
© 2002 Elsevier Science B.V. All rights reserved.

Keywords Streptozotocin-diabetes, Stobadine; Vitamin E, Ca^{2+}-ATPase, Protein glycation, Lipid peroxidation

---

1. Introduction

A number of mechanisms, including hyperglycemia, glycosylation of proteins and oxidative stress, have been proposed to contribute to the pathogenesis of cellular

---

[*] Corresponding author and the leader of ADIC Study Group
E-mail address karasu@med.gari.edu.tr (Ç Karasu)

0925-4439/02/$ - see front matter © 2002 Elsevier Science B V All rights reserved
PII S0925-4439(02)00141-2

dysfunction leading to cardiovascular, hepatic and other complications of diabetes [1,2]. Hyperglycemia has been shown to generate reactive oxygen species (ROS) such as superoxide radicals from autooxidation of glucose, and resultant increase in cellular lipid peroxidation in diabetic patients and animals [3,4]. Excess production of ROS may lead to cellular injury through nonspecific modification and disruption of proteins, phospholipids and nucleic acids [5]. Critical sites of ROS attack are the cell membrane and the membranes of intracellular organelles. The disruptive effect of ROS involves membrane lipid peroxidation and membrane protein modification, which may produce alterations in the membrane structure and function including fluidity, permeability, enzyme activity, ion channels and transport, and receptor proteins. Data obtained from animals and patients with diabetes showed that abnormal intracellular calcium metabolism is widespread in tissues [6], and intracellular calcium levels are increased in many tissues including heart [7–10]. Similarly, hepatocyte calcium sequestration and turnover are also increased in both acute and chronic experimentally induced diabetes [11,12]. The activities of membrane ATPases (i.e. Ca^{2+},Mg^{2+}-ATPase and Na^{+},K^{+}-ATPase) has been shown to be abnormal in diabetic state. Decreased Ca^{2+}-ATPase activity has been reported in diabetic heart [7,8,10]. In contrast, streptozotocin (STZ)-induced diabetes led to an increase in hepatic plasma membrane Ca^{2+}-ATPase activity of rats [14]. The studies imply that the nature of the alterations is tissue-specific and may depend on the level of blood glucose or insulin, or both. Membrane Ca^{2+},Mg^{2+}-ATPase is responsible for the fine-tuning of intracellular calcium and the Na^{+}–Ca^{2+} exchanger for rapid ejection of the excess calcium that has entered the cell [15]. Insufficient Ca^{2+},Mg^{2+}-ATPase activity has been suggested as contributing factor in the development of diabetic cardiomyopathy [7,8]. The effects of ROS on the enzyme may be very specific and may include selective alterations of its active sites resulting in inhibition of its activity [16–19].

Supplementation with antioxidants has been shown to decrease oxidative stress and complications in animal models of diabetes [20,21] and in diabetic patients [22]. Diabetes-induced defects in the homeostasis and the transport of intracellular calcium has been shown to decrease or recover by the treatment of diabetic animals with some antioxidant compounds, such as *N*-acetyl cysteine, beta-carotene, vitamin E, trolox C and pyridoxine [19,23,24]. Stobadine (ST), (−)-*cis*-2,8-dimethyl-2,3,4,4a,5,9b-hexa-hydro-1*H*-pyrido[4,3-b] indole, was shown to be able to scavenge hydroxyl, alkoxyl and peroxyl radicals, weakly superoxide, and to quench singlet oxygen, to repair oxidized amino acids and to preserve oxidation of SH groups by one-electron donation [25]. It was demonstrated that in free radical generating systems in vitro, ST and some other lipophilic and water-soluble antioxidants, including butylated hydroxytoluene, lipoic acid and vitamin E, are able to decrease the effects of oxidative stress on tissue Ca^{2+}-ATPase activity and calcium accumulation [16,18,24,26]. We recently showed that the treatment of diabetic rats with a low dose of ST attenuates tissue markers of oxidative stress and other diabetes-induced abnormalities in brain [27], heart [28] and aorta [29]. Since the question of the effect of ST on calcium homeostasis in diabetes mellitus has not yet been addressed, the main purpose of the present study was to evaluate the effects of ST on cardiac and hepatic calcium metabolism in STZ-diabetic rats. For this purpose, the amount of calcium and the activity of Ca^{2+}-ATPase in heart and liver microsomes of normal and STZ-diabetic rats, treated or untreated with ST, were determined. Secondly, we compared the effect of ST treatment alone with that of vitamin E. Since different antioxidant compounds may act synergistically and some combinations may be more effective than any one compound alone, the effects of ST plus vitamin E treatment were also evaluated and compared with the effects of treatment with each agent alone. The effects of ST and vitamin E on plasma triacylglycerol levels, lipid peroxidation and tissue protein glycation were also measured to elucidate the underlying mechanisms.

2. Materials and methods

2.1. Induction of diabetes and treatment protocols

Male Wistar rats, body weight 250–300 g, were fed a standard rat chow diet and had access to water ad libitum. Diabetes was induced by a single intraperitoneal injection of STZ (55 mg/kg body weight) to animals fasted overnight. Diabetes was verified 48 h later by measuring tail vein blood glucose, and the rats with blood glucose of 300 mg/dl or more were considered diabetic. Two days after injection of STZ or vehicle, rats were divided into the following groups: (1) untreated diabetic rats ($n=12$); (2) diabetic rats treated with ST (24.7 mg/kg/day, orally) ($n=11$); (3) diabetic rats treated with vitamin E (alpha-tocopheryl acetate, 400–500 IU/kg/day, orally) ($n=11$); (4) diabetic rats treated with both ST and vitamin E, as given in protocols 2 and 3 ($n=10$); (5) untreated control rats ($n=9$); (6) control rats treated with ST as given in protocol 2 ($n=5$); (7) control rats treated with vitamin E, as given in protocol 3 ($n=5$); (8) control rats treated with ST plus vitamin E as given in protocol 4 ($n=5$). The dose regimen of ST or vitamin E was chosen according to some previous studies [20,25]. The animals were treated for a period of 10 weeks beginning 48 h after either vehicle or STZ injection. “The principles of laboratory animal care” (NIH publication no. 85-23, revised 1985) were observed.

2.2. Measurement of blood glucose, triacylglycerol and thiobarbituric acid reactive substances (TBARS)

Blood glucose and triacylglycerol concentrations were measured by Accutrend® GCT meter (Roche Diagnostics).

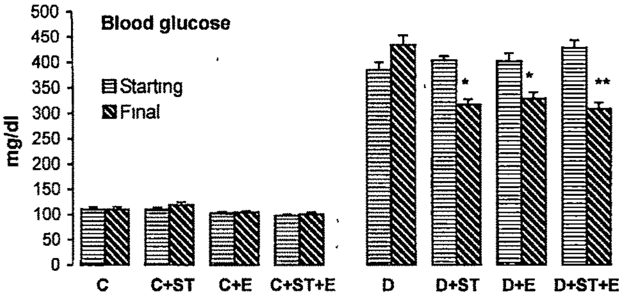

Fig. 1. Blood glucose levels of control (C) and diabetic (D) animals untreated or treated with stobadine (ST), vitamin E (E) or stobadine plus vitamin E (ST+E). Data are reported as means ± S.E. The blood glucose concentrations of all diabetic animals were significantly different from the control animals untreated or treated with antioxidants Start: 2 days later of STZ injection. Final: at the end of the treatment period $*P<0.05$, $**P<0.01$ vs starting within group.

TBARS, end products of lipid peroxidation, were measured fluorometrically in plasma [30].

2.3. Membrane-enriched microsome preparation

Heart and liver tissues were weighed and homogenised in six volumes of freshly prepared buffer A containing: 0.3 mol/l sucrose, 10 mmol/l HEPES–HCl pH 7.4 and 2 mmol/l dithiothreitol. A Teflon/glass homogeniser (Omni mixer homogeniser model 18074, Omni Int., CT, USA) was used for homogenisation of tissues. The homogenates were centrifuged at $85{,}000 \times g$ for 75 min, the supernatant discarded and the pellets were resuspended in the original volume of buffer A containing 0.6 mol/l KCl (using four strokes) and centrifuged again at $85{,}000 \times g$ for 75 min. The pellets were then resuspended in the original volume of buffer A. After centrifugation at $85{,}000 \times g$ for 75 min (Beckman L 7, Beckman Instruments Inc., Fullerton, CA), the pellets were suspended in buffer A (using four strokes) at a protein concentration of 2–7 mg/ml. Samples were kept frozen at − 60 °C until further use. Isolation procedure was performed at +4 °C [31].

2.4. Determination of Ca^{2+}-ATPase activity

Ca^{2+}-ATPase activity was measured spectrophotometrically (Pye Unicam SP8-100 UV spectrophotometer, PYE Unicam Ltd., Cambridge, England), as described previously [32]. The incubation medium contained: 120 mmol/l KCl, 60 mmol/l HEPES, pH 7.0 (at 37 °C), 1 mmol/l MgCl$_2$, 0.5 mmol/l K$_2$-ATP, 0.2 mmol/l NADH, 0.5 mmol/l PEPA, 1 IU pyruvate kinase, 1 IU lactate dehydrogenase/ml and 500 μmol/l EGTA. After preincubation of the assay medium (total volume of 1 ml) for 4 min at 37 °C, 75-μg ATPase was added to the medium. After 2 min, the reaction was started by addition of 600 μmol/l CaCl$_2$. Determination of ATPase activity was followed by continuous measurement of absorbance at 365 nm.

2.5. Determination of tissue calcium levels and protein glycation

Tissue calcium levels were analysed by atomic absorption spectrophotometry (Perkin Elmer 2380) according to the wet-ashing procedure with nitric acid.

Protein glycation in microsomal fractions was measured as described previously [33].

2.6. Drugs and statistical analysis

All chemicals except ST were purchased from Sigma Chemical (St. Louis, MO, USA). ST dipalmitate was obtained from the Slovak Academy of Sciences. Data are expressed as mean ± S.E. They were first subjected to Bartlett's test for homogeneity of variances and were given a log transformation if necessary. One-way analysis of variance was then performed, followed by the Student–Neuman–Keuls test to estimate the significance of differences for individual between-group comparisons. For the statistical evaluation of starting and final blood glucose concentrations within groups, Student's t test was used.

3. Results

The final blood glucose concentrations of untreated diabetic rats were about four times higher than in normal control rats (Fig. 1). A treatment with each agent alone produced a significant fall in blood glucose levels of diabetic animals. The magnitude of the blood glucose lowering effect of ST treatment was found to be comparable to the effects of vitamin E treatment. Combination of ST and vitamin E provided some further benefit on blood glucose control; nevertheless, at the end of the treatments, diabetic rats were still hyperglycaemic when compared with normal control rats (Fig. 1).

Plasma triacylglycerol concentrations significantly increased in untreated diabetic rats (Fig. 2). Single treatment with ST resulted in a marked decrease in plasma triacylgly-

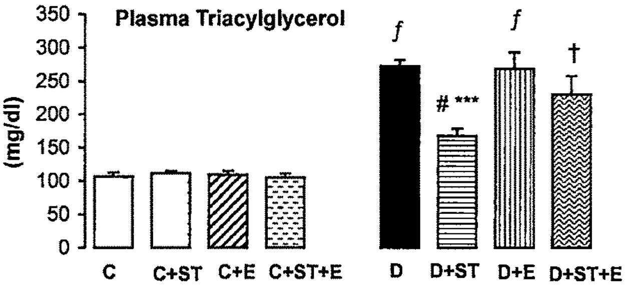

Fig. 2. Plasma triacylglycerol levels of control (C) and diabetic (D) animals untreated or treated with stobadine (ST), vitamin E (E) or stobadine plus vitamin E (ST+E). Data are reported as means ± S.E $^{\#}P<0.05$, $^{\dagger}P<0.01$, $^{f}P<0.001$ vs. untreated-control (C) animals $**P<0.01$, $***P<0.001$ vs. untreated-diabetic (D) animals

cerols while vitamin E alone was unable to induce a significant reduction in elevated triacylglycerols of diabetic rats (Fig. 2). Combined treatment has no further effect on the decreasing of triacylglycerol levels of diabetic animals.

The levels of TBARS, end products of lipid peroxidation, were markedly elevated in plasma of diabetic rats compared to those in controls (Fig. 3). This increase was partially prevented by treatment with either ST or vitamin E alone. In the prevention of plasma lipid peroxidation, the combined therapy was significantly more effective than treatment with a single agent, and it provided almost normalised plasma TBARS in diabetic animals (Fig. 3).

In normal control rats, treatment with each antioxidant studied, as well as their combination, led to a significant reduction of cardiac protein glycation. In these animals, hepatic protein glycation was also inhibited by ST alone, yet not by vitamin E. Glycation of proteins significantly increased in heart and liver of untreated diabetic rats (Fig. 4). In heart of diabetic rats, an increase in protein glycation was significantly but not completely prevented by vitamin E treatment; while this vitamin completely prevented diabetes-induced changes in glycation of hepatic proteins. ST, when given alone, was also effective in the prevention of protein glycation increase in both diabetic heart and liver; however, in comparison with vitamin E, the inhibitory effect of ST was moderate. When compared with the effect of viatamin E treatment alone, the combination of the two antioxidants did not provide an additional benefit on either cardiac or hepatic protein glycation of diabetic rats (Fig. 4).

Total calcium levels were markedly increased in heart and liver of untreated diabetic rats (Fig. 5). In the heart, treatment with either ST or vitamin E resulted in a significant decrease in calcium levels in both nondiabetic control and diabetic rats. In the treatment with vitamin E alone or two agents together, the calcium levels of the diabetic heart were found to be lower than those of normal control animals. In the liver, neither ST nor vitamin E treatment did significantly change calcium levels of normal control rats, but in diabetic rats calcium overload was completely prevented (Fig. 5).

Microsomal Ca^{2+}-ATPase activity significantly decreased in heart and liver of untreated diabetic rats (Fig. 6).

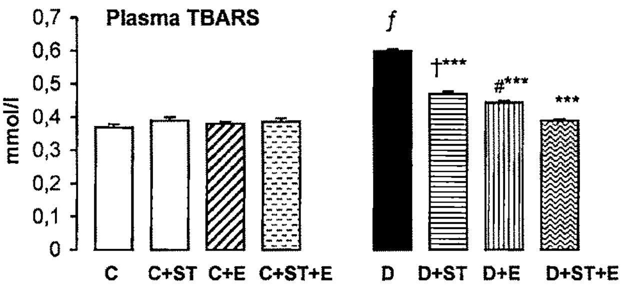

Fig 3 Effects of stobadine (ST) and vitamin (E) treatments on plasma lipid peroxidation levels (Thiobarbituric acid reactive substances (TBARS) of the animals. Data are reported as means ± S E $^{\#}P<0.05$, $^{\dagger}P<0.01$, $^{f}P<0.001$ vs. untreated-control (C) animals $^{**}P<0.01$, $^{***}P<0.001$ vs. untreated-diabetic (D) animals

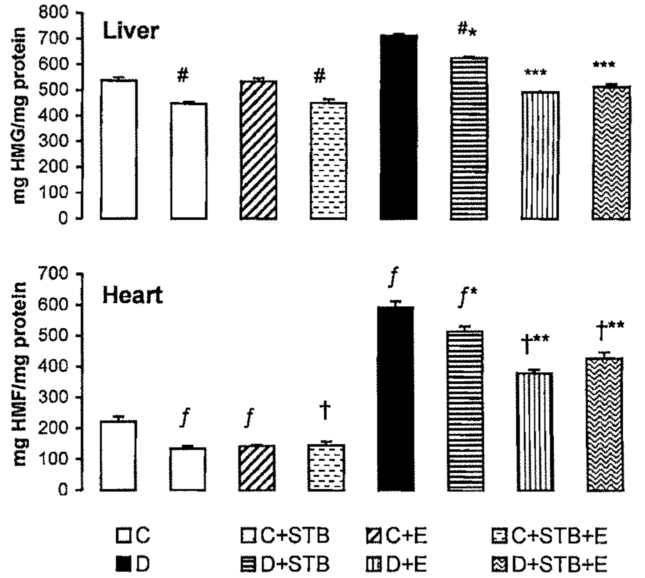

Fig 4 Effects of stobadine (ST) and vitamin E (E) treatments on the glycation of proteins in liver and heart of the animals. Data are reported as means ± S.E $^{\#}P<0.05$, $^{\dagger}P<0.01$, $^{f}P<0.001$ vs untreated-control (C) animals $^{*}P<0.05$, $^{**}P<0.01$, $^{***}P<0.001$ vs. untreated-diabetic (D) animals

The inhibitory effect of diabetes on Ca^{2+}-ATPase activity was observed to be higher in heart than that in liver. ST alone or its combination with vitamin E significantly increased microsomal Ca^{2+}-ATPase activity in the heart of normal rats. However, neither treatment with ST nor vitamin E alone, nor their combination did change cardiac Ca^{2+}-ATPase activity in diabetic heart. In normal rats, neither antioxidant had a significant effect on hepatic Ca^{2+}-ATPase activity. Hepatic Ca^{2+}-ATPase activity of diabetic rats was

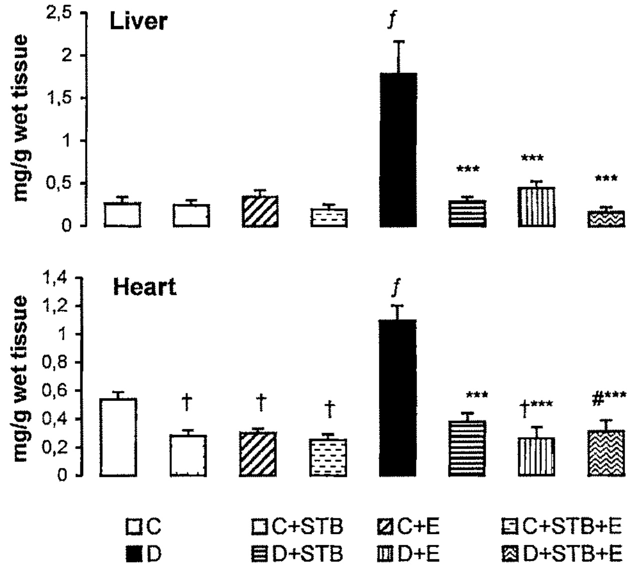

Fig 5 Tissue calcium concentrations in control (C) and diabetic (D) animals untreated or treated with stobadine (ST), vitamin E (E) or stobadine plus vitamin E (ST + E) Data are reported as means ± S E $^{\#}P<0.05$, $^{\dagger}P<0.01$, $^{f}P<0.001$ vs untreated-control (C) animals $^{*}P<0.05$, $^{**}P<0.01$, $^{***}P<0.001$ vs. untreated-diabetic (D) animals

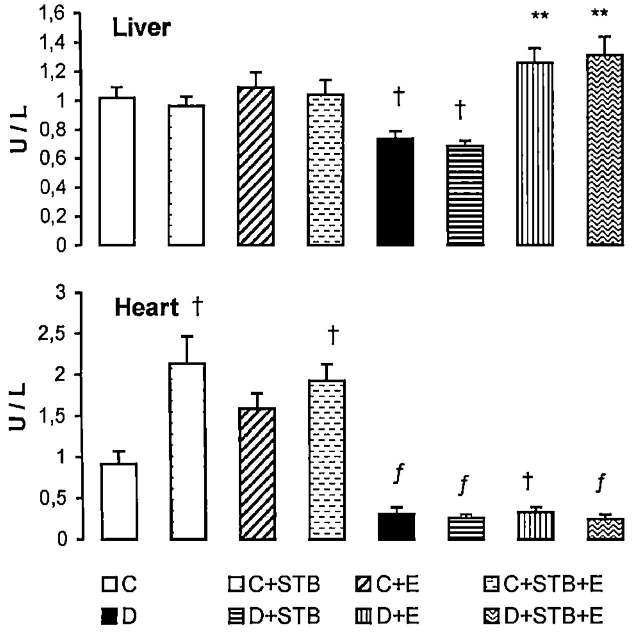

Fig 6 Microsomal Ca^{2+}-ATPase activity in control (C) and diabetic (D) animals untreated- or treated with stobadine (ST), vitamin E (E) or stobadine plus vitamin E (ST+E). Data are reported as means ± S E $^{\#}P<0.05$, $^{\dagger}P<0.01$, $^{f}P<0\ 001$ vs untreated-control (C) animals $^{*}P<0.05$, $^{**}P<0\ 01$, $^{***}P<0\ 001$ vs untreated-diabetic (D) animals.

not changed by the treatment with single ST, while vitamin E alone completely prevented diabetes-induced inhibition in microsomal Ca^{2+}-ATPase activity in liver (Fig. 6).

4. Discussion

Abundant information is now available on changes in plasma membrane and subcellular organelles, which are responsible for the impaired intracellular calcium homeostasis in diabetic cardiomyopathy and other complications of diabetes mellitus [6,7,9,10]. Some of these include abnormalities in the following variables: calcium binding, influx of calcium through the L-type calcium channels, Na^{+},K^{+}-ATPase activity, $Na^{+}-Ca^{2+}$ exchange, $H^{+}-Na^{+}$ exchange and Ca^{2+},Mg^{2+}-ATPase activity etc. The Ca^{2+}-ATPase is the major active calcium transport protein responsible for the maintenance of normal intracellular calcium levels in a variety of cell types. Maintenance of the cation gradient by Ca^{2+}-ATPase is of fundamental importance in the control of hydration, volume, nutrient uptake and fluidity of cells, and is also essential for the contractility and excitability properties of muscles [6,7]. In the present study, microsomal Ca^{2+},Mg^{2+}-ATPase activity was depressed by STZ-diabetes in heart and liver of rats. This event was accompanied to increased total calcium levels. Our findings are in agreement with previous observations showing that the membrane abnormalities in Na^{+},K^{+}-ATPase, $Na^{+}-Ca^{2+}$ exchange and Ca^{2+}-pump activities led to the occurrence of intracellular calcium overload in experimental rat models of diabetes [7,10,13,34]. Depressed myofibrillar and sarcolemmal Ca^{2+}-ATPase activity and sarcoplasmic reticulum calcium uptake were reported as important mechanisms responsible for the cardiac dysfunction and cardiomyopathy exhibited by insulin-deficient (Type I) diabetic animals [7,10,13,34].

The increased intracellular concentration of calcium may be explained by the osmotic activity of high glucose (cell shrinkage), demonstrated to activate G protein(s), most likely through a stretch receptor, which in turn stimulates calcium channels inhibitable by verapamil, nifedipine and amlodipine, thus permitting a calcium influx into cardiac myocytes [9]. The increased cardiac affinity for calcium in diabetic rats was also reported to be due to changes in sarcolemmal lipid bilayer composition secondary to diabetes-induced hyperlipidaemia [35]. Diabetes-induced hyperlipidemia and the alterations in membrane phospholipids and fatty acids have been shown to depress membrane-bound enzyme activities, which influence intracellular calcium metabolism resulting in cardiac dysfunction [34]. As indicated before, plasma membrane and the membranes of intracellular organelles are crucial targets of ROS attack. Oxidative insult was found to lead to a decrease in Ca^{2+}-ATPase activity in heart [36,37] or brain microsomes [18]. Decreased membrane fluidity induced by increased oxidative stress has been linked with the aforementioned abnormalities in calcium metabolism [18]. The present study provided once again evidence that there are significant increase in plasma triacylglycerol levels and the peroxidation of lipids in diabetic animals. As it is well known, hyperglycemia results in increased oxidative stress from excessive ROS production from the auto-oxidation of glucose and glycated proteins [2,5,38]. The increased ROS activity initiates peroxidation of lipids and MDA accumulation, which in turn can stimulate glycation of proteins in diabetes [4,38]. Another possibility involves the modification of enzyme molecules either by direct oxidation or by modification mediated by products of lipid peroxidation [39]. A decrease in ATPase enzyme activity in any diabetic tissue could be due to excessive nonenzymatic glycation of the enzyme itself and/or of calmodulin [40]. Ca^{2+}-ATPase was shown to be particularly sensitive to cross-linking and the concomitant decrease in protein rotational mobility due to protein aggregation [36]. In the present study, cardiac and hepatic protein glycation was markedly increased in STZ-diabetic rats; in the light of previous observations, both glycosylation of enzyme proteins and/or inhibition of its activity by lipid peroxidation products seem to be major contributing factors associated with abnormal calcium homeostasis in diabetic animals.

In the present study, we demonstrated for the first time that 10 weeks of ST treatment completely prevented cardiac and hepatic calcium accumulation without a significant amelioration in Ca^{2+}-ATPase activity in STZ-diabetic rats. The magnitude of this effect of ST was parallel with the same effect of vitamin E in both tissues; a combination of ST plus vitamin E did not produce a further effect on total calcium amount in diabetic tissues. On the other hand, the effect of each antioxidant on microsomal Ca^{2+}-ATPase activity was tissue-specific. In heart of normal control rats, ST treatment alone led to an increase in Ca^{2+}-ATPase activity, but did not produce a significant change in depressed Ca^{2+}-ATPase activity in diabetic rats. In liver, however, ST treatment alone had no significant effect on Ca^{2+}-ATPase activity in either control or diabetic animals. In diabetic animals, vitamin E, although unable to prevent Ca^{2+}-ATPase depression in heart, completely protected hepatic Ca^{2+}-ATPase activity from the destructive effect of STZ-diabetes. In addition, neither ST nor vitamin E did alter hepatic Ca^{2+}-ATPase activity in normal animals.

Previous studies have reported that supplementation with some antioxidants prevents lipid peroxidation, hemoglobin glycosylation and inhibition of Na^+,K^+-ATPase and/or Ca^{2+}-ATPase activity caused by hyperglycemia in various cells [19,23,24]. The exact mechanism(s) of the effects of the both antioxidants on abnormal intracellular calcium regulation of diabetic heart and liver are not fully known. As demonstrated previously, ST prevents the decrease in membrane fluidity and nonspecifically inhibits various excitable channels, and diminishes in a concentration-dependent manner calcium (L-type) inward currents [25] that may account for its preventive effect on calcium accumulation in diabetic tissues. In endoplasmic reticulum membranes of synaptosomes and erythrocytes, ST has been shown to attenuate calcium permeability already increased by a free radical generating system in vitro [16,18]. In this in vitro system, brain Ca^{2+}-ATPase activity was protected by ST, and the efficiency of ST to prevent calcium transport changes was demonstrated to depend on the presence of glutathione and was similar to that of a good chain-breaking antioxidant, butylated hydroxytoluene [18]. In the aforementioned study, in contrast to ST, vitamin E was shown to be less potent to confer the defence against ROS-induced changes in calcium regulation [18]. It has been suggested that inhibition of Ca^{2+}-ATPase is not based on direct protein modifications, but is rather mediated by changes in membrane fluidity and protein–lipid interaction [18]. In the present study, we observed that in vivo treatment with a low dose of ST partially prevented glycation of cardiac and liver proteins and the peroxidation of plasma lipids. These effects of ST treatment alone were less potent than the corresponding effects of vitamin E treatment in diabetic animals. It has been shown that ST inhibits protein glycation and lipid peroxidation [25,41,42]. The inhibitory effect of ST on hyperglycemia-induced lipid peroxidation could be a result of the scavenging of ROS. ST was shown to be able to scavenge hydroxyl, alkoxyl and peroxyl radicals, weakly superoxide, and to quench singlet oxygen, to repair oxidized amino acids and to preserve oxidation of SH groups by one-electron donation [25]. The protein glycation-inhibiting effect of ST has been demonstrated in an experimental in vitro glycation model [42]. Since ST did not affect the covalent binding of glucose, the protective effect of ST has been attributed to its ability to eliminate free radical intermediates of glyco-oxidation reactions, operative after the preceding glycation step [42,43]. ST inhibits glucose-induced chromo- and fluorophore formation, interferes with metal-catalysed oxidation reaction following after the glycation step and limits the damage from glycation-induced processes [43]. Blood-glucose-lowering effect of ST treatment, started 2 days later of STZ injection, might be directly related to its free radical (peroxyl radicals) scavenging properties, which may protect pancreatic beta cells against the STZ toxicity [25].

Vitamin E treatment alone completely prevented protein glycation in diabetic liver, which was parallel with the protection of microsomal Ca^{2+}-ATPase. This implies that impaired Ca^{2+}-ATPase is more likely a consequence of increased protein glycation in diabetic tissue. This phenomenon, however, may be valid for diabetic liver only. In the heart of diabetic animals, the findings suggest that other factors are also involved in the regulation of calcium homeostasis affected by ST and vitamin E These factors seem unlikely to be directly linked with lipid peroxidation since both antioxidants significantly prevented overproduction of lipid hydroperoxides both in plasma (as observed in this study) and in heart [28] of diabetic animals. In earlier studies, other investigators found that administration of vitamin E in a combination with other antioxidants, *N*-acetyl cysteine, beta-carotene and vitamin C, prevented both diabetes- and galactosemia-induced elevations in oxidative stress, and protected myocardial and retinal Na^+,K^+-ATPase and Ca^{2+}-ATPases against oxidative damage [19,44]. Another report stated that pre-treatment of animals with vitamin E attenuated depression in sarcoplasmic reticulum calcium transport, intracellular calcium accumulation and heart dysfunction in catecholamine-induced cardiomyopathy [26]. Vitamin E can block the glycation of proteins by inhibiting MDA formation [38]. However, some reports suggest that the Ca^{2+}-releasing and/or -retaining effects of alpha-tocopherol may be independent of pro- and/or antioxidant activities [45].

Our study provided the first evidence that a low dose of ST is able to lower blood glucose and triacylglycerol levels and to prevent lipid peroxidation, protein glycation and tissue calcium accumulation in STZ-diabetic rats. The inhibitory effect of ST on calcium overload seems to be dependent largely on its aforementioned beneficial effects but is unlikely to be directly linked with the membrane Ca^{2+}-ATPase activity since ST treatment is unable to prevent Ca^{2+}-ATPase reduction in diabetic heart and liver. The increasing effect of ST on cardiac Ca^{2+}-ATPase activity in normal control rats may be attributed to its lowering effect on calcium amount in this tissue. On comparing the two compounds, vitamin E was found to be more effective than ST in the prevention of lipid peroxidation and protein glycation. These antioxidants provide more benefits only in the prevention of diabetes-induced hyperglycemia and lipid peroxidation when used in combination for the treatment of diabetes. In addition, ST is a potent inhibitor of plasma triacylglycerol levels. This study describes potential mechanisms on cellular effects of ST in the presence of hyperglycemia that may delay or inhibit the development of diabetic complications. The use of both antioxidants together can provide a better control on hyperglycemia-induced oxidative stress.

Acknowledgements

This study was supported by the "Turkish Scientific and Research Council" (TUBITAK-SBAG-2397).

References

[1] S M Strowing, P. Raskin, Glycemic control and the complications of diabetes: after the diabetes control and complications trial, Diabetes Rev 3 (1995) 237–257

[2] J W. Baynes, S R Thorpe, The role of oxidative stress in diabetic complications, Curr. Opin Endocrinol. 3 (1996) 277–284

[3] K.C Chang, S Y Chung, W S Chong, J.S. Suh, S.H. Kim, H.K Noh, B.W. Seong, H J. Ko, K W Chun, Possible superoxide radical-induced alteration of vascular reactivity in aortas from streptozotocin-treated rats, J. Pharmacol Exp Ther. 266 (1993) 992–1000

[4] S K Jain, Hyperglycemia can cause membrane lipid peroxidation and osmotic fragility in human red blood cells, J. Biol. Chem. 264 (1989) 21340–21345

[5] J.V Hunt, R T Dean, S.P Wolff, Hydroxyl radical production and autoxidative glycosylation: glucose autoxidation as the cause of protein damage in the experimental glycation model of diabetes mellitus and ageing, Biochem. J. 256 (1988) 205–212.

[6] J. Levy, J.R Gavin III, J R. Sower, Diabetes mellitus: a disease of abnormal cellular calcium metabolism? Am J Med 96 (1994) 260–273.

[7] L S. Golfman, N. Takeda, N S. Dhalla, Cardiac membrane Ca^{2+}-transport in alloxan-induced diabetes in rats, Diabetes Res. Clin Pract. 3 (1996) S73–S77 (Suppl)

[8] L Golfman, I.M Dixon, N. Takeda, A Lukas, K Dakshinamurti, N.S. Dhalla, Cardiac sarcolemmal Na^{+}–Ca^{2+} exchange and Na^{+}–K^{+} ATPase activities and gene expression in alloxan-induced diabetes in rats, Mol. Cell Biochem 188 (1998) 91–101.

[9] M. Smogorzewski, V. Galfayan, S.G Massry, High glucose concentration causes a rise in $[Ca^{2+}]_i$ of cardiac myocytes, Kidney Int 53 (1998) 1237–1243

[10] Y Hattori, N Matsuda, J Kimura, T Ishitani, A Tamada, S. Gando, O Kemmotsu, M. Kanno, Diminished function and expression of the cardiac Na^{+}–Ca^{2+} exchanger in diabetic rats implication in Ca^{2+} overload, J. Physiol 15 (527 Pt. 1) (2000) 85–94

[11] K M. Chan, K D Junger, The effect of streptozocin-induced diabetes on the plasma membrane calcium uptake activity of rat liver, Diabetes 33 (1984) 1072–1077

[12] R.K. Studer, L. Ganas, Effect of diabetes on hormone-stimulated and basal hepatocyte calcium metabolism, Endocrinology 125 (1989) 2421–2433

[13] T. Misra, J.S Gilchrist, J C. Russell, G N Pierce, Cardiac myofibrillar and sarcoplasmic reticulum function are not depressed in insulin-resistant JCR·LA-cp rats, Am J Physiol 276 (1999) H1811–H1817

[14] H Takahashi, T. Murata, Y. Hanahisa, M. Yamaguchi, Streptozotocin-induced diabetes increases (Ca^{2+}–Mg^{2+})-ATPase activity in hepatic plasma membranes of rats involvement of protein kinase C, Mol. Cell. Biochem. 178 (1998) 311–316

[15] M.P.E Van Heeswijk, J.A.M Greertsen, C.H. Van Os, Kinetic properties of the ATP-dependent Ca^{2+}-dependent Ca^{2+} pump and Na^{+}/Ca^{2+} exchange system in basolateral membranes from rat kidney cortex, J Membr. Biol. 79 (1984) 19–31

[16] K.A. Clinch, F.F. Vincenzi, T T Rohn, T R. Hinds, ST protects ion pump ATPases from free radical inhibition, Proc. West. Pharmacol Soc 36 (1993) 209–214

[17] P Racay, P. Kaplan, V Mezesova, J. Lehotsky, Lipid peroxidation both inhibits Ca^{2+}-ATPase and increases Ca^{2+} permeability of endoplasmic reticulum membrane, Biochem. Mol Biol Int 41 (1997) 647–655

[18] J Lehotsky, P Kaplan, P. Racay, M. Matejovicova, A Drgova, V. Mezesova, Membrane ion transport system during oxidative stress in rodent brain protective effect of ST and other antioxidants, Life Sci. 65 (1999) 1951–1958

[19] R.A Kowluru, R.L Engerman, T.S Kern, Diabetes-induced metabolic abnormalities in myocardium: effect of antioxidant therapy, Free Radic. Res 32 (2000) 67–74.

[20] Ç Karasu, G. Ozansoy, O Bozkurt, D Erdoğan, S. Omeroğlu, Atioxidant and triglyceride-lowering effects of vitamin E associate with the prevention of abnormalities in the reactivity and morphology of aorta from streptozotocin-diabetic rats, Metabolism 46 (1997) 872–879

[21] G. Koçak, F Aktan, O Canbolat, C Özoğul, Ş Elbeğ, N. Yıldızoğlu-Arı, Ç. Karasu, Alpha-lipoic acid treatment ameliorates metabolic parameters, blood pressure, vascular reactivity and morphology of vessels already damaged by streptozotocin-diabetes (The ADIC Study Group), Diabet. Nutr Metab 13 (2000) 308–319.

[22] S.K. Jain, R. McVie, T. Smith, Vitamin E supplementation restores glutathione and malondialdehyde to normal concentrations in erythrocytes of type-1 diabetic children, Diabetes Care 23 (2000) 1389–1394.

[23] S.K. Jain, G Lim, Pyridoxine and pyridoxamine inhibits superoxide radicals and prevents lipid peroxidation, protein glycation, and (Na^{+}+K^{+})-ATPase activity reduction in high glucose-treated human erythrocytes, Free Radic. Biol Med 30 (2001) 232–237.

[24] S K. Jain, G Lim, Lipoic acid decreases lipid peroxidation and protein glycation and increases (Na^{+}+K^{+})- and Ca^{++}-ATPase activities in high glucose-treated human erythrocytes, Free Radic Biol Med 29 (2000) 1122–1128.

[25] L Horakova, S. Stolc, Antioxidant and pharmacodynamic effects of pyridoindole ST, Gen. Pharmacol 30 (1998) 627–638

[26] P S Tappia, T. Hata, L. Hozaima, M S Sandhu, V Panagia, N S. Dhalla, Role of oxidative stress in catecholamine-induced changes in cardiac sarcolemmal Ca^{2+} transport, Arch Biochem Biophys 387 (2001) 85–92.

[27] Ç Karasu, N. Ulusu, A Avcı, M Sahıllı, O. Canbolat, G. Ozansoy, N Arı, S Stefek, S Stolc, A. Gojdosik, Effects of ST treatment on pentose phosphate pathway, glutathione-dependent enzymes, superoxide dismutase, and lipid peroxidation in the brain of diabetic rat, comparison with vitamin E Diabetologia (Suppl. 1) (2001) A155, 592.

[28] M. Stefek, R. Sotnikova, L. Okruhlicova, K Volkovova, J Kucharska, A Gajdosik, A Gajdosikova, D. Mihalova, R Hozova, N Tribulova, A Gvozdjakova, Effect of dietary supplementation with the pyridoindole antioxidant ST on antioxidant state and ultrastructure of diabetic rat myocardium, Acta Diabetol. 37 (2000) 111–117.

[29] R. Sotnikova, M. Stefek, L Okruhlicova, J Navarova, V Bauer, A. Gajdosik, A. Gajdosikova, Dietary supplementation of the pyridoindole antioxidant ST reduces vascular impairment in streptozotocin-diabetic rats, Methods Find. Exp. Clin. Pharmacol 23 (2001) 121–129.

[30] K. Yagi, Lipid peroxides and human disease, Chem Phys Lipids 45 (1987) 337–351

[31] D. Borchman, N A Delamere, C A. Peterson, Ca^{2+}-ATPase activity in the rabbit and bovine lens, Invest. Ophthalmol Visual Sci 29 (1988) 982–987

[32] V. Nigli, E S Adunyah, J.T Penniston, E Carafoli, Purified (Ca^{2+}–Mg^{2+})ATPase of the erythrocyte membrane· reconstitution and effect

of calmoduline and phospholipids, J Biol Chem 256 (1981) 395–401

[33] R Fluckiger, K.H Winterhalter, In vitro synthesis of HbA$_1$C, FEBS Lett 71 (1976) 356

[34] Y Kuwahara, T Yanagishita, N Konno, T. Katagiri, Changes in microsomal membrane phospholipids and fatty acids and in activities of membrane-bound enzyme in diabetic rat heart, Basic Res Cardiol. 92 (1997) 214–222.

[35] H. Kashihara, Z Q Shi, J Z Yu, J H McNeill, G F Tibbits, Effects of diabetes and hypertension on myocardial Na$^+$–Ca^{2+} exchange, Can. J Physiol Pharm 78 (2000) 12–19.

[36] R I Viner, G.K. Arkadi, T D Williams, C Schoneich, D J Bigelow, Identification of oxidation-sensitive peptides within the cytoplasmic domain of the sarcoplasmic reticulum Ca^{2+}-ATPase, Biochemistry 36 (1997) 7706–7716.

[37] A. Ziegelhoffer, T Ravingerova, J Styk, J Sebokova, I Waczulikova, A Breier, A Dzurba, K Volkovova, J. Carsky, L. Turecky, Mechanisms that may be involved in calcium tolerance of the diabetic heart, Mol Cell Biochem 176 (1997) 191–198

[38] S K Jain, M. Palmer, The effect of oxygen radicals metbolites and vitamin E on glycosylation of proteins, Free Radic Biol Med. 22 (1997) 593–596.

[39] W G Siems, S.J. Hapner, F J. van Kuijk, 4-Hydroxynonenal inhibits Na$^+$-K$^+$-ATPase, Free Radic Biol Med 20 (1996) 215–223.

[40] F.L G Flecha, M C Bermudez, N V Cedola, J J. Gagliardino, J P.F Rossi, Decreased Ca^{2+}-ATPase activity after glycosylation of erythrocyte membranes in vivo and in vitro, Diabetes 39 (1990) 707–711

[41] O Odrejiskova, L Horakova, I Juranek, A Ziegelhoeffer, S Stolc, Effect of stobadine on lipid peroxidation in brain and heart after ischemia and reperfusion of the brain, Life Sci. 65 (1999) 1959–1961

[42] M Stefek, L Krizanova, Z Trnkova, Oxidative modification of serum albumin in an experimental glycation model of diabetes mellitus in vitro. effect of the pyridoindole antioxidant ST, Life Sci 65 (1999) 1995–1997

[43] M Stefek, I Drozdikova, K Vajdova, The pyridoindole antioxidant stobadine inhibited glycation-induced absorbance and fluorescence changes in albumin, Acta Diabetol 33 (1996) 35–40

[44] R A Kowluru, T S Kern, R L. Engerman, D Armstrong, Abnormalities of retinal metabolism in diabetes or experimental galactosemia III Effects of antioxidants, Diabetes 45 (1996) 1233–1237

[45] R Guidoux, P Lambelet, J Phoenix, Effects of oxygen and antioxidants on the mitochondrial Ca^{2+}-retention capacity, Arch Biochem Biophys. 306 (1993) 139–147

ELSEVIER

Biochimica et Biophysica Acta 1588 (2002) 79–84

BIOCHIMICA ET BIOPHYSICA ACTA
BBA
www.bba-direct.com

Thiamine-responsive pyruvate dehydrogenase deficiency in two patients caused by a point mutation (F205L and L216F) within the thiamine pyrophosphate binding region

Etsuo Naito[a,*], Michinori Ito[a], Ichiro Yokota[a], Takahiko Saijo[a], Junko Matsuda[a], Yukiko Ogawa[a], Seiko Kitamura[a], Eiko Takada[b], Yoshihiro Horii[c], Yasuhiro Kuroda[a]

[a]*Department of Pediatrics, School of Medicine, University of Tokushima, Kuramoto Cho 3, Tokushima 770-8503, Japan*
[b]*Department of Pediatrics, Saitama Medical Center, Saitama Medical School, Saitama, Japan*
[c]*Department of Pediatrics, Yamashiro Hospital, Kyoto, Japan*

Received 24 January 2002; received in revised form 17 April 2002, accepted 23 May 2002

Abstract

The human pyruvate dehydrogenase complex (PDHC) catalyzes the thiamine-dependent decarboxylation of pyruvate. Thiamine treatment is very effective for some patients with PDHC deficiency Among these patients, five mutations of the pyruvate dehydrogenase $(E_1)\alpha$ subunit have been reported previously: H44R, R88S, G89S, R263G, and V389fs All five mutations are in a region outside the thiamine pyrophosphate (TPP)-binding region of the $E_1\alpha$ subunit. We report the biochemical and molecular analysis of two patients with clinically thiamine-responsive lactic acidemia. The PDHC activity was assayed using two different concentrations of TPP. These two patients displayed very low PDHC activity in the presence of a low (1×10^{-4} mM) TPP concentration, but their PDHC activity significantly increased at a high (0.4 mM) TPP concentration Therefore, the PDHC deficiency in these two patients was due to a decreased affinity of PDHC for TPP. Treatment of both patients with thiamine resulted in a reduction in the serum lactate concentration and clinical improvement, suggesting that these two patients have a thiamine-responsive PDHC deficiency. The DNA sequence of these two male patients' X-linked $E_1\alpha$ subunit revealed a point mutation (F205L and L216F) within the TPP-binding region in exon 7.

© 2002 Elsevier Science B V. All rights reserved.

Keywords Lactic acidemia; Pyruvate dehydrogenase complex deficiency; $E_1\alpha$ subunit, Thiamine pyrophosphate, Thiamine treatment, TPP binding region

1. Introduction

The human pyruvate dehydrogenase complex (PDHC) catalyzes the thiamine-dependent decarboxylation of pyruvate, and plays an important role in energy metabolism of the cell since it is an essential and rate-limiting enzyme connecting glycolysis with the tricarboxylic acid cycle and oxidative phosphorylation. Defects in PDHC are a common cause of primary lactic acidemia. Clinical symptoms can vary considerably in patients with PDHC deficiencies [1]. Thiamine treatment is very effective for some patients with PDHC deficiency. The majority of PDHC deficiencies result from mutations in the X-linked pyruvate dehydrogenase $(E_1)\alpha$ subunit gene [2,3]. The E1 component also contains a thiamine pyrophosphate (TPP) binding site that is shared by the α and β subunits [1,2]. In this study, we describe two male patients with a point mutation (F205L and L216F) within the TPP-binding region of the $E_1\alpha$ subunit.

2. Materials and methods

2.1. Patients

2.1.1. Patient 1

A boy weighing 1464 g at birth was born at 34 weeks of gestation. At 10 months of age, he suddenly developed marked generalized muscle hypotonia and weakness, while suffering from examthema subitum. He was admitted to the hospital for evaluation. On admission, his blood lactate concentrations ranged between 8.1 and 6.9 mM, and his pyruvate concentrations between 1.1 and 0.76 mM with lactate/pyruvate ratios between 7.4 and 9.2. The concentrations of lactate and pyruvate in the cerebrospinal fluid

---

[*] Corresponding author Tel.: +81-88-633-7134; fax. +81-88-631-8697
E-mail address enaito@clin.med.tokushima-u.ac.jp (E Naito)

0925-4439/02/$ - see front matter © 2002 Elsevier Science B V All rights reserved
PII S0925-4439(02)00142-4

(CSF) were significantly elevated at 8.2 and 1.2 mM, respectively. Amino acid analysis of his plasma showed an elevated alanine concentration of 1497 μmol/l (normal range, 320 to 480). He responded to 100 mg/day of thiamine. His blood lactate and pyruvate concentrations decreased to 2.7 and 0.4 mM, respectively. After treatment with a high dose of thiamine, the muscle weakness improved, and he was able to walk. He no longer developed generalized muscle hypotonia and weakness during febrile illness, and his condition remained relatively stable at the age of 2 years and 10 months. CT and MRI scans of the patient's brain showed no abnormalities.

2.1.2. Patient 2

The second patient was an 8-year-old boy, the second child of healthy unrelated parents; his sister was healthy. He was clinically normal at birth and during his first 2 years of life. At 24 months, he developed an ataxic gait and muscle weakness during a febrile illness, and he could not walk. He was admitted to the hospital for evaluation. On admission, his blood lactate (6.2 mM) to blood pyruvate (0.6 mM) ratio was 10.3. The concentration of lactate and pyruvate in the CSF were elevated at 5.1 and 0.64 mM, respectively. An MRI of the brain showed a bilateral hypointense signal on the T1 weighted images in the basal ganglia. He received 60 mg/day of thiamine. After the start of thiamine therapy, his blood lactate and pyruvate concentrations decreased to the normal range, and he was able to walk without support. His muscle weakness and ataxia decreased and he did not develop metabolic acidosis during febrile illnesses. The abnormality on the brain MRI improved. He showed normal development with only a slight gait disturbance after the age of 6 years and was admitted to an elementary school.

2.2. Enzymatic assays

Lymphoblastoid cell lines derived from two patients with clinically thiamine-responsive lactic acidemia were established and cultured in RPMI 1640 medium (Nissui, Tokyo) containing 3×10^{-3} mM thiamine-HCl as previously described [4]. The activities of the PDHC and E1 in cultured lymphoblastoid cells were assayed at two different concentrations of TPP (0.4 and 1×10^{-4} mM) [4]. The concentration of TPP in normal human blood is 1×10^{-4} mM [5]. Protein concentrations were measured by the method of Lowry et al. [6] with bovine serum albumin as a standard.

2.3. Assay of rate of [1-^{14}C]pyruvate decarboxylation

The rate of [1-^{14}C]pyruvate decarboxylation was measured by a modification of the method of Naito et al. [7]. Briefly, intact lymphoblastoid cells were harvested, washed, and suspended with PBS. After preincubation with or without thiamine-HCl (4 mM) for 60 min, the cells were incubated in 0.2 ml of PBS containing 2.5 mM [1-^{14}C]pyruvate (0.1 mCi/mmol) in closed vessels at 37 °C for 30 min.

2.4. Molecular analysis of the PDHC-$E_1\alpha$ gene

The great majority of PDHC deficiencies result from mutations in the $E_1\alpha$ subunit gene [3]. Mutation analysis of the $E_1\alpha$ gene was performed using genomic DNA from cultured lymphoblastoid cells. For genetic analysis of the 11 exons of the $E_1\alpha$ gene, individual exons of the gene were amplified using primer pairs and conditions as described previously [8]. These fragments, used to detect single-strand conformation polymorphisms (SSCP), were sequenced directly using appropriate amplification primers. SSCP analysis was performed using the GeneGel Exel kit (Amersham Pharmacia Biotech UK Ltd., Bucks, UK). Sequence analysis was performed by an automated ABI 377 autosequencer using a dye-terminator kit (Applied Biosystems, Norwalk, CT).

3. Statistical analysis

Statistical analysis of the biochemical data was performed using Student's *t*-test. A value of $P < 0.05$ was accepted as statistically significant.

4. Results

4.1. Activities of PDHC

Two thiamine-responsive patients showed apparently low activity of PDHC in the presence of low (1×10^{-4} mM) TPP, as shown in Table 1, but their PDHC activities significantly increased at a high (0.4 mM) TPP concentration. Most strikingly, the PDHC activity of patient 2 increased to within the normal range. The mother of patient 2 also had a low activity of PDHC under low TPP concentrations, but the PDHC activity was normal at a high TPP concentration. Therefore, the PDHC deficiency in these two patients and the mother of patient 2 was due to a decreased affinity of PDHC for TPP.

Table 1
Activities of PDHC in cultured lymphoblastoid cells

	PDHC (nmol/min/mg protein)[a]	
	With 1×10^{-4} mM TPP	With 0.4 mM TPP
Patient 1	0.05 ± 0.02* (4)	2.65 ± 0.38** (4)0
Patient 2	1.82 ± 0.11* (4)	3.24 ± 0.33 (4)
Mother of Patient 2	2.34 ± 0.21* (3)	4.34
Controls	3.99 ± 0.31 (6)	4.01 ± 0.66 (10)

PDHC, pyruvate dehydrogenase complex, TPP: thiamine pyrophosphate

[a] DCA-activated PDHC values are the means ± S.D. of (*n*) determinations or the result of a single determination

* $P < 0.001$ vs. controls

** $P < 0.01$ vs. controls.

4.2. Affinity of PDHC for TPP

We investigated the affinities of normal and mutant PDHC for TPP. As shown in Fig. 1, normal cells showed approximately 50% of maximal PDHC activity in the absence of TPP, and the addition of 1×10^{-5} mM TPP restored full activity, with no further change in PDHC activity at higher concentrations of TPP. However, cells from the two thiamine-responsive patients showed significantly lower PDHC activity at the 1×10^{-3} mM TPP concentration. The addition of a high concentration (0.4 mM) of TPP restored activity to 66% and 81%, respectively, of the maximal PDHC activity of normal cells.

4.3. Affinity of E1 for TPP

To investigate the affinity of E1 for TPP, we measured the activities of DCA-activated E1 in the presence of 0.4 and 1×10^{-4} mM TPP (Table 2). There was no difference in the E1 activity of normal controls in the presence of 0.4 and 1×10^{-4} mM TPP. In contrast, the activity of DCA-activated E1 of the two patients was significantly lower in the presence of 1×10^{-4} mM TPP, and the addition of a high TPP concentration (0.4 mM) increased the average activity to 36% and 64%, respectively, of the controls. Thus, the E1 of these two patients also showed decreased affinity for TPP.

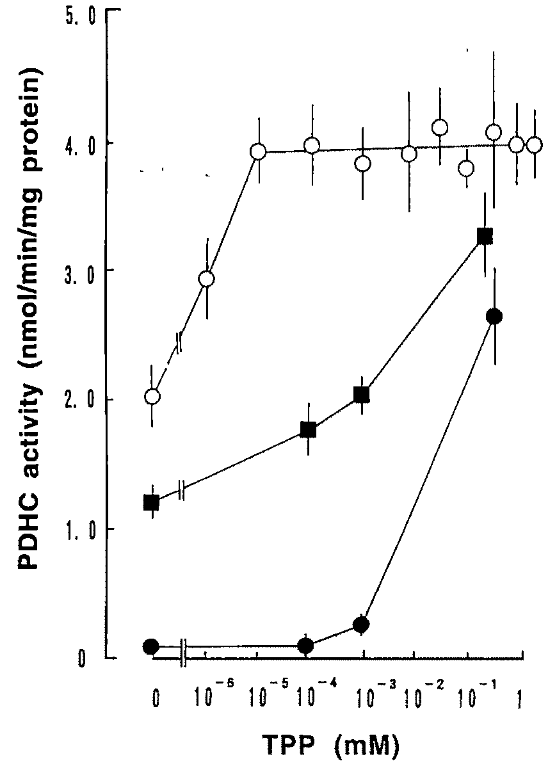

Fig. 1. Effect of TPP on the activity of DCA-activated PDHC in cultured lymphoblastoid cells from normal subjects and two patients with thiamine-responsive lactic acidemia. The activity of PDHC in cultured lymphoblastoid cells is shown at various concentrations of TPP. ○, normal controls, ●, patient 1, ■, patient 2.

Table 2
Activities of E1 in cultured lymphoblastoid cells

	E1 activity (nmol/h per mg protein)[a]	
	With 1×10^{-4} mM TPP	With 0.4 mM TPP
Patient 1	0.23 ± 0.13* (3)	1.41 ± 0.51** (3)
Patient 2	0.61 ± 0.27* (3)	2.54 ± 0.30 (3)
Controls	3.17 ± 0.19 (5)	3.95 ± 1.06 (7)

E1: pyruvate dehydrogenase; TPP: thiamine pyrophosphate.

[a] DCA-activated E1 values are the means ± S.D. of (n) determinations or the result of a single determination.

* $P < 0.001$ vs controls.

** $P < 0.01$ vs controls.

4.4. Rate of [1-^{14}C]pyruvate decarboxylation in intact lymphoblastoid cells

During incubation without thiamine-HCl, intact lymphoblastoid cells from the two patients with thiamine-responsive PDHC deficiency showed decreased decarboxylation rates of 25% and 22%, respectively, of the controls. However, during incubation with 4 mM thiamine-HCl, the decarboxylation rate of these two patients increased markedly to 45% and 49%, respectively, of the controls. In contrast, the decarboxylation rate of the normal controls scarcely increased (Table 3). Thus, pyruvate decarboxylation by intact lymphoblastoid cells from these two patients were also thiamine-responsive.

4.5. Mutation analysis of the E$_1$α subunit

DNA sequence analysis of the two patients' X-linked E$_1$α subunit revealed a substitution within the TPP-binding region in exon 7 of the E$_1$α subunit. The genomic sequence of patient 1 had a C → G point mutation at nucleotide 615, resulting in the substitution of leucine for phenylalanine at position 205 (F205L), and the genomic sequence of patient 2 had an A → C point mutation at nucleotide 648, resulting in the substitution of phenylalanine for leucine at position 216 (L216F) as shown in Fig. 2. The genomic sequence of the mother of patient 2 yielded A and C at nucleotide 648,

Table 3
Rate of [1-^{14}C]pyruvate decarboxylation in intact lymphoblastoid cells

	Pyruvate decarboxylation (nmol/h/mg protein)	
	Without thiamine-HCl	With thiamine-HCl
Patient 1	19.9 ± 6.3* (4)	35.9 ± 5.3* (4)
Patient 2	17.2 ± 4.0* (3)	38.9 ± 5.2* (4)
Controls	78.6 ± 7.2 (4)	80.0 ± 5.8 (3)

HCl: hydrochloride.

Values are the means ± S.D. of (n) determinations or the result of a single determination.

* $P < 0.001$ vs controls.

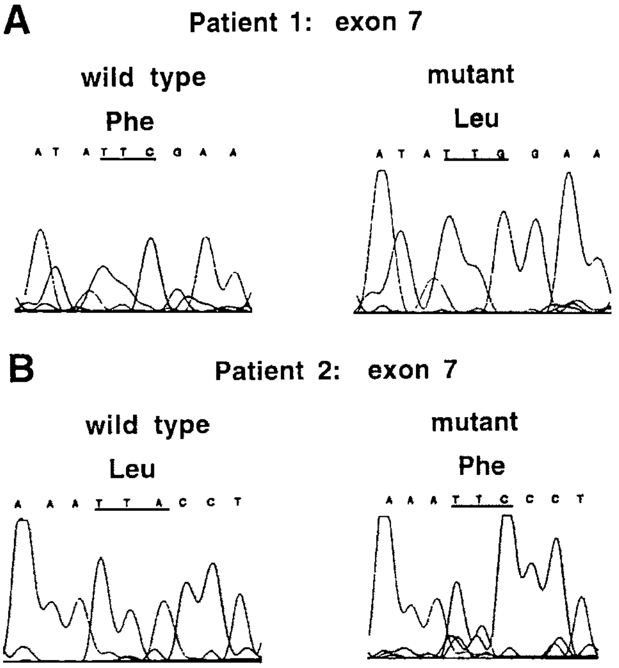

Fig 2 Amplified genomic fragments for the 11 exons of the $E_1\alpha$ subunit gene from two patients were sequenced and analyzed (A) The genomic sequence for exon 7 of patient 1 has a C→G point mutation at nucleotide 615, resulting in a substitution of leucine for phenylalanine at position 205 (F205L) (B) The genomic sequence for exon 7 of patient 2 has an A→C point mutation at nucleotide 648, resulting in a substitution of phenylalanine for leucine at position 216 (L216F)

resulting in a heterozygote for the L216F mutation (data not shown).

5. Discussion

Defects in PDHC are an important cause of congenital lactic acidemia in children. The great majority of PDHC deficiencies result from mutations in the X-linked $E_1\alpha$ subunit gene [2,3]. The E1 subunit also contains a TPP binding site that is shared by the α and β subunits [1,2]. Therefore, the $E_1\alpha$ subunit plays an important role in the thiamine-dependent decarboxylation of pyruvate. It has been pointed out that the $E_1\alpha$ subunit carries the TPP binding motif GDG X26/27 NN common to all TPP-utilizing enzymes [1,9], and it is thought to be the region from amino acid 195 in exon 6 to amino acid 225 in exon 7 [9]. Thiamine treatment is very effective for some patients with PDHC deficiency. Among these patients with PDHC deficiency responding to thiamine therapy, five mutations in the $E_1\alpha$ subunit gene have been reported previously: H44R, R88S, G89S, R263G, and V389fs [4,10–12]. All five mutations are in a region outside the TPP-binding site of the $E_1\alpha$ subunit. Recently, the roles of specific amino acid residues in these two mutations (H44R and R263G) were investigated using site-directed mutagenesis, and two mutations had an increase in their apparent K_m value for TPP [13,14]. Therefore, thiamine responsiveness of these two mutations is supported by a change in the K_m value for TPP observed in the recent study [13,14].

In this study, we described two clinically thiamine-responsive male patients who had a point mutation (F205L and L216F) within the TPP-binding region of the $E_1\alpha$ subunit. Unfortunately, it was not possible to analyze the mother of patient 1 for the F205L mutation. We therefore do not know if this is a new or inherited mutation, although this mutation had been identified previously in two patients [15,16]. One patient was a male who died at age 18 months, with evidence of Leigh disease at autopsy [15]. Another male patient (patient 3929) was a 3-year-old child with Leigh disease and psychomotor retardation [16]. Both male patients showed evidence of Leigh disease and the PDHC activities of these two patients were 25% and 36% of the normal controls. The PDHC activities of our patient 1 were 1% and 66% of the normal controls at two different concentrations of TPP as shown in Table 1. In male patients with the same mutation (F205L), their cultured cells showed quite different PDHC activity. These differences might have been due to differences in the TPP concentration in these assays of PDHC activity, or differences in the thiamine concentration in the culture medium, or differences in the cultured cells (skin fibroblasts and lymphoblastoid cells). The concentration of thiamine-HCl in the culture medium used for our studies was 3×10^{-3} mM, but there are culture media with various concentrations of thiamine-HCl ranging from 3×10^{-5} to 3×10^{-2} mM [11]. We previously reported that the PDHC activities of the patient with thiamine-responsive PDHC deficiency (R263G mutation) in the presence of 1×10^{-4} mM TPP was increased to about two times by culturing cells in high-thiamine (0.4 mM) medium [11]. Thus, it is possible that the PDHC activity in the cultured cells with these thiamine-responsive mutations might depend not only on the concentration of TPP in the reaction mixture, but also on the concentration of thiamine in the culture medium or within the cultured cells.

The L216F mutation of patient 2 is novel [3]. The L216F mutation was inherited from his mother, because it was found in the genomic DNA of his mother, and the PDHC activity of his mother was significantly decreased in the presence of low TPP concentration. We believe that the F205L and L216F mutations were the cause of their disease: aside from the presence of an appropriate defect in thiamine-responsive PDHC and E1 activities, no other mutations were found in the $E_1\alpha$ subunit gene, and these two mutations were not present in the genomic DNA from 50 unrelated controls. A comparison of the PDH $E_1\alpha$ amino acid sequence from a variety of different sources (pig heart, rat liver, mouse liver, and yeast) shows that the amino acid 205 and 216 is phenylalanine and leucine, respectively [17–20].

PDHC deficiency is generally diagnosed by measuring the activity of PDHC in the presence of a high concentration of TPP (0.1–0.7 mM) [11]. Two thiamine-responsive patients showed apparently low activity of PDHC in the presence of low (1×10^{-4} mM) TPP, as shown in Table 1, but their PDHC activities significantly increased at a high (0.4 mM) TPP concentration. Most strikingly, the PDHC activity of patient 2 increased to within the normal range. Therefore, in order to diagnose this type of thiamine-responsive PDHC deficiency and to prevent a diagnostic error, it is important to measure the activity of PDHC in the presence of a low (1×10^{-4} mM) as well as a high TPP concentration.

Among the patients with PDHC deficiency caused by mutations within the TPP-binding region, five mutations have been reported previously: A199T, F205L, M210V, W214R, and P217L [3,15,16,21–23]. Because the PDHC activity in patients with these mutations was not measured in the presence of low TPP concentrations, no one knows whether or not these patients have thiamine-responsive PDHC deficiency. These patients are all male, and all the mutations except for the M210V mutation caused Leigh disease. Therefore, it is possible that the PDHC deficiency caused by mutations within the TPP-binding region might lead to Leigh disease. However, our two patients had not developed Leigh disease by the time of their diagnosis. High-dose thiamine therapy might have been effective in preventing Leigh disease in our patient. Recently, the roles of two mutations (M210V and P217A) within the TPP-binding region were investigated using site-directed mutagenesis [24]. The apparent K_m for M210V mutation increased significantly, but P217A mutation did not affect the apparent K_m value for TPP. Thus, the different substitutions within the TPP-binding region can cause different functional defects in the E1 enzyme.

No effective therapy for congenital lactic acidemia has been established. In this study, the clinical symptoms in our two patients were improved by high-dose thiamine therapy. The clinical thiamine responsiveness in our patients was confirmed by in vitro studies showing a thiamine-responsive functional defect in the activities of PDHC and E1 in the lymphoblastoid cells and the decarboxylation rate in intact cultured lymphoblastoid cells. The DCA-activated PDHC activity in the lymphoblastoid cells was maximal in the presence of a high concentration of TPP. These data suggest that the concomitant administration of a high dose of thiamine and DCA may be required to achieve maximal PDHC activity in patients with thiamine-responsive PDHC deficiency, especially in patients with an acidotic crisis.

References

[1] B.H. Robinson, Lactic acidemia (disorders of pyruvate carboxylase, pyruvate dehydrogenase), in C R Scriver, A.L. Beaudet, W.S Sly, D Valle (Eds), The Metabolic and Molecular Bases of Inherited Disease, 8th edn., McGraw-Hill, New York, 2001, pp. 2275–2295.

[2] B H. Robinson, N MacKay, K. Chun, M Ling, Disorders of pyruvate carboxylase and the pyruvate dehydrogenase complex, J. Inherit Metab. Dis. 19 (1996) 452–462

[3] W Lissens, D L Meirleir, S. Sebeca, I Liebaers, G.K. Brown, R M Brown, M Ito, E Naito, Y Kuroda, D S Kerr, I.D Wexler, M.S Patel, B H Robinson, A Seyda, Mutation in the X-linked pyruvate dehydrogenase(E1) α subunit gene (PDHA1) in patients with a pyruvate dehydrogenase complex deficiency, Human Mutat 15 (2000) 209–219.

[4] E. Naito, M Ito, E. Takeda, I. Yokota, S Yoshijima, Y Kuroda, Molecular analysis of abnormal pyruvate dehydrogenase in a patient with thiamine-responsive congenital lactic acidemia, Pediatr. Res 36 (1994) 340–346.

[5] N Kitamori, Y Itokawa, Pharmacokinetics of thiamin after oral administration of thiamin tetrahydrofurfuryl disulfide to humans, J Nutr Sci Vitaminol 39 (1993) 465–472

[6] O.H. Lowry, N J Rosebrough, A L Farr, R J. Randall, Protein measurement with the Folin phenol reagent, J. Biol Chem 193 (1951) 265–275

[7] E Naito, Y. Kuroda, E Takeda, I. Yokota, H Kobashi, M Miyao, Detection of pyruvate metabolism of skin fibroblasts with dichloroacetate, Pediatr Res 23 (1988) 561–564.

[8] J. Matsuda, M Ito, E Naito, I Yokota, Y Kuroda, DNA diagnosis of pyruvate dehydrogenase deficiency in female patients with congenital lactic acidaemia, J Inherit Metab Dis. 18 (1995) 534–546

[9] B.H. Robinson, K Chun, The relationships between transketolase, yeast pyruvate decarboxylase and pyruvate dehydrogenase of the pyruvate dehydrogenase complex, FEBS Lett 328 (1993) 99–102

[10] E Naito, M Ito, I Yokota, T. Saijo, S Chen, M. Maehara, Y. Kuroda, Concomitant administration of sodium dichloroacetate and thiamine in West syndrome caused by thiamine-responsive pyruvate dehydrogenase complex deficiency, J Neurol. Sci 171 (1999) 56–59

[11] E Naito, M Ito, I Yokota, T Saijo, J Matsuda, H. Osaka, S. Kimura, Y. Kuroda, Biochemical and molecular analysis of an X-linked case of Leigh syndrome associated with thiamin-responsive pyruvate dehydrogenase deficiency, J Inherit Metab. Dis. 20 (1997) 539–548

[12] C Marsac, C Benelli, I Desguerre, M. Diry, F. Fouque, L De Meirleir, G Ponsot, S. Seneca, F Poggi, J M Saudubray, M T Zabot, D Fontan, W. Lissens, Biochemical and genetic studies of four patients with pyruvate dehydrogenase $E_1\alpha$ deficiency, Hum. Genet 99 (1997) 785–792

[13] S.J Jacobia, L.G Korotchkina, M S. Patel, Characterization of a missense mutation at histidine-44 in a pyruvate dehydrogenase-deficient patient, Biochim. Biophys Acta 1586 (2002) 32–42

[14] S J Jacobia, L.G. Korotchkina, M.S. Patel, Differential effects of two mutations at arginine-234 in the α subunit of human pyruvate dehydrogenase, Arch. Biochem Biophys 395 (2001) 121–128.

[15] H -H.M Dahl, G K Brown, Pyruvate dehydrogenase deficiency in a male caused by a point mutation (F205L) in the $E_1\alpha$ subunit, Human Mutat 3 (1994) 152–155.

[16] K Chun, N MacKay, R. Petrova-Benedict, A Federico, A Fois, D E.C. Cole, E Robinson, B.H Robinson, Mutations in the X-linked $E_1\alpha$ subunit of pyruvate dehydrogenase: exon skipping, insertion of duplicate sequence, and missense mutations leading to the deficiency of the pyruvate dehydrogenase complex, Am J. Hum. Genet 56 (1995) 558–569.

[17] Y. Urata, K Koike, S Goto, M. Koike, Novel separation and amino acid sequences of α and β subunits of pig heart pyruvate dehydrogenase, J. Nutr Sci Vitaminol 37 (1991) 257–267

[18] S Matsuda, K Nakano, S Ohta, T Saheki, Y Kawanishi, T Miyata, The α-ketoacid dehydrogenase complexes Sequence similarity of rat pyruvate dehydrogenase with *Escherichia coli* and *Azotobacter vinelandii* α-ketoglutarate dehydrogenase, Biochim Biophys Acta 1089 (1991) 1–7

[19] J Fitzgerald, W.M. Hutchison, H.-H M Dahl, Isolation and characterisation of the mouse pyruvate dehydrogenase $E_1\alpha$ genes, Biochim Biophys. Acta 1131 (1992) 83–90

[20] R H. Behal, K S Browning, L J. Reed, Nucleotide and deduced amino acid sequence of the alpha subunit of yeast pyruvate dehydrogenase, Biochem. Biophys Res Commun 164 (1989) 941–946

[21] K Chun, N. MacKay, R Petrova-Benedict, B H. Robinson, Mutations in the X- linked $E_1\alpha$ subunit of pyruvate dehydrogenase leading to deficiency of the pyruvate dehydrogenase complex, Hum. Mol Genet 2 (1993) 449–454.

[22] A. Tripatara, D.S. Kerr, M.M. Lusk, M. Koli, J Tan, M.S Patel, Three new mutations of the pyruvate dehydrogenase alpha subunit· a point mutation (M181V), 3 bp deletion (-R282), and 16 bp insertion/frameshift (K358SVS > TVDQS), Human Mutat 8 (1996) 180–182

[23] S G Hemalatha, D S Kerr, I.D Wexler, M M Lusk, M Kaung, Y Du, M Koli, M. Schelper, M.S Patel, Pyruvate dehydrogenase deficiency due to a point mutation (P188L) within the thiamine pyrophosphate binding loop of the $E_1\alpha$ subunit, Hum Mol Genet 4 (1995) 315–318

[24] A. Tripatara, L G Korotchkina, M.S Patel, Characterization of point mutations in patients with pyruvate dehydrogenase deficiency role of methionine-181, proline-188, and arginine-349 in the α subunit, Arch Biochem Biophys 367 (1999) 39–50

ELSEVIER

Biochimica et Biophysica Acta 1588 (2002) 85–93

BIOCHIMICA ET BIOPHYSICA ACTA

BBA

www.bba-direct.com

Selenoprotein expression in endothelial cells from different human vasculature and species

S. Miller[a], S.W. Walker[a], J.R. Arthur[b], M.H. Lewin[a], K. Pickard[b], F. Nicol[b], A.F. Howie[a], G.J. Beckett[a,*]

[a]*Clinical Biochemistry, University of Edinburgh, Royal Infirmary, Lauriston Place, Edinburgh EH3 9YW, UK*
[b]*Rowett Research Institute Bucksburn, Aberdeen AB21 9SB, UK*

Received 17 December 2001; received in revised form 11 April 2002, accepted 23 May 2002

Abstract

Selenium (Se) can protect endothelial cells (EC) from oxidative damage by altering the expression of selenoproteins with antioxidant function such as cytoplasmic glutathione peroxidase (cyGPX), phospholipid hydroperoxide glutathione peroxidase (PHGPX) and thioredoxin reductase (TR). If the role of Se on EC function is to be studied, it is essential that a model system be chosen which reflects selenoprotein expression in human EC derived from vessels prone to developing atheroma. We have used [^{75}Se]-selenite labelling and selenoenzyme measurements to compare the selenoproteins expressed by cultures of EC isolated from different human vasculature with EC isolated from bovine and porcine aorta. Only small differences were observed in selenoprotein expression and activity in EC originating from human coronary artery, human umbilical vein (HUVEC), human umbilical artery and the human EC line EAhy926. The selenoprotein profile in HUVEC was consistent over eight passages and HUVEC isolated from four cords also showed little variability. In contrast, EC isolated from pig and bovine aorta showed marked differences in selenoprotein expression when compared to human cells This study firmly establishes the suitability and consistency of using HUVEC (and possibly the human cell line EAhy926) as a model to study the effects of Se on EC function in relation to atheroma development in the coronary artery Bovine or porcine EC appear to be an inappropriate model.

© 2002 Elsevier Science B.V All rights reserved.

Keywords Selenium; Atherosclerosis, Endothelium, Selenoprotein

1. Introduction

The intake of selenium (Se) can to be inversely correlated with the incidence of atherosclerosis and coronary heart disease [1,2]. Oxidative damage to the endothelium is thought to be a primary event in the pathogenesis of atherosclerosis and Se, added as selenite, can protect the EC from such damage by altering the expression of specific selenoproteins [3,4]. The intracellular selenoproteins identified to date as having a potential antioxidant function include cytoplasmic glutathione peroxidase (cyGPX), phospholipid hydroperoxide glutathione peroxidase (PHGPX) and isoenzymes of thioredoxin reductase (TR).

Labelling cells with [^{75}Se]-selenite provides a sensitive method for assessing the expression of selenoproteins. Since equilibration of exogenous [^{75}Se]-selenite with the endogenous pool of Se and selenoproteins can take in excess of 24 h [5,6], such labelling experiments require incubation with [^{75}Se]-selenite for 36–48 h. Using these techniques to detect selenoproteins in human umbilical vein endothelial cells (HUVEC), TR has been identified as the predominant selenoprotein comprising 43% of the total selenoproteins [6]. Both cyGPX and PHGPX are also expressed by cultured EC obtained from a number of species including humans [4,7,8] but the relative activities of TR in EC isolated from different species have not been defined.

The culture of EC derived from the large vasculature is a well-established model for the study of the endothelium. Ideally, EC isolated from human coronary arteries would be preferred for studies relating to cardiovascular disease in man since atheroma is common in these vessels and is a major cause of morbidity and mortality. In practice, the human umbilical vein is often the chosen source of EC for the study of human endothelial function because of its accessibility.

---

[*] Corresponding author Tel +44-131-536-2702; fax: +44-131-536-2758

E-mail address G.J Beckett@ed.ac.uk (G.J Beckett)

0925-4439/02/$ - see front matter © 2002 Elsevier Science B.V All rights reserved
PII S0925-4439(02)00143-6

Moreover, it is a non-branching vessel with a large intimal surface area, making it technically easy to isolate cells. Unfortunately, the viability of isolated EC can be modified by several factors including foetal stress, maternal anaesthesia, smoking and other toxins [9,10]. The use of HUVEC and other primary cultures of EC is also complicated by genetic variability between preparations, limited population doublings and the requirement for specialised growth factors. Arterial and venous EC show differences in the production of angiotensin-converting enzyme [11] and their response to cytokine stimulation [12]. These observations have led to the suggestion that HUVEC, despite being widely used by researchers in the field of vascular disease, may not be the most suitable model for studying human cardiovascular disease [13–15].

Bovine aortic endothelial cells (BAEC) and porcine aortic endothelial cells (PAEC) are also often used as models to study EC function. PAEC may be a suitable alternative to HUVEC since there are similarities between the porcine and human cardiovascular system [16]. In addition, porcine aorta is subject to atheroma formation and has been used as a model for the study of this process [17]. However, variation between EC isolated from different species has been acknowledged to occur; for example, PAEC, unlike HUVEC and BAEC, do not express Factor VIII-related antigen [17].

The EC line EAhy926, established by hybridising primary HUVEC with A549 human lung tumour cells [18], has been used in a number of studies of EC function. EAhy926 retain many of the differentiated functions common to primary EC beyond 100 passages. These functions include: the expression of von Willebrand Factor [18]; prostacyclin formation [19]; expression of endothelin-1 [20]. The selenoprotein profile of EAhy926 cells has not been previously determined, but such work is essential in order to establish whether this convenient cell line would provide a suitable model for future studies of selenoprotein expression in EC.

If the role of Se on EC function is to be studied, it is essential that a model system be chosen which reflects the selenoprotein expression and function of human EC derived from vessels prone to developing atheroma. The experiments reported here use [^{75}Se]-selenite labelling and enzyme measurements to compare the selenoproteins expressed by cultures of EC isolated from different human vasculature with EC isolated form bovine and porcine aorta. The selenoprotein profile of the human EC cell line EAhy926 has also been studied.

2. Methods

2.1. Isolation and culture of EC

2 1.1. HUVEC and human umbilical artery endothelial cells (HUAEC)

Human umbilical cords (> 100 mm in length) were obtained at normal deliveries or Caesarean section from nonsmoking women. Immediately after delivery, the cords were placed into sterile Earle's balanced salt solution (EBSS) containing penicillin (100 units/ml), streptomycin (100 μg/ml) and amphotericin B (2.5 μg/ml) and kept at 4 °C. EC were isolated within 20 h of delivery using a method adapted from that described previously by Anema et al. [6] and Jaffe et al. [21]. Cells were cultured in Endothelial Growth Medium-2 (EGM-2: Biowhittaker, Berkshire, UK) containing penicillin (100 units/ml), streptomycin (100 μg/ml) and amphotericin B (2.5 μg/ml) at 37 °C in an atmosphere of 5% CO_2, 95% air.

The cells showed the morphology characteristic of EC in culture previously described by Jaffe et al. [21]. Cells also synthesised von Willebrand Factor as determined by an indirect immuno-fluorescent detection system.

2 1.2 Human coronary arterial endothelial cells (HCAEC)

These were purchased from Biowhittaker, and tested positive for the presence of von Willebrand Factor and acetylated LDL (an alternative method for the specific characterisation of EC in culture) [22]. The HCAEC also displayed the characteristic morphology of EC. HCAEC were maintained in EGM-2 containing penicillin (100 units/ml), streptomycin (100 μg/ml) and amphotericin B (2.5 μg/ml), and cultured at 37 °C in an atmosphere of 5% CO_2, 95% air.

2.1.3. EAhy926 EC line

EAhy926 cells were kindly donated by Professor Cora-Jean Edgell of the University of North Carolina, North Carolina, USA. The cells were maintained in high glucose (4.5 g/l) Dulbeco's Modified Eagle's medium (DMEM) containing 10% foetal bovine serum (FBS), 5 mM hypoxanthine , 0.02 mM aminopterin, 0.8 mM thymidine, penicillin (100 units/ml), streptomycin (100 μg/ml) and amphotericin B (2.5 μg/ml). The cells were incubated at 37 °C in an atmosphere of 5% CO_2, 95% air and were passaged weekly using 0.25% trypsin–0.02% EDTA solution. EAhy926 cells displayed the characteristic morphology of EC in culture and stained positive for vWF.

2.1.4. BAEC

These were purchased from Biowhittaker. The certificate of analysis supplied with this product stated that the BAEC tested positive for acetylated LDL. The cells were maintained in EGM (Biowhittaker) containing penicillin (100 units/ml), streptomycin (100 μg/ml) and amphotericin B (2.5 μg/ml) and incubated at 37 °C in an atmosphere of 5% CO_2, 95% air.

2.1.5. PAEC

Porcine aorta was obtained within 5–10 min of slaughter from pigs aged under 2 years and was immediately placed into sterile EBSS at 4 °C containing penicillin (100 units/ml), streptomycin (100 μg/ml) and amphotericin B (2.5 μg/ml). EC were isolated within 2–3 h of dissection using a method adapted from that previously described by Slater and Sloan [16]. Briefly, segments of about 5–10 cm were cut and any

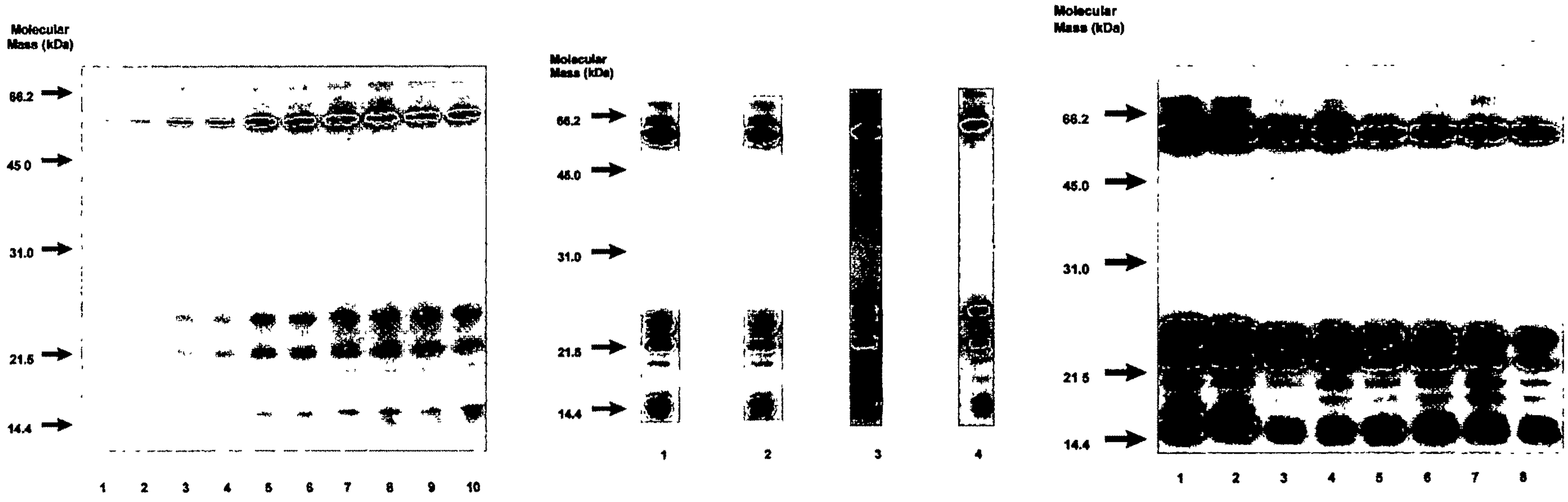

Fig. 1 Left Autoradiograph of an SDS-PAGE gel of the intracellular selenoproteins of HUVEC labelled with [^{75}Se]-selenite (0 02 MBq/ml) for various lengths of time over a 96-h period Duplicate flasks of HUVEC were labelled for each time point Lanes 1, 2. 12 h, lanes 3, 4: 24 h; lanes 5, 6 48 h; lanes 7, 8: 72 h, lanes 9, 10: 96 h Each lane was loaded with 25-μg protein. Middle Autoradiographs of four SDS-PAGE gels showing the intracellular selenoproteins from four different preparations of HUVEC labelled with [^{75}Se]-selenite (0 02 MBq/ml) for 48 h. Each lane was loaded with 25 μg of protein Right Autoradiograph of an SDS-PAGE gel of a single isolation of HUVEC at different passages each labelled with [^{75}Se]-selenite (0 02 MBq/ml) for 48 h Lanes 1 to 8 represent passages 1 to 8, respectively. Each lane was loaded with 25 μg of protein

minor vessels were ligated. The segments were washed with approximately 25 ml of EBSS (prewarmed to 37 °C). One end of the aorta was then clamped shut and the opposite end infused with 0.1% collagenase in EBSS (approximately 10 ml). This end was then closed and the cord incubated at 37 °C in an atmosphere of 5% CO$_2$, 95% air. After 15 min the segment was gently massaged and the contents collected into a sterile universal container. The vessel was then cut along its longitudinal axis and the luminal surface gently scraped gently with a sterile stainless steel scalpel blade angled at approximately 60° to the intimal surface. The blade was washed with EBSS and the washings added to the cell suspension previously collected. The sample was then centrifuged at 450 × *g* for 10 min and the resulting cell pellet was washed with the culture medium [M199 containing 20% FBS, penicillin (100 units/ml), streptomycin (100 μg/ml) and amphotericin B (2.5 μg/ml)]. The cells were resuspended into a 25-cm^2 flask and incubated at 37 °C in an atmosphere of 5% CO$_2$, 95% air. The growth medium was changed and replaced after 24 h and then on alternate days. Cells displayed the characteristic morphology of EC.

2.2. *Time-course of [^{75}Se]-labelling in HUVEC*

HUVEC were isolated and maintained as described previously. For labelling with ^{75}Se-selenite, cells were grown to confluence and the culture medium was changed and replaced with fresh medium containing [^{75}Se]-selenite (0.02 MBq/ml). At time 0, 12, 24, 48, 72 and 96 h, the medium was removed from all the flasks and the cells were washed three times with EBSS (4 °C). The cells were harvested into 20 ml of EBSS by scraping and centrifuged at 2000 × *g* for 10 min at 4 °C. The supernatant was aspirated and the cell pellet resuspended in 200 μl of 60 mM Tris buffer, pH 7.8, containing 1 mM EDTA and 1 mM dithiothreitol (Tris buffer). The cells were then lysed by sonication whilst kept at 4 °C on ice.

Protein concentrations were measured using the Bradford assay [23] and the samples were diluted to a common protein concentration with Tris buffer. The cell lysates were subjected to SDS-polyacrylamide gel electrophoresis to separate the [^{75}Se]-labelled proteins present in 25 μg of protein. The resulting gel was dried and the [^{75}Se]-labelled selenoproteins were visualised by autoradiography using Kodak X-OMAT XAR-5 film.

2.3. *The effect of passage number on [^{75}Se]-labelling in HUVEC*

The intracellular [^{75}Se]-selenoprotein profiles of eight passages of a preparation of HUVEC isolated from a single umbilical vein were compared. HUVEC were isolated and maintained as described above. The HUVEC from the primary isolate (passage zero) were grown to confluence and passaged into at least three T75 flasks (passage one). At confluence, HUVEC in two of the T75 flasks were labelled with [^{75}Se]-selenite (0.02 MBq/ml) for 48 h, whilst the third was subcultured further to provide passage two. This procedure was continued until cells had reached passage eight, at which point distinct morphological changes were observed, such as significant cell enlargement and a partial loss of the characteristic cobblestone appearance.

After a 48-h labelling period, cells from each passage were harvested and stored at − 20 °C. Samples were thawed, lysed and prepared for separation using SDS-PAGE as described above.

2.4. *The [^{75}Se]-labelling of vascular EC isolated from different vasculature*

The intracellular selenoprotein profile of HUVEC, HCAEC, HUAEC, EAhy926, BAEC and PAEC were compared. Each cell type was isolated and maintained as previously described above and labelled for 48 h with [^{75}Se]-selenite (0.02 MBq/ml) prior to SDS-PAGE electrophoresis. For HUVEC, the selenoprotein profiles in

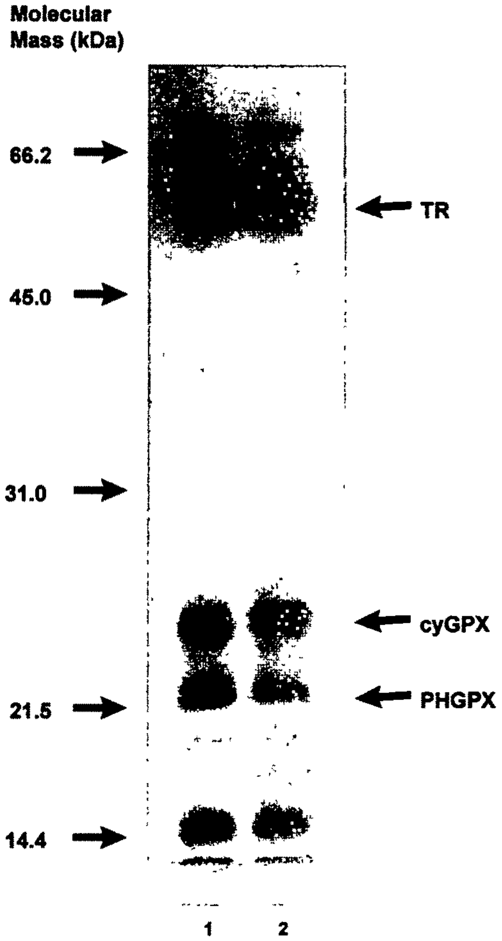

Fig. 2. Autoradiograph of an SDS-PAGE gel of the intracellular selenoproteins of HUVEC and HCAEC labelled with [^{75}Se]-selenite (0.02 MBq/ml) for 48 h. Lane 1, HUVEC, lane 2, HCAEC. Each lane was loaded with 25-μg protein. The selenoprotein bands representing cyGPX, PHGPX and TR are indicated.

four different preparations of cells isolated from four different cords were also compared.

2.5. Glutathione peroxidase and TR in EC

For each cell type the activities of TR, cGPX and PHGPX were measured in parallel subcultures of EC grown in triplicate 75-cm^2 flasks using the same culture medium as was used for the ^{75}Se labelling experiments. The activity of the selenoenzymes in EAhy926 cells was measured in cells grown in the DMEM culture medium specified above in the presence or absence of 40 nM selenite. After culture, cells were harvested by scrapping and lysed in 0.125 M potassium phosphate buffer (pH 7.4) by sonication on ice. TR concentration was measured by an in-house radioimmunoassay using antiserum raised against human placental TR. The activity of TR was determined using 5,5′-dithiobis 2-nitrobenzoic acid (DTNB) as substrate in the presence and absence of 720 nM gold thioglucose [24]. The activities of cyGPX and PHGPX activity were determined as described previously [25].

2.6. Se content of culture medium

The Se content of the culture medium used for each cell type was determined using a fluorometric assay as described by Olsen et al. [26].

2.7. Statistical analysis

An unpaired Student's *t* test (with Welch correction when appropriate) was used to test for significant differences between the levels of TR, cyGPX and PHGPX.

3. Results

3.1. [^{75}Se]-labelling in HUVEC

Fig. 1 (left panel) shows the autoradiograph of a SDS-PAGE gel demonstrating the changes in [^{75}Se]-labelling over time. Selenoproteins were only faintly labelled after a 12-h exposure to [^{75}Se]-selenite. The intensity of labelling of all selenoproteins increased up until 48 h, at which time a steady state of labelling was achieved. Three major [^{75}Se]-labelled selenoproteins were observed with mean molecular masses of 58.1, 21.7 and 24.4 kDa. A selenoprotein of approximately 15 kDa was also moderately expressed. A number of minor labelled selenoproteins were observed.

No distinct variations in the pattern of intracellular [^{75}Se]-labelled selenoproteins between four different preparations of HUVEC were observed (Fig. 1, centre panel) and similarly the selenoprotein profile did not change over eight passages in HUVEC obtained form a single cord (Fig. 1, right panel).

Using antiserum to rat TR and human TR, we have previously identified by Western blotting the 58.1-kDa [^{75}Se]-labelled band in HUVEC as TR. Western blotting with antiserum to rat testis PHGPX demonstrated an immunoreactive band that co-migrated with the 21.7-kDa [^{75}Se]-labelled band. The same approach using antiserum to human cyGPX failed to visualise an immunoreactive band in HUVEC. However, purified human cyGPX (Sigma Chemical Co., Poole, UK) co-migrated with an identical Rf to the 24.4-kDa protein [^{75}Se]-labelled band on the SDS-PAGE gel. The 58-, 21.7- and 24.4-kDa ^{75}Se-selenoproteins observed on the autoradiograph of the SDS-PAGE gels were thus considered to represent TR, PHGPX and cyGPX, respectively.

3.2. Selenoproteins expressed by human EC and the cell line EAhy926

The pattern of [^{75}Se]-labelled selenoproteins found in HCAEC and HUVEC were almost identical (Fig. 2). TR appeared to be expressed to a higher degree in HCAEC than in HUVEC and mass measurements (Table 1) confirmed this. No significant difference was observed in the activities of cyGPX or PHGPX between HCAEC and HUVEC (Table 1).

The [^{75}Se]-selenoprotein expression in venous EC and arterial EC isolated from the same umbilical cord differed only slightly. In HUVEC an additional selenoprotein with a molecular mass of approximately 27 kDa was labelled,

Table 1
Selenoproteins expressed by EC and the EC line EAhy926

	HUVEC	HCAEC	EAhy926	BAEC
CyGPX activity (mU/mg protein)	86 ± 0.7	88 ± 0.03	23 ± 0.5** *158 ± 24.5**	115 ± 7.0
PHGPX activity (mU/mg protein)	7.15 ± 2.09	8.36 ± 0.01	4.41 ± 1.86 *12.5 ± 3.0*	4.54 ± 0.76
TR concentration (ng/mg protein)	721 ± 63	1245 ± 335*	871 ± 149 *1002 ± 267*	ND
TR activity (mU/mg protein)	8.9 ± 0.60	24.4 ± 0.34**	11.7 ± 1.37	1.06 ± 0.16**

Results for EAhy926 are given for cells grown in basal culture medium and results in italics are from cells grown in basal medium supplemented with 40 nM sodium selenite

TR was not detectable (ND) in BAEC because of the lack of cross-reactivity of the antisera with bovine TR.

* Results significantly different from HUVEC, $P < 0.05$

** Results significantly different from HUVEC, $P < 0.001$

which was not observed in HUAEC. TR expression in HUAEC also appeared to be slightly greater than in HUVEC (Fig. 3).

The pattern of selenoprotein expression in EAhy926 cells closely resembled that observed in HUVEC (Fig. 4). The levels of TR and PHGPX in HUVEC were not significantly different to the levels found in EAhy926 cells grown in the basal medium or when supplemented with 40 nM selenite (Table 1). The activity of cyGPX in EAhy926 grown in basal medium was significantly lower than that found in HUVEC, however, EAhy926 cells supplemented with 40 nM selenite had significantly higher activities of cyGPX than HUVEC (Table 1). Supplementation with 40 nM selenite significantly ($P < 0.05$) increased the expression of TR, cyGPX and PHGPX in EAhy926 cells.

3.3. Selenoprotein expression in BAEC and PAEC

Compared to HUVEC, PAEC showed quite distinct differences in the pattern of [^{75}Se]-labelled selenoproteins (Fig. 5, left panel). TR was not the most prominently labelled selenoprotein in PAEC but rather a selenoprotein of 15 kDa.

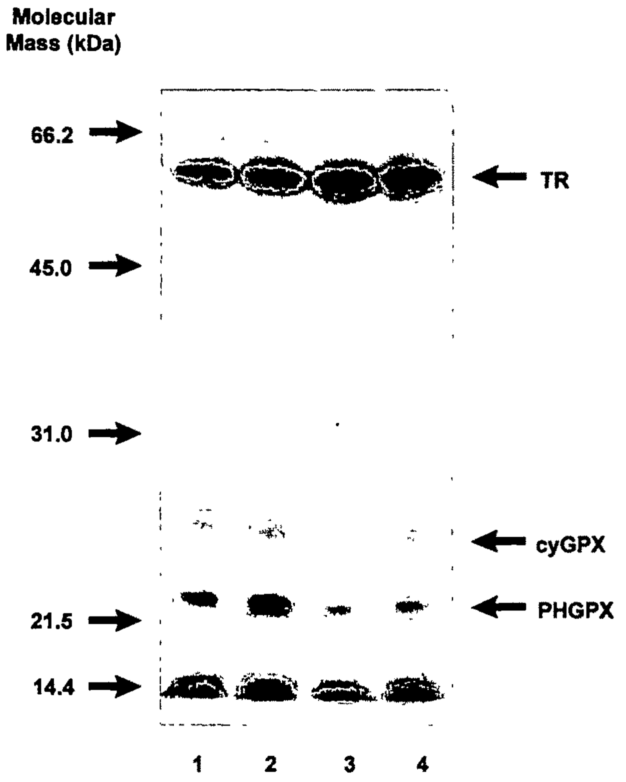

Fig. 3. Autoradiograph of an SDS-PAGE gel of the intracellular selenoproteins of HUVEC and HUAEC labelled with [^{75}Se]-selenite (0.02 MBq/ml) for 48 h. Both HUVEC and HUAEC were isolated from a single umbilical cord and samples were taken from duplicate flasks. Lanes 1 and 2, HUVEC, lanes 3 and 4, HUAEC. Each lane was loaded with 25-µg protein. The selenoprotein bands representing cyGPX, PHGPX and TR are indicated.

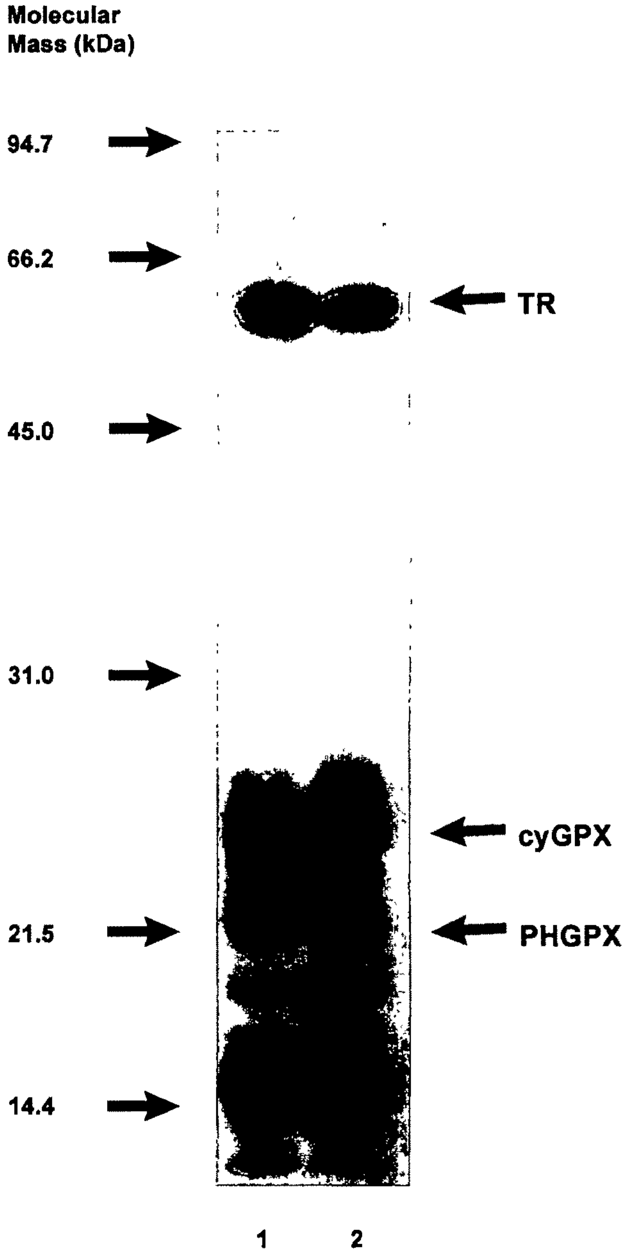

Fig. 4. Autoradiograph of an SDS-PAGE gel of the intracellular selenoproteins of HUVEC and EAhy926 cells labelled with [^{75}Se]-selenite (0.02 MBq/ml) for 48 h. Lane 1, HUVEC, lane 2, EAhy926 cells. Both lanes were loaded with 25-µg protein. The selenoprotein bands representing cyGPX, PHGPX and TR are indicated.

The [^{75}Se]-labelling of many selenoproteins in BAEC was significantly less than in HUVEC (Fig. 5, right panel). In particular, the expression of the TR band was much less in BAEC than HUVEC, an observation that was confirmed by activity measurements of TR (Table 1).

3.4. Se content of culture medium

The EGM2 used for the culture of HUVEC, HCAEC and HUAEC had a Se content of 30 ± 2 nM, which was not significantly different to the Se content of EGM used for the

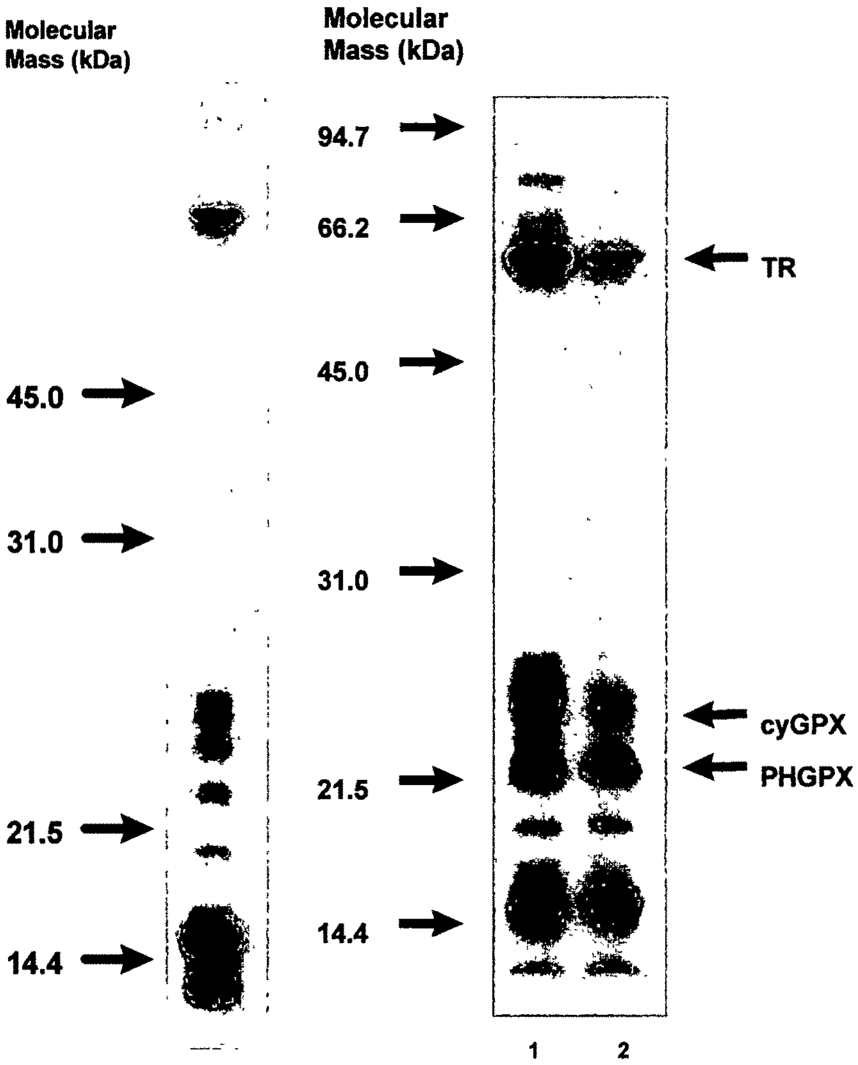

Fig 5 Left. Autoradiograph of an SDS-PAGE gel of PAEC labelled with [^{75}Se]-selenite (0.02 MBq/ml) for 48 h The lane was loaded with 25 µg of protein Right Autoradiograph of an SDS-PAGE gel of the intracellular selenoproteins of HUVEC and BAEC labelled with [^{75}Se]-selenite (0 02 MBq/ml) for 48 h Lane 1, HUVEC; lane 2, BAEC. Both lanes were loaded with 25-µg protein. The selenoprotein bands representing cyGPX, PHGPX and TR are indicated

culture of BAEC (43 ± 10 nM). In both of these culture media, Se is present as selenious acid. The Se content of the DMEM/10% FCS/HAT culture medium used for the culture of EAhy926 cells was 18 ± 2 nM, with the Se provided by the FBS in the form of selenoprotein. The basal M199 medium used to culture PAEC had no detectable Se content, however, since these cells are grown in the presence of 20% FBS, the final concentration of Se in this culture medium was 36 ± 2 nM present as selenoprotein.

4. Discussion

These studies indicate that for HUVEC, an incubation period of at least 48 h must be employed to achieve maximal ^{75}Se labelling of selenoproteins (Fig. 1, left panel). This contrasts with human thyrocytes where [^{75}Se]-labelling reaches a steady state by 27 h [5]. This difference may be due to the variability in selenoprotein turnover between tissues and possibly different rates of [^{75}Se]-selenite uptake between cell types.

In primary culture, HUVEC have a limited replication potential, tending to senesce [27] and, in addition, the activities of some enzymes have been reported to vary with successive passages [28]. We observed no differences in the [^{75}Se]-selenoprotein labelling of HUVEC throughout eight passages of the same preparation under identical growth conditions (Fig. 1, right panel), arguing that the expression of selenoproteins in HUVEC remains constant over at least eight passages. In addition, we found that the selenoprotein profile in four individual preparations of HUVEC showed no marked variability between preparations (Fig. 1, centre). We have also confirmed our previous observation that HUVEC show dominant expression of the 58.1-kDa selenoprotein, TR [6]. Two other major [^{75}Se]-selenoproteins expressed by HUVEC, which were labelled to a much lesser extent than TR, had molecular masses of 21.7 and 24.4 kDa and were provisionally identified as cyGPX and PHGPX, respectively. Since identification was based on co-migration with purified material and by Western blotting, we cannot exclude the possibility that selenoproteins with identical molecular mass co-migrate with these peroxidases on the SDS-PAGE system.

EC show functional differences according to the vascular bed from which they are derived. Arterial EC differ from venous EC in a number of aspects, such as the production of angiotensin-converting enzyme, ability to form prostacyclin [11] and their cell adhesion molecule response to cytokine stimulation [12]. We compared selenoprotein expression in a range of primary human EC cells using similar culture conditions that included keeping the concentration and chemical form of Se in the culture medium constant. The [^{75}Se]-selenoprotein profiles of HUVEC and HCAEC were remarkably similar, with the only observable difference being a slight increased expression of TR in HCAEC that was confirmed by assay of TR concentration. The [^{75}Se]-labelled selenoprotein profiles of EC isolated from the human umbilical vein (which is arterial-like in the umbilical cord) and human umbilical artery of the same umbilical cord were also very similar. The most obvious difference was that HUVEC expressed an additional selenoprotein (27 kDa) when compared to HUAEC (Fig. 2). We did not characterise this selenoprotein but it has a molecular mass similar to type I iodothyronine deiodinase [29].

Distinct differences in the pattern of selenoprotein expression between human EC and EC isolated from bovine and porcine vascular beds were observed. In HUVEC and other human EC studied, TR was the dominantly [^{75}Se]-labelled selenoprotein. In PAEC the expression of TR was relatively weak, the predominant selenoprotein having an approximate molecular mass of 15 kDa (Fig. 5 left panel). This 15-kDa [^{75}Se]-selenoprotein was also found in HUVEC but labelled to a lesser extent. The identity of the 15-kDa selenoprotein was not established, although its electrophoretic mobility is consistent with it being either the uncharacterised 15-kDa selenoprotein described by Gladyshev et al. [30] or the Se-containing protein, epidermal fatty acid-binding protein (E-FABP) [30]. Masouyé et al. [31] have demonstrated the presence of E-FABP in HUVEC but they were unable to detect the protein in the endothelium of the umbilical vein from which the EC were isolated, suggesting that the expression of E-FABP may be induced by cell culture.

The pattern of [^{75}Se]-selenoprotein expression in BAEC also differed considerably from that observed in HUVEC (Fig. 5, right panel). The [^{75}Se]-labelling of the majority of selenoproteins was significantly lower in BAEC compared to HUVEC and TR expression and activity was considerably lower in BAEC than in HUVEC (Table 1). The expression of selenoproteins is modified by the Se status of the cell. However, the Se content and the chemical form of Se (ie selenious acid) present in the culture medium for HUVEC (EGM2) and BAEC (EGM) were identical. This suggests that differing selenoprotein profiles seen in HUVEC and BAEC is not a consequence of altered Se status.

The selenoprotein profile found for EAhy926 cells was very similar to HUVEV and HCAEC, however, the activity of cyGPX in EAhy926 grown in basal medium was significantly lower than in HUVEV or HCAEC (Table 1). Inclusion of 40 nM selenite into the basal culture medium resulted in significant increases in the expression of each of the selenoenzymes, such that cyGPX activity increased to levels that were significantly higher than that found in HUVEC (Table 1). These data suggest that the small differences in selenoenzyme activity observed between HUVEC and EAhy926 grown in basal medium are due to the limiting supply of Se in the basal medium used to culture EAhy926. This basal medium has Se included as selenoprotein incorporated into the FBS. The Se in extracellular selenoproteins is not readily available to the cell whilst selenite is rapidly taken up by the cell and utilised for selenoprotein synthesis.

This study has firmly established the suitability and consistency of using EC from the human umbilical vein as a model to study the effects of Se on EC function in relation to atheroma development in the coronary artery. EC isolated from pig and bovine aorta showed marked differences in selenoprotein profile when compared to human cells, particularly as regards the expression of the antioxidant enzyme TR. Only small differences were observed in selenoprotein expression and activity in EC originating from the coronary artery and other various human vasculature and the human cell line EAhy926.

We conclude that whilst the most appropriate cell culture model for the study of selenoprotein expression in atherosclerotic disease in man might be HCAEC, the supply of such cells is limited and even then the cells are often isolated from diseased vessels. Our studies suggest that HUVEC and possibly EAhy926 cells are suitable alternative model systems to HCAEC in which the role of selenoproteins in protecting against atheroma formation can be studied.

Acknowledgements

This work was supported by grant PG/96017 awarded by the British Heart Foundation. MHL was supported through an MRC Research studentship. JRA, KP and FN are supported by The Scottish Executive Rural Affairs Department (SERAD).

References

[1] F J Kok, G van Poppel, J Melse, E Verheul, E G Schouten, D.H Kruyssen, et al , Atherosclerosis 86 (1991) 85–90

[2] P Suadicani, H O. Hein, F Gyntelberg, Atherosclerosis 96 (1992) 33–42.

[3] H. Ochi, I. Morita, S Murota, Arch Biochem Biophys 294 (1992) 407–411.

[4] J.P. Thomas, P.G. Geiger, A.W. Girotti, J. Lipid Res 34 (1993) 479–489

[5] S. Beech, S W. Walker, J.R. Arthur, F. Nicol, G.J. Beckett, in: M Anke, D. Meissner, C.F Mills (Eds.), Trace Elements in Man and Animal, TEMA 8, Verlag Media Touristik, Gersdorf, 1994, pp 1062–1065.

[6] S.M. Anema, S.W. Walker, A F Howie, J.R. Arthur, F. Nicol, G.J Beckett, Biochem J. 342 (1999) 111–117

[7] L Jornot, A.F. Junod, Biochem J. 306 (1995) 581–587

[8] M.M. Ricetti, G C Guidi, G. Bellisola, R. Marrocchella, A Rigo, G Perona, Biol Trace Elem. Res 46 (1994) 113–123

[9] M A. Gimbrone, R.S Cotran, J Folkman, J Cell Biol 60 (1974) 673–684.

[10] B Tu, A. Wallin, P. Moldeus, I.A. Cotgreave, Pharmacol. Toxicol 75 (1994) 82–90

[11] A.R. Johnson, Human pulmonary endothelial cells in culture, J Clin. Invest. 65 (1980) 841–850.

[12] I.A. Hauser, D R. Johnson, J.A. Madri, J. Immunol. 151 (1993) 5172–5185.

[13] L Jornot, A F Junod, Biochem. J 326 (1997) 117–123

[14] P. Milner, K A Kirkpatrick, V. Ralevic, V. Toothill, J. Pearson, G Burnstock, Proc R Soc. Lond, B Biol. Sci. 241 (1990) 245–248

[15] B Zhao, W.D. Ehringer, R. Dierichs, F.N Miller, Eur J. Clin. Invest 27 (1997) 48–54

[16] D.N. Slater, J.M Sloan, The porcine endothelial cell in tissue culture, Atherosclerosis 21 (1975) 259–272.

[17] A M. Rosenthal, A I. Gotlieb, in: H M Piper (Ed), Cell Culture Techniques in Heart and Vessel Research, Springer-Verlag, Berlin, 1990, pp 117–129.

[18] C.S Edgell, C.C McDonald, J B Graham, Proc Natl Acad Sci. U. S A. 80 (1983) 3734–3737

[19] J.E. Suggs, M.C Madden, M. Friedman, C S Edgell, Blood 68 (1986) 825–829.

[20] O. Saijonmaa, T. Nyman, U Hohenthal, F. Fyhrquist, Biochem. Biophys Res. Commun 181 (1991) 529–536

[21] E.A Jaffe, R.L Nachman, C.G Becker, C R Minick, J. Clin Invest. 52 (1973) 2745–2756

[22] J C. Voyta, D P Via, C.E Butterfield, B.R. Zetter, J. Cell Biol. 99 (1984) 2034–2040

[23] M M Bradford, Anal Biochem. 72 (1976) 248–254.

[24] K E. Hill, G.W McCollum, R.F. Burk, Anal Biochem 253 (1997) 123–125.

[25] G.J. Beckett, F Nicol, D Proudfoot, K Dyson, G. Loucaides, J.R. Arthur, Biochem J 266 (1990) 743–747.

[26] O.E. Olsen, I.S Palmer, H.H Carey, J Assoc Off Anal. Chem 58 (1975) 117–121.

[27] A. Ager, J.L Gordon, S Moncada, J D Pearson, J A Salmon, M.A Trevethick, J. Cell Physiol. 110 (1992) 9–16

[28] T D. Oberley, J.L. Schultz, N Li, L W. Oberley, Free Radic. Biol. Med 19 (1995) 53–65

[29] D.L. St Germain, V A Galton, Thyroid 7 (1997) 655–668

[30] V N. Gladyshev, K Jeang, J.C. Wooton, D L. Hatfield, J. Biol Chem 273 (1998) 8910–8915.

[31] I. Masouyé, G. Hagens, T H. Van Kuppevelt, P. Maden, J. Saurat, J H Veercamp, et al., Circ. Res 81 (1997) 297–303.

ELSEVIER

Biochimica et Biophysica Acta 1588 (2002) 94–101

BIOCHIMICA ET BIOPHYSICA ACTA

BBA

www.bba-direct com

Mitochondrial dysfunction is an early indicator of doxorubicin-induced apoptosis

Pattie S. Green, Christiaan Leeuwenburgh*

University of Florida, Biochemistry of Aging Laboratory, P O Box 118206, Gainesville, FL 32611, USA

Received 31 January 2002; received in revised form 23 April 2002; accepted 24 May 2002

Abstract

Generation of reactive oxygen species and mitochondrial dysfunction has been implicated in doxorubicin-induced cardiotoxicity. This study examined pro-apoptotic mitochondrial cell death signals in an H9C2 myocyte rat cell line and in isolated rat heart mitochondria exposed to doxorubicin. Mitochondrial and cellular viability were assessed using an MTT viability assay (formazan product formed by functional mitochondrial dehydrogenases) and calcein AM dye (fluoresces upon cleavage by cytosolic esterases) Mitochondrial dysfunction followed by cell death was observed using nM concentrations of doxorubicin. Significant doxorubicin-induced cell death was not apparent until after 6 h following doxorubicin exposure using the calcein AM assay. The involvement of apoptosis is evidenced by an increase in TUNEL (terminal (TdT)-mediated dUTP-biotin nick end labeling)-positive nuclei following doxorubicin treatment. Furthermore, doxorubicin administered to isolated mitochondria induced a rapid increase in superoxide production, which persisted for at least 1 h and was followed by increased cytochrome *c* efflux In addition, caspase-3 activity was increased with doxorubicin administration in the H9C2 myocyte cell line. An oxidant-mediated threshold of mitochondrial death may be required for doxorubicin-induced apoptosis.

© 2002 Elsevier Science B.V. All rights reserved.

Keywords Mitochondrion; Hydrogen peroxide; Cytochrome *c*, Caspase, TUNEL

1. Introduction

Doxorubicin is a powerful anthracycline antibiotic used to treat a multitude of human neoplasms; however, cardiac toxicity compromises the clinical usefulness of the drug [1,2]. It is believed that mitochondria play a significant role in this toxicity as isolated heart mitochondria and myocytes have been shown to give rise to increased levels of oxygen radicals after doxorubicin treatment [3–8]. The chronic side effects of doxorubicin are irreversible and devastating for the patient and include the development of cardiomyopathy and ultimately congestive heart failure [1,2]. Although recent evidence shows that less toxic doses of doxorubicin can be used effectively, heart failure in doxorubicin treated patients can go undetected for many years [9]. Therefore, it is essential to identify the mechanisms by which doxorubicin is cardiotoxic so that interventions to prevent the cardiotoxic effects of doxorubicin can be developed.

Doxorubicin-induced cardiomyopathy is partially caused by increased oxidant production in the heart [6,10–14]. The mitochondria are believed to be a primary sink for doxorubicin and specific dehydrogenase systems produce superoxide anions [7]. Single electrons are shuttled to doxorubicin, giving rise to oxygen radicals through the auto-oxidation of doxorubicin and semiquinones [7,15]. Moreover, Kotamraju et al. [6] recently showed that hydrogen peroxide produced from the superoxide anion might be the key oxidant responsible for doxorubicin-induced apoptosis in endothelial cells and cardiomyocytes.

Mitochondria play a pivotal role in regulating apoptosis by mechanisms such as release of cytochrome *c* that results in the activation of caspases and subsequent cell death [16,17]. The mitochondria respond to several signals (i.e. reactive oxygen species, altered redox status, and increases in calcium levels), which trigger the release of caspase-activating proteins, such as cytochrome *c* and apoptosis-inducing factor [18]. The release of cytochrome *c* from the mitochondria into the cytosol can result in the activation of caspase-9, which is responsible for activating effector caspases, such as caspase-3, to induce cell death.

---

* Corresponding author. Tel.: +1-352-392-9575x1356, fax +1-352-392-0316

E-mail address. cleeuwen@ufl edu (C Leeuwenburgh)

0925-4439/02/$ - see front matter © 2002 Elsevier Science B.V. All rights reserved.
PII: S0925-4439(02)00144-8

This study examined doxorubicin-induced mitochondrial dysfunction and pro-apoptotic markers in a rat cardiac myocyte cell line and in isolated mitochondria from rat heart. In this study, we show that mitochondrial dysfunction may be an important early step in the regulation of doxorubicin-induced release of cytochrome *c* from the mitochondria. Our results show that when H9C2 cells are exposed to very low (nM) concentrations of doxorubicin, a rapid decline in mitochondrial reduction potential precedes cell death by approximately 6 h, implicating mitochondrial dysfunction as an early event in doxorubicin-induced cardiotoxicity. In addition, we show that doxorubicin treatment to isolated mitochondria causes a rapid increase in radical production, which can be maintained for over 1 h. Understanding the time-course of doxorubicin toxicity and the underlying causes of doxorubicin-induced cardiomyopathy may lead to specific therapeutic interventions that can attenuate these effects.

2. Methods

2.1. Cell culture

H9C2 cells (ATCC, Rockville, MD) were maintained in DMEM supplemented with 10% FBS in 95% air:5% CO_2 using standard culture methods. Cells were plated 24 h prior to doxorubicin treatment at a density of 150 cells/mm^2.

All studies were conducted in the presence of 10% FBS. Although growth factors and other possible confounding factors are present in the serum, removing the serum from the experiments could also confound interpretation through altering the baseline viability of the cultures and causing apoptotic changes independently of the doxorubicin treatment.

2.2. Viability assay

Cells were rinsed once with PBS followed by incubation at (37 °C) with 25 μM calcein AM and 1 mg/ml propidium iodide for 15 min. Fluorescence was measured at ex 485/em 530 and ex 480/em 620, respectively. 3-(4,5-Dimethylthiazol-2-yl)-2,5-diphenyltetrazolium bromide (MTT) reduction was determined by incubating cells with 0.25 mg/ml MTT in the culture media at 37 °C for 3 h. Formazan crystals were solubilized by overnight incubation in 50% *N,N*-dimethyl formamide, 20% sodium dodecyl sulfate, pH 4.8 and absorbance determined at 575 nm.

2.3. Mitochondrial isolation

Mitochondria were immediately isolated from the ventricles of a rat heart as previously described [19]. Briefly, tissue was weighed and minced in 10 volumes of isolation buffer (0.225 M mannitol, 0.075 M sucrose, 0.2% fatty acid free bovine serum albumin, pH 7.4). The tissue was homogenized in a Potter-Elvehjem glass homogenizer and centrifuged for 7 min at 480×*g*. The resulting supernatant was stored on ice while the pellet was resuspended in 5 ml of isolation buffer and centrifuged for 7 min at 480×*g*. The combined supernatants were centrifuged for 7 min at 7700×*g*. The supernatant was decanted and the mitochondrial pellet was resuspended in 5 ml of wash buffer (0.225 M mannitol, 0.075 M sucrose, 0.001 M EGTA, pH 7.4) using a cotton swab so as not to break the mitochondria and then centrifuged for 7 min at 7700×*g*. The final mitochondrial pellet was resuspended in 1 ml of storage buffer (0.25 M sucrose, 0.002 M EDTA pH 7.4) and immediately used for experiments.

2.4. Superoxide anion measurement

Superoxide anion generation in isolated rat heart mitochondria was determined immediately following the isolation procedure. Briefly, mitochondria (0.5 mg/ml) were incubated with buffer (6 mM succinate, 70 mM sucrose, 220 mM mannitol, 2 mM, Hepes, 25 mM KH_2PO_4, 2.5 mM $MgCl_2$, 0.5 mM EDTA, 5 μg/ml catalase, pH 7.4) and 10 μM doxorubicin at 37 °C. At the indicated time points, 40 μM acetylated cytochrome *c* was added and the change in absorbance at 550 nm was measured for 1 min at 37 °C with a Beckman spectrophotometer. Background absorbance for all groups was determined by the addition of SOD (1000 units/ml).

2.5. Markers for apoptosis

TUNEL (terminal (TdT)-mediated dUTP-biotin nick end labeling) staining was performed using ApoTag Plus kit (Intergen Company, Purchase, NY) according to the manufacturer's instructions. Caspase-3-like activity was measured using the synthetic peptide *N*-acetyl-DEVD-AMC (BD PharMingen, San Diego, CA). This assay detects activated caspase-3 and, to a lesser extent, caspase-6, -7, and -8. Although the caspase-3 assay can detect caspase-8, the difference in sensitivity for the two caspases in the assay (the assay is 20-fold more sensitive for caspase-3) argues that a substantial portion of the signal is caspase-3. Caspase-1 like activity was measured using the synthetic peptide *N*-acetyl-YVAD-AMC (BD PharMingen). Active caspases will cleave the AMC from the peptide and the free AMC will fluoresce. Standards of active caspase-3 and caspase-1 were also prepared. Briefly, 1 ml of assay buffer (20 mM HEPES, 10% glycerol, 2 mM DTT (2 μl of a 1 M solution) and 14 μl of peptide/ml of buffer) and 50 μl of sample were added to a microcentrifuge tube and protected from the light. Samples were incubated at 37 °C for 60 min (caspase-3) or 120 min (caspase-1); after which fluorescence was measured on a spectrofluorometer with an excitation wavelength of 380 nm and an emission wavelength of 440 nm. Cytosolic cytochrome *c* was quantified using an

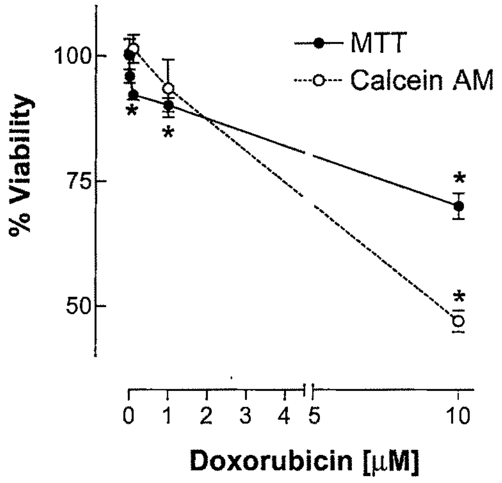

Fig 1 Doxorubicin exposure reduces viability of H9C2 cells. H9C2 cells were exposed to very low (nM) and high concentrations (10 μM) of doxorubicin Mitochondrial viability was determined using the MTT conversion assay and cellular viability was determined by the Calcein AM assay 20 h after addition of doxorubicin (see Methods). There was an immediate reduction (nm concentrations) in mitochondrial function determined by MTT conversion rate. Both the 100 nM, 1 μM, and 10 μM concentrations of doxorubicin are significantly ($P<0.05$) different from control In contrast, the calcein assay (cellular viability) was not significant until 10 μM of doxorubiucin Data were normalized to untreated cells as 100% and shown as mean±S E. for 8 wells per group versus vehicle-treated cells. *$P<0.05$ vs control

ELISA kit from R&D Systems (Minneapolis, MN). The cytochrome *c* assay is calibrated against a highly purified natural rat cytochrome *c* protein isolated from rat heart. Based upon amino acid analysis, the molecular weight of this protein is 12.1 kDa and contains less than 5% of the reduced form of cytochrome *c*. This immunoassay recognizes both the oxidized and reduced forms of cytochrome *c*. Moreover, the cross-reactivity is approximately 7.2% and the limit of detection is 0.5 ng/ml, while the intra-assay and inter-assay precision is between 1% and 4%. Results were reported as arbitrary fluorescence units normalized to milligrams of protein.

2.6. Protein concentration

Cytosolic and mitochondrial protein concentrations were determined using the method developed by Bradford [20].

2.7. Statistical analysis

All experiments were performed successfully at least three times. Unpaired *t* tests were used for comparisons between two groups and analysis of variance with a Tukey post hoc test was used for multiple comparisons. Analysis of variance with repeated measure was performed when multiple time points were recorded from the same sample. All statistics were calculated using a statistical package from Prism (San Diego, CA). A *P* value of <0.05 was considered significant.

3. Results

3.1. Toxic effects of doxorubicin treatment in an H9C2 cultured myocyte cell line

We evaluated the role of oxidant production, mitochondrial dysfunction, and apoptosis in doxorubicin toxicity using a myocyte cell line as well as isolated heart mitochondria. Doxorubicin exposure resulted in dose-dependent toxicity in the H9C2 cardiac myocyte cell line as determined by both the MTT and calcein AM viability assay (Fig. 1). The conversion of MTT to a formazan product by mitochondrial dehydrogenases was used as an index of mitochondrial viability, and the calcein AM assay, which depends upon cleavage by cytosolic esterase activity, was used as an indicator of cellular viability. There was a significant reduction in mitochondrial function using nanomolar concentrations of doxorubicin although loss of viability required micromolar concentrations, indicating that low concentrations of doxorubicin are sufficient to cause significant mitochondrial dysfunction, but not a significant loss in cell number (Fig. 1). Greater reduction in mitochondrial function was seen with a concentration of 10 μM. This dose reduced MTT conversion by about 30%, which corresponded to a significant decline in cell viability, suggesting that this dose caused not only damage to the mitochondrial population but also may have induced an increased rate of apoptosis. We continued to use 10 μM concentration of doxorubicin in our experiments since similar levels are seen transiently in plasma following pharmaceutical use in patients. Time course analysis revealed a reduction in

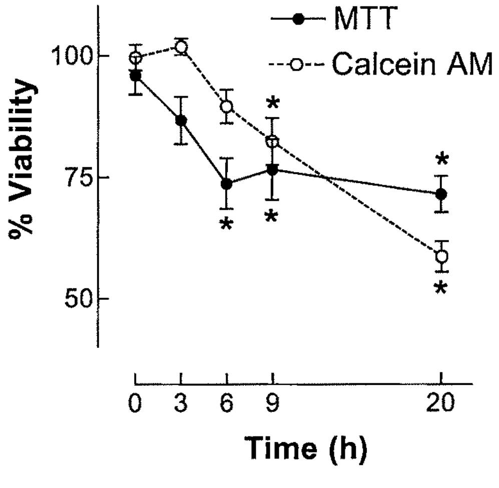

Fig 2. Doxorubicin exposure of H9C2 cells results in inhibition of mitochondrial MTT conversion prior to cell death H9C2 were exposed to 10 μM doxorubicin and viability was determined after 3, 6, 9, and 20 h. Mitochondrial function determined by the MTT viability assay was reduced more rapidly as compared to cellular viability Data were normalized to untreated control cells at each time point and shown as mean±S E for 4–6 wells per group *$P<0.05$ vs. control

MTT conversion as early as 3 h in some experiments but reproducibly was lower 6 h following exposure to 10 μM doxorubicin (Fig. 2). In contrast, using the calcein AM assay, the toxic effects of 10 μM doxorubicin were not seen until 9 h of exposure (Fig. 2). The difference in the time course of these viability markers indicates that mitochondrial dysfunction is an early event in doxorubicin toxicity in these cells.

3.2. Evidence for doxorubicin-induced apoptosis in the H9C2 cell line

H9C2 cells were exposed to low (1 nM) and high concentrations (10 μM) of doxorubicin for 20 h. Exposure of H9C2 cells to 10 μM of doxorubicin for 20 h resulted in a 45% increase in TUNEL-positive cells (Fig. 3). This is notable as there was an overall decrease in total nuclei,

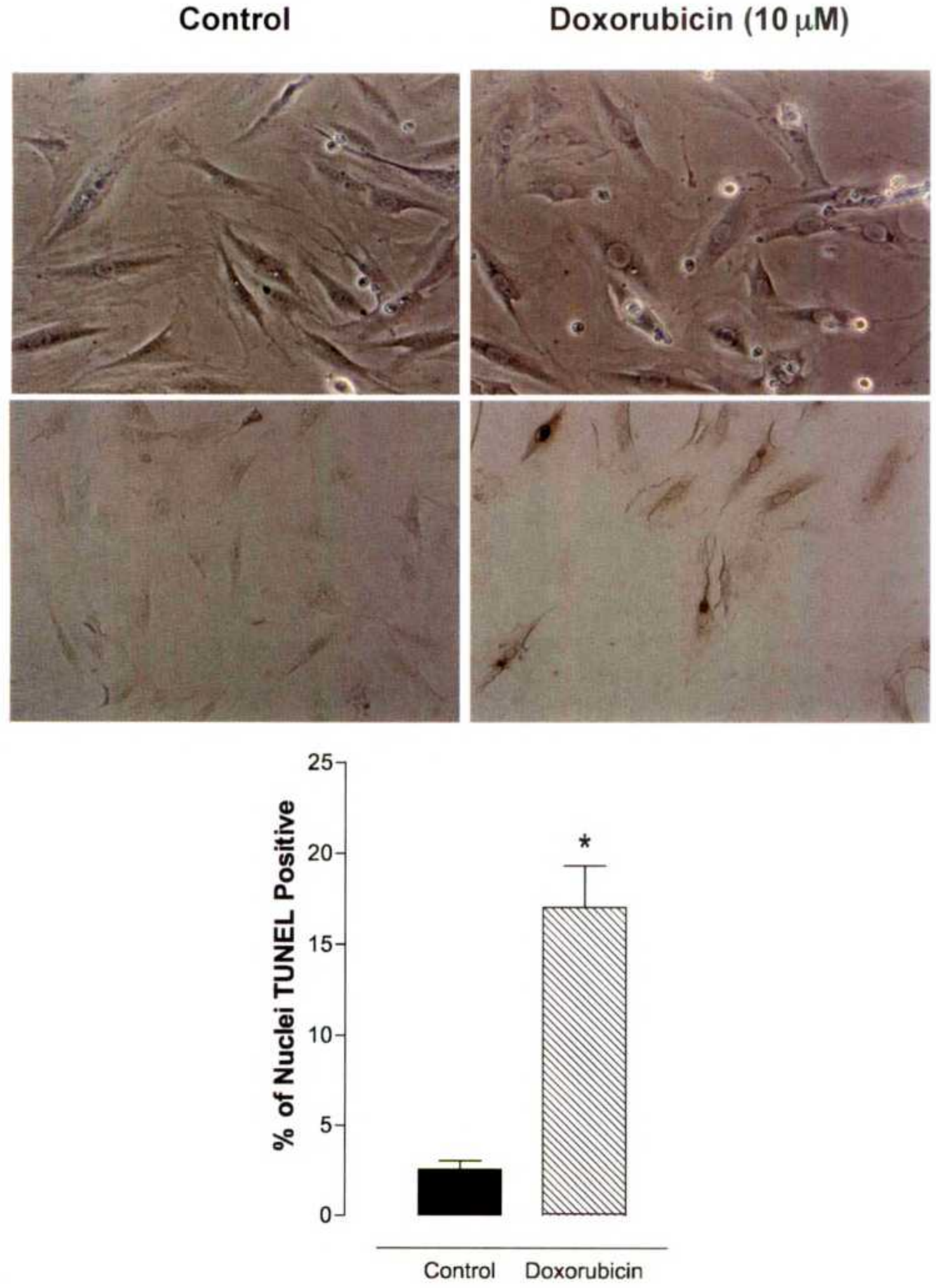

Fig. 3. Doxorubicin exposure increases cell death and TUNEL-positive nuclei in H9C2 cells. Top panels show photomicrographs of doxorubicin-treated H9C2 cells. H9C2 cells were plated at a density of 5000 cells per well in a 16-well slide and were exposed to 10 μM doxorubicin for 20 h. The top two panels are phase-contrast micrographs taken prior to TUNEL staining and the bottom two panels show the results of the TUNEL stain. Noticed marked swelling of H9C2 cells and an increase in the size of the nuclei occurred. The TUNEL analysis was quantified and bottom figure depicts the percent of total nuclei stained positive. Shown are mean ± S.E. for n=8 wells per group. *P<0.001 vs. control.

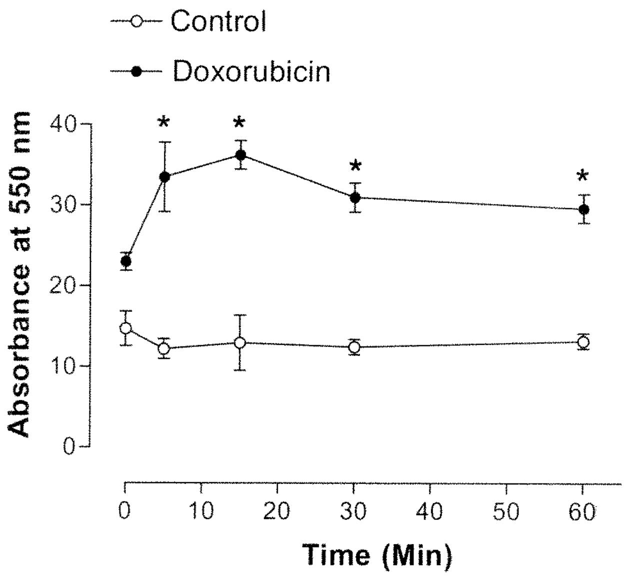

Fig. 4. Doxorubicin rapidly increased superoxide anion production in isolated rat heart mitochondria. Mitochondria were isolated from a Sprague–Dawley rat heart to obtain sufficient amounts of mitochondria to determine superoxide production. Following the isolation, mitochondria (0.5 mg/ml) were treated with 10 μM doxorubicin and cytochrome *c* reduction was monitored at the different time points. Superoxide production increased rapidly and was sustained for at least 1 h. Shown are mean±S.E. for n=4. *P<0.05 vs control.

strongly suggesting the involvement of apoptosis in doxorubicin toxicity in these cells. In addition, profound swelling of myocytes and cell nuclei was observed upon doxorubicin administration. A further indication of apoptosis, 10 μM doxorubicin caused an increase in nuclei with chromatin condensation visualized by propidium iodide staining (data not shown). With 1 μM doxorubicin, only 5.6% of nuclei were TUNEL positive (data not shown). There was no effect of lower concentrations of doxorubicin (1 nM) on TUNEL staining. These results indicate that the increase in apoptotic nuclei occurs in a similar dose range as the loss in cell number, indicating the importance of apoptosis in doxorubicin toxicity in these cells.

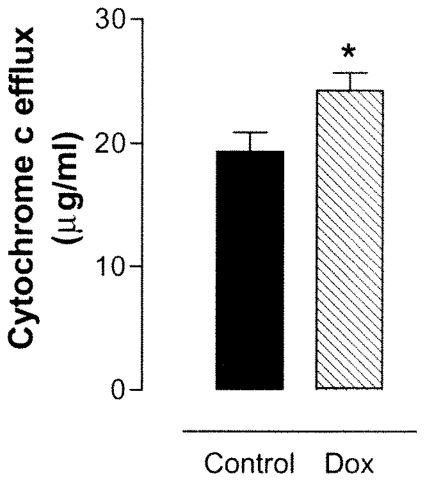

Fig. 5. Doxorubicin treatment increases cytochrome *c* efflux from isolated rat heart mitochondria. Mitochondria were incubated with doxorubicin (10 μM) for 3 h at 37 °C. Mitochondria were pelleted by centrifugation at 7700×g for 7 min and cytochrome *c* concentration in the supernatant was determined using an ELISA. Shown are mean±S.E. for n=4. *P<0.05 vs. control.

3.3. Effects of doxorubicin on isolated rat mitochondria

We used mitochondria isolated from rat hearts, since using our cell line it would have been very difficult to isolate sufficient mitochondrial protein for assay analysis. Further, H9C2 cells are rat heart derived; therefore, the mitochondria are from a similar source. Doxorubicin exposure (10 μM) resulted in a remarkable increase in superoxide anion production by isolated rat heart mitochondia (Fig. 4). The increase in superoxide production was rapid (within 5 min) and peaked at 15 min following treatment. This increase in superoxide production persisted through 1 h of exposure. The very modest decline in superoxide production (15% after 30 min) is not statistically significant (P=0.18)

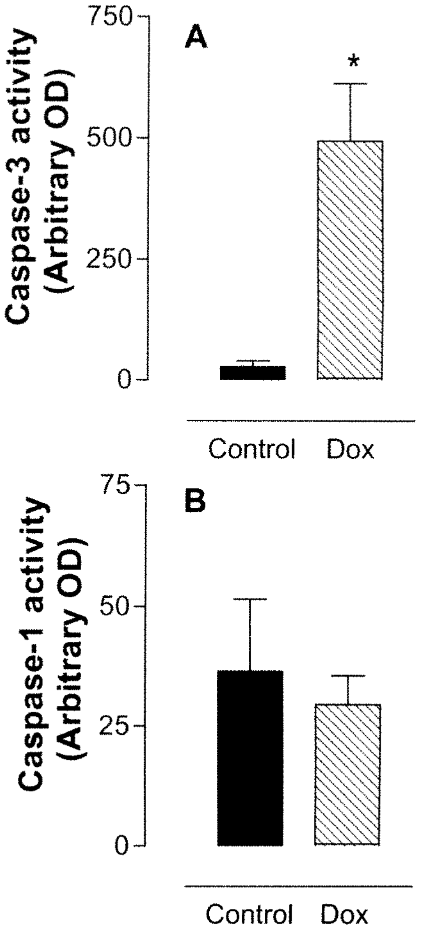

Fig. 6. Doxorubicin treatment increases caspase-3, but not caspase-1, activities in H9C2 cells. Cells were treated with 10 μM doxorubicin for 6 h. Caspase-3 (A) and caspase-1 (B) activities were determined in the cytosolic fraction as described in Methods. Shown are mean±S.E. for n=7. *P<0.01 vs control.

and may represent normal variability in the assay. Alternatively, superoxide production may be decreasing from the peak in the doxorubicin-treated mitochondria and be due to destruction of mitochondria. These data demonstrate the intensity of the oxidative burst to produce superoxide anions due to doxorubicin treatment.

3.4. Markers of apoptosis

Doxorubicin treatment of isolated mitochondria showed a significant increase in cytochrome *c* efflux into the assay supernatant (Fig. 5), implicating mitochondrial dysfunction and activation of permeability transition due to doxorubicin toxicity. The high background levels of cytochrome *c* (Fig. 5) could be attributed to (1) significant levels of cytochrome *c* being present in the cytosol, (2) leakage (structural damage) during the isolation procedures, and (3) activation of permeability transition. However, the differences observed between control and the treatment group indicates a greater release of cytochrome *c* due to doxorubicin. Furthermore, caspase-3, a major "effector caspase", was significantly elevated in the H9C2 cardiac cell line following doxorubicin treatment (Fig. 6A). In contrast, caspase-1 activity (Fig. 6B), a mitochondrial independent pathway, was not affected by doxorubicin treatment. These results suggest that the mitochondrial-mediated pathway is important in inducing apoptosis under these conditions (see Discussion).

4. Discussion

Doxorubicin (adriamycin) is an anthracycline antibiotic that is used as a potent anticancer agent; however, it is exceptionally cytotoxic to the heart. Toxicity is believed to occur by doxorubicin-induced mitochondrial dysfunction and subsequent oxidant production. [21,22]. The heart is especially prone to oxidative damage due to high levels of enzymes with reductase and dehydrogenase properties, such as NADPH dehydrogenase and endothelial nitric oxide synthase (NOS), which play major roles in transferring electrons to generate oxidant species [5,6]. In our study, doxorubicin treatment of cultured myocytes induced apoptosis as determined by TUNEL staining of nuclei and caspase-3 activation. Interestingly, a rapid decline in mitochondrial reduction potential precedes cell death by approximately 6 h, implicating mitochondrial dysfunction as an early event in doxorubicin-induced cardiotoxicity. In support of this hypothesis, we also found that doxorubicin results in a very rapid (within 5 min) increase in superoxide production in isolated rat heart mitochondria and this is followed by release of the pro-apoptotic protein cytochrome *c*. Our experiments differ from the literature in that we examined rapid effects on mitochondrial function that were shown to precede myocyte death/apoptosis. Our results not only indicate that doxorubicin treatment can lead to oxidative stress, mitochondrial dysfunction, and apoptosis, but describe a temporal relationship between these variables. Thus, very low (nM) concentrations of doxorubicin caused a rapid decline in mitochondrial reduction potential, which precedes cell death by approximately 6 h, implicating mitochondrial dysfunction as an early event in doxorubicin-induced myocyte apoptosis.

We showed that mitochondria isolated from rat heart treated with pharmacological levels of doxorubicin produce a ~4-fold greater amount of O_2^- compared to nontreated mitochondria and superoxide production persisted through 1 h of exposure. The rapid and sustained oxidant production could cause oxidative stress. Indeed, Luo et al. [23] showed that reactive aldehydes (malondialdehyde, hexanal and 4-hydroxy-non-2-enal) in rat plasma and heart tissues increased significantly following doxorubicin treatment. Importantly, changes occurred early, peaked around 2 h after doxorubicin administration, and the levels declined or returned to baseline value within 8–24 h [23]. Oxidative stress after doxorubicin treatment could therefore be directly responsible for the development of functional abnormalities also documented by echocardiography abnormalities in this study [23].

Which oxidant is responsible for oxidative stress continues to be a heavily debated topic. NO can rapidly scavenge superoxide produced in the mitochondria, because NO outcompetes the superoxide scavenging enzyme superoxide dismutase (SOD) for O_2^-. Therefore, O_2^- produced during doxorubicin toxicity and scavenged by NO may produce the strong oxidant peroxynitrite ($ONOO^-$). There are studies that support superoxide anion as the major cause for oxidative stress, whereas others suggest that hydrogen peroxides and peroxynitrite are more relevant oxidants inducing oxidative stress. In support of a primary role of superoxide production in doxorubicin toxicity, the overexpression of manganese superoxide dismutase has been shown to be cardioprotective in mice five days after doxorubicin treatment [14]. However, other studies suggest that doxorubicin-induced hydrogen peroxide formation is responsible for the toxicity [13]. Hydrogen peroxide production is also directly related to the production of the superoxide anion. Furthermore, hydrogen peroxide production could function as a gene regulator and increase transcription of eNOS [5,6], thereby increasing NO. Alternatively, studies have shown that doxorubicin interacts with eNOS (reductase enzyme moiety) and produce additional superoxide radicals [4–6,24]. We recently demonstrated that there is an increase in plasma iron levels after doxorubicin treatment, suggesting that hydroxyl radical formation is also a likely candidate for free radical damage [25]. Although there is debate over which specific radical is responsible for oxidative damage, it is likely a combination of all these oxidants and their respective reactions are involved in the pathophysiological events leading to cardiomyopathies.

Since oxidants are a major factor in reducing cellular ATP, glutathione, and other reducing equivalents, such as NADPH, they increase the susceptibility of the mitochondria to undergo permeability transition. We show that mitochondrial dysfunction was prevalent in the early stages of doxorubicin treatment and may have been directly responsible for the apoptotic cell death observed. Moreover, we believe that a threshold of mitochondrial destruction needs to be reached before a cell will die. Very low levels of doxorubicin caused a reduction in mitochondrial function, but not cell death.

Additional in vitro studies will determine if the mechanism of doxorubicin action on apoptosis is the same using various doses for longer time periods in the H9C2 cells. These studies would use lower concentrations (e.g. 0.1–2 μM) to study the effects on cardiomyocyte apoptosis. However, long-term use of doxorubicin in cell culture and specifically mitochondria may be very difficult and different from its use in vivo. Chronic, low concentration studies in isolated mitochondria are not feasible due to difficulties in maintaining mitochondrial viability for longer than 2 h. In addition, in vivo and in vitro studies are needed using a low chronic dosage since other death pathways of apoptosis, such as the receptor-mediated pathway, may also be very relevant. In vivo studies use an acute dose of 20 mg/kg of doxorubicin in animals or lower chronic doses, which are all likely to increase plasma levels greater than 10 μM transiently and may only represent clinical conditions for a short period of time. However, some of the effects described in our study are rapid, and therefore could occur in patients since high concentrations could be reached transiently.

Others have also shown that doxorubicin can cause apoptosis in the rat heart [26]. In addition, apoptosis occurs in cell culture models and isolated myocytes exposed to doxorubicin [6,27,28]. The production of oxidant radicals, specifically hydrogen peroxides [6], is able to increase cytochrome *c* release and induce apoptosis. We found significant release of cytochrome *c* levels in myocytes treated with doxorubicin. Although apoptosis can occur via cytochrome *c*-independent mechanisms, it is well established that in most cell types, once cytochrome *c* is released it interacts with Apaf-1 and procaspase-9, leading to the generation of active caspase-9, which is capable of proteolytically activating caspase-3. Active caspase-3 can then initiate the apoptotic degradation phase [16]. We observed significant increases in caspase-3 activity, but not in caspase-1 activity, which is a well-known cytochrome *c*-independent caspase.

However, there are several other pathways that can activate caspase-3. For example, caspase-8 is able to activate caspase-3, and therefore this receptor-mediated pathway may also be intricately involved in the cell death observed. However, under these in vitro experimental conditions we believe that the activity of caspase-3 is mainly attributed to the mitochondrial pathway. We expect that investigating chronic doxorubicin toxicity in animals may give more insight on activation of receptor mediated pathways, since doxorubicin has also been shown to activate cytokines [29] and could have effected caspase-1 and caspase-8, which are thought to be primarily activated by receptor-mediated pathways. Since systemic alterations could occur after doxorubicin treatment, responses of receptor-mediated pathways need more investigation. Furthermore, caspase-12, an endoplasmic reticulum-mediated pathway, has received attention since it can be activated by endoplasmic reticulum-mediated stress and releases calcium, which activates caspase-12. Once caspase activation occurs, it may be responsible for cytoskeletal alterations that can result in cell shrinkage and negatively affect tension development [30], two events important for the development of chronic cardiomyopathies.

Therefore, other research efforts will further explore the use of specific antioxidants and caspase inhibitors to prevent apoptosis. Ebselen and lipoic acid could provide a sufficient water and lipid soluble antioxidant buffer to reduce oxidative stress and apoptosis. In addition, the prodomain of proximal caspases contains a *ca*spase *r*ecruitment *d*omain (CARD) for the activation or inhibition of caspases. For example, ARC (*a*poptosis *r*epressor with a CARD) interacts with caspase-2 and -8 and functions as an inhibitor [31]. Alternatively, ARC has also been shown to block mitochondrial cytochrome *c* release and prevents caspase-3 activation, possibly by binding to voltage dependent anion channels in the mitochondria [32,33], presenting another avenue to inhibit caspase activation. In addition, we will attempt to use longer periods of doxorubicin treatment using lower concentrations to reflect the chronic use of doxorubicin by patients with lymphomas. These efforts to prevent mitochondrial dysfunction and release of cytochrome *c* from the mitochondria and/or inhibit caspase-3 activation may prove successful in preventing some of the cardiotoxic effects of doxorubicin.

Acknowledgements

We would like to thank Sharon Phaneuf for input and discussion on this manuscript. The American Heart Association, Florida-Puerto Rico Affiliate Grant 30334B supported this research.

References

[1] M.G. Mott, Ann. N. Y. Acad Sci. 824 (1997) 221–228.
[2] K Shan, A.M Lincoff, J B. Young, Ann Intern. Med 125 (1996) 47–58.
[3] S. Barogi, A. Baracca, M. Cavazzoni, G P. Castelli, G Lenaz, Mech. Ageing Dev. 113 (2000) 1–21.
[4] B. Kalyanaraman, K M Morehouse, R.P. Mason, Arch Biochem. Biophys. 286 (1991) 164–170
[5] S.V Kalivendi, S Kotamraju, H. Zhao, J. Joseph, B. Kalyanaraman, J Biol Chem. 28 (2001) 28.
[6] S. Kotamraju, E A Konorev, J. Joseph, B Kalyanaraman, J. Biol. Chem. 275 (2000) 33585–33592.
[7] H. Nohl, L Gille, K. Staniek, Z. Naturforsch., C 53 (1998) 279–285.

[8] H. Nohl, FEBS Lett 214 (1987) 269–273.

[9] P.K. Singal, N. Iliskovic, N Engl. J. Med. 339 (1998) 900–905.

[10] Y.J. Kang, Y. Chen, A. Yu, M. Voss-McCowan, P.N. Epstein, J. Clin Invest. 100 (1997) 1501–1506.

[11] J.H. Doroshow, G.Y Locker, J. Baldinger, C.E. Myers, Res. Commun Chem. Pathol. Pharmacol. 26 (1979) 285–295

[12] J.H. Doroshow, Cancer Res. 43 (1983) 460–472.

[13] Y.J. Kang, Y. Chen, P.N. Epstein, J. Biol. Chem 271 (1996) 12610–12616.

[14] H C. Yen, T.D. Oberley, S. Vichitbandha, Y S. Ho, D.K. St Clair, J Clin. Invest 98 (1996) 1253–1260.

[15] H. Nohl, Eur. J. Biochem 169 (1987) 585–591.

[16] D. Green, G. Kroemer, Trends Cell Biol. 8 (1998) 267–271.

[17] R.C Duke, D.M Ojcius, J.D Young, Sci. Am. 275 (1996) 80–87.

[18] S. Matsuyama, J.C Reed, Cell Death Differ. 7 (2000) 1155–1165.

[19] C. Leeuwenburgh, P.A. Hansen, J.O Holloszy, J.W. Heinecke, Free Radic. Biol. Med 27 (1999) 186–192.

[20] M M. Bradford, Anal. Biochem 72 (1976) 248–254.

[21] E.L. De Beer, A.E. Bottone, E.E. Voest, Eur. J Pharmacol. 415 (2001) 1–11.

[22] P. Perego, E. Corna, M. De Cesare, L. Gatti, D. Polizzi, G. Pratesi, R. Supmo, F Zunmo, Curr. Med Chem. 8 (2001) 31–37.

[23] X. Luo, Y. Evrovsky, D Cole, J. Tnnes, L.N. Benson, D.C. Lehotay, Biochim Biophys Acta 1360 (1997) 45–52

[24] B. Kalyanaraman, R C. Sealy, B.K. Sinha, Biochim. Biophys Acta 799 (1984) 270–275

[25] T. Phillips, A. Childs, J. Goldstein, C. Leeuwenburgh, FASEB 15 (5) (2001) A1133Part 2 (889 7)

[26] O J Arola, A. Saraste, K. Pulkki, M. Kallajoki, M. Parvinen, L M. Voipio-Pulkki, Cancer Res 60 (2000) 1789–1792

[27] D Kumar, L Kirshenbaum, T. Li, I Danelisen, P Singal, Ann N Y. Acad. Sci. 874 (1999) 156–168

[28] M Yamaoka, S. Yamaguchi, T. Suzuki, M. Okuyama, J Nitobe, N Nakamura, Y. Mitsui, H. Tomoike, J. Mol. Cell. Cardiol. 32 (2000) 881–889.

[29] M. Sasaki, D. Kobayashi, N. Watanabe, Jpn. J Cancer Res 92 (2001) 983–988.

[30] J. Chen, K.R. Chien, J Clin. Invest 103 (1999) 1483–1485

[31] T. Koseki, N. Inohara, S. Chen, G. Nunez, Proc Natl Acad Sci. U S. A. 95 (1998) 5156–5160

[32] D. Ekhterae, Z. Lin, M.S. Lundberg, M T. Crow, F.C. Brosius 3rd, G. Nunez, Circ. Res. 85 (1999) e70–e77.

[33] M. Neuss, R. Monticone, M.S. Lundberg, A T. Chesley, E Fleck, M.T. Crow, J Biol. Chem 276 (2001) 33915–33922

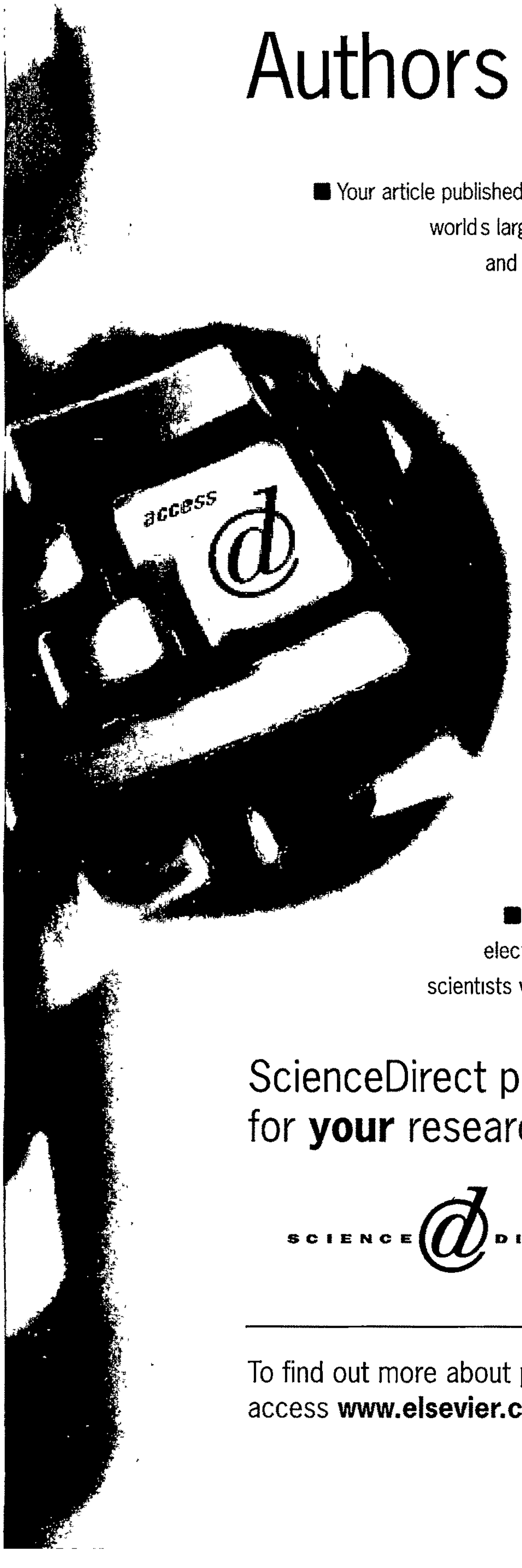

Authors did you know...

- Your article published with Elsevier Science is also included in ScienceDirect, the world's largest scientific network, reaching over 9 million scientists and researchers at **www.sciencedirect.com.**

- If your institute or organisation currently subscribes to ScienceDirect, you now have access to the full text of those journals in your subscription package at your desktop.

- ScienceDirect allows you to keep track of citations to your article via e-mail. You can set up a personal profile to ensure you are kept up-to-date with publications in your specialist areas of research.

- The publication of your article is announced in advance to thousands of registrants to our FREE e-mail alerting service **ContentsDirect.** Find out more by accessing **www.elsevier.com/locate/contentsdirect**

- Your article will be available in the ScienceDirect electronic archive and as such accessible to the millions of scientists visiting our database for an unlimited period of time.

ScienceDirect provides the articles **you** need for **your** research – **www.sciencedirect.com**

SCIENCE DIRECT® SCIENCE DIRECT® WEB editions

To find out more about publishing your article with Elsevier Science, access **www.elsevier.com/homepage/authors** find submit track alerts personalise

authorGATEWAY

from Elsevier Science

The integrated online entry point for all your submission needs

- Find your journal - search by title, keyword or editor; browse by subject area or title.
- Submit your paper - access comprehensive instructions about getting published, including online submission where available.
- Track your paper - track the status of your paper from acceptance to publication (this service was formerly known as OASIS)
- Set up alerts for your favourite journals - receive tables of contents by email from ContentsDirect.
- Personalise your homepage - create your own unique homepage with quick links to your papers, journals and email alerts.

http://authors.elsevier.com

helping you get published

For more information about the Author Gateway contact Author Support at: authorsupport@elsevier.com

CONTENTS

(continued from back cover)

Thiamine-responsive pyruvate dehydrogenase deficiency in two patients caused by a point mutation (F205L and L216F) within the thiamine pyrophosphate binding region
E. Naito, M. Ito, I. Yokota, T. Saijo, J. Matsuda, Y. Ogawa, S. Kitamura, E. Takada, Y. Horii and Y. Kuroda (Japan) 79

Selenoprotein expression in endothelial cells from different human vasculature and species
S. Miller, S.W. Walker, J.R. Arthur, M.H. Lewin, K. Pickard, F. Nicol, A.F. Howie and G.J. Beckett (UK) 85

Mitochondrial dysfunction is an early indicator of doxorubicin-induced apoptosis
P.S. Green and C. Leeuwenburgh (USA) 94

Information for Contributors can be found in http://www.bba-direct com

This journal is in the *ADONIS Service*, whereby copies of individual articles can be printed out from CD-ROM on request. An explanatory leaflet can be obtained by writing to ADONIS B.V , P.O Box 993, 1000 AZ Amsterdam, The Netherlands. Or you can contact ADONIS by e-mail info@adonis.nl or visit the website at www adonis.nl

OASIS: **O**n-line **A**rticle **S**tatus **I**nformation **S**ystem **(http://www.elsevier.com/oasis)**
Authors of articles which are currently in production at Elsevier can obtain the following information on the status of their article:

- general production status (in preparation, in proof, in issue)
- date of publication and offprints dispatch date
- issue, volume and page numbers

This journal is a part of **ContentsDirect**, the ***free*** alerting service which sends tables of contents by e-mail for Elsevier Science books and journals. You can register for **ContentsDirect** online at·
http://contentsdirect.elsevier.com

BIOCHIMICA ET BIOPHYSICA ACTA
MOLECULAR BASIS OF DISEASE

VOL. 1588 NO. 1 9 OCTOBER 2002

(Abstracted/indexed in Biological Abstracts - Chemical Abstract - Current Contents / Life Sciences - EMBASE/Excerpta Medica - Index Chemicus - Index Medicus / MEDLINE - Science Citation Index - Sociedad Iberoamericana de Información Científica (SIIC) Data Bases)

CONTENTS

Regular papers

Induction and expression of *βig-h3* in pancreatic cancer cells
D. Schneider, J. Kleeff, P.O. Berberat, Z. Zhu, M. Korc, H. Friess and M.W. Büchler (Switzerland, Germany, USA) 1

Respiratory function in cybrid cell lines carrying European mtDNA haplogroups: implications for Leber's hereditary optic neuropathy
V. Carelli, L. Vergani, B. Bernazzi, C. Zampieron, L. Bucchi, M.L. Valentino, C. Rengo, A. Torroni and A. Martinuzzi (Italy) 7

Cholesterol crystallite nucleation in supersaturated model biles from a thermodynamic standpoint
C.-L. Liu and W.I. Higuchi (Taiwan, ROC, USA) 15

3,4-Methylenedioxymethamphetamine (''Ecstasy'') induces apoptosis of cultured rat liver cells
C. Montiel-Duarte, M. Varela-Rey, J.A. Osés-Prieto, M.J. López-Zabalza, G. Beitia, E. Cenarruzabeitia and M.J. Iraburu (Spain) 26

Telethonin protein expression in neuromuscular disorders
M. Vainzof, E.S. Moreira, O.T. Suzuki, G. Faulkner, G. Valle, A.H. Beggs, O. Carpen, A.F. Ribeiro, E. Zanoteli, J. Gurgel-Gianneti, A.M. Tsanaclis, H.C.A. Silva, M.R. Passos-Bueno and M. Zatz (Brazil, Italy, USA, Finland) 33

The CD23b promoter is a target for NF-AT transcription factors in B-CLL cells
C. Kneitz, M. Goller, H.-P. Tony, A. Simon, C. Stibbe, T. König, E. Serfling and A. Avots (Germany) 41

Functional interaction of lithocholic acid conjugates with M3 muscarinic receptors on a human colon cancer cell line
K. Cheng, Y. Chen, P. Zimniak, J.-P. Raufman, Y. Xiao and H. Frucht (USA) 48

Molecular understanding of aluminum-induced topological changes in $(CCG)_{12}$ triplet repeats: relevance to neurological disorders
K.S. Latha, S. Anitha, K.S.J. Rao and M.A. Viswamitra (India) 56

Frequency of duplications in the D-loop in patients with mitochondrial DNA deletions
C.H. Tengan, C. Ferreiro-Barros, M. Cardeal, M.A.T. Fireman, A.S.B. Oliveira, B.H. Kiyomoto and A.A. Gabbai (Brazil) 65

In vivo treatment with stobadine prevents lipid peroxidation, protein glycation and calcium overload but does not ameliorate Ca^{2+}-ATPase activity in heart and liver of streptozotocin-diabetic rats: comparison with vitamin E
T.A.D.I.C.A.D.-I.C.S. Group, B. Pekiner, N.N. Ulusu, N. Das-Evcimen, M. Sahilli, F. Aktan, M. Stefek, S. Stolc and Ç. Karasu (Turkey, Slovak Republic) 71

(continued on inside back cover)

Also available on
SCIENCE DIRECT®
www.sciencedirect.com

0925-4439(20021009)1588:1;1-6

ALSO AVAILABLE ONLINE:

http://www.bba-direct.com

BIOCHIMICA ET BIOPHYSICA ACTA

BBA

MOLECULAR BASIS OF DISEASE

ELSEVIER

BIOCHIMICA ET BIOPHYSICA ACTA

BBA

Founded in 1947 by H.G.K. Westenbrink
Managing Editor, 1947-1964

HONORARY EXECUTIVE EDITOR
E.C. Slater (Southampton, UK)

EDITOR-IN-CHIEF: Peter C. van der Vliet (Utrecht, The Netherlands)

EXECUTIVE EDITORS:

Bioenergetics (including *Reviews on Bioenergetics*): **P.R. Rich** (London, UK) and **M. Wikström** (Helsinki, Finland)
Biomembranes (including *Reviews on Biomembranes*): **A.G. Lee** (Southampton, UK) and **P.L. Yeagle** (Storrs, CT, USA)
Molecular and Cell Biology of Lipids: **D.E. Vance** (Edmonton, AB, Canada) and **F. Spener** (Münster, Germany)
Proteins and Proteomics: **A. Fink** (Santa Cruz, CA, USA), **Y. Lindqvist** (Stockholm, Sweden) and
F. Lottspeich (Martinsried bei München, Germany)
Molecular Cell Research: **E.L.F. Holzbaur** (Philadelphia, PA, USA) and **N. Pfanner** (Freiburg, Germany)
Gene Structure and Expression: **C.L. Peterson** (Worcester, MA, USA) and **P.C. van der Vliet** (Utrecht, The Netherlands)
Molecular Basis of Disease: **P.E. Fraser** (Toronto, ON, Canada) and **J.R. Riordan** (Scottsdale, AZ, USA)
General Subjects: **M. Fukuda** (La Jolla, CA, USA), **C.G. Gahmberg** (Helsinki, Finland) and **S.S. Krag** (Baltimore, MD, US
Reviews on Cancer: **N.C. Jones** (Manchester, UK) and **G. Evan** (San Francisco, CA, USA)

Publication information: *Biochimica et Biophysica Acta* full subscription for 2002 consists of Volumes 1553-1603. Subscription prices are available upon requ from the Publisher or from the Regional Sales Office nearest you or from this journal's website (http://www.bba-direct.com) Further information is available this journal and other Elsevier Science products through Elsevier's website (http //www.elsevier com). Subscription are accepted on a prepaid basis only and entered on a calendar year basis. Issues are sent by standard mail (surface within Europe, air delivery outside Europe) Priority rates are available upon reque Claims for missing issues should be made within six months of the date of dispatch

BBA – Publication schedule for 2002
BBA is published according to a volume-numbering scheme that embraces all section of the journal
Full subscription: 51 volumes

BIO-ENERGETICS including Reviews on Bioenergetics 5 volumes:	BIO-MEMBRANES including Reviews on Biomembranes 10 volumes.	GENE STRUCTURE AND EXPRESSION 6 volumes	GENERAL SUBJECTS 6 volumes.	MOLECULAR AND CELL BIOLOGY OF LIPIDS 6 volumes.	MOLECULAR BASIS OF DISEASE 3 volumes:	MOLECULAR CELL RESEARCH 5 volumes.	PROTEINS AND PROTEOMICS 8 volumes.	REVIEWS ON CANCER 2 volumes·
1553–1557 (15 issues)	1558–1567 (20 issues)	1574–1579 (18 issues)	1568–1573 (18 issues)	1580–1585 (18 issues)	1586–1588 (9 issues)	1589–1593 (15 issues)	1594–1601 (16 issues)	1602–160 (4 issues)

Submission
Authors should submit their manuscripts (four copies) to one of the appropriate Executive Editors at either of the following Editorial Offices
BBA Editorial Secretariat, P O. Box 1345, 1000 BH Amsterdam, The Netherlands Tel.. (+31) 20 4853510, Fax: (+31) 20 4853506; E-mail: bba@elsevier
BBA Editorial Secretariat, 275 Washington Street, Newton, MA 02458, USA Tel (+1) (617) 630-2244; Fax: (+1) (617) 630-2245; E-mail: us_bba@elsevier

Although most published *Review* articles are submitted on the invitation of the Executive Editor(s), authors of suitable (mini) reviews may also submit th work unsolicited (four copies) by sending their paper(s) to one of the Executive Editors of the appropriate section.

For detailed instructions on the preparation of electronic artwork, consult the Author Gateway from Elsevier Science at http //authors.elsevier com

Author enquiries
For enquiries relating to the submission of articles (including electronic submission where available) please visit the Author Gateway from Elsevier Science http //www.authors elsevier com The Author Gateway also provides the facility to track accepted articles and set up e-mail alerts to inform you of when article's status has changed, as well as detailed artwork guidelines, copyright information, frequently asked questions and more

Contact details for questions arising after acceptance of an article, especially those relating to proofs, are provided after registration of an article for publicatio

Authors in Japan please note: Upon request, Elsevier Science K K. will provide authors with a list of people who can check and improve the English of th paper (*before submission*). Please contact our Tokyo office: Elsevier Science K K., 9-15 Higashi-Azabu 1-chome, Minato-ku, Tokyo 106-0044; Tel.: (03)-55 5032, Fax (03)- 5561-5045

Colour figures
Colour figures are published at the author's expense: €340 for the first page and € 227 each subsequent page, excluding sales tax

BBA has no page charges and 25 offprints are provided free to the corresponding author of each published paper.

B' 10.03.03'

BIOCHIMICA ET BIOPHYSICA ACTA

BBA

VOL. 1588
(2002)

BIOCHIMICA ET BIOPHYSICA ACTA

Founded in 1947 by H.G.K. Westenbrink, Managing Editor, 1947-1964

HONORARY EXECUTIVE EDITOR: E.C. Slater (Southampton, UK)

EDITOR-IN-CHIEF: Peter C. van der Vliet (Utrecht, The Netherlands)

EXECUTIVE EDITORS:

Bioenergetics (including *Reviews on Bioenergetics*): **P.R. Rich** (London, UK) and **M. Wikström** (Helsinki, Finland)
Biomembranes (including *Reviews on Biomembranes*): **A.G. Lee** (Southampton, UK) and **P.L. Yeagle** (Storrs, CT, USA)
Molecular and Cell Biology of Lipids: **D.E. Vance** (Edmonton, AB, Canada) and **F. Spener** (Münster, Germany)
Proteins and Proteomics: **A. Fink** (Santa Cruz, CA, USA), **Y. Lindqvist** (Stockholm, Sweden) and **F. Lottspeich** (Martinsried bei München, Germany)
Molecular Cell Research: **E.L.F. Holzbaur** (Philadelphia, PA, USA) and **N. Pfanner** (Freiburg, Germany)
Gene Structure and Expression: **C.L. Peterson** (Worcester, MA, USA) and **P.C. van der Vliet** (Utrecht, The Netherlands)
Molecular Basis of Disease: **P.E. Fraser** (Toronto, ON, Canada) and **J.R. Riordan** (Scottsdale, AZ, USA)
General Subjects: **M. Fukuda** (La Jolla, CA, USA), **C.G. Gahmberg** (Helsinki, Finland) and **S.S. Krag** (Baltimore, MD, USA)
Reviews on Cancer: **N.C. Jones** (Manchester, UK) and **G. Evan** (San Francisco, CA, USA)

A.D. Albert (Storrs, CT, USA)
J.M. Allen (London, UK)
T.M. Allen (Edmonton, AB, Canada)
K. Altendorf (Osnabruck, Germany)
T. Arakawa (Thousand Oaks, CA, USA)
P.A. Baeuerle (Martinsried, Germany)
C. Balny (Montpellier, France)
R. Beckmann (Berlin, Germany)
U. Beisiegel (Hamburg, Germany)
D.J. Benos (Birmingham, AL, USA)
P. Bernardi (Padua, Italy)
R. Bernards (Amsterdam, The Netherlands)
A.J.M. Berns (Amsterdam, The Netherlands)
H. Beug (Vienna, Austria)
C.L. Bevins (Cleveland, OH, USA)
C. Birchmeier (Berlin, Germany)
T. Bisseling (Wageningen, The Netherlands)
C. Borner (Freiburg, Germany)
J.L. Bos (Utrecht, The Netherlands)
I. Braakman (Utrecht, The Netherlands)
U. Brandt (Frankfurt am Main, Germany)
R.J. Bridges (Pittsburgh, PA, USA)
C.L. Brooks, III (La Jolla, CA, USA)
D.D. Busath (Provo, UT, USA)
M. Busslinger (Vienna, Austria)
F. Carrière (Marseille, France)
J.E. Celis (Copenhagen, Denmark)
G. Cevc (Munchen, Germany)
H. Chap (Toulouse, France)
A.H. Chishti (Boston, MA, USA)
R. Cogdell (Glasgow, UK)
N.H. Colburn (Frederick, MD, USA)
H.W. Cook (Halifax, NS, Canada)
P.F. Cook (Norman, OK, USA)
C. Cooper (Colchester, UK)
W.A. Cramer (West Lafayette, IN, USA)
B. de Crombrugghe (Houston, TX, USA)
R.D. Cummings (Oklahoma, OK, USA)
D.T. Curiel (Birmingham, AL, USA)
D.A. Day (Canberra, Australia)
J.P. Dekker (Amsterdam, The Netherlands)
B. De Strooper (Leuven, Belgium)
B. Desvergne (Lausanne, Switzerland)
G. Dickson (Egham, UK)
K.T. Douglas (Manchester, UK)
G.F. Draetta (Milan, Italy)
H.B. Dunford (Edmonton, AB, Canada)
D.H. Ellison (Portland, OR, USA)
T. Endo (Tokyo, Japan)
R.M. Epand (Hamilton, ON, Canada)
J. Fidy (Budapest, Hungary).
A. Fontana (Padua, Italy)
M. Fontecave (Grenoble, France)
J.-C. Fruchart (Lille, France)
J.T. Gallagher (Manchester, UK)
G. Geba (New Haven, CT, USA)
R. Geyer (Giessen, Germany)
T.E. Golde (Jacksonville, FL, USA)
F.M. Goñi (Bilbao, Spain)
Y. Goto (Osaka, Japan)
L.I. Grossman (Detroit, MI, USA)
A.P. Halestrap (Bristol, UK)
T.D. Heath (Madison, WI, USA)
J. Heberle (Julich, Germany)
D. Hoekstra (Groningen, The Netherlands)
J. Horwitz (Los Angeles, CA, USA)
R.A. Houghten (San Diego, CA, USA)
G. Hubner (Halle/Saale, Germany)
R.C. Hughes (Mill Hill, UK)
S.W. Hui (Buffalo, NY, USA)
T. Hunter (La Jolla, CA, USA)
M. Ikeda-Saito (Cleveland, OH, USA)
A.N. Imbalzano (Worcester, MA, USA)
T. Iwatsubo (Tokyo, Japan)
H.R. de Jonge (Rotterdam, The Netherlands)
R.L. Juliano (Chapel Hill, NC, USA)
W. Junge (Osnabruck, Germany)
C. Kaltschmidt (Witten, Germany)
S.E. Kearsey (Oxford, UK)
T. Kiefhaber (Basel, Switzerland)
J.A. Killian (Utrecht, The Netherlands)
K. Kimata (Aichi, Japan)
K.H. Kinne (Dortmund, Germany)
M. Kiso (Gifu, Japan)
W.N. Konings (Groningen, The Netherlands)
J.M. Kooter (Amsterdam, The Netherlands)
I. Kudo (Tokyo, Japan)
K. Kuwajima (Tokyo, Japan)
W. Lamers (Amsterdam, The Netherlands)
T. Levade (Toulouse, France)
R. Luhrmann (Gottingen, Germany)
G.I. Makhatadze (Lubbock, TX, USA)
B. Mannervik (Uppsala, Sweden)
W. Mantele (Frankfurt am Main, Germany)
C.J. Marshall (London, UK)
W.F. Marzluff (Chapel Hill, NC, USA)
F. McCormick (San Francisco, CA, USA)
R.N. McElhaney (Edmonton, AB, Canada)
M.G. McNamee (Davis, CA, USA)
R. Mendelsohn (Newark, NJ, USA)
J. Moody (Plymouth, UK)
C.P. Moran Jr. (Atlanta, GA, USA)
O.G. Mouritsen (Odense, Denmark)
S. Nagata (Osaka, Japan)
P.E. Nielsen (Copenhagen, Denmark)
K.H. Nierhaus (Berlin, Germany)
E.A. Nigg (Martinsried bei Munchen, Germany)
B. Nordén (Gothenburg, Sweden)
N. Oppenheimer (San Francisco, CA, USA)
J.F. Oram (Seattle, WA, USA)
N. Osheroff (Nashville, TN, USA)
R.P. Oude Elferink (Amsterdam, The Netherlands)
E. Padan (Jerusalem, Israel)
S. Parthasarathy (Atlanta, GA, USA)
M. Peters-Golden (Ann Arbor, MI, USA)
D.W. Pettigrew (College Station, TX, USA)
J. Philo (Thousand Oaks, CA, USA)
J.J.H.H.M. de Pont (Nijmegen, The Netherlands)
T. Pozzan (Padua, Italy)
N.C. Price (Glasgow, UK)
U.R. Rapp (Wurzburg, Germany)
N. Ridgway (Halifax, NS, Canada)
J.-L. Rigaud (Paris, France)
G.T. Robillard (Groningen, The Netherlands)
S. Rose-John (Kiel, Germany)
E. Rozengurt (Los Angeles, CA, USA)
F. Sachs (Buffalo, NY, USA)
M.S.P. Sansom (Oxford, UK)
S. Schuldiner (Jerusalem, Israel)
H.H. Schulz (New York, NY, USA)
K. Schulze-Osthoff (Munster, Germany)
J.M. Seddon (London, UK)
R. Serrano (Valencia, Spain)
D.L. Severson (Calgary, AB, Canada)
T. Shimizu (Tokyo, Japan)
H. Sjostrom (Copenhagen, Denmark)
S.T. Smale (Los Angeles, CA, USA)
S. Spiegel (Washington, DC, USA)
W.D. Stein (Jerusalem, Israel)
B. Svensson (Copenhagen, Denmark)
G. Tigyi (Memphis, TN, USA)
K.F. Tipton (Dublin, Ireland)
J. Travis (Athens, GA, USA)
L.-C. Tsui (Toronto, ON, Canada)
B. Tümmler (Hannover, Germany)
G. van Meer (Amsterdam, The Netherlands)
M.H. Vos (Palaiseau, France)
K.H. Vousden (Frederick, MD, USA)
E. Wahle (Halle/Saale, Germany)
M.J. Waring (Cambridge, UK)
D. Wemmer (Berkeley, CA, USA)
R. Wetzel (Knoxville, TN, USA)
G.R. Willsky (Buffalo, NY, USA)
D.C. Wilton (Southampton, UK)
P. Workman (Sutton, UK)
R.F.A. Zwaal (Maastricht, The Netherlands)

BIOCHIMICA ET BIOPHYSICA ACTA

BBA

INTERNATIONAL JOURNAL OF BIOCHEMISTRY, BIOPHYSICS
AND MOLECULAR BIOLOGY

VOL. 1588 (2) (2002)

MOLECULAR BASIS OF DISEASE

Executive Editors: P.E. Fraser (Toronto, Canada) and
J.R. Riordan (Scottsdale, AZ, USA)

Section Editors:
C.L. Bevins
R.J. Bridges
B. De Strooper
G. Dickson
D.H. Ellison
G. Geba
T.E. Golde
R.A. Houghten
T. Iwatsubo
H.R. de Jonge
R.P. Oude Elferink
B. Tümmler

ELSEVIER
Amsterdam – London – New York – Oxford – Paris – Shannon – Tokyo

© 2002 Elsevier Science B V All rights reserved

This journal and the individual contributions contained in it are protected under copyright laws by Elsevier Science B V., and the following terms and conditions apply to their use:

Photocopying
Single photocopies of single articles may be made for personal use as allowed by national copyright laws. Permission of the Publisher and the payment of a fee is required for all other photocopying, including multiple or systematic copying, copying for advertising or promotional purposes, resale, and all forms of document delivery. Special rates are available for educational institutions that wish to make photocopies for non-profit educational classroom use

Permissions may be sought directly from Elsevier Science via their homepage (http://www.elsevier.com) by selecting "Customer support" and then "Permissions" Alternatively you can send an e-mail to permissions@elsevier.co uk, or fax to (+44) 1865 853333

In the USA, users may clear permissions and make payments through the Copyright Clearance Center, Inc , 222 Rosewood Drive, Danvers, MA 01923, USA; phone· (+1) (978) 7508400, fax· (+1) (978) 7504744, and in the UK through the Copyright Licensing Agency Rapid Clearance Service (CLARCS), 90 Tottenham Court Road, London W1P 0LP, UK, phone· (+44) 20 7631 5555, fax· (+44) 20 7631 5500 Other countries may have a local reprographic rights agency for payments

Derivative Works
Subscribers may reproduce tables of contents of prepare lists of articles including abstracts for internal circulation within their institutions. Permission of the Publisher is required for resale or distribution outside the institution
Permission of the Publisher is required for all other derivative works, including compilation and translations.

Electronic Storage or Usage
Permission of the Publisher is required to store or use electronically any material contained in this journal, including any article or part of an article.

Except as outlined above, no part of this publication may be reproduced, stored in a retrieval system of transmitted in any form of by any means, electronic, mechanical, photocopying, recording or otherwise, without prior written permission of the Publisher

Address permission requests to Elsevier Science Global Rights Department, at the mail, fax and e-mail addresses noted above.

Notice
No responsibility is assumed by the Publisher for any injury and/or damage to persons or property as a matter of products liability, negligence or otherwise, or from any use or operation of any methods, products, instructions or ideas contained in the material herein. Because of the rapid advances in the medical sciences, in particular, independent verification of diagnoses and drug dosages should be made.

Although all advertising material is expected to conform to ethical (medical) standards, inclusion in this publication does not constitute a guarantee or endorsement of the quality or value of such product or of the claims made of it by its manufacturer.

Advertising Information
Advertising orders and enquiries can be sent to **USA, Canada and South America** Mr Tino DeCarlo, The Advertising Department, Elsevier Science Inc , 360 Park Avenue South, New York, NY 10010-1710, USA, phone (+1) (212) 633 3815, fax· (+1) (212) 633 3820, e-mail: t decarlo@elsevier com. **Japan·** The Advertising Department, Elsevier Science K.K , 9-15 Higashi-Azabu 1-chome, Minato-ku, Tokyo 106-0044, Japan, phone (+81) (3) 5561 5033; fax (+81) (3) 5561 5047 **Europe and ROW** Commercial Sales Department, Elsevier Science Ltd , The Boulevard, Langford Lane, Kidlington, Oxford, OX5 1GB, UK, phone. (+44) 1865 843016, fax (+44) 1865 843976; e-mail. media@elsevier com

Orders, claims, and product enquiries: please contact the Customer Support Department at the Regional Sales Office nearest you
New York: Elsevier Science, PO Box 945, New York, NY 10159-0945, USA, phone· (+1) (212) 633 3730 [toll free number for North American customers 1-888-4ES-INFO (437-4636)], fax· (+1) (212) 633 3680, e-mail· usinfo-f@elsevier.com
Amsterdam: Elsevier Science, PO Box 211, 1000 AE Amsterdam, The Netherlands; phone: (+31) 20 4853757; fax. (+31) 20 4853432; e-mail nlinfo-f@elsevier.com
Tokyo: Elsevier Science, 9-15 Higashi-Azabu 1-chome, Minato-ku, Tokyo 106-0044, Japan; phone: (+81) (3) 5561 5033; fax: (+81) (3) 5561 5047, e-mail· info@elsevier co jp
Singapore Elsevier Science, 3 Killiney Road, #08-01 Winsland House I, Singapore 239519; phone: (+65) 6349 0200; fax: (+65) 6733 1510, e-mail· asiainfo@elsevier.com.sg
Rio de Janeiro: Elsevier Science, Rua Sete de Setembro 111/16 Andar, 20050-002 Centro, Rio de Janeiro-RJ, Brazil, phone (+55) (21) 509 5340; fax (+55) (21) 507 1991, e-mail. elsevier@campus.com br [Note (Latin America). for orders, claims and help desk information, please contact the Regional Sales Office in New York as listed above]

USA mailing notice: *Biochimica et Biophysica Acta (Molecular Basis of Disease)* (ISSN 0925–4439) is published monthly except in February, May and September by Elsevier Science B V (PO Box 211, 1000 AE Amsterdam, The Netherlands)
Annual subscription price in the USA US$ 1165 00 (valid in North, Central and South America), including air speed delivery Second class Periodicals postage paid at Jamaica, NY 11431
USA POSTMASTER: Send address changes to *Biochimica et Biophysica Acta (Molecular Basis of Disease)*, Publications Expediting, Inc ,200 Meacham Avenue, Elmont, NY 11003.
AIRFREIGHT AND MAILING in the USA by Publications Expediting, Inc , 200 Meacham Avenue, Elmont, NY 11003.

Printed in The Netherlands
∞ The paper used in this publication meets the requirements of ANSI/NISO Z39 48-1992 (Permanence of Paper).

ELSEVIER

Biochimica et Biophysica Acta 1588 (2002) 103–105

BIOCHIMICA ET BIOPHYSICA ACTA
BBA
www.bba-direct.com

Lack of association between the uncoupling protein-2 Ala55Val gene polymorphism and phenotypic features of the Metabolic Syndrome

Roland Rosmond[a,b,*], Claude Bouchard[b], Per Björntorp[c]

[a]Department of Clinical Chemistry, Sahlgrenska University Hospital, S-413 45 Goteborg, Sweden
[b]Pennington Biomedical Research Center, Baton Rouge, LA, USA
[c]Department of Cardiovascular Diseases, Sahlgrenska University Hospital, Goteborg, Sweden

Received 13 February 2002; received in revised form 29 May 2002, accepted 3 June 2002

Abstract

The uncoupling protein (UCP) 2 gene is expressed in adipose tissues and skeletal muscles, which are important sites for variations in energy expenditure. The objective of the current study was to examine the potential impact of a C→T substitution in exon 4, resulting in an alanine to valine substitution at codon 55, on the Metabolic Syndrome in 284 unrelated Swedish men born in 1944. The subjects were genotyped using PCR amplification of the exon 4 region of the UCP2 gene followed by digestion with the restriction enzyme *Ecl*HK1 The allelic frequencies were 0.56 for allele Ala and 0.44 for allele Val. No association was found between the Ala55Val SNP and obesity and blood levels of insulin, glucose, and lipids as well as blood pressure and circulating hormones. From these data, we conclude that the C→T substitution in exon 4 of the UCP2 gene does not contribute to the predisposition to be affected by the Metabolic Syndrome

© 2002 Elsevier Science B V All rights reserved.

Keywords. Ala55Val, Obesity, UCP2, SNP; Hormone, Lipid; Blood pressure

1. Introduction

The mitochondrial uncoupling proteins (UCP) are thought to play an important role in the molecular basis for energy expenditure. However, the precise function of these proteins in human metabolism is still unclear [1]. In newborn infants, UCP1 is potentially a major contributor to the energy expenditure [1], but is unlikely to be involved in weight regulation in adult humans. In 1997, two new mitochondrial UCPs, UCP2 and UCP3, were discovered. It has been proposed that UCP2 and UCP3 have thermogenic properties and that they may thus be involved in energy metabolism [2,3]. The UCP2–UCP3 gene cluster maps to 11q13 in humans [4]. A number of single nucleotide polymorphisms (SNPs) in the UCP1, UCP2 and UCP3 genes have been identified, and they have been studied for linkages and associations with obesity traits [1]. In Pima Indians, a C→T substitution in exon 4 of the UCP2 gene, resulting in an alanine to valine substitution at codon 55, has been found to be associated with metabolic rate during sleep and over 24 h [4]. In addition, the valine substitution in the homozygous state exhibits an enhanced metabolic efficiency and a lower fat oxidation rate [5]. However, several studies do not support an impact of the UCP2 Ala55Val SNP on either obesity or Type 2 diabetes [1].

There is a clustering of risk factors, including obesity, hypertension, glucose intolerance, diabetes mellitus, and hyperlipidemia, which is observed more frequently in some individuals than by chance alone. This has led to the suggestion that this cluster represents a single syndrome, which has been referred to as the Metabolic Syndrome [6]. Hence, the objective of the present study was to evaluate the potential impact of the Ala55Val variant of the UCP2 gene on obesity and blood levels of insulin, glucose, and lipids as well as blood pressure and circulating hormones, including salivary cortisol.

2. Subjects and methods

The subjects (n=284) were randomly selected from a larger geographically defined total population cohort of men

---

[*] Corresponding author. Department of Clinical Chemistry, Sahlgrenska University Hospital, S-413 45 Göteborg, Sweden Tel: +46-31-342-6272, fax. +46-31-82-8458

E-mail address rolandrosmond@hotmail.com (R Rosmond)

0925-4439/02/$ - see front matter © 2002 Elsevier Science B V All rights reserved
PII S0925-4439(02)00152-7

born in Gothenburg, Sweden in 1944. The design has been described elsewhere [7]. All subjects gave written informed consent before participating in the study, which was approved by the Ethics Committee of Göteborg University.

Body mass index (BMI, kg/m^2), waist-to-hip ratio (WHR), and abdominal sagittal diameter were measured as described previously [7]. Salivary cortisol was measured repeatedly over a random working day. Endocrine measurements, beside cortisol, included testosterone, insulin-like growth factor I, and leptin as described previously [7]. Blood levels of insulin, glucose, triglycerides, total, high (HDL) and low (LDL) density lipoprotein cholesterol were measured in the overnight fasting state as described previously [7]. The serum lipids were determined by an enzymatic procedure in a Cobas Fara II (Roche Molecular Biochemicals, Mannheim, Germany). Two blood pressure readings were recorded on the right arm with the participants sitting, using a random-zero mercury sphygmomanometer, after 5 min resting, with the auscultation site at heart level, a peak inflation level of 30 mm Hg above radial pulse disappearance, and a cuff-deflation rate of 2–3 mm Hg/s. Values were recorded to the nearest even digit. Heart rate was recorded simultaneously, and systolic and diastolic blood pressure was calculated as the mean of the two measurements.

Genotyping of the DNA sequence variant in exon 4 was carried out by PCR and restriction enzyme digestion. Genomic leukocyte DNA (150 ng in a final volume of 10 µl) was amplified by PCR (annealing temperature: 56 °C) using primers described previously [4]. The PCR reaction product was digested at 37 °C for 3–4 h with 2 U of the restriction enzyme *Ecl*HK1, and the fragments were separated on a 3% agarose gel.

All statistical analyses were performed using SPSS for Windows, release 10.0 (SPSS Inc., Chicago, IL). *P* values are two-sided throughout, and a $P<0.05$ was considered significant. Analyses were carried out with the General Linear Model, with genotype as independent factor and BMI and WHR as covariates whenever appropriate. All *P* values were adjusted for multiple tests by using the Spjotvoll–Stoline post hoc correction [8].

3. Results and discussion

The frequency of the Ala allele was 0.56 and that of the Val allele 0.44. The observed genotype frequencies were 29.3%, 54.2% and 16.5% for Ala/Ala, Ala/Val and Val/Val, respectively. Genotype frequencies were in a Hardy–Weinberg equilibrium (χ^2=1.6, *df*=2). The allelic frequencies are in accordance with those observed in other studies on Caucasian populations [9,10].

In the present study, there were no significant differences between the genotype groups with respect to phenotypes of obesity (BMI) and body fat distribution (WHR and abdominal sagittal diameter). Interestingly, the UCP2 knock-out mice is neither obese nor resistant to diet-induced obesity [11]. In fact, these mice have a normal body temperature regulation, suggesting that UCP2 is not vital in the maintenance of normal body weight [11].

However, it has been recently shown that UCP2-deficient *ob*/*ob* mice have increased serum insulin levels, and greatly decreased levels of glycemia [12]. In contrast, the results of our study indicate no significant difference in serum insulin levels and fasting glucose, either before or after adjusting for BMI and WHR, among the genotypes of UCP2 Ala55Val. Moreover, our data indicate no significant differences between the genotype groups regarding salivary cortisol, testosterone, insulin-like growth factor I, leptin, serum lipids and blood pressure (Table 1). Similar findings have previously been reported in another Swedish sample [10].

Although one study related the Ala55Val polymorphism to measures of energy expenditure [5], the majority of studies do not support a functional impact of the Ala55Val polymorphism on polygenic obesity or Type 2 diabetes [1].

In conclusion, the Ala55Val UCP2 SNP is not associated with any of the phenotypic features of the Metabolic Syndrome in a general Swedish population of middle-aged men. The Ala55Val variant might, however, influence different components of the Metabolic Syndrome in other ethnic groups.

Table 1

Differences in anthropometric, endocrine, metabolic and circulatory measurements between genotypes of the Ala55Val SNP in exon 4 of the UCP2 gene

	Genotypes		
	Ala55Ala (*n*=78)	Ala55Val (*n*=144)	Val55Val (*n*=44)
BMI (kg/m^2)	26.5±4.2	26.1±3.8	25.7±3.8
WHR	0.94±0.09	0.94±0.06	0.93±0.06
Abdominal sagittal diameter (cm)	22.8±4.0	22.7±3.5	22.3±3.5
Dexamethasone suppression test (nmol/l)	11.3±4.4	12.1±5.7	13.2±5.5
Testosterone (nmol/l)	19.5±5.2	19.8±5.6	19.6±5.7
Insulin-like growth factor I (µg/l)	214.6±67.9	199.5±64.7	209.6±61.1
Leptin (µg/l)	6.3±4.7	6.2±4.2	5.7±3.8
Fasting insulin (mU/l)	14.2±14.0	11.4±7.0	14.2±14.5
Fasting glucose (mmol/l)	4.5±1.0	4.6±0.9	4.6±1.2
Triglycerides (mmol/l)	1.8±1.1	1.8±1.1	1.7±0.9
Total cholesterol (mmol/l)	6.1±1.1	6.2±1.0	6.2±1.3
High-density lipoprotein cholesterol (mmol/l)	1.3±0.3	1.2±0.3	1.3±0.4
Low-density lipoprotein cholesterol (mmol/l)	4.0±1.0	4.1±1.0	4.2±1.2
Systolic blood pressure (mm Hg)	130.3±16.8	129.4±18.6	128.2±15.2
Diastolic blood pressure (mm Hg)	83.7±9.4	83.8±11.5	82.5±8.9
Heart rate (beats/min)	68.8±10.8	68.0±10.0	72.2±11.2

Data (mean±SD) were adjusted for BMI and WHR when appropriate. All *P* values are >0.20.

Acknowledgements

This study was supported by grants from the Swedish Medical Research Council (K97-19X-00251-35A) and the Pennington Biomedical Research Center. R. Rosmond would also like to acknowledge the Henning and Johan Throne-Holst Foundation for the support of a postdoctoral fellowship at the Pennington Biomedical Research Center. C. Bouchard is partially supported by the George A. Bray Chair in Nutrition.

References

[1] L T Dalgaard, O. Pedersen, Uncoupling proteins: functional characteristics and role in the pathogenesis of obesity and Type II diabetes, Diabetologia 44 (2001) 946–965

[2] C Fleury, M. Neverova, S. Collins, S Raimbault, O Champigny, C Levi-Meyrueis, F Bouillaud, M F. Seldin, R.S. Surwit, D Ricquier, C.H Warden, Uncoupling protein-2· a novel gene linked to obesity and hyperinsulinemia, Nat Genet. 15 (1997) 269–272.

[3] O. Boss, S. Samec, A. Paoloni-Giacobino, C. Rossier, A. Dulloo, J Seydoux, P. Muzzin, J.P Giacobino, Uncoupling protein-3: a new member of the mitochondrial carrier family with tissue-specific expression, FEBS Lett 408 (1997) 39–42.

[4] K. Walder, R.A. Norman, R L. Hanson, P Schrauwen, M Neverova, C P Jenkinson, J. Easlick, C.H. Warden, C. Pecqueur, S Raimbault, D Ricquier, M.H. Silver, A R. Shuldiner, G Solanes, B B. Lowell, W.K. Chung, R.L. Leibel, R. Pratley, E. Ravussin, Association between uncoupling protein polymorphisms (UCP2–UCP3) and energy metabolism/obesity in Pima indians, Hum. Mol Genet. 7 (1998) 1431–1435.

[5] A. Astrup, S Toubro, L T Dalgaard, S A. Urhammer, T I. Sorensen, O. Pedersen, Impact of the v/v 55 polymorphism of the uncoupling protein 2 gene on 24-h energy expenditure and substrate oxidation, Int. J. Obes Relat. Metab Disord. 23 (1999) 1030–1034

[6] P. Bjorntorp, The associations between obesity, adipose tissue distribution and disease, Acta Med. Scand., Suppl. 723 (1988) 121–134

[7] R Rosmond, Y C. Chagnon, G Holm, M Chagnon, L Perusse, K. Lindell, B. Carlsson, C. Bouchard, P. Björntorp, Hypertension in obesity and the leptin receptor gene locus, J Clin Endocrinol Metab 85 (2000) 3126–3131

[8] E Spjotvoll, M. Stoline, An extension of the T-method of multiple comparison to include the cases with unequal sample sizes, J. Am Stat Assoc 68 (1973) 976–978

[9] S A. Urhammer, L T. Dalgaard, T I. Sorensen, A.M Moller, T Andersen, A Tybjaerg-Hansen, T Hansen, J O Clausen, H Vestergaard, O Pedersen, Mutational analysis of the coding region of the uncoupling protein 2 gene in obese NIDDM patients: impact of a common amino acid polymorphism on juvenile and maturity onset forms of obesity and insulin resistance, Diabetologia 40 (1997) 1227–1230

[10] M. Klannemark, M Orho, L. Groop, No relationship between identified variants in the uncoupling protein 2 gene and energy expenditure, Eur J. Endocrinol 139 (1998) 217–223.

[11] D Arsenijevic, H. Onuma, C Pecqueur, S Raimbault, B.S Manning, B. Miroux, E Couplan, M.C. Alves-Guerra, M. Goubern, R Surwit, F. Bouillaud, D Richard, S. Collins, D. Ricquier, Disruption of the uncoupling protein-2 gene in mice reveals a role in immunity and reactive oxygen species production, Nat. Genet 26 (2000) 435–439.

[12] C.Y. Zhang, G Baffy, P Perret, S. Krauss, O Peroni, D. Grujic, T. Hagen, A J Vidal-Puig, O. Boss, Y B. Kim, X X. Zheng, M B Wheeler, G.I. Shulman, C.B. Chan, B B Lowell, Uncoupling protein-2 negatively regulates insulin secretion and is a major link between obesity, beta cell dysfunction, and type 2 diabetes, Cell 105 (2001) 745–755.

ELSEVIER

Biochimica et Biophysica Acta 1588 (2002) 106–112

BIOCHIMICA ET BIOPHYSICA ACTA
BBA
www.bba-direct.com

Expression and functional analysis of rat P23, a gut hormone-inducible isoform of trypsin, reveals its resistance to proteinaceous trypsin inhibitors

Shin-Ichi Fukuoka[*], Cornelio M. Nyaruhucha

Division of Food Science and Biotechnology, Graduate School of Agriculture, Kyoto University, Uji, Kyoto 611, Japan

Received 13 November 2001; received in revised form 16 May 2002, accepted 30 May 2002

Abstract

Rat P23 is an isoform of trypsin (ogens) synthesized by rat acinar cells. Expression of P23 is stimulated strongly by caerulein, an analogue of cholecystokinin (CCK). However, the physiological relevance of rat P23 in healthy and pathological conditions such as caerulein-induced pancreatitis is largely unknown. Using recombinant P23 trypsinogen and reconstitution analysis of zymogen autoactivation, unique inhibitor-resistance characteristics of P23 were elucidated. P23 cDNA was expressed in *Escherichia coli* periplasm, yielding recombinant P23 trypsinogen. Autoactivation of zymogen granule contents from caerulein-induced rat pancreas was also studied. Activation kinetics of P23 by enterokinase was similar to those of rat anionic trypsinogen, which is a major isoform of trypsinogen. Interestingly, rat pancreatic secretory trypsin inhibitor (PSTI), which protects against deleterious activation of trypsinogens in zymogen granules, failed to inhibit P23 trypsin even with four-fold molar excess, at which concentration it effectively inhibited rat anionic trypsin to almost 100%. P23 trypsin also showed marked resistance to proteinaceous trypsin inhibitors such as soybean trypsin inhibitor and aprotinin. P23 trypsin activated by enterokinase dramatically accelerated the cascade of autoactivation of anionic trypsinogen even in the presence of PSTI. Taken together with a previous observation that P23 is specifically upregulated 14-fold by 24-h caerulein infusion, these results suggest that elevated levels of P23 should be taken into consideration in the mechanism of trypsinogens within the pancreas in pathological conditions.

© 2002 Elsevier Science B.V. All rights reserved.

Keywords Trypsin, Gut, Rat P23

1. Introduction

P23 was found originally in rat exocrine pancreas by two-dimensional isoelectric focusing and SDS-PAGE to be an unidentified protein with M_r=23,000 and an isoelectric point (p*I*) of 6.2 [1]. P23 is expressed only in trace amounts (<0.4% of total secretory proteins) in the unstimulated pancreas while caerulein, an analog of the physiological pancreatic secretagogue cholecystokinin (CCK), causes an acute 14-fold induction of P23 protein synthesis, so that it comprises up to 2% of total secretory proteins [1]. By this criterion, P23 is the most strongly regulated protein of the rat exocrine pancreas. Molecular cloning using a specific antibody against P23 revealed that rat P23 cDNA encodes a novel isoform of trypsinogen, whose similarities in amino acid sequence to two anionic (trypsinogen 1 and 2) and one basic (trypsinogen 3) isoform previously identified in the rat pancreas are 67%, 68% and 72%, respectively [2]. P23 contains all the major structural features of other trypsins [2].

Thus far, the physiological role and hormonal regulation of P23 are relatively unknown. Here, we describe the experimental expression and functional analysis of rat P23 and its unique inhibitor resistance.

2. Materials and methods

2.1. Materials

Rat anionic trypsinogen and pancreatic secretory trypsin inhibitor (PSTI) were purified from pure rat pancreatic juice collected from rats under anesthesia as described in Ref. [3]. Purified bovine trypsin (Type III) was purchased from Sigma. Enterokinase was purchased from NEB. A synthetic trypsin substrate, benzoyl-arginine-*p*-nitroanilide (BApNA) and an expression inducer, isopropyl-beta-D(−)-thiogalactopyrano-

---

[*] Corresponding author. Tel +81-774-38-3754; fax: +81-774-38-3755.
E-mail address fukuoka@food2.food.kyoto-u.ac.jp (S.-I. Fukuoka)

0925-4439/02/$ - see front matter © 2002 Elsevier Science B.V. All rights reserved
PII: S0925-4439(02)00153-9

side (IPTG) were purchased from Wako Pure Chemicals. Protein concentration was determined using Bio-Rad protein assay reagent. Recombinant enterokinase and reagents for DNA manipulation were purchased from NEB. FOY-305 was provided from Ono Pharmaceutical Co., Ltd.

2.2. Construction of a P23 expression vector in Escherichia coli periplasm

Two oligonucleotide primers were used for polymerase chain reaction (PCR). The sense primer 5′-GATGACAAGCTTGTTGGAGGCTACA-3′, corresponding to amino acid residues 21–29 of P23, was designed to contain *Hin*dIII restriction sites. M13–20 primer was utilized as an antisense primer. PCR was performed using P23 cDNA cloned into pBluescript [2] as a template, with Taq/Pfu polymerases. Samples were amplified for 25 cycles under the following conditions: denaturation for 1 min at 94 °C, annealing for 1 min at 55 °C and extension for 1 min at 72 °C. A DNA fragment of approximately 750 bp was treated with *Hin*dIII, isolated by electrophoresis on a 0.7% agarose gel, and recovered with a Gene Clean kit (Bio 101). The fragment was subcloned into the prokaryotic expression vector pFlag-1 (IBI) at its *Hin*dIII site as described previously [4]. The DNA sequence was determined to confirm insertion and integrity of the P23 sequence. Restriction enzyme analysis was also performed to determine the orientation of the inserts. Both constructs with normal and reversed (as a control) orientations relative to the promoter in pFlag-1 were selected for the following expression study.

2.3. Expression of P23 protein in E. coli periplasm

E. coli JM109 strains were transformed by pFlag carrying P23 or reversed P23 inserts using a standard calcium chloride method. Transformants were selected on plates containing ampicillin (50 μg/ml). Plasmid DNA was purified from these transformants and restriction patterns were checked with several restriction enzymes for DNA integrity. Transformants were preincubated at 37 °C with vigorous shaking in LB media with ampicillin to achieve log phase growth, at which point IPTG was added (0.05 mM). Periplasmic expression and purification were performed as described in Ref. [4]. Briefly, cells were harvested by centrifugation after 3 h incubation with IPTG in the presence of 5 mM reduced glutathione. Cells were washed with a Tris–HCl buffer, pH 7.5 containing 1 mM EDTA, and then treated with lysozyme (0.1 mg/ml) in the same buffer at 4 °C for 30 min. Periplasmic proteins were recovered in the supernatant after centrifugation at 10,000×*g* for 20 min. Expressed P23 was purified further by two cycles of sedimentation with ammonium sulfate and by HPLC with a TSK3000 gel filtration column. Elution was monitored by measuring absorbance at 280 nm and performing SDS-PAGE. Fractions with a molecular weight of 23 kDa and trypsin activity were pooled and stored at −20 °C until use. A control transformant with a Flag-1 vector carrying a reversed P23 insert was treated in the same manner and the periplasmic fraction was mock-purified with ammonium sulfate and by HPLC and then used as a control solution for enzyme assay.

2.4. Enzyme assay

The recombinant P23, reversed P23 fraction or purified anionic trypsinogen (100 μg/ml) was activated with enterokinase (1 μg/ml) at 37 °C for 40 min, and then BApNA (2 mM) was added. The mixtures were incubated at 37 °C. At given time points, a portion of each reaction was collected and the reaction stopped by addition of acetic acid (20%). *p*-Nitroanilines liberated by trypsin activity were measured with a spectrophotometer at 410 nm. Dependency of the reactions on enterokinase activation was studied by performing the same reaction in the absence of enterokinase and comparing the results.

2.5. Effects of trypsin inhibitors on the recombinant P23 and native anionic trypsins

Recombinant P23 or purified anionic trypsinogen was activated with enterokinase as described above, and then various proteinaceous or synthetic trypsin inhibitors were added at various inhibitor/enzyme ratios. The reaction mixtures were incubated at 22 °C for 15 min to allow inhibitor/enzyme interaction, and then BApNA was added. Reactions were carried out and stopped as described earlier. Inhibitor-resistant trypsin activity was expressed as a percentage of the activity in control reactions without inhibitors.

2.6. In vitro studies of acceleration of autoactivation by rat P23 trypsin

Highly purified rat anionic trypsinogen (90 μg/ml) was incubated with recombinant P23 trypsinogen (10 μg/ml) for various periods of time in the presence or absence of enterokinase (0.1 μg/ml) and/or purified rat PSTI (2 μg/ml) at 37 °C. Experiments conducted without addition of P23 trypsinogen were controlled by addition of an equivalent amount of anionic trypsinogen (10 μg/ml), in order to maintain a total of 100 μg/ml trypsinogen in the reaction mixtures. The amount of P23 trypsinogen to be added was estimated to be similar to those found in rat pancreatic secretions after 24-h stimulation by caerulein (about one-tenth of total anionic trypsinogens) [1]. The amount of PSTI to be added was made to be similar to physiological conditions, which effectively inhibits about 5% of total trypsin activity in pancreatic secretions [5]. At given time points, portions of the samples were collected and assayed with BApNA for activated trypsin activity. Trypsin-like activity of enterokinase toward BApNA was negligible.

3. Results

3.1. Expression of P23 trypsinogen as a secretory protein in E. coli periplasm

E. coli transformed with pFlag-1 carrying P23 cDNA produced a protein with a molecular mass corresponding to a trypsinogen (23 kDa) in the periplasm, representing about 10% of all periplasmic proteins upon IPTG induction (Fig. 1, lane 1 vs. 2). As a control, *E. coli* with pFlag-1 carrying reverse-oriented P23 cDNA did not express any significant protein at the corresponding molecular weight with or without IPTG (Fig. 1, lanes 3 and 4). Western blotting using polyclonal anti-dog trypsinogen antibody was weakly positive, confirming that the 23-kDa band in lane 2 is a trypsinogen-related molecule (data not shown). A large portion (>90%) of the expressed P23 protein remained in insoluble forms in the bacteria even after lysis with 1% Triton X-100. SDS-PAGE with beta-mercaptoethanol showed that inclusion bodies contained a protein with a molecular mass of about 25 kDa, suggesting that the soluble form of P23 was translocated to the periplasm and an Omp A signal peptide (with a predicted size of 2046 Da for 21 amino acids) was released, resulting in formation of a proenzyme (P23 trypsinogen) form in the periplasm. The apparent low efficiency of translocation may be due to saturation of the *E. coli* translation machinery with a high level of exogenous protein expression. The expressed P23 trypsinogen in the periplasm was further purified by two rounds of ammonium sulfate precipitation and HPLC gel filtration, producing a homogenous sample to be used for enzymatic assays.

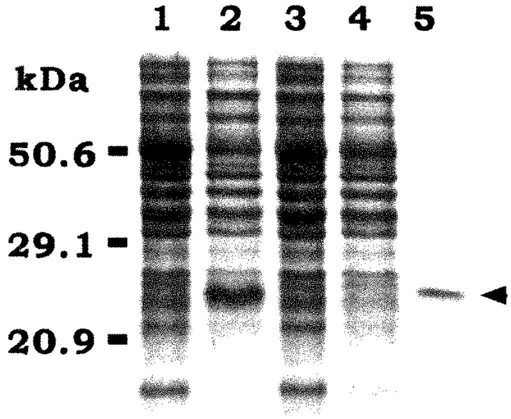

Fig. 1. Expression of recombinant P23 trypsinogen in *E. coli* periplasm. *E. coli* transformed with pflag-1 carrying P23 cDNA (lanes 1 and 2) or reverse-oriented p23 cDNA (lanes 3 and 4) were incubated in LB media with (lanes 2 and 4) or without (lanes 1 and 3) IPTG. Cells were harvested and the periplasmic fractions were subjected to 10% SDS-PAGE. Apparent molecular weight shown by prestained molecular markers are indicated as kDa at far left. P23 trypsinogen purified by ammonium sulfate precipitation/HPLC gel filtration is indicated in lane 5 with an arrow head.

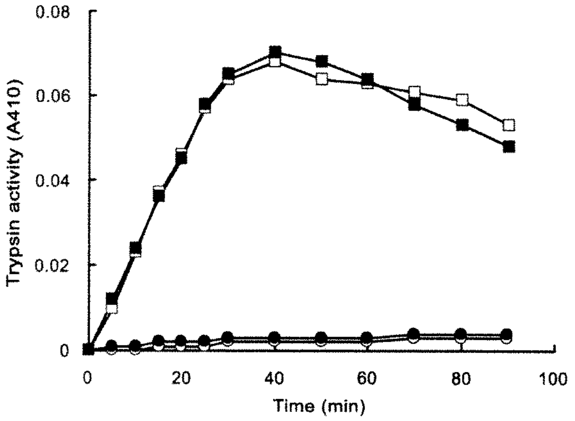

Fig. 2. Enterokinase-dependent activation of rat anionic and p23 trypsinogens. Recombinant rat P23 trypsinogen (closed symbols) or purified rat anionic trypsinogen (open symbols) (100 μg/ml) were incubated in the presence (square) or absence (circle) of enterokinase (1 μg/ml). Samples were taken at given incubation times, mixed with BApNA (2 mM) as a substrate and incubated again at 37 °C for 15 min. *p*-Nitroanilides liberated by trypsin cleavage were measured with a spectrophotometer (Beckman DU-650) at 410 nm. Trypsin activity was expressed as the rate of A410 increase per minute.

3.2. Enteropeptidase-dependent activation of P23 trypsinogen

Expressed P23 trypsinogen showed enteropeptidase-dependent activation, with a time-dependent profile similar to that of purified rat anionic trypsinogen (Fig. 2). A control preparation similarly purified from *E. coli* periplasm transformed with the reversed P23 cDNA did not show any significant trypsin activity either in the presence or absence of enteropeptidase, indicating efficient separation of recombinant P23 from endogenous *E. coli* proteases by the purification (data not shown).

3.3. Inhibition of P23 trypsin with various trypsin inhibitors

The effect of various trypsin inhibitors on P23 trypsin was compared with their effects on rat anionic trypsin and bovine trypsin. Increasing concentrations of inhibitors were incubated with 100 μg/ml of each trypsin, and then the remaining resistant trypsin activities were measured. Rat anionic and bovine trypsins were completely inhibited by equimolar (100 μg/ml) soybean trypsin inhibitor (SBTI), whereas P23 was inhibited by 20–30% with the same concentration of SBTI (Fig. 3A). Similar results were obtained when P23 was mixed with rat pancreatic secretory trypsin inhibitor (rPSTI), a physiological inhibitor present together with trypsinogens in the zymogen granules, possibly to prevent premature trypsin activation. In the presence of a four-fold molar excess of rPSTI (100 μg/ml), control trypsins were inhibited completely, whereas more than 95% of the original P23 activity remained (Fig. 3B). A very similar profile was obtained when these trypsins were challenged by bovine pancreatic trypsin inhibitor (BPTI),

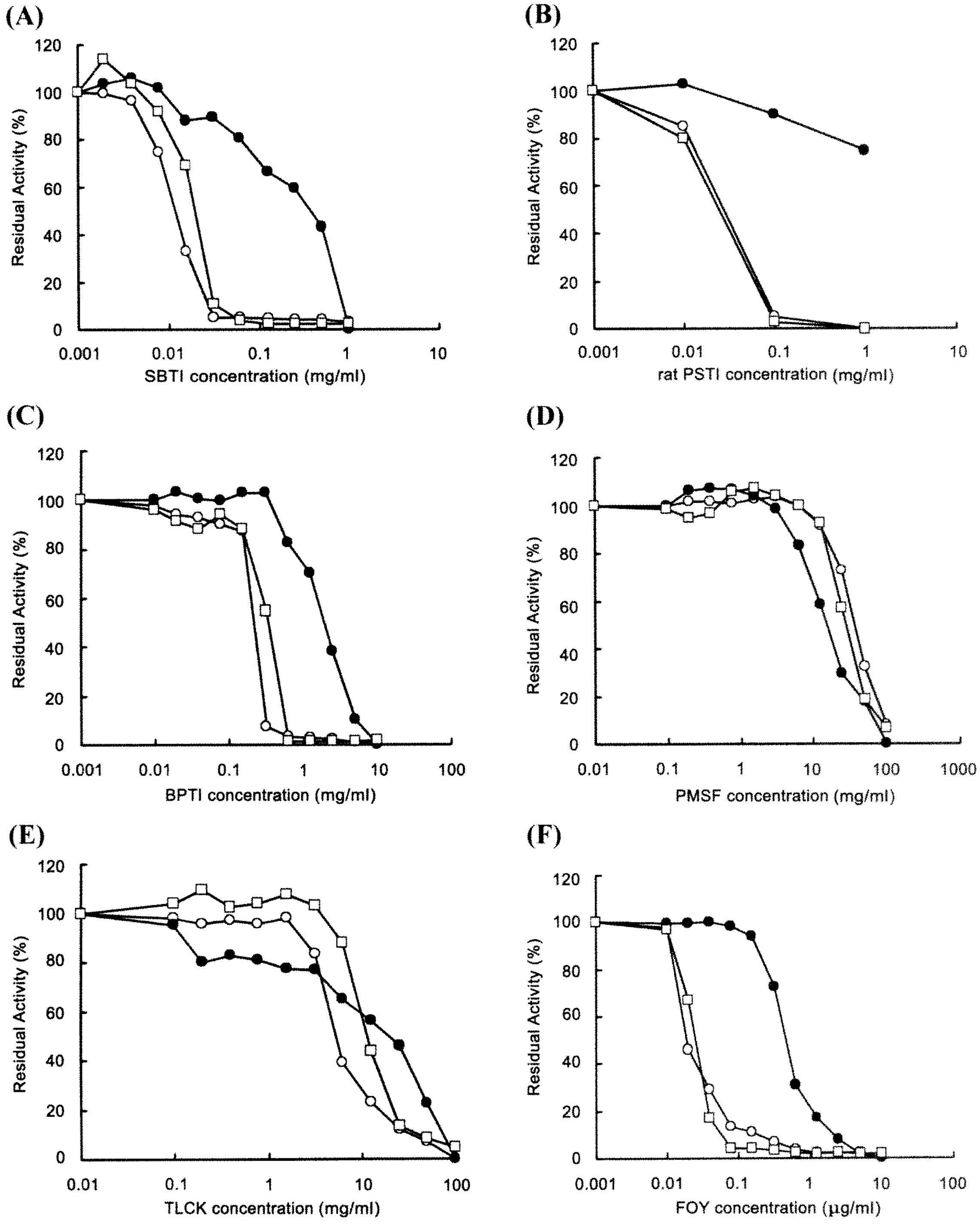

Fig. 3. Inhibition profiles of rat p23 trypsin, rat anionic trypsin and bovine trypsin with various trypsin inhibitors. One hundred microgram per milliliter each of recombinant p23 trypsin (closed circle), purified rat anionic trypsin (open circle), or bovine trypsin (open square) was activated with enterokinase (1 μg/ml) as described and then incubated with one of the given trypsin inhibitors at various concentrations as indicated at 22 °C for 15 min. Residual trypsin activity was assayed using BApNA and expressed as a percentage of total activity without the inhibitor. (A) Soybean trypsin inhibitor (SBTI), (B) rat pancreatic secretory trypsin inhibitor (rPSTI), (C) bovine pancreatic trypsin inhibitor (BPTI/aprotinin), (D) phenylmethylsulfonylfluoride (PMSF), (E) *p*-toluenesulfonyl-l-lysine chloromethyl ketone (TLCK), (F) FOY-305 (*n*,*n*-dimethylcarbamoylmethyl 4-(4-guanidinobenzoyloxy) phenylacetate methane sulfate). Data are expressed as the mean of three experiments, all of which varied less than 5%.

also known as aprotinin or Trasylol, a strong, widely used trypsin inhibitor in both experimental and clinical settings (Fig. 3C). However, P23 was sensitive to synthetic serine protease inhibitors such as PMSF (Fig. 3D) and TLCK (Fig. 3E) at concentrations comparable to those used to inhibit rat anionic trypsin and bovine trypsin, confirming that P23 is a member of the serine protease family. When FOY-305, a low molecular weight inhibitor, was used, rat P23 trypsin was more resistant than rat anionic and bovine trypsins (Fig. 3F), but was almost completely inhibited at higher FOY-305 concentrations.

3.4. In vitro studies of autoactivation acceleration by rat P23 trypsin

Based on the observation that P23 trypsin shows resistance to PSTI, which is thought to protect against trypsinogen autoactivation, an experiment to assess the ability of increased levels inhibitor-resistant P23 trypsinogen to induce autoactivation was performed in vitro.

When purified anionic trypsinogen was incubated with or without purified recombinant P23 trypsinogen (at 9:1 molar ratio) at 37 °C up to 16 h, trypsin autoactivation was not detected in either sample (Fig. 5). This finding indicates that purified trypsinogens are stable and not activated spontaneously under such conditions. When a small amount of enterokinase, an artificial initiator of activation, was added, anionic trypsinogens, with or without P23 trypsinogen, were all activated very quickly. When similar experiments were performed in the presence of purified PSTI, a physiological inhibitor of trypsin autoactivation, anionic trypsinogen was only slowly activated by enterokinase, indicating that PSTI attenuates the initial rate of trypsin autoactivation. On the other hand, when P23 trypsinogen was present in the reaction mixture, trypsin activation was accelerated dramatically, suggesting that P23 trypsinogen was activated by enterokinase to P23 trypsin, a PSTI-resistant enzyme that could promote the cascade of trypsin autoactivation free from PSTI control. The autoactivation promoted by the activated P23 trypsin was observed to overcome PSTI inhibitory effects on the other trypsinogens after an initial period of time. In conclusion, these results indicate that P23 trypsinogen is stable and does not promote trypsin autoactivation by itself but requires activation by an independent initiator (enterokinase, present in this experimental case but absent in the exocrine pancreas).

4. Discussion

Based on observations presented here, rat P23 trypsin (ogen) appears to be a unique isoform of trypsin, which is resistant to proteinaceous trypsin inhibitors such as PSTI and SBTI. A similar isoform of trypsin has been described in human pancreatic secretions and named mesotrypsin, due to its p*I* of 5.95, which is 'meso', or in the middle, between other acidic and basic trypsins [6,7]. Human mesotrypsin is a minor species of pancreatic digestive enzyme and shows resistances to naturally occurring trypsin inhibitors similar to those exhibited in P23. Structural and functional analyses suggest that rat P23 trypsinogen is a functional homologue of human mesotrypsinogen. However, the degree to which human mesotrypsinogen is regulated by CCK or its analogues should be investigated further. Structural comparison of rat P23 and human mesotrypsinogen revealed several unique characteristics. Upon comparison of rat P23 or human mesotrypsin to other known trypsin isoforms, it is found that the catalytic triad of His-63, Asp-107 and Ser-201 (numbers are based on the rat P23 sequence), as well as an obligatory Asp at position 194, are all conserved.

However, at amino acid 198, close to the active center of the enzyme, an Asp residue is found in P23, rather than an Asn, which is conserved throughout all known rat and human trypsins (Fig. 4). This substitution may change the

				195						201	
Rat P23 trypsinogen	-Gly-	Gly-	Lys-	Asp-	Ser-	Cys-	Asp-	Gly-	Asp-	Ser-	Gly-
Rat Ta1	-	-	-	-	-	-	Asn	-	-	-	-
Rat Ta2	-	-	-	-	-	-	Asn	-	-	-	-
Rat Tc	-	-	-	-	-	-	Asn	-	-	-	-
Human trypsin 1	-	-	-	-	-	-	Asn	-	-	-	-
Human trypsin 2	-	-	-	-	-	-	Asn	-	-	-	-
Human mesotrypsin	-	-	-	-	-	-	Asn	Arg	-	-	-

Fig. 4. Comparison of amino acid sequences of various trypsin active sites. Number corresponding to amino acid residues in rat p23 trypsinogen are indicated at the top. Residue 195 is an obligatory Asp that determines substrate specificity toward basic amino acids and is conserved in all rat and human trypsins. Residue 200 is the active serine in the triad and is also conserved in all rat and human trypsins. Note the unique Asp-198, instead of Asn, in rat p23 and the unique Arg-199 in human mesotrypsinogen, which may be responsible for their altered interactions with trypsin inhibitors. Ta, anionic trypsin (two different anionic trypsins have been described in rats); Tc, cationic trypsin.

electrical and steric environment in the active center. A similar, in terms of site, but different, in terms of amino acid charge, substitution has been found in human mesotrypsin, which has an Arg instead of the conserved Gly in position 199.

Based upon an X-ray crystallographic structure of a complex between rat trypsin and BPTI [8], the Asp→Asn mutation at position 198 was modeled using the software Quanta (Molecular Simulations). The Van der Waals radii of Asp-198 in rat P23 and Arg-17 in BPTI were found to overlap for all possible rotations (data not shown). This suggests that the two residues cannot co-exist in the complex as it is currently structured, and would disrupt the binding between the enzyme and inhibitor. Further analysis of the change of the microscopic molecular environment in the active center of P23 and mesotrypsin could explain why they are not inhibited by large proteinaceous trypsin inhibitors such as PSTI, BPTI and SBTI, but can be blocked using small synthetic trypsin inhibitors such as PMSF and TLCK.

The fact that P23, a hormone-inducible trypsin isoform, exhibits marked inhibitor resistance implies that it may perform several physiologically relevant functions. If levels of rat P23 trypsin are increased by a specific stimulus such as CCK, caerulein or by pathogenic conditions, the inhibitor-resistant trypsin may cause potentially deleterious effects upon autoactivation within pancreatic tissues, especially in the setting of pancreatitis. Caerulein-induced pancreatitis is a widely acknowledged model as an experimental pancreatitis [9]. Supramaximal doses of CCK, caerulein or cholinergic agonists have been found to induce pancreatic damage manifested by edema, increased serum levels of pancreatic enzymes, inflammation and necrosis in rats [10], mice [11] and even healthy human [12]. Although molecular mechanisms that initiate or apply the form of pancreatitis are largely unknown, it has been pointed out that premature activation of pancreatic zymogens within pancreatic tissues is a key step for progression of the pathological consequence [9]. When P23 is turned out to be unique PSTI-resistant trypsin, one can speculate that activated P23 trypsin is able to further cleave trypsinogens to trypsins in the presence of PSTI or other endogenous trypsin inhibitors, and thus promote the activation cascade. Rat PSTI mRNA expression has been shown to be upregulated by CCK [13], it only occurs by one- to two-fold and is much less responsible than the expression of P23 induced by CCK analogue. Parallel regulation of anionic trypsinogen and PSTI was also observed under various dietary conditions in rats [14]. However, the ratio between the rates of P23 and PSTI expression might be much higher (P23≫PSTI) in the setting of caerulein–infusion, resulting in insufficient amounts of PSTI to attenuate the cascade of trypsin autoactivation promoted by activated P23. In vitro studies shown in Fig. 5 demonstrate the possibilities that imbalance between P23 and PSTI cause the promotion of trypsinogen activation cascade.

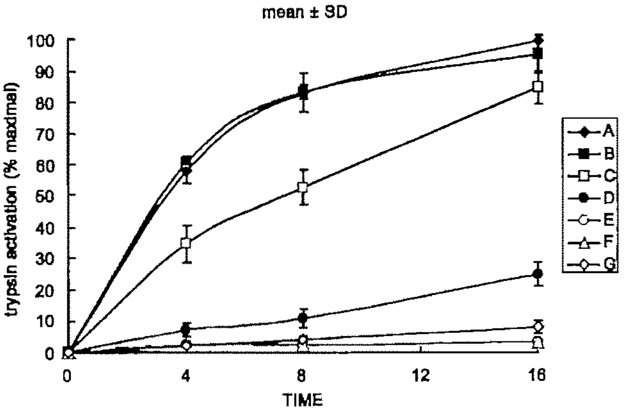

Fig. 5. In vitro studies of autoactivation acceleration by rat P23 trypsin. Highly purified rat anionic trypsinogen (Ta) (90 μg/ml) was incubated with recombinant P23 trypsinogen (10 μg/ml) in the presence or absence of enterokinase (0.1 μg/ml) and/or purified rat PSTI (2 μg/ml) at 37 °C: (A), (C) and (E). The experiments lacking P23 trypsinogen were compensated by addition of an equivalent amount of anionic trypsinogen (10 μg/ml) in order to maintain a total of 100 μg/ml trypsinogen in every reaction mixture: (B), (D) and (F). Increment of P23 trypsinogen (10 μg/ml) alone was also measured in the presence of enterokinase (0.1 μg/ml) and purified rat PSTI (2 μg/ml): (G). At given time points, portions of the samples were collected and assayed with BApNA for activated trypsin activity. (A) Ta+enterokinase+P23; (B) Ta+enterokinase; (C) Ta+enterokinase+PSTI+P23; (D) Ta+enterokinase+PSTI; (E) Ta+P23; (F) Ta alone; (G) P23+enterokinase+PSTI. Data are expressed as percentages of maximal activation and reported as the means of four experiments ± 1 S.D.

In conclusion, rat P23 is found to be a unique PSTI-resistant trypsin. Taken together with the fact that P23 is upregulated 14-fold after 24-h caerulein infusion, these results suggest that rat P23 plays an important role in the progression of the experimental animal model of caerulein-induced pancreatitis. An in vitro autoactivation assay system and recombinant P23 will be useful tools for further investigation of the mechanism underlying its pathogenesis.

References

[1] J. Schich, K. Horst, G. Scheele, Hormonal stimulation in the exocrine pancreas results in coordinate and anticoordinate regulation of protein synthesis, J. Cell Biol. 99 (1984) 1569–1574.

[2] H. Lütcke, U. Rausch, P. Vasiloudes, G.A. Scheele, H.F. Kern, A fourth trypsinogen (P23) in the rat pancreas induced by CCK, Nucleic Acids Res. 17 (1989) 6736.

[3] K. Iwai, S. Fukuoka, T. Fushiki, M. Tsujikawa, M. Hirose, S. Tsunasawa, F. Sakiyama, Purification and sequencing of a trypsin-sensitive cholecystokinin-releasing peptide from rat pancreatic juice, J. Biol. Chem. 262 (1987) 8956–8959.

[4] C.N.M. Nyaruhucha, M. Kito, S. Fukuoka, Identification and expression of the cDNA-encoding human mesotrypsin(ogen), an isoform of trypsin with inhibitor resistance, J. Biol. Chem. 272 (1997) 10573–10578.

[5] S. Fukuoka, H. Kwajiri, T. Fushiki, K. Takahashi, K. Iwai, Localization of pancreatic enzyme secretion-stimulating activity and trypsin inhibitory activity in zymogen granule of the rat pancreas, Biochim. Biophys. Acta 884 (1986) 18–24.

[6] H. Rinderknecht, I.G. Renner, C. Carmack, Trypsinogen variants in pancreatic juice of healthy volunteers, chronic alcoholics, and patients with pancreatitis and cancer of the pancreas, Gut 20 (1979) 886–891.

[7] H. Rinderknecht, I.G. Renner, S.B. Abramson, C. Carmack, Mesotrypsin: a new inhibitor-resistant protease from a zymogen in human pancreatic tissue and fluid, Gastroenterology 86 (1984) 681–692.

[8] J.J. Perona, C.A. Tsu, C.S. Craik, R.J. Fletterick, Crystal structures of rat anionic trypsin complexed with the protein inhibitors APPI and BPTI, J. Mol. Biol. 230 (1993) 919–933.

[9] F.S. Gorelick, G. Adler, H.F. Kern, Cerulein-induced pancreatitis, The Pancreas: Biology, Pathobiology, and Disease, 2nd edn., Raven Press, New York, 1993, pp. 501–526, (Article in book) Chapter 25.

[10] M. Lampel, H. Kern, Acute interstitial pancreatitis in the rat induced by excessive doses of pancreatic secretagogue, Virchows Arch., A Pathol. Anat. Histopathol. 373 (1977) 97–117.

[11] C. Niederau, C.D. Ferrell, J.H. Grendell, Caerulein-induced acute necrotizing pancreatitis in mice: protective effects of proglumide, benzotript, and secretin, Gastroenterology 88 (1985) 1192–1204.

[12] W.H. Marsh, G.A. Vukov, E.C. Conradi, Acute pancreatitis after cutaneous exposure to an organophosphate insecticide, Am. J. Gastroenterol. 83 (1988) 1158–1160.

[13] K. Miyasaka, A. Funakoshi, E. Nakamura, H. Teraoka, Regulation of gene expression of pancreatic secretory trypsin inhibitor-61 and -56 by bile and pancreatic juice in rats, Pancreas 11 (1995) 246–255.

[14] R. Graf, F. Valeri, R. Gassmann, S. Hailemariam, T.W. Frick, D. Bimmler, Adaptive response of the rat pancreas to dietary substrates: parallel regulation of trypsinogen and pancreatic secretory trypsin inhibitor, Pancreas 21 (2000) 181–190.

ELSEVIER

Biochimica et Biophysica Acta 1588 (2002) 113–118

BIOCHIMICA ET BIOPHYSICA ACTA
BBA
www.bba-direct.com

Protective effect of D-glucose, L-leucine and fetal calf serum against oxidative stress in neonatal pancreatic islets

Luiz F. Stoppiglia, Tatiane A. Nogueira, Adriana R. Leite, Everardo M. Carneiro,
Antonio C. Boschero *

*Departamento de Fisiologia e Biofísica, Instituto de Biologia, Universidade Estadual de Campinas (UNICAMP), CP 6109,
Campinas 13083-970, SP, Brazil*

Received 14 January 2002; received in revised form 23 April 2002; accepted 3 June 2002

Abstract

B-cell destruction during the onset of diabetes mellitus is associated with oxidative stress. In this work, we investigated the mechanisms of defense against oxidative stress present in neonatal islets and their modulation by D-glucose, L-leucine and fetal calf serum (FCS). Culturing neonatal rat islets in the presence of low D-glucose concentrations (2.8–5.6 mmol/l) and 1 mmol/l H_2O_2 increased the D-glucose uptake by islets sixfold compared to control levels. This effect was dose-dependently inhibited by D-glucose or FCS and by high concentrations of L-leucine. These supplements allowed islets to increase cytoplasmic catalase (CAT) activity only in response to H_2O_2, with no decrease in NO formation. Although L-leucine increased CAT activity and restored D-glucose uptake, it did not prevent damage to the islets. These data indicate that the most important H_2O_2 scavenger system in the islets is CAT and that this system can be modulated by metabolic substrates.

© 2002 Elsevier Science B.V. All rights reserved.

Keywords: Neonatal pancreatic islet; D-Glucose; L-Leucine; Fetal calf serum; Oxidative stress; H_2O_2; Catalase

1. Introduction

Pancreatic B-cells have low expression of reactive oxygen species (ROS) scavenger enzymes such as superoxide dismutase (SOD), catalase (CAT) and gluthathione peroxidase (GPx) [1], and oxidative stress in these cells is common [2]. The onset of type 1 diabetes is partly mediated by H_2O_2 released from activated lymphocytes that infiltrate islets [3–5]. In contrast, type 2 diabetes evolves to advanced clinical complications through islet damage and loss of insulin secretion, mediated by gluco-lipo-toxicity, TNFα cytotoxicity, and recognition of advanced glycated ends (AGEs) by islet resident macrophages and their subsequent activation [6–8].

Oxidative stress in B-cells occurs through different pathways [9]. Since B-cells express CuZnSOD (cytoplasm) and MnSOD (mitochondrial matrix) [10], they decompose ROS into H_2O_2 [11] but are unable to remove H_2O_2 because they lack a powerful peroxidase activity. Thus, H_2O_2 may accumulate in the cytoplasm and inhibit its own diffusion from the mitochondrial matrix [12]. Within the matrix, H_2O_2 causes lipid peroxidation [9] and provokes the cross-linking of thiol residues of inner mitochondrial membrane (IMM) and matrix proteins. Following oxidation, the ADP/ATP translocator, the major component of IMM proteins, interacts with proteins such as the voltage-dependent anion channel (VDAC) of the external mitochondrial membrane (EMM), cyclophilin D from the matrix, and ER proteins of the Bax and Bcl-2 families [12]. They form membrane permeability transition pores (MPTP) responsible for the decrease in IMM voltage, mitochondrial swelling and respiratory inefficiency [13].

In addition, cytoplasmic indicators of oxidative stress such as NIK and MEKK1 activate the transcription of iNOS and apoptotic genes [16–18]. iNOS uses NADPH, O_2 and L-arginine to increase NO production several fold [16,19], which in turn down-regulates the glycolytic and citric acid pathways [20,21], decreases cytochrome *c* oxidase complex

---

Abbreviations: SOD, superoxide dismutase; CAT, catalase; GPx, gluthathione peroxidase; TPx, thioredoxin peroxidase; BSA, bovine serum albumin; EDTA, ethylenediamine tetraacetic acid; EGTA, ethylene glycol-bis(β-aminoethyl ether)-*N,N,N',N'*-tetraacetic acid; DTT, dithiothreithiol

* Corresponding author. Tel.: +55-19-3788-6202; fax: +55-19-3289-3124

E-mail address: boschero@unicamp.br (A.C. Boschero).

0925-4439/02/$ - see front matter © 2002 Elsevier Science B.V. All rights reserved.
PII: S0925-4439(02)00154-0

(COX) free-eletron scavenger activity [22,23] and alters nuclear signaling by increasing DNA exposure [24,25].

Enhanced generation of H_2O_2 and ROS in islets stimulates the transcription of apoptotic genes that results in mitochondrial and nuclear DNA fragmentation, inhibition of protein synthesis and reduction in islet cell mass. All of these processes can be prevented by fetal calf serum (FCS) or its components such as IGF-1, IGF-2 and GH [26,27].

In this work, we analyzed the effect of chronic exposure to D-glucose, L-leucine and FCS on the H_2O_2 scavenging system of neonatal rat islets. Our results indicate that all three components increase the rate of H_2O_2 degradation when H_2O_2 is present in culture media. Almost all the peroxidase activity detected was due to CAT. None of these substances reduced NO formation by islets exposed to H_2O_2. Finally, D-glucose and FCS, but not L-leucine, protected the islets against exposure to H_2O_2.

2. Material and methods

2.1. Islets isolation and culture

Neonatal (1–2 days old) and adult (4–6 months old) Wistar rats were purchased from the State University of Campinas animal facilities. After decapitation, neonatal [28] and adult [29] islets were isolated by collagenase (EC 3.4.24.3) digestion of pancreata in Hanks balanced salt solution. Islets were handpicked under a microscope, washed twice in sterile Hanks solution and cultured in RPMI 1640 medium (Sigma) supplemented with 2 g $NaHCO_3$/l and 1% penicillin/streptomycin, pH 7.4, and other supplements as indicated in the legends. Approximately 1000 islets/dish were maintained at 37 °C in a humidified atmosphere with 3% CO_2 for different periods of time. The medium was renewed every 48 h, as required.

2.2. NO production

NO formation was quantified by measuring the nitrite content of islet extracts. The islets in each dish were transferred to Eppendorf tubes containing 100 μl of Hanks solution (4 °C) and sonicated. The NO_2^- concentrations of total extracts were measured colorimetrically using a modified Griess reagent (1 part of 15 mg of sulfanilamide/ml in pure H_3PO_4 + 1 part of 1.5 mg NEED/ml in H_2O), using $NaNO_2$ dissolved in Hanks solution as standard. Absorbances were calculated as the difference between the readings at 540 and 600 nm. Assays were done immediately after recovery the islets from the dishes. NO_2^- levels were expressed as $[NO_2^-]$/[total protein] ratio.

2.3. D-Glucose uptake

D-Glucose concentrations in the media were determined using a commercial glucose enzymatic kit (Biotrol Diagnostic, Chennevières-lès-Louvres, France). D-Glucose uptake by the islets was measured as the variation in D-glucose concentrations in 10 ml of medium containing 5.6 mmol of D-glucose/l + 5% FCS at the end of 12 h in culture. Samples for D-glucose measurements were taken after filtration of the media through 0.45-μm pore filters (Millipore) to remove cells. The results were expressed as the D-glucose consumed/total protein content of islets in each dish. Extracts were prepared in Hanks solution by mechanical high-speed disruption of islets, at the end of the culture.

2.4. Peroxidase activity

Islet extracts were centrifuged at 10000g × 6 min to remove cellular membranes and organelles. The protein concentration of the liquid phase was measured (Biorad) and adjusted to 100 μg/ml by adding Hanks solution. H_2O_2 was added to each sample to a final concentration of 2.3 mmol/l and its concentration was then measured 0, 5, 10, 20, 30, 40 and 60 min later using a colorimetric reaction (Glucose Enzymatic Colour Liquide), against an H_2O_2 standard curve. The values were fitted to single exponential decay curves using the expression $[H_2O_2](t)=[H_2O_2]_{t=0} \times e^{-kt}$. The peroxidase activity of each sample was expressed as the k value (decay constant) obtained with given protein concentrations (100 μg/ml). Since the experiments with pure CAT showed a nonlinear crescent relationship between enzyme concentration and peroxidase activity, activities were not normalized.

2.5. Enzymatic kinetics

The velocity of H_2O_2 decomposition by islet protein or pure CAT (EC 1. 11.1.6, H_2O_2 oxidoreductase) (Sigma) was determined in Eppendorf tubes containing either islet protein or CAT dissolved is Hanks solution alone with increasing concentrations of H_2O_2 (0 to 300 mmol/l). Aliquots of the medium were taken 1, 2, 3 and 4 min after H_2O_2 addition, diluted with acidified Hanks solution (pH 1.0) and assayed for H_2O_2, as stated. Initial H_2O_2 concentrations and the degradation rate were determined by linear regression over the data. K_m values were calculated from Boltzman sigmoidal curves fitted to the points.

2.6. Statistical analysis

The results were expressed as the means ± S.E. and the significance of differences was assessed by Student's t test. A value of $P<0.05$ indicated significance.

3. Results

Peroxidase activity in neonatal islets was approximately three times greater than adult islets ($k = 0.111 \pm 0.007$ min^{-1} vs. $k = 0.034 \pm 0.004$ min^{-1}, respectively, at 100 μg protein/

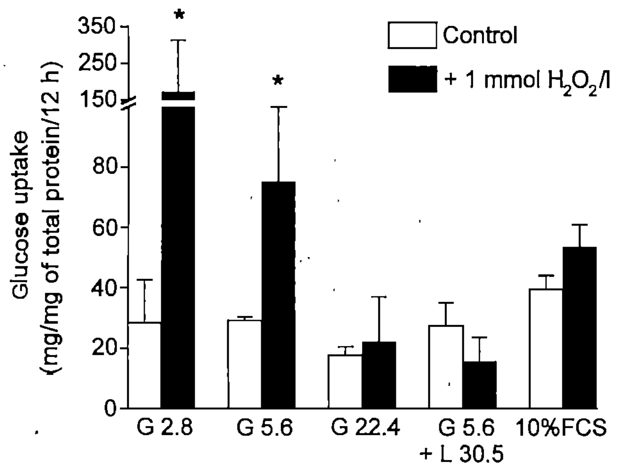

Fig. 1. Effect of H_2O_2 on D-glucose use by cultured neonatal islets. Islets were cultured for 4 days in RPMI medium with or without 1 mmol of H_2O_2/l and different concentrations of D-glucose (G; 2.8, 5.6 and 22.4 mmol/l) + 5% FCS, L-leucine (L; 30.5 mmol/l) + 5.6 mmol of D-glucose/l and 5% FCS or FCS (10%) + 5.6 mmol D-glucose/l. This medium was subsequently replaced by one containing 5.6 mmol of D-glucose/l and 5% FCS. The bars represent cumulative D-glucose use for 12 h as described in Section 2. The values are the means ± S.E. of six independent experiments. $^*P < 0.05$ vs. the respective control.

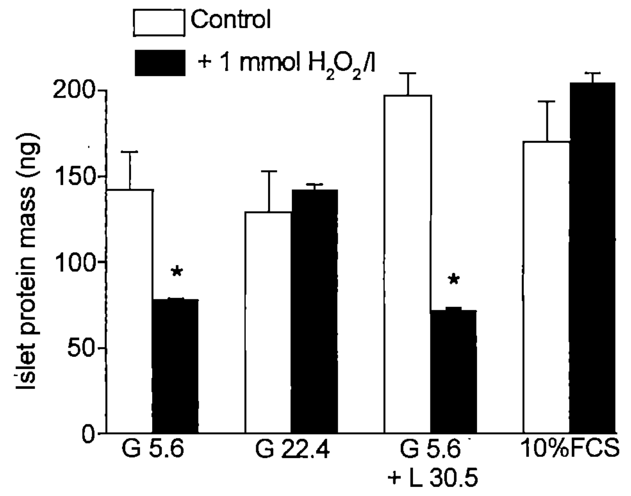

Fig. 3. Effect of H_2O_2 on protein mass of cultured neonatal islets. Islets were cultured for 4 days in RPMI medium with or without 1 mmol of H_2O_2/l and different concentrations of D-glucose (G; 5.6 and 22.4 mmol/l) + 5% FCS, L-leucine (L; 30.5 mmol/l) + 5.6 mmol of D-glucose and 5% FCS or FCS (10%) + 5.6 mmol of D-glucose/l. Subsequently, groups of 200 islets were sonicated in 100 µl of Hanks solution and the protein concentration was measured by a colorimetric assay. The bars represent the means ± S.E. of six independent experiments. $^*P < 0.05$ vs. the respective control.

ml, $n = 4$; $P < 0.05$). This activity was almost attributed to hydrophilic proteins since the removal of membranes and organelles from islet extracts did not alter the ability to decompose H_2O_2 ($k = 0.24 \pm 0.02$ min^{-1} for the liquid phase vs. $k = 0.22 \pm 0.02$ min^{-1} for the total extract, at 200 µg protein/ml, $n = 4$; NS). Heating the extracts at 100 °C for 5 min reduced peroxidase activity to less than 3% of normal values, indicating that heat-denatured proteins are responsible for H_2O_2 degradation.

The presence of 1 mmol H_2O_2/l in culture medium containing low concentrations of D-glucose (2.8 mmol/l) dramatically increased the uptake of this sugar by neonatal islets (Fig. 1). This effect was significantly reduced by physiological concentrations of D-glucose (5.6 mmol/l)

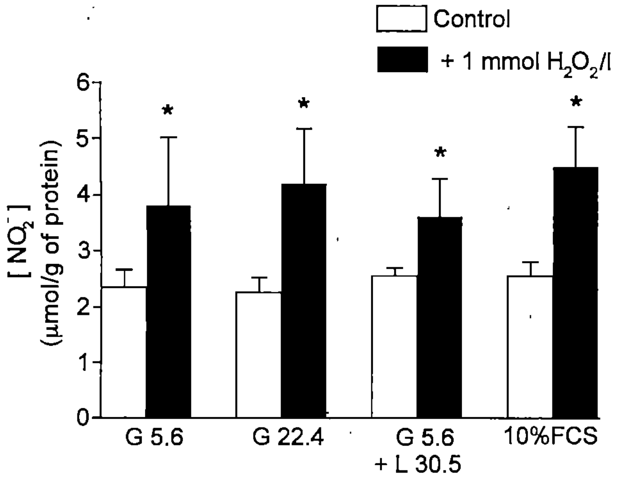

Fig. 2. Effect of H_2O_2 on nitrite production by cultured neonatal islets. Islets were cultured for 4 days in RPMI with or without 1 mmol of H_2O_2/l and different concentrations of D-glucose (G; 2.8, 5.6 and 22.4 mmol/l) + 5% FCS, L-leucine (L; 30.5 mmol/l) + 5.6 mmol of D-glucose/l and 5% FCS or FCS (10%) + 5.6 mmol of D-glucose/l. After culture, the islets were sonicated and NO_2^- concentrations within the cells were measured as described in Section 2. The values are the means ± S.E. of six independent experiments. $^*P < 0.05$ vs. the respective control.

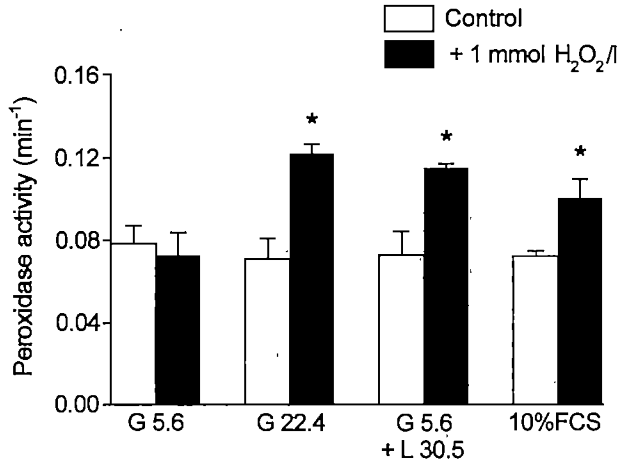

Fig. 4. Effect of H_2O_2 on peroxidase activity of cultured neonatal islets. Islets were cultured for 4 days in RPMI medium with or without 1 mmol H_2O_2/l and different concentrations of D-glucose (G; 2.8, 5.6 and 22.4 mmol/l) + 5% FCS, L-leucine (L; 30.5 mmol/l) + 5.6 mmol of D-glucose/l and 5% FCS or FCS (10%) + 5.6 mmol of D-glucose/l. The islets were subsequently sonicated and the peroxidase activity in the extract was measured as described in Section 2. The bars are the means ± S.E. of 10 independent experiments. $^*P < 0.05$ vs. the respective control.

Table 1
Effects of different concentrations of D-glucose and FCS on the peroxidase activity of islet extracts

Agents		Peroxidase activity (%)
D-Glucose (mmol/l)	FCS (%)	
2.8	5	116 ± 9
5.6	5	100
11.2	5	110 ± 30
22.4	5	70 ± 20 *
5.6	2	130 ± 6 *
5.6	5	100
5.6	7	85.4 ± 0.1 *
5.6	10	60 ± 20 *

The values are the means ± S.E. of four experiments.

* $P<0.05$ compared to the respective controls (5.6 mmol/l for D-glucose and 5% for FCS).

and abolished by 22.4 mmol of D-glucose/l, by the combination of D-glucose (5.6 mmol/l) plus L-leucine (30.5 mmol/l) and by 10% FCS (Fig. 1). H_2O_2 per se did not affect the D-glucose concentration in the incubation medium.

Exposure to 1 mmol of H_2O_2/l also increased nitrite production by the islets. This occurred even in the presence of D-glucose, L-leucine or FCS (Fig. 2). There was no correlation between D-glucose uptake and nitrite production, indicating that NO formation may not be responsible for increased D-glucose uptake by islets exposed to H_2O_2.

Culturing the islets in the presence of 1 mmol of H_2O_2/l and 5.6 mmol of D-glucose/l reduced the islet mass by 50% compared to the controls (absence of H_2O_2). High D-glucose (22.4 mmol/l) or FCS (10%), but not L-leucine (30.5 mmol/l), protected islet against damage by H_2O_2 (Fig. 3). Fig. 4 shows that the peroxidase activity of islet extracts was significantly increased by the exposure to H_2O_2, however, this increased activity was dependent on the presence of high D-glucose, L-leucine or FCS.

Unexpectedly, incubation of islets with high D-glucose and FCS concentrations in the absence of H_2O_2 dose-dependently reduced the peroxidase activity of islet extracts (Table 1).

In the next series of experiments, we investigated the enzyme responsible for H_2O_2 degradation in islet extracts. Fig. 5A shows that the enzyme activity of the extract did not change during successive challenges with H_2O_2, and that the incubation of samples with thiol reductants such as L-cysteine (1 mmol/l), 2-mercaptoethanol (1 mmol/l) or dithiothreithiol (DTT) (0.5 mmol/l) between two H_2O_2 additions did not affect the peroxidase activity of the extracts. Fig. 5B illustrates that addition of different inhib-

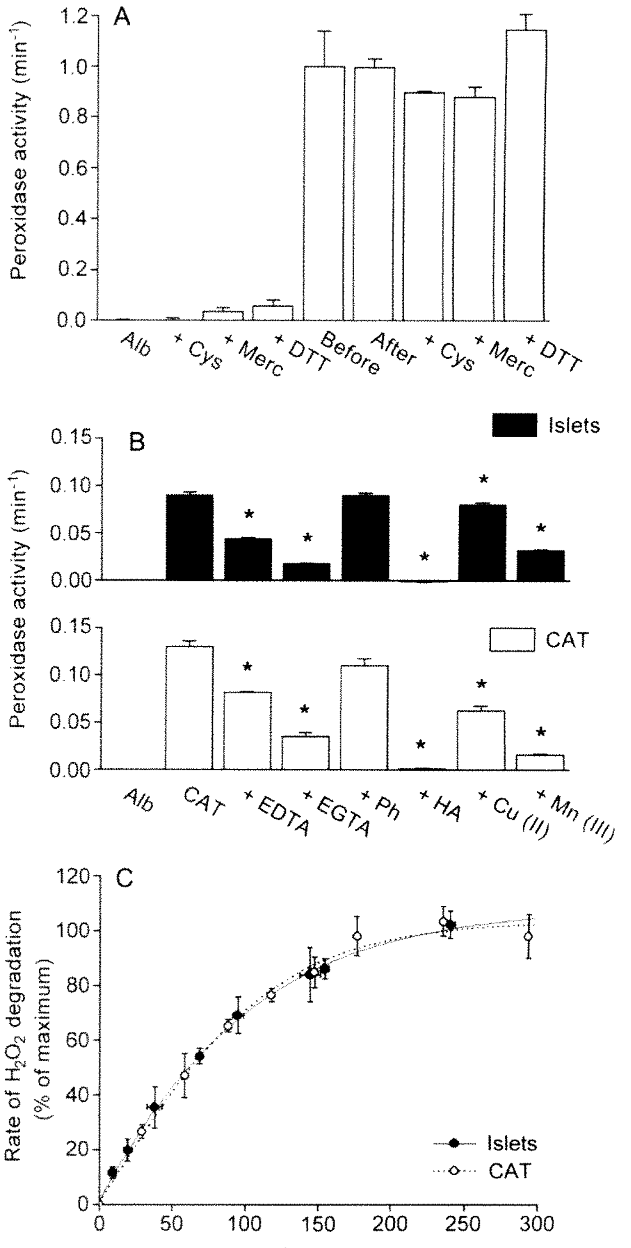

Fig. 5. Nature of the peroxidase activity in pancreatic neonatal islets. Islets were cultured in RPMI medium containing 5.6 mmol of D-glucose/l and 5% FCS. (A) represents the peroxidase activity of islet extracts (200 μg of protein/ml), the first challenge with H_2O_2 (before) and at the second challenge after a 30-min incubation with the following substances at the indicated final concentrations (pH adjusted to 7.4) in Hanks solution: none (After), 1 mmol of L-cysteine/l (Cys), 1 mmol of 2-mercaptoethanol/l (Merc) and 0.5 mmol of DTT/l (DTT). Negative controls were BSA (Alb; 100 μg/ml) without or with the same additions. The values are the means ± S.E. of six independent experiments. (B) (upper panel) represents the peroxidase activity of islet extracts (500 μg of protein/ml) in the presence of EDTA (40 mmol/l), EGTA (40 mmol/l), phenantroline (Ph) (10 mmol/l), hydroxylamine (HA) (10 mmol/l), and saturated $CuCO_3$ and $Mn_2(CO_3)_3$ (pH adjusted to 7.4). BSA (Alb) (100 μg/ml) was used as negative control. Identical experiments were done with purified catalase (lower panel). The values are the means ± S.E. of six independent experiments. * $P<0.05$ vs. control values (no additions). (C) represents the rate of H_2O_2 degradation measured at increasing concentrations of H_2O_2 using islet extracts or purified catalase (5.4 μg/ml). The K_m for the islet extracts and purified catalase were 70 ± 1 and 70 ± 0.8 mmol/l, respectively ($n=5$).

itors of CAT similarly reduced the peroxidase activity of islet extracts (upper panel) and of purified CAT (lower panel). Finally, the rate of H_2O_2 degradation for islet extracts and purified CAT had identical kinetics with K_m close to 70 mmol/l (Fig. 5C). The optimal pH for the islet extracts and purified CAT was 8.5.

4. Discussion

The best known ROS scavenging system in pancreatic islets consists of: COX, which avoids the leakage of free electrons from the respiratory chain [23]; SOD isoforms, which convert ROS into H_2O_2 in the cytoplasm or inside mitochondria; glutathione/glutathione reductase, which uses NAD(P)H as an electron source to regenerate glutathione within mitochondria; and CAT, which decomposes H_2O_2 into $H_2O + 1/2\ O_2$ [1]. We have also recently observed the presence of thioredoxin peroxidase (TPx) in islets that may represent another system for cytoplasmic H_2O_2 degradation (unpublished data).

As shown here, neonatal islets were protected better against oxidative stress than adult islets because of their more active peroxidase system. This greater protective ability against oxidative stress may be linked to higher circulating levels of growth factors in neonatal rats, thus allowing the islets to increase the rate of H_2O_2 degradation, if H_2O_2 is generated in large amounts (Fig. 4). Since this peroxidase system is almost totally localized in the water-soluble cell fraction, it is likely to be different from the peroxidase system of mitochondrial membranes [14].

Oxidative stress induced by H_2O_2 uncouples mitochondria by forming MPTP [14]. Thus, islets exposed chronically to H_2O_2 would be expected to metabolize higher amounts of D-glucose than controls in order to generate similar quantities of ATP, even at a nonstimulatory D-glucose concentration. In the presence of stimulatory concentrations, more ATP would be required for synthesis, maturation and translocation of insulin to the membrane [30]. The addition of D-glucose, L-leucine or FCS to the media containing H_2O_2 enhanced H_2O_2 degradation within the islets, thus decreasing the metabolic demand for ATP synthesis (Figs. 1 and 4).

NO has recently been associated with a reduction in COX activity that could increase ROS and H_2O_2 formation [23]. NO also reacts with ROS or H_2O_2 generated in mitochondria to form $ONOO^-$, an even more active radical [21]. Oxidative stress causes IkB heterodimer phosphorylation, subsequent NF-kB translocation to the nucleus and transcription of iNOS, in a positive feedback mechanism [17,31]. Since D-glucose, L-leucine and FCS did not decrease NO production in islets, with or without H_2O_2 in the culture media (Fig. 2), they probably failed to reduce iNOS expression. However, even with greater NO production, glucose uptake by islets was normalized in the presence of high concentrations of D-glucose, L-leucine and FCS (Fig. 1), indicating that increased NO production was not sufficient to induce mitochondria damage [21,32,33].

Thiol-reducing enzymes probably participate strong in H_2O_2 degradation by accelerating the reaction $2R\text{-}SH + H_2O_2 \Rightarrow RSSR + 2H_2O$ [15]. These enzymes and cofactors such as glutathione are reduced to the R-SH form by small thiol molecules such as L-cysteine, 2-mercaptoethanol and DTT [34]. However, treatment of samples with these thiol groups after exposure to H_2O_2 did not alter peroxidase activity, indicating that at the high concentrations of H_2O_2 used in our experiments [4], these enzymes and cofactors have a marginal participation in the degradation of H_2O_2 (Fig. 5A). To investigate the nature of peroxidase activity in islets, we used nonspecific inhibitors of metal-dependent enzymes such as ethylenediamine tetraacetic acid (EDTA), ethylenediamine tetraacetic acid (EGTA), Cu^{2+}, Mn^{3+}, phenantroline and hydroxylamine [35,36]. The variations in the peroxidase activity of islet extracts with each inhibitor mimicked the variations seen with purified CAT. These results, which were confirmed by the enzyme kinetics, strong indicated that this peroxidase was CAT (Fig. 5B,C).

Antioxidant systems must be regenerated by electron donors such as NAD(P)H, $FADH_2$, glutathione, DTT or other thiol groups from soluble (e.g. thioredoxin) or membrane-bound proteins (EMM) [15,34]. In normal cells, the concentration of H_2O_2 is in the range of 1 μmol/l, and CAT has to be coupled to NADPH to be active. In contrast, in the range of 1 mmol of H_2O_2/l, as used in our experiments and usually found in lymphocyte-infiltrated islets [3], CAT no longer requires NADPH [37]. NADPH levels, kept elevated by metabolic substrates (D-glucose and L-leucine), reduced the peroxidase activity in islets (Table 1). Thus, the decreasing amount of CAT seen in the presence of increasing concentrations of D-glucose or FCS may correlate with an increase in its individual molecules activity [37,38].

The increase in peroxidase activity produced by FCS suggests another possible mechanism in the regulation of scavenging systems. FCS is known to preserve islets by suppressing apoptotic genes and stimulating the transcription of anti-apoptotic ones [39]. This is the case of some Bcl-2 family proteins that inhibit the formation of MPTP [27]. Proteins with increased expression in response to growth factors may exert other protective effects against oxidative stress that cannot be explained simply by increasing CAT activity (Figs. 3 and 4). Our data indicate that, in the case of severe oxidative stress induced by H_2O_2 in islets, high concentrations of D-glucose, but not L-leucine (which shares the mitochondrial part of the metabolic pathway with D-glucose), may exert an FCS-like protection through some as yet unknown mechanism [38,40].

Acknowledgements

The authors thank L.D. Teixeira for technical assistance and Dr. S. Hyslop for editing the English. This work was partially supported by the Brazilian foundations CAPES, CNPq/PRONEX and FAPESP.

References

[1] M. Tiedge, S. Lortz, J. Drinkgern, S. Lenzen, Diabetes 46 (1997) 1733–1742.

[2] H. Kaneto, Y. Kajimoto, J. Miyagawa, T. Matsuoka, Y. Hujitami, Y. Umayahara, T. Hanafusa, Y. Matsuzawa, Y. Yamasaki, M. Hori, Diabetes 48 (1999) 2398–2406.

[3] S. Sreenan, A.J. Pick, M. Levisetti, A.C. Baldwin, W. Pugh, K.S. Polonki, Diabetes 48 (1999) 989–996.

[4] F. Horio, M. Fukuda, H. Katoh, M. Petruzzelli, N. Yano, C. Rittershaus, S. Bonner-Weir, M. Hatori, Diabetologia 37 (1994) 22–31.

[5] M.L. Lang, M.A. Kerr, Biochem. Biophys. Res. Commun. 276 (2000) 749–755.

[6] P.J. Beisswenger, B.S. Szwergold, K.T. Yeo, Clin. Lab. Med. 21 (2001) 53–78.

[7] M. Shimabukuro, M. Ohneda, Y. Lee, R.H. Unger, J. Clin. Invest. 100 (1997) 290–295.

[8] N. Sekine, T. Ishikawa, T. Okazaki, M. Hayashi, C.B. Wollheim, T. Fujita, J. Cell. Physiol. 184 (2000) 46–57.

[9] D.L. Eizirik, M. Flodstrom, A.E. Karlsen, N. Welsh, Diabetologia 38 (1996) 875–890.

[10] J.C. Copin, L.F. Reola, D.I. Chan, Y. Li, C.J. Epstein, P.H. Chan, J. Neurotrauma 13 (1996) 233–244.

[11] M.E. Murphy, H. Sies, Proc. Natl. Acad. Sci. U. S. A. 88 (1991) 10860–10864.

[12] A.L. Lehninger, A.E. Vercesi, E.A. Bababunmi, Proc. Natl. Acad. Sci. U. S. A. 75 (1978) 1690–1694.

[13] A.J. Kowaltowski, R.F. Castilho, M.T. Grijalba, E.J.H. Bechara, A.E. Vercesi, J. Biol. Chem. (1996) 2929–2934.

[14] A.J. Kowaltowski, A.E. Vercesi, G. Fiskum, Cell Death Differ. 7 (2000) 903–910.

[15] A.J. Kowaltowski, L.E.S. Netto, A.E. Vercesi, J. Biol. Chem. 273 (1998) 12766–12769.

[16] M.A. Marletta, J. Biol. Chem. 17 (1993) 12231–12234.

[17] F. Delfino, W.H. Walker, Mol. Cell. Endocrinol. 157 (1999) 1–9.

[18] A.L. Scarin, M.R. Heitmeier, J.A. Corbett, Endocrinology 139 (1998) 5050–5057.

[19] A. Rabinovitch, W.L. Suarez-Pinzon, K. Strynadka, R. Schulz, J.R.T. Lakey, G.L. Warnock, R.V. Rajotte, J. Clin. Endocrinol. Metab. 4 (1994) 1058–1062.

[20] Y. Tsuura, H. Ishida, T. Shinomura, M. Nishimura, Y. Seino, Biochem. Biophys. Res. Commun. 252 (1998) 34–38.

[21] L. Castro, M. Rodriguez, R. Radi, J. Biol. Chem. 269 (1994) 29409–29415.

[22] G.C. Brown, Biochim. Biophys. Acta 1504 (2001) 46–57.

[23] H. Yamasaki, H. Shimoji, Y. Ohshiro, Y. Sakihama, Nitric Oxide 5 (2001) 261–270.

[24] C. Szabó, Free Radic. Biol. Med. 6 (1996) 869–885.

[25] K. Ueda, Annu. Rev. Biochem. 54 (1985) 73–100.

[26] Z. Ling, J.C. Hannaert, D. Pippelers, Diabetologia 37 (1994) 15–21.

[27] J. Petrik, E. Arany, T.J. McDonald, D.J. Hill, Can. J. Diabetes Care 22 (1998) 63–67.

[28] E.C. Vieira, E.M. Carneiro, M.Q. Latorraca, V. Delguingaro-Augusto, M.E.C. Amaral, J.R. Bosqueiro, A.C. Boschero, J. Nutr. Biochem. 12 (2001) 285–291.

[29] C.B. Collares-Buzato, A.R. Leite, A.C. Boschero, Pancreas 23 (2001) 177–185.

[30] P. Rorsman, Diabetologia 40 (1997) 487–495.

[31] M. Flodström, N. Welsh, D. Eizirik, FEBS Lett. 385 (1996) 4–6.

[32] C.A. Delaney, M.H.L. Green, J.E. Lowe, I.C. Green, FEBS Lett. 3 (1993) 291–295.

[33] G.L. Wilson, N.J. Patton, S.P. Ledoux, Diabetes 46 (1997) 1291–1295.

[34] L.E.S. Netto, H.Z. Chae, S. Kang, S.G. Rhee, E.R. Stadtman, J. Biol. Chem. 271 (1996) 15315–15321.

[35] D.L. Eizirik, M.A. Lúcio, A.C. Boschero, M.E. Hoffmann, J. Free Radic. Biol. Med. 2 (1986) 189–192.

[36] P. Nicholls, Biochem. J. 90 (1964) 331–343.

[37] F. Hoffschir, L.D. Grosjean, P.X. Petit, S. Nocentini, B. Dutrillaux, A. Sarasin, M. Vuillaume, Free Radic. Biol. Med. 5 (1998) 809–816.

[38] D. Putnam, A.S. Arvai, Y. Bourne, J. Tainer, J. Mol. Biol. 296 (2000) 295–309.

[39] M. Federici, M. Hribal, L. Perego, M. Ranalli, Z. Caradonna, C. Perego, L. Usellini, R. Nano, P. Bonini, F. Bertuzzi, L.N.J.L. Marlier, A.M. Davalli, O. Caradente, A.E. Pontiroli, G. Melino, P. Marchetti, R. Lauro, G. Sesti, F. Folli, Diabetes 50 (2001) 1290–1301.

[40] G.C. Webb, M.S. Akbar, C. Zhao, D.F. Steiner, Proc. Natl. Acad. Sci. U. S. A. 11 (2000) 5773–5778.

ELSEVIER

Biochimica et Biophysica Acta 1588 (2002) 119–125

BIOCHIMICA ET BIOPHYSICA ACTA
BBA
www.bba-direct.com

Functional characterization of *PCCA* mutations causing propionic acidemia

Sonia Clavero, Mª Angeles Martínez, Belén Pérez, Celia Pérez-Cerdá, Magdalena Ugarte *, Lourdes R. Desviat

Dpto. Biología Molecular, Centro de Biología Molecular "Severo Ochoa", CSIC-UAM, Universidad Autónoma de Madrid, Campus de Cantoblanco, 28049 Madrid, Spain

Received 25 March 2002; received in revised form 22 May 2002; accepted 3 June 2002

Abstract

Propionic acidemia (PA, MIM 232000 and 232050) is caused by a deficiency of mitochondrial biotin-dependent propionyl-CoA carboxylase (PCC, EC 6.4.1.3), a heteropolymeric enzyme composed of α and β subunits, which are encoded by the *PCCA* and *PCCB* genes, respectively. The PCCA protein (α subunit) is responsible for the formation of carboxybiotin upon hydrolysis of ATP and contains a C-terminal biotin-binding domain and a biotin carboxylase domain, defined by homology with other biotin-dependent carboxylases, some of them characterized structurally. More than 24 mutations have been found in the *PCCA* gene in patients with PA, among them 14 missense mutations and one in-frame deletion, for which the precise molecular effect is unknown. In this study, we have established the pathogenicity of 11 *PCCA* mutations (10 missense and an in-frame deletion) by expression studies in deficient fibroblasts and in a cell-free in vitro system, and analyzed the effect of each mutation on PCC activity, protein stability and domain structure. The results show that most mutant proteins show an increased turnover and are functionally deficient, suggesting that the structural alterations they cause are incompatible with normal assembly to produce a stable, functional PCC oligomer. These results are discussed in the context of the genotype–phenotype correlations in *PCCA*-deficient PA patients.

© 2002 Elsevier Science B.V. All rights reserved.

Keywords: Propionic acidemia; PCCA; Mutation; Expression analysis; Genotype–phenotype correlation

---

1. Introduction

Propionic acidemia (PA, MIM 232000 and 232050) results from a genetic deficiency of propionyl-CoA carboxylase (PCC, EC 6.4.1.3), a mitochondrial, biotin-dependent enzyme involved in the degradation of branched-chain amino acids, odd-number chain length fatty acids and other metabolites [1]. The enzyme is composed of two types of subunits, α and β, encoded by the genes *PCCA* and *PCCB*, respectively. Both subunits are synthesized as larger precursors with mitochondrial leader peptides at the amino terminus [2].

The cDNAs for the α and β subunits have been cloned [3–5] and the structure of the genes elucidated [6,7]. The *PCCA* gene comprises 24 exons and the translation initiation codon has recently been redefined 75 nucleotides upstream of the originally reported, which accounts for 25 extra amino acids in the amino terminal region of the protein, although the mature protein is predicted to be the same [6]. The *PCCB* gene contains 15 exons [7].

Mutations in either gene cause PA [8], which in most affected patients presents as a life-threatening ketoacidosis during neonatal period, although in other cases there is a late onset with milder symptoms. Up to date, no clear correlation has been found between the degree of enzyme deficiency in patients' fibroblasts, the clinical outcome and the genotype [9]. Recently, an animal model of PA was generated by creating *PCCA* knockout mice and also a transgenic strain expressing low levels of PCCA exclusively in the liver, both useful for the further understanding of PA pathogenesis and to test successful therapies of the disease [10].

PCC catalyses the ATP-dependent carboxylation of propionyl-CoA to D-methylmalonyl CoA. In the first half-reaction, catalysed by the α subunit, bicarbonate is

---

* Corresponding author. Tel.: +34-91-7347011; fax: +34-91-7347797.
E-mail address: mugarte@cbm.uam.es (M. Ugarte).

0925-4439/02/$ - see front matter © 2002 Elsevier Science B.V. All rights reserved.
PII: S0925-4439(02)00155-2

transferred to biotin upon hydrolysis of ATP to form carboxybiotin. The β subunit is responsible for the subsequent transfer of the carboxyl group of carboxybiotin to propionyl-CoA. In the α subunit, two functional domains have been identified by homology with other biotin-dependent carboxylases. They include a putative biotin carboxylase domain containing the ATP and bicarbonate-binding sites, and a C-terminal biotin-binding domain with the conserved A-M-K-M motif [11,12]. The homologous proteins biotin carboxylase and biotin carboxyl carrier protein (BCCP), subunits of acetyl-coA carboxylase from *Escherichia coli*, have been crystallized recently [13,14], providing a structural framework to study the effect of *PCCA* mutations.

Several expression studies have addressed the effect of *pccb* gene mutations on assembly and activity of the PCC enzyme [15–19]. However, extensive information on the effect of missense *pcca* mutations is still lacking, with only two reports describing defective biotinylation for the G668R mutation [12] and a reduced intramitochondrial stability of M373K [20]. In the present study, we report the expression of 11 *PCCA* mutations (10 missense and 1 in-frame deletion) in deficient fibroblasts and in a cell-free system with coupled import into rat liver mitochondria, with the aim of gaining further insight into the structure–function relationship of human PCCA protein and into the genotype–phenotype correlations in PA.

2. Methods

Primary fibroblasts from a *PCCA*-deficient patient carrying IVS21+3del4 mutation in homozygous fashion, were stably transformed by lipofection followed by phenotypic selection using the T22 plasmid which contains SV40 DNA sequences (kindly supplied by Dr. P.H. Gallimore) [21]. Previous studies had shown the absence of functional PCCA protein and undetectable PCC activity in the primary fibroblasts [22], which was also confirmed in the transformed cells. These cells were used in the transfection experiments with the expression vectors pCMVA45-12 and pRcCMVB52 (provided by Dr. Leclerc and Prof. Gravel), which code for the *PCCA* and *PCCB* cDNAs, respectively. Vectors containing the desired mutations were prepared by PCR mutagenesis using the Quickchange mutagenesis kit (Stratagene). *PCCA* mutations are named according to the recently defined novel initiation codon [6]. For the delEx21 mutation, caused by the effect of different mutations in exon 21 splice acceptor and donor sites [22], two oligos: 5′-GCACTCAGAGGACTGTCCAGTACAAGGTGAATA TCTTAAC-3′ and its complementary were used to delete nucleotides 1846–1899 comprising exon 21 from *PCCA* cDNA. The resulting cDNA codes for a PCCA protein lacking 18 amino acids (residues 616–634). For each of the other point mutations, two mutagenic oligos, sense and complementary antisense, were designed with 13–15 bases of correct sequence on both sides of the mutation. Sequence analysis confirmed the identity of the mutant clones.

Transfection was achieved by lipofection using Gene Porter™ (Gene Therapy System) as transfection reagent and following the manufacturer's recommendations. 0.6 × 10^6 cells were plated in 25-cm^2 flasks and transfected with 30 μl of lipid and a mixture of DNA containing 2 μg of each *PCCA* (wild-type or mutant) and *PCCB* constructs in serum-free medium. After 5 h incubation at 37 °C, the medium was replaced by MEM with 10% fetal calf serum. Cells were harvested 72 h after transfection and PCC activity assayed [23].

For the detection of biotin-bound proteins, transfected fibroblasts were harvested by trypsinization, resuspended in sucrose buffer (0.25 M sucrose, 10 mM Tris–HCl pH 7.4, EDTA 2 mM, PMSF 0.2 mM) and disrupted with a Teflon Potter homogenizer. Mitochondria were isolated by differential centrifugation at 4 °C [24], suspended in sucrose buffer and protein concentration determined by the Bradford assay. Equal amounts of total protein (100 μg) from each sample were loaded on a denaturing 6% polyacrylamide gel. After electrophoresis, proteins were transferred to PVDF membranes (Immobilon™-P, Millipore) and the biotin-containing proteins were detected with an avidin alkaline phosphatase conjugate (Pierce), using NBT/BCIP (Pierce) as alkaline phosphatase substrate for color development.

For in vitro transcription and translation, we used the pGEM-PCCA vector [20]. Mutations were introduced in the cloned *PCCA* cDNA using the Quickchange mutagenesis kit (Stratagene). One microgram of the resulting plasmids, normal or mutant, were used with the TnT Coupled Transcription/Translation kit (Promega) in the presence of [^{35}S]-Methionine+[^{35}S]-Cysteine (*Promix* L-[^{35}S] in vitro cell labelling mix, Amersham Pharmacia Biotech) for 60 min at 28 °C, following the manufacturer's protocol. Rat liver mitochondria were prepared according to previously described methods [25] and were used at 30–40 mg/ml in HMS buffer (2 mM HEPES, pH 7.4, 220 mM D-mannitol, 70 mM sucrose). Mitochondrial import was carried out with equal volumes of translation product and mitochondria, incubated at 30 °C for 60 min. The mitochondrial pellet was then separated from the supernatant by centrifugation, washed twice with HMS buffer, resuspended in the same buffer and further incubated at 37 °C, removing aliquots at different time points up to 24 h. After boiling in SDS buffer, samples were subjected to SDS-PAGE electrophoresis. The radioactive proteins were visualized after SDS-PAGE and fluorography. The bands were quantitated by laser densitometry.

Structural analysis of PCCA mutations was performed using homologous crystallized proteins available in the PDB database. The biotin carboxylase subunit of *E. coli* acetyl-CoA carboxylase (PDB coordinates 1DV2) [13] was used as a template for the biotin carboxylase domain of PCC (amino acids 64–513). Both the *E. coli* BCCP (PDB coordinates 1BDO) [14] and the 1.3 S subunit of the *Propionibacterium*

Table 1
PCC activities in *PCCA*-deficient fibroblasts transfected with wild-type or mutant *PCCA* constructs

Transfected construct(s)	PCC activity (pmol/min/mg protein)	Relative PCC activity[a] (%)
pRC/CMV	31.1 ± 10.4	–
pCMV-PCCA	580.8 ± 171.4	–
pCMV-PCCA + pCMV-PCCB	3432 ± 232.9	100
pCMV-PCCB + pCMV-PCCA with mutations:		
A75P	917.5 ± 53	26.7
R77P	125 ± 26.9	3.6
A138T	322.3 ± 37.1	9.4
I164T	544.7 ± 70.2	15.8
M229K	96.5 ± 34.6	2.8
D368G	148.6 ± 32	4.3
M373K	122.5 ± 55.9	3.5
G379V	185 ± 7.1	5.4
G631R	113.5 ± 27.6	3.3
G668R	48 ± 5.7	1.4
delEx21	36.3 ± 13.5	1.0
Control transformed fibroblasts	1123 ± 455	–

The data show the mean ± S.D. from at least two independent experiments.

[a] Residual activity relative to that obtained with cotransfection with wild-type *PCCA* and *PCCB* constructs.

shermanii transcarboxylase complex (PDB coordinates 1DCZ) [26] were used as templates for the biotinylation domain of PCCA (amino acids 621–728). Models were displayed using WebLab Viewer software (Molecular Simulations).

3. Results

3.1. Transient transfection in PCCA-deficient fibroblasts

The introduction of wild-type *PCCA* cDNA in the deficient fibroblasts resulted in a partial restoration of PCC activity (580 ± 171 pmol/min/mg protein). However, when both wild-type *PCCA* and *PCCB* cDNAs were cotransfected, enzyme activity levels were higher than for control transformed fibroblasts (3432 ± 232.9 pmol/min/mg protein versus 1123 ± 455 pmol/min/mg protein, respectively) (Table 1). This demonstrates that both subunits have been efficiently expressed, imported into mitochondria and assembled and that coordinated overexpression of both subunits is necessary to achieve maximal enzyme activity.

A total of 11 *PCCA* mutations were analyzed by transient transfection in *PCCA*-deficient fibroblasts, with cotransfection of wild-type *PCCB*. They include 10 missense mutations (A75P, R77W, A138T, I164T, M229K, D368G, M373K, G379V, G631R and G668R) and 1 in-frame deletion of 18 amino acids corresponding to exon 21 (delEx21), skipped in the mRNA as a consequence of different mutations in the splice donor and acceptor sites [22]. In all cases, PCC activity was clearly diminished compared to the results obtained with wild-type *PCCA*, demonstrating the pathogenicity of the mutations tested. Most mutant proteins resulted in < 5% residual activity; only those carrying A75P, A138T and I164T substitutions showed a low–intermediate PCC activity (26.7%, 9.4% and 16%, see Table 1).

Examination of the pattern of biotinylated mitochondrial proteins in transfected fibroblasts demonstrated similar amounts of α-PCC subunit for wild type and all mutations tested except for G668R (Fig. 1). No biotinylated G668R protein is detected, in accordance with previous reports showing it is defective in biotin binding [27]. A slightly smaller molecular weight is observed for the delEx21 mutant protein, which has an internal deletion of 18 amino acids.

3.2. Mitochondrial import and stability after in vitro synthesis

The cell-free transcription–translation assay of human *PCCA* cDNA cloned in the pGEM vector yields a major radioactive product with a molecular mass of 72 kDa on SDS-PAGE, as predicted for the precursor α-PCC protein, and which can be efficiently imported into rat liver mitochondria and processed to the mature form [20].

The different PCCA mutations described above were analyzed for mitochondrial import and stability after in vitro synthesis. G668R was not assayed as its major pathogenic effect is clearly a defect in biotynilation and M373K has already been analyzed by this method [20]. The remaining mutant proteins were synthesized, imported into mitochondria and converted into the mature form with comparable

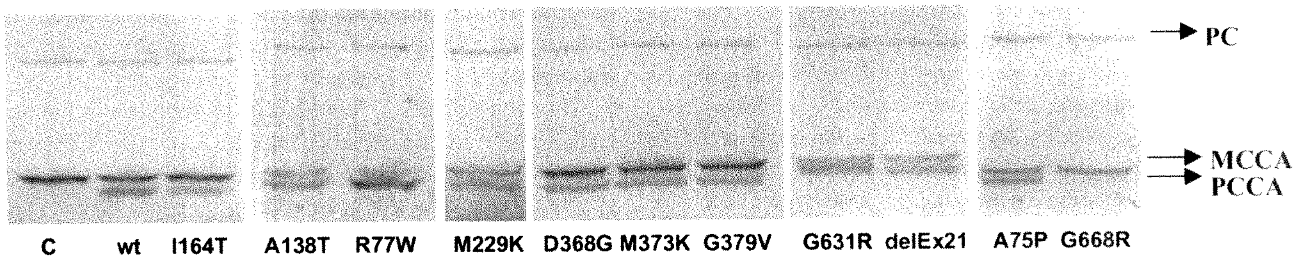

Fig. 1. Detection of biotinylated proteins in mitochondrial extracts of *PCCA*-deficient fibroblasts transfected with wild-type (wt) and mutant constructs. C, control of non-transfected deficient fibroblasts. PC, pyruvate carboxylase. MCCA, α-subunit of methylcrotonyl-CoA carboxylase.

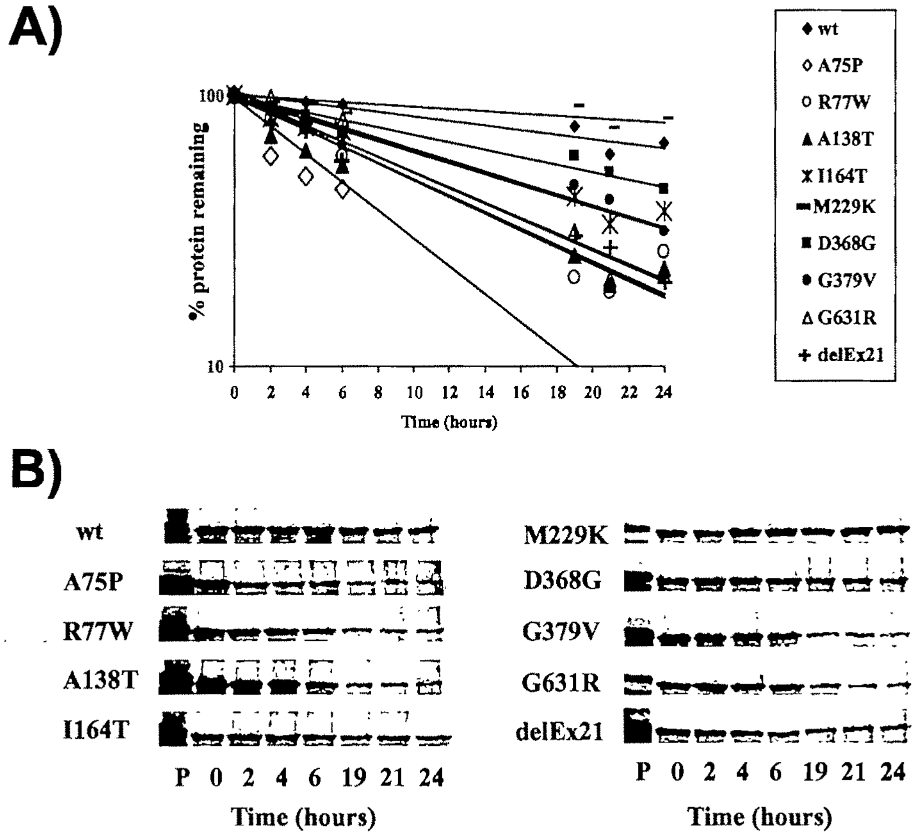

Fig. 2. Analysis of the intramitochondrial stability of wild-type and mutant PCCA proteins after in vitro synthesis and import into rat liver mitochondria. (A) Semilogarithmic plot of the mitochondrial degradation time courses of wild-type and mutant PCCA proteins. Labelled PCCA protein was quantitated by laser densitometry after SDS-PAGE and fluorography and the amount of residual mature PCCA expressed in percentages of the amount of imported protein in the sample at time 0. The results represent the mean from at least two experiments. (B) SDS-PAGE analysis of labelled wild-type and mutant PCCA protein turnover in mitochondria in a representative experiment. P, in vitro synthesized PCCA precursor before mitochondrial import.

efficiency to the normal protein. However, the intramitochondrial stability of most mutant proteins was clearly diminished compared to wild-type protein (Fig. 2). Only the mutant protein carrying M229K remains stable over the 24-h period; the rest are degraded more rapidly than the wild-type protein. This effect is very pronounced for A75P. Results from a representative experiment are shown in Fig. 2B.

4. Discussion

4.1. Functional effect of PCCA mutations

We have used a transformed deficient cell line to investigate the effect of mutations in the *PCCA* gene. The use of transformed cells was necessary to generate sufficient quantity of cells for repeated expression assays. We have shown that it is possible to complement the enzyme defect by transfecting with wild-type *PCCA* cDNA, as already reported [28]. However, normal levels of activity were never achieved (only around 50%). This limitation was overcome by cotransfection with wild-type *PCCB* cDNA, which resulted in 3- to 4-fold higher PCC activity than in control transformed fibroblasts. The overexpression of only one subunit probably interferes with the overall assembly and activity of the PCC complex, which may depend on a critical stoichiometric balance between the two subunits, as has been argued for other enzymatic complexes [21].

To prove that the mutations identified in patients within the *PCCA* coding sequence are responsible for the PCC deficiency, we introduced the mutations in the cDNA cloned in a pCMV expression vector and tested them in a transient expression system. All normal and mutant cDNAs produced significant levels of biotinylated proteins (except mutant G668R, defective in biotinylation), although the enzymatic activity was partially or severely diminished.

The crystallized *E. coli* biotin carboxylase subunit of acetyl-CoA carboxylase and both the *E. coli* BCCP protein and the 1.3 S subunit of *P. shermanii* transcarboxylase were used as models to study the structural effect of the *PCCA* mutations (Figs. 3 and 4). All mutated residues are well conserved in homologous proteins. Biotin carboxylase belongs to a large family of proteins characterized by an ATP-grasp fold [29]. The residues involved in *PCCA* mutations mapping to this domain were all found to cluster together in the three-dimensional structure, with the exception of M229K (Fig. 3). Residue M229 forms part of a hydrophobic pocket well conserved in all biotin carboxylases and in related structures, namely D-Ala:D-Ala ligase and glutathione synthase [30], which is involved in the interaction with the adenine moiety of the ATP. M229 lies within approximately 4.5 Å of the ATP [13]. It has been suggested that the substitution for Lys destabilizes the pocket and reduces ATP binding, although the protein is stable and binds biotin, as shown in patients' fibroblasts [27]. The remaining biotin carboxylase domain *PCCA* mutations (A75P, R77W, A138T, I164T, D368G M373K and G379V) map in close proximity in the crystalline structure (Fig. 3), clearly defining a region probably important for function and/or stability of the α subunit. This region lies exactly opposite away from the active site, which was defined after modelling the relative positions of bound biotin and ATP in *E. coli* biotin carboxylase [13]. A direct effect on catalysis is therefore unlikely, and the mutations are most likely affecting the structure of the protein. This structural alteration may affect the active site, but in vivo, the abnormally folded proteins are probably recognized and rapidly degraded as has been described in other diseases [31]. This is consistent with the fact that no protein is detected in patient's cells and with the observed accelerated mutant protein turnover after in vitro synthesis and mitochondrial import. Only after overexpression of the proteins in the transfection experiments is it possible to detect the biotinylated mutant proteins in levels comparable to wild-type protein. These results confirm that the folding of the biotin carboxylase domain does not influence the biotinylation reaction. In fact, most of the PCCA protein does not seem to play a role in this, as the C-terminal 67 residues alone can act as a substrate for biotinylation by the BirA protein of *E. coli* [12]. However, in the expression experiments, the correctly biotinylated mutant proteins are defective in enzymatic activity. The defect in folding/structure could also be affecting the normal assembly with the β-subunit to produce a functional PCC oligomer. The putative folding defects may be analyzed by transient transfection of cells grown at lower temperature, improving folding and thus allowing to measure the effect (if any) of the mutations on the catalytic activity. This interesting experimental approach has been reported for several disease-causing mutations [32].

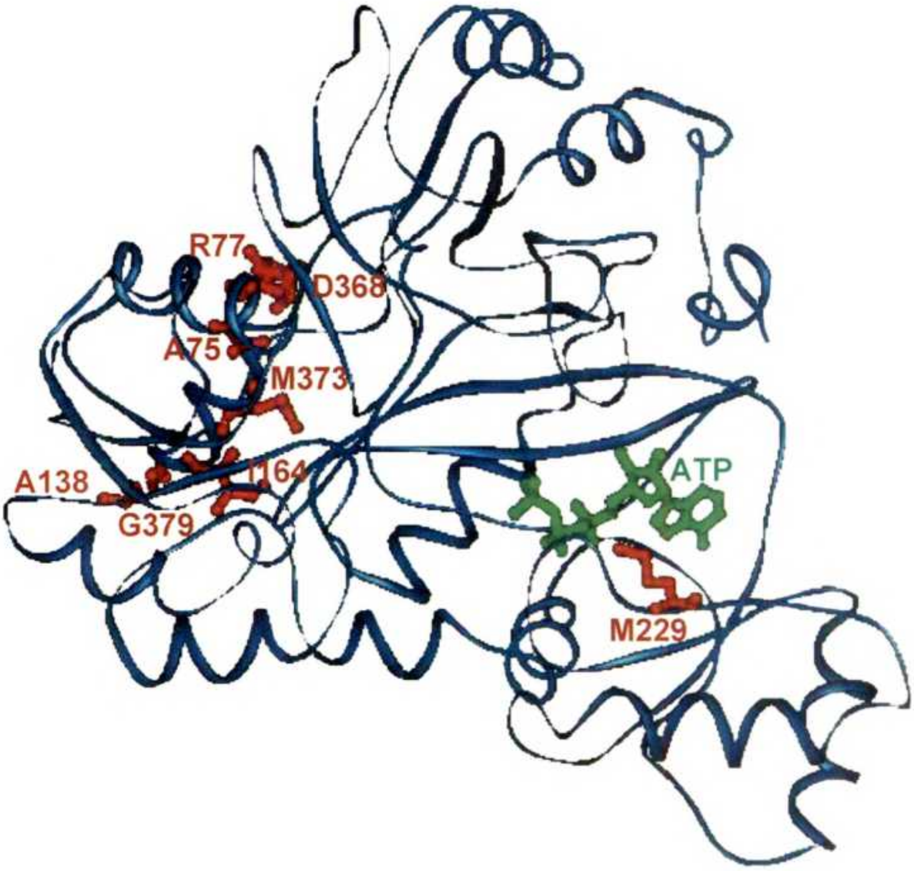

Fig. 3. Modelling of the PCCA biotin carboxylase domain against the *E. coli* biotin carboxylase subunit of acetyl-CoA carboxylase complexed with ATP (PDB accession number 1DV2). The PCCA missense mutations found in the biotin carboxylase domain are positioned by alignment with the *E. coli* sequence where the normal residues are displayed as red ball and stick structures.

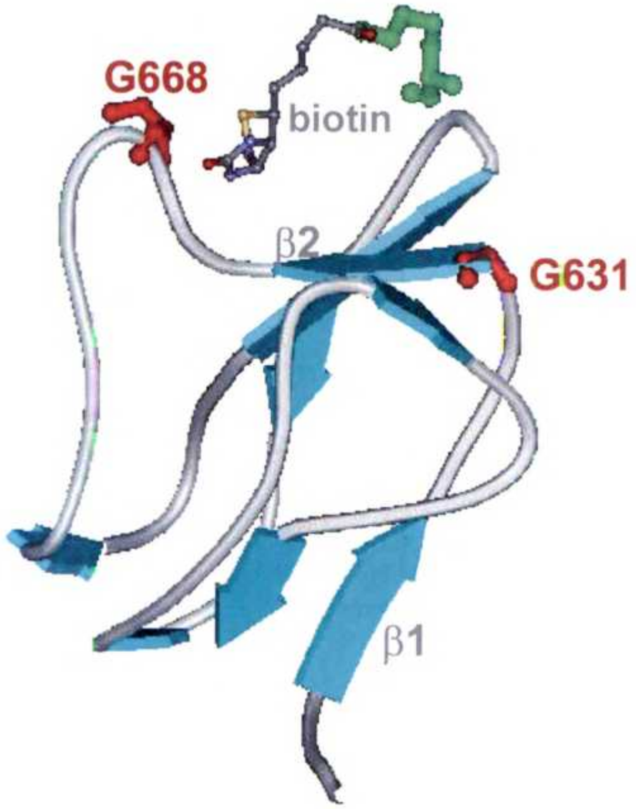

Fig. 4. Modelling of the PCC biotinylation domain against the *E. coli* BCCP of acetyl-CoA carboxylase (PDB accession number 1BDO). PCCA mutations are identified by alignment and normal residues involved are represented as red ball and stick structures.

Mutations G631R and G668R as well as delEx21 map to the biotinylation domain (Fig. 4). No biotinylated protein nor residual activity is detectable with the G668R mutation. It is highly probable that the protein is unstable, as in BCCP it has been described that the apoenzyme is less stable than the holoenzyme, and that biotin binding induces a conformational change resulting in increased protease resistance [33]. Both the deletion of exon 21 which eliminates beta strands β1 and β2, and mutation G631R, are compatible with a normal biotinylation of the PCCA protein, as seen in the expression studies, although the mutant proteins are inactive. Residue G631 is very well conserved in acetyl-CoA carboxylases from different species and in related structures corresponding to lipoyl domains of pyruvate dehydrogenase, glycine decarboxylase and 2-oxoglutarate dehydrogenase from different species. Both G631R and delEx21 result in proteins with an accelerated turnover in rat liver mitochondria after in vitro synthesis, which may also be the main molecular effect in the patient's cells.

4.2. Genotype–phenotype correlations

The clinical spectrum of PCC deficiency is extremely broad, and, in the case of *PCCA*-deficient patients, the establishment of genotype–phenotype correlations is hampered by the extensive genetic heterogeneity and by the fact that most patients are compound heterozygotes (Table 2).

M373K and G631R changes are present in homozygous patients presenting a severe phenotype. This is in accordance with the expression assays where they exhibit null activity and accelerated protein turnover. The mild phenotype of the patients with A138T (homozygous) and I164T (hemyzygous, with a frameshift mutation on the second allele) is also in agreement with the partial residual activity recovered after transient expression (9% and 16%, respectively). Although steady-state protein is undetectable in patients' fibroblasts, newly synthesized or residual protein with partial activity could contribute to the milder phenotypic expression of the disease. This may also be the case of A75P, associated with 26.7% residual activity, but which in contrast is the least stable after mitochondrial import in the cell-free system (Fig. 2). A75P is present in a heterozygous patient, with a moderate psychomotor delay. In this case, the contribution of each mutant allele (A75P and G379V) to the phenotype is difficult to evaluate.

The skipping of exon 21 in the mRNA produces an in-frame deletion of 18 amino acids (616–634) in the PCCA protein. Expression of the cDNA with the corresponding

Table 2
Genotypes, clinical presentation and biotinylation status of αPCC subunit of PA patients bearing PCCA mutations expressed in this work

Patient	Genotype	Clinical presentation	Percentage PCC activity in patients' fibroblasts	Biotinylated αPCC subunit in fibroblasts	Reference
3131 (BE)	A75P/G379V	Moderate	no data	No	[27]
SAG	R77W/delEx21	Mild	3.5	Yes[a]	[9]
JMMO	A138T/A138T	Mild	4	No	[9]
ESG	I164T/S147fs	Mild	4	No	[9]
2967 (AG)	M229K/ND	Mild	0.6[b]	Yes	[27]
3144 (NM)	D368G/delEx20-21	Severe	2	No	[27]
JN	M373K/M373K	Severe	2	No	[20]
MSH	delEx21/delEx21	Moderate	1.3	No	[9]
DFH, JCS, TC	G631R/G631R	Severe	≤ 1	No	[9]; this work
3135	G668R/delEx22	Severe	no data	No	[27]

Mild: patient alive with near-normal development. Moderate: Patient alive with moderate psychomotor delay. Severe: patient dead or severely retarded.

[a] Yes: faint band of αPCC of normal size.

[b] PCC activity measured in patient's leukocytes.

deletion produces a protein devoid of enzymatic activity and rapidly degraded intramitochondrially. However, patient MSH, homozygous for this change, presents a moderate phenotype. In this patient, the genomic lesion is a short deletion (four nucleotides) in position +3 in the 5′ splicing donor site. Although a standard RT-PCR did not detect the presence of a correctly spliced transcript [22], this cannot be excluded as the invariant GT is conserved and the Shapiro splicing score is reduced to only 75%. Real-time PCR experiments and/or in vitro splicing analysis with minigenes could be employed to study this possibility, which could explain a less severe phenotypic expression in patients.

Patient AG with a mild phenotype carries mutation M229K and a yet unidentified mutation not expressed in the cDNA on the second allele, so the patient can be considered hemizygous (M229K plus a functionally "null" allele). M229K mutant protein is the only one of our series that is stable after import to mitochondria (Fig. 2), which is consistent with the detection of normal amounts of biotinylated protein in patients' cells. However, no residual activity is detectable in the PCC assay, which does not allow the analysis of the affinity for ATP.

In summary, the high genetic heterogeneity in the *pcca* gene defies the drawing of simplistic conclusions on the genotype–phenotype correlations. The characterization of other mutations, newly identified as more patients are analyzed, is necessary to get a deeper understanding on the structure and function of PCC and the relationship to disease phenotype.

Acknowledgements

The authors wish to thank C. Hernández, A. Sánchez and R. Navarrete for their helpful technical assistance. This work was supported by grants from Fondo de Investigaciones Sanitarias (01/0405). The financial support of Fundación Ramón Areces to the Centro de Biología Molecular "Severo Ochoa" is gratefully acknowledged. S.C. was supported by Comunidad Autónoma de Madrid and M.A.M. was supported by Fondo de Investigaciones Sanitarias.

References

[1] W.A. Fenton, R.A. Gravel, L.E. Rosenberg, in: C.R. Scriver, A.L. Beaudet, W. Sly, D. Valle (Eds.), The Metabolic and Molecular Bases of Inherited Disease, 8th ed., McGraw-Hill, New York, 2001, pp. 2165–2190.
[2] L.E. Rosenberg, W.A. Fenton, A.L. Horwich, F. Kalousek, J.P. Kraus, Ann. N.Y. Acad. Sci. 488 (1986) 99–108.
[3] T. Ohura, K. Narisawa, K. Tada, J. Inherit. Metab. Dis. 16 (1993) 863–867.
[4] J. Stankovics, F.D. Ledley, Am. J. Hum. Genet. 52 (1993) 144–151.
[5] A. Lamhonwah, D. Leclerc, M. Loyer, R. Clarizio, R.A. Gravel, Genomics 19 (1994) 500–505.
[6] E. Campeau, L.R. Desviat, D. Leclerc, X. Wu, B. Perez, M. Ugarte, R.A. Gravel, Mol. Genet. Metab. 74 (2001) 238–247.
[7] P. Rodríguez-Pombo, J. Hoenicka, S. Muro, B. Pérez, C. Pérez-Cerdá, E. Richard, L.R. Desviat, M. Ugarte, Am. J. Hum. Genet. 63 (1998) 360–369.
[8] M. Ugarte, C. Pérez-Cerdá, P. Rodríguez-Pombo, L.R. Desviat, B. Pérez, E. Richard, S. Muro, E. Campeau, T. Ohura, R.A. Gravel, Hum. Mutat. 14 (1999) 275–282.
[9] C. Pérez-Cerdá, B. Merinero, P. Rodríguez-Pombo, B. Pérez, L.R. Desviat, S. Muro, E. Richard, M.J. García, J. Gangoiti, P. Ruiz-Sala, P. Sanz, P. Briones, A. Ribes, M. Martínez-Pardo, J. Campistol, M. Pérez, R. Lama, M.L. Murga, T. Lema-Garrett, A. Verdú, M. Ugarte, Eur. J. Hum. Genet. 8 (2000) 187–194.
[10] T. Miyazaki, T. Ohura, M. Kobayashi, Y. Shigematsu, S. Yamaguchi, Y. Suzuki, I. Hata, Y. Aoki, X. Yang, C. Minjares, I. Haruta, H. Uto, Y. Ito, U. Muller, J. Biol. Chem. 276 (2001) 35995–35999.
[11] D. Samols, C.G. Thornton, V.L. Murtif, G.K. Kumar, F.C. Haase, H.G. Wood, J. Biol. Chem. 263 (1988) 6461–6464.
[12] A. Leon-del-Rio, R.A. Gravel, J. Biol. Chem. 269 (1994) 22964–22968.
[13] J.B. Thoden, C.Z. Blanchard, H.M. Holden, G.L. Waldrop, J. Biol. Chem. 275 (2000) 16183–16190.
[14] F.K. Athappilly, W.A. Hendrikson, Structure 3 (1995) 1407–1419.
[15] T.L. Kelson, T. Ohura, J.P. Kraus, Hum. Mol. Genet. 5 (1996) 331–337.
[16] K. Ravn, M. Chloupkova, E. Christensen, N.J. Brandt, H. Simonsen, J.P. Kraus, I.M. Nielsen, F. Skovby, M. Schwartz, Am. J. Hum. Genet. 67 (2000) 203–206.
[17] M. Chloupkova, K. Ravn, M. Schwartz, J.P. Kraus, Mol. Genet. Metab. 71 (2000) 623–632.
[18] S. Muro, B. Pérez, P. Rodríguez-Pombo, L.R. Desviat, C. Pérez-Cerdá, M. Ugarte, J. Inherit. Metab. Dis. 23 (2000) 300–304.
[19] S. Muro, B. Perez, L.R. Desviat, P. Rodríguez-Pombo, C. Perez-Cerda, S. Clavero, M. Ugarte, Mol. Genet. Metab. 74 (2001) 476–483.
[20] E. Richard, L.R. Desviat, B. Pérez, C. Pérez-Cerdá, M. Ugarte, Biochim. Biophys. Acta 1453 (1999) 351–358.
[21] R.M. Brown, L.J. Otero, G.K. Brown, Hum. Mol. Genet. 6 (1997) 1361–1367.
[22] E. Richard, L.R. Desviat, B. Pérez, C. Pérez-Cerdá, M. Ugarte, Hum. Genet. 101 (1997) 93–96.
[23] T. Suormala, H. Wick, J.P. Bonjour, E.R. Baumgartner, Clin. Chim. Acta 145 (1985) 151–162.
[24] S.E. Old, D.C. DeVivo, Ann. Neurol. 26 (1989) 746–754.
[25] J. Loewenstein, H.R. Scholte, E.M. Wit-Peeters, Biochim. Biophys. Acta 223 (1970) 432–436.
[26] D.V. Reddy, B.C. Shenoy, P.R. Carey, F.D. Sonnichsen, Biochemistry 39 (2000) 2509–2516.
[27] E. Campeau, L. Dupuis, A. Leon-del-Rio, R.A. Gravel, Mol. Genet. Metab. 67 (1999) 11–22.
[28] C. Pérez-Cerdá, L.R. Desviat, B. Perez, M. Ugarte, P. Rodriguez-Pombo, Mol. Genet. Metab. 75 (2002) 276–279.
[29] M.Y. Galperin, E.V. Koonin, Protein Sci. 6 (1997) 2639–2643.
[30] P.J. Artymiuk, A.R. Poirrette, D.W. Rice, P. Willett, Nat. Struct. Biol. 3 (1996) 128–132.
[31] P. Bross, T.J. Corydon, B.S. Andresen, M.M. Jorgensen, L. Bolund, N. Gregersen, Hum. Mutat. 14 (1999) 186–198.
[32] N. Gregersen, P. Bross, M.M. Jorgensen, T.J. Corydon, B.S. Andresen, J. Inherit. Metab. Dis. 23 (2000) 441–447.
[33] A. Chapman-Smith, B.E. Forbes, J.C. Wallace, J.E. Cronan Jr., J. Biol. Chem. 272 (1997) 26017–26022.

ELSEVIER

Biochimica et Biophysica Acta 1588 (2002) 126–134

BIOCHIMICA ET BIOPHYSICA ACTA
BBA
www.bba-direct.com

Age-related changes in cartilage endogenous osteogenic protein-1 (OP-1)

Susan Chubinskaya[a,b,*], Bhavna Kumar[a], Charis Merrihew[a], Katherine Heretis[a],
David C. Rueger[c], Klaus E. Kuettner[a,d]

[a]*Department of Biochemistry, Rush Medical College, Rush-Presbyterian-St. Luke's Medical Center, 1653 W. Congress Parkway, Chicago, IL 60612, USA*
[b]*Section of Rheumatology, Rush Medical College, Rush-Presbyterian-St. Luke's Medical Center, 1653 W. Congress Parkway, Chicago, IL 60612, USA*
[c]*Stryker Biotech, 35 South Street, Hopkinton, MA 01742, USA*
[d]*Department of Orthopedic Surgery, Rush Medical College, Rush-Presbyterian-St. Luke's Medical Center, 1653 W. Congress Parkway, Chicago, IL 60612, USA*

Received 1 April 2002; received in revised form 25 June 2002; accepted 27 June 2002

Abstract

Articular cartilage has a poor reparative capacity. This feature is exacerbated with aging and during degenerative joint conditions, contributing to loss of motion and impairment of quality of life. This study focused on osteogenic protein-1 (OP-1) and its ability to serve as a repair-stimulating factor in articular cartilage. The purpose of this work was to develop a quantitative method for the assessment of the content of OP-1 protein in extracts from human articular cartilage and to investigate the changes in OP-1 mRNA expression and protein levels with aging of normal adult cartilage. Full thickness cartilage was dissected from femoral condyles of donors with no history of joint disease within 24 h of death. Levels of OP-1 mRNA expression were measured by a semi-quantitative reverse transcription-polymerase chain reaction (RT-PCR) method; concentration of OP-1 protein was detected by new sandwich enzyme-linked immunosorbent assay (ELISA); qualitative changes in OP-1 forms were evaluated by Western blots with various anti-OP-1 antibodies. The sensitivity of the ELISA method allowed the detection of picogram quantities of OP-1 in cartilage extracts. We found that (1) concentration of OP-1 in normal cartilage is within the range of biological activity of OP-1 in vitro; and (2) during aging of human adult, articular cartilage, levels of OP-1 protein and message are dramatically reduced (more than 4-fold; $p<0.02$). The major qualitative changes affected primarily mature OP-1. The results of the current study suggest the possibility that OP-1 may be critical for chondrocytes to maintain their normal homeostasis and could also serve as a repair factor during joint disease or aging.

© 2002 Elsevier Science B.V. All rights reserved.

Keywords: Human articular cartilage; Aging; Bone morphogenetic protein; Osteogenic protein-1; ELISA; PCR

1. Introduction

Osteoarthritis (OA) is a debilitating joint disease affecting primarily the elderly. OA is rare in young adults, developing symptomatically and radiographically in adults by their late 40s and 50s, and then, rapidly increases in prevalence from age 60 to 70 [1]. However, the mechanisms that turn normal aging of articular cartilage into the pathological OA process are currently unknown. In general, as any biological tissue or organ ages, function gradually declines and susceptibility to disease and injury increases [2]. During the last decade, a number of age-related changes in cartilage have been documented: (1) an increased denaturation of collagen type II [3]; (2) a decline in synthesis of DNA [4], proteoglycans (PG) and link protein [5–8]; (3) an increased sulfation of chondroitin sulfate [9]; (4) accumulation of hyaluronan [10] and cartilage intermediate layer protein [11]; (5) structural changes in fibromodulin [12]; (6) a decreased capability of assembling large molecular size aggregates [7]; (7) elevated levels of transglutaminase activity that promotes a pathologic matrix mineralization and cartilage degeneration [13]; and (8) increased apoptosis [14]. Importantly, with aging, the responsiveness of articular cartilage to different growth factors, such as transforming growth factor-β (TGF-β) [6,15], insulin-like growth factor-1 (IGF-1) [16], epidermal growth factor (EGF) [4], osteogenic protein-1 (OP-1) [17] and others, was also changed.

While the underlying causes of articular cartilage degeneration seen with age have not been identified, there is increasing evidence that cytokines and growth factors,

---

[*] Corresponding author. Department of Biochemistry, Rush Medical College, Rush-Presbyterian-St. Luke's Medical Center, 1653 W. Congress Parkway, Chicago, IL 60612, USA. Tel.: +1-312-942-6699; fax: +1-312-942-3053.

E-mail address: schubins@rush.edu (S. Chubinskaya).

0925-4439/02/$ - see front matter © 2002 Elsevier Science B.V. All rights reserved.
PII: S0925-4439(02)00158-8

especially those expressed endogenously in cartilage, play a critical mediatory role. Since growth factors, and particularly members of the bone morphogenetic protein family (BMP), are important regulators of matrix production that can also inhibit certain degradative processes, it is not difficult to envision how a loss in the biologically active endogenous growth factor could play a role in the development of matrix damage.

BMPs were originally identified as proteins capable of inducing ectopic endochondral bone formation in subcutaneous implants [18,19]. Subsequent molecular cloning revealed that the BMP family consists of a large number of related molecules that belong to the TGF-β superfamily. Although BMPs were initially found in the bone matrix, it is now clear that they are expressed in a variety of tissues. OP-1 is the seventh member of this family (BMP-7). It is synthesized as a large precursor, approximately three times larger than a mature protein, and is ultimately processed proteolytically at the C-terminal region to yield a mature disulfide-linked dimer. OP-1 is the most closely related to BMP-6 and BMP-5 (88% and 87% homology), and to a lesser extent to BMP-2 and BMP-4 (60% and 58%), with some homology to BMP-3 (42%) and TGF-β (about 30%) [20,21]. Originally, OP-1 was purified from bovine demineralized bone [22] with its recombinant form being subsequently cloned from human cDNA libraries in Chinese hamster ovary (CHO) cells [23]. The critical importance of BMPs for cartilage and bone formation was demonstrated using the transgenic approach: lack of some BMP genes caused skeletal abnormalities and eventually the lethality of mouse embryos [24,25]. Recent studies from our department [17,26–28] have focused on the potential role of exogenous OP-1 in human and bovine cartilage homeostasis and repair. We showed that human recombinant OP-1 caused a significant anabolic response in articular cartilage. It induced the synthesis of major matrix components (aggrecan and collagen type II) in human chondrocytes of different age [17,26] with continued expression of the chondrocyte phenotype. In addition, OP-1 has been shown to induce the synthesis of hyaluronan, its receptor CD44 and hyaluronan synthase-2, to promote the formation and retention of the extracellular matrix [28], and to counteract catabolic events, such as interleukin-1 (IL-1), fibronectin and collagen fragment-induced human cartilage degeneration [26,27,29]. When the effect of OP-1 on the Fn-f-challenged cartilage was compared to that of TGF-β, it was found that TGF-β was not able to block Fn-f-mediated PG depletion, but by itself promoted a decrease in cartilage PG content [27]. Importantly, recombinant OP-1 did not lead to chondrocyte proliferation and differentiation in human and bovine adult articular cartilage during short-term culture [17,30].

Noteworthy, we previously showed [31] that OP-1 is endogenously expressed by human adult articular chondrocytes. Moreover, in human articular cartilage, OP-1 is present in two forms, unprocessed, pro-form, and processed, mature-form, that are distributed in the inverted manner. Mature OP-1 is immunolocalized primarily in the superficial layer of cartilage, while pro-OP-1 is detected in the deep layer. The endogenous expression of OP-1 by articular chondrocytes indicates that articular cartilage has the potential to repair and might suggest the unique role of this BMP in tissue protection and regeneration. This is supported by recent data [32] where overexpression of OP-1 in mice led to the increased synthesis of matrix macromolecules, collagen type II and PGs.

The purpose of the current study was to investigate changes in endogenous OP-1 (protein and mRNA) with aging of human articular cartilage. We hypothesized that with aging, there will be a decline in the levels of endogenous OP-1, primarily, mature form of the protein, that might contribute to the elevated susceptibility of cartilage to the degenerative processes. To assess quantitatively the concentration of total endogenous OP-1 protein in cartilage extracts, we developed a sandwich OP-1 enzyme-linked immunosorbent assay (ELISA). We present here a quantitative data on age-related changes in endogenous OP-1 mRNA and protein and provide a qualitative analysis of these changes.

2. Materials and methods

2.1. Reagents

Human recombinant pro- and mature-OP-1, BMP-6, anti-pro (R2854) and anti-mature (1B12) OP-1 antibodies were provided by Stryker Biotech (Hopkinton, MA). Two other, anti-mature OP-1 antibodies (sc-9305 and MAB 354) were purchased from Santa Cruz Biotechnology (Santa Cruz, CA) and R&D Systems (Minneapolis, MN). Electrophoresis grade reagents were purchased from Bio-Rad (Hercules, CA). Chemicals, either reagent or molecular biology grade, were purchased from Sigma (St. Louis, MO) unless otherwise noted. Keratanase (Ker; *Pseudomonas* sp.; EC 3.2.1.103), keratanase II (Ker II; *Bacillus* sp. Ks 36) and chondroitinase ABC (CHase; *Proteus vulgaris*; EC 4.2.2.2) were obtained from Seikagaku, Japan. Hyaluronidase (bovine testicular) was purchased from Sigma and Collagenase P (*Clostridium histolyticus*) was purchased from Boehringer Mannheim.

2.2. Tissue acquisition

Full thickness normal human articular cartilage was dissected from load bearing regions of femoral condyles of donors with no history of joint disease within 24 h of death. Samples from men and women ranging from 20 to 80 years old were obtained, with institutional approval, through the Regional Organ Bank of Illinois according to their protocol. After opening the joint, the surface of the cartilage was grossly examined. Although all cartilages were obtained from normal donors, not all of them appeared to be normal. Some samples revealed degenerative morphological changes. All cartilages were processed for either messenger RNA or protein extraction.

2.3. OP-1 antibodies

We used four different antibodies for this study. Antibodies obtained from Stryker Biotech (R2854 and 1B12) were previously described and specificity toward OP-1 was tested [31,33–35]. The polyclonal antibody R2854 was raised in rabbits against the monomeric pro-domain of the OP-1 molecule. For the detection of the mature domain of OP-1, we utilized three antibodies that were available to us either from commercial sources or from Stryker Biotech. Two monoclonal antibodies, 1B12 and MAB354, were raised against the monomeric mature domain of OP-1. A third, polyclonal antibody sc-9305 was raised against a 15-amino-acid synthetic peptide within the N-terminus of the mature OP-1 domain. The specificity of all antibodies was tested by the companies that produced these antibodies. However, taking into consideration the high homology between OP-1 and BMP-6 and the fact that the recombinant BMP-6 was cloned after the anti-OP-1 antibodies were produced, all antibodies used for the current study were tested for cross-reactivity with BMP-6 (Fig. 1).

2.4. Cartilage extraction

Five hundred milligrams of fresh donor cartilage was lyophilized overnight and the dry weight of the tissue was determined. Samples were pulverized in liquid nitrogen and 150 mg (dry weight) of cartilage tissue was extracted with 3.5 ml of ice-cold 1 M GuHCl buffer, pH 7.5, containing 10 mM $CaCl_2$, 50 mM Tris, and protease inhibitors (Protease inhibitor cocktail tablets, one tablet per 10 ml of ice-cold 1 M GuHCl buffer; Roche Diagnostics, Indianapolis, IN). The extraction was performed at 4 °C for 4 h with rotation. Supernatants were centrifuged at 2500 rpm for 10 min at 4 °C, dialyzed for 2 days in water (12,000–14,000 MW cutoff) and stored at 4 °C. To prove the efficiency of the extraction, the cartilage tissue underwent a second extraction after the supernatants were removed. These extracts were also analyzed by Western blotting and ELISA.

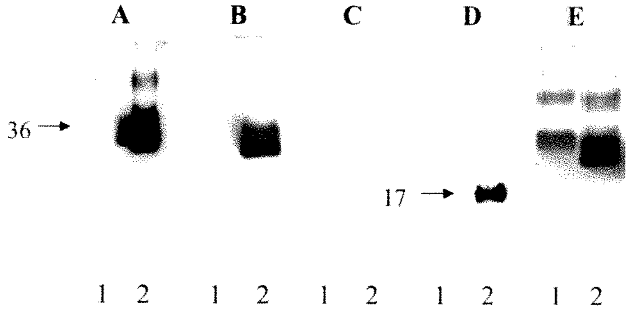

Fig. 1. Specificity of different anti-OP-1 antibodies as detected by Western blotting. (A) Anti-mature OP-1 antibody sc-9305 (Santa Cruz Biotechnology); (B) anti-mature OP-1 antibody 1B12 (Stryker Biotech); (C) anti-pro-OP-1 antibody R2854 (Stryker Biotech); (D) anti-mature OP-1 antibody MAB354 (R&D Systems); (E) antibody that recognizes both BMP-6 and BMP-7. Lane 1, recombinant BMP-6; Lane 2, recombinant BMP-7. A, B, C, and E—proteins were loaded under non-reduced conditions; D—proteins were reduced with 10% β-mercaptoethanol. Immunoreactive band at 36 kDa corresponds to mature OP-1 dimer; band at 17 kDa corresponds to mature OP-1 monomer; bands above 36 kDa correspond to the aggregates of the recombinant proteins. These data prove the specificity of the antibodies toward OP-1 protein.

2.5. SDS-PAGE and Western blot analysis

2.5 mg dry weight of each sample (lyophilized) was solubilized in a buffer containing 10 mM Tris, pH 6.5, 1% SDS, 10% glycerol, 0.016% bromphenol blue. Samples were loaded onto SDS-PAGE gel under reduced (with 2-mercaptoethanol) or non-reduced conditions. Western blots were performed following 12% SDS-PAGE gels. To reduce non-specific binding, blots were incubated with blocking solution containing 5% non-fat dry milk (Bio-Rad) in Tris-buffered saline with 0.05% Tween 20 (TBS/Tween) (Bio-Rad) for 1 h at room temperature. The blots were incubated with primary antibody at suggested dilutions in TBS/Tween: 1:250 for R2854 and MAB354 anti-OP-1 antibodies, and 1:100 for sc-9305 antibody. As a secondary antibody, either ImmunoPure goat anti-mouse IgG (Pierce, Rockford, IL) or donkey anti-rabbit IgG (Pierce) conjugated with horseradish peroxidase at 1:10,000 dilutions in TBS/Tween was used. The blots were developed with the Enhanced Chemiluminescent (ECL-Plus) kit for Western blotting (Amersham Pharmacia Biotech, England). Specificity of the binding was compared with the binding of the antibodies to recombinant pro- or mature OP-1. Secondary antibodies were also tested for non-specific binding. The densities of specific immunoreactive bands was scanned by Fluor-S MultiImager (Bio-Rad) and quantified by Quantity One Software program (Bio-Rad).

2.6. Chemiluminescent sandwich ELISA

For sandwich ELISA, two anti-OP-1 antibodies, polyclonal sc-9305 and monoclonal 1B12, were used. Polyclonal anti-OP-1 antibody was utilized as a coating antibody. Plates were coated with 50 ng/well of this antibody in TBS, pH 7.5, and incubated overnight at 4 °C. Non-specific binding was blocked with 200 μl/well blocking solution (5% non fat dry milk in TBS/Tween, pH 7.5) for 2 h at room temperature. To generate a standard curve, mature recombinant OP-1 was diluted in TBS/Tween at different concentrations ranging from 10 to 0.01 ng/ml. Either OP-1 standard (100 μl) or cartilage extract was added to the plate and incubated for 1 h at room temperature. Second anti-OP-1 antibody (1B12) was applied at 1:1000 dilution in TBS/Tween and incubated at room temperature for 1 h. ImmunoPure goat anti-mouse IgG peroxidase conjugated antibody (Pierce) was used at 1:10,000 dilution as a secondary antibody. The reaction was developed with Supersignal ELISA Femto Maximum Sensitivity Substrate (Pierce).

The data were obtained through chemiluminescent ELISA plate reader Victor2 (Wallac) as relative light units (RLU).

2.7. Reverse transcription-polymerase chain reaction (RT-PCR)

Total RNA was extracted directly from cartilage tissue with acid-guanidinium thiocyanate as previously described [36]. Specific primer pairs were constructed for OP-1 [31] and glyceraldehyde-3-phosphate dehydrogenase (GAPDH). These primer pairs were designed to yield PCR products of different sizes (319 base pairs [bp] for GAPDH and 313 bp for OP-1). OP-1 primers used for nested RT-PCR: (a) 21-mer, antisense, location 1810–1830, 5′-TTTTCCTTTCGC-ACAGACACC-3′; (b) 20-mer, sense, location 1328–1347, 5′-TGCCATCTCCGTCCTCTACT-3′; and (c) 23-mer, sense, location 1518–1540, 5′-TTCCCCTCCCTATCCCCAACTT-T-3′. The specificity of the primers was previously proven [31]. GAPDH primers were: sense, 5′-GGTATCGTGGAAG-GACTCAT-3′ and antisense, 5′-ACCACCTGGTGCTCA-GTGTA-3′. Approximately 1 μg of total RNA was trans- cribed using reverse transcriptase as described by Cs-Szabo et al. [36]. Five microliters of the resulting cDNA was am-plified by PCR using *Taq* DNA polymerase (Promega, Madi-son, WI) in the presence of specific upstream and down-stream primers [15 pM each; primers (a) and (b) for OP-1 gene]. 0.5 microliters of the first amplification product and a second sense primer [primer (c); nested primer] was used for a subsequent amplification step. To perform RT-PCR at the optimal conditions and to stay within the logarithmically linear product formation, 30 cycles were chosen (45 s at 95 °C, 30 s at 57 °C of annealing temperature and 45 s at 72 °C for the primers used), followed by the final extension for 5 min at 72 °C. PCR products were separated in 3% Metaphor agarose gels (FMC BioProducts, Rockland, ME) and visualized by ethidium bromide staining. Densities of the bands were measured using Fluor S MultiImager (Bio-Rad) with attached Quantity one software program (Bio-Rad). The densities of the OP-1 bands were normalized to the densities of the GAPDH bands to control variability among samples.

2.8. Statistical analysis

All results shown are mean ± S.D. of at least three separate experiments, with triplicate determination for each point. Covariation significance was determined by Pearson correlation of normal data.

3. Results

3.1. Antibody specificity

For the current study, we have used either commercially available antibodies or antibodies produced by Stryker Biotech. Although the specificity of these antibodies was previously proven, we have tested their cross-reactivity to the closely related member of the BMP family, BMP-6, of which the recombinant form became recently available. As a positive control, human recombinant processed (mature) OP-1 dimer was used (molecular weight is 36 kDa for dimer and 17 kDa for the reduced monomer). It is important to mention that with storage, recombinant OP-1 might form higher molecular weight aggregates that could be detected by the antibodies as a higher molecular weight band. In Fig. 1A–C, and E, BMP-6 and -7 were loaded onto the gels under non-reduced conditions; while in Fig. 1D, these proteins were reduced with 10% β-mercaptoethanol. As shown in Fig. 1, anti-mature OP-1 antibodies sc-9305 (Fig. 1A), 1B12 (Fig. 1B) and MAB354 (Fig. 1D) clearly recognized mature form of OP-1, both a dimer (36 kDa) and a monomer (17 kDa); none of the antibodies cross-reacted to BMP-6. Anti-pro-OP-1 antibody R2854 (Fig. 1C) showed no specific binding neither to BMP-6, nor to mature OP-1. As we showed previously [31], this antibody reacts only with pro-domain of OP-1. As a control, antibody that cross-reacts with both BMPs, BMP-6 and BMP-7, is shown in Fig. 1E.

3.2. OP-1 ELISA method

To quantify antigenic endogenous OP-1 present in tissue extracts and culture media, a sandwich ELISA method has been developed. Several parameters have been tested: different combinations of anti-OP-1 antibodies, effect of pH, various extraction buffers, enzyme digestions, normalization to the protein content or dry weight, etc. We found that the highest sensitivity of the method was achieved when the combination of polyclonal peptide antibody sc-9305 (coating antibody) and monoclonal 1B12 antibody was used. Standard curves were originated by utilizing human recombinant mature OP-1 at different dilutions ranging from 0.01 to 10 ng/ml (Fig. 2). The conformation of OP-1 epitope and therefore the sensitivity of the method depend also on the pH of the buffer used for ELISA. A wide range of pH values for TBS/Tween buffer was tested (Fig. 3). Since the extraction buffer has a neutral pH and at neutral pH the ELISA readings were in the middle range, this pH was chosen as a standard for OP-1 ELISA. To address the question of whether cartilage extracts have to be dialyzed before the assessment by ELISA, we have tested the effect of two extraction buffers (1 M GuHCl and lysis buffer) on ELISA readings. As shown in Fig. 4A, the presence of 1 M GuHCl buffer inhibited the binding of OP-1 by 50% or more, while the lysis buffer did not affect the ELISA results (Fig. 4B). However, when the same cartilage specimens were extracted with both buffers and then analyzed by ELISA, we found that more antigenic OP-1 could be extracted from cartilage tissue with GuHCl buffer than with lysis buffer (Table 1). To overcome this problem, GuHCl buffer was selected as an extraction buffer, and all samples had to be dialyzed before further analysis.

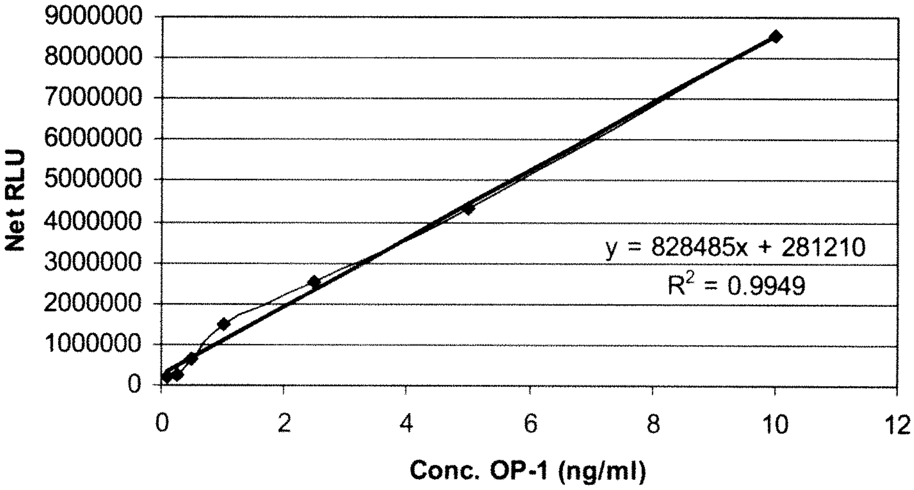

Fig. 2. Typical standard curve with human recombinant OP-1 generated by chemiluminescent sandwich ELISA method.

To standardize the ELISA method and to address the possible decline in cell numbers and depletion of matrix molecules that influence cartilage extractability with aging, before extraction, 500 mg of tissue (wet weight) was always lyophilized (to avoid the influence of matrix), pulverized in liquid nitrogen and extracted with 1 M GuHCl in a ratio of 150 mg (dry weight) of tissue per 3.5 ml of buffer. A repeated extraction of the remaining tissue with 4 M GuHCl buffer showed no extractable OP-1 left as detected by ELISA. To confirm quantitatively that 1 M GuHCl buffer extracts the most of the antigenic OP-1, aliquots of the same cartilage sample were extracted with a variety of extraction buffers including: (1) 1 M GuHCl, 0.005 M EDTA, 0.05 M NaCl; (2) 50 mM Tris, 1 M GuHCl; (3) 50 mM Tris, 4 M GuHCl; (4) 50 mM Tris, 20 mM Na_2HPO_4; (5) 50 mM Tris, 1% SDS; (6) 50 mM Tris, 0.15 M β-mercaptoethanol; (7) 50 mM Tris, 0.1 M NaCl, 8 M urea; and (8) 50 mM Tris, 1 M NaCl, 8 M urea. The choice of the dissociative/extraction agents was based on the specifics of the extraction of BMPs and the ability of BMPs to bind the components of cartilage extracellular matrix [19]. All these extracts were quantitatively analyzed by ELISA. 1 M GuHCl buffer was found to be the most appropriate for OP-1 extraction from human adult articular cartilage.

While seeking the most sensitive ELISA conditions, different enzymatic treatments of cartilage extracts were performed. Cartilage extracts were treated for 1 h at 37 °C with hyaluronidase (1 mg/ml), collagenase (5 mg/ml), chondroitinase ABC (0.1 U/ml), keratanase (0.1 U/ml), keratanase II (0.001 U/ml) and combinations of these enzymes and analyzed by ELISA. The values in the treatment groups were compared to control groups (no prior digestion) (Table 1). We found no significant differences between the groups in ELISA readings. Therefore, enzymatic digestion is not included in the standard protocol for ELISA. The high sensitivity of this method was achieved by utilizing Chemiluminescent Supersignal ELISA Femto Maximum Sensitivity Substrate (Pierce).

3.3. Cartilage ELISA results

Extracts from all cartilage samples were analyzed with the sandwich ELISA method described above. We found that with increasing age, the content of endogenous OP-1 protein significantly declined ($p < 0.02$; Fig. 5). Age of the donors and the levels of OP-1 protein showed a significant covariation (Pearson correlation, $p < 0.02$). Although cartilage samples were obtained from organ donors with no history of joint disease, not all of them appeared to be normal. It is noteworthy, that a decrease in the levels of OP-1 protein with age was found not only in the group that

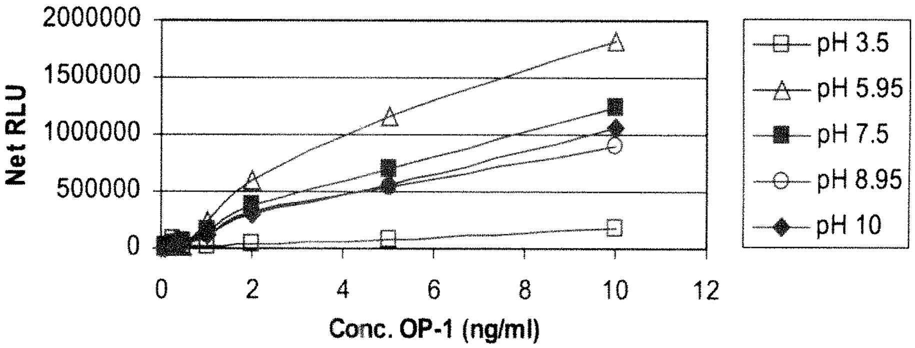

Fig. 3. Effect of pH of the TBS/Tween buffer on a standard curve generated by OP-1 sandwich ELISA.

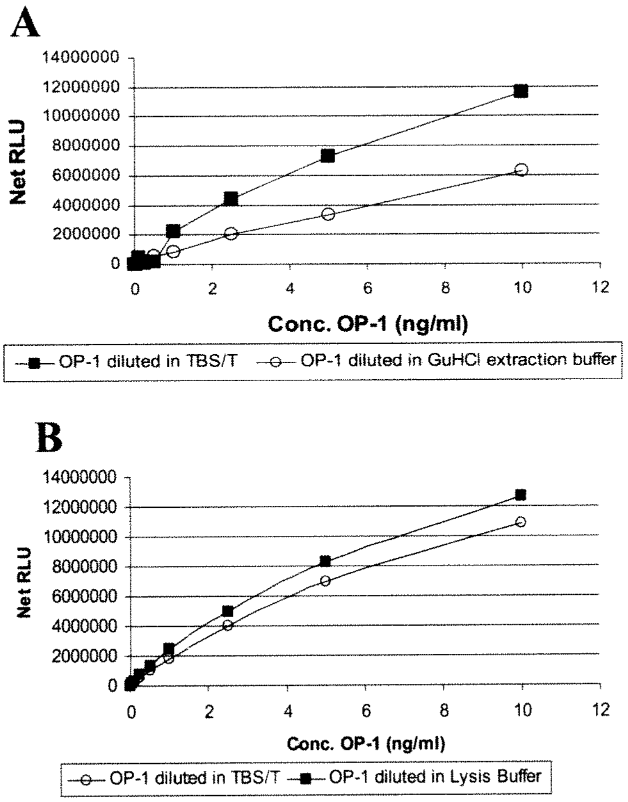

Fig. 4. Effect of 1 M GuHCl extraction buffer (A) and lysis extraction buffer (B) on a standard curve generated by OP-1 ELISA. Closed squares, human recombinant OP-1 diluted in TBS/Tween buffer; opened circles, human recombinant OP-1 diluted in lysis buffer.

consisted of normal tissues and tissues exhibiting early degenerative changes, but also in the subgroup of normal cartilages only. When specimens with normal histomorphological appearance were secluded in a separate subgroup and analyzed for the content of OP-1 protein, the same statistical differences were detected (open circles for normal cartilages only, Fig. 5).

3.4. Western Blot analysis

For Western blotting, representative samples were taken from each age decade and analyzed with anti-mature OP-1 antibody. The gels were scanned and the densities of the immunoreactive bands were measured. Two major OP-1 bands were present in all tested cartilages regardless of the age of donors (Fig. 6A). These bands represented fully processed mature OP-1 form (molecular weight is 36 kDa) and the partially processed intermediate form of the OP-1 protein (molecular weight is 75 kDa). Semi-quantitative densitometric analysis of each of the bands demonstrated a decrease in the intensity of these bands with age, which

Table 1
Effect of enzymatic digestion on the content of endogenous OP-1 in extracts from the same cartilage specimen as detected by ELISA (mean ± S.D.)

Type of treatment	ELISA (ng/ml)
1 M GuHCl buffer only	0.03 ± 0.0027
1 M GuHCl buffer ± CHase, Ker, Ker II	0.027 ± 0.0019
1 M GuHCl buffer ± CHase, Collagenase	0.022 ± 0.0024
1 M GuHCl buffer ± Hyaluronidase	0.025 ± 0.0027
1 M GuHCl buffer ± Collagenase	0.0181 ± 0.0011
Lysis buffer	0.017 ± 0.0013
Lysis buffer ± CHase, Collagenase	0.017 ± 0.0009

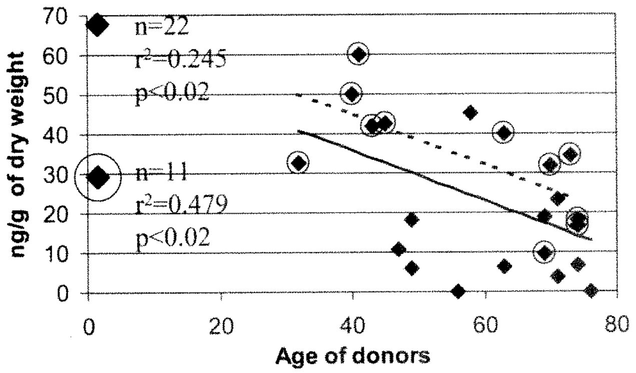

Fig. 5. Concentration of endogenous OP-1 protein detected by sandwich ELISA method in extracts from all tested human adult articular cartilages (solid squares) or in extracts from normal cartilages only (open circles).

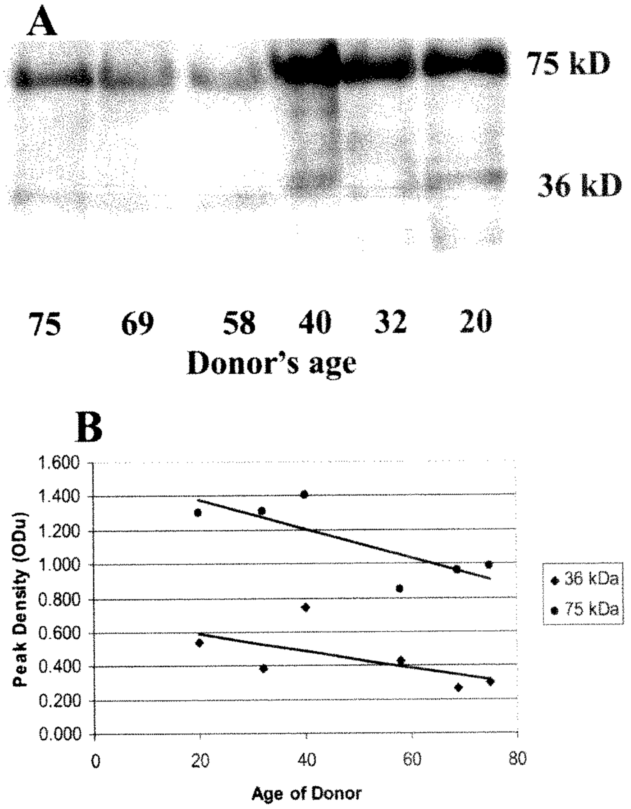

Fig. 6. Changes in OP-1 protein with age detected by Western blotting. (A) Representative Western blot with anti-mature OP-1 antibody of cartilage extracts from each age decade. Band at 75 kDa indicates a hemidimer form of OP-1 that consists of OP-1 mature dimer and one attached pro-domain [35]; band at 36 kDa corresponds to the mature OP-1 dimer. (B) Semi-quantitative image analyses of the Western blot described in A. Trendlines indicate the changes in the intensity of the major OP-1 immunoreactive bands.

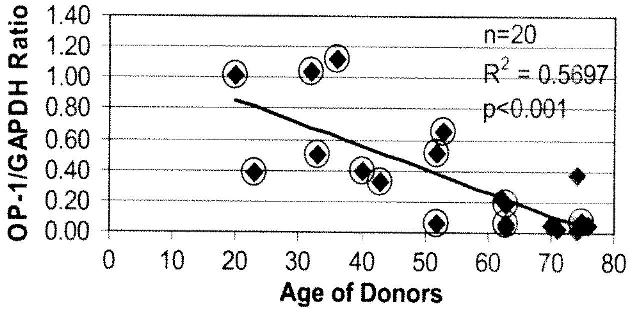

Fig. 7. Graphical illustration of the changes in OP-1 mRNA expression with aging of human adult articular cartilage. Semi-quantitative analysis of the PCR bands. The levels of OP-1 message normalized to the levels of GAPDH message. Solid squares represent all tested cartilage samples; open circles represent a subgroup of normal cartilages.

correlated to ELISA findings (Fig. 6B). Western blot results were normalized to tissue dry weight, as were ELISA data.

3.5. RT-PCR results

For PCR analysis, total RNA was extracted directly from cartilage tissue without previous chondrocyte isolation or culture. Aliquots of the same mRNA were used for nested RT-PCR with OP-1 and GAPDH specific primer sets. Both PCR products were amplified with the same number of cycles. GAPDH was chosen as the normalization factor, since it is a housekeeping gene. We found that with aging levels of GAPDH mRNA expression in normal cartilage did not vary for more than 10%. As it was identified on the protein level, OP-1 mRNA expression in articular cartilage decreased with the increasing age of donors (Fig. 7; $p<0.001$).

4. Discussion

This study confirms an age-related decrease in the anabolic activity of human adult articular cartilage. The anabolic activity of cartilage was evaluated via the assessment of changes in endogenous OP-1, a BMP that is considered to be one of the most potent inducers of cartilage regeneration and repair. We observed greater than a 4-fold decline in OP-1 protein content between ages of 35 and 75 years. The data showed that there was a greater decline in OP-1 mRNA expression, where in some cartilages from older individuals, OP-1 message was barely detectable or was below the detection limit. Another important result of our study is that the concentration of endogenous OP-1 protein in normal articular cartilage is within the range of biological activity of OP-1 (50–100 ng/ml) in vitro, as we have shown previously [17,26–28].

One of the main difficulties in studying human tissue has been to distinguish between non-pathologically (normal) and pathologically progressive (degenerative) aging of articular cartilage. The uniqueness of the present study lies in the examination of age-related changes in human adult articular cartilage obtained from normal individuals through the collaboration with the Regional Organ Bank of Illinois in Chicago. For this study, cartilage from organ donors with no documented history of joint disease was selected. Although tissue was collected from normal individuals (not from patients), not all of the cartilages appeared normal. Some of them displayed degenerative changes described in detail in Chubinskaya et al. [37]. Therefore, tissue selected for the current study was divided into two subgroups. One group included the entire spectrum of cartilages, and one group consisted only of normal cartilages (normal histomorphological appearance). Critically, statistical changes in endogenous OP-1 with age were observed in both groups, suggesting that the decline in anabolic activity of human chondrocytes is associated not only with degenerative changes, but is truly an age-related process.

The decrease in endogenous OP-1 with aging of human articular cartilage is consistent with previous findings on changes in the levels of other growth factors and their receptors, for example, a decrease in mRNA expression of TGF-β1, 2 and 3 in aging equine articular cartilage [6] and increase in EGF synthesis and a decrease in the EGF-receptor mRNA by rat articular chondrocytes [4]. However, our study is the first to show an age-related decrease in endogenous OP-1 in human adult articular cartilage. Also, in the current study, we evaluated changes in both levels, message and protein, and found that there was a decrease in OP-1 mRNA and protein expression with age.

Even though it is apparent that elderly people have decreased levels of OP-1, it still remains unclear whether this phenomenon is a result of aging per se or is due to other age-related variables. The decrease in OP-1 protein in part could be due to the suppression of mRNA expression (as we demonstrated in this study), but also due to many other processes including but not limiting a general slower metabolic activity of older cells, increased degradation of OP-1 due to an activation of catabolic events in cartilage, increase in OP-1 binding proteins, changes in OP-1 receptors or other members of the BMP signaling pathway, etc. Although degradation of OP-1 protein could be one of the reasons in the decline of OP-1, we have not noticed an accumulation of the degradation products in cartilage matrix. As a consequence of aging, catabolic events could be induced and different proteinases present in cartilage could be activated leading to a degradation of a number of matrix proteins including mature OP-1. Also mature OP-1 might undergo autodegradation and might be degraded by serine proteinases.

The results obtained by Western blot analysis suggest that the predominant form of OP-1 in cartilage is the intermediate form (75 kDa), although some OP-1 is also present in the mature (active) form (36 kDa). Since 75 kDa is a partially processed form of OP-1 that contains in its structure one bound pro-domain and one non-covalently associated pro-domain in addition to two mature domains [35], we do not expect this form to be biologically active. By analogy to TGF-β, pro-domain could function as a latency-associated protein that prevents binding of mature BMP molecule to its receptors [39]. However, the function of pro-domain is well described only for TGF-β, and it remains unclear whether pro-domain in other BMPs plays a similar role in preventing the biological activity of these molecules.

The effect of binding proteins on endogenous OP-1 pathway in cartilage is largely unknown. If there is an increase in BMP binding proteins with age as it is documented for IGF-1 binding proteins [38], the decline in OP-1 with age could be attributed by this phenomenon. The exploration of OP-1 binding proteins in human adult articular cartilage and their effect on different cartilage matrix molecules might shed the light on the entire OP-1/BMP pathway role in aging and disease. As it was shown by Martin et al. [38], an elevation of IGF binding proteins in rat articular chondrocytes was one of the reasons for the suppression of the synthetic activity of cells with age in response to IGF-1. Also our preliminary experiments indicate that BMP binding proteins added to cultures of human articular chondrocytes suppress OP-1 and lead to a decline in PG synthesis (unpublished data).

The results obtained in the present study confirm an age-related decline in endogenous OP-1, one of the most potent naturally occurring agents produced by chondrocytes that could counteract cartilage destruction and/or facilitate its repair. These data prompted us to develop a hypothesis that a decrease in endogenous OP-1 metabolism with aging may lead to an elevated susceptibility of cells to catabolic processes thus contributing/promoting cartilage degeneration. Further work is needed to confirm this hypothesis and to understand the function of endogenous OP-1 in cartilage. The availability of quantitative and qualitative methods described here will provide necessary tools for answering these and other questions and could be useful in monitoring therapies and/or disease prognosis. The results of this study suggest future means of using OP-1 to stimulate normal phenotypic activity in articular chondrocytes and maintain/restore function in affected joints.

Acknowledgements

Regional Organ Bank of Illinois and donor's families are gratefully acknowledged. This work was supported by the NIH SCOR Grant P50 AR 39239-11, NIH/NIAMS Grant AR47654, and Stryker Biotech Grant KK-001.

References

[1] D Hamerman, Aging and osteoarthritis basic mechanisms, J. Am. Geriatr Soc 41 (1993) 760–770

[2] J A. Buckwalter, S.L -Y. Woo, V M Goldberg, E C Hadley, F. Booth, T R. Oegema, D.R Eyre, Current concepts review soft-tissue aging and musculoskeletal function, J B J S. 75-A (1993) 1533–1548.

[3] A P. Hollander, I. Pidoux, A Reiner, C. Rorabeck, R Bourne, A R Poole, Damage to type II collagen in aging and osteoarthritis starts at the articular surface, originates around chondrocytes, and extends into the cartilage with progressive degeneration, J Clin Invest 96 (6) (1995) 2859–2869.

[4] D. Ribault, M. Habib, K Abdel-Majid, A Barbara, D Mitrovic, Age-related decrease in the responsiveness of rat articular chondrocytes to EGF is associated with diminished number and affinity for the ligand of cell surface binding sites, Mech Ageing Dev 100 (1) (1998) 25–40.

[5] J. DeGroot, N Verzijl, R A Bank, F P J G Lafeber, J W J Bijlsma, J M. TeKoppele, Age-related decrease in proteoglycan synthesis of human articular chondrocytes the role of nonenzymatic glycation, Arthritis Rheum 42 (5) (1999) 1003–1009

[6] J. Iqbal, J Dudhia, J L Bird, M.T Bayliss, Age-related effects of TGF-β on proteoglycan synthesis in equine articular cartilage, Biochem Biophys Res Commun 274 (2) (2000) 467–471.

[7] G Verbruggen, M Cornelissen, K F. Almqvist, L Wang, D Elewaut, C Broddelez, L de Ridder, E M Veys, Influence of aging on the synthesis and morphology of the aggrecan synthesized by differentiated human articular chondrocytes, Osteoarthr Cartil 8 (3) (2000) 170–179

[8] M.C Bolton, J Dudhia, M T Bayliss, Age-related changes in the synthesis of link protein and aggrecan in human articular cartilage· implications for aggregate stability, Biochem J. 337 (Pt 1) (1999) 77–82

[9] M.P Brown, L A West, K A Merritt, A.H Plaas, Changes in sulfation patterns of chondroitin sulfate in equine articular cartilage and synovial fluid in response to aging and osteoarthritis, Am J Vet Res 59 (6) (1998) 786–791.

[10] D Platt, J L. Bird, M.T Bayliss, Ageing of equine articular cartilage structure and composition of aggrecan and decorin, Equine Vet J. 30 (1) (1998) 43–52

[11] P. Lorenzo, M T Bayliss, D Heinegard, A novel cartilage protein (CILP) present in the mid-zone of human articular cartilage increases with age, J Biol Chem 273 (36) (1998) 23463–23468.

[12] P J Roughley, R J. White, G Cs-Szabo, J S Mort, Changes with age in the structure of fibromodulin in human articular cartilage, Osteoarthr Cartil 4 (3) (1996) 153–161

[13] A.K. Rosenthal, B A. Derfus, L A Henry, Transglutaminase-mediated activity in aging articular chondrocytes and articular cartilage vesicles, Arthritis Rheum 40 (1997) 966–970

[14] C.S Adams, W E Horton Jr, Chondrocyte apoptosis increases with age in the articular cartilage of adult animals, Anat Rec 250 (4) (1998) 418–425

[15] P A Guerne, F Blanco, A Kaelin, A Desgeorges, M Lotz, Growth factor responsiveness of human articular chondrocytes in aging and development, Arthritis Rheum 38 (7) (1995) 960–968

[16] H. Messai, Y. Duchossoy, A M. Khatib, A Panasyuk, D R Mitrovic, Articular chondrocytes from aging rats respond poorly to insulin-like growth factor-1 an altered signaling pathway, Mech. Ageing Dev 115 (1–2) (2000) 21–37

[17] J. Flechtenmacher, K Huch, E J -M A Thonar, J A Mollenhauer, S R Davies, T.M Schmid, W. Puhl, T.K Sampath, M B Aydelotte, K E Kuettner, Recombinant human osteogenic protein 1 is a potent stimulator of the synthesis of cartilage proteoglycans and collagens by human articular chondrocytes, Arthritis Rheum. 39 (1996) 1896–1904

[18] M.R Urist, A Mikulski, A. Lietze, Solubilized and insolubilized bone morphogenetic protein, Proc Natl Acad Sci U. S. A 76 (1979) 1828–1832.

[19] T.K. Sampath, A H Reddi, Dissociative extraction and reconstitution of extracellular matrix components involved in local bone differentiation, Proc Natl Acad Sci U S. A 78 (1981) 7599–7603

[20] S.D Cook, D C. Rueger, Osteogenic protein-1 Biology and applications, Clin Orthop. Relat Res 324 (1996) 29–38

[21] T.K Sampath, D C. Rueger, Structure, functions, and orthopedic applications of osteogenic protein-1 (OP-1), Complicat. Orthop (1994) 101–107, Winter

[22] T K Sampath, J E Coughlin, R M Whetstone, D Banach, C

Corbett, R.J Ridge, E Ozkaynak, H Oppermann, D.C Rueger, Bovine osteogenic protein is composed of dimers of OP-1 and BMP-2A, two members of transforming growth factor-β superfamily, J Biol Chem 265 (22) (1990) 13198–13205

[23] E. Ozkaynak, D C Rueger, E A. Drier, C. Corbett, R.J Ridge, T K Sampath, H. Oppermann, OP-1 cDNA encodes an osteogenic protein in the TGF-β family, EMBO J 9 (1990) 2085–2093

[24] A T. Dudley, K M Lyons, E J. Robertson, A requirement for bone morphogenetic protein-7 during development of the mammalian kidney and eye, Genes Dev 9 (1995) 2795–2807

[25] G Luo, C Hofmann, A.L J J Bronckers, M. Sohocki, A. Bradley, G Karsenty, BMP-7 is an inducer of nephrogenesis, and is also required for eye development and skeletal patterning, Genes Dev 9 (1995) 2808–2820

[26] K Huch, B Wilbrink, J Flechtenmacher, H E. Koepp, M B Aydelotte, T K Sampath, K E Kuettner, J A Mollenhauer. E J -M A Thonar, Effects of recombinant human osteogenic protein 1 on the production of proteoglycan, prostaglandin E2, and interleukin-1 receptor antagonist by human articular chondrocytes cultured in the presence of interleukin-1β, Arthritis Rheum 40 (1997) 2157–2161

[27] H.E Koepp, K.T Sampath, K E Kuettner, G A Homandberg, Osteogenic protein-1 (OP-1) blocks cartilage damage caused by fibronectin fragments and promotes repair by enhancing proteoglycan synthesis, Inflamm Res 47 (1999) 1–6

[28] Y Nishida, C B Knudson, W. Eger, K E Kuettner, W Knudson, Osteogenic protein-1 stimulates cell-associated matrix assembly by normal human articular chondrocytes upregulation of hyaluronan synthase, CD 44 and aggrecan, Arthritis Rheum 43 (2000) 206–214

[29] L Jennings, L. Madsen, J Mollenhauer, The effect of collagen fragments on the extracellular matrix metabolism of bovine and human chondrocytes, Connect. Tissue Res. 42 (1) (2001) 71–86.

[30] P Chen, S Vukicevic, T K Sampath, F.P Luyten, Bovine articular chondrocytes do not undergo hypertrophy when cultured in the presence of serum and osteogenic protein-1, Biochem Biophys Res Commun 197 (1993) 1253–1259.

[31] S Chubinskaya, C Merrihew, G Cs-Szabo, J Mollenhauer, J McCartney, D C. Rueger, K E Kuettner, Human articular chondrocytes express osteogenic protein-1, J Histochem Cytochem 48 (2) (2000) 239–250

[32] C. Hidaka, M Quitoriano, R F Warren, R G Crystal, Enhanced matrix synthesis and in vitro formation of cartilage-like tissue by genetically modified chondrocytes expressing BMP-7, J Orthop Res. 19 (2001) 751–758

[33] S Vukicevic, V Latin, P Chen, R Batorsky, A H. Reddi, T K Sampath, Localization of osteogenic protein-1 (bone morphogenetic protein-7) during human embryonic development high affinity binding to basement membranes, Biochem Biophys Res Commun. 198 (1994) 693–700.

[34] M N. Helder, H Karg, T.J.M Bervoets, S Vukicevic, E H Burger, R N D'Souza, J H M Woltgens, G. Karsenty, A L J J Bronckers, Bone morphogenetic protein-7 (osteogenic protein-1, OP-1) and tooth development, J Dent Res 77 (1998) 545–554

[35] W K Jones, E A. Richmond, K White, H Sasak, W Kusmik, J Smart, H. Oppermann, D C Rueger, R F Tucker, Osteogenic protein-1 (OP-1) expression and processing in Chinese hamster ovary cells isolation of a soluble complex containing the mature and pro-domains of OP-1, Growth Factors 11 (1994) 215–225

[36] G Cs-Szabo, L I Melching, P J Roughley, T.T. Glant, Changes in messenger RNA and protein levels of proteoglycans and link protein in human osteoarthritic cartilage samples, Arthritis Rheum 40 (1997) 1037–1045

[37] S Chubinskaya, K E Kuettner, A A Cole, Expression of matrix metalloproteinases in human normal and damaged articular cartilage from knee and ankle joints, Lab Invest. 79 (12) (1999) 1669–1677

[38] J.A Martin, S.M Ellerbroek, J.A. Buckwalter, Age-related decline in chondrocyte response to insulin-like growth factor-1. the role of growth factor binding proteins, J Orthop Res. 15 (1997) 491–498.

[39] E Piek, C.-H Heldin, P ten Dijke, Specificity, diversity, and regulation in TGF-β superfamily signaling, FASEB J 13 (1999) 2105–2124

ELSEVIER

Biochimica et Biophysica Acta 1588 (2002) 135–138

BIOCHIMICA ET BIOPHYSICA ACTA
BBA
www.bba-direct.com

The peak height ratio of *S*-sulfonated transthyretin and other oxidized isoforms as a marker for molybdenum cofactor deficiency, measured by electrospray ionization mass spectrometry

Masahiko Kishikawa[a], Jörn Oliver Sass[b,1], Nobuo Sakura[c], Toyofumi Nakanishi[a], Akira Shimizu[a,*], Masanori Yoshioka[d]

[a]*Department of Clinical Pathology, Osaka Medical College, 2-7 Daigakucho, Takatsuki, Osaka 569-8686, Japan*
[b]*University of Innsbruck Children's Hospital, Anichstr 35, A-6020 Innsbruck, Austria*
[c]*Department of Pediatrics, Hiroshima University School of Medicine, Hiroshima 734-0037, Japan*
[d]*Department of Analytical Chemistry, Faculty of Pharmaceutical Sciences, Setsunan University, Hirakata, Osaka 573-0101, Japan*

Received 14 November 2001; received in revised form 7 May 2002; accepted 13 June 2002

Abstract

Molybdenum cofactor deficiency is a fatal neurological disorder, which follows an autosomal-recessive trait and is characterized by combined deficiency of the enzyme, sulfite oxidase, xanthine dehydrogenase and aldehyde oxidase. Early detection of molybdenum cofactor-deficient patients is essential for their proper care and genetic counseling of families at risk. We demonstrate the use of *S*-sulfonated transthyretin (TTR) as a marker for molybdenum cofactor deficiency. Plasma or sera obtained from 4 patients with molybdenum cofactor deficiency and 57 controls were studied by electrospray ionization mass spectrometry (ESIMS) following selective enrichment of TTR by immunoprecipitation using protein G/A agarose. The data obtained from molybdenum cofactor deficiency samples indicated a strong increase in the peak height of *S*-sulfonated TTR. A more significant difference was revealed if the peak height ratio of *S*-sulfonated TTR and the sum of the other oxidized TTR were determined. By accurate determination of the ratio, the samples of molybdenum cofactor deficiency patients could clearly be distinguished from controls without molybdenum cofactor deficiency.

© 2002 Elsevier Science B.V. All rights reserved.

Keywords: *S*-sulfonated; Immunoprecipitation; Protein G/A agarose; Mass spectrometry; Posttranslational modification; Molybdenum cofactor deficiency

1. Introduction

We reported previously a unique isoform of serum transthyretin (TTR), which was *S*-sulfonated by excessive sulfite *in vivo* in a patient with molybdenum cofactor deficiency (MCD) [1]. Molybdenum cofactor is essential for the function of the enzymes sulfite oxidase, xanthine dehydrogenase and aldehyde oxidase [2]. MCD and isolated sulfite oxidase deficiency result in a severe clinical phenotype, which is, in most cases, characterized by nontreatable convulsions presenting early after birth. Besides neurological symptoms and anatomic brain anomalies, ectopic lenses, dysmorphic signs, hypertonicity and hypotonia are frequent features. Due to the lack of sulfite oxidase activity, sulfite accumulates and sulfate production decreases. The presence of elevated levels of sulfite leads to the accumulation of *S*-sulfocysteine formed by a direct reaction of sulfite with cysteine [2]. The formation of protein-sulfonated compounds ($RS-SO_3^-$) in the albumin and fibronectin of several animal species exposed to sulfur dioxide or to sulfite/hydrogen sulfite has been reported [3]. TTR contains a single free cysteine at position 10. We predicted the elevation of *S*-sulfonated TTR in the sera of sulfite oxidase-deficient patients, and demonstrated it in a single case of MCD by electrospray ionization mass spectrometry (ESIMS) [1]. To reveal the modified structure of TTR, ESIMS with immunoprecipitated TTR was successfully applied [4].

The *S*-sulfonated TTR signals were also clearly high in additional MCD samples, in contrast to most control samples that presented low *S*-sulfonated TTR peaks. However, elevated *S*-sulfonated TTR was also observed in some of the

---

[*] Corresponding author. Tel.: +81-726-84-6448; fax: +81-726-84-6548. *E-mail address:* shimizu@poh.osaka-med.ac.jp (A. Shimizu).

[1] Present address: Laboratory of Metabolism, University of Freiburg Children's Hospital, Mathildenstr. 1, D-79106 Freiburg, Germany.

0925-4439/02/$ - see front matter © 2002 Elsevier Science B.V. All rights reserved.
PII: S0925-4439(02)00156-4

control samples, although those patients did not have MCD. Commercially obtained TTR also showed a rather high peak of *S*-sulfonated TTR (~ 15%). High peaks of *S*-sulfonated TTR were often detected (ca. 20%) in TTR prepared from rabbit sera. Our original ESIMS method with immunoprecipitated TTR has been applied in several institutions to detect TTR variants in sera from patients with familial amyloidotic polyneuropathy [5–7]. In some of the samples, which were studied in this regard and were not from MCD patients, rather high signals corresponding to *S*-sulfonated TTR, which is 80 Da larger than free TTR, were also reported [6]. To distinguish MCD from these ambiguous cases, we here describe an improved method for sample preparation and calculation of results.

2. Materials and methods

2.1. Specimens

Plasma or sera of 4 patients with MCD as diagnosed on the basis of clinical features, metabolite studies, enzyme assays in cultured skin fibroblasts and mutation analysis, and 57 samples obtained from children with a variety of diagnoses, but neither MCD nor isolated sulfite oxidase deficiency, were analyzed. One case of MCD was already reported previously [1]. The ages of the MCD patients at the time of sampling were 3 days, 3 months, 2 and 3 years. The ages of the controls were distributed from 1 month to 13 years.

2.2 Sample preparation

We previously reported a convenient method for preparing protein samples for application to soft ionization MS [8–10]. The test serum was mixed with antiserum against the target protein, and the generated immunoprecipitates were subsequently washed with 0.15 M sodium chloride and water. The mixture was applied directly to on-line high performance liquid chromatography (HPLC)/ESIMS. Most samples were successfully analyzed by this method. However, the preparation method was not good enough to determine an accurate ratio for the *S*-sulfonated TTR and TTR isoforms. The remaining albumin in immunoprecipitates coeluted with *S*-sulfonated TTR in the HPLC system, and disturbed the measurement of this fraction. To wash out serum protein extensively, we used protein G/A agarose to form large immune complex particles. Protein G plus/Protein A Agarose (50 µl of suspension) (Oncogene Research Products, cat# IP05, lot# D14269, Boston, MA) was washed three times with 0.5 ml of 0.15 M sodium chloride. Antihuman TTR (prealbumin) antiserum (25 µl) (SIGMA, lot# 19H4822, St. Louis, MO) was added to the agarose, and the mixture was

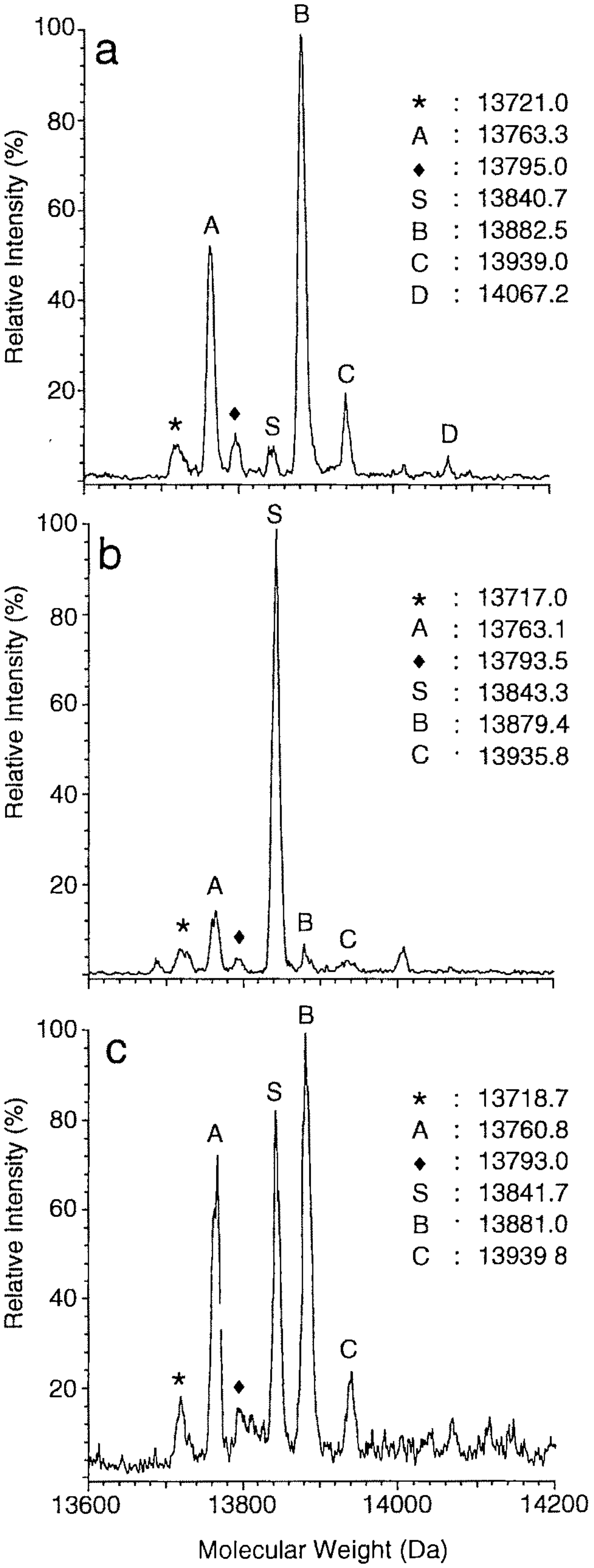

Fig 1 Deconvoluted ESIMS spectra of TTR from a control infant (a), a patient with MCD (b), and a second infant without MCD (c), but with a rather high peak of *S*-sulfonated TTR A, free TTR, B, TTR conjugated with cysteine; C, TTR conjugated with cysteinylglycine, D, TTR conjugated with glutathione; S, *S*-sulfonated TTR, *, modified TTR in which a side chain of cysteine residue is cleaved, and changed to glycine The assignment of each peak was discussed in a previous paper [10] ◆, the observed molecular mass corresponds to TTR in which cysteine is oxidized

shaken for 30 min at room temperature. The resulting agarose–antibody complex was washed with 0.5 ml 0.15 M sodium chloride four times. Subsequently, a 10 μl sample serum was mixed with the washed complex and shaken for 30 min. The generated precipitates were washed with 0.5 ml of 0.15 M sodium chloride seven times. Each washing step consisted of turning the tube over several times, centrifuging for 5 s with a centrifuge and discarding the supernatant. Finally, the precipitate was suspended in 20 μl of 2% acetic acid and the agarose was removed by filtration, using an ultrafree-MC centrifugal 0.45 μm filter unit (Millipore, Bedford, MA). The filtration was repeated twice and the pooled filtrate was applied to LC/ESIMS.

2 3. Reversed-phase HPLC and mass spectrometry

On-line HPLC/ESIMS was used, with a PLRP-S reversed-phase column (1 × 50 mm, 1000 Å, 8 μm; Michrom Bioresources, Pleasanton, CA), as reported previously [4]. An ESI mass spectrometer, TSQ7000 (Thermo Quest, San Jose, CA) was utilized [4]. The scanning range was *m/z* 500–2000 in 3 s. Calibration was performed using the peptide Met–Arg–Phe–Ala and multiple charged ions of horse apo myoglobin, according to the manufacturer's instructions.

2.4. Calculation of the TTR ion peaks on ESIMS

The ratios of TTR isoforms' ion peak heights were determined on deconvoluted spectra, which were a summation of scans covering the whole TTR elution. The ratio of the peak heights of *S*-sulfonated TTR and the sum of the peak heights of the TTR conjugates with cysteine, cysteinylglycine and glutathione were calculated. Note the marks used in Fig. 1: (S)/(B + C + D).

3. Results

Deconvoluted ESIMS spectra of TTR prepared by immunoprecipitation using protein G/A agarose are shown in Fig. 1. The spectrum of TTR from a control infant (Fig. 1a) shows several peaks, which were similar to those previously reported by the original preparation method [4,10]. The observed mass of each peak corresponded to the theoretical molecular weight as assigned in the figure. The assignment of each peak was as reported previously [10]; the peak 80 Da larger than unmodified TTR was assigned to *S*-sulfonated TTR (S). The two major peaks in the control sample corresponded to free TTR (A) and TTR conjugated with cysteine (B). Samples of most of the remaining controls presented with patterns similar to that in Fig. 1a. The spectrum from a patient with MCD (Fig. 1b) showed a prominent *S*-sulfonated TTR peak, while the peaks of other oxidized forms of TTR and free TTR were relatively low. A similar pattern was reported for this patient using the earlier pretreatment method [1]. Spectra obtained from the other three MCD patients using the new method were nearly identical to that shown in Fig. 1b.

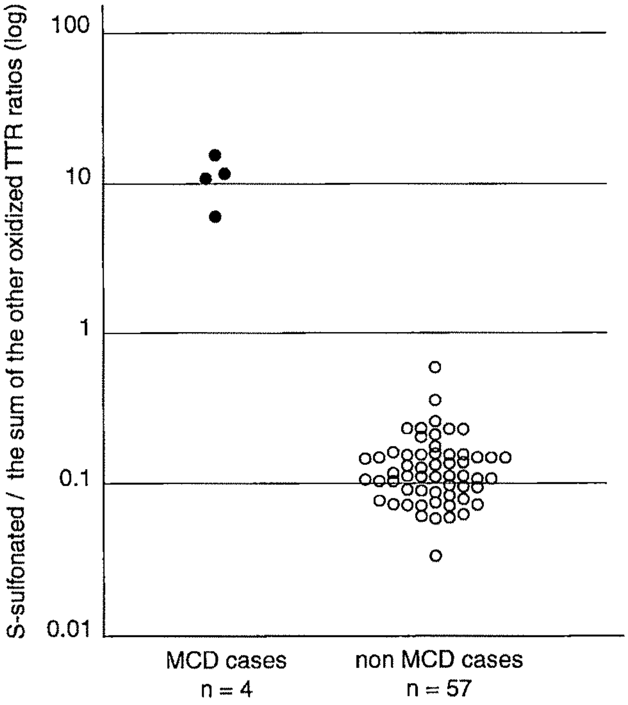

Fig 2. Comparison of the ratio of peak height between patients with MCD and controls, calculated by the equation: (peak height of *S*-sulfonated TTR)/(the sum of the peak heights TTR conjugated with cysteine, cysteinylglycine and glutathione). Note the marks used in Fig 1 (S)/(B + C + D)

Analysis of samples from most of the remaining controls showed some with patterns similar to that in Fig. 1a, but others with significantly higher signals of *S*-sulfonated TTR, as shown in Fig. 1c. However, a critical difference was noted between the spectra obtained from these controls and those of patients with MCD. Controls with high signals of *S*-sulfonated TTR also showed increased signals of TTR conjugated with cysteine, cysteinylglycine, and (sometimes) glutathione, while patients with MCD showed a specific elevation of *S*-sulfonated TTR. Thus, the significance of the elevated *S*-sulfonated TTR in any one individual is more accurately documented by calculating the peak height ratio of *S*-sulfonated TTR to that of the other oxidized derivatives (S)/(B + C + D). The mean and S.D. of the ratio for MCD cases ($n = 4$) and controls ($n = 57$) were 11.0 ± 3.8 and 0.14 ± 0.09, respectively (see Fig. 2).

No significant difference was found among the peak height ratios (*S*-sulfonated TTR)/(all oxidized isoforms in TTR) obtained from controls of different ages.

4. Discussion

Using an immunoprecipitation method previously reported by us [4], serum protein was not removed completely because of the washing limit for small amounts of precipitates (often invisible). On reversed-phase HPLC, *S*-

sulfonated TTR was eluted slightly later than the other isoforms of TTR, and co-migrated with the remaining serum protein, mainly albumin. Using the immunoprecipitation method with the help of protein G/A agarose, we obtained clearly visible precipitates, making the washing steps easy to perform Sufficient washing removed the remaining albumin, and high-quality spectra were obtained for a wide range of TTR peaks on HPLC chromatography, which gave an accurate peak height ratio of the signal of *S*-sulfonated TTR to the sum of the signals of other TTR isoforms. With this improved procedure, we found a clear difference in the ratio (peak height of *S*-sulfonated TTR)/(sum of peak heights of total oxidized TTR) between MCD patients and controls.

S-sulfocysteine has been used for the diagnosis of sulfite oxidase deficiency. However, it is a strongly acidic and relatively unstable amino acid, which tends to be lost when urine is desalted with the H^+-form of a sulfonated ion-exchange resin [11]. In common routine amino acid analysis by ion-exchange chromatography, *S*-sulfocysteine elutes on a position corresponding to a void volume of chromatography, and is not separated from phosphoserine. *S*-sulfocysteine in urine can accurately be monitored by mass spectral analysis [2], and quantitation of this metabolite is now available as a service through the Duke University Mass Spectrometry Laboratory [12]. The assessment of peak height ratios proposed in this paper may represent a valuable additional diagnostic marker. By our experiences, TTR in plasma or sera can stay at ambient temperature for at least 1 week. *S*-sulfonated TTR in plasma or sera may be more stable than *S*-sulfocysteine in urine.

In some control samples, the peak height of *S*-sulfonated TTR was elevated in addition to that of other oxidized TTR isoforms. The mechanism of *S*-sulfonated TTR formation in control samples is unknown. We previously characterized a unique isoform of TTR, which was 46 Da smaller than free TTR [10]. The peak is marked by an asterisk in Fig. 1. To characterize this isoform, the component TTR-46 prepared by reversed phase HPLC was cleaved with trypsin. The peptides were analyzed by LC/ESIMS, and using reconstructed ion chromatograms, the ions corresponding to all normal expected peptides, and the ions 46 Da smaller than all normal peptides were plotted. A clear ion, 46 Da smaller than mass of normal T1 + 2(M + 2H: 729.9), was detected, but an ion corresponding to normal T1 + 2 was not detected. The collision-induced dissociation (CID) spectra of the abnormal ion suggested that Cys-10 is substituted by Gly [10]. The amino-terminal sequence of TTR-46 was also studied with a protein sequencer, and the first 15 residues were the same as normal sequence except position 10, which showed Gly instead of Cys [10]. It is possible that *S*-sulfonated TTR and TTR-Gly-10 are formed by an unknown common pathway, although additional experiments are needed to clarify this issue.

A European survey group has suggested that MCD is more common than generally thought, and that patients may well be overlooked because of a lack of awareness [13]. Although work with additional patient samples is needed to determine the general applicability of the assay described here, the study of TTR by ESIMS may represent a promising method for MCD screening. It may prove to be of special value in the diagnosis of patients with isolated sulfite oxidase deficiency, because that disorder is not associated with disturbed purine metabolism, as in patients with MCD deficiency, where low uric acid values can help establish the diagnosis [2].

Acknowledgements

This study was supported by a 1998–2000 and a 2001–2002 grant-in-aid (to M.K.) from the Ministry of Education, Science, Sports and Culture of Japan. We are grateful to Univ.-Prof. Dr. Wolfgang Sperl, Children's Hospital of Salzburg, Austria, and to Dr. Hartmut Koch, St. Marienhospital Vechta, Germany, for plasma of MCD patients.

References

[1] M Kishikawa, T Nakanishi, A Shimizu, M. Yoshino, Pediatr Res 47 (2000) 492–494

[2] J L Johnson, M Duran, in: C.R Scriver, A L Beaudet, W S Sly, D Valle (Eds), The Metabolic and Molecular Bases of Inherited Disease, McGraw-Hill, New York, 2001, pp 3163–3177.

[3] D B Menzel, D.A Keller, K.H Leung, Adv Exp Med Biol 197 (1986) 477–492

[4] M Kishikawa, T Nakanishi, A. Miyazaki, A Shimizu, M Nakazato, K Kangawa, H Matsuo, J Mass Spectrom 31 (1996) 112–114

[5] Y Ando, P I Ohlsson, O B Suhr, N Nyhlin, T Yamashita, G Holmgren, A. Danielsson, O Sandgren, M. Uchino, M Ando, Biochem Biophys. Res Commun 228 (1996) 480–483

[6] R Theberge, L Connors, M. Skinner, J Skare, C E Costello, Anal Chem. 71 (1999) 452–459.

[7] S Ikeda, T Tokuda, A Nakamura, I Ueno, T Taketomi, N Yanagisawa, Y.F Li, Amyloid 4 (1997) 104–107

[8] T Nakanishi, N Okamoto, K Tanaka, A Shimizu, Biol. Mass Spectrom 23 (1994) 230–233

[9] T Nakanishi, M. Kishikawa, A Miyazaki, A. Shimizu, Y Ogawa, S. Sakoda, T Ohi, H Shoji, J Neurosci. Methods 81 (1998) 41–44

[10] M Kishikawa, T Nakanishi, A. Miyazaki, A Shimizu, Amyloid 6 (1999) 48–53

[11] H.J Bremer, M Duran, J P Kamerling, H. Przyrembel, S K Wadman, Disturbances of Amino Acid Metabolism: Clinical Chemistry and Diagnosis, Urban and Schwarzenberg, Baltimore, 1981.

[12] URL http //www duke edu/~mdfeezor/MSHome/MCDSulfo html.

[13] H A Simmonds, G F Hoffmann, J L Perignon, V Micheli, A H. van Gennip, Lancet 353 (1999) 675–676.

ELSEVIER

Biochimica et Biophysica Acta 1588 (2002) 139–148

BIOCHIMICA ET BIOPHYSICA ACTA
BBA
www.bba-direct.com

Selective inhibition of CYP27A1 and of chenodeoxycholic acid synthesis in cholestatic hamster liver

Yasushi Matsuzaki [a,*], Bernard Bouscarel [b], Tadashi Ikegami [a], Akira Honda [a,c], Mikio Doy [c], Susan Ceryak [b], Sugano Fukushima [a], Shigemasa Yoshida [a], Junichi Shoda [a], Naomi Tanaka [a]

[a] *Department of Gastroenterology and Hepatology, Institute of Clinical Medicine, University of Tsukuba, 1-1-1 Tennodai, Tsukuba City, 305-8575 Ibaraki, Japan*
[b] *Department of Medicine, The George Washington University, Washington, DC, USA*
[c] *Ibaraki Prefectural Institute of Public Health, Mito, Ibaraki, Japan*

Received 18 April 2002; received in revised form 20 June 2002; accepted 20 June 2002

Abstract

The aim of this study was to explore the regulation of serum cholic acid (CA)/chenodeoxycholic acid (CDCA) ratio in cholestatic hamster induced by ligation of the common bile duct for 48 h. The serum concentration of total bile acids and CA/CDCA ratio were significantly elevated, and the serum proportion of unconjugated bile acids to total bile acids was reduced in the cholestatic hamster similar to that in patients with obstructive jaundice. The hepatic CA/CDCA ratio increased from 3.6 to 11.0 ($P<0.05$) along with a 2.9-fold elevation in CA concentration ($P<0.05$) while the CDCA level remained unchanged. The hepatic mRNA and protein level as well as microsomal activity of the cholesterol 7α-hydroxylase, 7α-hydroxy-4-cholesten-3-one 12α-hydroxylase and 5β-cholestane-3α,7α,12α-triol 25-hydroxylase were not significantly affected in cholestatic hamsters. In contrast, the mitochondrial activity and enzyme mass of the sterol 27-hydroxylase were significantly reduced, while its mRNA levels remained normal in bile duct-ligated hamster. In conclusion, bile acid biosynthetic pathway via mitochondrial sterol 27-hydroxylase was preferentially inhibited in bile duct-ligated hamsters. The suppression of CYP27A1 is, at least in part, responsible for the relative decreased production of CDCA and increased CA/CDCA ratio in the liver, bile and serum of cholestatic hamsters.

© 2002 Elsevier Science B.V. All rights reserved

Keywords: Bile acid synthesis; Cholestasis; Cholesterol 7α-hydroxylase (CYP7A1); 7α-Hydroxy-4-cholesten-3-one 12α-hydroxylase (CYP8B1); 5β-Cholestane-3α,7α,12α-triol 25-hydroxylase (CYP3A)

---

1. Introduction

The total serum bile acid concentration increases in patients with various hepatobiliary diseases: e.g., acute and chronic hepatitis, liver cirrhosis and intra- and extrahepatic cholestasis [1–3]. However, the composition of serum bile acids in patients with cholestasis is very different from that in patients with other hepatobiliary diseases. In cholestasis, the ratio of the serum concentration of the primary bile acid cholic acid (CA), to chenodeoxycholic acid (CDCA) increases to more than one [1–3], while the proportion of unconjugated bile acids is reduced [2,3]. However, the mechanism(s) responsible for the altered bile acid biosynthesis under cholestatic conditions remains unknown.

Production of CA and CDCA from cholesterol is principally regulated by two key enzymes, namely microsomal cholesterol 7α-hydroxylase (CYP7A1) and mitochondrial sterol 27-hydroxylase (CYP27A1) [4]. CYP7A1 is the first and rate-limiting enzyme in the classic pathway, while CYP27A1 is the key enzyme in the alternative pathway as depicted in Fig. 1. The microsomal 7α-hydroxy-4-cholesten-3-one 12α-hydroxylase (CYP8B1) is an additional key enzyme involved in bile acid biosynthesis [5]. This enzyme is known to catalyze 12α-hydroxylation of 7α-hydroxy-4-cholesten-3-one which is an intermediate in the classic pathway. The role of CYP8B1 in the alternative pathway has not been clarified, while it is believed that the alternative pathway is mostly involved in CDCA synthesis [6]. However, recent studies have suggested that 27-hydroxycholesterol could be

---

* Corresponding author. Tel.: +81-298-53-3138; fax: +81-298-53-3138.
E-mail address: ymatsuzaki-gi@umin.ac.jp (Y. Matsuzaki).

0925-4439/02/$ - see front matter © 2002 Elsevier Science B.V. All rights reserved.
PII: S0925-4439(02)00157-6

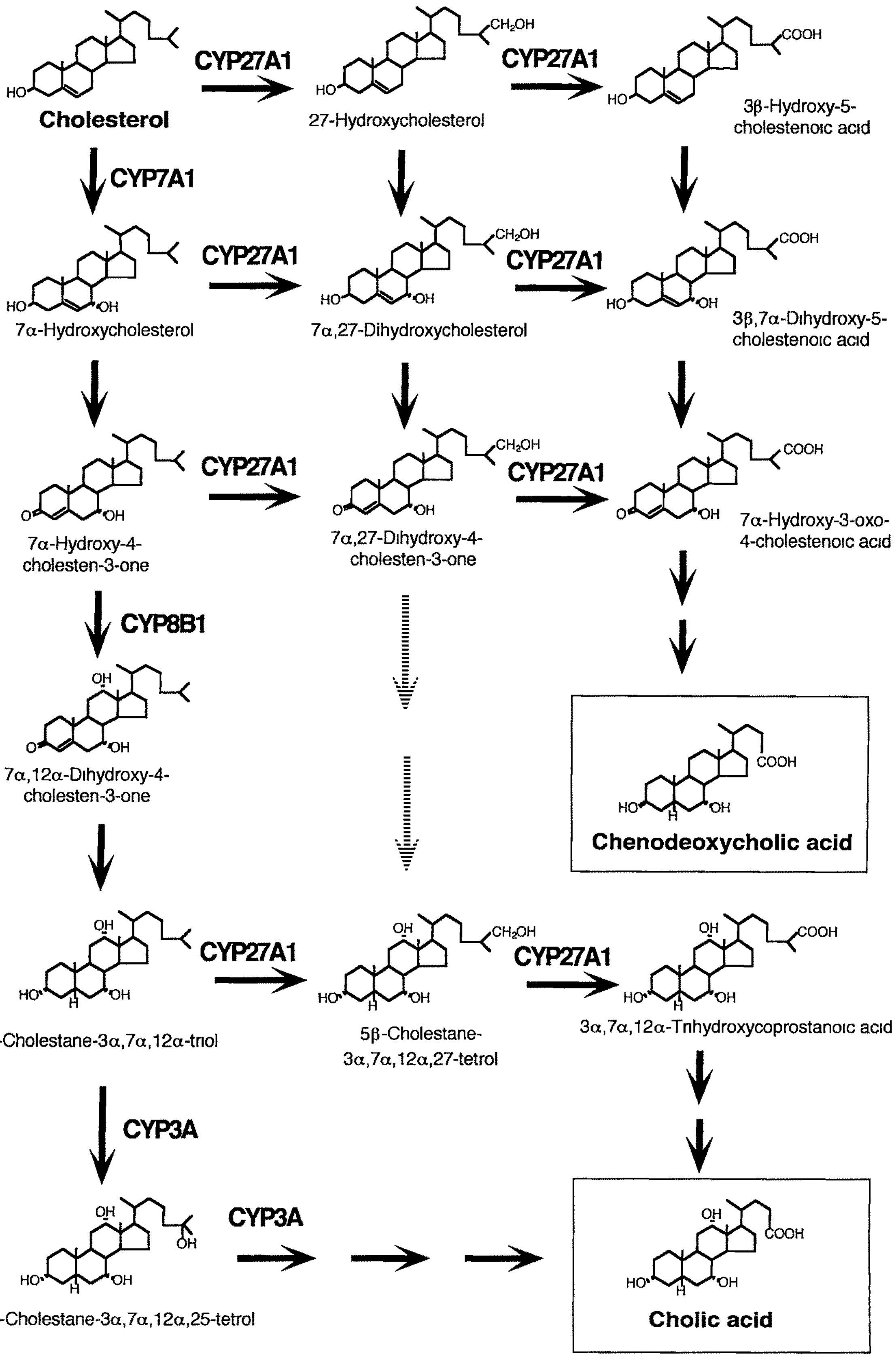
Cholesterol
CYP27A1
27-Hydroxycholesterol
CYP27A1
3β-Hydroxy-5-cholestenoic acid
CYP7A1
7α-Hydroxycholesterol
CYP27A1
7α,27-Dihydroxycholesterol
CYP27A1
3β,7α-Dihydroxy-5-cholestenoic acid
7α-Hydroxy-4-cholesten-3-one
CYP27A1
7α,27-Dihydroxy-4-cholesten-3-one
CYP27A1
7α-Hydroxy-3-oxo-4-cholestenoic acid
CYP8B1
7α,12α-Dihydroxy-4-cholesten-3-one
Chenodeoxycholic acid
5β-Cholestane-3α,7α,12α-triol
CYP27A1
5β-Cholestane-3α,7α,12α,27-tetrol
CYP27A1
3α,7α,12α-Trihydroxycoprostanoic acid
CYP3A
5β-Cholestane-3α,7α,12α,25-tetrol
CYP3A
Cholic acid
HO
OH
O
H
CH₂OH
COOH

Fig 1 Bile acid biosynthesis from cholesterol initiated either by a series of ring modifications (classic pathway) or by side chain hydroxylation (alternative pathway). Solid arrows represent known enzymatic steps while broken arrows represent putative reactions that have yet to be confirmed

converted into CA [7,8] while 3β-hydroxy-5-cholestenoic acid was not [7]. Thus, CA and CDCA are synthesized by both pathways, and CYP8B1 appears to be the most important enzyme regulating the ratio of CA to CDCA under normal conditions [5,8].

In certain pathological conditions, however, CYP27A1 can also be important in determining CA/CDCA ratio. Cerebrotendinous xanthomatosis (CTX) is a recessively inherited disorder caused by mutations in *CYP27A1* gene located on human chromosome 2 [9–12]. In this disease, the pool size of CDCA is markedly reduced while that of CA is almost normal [13]. When CYP27A1 is defective, not only 27-hydroxylation of cholesterol in the alternative pathway but also 27-hydroxylation of 5β-cholestane-3α,7α-diol and 5β-cholestane-3α,7α,12α-triol in the classic pathway is blocked [14]. Therefore, in CTX, only the microsomal 5β-cholestane-3α,7α,12α-triol 25-hydroxylase (CYP3A) pathway is intact for side chain hydroxylation, resulting in CA being the only bile acid synthesized [15,16] (Fig. 1).

In the present study, we selected the cholestatic hamster with the common bile duct ligated for 48 h as model. This model was chosen since it has both the hepatic capacity for cholesterol biosynthesis [17], as well as a bile acid composition [18] similar to that found in human. In this study, we compared the bile acid concentration and composition in serum, bile and liver tissue, as well as CYP7A1, CYP27A1, CYP8B1 and CYP3A protein expression and activity in bile duct-ligated and sham-operated hamsters. The results from the present study showed that in the cholestatic hamster, the increased serum CA/CDCA ratio was mainly due to the reduced hepatic CDCA production probably derived, at least in part, from the suppression of the mitochondrial CYP27A1 protein expression and activity.

2. Materials and methods

2.1 Chemicals

7α-Hydroxycholesterol was obtained from Steraloids (Wilton, NH). 27-Hydroxycholesterol was synthesized from diosgenin [19] and purified by preparative thin-layer chromatography (TLC). 7α-Hydroxy-4-cholesten-3-one and 7α,12α-dihydroxy-4-cholesten-3-one were gifts from Dr. T. Hoshita and Dr. K. Kihira (Pharmaceutical Institute, Hiroshima University, Hiroshima, Japan). 5β-Cholestane-3α,7α,12α-triol was prepared by electrolytic coupling of cholic acid with isovaleric acid according to Bergström and Krabisch [20]. 5β-Cholestane-3α,7α,12α,25-tetrol was synthesized from CA by the method of Dayal et al. [21]. [25,26,26,26,27,27,27-$^2H_7$]cholesterol was obtained from MSD Isotopes (Montreal, Canada). [$^2H_7$]7α-hydroxycholesterol and [$^2H_7$]27-hydroxycholesterol were prepared by previously described methods [22,23]. [2,2,4,4-$^2H_4$]CA, [2,2,4,4-$^2H_4$]DCA, and [2,2,4,4-$^2H_4$]LCA were obtained from MSD Isotopes, [11,11,12,12-$^2H_4$]CDCA and [11,11,12,12-$^2H_4$]UDCA were supplied by the Research Laboratories of Nippon Kayaku Co. and Tokyo Tanabe Co. (Tokyo, Japan), respectively. Leupeptin, phenylmethylsulfonyl fluoride and soybean trypsin inhibitor were purchased from Sigma Chemical Co. (St. Louis, MO) The human anti-cholesterol 7α-hydroxylase antibody was a gift from Dr. T. Tanabe (National Cardiovascular Disease Center, Osaka, Japan). The rat anti-sterol 27-hydroxylase antibody was a gift from Dr. D.W. Russell, University of Texas Southwestern Medical Center, Dallas, TX.

2 2. Patients

We studied 20 human subjects. Eight had untreated extrahepatic obstructive jaundice and the other 12 were without hepatobiliary diseases. All patients provided written informed consent and this study was conducted according to the Declaration of Helsinki. Blood samples were obtained in the morning before breakfast after overnight fasting, and the plasma and/or serum was stored at − 20 °C until analysis.

2 3. Animals

Adult male Golden Syrian hamsters (100–130 g body weight) were purchased from Harlan Sprague Dowley, fed a standard rodent chow diet and maintained on a 12·12 h light–dark cycle.

2.4. Surgical procedure

After fasting for 24 h, hamsters were anesthetized with sodium nembutal (50 mg/kg body weight). The ligation of the common bile duct was performed as previously described [24]. Briefly, the abdomen was opened with a midline incision, the common bile duct was dissected from the surrounding tissue, and three ligations with silk thread were performed. The bile duct was cut between the second and third ligation from the gallbladder. Four hundred microliters of antibiotic solution (300,000 U/ml) containing penicillin G benzathine and penicillin G procaine (Durapen Vedco, Syracuse, NY) were poured over the peritoneal cavity to avoid infection. The incision of the abdominal wall was closed by using separate sutures for the muscle layer and the skin. Control hamsters underwent sham operation in which the bile duct was not ligated. The hamsters were maintained under fasting conditions for 24 h after surgery. Cholestasis was suggested by the appearance of green urine and the presence of an enlarged gallbladder. After 48 h, the animals were sacrificed at noon and blood was collected by direct puncture of the heart. Livers were then immediately frozen and stored at − 70 °C until used. Serum and gallbladder bile were stored at − 20 °C until analysis. All animals received humane care in compliance with the George Washington University guidelines.

2.5. Bile acid analyses

2.5.1. Serum and biliary bile acids

Bile acid concentrations and profile in serum and gallbladder bile were determined by high-performance liquid chromatography (HPLC) combined with a 3α-hydroxysteroid dehydrogenase-immobilized column according to the method of Okuyama et al. [25]. Either serum or bile was diluted with 100 mM potassium phosphate buffer (pH 7.2), and 5β-pregnane-3α,17α,20α-triol was added as an internal standard. The mixture was incubated at 64 °C for 30 min. Bile acids were then extracted with a Bond Elut C_{18} cartridge (Varian, Harbor City, CA). After evaporation, the residue was dissolved in methanol, filtered through an Ultra-Free C3HV filter (0.45 μm; Millipore, Bedford, MA), and analyzed by HPLC.

2 5.2. Hepatic bile acids

Bile acid concentrations and profile in liver tissue were determined by gas-chromatography mass-spectrometry (GC-MS) according to our previously described method [26]. Briefly, the liver specimen (10 mg wet weight) was washed carefully with saline to remove biliary bile acids. After addition of deuterium-labeled bile acids as internal standards and solubilization in 5% NaOH at 80 °C for 30 min, bile acids were extracted by a Bond Elut C_{18} cartridge and subjected to solvolysis and enzymatic hydrolysis The resulting deconjugated bile acids were converted into the ethyl ester dimethylethylsilyl (DMES) ether derivatives and quantified by high-resolution GC-MS with selected-ion monitoring (SIM).

2 6. Assays for enzyme activities

2.6.1. CYP7A1 and CYP27A1 activities

Hepatic microsomes and mitochondria were prepared by differential ultracentrifugation [27], and the protein determined according to the method of Lowry et al. [28]. The activities of microsomal 7α-hydroxylation of cholesterol and mitochondrial 27-hydroxylation of cholesterol were measured by high-resolution GC-MS with SIM using $[^2H_7]$7α-hydroxycholesterol and $[^2H_7]$27-hydroxycholesterol as internal recovery standards [29].

2 6.2. CYP8B1 activity

Microsomal 12α-hydroxylase activity was assayed as described by Noshiro et al. [30] with minor modifications. Microsomes were incubated for 10 min at 37 °C with 7α-hydroxy-4-cholesten-3-one (6 μg dissolved in 5 μl of isopropanol), NADPH (1 mM), and 100 mM potassium phosphate buffer (pH 7.4) containing 0.1 mM EDTA in a total volume of 0.3 ml. The incubation was stopped by the addition of 5 ml of benzene. The formation of 7α,12α-dihydroxy-4-cholesten-3-one was quantified by HPLC [30].

2.6 3 CYP3A activity

CYP3A activity was determined by assaying CYP3A activity as described previously [31]. Microsomes were incubated for 20 min at 37 °C with 5β-cholestane-3α,7α,12α-triol (25 nmol dissolved in 10 μl of acetone), NADPH (1.2 mM), glucose-6-phosphate (3.6 mM), 2 units of glucose-6-phosphate dehydrogenase, and 100 mM potassium phosphate buffer (pH 7.4) containing 0.1 mM EDTA in a total volume of 0.5 ml. The reaction was stopped by adding 2 ml of ethyl acetate. After the addition of 1 μg of 5β-cholestane-3α,7α,12α,27-tetrol as an internal recovery standard, tetrols were extracted twice with 2 ml of ethyl acetate, purified by a Bond Elut SI cartridge, derivatized to trimethylsilyl (TMS) ether and quantified by high-resolution GC-MS with SIM.

2.7. Determination of CYP7A1 and CYP27A1 protein expression level

Proteins from microsomal or mitochondrial fractions (25–50 μg) were separated by SDS-polyacrylamide gel electrophoresis (PAGE) according to the procedure of Laemmli [32]. After electrophoresis, the proteins were transferred onto a polyvinylidine difluoride membrane (Immobilon-P, Millipore). Transferred microsomal fraction was probed with a rabbit anti-human CYP7A1 antibody (1.1000) and transferred mitochondrial fraction was probed with a rabbit anti-rat CYP27A1 antibody (1:1500), respectively, followed by a donkey horseradish peroxidase-labeled anti-rabbit immunoglobulin G (1:3000) (Amersham, Arlington Heights, IL). The immunoreactive proteins were visualized by enhanced chemiluminescence using a kit from Amersham. After being exposed to the membrane, the Hyperfilm (Amersham) was analyzed by densitometric scanning.

2.8. Determination of steady-state mRNA levels of CYP7A1 and CYP27A1

Total RNA was obtained from the stored frozen liver tissues by the method of Chomczynski and Sacchi [33] with minor modifications using RNA-Zol B reagent (Tel-Test Inc., TX). Complementary DNAs (cDNAs) were synthesized from total RNA with M-MLV reverse transcriptase by the random primer method. PCR was performed using 50 pmol of each primer, 200 ng of cDNA template, 1.25 units of Taq DNA polymerase, 200 nmol/l deoxynucleoside triphosphate, in the reaction buffer (10 mmol/l Tris–HCl, pH 8.3, 50 mmol/l KCl, 1.5 mmol/l $MgCl_2$, and 0 01% gelatin) using a DNA thermal cycler (Gene-Amp PCR system 2400; Perkin Elmer, Norwalk, CT). PCR was subjected to the respective cycles (CYP7A1, 30; CYP27A1, 35; and glyceraldehyde-3-phosphate dehydrogenase (G3PDH), 26) at 94, 55, and 72 °C for 1 min each, respectively. PCR primers were designated by referring to cDNA sequences for rat G3PDH, human, rat and rabbit CYP7A1, and human and rat CYP27A1. Primer designs were as follows: hamster CYP7A1, sense 5′-CAC/TCT/CCA/TCT/TGA/GGA/CGG-3′, antisense 5′-GTG/GCA/AAA/TTC/CCA/AGC/CTG-3′; hamster CYP27A1, sense 5′-ACC/TTC/CTC/CCC/AAG/TGG/AC-3′, antisense 5′-CAG/AAC/ACA/AAC/TGG/GTG/TTC-3′; G3PDH, sense 5′-GAA/CGG/GAA/GCT/CAC/TGG/CAT/GGC-3′, antisense 5′-CAG/CAA/CAG/GGT/GGT/GGA/CCT/CA-3′. Aliquots of the reaction mixture were electrophoresed on a 2% agarose gel. PCR products were stained by SYBR-GREEN I (Molecular Probe Inc., Eugene, OR) according to the manufacturer's instructions and semi-quantified using a multi-bioimager (STORM, Molecular Dynamics Inc., Sunnyvale, CA). The data were expressed relative to the amounts of G3PDH mRNA present in each specimen.

2.9. Histological examination

Liver specimens from both sham-operated and 2-day bile duct-ligated hamsters were fixed in 2% paraformaldehyde and mounted. Specimens were evaluated both by light and electron microscopy.

2.10. Statistical analysis

Data are reported as the mean ± SD. The statistical significance between the results in the different groups was evaluated by the Student's two-tailed *t*-test. For all comparisons, significance was accepted at the level of $P < 0.05$.

Table 1

Serum and biliary bile acid profile in sham-operated and bile duct-ligated hamsters

	Sham ($n = 5$)		BDL ($n = 5$)	
	Serum (%)	Bile (%)	Serum (%)	Bile (%)
CA				
F	33 ± 17	0.3 ± 0.2	0.2 ± 0.0	0.8 ± 0.5
G	16 ± 8	33 ± 8	40 ± 1	38 ± 3
T	11 ± 9	37 ± 9	45 ± 2	41 ± 8
CDCA				
F	17 ± 10	0.1 ± 0.1	<0.1	<0.1
G	5 ± 5	8 ± 4	4 ± 1	8 ± 3
T	8 ± 3	13 ± 5	9 ± 1	8 ± 1
DCA				
F	9 ± 9	<0.1	<0.1	<0.1
G	2 ± 2	3 ± 2	0.1 ± 0.0	2 ± 1
T	<0.1	4 ± 3	<0.1	2 ± 1
LCA				
F	<0.1	0.1 ± 0.0	<0.1	<0.1
G	<0.1	0.4 ± 0.2	<0.1	<0.1
T	<0.1	0.7 ± 0.5	<0.1	<0.1
UDCA				
F	<0.1	<0.1	0.9 ± 0.4	0.4 ± 0.4
G	<0.1	<0.1	<0.1	<0.1
T	<0.1	<0.1	0.7 ± 0.4	<0.1
Total	100	100	100	100

Serum and bile were collected from hamsters 2 days after sham operation (Sham) or bile duct ligation (BDL). F, Unconjugated bile acid; G, glycine-conjugated bile acid; T, taurine-conjugated bile acid. Data are expressed as mean ± SD.

3. Results

Fig. 2 summarizes the data comparing the effects of cholestasis on the serum bile acid concentration and composition in human vs. hamster. Serum total bile acid concentration was elevated 34-fold ($P < 0.01$) in patients with obstructive jaundice while the elevation was 116-fold ($P < 0.01$) in hamsters 48 h after bile duct ligation. CA/CDCA ratio was increased from 0.30 to 1.54 ($P < 0.01$) in patients and from 2.0 to 6.8 ($P < 0.01$) in hamsters. The pool

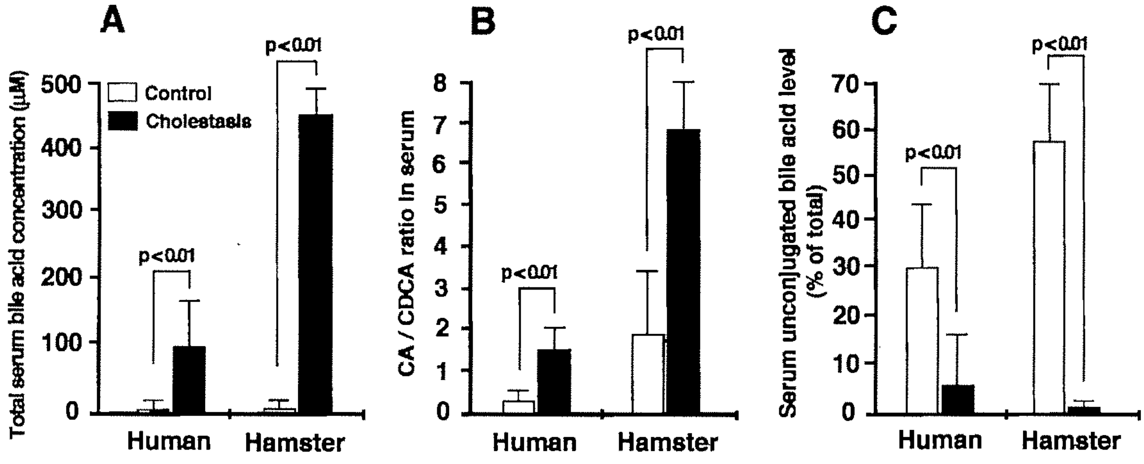

Fig. 2. Effects of cholestasis on total bile acid concentration (A), ratio of cholic to chenodeoxycholic acid concentration (B) and proportion of unconjugated to total bile acid concentration (C) in human and hamster sera. Solid bars represent patients with extrahepatic obstructive jaundice ($n = 8$) or hamster 2 days after bile duct ligation ($n = 5$), while open bars represent control humans ($n = 12$) or sham-operated hamsters ($n = 5$).

Table 2
Serum, hepatic and biliary bile acid concentrations in sham-operated and bile duct-ligated Hamsters

	Sham			BDL		
	Serum ($n=5$) [μM]	Liver ($n=4$) [nmol/g]	Bile ($n=5$) [mM]	Serum ($n=5$) [μM]	Liver ($n=4$) [nmol/g]	Bile ($n=5$) [mM]
CA	2.4 ± 1.0	231 ± 236	94 ± 24	386 ± 12[†]	680 ± 227[‡]	6.3 ± 1.0[†]
CDCA	1.2 ± 1.0	63 ± 57	29 ± 12	57 ± 10[†]	68 ± 26	1.3 ± 0.2[†]
DCA	0.4 ± 0.3	56 ± 50	10 ± 5	0.3 ± 0.2	82 ± 54	0.3 ± 0.2[§]
LCA	< 0.1[a]	7.8 ± 8.8	1.6 ± 0.7	< 0.1[a]	16 ± 13	< 0.01[a,†]
UDCA	< 0.1[a]	29 ± 27	0.04 ± 0.02	7.6 ± 3.6[§]	18 ± 13	0.03 ± 0.02
Total	3.9 ± 2.5	387 ± 112	134 ± 14	452 ± 38[†]	864 ± 105[†]	7.9 ± 1.0[†]
CA/CDCA	2.0 ± 1.9	3.6 ± 1.4	2.8 ± 1.0	6.8 ± 1.4[§]	11.0 ± 5.8[‡]	5.0 ± 1.2[‡]

Serum, liver and bile were collected from hamsters 2 days after sham operation (Sham) or bile duct ligation (BDL). Data are expressed as mean ± SD.

[†] $P<0.001$ vs. sham-operated hamsters.

[‡] $P<0.05$ vs. sham-operated hamsters.

[§] $P<0.01$ vs. sham-operated hamsters.

[a] Limit of detection.

of unconjugated bile acids was reduced from 29% to 5.2% ($P<0.01$) in patients and from 59% to 1.1% ($P<0.01$) in hamsters.

The respective serum and biliary bile acid compositions in bile duct-ligated and sham-operated hamsters are shown in Table 1. In sham-operated hamsters, the proportion of serum unconjugated bile acids (59%) was significantly greater than that in bile (0.5%). In contrast, these proportions were rather similar (1.1% vs. 1.2%) in bile duct-ligated hamsters. The ratios of glycine-conjugated to taurine-conjugated bile acids was not significantly different between bile duct-ligated and sham-operated hamsters.

Table 2 reports the respective serum, hepatic and biliary bile acid concentrations, as well as the CA/CDCA ratios in the bile duct-ligated and sham-operated hamsters. After bile duct ligation, in contrast to a markedly increased serum CA and CDCA concentration, these bile acid concentrations were significantly decreased in gallbladder bile. However, the serum and bile CA/CDCA ratios were both significantly elevated in bile duct-ligated hamsters. The highest CA/CDCA ratio was observed in bile duct-ligated hamster liver tissue. In this model, the hepatic CA concentration was increased 2.9-fold ($P<0.05$) while the other bile acid levels were not significantly different from those in control liver.

Table 3 shows the activity of hepatic key enzymes involved in bile acid biosynthesis. Microsomal CYP7A1, CYP8B1 and CYP3A activities were similar in both bile

Table 3
Hepatic activities of mitochondrial CYP27A1, and microsomal CYP7A1, CYP8B1 and CYP3A in sham-operated, bile duct-ligated and cholestyramine-treated hamsters

Enzymes	Sham ($n=5$)	BDL ($n=5$)	CHY ($n=4$)
	pmol/min/mg protein		
Mitochondrial			
CYP27A1	1.7 ± 0.3	0.8 ± 0.3 *	1.7 ± 0.8
Microsomal			
CYP7A1	1.6 ± 1.0	1.4 ± 0.6	4.7 ± 2.3[†]
CYP8B1	10 ± 6	11 ± 3	ND
CYP3A	38 ± 16	25 ± 12	ND

Livers were obtained from hamsters 2 days after either sham operation (Sham), bile duct ligation (BDL) or fed a 4% cholestyramine containing diet for 1 week (CHY). Specific activities of CYP27A1, CYP7A1, CYP8B1 and CYP3A were determined by measuring 27- and 7α-hydroxylations of cholesterol, 12α-hydroxylation of 7α-hydroxy-4-cholesten-3-one and 25-hydroxylation of 5β-cholestane-3α,7α,12α-triol, respectively. Data are expressed as mean ± SD.

ND, not determined.

* $P<0.005$ vs. sham-operated hamsters.

[†] $P<0.05$ vs. sham-operated hamsters.

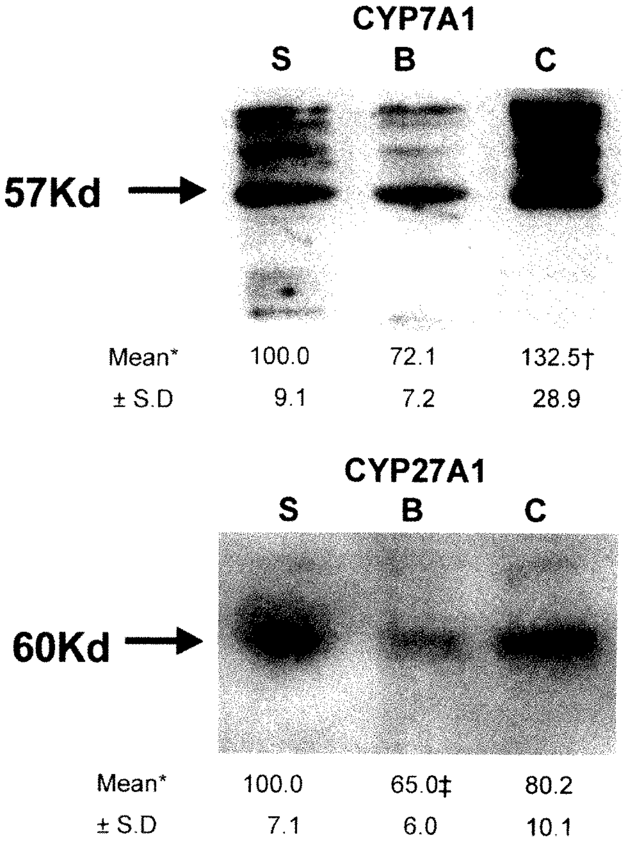

Fig. 3. Western blot of hamster liver microsomal CYP7A1 and mitochondrial CYP27A1. S, sham-operated ($n=4$); B, bile duct-ligated ($n=4$); C, cholestyramine-treated ($n=4$). *, Percentage of sham operation. †$P<0.001$, compared to bile duct ligation, ‡$P<0.05$, compared to sham operation.

duct-ligated and sham-operated hamsters. In contrast, the mitochondrial activity of CYP27A1 was decreased by 53% ($P < 0.005$) in the bile duct-ligated hamsters. In the present study, we also used hamsters fed a diet containing 4% cholestyramine known to activate hamster microsomal CYP7A1 [34,35] as control (Table 3). The protein expression levels of CYP7A1 and CYP27A1 were determined by Western blotting method using specific antibodies against the human CYP7A1 and rat CYP27A1. As shown in Fig. 3, CYP7A1 protein expression level did not change significantly while that of CYP27A1 was significantly decreased in the bile duct-ligated hamsters. This is in agreement with the above reported results on these enzymes' specific activities. We also determined the steady-state mRNA expression levels for CYP7A1 and CYP27A1 by semi-quantitative RT-PCR (Fig. 4). However, bile duct ligation for 2 days did not change the mRNA expression levels of either of these two enzymes.

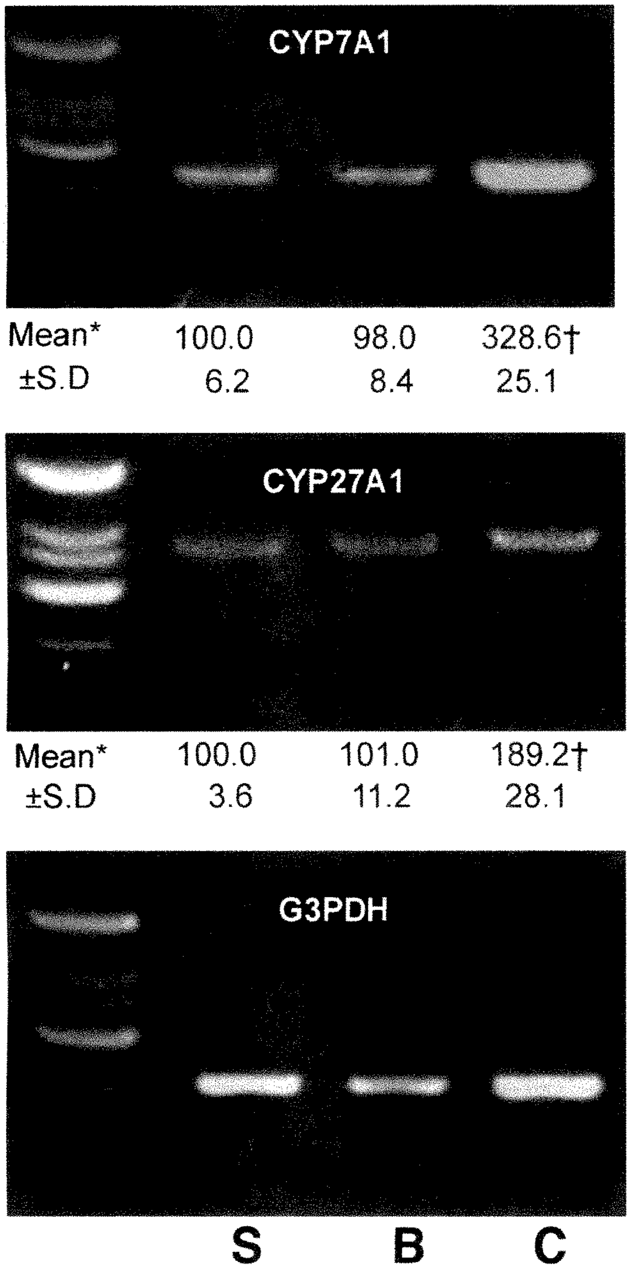

Fig. 4. Relative amount of steady-state mRNA for CYP7A1, CYP27A1 and G3PDH in the livers of sham-operated, bile duct-ligated and cholestyramine-treated hamsters S, sham-operated ($n = 4$); B, bile duct-ligated ($n = 4$); C, cholestyramine-treated ($n = 4$). *, Ratio of mRNA expression level between respective enzymes and G3PDH, percentage of sham operation. †$P < 0.001$, compared to sham operation.

Histological examination suggested dilatation of the hepatic ducts as well as increased biliary ductule proliferation in the bile duct-ligated hamster liver. This was accompanied by infiltration of neutrophils and mononuclear cells. However, neither hepatic necrosis nor periportal or portal fibrosis was found. The electron microscopic findings of liver sections 48 h after bile duct ligation were characterized by swollen hepatocytes and a marked decreased or complete disappearance of glycogen rosettes. The endoplasmic reticulum was dilated while the mitochondria showed no significant pathological change in either form or number. With respect to the canal of Hering, the epithelium showed irregular nuclei in shape and size.

4. Discussion

Our cholestatic hamster model showed a significantly increased serum CA/CDCA ratio and a markedly decreased ratio of unconjugated to total bile acids, which are characteristic features of patients with cholestatic liver diseases. These results are different from those reported in the bile duct-ligated rats. In the cholestatic rat model, the synthesis of CA is either not changed [36] or decreased [37], whereas the β-muricholic acid production is markedly enhanced [36,38,39], and the CA/β-muricholic acid ratio reduced [36,39]. Since β-muricholic acid is formed from CDCA [39], CA/β-muricholic acid ratio in the rat relates to the CA/CDCA ratio in human and hamster. The effect of bile duct ligation on the total bile acid synthesis appears to be different between rats and hamsters. In bile duct-ligated rats, CYP7A1 activity was significantly up-regulated [37,40,41], whereas CYP7A1 activity was not changed in our hamster model. Similar results were also reported in rhesus monkeys [42] and humans [43] where total bile acid synthesis was suppressed during biliary obstruction. Thus, there are considerable species-specific differences in bile acid metabolism, and the hamster may be a better model than the rat for studying bile acid metabolism relevant to patients with obstructive jaundice.

Abnormal flow from hepatocyte canaliculi to sinusoids is one of the important reasons for the increased level of serum total bile acids. Actually, in bile duct-ligated hamsters, the serum bile acid composition, including CA/CDCA ratio and glycine- and taurine-conjugation pattern, were very similar to that found in bile (Table 1). However, the elevated serum CA/CDCA ratio in bile duct-ligated hamsters cannot be solely explained by this abnormal back flow from bile or hepatocytes to serum. The reason is that not only in serum but also in the liver and bile, the CA/CDCA ratio was significantly increased in the bile duct-ligated hamsters. Therefore, altered bile acid synthesis in the cholestatic liver, i.e. enhanced CA synthesis and/or decreased CDCA production is strongly suggested.

When we measured the activity and protein expression level of CYP7A1 and CYP27A1, two key enzymes in the classic and alternative bile acid biosynthetic pathways, respectively, CYP7A1 was not affected but CYP27A1 was significantly down-regulated following bile duct ligation. These results lend support to our hypothesis that in contrast to the bile duct-ligated rats, the total bile acid synthesis was not increased in the bile duct-ligated hamsters. A recent report by Pandak et al. [8] demonstrated that CYP8B1 was capable of 12α-hydroxylating bile acid intermediates from both the classic and alternative pathways. In addition, these authors described CYP8B1 to be the sole regulator of the CA/CDCA ratio. However, as seen in CTX patients, CYP27A1 is also an important enzyme in determining CA/CDCA ratio under pathological conditions. In fact, decreased CYP27A1 activity without change of CYP8B1 activity was observed in bile duct-ligated hamsters and was associated with an increased CA/CDCA ratio. Recent reports show that induction of *CYP3A* family of genes is one of the important mechanisms for detoxification of hydrophobic bile acids in cholestasis [44,45]. The retained activity of CYP3A that is also a key enzyme in the alternative side chain cleavage pathway in CA biosynthesis [46] may explain why the production of CA was not reduced as much as that of CDCA in the bile duct-ligated hamster model.

An interesting observation concerns the regulation of CYP7A1 in cholestasis. In spite of a significantly increased hepatic total bile acid concentration, CYP7A1 was not down-regulated in the cholestatic liver. CDCA is a physiological ligand for the farnesoid X receptor (FXR), an orphan nuclear receptor [47–49]. The binding of CDCA to the receptor leads to the repression of CYP7A1 gene transcription. Our results showed that the hepatic CA concentration was increased while that of CDCA remained unchanged in the bile duct-ligated hamster, which is similar to what is observed in the liver of patients with jaundice of short duration [50]. This may be one of the reasons for the lack of suppression of CYP7A1 activity and expression in bile duct-ligated hamster, although another orphan nuclear receptor, LXRα [51] may also play an important role in the regulation of CYP7A1 in cholestasis.

In contrast to microsomal CYP7A1, CYP8B1 and CYP3A enzymes, mitochondrial CYP27A1 activity and protein level were significantly reduced in the liver of cholestatic hamsters. Although the regulation of CYP27A1 has not yet been clarified, Segev et al. [52] recently reported that the human *CYP27A1* gene had a TATA-less promoter and its transcription was initiated at a cluster of sites. Dexamethasone up-regulates and cyclosporin A down-regulates CYP27A1 at the transcriptional level, while CA inhibits CYP27A1 post-transcriptionally by affecting the stability of its mRNA [52]. It is important to know that there may be species-specific differences in the control of *CYP27A1* gene expression because in rat hepatocytes CA repressed the transcription of *CYP27A1* gene [53].

There are at least two hypotheses to explain the mechanism(s) of decreased CYP27A1 activity in bile duct-ligated hamster. First, as shown in human [52] and rat [53], CYP27A1 might be inhibited by an increased hepatic CA concentration in cholestasis. Hamster hepatic CYP27A1 showed both reduced specific activity and protein expression level without decreased steady-state mRNA level, suggesting CYP27A1 to be post-transcriptionally down-regulated. In the rat extrahepatic cholestatic model, the activity, protein and mRNA levels of the sodium-dependent taurocholate cotransporting polypeptide (ntcp) were markedly reduced [54]. In contrast, 6β-hydroxylations of CDCA and LCA were significantly up-regulated and these hydrophobic bile acids were metabolized to less cytotoxic β-muricholic acid [37,40]. Thus, in the rat model, a signal seems to be generated under cholestatic conditions to regulate bile acid uptake and synthesis, and to diminish the accumulation of potentially hepatotoxic bile acids in rats. Humans and hamsters do not synthesize β-muricholic acid, but rather reduce the formation of CDCA by down-regulating CYP27A1 as a protective mechanism, which parallels the formation of β-muricholic acid in the rat.

Second, hydrophobic bile acids including CDCA are known to cause cellular ATP depletion due to impairment of mitochondrial function in rat hepatocytes [55]. Although the hepatic concentration of bile acids other than CA were not elevated in the cholestatic hamster model, that of CDCA has been suggested to be transiently increased in the earlier period after bile duct ligation. CDCA has also been shown by us [24,56], as well as by others [57] to activate various signal transduction pathways. It is therefore a possibility that this bile acid can be responsible for the decreased CYP27A1 protein expression and/or activity through its regulation of signaling mechanisms. The role for a regulatory mechanism is supported by the fact that while the glycogen rosettes were markedly decreased, there was no significant pathological change in either mitochondrial shape or number in the cholestatic hamster liver.

In summary, the hamster hepatic mitochondrial CYP27A1 was post-transcriptionally down-regulated while the microsomal CYP7A1 and CYP8B1 were not affected by bile duct ligation. This could explain, at least in part, the increased serum CA/CDCA ratio and the decreased CDCA production observed in cholestatic hamsters.

Acknowledgements

This work was supported by a grant from the Ministry of Education, Science and Culture of Japan #12670457

(Matsuzaki, Y.) and from the National Institutes of Health DK46954 (Bouscarel, B.), respectively.

References

[1] J.B. Carey Jr., The serum trihydroxy–dihydroxy bile acid ratio in liver and biliary tract disease, J. Clin. Invest. 37 (1958) 1494–1503.

[2] I. Makino, S. Nakagawa, K. Mashimo, Conjugated and unconjugated serum bile acid levels in patients with hepatobiliary diseases, Gastroenterology 56 (1969) 1033–1039.

[3] T. Osuga, Y. Matsuzaki, N. Tanaka, T. Beppu, K. Mitamura, M. Imawari, J. Shoda, Clinical application of serum bile acid determination in gastrointestinal and liver diseases, Proceedings of the First International Symposium on Bile acids in Hepatobiliary and Gastrointestinal Diseases, 1983, pp. 79–90.

[4] Z.R. Vlahcevic, W.M. Pandak, D.M. Heuman, P.B. Hylemon, Function and regulation of hydroxylases involved in the bile acid biosynthesis pathways, Semin. Liver Dis. 12 (1992) 403–419.

[5] Z.R. Vlahcevic, G. Eggertsen, I. Björkhem, P.B. Hylemon, K. Redford, W.M. Pandak, Regulation of sterol 12α-hydroxylase and cholic acid biosynthesis in the rat, Gastroenterology 118 (2000) 599–607.

[6] I. Björkhem, Mechanism of bile acid biosynthesis in mammalian liver, in: H. Danielsson, J. Sjövall (Eds.), In Sterols and Bile Acids, Elsevier, Amsterdam, Netherlands, 1985, pp. 231–278.

[7] Y. Ayaki, E. Kok, N.B. Javitt, Cholic acid synthesis from 26-hydroxycholesterol and 3-hydroxy-5-cholestenoic acid in the rabbit, J. Biol. Chem. 264 (1989) 3818–3821.

[8] W.M. Pandak, P. Bohdan, C. Franklund, D.H. Mallonee, G. Eggertsen, I. Björkhem, G. Gil, Z.R. Vlahcevic, P.B. Hylemon, Expression of sterol 12α-hydroxylase alters bile acid pool composition in primary rat hepatocytes and in vivo, Gastroenterology 120 (2001) 1801–1809.

[9] J.J. Cali, C.-L. Hsieh, U. Francke, D.W. Russell, Mutations in the bile acid biosynthetic enzyme sterol 27-hydroxylase underlie cerebrotendinous xanthomatosis, J. Biol. Chem. 266 (1991) 7779–7783.

[10] E. Leitersdorf, A. Reshef, V. Meiner, R. Levitzki, S. Pressman-Schwartz, E.J. Dann, N. Berkman, J.J. Cali, L. Klapholz, V.M. Berginer, Frameshift and splice-junction mutations in the sterol 27-hydroxylase gene cause cerebrotendinous xanthomatosis in Jews or Moroccan origin, J. Clin. Invest. 91 (1993) 2488–2496.

[11] K.S. Kim, S. Kubota, M. Kuriyama, J. Fujiyama, I. Björkhem, G. Eggertsen, Y. Seyama, Identification of new mutations in sterol 27-hydroxylase gene in Japanese patients with cerebrotendinous xanthomatosis (CTX), J. Lipid Res. 35 (1994) 1031–1039.

[12] M.-H. Lee, S. Hazard, J.D. Carpten, S. Yi, J. Cohen, G.T. Gerhardt, G. Salen, S.B. Patel, Fine-mapping, mutation analyses, and structural mapping of cerebrotendinous xanthomatosis in U.S. pedigrees, J. Lipid Res. 42 (2001) 159–169.

[13] G. Salen, S. Shefer, G.S. Tint, G. Nicolau, B. Dayal, A.K. Batta, Biosynthesis of bile acids in cerebrotendinous xanthomatosis, J. Clin. Invest. 76 (1985) 744–751.

[14] K. Okuda, O. Masumoto, Y. Ohyama, Purification and characterization of 5β-cholestane-3α, 7α, 12α-triol 27-hydroxylase from female rat liver mitochondria, J. Biol. Chem. 263 (1988) 18138–18142.

[15] S. Shefer, F.W. Cheng, B. Dayal, S. Hauser, G.S. Tint, G. Salen, E.H. Mosbach, A 25-hydroxylation pathway of cholic acid biosynthesis in man and rat, J. Clin. Invest. 57 (1976) 897–903.

[16] G. Salen, S. Shefer, F.W. Cheng, B. Dayal, A.K. Batta, G.S. Tint, Cholic acid biosynthesis, J. Clin. Invest. 63 (1979) 38–44.

[17] D.K. Spady, S.D. Turley, J.M. Dietschy, Dissociation of hepatic cholesterol synthesis from hepatic low-density lipoprotein uptake and biliary cholesterol saturation in female and male hamsters of different ages, Biochim. Biophys. Acta 753 (1983) 381–392.

[18] D.K. Spady, E.F. Stange, E. Bilhartz, M. Dietschy, Bile acids regulate hepatic low density lipoprotein receptor activity in the hamster by altering cholesterol flux across the liver, Proc. Natl. Acad. Sci. U. S. A., 83 (1986) 1916–1920.

[19] H.-S. Kim, W.K. Wilson, D.H. Needleman, F.D. Pinkerton, D.K. Wilson, F.A. Quiocho , G.J. Schroepfer Jr., Inhibitors of sterol synthesis. Chemical synthesis, structure, and biological activities of (25R)-3β,26-dihydroxy-5α-cholest-8(14)-en-15-one, a metabolite of 3β-hydroxy-5α-cholest-8(14)-en-15-one, J. Lipid Res. 30 (1989) 247–261.

[20] S. Bergström, L. Krabisch, Preparation of some hydroxy coprostanes, 3α,7α- and 3α,12α-dihydroxy coprostane, Acta Chem. Scand. 11 (1957) 1067.

[21] B. Dayal, S. Shefer, G.S. Tint, G. Salen, E.H. Mosbach, Synthesis of 5β-cholestane-3α, 7α, 12α, 25-tetrol and 5β-cholestane-3α, 7α, 12α, 24ξ, 25-pentol, J. Lipid Res. 17 (1976) 74–77.

[22] A. Honda, J. Shoda, N. Tanaka, Y. Matsuzaki, T. Osuga, N. Shigematsu, M. Tohma, H. Miyazaki, Simultaneous assay of the activities of two key enzymes in cholesterol metabolism by gas chromatography-mass spectrometry, J. Chromatogr. 565 (1991) 53–66.

[23] J. Shoda, M. Axelson, J. Sjövall, Synthesis of potential C27-intermediates in bile acid biosynthesis and their deuterium-labeled analogs, Steroids 58 (1993) 119–125.

[24] Y. Matsuzaki, B. Bouscarel, M. Le, S. Ceryak, T.W. Gettys, J. Shoda, H. Fromm, Effect of cholestasis on regulation of cAMP synthesis by glucagon and bile acids in isolated hepatocytes, Am. J. Phys. 273 (1997) G164–G174.

[25] S. Okuyama, N. Kokubo, S. Higashidate, D. Uemura, Y. Hirata, A new analytical method of individual bile acids using high performance liquid chromatography and immobilized 3α-hydroxysteroid dehydrogenase in column form, Chem. Lett. 89 (1981) 1963–1973.

[26] A. Honda, T. Yoshida, N. Tanaka, Y. Matsuzaki, B. He, J. Shoda, T. Osuga, Increased bile acid concentration in liver tissue with cholesterol gallstone disease, J. Gastroenterol. 30 (1995) 61–66.

[27] A. Honda, G. Salen, Y. Matsuzaki, A.K. Batta, G. Xu, E. Leitersdorf, G.S. Tint, S.K. Erickson, N. Tanaka, S. Shefer, Differences in hepatic levels of intermediates in bile acid biosynthesis between CYP27$^{-/-}$ mice and CTX, J. Lipid Res. 42 (2001) 291–300.

[28] O.H. Lowry, N.J. Rosebrough, A.L. Farr, R.J. Randall, Protein measurement with the Folin phenol reagent, J. Biol. Chem. 193 (1951) 265–275.

[29] A. Honda, G. Salen, S. Shefer, A.K. Batta, M. Honda, G. Xu, G.S. Tint, Y. Matsuzaki, J. Shoda, N. Tanaka, Bile acid synthesis in the Smith–Lemli–Opitz syndrome: effects of dehydrocholesterols on cholesterol 7α-hydroxylase and 27-hydroxylase activities in rat liver, J. Lipid Res. 40 (1999) 1520–1528.

[30] M. Noshiro, H. Ishida, S. Hayashi, K. Okuda, Assays for cholesterol 7α-hydroxylase and 12α-hydroxylase using high performance liquid chromatography, Steroids 45 (1985) 539–549.

[31] A. Honda, G. Salen, S. Shefer, Y. Matsuzaki, G. Xu, A.K. Batta, G.S. Tint, N. Tanaka, Regulation of 25- and 27-hydroxylation side chain cleavage pathways for cholic acid biosynthesis in humans, rabbits and mice: assay of enzyme activities by high-resolution gas chromatography-mass spectrometry, J. Lipid Res. 41 (2000) 442–451.

[32] U.K. Laemmli, Cleavage of structural proteins during the assembly of the head of bacteriophage T4, Nature 227 (1970) 680–685.

[33] P. Chomczynski, N. Sacchi, Single-step method of RNA isolation by acid guanidinium thiocyanate-phenol-chloroform extraction, Anal. Biochem. 162 (1987) 156–159.

[34] L.J. Schoenfield, G.G. Bonorris, P. Ganz, Induced alterations in the rate-limiting enzymes of hepatic cholesterol and bile acid synthesis in the hamster, J. Lab. Clin. Med. 82 (1973) 858–868.

[35] J. Shoda, N. Tanaka, B. He, A. Honda, T. Yoshida, Y. Matsuzaki, T. Osuga, Novel sterol 7α-hydroxylases active towards not cholesterol but side-chain oxygenated steroids in liver microsomes, Gastroenterol. Jpn. 28 (1993) 438.

[36] T. Kinugasa, K. Uchida, M. Kadowaki, H. Takase, Y. Nomura, Y. Saito, Effect of bile duct ligation on bile acid metabolism in rats, J. Lipid Res. 22 (1981) 201–207.

[37] J. Gustafsson, Effect of biliary obstruction on 26-hydroxylation of C27-steroids in bile acid synthesis, J. Lipid Res. 19 (1978) 237–243.

[38] T.A. Mahowald, J.T. Matschiner, S.L. Hsia , E.A. Doisy Jr., W.H. Elliott, E.A. Doisy, Bile acids: III. Acid I; the principal bile acid in urine of surgically jaundiced rats, J. Biol. Chem. 225 (1957) 795–802.

[39] H. Greim, D. Trülzsch, J. Roboz, K. Dressler, P. Czygan, F. Hutterer, F. Schaffner, H. Popper, Mechanism of cholestasis: 5. Bile acids in normal rat livers and in those after bile duct ligation, Gastroenterology 63 (1972) 837–845.

[40] H. Danielsson, Effect of biliary obstruction on formation and metabolism of bile acids in rat, Steroids 22 (1973) 567–579.

[41] S. Dueland, J. Reichen, G.T. Everson, R.A. Davis, Regulation of cholesterol and bile acid homeostasis in bile-obstructed rats, Biochem. J. 280 (1991) 373–377.

[42] R.N. Redinger, S.M. Strasberg, D.M. Small, Primate biliary physiology: IX. Effects of acute biliary obstruction on biliary lipid metabolism in the monkey, Am. J. Phys. 226 (1974) 776–783.

[43] M. Bertolotti, L. Carulli, M. Concari, P. Martella, P. Loria, E. Tagliafico, S. Ferrari, M. Del Puppo, B. Amati, E. De Fabiani, M. Crestani, C. Amorotti, A. Manenti, F. Carubbi, A. Pinetti, N. Carulli, Suppression of bile acid synthesis, but not of hepatic cholesterol 7α-hydroxylase expression, by obstructive cholestasis in humans, Hepatology 34 (2001) 234–242.

[44] J.L. Staudinger, B. Goodwin, S.A. Jones, D. Hawkins-Brown, K.I. Mackenzie, A. LaTour, Y. Liu, C.D. Klaassen, K.K. Brown, J. Reinhard, T.M. Willson, B.H. Koller, S.A. Kliewer, The nuclear receptor PXR is a lithocholic acid sensor that protects against liver toxicity, Proc. Natl. Acad. Sci. U. S. A. 98 (2001) 3369–3374.

[45] W. Xie, A. Radominska-Pandya, Y. Shi, C.M. Simon, M.C. Nelson, E.S. Ong, D.J. Waxman, R.M. Evans, An essential role for nuclear receptors SXR/PXR in detoxification of cholestatic bile acids, Proc. Natl. Acad. Sci. U. S. A. 98 (2001) 3375–3380.

[46] A. Honda, G. Salen, Y. Matsuzaki, A.K. Batta, G. Xu, E. Leitersdorf, G.S. Tint, S.K. Erickson, N. Tanaka, S. Shefer, Side chain hydroxylations in bile acid biosynthesis catalyzed by CYP3A are markedly upregulated in Cyp27$^{-/-}$ mice but not in cerebrotendinous xanthomatosis, J. Biol. Chem. 276 (2001) 34579–34585.

[47] H. Wang, J. Chen, K. Hollister, L.C. Sowers, B.M. Forman, Endogenous bile acids are ligands for the nuclear receptor FXR/BAR, Mol. Cell 3 (1999) 543–553.

[48] M. Makishima, A.Y. Okamoto, J.J. Repa, H. Tu, R.M. Learned, A. Luk, M.V. Hull, K.D. Lustig, D.J. Mangelsdorf, B. Shan, Identification of a nuclear receptor for bile acids, Science 284 (1999) 1362–1365.

[49] D.J. Parks, S.G. Blanchard, R.K. Bledsoe, G. Chandra, T.G. Consler, S.A. Kliewer, J.B. Stimmel, T.M. Willson, A.M. Zavacki, D.D. Moore, J.M. Lehmann, Bile acids: natural ligands for an orphan nuclear receptor, Science 284 (1999) 1365–1368.

[50] H. Greim, D. Trülzsch, P. Czygan, J. Rudick, F. Hutterer, F. Schaffner, H. Popper, Mechanism of cholestasis: 6. Bile acids in human livers with or without biliary obstruction, Gastroenterology 63 (1972) 846–850.

[51] B.A. Janowski, M.J. Grogan, S.A. Jones, G.B. Wisely, S.A. Kliewer, E.J. Corey, D.J. Mangelsdorf, Structural requirements of ligands for the oxysterol liver X receptors LXRα and LXRβ, Proc. Natl. Acad. Sci. U. S. A. 96 (1999) 266–271.

[52] H. Segev, A. Honigman, H. Rosen, E. Leitersdorf, Transcriptional regulation of the human sterol 27-hydroxylase gene (CYP27) and promoter mapping, Atherosclerosis 156 (2001) 339–347.

[53] Y.P. Rao, Z.R. Vlahcevic, R.T. Stravitz, D.H. Mallonee, J. Mullick, N.G. Avadhani, P.B. Hylemon, Down-regulation of the rat hepatic sterol 27-hydroxylase gene by bile acids in transfected primary hepatocytes: possible role of hepatic nuclear factor 1α, J. Steroid Biochem. Mol. Biol. 70 (1999) 1–14.

[54] C. Gartung, M. Ananthanarayanan, M.A. Rahman, S. Schuele, A. Nundy, C.J. Soroka, A. Stolz, F.J. Suchy, J.L. Boyer, Down-regulation of expression and function of the rat liver Na^+/bile acid cotransporter in extrahepatic cholestasis, Gastroenterology 110 (1996) 199–209.

[55] J.R. Spivey, S.F. Bronk, G.J. Gores, Glycochenodeoxycholate-induced lethal hepatocellular injury in rat hepatocytes: role of ATP depletion and cytosolic free calcium, J. Clin. Invest. 92 (1993) 17–24.

[56] B. Bouscarel, Y. Matsuzaki, M. Le, T.W. Gettys, H. Fromm, Changes in G protein expression account for impaired modulation of hepatic cAMP formation after BDL, Am. J. Phys. 274 (1998) G1151–G1159.

[57] B.A. Jones, Y.P. Rao, R.T. Stravitz, G.J. Gores, Bile salt-induced apoptosis of hepatocytes involves activation of protein kinase C, Am. J. Phys. 272 (1997) G1109–G1115.

ELSEVIER

Biochimica et Biophysica Acta 1588 (2002) 149–158

BIOCHIMICA ET BIOPHYSICA ACTA

BBA

www.bba-direct.com

The role of oxidative stress in the ochratoxin A-mediated toxicity in proximal tubular cells

G.J. Schaaf[a], S.M. Nijmeijer[a], R.F.M. Maas[a], P. Roestenberg[a],
E.M. de Groene[b], J. Fink-Gremmels[a,*]

[a]*Department of Veterinary Pharmacology, Pharmacy and Toxicology (VFFT) Faculty of Veterinary Medicine, Utrecht University, P.O. Box 80152 NL 3508 TD, Utrecht, The Netherlands*
[b]*Unilever Health Institute, P.O. Box 114, 3130 AC Vlaardingen, The Netherlands*

Received 6 December 2001; received in revised form 4 June 2002; accepted 26 June 2002

Abstract

Balkan endemic nephropathy (BEN), a disease characterized by progressive renal fibrosis in human patients, has been associated with exposure to ochratoxin A (OTA). This mycotoxin is a frequent contaminant of human and animal food products, and is toxic to all animal species tested. OTA predominantly affects the kidney and is known to accumulate in the proximal tubule (PT). The induction of oxidative stress is implicated in the toxicity of this mycotoxin.

In the present study, primary rat PT cells and LLC-PK_1 cells, which express characteristics of the PT, were used to investigate the OTA-mediated oxidative stress response. OTA exposure of these cells resulted in a concentration-dependent elevation of reactive oxygen species (ROS) levels, depletion of cellular glutathione (GSH) levels and an increase in the formation of 8-oxoguanine.

The OTA-induced ROS response was significantly reduced following treatment with α-tocopherol (TOCO). However, this chain-braking anti-oxidant did not reduce the cytotoxicity of OTA and was unable to prevent the depletion of total GSH levels in OTA-exposed cells. In contrast, pre-incubation of the cell with *N*-acetyl-L-cysteine (NAC) completely prevented the OTA-induced increase in ROS levels as well as the formation of 8-oxoguanine and completely protected against the cytotoxicity of OTA. In addition, NAC treatment also limited the GSH depletion in OTA-exposed PT- and LLC-PK_1 cells.

From these data, we conclude that oxidative stress contributes to the tubular toxicity of OTA. Subsequently, cellular GSH levels play a pivotal role in limiting the short-term toxicity of this mycotoxin in renal tubular cells.

© 2002 Elsevier Science B.V. All rights reserved.

Keywords: 8-Oxoguanine; Nephrotoxicity; Ochratoxin A; Oxidative damage; Proximal tubule cell; Reactive oxygen species

1. Introduction

Ochratoxin A (OTA) is produced by *Aspergillus* and *Penicillium* strains, and is a frequent contaminant of feed and foodstuffs. Epidemiological studies associate OTA with Balkan endemic nephropathy (BEN), a progressive renal fibrosis, and tumors of the urinary tract. However, the etiology of the disease still remains unclear [1–3]. In animals, OTA was shown to induce a tubulo-interstitial nephropathy similar to BEN [4–6] as well as renal adenoma and carcinoma [7]. Other toxic effects associated with OTA include immunosuppression, hepatotoxicity and teratogenicity (for a review, see Refs. [8–12]).

OTA is known to affect multiple sites of the nephron: acute exposure mainly affects the postproximal parts, while chronic exposure leads predominantly to damage of the proximal tubule (PT) [13]. The exact mechanism of OTA toxicity has not been elucidated as of yet. OTA contains a chlorinated dihydroisocoumarin moiety linked to L-phenylalanine. The observed inhibition of protein synthesis by OTA [14] results from competition with phenylalanine during the aminoacetylation reaction of phenylalanine–tRNA [12]. The inhibition of protein synthesis is thought to underlie most toxic effects of OTA, but protein inhibition alone cannot explain the diverse but apparent site-specific toxic effects. Several studies propose the involvement of oxidative stress to the toxicity of OTA [5,15–17]. Initially,

---

[*] Corresponding author. Tel.: +31-30-253-5453; fax: +31-30-253-4125/5077.
E-mail address: j.fink@vfft.vet.uu.nl (J. Fink-Gremmels).

0925-4439/02/$ - see front matter © 2002 Elsevier Science B.V. All rights reserved.
PII: S0925-4439(02)00159-X

Rahimtula et al. [17] have shown that OTA induces lipid peroxidation (LPO) in subcellular fractions. Further evidence showing that OTA is a potent pro-oxidant was provided by Belmadani et al. [15] who reported that OTA induced LPO in primary cultures of brain cells. In addition, the formation of reactive oxygen species (ROS) was significantly increased after exposure of foetal rat telencephalon cells to high OTA concentrations [18]. The kidney is a prominent site for intense oxidative processes in the body and ROS play an important role in the pathogenesis of a variety of renal diseases [19]. Thus, we investigated the relation between the OTA-induced oxidative response and toxicity in its main target cells, renal PT cells, using primary rat proximal tubular cells (PT cells) and continuous proximal tubular cells (LLC-PK$_1$). Primary cells resemble the in vivo PT cell closely by expressing PT-specific functions including phase I and II biotransformation and organic anion and cation transport [20]. LLC-PK$_1$ cells are widely used as in vitro model of cultured tubular epithelial cells, as they have retained several characteristics of the PT cell [21]. In contrast to the primary cells, the LLC-PK$_1$ cells have lost some differentiated functions, including organic anion transport [22]. The OTA-induced stress response was monitored at several levels in these cells, as ROS can attack almost any cellular structure or molecule, including membrane lipids, proteins and DNA [23,24]. The effects of exposure of the cells to OTA on ROS production and cell viability were assessed with respect to concentration- and time-dependency. Furthermore, the effects of the mycotoxin on cellular glutathione (GSH) levels and the formation of 8-oxoguanine were investigated. The established anti-oxidants α-tocopherol (TOCO) and *N*-acetyl-L-cysteine (NAC) were used to determine the contribution of oxidative stress to DNA damage and cytotoxicity induced by OTA.

2. Materials and methods

2.1. Materials

Dimethylthiazol diphenyl tetrazolium bromide (MTT), NAC, OTA and TOCO were obtained from Sigma (St. Louis, MO, USA). 2′,7′-Dichlorodihydrofluorescein diacetate (H_2DCF-DA) was obtained from Molecular Probes (Leiden, The Netherlands). DMEM/F12 and medium 199 culture media and supplement G (insulin 10 mg/l, transferrin 5.5 mg/l, sodium-selenite 6.7 μg/l) were obtained from Life Technologies (Breda, The Netherlands). All other chemicals were of analytical grade and purchased from Sigma (St. Louis, MO, USA). OTA, TOCO and H_2DCF-DA were dissolved in DMSO and diluted in culture medium to the concentrations described in the text. NAC was diluted in ethanol/H_2O (1:1; v/v). Solvent concentrations were 0.1% (v/v) unless specified otherwise. OTA dilutions were prepared in serum-free medium.

2.2. Cell culture

2.2.1. Isolation of rat PT cells

Rat PT cells were isolated as described previously [20]. Cell yield was 30–50 × 10^6 cells/rat and cell viability was routinely higher than 70% as judged by trypan blue exclusion. Cells were seeded on collagen (rat tail type IV) precoated 60 mm culture dishes (1 × 10^6 cells/dish) in culture medium containing serum (10% FCS) for 24 h. After 24 h, non-attached cells were removed, pelleted and re-plated (in the same culture dishes) in fresh serum-free culture medium to increase attachment efficiency. Medium was then changed every 3 days with serum-free DMEM/F12 supplemented with 10 mg/l insulin, 5.5 mg/l transferrin, 6.7 μg/ml sodium selenite (supplement G; 1 × concentrated), 10 U/ml penicillin and 10 μg/ml streptomycin. OTA, H_2DCF-DA and TOCO were dissolved in DMSO; NAC was dissolved in H_2O/ethanol (1:1, v/v). The stock solutions were further diluted in culture medium, so that solvent concentrations never exceeded 0.1% (v/v).

2.2.2. LLC-PK$_1$ cells

LLC-PK$_1$ cells, obtained from ATCC (number CL-101) were routinely seeded at 4 × 10^5 cells/75 cm^2 flask and were subcultured every 6–7 days. Two days before experiments, cells were plated at a density of 2.7 × 10^4 cells/cm^2 culture area in medium 199 supplemented with 5% FCS, 2 mM L-glutamine, 100 U/ml penicillin and 100 μg/ml streptomycin. Cells were maintained in a 5% CO_2 humidified atmosphere at 37 °C.

2.3. Determination of ROS production

Cells were seeded in 96-well culture plates at 1 × 10^4 cells/well and allowed to grow for 48 h. In the dose-response experiments, cells were then incubated for 2 h at 37 °C cells in serum-free medium containing 20 μM H_2DCF-DA. After aspiration of H_2DCF-DA, the cells were rinsed once and were subsequently exposed to increasing concentrations of OTA (0–200 μM) in serum- and phenol red-free medium. ROS production was measured after 24 h incubation on a Cytofluor 2300 (Fluorescence Measurement System, Millipore, Bedford, MA, USA) with an excitation wavelength of 485 nm and an emission wavelength of 538 nm. In the experiments with the anti-oxidants, cells were incubated 48 h after plating with increasing concentrations of TOCO (0–12.5 μM) or NAC (0–4 mM). Following the 24-h pre-incubation period, the cells were treated with H_2DCF-DA as described above. After removal of H_2DCF-DA, cells were exposed to a fixed OTA concentration (100 μM) in the presence of increasing concentrations of TOCO or NAC. The ROS levels were determined 24 h later as described above. The incubation volumes were 50 μl/well unless specified otherwise. Relative ROS production was expressed as the ratio of fluorescence of the treated samples over the response in the appropriate controls [$(\text{fluorescence}_{\text{treatment}}/\text{fluorescence}_{\text{control}})100\%$].

2.4. Determination of cell viability

Cell viability was assessed by measuring the reduction of MTT to formazan by the mitochondrial enzyme succinate dehydrogenase [25]. Cells were seeded on 96-well plates at 1×10^4 cells/well. In the dose-response experiments, cells were exposed to increasing concentrations of OTA (0–200 μM) for 4 and 24 h. Then 0.6 mg/ml MTT solution (final concentration in medium; 3 mg/ml stock dissolved in PBS) was added to the wells. Plates were then incubated for 2 h at 37 °C in a humidified atmosphere. The reaction was terminated by discarding the incubation solutions followed by dissolving the formazan product in 50 μl acidic isopropanol (containing 0.1 M HCl). Absorbance at 595 nm was determined on a Biorad 3550 microplate reader (Biorad, Veenendaal, The Netherlands).

In the experiments with the anti-oxidants, cells were incubated 48 h after plating with increasing concentrations of TOCO (0–12.5 μM) or NAC (0–4 mM). Following the 24-h pre-incubation period, cells were exposed to a fixed OTA concentration (100 μM) in the presence of increasing concentrations of TOCO or NAC. Cell viability was determined 24 h later as described above. The incubation volumes were 50 μl/well unless specified otherwise.

Cell viability was expressed as the relative formazan formation in treated samples as compared to that in solvent-treated controls [(A_{595} treated cells/A_{595} of appropriate control)100%, after correction for background absorbance]. IC$_{50}$ values, defined as the concentrations inducing 50% loss of cell viability, were estimated from the figures. IC$_{50}$ values (24 h OTA incubation) were calculated after fitting the cell viability data with Slide Write plus software, version 4.0 (BIS Netherlands, Ridderkerk, The Netherlands).

2.5. Determination of cellular GSH levels

Total cellular GSH (reduced GSH, GSSG and GSSR) measurements were based on the method described by Griffith [26]. Cells were seeded at 5×10^4 cells/well in 24-well plates (for rat PT cells, the plates were coated with collagen type I as previously described [20]). The (pre-) incubation volumes were 500 μl. Cells were either pre-incubated for 24 h with solvent (0.1% DMSO or ethanol), 5 μM TOCO, 2 mM NAC (PT cells) or 4 mM NAC (LLC-PK$_1$). Initially, for measurements of solvent controls, cells were treated with either 0.1% (v/v) DMSO (vehicle for TOCO) or 0.1% (v/v) ethanol/ddH$_2$O [1:1] (vehicle for NAC) and results interpreted independently. However, replicate measurements (two groups of triplicate measurements) showed that these solvent control groups did not differ significantly and are thus presented as one group (solvent in Table 1). Following the pre-incubation period, cells were exposed to OTA (0, 6.25 or 100 μM). After 24 h, the incubation medium was aspirated and cells were harvested in 100 μl cold harvest buffer [Triton X-100 0.05% (w/v), EDTA 0.05 mM in PBS]. The amount of protein was determined in 10 μl of this suspension, while 10 μl sulfosalicylic acid 25% (w/v) was added to the remaining 90 μl sample. After centrifugation of the samples (12,000 × g, 5 min 4 °C), 20 μl triethanolamine (T-1377, Sigma) was added. GSH levels were determined in a mixture containing 5.3 mM NADPH and 0.6 mM 5-5′ dithio-bis (2-nitrobenzoic acid) [DTNB]. After incubation for 5 min at 30 °C, 25 μl sample or GSH standard (0, 0.5, 1.0, 2.0 and 3.0 mg/ml) was added. The reaction was initiated with glutathione reductase (0.5 U/sample) and the increase in absorption at 412 nm and 30 °C was determined. Specific activity was calculated by comparison to a standard curve. Activity was expressed as nanomoles per milligram total cellular protein.

Table 1
The effect of anti-oxidant treatment on GSH levels (nmol/mg protein) in rat PT- and LLC-PK$_1$ cells exposed to OTA for 4 and 24 h

OTA	Anti-oxidant	PT cells		LLC-PK$_1$	
		4 h OTA	24 h OTA	4 h OTA	24 h OTA
OTA 0 μM					
	Solvent[a]	3.2 ± 1.3	1.5 ± 0.4	22.9 ± 3.3	15.8 ± 2.1
	TOCO	4.1 ± 0.7	2.0 ± 0.9	26.6 ± 2.4	23.8 ± 2.1 [*]
	NAC	28.2 ± 4.4 [*]	21.1 ± 2.0 [*]	26.8 ± 2.5	16.5 ± 2.3
OTA 6.25 μM					
	Solvent[a]	3.7 ± 1.2	2.0 ± 2.3	20.4 ± 4.0	12.2 ± 6.8
	TOCO	4.9 ± 1.4	1.9 ± 1.3	23.5 ± 3.7	9.0 ± 3.8
	NAC	38.2 ± 4.5 [*,#]	15.5 ± 3.9 [*,#]	31.1 ± 4.0[#]	24.1 ± 6.5
OTA 100 μM					
	Solvent[a]	5.5 ± 1.5	ND	18.2 ± 2.0	3.4 ± 2.3 [*,#]
	TOCO	5.2 ± 1.2	ND	21.6 ± 1.7	5.9 ± 1.2 [*]
	NAC	30.4 ± 4.1 [*,$]	3.8 ± 0.9 [*,$]	28.4 ± 2.5[$]	8.3 ± 8.8 [*]

Cells were pre-incubated for 24 h with 5 μM TOCO, 2 mM NAC (PT cells) or 4 mM (LLC-PK$_1$) NAC. Following pre-incubation with the anti-oxidant, OTA was added and GSH levels were determined 4 and 24 h later. The data represent means ± S.D. from triplicate measurements from at least two independent experiments. Symbols indicate significant difference ($P < 0.05$). ND: below limit of detection (<30 pmol/mg protein).

[a] Solvent-treated cells refer to cells treated with 0.1% (v/v) DMSO (vehicle for TOCO) or 0.1% (v/v) ethanol/ddH$_2$O [1:1] (vehicle for NAC).

[*] Significantly different from GSH levels in non-exposed (0 μM OTA) solvent-treated cells.

[#] Significantly different GSH levels in solvent-treated cells exposed to 6.25 μM OTA.

[$] Significantly different GSH levels in solvent-treated cells exposed to 100 μM OTA.

2.6. Detection of OTA-induced oxidative DNA damage

LLC-PK$_1$ cells were seeded at 5×10^4 cells/chamber on LabTek 8-chamber slides (Nalgene, cat. no. 177445, Life Technologies, Breda, The Netherlands) 2 days before the start of the experiment. As reference, cells were exposed to methylene blue (2 mM; MB) for 1 h followed by 30 min exposure to ambient light, a treatment known to generate primarily 8-oxoguanine adducts [27]. For experiments involving OTA, LLC-PK$_1$ cells were either pre-incubated with solvent (0.1% EtOH) or with 4 mM NAC for 24 h. Cells were then exposed to 15 μM OTA for 4 and 24 h. The cells were fixed using cold 4% paraformaldehyde for 30 min. The Biotrin OxyDNA assay (Biotrin, cat. no. BIO81-DNA, Dublin, Ireland) was used to detect the formation of 8-oxyguanine adducts. The Biotrin OxyDNA assay was performed according to the manufacturers' instructions. Micrographs were taken immediately following the experiments using a fluorescence microscope (Olympus BX60, Hamburg, Germany; with a U-MNB fluorescence filter wheel, excitation wavelength between 470 and 490 nm, emission wavelength 520 and 550 nm, magnification × 20).

2.7. Protein determination

Total cellular protein was determined according to the method described by Lowry et al. [28].

2.8. Statistical analysis

Significance of differences between different data groups was first determined using a one-way ANOVA analysis within a study and then by *t*-test pairwise comparison (Bonferroni) of the groups of data using SYSTAT 8.0. Differences were considered significant if $P < 0.05$.

3. Results

3.1. OTA-induced production of ROS

Fig. 1 shows that OTA concentration-dependently induced the formation of ROS in both cell types. ROS levels of primary rat PT cells were already significantly elevated above the levels in solvent-treated (DMSO) controls after 4 h of incubation with 12.5 μM OTA (Fig. 1A).

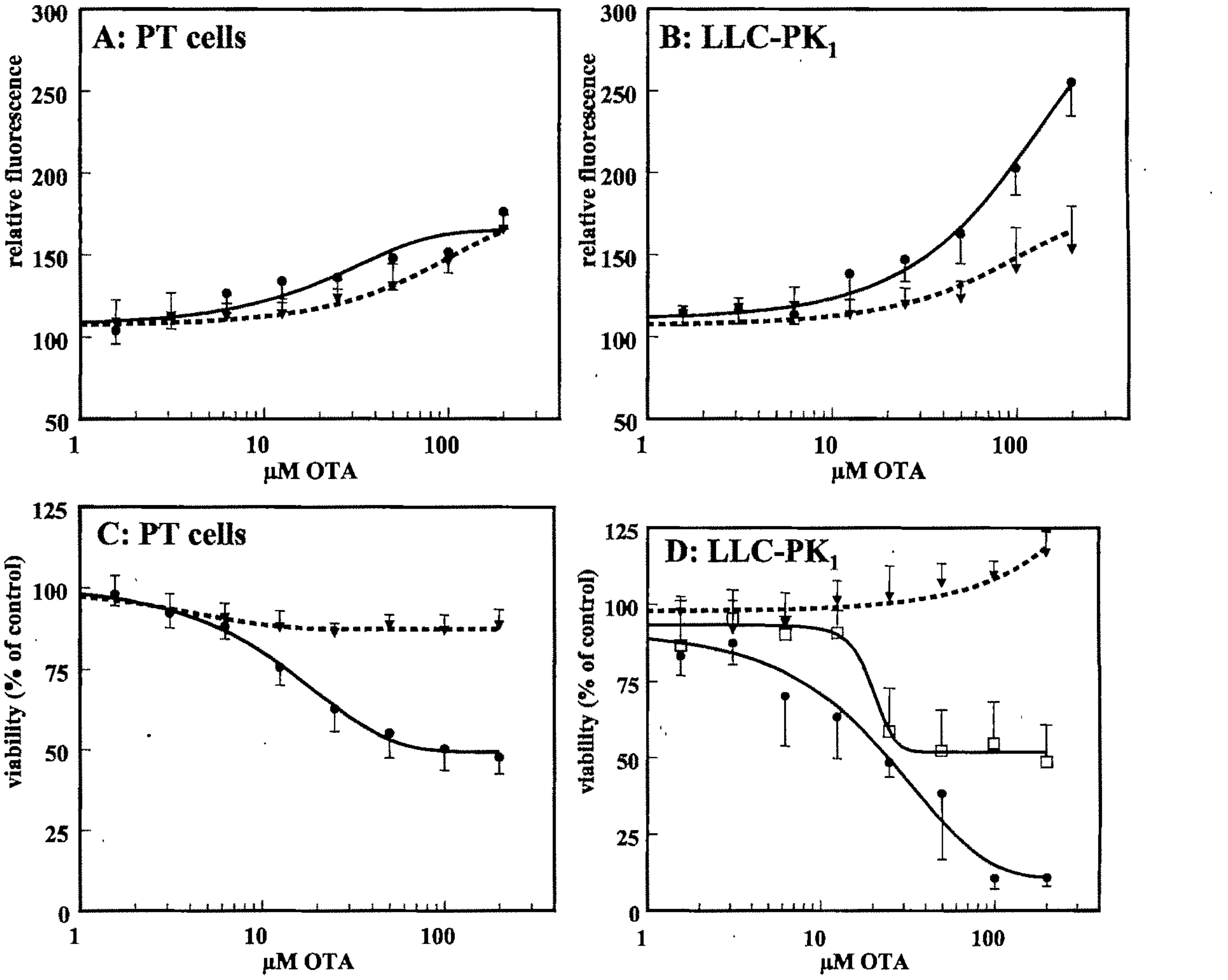

Fig. 1. OTA-induced ROS formation (A and B) and loss of cell viability (C and D) in primary PT cells and LLC-PK$_1$. Primary PT (A and C) and LLC-PK$_1$ cells (B and D) were exposed to increasing concentrations of OTA and the ROS production (A and B) or cell viability (C and D) after 4 h (- -▼- -) and 24 h (—●—) of incubation with OTA was measured as described in the Materials and Methods section. The effect of serum (10% FCS) (—□—) on cell viability after exposure of LLC-PK$_1$ cells for 24 h to increasing concentrations of OTA was also determined (D). The data are expressed as relative response as compared to DMSO-treated controls (100%) and represent means ± S.D. from quadruplicate measurements from at least two independent experiments. The results of statistical analysis are delineated in the text.

After 24 h, the ROS production was significantly elevated by OTA concentrations as low as 3.1 μM. In contrast, a significant increase of ROS levels was observed following exposure of continuous LLC-PK$_1$ cells to a minimal effective concentration of 25 μM OTA after 4 h and 12.5 μM OTA after 24 h, respectively (Fig. 1B). These data indicate that this mycotoxin induces a ROS response in a concentration- and time-dependent manner. The time-dependent increase in ROS levels was more pronounced in LLC-PK$_1$ cells as compared to the primary PT cells. In LLC-PK$_1$ cells, the formation of ROS induced by OTA concentrations >50 μM after 24 h incubation was significantly increased as compared to the ROS response evoked by equimolar concentrations OTA after 4 h. In contrast, the ROS response to OTA in rat PT cells after 24 h exposure did not differ statistically from that after 4 h.

3.2. Cytotoxicity of OTA

The cell viability of primary rat PT cells incubated for 4 h with increasing concentrations of OTA in serum-free medium decreased slightly, but this decrease was not significant. However, 24 h OTA exposure in serum-free medium clearly decreased cell viability in a concentration-dependent manner (Fig. 1C). Loss of cell viability was also time-dependent as viability after 24 h exposure to OTA was significantly lower in PT cells than after 4 h incubation for OTA concentrations of 12.5 μM and higher.

This concentration- and time-dependent loss of cell viability following OTA exposure was also observed in LLC-PK$_1$ cells. Interestingly, OTA-induced ROS production clearly preceded the loss of cell viability in LLC-PK$_1$ cells as cell viability was unaffected after 4 h incubation with OTA, while a distinct ROS response was observed at OTA concentrations exceeding 50 μM (Fig. 1D). In contrast, cell viability was even slightly increased after 4 h exposure to high OTA concentrations (100 and 200 μM) in serum-free medium ($P < 0.05$ as compared to vehicle-treated cells). However, exposure to increasing concentrations of OTA for 24 h in serum-free medium resulted in a loss of cell viability in LLC-PK$_1$ cells (Fig. 1D). Loss of cell viability after 24 h was significantly different from that after 4 h OTA incubation at 12.5 μM and higher. However, the presence of serum in the incubation medium attenuated the cytotoxicity of OTA (data not shown).

In serum-free medium, the calculated IC$_{50}$ values following 24 h exposure to OTA were approximately 83 and 25 μM for PT cells and LLC-PK$_1$ cells, respectively, whereas in the presence of 10% serum, the IC$_{50}$ was approximately 50 μM. A concentration close to the IC$_{50}$ values for both cell types (100 μM for rat PT cells; 25 μM for LLC-PK$_1$) were chosen for successive experiments investigating the mechanism of OTA-mediated toxicity. The subsequent experiments were performed in serum-free medium.

3.3. Influence of anti-oxidants on the OTA-induced ROS response

Cells were pre-incubated for 24 h with the selected anti-oxidative agent and subsequently challenged with OTA still in the presence of the anti-oxidant. Treatment of rat PT cells with several concentrations (1.56–12.5 μM) of TOCO significantly decreased the OTA-induced ROS response (Fig. 2A; hatched bars). Treatment with 6.25 and 12.5 μM TOCO completely prevented the OTA-induced ROS response. Similarly, the ROS production in rat PT cells treated with 1, 2 and 4 mM NAC following exposure to OTA was not statistically different from the basal ROS levels in solvent-treated control cells (Fig. 2B; hatched bars).

In LLC-PK$_1$ cells treated with increasing concentrations (1.56–12.5 μM) TOCO and exposed to OTA, the formation of ROS was not different from that in solvent-treated cells, but was significantly in comparison with the response in cells exposed to OTA alone (Fig. 2C; hatched bars). Treatment of LLC-PK$_1$ cells with 0.5–4 mM NAC significantly decreased the OTA-mediated elevation of ROS levels at all NAC concentrations tested, in a dose-dependent manner. Treatment with 4 mM NAC appeared to completely prevent loss of cell viability in cells exposed to 25 μM OTA.

3.4. Influence of anti-oxidants on the OTA-induced loss of cell viability

In addition to monitoring the effects of anti-oxidants on the OTA-induced ROS response, the effects of TOCO and NAC on the cell viability were determined. As depicted in Fig. 2A (black bars), the treatment of the cells with TOCO up to 12.5 μM could not prevent the OTA-induced loss of cell viability in rat PT cells. In contrast, NAC treatment showed a clear dose-dependent protective effect in rat PT cells and at the tested concentrations between 0.5 and 4 mM NAC (Fig. 2B; black bars).

Similarly as observed in PT cells, TOCO up to 12.5 μM was unable to protect LLC-PK$_1$ cells against the cytotoxicity of OTA (Fig. 2C; black bars). In contrast, NAC treatment provided a dose-dependent protection of LLC-PK$_1$ cells against the cytotoxicity of OTA (Fig. 2D; black bars). In fact, the viability of the cells treated with 4 mM NAC followed by exposure to OTA was not statistically different from that of solvent-treated controls.

3.5. The role of GSH

Incubation with NAC strongly elevated GSH levels in control PT cells, while TOCO incubation did not affect basal GSH levels (Table 1). Exposure for 4 h to OTA did not statistically affect GSH levels. The GSH levels of NAC-treated PT cells were significantly higher after exposure to 6.25 and 100 μM OTA as compared to solvent- and TOCO-

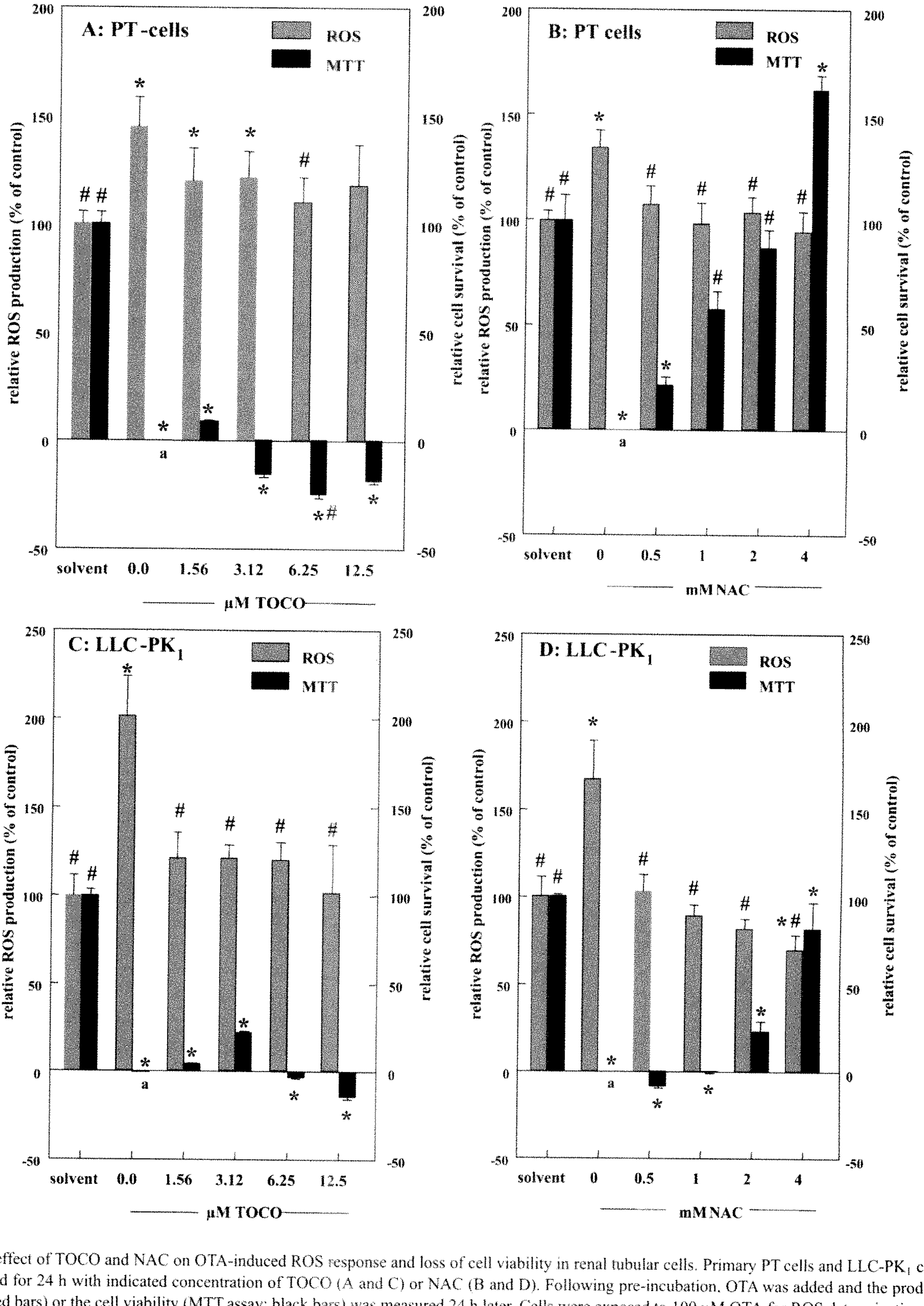

Fig. 2. The effect of TOCO and NAC on OTA-induced ROS response and loss of cell viability in renal tubular cells. Primary PT cells and LLC-PK$_1$ cells were pre-incubated for 24 h with indicated concentration of TOCO (A and C) or NAC (B and D). Following pre-incubation, OTA was added and the production of ROS (hatched bars) or the cell viability (MTT assay; black bars) was measured 24 h later. Cells were exposed to 100 µM OTA for ROS determinations (A–D). For determination of the effect on cell viability (MTT assay), PT cells were exposed to 100 µM OTA (A and B), while LLC-PK$_1$ cells were incubated with 25 µM OTA for 24 h (C and D). The OTA concentrations were chosen on the basis of the IC$_{50}$ values in the respective cell types. The data represent the relative response in treated cells as compared to the response in solvent-treated cells (100%). The results of the MTT assay are expressed as protection against the OTA-induced loss of viability; therefore, the viability of the cells exposed to OTA alone (0 µM TOCO or NAC) was set at 0% (indicated in the figure as "a"). The data represent means ± S.D. of quadruplicate measurements from at least two independent experiments. * Significantly different from response in solvent-treated cells ($P < 0.05$). # Significantly different from the response in OTA-alone treated cells ($P < 0.05$).

treated cells (Table 1). TOCO treatment did affect the OTA-induced GSH depletion.

A similar pattern was observed after 24 h exposure to OTA, although the GSH levels were below the limit of detection (< 30 pmol/mg protein) after exposure to 100 μM OTA, indicating significant depletion of GSH (Table 1). Moreover, an evident decrease of GSH levels following 24 h OTA exposure was observed in NAC-treated PT cells. TOCO treatment did not result in preservation of the GSH levels in OTA-exposed cells.

In LLC-PK$_1$ cells, GSH levels were not statistically affected after 4 h incubation with OTA, similarly as observed in PT cells (Table 1). Table 1 shows that NAC treatment resulted in significantly higher GSH levels after 4 h exposure to 6.25 and 100 μM OTA, as compared to solvent-treated cells. TOCO treatment had no effect on the GSH levels in OTA exposed LLC-PK$_1$ cells.

The decrease in GSH levels in LLC-PK$_1$ cells following 24 h OTA exposure was more pronounced at 100 μM OTA than that at 6.25 μM OTA suggesting a dose-dependent trend (Table 1). TOCO treatment appeared to have slightly increased the basal GSH levels, but was unable to preserve GSH levels after 24 h exposure to OTA. The GSH levels of TOCO-treated cells decreased to the same extent as in solvent-treated cells after exposure to OTA. Table 1 shows that NAC treatment resulted in significantly higher GSH levels after 24 h incubation with 6.25 μM OTA as compared to solvent- and TOCO-treated cells, although this effect was only significant as compared to TOCO-treated cells (Table 1). Taken together, these results illustrate that NAC treatment preserved GSH levels in OTA-exposed PT- and LLC-PK$_1$ cells. This protective effect by NAC treatment was more pronounced in PT cells as compared to NAC-treated LLC-PK$_1$ cells.

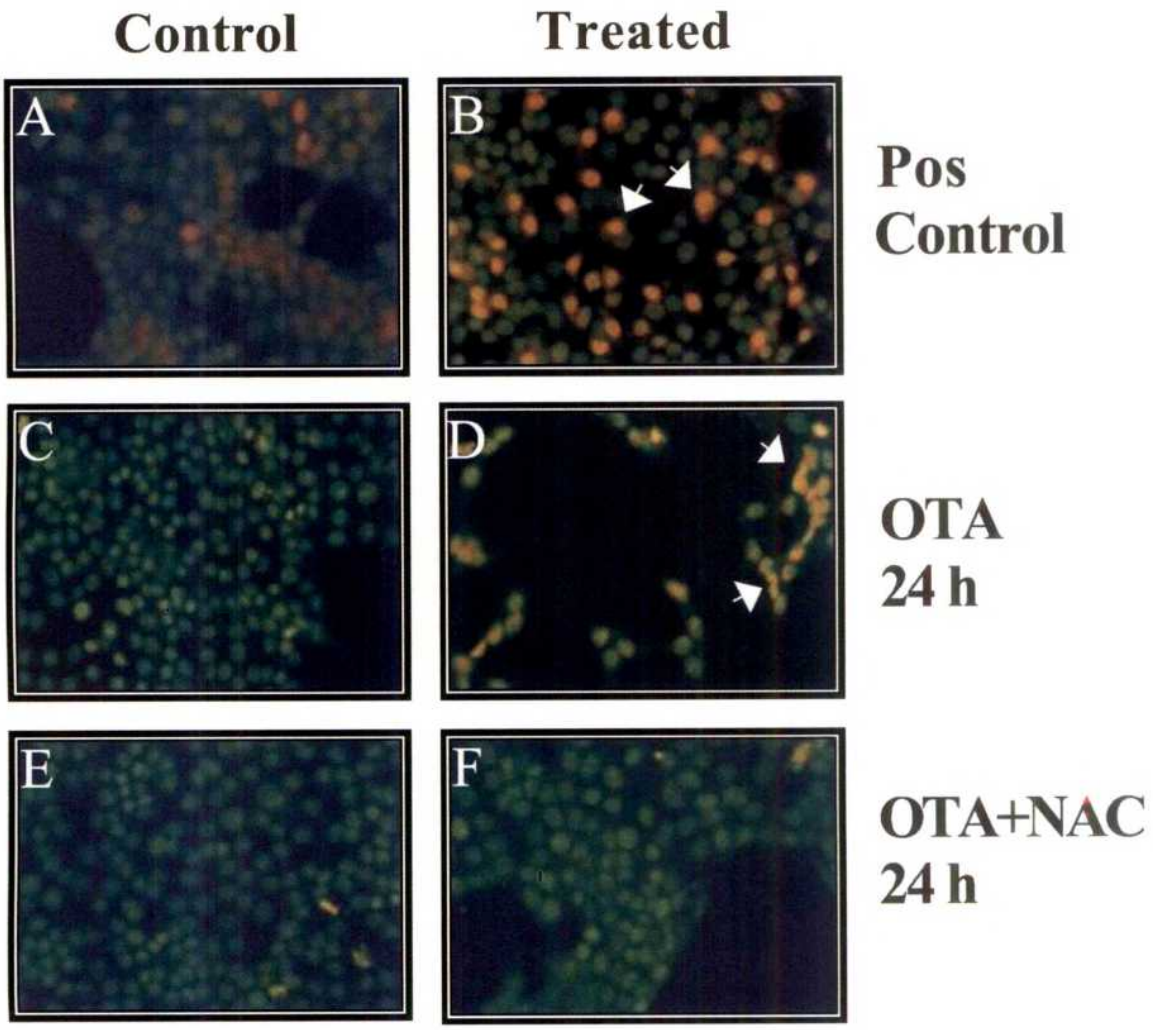

Fig. 3. Formation of 8-oxoguanine adducts in OTA-exposed LLC-PK$_1$ cells. (A and B) LLC-PK$_1$ cells were exposed for 1 h to solvent (panel A) or 2 mM methylene blue (Pos Control) (panel B) followed by 30 min exposure to ambient light. Formation of 8-oxoguanine was assessed using the Biotrin oxyDNA assay kit as described in the Materials and Methods section. (C and D) LLC-PK$_1$ cells were exposed for 24 h to solvent (panel C) or 15 μM OTA (panel D) for 24 h and assessed for 8-oxoguanine formation. (E and F) Cells were treated with 4 mM NAC for 24 h before 24 h exposure to solvent (panel E) or 15 μM OTA (panel F). The fixed cultures were then assayed for the formation of 8-oxoguanine adducts. The arrows indicate representative 8-oxoguanine positive cells. The presented micrographs were taken from representative areas from one of two independent experiments. Original magnification: × 20.

treated cells (Table 1). TOCO treatment did affect the OTA-induced GSH depletion.

A similar pattern was observed after 24 h exposure to OTA, although the GSH levels were below the limit of detection (< 30 pmol/mg protein) after exposure to 100 μM OTA, indicating significant depletion of GSH (Table 1). Moreover, an evident decrease of GSH levels following 24 h OTA exposure was observed in NAC-treated PT cells. TOCO treatment did not result in preservation of the GSH levels in OTA-exposed cells.

In LLC-PK$_1$ cells, GSH levels were not statistically affected after 4 h incubation with OTA, similarly as observed in PT cells (Table 1). Table 1 shows that NAC treatment resulted in significantly higher GSH levels after 4 h exposure to 6.25 and 100 μM OTA, as compared to solvent-treated cells. TOCO treatment had no effect on the GSH levels in OTA exposed LLC-PK$_1$ cells.

The decrease in GSH levels in LLC-PK$_1$ cells following 24 h OTA exposure was more pronounced at 100 μM OTA than that at 6.25 μM OTA suggesting a dose-dependent trend (Table 1). TOCO treatment appeared to have slightly increased the basal GSH levels, but was unable to preserve GSH levels after 24 h exposure to OTA. The GSH levels of TOCO-treated cells decreased to the same extent as in solvent-treated cells after exposure to OTA. Table 1 shows that NAC treatment resulted in significantly higher GSH levels after 24 h incubation with 6.25 μM OTA as compared to solvent- and TOCO-treated cells, although this effect was only significant as compared to TOCO-treated cells (Table 1). Taken together, these results illustrate that NAC treatment preserved GSH levels in OTA-exposed PT- and LLC-PK$_1$ cells. This protective effect by NAC treatment was more pronounced in PT cells as compared to NAC-treated LLC-PK$_1$ cells.

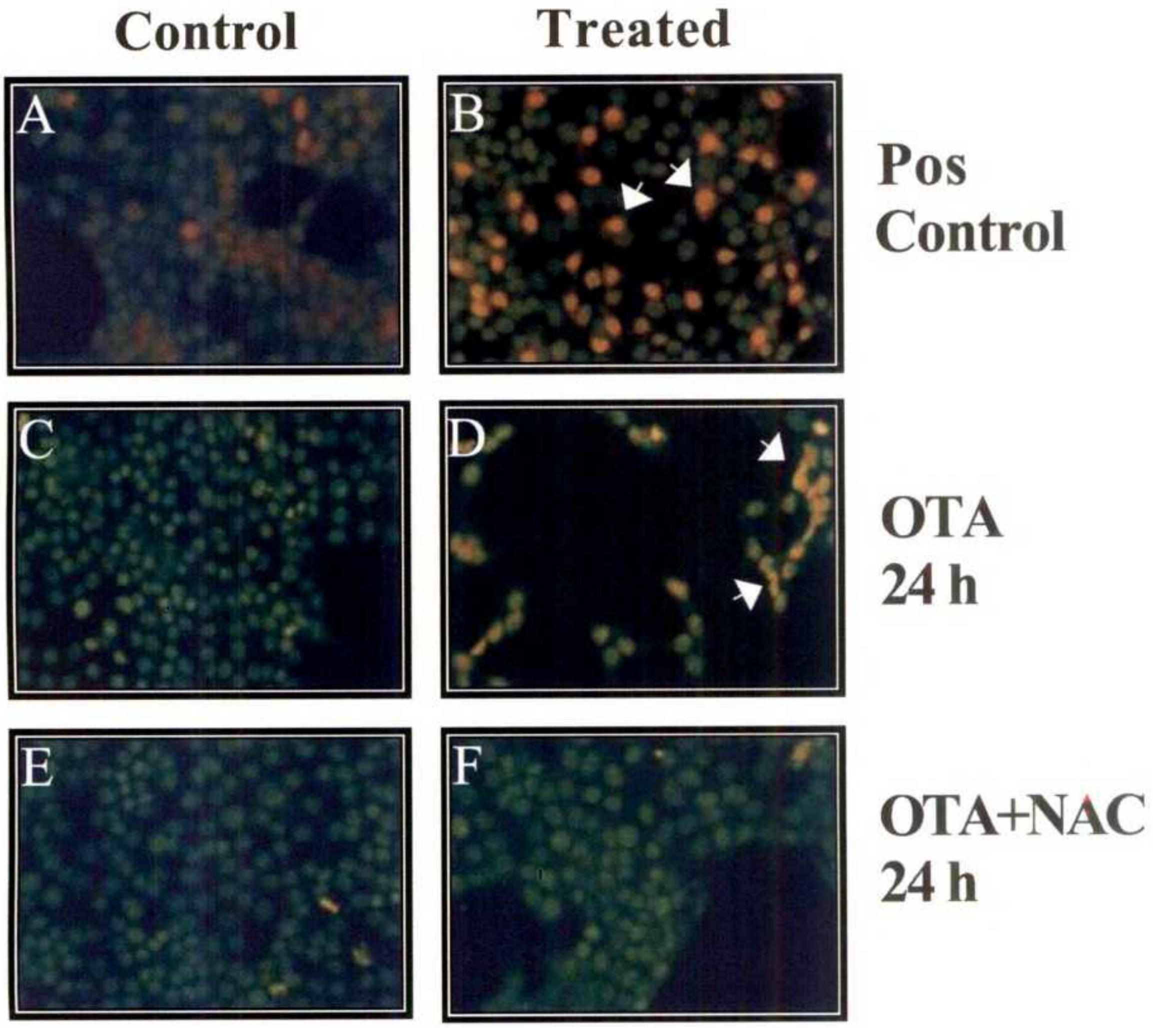

Fig. 3. Formation of 8-oxoguanine adducts in OTA-exposed LLC-PK$_1$ cells. (A and B) LLC-PK$_1$ cells were exposed for 1 h to solvent (panel A) or 2 mM methylene blue (Pos Control) (panel B) followed by 30 min exposure to ambient light. Formation of 8-oxoguanine was assessed using the Biotrin oxyDNA assay kit as described in the Materials and Methods section. (C and D) LLC-PK$_1$ cells were exposed for 24 h to solvent (panel C) or 15 μM OTA (panel D) for 24 h and assessed for 8-oxoguanine formation. (E and F) Cells were treated with 4 mM NAC for 24 h before 24 h exposure to solvent (panel E) or 15 μM OTA (panel F). The fixed cultures were then assayed for the formation of 8-oxoguanine adducts. The arrows indicate representative 8-oxoguanine positive cells. The presented micrographs were taken from representative areas from one of two independent experiments. Original magnification: × 20.

from the tubular cell. Our results, therefore, point toward a central role for GSH in the protection against OTA-induced cellular toxicity.

We are the first to show that OTA induces the formation of 8-oxoguanine in vitro, providing unequivocal evidence of oxidative DNA damage. Oxidative base modifications may result in mutations, whereas oxidation of deoxyribose moieties may induce base release or DNA strand breaks (Ref. [24] and references therein). Singlet oxygen selectively reacts with guanine and predominantly forms 8-oxoguanine, which is also one of the products formed after attack of DNA by the hydroxyl radical [24,27].

In contrast, Gautier et al. [39] found no evidence for 8-oxoguanine formation in rats treated with OTA (up to 2 mg/kg body wt). The latter authors ascribe the discrepancy between the generation of ROS in vitro and in vivo and the resultant oxidative damage to the protective activity of GSH and TOCO. Furthermore, those authors suggest that the maximal plasma concentrations (15 μM) were below the minimal OTA concentration (30 μM) required to induce LPO in vitro and were consequently too low to induce 8-oxoguanine formation in the rats.

Formation of 8-oxoguanine adducts occurred in a time-dependent manner, which correlates well with the OTA-induced production of ROS in these cells. Using the same method as described in this study, Morin et al. [30,31] showed the formation of 8-oxoguanine in cell cultures treated with pro-oxidants. The OTA concentrations elevating the ROS levels and inducing the formation of 8-oxoguanine were of the same order of magnitude. Recently, Griffith [38] showed that OTA in the presence of Fe(III)-porphyrin facilitates single-strand cleavage of supercoiled plasmid DNA through the production of ROS (i.e. hydroxyl radical HO). The author proposes that OTA is oxidized to a (hydro-) quinone. Quinones are known to redox cycle, thus creating free radicals that bind covalently to a variety of cellular macromolecules [40]. The formation of the (hydro-) quinone of OTA implicates the reported involvement of oxidative metabolism in the genotoxicity of OTA [41] and could help to explain the previously described CYP450-dependent mutagenicity of OTA and its metabolites [42]. Redox cycling causes the oxidation of reducing equivalents in the cell, including GSH, and may thus contribute to the observed depletion of GSH in the present study. Moreover, Gautier et al. [43] have shown that most, if not all, of the DNA adducts attributed to OTA and its metabolites do not contain an OTA-moiety, further implicating oxidative stress as important determinant in the OTA-induced DNA damage. OTA and its metabolites have also been observed to induce the formation of DNA adducts in rats and mice [34,44–46]. Interestingly, DNA adduct formation was reduced by pre-treatment of mice with vitamins A, C and E, indicating the involvement of oxidative stress in OTA-mediated DNA damage [46].

The results of the present study show that OTA induced a comparable response in the two PT cell models, the primary PT- and the continuous LLC-PK$_1$ cells. In addition, the effects of TOCO and NAC on the OTA-mediated toxicity were similar and differed only quantitatively. Particularly, NAC showed a more potent protection in PT cells that can be explained by its more pronounced effect on the GSH levels in the primary cells. This suggests that the primary PT cells are slightly less sensitive to the actions of OTA, as judged by the lower maximal ROS response, the higher IC$_{50}$ and the more potent NAC protection in the primary PT cells.

In conclusion, cultured renal tubular cells respond to OTA exposure by elevation of ROS levels, depletion of GSH levels and an increase in oxidative DNA damage, which are indicators of oxidative stress. Taking our results obtained with TOCO and NAC into account, it may be hypothesized that the OTA-induced oxidative stress contributes to both the DNA damage and cytotoxicity. The effects of TOCO indicate that OTA-induced LPO does not contribute profoundly to the observed loss of cell viability. The strong protective effect of GSH indicates that oxidative-stress-related protein damage is a major determinant in OTA-mediated toxicity. To which extent the ROS formation contributes to other toxic effects, in particular by disrupting protein synthesis, affecting intracellular calcium handling, or inducing mitochondrial dysfunctioning etc., requires further exploration. Furthermore, OTA-related ROS formation may induce epigenetic effects.

Acknowledgements

This work was supported by grant C95.1535 from the Dutch Kidney Foundation.

References

[1] Z. Bozic, V. Duancic, M. Belicza, O. Kraus, I. Skljarov, Balkan endemic nephropathy: still a mysterious disease, Eur. J. Epidemiol. 11 (1995) 235–238.

[2] V. Stefanovic, Balkan endemic nephropathy: a need for novel aetiological approaches, QJM, (1997) 457–463.

[3] A. Horvath, B.L. Upham, V. Ganev, J.E. Trosko, Determination of the epigenetic effects of ochratoxin in a human kidney and a rat liver epithelial cell line, Toxicon 40 (2002) 273–282.

[4] D. Benford, C. Boyle, W. Dekant, R. Fuchs, D.W. Gaylor, G. Hard, D.B. Mc. Gregor, J.J. Pitt, R. Plestina, G. Shephard, U. Solfrizzo, P.J.P. Verger, R. Walker, Ochratoxin A, Safety Evaluation of Certain Mycotoxins in Food, WHO Food Additives, Series 47, vol. 74 WHO, Geneve, 2001, pp. 281–415.

[5] I. Baudrimont, A.M. Betbeder, A. Gharbi, A. Pfohl-Leszkowicz, G. Dirheimer, E.E. Creppy, Effect of superoxide dismutase and catalase on the nephrotoxicity induced by subchronical administration of ochratoxin A in rats, Toxicology 89 (1994) 101–111.

[6] A. Kane, E.E. Creppy, R. Roschenthaler, G. Dirheimer, Changes in urinary and renal tubular enzymes caused by subchronic administration of ochratoxin A in rats, Toxicology 42 (1986) 233–243.

[7] NTP, Technical report on the toxicology and carcinogenesis studies of ochratoxin A (Case no. 303-47-9) in F344/N rats (Gavage studies), US Department of Health and Human services, NIH Publication no. 89-2813, Research Triangle Park, NC., 1989.

[8] P. Krogh, N.H Axelsen, F Elling, N. Gyrd-Hansen, B. Hald, J Hyldgaard-Jensen, A.E. Larsen, A. Madsen, H.P Mortensen, T Moller, O K Petersen, U. Ravnskov, M Rostgaard, O Aalund, Experimental porcine nephropathy. Changes of renal function and structure induced by ochratoxin A-contaminated feed, Acta Pathol. Microbiol Scand [A] 82 (1974) 1–21.

[9] P Krogh, Role of ochratoxin in disease causation, Food Chem. Toxicol 30 (1992) 213–224

[10] A.E. Pohland, S. Nesheim, L Friedman, Ochratoxin A· a review, Pure Appl Chem 64 (1992) 1029–1046

[11] F S. Chu, Mycotoxins food contamination, mechanism, carcinogenic potential and preventive measures, Mutat Res 259 (1991) 291–306

[12] G Dirheimer, E.E. Creppy, Mechanism of action of ochratoxin A, IARC Sci. Publ. 115 (1991) 171–186

[13] M. Gekle, S. Silbernagl, Renal toxicodynamics of ochratoxin A. a pathophysiological approach, Kidney Blood Press Res 19 (1996) 225–235

[14] J. Fink-Gremmels, A. Jahn, M.J. Blom, Toxicity and metabolism of ochratoxin A, Nat. Toxins 3 (1995) 214–220.

[15] A. Belmadani, P.S. Steyn, G Tramu, A.M Betbeder, I Baudrimont, E.E. Creppy, Selective toxicity of ochratoxin A in primary cultures from different brain regions, Arch Toxicol 73 (1999) 108–114.

[16] R.F Omar, B.B Hasinoff, F. Mejilla, A D Rahimtula, Mechanism of ochratoxin A stimulated lipid peroxidation, Biochem Pharmacol 40 (1990) 1183–1191

[17] A.D Rahimtula, J.C Bereziat, V Bussacchini-Griot, H. Bartsch, Lipid peroxidation as a possible cause of ochratoxin A toxicity, Biochem. Pharmacol 37 (1988) 4469–4477.

[18] F Monnet-Tschudi, O. Sorg, P. Honegger, M G Zurich, A.C Huggett, B. Schilter, Effects of the naturally occurring food mycotoxin ochratoxin A on brain cells in culture, Neurotoxicology 18 (1997) 831–839

[19] F Shiraishi, L.M. Curtis, L. Truong, K Poss, G.A Visner, K Madsen, H.S Nick, A. Agarwal, Heme oxygenase-1 gene ablation or expression modulates cisplatin-induced renal tubular apoptosis, Am J. Physiol Renal Physiol. 278 (2000) F726–F736.

[20] G J. Schaaf, E M. de Groene, R.F. Maas, J.N. Commandeur, J. Fink-Gremmels, Characterization of biotransformation enzyme activities in primary rat proximal tubular cells, Chem -Biol. Interact 134 (2001) 167–190

[21] R N. Hull, W R Cherry, G.W. Weaver, The origin and characteristics of a pig kidney cell strain, LLC-PK, In Vitro 12 (1976) 670–677

[22] C Fauth, B Rossier, F Roch-Ramel, Transport of tetraethylammonium by a kidney epithelial cell line (LLC-PK1), Am J. Physiol. 254 (1988) F351–F357.

[23] S.M Cardoso, C. Pereira, R. Oliveira, Mitochondrial function is differentially affected upon oxidative stress, Free Radic Biol Med 26 (1999) 3–13.

[24] L.L de Zwart, J.H Meerman, J N Commandeur, N.P. Vermeulen, Biomarkers of free radical damage applications in experimental animals and in humans, Free Radic. Biol. Med. 26 (1999) 202–226

[25] F. Denizot, R Lang, Rapid colorimetric assay for cell growth and survival Modifications to the tetrazolium dye procedure giving improved sensitivity and reliability, J Immunol Methods 89 (1986) 271–277

[26] O W Griffith, Determination of glutathione and glutathione disulfide using glutathione reductase and 2-vinylpyridine, Anal. Biochem. 106 (1980) 207–212

[27] M. Cooke, I. Podmore, K Herbert, J Lunec, S. Thomas, UV-mediated DNA damage and its assessment, Toxicol. Ecotoxicol. News 3 (1996) 101–109

[28] O H. Lowry, N.J. Rosebrough, A L. Farr, R J. Randall, Protein measurement with Folin phenol reagent, J. Biol Chem 193 (1951) 265–275.

[29] H. Kasai, Analysis of a form of oxidative DNA damage, 8-hydroxy-2′-deoxyguanosine, as a marker of cellular oxidative stress during carcinogenesis, Mutat Res. 387 (1997) 147–163

[30] J.P Morin, T. Maziere, F Manning, G. Ryan, Impact of TNF-alfa on compartmentalized and adjacent endothelial/epithelial cell co-cultures, Joint meeting IVTIP and Biotechnology Program 4th Framework of European commission DG XII Innsbruck, 2000

[31] J P Morin, T. Maziere, F. Manning, S. Bonner, In situ detection of oxidative DNA damage in cultured cells using histofluorescent detection of 8-oxoguanine, Joint meeting IVTIP and Biotechnology Program 4th Framework of European commission DG XII Innsbruck, 2000

[32] R.F Omar, A D Rahimtula, H. Bartsch, Role of cytochrome P-450 in ochratoxin A-stimulated lipid peroxidation, J Biochem. Toxicol 6 (1991) 203–209.

[33] R.F Omar, H V Gelboin, A D Rahimtula, Effect of cytochrome P450 induction on the metabolism and toxicity of ochratoxin A, Biochem Pharmacol. 51 (1996) 207–216

[34] A Pfohl-Leszkowicz, Y. Grosse, A Kane, A. Gharbi, I. Baudrimont, S Obrecht, E E. Creppy, G Dirheimer, Is the oxidative pathway implicated in the genotoxicity of ochratoxin A? in· E E. Creppy, M Castegnaro, G Dirheimer (Eds), Human Ochratoxicosis and Related Pathologies, Colloque INSERM, vol 231, J. Libbey Eurotext, London, 1993, pp 129–140

[35] S.L Hempel, G R Buettner, Y.Q O'Malley, D A. Wessels, D M Flaherty, Dihydrofluorescein diacetate is superior for detecting intracellular oxidants· comparison with 2′,7′-dichlorodihydrofluorescein diacetate, 5(and 6)-carboxy-2′,7′-dichlorodihydrofluorescein diacetate, and dihydrorhodamine 123, Free Radic. Biol Med. 27 (1999) 146–159.

[36] J Chaudiere, R. Ferrari-Iliou, Intracellular antioxidants from chemical to biochemical mechanisms, Food Chem Toxicol 37 (1999) 949–962.

[37] M.D. Aleo, R.D Wyatt, R.G Schnellmann, Mitochondrial dysfunction is an early event in ochratoxin A but not oosporein toxicity to rat renal proximal tubules, Toxicol Appl Pharmacol 107 (1991) 73–80.

[38] O.W. Griffith, Biologic and pharmacologic regulation of mammalian glutathione synthesis, Free Radic Biol. Med 27 (1999) 922–935

[39] J.C. Gautier, D Holzhaeuser, J Markovic, E. Gremaud, B Schilter, R.J. Turesky, Oxidative damage and stress response from ochratoxin a exposure in rats, Free Radic. Biol. Med 30 (2001) 1089–1098.

[40] M S. Peter, Chemical modifications of biopolymers by quinones and quinone methides, Angew Chem. 101 (1989) 572–587

[41] S. Obrecht-Pflumio, Y. Grosse, A Pfohl-Leszkowicz, G Dirheimer, Protection by indomethacin and aspirin against genotoxicity of ochratoxin A, particularly in the urinary bladder and kidney, Arch Toxicol. 70 (1996) 244–248

[42] E.M de Groene, I.G Hassing, M J. Blom, W Seinen, G J Fink-Gremmels, J. Horbach, Development of human cytochrome P450-expressing cell lines. application in mutagenicity testing of ochratoxin A, Cancer Res 56 (1996) 299–304

[43] J Gautier, J Richoz, D.H. Welti, J. Markovic, E. Gremaud, F P. Guengerich, R.J. Turesky, Metabolism of ochratoxin A. absence of formation of genotoxic derivatives by human and rat enzymes, Chem Res. Toxicol 14 (2001) 34–45

[44] A. Pfohl-Leszkowicz, Y. Grosse, A Kane, E E. Creppy, G Dirheimer, Differential DNA adduct formation and disappearance in three mouse tissues after treatment with the mycotoxin ochratoxin A, Mutat. Res. 289 (1993) 265–273

[45] A Pfohl-Leszkowicz, Y Grosse, A. Kane, M. Castegnaro, E.E Creppy, G Dirheimer, Preponderance of DNA adducts in kidney after ochratoxin A exposure, in. E.E. Creppy, M Castegnaro, G. Dirheimer (Eds), Human Ochratoxicosis and Related Pathologies, Colloque INSERM, vol. 231, J. Libbey Eurotext, London, 1993, pp. 199–207.

[46] Y. Grosse, L. Chekir-Ghedira, A. Huc, S Obrecht-Pflumio, G. Dirheimer, H Bacha, A Pfohl-Leszkowicz, Retinol, ascorbic acid and alpha-tocopherol prevent DNA adduct formation in mice treated with the mycotoxins ochratoxin A and zearalenone, Cancer Lett 114 (1997) 225–229

ELSEVIER

Biochimica et Biophysica Acta 1588 (2002) 159–164

BIOCHIMICA ET BIOPHYSICA ACTA

BBA

www.bba-direct.com

Time-course of oxygen free radical production in acinar cells during acute pancreatitis induced by pancreatic duct obstruction

A. Uruñuela[a], S. Sevillano[a], A.M. de la Mano[a], M.A. Manso[a], A. Orfao[b], I. de Dios[a,*]

[a]Departamento de Fisiología y Farmacología, Edificio Departamental, Campus Miguel de Unamuno, University of Salamanca, 37007 Salamanca, Spain
[b]Flow Cytometry Service, University of Salamanca, Salamanca, Spain

Received 31 January 2002; received in revised form 19 April 2002; accepted 26 June 2002

Abstract

The time-course of oxygen free radicals (OFR) generation within acinar cells was studied at different stages of acute pancreatitis (AP) induced in rats by duct obstruction (PDO) for 48 h by flow cytometry, using dihydrorhodamine-123 (DHR) as fluorescent dye. Parallel measurements of the most common markers of oxidative stress such as glutathione (GSH) depletion and malondialdehyde (MDA) levels in pancreas were also performed. OFR production significantly increased within acinar cells at early stages of AP, concomitant with a marked depletion in pancreatic GSH. Lipid peroxidation was significantly enhanced 6 h after PDO, suggesting that the antioxidant defence system of the cell is overwhelmed by OFR production. Both MDA and OFR production in acinar cells decreased to normal values at late AP stages, thus allowing the recovery of pancreatic GSH levels 48 h after PDO. Among the two types of acinar cells differentiated by flow cytometry, R1 and R2, it was the R2 population that showed higher values of DHR dye. However, no differences between the two cell types were found regarding the amount of OFR generation. Our results demonstrate that individual acinar cells significantly contribute to produce large amounts of OFR at early stages of AP. The two existing populations of acinar cells displayed similar behaviour regarding oxidative stress over the course of the disease.

© 2002 Elsevier Science B.V. All rights reserved.

Keywords: Acinar cell; Acute pancreatitis; Oxidative stress; Oxygen free radical; Rat

1. Introduction

Acute pancreatitis (AP) is an inflammatory disease whose pathophysiology remains poorly understood. It is usually considered to be an autodigestive disease, in which, in addition to premature intracellular protease activation [1], other mechanisms such as oxidative stress have also been shown to be involved in the development of the disease [2,3]. Since Sanfey et al. [4] suggested the possible role of oxygen free radicals (OFR) in AP, many studies have been carried out in order to investigate the role of oxidative stress in different experimental models of AP [5–10]. Under healthy conditions, OFR are generated by aerobic cells as by-products of a number of metabolic reactions, but they are quickly removed by a system of enzymatic and non-enzymatic antioxidants within the cell. If OFR production exceeds the cellular antioxidant defence mechanisms, oxidative stress develops. This leads to disturbances in cellular homeostasis since these OFR can cause biochemical and functional alterations at different cellular levels, such as lipid peroxidation [11], protein oxidation [12] or DNA damage [13], among other toxic effects. Glutathione (GSH) is one of the most important cellular antioxidants [14], which is generally depleted under situations in which OFR production is enhanced, as occurs in AP [7–9]. On this basis, the oxidative state of the pancreas is routinely evaluated by indirect measurements on extracts of tissue. Pancreatic GSH levels and concentration of malondialdehyde (MDA), as a product of membrane lipid peroxidation [15] are widely considered as indices of the cellular redox estate. However, direct analysis of oxidative stress on individual acinar cells have not been performed. Two different populations of acinar cells have recently been reported in rat pancreas [16–19]. Differences in the light scatter properties and in the plasma membrane glycoconjugates were found [16,17]. In addition, they showed different behaviour regarding the enzyme load and intracellular Ca^{2+} content in rats with AP induced by pancreatic duct obstruction (PDO) [19]. In this

---

* Corresponding author. Fax: +34-923-294673.
E-mail address: bel@gugu.usal.es (I. de Dios).

0925-4439/02/$ - see front matter © 2002 Elsevier Science B.V. All rights reserved.
PII: S0925-4439(02)00160-6

study, the time-course of OFR generation has been analyzed in individual acinar cells during 48 h after inducing AP in order to evaluate the relative contributory role of both types of acinar cells to oxidative damage in the pancreas at the different stages of pancreatitis. The results were associated with the depletion of GSH and production of MDA in the whole pancreas.

2. Materials and methods

2.1. Chemicals

Collagenase type VII, soybean trypsin inhibitor (STI), amino acid admixture, bovine serum albumine (BSA), dihydrorhodamine-123 (DHR), *N*-(2-hydroxyethyl) piperazine-*N*′-(2-ethanesulfonic acid) (Hepes), GSH, β-nicotinamide adenine dinucleotide phospate reduced form (NADPH), glutathione reductase type III, ethylenediamine-tetraacetic acid (EDTA) and 5,5′-dithio-bis(2-nitrobenzoic acid) (DTNB) were supplied by Sigma Chemical Co. (Spain). Other standard analytical grade laboratory reagents were obtained from Merck (Germany).

2.2. Surgical procedure

Male Wistar rats weighing 250–300 g were used. After 12 h fasting, the rats were anaesthetized with ether and acute pancreatitis was induced by ligation of the common bile–pancreatic duct at the distal part, close to its exit to the duodenum. Afterwards, the abdomen was closed with 5–0 polyester sutures and the animals were again placed in their cages with free access to food and water. Sham-operated rats were used as controls; in these animals, bile–pancreatic duct was dissected but not ligated. Post-operative analgesia was maintained in all animals by subcutaneous injections of buprenorphine (0.2 mg/kg/8 h).

2 3 Animal groups

Rats were randomly divided into different groups. Controls and rats with PDO for 1.5 h ($n=12$), 3 h ($n=11$), 6 h ($n=13$), 12 h ($n=15$), 24 h ($n=12$) and 48 h ($n=11$) were prepared. Intact animals were considered as 0 h PDO ($n=12$). At each stage, samples were collected under anaesthesia with sodium pentobarbital (3 mg/100 g of body weight). Different animals from each group were used to analyze the oxidative stress either in isolated pancreatic acinar cells or in pancreatic homogenates. The study protocol was approved by the Ethics Committee of the University of Salamanca.

2.4. Collection of samples

Laparotomy was performed and the peritoneal fluid (ascites) was collected by aspiration. Blood samples were taken by cardiac puncture to determine hematocrit and plasma amylase activity. Finally, the entire pancreas was removed to determine the percentage of fluid, MDA content and GSH levels or for isolation of pancreatic cells.

2.5. Assays

2.5.1. Pancreatitis indicators

Amylase activity was determined in plasma and ascites using the method of Noelting and Bernfeld [20]. To measure the hematocrit, heparinized blood was centrifuged at 4000 × *g* for 5 min in microhematocrit tubes. The amount of tissue fluid was calculated by drying the pancreas at 100 °C for 72 h.

2 5 2. Measurements of GSH and MDA in pancreas

After homogenizing the pancreas in 5%–5 sulfosalicylic acid, the GSH content was measured using the specific technique described by Tietze [21], based on the spectrophotometric monitoring of GSH-mediated reduction of DTNB at 412 nm.

For MDA measurement, pancreata were homogenized in 0.9% NaCl. The concentration of MDA was quantified by thiobarbituric acid reaction [22].

2.5.3. Preparation of isolated cells

Acinar cells were isolated as previously described [16]. After a median laparotomy, the bile duct was ligated at its exit from the liver and the main pancreatic duct was cannulated at its exit into the duodenum to perfuse 5 ml of 25 mM HEPES solution pH 7.4 containing collagenase (40 U/ml), 0.1 mg/ml STI, 100 mM NaCl, 5 mM KCl, 1 mM $MgCl_2$, 1 mM $CaCl_2$, 14 mM D-glucose, 2 mM glutamine, 2% (w/v) BSA and 2% (w/v) amino acid admixture. The solution was pre-incubated with 95% O_2 and 5% CO_2 and all further incubations were performed with this gas phase The pancreas was digested at 37 °C in a shaking bath (200 cycles/min) during 20 min and washed with fresh collagenase solution every 5 min. Following gentle pipetting through tips of decreasing diameter (3–1 mm), cells were filtered through a double layer of muslin gauze and then centrifuged at 30 × *g* for 30 s at 4 °C. The supernatant was collected and centrifuged at 500 × *g*, 5 min at 4 °C. The supernatant was discarded and the cell pellet resuspended in HEPES buffer without collagenase and centrifuged again at 500 × *g* for 5 min at 4 °C. The pellet was resuspended in HEPES buffer without collagenase at a concentration of 10^7 cells/ml. The labelling of isolated cells with specific antisera against digestive enzymes assessed the purity of acinar cells as 99% [16].

2.5 4 Analysis of OFR generation in acinar cells

Oxidative stress in individual acinar cells was measured by using DHR. DHR easily crosses cell membranes and upon oxidation by OFR, turns into rhodamine-123 and becomes fluorescent [23].

Table 1
Hematocrit, percentage of fluid, volume of ascites and amylase activity in ascites and plasma

	Hematocrit (%)	Percentage of fluid	Volume of ascites (ml)	Amylase in ascites (U/dl)	Amylase in plasma (U/dl)
PDO 0 h (n=7–12)	43.22 ± 0.46	72.65 ± 0 72	0 63 ± 0 11	0 02 ± 0 01	5.38 ± 0 3
PDO 1.5 h (n=5–7)	46.19 ± 0.97 (*)	76.8 ± 0.96 (*)	1 12 ± 0 19	0 56 ± 0 10 (*)	7.49 ± 0 57
PDO 3 h (n=5)	49 58 ± 0.77 (***)	78 10 ± 1.36 (***)	1 82 ± 0 73 (*)	0 83 ± 0.22 (**)	10.39 ± 0 76 (***)
PDO 6 h (n=5)	52 21 ± 1.02 (***)	81 50 ± 1 07 (***)	4.04 ± 1.15 (***)	1 96 ± 0.30 (***)	13 81 ± 1 37 (***)
PDO 12 h (n=5–8)	49 00 ± 0.64 (***)	79.73 ± 0 81 (***)	3.95 ± 0 73 (***)	3 01 ± 0 51 (***)	16 04 ± 1 50 (***)
PDO 24 h (n=5–7)	44 91 ± 1.42	79.80 ± 0 54 (***)	1 01 ± 0.14	0.31 ± 0 10	14 96 ± 1 55 (***)
PDO 48 h (n=5–6)	43 60 ± 0.75	81.14 ± 1 81 (***)	0 04 ± 0.11	0.09 ± 0 02	8.10 ± 0 40

Values are mean ± S.E , n represents the number of animals Statistical test showed significant differences with respect to 0 h PDO * $P<0.05$, ** $P<0.001$, *** $P<0\ 01$

A suspension of 100 μl of acinar cells (10^6) were loaded with 25 mM DHR for 20 min at 4 °C in the dark. After washing twice with HEPES buffer, the intracellular green fluorescence (Fl1) due to DHR dye, was measured using a FACScalibur dual laser flow cytometer (Becton/Dickinson, San Jose, CA), equipped with a double discrimination module. The argon-ion laser emitting light at 488 nm and 15 mW was used. Calibration of the instrument was performed on a daily basis using Calibrite beads (Becton/Dickinson). Leukocytes infiltrating the pancreas were excluded on the basis of their unique high-light scatter properties [forward or low light scatter (FSC)/side or 90° light scatter (SSC)]. At each stage studied, cells from sham-operated and PDO-rats were measured in parallel, in order to express the changes in the intensity of Fl1 in pancreatic cells from PDO-rats as percentages of values obtained in sham-operated rats. The Paint-a-Gate 3.0 software programme was used for data acquisition and analysis. In each experiment, the mean value per individual cell was obtained from the analysis of at least 10,000 cells.

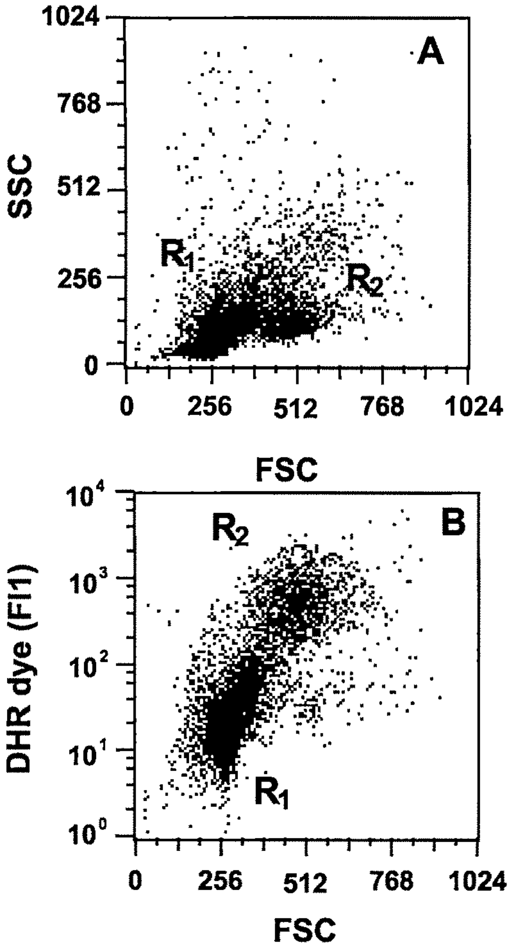

Fig 1 Flow cytometric distribution of acinar cells according to FSC/SSC (A), and to FSC/DHR dye (Fl1) (B) Dot plots are representative examples of one experiment Acinar cells were from rats with PDO for 6 h.

2.6. Statistical analysis

Results are expressed as mean ± S.E. analysis of variance (ANOVA) followed by Fisher test was applied in order to establish whether the differences between controls and rats with PDO for different times were statistically significant. Paired Student's t-test was applied to the results

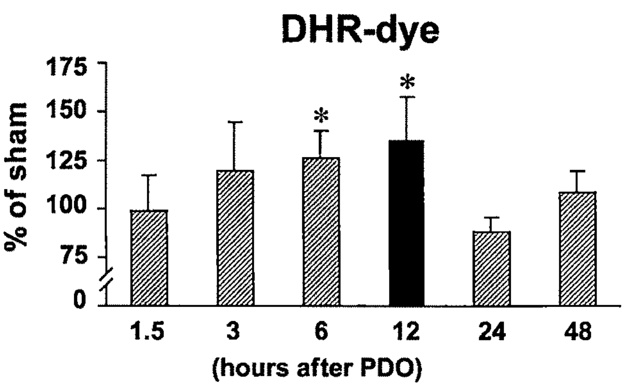

Fig. 2 Flow cytometry analysis of intracellular generation of OFR in individual acinar cells from rats with PDO for 1 5 h (n=5), 3 h (n=5), 6 h (n=8), 12 h (n=7), 24 h (n=5) and 48 h (n=5), using DHR as fluorescent dye. Data are expressed as means of percentages of values obtained in sham-operated rats ± S E n—number of animals. ANOVA test followed by Fisher test showed statistically significant vs controls (* $P<0\ 05$)

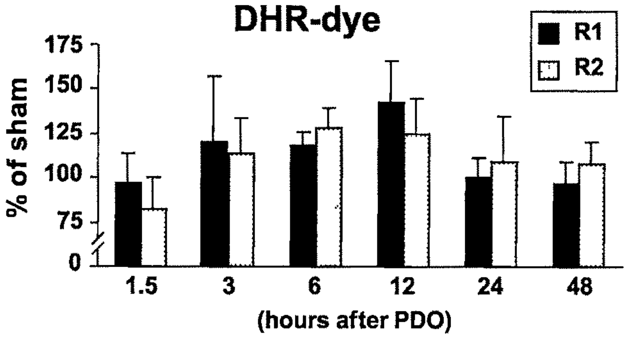

Fig 3 Flow cytometric analysis of intracellular OFR in R1 and R2 acinar cells from rats with PDO for 1.5 h ($n=5$), 3 h ($n=5$), 6 h ($n=8$), 12 h ($n=7$), 24 h ($n=5$) and 48 h ($n=5$), using DHR as fluorescent dye Data are expressed as means of percentages of values obtained in sham-operated rats ± S E n—number of animals Paired Student's t test showed no significant differences between R1 and R2 cells.

obtained in the two acinar cell populations, R1 and R2. In all cases, P values lower than 0.05 were considered to be statistically significant.

3. Results

As can be seen in Table 1, progressive increases in hematocrit, percentage of fluid in pancreatic tissue and amylase activity in ascites and plasma were observed from 1.5 to 12 h after PDO. The highest values were reached 6 and 12 h after PDO ($P<0.001$). Hematocrit, volume of peritoneal fluid and amylase activity in ascites returned to control values 24 h after PDO, whereas plasma amylase activity still remained increased at this stage.

Fig. 1 shows a representative example of the flow cytometric distribution of pancreatic acinar cells according to FSC (forward or low light angle scatter) vs. SSC (side or 90 °C light scatter) (Fig. 1A) and FSC vs. DHR dye (Fig. 1B). Two well-differentiated populations of cells could be observed on the basis of FSC, which are referred to as R1 and R2. Since R2 cells showed higher values of FSC—a parameter related to size [24]—this minor population is made up of larger cells than R1. Regarding the intensity of fluorescence due to DHR, a great degree of heterogeneity could be observed in both populations. Nevertheless, R2 cells displayed higher values of DHR dye than R1 cells in all animal groups.

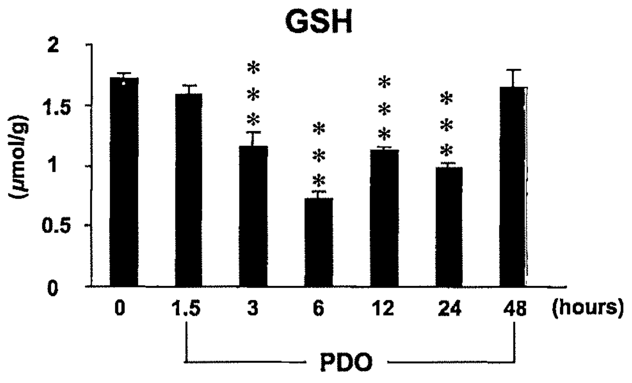

Fig 4 Pancreatic content of GSH in rats with PDO for 0 h ($n=12$), 1.5 h ($n=5$), 3 h ($n=6$), 6 h ($n=5$), 12 h ($n=8$), 24 h ($n=7$) and 48 h ($n=6$) Values are expressed as mean ± S E. n—number of animals. ANOVA test followed by Fisher test showed statistically significant differences vs rats without PDO (0 h) (***$P<0.001$)

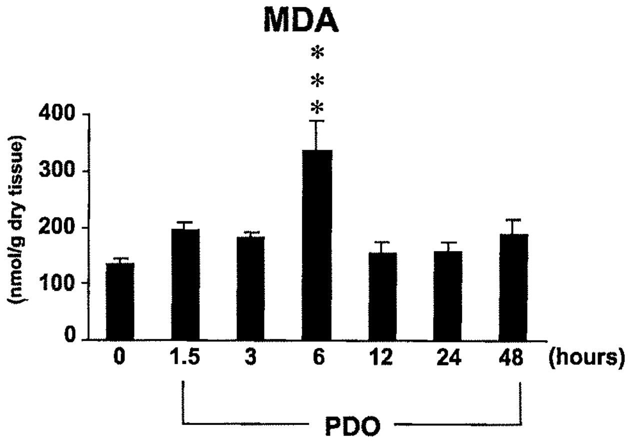

Fig 5 Tissue levels of MDA in rats with PDO for 0 h ($n=10$), 1.5 h ($n=7$), 3 h ($n=6$), 6 h ($n=5$), 12 h ($n=6$), 24 h ($n=6$) and 48 h ($n=5$). Values are expressed as mean ± S E. n—number of animals ANOVA test followed by Fisher test showed statistically significant differences vs rats without PDO (0 h) (***$P<0.001$)

Flow cytometric analysis of individual acinar cells (Fig. 2) revealed an increase in the mean fluorescence intensity due to DHR from 3 h after PDO, although statistical significance ($P<0.05$) was not reached until 6 and 12 h after PDO.

Regarding the changes in DHR-fluorescence respect to the values obtained in sham-operated rats, no significant differences between R1 and R2 cells were found at different times of PDO (Fig. 3).

The content of total GSH in pancreatic tissue is shown in Fig. 4. Significantly ($P<0.001$) decreased concentrations of GSH were found from 3 to 24 h after PDO. Normal GSH values were reached 48 h after PDO.

A significant ($P<0.001$) increase in MDA concentrations (Fig. 5) was observed in pancreas from rats subjected to PDO for 6 h.

4. Discussion

The role of oxidative stress in AP has been widely studied in several animal models [5–10]. However, little data are available regarding AP induced by PDO, even though this experimental design represents a useful model to study gallstone-induced pancreatitis—the most common etiology of the disease in humans [25]. Although it is accepted that the biochemical alterations that lead to AP are initiated within acinar cells at early stages [26], the evaluation of the OFR and its role in AP is generally performed in homogenates of pancreatic tissue [6,9–11]. Therefore, our major goal was to evaluate the individual contribution of acinar cells to OFR production at different stages of AP induced by PDO and correlate the results with the pancreatic GSH content, as a major reductant factor in oxidant–reductant processes.

In this study, intracellular OFR generation was monitored by flow cytometry using DHR as fluorogenic dye. DHR is usually considered as a useful tool for depicting the production of O_2^-, H_2O_2, and $OONO^-$ [23]. Flow cytometric analysis of acinar cells loaded with DHR revealed a progressive enhancement of OFR production from 3 to 12 h after PDO, which was concomitant with the progressive development of AP, as revealed by the different parameters used for diagnosing the severity of the disease. Nevertheless, OFR are characterized by an extremely short half-life because they attack nearby substrates such as proteins, lipids and DNA [11–13]. Therefore, the production of OFR at earlier stages of AP should not be ruled out. This notion is supported by Reinheckel et al.'s [27] reports who found oxidized proteins in pancreas as a result of oxidative stress 1 h after inducing AP by both taurocholate and cerulein [28], even before pancreatic edema and hyperamylasemia were observed. In the current study, lipid peroxidation, expressed in terms of MDA concentration, also seems to have started 1.5 h after PDO, but it was 6 h after PDO when the highest MDA levels were found. Reinheckel et al. reported that protein oxidation precedes the formation of the lipid peroxidation product MDA, suggesting independent pathways for the oxidative damage exerted on different cellular substrates. Protection against OFR requires enzymatic and non-enzymatic antioxidants [29] such as GSH. Our results show that the enhanced lipid peroxidation observed 6 h after inducing AP is concomitant with the maximum depletion of GSH and the highest increases in DHR dye in acinar cells. These data indicate that at this stage of AP, a large OFR production takes place in acinar cells which overwhelms OFR neutralization by the antioxidant defence system in acinar cells and suggests that MDA generation might require higher amounts of OFR than protein oxidation. Peroxidation of lipids of membranes would lead to disturbances in membrane organization and cellular damage observed by electron microscopy in previous studies [19]. Furthermore, some of the products resulting from lipid peroxidation may act as co-factors or activators of other pathological mechanisms, like phospholipase A_2 [30], an enzyme whose serum levels correlate with the severity of AP and which seems to be involved in lung damage occurring during AP [31]. In the light of the OFR increases in acinar cells and the reduced GSH levels, MDA increase could have been expected 12 h after PDO. However, as occurs in other experimental models of AP [28,32], a single peak of MDA was observed 6 h after PDO. Currently, we cannot explain this finding but as an asynchronous oxidation of proteins and lipid was described by Reinheckel et al. [27,28], a later attack of OFR to a new target while MDA is metabolized could be a possibility.

Activated neutrophil system, xanthine oxidase (XOD) and mitochondrial dysfunction are among the mechanisms responsible for inducing oxidative stress [33]. Although neutrophils that infiltrate into the pancreas from early stages of AP can contribute to the generation of OFR [34], our results indicate that acinar cells—themselves—are able to significantly increase OFR production, thereby acting as messengers to directly and/or indirectly enhance the activation of intracellular proteases and the inflammatory reaction during the development of AP.

From 24 h after PDO, individual acinar cells no longer showed increased values of fluorescence due to DHR Morphological alterations [18] and depletion of ATP levels in acinar cells [8,9] indicate that mitochondria are early targets of cell damage in AP. Taking into account that these organelles are the main source of OFR [35], our results can be explained by a severe mitochondrial injury at late stages of AP in many acinar cells, rendering them incapable of producing more OFR because of impairment in the energy metabolism. Furthermore, DHR is a dye which easily crosses all membranes and becomes fluorescent upon oxidation generating rhodamine-123, also located in the mitochondria [23]; if these organelles are severely injured, cells could fail to take up the dye.

GSH levels returned to normal values 48 h after PDO. Since we measure total glutathione, this could be attributed to an enhanced oxidized glutathione (GSSG). Nevertheless, it has been reported that this does not occur during AP induced by duct obstruction [9]. We suggest that the GSH turnover supplies GSH to the pancreas from other organs, such as the liver, the main source of GSH in the body. Since OFR are not generated at late stages of AP, GSH may not be used as reductant factor, thus allowing the recovery of GSH levels in pancreatic tissue.

Despite the mean values of DHR dye in acinar cells, and GSH and MDA pancreatic contents returning to control values at late stages of AP induced by PDO, the improvement of the disease should not be considered in the light of the severe morphological alterations at 24 and 48 h after PDO observed by electron microscopy studies [16–19].

Flow cytometric studies revealed the existence of two well-differentiated populations of acinar cells, R1 and R2, on the basis of light scatter properties. The two cell types have been shown to react distinctly to AP induction as regards enzyme load [16] and intracellular Ca^{2+} concentrations [19]. In the present study, both in controls and PDO-rats, R2 cells showed higher values of fluorescence intensity due to DHR, a finding that suggests either higher oxidative capacity and/or higher respiratory metabolism than R1 cells. Accordingly, we expected both populations to behave in a different way with regard to oxidative metabolism. However, no differences between them could be observed. Both populations of acinar cells displayed similar behaviour in all stages of AP induced by PDO, which suggests that oxidative stress within acinar cells does not totally correlate with other pathological mechanisms involved in the development of AP, such as Ca^{2+} homeostasis or enzyme overload.

In conclusion, our study clearly shows that acinar cells produce large amounts of OFR at early stages of PDO-induced AP in rats, which may contribute to the oxidative injury of the pancreas. In addition, we have shown that the two existing populations of acinar cells display a similar behaviour regarding oxidative stress during different stages of AP. Further studies are needed to clarify the relationship between the different events related to oxidative stress and other intracellular pathological events involved in the development of acute pancreatitis.

Acknowledgements

This study was supported by grants from CICYT and European Commission (1FD97-1724) and FISSS, Spain (00/0512). Thanks are due to Mark Anderson for revising the manuscript.

References

[1] M.L. Steer, A.K Saluja, in V.L.W. Go, E.P DiMagno, J.D. Gardner, E. Lebenthal, H.A. Rebar, G A Scheele (Eds), The Pancreas Biology, Pathophysiology and Disease, 2nd ed, Raven, New York, 1993, pp 489–499

[2] J.M Braganza, in C Rice-Evans, T Dormandy (Eds.), Free Radicals. Chemistry, Pathology and Medicine, Richelieu Press, London, 1988, pp. 357–381

[3] M.H. Schonberg, M Büchler, H G. Beger, Hepato-Gastroenterol. 41 (1994) 313–319

[4] H Sanfey, G B Bulkley, J L Cameron, Ann. Surg. 200 (1984) 405–413.

[5] M H Schonberg, M. Buchler, H Schadlich, M Younes, B. Bultmann, H G Beger, Klin Wochenschr. 67 (1989) 166–170.

[6] L Czakó, T. Takács, I.S Varga, L. Tiszlavicz, D Quy Hai, P Hegyi, B. Matkovics, J. Lonovics, Dig Dis Sci 43 (1998) 1770–1777

[7] P Kruse, M E Anderson, S Loft, Free Radic Biol Med 30 (2001) 309–317

[8] R. Lüthen, C Niederau, J H Grendell, Am J Physiol. 268 (1995) G592–G604.

[9] R Luthen, J H Grendell, C Niederau, D Haussinger, Int J Pancreatol. 24 (1998) 193–202

[10] T Koiwai, H Oguchi, S Kawa, Y Yanagisawa, T Kobayashi, T Homma, Int. J Pancreatol. 5 (1989) 135–143.

[11] A. Nonaka, T Manabe, T. Kyogoku, K Tamura, T Tobe, Digestion 47 (1990) 130–137

[12] E R Stadman, Ann Rev. Biochem 62 (1993) 797–821

[13] H Wiseman, B Halliwel, Biochem. J. 313 (1996) 17–29.

[14] J. Meister, Biol. Chem 269 (1999) 9397–9400.

[15] B. Chance, H Sies, A Boveris, Physiol. Rev 59 (1979) 527–605.

[16] A Uruñuela, M A Manso, R M. Pinto, A. Orfao, I. De Dios, Clin Sci. 98 (2000) 143–150

[17] R.M. Pinto, I De Dios, A. Uruñuela, A. Orfao, M A. Manso, Eur J Cell Biol. 79 (2000) 62–69.

[18] I. De Dios, A Uruñuela, R.M Pinto, A Orfao, M.A Manso, Cell Tissue Res. 300 (2000) 307–314

[19] A. Uruñuela, M.A Manso, A M. de la Mano, S Sevillano, A Orfao, I De Dios, Clin Sci 102 (2002) 615–622

[20] G. Noelting, P. Bernfeld, Helv Chim Acta 31 (1948) 286–290

[21] F. Tietze, Anal. Biochem. 27 (1969) 502–522.

[22] H Ohkawa, N Ohishi, K. Yagi, Anal. Biochem 95 (1979) 351–358

[23] G Rothe, A. Emmendorffer, A Oser, J Roesler, G Valet, J. Immunol Methods 138 (1991) 133–135

[24] G C Salzman, S.B Singham, R G Jonston, C.F. Bohren, in· M.R Melamed, T Lindmo, M L Mendelshon (Eds.), Flow Cytometry and Sorting, Wiley-Liss, New York, 1990, pp. 81–107

[25] P A Banks, in. W S. Haubrich, F. Schaffuer, J.E Berk (Eds.), Bockus Gastroenterology, W B Saunders, Philadelphia, 1995, pp 2888–2917

[26] R Bialek, R. Willemer, R Arnold, G Adler, Scand. J Gastroenterol 26 (1991) 190–196

[27] T Reinheckel, B. Nedelev, J Prause, W Augustin, H U. Schulz, H Lippert, W Halangk, Free Radic Biol 24 (1998) 393–400

[28] T Reinheckel, J Prause, B Nedelev, W. Augustin, H U Schulz, H Lippert, W Halangk, Digestion 60 (1999) 56–62.

[29] B A Freeman, J.D Crapo, Lab. Invest 47 (1982) 412–426

[30] F R Ungemach, Chem Phys Lipids 45 (1987) 171–205

[31] P G Lankisch, G. Rahlf, H Koop, Dig. Dis. Sci 28 (1983) 111–116.

[32] A Dabrowski, A Gabryelewicz, Scand J Gastroenterol 29 (1994) 943–948

[33] J M Braganza (Ed.), The Pathogenesis of Pancreatitis, Manchester Univ. Press, Manchester, 1991

[34] T Ito, A. Nakao, W Kishimoto, M. Nakano, H. Takagi, Pancreas 12 (1996) 173–177.

[35] E. Gottlieb, G Matthew, V Heiden, C B. Thompson, Mol Cell Biol 20 (2000) 5680–5689

ELSEVIER

Biochimica et Biophysica Acta 1588 (2002) 165–172

BIOCHIMICA ET BIOPHYSICA ACTA
BBA
www.bba-direct.com

Human colon adenocarcinoma is associated with specific post-translational modifications of versican and decorin

Achilleas D. Theocharis *

Department of Chemistry, Section of Organic Chemistry, Biochemistry and Natural Products, Laboratory of Biochemistry, University of Patras, 261 10 Patras, Greece

Received 14 March 2002; received in revised form 11 June 2002; accepted 26 June 2002

Abstract

In this study, the amounts and the fine structural characteristics of versican and decorin present in human colon adenocarcinomas (HCC) were investigated and compared with those in human normal colon (HNC). HCC is characterized by significant increase in the amounts of versican and decorin (13- and 8-fold in terms of protein, respectively). These two proteoglycans (PGs) were the predominant in HCC (86% of total uronic acid). In HNC, versican and decorin contained both chondroitin sulfate/dermatan sulfate chains (CS/DS), with DS to be the predominant one (90–93%). The molecular sizes (M_rs) estimated for DS and CS chains were 25–28 and 21–28 kDa, respectively. In CS/DS chains isolated from both versican and decorin, 4-sulfated disaccharides accounted for 79–86% of total disaccharide units, respectively, whereas lower amounts of 6- and non-sulfated units were also recorded. In contrast, the tumor-associated versican and decorin were of smaller hydrodynamic size with lower glycosaminoglycan (GAG) content per PG molecule as compared with those found in HNC. In HCC, both PGs contained mainly CS chains (up to 86%) and the M_rs of CS and DS chains were also found to be of smaller size (12 and 16 kDa, respectively). The sulfation patterns of CS/DS chains from both PGs were also significantly different. They were composed mainly of 6-sulfated disaccharides (63–70%), whereas 4-sulfated units accounted for 23–31%. A significant increase in the proportion of non-sulfated disaccharides was also recorded. These findings indicate that the colon adenocarcinoma is characterized by a remarkable increase in the concentration of versican and decorin. Furthermore, these PGs are significantly modified at the post-translational level, i.e. the type, length and the sulfation pattern of their GAG chains. These specific structural alterations of versican and decorin may influence the biology of cancer cells in HCC.

© 2002 Elsevier Science B.V. All rights reserved.

Keywords: Colon carcinoma; Proteoglycan; Versican; Decorin; Glycosaminoglycan; Sulfation pattern

1. Introduction

Proteoglycans (PGs) are macromolecules composed of a core protein onto which variable number of glycosaminoglycan (GAG) chains are covalently attached. They are key bioactive molecules and are directly implicated in a large variety of human diseases. Several studies indicated that significant changes in PG content occur in the tumor stroma of epithelial neoplasms and that these alterations support tumor growth and invasion [1]. Colon carcinoma is a common epithelial neoplasm, which is characterized by increased levels of versican and decorin [2]. These PGs contain chondroitin sulfate (CS)/dermatan sulfate (DS) chains and are abnormally expressed in a wide variety of malignant tumors. Versican is a member of the hyalectan family and play important roles in forming hyaluronan (HA)-rich matrix, which would provide cells with anti-adhesive environment [3–5]. The deposition of versican in the tumor stroma, particularly in HA-rich regions, probably supports the cancer cell growth. The abnormal expression of versican occurs as a consequence of hypomethylation of its control genomic region and abrogation of versican expression by antisense oligodeoxynucleotides can revert the malignant phenotype. Decorin, a prototype member of the small leucine-rich PG family [1,2,6], is emerging as a powerful modulator of cell growth by affecting several key elements including matrix assembly, binding of growth factors and tyrosine kinase activity [7–9]. Decorin levels are suppressed in most transformed cells [10], but markedly increased in the peritumorous stroma of colon cancer [11]. The latter may represent a natural biological response of the host cells to the

---

* Fax. +30-610-997690

0925-4439/02/$ - see front matter © 2002 Elsevier Science B.V. All rights reserved.
PII S0925-4439(02)00161-8

invading neoplastic cells [12]. Many of the above biological properties of these matrix PGs reside to the specific structural characteristics of their GAG chains. Remarkable structural alterations of GAG chains have been recorded in a variety of neoplasms of the gastrointestinal tract and pancreas [13,14]. Particularly, poorly differentiated colon adenocarcinoma is characterized by significant increase of HA-derived Δ-disaccharides and 6- and non-sulfated disaccharides as determined by high-performance capillary electrophoresis (HPCE) [13].

The aim of this study was to determine in deep detail the fine structural characteristics of the GAG moieties of versican and decorin in human colon carcinoma (HCC). The results reveal that the poorly differentiated colon adenocarcinoma is characterized by significant increase in the concentration of versican and decorin. In normal colon these PGs contain primarily DS chains, whereas in colon carcinoma they are mainly substituted with CS chains. Furthermore, in cancerous tissue, both GAGs exhibit smaller molecular size and a quite different sulfation pattern.

2. Materials and methods

2.1 Chemicals

Sepharose CL-4B, CL-6B and DEAE-Sephacel were obtained from Pharmacia Chemicals (Uppsala, Sweden). Papain twice crystallized (EC 3.4.22.2), cetylpyridinium chloride (CPC), chondroitinase ABC (EC 4.2.2.5), chondroitinase AC II (EC 4.2.2.4), heparin lyase II (heparitinase II, no EC number), GAG standards and standard preparations of differently sulfated Δ-disaccharides from heparin and heparan sulfate were from Sigma Chemical Co. (St. Louis, MO, USA). Chondroitinase B (EC 4.2.2.5), heparin lyases I and III (EC 4.2.2.7 and 4.2.2.8, respectively) and standard preparations of variously sulfated Δ-disaccharides from CS, DS, HA as well as monoclonal antibodies 2–B–1 against versican and 6–B–6 against decorin were purchased from Seikagaku Kogyo. All chemicals used were of the best commercially available grade.

2.2 Analytical methods

GAGs were detected in column fractions by the DMB method [15] and uronic acid (UA) was determined by the Bitter–Muir modified carbazole reaction [16]. Protein content was determined by the method of Bradford [17]. Unsaturated disaccharides released following treatment of GAGs with chondroitinase ABC were determined by high-performance liquid chromatography (HPLC) [18].

2.3. Tissue source—patients

Colon carcinomas were collected from patients (five males/three females) aged 45–65 years, who underwent colectomy for colon adenocarcinoma in the University Hospital of Patras. Specimens were taken directly from operating rooms. Specimens of normal colon, which included mucosa and submucosa, were also collected from the normal regions of the same patient. All specimens were immediately stored at − 70 °C. Pathological examination of the neoplastic tissue showed poorly differentiated adenocarcinoma in six out of eight cases. The poorly differentiated carcinomas were located in the descending and sigmoid colon and were of stage C1 (two cases out of six) and C2 (four cases out of six) according to the modified Duke's classification of colon carcinoma. Normal tissue specimens were free from specific histopathological evidence.

2.4. Extraction, isolation and characterization of versican and decorin

The poorly differentiated carcinomas and the respective normal specimens ($n = 6$) were finely diced and extracted separately, by gentle shaking with 10 vol. of 4 M guanidine-HCl–0.05 M sodium acetate, pH 5.8, containing protease inhibitors for 24 h at 4 °C [19,20]. The extraction mixture was filtered and the filtrate was retained. The residues were re-extracted with 10 vol. of the same extracting solution. The extracts were concentrated by ultrafiltration on a YM-10 Amicon filter and then dialyzed against 0.15 M sodium chloride containing the above described protease inhibitors. Consequently, the PGs were isolated by precipitation with CPC, extraction of the CPC-PGs complex with 2 M sodium chloride and re-precipitation with ethanol [21].

PGs were dissolved in 4 M guanidine-HCl–0.05 M sodium acetate pH 5.8, in the presence of protease inhibitors and aliquots were obtained for chemical analyses. The remainder were subjected to dissociative cesium chloride density gradient ultracentrifugation (starting density = 1.42 g/ml). Ultracentrifugation was performed for 48 h at 10 °C, in a Beckman L2-65B centrifuge with an 8 × 12 ml T 65 fixed angle rotor at 37,000 rpm. After centrifugation, the tubes were frozen and cut into three fractions as follows: bottom 3 ml (D_1, density >1.53 g/ml), middle 6 ml (D_2, density 1.36–1.53 g/ml) and top 3 ml (D_3, density < 1.36 g/ml). The fractions were analyzed for uronic acid, hexosamine and protein. The isolated proteoglycans of high buoyant density (D_1 fraction) and low buoyant density (D_2 fraction) were dialyzed against 10 M formamide–0.05 M sodium acetate, pH 6.0, containing 0.2% Triton X-100 and all above described inhibitors [22] and applied to a DEAE-Sephacel microcolumn (3 ml) equilibrated with the same buffer. HA were eluted by washing of the column with 3 vol. of the same buffer containing 0.3 M NaCl. PGs were fractionated by elution of the column with 10 vol. of a linear gradient ranging from 0.3 to 0.85 M NaCl in formamide buffer. HSPGs were eluted with ~ 0.4–0.5 M NaCl and were completely separated from CS/DSPGs, which were eluted with 0.55–0.7 M NaCl in each case. CS/DSPGs were pooled as indicated by bars and concentrated.

CS/DSPGs were further fractionated by gel filtration chromatographies on analytical Sepharose CL-4B and -6B columns (110 × 0.6 cm), equilibrated and eluted with 4 M guanidine-HCl–0.15 M sodium acetate, pH 5.8. The average molecular weight (M_r) of the proteoglycans was estimated using proteoglycan standards for calibrating the columns [23].

Identification of PGs was performed by Western blotting. PGs were electrophoresed in 4–20% (w/v) acrylamide gradient gels, containing SDS (SDS-PAGE) according to the method of Laemmli [24]. Separate gels were stained with Coomassie R-250 and Toluidine blue. The electrophoresed samples were transferred to polyvinylidenedifluoride membranes (Immobilon-P) at constant current 80 mA at 4 °C for 20 h in 0.05 M Tris–HCl, pH 8.3. The membranes were washed with 0.14 M NaCl in 0.01 M phosphate buffer, pH 7.2, containing 0.1% Tween 20 (PBS-T) and blocked with 5% dry defatted milk in PBS-T. They were immersed in antiserum against either versican (monoclonal antibody, clone 2–B–1) [25,26], decorin (monoclonal antibody, clone 6–B–6) and biglycan (polyclonal antibody) [27], diluted 1:1000 in PBS-T and incubated for 60 min at room temperature. The membranes were washed and incubated with peroxidase-labelled secondary antibodies (rabbit anti-mouse/goat anti-rabbit) diluted 1:2000 in PBS-T for 60 min at room temperature. The membranes were washed and the immunoreacted bands were visualized by the enhanced chemilumiscence technique (ECL, Amersham) according to the instructions of the manufacturer.

2.5. Isolation and characterization of GAGs

Aliquots of isolated PGs were digested with papain and the GAGs were released from remaining peptide fragments by treatment with 0.05 M NaOH/1 M sodium borohydride at 45 °C for 48 h under vacuum [28,29]. Characterization and quantitation of GAGs were performed following acetate cellulose electrophoresis [30], gel filtration on analytical columns of Sepharose CL-6B and HPLC analyses before and after treatment with a mixture of heparin lyases I, II and III and/or chondroitinases ABC and AC II [31]. Disaccharide composition and sulfation pattern of GAGs were estimated following digestion with chondroitinase ABC and HPLC analysis [18]. Gel filtration of GAGs was performed

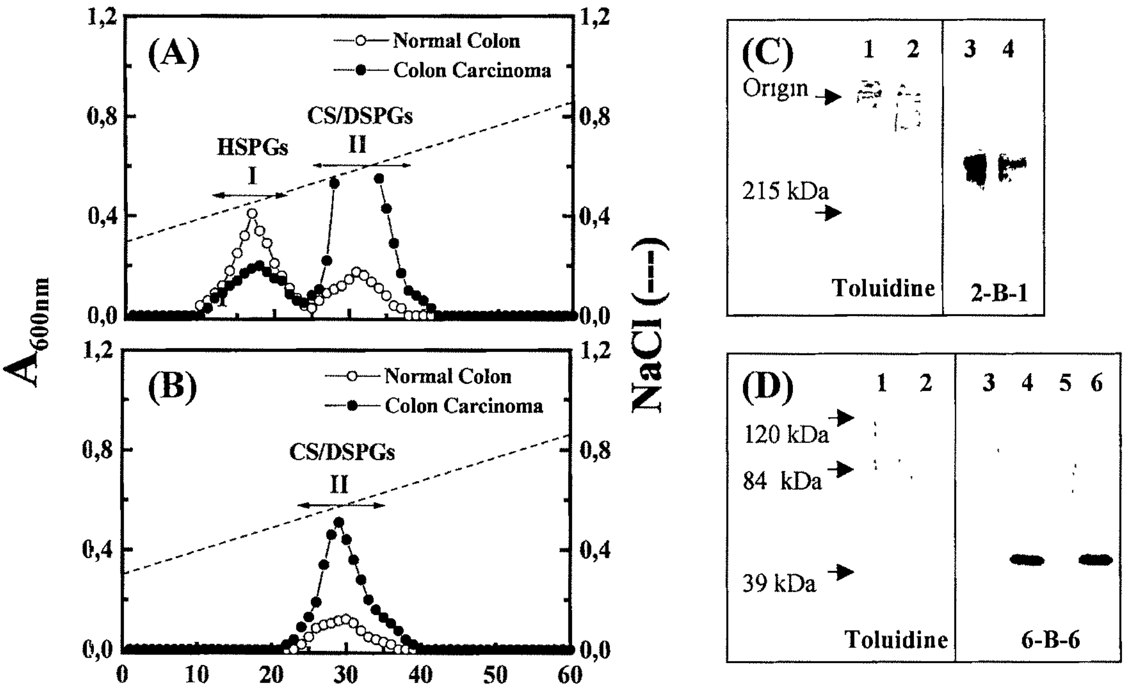

Fig 1 Fractionation of NPGs-D_1 and CPGs-D_1 (A) and NPGs-D_2 and CPGs-D_2 (B) from normal colon (O) and colon carcinoma (●), respectively, by anion-exchange chromatography on DEAE-Sephacel microcolumn (3 ml bed volume) The column was elute stepwise with 3 vol of the formamide buffer described in the text containing 0 3 M NaCl and 10 vol of a NaCl linear gradient ranging from 0 3 to 0.85 M Fractions of 0 5 ml were collected and aliquots were precipitated by the addition of 4 vol of ethanol Precipitates were dissolved in distilled water and analyzed for their GAG content by the DMB method. (C) SDS-PAGE (lanes 1 and 2) and immunoblot analyses (lanes 3 and 4) of CS/DSPGs isolated from NPGs-D_1 (lanes 1 and 3) and CPGs-D_1 (lanes 2 and 4) CS/DSPGs were electrophoresed without any treatment in 4–20% gradient gels and they were stained with Toluidine blue (lanes 1 and 2) Immunostaining was performed in CS/DSPGs which had been digested with chondroitinase ABC using the monoclonal antibody 2–B–1 against versican (lanes 3 and 4). (D) SDS-PAGE (lanes 1 and 2) and immunoblot analyses (lanes 3–6) of CS/DSPGs isolated from NPGs-D_2 (lanes 1, 3 and 4) and CPGs-D_2 (lanes 2, 5 and 6) CS/DSPGs were electrophoresed without any treatment in 4–20% gradient gels and they were stained with Toluidine blue (lanes 1 and 2) Immunostaining was performed in CS/DSPGs before (lanes 3 and 5) and after digestion (lanes 4 and 6) with chondroitinase ABC using the monoclonal antibody 6–B–6 against decorin The figure indicates a representative case of normal ($n = 6$) and cancerous specimens ($n = 6$) examined

on analytical Sepharose CL-6B column (110 × 0.6 cm), equilibrated and eluted with 0.5 M sodium acetate, pH 7.0. The M_rs of the CS and DS chains were estimated by the construction of the *secondary profile* according to a recent study [32], using CS molecular weight standards for calibrating the column. In brief, the mixture of isolated CS/DS was digested with chondroitinase B and the profile, upon gel chromatography on Sepharose CL-6B, was compared to that of the initial undigested sample. The absolute amounts or percentage of uronic acid measured in each fraction of the chromatographies before and after treatment with chondroitinase B were subtracted, fraction by fraction, and the differences were obtained. The positive differences were used to construct the *secondary profile*, which represented the uronic acid content of the fractions removed after the enzymatic digestion, i.e. the elution profile of intact DS chains, and thus the size distribution of DS was obtained and its M_r was calculated.

2.6. Statistical analysis

Statistical analysis was performed by the *t*-test using the microcal origin software (version 3.2).

3. Results

3.1. Isolation and characterization of versican and decorin

The extracts of each specimen from normal colon and colon carcinoma ($n = 6$) were analyzed separately for their uronic acid contents. These analyses indicated that the dissociative extraction of normal and cancerous specimens removed up to 83–87% of total uronic acid in both tissues. PGs from each specimen were isolated separately following CPC and ethanol precipitation and further subjected to equilibrium–density-gradient fractionation under dissociative conditions. The gradient was divided into three fractions and the distribution of uronic acid and protein was determined. The top fractions of buoyant density (D_3, $P < 1.36$ g/ml) from both normal and cancerous tissues contained about 2% of total uronic acid and were not further examined. The specimens of normal colon contained mainly (87–91% of total uronic acid) PGs of high buoyant density (NPGs-D_1, $P > 1.53$ g/ml) and a small proportion (7–11% of total uronic acid) of PGs of low buoyant density (NPGs-D_2, $1.36 < P < 1.53$ g/ml). In colon carcinoma, the PGs of high buoyant density (CPGs-D_1) represented the 80–83% of total uronic acid and those of low buoyant density PGs (CPGs-D_2) accounted for 15–18% of total uronic acid.

NPGs-D_1 and CPGs-D_1 were further fractionated by ion-exchange chromatography on DEAE-Sephacel column. A typical profile of these chromatographies is shown in Fig. 1A. The column was eluted with 10 vol. of a NaCl linear gradient ranging from 0.3 to 0.85 M and two populations were resolved in each case. The column recoveries exceeded 93% and the elution patterns were reproducible. As assessed following treatments of the isolated populations with a mixture of heparin lyases as well as with chondroitinases ABC and AC II, and analyses by HPLC and cellulose acetate electrophoresis, population I contained HSPGs, whereas population II contained a mixture of CS/DSPGs (Fig. 1A). Similarly to NPGs-D_1 and CPGs-D_1, PGs present in fractions NPGs-D_2 and CPGs-D_2 were isolated following ion-exchange chromatography. NPGs-D_2 and CPGs-D_2 fractions were chromatographed on DEAE-Sephacel column and only population II of CS/DSPGs, which was eluted with 0.55–0.7 M NaCl, was recorded in each case (Fig. 1B).

The isolated CS/DSPGs were further analyzed by SDS-PAGE and immunoblotting using specific antibodies against several types of matrix CS/DSPGs. Analyses were performed before or/and after they had been digested with chondroitinase ABC. SDS-PAGE of intact populations NPGs-D_1 and CPGs-D_1 showed the presence of a large size population, which remained in the top of the stacking gel (Fig. 1C, lanes 1 and 2). Immunoblotting following treatment of the populations NPGs-D_1 and CPGs-D_1 with chondroitinase ABC revealed the presence of two core proteins with M_rs>215 kDa in each tissue specimen, which

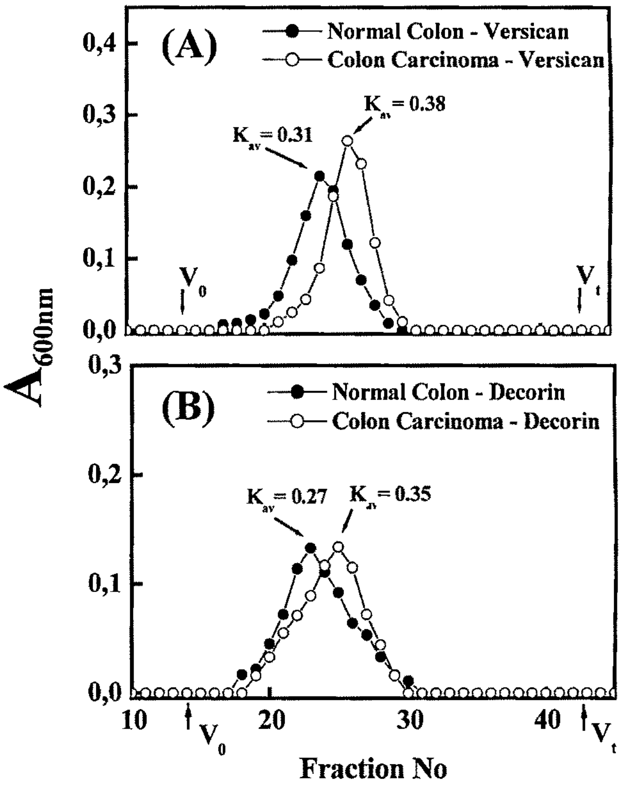

Fig. 2. Gel chromatography of pooled versican (A) and decorin (B) isolated from normal colon (○) and colon carcinoma (●), on Sepharose CL-4B and Sepharose CL-6B (110 × 0.6 cm i.d.), respectively. The columns were eluted with 4 M guanidine-HCl–0.15 M sodium acetate, pH 5.8, and fractions of 0.9 ml were collected. Aliquots of the fractions were precipitated by the addition of 4 vol. of ethanol, dissolved in distilled water and analyzed by the DMB method.

reacted only with the monoclonal antibody 2–B–1 against versican (Fig. 1C, lanes 3 and 4). In the isolated populations, NPGs-D$_2$ and CPGs-D$_2$, the presence of a single population with apparent molecular size (estimated using protein standards) of ~ 100 kDa for NPGs-D$_1$ and ~ 80 kDa for CPGs-D$_1$ was identified by SDS-PAGE (Fig. 1D, lanes 1 and 2). Immunoblot analyses of these populations before and after treatment with chondroitinase ABC, using specific antibodies for the matrix CS/DSPGs described in Material and methods revealed the only presence of decorin with a core protein of ~ 40 kDa in these populations (Fig. 1D, lanes 3–6).

Both versican and decorin present in each tissue specimen were quantitated in terms of uronic acid and protein (Table 1). HCC was found to contain significantly increased amounts of versican (13-fold, 620 ± 45 μg of protein/g w/w of tissue) in comparison to human normal colon (HNC) (45 ± 7 μg of protein/g w/w of tissue). Furthermore, the ratio of uronic acid to protein in versican isolated from HCC (0.4) was decreased 40% as compared to that from HNC (0.65). Decorin amounts were also markedly increased in colon carcinoma (8-fold, 413 ± 30 μg of protein/g w/w of tissue) in comparison to normal colon (48 ± 5 μg of protein/g w/w of tissue) and a 40% decrease in the ratio of uronic acid to protein was also estimated in cancerous specimens (0.25 in normal colon and 0.15 in colon carcinoma) (Table 1). The analyses indicated no significant intrabatch differences in the concentrations of versican and decorin between the various normal and cancerous specimens examined as shown by the low variability in each group. For this reason, versican and decorin from each group were separately pooled and further structural analyses were performed on pooled versican and decorin from HNC and HCC.

Gel chromatography of versican contained in HNC and HCC on a Sepharose CL-4B column revealed the presence of a homogeneous population in each case with K_{av} values of 0.31 (M_r of 800 kDa) and 0.38 (M_r of 580 kDa), respectively (Fig. 2A). The respective chromatography of decorin on Sepharose CL-6B column also revealed the presence of homogenous populations in each case with K_{av} of 0.27 for normal tissue (M_r of 80 kDa) and 0.35 for colon carcinoma (M_r of 56 kDa) (Fig. 2B). These results indicated a 30% decrease in the molecular mass of both versican and decorin in HCC.

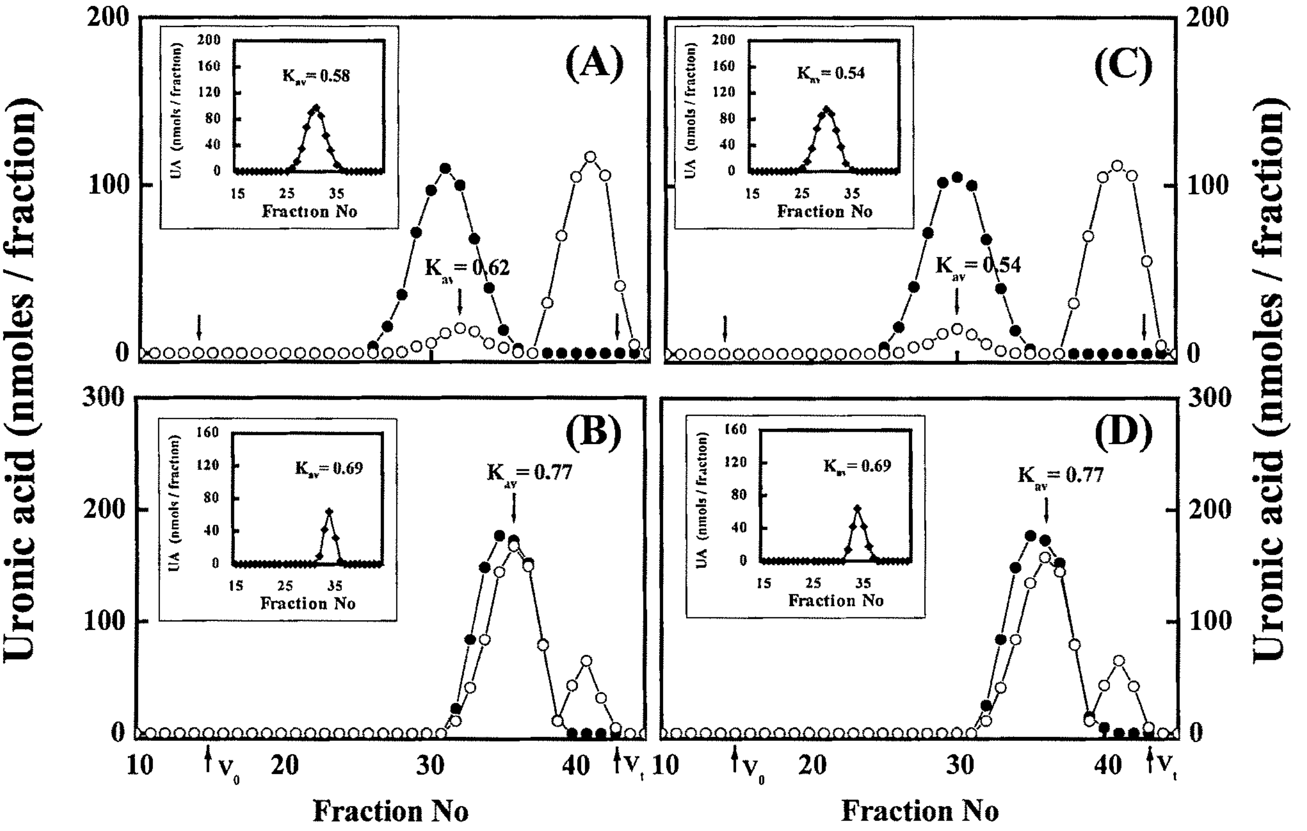

Fig 3. Gel chromatography of CS/DS chains isolated from pooled versican (A) and (B) and decorin (C) and (D) from normal colon (A) and (C) and colon carcinoma (B) and (D) on an analytical Sepharose CL-6B column (110 × 0 6 cm i d), before (●) and after (O) treatment with chondroitinase B. The column was eluted with 0 5 M sodium acetate, pH 7 0 Fractions of 0 9 ml were collected and analyzed for their uronic acid content (Insets) Secondary profile of DS chains, obtained from the positive differences of uronic acid in each fraction of the sample before and after digestion with chondroitinase B

Table 1
Structural characteristics of versican and decorin isolated from human normal colon and poorly differentiated colon adenocarcinoma

PGs composition	Versican		Decorin	
	Normal colon	Colon carcinoma	Normal colon	Colon Carcinoma
Uronic acid	29 ± 4	248 ± 30	12 ± 3	62 ± 7
Protein	45 ± 7	620 ± 45	48 ± 5	413 ± 30
Uronic acid/protein (w/w)	0.65	0.40	0.25	0.15
M_r of PGs (kDa)	800	580	80	56
CS[a]	10	86	7	77
DS[b]	90	14	93	23
M_r of CS (kDa)	21	12	28	12
M_r of DS (kDa)	25	16	28	16
Non-sulfated disaccharides[c]	3	7	2	6
4-Sulfated disaccharides[c]	79	23	86	31
6-Sulfated disaccharides[c]	18	70	12	63

The results are expressed as μg/g wet weight of tissue. Values are the means ± S.D. of the normal colon specimens ($n = 6$) and colon carcinoma specimens ($n = 6$) examined.

[a] Percentage composition estimated in the pooled versican and decorin. CS was estimated as the chondroitinase B resistant material.

[b] Percentage composition estimated in the pooled versican and decorin. DS was estimated as the chondroitinase B degradable material.

[c] Percentage composition estimated in the pooled versican and decorin.

3.2. Characterization of GAG chains of versican and decorin

In order to examine the composition and fine chemical structures of GAG chains attached into versican and decorin, they were released following papain digestion and alkaline borohydride treatment. GAGs were then chromatographed on an analytical Sepharose CL-6B column before and after exhaustive digestion with chondroitinase B, an enzyme that is specific for the degradation of DS-type sequences. The products of digestion were eluted close to the V_t of the column. In versican and decorin isolated from normal colon, the enzyme degraded significant amounts of the mixture of CS/DS chains (about 90–93% of total uronic acid), indicating the prominent presence of DS in both versican (Fig. 3A) and decorin (Fig. 3C). A minor proportion (about 7–10% of total uronic acid) of the sample, which was resistant to degradation with chondroitinase B represents CS chains (Fig. 3A and C, Table 1). In contrast to normal tissue, the chondroitinase B degraded only minor amounts of the mixture of CS/DS chains attached into versican (Fig. 3B) and decorin (Fig. 3D) in HCC. In both versican and decorin from cancerous tissue, CS is the predominant GAG (86% of total uronic acid in versican and 77% in decorin), whereas DS accounts for 14–23% of total uronic acid, respectively (Table 1).

The CS chains isolated from versican and decorin from HNC after digestion of CS/DS chains with chondroitinase B were eluted as single peaks with K_{av} of 0.62 and 0.54 corresponding to M_rs of 21 and 28 kDa, respectively (Fig. 3A and C, Table 1). The CS chains isolated from both versican and decorin from HCC were of smaller size (M_r of 12 kDa in both PGs) (Fig. 3B and D, Table 1). The *secondary profiles* of DS present in versican and decorin were constructed (Fig. 2A–D insets) as described in Materials and methods. From these secondary profiles, the M_rs of DS chains were calculated. DS chains belonging to both versican and decorin from HCC were of smaller molecular size (M_r of 16 kDa) as compared to those from normal tissues (M_r of 25 kDa for versican and 28 kDa for decorin) (Fig. 3A–D insets, Table 1).

Analyses for the sulfation pattern of the GalGAG chains are presented in Table 1. In versican and decorin isolated from HNC, 4-sulfated disaccharides predominated (79–86% of total disaccharides, respectively). Lower amounts of 6-sulfated (18–12% of total disaccharides in versican and decorin, respectively) and non-sulfated units (3–2%) were also recorded in the normal tissue (Table 1). In contrast, in HCC the sulfation patterns of both versican and decorin were significantly altered. Particularly, the relative proportions of 6-sulfated and non-sulfated disaccharides were markedly increased in both versican and decorin and accounted for 70–63% and 7–6% of total disaccharides, respectively (Table 1).

4. Discussion

Previous studies [33,34] have demonstrated that HCC is characterized by the increased production of a structurally altered CS by the connective tissue surrounding the neoplastic cells. Other studies [11] have shown that HCC contained increased levels of decorin-bearing CS chain, in which the non- and 6-sulfated disaccharides are the predominant units, as detected by specific antibodies. The abnormal expression of versican in the cancerous tissue has been also demonstrated [11,35,36]. In a recent study, we showed that the poorly differentiated colon adenocarcinoma and other epithelial cancers are associated with specific compositional and structural modifications of GAGs [13].

The goal of the present study was to examine in deep detail the fine structural characteristics of GAGs attached on the abnormal expressed PGs versican and decorin in human colon cancer and to compare them with normal tissue.

The results indicated that HNC contained versican and decorin, which are primarily substituted with DS side chains. HCC contained significantly elevated amounts of versican (13-fold increase of protein amounts) and decorin (8-fold increase of protein amounts). CS chains are the major GAG attached in both PGs in HCC. The ratios of uronic acid to protein for versican and decorin in the diseased tissue (0.40 and 0.15, respectively) were markedly decreased (~ 40%) as compared to those of normal tissue (0.65 and 0.25, respectively). Additionally, in colon carcinoma, versican and decorin exhibited lower M_rs (~ 30%) than in normal colon. Both of these observations suggest a poverty in GAG content of versican and decorin isolated from colon carcinoma. This is probably due to the reduced M_rs of CS and DS chains and not to fewer GAG chains per core protein. Actually CS and DS found in cancerous tissue exhibited a similar magnitude decrease (~ 40–50%) in their hydrodynamic sizes (12 and 16 kDa, respectively) in comparison to those of normal colon (21–28 and 25–28 kDa, respectively). Further structural modifications, concerning the sulfation patterns of both PGs, were also documented. In normal tissue CS/DS chains of versican and decorin are mainly composed of 4-sulfated disaccharides, whereas the sulfation profile of CS/DS chains is significant altered in the diseased tissue, showing a marked increase in the proportions of non- and 6-sulfated disaccharides. The latter one being the predominant type of disaccharide units in colon carcinoma. The reduced proportion of DS, a type of GAG containing iduronic acid, in the cancerous tissue may be explained by the presence of 4-sulfate units in low amounts in CS/DS chains, since the C-4 sulfation is a prerequisite for the C_5 epimerase that converts the glucuronic acid to iduronic acid [37].

Remarkable alterations in the biosynthesis of glycan moieties of (glyco)proteins and PGs have been also documented during maturation of several tissues as well as in the development of malignancies [38–40]. In colon adenocarcinoma, several genes involved in the biosynthesis of *O*-glycans are abnormally expressed, resulting to the synthesis of structural and antigenic altered *O*-glycans by cancer cells [40]. The sulfation pattern of GAGs is also suggested as key mediator of several biological events. It has been proposed [41] that the increase in the ratio of 6-sulfated chondroitin to 4-sulfated chondroitin represents a general phenomenon that is occurred in immature tissues, which containing proliferating and differentiated cells and it is suggested to influence some developmentally significant events such as cellular adhesion, migration and neurite outgrowth [42,43]. As shown by recent studies, the type and the sulfation patterns of versican and decorin present in the extracellular matrix is of great importance for the migration of the cells through the matrix. Perissinotto et al. [44] demonstrated that versican promotes the migration of neural crest cells, lining their migratory routes and this function is mediated by both the core protein and the GAG side chains. Versican purified from the migratory routes of neural crest cells is primarily substituted with 6-sulfated chondroitin. The substitution of versican with DS chains is suggested to be responsible for the 'repulsion-like' effects exerted on the migration of neural crest cell. Identical effects have been also documented for aggrecan, the homologous PG of versican, which inhibits the migration of neural crest cells. In this inhibitory effect of aggrecan, keratan sulfate (KS) side chains may play central role [45,46]. Furthermore, Merle et al. [47] showed that decorin inhibits the migration of MG-63 osteosarcoma cells and this phenomenon is depended of both core protein and GAG chain and is differentially mediated by its GAG side chains. Particularly, it was demonstrated that decorin bearing DS chain was 20-fold more effective in inhibiting migration of cells than decorin bearing CS chains.

The above described observations suggest that the specific structural alterations of versican and decorin described in this study may influence the biology of cancer cells in colon carcinoma. The remarkable substitution of both PGs in the stroma of colon carcinoma with CS chains and 6-sulfated disaccharides may contribute to the growth, proliferation and migration of cancer cells through a mechanism similar to that observed in neural crest and osteosarcoma cells migration. Further studies to demonstrate the functional relevance of the alterations observed in the biosynthesis of versican and decorin in colon carcinoma are under progress. It is becoming important to clarify the possible relation of the modified glycanation of the extracellular matrix PGs with the cancer cells proliferation and migration.

Acknowledgements

The author wishes to thank Dr. N.K. Karamanos, Dr. D.A. Theocharis and Dr. D.H. Vynios for support and constructive criticism of this work and Professor D. Heinegard for providing the polyclonal antibody against biglycan described in the text.

References

[1] R V. Iozzo, Ann Rev Biochem 67 (1998) 609–652

[2] R.V Iozzo, I Cohen, Experientia 49 (1993) 447–455.

[3] R G LeBaron, D R Zimmermann, E Ruoslahti, J Biol Chem 267 (1992) 10003–10010

[4] M Yamagata, S Suzuki, S.K Akiyama, K M Yamada, K Kimata, J Biol Chem 264 (1989) 8012–8018.

[5] M Yamagata, K M Yamada, M Yoneda, S Suzuki, K Kimata, J Biol Chem 261 (1986) 13526–13535

[6] H Kresse, H Hausser, E Schonherr, Experientia 49 (1993) 403–416

[7] E Ruoslahti, Y Yamaguchi, Cell 64 (1991) 867–869

[8] M Stander, U Naumann, W Wick, M. Weller, Cell Tissue Res 296 (1999) 221–227

[9] R V Iozzo, J Biol Chem 274 (1999) 18843–18846

[10] D.L. Coppock, C. Kopman, S Scandalis, S Gilleran, Cell Growth Differ 4 (1993) 483–493

[11] R Adany, R Heimer, B Caterson, J.M Sorell, R V Iozzo, J Biol Chem 265 (1990) 11389–11396.

[12] R.V Iozzo, Crit Rev Biochem Mol. Biol 32 (1997) 141–174

[13] A D Theocharis, D A Theocharis, Biomed. Chromatogr. 16 (2002) 157–161.

[14] A.D. Theocharis, M.E Tsara, N. Papageorgakopoulou, D D Karavias, D A Theocharis, Biochim. Biophys. Acta 1502 (2000) 201–206

[15] R.W Farndale, C.A. Sayers, A J. Barrett, Connect. Tissue Res 9 (1982) 247–248.

[16] T. Bitter, H Muir, Anal Biochem 4 (1962) 330–334.

[17] M.M Bradford, Anal Biochem 72 (1976) 248–254

[18] N.K. Karamanos, A. Syrokou, P Vanky, M. Nurminen, A Hjerpe, Anal Biochem 221 (1994) 189–199

[19] S.W. Sajera, V.C. Hascall, J. Biol Chem 244 (1969) 77–87

[20] T R. Oegema, V.C. Hascall, D.D Dziewiatkowski, J. Biol. Chem 250 (1975) 6151–6159.

[21] D C Gowda, V.P. Bhavanandan, E A. Davidson, J Biol Chem 261 (1986) 4926–4934.

[22] M. Yanagishita, V C Hascall, J. Biol. Chem 258 (1983) 12847–12856.

[23] D H. Vynios, C.P. Tsiganos, Biochim Biophys Acta 1033 (1990) 139–147

[24] U.K. Laemmli, Nature 277 (1970) 680–685

[25] Z. Isogai, T. Shinomura, N Yamakawa, J Takeuchi, T Tsuji, D Heinegard, K. Kimata, Cancer Res. 56 (1996) 3902–3908.

[26] A.D Theocharis, I Tsolakis, A Hjerpe, N K Karamanos, Atherosclerosis 154 (2001) 367–376.

[27] A D Theocharis, N.K Karamanos, N Papageorgakopoulou, C.P. Tsiganos, D.A Theocharis, Biochim. Biophys Acta 1569 (2002) 117–126

[28] A D. Theocharis, M Tsara, N Papageorgakopoulou, D.H. Vynios, D A Theocharis, Biochim Biophys Acta 1528 (2001) 81–85

[29] D M Carlson, J Biol. Chem 243 (1968) 616–626

[30] M.E. Tsara, N. Papageorgacopoulou, D D. Karavias, D.A Theocharis, Anticancer Res 15 (1995) 2107–2112.

[31] A D Theocharis, I Tsolakis, T. Tsegenidis, N K Karamanos, Atherosclerosis 145 (1999) 359–368.

[32] D A. Theocharis, N Papageorgakopoulou, D H. Vynios, S Th. Anagnostides, C.P. Tsiganos, J. Chromatogr, B 754 (2001) 297–309

[33] R.V. Iozzo, T.N Wight, J. Biol Chem 257 (1982) 11135–11144

[34] R V Iozzo, R P. Bolender, T N Wight, Lab Invest. 47 (1982) 124–138

[35] R Adany, R V Iozzo, Biochem Biophys. Res. Commun. 171 (1990) 1402–1413

[36] R V Iozzo, Lab. Invest 73 (1995) 157–160

[37] A. Malmstrom, L. Costel, L -A Fransson, A Hagner-McWhirter, G. Westergren-Thorsson, Dermatan Sulfate Proteoglycans Chemistry, Biology and Chemical Pathology, Portland Press, London, 1993, pp 129–137

[38] M T. Bayliss, D. Osborne, S Woodhouse, C Davidson, J Biol Chem 274 (1999) 15892–15900.

[39] K. Furukawa, K Takamiya, M Okada, M Inoue, S. Fukumoto, K Furukawa, Biochim Biophys Acta 1525 (2001) 1–12

[40] I. Brockhausen, Biochim Biophys Acta 1473 (1999) 67–95

[41] H. Kitagawa, K Tsutsumi, Y. Tone, K Sugahara, J. Biol Chem 272 (1997) 31377–31381

[42] M E Herndon, A D Lander, Neuron 4 (1990) 949–961

[43] A Faissner, A Clement, A. Lochter, A Streit, C. Mandl, M Schachner, J. Cell Biol 126 (1994) 783–799

[44] D Perissinotto, P. Iacopetti, I Bellina, R Doliana, A Colombatti, Z Pettway, M. Bronner-Fraser, T. Shinomura, K Kimata, M Morgelin, J Lofberg, R Perris, Development 127 (2000) 2823–2842

[45] R Perris, D Perissinotto, Z Pettway, M Bronner-Fraser, M. Morgelin, K Kimata, FASEB 10 (1996) 293–301.

[46] R. Perris, TINS 20 (1997) 23–31

[47] B Merle, L. Durussel, P D Delmas, P Clezardin, J. Cell Biochem 75 (1999) 538–546.

ELSEVIER

Biochimica et Biophysica Acta 1588 (2002) 173–178

BIOCHIMICA ET BIOPHYSICA ACTA
BBA
www.bba-direct com

Effect of imipramine on 1-methyl-4-phenylpyridinium ion-induced hydroxyl radical generation in rat striatum

Toshio Obata *, Toru Egashira

Department of Pharmacology and Therapeutics, Oita Medical University, 1-1, Idaigaoka, Hasama-machi, Oita 879-5593, Japan

Received 8 April 2002; received in revised form 20 June 2002, accepted 26 June 2002

Abstract

We examined the effect of imipramine (a tricyclic antidepressant drug) on hydroxyl radical (•OH) generation induced by 1-methyl-4-phenylpyridinium ion (MPP^+) in extracellular fluid of rat striatum, using a microdialysis technique. Imipramine enhanced the formation of •OH trapped as 2,3-dihydroxybenzoic acid (DHBA) induced by MPP^+ (5 mM). Introduction of imipramine (0.1, 0.5 and 1 0 mM) dose-dependently increased the level of dopamine (DA) release. Concomitantly, imipramine enhanced DA efflux and the level of DHBA induced by MPP^+, as compared with MPP^+-treated control. When corresponding experiments were performed with reserpinized rats, there were small increases in the levels of DA and nonsignificant increase in the formation of DHBA. When iron (II) was administered to imipramine (1 mM)-treated animals, a marked elevation of DHBA was observed, compared with MPP^+-only treated animals. A positive linear correlation was observed between iron (II) and DHBA ($R^2 = 0.985$) in the dialysate. These results indicate that imipramine enhances generation of •OH induced by MPP^+ during enhanced DA overflow.

© 2002 Elsevier Science B.V All rights reserved.

Keywords Imipramine. 1-Methyl-4-phenylpyridinium ion (MPP^+); Dopamine, Hydroxyl radical, Parkinson's disease

1. Introduction

Various antidepressant drugs have been developed and their antidepressive effects have been observed in animal model [1]. It has been demonstrated that tricyclic antidepressant drugs inhibit monoamine oxidase (MAO; EC 1.4.3.4) in vitro [2–4]. MAO exists in two forms, form A (MAO-A) and form B (MAO-B), based on its substrate specificity and sensitivity to inhibitors [5,6]. MAO-A preferentially deaminates 5-hydroxytryptamine (5-HT), whereas MAO-B deaminates β-phenylethylamine (β-PEA). 1-Methyl-4-phenyl-1,2,3,6-tetrahydropyridine (MPTP) produces a parkinsonian syndrome after its conversion to 1-methyl-4-phenylpyridinium ion (MPP^+) by MAO-B in the brain [7,8]. It has been shown that MAO-A is the major enzyme responsible for the deamination of dopamine (DA) in the rat striatum [9]. Although there are many papers showing that DA autoxidation and oxidative stress may be involved in Parkinson's disease [10–12], the etiology of Parkinson's disease still remains obscure.

Autoxidation and MAO-dependent oxidation of DA can lead to the formation of reactive cytotoxic free radicals whose generation could be influenced by the antidepressants because these antidepressants could inhibit catecholamine uptake and MAO activities. We as well as others reported that MPP^+ induces a massive release of DA in the striatum, which leads to increased free radicals [11,13,14]. In dopaminergic nerve cells, free radicals are mainly generated by MAO via deamination of DA and nonenzymatically by the autoxidation of DA [15]. The present study focuses on the effect of imipramine (tricyclic antidepressant drug) on hydroxyl radical (•OH) generation induced by MPP^+ in rat striatum.

2. Materials and methods

2.1. Animals

Adult female Wistar rats weighing 300–400 g were kept in an environmentally controlled room (20–23 °C, 50–60%

Abbreviations MPP^+, 1-methyl-4-phenylpyridinium ion, •OH, hydroxyl radical, DHBA, dihydroxybenzoic acid, DA, dopamine; MAO, monoamine oxidase, GSH, Glutathione

* Corresponding author Tel.. +81-97-586-5724; fax. +81-97-586-5729
E-mail address tobata@oita-med ac.jp (T. Obata)

0925-4439/02/$ - see front matter © 2002 Elsevier Science B.V. All rights reserved
PII: S0925-4439(02)00162-X

humidity, illuminated from 07:00 to 19:00) and fed food and water ad libitum. At the end of the experiments the rats were sacrificed using an overdose of anesthetic. All procedures in dealing with the experimental animals met the guideline principles stipulated by the Physiological Society of Japan and the Animal Ethics Committee of the Oita Medical University.

2.2. Chemicals

Imipramine hydrochloride was purchased from Ciba-Geigy (Takarazuka, Japan). MPP$^+$ was purchased from Research Biochemicals Inc., MA, USA. Sodium salicylate and its hydroxylated metabolites were purchased from Sigma Chemical Co. (St. Louis, MO, USA). All other chemicals were obtained from Wako Pure Chemical Industries (Osaka, Japan). The two radiochemical substrates used in this study, 5-hydroxytryptamine binoxalate ([2-^{14}C]-5-HT; 1.48–2.22 Gbq/mmol) and β-phenylethylamine hydrochloride ([ethyl-1-^{14}C]-β-PEA, 1.48–2.22 Gbq/mmol), were purchased from Dupont NEN (New England Nuclear) Products (Boston, MA, USA). In the case of reserpinized rats, reserpine (5 mg/kg; Daiichi Pharmaceutical, Japan) was injected intravenously into the rats 24 h before the experiments.

2.3. Experimental protocol

2.3.1. Assay of MAO activity

The rats were killed by decapitation and the brains were quickly removed and homogenated in 10 ml of 10 mM phosphate buffer, pH 7.4, containing 0.32 mM sucrose solution. To examine the effects of imipramine on MAO activity in vitro, the enzyme was preincubated for 20 min at 25 °C with imipramine (0.001 to 1.0 mM) before adding the substrates. Final concentrations of substrate (5-HT for MAO-A, and β-PEA for MAO-B) were 100 and 10 μM, respectively. The remaining MAO activity was measured by adding 20 μl of substrate solution and the mixture was incubated for 20 min at 37 °C. The reaction was stopped by adding 2 N HCl (200 μl). The reaction products were extracted with ethyl acetate–benzene mixture (1:1, v/v) saturated with water, and the radioactivity in the extract was measured using Beckmann LS-9000 scintillation counter. The protein concentrations of the enzyme preparations were measured according to the method of Lowry et al. [16] using bovine serum albumin as a standard. The data were corrected using protein concentration, and expressed as percent, compared to control (100%). One hundred percent of MAO-A and -B activities were 0.072 ± 0.03 and 1.02 ± 0.05 nmol/min/mg protein, respectively.

2.3.2. Microdialysis experiments

The rats were anaesthetized with chloral hydrate (400 mg/kg, i.p.), and the level of anaesthesia was maintained by intraperitoneal injection of chloral hydrate (20 mg/kg). Ringer's solution containing 147 mM NaCl, 2.3 mM CaCl2 and 4 mM KCl, pH 7.0, was used for perfusion (1 μl/min) through a microdialysis probe into the striatum. The recovery rate of 0.1 μM DA was 20.8 ± 0.9% at flow rate of 1 μl/min. The microdialysis probe was pre-washed with Ringer's solution for at least 30 min prior to stereotaxical implantation in the striatum (stereotaxic coordinates: AP: 1.0, R/L: 2.5, H: − 7 mm from dura matter) [17]. Thereafter, sodium salicylate in Ringer's solution (0.5 nmol/μl/min) was perfused by a microinjection pump (Carnegie Medicine CMA/100, Stockholm, Sweden) to trap •OH radicals [18,19] in the striatum, and basal levels of dihydroxybenzoic acid (DHBA) were determined during a definite period. Brain dialysate (1 μl/min) was collected every 15 min in small tubes containing 15 μl of 0.1 N HClO$_4$ to prevent amine oxidation and assayed immediately for DHBA by high-performance liquid chromatography with electrochemical (HPLC-EC) procedure [18–20]. The dialysate samples were promptly injected into an HPLC-EC system equipped with a glassy carbon working electrode (Eicom, Kyoto, Japan) and an analytic reverse-phase column on an Eicompak MA-5ODS column (5 μm, 4.6 ± 150 mm; Eicom). The working electrode was set at a detection potential of 0.75 V.

2.4. Statistical analysis

All values are presented as means ± S.E. The significance of difference was determined by using ANOVA with Fisher's post-hoc test. A P value of less than 0.05 was regarded as being statistically significant.

3. Results

3.1. Effect of imipramine on MAO activity in vitro

To determine the mechanism by which MAO activity was inhibited by imipramine, the effects of various concen-

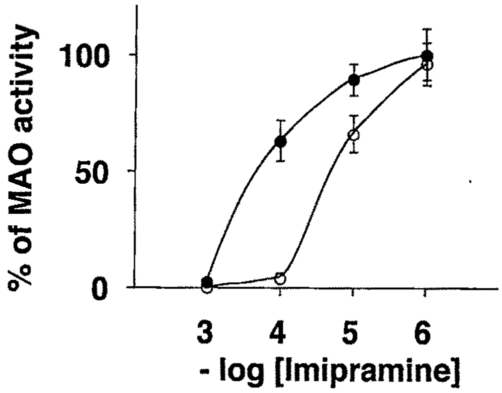

Fig 1 Inhibition of MAO activity in rat brain by imipramine After incubation at 25 °C for 20 min with imipramine (0.001, 0.01, 0.1 and 1 mM), MAO activities were determined using 100 μM 5-HT (closed circle) or 10 μM β-PEA (open circle) as substrate at 37 °C for 20 min. Values are expressed as percent control. The results are mean ± S.E. for five animals

trations of imipramine on MAO in rat brain homogenates were studied in vitro using 5-HT and β-PEA as substrates. Imipramine (0.001, 0.01, 0.1 and 1 mM) inhibited both MAO-A and -B activities in a dose-dependent manner. When the brain homogenates were preincubated at 25 °C for 20 min with imipramine, the residual activity of MAO-A and MAO-B activities with 100 μM imipramine were 63% and 4%, respectively (Fig. 1). However, 1 mM imipramine completely inhibited both MAO activities.

3.2. *Effect of imipramine on •OH generation induced by MPP$^+$*

After a 60-min washout with pH 7.4 Ringer's solution, the striatum was infused with MPP$^+$ (5 mM) for 15 min (total dose 75 nmol). When 1 mM imipramine was introduced into the dialysate, time-dependent changes in the level of DA and the formation of DHBA from •OH were monitored in the dialysates from rat brain after MPP$^+$ treatment. Although imipramine (1 mM) alone did not induced DA efflux, imipramine (1 mM) enhanced the level of DA induced by MPP$^+$ (Fig. 2A). Introduction of imipramine drastically enhanced MPP$^+$-induced DA release with concomitant increase in •OH formation trapped as DHBA in the brain dialysate, compared with MPP$^+$-only treated animals. At 90 and 105 min, imipramine significantly increased DHBA formation as shown in Fig. 2B ($P<0.05$). When corresponding experiments were performed with reserpinized rats, small increases in the level of DA (Fig. 3A) and nonsignificant increase in the formation of DHBA were

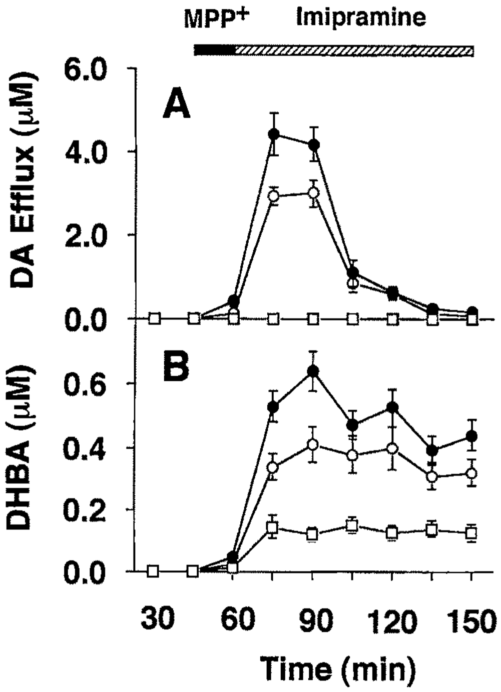

Fig 2 Effect of MPP$^+$ on the release of DA and the formation of •OH after imipramine treatment in the striatum of rats. After a 60-min washout with Ringer's solution (pH 7 4), striatum was infused with MPP$^+$ (5 mM) for 15 min (solid bat, total dose, 75 nmol) to evoke the release of DA (A) Then, at 60 min after probe implantation, sodium salicylate (hatched bar, 0 5 nmol/μl/min) was infused through the microdialysis probe for 90 min to trap •OH (B) Brain dialysates were collected every 15 min in 0 1 N HClO$_4$ and immediately assayed by an HPLC-EC. MPP$^+$ (open circle), MPP$^+$ and 1 mM imipramine (closed circle), and no MPP$^+$ (rectangle) were compared Values are means ± S E for five animals Both the total DA efflux and DHBA formation elicited by imipramine were significantly elevated over that of MPP$^+$ alone group ($P<0$ 05 for MPP$^+$ alone vs MPP$^+$ and 1 mM imipramine. ANOVA and Fisher's test)

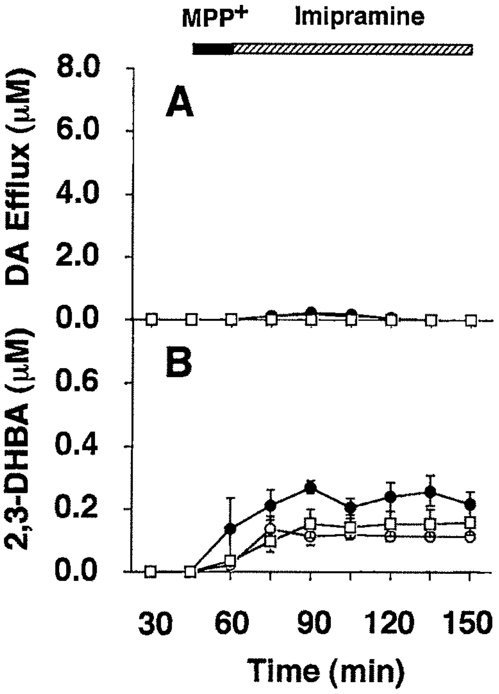

Fig 3 Effect of MPP$^+$ on the release of DA and the formation of •OH after imipramine treatment by reserpinized rats Experimental conditions and symbols are the same as for Fig 2

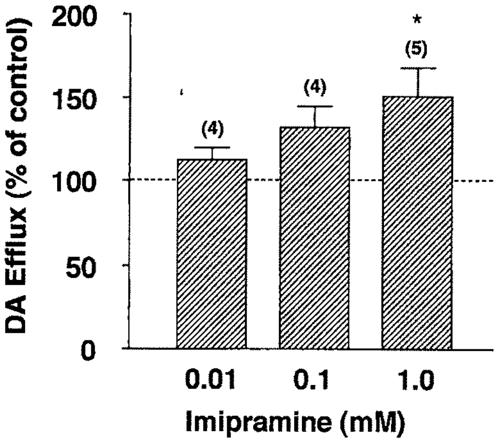

Fig 4 Dose-dependent effects of imipramine on the level of DA in the MPP$^+$-treated rat striatum The level of DA measured at 30–45 min after application of various concentrations of imipramine (as indicated abscissa) (hatched column) are given as a percentage of the value measured just before application of imipramine Each column and vertical bar indicates mean ± S.E The number in the parentheses indicates the number of animal * $P<0$ 05 versus the level of DA immediately before application of imipramine (ANOVA and Fisher's test)

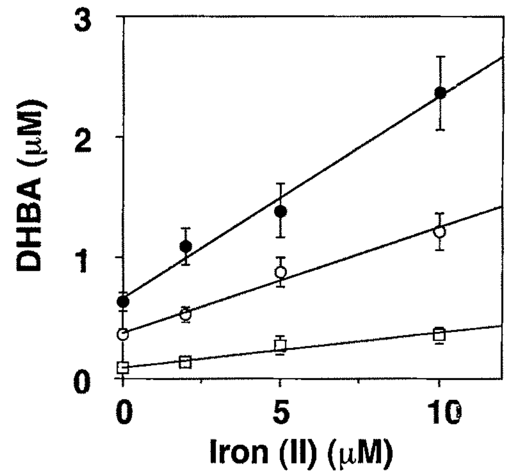

Fig 5 Cumulative dose–response relationship between iron (II) and the formation of •OH products of salicylic acid with and without MPP$^+$ treatment Iron (II) and sodium salicylate (0 5 nmol/μl/min) were infused through the dialysis probe. Three different concentrations of iron (II) (2, 5 and 10 μM) were infused through the probe placed in the imipramine (1 mM)-treated rats, and the levels of DHBA were measured. The ordinate shows the cumulative level of DHBA output over 90 min. MPP$^+$ (open circle), MPP$^+$ and 1 mM imipramine (closed circle), MPP$^+$ and no MPP$^+$ (rectangle) were compared Values are means ± S E for four animals

observed (Fig. 3B). As shown in Fig. 4, imipramine (0.01, 0.1 and 1.0 mM) dose-dependently increased the level of DA release. At 1 mM of imipramine, the increase in DA was statistically significant ($P < 0.05$, $n = 5$). To confirm whether the •OH generation was based on a Fenton-type reaction, iron (II) was infused through the dialysis probe. When iron (II) (2, 5 and 10 μM) was administered to MPP$^+$-pretreated animals, iron (II) clearly produced a dose-dependent increase in the levels of DHBA, showing a positive linear correlation between iron (II) and •OH formation trapped as DHBA ($R^2 = 0.985$) in the dialysate, as compared with the iron (II)-only treated group (Fig. 5). The data suggest that the effect of imipramine on •OH formation was based on the Fenton-type reaction.

4. Discussion

We have demonstrated that imipramine (a tricyclic antidepressant drug) enhances generation of •OH induced by MPP$^+$ in the extracellular space of the striatum. It is known that tricyclic antidepressant drugs inhibited MAO activities and that, in vitro, these drugs are more potent inhibitors of MAO-B than MAO-A [3,4]. MAO is a brain enzyme that plays a role in the metabolism of various catecholamine. Both MAO-A and MAO-B activities in rat brain were inhibited by imipramine (Fig. 1). Kato et al. [21] reported that MAO inhibitor caused the accumulation of DA in the extracellular fluid. We previously reported [3] that the level of the oxidized DA metabolite DOPAC decreased following the administration of imipramine. This result indicates that imipramine increased the level of DA. MAO is one of the enzymes metabolizing various neurotransmitter monoamines [14]. If MPP$^+$ or its related compound(s) is responsible for inducing Parkinson disease, inhibition of MAO-B may lead to induce protective effect against •OH formation [22]. It was reported that the MAO-B inhibitors can diminish neuronal cell death [23]. In rat brain, MPP$^+$ is a more potent MAO-A inhibitor than MAO-B [24], and MAO-A is predominantly responsible for striatal DA oxidation [21]. On the contrary, in human brain, MAO-B is responsible for DA oxidation [25,26]. The DA that accumulates in the extracellular fluid following administration of antidepressants can undergo autoxidation, which in turn leads (possibly by an indirect mechanism) to the formation of cytotoxic •OH free radicals. As shown in the present study, the antidepressant inhibited MAO activities in vitro. Antidepressant drugs have heretofore been considered effective in the treatment of depression because they inhibit the active uptake of amines in the presynaptic cells of the brain [27,28]. Imipramine is also potent inhibitors of DA reuptake. Regardless of their specific mechanisms of action, the consequence is increased extracellular levels of DA. This may explain the observed increase in •OH. Both nonenzymatic and enzymatic mechanisms may contribute to free radical formation induced by antidepressant drugs in the striatum in vivo.

The concentration profile of the administered compounds in the surrounding interstitial space is unknown: in general, the extracellular concentration of a compound given through the probe would never reach the concentration in the dialysis probe. This is an unavoidable limitation of the microdialysis technique that should be kept in mind when interpreting the experimental data. Introduction of imipramine (1 mM) drastically increased the DA efflux and the level of DHBA induced by MPP$^+$ (Fig. 2). Although there are many reports about the effect of MPP$^+$ on •OH generation, the mechanism of •OH generation by MPP$^+$ is obscure. Free radical formation enhanced by MPP$^+$ in the striatum appeared to be dose-dependent and positively correlated with amounts of sustained DA overflow [13]. DA is known to be autoxidated in the presence of oxygen and transition metal [12,29]. When imipramine concentration in the perfusate was increased, DA efflux was enhanced with concomitant increase in •OH formation. Our obtained data demonstrated that sustained DA overflow elicited by imipramine in the striatum also led to enhanced MPP$^+$-induced •OH formation. These data are consistent with the notion that DA autoxidation and sustained DA turnover can lead to free radical formation, which in turn causes oxidative damage in the iron-enriched nigral neuron during senescence and Parkinson's diseases [12,13]. This evoked DA overflow was enhanced by imipramine. The levels of DA and DHBA in reserpinized rats were drastically reduced, as compared with that of imipramine and MPP$^+$-treated groups (Fig. 3). The results also suggest that the mechanism of imipramine and MPP$^+$-induced •OH formation was via DA efflux. The present study demonstrated that imipramine increased •OH formation in the extracellular space of the striatum with concomitant DA release. Therefore, imipramine increased the •OH formation trapped as DHBA. Moreover, to confirm whether the imipramine-evoked •OH generation in the MPP$^+$-treated rats was based on the Fenton-type reaction, the DHBA formation was measured in the presence of iron in imipramine- and MPP$^+$-treated rats. Iron (II) clearly produced a dose-dependent increase in the levels of DHBA (Fig. 5). This finding indicates that extracellular DA is needed for the observed effect of Fenton-type reaction.

MPP$^+$ causes a sustained DA release into extraneuronal space, generating oxygen free radicals with extracellular DA autoxidation [11]. This could lead to the formation of •OH radicals, which may induce lipid peroxidation, protein cross-linking and DNA damage, mediated by base pair mutation [30]. If toxic species are being produced on Parkinson's disease, they would normally be inactivated by a variety of protective mechanisms, but the mechanisms, however, may be impaired in the substantia nigra of patients with Parkinson's disease; reduced levels of, e.g., catalase and glutathione (GSH) [31]. The enzyme MAO is one of the enzymes metabolizing various neurotransmitter monoamines [14]. Among MAO-B inhibitors, L-deprenyl is widely used for the treatment of patients with Parkinson's disease. Inhibition of MAO-B may be involved in its protective effect [22], if MPP$^+$ or related compound(s) is responsible for inducing Parkinson's disease. It is clear that MAO-B is responsible for the production of MPP$^+$. Therefore, the MAO-B inhibitors can diminish neuronal cell death [23].

DA is known to be autoxidized in the presence of oxygen and iron (II), and to be converted to semiquinone, quinone, zwitteric 5,6-dihydroxyindoles and melanin [11]. The DA efflux was enhanced imipramine and MPP$^+$ administration. DA is known to undergo autoxidation in the presence of oxygen and iron (II) [13,29]. Normally, iron (III) is bound to endogenous chelators such as ADP and, in the absence of a significant amount of ferritin in the substantia nigra, could be chelated by melanin. Increased concentrations of DA could serve as the catalyst for the conversion of iron (III) to iron (II) by melanin and, in the presence of H_2O_2, results in further formation of •OH, depending on the environmental conditions [32]. The production of •OH in the presence of melanin is significantly greater when iron (III) is predominant [32], and is further demonstrated by the greater lipid peroxidation of rat cerebral cortex in the presence of iron (II) and higher DA melanin concentrations [33]. An enhanced generation of cytotoxic •OH radicals through DA accumulation could accelerate the MPP$^+$-induced degeneration of nigral neurons. Accordingly, imipramine enhances generation of •OH induced by MPP$^+$ during enhanced DA overflow.

In conclusion, a tricyclic antidepressant drug may play a key role in •OH formation by the release of DA from nigrostriatal nerves in the brain by the action of MPP$^+$. The results in the experiment may be useful for elucidating the actual mechanism of free radical formation in the pathogenesis of neurodegenerative brain disorders including Parkinson's disease, Alzheimer's disease and traumatic brain injuries.

Acknowledgements

We are thankful to Prof. Lars Oreland (Department of Neuroscience, Section of Pharmacology, Box 593 Biomedical Centre, Uppsala University, 751-24, Uppsala, Sweden) for valuable discussions.

References

[1] C Prakash, D Cui, Metabolism and excretion of a new antianxiety drug candidate, CP-93, 393, in cynomolgus monkeys identification of the novel pyrimidine ring cleaved metabolites, Drug Metab. Dispos 25 (1997) 1395–1406.

[2] D.J Edwards, M O Burns, Effects of tricyclic antidepressants upon human platelet monoamine oxidase, Life Sci. 15 (1974) 2045–2058

[3] T. Obata, T Inada, Y. Yamanaka, Intracranial microdialysis of salicylic acid to detect hydroxyl radical generation by antidepressant drugs in the rat, Neurosci. Res. Commun. 21 (1997) 223–229

[4] J.A. Roth, C N Gillis, Deamination of beta-phenylethylamine by monoamine oxidase-inhibition by imipramine, Biochem. Pharmacol 23 (1974) 2537–2545

[5] N.H Neff, H.-Y.T. Yang, Another look at the monoamine oxidases and the monoamine oxidase inhibitor drugs, Life Sci 14 (1974) 2061–2074.

[6] M.B H. Youdim, J.P. Finberg, New directions in monoamine oxidase A and B selective inhibitors and substrates, Biochem Pharmacol. 41 (1991) 155–1562.

[7] K. Chiba, A Trevor, N Castagnoli Jr, Metabolism of the neurotoxic tertiary amine, MPTP, by brain monoamine oxidase, Biochem Biophys Res. Commun. 120 (1984) 574–578

[8] S.P Markey, J.N. Johannessen, C.C Chiueh, R S. Burns, M.A. Herkenham, Intraneuronal generation of a pyridinium metabolite may cause drug-induced parkinsonism, Nature 311 (1984) 464–467.

[9] C J Fowler, M.S. Beneditti, The metabolism of dopamine by both forms of monoamine oxidase in the brain and its inhibition by cimoxatone, J Neurochem. 40 (1983) 1534–1541.

[10] C.C. Chiueh, R.-M Wu, K.P. Mohanakumar, L.M. Sternberger, G Krishna, T. Obata, D.L. Murphy, In vivo generation of hydroxyl radicals and MPTP-induced dopaminergic toxicity in the basal ganglia, Ann. N Y Acad. Sci. 738 (1994) 25–36.

[11] M. Gerlach, D. Ben-Shachar, P. Riederer, M B.H. Youdim, Altered brain metabolism of iron as a cause of neurodegenerative diseases? J. Neurochem. 63 (1994) 793–807.

[12] P. Riederer, E. Sofic, W-D. Rausch, B. Schmidt, G P. Reynolds, K Jellinger, M B.H. Youdim, Transition metals, ferritin, glutathione, and ascorbic acid in parkinsonian brains, J Neurochem 52 (1989) 515–520

[13] C.C Chiueh, G Krishna, P Tulsi, T Obata, K Lang, S-J Huang, D.L. Murphy, Intracranial microdialysis of salicylic acid to detect hydroxyl radical generation through dopamine autooxidation in the caudate nucleus. effects of MPP$^+$, Free Radic Biol. Med. 13 (1992) 581–583

[14] H. Kinemuchi, C J. Fowler, K F Tipton, The neurotoxicity of 1-methyl-4-phenyl-1,2,3,6-tetrahydropyridine (MPTP) and its relevance to Parkinson disease, Neurochem. Int 11 (1987) 359–373

[15] B Fornstedt, E Pileblad, A Carlsson, In vivo autoxidation of dopamine in guinea pig striatum increases with age, J. Neurochem 55 (1990) 655–659.

[16] O H. Lowry, N J Rosebrough, A L. Farr, R J Randall, Protein measurement with the folin phenol reagent, J Biol Chem 193 (1951) 265–275

[17] G. Paxinos, C Watson, The Rat Brain Stereotaxic Coordinates, 2nd ed , Academic Press, Sydney, 1982.

[18] R.A. Floyd, J.J. Watson, P.K. Wong, Sensitive assay of hydroxyl free radical formation utilizing high pressure liquid chromatography with electrochemical detection of phenol and salicylate hydroxylation products, J Biochem. Biophys Methods 10 (1984) 221–235

[19] B Halliwell, H. Kaur, M Ingleman-Sundberg, Hydroxylation of salicylate as an assay for hydroxyl radicals: a cautionary note, Free Radic. Biol. Med 10 (1991) 439–441

[20] N. Ozaki, D. Nakahara, N Kaneda, K. Kiuchi, T Okada, Y Kasahara, T Nagatsu, Acute effects of 1-methyl-4-phenylpyridinium ion (MPP$^+$) on dopamine and serotonin metabolism in rat striatum as assayed in vivo by a micro-dialysis technique, J. Neural Transm 70 (1987) 241–250

[21] T. Kato, B Dong, K Ishii, H Kinemuchi, Brain dialysis: in vivo metabolism of dopamine and serotonin by monoamine oxidase A but not B in the striatum of unrestrained rats, J Neurochem. 46 (1986) 1277–1282

[22] D A Di Monte, J.E Royland, A Anderson, K. Castagnoli , N Castagnoli Jr , J W Langston, Inhibition of monoamine oxidase contributes to the protective effect of 7-nitroindazole against MPTP neurotoxicity, J. Neurochem 69 (1997) 1771–1773

[23] C Mytilineou, E.K. Leonardi, P Radcliffe, E H. Heinonen, S K Han, P Werner, G Cohen, C W. Olanow, Deprenyl and desmethylselegiline protect mesencephalic neurons from toxicity induced by glutathione depletion, J Pharmacol. Exp Ther 284 (1998) 700–706.

[24] H. Kinemuchi, Y Arai, Y Toyoshima, Participation of brain monoamine oxidase B form in the neurotoxicity of 1-methyl-4-phenyl-1,2,3,6-tetrahydropyridine relationship between the enzyme inhibition and the neurotoxicity, Neurosci Lett. 58 (1985) 195–200.

[25] C J Fowler, L Oreland, J. Marcusson, B Winblad, Titration of human brain monoamine oxidase-A and -B by clorgyline and L-deprenyl, Naunyn-Schmiedeberg's Arch Pharmacol 311 (1980) 263–272

[26] C J Fowler, S B Ross, Selective inhibitors of monoamine oxidase A and B. biochemical, pharmacological, and clinical properties, Med. Res Rev. 4 (1984) 323–358

[27] A. Coppen, Indoleamines and affective disorders, J Psychiatr Res. 9 (1972) 163–171

[28] A J. Prange Jr , I.C Wilson, C.W. Lynn, L.B Alltop, R.A Stikeleather, L-Tryptophan in mania Contribution to a permissive hypothesis of affective disorders, Arch Gen Psychiatry 30 (1974) 56–62

[29] T. Obata, Reserpine prevent hydroxyl radical formation by MPP$^+$ in rat striatum, Brain Res 828 (1999) 68–73

[30] P C Dedon, J.P Plastaras, C A Rouzer, L.J Marnett, Indirect mutagenesis by oxidative DNA damage: formation of the pyrimidopurinone adduct of deoxyguanosine by base propenal, Proc Natl Acad Sci U. S. A. 95 (1998) 11113–11116.

[31] T.L Perry, V.W Yong, Idiopathic Parkinson's disease, progressive supranuclear palsy and glutathione metabolism in the substantia nigra of patients, Neurosci Lett 67 (1986) 269–274

[32] B Pilas, T Sarna, B Kalyanaraman, H M Swartz, The effect of melanin on iron associated decomposition of hydrogen peroxide, Free Radic Biol Med 4 (1988) 285–293.

[33] D Ben-Shachar, P Riederer, M B H. Youdim, Iron–melanin interaction and lipid peroxidation: implications for Parkinson's disease, J Neurochem 57 (1991) 1609–1614.

ELSEVIER

Biochimica et Biophysica Acta 1588 (2002) 179–188

BIOCHIMICA ET BIOPHYSICA ACTA
BBA
www.bba-direct.com

Differential expression of protein kinase C isoenzymes related to high nitric oxide synthase activity in a T lymphoma cell line

Gabriela Gorelik, María Laura Barreiro Arcos, Alicia J. Klecha, Graciela A. Cremaschi *

Centro de Estudios Farmacológicos y Botánicos (CEFYBO)-CONICET, Serrano 669 (1414) Buenos Aires, Argentina

Received 5 October 2001; received in revised form 27 June 2002; accepted 18 July 2002

Abstract

Protein kinase C (PKC) is critical for T lymphocyte activation and proliferation, while nitric oxide synthase (NOS) may function both as an activator or inhibitor of T cell apoptosis. Both enzymatic activities were studied in T lymphoma cells in comparison to normal and activated T lymphocytes. Here we show a higher translocation of PKC in BW5147 lymphoma cells than in mitogen-stimulated T lymphocytes. Tumor cells overexpressed PKC ζ isoform, while high levels of the PKC β isotype were found in mitogen-stimulated T lymphocytes. Moreover, tumoral T cells showed high NOS activity, almost undetectable in normal or stimulated T lymphocytes. PKC and NOS inhibitors or the intracellular delivery of an anti-PKC ζ antibody diminished both NO production and proliferation in tumor cells.

These results suggest that atypical PKC ζ isoform expression and its association with NOS activity regulation would participate in the multistep process leading to BW5147 cell malignant transformation.

© 2002 Elsevier Science B.V. All rights reserved.

Keywords: NOS activity; PKC activity; PKC isoenzyme; T lymphocyte; T lymphoma cell line; Proliferation

1. Introduction

The knowledge of the signaling events that control cellular growth and differentiation is of paramount importance to understand the mechanisms involved in malignant transformation. Particularly, in lymphoid cells, it has been suggested that deregulation of intracellular pathways participates in leukemic disorders [1]. Phosphorylation and dephosphorylation of protein substrates by kinases and phosphatases, respectively, play prominent roles in the transduction of signals from cell membrane receptors to the nucleus. Physiological activation of T lymphocytes leading to differentiation and proliferation involves a complex series of intracellular signaling events that is initiated by protein tyrosine kinases (TPK) activation. The biochemical cascade downstream includes increased hydrolysis of inositol phospholipids, mediated by phospholipase C (PLC) γ1 phosphorylation, which gives rise to inositol triphosphate and diacylglicerol (DAG). These second messengers, in turn, increase intracellular Ca^{2+} concentrations and activate protein kinase C (PKC), respectively [2,3].

PKC represents a family of serine/threonine kinases that plays a central role in signal transduction as it is involved in the control of numerous cellular processes, such as proliferation and differentiation, as well as in carcinogenesis [4–6]. Although all PKCs require the lipid phosphatidylserine as a cofactor, differences in their structure and substrate requirements allowed isoform classification into three subclasses: the conventional or classical PKCs (cPKC) (α, βI, βII and γ), which are Ca^{2+}-dependent and activated by DAG and phorbol esters; the novel PKCs (nPKC) (δ, ε, η and θ), which can be activated by DAG and phorbol esters but are Ca^{2+}-independent; and the atypical isoforms (aPKC) (ζ and τ/λ), which are unresponsive to both Ca^{2+} and DAG or phorbol esters [5]. The existence of such a large family of PKC isoenzymes, which exhibits different tissue distribution, subcellular localization and biochemical properties, suggests that individual PKC isoforms may play specialized roles in cellular functions. In many cases, PKC isoforms exhibit distinct and even opposing cellular effects [7,8]. A differential expression of PKC isozymes has been described for distinct hemopoietic lineages [9] and their participation in determined cellular functions has also been assigned. In fact, modulation of α and β isoform levels was related to B lymphocyte differentiation [9] while particular activation of atypical PKC ζ was demonstrated to participate

---

* Corresponding author. Tel.: +54-11-4857-1434; fax +54-11-4856-2751.

E-mail address: grace@cefybo.edu.ar (G.A. Cremaschi).

0925-4439/02/$ - see front matter © 2002 Elsevier Science B.V. All rights reserved.
PII: S0925-4439(02)00163-1

in interleukin-2-mediated proliferation of T cells [10]. Also, PKC θ, an isoenzyme that was found predominantly in hematopoietic cells and skeletal muscle, was demonstrated to be expressed in T, but not in B lymphocytes, and played an important role in T lymphocyte activation as an essential component of the T-cell synapse [11,12].

On the other hand, nitric oxide (NO) is a physiologically important signal molecule in many cells and tissues, regulating a variety of biological functions, including immune processes [13]. The role of NO in the control of cell growth is controversial since both stimulation and inhibition have been demonstrated [14]. Also, NO exerts contrasting effects on apoptosis, depending on its concentration, flux and cell type, having, in some situations, an apoptotic effect while protecting cells against spontaneous or induced apoptosis in other [15]. The redox state of the cell seemed to be crucial for the ultimate action of NO on cell multiplication and survival. A protective antiapopatotic effect is commonly related to the endogenous NO production through NO synthases (NOS) and is frequently observed in lymphoid cells from B origin [16,17]. Cells from a wide variety of malignancies have a decreased ability to undergo apoptosis in response to some physiological stimuli and inhibition of apoptosis can result in the expression of cells with increased susceptibility to subsequent malignant transformation [1,18]. Furthermore, production of NO, as well as expression of different NOS isoenzymes, both at the protein and mRNA level, were demonstrated to be related to PKC activity in several cell types including tumor cells [19,20]. Production of NO downstream PKC was demonstrated to be induced by immunopotentiators in splenic lymphocytes [21].

The present study was undertaken to analyze PKC activity and isoenzyme expression and their relationship with NO production in a T lymphoma cell line. Also their contribution to cellular proliferation was analyzed. All these studies were performed in comparison to normal unstimulated and mitogen stimulated T cells. Here we report that tumor T cells show significantly higher levels of PKC ζ and increased NOS activity than resting or mitogen-stimulated normal T lymphocytes. Intracellular delivery of PKC ζ isoform-specific antibodies results in a decrease of both proliferation and NOS activity in tumor T cells. The implications of these results in neoplastic transformation are discussed.

2. Materials and methods

2.1. Cell suspensions and culture conditions

The tumor cell line BW5147 (a generous gift from Dr. A. Schimpl, Institute für Virologie und Immunobiologie der Universität Würzburg, Germany) is a T cell lymphoma that expresses H-2^k haplotype, CD3$^+$ and αβ T cell receptor, as tested routinely by flow cytometry with specific antibodies against the corresponding surface markers. These cells were cultured at an optimal concentration of 1–5 × 10^5 cells/ml, in RPMI 1640 medium (GIBCO BRL) supplemented with 10% fetal calf serum (FCS), 2 mM glutamine and antibiotics, with twice-weekly splitting once they have reached exponential growth. Where indicated, synchronized (kept for 24 h in FCS-deprived medium) BW5147 cells were used.

Aseptically prepared lymphoid cell suspensions from C3H (H-2^k) inbred mice lymph nodes were obtained from nylon wool purification of T cells as described before [22,23]. T cell purification was higher than 97% as checked by lysis with anti-Thy plus complement and by indirect immunofluorescence. Cells, at a concentration of 1 × 10^6 cells/ml, were cultured in the same medium as tumor cells, alone or in the presence of 2 μg/ml of concanavalin A (Con A), as previously described [22].

Cells were settled at a final volume of 0.2 ml in 96-well flat-bottom microtiter plates (Nunc™) for microcultures or were kept in T-25 or T-75 culture flasks (Corning, NY) for macrocultures. Cells were cultured for different times and inhibitors were added at the beginning of the culture where indicated.

2.2 Proliferation assays

Proliferation was evaluated on microcultures and controlled in 0.2-ml aliquots of macrocultures established for enzymatic assays.

The proliferation kinetics of BW5147 cells was determined on BW5147 synchronized cells after re-culturing them in FCS-rich medium. Cells were pulsed with [^{3}H]thymidine ([^{3}H]TdR, NEN, 20 Ci/mmol) for the last 6 h of incubation, as described before [22]. Results are expressed as dpm values in experimental cultures subtracting the dpm control values obtained on BW5147 synchronized cells. The percentage of inhibition (% inh) for experimental cultures performed in the presence of inhibitors was calculated as:

$$\%\ \text{inh} = \left[1 - \frac{\text{dpm BW5147 cells} + \text{inhibitor} - \text{dpm control}}{\text{dpm BW5147 cells} - \text{dpm control}}\right] \times 100$$

For Con A-stimulated T lymphocytes, cultures were pulsed with [^{3}H]TdR as indicated for BW5147 and cultures of unstimulated cells were used as controls. The action of inhibitors upon Con A-stimulated T cells was evaluated as indicated for BW5147 cells.

It is worth noting that inhibitors alone do not significantly modify either the basal control values of BW5147 (synchronized BW5147 cells) or the unstimulated cultures of normal T lymphocytes.

2.3. PKC assay

Synchronized BW51457 cells (0.5 × 10^7 cells/sample) were re-cultured for different times in FCS-rich medium alone or in the presence of the indicated drugs and were immediately frozen in liquid N_2. Normal or Con A-stimulated T cells (1×10^7 cells/sample) were incubated alone or with inhibitors for the indicated times and processed as tumor cells. PKC was purified from total cell extracts or from subcellular fractions as previously described [24]. PKC activity was assayed by measuring the incorporation of ^{32}P from [γ-^{32}P]-ATP into histone H_1 [24]. Incubations were conducted in a final volume of 85 µl at 30 °C for 30 min. In the final concentrations, the assay mixture contained 25 µM ATP (0.4 µCi), 10 mM Mg acetate, 5 mM β-mercaptoethanol, 50 µg of histone H_1, 20 mM HEPES, pH = 7.5, 10 µg/ml of phosphatidylserine vesicles and in the presence or absence of 0.2 mM $CaCl_2$. The incorporation of [^{32}P]-phosphate into histone was linear for at least 30 min. The reaction was stopped by the addition of 2 ml of ice-cold 5% trichloroacetic acid with 10 mM H_3PO_4. The radioactivity retained on GF/C glass fiber filters after filtration was determined by counting the filters in 2 ml of scintillation fluid. PKC activity was determined after subtracting the ^{32}P-incorporation in the absence of Ca^{2+} and phospholipids. Data were expressed as picomoles of phosphate incorporated into the substrate per minute and per 10^7 cells (pmol/min/10^7 cells). The selective PKC substrate peptide, MBP(4–14) [25] (GIBCO BRL), was also used to measure PKC activity purified from subcellular lymphoid fractions, following the instructions of the PKC assay system from GIBCO BRL. PKC specificity was confirmed by the PKC pseudosubstrate inhibitor peptide PKC (19–36) provided by GIBCO BRL.

2.4. NOS activity determination

NOS activity was measured by production of [U-^{14}C]-citrulline from [U-^{14}C]-arginine [26]. Briefly, cells were incubated in 500-µl RPMI-1640, in the presence of [U-^{14}C]-arginine (0.5 µCi). After incubation, cells were disrupted by sonication (Vibra-cell, Sonics and Materials) in a medium containing 10 mmol/l EGTA, 0.1 mmol/l citrulline, 0.1 mmol/l dithiothreitol and 20 mmol/l HEPES, pH 7.5. After centrifugation at 20,000 × g for 10 min, supernatants were applied to 2-ml columns of Dowex AG 50WX-8 (sodium form, Bio-Rad) and [U-^{14}C]-citrulline was eluted with 3 ml of water and quantified by liquid scintillation counter.

2.5. Immunoblot analysis of PKC isoenzymes

Samples of whole cell lysates from tumor and normal T lymphocytes were prepared by dissolving cellular pellets in SDS-sample buffer (2% SDS, 10% (v/v) glycerol, 62.5 mM Tris–HCl, pH = 6.8, 0.2% bromophenol blue, 1% (v/v) 2-mercaptoethanol) at a final concentration of 10 mg/ml. Equal amounts of proteins were separated by SDS-PAGE on 10% polyacrylamide gels and transferred to nitrocellulose membranes. Where indicated, cytosol and particulate fractions of unstimulated or stimulated cells, obtained as described by Meller et al. [27], representing 2×10^6 cell equivalents per 10 µl and supplemented with 2.5-µl 5 × SDS sample buffer, were analyzed by SDS-PAGE and immunoblotted, as above.

Nonspecific binding sites in nitrocellulose membranes were blocked with blocking buffer (5% nonfat dried milk, containing 0.1% Tween-20 in 100 mM Tris–HCl, pH = 7.5 and 0.9% NaCl) for 1 h. The nitrocellulose was subsequently incubated with protein G-purified anti-peptide antibodies to specific PKC isoforms for 18 h. Anti-PKC isoenzyme specific antibodies from GIBCO BRL are polyclonal antibodies raised against specific peptides from each isoenzyme. The α-, β- and γ-specific antibodies were raised against the peptides corresponding to amino acids 313–326, 313–329 and 306–318, respectively, derived from murine cDNA sequences. The δ-, ε- and ζ-specific antibodies were raised against C-terminal peptides corresponding to amino acids 662–673, 726–737 and 577–592, respectively. The anti-PKC θ antibody (C-18, from Santa Cruz Biotechnologies) specific for an epitope mapping at the carboxy terminus of nPKC θ of mouse origin was also used. Negative controls were incubated in the presence of immunogenic peptides at a concentration 2 µg/ml antibody to 1 µg/ml peptide. The membrane was then incubated with a monoclonal anti-rabbit IgG alkaline phosphatase conjugate (Sigma Chemical Co.) for 1 h. Immunoreactive bands were visualized using nitroblue tetrazolium (NBT) and 5-bromo-4-chloro-3-indolyl-phosphate (BCIP). As molecular weight markers, a Full Range Rainbow (Amersham Pharmacia) was used. Anti-actin antibody (rabbit polyclonal, against actin of human origin, but cross-reactive to mouse actin, from Santa Cruz Biotechnol.) was used as a control for protein loaded. Densitometric analysis was performed by UN-SCAN-IT (version 5.1, Silk Scientific Corporation) software. Densitometric values of actin (arbitrary units) for each gel were normalized relative to each other and PKC densitometry values (arbitrary units) in each lane were divided by the corresponding normalized actin value.

2.6. Intracellular delivery of anti-PKC ζ antibody in normal and tumor T cells

Anti-PKC ζ antibody against the C-terminal region of PKC (GIBCO BRL) was introduced into normal or BW5147 tumor T cells after permeabilization with lysolecithin as described [28]. Briefly, BW5147 cells were equilibrated in 7% FCS-containing medium for 24 h. Normal cells or tumor cells, cultured as indicated, were washed with serum-free medium and 0.1-ml glycerol in PBS at 37 °C was added. After 6 min on ice, 4 µl of a 1 mg/ml lysolecithin (Sigma) solution in water was added, and the incubation continued for an additional 5 min. Cells were then brought to 37 °C and 0.1 ml of a dilution of antibody (alone or preincubated with 3 × concentration of the corresponding peptide) was added. After 10 additional minutes at 37 °C, during which the cells reseal, 0.1 ml of medium containing 21% FCS was added. Cells were brought back to

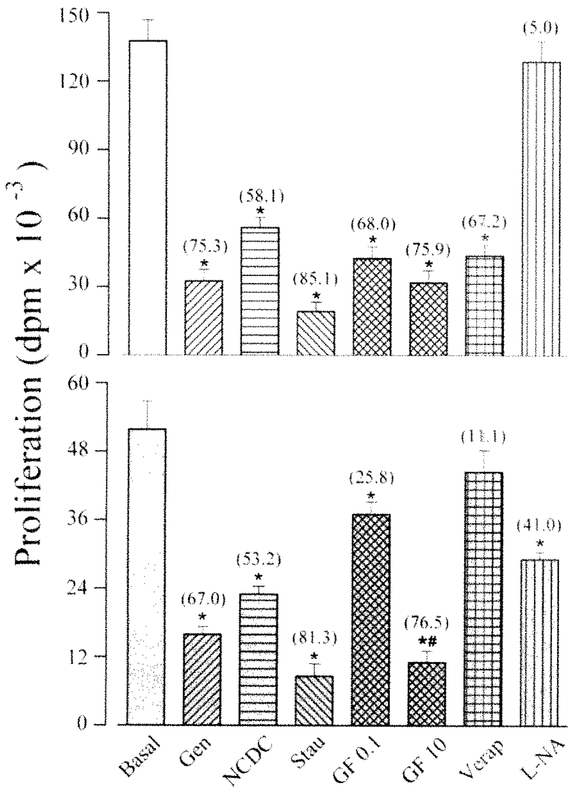

Fig. 1. Effect of different enzymatic and calcium blockers on Con A-stimulated and tumor T cell proliferation. Purified T lymphocytes were prepared aseptically following the indicated procedures and stimulated with Con A (2 μg/ml), for 72 h (☐). Cells were cultured in the absence (basal) or presence of the drugs mentioned above. BW5147 synchronized cells (▩) were incubated for 24 h in FCS-rich medium alone (basal) or with the indicated blockers. The following blockers, added at the beginning of culture, were used: genistein (GEN) (30 μg/ml), NCDC (10 μM), staurosporine (STAU) (0.1 μM), GF109203X (GF) (0.1 or 10 μM), verapamil (VER) (0.1 mM) and L-NAME (L-NA) (5 mM). Proliferation was evaluated by [^{3}H]TdR incorporation. Percentage of inhibition of cellular proliferative activity, calculated as described in Materials and methods, is shown between brackets. Results shown are the mean ± SD of three independent experiments performed in triplicate. * Differs significantly from the corresponding basal value with at least $P<0.01$. #Differs significantly from the other values of BW5147 cells with at least $P<0.05$.

the 7% FCS-containing medium. Incubations were continued for 72 h, in the presence of 2 μg/ml Con A, for normal T cells or 24 h for BW5147 cells. Control untreated cells were submitted to the same permeabilization schedule than intracellular antibody-delivered cells. Proliferation was evaluated by [^{3}H]TdR incorporation by adding the radioligand substrate 6 h prior to culture finalization. NOS enzymatic activity was evaluated immediately upon the ending time of incubation, as indicated before.

2.7. Drugs

The following drugs were used in cultures at the final concentrations indicated in Results. The protein kinase inhibitors staurosporine, the selective PKC inhibitor GF-109203X (bisindolylmaleimide), the PLC blocker 2-nitro-4-carboxyphenyl-*N*,*N*-diphenylcarbamate (NCDC) and the TPK inhibitor genistein (all from Sigma) were dissolved in DMSO. N^G-Nitro-L-arginine methyl ester (L-NAME) (RBI, USA) was dissolved in water. Stock solutions were freshly prepared before use. All drugs were further diluted (at least 1:1000 or more) in RPMI 1640 medium to achieve the concentrations indicated in Results.

2.8. Statistical analysis

The Student's *t*-test for unpaired values was used to determine the levels of significance. When multiple comparison were necessary after analysis of variance, the Student–Newman–Keuls test was applied. Differences between means were considered significant if $P \leq 0.05$.

3. Results

3.1. Blockers of intracellular pathways involved in T lymphocyte activation displayed different actions on mitogen-stimulated and tumor T cell proliferation

In order to analyze differences in the enzymatic intracellular pathways involved in both mitogen-induced and tumor T cell proliferation, the effect of TPK, PLC, PKC and calcium blockers was analyzed. As shown in Fig. 1, the blockade of TPK by genistein, at a dose that has no effect on cellular viability, PLC by NCDC or PKC by either staurosporine or the more selective GF109203X inhibit both normal and tumor cell proliferation. It is worth noting that

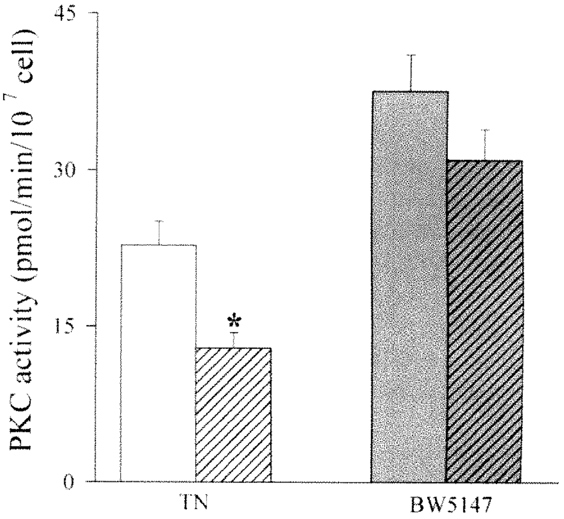

Fig. 2. Calcium dependence of PKC total activity in normal and tumor T cells. PKC total activity was purified from normal T lymphocytes (TN, white bars) or tumor BW5147 cells (gray bars) and was measured, in the presence (open bars) or in the absence of Ca^{2+} (dashed bars), using the substrate MBP (4–14), as described in Materials and methods. Results shown are the mean ± SD from four independent experiments performed in duplicate. * Differs significantly from the corresponding basal value with $P<0.01$.

GF109203X is a potent inhibitor of cPKC (IC50 ≅ 0.01 – 0.02 μM), but a weak inhibitor of nPKC (IC50 ≅ 0.1 – 0.2 μM) or aPKC (IC50 for PKC ζ ≅ 6.0 μM) [7]. So, the fact that this blocker exerted a significant higher effect at 10 μM than 0.1 μM concentration could be related to the different IC50 s. Furthermore, the calcium blocker verapamil, although efficiently inhibiting Con A-stimulated proliferation, had little effect on T lymphoma cell growth.

To assess the role of cell-specific pathways for NO in normal and tumor cells, the action of the NOS competitive blocker, L-NAME, was also determined. Fig. 1 also shows that L-NAME was able to abrogate tumor, but not normal, T cell proliferation.

3.2. PKC and NOS activities in normal, activated and tumor T cells

To compare PKC activity on both normal and tumor cells and to evaluate the balance between calcium-dependent and independent PKC isoforms, enzymatic activity was measured on whole cell extracts in the presence or absence of Ca^{2+} using the specific PKC substrate, MBP (4–14) peptide. As shown in Fig. 2, total PKC activity was higher in tumor than in normal T cells, and it was unaffected in the absence of Ca^{2+}. In normal T cells a decrease of approximately 43% was observed in the absence of Ca^{2+}.

To analyze differences in PKC translocation to plasma membrane, related to cellular proliferation in both normal and tumor T lymphocytes, PKC enzymatic activity was measured on both soluble and particulate fractions from mitogen-stimulated normal and tumor T cell, at different times during the kinetics of proliferation. For this purpose BW5147 synchronized cells were induced to proliferate by re-culturing them in FCS-rich medium. Resting normal T lymphocytes were activated by Con A in vitro as indicated before. As shown in Fig. 3 and in accordance to Fig. 2, total PKC activity was higher on synchronized tumor (basal) than in normal T cells. Within 15-min exposure to FCS, synchronized BW5147 cells displayed an early and significant increment in membrane PKC activity that was accompanied by the decrease in cytosolic PKC (Table in Fig. 3). The increment in phosphorylated substrate was observed

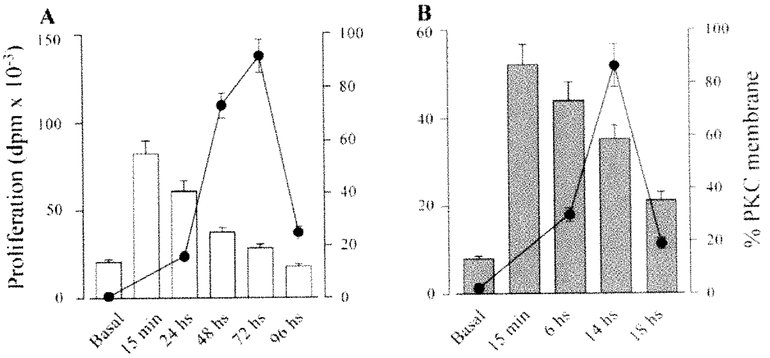

Cell type	Treatment	PKC[a] (pmol/10^7 cell) Cytosol / Membrane	Proliferation[b] (dpm)
T Normal	---	12.7 ± 0.8 / 2.3 ± 0.3	1034 ± 108
	Con A	6.1 ± 0.7 / 7.4 ± 0.7*	137524 ± 9370*
BW5147	Without FCS	29.4 ± 2.9 / 4.5 ± 0.5	1209 ± 235
	With FCS	4.0 ± 0.4 / 26.7 ± 1.8*#	51875 ± 4612*

Fig. 3. PKC activity and proliferation of normal, mitogen-stimulated and tumor T cells. Panel A: Normal T lymphocytes were kept in culture alone (basal) or in the presence of Con A (2 μg/ml) for the indicated times. Proliferation (curve) was evaluated by [^{3}H]TdR incorporation, in 0.2-ml aliquots of macrocultures established for enzymatic PKC activity determination. Results shown are the mean ± SD of three independent experiments performed in triplicate. PKC activity in membrane fractions was determined using MBP (4–14) as described in Materials and methods and percent of total (cytosol + membrane) PKC activity (bars) from the three experiments performed in duplicate were calculated. Panel B: BW5147 cells, synchronized by 24-h culture in FCS-deprived medium, were recultured in FCS-rich RPMI 1640 medium as indicated before. Proliferation (curve) was evaluated by 6 h lasting pulses of [^{3}H]TdR, as indicated in panel A, on BW5147 synchronized (without FCS, basal) and after resetting them in FCS-rich medium for the indicated times. Results shown are the mean ± SD of three experiments performed in triplicate. Percentages of total PKC activity corresponding to membrane purified fractions determined as in Panel A are shown in the bar graphic.

A summary of both PKC activity (pmol/10^7 cells) and proliferation (dpm) is shown in the adjoining table. (a) PKC activity values from purified cytosol and membrane fractions corresponding to basal or 15 min treatment with Con A (normal T cells) or with FCS-rich medium (BW5147 cells) are shown. Results are the mean ± SD of three experiments performed in duplicate. (b) Mean dpm ± SD of [^{3}H]TdR incorporation corresponding to basal or to the peak of proliferation (72 h for Con A-treated T lymphocytes or 14 h for BW5147 cells). * Differs from basal values with at least $P<0.01$. *#Differs from basal values and from Con A-stimulated T cells with at least $P<0.01$.

both when using histone H_1 (data not shown) or the specific PKC peptide MBP (4–14). This membrane PKC activity diminished but stayed higher than basal values after the peak of proliferation. It is worth noting that exponentially growing BW5147 cells displayed similar values for total PKC activity, with most of this activity (80–90%) in membrane fractions.

On the other hand, mitogenic stimulation of resting normal T lymphocytes also induced an early translocation of PKC (within 15 min), but to a lesser extent to that found in tumor cells. Membrane PKC returns to basal levels after the peak of proliferation.

With respect to NOS activity, we found very low levels in normal T cells (Fig. 4), with a slight nonsignificant increase upon physiologic activation. On the contrary, BW5147 cells showed an important basal NOS activity, which was blunted by L-NAME (Fig. 4); an effect that was reverted by L-arginine (data not shown). To analyze the relationship between high PKC and NOS activities in BW5147 cells, the effect of PKC blockers on NOS was also determined. As can be seen in Fig. 4, both staurosporine and GF109203X in high doses were able to inhibit, similarly, NOS activity in tumor cells.

3.3. PKC isoform expression in mitogen-activated and tumor T cells

In order to asses that differences in PKC activity could be related to distinct isoenzyme expression, PKC isoform profile was analyzed on both tumor and resting or mitogen-stimulated T cells by Western blot analysis. The expression of cPKC α and β, nPKC δ, θ and ε, and the atypical PKC ζ isoform in lysates from naive or Con A-stimulated T cells and exponentially growing BW5147 cells was measured. A representative plot of the levels of PKC isoenzymes in the different cell types is shown in Fig. 5 (Panel A). As can be seen, resting T cells express the cPKC α and β and the nPKC θ, but not γ (data not shown) isoform with barely detectable amounts of PKC δ and ζ. As an example of PKC translocation upon cellular activation, within 15 min of mitogenic stimulation, membrane levels of cPKC β isoform were increased in membrane fractions (Fig. 5, Panel B). Also, after 72 h of Con A treatment, a significant increase in levels of cPKC α and β was observed. On the contrary, exponentially growing BW5147 cells showed only vanishing amounts of the β isoform and an increased expression of PKC ζ (Fig. 5, Panel A). Whereas levels of α, γ, δ and ε isoforms were identical to those found in activated normal T lymphocytes of the same H-2 haplotype (Fig. 5A), expression of the θ isotype was not found. It is worth noting that all the bands were detected at the positions corresponding to PKC isoenzymes from T lymphoid cells previously described [29]. PKC ζ translocation to the particulate fraction was obtained upon 15-min stimulation of synchronized BW5147 cells with FCS (Fig. 5, Panel B).

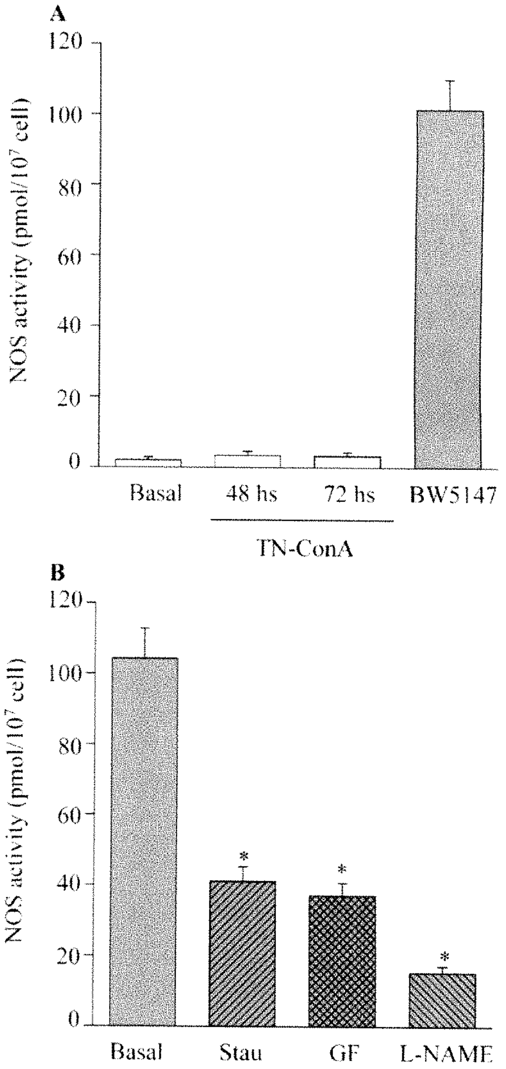

Fig 4. NOS activity in normal, mitogen-stimulated and tumor T cells. Panel A: NOS activity was measured by the conversion of [^{14}C]-arginine to [^{14}C]-citrulline as indicated in Materials and methods in normal T lymphocytes (▭, basal or Con A-stimulated for 48 or 72 h, or BW5147 (▩) cells. Panel B: Effect of the PKC blockers, staurosporine (Stau, 0.1 μM) or GF 09203X (GF, 10 μM) and the NOS blocker, L-NAME (5mM), on BW5147 cells incubated alone (Basal) or in the presence of the indicated blocker concentrations for 24 h is shown. Results are the mean ± SD of $n = 4$ experiments. * Differs significantly from basal values with at least $P < 0.05$.

3.4. Effect of the intracellular delivery of anti-PKC ζ isoform antibody on BW5147 proliferation and NOS activity

In order to determine the involvement of PKC ζ in the high proliferative rate and NOS activity from tumor T cells, the effect of intracellular delivering of a specific antibody against the C-terminal region of PKC ζ, was assessed. Anti-PKC ζ antibody (Fig. 6) was able to diminish, in the concentrations tested, both proliferation and NOS activity in BW5147 cells, but not in normal activated T lymphocytes. It is worth noting that no differences from basal values with dilutions higher than 1:500 (data not shown)

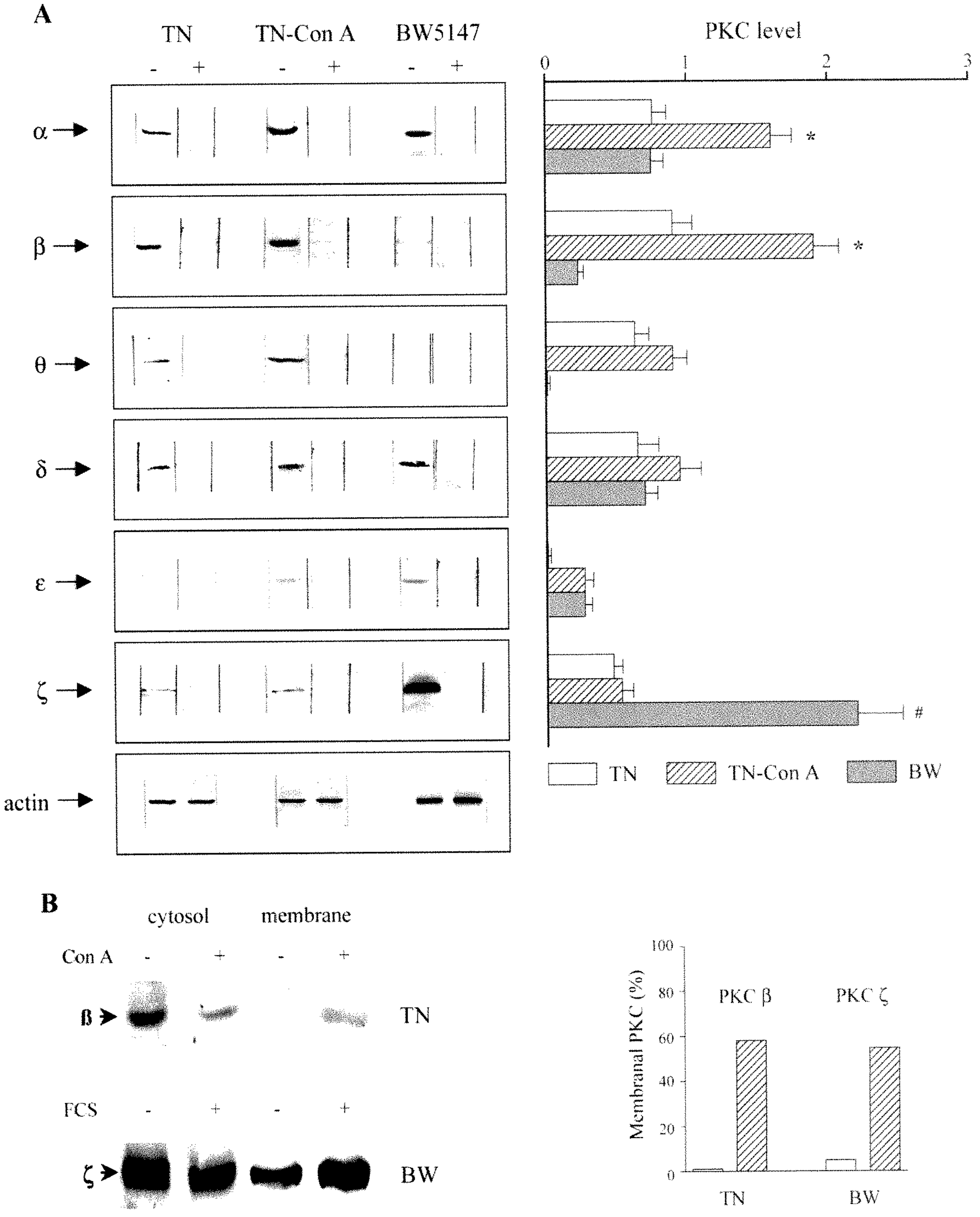

Fig. 5. PKC isotype expression in normal (TN), Con A-stimulated (TN-Con A) or BW5147 T cells. Panel A: The data show the Western blot analysis of PKC α, β, θ, δ, ε and ζ isotypes. Specificity of anti-PKC antibodies was assessed by performing Western blot analyses in the absence (−) or presence (+) of the corresponding peptide against which the antibodies had been raised. Results, corresponding to TN, TN-Con A (culturing time 72 h) and BW5147 total cells, are representative of seven independent experiments. Anti-actin antibodies were tested on same samples used for PKC isoform analysis as control for protein loading in three of these experiments. Also, PKC levels for each isoenzyme (bar graph) were calculated in relation to the expression level of actin in the same sample as described in Materials and methods. Results shown are the mean ± SD of $n = 3$ experiments. Statistic analysis was performed within each isoenzyme group. * Differs significantly from TN and BW values with at least $P < 0.01$. #Differs significantly from TN and TN-Con A values with at least $P < 0.001$. Panel B: Subcellular distribution of PKC β and ζ isoenzymes in normal and tumor T cells, respectively, upon cellular activation. Freshly isolated T lymphocytes or synchronyzed BW5147 cells were either left unstimulated (−) or stimulated (+) with Con A (2 μg/ml) or FCS (10%), respectively, for 15 min. Cytosol and membrane fraction of 2×10^6 cell equivalents were analyzed by SDS-PAGE followed by immunoblotting with the indicated antibodies. Arrows indicate the position of the corresponding PKC protein bands. The relative intensity of the different PKC bands was quantitated by densitometry and the percentage of the membranal PKC out of the sum of cytosolic plus membranal PKC was calculated in each case and represented in the bar graph. It is worth noting that both Western blots and the bar graph are one representative out of three experiments.

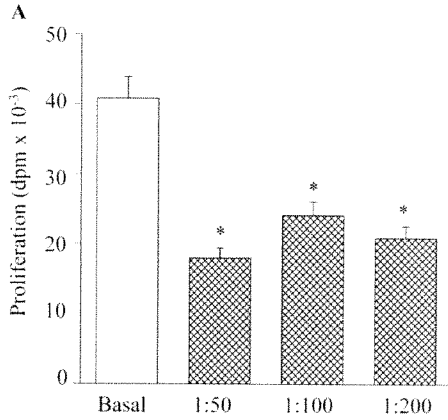

B

Cell type	Addition	Proliferation (dpm)	NOS activity (pmol / 10^7 cell)
	none	38752 ± 3410	91.0 ± 7.8
BW5147	Anti-PKCζ	19376 ± 1744*	47.5 ± 3.6*
	Anti-PKCζ + peptide	41276 ± 3343	95.3 ± 6.9
TN-ConA	none	98234 ± 8841	5.9 ± 0.6
	Anti-PKCζ	88428 ± 7074	6.1 ± 0.5

Fig. 6. Effect of intracellular delivery of an anti-PKC ζ antibody on cellular proliferation and NOS activity. Panel A: BW5147 cells were permeabilized with lysolecithin and incubated in the absence or presence of different dilutions of the anti-PKC ζ for 10 min and resealed. After 24 h of incubation, cellular proliferation was assessed as described before. Panel B: both normal or tumor cells were permeabilized, as indicated in panel A, and incubated in the absence or presence of anti-PKC ζ antibody (in a concentration 1:200) or anti-PKC ζ plus PKC ζ peptide (1:3). After resealing, BW5147 cells were incubated for 24 h and normal cells were stimulated with Con A (TN-Con A) for 72 h. Proliferation and NOS activity were measured as described. Results shown are the mean ± SD of three independent experiments. * Differs significantly from the corresponding basal (none) values with at least $P<0.05$.

were found in tumor cells. These effects were blunted by pretreatment of the antibody with the specific immunogenic ζ peptide (Fig. 6).

4. Discussion

Both PKC and NOS activities play important roles in the regulation of cellular functions. In this work the involvement of these enzymatic pathways in the proliferation of a T lymphoma cell line was studied in comparison to normal and mitogen-stimulated T lymphocytes. Tumor BW5147 cells exhibit higher total PKC activity and membrane PKC translocation than normal or mitogen-stimulated T cells. In normal T lymphocytes, PKC activity was diminished in the absence of calcium, while it was almost unmodified in tumor cells, thus pointing to a prevalence of calcium-independent PKC isoform activity in tumor cells in comparison to normal lymphocytes. It is worth noting that the calcium blocker verapamil inhibits Con A-induced proliferation of normal cells, but has not a significative effect in the proliferation of BW5147 cells. PKC inhibitors or blockers of the upstream signaling pathways, namely, TPK and PLC, are capable of inhibiting both mitogen-stimulated and tumor T cell proliferation. GF109203X, a potent inhibitor of cPKC but a weak inhibitor of calcium-independent isoforms, was able to efficiently block tumor cell proliferation at high doses, while equally inhibiting Con A-stimulated proliferation at low and high doses. These results indicate that different PKC isoforms would have differential hierarchical participation in normal and tumor T cell activation. The higher PKC translocation observed in tumor cells with respect to the physiologic translocation induced by the mitogenic stimulus would point to the participation of this intracellular transduction mechanism in the sustained proliferation of BW5147 cells. In fact, a correlation has been proposed between PKC activity and the rate of cellular growth, as well as a parallelism between PKC inhibition and induction of cellular differentiation in lymphoid cells [4].

Several experimental evidences indicate that PKC isoenzymes are localized in specific tissues and that different isoforms are related to lymphoid proliferation or differentiation [4,9,10], so the pattern of PKC isoenzymes was studied on both normal and tumor T cells. We found that normal and activated T lymphocytes display the calcium-dependent α and β PKC isoforms, as well as the nPKC θ, and detectable levels of ε and ζ, with no expression of the γ isoenzyme. Similarly, Mischak et al. [9] found the expression of mRNA encoding for α and β, but not γ isoforms, with low levels of PKC ε and ζ, in resting murine T lymphocytes and a close correlation between protein expression and mRNA levels. With respect to the θ isoform, its expression and role in T cell activation was already demonstrated [27]. The expression of cPKC α and β was progressively up-regulated by Con A stimulation and this correlates with cell proliferation. Several stimuli, including mitogens, were demonstrated to induce changes in T lymphocyte PKC isoenzyme expression, both at protein and mRNA levels [30–32]. These changes were time- and cell-type-dependent. Thus, a decrease in PKC β protein levels within 24 h of mitogen stimulation [30] and an earlier but transient loss of β and α PKC mRNA were described in murine thymocytes [31]. Despite this, Isakov et al. [32] demonstrate that mitogen stimulation of human mature T cells is followed by a four- to fivefold increase in PKC α and β mRNA, peaking at 48 h and correlating with cellular proliferation, which is in agreement with our results. Differences from the data of Strulovici [30] could be related with the distinct T cell populations studied.

BW5147 cells have barely detectable levels of the β isoform, with similar levels of α and δ isoforms, and no detectable levels of the γ and θ isoenzymes. Interestingly, we found an increased expression of the atypical calcium-independent ζ isoenzyme. These results are in agreement with the fact that cellular proliferation is mainly calcium-independent in BW5147 cells, and PKC activity involves calcium-independent isoforms, as it was not modified in the presence of EGTA. Goodnight et al. [33] have described elevated expression of PKC ζ in B lymphocytic neoplasms at both mRNA and protein levels. Also, a high expression of the β isoform has been related to accelerated leukemic cell differentiation [34], while final differentiation of B lymphocytes into antibody-secreting plasma cells is accompanied by a loss in this isoenzyme [9]. Taken together, these facts and our results, it is possible that the increase in PKC β isoform observed during mitogenic stimulation of T cells would allow an efficient but limited activation, leading to differentiation to immune effector cells, while low levels of this isoenzyme, together with high levels of the ζ isoform, would be responsible for the hyperproliferative pattern of BW5147 cell line.

On the other hand, the NOS blocker L-NAME impaired tumor, but not normal T cell proliferation. Also, BW5147 cells exhibit high NOS activity, while a low basal activity was found in resting normal T cells, which was not increased by mitogenic stimulation. High NOS activity levels in tumor cells were blunted by L-NAME and were partially impaired by PKC blockers, thus indicating that PKC activity is, in part, responsible for NOS activity in BW5147 cells. High levels of endogenous NOS activity would allow the survival of tumor cells, protecting them from apoptotic mechanisms. Furthermore, intracellular delivery of an antibody directed to the most abundant PKC isoform in BW5147 cells, an anti-PKC ζ antibody, not only diminished cellular proliferation, but also lowered NOS activity in tumor cells, with no effect on mitogen-activated T lymphocytes. Other authors have previously demonstrated that intracellular delivery of antibodies directed to the C-terminal region of specific PKC isoforms are able to modify physiological functions of different cell types [28], including T lymphocytes [35]. In support to our results, overexpression of PKC ζ isoform was demonstrated to markedly increase the inducible NOS isoenzyme expression in rat mesangial cells [36]. The fact that anti-PKC ζ antibody was not able to completely abrogate NOS activity or proliferation of BW5147 cells indicates that probably other isoforms could be involved in these functions, but nevertheless, they point to a role for the PKC ζ isoenzyme. Actually, PKC activation by phorbol esters, which activates cPKC and nPKC but not aPKC, was demonstrated to increase NOS expression and/or activity in several cell types [19,20,26,37].

Experimental evidence showed that aPKCs play important roles in controlling cell growth and survival [38]. In fact, it was demonstrated that PKC ζ is critical for mitogenic signal transduction in oocytes [39], while aPKC τ was shown to protect human leukemic cells from drug-induced apoptosis [40]. Furthermore, Tsutsumi et al. [41] demonstrated the down-regulation of PKC ζ RNA following cross-linking of membrane IgM on B lymphoma cells, and growth arrest and apoptosis were induced in a B cell line by cross-linking of surface immunoglobulin [42]. There are also evidences that endothelial NOS autocrine is able to protect T lymphocytes from apoptosis [43].

For the first time, shown here are evidences that strengthened the crosstalk of PKC and NOS enzymatic pathways in T lymphoid cells and their participation in cellular proliferation. Although further studies would be necessary to analyze the role of other isoforms, our results would indicate that hyperproliferation of BW5147 cells is related to PKC hyperactivity, with a major participation of calcium-independent isoenzymes and particularly of PKC ζ. This activity is in part responsible for inducing NOS activation that would protect BW5147 cells from apoptotic signals, contributing in this way to cellular survival. Our findings also suggest that the PKC ζ member of the PKC multigene family participates in the multistep process of BW5147 cell growth, leading to the malignant phenotype.

Acknowledgements

The authors wish to thank Dr. A.M. Genaro for her helpful discussion of the manuscript.

This work was supported by the "R. Carrillo-A. Oñativia" grant from the Ministerio de Salud de la Nación, República Argentina.

References

[1] C.L. Sawyus, C.T. Denny, O.N. Wilte, Cell 64 (1991) 337–350.
[2] A. Weiss, D. Littman, Cell 76 (1994) 263–274.
[3] M. Szamel, A. Appel, R. Schwinzer, K. Resch, J. Immunol. 160 (1998) 2207–2214.
[4] M.J. Clemens, I. Trayner, J. Menaya, J. Cell Sci. 103 (1992) 881–887.
[5] Y. Nishizuka, FASEB J. 9 (1995) 484–496.
[6] G.C. Mayne, A.W. Murray, J. Biol. Chem. 273 (1998) 24115–24121.
[7] K.J. Way, E. Chou, G.L. King, Trends Pharmacol. Sci. 21 (2000) 181–187.
[8] E.C. Dempsey, A.C. Newton, D. Mochly-Rosen, A.P. Fields, M.E. Reylad, P.A. Insel, R.O. Messing, Am. J. Physiol., Lung Cell. Mol. Physiol. 279 (2000) L429–L438.
[9] H. Mischak, W. Kolch, J. Goodnight, W.F. Davidson, U. Rapp, S. Rose-John, J.F. Mushinski, J. Immunol. 147 (1991) 3981–3987.
[10] J. Gomez, C. Pitton, A. Garcia, A. Martinez de Aragon, A. Silva, A. Rebollo, Exp. Cell Res. 218 (1995) 105–113.
[11] A. Altman, N. Isakov, G. Baier, Immunol. Today 21 (2000) 567–573.
[12] N. Meller, A. Altman, N. Isakov, Stem Cells 16 (1998) 178–192.
[13] B. Brune, A. von Knethen, K.B. Sandau, Eur. J. Pharmacol. 351 (1998) 261–272.
[14] C. Sciorati, G. Nisticò, J. Meldolesi, E. Clementi, Br. J. Pharmacol. 122 (1997) 687–697.
[15] J.P. Kolb, Leukemia 14 (2000) 1685–1694.
[16] J.B. Mannick, K. Asano, K. Izumi, E. Kieff, J.S. Stamler, Cell 79 (1994) 1137–1146.
[17] A.M. Genaro, S. Hortelano, A. Alvarez, A. Martinez, L. Bosca, J. Clin. Invest. 95 (1995) 1884–1890.
[18] C.B. Thompson, Science 267 (1995) 1456–1462.
[19] Y. Hirose, C.V. Rao, B.S. Reddy, Int. J. Oncol. 18 (2001) 141–146.

[20] I. Momose, M. Terashima, Y. Nakashima, M. Sakamoto, H. Ishino, T. Nabika, Y. Hosokawa, Y. Tanigawa, Biochim. Biophys. Acta 1498 (2000) 19–31.

[21] S. Goenka, T. Das, G. Sa, P.K. Ray, Biochem. Biophys. Res. Commun. 250 (1998) 425–429.

[22] C.A. Cazaux, L. Sterin-Borda, G. Gorelik, G.A. Cremaschi, FEBS Lett. 364 (1995) 120–124.

[23] A.M. Genaro, E. Borda, G.A. Cremaschi, L. Sterin-Borda, M. Braun, Immunopharmacology 11 (1986) 129–140.

[24] A.M. Genaro, L. Boscá, J. Immunol. 151 (1993) 1832–1843.

[25] I. Yasuda, A. Kishimoto, S. Tanaka, M. Tominaga, A. Sakurai, Y. Nishizuka, Biochem. Biophys. Res. Commun. 166 (1990) 1220–1227.

[26] S. Hortelano, A.M. Genaro, L. Boscá, FEBS Lett. 320 (1993) 135–139.

[27] N. Meller, Y. Elitzur, N. Isakov, Cell. Immunol. 193 (1999) 185–193.

[28] U. Leli, P.J. Parker, T.B. Shea, FEBS Lett. 297 (1992) 91–94.

[29] C. Keenan, D. Kelleher, A. Long, Eur. J. Immunol. 25 (1995) 13–17.

[30] B. Strulovici, S.D. Isaakani, G. Baxter, J. Knopf, L. Sultzman, H. Cherwinsky, J. Nestor, D.R. Webb, J. Ransom, J. Biol. Chem. 266 (1991) 168–173.

[31] J. Freire-Moar, H. Cherwinsky, F. Hwang, J. Ransom, D. Webb, J. Immunol. 147 (1991) 405–409.

[32] N. Isakov, M.I. Mally, A. Altman, Mol. Immunol. 29 (1991) 927–933.

[33] J. Goodnight, H. Mischak, J.F. Mushinski, Mol. Carcinog. 11 (1994) 131–137.

[34] E. Melloni, S. Pontremoli, B. Sparatore, M. Patrone, F. Grossi, P.A. Marks, R.A. Rifkind, Proc. Natl. Acad. Sci. U. S. A. 87 1990, 4417–4420.

[35] M. Szamel, U. Ebel, P. Uciechowski, V. Kaever, K. Resch, Biochim. Biophys. Acta 1356 (1997) 237–248.

[36] B.W. Miller, L.D. Baier, A.R. Morrison, Am. J. Physiol. 273 (1997) C130–C136.

[37] J. Kang, M. Yang, I. Jou, E. Joe, Neurosci. Lett. 299 (2001) 205–208.

[38] J. Moscat, M.T. Diaz-Meco, EMBO Rep. 11 (2000) 399–403.

[39] E. Berra, M.T. Diaz-Meco, I. Dominguez, M.M. Municio, L. Sanz, J. Lozano, R.S. Chapkin, J. Moscat, Cell 74 (1993) 555–563.

[40] N.R. Murray, A. Fields, J. Biol. Chem. 272 (1997) 27521–27524.

[41] A. Tsutsumi, J. Freire-Moar, J.T. Ransom, Cell. Immunol. 142 (1992) 303–312.

[42] S. An, K.A. Knox, FEBS Lett. 386 (1996) 115–122.

[43] C. Sciorati, P. Rovere, M. Ferrarini, S. Heltai, A.A. Manfredi, E. Clementi, J. Biol. Chem. 272 (1997) 23211–23215.

ELSEVIER

Biochimica et Biophysica Acta 1588 (2002) 189–194

BIOCHIMICA ET BIOPHYSICA ACTA
BBA
www.bba-direct.com

Correction of the copper transport defect of Menkes patient fibroblasts by expression of two forms of the sheep Wilson ATPase

Paul J. Lockhart[a], Sharon La Fontaine[a], Stephen D. Firth[a], Mark Greenough[b], James Camakaris[b], Julian F.B. Mercer[a,*]

[a]*Center for Cellular and Molecular Biology, School of Biological and Chemical Sciences, Deakin University, Building L, Burwood Campus, 221 Burwood Highway, Victoria 3125, Australia*
[b]*Department of Genetics, University of Melbourne, Parkville 3052, Australia*

Received 14 March 2002; received in revised form 2 July 2002; accepted 25 July 2002

Abstract

The Wilson disease (WD) protein (ATP7B) is a copper-transporting P-type ATPase that is responsible for the efflux of hepatic copper into the bile, a process that is essential for copper homeostasis in mammals. Compared with other mammals, sheep have a variant copper phenotype and do not efficiently excrete copper via the bile, often resulting in excessive copper accumulation in the liver. To investigate the function of sheep ATP7B and its potential role in the copper-accumulation phenotype, cDNAs encoding the two forms of ovine ATP7B were transfected into immortalised fibroblast cell lines derived from a Menkes disease patient and a normal control. Both forms of ATP7B were able to correct the copper-retention phenotype of the Menkes cell line, demonstrating each to be functional copper-transporting molecules and suggesting that the accumulation of copper in the sheep liver is not due to a defect in the copper transport function of either form of sATP7B.
© 2002 Elsevier Science B.V. All rights reserved.

Keywords: Copper metabolism; P-type ATPase; ATP7B

1. Introduction

Copper homeostasis is important because copper is an essential trace element but is toxic in excess, so organisms require mechanisms to maintain intracellular copper at the required level [1]. In humans and other mammals, the liver is the major organ involved in the regulation of overall copper status, with excess copper being excreted from the body in the bile [2]. The importance of the biliary excretion pathway is illustrated by the human copper toxicosis disorder Wilson disease (WD). Patients with this disease cannot excrete copper into the bile, resulting in hepatic copper accumulation and if untreated, fatal copper toxicosis. A second feature of most, but not all WD patients, is very low serum ceruloplasmin levels [3]. The gene that is defective in WD patients encodes a copper-transporting P-type ATPase (ATP7B) [4–6]. ATP7B has two functional roles in copper homeostasis in the liver. The first is the transport of copper into the lumen of the Golgi apparatus for incorporation into secreted copper-dependent enzymes, primarily ceruloplasmin [7]. The second role of ATP7B is the excretion of excess copper into the bile. This involves copper-induced trafficking of ATP7B from the trans-Golgi network (TGN) or late endosomic vesicles, to vesicles and the apical biliary canalicular membrane when copper is present in excess [8–10]. The dual roles of ATP7B may explain the heterogeneity in clinical features of patients presenting with WD, with different ATP7B alleles affecting either copper transport or intracellular location/trafficking of ATP7B [8]. Recently, a cell culture system was utilised to distinguish ATP7B variants in which copper transport was disrupted from those in which intracellular trafficking was impaired [11].

Sheep have a variant copper phenotype when compared with other mammals. The species is prone to copper deficiency due to the formation of copper-chelating thiomolybdates in the rumen [12]. However, sheep are prone to copper toxicosis due to a reduced capacity to excrete copper in the bile. Unlike most mammals, the rate of biliary copper excretion is not responsive to copper intake [13]. Analogous

---

[*] Corresponding author. Tel.: +61-3-9251-7329; fax: +61-3-9251-7328.
E-mail address: jmercer@deakin.edu.au (J.F.B. Mercer).

0925-4439/02/$ - see front matter © 2002 Elsevier Science B.V. All rights reserved.
PII: S0925-4439(02)00164-3

to WD patients, the intake of moderate dietary levels of copper can result in elevated hepatic copper concentrations, liver failure and death [14]. Unlike most WD patients, the level of copper and holoceruloplasmin in sheep plasma is similar to the normal human range [15]. We are investigating the molecular basis of the sheep copper phenotype. In previous studies, we cloned the sheep *ATP7B* (*sATP7B*) cDNA, but did not find any obvious abnormality of structure or expression that would suggest that sheep have a defect in ATP7B. However, we identified a novel form of the *ATP7B* cDNA which had an alternative N-terminal region, generated by alternate splicing [16]. The form corresponding to published ATP7B orthologues (normal sATP7B) encodes an 18-amino-acid N-terminal sequence, which is replaced by a novel 79-amino-acid sequence in the alternate sATP7B protein. Both forms of sATP7B localise to the TGN and undergo copper-induced trafficking to a vesicular compartment when expressed in CHO cells [17].

In this study, we examined the copper-translocating activity of each form of sATP7B to determine if the sheep copper phenotype might be related to alterations in this activity in either form of sATP7B. The copper transport function of both forms of sATP7B was examined in vitro by the generation of fibroblast cell lines from a Menkes disease patient and a normal control, which expressed cDNA-derived sATP7B. Although exogenously expressed ATP7B does not undergo copper-induced trafficking in this cell line, the copper transport function of introduced ATPases can be accurately assessed by measuring efflux of radiolabeled copper from the cell. Our results indicate that both forms of sATP7B correct the copper accumulation defect of Menkes patient fibroblasts and therefore are functional copper-transport proteins.

2. Materials and methods

2.1. Cell culture, constructs and antibodies

The generation and characterisation of immortalised fibroblasts derived from a Menkes disease patient (Me32a-T22/2L) and control cell line (GM847) has been previously described. The Me32a MNK gene has a 4-base-pair (bp) deletion within exon 6, resulting in a prematurely terminated protein between metal binding sites 5 and 6, and complete loss of the protein as determined by Western blot utilising a polyclonal antibody directed against all six metal binding sites [18]. Cells were maintained at 37 °C in basal medium (approximately 1 μM copper), which consisted of Eagle's basal medium (BME) (Trace BioSciences) supplemented with 2 mM L-glutamine, 0.2 mM proline, 1.2 mM $NaHCO_3$, 20 mM HEPES and 10% foetal calf serum (Commonwealth Serum Laboratories). The generation of the constructs pNORM and pALT, encoding the normal and alternate forms of sheep ATP7B cloned into a low-copy number mammalian expression vector was reported previously, as was the production, purification and characterisation of antibodies specific for each form of sheep ATP7B [17].

2.2. Cell transfection and expression analysis

The transfection of cells was performed essentially as described previously [17]. Briefly, stable transfection of cultured cells was performed with 20 μg of linear plasmid DNA and Superfect reagent (Qiagen) according to the manufacturer's protocols. Following 3 weeks of G418 selection (Gibco, 400 μg/ml), resistant colonies were detached, expanded and maintained as a mixed population of G418-resistant cells. Approximately 60–80% of the G418-resistant population expressed sATP7B, as determined by immunofluorescence analysis (see below). The transfected cell populations were routinely cultured in the presence of G418 (200 μg/ml) to maintain selective pressure for expression of the ATP7B transgene. The generation and characterisation of Me32a-T22/2L cells expressing mouse Atp7b was reported previously [18]. Total RNA was prepared from cells and the expression of each ATP7B transcript was analysed utilising a ribonuclease protection assay (RPA) as described previously [16]. Total protein extracts were prepared from approximately 5×10^6 cells as previously described [19]. The protein concentration was estimated by absorbance at 280 nm and approximately 15 μg of each sample was separated by SDS-PAGE on 7.5% gels (Bio-Rad) under reducing conditions and transferred to nitrocellulose membranes (Millipore). Immunoblot analysis was carried out using the BM Chemiluminescence Kit (Boehringer Mannheim) according to the manufacturer's protocols. Filters were incubated overnight at 4 °C in blocking buffer and incubated for 1–5 h with the appropriate affinity-purified primary antibody at room temperature. After four washes in blocking solution, filters were incubated for 1 h with horseradish peroxidase-conjugated sheep anti-rabbit IgG (Amrad Pharmacia Biotech) and immunoreactive proteins were visualised by chemiluminescence.

2.3. Immunofluorescence microscopy

Immunofluorescence analysis of cells was carried out essentially as described previously [20]. Where appropriate, copper (as $CuCl_2$) was added to the growth medium. In general, cells were grown to 60% confluence on glass cover slips, fixed with 4% paraformaldehyde in PBS for 5 min, permeabilised with 0.1% Triton X-100 in PBS for 5 min at room temperature and placed in blocking solution (1% BSA/1% gelatin in PBS) overnight at 4 °C. Primary antibodies consisted of affinity-purified anti-normal and anti-alternate sheep ATP7B antibodies (1:100 or 1:50) and an affinity-purified anti-mouse Atp7b (1:50) antibody described previously [18]. The secondary antibody was affinity-purified FITC-conjugated sheep anti-rabbit IgG (Amrad Pharmacia Biotech, 1:400). The cover slips were mounted onto glass slides using 2.6% DABCO (1,4-diazabicyclo-(2.2.2) octane, Sigma) in 100% glycerol and analysed using a Zeiss axioskop fluorescence microscope with a CCD camera (Photometrics) and V for Windows software (Digital Optics).

2.4. ^{64}Cu accumulation and retention studies

Copper accumulation studies were performed as described [18]. Briefly, cells were cultured in basal medium and transferred to BME supplemented with 2% foetal calf serum and trace amounts of ^{64}Cu (approximately 0.5 μM as $CuCl_2$; Australian Radioisotopes). For accumulation studies, cells were incubated for 24 h at 37 °C, washed twice in cold BME, and harvested by homogenisation in 0.1% SDS. For retention experiments, cells were treated as above but with an 8-h incubation in BME containing 2% foetal calf serum but lacking ^{64}Cu. The cells then were washed twice with cold BME and harvested in 0.1% SDS. The amount of ^{64}Cu in the cell lysates was measured using an LKB-Wallac Ultragamma counter and the protein content of the extracts was determined by protein assay [21].

3. Results

3.1. Transfection and expression analysis of sheep ATP7B in Menkes patient and control fibroblasts

Expression constructs encoding the normal (pNORM) and alternate (pALT) sATP7B cDNAs were transfected into immortalised fibroblast cell lines, one control, GM847 and one derived from a Menkes disease patient, Me32a-T22/2L.

To confirm expression of the sheep *ATP7B* cDNA, total RNA was extracted from 5×10^6 cells and 3 μg was analysed by a RPA. A protected fragment of the expected size (approximately 180 bp) was observed in Me32a-T22/2L and GM847 cells transfected with pNORM, but not in the corresponding untransfected cells or those transfected with pALT (Fig. 1). Similarly, a protected fragment of expected size (approximately 340 bp) was detected in cells transfected with pALT but not in untransfected cells or pNORM-transfected cells (Fig. 1).

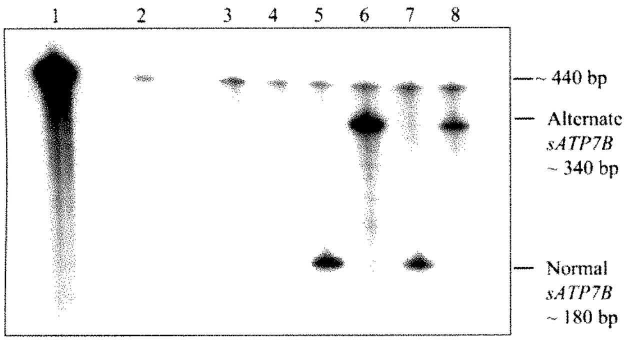

Fig. 1. RPA of *sATP7B* expression in transfected fibroblast cells. Total RNA was isolated from transfected cells and 3 μg was analysed by RPA as described in the Materials and methods. Lane 1 shows the size of the full-length, undigested probe and lane 2 the probe treated with ribonuclease. The RNA samples are: lane 3, untransfected Me32a Menkes patient fibroblasts; lane 4, untransfected GM847 normal fibroblasts; lane 5, Me32a transfected with pNORM; lane 6, Me32a transfected with pALT; lane 7, GM847 transfected with pNORM; lane 8, GM847 transfected with pALT. The approximately 340 and 180 bp protected fragments correspond to the alternative and normal *sATP7B* transcripts, respectively.

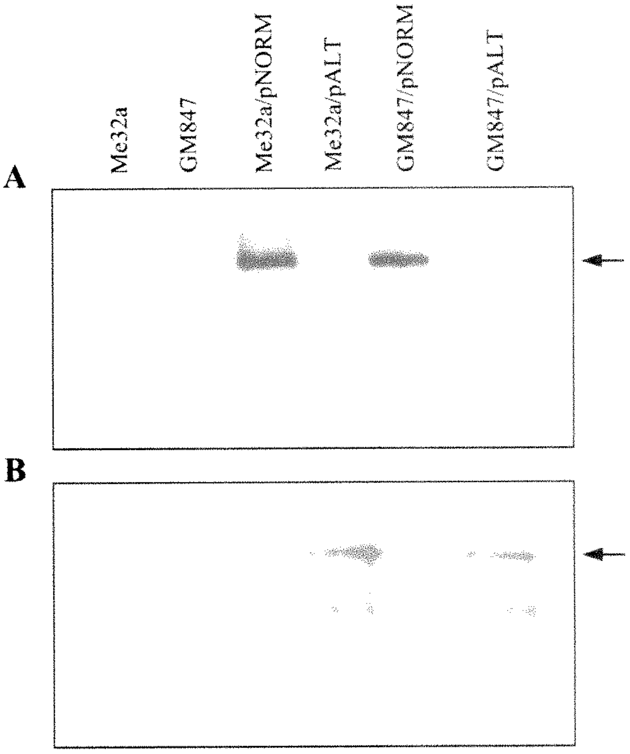

Fig. 2. Western blot analysis of sATP7B expressed in fibroblast cells. Approximately 15 μg of total protein extract from fibroblast cells was fractionated by SDS-PAGE (7.5%) and duplicate gels were transferred to nitrocellulose membranes. Sheep ATP7B was detected with affinity-purified anti-normal sATP7B (A, 1:100) or anti-alternate sATP7B antibody (B, 1:50) and enhanced chemiluminescence. The samples are: Me32a, untransfected Me32a Menkes patient fibroblasts; GM847, untransfected GM847 normal fibroblasts; Me32a/pNORM, Me32a transfected with pNORM; Me32a/pALT, Me32a transfected with pALT; GM847/pNORM, GM847 transfected with pNORM; GM847/pALT, GM847 transfected with pALT. The position of the approximately 160 kDa sATP7B protein is indicated.

Western blot analysis was carried out to confirm the expression of sheep ATP7B and to determine the relative level of protein expression. Approximately 15 μg of whole cell protein extract from the transfected and control cell lines was analysed. A protein of the expected size (approximately 180 kDa) was detected in the appropriate cell lines following analysis with either the anti-normal or anti-alternate ATP7B antibody (Fig. 2). There was no evidence of ATP7B protein in the untransfected cell lines. This result was expected as these cells do not express detectable levels of endogenous human ATP7B mRNA [18] and the sheep ATP7B antibodies do not cross-react with human ATP7B or human ATP7A (data not shown). The lower molecular

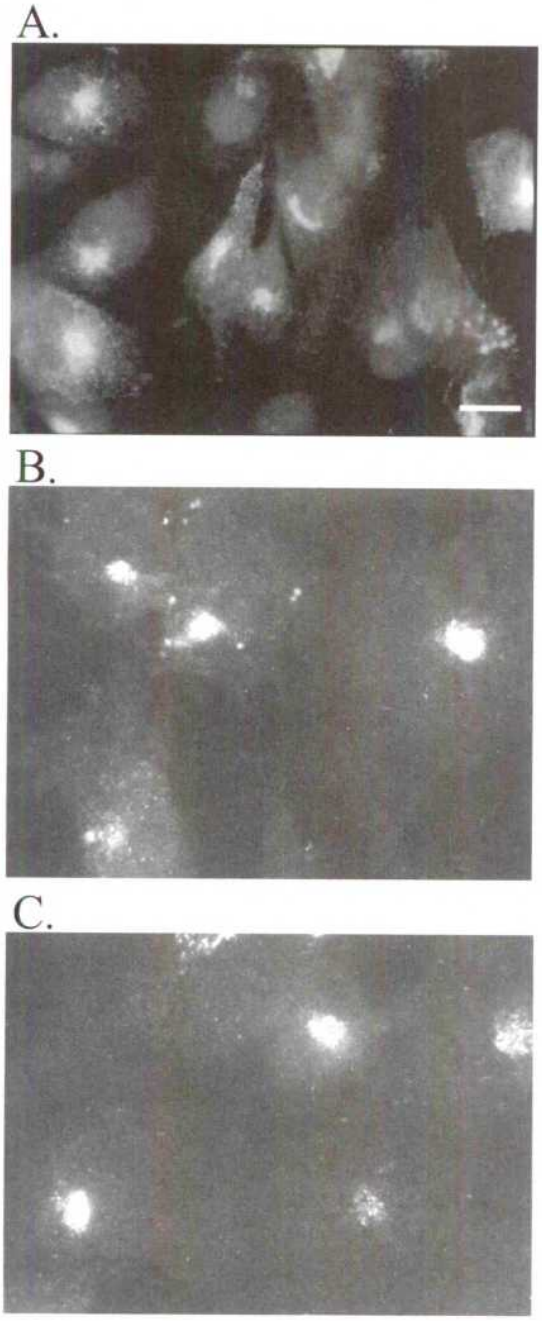

Fig. 3. Immunofluorescence microscopy analysis of ATP7B expressed in fibroblast cells. Transfected Menkes patient fibroblast cells expressing normal sATP7B (A), alternate sATP7B (B) or mouse Atp7b (C) were grown in basal media. The cells were fixed with 4% paraformaldehyde and permeabilised with 0.1% Triton X-100 before staining by indirect immunofluorescence with affinity-purified antibodies raised against normal sATP7B (1:100), alternate sATP7B (1:50) and mouse Atp7b (1:50). Primary antibodies were detected using affinity-purified FITC-conjugated sheep antibodies to rabbit IgG. Bar: 10 μm (× 60 objective).

weight bands observed with the anti-alternate sATP7B antibody probably represent non-specific background, since they also were visible in the untransfected samples following an increased exposure time (data not shown).

3.2. Intracellular distribution of sheep ATP7B in Menkes patient and control fibroblasts

Immunofluorescence analysis was used to confirm expression and assess the intracellular distribution of each form of the sheep ATP7B protein in Menkes patient and control fibroblasts. In basal medium, each form of sheep ATP7B was similarly localised to the perinuclear region of transfected Menkes patient cells (Fig. 3A,B). A similar distribution was observed for each form of sATP7B in the control cell line (data not shown). This localisation of sATP7B was similar to that of murine Atp7b when expressed in the same cell line (Fig. 3C) and was consistent with previous studies, which demonstrated that sheep, mouse and human ATP7B is located at the TGN [17,18,22].

3.3. Copper accumulation and retention studies in transfected fibroblasts

Copper transport studies were carried out to determine if the sheep ATP7B proteins could correct the abnormal copper accumulation of Menkes patient fibroblasts, as was reported for mouse and human ATP7B [18,23]. Following a 24-h incubation in media containing approximately 0.5 μM ^{64}Cu, the parental Me32a cell line accumulated approximately three-fold more copper than the control GM847 cell line (Table 1). The copper accumulation in Me32a cells transfected with either form of sheep ATP7B was significantly reduced in comparison to the non-transfected Me32a cells and was comparable to, or lower than the copper accumulation of the control cell line GM847 (Table 1). Further, the copper accumulation of normal fibroblasts (GM847) transfected with either form of sheep ATP7B

Table 1

Copper accumulation and efflux by fibroblasts expressing sATP7B

Cell line	24 h Copper accumulation (pmol Cu/μg protein, mean ± S.D.)	Percentage copper retention (mean ± S.D.)
Me32a	0.65 ± 0.04	76 ± 1.2
GM847	0.25 ± 0.01	49 ± 1.7
Me32a–pNORM	0.2 ± 0.03	36 ± 1.5
Me32a–pALT	0.006 ± 0.001	30 ± 2
GM847–pNORM	0.006 ± 0.001	34 ± 3.5
GM847–pALT	0.006 ± 0.001	32 ± 1.7

Transfected and untransfected Menkes patient fibroblast (Me32a) and control fibroblast cells (GM847) were grown in ^{64}Cu-containing media for 24 h and the amount of copper accumulated in the cells was determined. The percentage copper retention represents the amount of copper retained in the cells after a further 8 h incubation in media lacking ^{64}Cu, expressed as a percentage of the amount of ^{64}Cu accumulated in cells during the 24-h period. The samples are: Me32a, untransfected Menkes patient fibroblasts; GM847, untransfected normal fibroblasts; Me32a–pNORM, Me32a transfected with pNORM; Me32a–pALT, Me32a transfected with pALT; GM847–pNORM, GM847 transfected with pNORM; GM847–pALT, GM847 transfected with pALT. Values represent the mean ± S.D. of three independent measurements.

was significantly reduced in comparison to the non-transfected GM847 cells. After a further 8-h incubation in medium without ^{64}Cu, the amount of radioactive copper retained within the cells was determined, to give an indirect measure of copper efflux. The results demonstrated that Menkes or normal cells transfected with either form of sheep ATP7B retained significantly less copper than the parental cell lines (Table 1), suggesting that sheep ATP7B corrected the copper transport defect in these cells by enhancing copper efflux, rather than by decreasing copper uptake.

4. Discussion

The results of previous studies of the structure and expression of *sATP7B* suggested that the gene could encode a functional protein [16]. Similarly, in vitro analysis of sATP7B demonstrated interaction with the copper chaperone SAH [24] and copper-induced trafficking in Chinese hamster ovary (CHO) cells [17], properties required for correct functioning of ATP7B. However, copper homeostasis mediated by ATP7B is proposed to involve copper transport across cellular membranes in addition to ligand-induced trafficking of the molecule when copper is in excess [8]. In this study, we demonstrated that the two forms of sATP7B are functional copper-transporting molecules.

A diagnostic feature of Menkes disease is that cultured cells derived from an affected individual hyper-accumulate copper [25,26]. The functional complementation of the copper accumulation phenotype of Menkes patient fibroblasts by ATP7A and ATP7B has demonstrated that these cells constitute a valuable model for analysis of the copper transport function of CPx-type ATPases [18,23]. RNA and protein analysis confirmed the successful transfection and expression of cDNA-derived sATP7B in Menkes and control fibroblasts. A significant level of sATP7B mRNA and protein was detected in transfected fibroblasts, but not in untransfected cells (Figs. 1 and 2).

Immunofluorescence analysis was used to assess the intracellular distribution of sATP7B in the Menkes and control fibroblasts and demonstrated that the two proteins were similarly localised within the cell. In basal medium, each form of sATP7B was localised to the perinuclear region in transfected Menkes patient cells (Fig. 3). This localisation was observed in cells expressing different levels of the recombinant protein and was consistent with previous studies which indicated that ATP7B is located at the TGN in basal copper conditions [17,22]. The addition of 200 μM copper to the medium did not appear to significantly alter the localisation of sATP7B in the transfected cells (data not shown). A similar apparent lack of response to copper was observed when the cDNA-derived murine Atp7b protein was expressed in the Me32a and GM847 cell lines [18], suggesting that normal trafficking of ATP7B does not take place in these fibroblast cells. In contrast, a significant proportion of human ATP7B expressed in *mottled* mice fibroblasts and HepG2 cells underwent a copper-induced relocalisation to a vesicular, cytoplasmic compartment [22,23]. It is difficult to reconcile these conflicting results, but they do suggest that the cell type utilised for in vitro studies may significantly influence the extent to which copper-induced relocalisation of ATP7B is detectable.

Copper transport studies demonstrated that both forms of sATP7B corrected the copper accumulation of Menkes patient fibroblasts. Following a 24-h incubation in medium containing trace amounts of ^{64}Cu, the parental Me32a cell line accumulated approximately three-fold more copper than the control GM847 cell line (Table 1). The copper accumulation in Me32a cells transfected with either form of sATP7B was reduced in comparison to the non-transfected Me32a cells and was comparable to the copper accumulation of the control GM847 cell line. The reduced copper accumulation of the Me32a cells transfected with pALT, in comparison to pNORM, might have been due to higher expression levels of alternate sATP7B, as suggested by the intensity of the protected fragment in the RPA analysis (Fig. 1). Alternatively, the difference may be the result of a larger proportion of the G418-resistant population expressing pALT in comparison to pNORM. Similarly, the copper accumulation of normal fibroblasts (GM847) transfected with either form of sATP7B was significantly reduced in comparison to the non-transfected GM847 cells. These observations were analogous to those reported for functional murine and human ATP7B expressed in Menkes and mottled fibroblasts [18,23]. After a further 8 h incubation in medium without ^{64}Cu, the amount of radioactive copper retained within the cells was determined, to give an indirect measure of copper efflux. The transfected Me32a and GM847 cells expressing sATP7B retained similar proportions of copper as the non-transfected control cell line, and this was substantially less than the non-transfected Me32a cell line (Table 1). This result suggests that sATP7B corrected the copper transport defect in these cells by enhancing copper efflux, rather than by decreasing copper uptake. These results demonstrate that both forms of sATP7B are functional copper-transport proteins that can reduce the intracellular copper content of fibroblasts by enhancing copper efflux. Taken together with our previous studies examining the structure, expression and localisation of sATP7B [16,17,24], these results suggest that the copper toxicosis syndrome of sheep may not result from defects in the copper transport or localisation of either form of sheep *ATP7B*. It is important to note that these studies utilised a non-polarised cell culture system and the sheep ATP7B proteins may have properties distinct from other mammalian copper ATPases that are only apparent in hepatic cells which have an apical (canalicular) and basolateral surface. Furthermore, the specific identity of the compartment to which ATP7B traffics in response to elevated copper is yet to be determined. If this is found to be different for the two forms of sATP7B, it may suggest distinct roles for these proteins in copper homeostasis. Future studies will be directed toward comparison of the sheep proteins in a polarised hepatic cell line.

Acknowledgements

We thank Rosario Reyes for invaluable technical support and express our sincere appreciation for the advice and support given by our laboratory colleagues. This work was supported in part by the National Health and Medical Research Council of Australia (NH and MRC), the Australian Research Council and the International Copper Association. S.L. is supported by an NH&MRC R. Douglas Wright Award.

References

[1] C.D. Vulpe, S. Packman, Annu. Rev. Nutr. 15 (1995) 293–322.

[2] M.C. Linder, Biochemistry of Copper, Plenum, New York, 1991.

[3] D.M. Danks, in: C.R. Scriver, A.L. Beaudet, W.M. Sly, D. Valle (Eds.), The Metabolic and Molecular Basis of Inherited Disease, vol. 1, 7th ed., McGraw-Hill, New York, 1995, pp. 2211–2235.

[4] P.C. Bull, G.R. Thomas, J.M. Rommens, J.R. Forbes, D.C. Cox, Nat. Genet. 5 (1993) 327–337.

[5] R.E. Tanzi, K. Petrukhin, I. Chernov, J.L. Pellequer, W. Wasco, B. Ross, D.M. Romano, E. Parano, L. Pavone, L.M. Brzustowicz, M. Devoto, J. Peppercorn, A.I. Bush, I. Sternlieb, M. Pirastu, J.F. Gusella, O. Evgrafov, G.K. Penchaszadeh, B. Honig, I.S. Edelman, M.B. Soares, I.H. Scheinberg, T.C. Gilliam, Nat. Genet. 5 (1993) 344–350.

[6] Y. Yamaguchi, M.E. Heiny, J.D. Gitlin, Biochem. Biophys. Res. Commun. 197 (1993) 271–277.

[7] K. Terada, T. Nakako, X.-L. Yang, M. Iida, N. Aiba, Y. Minamiya, M. Nakai, T. Sakaki, N. Miura, T. Sugiyama, J. Biol. Chem. 373 (1998) 1815–1820.

[8] M. Schaefer, R.G. Hopkins, M.L. Failla, J.D. Gitlin, Am. J. Physiol. 276 (1999) G639–G646.

[9] H. Roelofsen, H. Wolters, M.J. Van Luyn, N. Miura, F. Kuipers, R.J. Vonk, Gastroenterology 119 (2000) 782–793.

[10] M. Harada, S. Sakisaka, T. Kawaguchi, R. Kimura, E. Taniguchi, H. Koga, S. Hanada, S. Baba, K. Furuta, R. Kumashiro, T. Sugiyama, M. Sata, Biochem. Biophys. Res. Commun. 275 (2000) 871–876.

[11] J.R. Forbes, D.W. Cox, Hum. Mol. Genet. 9 (2000) 1927–1935.

[12] E.J. Underwood, Trace Elements in Human and Animal Nutrition, 4th ed., Academic Press, New York, 1977.

[13] K.M. Weber, R.C. Boston, D.D. Leaver, Aust. J. Agric. Res. 31 (1980) 773–790.

[14] J. Ishmael, C. Gopinath, J.M. Howell, Res. Vet. Sci. 12 (1971) 358–366.

[15] J.M. Howell, J.M. Gawthorne, Copper in Animals and Man, CRC Press, Boca Raton, 1987.

[16] P.J. Lockhart, S.A. Wilcox, H.-H. Dahl, J.F.B. Mercer, Biochim. Biophys. Acta 1491 (2000) 229–239.

[17] P.J. Lockhart, J.F.B. Mercer, Eur. J. Cell Biol. 80 (2001) 349–357.

[18] S. La Fontaine, S.D. Firth, J. Camakaris, A. Englezou, M.B. Theophilos, M.J. Petris, M. Howie, P.J. Lockhart, M. Greenough, H. Brooks, R.R. Reddel, J.F. Mercer, J. Biol. Chem. 273 (1998) 31375–31380.

[19] J. Camakaris, M.J. Petris, L. Bailey, P. Shen, P. Lockhart, T.W. Glover, C.L. Barcroft, J. Patton, J.F.B. Mercer, Hum. Mol. Genet. 4 (1995) 2117–2123.

[20] M.J. Petris, J.F.B. Mercer, J.G. Culvenor, P. Lockhart, P.A. Gleeson, J. Camakaris, EMBO 15 (1996) 6084–6095.

[21] M.M. Bradford, Anal. Biochem. 72 (1976) 248–254.

[22] I.H. Hung, M. Suzuki, Y. Yamaguchi, D.S. Yuan, R.D. Klausner, J.D. Gitlin, J. Biol. Chem. 272 (1997) 21461–21466.

[23] A.S. Payne, E.J. Kelly, J.D. Gitlin, Proc. Natl. Acad. Sci. U. S. A. 95 (1998) 10854–10859.

[24] P.J. Lockhart, J.F.B. Mercer, Biochim. Biophys. Acta 1490 (2000) 11–20.

[25] T.J. Goka, R.E. Stevenson, P.M. Hefferan, R.R. Howell, Proc. Nat. Acad. Sci. U. S. A. 73 (1976) 604–606.

[26] N. Horn, Lancet 1 (1976) 1156–1158.

Information for Contributors can be found in http://www.bba-direct.com

This journal is in the *ADONIS Service*, whereby copies of individual articles can be printed out from CD-ROM on request. An explanatory leaflet can be obtained by writing to: ADONIS B.V., P.O. Box 993, 1000 AZ Amsterdam, The Netherlands. Or you can contact ADONIS by e-mail : info@adonis.nl or visit the website at www.adonis.nl

OASIS: **O**n-line **A**rticle **S**tatus **I**nformation **S**ystem **(http://www.elsevier.com/oasis)**
Authors of articles which are currently in production at Elsevier can obtain the following information on the status of their article:

- general production status (in preparation, in proof, in issue)
- date of publication and offprints dispatch date
- issue, volume and page numbers

This journal is a part of **ContentsDirect**, the ***free*** alerting service which sends tables of contents by e-mail for Elsevier Science books and journals. You can register for **ContentsDirect** online at: **http://contentsdirect.elsevier.com**

BIOCHIMICA ET BIOPHYSICA ACTA
MOLECULAR BASIS OF DISEASE

VOL. 1588 NO. 2 20 NOVEMBER 2002

(Abstracted/Indexed in: Biological Abstracts - Chemical Abstract - Current Contents / Life Sciences - EMBASE/Excerpta Medica - Index Chemicus - Index Medicus / MEDLINE - ***Science Citation Index - Sociedad Iberoamericana de Información Científica (SIIC) Data Bases)***

CONTENTS

Regular papers

Lack of association between the uncoupling protein-2 Ala55Val gene polymorphism and phenotypic features of the Metabolic Syndrome
R. Rosmond, C. Bouchard and P. Björntorp (Sweden, USA) 103

Expression and functional analysis of rat P23, a gut hormone-inducible isoform of trypsin, reveals its resistance to proteinaceous trypsin inhibitors
S.-I. Fukuoka and C.M. Nyaruhucha (Japan) 106

Protective effect of D-glucose, L-leucine and fetal calf serum against oxidative stress in neonatal pancreatic islets
L.F. Stoppiglia, T.A. Nogueira, A.R. Leite, E.M. Carneiro and A.C. Boschero (Brazil) 113

Functional characterization of *PCCA* mutations causing propionic acidemia
S. Clavero, M.A. Martínez, B. Pérez, C. Pérez-Cerdá, M. Ugarte and L.R. Desviat (Spain) 119

Age-related changes in cartilage endogenous osteogenic protein-1 (OP-1)
S. Chubinskaya, B. Kumar, C. Merrihew, K. Heretis, D.C. Rueger and K.E. Kuettner (USA) 126

The peak height ratio of *S*-sulfonated transthyretin and other oxidized isoforms as a marker for molybdenum cofactor deficiency, measured by electrospray ionization mass spectrometry
M. Kishikawa, J.O. Sass, N. Sakura, T. Nakanishi, A. Shimizu and M. Yoshioka (Japan, Austria) 135

Selective inhibition of CYP27A1 and of chenodeoxycholic acid synthesis in cholestatic hamster liver
Y. Matsuzaki, B. Bouscarel, T. Ikegami, A. Honda, M. Doy, S. Ceryak, S. Fukushima, S. Yoshida, J. Shoda and N. Tanaka (Japan, USA) 139

The role of oxidative stress in the ochratoxin A-mediated toxicity in proximal tubular cells
G.J. Schaaf, S.M. Nijmeijer, R.F.M. Maas, P. Roestenberg, E.M. De Groene and J. Fink-Gremmels (The Netherlands) 149

Time-course of oxygen free radical production in acinar cells during acute pancreatitis induced by pancreatic duct obstruction
A. Urunuela, S. Sevillano, A.M. De la Mano, M.A. Manso, A. Orfao and I. De Dios (Spain) 159

Human colon adenocarcinoma is associated with specific post-translational modifications of versican and decorin
A.D. Theocharis (Greece) 165

Effect of imipramine on 1-methyl-4-phenylpyridinium ion-induced hydroxyl radical generation in rat striatum
T. Obata and T. Egashira (Japan) 173

Differential expression of protein kinase C isoenzymes related to high nitric oxide synthase activity in a T lymphoma cell line
G. Gorelik, M.L. Barreiro Arcos, A.J. Klecha and G.A. Cremaschi (Argentina) 179

Correction of the copper transport defect of Menkes patient fibroblasts by expression of two forms of the sheep Wilson ATPase
P.J. Lockhart, S. La Fontaine, S.D. Firth, M. Greenough, J. Camakaris and J.F.B. Mercer (Australia) 189

Also available on
SCIENCE DIRECT®
www.sciencedirect.com

0925-4439(20021120)1588:2;1-R

ALSO AVAILABLE ONLINE:

http://www.bba-direct.com

BIOCHIMICA ET BIOPHYSICA ACTA

BBA

MOLECULAR BASIS OF DISEASE

ELSEVIER

BIOCHIMICA ET BIOPHYSICA ACTA

BBA

Founded in 1947 by H.G.K. Westenbrink
Managing Editor, 1947-1964

HONORARY EXECUTIVE EDITOR
E.C. Slater (Southampton, UK)

EDITOR-IN-CHIEF: Peter C. van der Vliet (Utrecht, The Netherlands)

EXECUTIVE EDITORS:

Bioenergetics (including *Reviews on Bioenergetics*): **P.R. Rich** (London, UK) and **M. Wikström** (Helsinki, Finland)
Biomembranes (including *Reviews on Biomembranes*): **A.G. Lee** (Southampton, UK) and **P.L. Yeagle** (Storrs, CT, USA)
Molecular and Cell Biology of Lipids: **D.E. Vance** (Edmonton, AB, Canada) and **F. Spener** (Münster, Germany)
Proteins and Proteomics: **A. Fink** (Santa Cruz, CA, USA), **Y. Lindqvist** (Stockholm, Sweden) and **F. Lottspeich** (Martinsried bei München, Germany)
Molecular Cell Research: **E.L.F. Holzbaur** (Philadelphia, PA, USA) and **N. Pfanner** (Freiburg, Germany)
Gene Structure and Expression: **C.L. Peterson** (Worcester, MA, USA) and **P.C. van der Vliet** (Utrecht, The Netherlands)
Molecular Basis of Disease: **P.E. Fraser** (Toronto, ON, Canada) and **J.R. Riordan** (Scottsdale, AZ, USA)
General Subjects: **M. Fukuda** (La Jolla, CA, USA), **C.G. Gahmberg** (Helsinki, Finland) and **S.S. Krag** (Baltimore, MD, USA)
Reviews on Cancer: **N.C. Jones** (Manchester, UK) and **G. Evan** (San Francisco, CA, USA)

Publication information: *Biochimica et Biophysica Acta* full subscription for 2002 consists of Volumes 1553-1603. Subscription prices are available upon request from the Publisher or from the Regional Sales Office nearest you or from this journal's website (http://www.bba-direct.com). Further information is available on this journal and other Elsevier Science products through Elsevier's website (http://www.elsevier.com). Subscription are accepted on a prepaid basis only and are entered on a calendar year basis. Issues are sent by standard mail (surface within Europe, air delivery outside Europe). Priority rates are available upon request. Claims for missing issues should be made within six months of the date of dispatch.

BBA – Publication schedule for 2002
BBA is published according to a volume-numbering scheme that embraces all section of the journal.
Full subscription: 51 volumes

BIO-ENERGETICS including Reviews on Bioenergetics	BIO-MEMBRANES including Reviews on Biomembranes	GENE STRUCTURE AND EXPRESSION	GENERAL SUBJECTS	MOLECULAR AND CELL BIOLOGY OF LIPIDS	MOLECULAR BASIS OF DISEASE	MOLECULAR CELL RESEARCH	PROTEINS AND PROTEOMICS	REVIEWS ON CANCER
5 volumes:	10 volumes:	6 volumes:	6 volumes:	6 volumes:	3 volumes:	5 volumes:	8 volumes:	2 volumes:
1553–1557 (15 issues)	1558–1567 (20 issues)	1574–1579 (18 issues)	1568–1573 (18 issues)	1580–1585 (18 issues)	1586–1588 (9 issues)	1589–1593 (15 issues)	1594–1601 (16 issues)	1602–1603 (4 issues)

Submission
Authors should submit their manuscripts (four copies) to one of the appropriate Executive Editors at either of the following Editorial Offices:
BBA Editorial Secretariat, P.O. Box 1345, 1000 BH Amsterdam, The Netherlands. Tel.: (+31) 20 4853510; Fax: (+31) 20 4853506; E-mail: bba@elsevier.com
BBA Editorial Secretariat, 275 Washington Street, Newton, MA 02458, USA. Tel.: (+1) (617) 630-2244; Fax: (+1) (617) 630-2245; E-mail: us_bba@elsevier.com

Although most published *Review* articles are submitted on the invitation of the Executive Editor(s), authors of suitable (mini) reviews may also submit their work unsolicited (four copies) by sending their paper(s) to one of the Executive Editors of the appropriate section.

For detailed instructions on the preparation of electronic artwork, consult the Author Gateway from Elsevier Science at http://authors.elsevier.com

Author enquiries
For enquiries relating to the submission of articles (including electronic submission where available) please visit the Author Gateway from Elsevier Science at http://www.authors.elsevier.com. The Author Gateway also provides the facility to track accepted articles and set up e-mail alerts to inform you of when an article's status has changed, as well as detailed artwork guidelines copyright information, frequently asked questions and more.

Contact details for questions arising after acceptance of an article, especially those relating to proofs, are provided after registration of an article for publication.

Authors in Japan please note: Upon request, Elsevier Science K.K. will provide authors with a list of people who can check and improve the English of their paper (*before submission*). Please contact our Tokyo office: Elsevier Science K.K., 9-15 Higashi-Azabu 1-chome, Minato-ku, Tokyo 106-0044; Tel.: (03)-5561-5032; Fax: (03)- 5561-5045.

Colour figures
Colour figures are published at the author's expense: € 340 for the first page and € 227 each subsequent page, excluding sales tax.

BBA has no page charges and 25 offprints are provided free to the corresponding author of each published paper.

10.03.03.

BIOCHIMICA ET BIOPHYSICA ACTA

BBA

VOL. 1588
(2002)

BIOCHIMICA ET BIOPHYSICA ACTA

Founded in 1947 by H.G.K. Westenbrink, Managing Editor, 1947-1964

HONORARY EXECUTIVE EDITOR: E.C. Slater (Southampton, UK)

EDITOR-IN-CHIEF: Peter C. van der Vliet (Utrecht, The Netherlands)

EXECUTIVE EDITORS:

Bioenergetics (including *Reviews on Bioenergetics*): **P.R. Rich** (London, UK) and **M. Wikström** (Helsinki, Finland)
Biomembranes (including *Reviews on Biomembranes*): **A.G. Lee** (Southampton, UK) and **P.L. Yeagle** (Storrs, CT, US
Molecular and Cell Biology of Lipids: **D.E. Vance** (Edmonton, AB, Canada) and **F. Spener** (Münster, Germany)
Proteins and Proteomics: **A. Fink** (Santa Cruz, CA, USA), **Y. Lindqvist** (Stockholm, Sweden) and **F. Lottspeich** (Martinsried bei München, Germany)
Molecular Cell Research: **E.L.F. Holzbaur** (Philadelphia, PA, USA) and **N. Pfanner** (Freiburg, Germany)
Gene Structure and Expression: **C.L. Peterson** (Worcester, MA, USA) and **P.C. van der Vliet** (Utrecht, The Netherlands)
Molecular Basis of Disease: **P.E. Fraser** (Toronto, ON, Canada) and **J.R. Riordan** (Scottsdale, AZ, USA)
General Subjects: **M. Fukuda** (La Jolla, CA, USA), **C.G. Gahmberg** (Helsinki, Finland) and **S.S. Krag** (Baltimore, MD, US
Reviews on Cancer: **N.C. Jones** (Manchester, UK) and **G. Evan** (San Francisco, CA, USA)

A.D. Albert (Storrs, CT, USA)
J.M. Allen (London, UK)
T.M. Allen (Edmonton, AB, Canada)
K. Altendorf (Osnabrück, Germany)
T. Arakawa (Thousand Oaks, CA, USA)
P.A. Baeuerle (Martinsried, Germany)
C. Balny (Montpellier, France)
R. Beckmann (Berlin, Germany)
U. Beisiegel (Hamburg, Germany)
D.J. Benos (Birmingham, AL, USA)
P. Bernardi (Padua, Italy)
R. Bernards (Amsterdam, The Netherlands)
A.J.M. Berns (Amsterdam, The Netherlands)
H. Beug (Vienna, Austria)
C.L. Bevins (Cleveland, OH, USA)
C. Birchmeier (Berlin, Germany)
T. Bisseling (Wageningen, The Netherlands)
C. Borner (Freiburg, Germany)
J.L. Bos (Utrecht, The Netherlands)
I. Braakman (Utrecht, The Netherlands)
U. Brandt (Frankfurt am Main, Germany)
R.J. Bridges (Pittsburgh, PA, USA)
C.L. Brooks, III (La Jolla, CA, USA)
D.D. Busath (Provo, UT, USA)
M. Busslinger (Vienna, Austria)
F. Carrière (Marseille, France)
J.E. Celis (Copenhagen, Denmark)
G. Cevc (München, Germany)
H. Chap (Toulouse, France)
A.H. Chishti (Boston, MA, USA)
R. Cogdell (Glasgow, UK)
N.H. Colburn (Frederick, MD, USA)
H.W. Cook (Halifax, NS, Canada)
P.F. Cook (Norman, OK, USA)
C. Cooper (Colchester, UK)
W.A. Cramer (West Lafayette, IN, USA)
B. de Crombrugghe (Houston, TX, USA)
R.D. Cummings (Oklahoma, OK, USA)
D.T. Curiel (Birmingham, AL, USA)
D.A. Day (Canberra, Australia)
J.P. Dekker (Amsterdam, The Netherlands)
B. De Strooper (Leuven, Belgium)
B. Desvergne (Lausanne, Switzerland)
G. Dickson (Egham, UK)
K.T. Douglas (Manchester, UK)
G.F. Draetta (Milan, Italy)
H.B. Dunford (Edmonton, AB, Canada)
D.H. Ellison (Portland, OR, USA)
T. Endo (Tokyo, Japan)
R.M. Epand (Hamilton, ON, Canada)
J. Fidy (Budapest, Hungary).
A. Fontana (Padua, Italy)
M. Fontecave (Grenoble, France)
J.-C. Fruchart (Lille, France)
J.T. Gallagher (Manchester, UK)
G. Geba (New Haven, CT, USA)
R. Geyer (Giessen, Germany)
T.E. Golde (Jacksonville, FL, USA)
F.M. Goñi (Bilbao, Spain)
Y. Goto (Osaka, Japan)
L.I. Grossman (Detroit, MI, USA)
A.P. Halestrap (Bristol, UK)
T.D. Heath (Madison, WI, USA)
J. Heberle (Jülich, Germany)
D. Hoekstra (Groningen, The Netherlands)
J. Horwitz (Los Angeles, CA, USA)
R.A. Houghten (San Diego, CA, USA)
G. Hübner (Halle/Saale, Germany)
R.C. Hughes (Mill Hill, UK)
S.W. Hui (Buffalo, NY, USA)
T. Hunter (La Jolla, CA, USA)
M. Ikeda-Saito (Cleveland, OH, USA)
A.N. Imbalzano (Worcester, MA, USA)
T. Iwatsubo (Tokyo, Japan)
H.R. de Jonge (Rotterdam, The Netherlands)
R.L. Juliano (Chapel Hill, NC, USA)
W. Junge (Osnebrück, Germany)
C. Kaltschmidt (Witten, Germany)
S.E. Kearsey (Oxford, UK)
T. Kiefhaber (Basel, Switzerland)
J.A. Killian (Utrecht, The Netherlands)
K. Kimata (Aichi, Japan)
K.H. Kinne (Dortmund, Germany)
M. Kiso (Gifu, Japan)
W.N. Konings (Groningen, The Netherlands)
J.M. Kooter (Amsterdam, The Netherlands)
I. Kudo (Tokyo, Japan)
K. Kuwajima (Tokyo, Japan)
W. Lamers (Amsterdam, The Netherlands)
T. Levade (Toulouse, France)
R. Lührmann (Göttingen, Germany)
G.I. Makhatadze (Lubbock, TX, USA)
B. Mannervik (Uppsala, Sweden)
W. Mäntele (Frankfurt am Main, Germany)
C.J. Marshall (London, UK)
W.F. Marzluff (Chapel Hill, NC, USA)
F. McCormick (San Francisco, CA, USA)
R.N. McElhaney (Edmonton, AB, Canada)
M.G. McNamee (Davis, CA, USA)
R. Mendelsohn (Newark, NJ, USA)
J. Moody (Plymouth, UK)
C.P. Moran Jr. (Atlanta, GA, USA)
O.G. Mouritsen (Odense, Denmark)
S. Nagata (Osaka, Japan)
P.E. Nielsen (Copenhagen, Denmark)
K.H. Nierhaus (Berlin, Germany)
E.A. Nigg (Martinsried bei München, Germany)
B. Nordén (Gothenburg, Sweden)
N. Oppenheimer (San Francisco, CA, USA)
J.F. Oram (Seattle, WA, USA)
N. Osheroff (Nashville, TN, USA)
R.P. Oude Elferink (Amsterdam, The Netherlands)
E. Padan (Jerusalem, Israel)
S. Parthasarathy (Atlanta, GA, USA)
M. Peters-Golden (Ann Arbor, MI, USA)
D.W. Pettigrew (College Station, TX, USA)
J. Philo (Thousand Oaks, CA, USA)
J.J.H.H.M. de Pont (Nijmegen, The Netherlands)
T. Pozzan (Padua, Italy)
N.C. Price (Glasgow, UK)
U.R. Rapp (Würzburg, Germany)
N. Ridgway (Halifax, NS, Canada)
J.-L. Rigaud (Paris, France)
G.T. Robillard (Groningen, The Netherlands)
S. Rose-John (Kiel, Germany)
E. Rozengurt (Los Angeles, CA, USA)
F. Sachs (Buffalo, NY, USA)
M.S.P. Sansom (Oxford, UK)
S. Schuldiner (Jerusalem, Israel)
H.H. Schulz (New York, NY, USA)
K. Schulze-Osthoff (Münster, Germany)
J.M. Seddon (London, UK)
R. Serrano (Valencia, Spain)
D.L. Severson (Calgary, AB, Canada)
T. Shimizu (Tokyo, Japan)
H. Sjöström (Copenhagen, Denmark)
S.T. Smale (Los Angeles, CA, USA)
S. Spiegel (Washington, DC, USA)
W.D. Stein (Jerusalem, Israel)
B. Svensson (Copenhagen, Denmark)
G. Tigyi (Memphis, TN, USA)
K.F. Tipton (Dublin, Ireland)
J. Travis (Athens, GA, USA)
L.-C. Tsui (Toronto, ON, Canada)
B. Tümmler (Hannover, Germany)
G. van Meer (Amsterdam, The Netherlands)
M.H. Vos (Palaiseau, France)
K.H. Vousden (Frederick, MD, USA)
E. Wahle (Halle/Saale, Germany)
M.J. Waring (Cambridge, UK)
D. Wemmer (Berkeley, CA, USA)
R. Wetzel (Knoxville, TN, USA)
G.R. Willsky (Buffalo, NY, USA)
D.C. Wilton (Southampton, UK)
P. Workman (Sutton, UK)
R.F.A. Zwaal (Maastricht, The Netherlands)

BIOCHIMICA ET BIOPHYSICA ACTA

BBA

INTERNATIONAL JOURNAL OF BIOCHEMISTRY, BIOPHYSICS
AND MOLECULAR BIOLOGY

VOL. 1588 (3) (2002)

MOLECULAR BASIS OF DISEASE

Executive Editors: P.E. Fraser (Toronto, Canada) and
J.R. Riordan (Scottsdale, AZ, USA)

Section Editors:
C.L. Bevins
R.J. Bridges
B. De Strooper
G. Dickson
D.H. Ellison
G. Geba
T.E. Golde
R.A. Houghten
T. Iwatsubo
H.R. de Jonge
R.P. Oude Elferink
B. Tümmler

ELSEVIER
Amsterdam – London – New York – Oxford – Paris – Shannon – Tokyo

© 2002 Elsevier Science B.V. All rights reserved.

This journal and the individual contributions contained in it are protected under copyright laws by Elsevier Science B.V., and the following terms and conditions apply to their use:

Photocopying
Single photocopies of single articles may be made for personal use as allowed by national copyright laws. Permission of the Publisher and the payment of a fee is required for all other photocopying, including multiple or systematic copying, copying for advertising or promotional purposes, resale, and all forms of document delivery. Special rates are available for educational institutions that wish to make photocopies for non-profit educational classroom use.

Permissions may be sought directly from Elsevier Science via their homepage (http://www.elsevier.com) by selecting "Customer support" and then "Permissions". Alternatively you can send an e-mail to: permissions@elsevier.co.uk, or fax to: (+44) 1865 853333.

In the USA, users may clear permissions and make payments through the Copyright Clearance Center, Inc., 222 Rosewood Drive, Danvers, MA 01923, USA; phone: (+1) (978) 7508400, fax: (+1) (978) 7504744, and in the UK through the Copyright Licensing Agency Rapid Clearance Service (CLARCS), 90 Tottenham Court Road, London W1P 0LP, UK; phone: (+44) 20 7631 5555; fax: (+44) 20 7631 5500. Other countries may have a local reprographic rights agency for payments.

Derivative Works
Subscribers may reproduce tables of contents of prepare lists of articles including abstracts for internal circulation within their institutions. Permission of the Publisher is required for resale or distribution outside the institution.
Permission of the Publisher is required for all other derivative works, including compilation and translations.

Electronic Storage or Usage
Permission of the Publisher is required to store or use electronically any material contained in this journal, including any article or part of an article.

Except as outlined above, no part of this publication may be reproduced, stored in a retrieval system of transmitted in any form of by any means, electronic, mechanical, photocopying, recording or otherwise, without prior written permission of the Publisher.

Address permission requests to: Elsevier Science Global Rights Department, at the mail, fax and e-mail addresses noted above.

Notice
No responsibility is assumed by the Publisher for any injury and/or damage to persons or property as a matter of products liability, negligence or otherwise, or from any use or operation of any methods, products, instructions or ideas contained in the material herein. Because of the rapid advances in the medical sciences, in particular, independent verification of diagnoses and drug dosages should be made.

Although all advertising material is expected to conform to ethical (medical) standards, inclusion in this publication does not constitute a guarantee or endorsement of the quality or value of such product or of the claims made of it by its manufacturer.

Advertising Information
Advertising orders and enquiries can be sent to: **USA, Canada and South America**: Mr Tino DeCarlo, The Advertising Department, Elsevier Science Inc., 360 Park Avenue South, New York, NY 10010-1710, USA; phone: (+1) (212) 633 3815; fax: (+1) (212) 633 3820; e-mail: t.decarlo@elsevier.com. **Japan**: The Advertising Department, Elsevier Science K.K., 9-15 Higashi-Azabu 1-chome, Minato-ku, Tokyo 106-0044, Japan; phone: (+81) (3) 5561 5033; fax: (+81) (3) 5561 5047. **Europe and ROW**: Commercial Sales Department, Elsevier Science Ltd., The Boulevard, Langford Lane, Kidlington, Oxford, OX5 1GB, UK; phone: (+44) 1865 843016; fax: (+44) 1865 843976; e-mail: media@elsevier.com

Orders, claims, and product enquiries: please contact the Customer Support Department at the Regional Sales Office nearest you:
New York: Elsevier Science, PO Box 945, New York, NY 10159-0945, USA; phone: (+1) (212) 633 3730 [toll free number for North American customers: 1-888-4ES-INFO (437-4636)]; fax: (+1) (212) 633 3680; e-mail: usinfo-f@elsevier.com
Amsterdam: Elsevier Science, PO Box 211, 1000 AE Amsterdam, The Netherlands; phone: (+31) 20 4853757; fax: (+31) 20 4853432; e-mail: nlinfo-f@elsevier.com
Tokyo: Elsevier Science, 9-15 Higashi-Azabu 1-chome, Minato-ku, Tokyo 106-0044, Japan; phone: (+81) (3) 5561 5033; fax: (+81) (3) 5561 5047; e-mail: info@elsevier.co.jp
Singapore: Elsevier Science, 3 Killiney Road, #08-01 Winsland House I, Singapore 239519; phone: (+65) 6349 0200; fax: (+65) 6733 1510; e-mail: asiainfo@elsevier.com.sg
Rio de Janeiro: Elsevier Science, Rua Sete de Setembro 111/16 Andar, 20050-002 Centro, Rio de Janeiro-RJ, Brazil; phone: (+55) (21) 509 5340; fax: (+55) (21) 507 1991; e-mail: elsevier@campus.com.br [Note (Latin America): for orders, claims and help desk information, please contact the Regional Sales Office in New York as listed above]

USA mailing notice: *Biochimica et Biophysica Acta (Molecular Basis of Disease)* (ISSN 0925–4439) is published monthly except in February, May and September by Elsevier Science B.V. (P.O. Box 211, 1000 AE Amsterdam, The Netherlands).
Annual subscription price in the USA US$ 1165.00 (valid in North, Central and South America), including air speed delivery. Second class Periodicals postage paid at Jamaica, NY 11431.
USA POSTMASTER: Send address changes to *Biochimica et Biophysica Acta (Molecular Basis of Disease)*, Publications Expediting, Inc., 200 Meacham Avenue, Elmont, NY 11003.
AIRFREIGHT AND MAILING in the USA by Publications Expediting, Inc., 200 Meacham Avenue, Elmont, NY 11003.

Printed in The Netherlands
④ The paper used in this publication meets the requirements of ANSI/NISO Z39.48-1992 (Permanence of Paper).

ELSEVIER

Biochimica et Biophysica Acta 1588 (2002) 195–202

BIOCHIMICA ET BIOPHYSICA ACTA

BBA

www.bba-direct.com

Quantitative evaluation of expression of iron-metabolism genes in ceruloplasmin-deficient mice

Kanji Yamamoto[a,b], Kunihiro Yoshida[c,*], Yuko Miyagoe[b], Aki Ishikawa[d], Kazunori Hanaoka[d], Shozo Nomoto[e], Kazuma Kaneko[a], Shu-ichi Ikeda[a], Shin'ichi Takeda[b]

[a] *The Third Department of Medicine, Shinshu University School of Medicine, Matsumoto 390-8621, Japan*

[b] *Department of Molecular Therapy, National Institute of Neuroscience, National Center of Neurology and Psychiatry, Kodaira, Tokyo 187-8502, Japan*

[c] *Division of Clinical and Molecular Genetics, Shinshu University Hospital, Asahi 3-1-1, Matsumoto 390-8621, Japan*

[d] *Department of Biosciences, School of Science, Kitasato University, Sagamihara, Kanagawa 228-8555, Japan*

[e] *Department of Laboratory Medicine, Shinshu University School of Medicine, Matsumoto 390-8621, Japan*

Received 22 March 2002; received in revised form 23 July 2002; accepted 25 July 2002

Abstract

Aceruloplasminemia is an autosomal recessive disorder caused by mutations in the ceruloplasmin (*CP*) gene, and is characterized by a unique combination of neurovisceral iron overload and iron deficiency anemia. We generated CP-deficient ($CP^{-/-}$) mice to investigate the functional involvement of CP in iron metabolism. The mice showed a marked iron overload in the liver and mild iron deficiency anemia. We examined the expression of iron-metabolism genes in the duodenum and liver using TaqMan RT-PCR. The divalent metal transporter 1 (*DMT1*), ferroportin 1 (*FPN1*), and hephaestin (*HEPH*) genes were not up-regulated in the duodenum from $CP^{-/-}$ mice. These data suggest that the mechanism of hepatic iron overload in aceruloplasminemia is quite different from that in hemochromatoses and atransferrinemia. In the liver, $CP^{-/-}$ mice showed no increase of gene expression for *DMT1* and transferrin receptors (*TFR* and *TFR2*), indicating that none of the known pathways of iron uptake is activated in hepatocytes of $CP^{-/-}$ mice. This result supports the hypothesis that CP mainly acts to release iron from cells in the liver.

© 2002 Elsevier Science B.V. All rights reserved.

Keywords: Ceruloplasmin; Iron overload; Divalent metal transporter 1; Ferroportin 1; Hephaestin; Transferrin receptor

1. Introduction

Aceruloplasminemia is an iron-overloading disorder caused by mutations in the ceruloplasmin (*CP*) gene, and is clinically characterized by diabetes mellitus, retinal degeneration, mild iron deficiency anemia, and neurological symptoms [1–4]. Laboratory findings include deficient serum CP, decreased serum iron, normal or decreased transferrin saturation rate, and increased serum ferritin. Marked hemosiderosis is seen in the liver, pancreas, and brain in affected individuals [4]. These findings strongly support that CP is involved in iron metabolism through its ferroxidase activity. However, the precise role of CP in iron homeostasis and mechanism of iron overload in aceruloplasminemia have remained unclear.

Iron is an element essential for a wide spectrum of biologic functions, whereas excess iron is toxic because of its insolubility at physiologic pH and its ability to generate reactive oxygen species. Iron homeostasis is maintained by the strict regulation of iron absorption from the intestine, rather than iron excretion [5]. Recently, several important molecules involved in iron transport have been identified by molecular genetic analyses of patients and animals with abnormal iron metabolism. They include hereditary hemochromatosis protein (HFE) [6], transferrin receptors (TFR [7] and TRF2 [8,9]), divalent metal transporter 1 [10,11] (DMT1, previously named NRAMP2 and DCT1), ferroportin 1 [12] (FPN1, also called IREG1 [13] or MTP1 [14]), and a CP homologue, hephaestin (HEPH) [15]. *DMT1*, *FPN1*, and *HEPH* are highly expressed in the intestine (mainly in the duodenum) and are considered to be a brush border transporter of ferrous iron, a basolateral iron exporter, and a basolateral multi-copper ferroxidase, respectively. The identification of these iron-metabolism proteins has contributed to enlarging our knowledge of iron homeostasis.

To elucidate iron kinetics in a CP-deficient state, we generated genetically CP-deficient ($CP^{-/-}$) mice. The mice

---

* Corresponding author. Tel.: +81-263-37-3215; fax: +81-263-37-3216.
E-mail address: kyoshida@hsp.md.shinshu-u.ac.jp (K. Yoshida).

0925-4439/02/$ - see front matter © 2002 Elsevier Science B.V. All rights reserved.

PII: S0925-4439(02)00165-5

were clinically well up to at least the age of 60 weeks, but showed a significant increase in iron storage in the liver not later than age 20 weeks. We examined the expression of iron-metabolism genes, *DMT1*, *FPN1*, *HEPH*, *TFR*, and *TFR2*, in the duodenum and liver of $CP^{-/-}$ mice to investigate iron kinetics in a CP-deficient state and to deduce functional involvement of CP in iron absorption and transport. We discuss the iron-overloading mechanism in aceruloplasminemia compared with other hereditary iron-overloading disorders.

2. Materials and methods

2.1. Generation of $CP^{-/-}$ mice

We generated a *CP* null allele by deletion of essential sequence from exon 1, as follows. A 6.5-kb mouse genomic DNA fragment containing exon 1 of the *CP* gene was isolated from a 129/SvJ mouse genomic library (Stratagene) and subcloned into Bluescript II SK+ vector (Stratagene). A pMC1neo polyA cassette (Stratagene) was then inserted between two *Bpu*1102I sites (+16 and −650, +1 denotes the translation start site) in the reverse orientation, followed by the insertion of the 1.8-kb herpes simplex virus thymidine kinase gene into the 3′-end of the genomic fragment (Fig. 1A). It was linearized by cleavage at the unique *Not*I site, before transfection by electroporation into E14 embryonic stem (ES) cells obtained from the inbred mouse strain 129/SvJ. Positive clones were selected by challenging the cultured ES cells with G418 (300 μg/ml) and ganciclovir (2 μM). Surviving colonies were then screened for the expected homologous recombination by PCR using LA *Taq* polymerase (TaKaRa) and primers; primer 1 (*CP* intron sequence outside the targeting vector): 5′-TAA GAT GCT GGA GAA GCC ACA GGA GAC TGT AG-3′, and primer

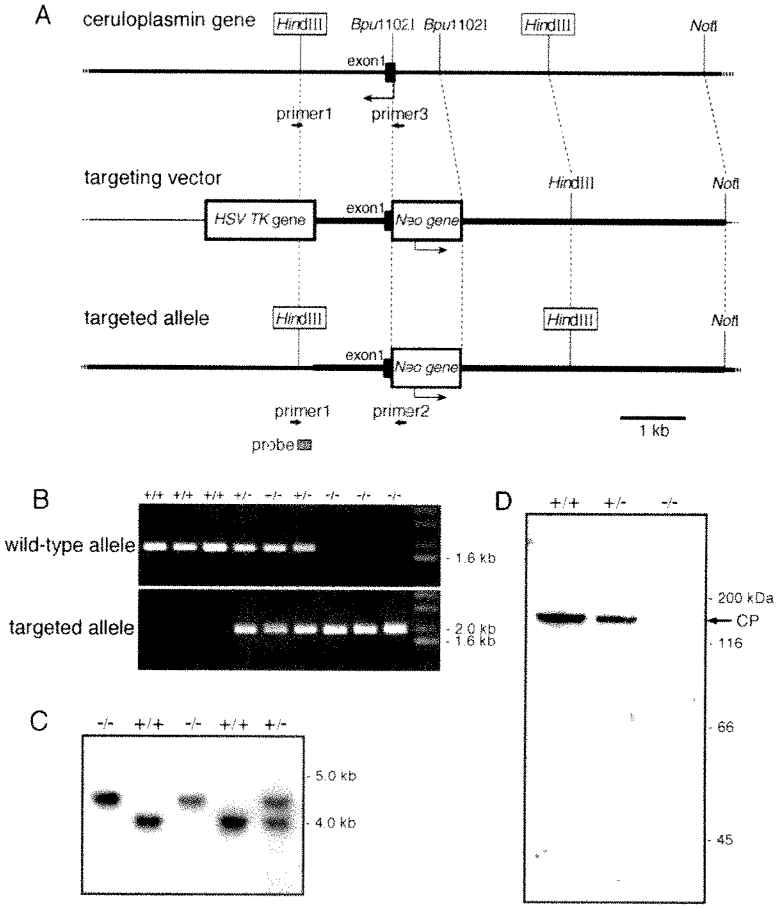

Fig. 1. Generation of $CP^{-/-}$ mice. (A) A schematic diagram of the *CP* gene (top), the *CP*-mutant targeting vector (middle), and the predicted structure of the *CP* null allele after homologous recombination (bottom). The restriction sites of *Bpu*1102I, *Hin*dIII, and *Not*I are shown. The *Hin*dIII-restriction sites (rectangles) generate the 4.0- and 4.4-kb restriction fragments diagnostic for wild-type and properly targeted alleles, respectively, as shown in (C). The *Neo* (neomycin resistance) and *HSV TK* (herpes simplex virus thymidine kinase) genes refer to the positive and negative selective markers, respectively. PCR primers and 3′ external probe are indicated. (B) PCR analysis for identification of the mouse genotype. The PCR product generated with primers 1 and 3 indicates the wild-type allele and that with primers 1 and 2 indicates the targeted allele. (C) Southern analysis of *Hin*dIII digest of genomic DNA isolated from mouse tail cuts. The bands of 4.4 and of 4.0 kb indicate mutant and wild-type *CP* alleles, respectively. (D) Immunoblot analysis of mouse serum with polyclonal anti-human CP antibody. CP protein is completely absent in serum from $CP^{-/-}$ mice.

2 (*neo* cassette sequence): 5′-CTG CGT GTT CGA ATT CGC CAA TGA CAA GAC GCT GG-3′. The PCR results were confirmed by Southern blot analysis of *Eco*RI- or *Hin*dIII-digested genomic DNA using the external probe (Fig. 1A). Probing with the *neo* gene confirmed the presence of a single mutant allele. Targeted ES cells containing one disrupted *CP* allele were injected into C57BL/6 blastocysts as described previously [16] and chimeric mice were derived from two independent clones. Heterozygous F_1 offspring from the ES clones were independently intercrossed to generate F_2 homozygous mice on the BALB/c strain background. To identify the genotype of the offspring, genomic DNA from the tails was amplified by PCR using oligonucleotide primers; primers 1 and 3 (sequence from exon 1): 5′-GCA ACA TTA AAT TGT GTC AGC CAA GC-3′ for wild-type allele amplification and primers 1 and 2 for targeted allele amplification (Fig. 1B). Southern blot analysis of *Hin*dIII-digested genomic DNA with the 3′ external probe that yielded a 4.0-kb band in the wild-type allele and a 4.4-kb band in the targeted allele was also performed to confirm the PCR results (Fig. 1C).

Mice fed ad libitum on a normal chow diet (containing 122 μg/g of iron and 77.2 μg/g of copper) were kept on a 12:12 light/dark cycle. Body weight was recorded once every 4 weeks.

2.2. Immunoblot analysis and measurement of serum ferroxidase activity

Liver tissue was homogenized and boiled for 6 min in a buffer containing 10% SDS, 70 mM Tris–HCl (pH 6.7), 10 mM EDTA, and 5% β-mercaptoethanol. Serum was added to an equal volume of buffer containing 4% SDS, 100 mM Tris–HCl (pH 6.7), and 10% β-mercaptoethanol, and boiled for 6 min. The liver or serum protein at 20 μg/lane was then separated on a 7.5% SDS-polyacrylamide gel and electrotransferred onto a polyvinylidene difluoride membrane (Millipore). The blot was then incubated with a rabbit polyclonal anti-human CP antibody (DAKO, A0031) at a 1:500 dilution. We had previously confirmed that this antibody could clearly detect both the secreted form and the glycosylphosphatidylinositol-anchored form [17] of mouse CP. Immune complexes on the blot were detected with a 1:3000 dilution of horseradish peroxidase-conjugated goat anti-rabbit IgG (BIO-RAD) and ECL Western blotting detection reagents (Amersham Pharmacia Biotech). Serum ferroxidase activity was measured using Fe^{2+} ions as the substrate, as described previously [18].

2.3. Histopathology

Under anesthesia with diethylether, organs were removed from 20-, 40- and 60-week-old $CP^{-/-}$ mice and $CP^{+/+}$ littermates used as controls. Tissues were fixed in 10% formalin, embedded in paraffin, sectioned, and mounted on slides for staining with hematoxylin and eosin. Other sets of slides were stained with potassium ferrocyanide (Berlin blue) to detect ferric iron in tissues, and counterstained with nuclear fast red.

2.4. Measurement of metal content

$CP^{-/-}$ mice and $CP^{+/+}$ littermates were anesthetized with diethylether and systemically perfused with saline from the left ventricle after thoracotomy to remove whole blood from organs. Iron and copper contents of tissues were analyzed as described previously [19]. Briefly, the tissues were collected into pre-weighed glass tube, reweighed to calculate the weight of wet specimen, then lyophilized and weighed again to calculate the weight of dried specimen. After sixfold wet tissue weight of nitric acid was added, the specimens were heated at 80 °C for 1 to 2 days, and dissolved with 2 ml of 50 mM hydrochloric acid under ultrasonic agitation at 50 °C. The supernatant of the centrifuged samples was analyzed by atomic absorption spectrophotometer after appropriate dilution with water. The iron and copper contents (μg/g of dry tissue) were calculated from the results of this analysis and the dilution factor. Hematological parameters and serum iron content were measured on other series of mice.

2.5. Quantitative TaqMan RT-PCR

Total RNA was isolated from tissues of 20- and 40-week-old $CP^{-/-}$ male mice and $CP^{+/+}$ male littermates using TRI Reagent (Sigma), and treated with RNase-free DNase (Stratagene). The RT reaction was performed with 1 μg of DNase-treated total RNA, random hexamers, and MMLV reverse transcriptase (Applied Biosystems) according to the manufacturer's instructions. TaqMan PCR primers and TaqMan probes used for quantification of *DMT1*, *FPN1*, *HEPH*, *TFR*, and *TFR2* cDNAs were designed using Primer Express Software (Applied Biosystems) (Table 1). The primers and probe for *DMT1* detected a total of two splice variants of *DMT1* mRNA, namely, the IRE (iron responsive element) form and the non-IRE form. These probes consist of an oligonucleotide with a 5′-reporter fluorescent dye (6-carboxyfluorescein) and a 3′-quencher dye (6-carboxy-tetramethyl-rhodamine). Each cDNA was amplified by PCR using each primer set and duodenum cDNA as the template for *DMT1*, *FPN1*, *HEPH*, and *TFR*, or liver cDNA for *TFR2*. The products were inserted into the pCR II vector (Invitrogen) and cloned. The serially diluted plasmids containing each cDNA were used as the standards for amplification. PCR reaction mixture was prepared according to the manufacturer's instructions and the amplification was carried out in MicroAmp optical 96-well reaction plates (Applied Biosystems) in the ABI Prism 7700 Sequence Detection System (Applied Biosystems). Each reaction was performed in triplicate. The cDNA quantities were normalized to the amount of glyceraldehyde-3-phosphate dehydrogenase (*GAPDH*) cDNA, which was quantified

Table 1
Sequence of TaqMan RT-PCR primers and probe used for quantification of gene expression

DMT1	primers	5′-AAC CAA CAA GCA GGT GGT TGA-3′ 5′-CTT TGT AGA TGT CCA CAG CCA GAG T-3′
	probe	5′-CCA TGC TGA CCT CTT TCC CAG TGA CAA C-3′
FPN1	primers	5′-AAG GAT TGA CCA GCT AAC CAA CA-3′ 5′-CAG CCA ATG ACT GGA GAA CCA-3′
	probe	5′-CCA TGG CTG TCG GCC AGA TTA TGA CAT-3′
HEPH	primers	5′-GCC TGG GCA CAG AGA CTG AT-3′ 5′-AAG GTG TGA GGA AAG AGC ATG AC-3′
	probe	5′-TTC GAG GGC AAC ACT GTG CAG CTT C-3′
TFR	primers	5′-CAG AAA GTT CCT CAG CTC AAC CA-3′ 5′-GTT CAA TTC AAC GTC ATG GGT AAG-3′
	probe	5′-AGC CAC TTC CGC TGC TGT ACG AAC C-3′
TFR2	primers	5′-AGC TGG GAC GGA GGT GAC TT-3′ 5′-TCC AGG CTC ACG TAC ACA ACA-3′
	probe	5′-AGG GCT ACC TCA GCG TGC TAC ACC TCA-3′

using Rodent GAPDH Control Reagents (VIC probe, Applied Biosystems).

2.6. Statistical analysis

Data were expressed as means ± standard deviations. We used the unpaired Student's t test to evaluate the differences in hematological parameters, serum and tissue metal content, serum ferroxidase activity, and gene expression level on quantitative TaqMan RT-PCR between $CP^{+/+}$ and $CP^{-/-}$ mice.

3. Results

3.1. Clinical phenotype of $CP^{-/-}$ mice

Immunoblot analysis of serum and liver showed that neither the 132-kDa full-length nor smaller sized truncated CP protein was detected in $CP^{-/-}$ mice (Fig. 1D), confirming that targeted disruption of the *CP* gene was completely attained. Serum ferroxidase activity was reduced in $CP^{+/-}$ mice [302.0 ± 85.6 vs. 523.5 ± 139.4 U/l ($P=0.002$); $CP^{+/-}$: $N=5$, $CP^{+/+}$: $N=11$] and negligible in $CP^{-/-}$ mice [53.7 ± 31.1 vs. 523.5 ± 139.4 U/l ($P=3.7\times10^{-7}$); $CP^{-/-}$: $N=16$, $CP^{+/+}$: $N=11$].

$CP^{+/-}$ and $CP^{-/-}$ mice appeared normal at birth. Of 228 offspring genotyped, 58 (25.4%) were wild-type ($CP^{+/+}$), 115 (50.4%) heterozygous for the *CP* null allele ($CP^{+/-}$), and 55 (24.1%) homozygous ($CP^{-/-}$). $CP^{-/-}$ mice developed and grew normally. They survived into their 60–80th weeks after birth. $CP^{-/-}$ mice did have mild microcytic anemia [12.6 ± 1.0 vs. 15.9 ± 0.3 g/dl ($P=0.0043$), 48.5 ± 4.0 vs. 55.8 ± 1.9 fl ($P=0.028$), and 28.5 ± 0.6 vs. 29.2 ± 0.4 g/dl ($P=0.097$) of hemoglobin content, mean corpuscular volume, and mean corpuscular hemoglobin concentration, respectively; 20-week-old mice; $CP^{-/-}$: $N=4$, $CP^{+/+}$: $N=5$] and lower serum iron content (Table 2).

3.2. Hepatic iron overload in $CP^{-/-}$ mice

Hematoxylin and eosin staining of the brain, duodenum, heart, kidney, liver, lung, pancreas, and retina of 20-, 40-, and 60-week-old $CP^{-/-}$ mice derived from two independent clones revealed no structural abnormalities (data not shown). Iron staining (Berlin blue staining) of the liver from $CP^{-/-}$ mice showed increased iron deposition (Fig. 2B), while little iron deposition was seen in the liver of $CP^{+/+}$ mice (Fig. 2A). Iron deposition was observed in the cytoplasm of both hepatocytes and Kupffer cells, not only at the periportal areas but also around the central veins (Fig. 2C). Iron staining of the brain, duodenum (Fig. 2D), heart, kidney, lung, pancreas, and retina showed no evidence of abnormal iron deposition up to at least the age of 60 weeks.

Although there was no significant difference in iron content between $CP^{+/+}$ and $CP^{-/-}$ mice in the cerebrum and duodenum, hepatic iron content of $CP^{-/-}$ mice was significantly (~ 3.4-fold) higher than that of $CP^{+/+}$ mice at both 20 and 40 weeks of age (Table 2). We also evaluated copper content of these organs, but no significant differences were found between $CP^{+/+}$ and $CP^{-/-}$ mice (data not shown).

3.3. Expression of iron-metabolism genes

The expression of iron-metabolism genes was measured by means of quantitative TaqMan RT-PCR. *DMT1*, *FPN1*, and *HEPH* mRNA were evaluated in the duodenum, which is the major site of iron absorption, and *DMT1*, *FPN1*, *HEPH*,

Table 2
Serum and tissue iron content in $CP^{+/+}$ and $CP^{-/-}$ mice

Age	Genotype	Serum iron [μg/dl]	Tissue iron [μg/g of dry tissue]		
			Cerebrum	Duodenum	Liver
20 w	$CP^{+/+}$	194.7 ± 18.0 (3)	70.6 ± 13.0 (7)	219.9 ± 124.2 (7)	419.1 ± 169.0 (7)
	$CP^{-/-}$	102.0 ± 32.5** (6)	73.3 ± 11.2 (7)	221.9 ± 123.7 (7)	1425.7 ± 557.2** (7)
40 w	$CP^{+/+}$	205.8 ± 31.8 (5)	72.0 ± 7.1 (6)	188.4 ± 19.3 (5)	539.0 ± 99.1 (6)
	$CP^{-/-}$	90 ± 58.3** (6)	76.2 ± 7.3 (5)	169.3 ± 30.7 (4)	1822.0 ± 903.1* (5)

The numbers of examined mice are shown in parenthesis. *$P<0.05$, **$P<0.01$ compared with the corresponding data of $CP^{+/+}$ mice.

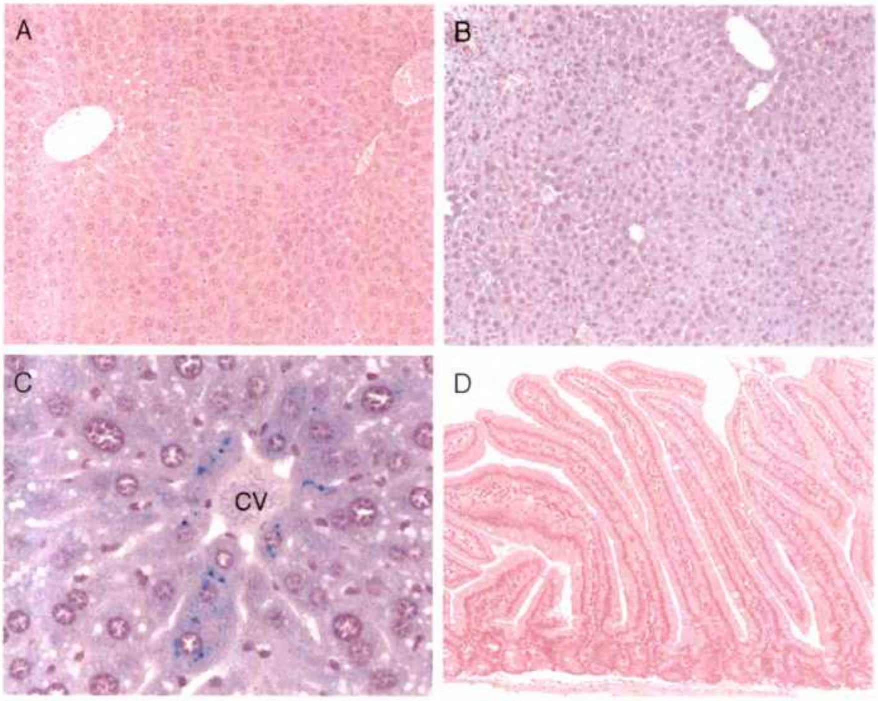

Fig. 2. Berlin blue iron stain counterstained with nuclear fast red of organs from 40-week-old mice. Liver sections of $CP^{+/+}$ (A) and $CP^{-/-}$ mice (B, C) and duodenum section of $CP^{-/-}$ mice (D) are shown. In the $CP^{-/-}$ mouse, markedly increased iron deposition is seen in the liver, where the cytoarchitecture is well preserved (B). Iron deposition was observed in the cytoplasm of both hepatocytes and Kupffer cells, not only at the periportal areas but also around the central veins (CV) (C). In the $CP^{-/-}$ mouse, neither structural abnormality nor abnormal iron deposition is seen in the duodenum (D).

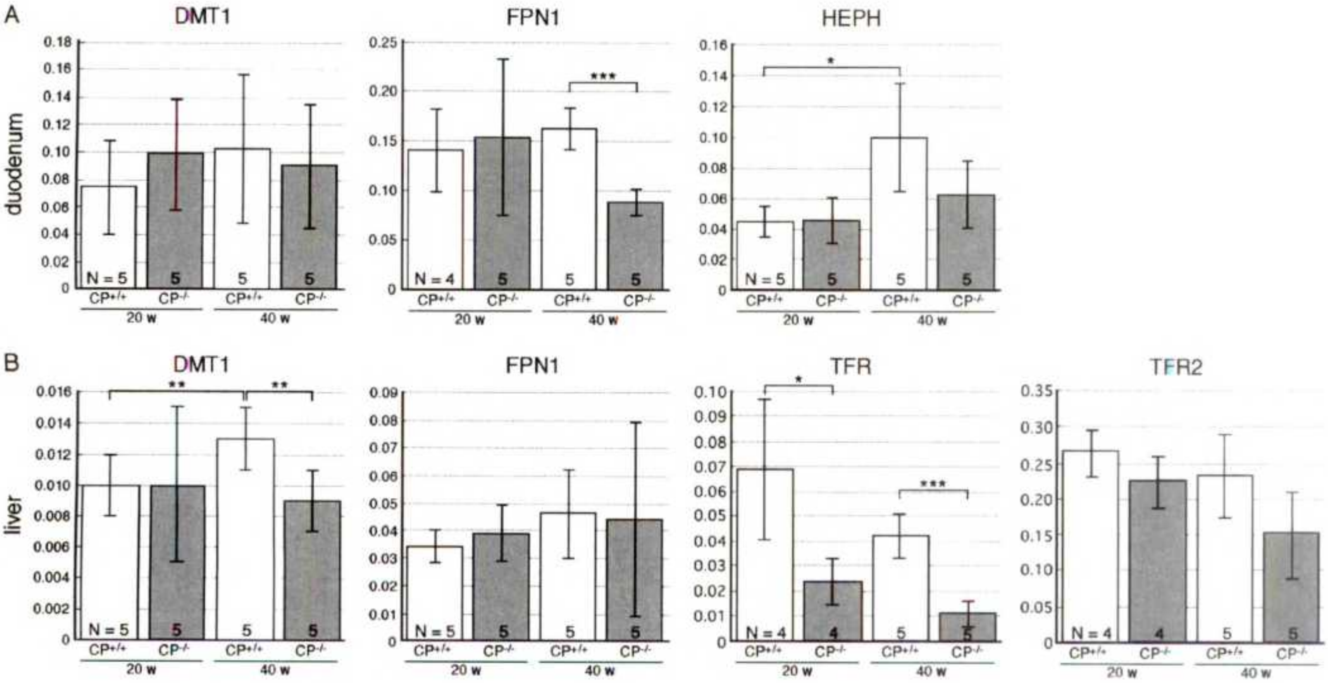

Fig. 3. Quantification of iron-metabolism gene expression by TaqMan RT-PCR. *DMT1*, *FPN1*, and *HEPH* mRNA were evaluated in duodenum (A) and *DMT1*, *FPN1*, *HEPH*, *TFR*, and *TFR2* mRNA were quantified in liver (B). Total RNA extracted from tissues of 20- and 40-week-old $CP^{+/+}$ and $CP^{-/-}$ male mice was used for reverse transcription and PCR amplification. The amount of each gene transcript relative to the *GAPDH* transcript is shown as mean ± standard deviations. $^{*}P<0.05$; $^{**}P<0.01$; $^{***}P<0.001$. Because *HEPH* gene expression was very low in the liver from both $CP^{+/+}$ and $CP^{-/-}$ mice, those results are not shown.

TFR, and *TFR2* mRNA in the liver. In the duodenum (Fig. 3A), there was no difference in the expression of the *DMT1*, *FPN1*, and *HEPH* genes between $CP^{+/+}$ and $CP^{-/-}$ mice at 20 weeks of age. Although the expression of these three genes had a tendency to increase with age in $CP^{+/+}$ mice, expression of the *DMT1* and *FPN1* genes tended to decrease and the *HEPH* gene showed a reduced rate of increase in $CP^{-/-}$ mice. There was a significant difference in the level of expression of the *FPN1* gene between $CP^{+/+}$ and $CP^{-/-}$ mice at 40 weeks of age ($P=0.0004$).

In the liver (Fig. 3B), expression of the *DMT1* gene in $CP^{-/-}$ mice was reduced in comparison with $CP^{+/+}$ mice at 40 weeks of age ($P=0.0085$). The levels of *FPN1* gene expression in the liver revealed no difference between $CP^{+/+}$ and $CP^{-/-}$ mice. CP deficiency significantly lowered *TFR* gene expression in the liver at both 20 ($P=0.044$) and 40 ($P=0.0004$) weeks of age. TaqMan RT-PCR showed a tendency towards lower *TFR2* gene expression in the liver from $CP^{-/-}$ than $CP^{+/+}$ mice, but this did not reach significance ($P=0.142$, 0.059 at 20 and 40 weeks of age, respectively). The expression levels of the *HEPH* gene were very low in the liver of both $CP^{+/+}$ and $CP^{-/-}$ mice at the age of either 20 or 40 weeks (data not shown).

4. Discussion

In the present study, we have generated $CP^{-/-}$ mice and investigated tissue iron storage and expression of iron-metabolism genes in the duodenum and liver. These $CP^{-/-}$ mice showed an iron overload in the liver in combination with hypoferremia and mild microcytic anemia, suggesting that abnormal iron kinetics in patients with aceruloplasminemia is faithfully modeled here. On the other hand, we found no evidence of abnormal iron overload in other organs including brain and pancreas up to the age of 60 weeks, where marked iron overload is observed in affected individuals [4]. Short life span and poor cerebral vascularization may be the reasons for absence of iron overload in the brain of $CP^{-/-}$ mice. Harris et al. [20] generated $CP^{-/-}$ mice independently, and found increased iron content in the liver and spleen, but not either hypoferremia or anemia in their $CP^{-/-}$ mice. The difference in hematological behavior is likely to have arisen due to targeting different strains of the mice; we generated $CP^{-/-}$ mice in the BALB/c strain background, whereas they used black Swiss–Webster mice [20].

Investigating the expression of the genes involved in iron transport in iron-depleting or iron-overloading conditions, although it is not a direct analysis of iron transport, may provide insights important for a better understanding of iron metabolism. Several studies have demonstrated that duodenal *DMT1* and *FPN1* expression is increased in patients with *HFE*-associated [13,21,22] or non-*HFE*-associated [21] hemochromatosis, *HFE*-deficient mice [23,24], hypotransferrinemic (homozygous *hpx*) mice [13,25], and iron-deficient states [11,13,14,26,27]. By contrast, up-regulation of the *DMT1* and *FPN1* genes was not found in the duodenum of $CP^{-/-}$ mice. This supports a previous ferrokinetic study by Harris et al. [20], which showed no difference in the rate of intestinal iron absorption between their $CP^{-/-}$ mice and control mice. The profile of duodenal *DMT1* expression in $CP^{-/-}$ mice is consistent with the manner of regulation through IRE/IRP (iron regulatory protein) system [28] since *DMT1* transcripts have IREs in the 3′-untranslated region (3′-UTR) and CP deficiency does not affect iron content in enterocytes. *FPN1* transcripts contain IRE in the 5′-UTR, but the modes of regulation other than those involving the IRE/IRP system have been speculated for duodenal *FPN1* expression [13,14]. Reduction of duodenal *FPN1* expression at the age of 40 weeks in $CP^{-/-}$ mice may be explained by that the iron store regulator acts more strongly than the erythropoietic regulator, although these regulators have not been clearly identified [5]. The profile of duodenal *DMT1* and *FPN1* expression in $CP^{-/-}$ mice suggests that the mechanism responsible for hepatic iron overload in aceruloplasminemia is quite different from that in hereditary hemochromatoses and atransferrinemia.

What mechanism functions in the process of tissue iron overload in CP-deficient state is open to discussion. To date, controversial results have accumulated on the role for CP in iron transport via its ferroxidase activity. Classical studies suggested that CP promotes iron efflux from the storage cells to plasma in vivo [29,30]. Some in vitro experiments were in favor of this possibility [31,32]. In addition, studies on human aceruloplasminemia and $CP^{-/-}$ mice strongly suggested an iron-releasing function of CP [1,20]. On the other hand, Fox et al. [33,34] and Qian et al. [35] demonstrated that CP has a role in iron uptake rather iron release. The different results might be partly due to experimental conditions, therefore, we are still awaiting a final answer on the role for CP in iron metabolism. The expression profile of iron-metabolism genes in the iron-overloaded liver of $CP^{-/-}$ mice may provide a clue to solve this intriguing issue. Hepatocytes have a transport system to take up both transferrin (TF)-bound and non-TF-bound iron [36]. TFR and TFR2 take TF-bound iron in hepatocytes, and DMT1 is involved in both TF-bound and non-TF-bound iron uptake [27,36]. In our study, hepatic *DMT1*, *TFR*, and *TFR2* expression in $CP^{-/-}$ mice was down-regulated in the face of enlarged iron store. The significant suppression of *DMT1* and *TFR* expression is in reasonable agreement with the regulation via IRE/IRP system because *DMT1* and *TFR* transcripts, but not *TFR2* transcripts [37], have IREs in 3′-UTR and are regulated directly by tissue iron status. More importantly, these results indicate that no known pathway of iron uptake is activated in hepatocytes in $CP^{-/-}$ mice. Thus, it is likely that CP mainly acts to release iron from hepatocytes and that its deficiency directly causes iron overload, although continued TFR2-mediated iron uptake may also contribute to hepatic iron accumulation. If this is not the case, we should presume that unknown CP-independent pathways of iron uptake will be activated in hepatocytes in a CP-deficient state.

Lastly, we should discuss on duodenal *HEPH* expression briefly. FPN1 requires an auxiliary ferroxidase activity to mediate iron release across the basolateral membrane of enterocytes. In a classical schema, CP was considered as a major ferroxidase in this compartment [38]. Harris et al. [20] showed that the rate of intestinal iron absorption was not affected in $CP^{-/-}$ mice. On the other hand, sex-linked anemia (*sla*) mice, which bear a mutation of the *HEPH* gene, have a block in intestinal iron transport and show moderate to severe microcytic hypochromic anemia [15]. Furthermore, we found no increase in duodenal *HEPH* expression in $CP^{-/-}$ mice. Taken together, it is concluded that CP is less critical than HEPH for intestinal iron absorption.

We have attempted to understand the iron-overloading mechanism in a CP-deficient state by evaluating the expression of iron-metabolism genes. Based on our data, aceruloplasminemia is characterized by a specific iron-overloading mechanism different from other disorders such as hereditary hemochromatosis and atransferrinemia. Further examination using each animal model may promote a better understanding of the pathogenesis peculiar to each iron metabolism disorder and may facilitate development of therapeutic approaches appropriate for each pathological condition.

Acknowledgements

The authors would like to thank S. Kameya for technical instruction and K. Kobayashi and K. Tsukita for their technical assistance. This work was supported by a Grant-in-Aid for Scientific Research (C) 12670599 from the Ministry of Education, Science, Sports, and Culture of Japan.

References

[1] J.D. Gitlin, Aceruloplasminemia, Pediatr. Res. 44 (1998) 271–276.

[2] K. Yoshida, K. Furihata, S. Takeda, A. Nakamura, K. Yamamoto, H. Morita, S. Hiyamuta, S. Ikeda, N. Shimizu, N. Yanagisawa, A mutation in the ceruloplasmin gene is associated with systemic hemosiderosis in humans, Nat. Genet. 9 (1995) 267–272.

[3] Z.L. Harris, Y. Takahashi, H. Miyajima, M. Serizawa, R.T. MacGillivray, J.D. Gitlin, Aceruloplasminemia: molecular characterization of this disorder of iron metabolism, Proc. Natl. Acad. Sci. U. S. A. 92 (1995) 2539–2543.

[4] H. Morita, S. Ikeda, K. Yamamoto, S. Morita, K. Yoshida, S. Nomoto, M. Kato, N. Yanagisawa, Hereditary ceruloplasmin deficiency with hemosiderosis: a clinicopathological study of a Japanese family, Ann. Neurol. 37 (1995) 646–656.

[5] C.N. Roy, C.A. Enns, Iron homeostasis: new tales from the crypt, Blood 96 (2000) 4020–4027.

[6] J.N. Feder, A. Gnirke, W. Thomas, Z. Tsuchihashi, D.A. Ruddy, A. Basava, F. Dormishian , R. Domongo Jr., M.C. Ellis, A. Fullan, L.M. Hinton, N.L. Jones, B.E. Kimmel, G.S. Kronmal, P. Lauer, V.K. Lee, D.B. Loeb, F.A. Mapa, E. McClelland, N.C. Meyer, G.A. Mintier, N. Moeller, T. Moore, E. Morikang, C.E. Prass, L. Quintana, S.M. Starnes, R.C. Schatzman, K.J. Brunke, D.T. Drayna, N.J. Rish, B.R. Bacon, R.K. Wolff, A novel MHC class I-like gene is mutated in patients with hereditary haemochromatosis, Nat. Genet. 13 (1996) 399–408.

[7] J.E. Levy, O. Jin, Y. Fujiwara, F. Kuo, N.C. Andrews, Transferrin receptor is necessary for development of erythrocytes and the nervous system, Nat. Genet. 21 (1999) 396–399.

[8] H. Kawabata, R. Yang, T. Hirama, P.T. Vuong, S. Kawano, A.F. Gombart, H.P. Koeffler, Molecular cloning of transferrin receptor 2. A new member of the transferrin receptor-like family, J. Biol. Chem. 274 (1999) 20826–20832.

[9] C. Camaschella, A. Roetto, A. Cali, M. De Gobbi, G. Garozzo, M. Carella, N. Majorano, A. Totaro, P. Gasparini, The gene TFR2 is mutated in a new type of haemochromatosis mapping to 7q22, Nat. Genet. 25 (2000) 14–15.

[10] M.D. Fleming, C.C. Trenor III, M.A. Su, D. Foernzler, D.R. Beier, W.F. Dietrich, N.C. Andrews, Microcytic anaemia mice have a mutation in Nramp2, a candidate iron transporter gene, Nat. Genet. 16 (1997) 383–386.

[11] H. Gunshin, B. Mackenzie, U.V. Berger, Y. Gunshin, M.F. Romero, W.F. Boron, S. Nussberger, J.L. Gollan, M.A. Hediger, Cloning and characterization of a mammalian proton-coupled metal-ion transporter, Nature 388 (1997) 482–488.

[12] A. Donovan, A. Brownlie, Y. Zhou, J. Shepard, S.J. Pratt, J. Moynihan, B.H. Paw, A. Drejer, B. Barut, A. Zapata, T.C. Law, C. Brugnara, S.E. Lux, G.S. Pinkus, J.L. Pinkus, P.D. Kingsley, J. Palis, M.D. Fleming, N.C. Andrews, L.I. Zon, Positional cloning of zebrafish ferroportin1 identifies a conserved vertebrate iron exporter, Nature 403 (2000) 776–781.

[13] A.T. McKie, P. Marciani, A. Rolfs, K. Brennan, K. Wehr, D. Barrow, S. Miret, A. Bomford, T.J. Peters, F. Farzaneh, M.A. Hediger, M.W. Hentze, R.J. Simpson, A novel duodenal iron-regulated transporter, IREG1, implicated in the basolateral transfer of iron to the circulation, Mol. Cell 5 (2000) 299–309.

[14] S. Abboud, D.J. Haile, A novel mammalian iron-regulated protein involved in intracellular iron metabolism, J. Biol. Chem. 275 (2000) 19906–19912.

[15] C.D. Vulpe, Y.M. Kuo, T.L. Murphy, L. Cowley, C. Askwith, N. Libina, J. Gitschier, G.J. Anderson, Hephaestin, a ceruloplasmin homologue implicated in intestinal iron transport, is defective in the sla mouse, Nat. Genet. 21 (1999) 195–199.

[16] Y. Nabeshima, K. Hanaoka, M. Hayasaka, E. Esumi, S. Li, I. Nonaka, Y. Nabeshima, Myogenin gene disruption results in perinatal lethality because of severe muscle defect, Nature 364 (1993) 532–535.

[17] B.N. Patel, S. David, A novel glycosylphosphatidylinositol-anchored form of ceruloplasmin is expressed by mammalian astrocytes, J. Biol. Chem. 272 (1997) 20185–20190.

[18] O. Erel, Automated measurement of serum ferroxidase activity, Clin. Chem. 44 (1998) 2313–2319.

[19] S. Nomoto, A simplified method for trace metal analysis of biological materials, J. UOEH. 9 (1987) 111–122 (Suppl.).

[20] Z.L. Harris, A.P. Durley, T.K. Man, J.D. Gitlin, Targeted gene disruption reveals an essential role for ceruloplasmin in cellular iron efflux, Proc. Natl. Acad. Sci. U. S. A. 96 (1999) 10812–10817.

[21] H. Zoller, R.O. Koch, I. Theurl, P. Obrist, A. Pietrangelo, G. Montosi, D.J. Haile, W. Vogel, G. Weiss, Expression of the duodenal iron transporters divalent-metal transporter 1 and ferroportin 1 in iron deficiency and iron overload, Gastroenterology 120 (2001) 1412–1419.

[22] H. Zoller, A. Pietrangelo, W. Vogel, G. Weiss, Duodenal metal-transporter (DMT-1, NRAMP-2) expression in patients with hereditary haemochromatosis, Lancet 353 (1999) 2120–2123.

[23] R.E. Fleming, M.C. Migas, X.Y. Zhou, J. Jiang, R.S. Britton, E.M. Brunt, S. Tomatsu, A. Waheed, B.R. Bacon, W.S. Sly, Mechanism of increased iron absorption in murine model of hereditary hemochromatosis: increased duodenal expression of the iron transporter DMT1, Proc. Natl. Acad. Sci. U. S. A. 96 (1999) 3143–3148.

[24] W.J.H. Griffiths, W.S. Sly, T.M. Cox, Intestinal iron uptake determined by divalent metal transporter is enhanced in HFE-deficient mice with hemochromatosis, Gastroenterology 120 (2001) 1420–1429.

[25] F. Canonne-Hergaux, J.E. Levy, M.D. Fleming, L.K. Montross, N.C. Andrews, P. Gros, Expression of the DMT1 (NRAMP2/DCT1) iron transporter in mice with genetic iron overload disorders, Blood 97 (2001) 1138–1140.

[26] F. Canonne-Hergaux, S. Gruenheid, P. Ponka, P. Gros, Cellular and subcellular localization of the Nramp2 iron transporter in the intestinal brush border and regulation by dietary iron, Blood 93 (1999) 4406–4417.

[27] D. Trinder, P.S. Oates, C. Thomas, J. Sadleir, E.H. Morgan, Localisation of divalent metal transporter 1 (DMT1) to the microvillus membrane of rat duodenal enterocytes in iron deficiency, but to hepatocytes in iron overload, Gut 46 (2000) 270–276.

[28] H. Gunshin, C.R. Allerson, M. Polycarpou-Schwarz, A. Rofts, J.T. Rogers, F. Kishi, M.W. Hentze, T.A. Rouault, N.C. Andrews, M.A. Hediger, Iron-dependent regulation of the divalent metal ion transporter, FEBS Lett. 509 (2001) 309–316.

[29] H.A. Ragan, S. Nacht, G.R. Lee, C.R. Bishop, G.E. Cartwright, Effect of ceruloplasmin on plasma iron in copper-deficient swine, Am. J. Physiol. 217 (1969) 1320–1323.

[30] H.P. Roeser, G.R. Lee, S. Nacht, G.E. Cartwright, The role of ceruloplasmin in iron metabolism, J. Clin. Invest. 49 (1970) 2408–2417.

[31] S.P. Young, M. Fahmy, S. Golding, Ceruloplasmin, transferrin and apotransferrin facilitate iron release from human liver cells, FEBS Lett. 411 (1997) 93–96.

[32] D.R. Richardson, Role of ceruloplasmin and ascorbate in cellular iron release, J. Lab. Clin. Med. 134 (1999) 454–465.

[33] C.K. Mukhopadhyay, Z.K. Attieh, P.L. Fox, Role of ceruloplasmin in cellular iron uptake, Science 279 (1998) 714–717.

[34] Z.K. Attieh, C.K. Mukhopadhyay, V. Seshadri, N.A. Tripoulas, P.L. Fox, Ceruloplasmin ferroxidase activity stimulates cellular iron uptake by a trivalent cation-specific transport mechanism, J. Biol. Chem. 274 (1999) 1116–1123.

[35] Z.M. Qian, Y.K. Tsoi, Y. Ke, M.S. Wong, Ceruloplasmin promotes iron uptake rather than release in BT325 cells, Exp. Brain Res. 140 (2001) 369–374.

[36] N.C. Andrews, Iron homeostasis: insights from genetics and animal models, Nat. Rev., Genet. 1 (2000) 208–217.

[37] R.E. Fleming, M.C. Migas, C.C. Holden, A. Waheed, R.S. Britton, S. Tomatsu, B.R. Bacon, W.S. Sly, Transferrin receptor 2: continued expression in mouse liver in the face of iron overload and in hereditary hemochromatosis, Proc. Natl. Acad. Sci. U. S. A. 97 (2000) 2214–2219.

[38] S. Osaki, D.A. Johnson, E. Frieden, The possible significance of the ferrous oxidase activity of ceruloplasmin in normal human serum, J. Biol. Chem. 241 (1966) 2746–2751.

ELSEVIER
Biochimica et Biophysica Acta 1588 (2002) 203–209
BIOCHIMICA ET BIOPHYSICA ACTA
BBA
www.bba-direct.com

Uptake of recombinant iduronate-2-sulfatase into neuronal and glial cells in vitro

A. Daniele[a], R. Tomanin[b], G.R.D. Villani[a], F. Zacchello[b], M. Scarpa[b], P. Di Natale[a,*]

[a]*Department of Biochemistry and Medical Biotechnologies, Medical School, University of Naples Federico II, Via Pansini, 5, 80131, Naples, Italy*
[b]*Department of Pediatrics and Center for Rare Diseases, University of Padua, Padua, Italy*

Received 18 February 2002; received in revised form 29 May 2002; accepted 1 August 2002

Abstract

Mucopolysaccharidosis type II (MPS II, Hunter syndrome) is a congenital storage disorder resulting from mutations on the iduronate-2-sulfatase (IDS) gene. The disease shows variable clinical phenotypes from severe to mild with progressive neurological dysfunction. The therapeutic options for treatment of MPS II are limited and currently no specific therapies are available; the problem is further compounded by difficulties in delivering therapeutic agents to the central nervous system (CNS). In this work, as a potential treatment for this disease, the transfer of the recombinant IDS enzyme into brain cells has been studied in vitro. Two different approaches to obtain recombinant IDS have been utilized: production of the recombinant enzyme by a transfected human clone (Bosc 23 cells); production of the recombinant enzyme by adenoviral transduction of neuronal (SK-N-BE) or glial (C6) cells. Our data indicate that the transfected as well as the infected cells produce a large amount of the IDS enzyme, which is efficiently endocytosed into neuronal and glial cells through the mannose 6-phosphate (M6P) receptor system. Somatic gene therapy appears therefore to be suitable to correct IDS deficiency in brain cells.
© 2002 Elsevier Science B.V. All rights reserved.

Keywords: Mucopolysaccharidosis type II; Hunter syndrome; Iduronate-2-sulfatase; Somatic gene therapy; Neuronal and glial cells

1. Introduction

Iduronate-2-sulfatase (IDS; E.C. 3.1.6.13) is a lysosomal enzyme involved in the catabolism of the mucopolysaccharides heparan and dermatan sulfate. In humans, the inherited deficiency of this enzymatic activity results in mucopolysaccharidosis type II (MPS II, Hunter syndrome) (for review, see Ref. [1]). Patients accumulate undegraded dermatan and heparan sulfate in the lysosomes of most cell types and this accumulation, particularly within cells of the neurological system, leads to a wide spectrum of clinical phenotypes, ranging from the mild form with late onset and absent or moderate mental retardation to the severe form characterized by progressive somatic and neurologic involvement. The 24-kb IDS gene is located on the Xq27/28 boundary and the 2.3-kb cDNA encodes a protein of 550 amino acids [2–4]. The IDS protein is synthesized as two precursor forms of 90 and 76 kDa; subsequent modification of N-linked sugar residues, with the addition of mannose 6-phosphate (M6P), targets newly synthesized IDS to lysosomal compartments where, after a proteolytic cleavage, it is converted into a 45- to 42-kDa mature polypeptide [5,6]. The cloning of IDS cDNA sequences has allowed the identification of a large variety of IDS locus alterations (for reviews, see Refs. [7,8]) with subsequent genotype/phenotype correlation for many of the described mutations. Moreover, some IDS mutant proteins have been characterized in expression studies [9–12].

Lysosomal enzymes are post-translationally processed to contain phosphorylated M6P residues. These bind to M6P receptors which target proteins to the lysosomes. Receptors are also present on the cell membrane and are able to bind circulating or extracellular lysosomal enzymes and deliver them to the lysosomes (for review, see Ref. [13]). Thus, enzyme replacement has been suggested for the treatment of lysosomal storage diseases. Despite substantial clinical and laboratory experimentation for the treatment of these disorders in which there is significant neurological involvement, little is known about the capacity of neuronal and glial cells to take up individual lysosomal enzymes from the extracellular medium and process them correctly within the lyso-

---

* Corresponding author. Tel.: +39-81-746-3202/3211; fax: +39-81-746-3150.
E-mail address: dinatale@cds.unina.it (P. Di Natale).

0925-4439/02/$ - see front matter © 2002 Elsevier Science B.V. All rights reserved.
PII: S0925-4439(02)00166-7

somes. Little research has been carried out to this regard; it has been reported that neurons and glial cells contain the appropriate M6P receptors necessary to take up all lysosomal enzymes from the extracellular medium and that extracellular α-L-iduronidase is indeed endocytosed [14]; moreover, it has been reported that a high percentage of M6P glycoproteins are present in rat brain [15]. However, no experiments have been done to assess the capacity of neuronal and glial cells, in vitro, to correctly process endocytosed lysosomal proteins. Thus, our aim was to extend these in vitro studies to the IDS enzyme; our experiments were designed to assess whether neuronal and glial cells could take up recombinant IDS from the extracellular medium, retain it intracellularly and process it correctly within the lysosomes. Two sources of recombinant IDS have been used: (1) enzyme secreted by transfected human Bosc 23 cells and (2) enzyme secreted by adenovirally transduced neuronal and glial cells, since the capacity of the recombinant vector AdRSVIDS to transduce human normal and Hunter fibroblasts has been previously demonstrated [16].

2. Materials and methods

2.1. Cell cultures

Bosc 23 (human kidney cells) were grown in Dulbecco's modified Eagle medium (DMEM). SK-N-BE (human neuroblastoma) and C6 (rat glioma) cell lines were grown in monolayers in RPMI 1640. All media were supplemented with 10% FCS, 100 U/ml penicillin, 100 μg/ml streptomycin, 2 mM L-glutamin (all purchased from Life Technologies, Italy). Cells were grown at 37 °C in a 5% CO_2/air atmosphere. SK-N-BE cells were treated with 5 μM trans retinoic acid (RA) (Sigma) for 3 days to induce differentiation [17].

2.2. Bosc 23 cells transfection

Ten micrograms of the plasmid pCXN [18] containing the IDS cDNA was introduced into Bosc 23 cells by electroporation using a BioRad Gene Pulser apparatus and a pulse of 250 V/960 μF. The cells were grown in nonselective medium for 48 h and then subcultured into medium containing 0.375 mg of active Geneticin (G418)/ml. After 2 weeks selection, G418-resistant colonies were harvested by tripsinisation, expanded in DMEM/G418, cloned in flat-bottomed 96-well tissue plates by limiting dilution, and assayed for IDS activity.

2.3. Adenovirus infection

The virus AdRSVIDS, previously described [16], carries in the E1 region of its genome the IDS cDNA driven by the RSV promoter. It was generated, purified and titred according to standard techniques [19].

RA-treated SK-N-BE neuronal cells and C6 glial cells were grown in 60-mm plates and infected with 20 or 50 pfu/cell of AdRSVIDS. The day before the infection, both cell lines were seeded; one additional plate of each line was seeded for counting. The next day, cells were counted just before the infection which was performed for 30 min at 37 °C in PBS^{++} containing an amount of virus dependent on the cell number and on the multiplicity of infection chosen. Mock samples were instead treated with PBS^{++} alone. All cells were afterwards refed and harvested 48 h later.

To assess the efficiency of adenovirus infection in both SK-N-BE and C6 cell lines, a control virus, AdHCMVSp1lacZ [20] expressing the *E. coli lacZ* reporter gene, was used, at 10-20-50-100 pfu/cell. X-gal staining, performed 48 h post-infection showed for both cell lines an efficiency of infection around 100% already at 50 pfu/cell, which was therefore taken as the maximum multiplicity to be used in the following experiments.

2.4. Enzyme analysis

Cell pellets were washed twice with 150 mM NaCl, resuspended in the same buffer and frozen–thawed six times. The protein content was determined in cell lysates according to Lowry et al. [21]. The IDS assay was performed as described: 2 μg of cellular proteins was incubated with 20 μl of the substrate 4-methylumbelliferyl-α-iduronide-2-sulfate (MU-αIdu-2S) and kept for 4 h at 37 °C, after which 10 μl of RLC (Rabbit Liver ConA fraction) was added and the reaction continued for 24 h more. The reaction was terminated by adding the appropriate stop buffer and the amount of product obtained was evaluated using a fluorometer with 365 nm excitation and 446 emission [22].

2.5. Endocytosis of recombinant IDS produced by stably transfected Bosc 23 cells into SK-N-BE neuronal and C6 glial cells. Effect of M6P

IDS Bosc 23 cell clones were grown to 70% confluency in 60-mm plates, after which fresh medium was added and left for 24 h, then removed and clarified by centrifugation at 200 × g for 5 min. The conditioned medium was then transferred onto recipient cells (RA-treated SK-N-BE cells or C6 cells) and cultures incubated for 2 days in the absence or in the presence of M6P. After 48 h endocytosis, the cells were trypsinized and the IDS activity measured in cell extracts.

In another set of experiments, IDS Bosc 23 cell clones were labeled for 2 h (pulse) with ^{35}S-Express Protein Labeling Mix; medium was changed and left for 24 h chase period. Chase medium was removed, clarified by centrifugation as described and added to SK-N-BE or C6 cells in the absence or in the presence of 5 mM M6P. After 48 h endocytosis, the cells were washed with PBS, lysed on ice for 30 min in 500 μl lysis buffer (10 mM EDTA pH 8, 0.1% Triton X-100, 0.2 mM PMSF, 1 mM pepstatin A and 1 mM leupeptin) and centrifuged for 15 min at 13 600 × *g*. Radiolabeled supernatants were treated overnight with 1 μl anti-IDS antiserum. Immune complexes were precipitated with 30 μl protein A-Agarose (Santa Cruz Biotechnology) for 1 h at 4 °C, washed four times with lysis buffer, analyzed by SDS-PAGE followed by fluorography.

2.6. Endocytosis of recombinant IDS produced by AdRSVIDS infected SK-N-BE and C6 cells into a second population of neuronal and glial cells. Effect of M6P

RA-treated SK-N-BE cells and C6 glial cells were grown to 70% confluency in 60-mm plates and were infected with 50 pfu/cell of AdRSVIDS; after 48 h, the medium was removed and clarified by centrifugation as described. The conditioned medium was then transferred onto recipient cells (a second population of untreated SK-N-BE or C6 cells) and cultures incubated for 2 days in the absence or in the presence of 5 mM M6P. After 48 h endocytosis, the cells were trypsinized and the IDS activity was measured in the cell extracts.

In another set of experiments, infected SK-N-BE and C6 cells were labeled for 2 h (pulse) with ^{35}S-Express Protein Labeling Mix; the medium was changed and left for 24 h chase period. The conditioned labeled medium was removed, clarified and added to a second population of untreated SK-N-BE or C6 cells in the absence or in the presence of 5 mM M6P. After 48 h endocytosis, the cells were treated exactly as described in Section 2.5.

3. Results

3.1. Generation of clonal cell lines expressing IDS

The pCXN expression vector containing the full-length cDNA for IDS was electroporated into Bosc 23 cells and stable clones selected using 0.375 mg of active Geneticin (G418)/ml; 24 clones were isolated and assessed for the level of IDS activity. Enzyme levels were between 205.3 and 496.0 nmol/4 h/mg. Clones C7, C10 and C18 showed the highest levels of IDS activity (Table 1), clone C10 resulting the best for IDS expression in the cells (4.5-fold the level of untreated cells) and in the medium (3.3-fold the level of untreated cells) (Table 1); it was therefore used for the production of recombinant IDS enzyme.

Table 1
IDS activity measured in three isolated clones of Bosc 23 cells after stable transfection with expression vector pCXN. Transfected cells were selected in G418

Bosc-23	Cells (nmol/4 h/mg)	Medium (nmol/4 h/ml)
Untransfected	108.5 ± 12.3	1.2 ± 0.3
C7-clone	336.1 ± 23.2	2.2 ± 0.5
C10-clone	496.0 ± 4.1	4.0 ± 1.1
C18-clone	393.2 ± 29.6	2.7 ± 1.2

IDS activity is given as nmol/4 h/mg and represents the mean ± S.D. of triplicate 60-mm plates.

Table 2.
Endocytosis of recombinant IDS from Bosc 23 cells into SK-N-BE neuronal and C6 glial cells. Effect of M6P

Experimental conditions	SK-N-BE (nmol/4 h/mg)	C6 (nmol/4 h/mg)
Control cells (means ± S.D.)	19.2 ± 0.15	23.2 ± 1.15
Cells + conditioned media (means ± S.D.)	69 ± 9.8	88 ± 10.4
Percentage versus controls	358	379
Cells + conditioned media + M6P (means ± S.D.)	23.2 ± 1.3	26.4 ± 2.1

SK-N-BE and C6 cells were treated for 2 days with conditioned medium from Bosc 23 cells in the absence or in the presence of 5 mM M6P. Control cells were maintained in unconditioned medium for the same time. IDS levels are given as nmol/4 h/mg and represent the mean ± S.D. of triplicate plates.

3.2. Endocytosis of recombinant IDS enzyme produced by stably transfected Bosc 23 cells into SK-N-BE and C6 cells. Evaluation of enzyme activity

To characterize the process by which neuronal SK-N-BE and C6 glial cells can acquire the lysosomal IDS enzyme, we performed an uptake cross-correction experiment to demonstrate active endocytosis. The basal levels of IDS in RA-treated SK-N-BE cells and C6 cells were 19.2 and 23.2 nmol/4 h/mg, respectively. To study neuronal uptake, the conditioned medium from C10 clone was used as a source of IDS for in vitro cultured SK-N-BE and C6 cells. Internalization of IDS was monitored after 48 h endocytosis: a significant increase in the enzyme activity was detected intracellularly in SK-N-BE (358.3%) and in C6 cells (379%) (Table 2). When the experiment was performed in the presence of 5 mM M6P, the IDS activity levels were similar to the basal levels (Table 2), indicating that endocytosis of IDS was mediated by the M6P receptor pathway. Taking into account the total enzyme units (35) measured in the extracellular medium and the total enzyme units (1.7 and 2.2) recovered in the recipient cells (SK-N-BE and C6, respectively), a mean value of 5.6% endocytosis was calculated.

3.3. Endocytosis of recombinant IDS enzyme produced by stably transfected Bosc 23 into SK-N-BE and C6 cells. Evaluation of enzyme maturation

To study the maturation of the IDS protein after endocytosis into SK-N-BE and C6 cells, the medium of the C10 clone, containing the labeled precursor forms of IDS, was added to SK-N-BE and C6 cells, in the absence or in the presence of M6P. The results are shown in Fig. 1; the precursor 76-kDa form in the absence of M6P was efficiently endocytosed, resulting in both cell types in the mature form of 43 kDa. The presence of 5 mM M6P again inhibited the uptake of the enzyme.

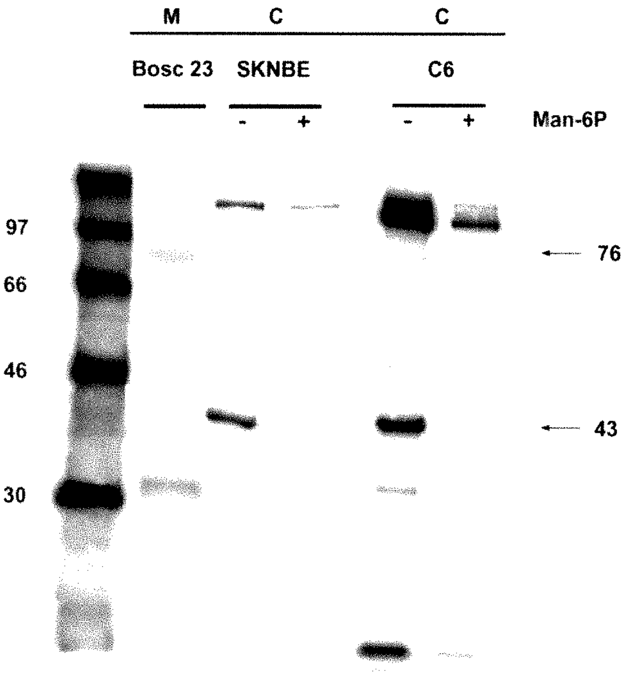

Fig. 1. Endocytosis of IDS produced by Bosc 23 cells into SK-N-BE neuronal and C6 glial cells. Effect of M6P. Bosc 23 cells, stably transfected with IDS cDNA construct, were labeled for 2 h (pulse) with ^{35}S-Express Protein Labeling Mix. After a subsequent period of 24 h (chase), the media, containing the precursor forms of the enzymes, were collected and concentrated to 0.5 ml by Millipore Centricon Centrifugal Filter Device or were directly added to RA-treated SK-N-BE and to C6 cells in the absence (−) or presence (+) of 5 mM M6P for 48 h endocytosis. IDS protein was immunoprecipitated from concentrated Bosc 23 medium or from homogenates of target cells, separated by SDS-PAGE and detected by fluorography. The mass (in kilodaltons) of the molecular weight markers is indicated on the left. M, medium; C, cell lysate. The arrows on the right indicate the 76-kDa precursor form and the 43-kDa mature IDS form.

3.4. Adenovirus infection of SK-N-BE neuronal and C6 glial cells

Triplicate 60-mm plates of neuronal SK-N-BE and C6 glial cells were infected with the viral vector AdRSVIDS at 20 and 50 pfu/cell, as described in Materials and Methods and the IDS activity was tested 48 h after infection. An IDS basal activity of 24 and 29 nmol/4 h/mg was observed in untreated SK-N-BE and C6 cells, respectively (Table 3); after infection with 20 pfu, an IDS increase above the basal level of 9.2-fold (intracellular) and 4.4-fold (extracellular) was found in SK-N-BE cells, while an increase of 8.5-fold (intracellular) and 7.1-fold (extracellular) was observed in C6 cells (Table 3). Infection with 50 pfu resulted in higher increases in the IDS activity: 18.1-fold and 10.6-fold in SK-N-BE (cells and medium, respectively); 16-fold and 15.6-fold in C6 (cells and medium, respectively) (Table 3).

Table 4
Endocytosis of recombinant IDS from AdRSVIDS infected SK-N-BE neuronal and C6 glial cells into a second population of untreated cells. Effect of M6P

Experimental conditions	SK-N-BE (nmol/4 h/mg)	C6 (nmol/4 h/mg)
Control cells (means ± S.D.)	24.7 ± 2.4	30.4 ± 3.6
Cells + conditioned media (means ± S.D.)	334 ± 42.1	435.9 ± 50.3
Percentage versus controls	1352.2	1433.8
Cells + conditioned media + M6P (means ± S.D.)	107 ± 25.6	112 ± 31.9

SK-N-BE and C6 cells were cultured for 48 h in conditioned medium from AdRSVIDS infected cells in the absence or in the presence of 5 mM M6P. Control cells for each cell type were maintained in unconditioned medium for the same time. IDS levels are given as nmol/4 h/mg and represent the mean ± S.D. of triplicate plates.

3.5. Endocytosis of recombinant IDS enzyme produced by AdRSVIDS infected SK-N-BE and C6 cells into a second population of untreated cells. Evaluation of enzyme activity

To evaluate whether the enzyme secreted from transduced neuronal SK-N-BE and C6 glial cells could be taken up by a second population of untreated cells, the conditioned medium from transduced cells was added to uninfected neuronal and glial cells. After 48 h, the target cells were tested for IDS activity. The results are shown in Table 4: the SK-N-BE cells, with a basal activity of 24.7 nmol/h/mg, after 48 h incubation with conditioned medium showed an activity of 334 nmol/4 h/mg, namely an increase of 1352%; the C6 cells, with a basal activity of 30.4 nmol/h/mg, after 48 h incubation with a conditioned medium showed an activity of 436 nmol/4 h/mg, namely an increase of 1434%. The presence of 5 mM M6P in the system blocked the IDS uptake (Table 4). Taking into account the total enzyme units (12.0 and 14.1) measured in the extracellular medium of SK-N-BE and C6, respectively, and the total enzyme units (8.8 and 10.5) recovered in the recipient cells, a mean value of 74% endocytosis was calculated.

Table 3
IDS activity in SK-N-BE neuronal cells and C6 glial cells after adenoviral infection

Experimental conditions	SK-N-BE cells (nmol/4 h/mg)	SK-N-BE medium (nmol/4 h/ml)	C6 cells (nmol/4 h/mg)	C6 medium (nmol/4 h/ml)
Control cells (untreated)	24 ± 2.4	1.13 ± 0.9	29 ± 3.5	0.9 ± 0.4
Infected cells (20 pfu)	221 ± 31.8	4.97 ± 2.1	246 ± 56.2	6.41 ± 2.6
Infected cells (50 pfu)	434 ± 83.1	12.0 ± 3.5	465 ± 75.5	14.1 ± 4.5

IDS activity, determined 48 h after infection, represents the mean ± S.D. of triplicate plates.

3.6. Endocytosis of recombinant IDS enzyme produced by AdRSVIDS infected SK-N-BE and C6 cells into a second population of untreated neuronal and glial cells. Evaluation of enzyme maturation

Immunoprecipitation experiments were performed to confirm the internalization of the IDS protein in untreated SK-N-BE and C6 cells. To this purpose, the conditioned medium by SK-N-BE and C6 was added to the same cells, in the absence or in the presence of M6P. The results are shown in Fig. 2; the recombinant IDS protein secreted into the culture medium was taken up by recipient cells and correctly processed to the mature form of 45 kDa. The presence of 5 mM M6P inhibited the uptake of the enzyme. It should be noted that, in contrast with the results shown in Fig. 1, the attempt to immunoprecipitate the precursor form in the conditioned medium of SK-N-BE and C6 cells was unsuccessful. Apparently, this precursor form obtained in neuronal cells after adenovirus infection contains some difference(s) with respect to the precursor form found after Bosc 23 transfection. A similar problem was encountered with the IDS protein expressed in another cell type [12].

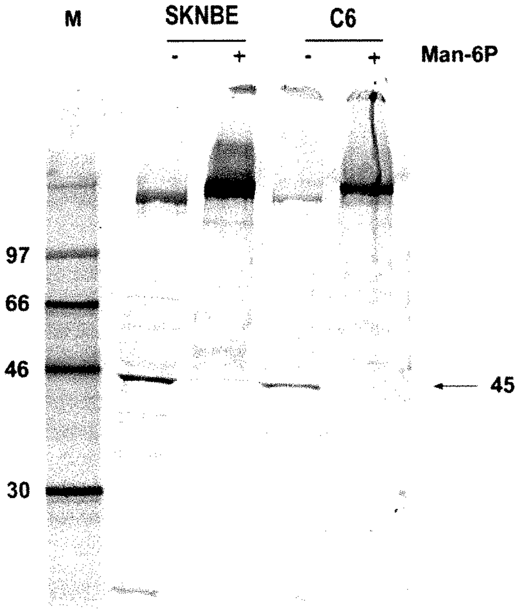

Fig. 2. Endocytosis of IDS produced by transduced SK-N-BE neuronal and C6 glial cells into a second population of untreated recipient cells. Effect of M6P. RA-treated SK-N-BE and C6 cells were infected with AdRSVIDS at 20 pfu/cell; 18 h later, the cells were labeled for 2 h (pulse) with ^{35}S-Express Protein Labeling Mix. After a subsequent period of 24 h (chase), the media, containing the precursor forms of the enzymes, were added to untreated SK-N-BE and C6 cells in the absence (−) or presence (+) of 5 mM M6P. After 48 h of endocytosis, IDS protein was immunoprecipitated from homogenates of target cells, separated by SDS-PAGE and detected by fluorography. The mass (in kilodaltons) of the molecular weight markers is indicated on the left. The arrow on the right indicates the 45-kDa mature IDS form.

4. Discussion

MPS II is a storage disorder with multiple sites of pathology, including the central nervous system (CNS). Currently, only symptomatic treatments are available; only a few patients, without severe neuropsychological impairment, have undergone bone marrow transplantation [23–25]. At present, MPS II is considered to be a candidate disorder for enzyme replacement therapy (ERT) and for gene therapy. In this respect, the in vitro correction of Hunter fibroblasts or lymphocytes [16,26–28] and in vivo autologous transplantation of genetically corrected peripheral blood lymphocytes [29] are currently the only options available to accomplish gene delivery of the correct gene sequence. However, the in vivo experiments on the CNS have been disappointing due to the blood-brain barrier and the in vitro experiments on CNS cells have never been performed, indicating the need for further investigation.

In this study, we have generated human kidney cells, Bosc 23, which overexpress and secrete human IDS following stable transfection with the IDS pCXN expression vector. After transfection, the IDS activity increased both in the cells and in the culture medium. The recombinant Bosc 23 cells were used as donor cells for in vitro cell-mediated enzyme replacement of neuronal SK-N-BE and C6 glial cells. We have demonstrated that the recombinant IDS enzyme produced by transfected Bosc 23 cells was efficiently taken up by neuronal and glial cells through the M6P receptor pathway. Metabolic labeling experiments have confirmed the enzymatic data demonstrating that the recombinant protein was not only properly glycosylated for uptake but also correctly processed into the brain cells in the mature form of 45–42 kDa.

At the same time, we have demonstrated that the replication defective adenovirus vector AdRSVIDS can be efficiently transduced into neuronal SK-N-BE and C6 cells; after infection, the enzymatic activity increased both intracellularly and in the extracellular medium. Furthermore, the experiments of metabolic labeling showed that the recombinant IDS enzyme, produced in neuronal and glial cells by the AdRSVIDS adenovirus vector, was endocytosed by a second population of the untreated cells and underwent correct processing to the 45–42-kDa mature form.

Previously, in vitro studies have shown that recombinant lysosomal enzymes, including IDS, are correctly localized in lysosomes of the transduced cells and normalize the substrate catabolism [14,16,26,27,30]; other studies on recombinant lysosomal proteins have indicated that these enzymes are properly glycosylated for uptake [14,26]. Recent data suggest that enzyme preparations containing phosphorylated β-glucuronidase are more effective than the non-phosphorylated enzyme in the clinical response to ERT in MPS VII mice [31]; on the other hand, overexpression resulting in intracellular aggregation may interfere with intracellular trafficking and optimal substrate degradation [32].

In conclusion, we have demonstrated that cultured CNS cells can be efficiently induced to produce or endocytose therapeutic levels of recombinant IDS enzyme and that the recombinant protein is subsequently correctly processed within the lysosomes. These results may have important implications both for enzyme replacement therapy and for gene therapy for neurological disorder of MPS II. In view of the considerable problem of the blood-brain barrier, a potential therapeutic approach could be based on intrathecal treatment of the recently obtained MPS II mouse model [33].

Acknowledgements

This work was supported by a grant from MURST (P. Di Natale, F. Zacchello), a grant from Italian MPS Association (P. Di Natale, M. Scarpa) and a grant from Regione Veneto (M. Scarpa).

References

[1] E.F. Neufeld, J. Muenzer, The mucopolysaccharidoses, in: C.R. Scriver, A.L. Beaudet, W.S. Sly, D. Valle (Eds.), The Metabolic and Molecular Bases of Inherited Disease, 8th ed., McGraw-Hill, New York, 2001, pp. 3421–3452.

[2] P.J. Wilson, C.P. Morris, D.S. Anson, T. Occhiodoro, J. Bielicki, P.R. Clements, J.J. Hopwood, Hunter syndrome: isolation of an iduronate-2-sulfatase cDNA clone and analysis of patient DNA, Proc. Natl. Acad. Sci. U. S. A. 87 (1990) 8525–8531.

[3] R.H. Flomen, P.M. Green, D.R. Bentley, F. Giannelli, Determination of the organization of coding sequences within the iduronate sulfatase (IDS) gene, Hum. Mol. Genet. 2 (1993) 5–10.

[4] P.J. Wilson, C.A. Meaney, J.J. Hopwood, C.P. Morris, Sequence of the human iduronate-2-sulfatase (IDS) gene, Genomics 17 (1993) 773–775.

[5] R. Froissart, G. Millat, M. Mathieu, D. Bozon, I. Maire, Processing of iduronate 2-sulfatase in human fibroblasts, Biochem. J. 309 (1995) 425–430.

[6] G. Millat, R. Froissart, I. Maire, D. Bozon, IDS transfer from overexpressing cells to IDS-deficient cells, Exp. Cell Res. 230 (1997) 362–367.

[7] J.J. Hopwood, S. Bunge, C.P. Morris, P.J. Wilson, C. Steglich, M. Beck, E. Schwinger, A. Gal, Molecular basis of mucopolysaccharidosis type II: mutations in the iduronate-2-sulphatase gene, Hum. Mutat. 2 (1993) 435–442.

[8] P. Di Natale, Mutations in sulfatase-deficient mucopolysaccharidoses, Curr. Top. Biochem. Res. 2 (2000) 207–217.

[9] K. Sukegawa, S. Tomatsu, T. Fukao, H. Iwata, X.Q. Song, Y. Yamada, S. Fukada, K. Isogai, T. Orij, Mucopolysaccharidosis Type II (Hunter disease): identification and characterization of eight point mutations in the iduronate-2-sulfatase gene in Japanese patients, Hum. Mutat. 6 (1995) 136–143.

[10] G. Millat, R. Froissart, S. Cudry, V. Bonnet, I. Maireand, D. Bozon, COS cell expression of P86L, P86R, P480L and P480Q Hunter's disease-causing mutations, Biochim. Biophys. Acta 1406 (1998) 214–218.

[11] G.R.D. Villani, A. Daniele, N. Balzano, P. Di Natale, Expression of five iduronate-2-sulfatase site-directed mutations, Biochim. Biophys. Acta 1501 (2000) 71–80.

[12] G. Bonuccelli, P. Di Natale, F. Corsolini, G.R.D. Villani, S. Regis, M. Filocamo, The effect of four mutations on the gene expression of iduronate-2-sulfatase in mucopolysaccharidosis type II, Biochim. Byophis. Acta 1537 (2001) 233–238.

[13] S. Kornfeld, I. Mellman, The biogenesis of lysosomes, Annu. Rev. Cell Biol. 5 (1989) 483–525.

[14] K. Stewart, O.A. Brown, A.E. Morelli, L.J. Fairbairn, L.S. Lasford, A. Cooper, C.E. Halton, T.M. Dexter, M.G. Castro, P.R. Lowenstein, Uptake of α-L-iduronidase produced by retrovirally transduced fibroblasts into neuronal and glial cells in vitro, Gene Ther. 4 (1997) 63–75.

[15] M. Jadot, L. Lin, D.E. Sleat, I. Sohar, M.S. Hsui, J. Pintari, F. Dubois, S. Wattiaux-De Coninck, R. Wattiaux, P. Lobel, Subcellular localization of mannose 6-phosphate glycoproteins in rat brain, J. Biol. Chem. 274 (1999) 21104–21113.

[16] C. Di Francesco, C. Cracco, R. Tomanin, L. Picci, F. Zacchello, P. Di Natale, J.J. Hopwood, F.L. Graham, M. Scarpa, In vitro correction of iduronate-2-sulfatase deficiency by adenovirus-mediated gene transfer, Gene Ther. 4 (1997) 442–448.

[17] T.B. Shea, I. Fischer, V.S. Sapirstein, Effect of retinoic acid on growth and morphological differentiation of mouse NB2a neuroblastoma cells in culture, Brain Res. 21 (1985) 307–314.

[18] H. Niwa, K. Yamamura, J. Miyazaki, Efficient selection for high-expression transfectants with a novel eukaryotic vector, Gene 108 (1991) 193–199.

[19] M. Hitt, A.J. Bett, C. Addison, L. Prevec, F.L. Graham, Techniques for human adenovirus vector construction and characterization, in: K.W. Adolph (Ed.), Methods in Molecular Genetics, vol. 7B, Academic Press, Orlando, FL, 1995, pp. 13–30.

[20] M.A. Morsy, E.L. Alford, A. Bett, F.L. Graham, C.T. Caskey, Efficient adenoviral vector-mediated ornithine transcarbamylase expression in deficient mouse and human hepatocytes, J. Clin. Invest. 92 (1993) 1580–1586.

[21] O.H. Lowry, N.J. Rosenbrough, A.L. Farr, K.J. Randall, Protein measurement with the Folin phenol reagent, J. Biol. Chem. 193 (1951) 265–276.

[22] Y.V. Voznyi, J.L.M. Keulemans, O.P. van Diggelen, A fluorimetric enzyme assay for the diagnosis of MPS II (Hunter disease), J. Inherit. Metab. Dis. 24 (2001) 675–680.

[23] W. Krivit, E.G. Shapiro, Bone marrow transplantation for storage diseases, in: R.J. Desnick (Ed.), Treatment of Genetic Diseases, Churchill-Livingstone, New York, 1991, pp. 203–211.

[24] E. McKinnis, S. Sulzbacher, J.C. Rutledge, J. Sanders, R. Scott, Bone marrow transplantation in Hunter syndrome, J. Pediatr. 129 (1996) 145–148.

[25] G. Coppa, O. Gabrielli, R. Cordiali, G.R.D. Villani, P. Di Natale, Bone marrow transplantation in a Hunter patient with P266H mutation, Int. J. Mol. Med. 4 (1999) 433–436.

[26] J. Bielicki, J.J. Hopwood, P.J. Wilson, D.S. Anson, Recombinant human iduronate-2-sulphatase: correction of mucopolysaccharidosis-type II fibroblasts and characterization of the purified enzyme, Biochem. J. 289 (1993) 241–246.

[27] S.E. Braun, E.L. Aronovich, R.A. Anderson, P.L. Crotty, R.S. McIvor, C.B. Whitley, Metabolic correction and cross-correction of mucopolysaccharidosis type II (Hunter syndrome) by retroviral-mediated gene transfer and expression of human iduronate-2-sulfatase, Proc. Natl. Acad. Sci. U. S. A. 90 (1993) 11830–11834.

[28] S.E. Braun, D. Pan, E.L. Aronovich, J.J. Jonsson, R.S. McIvor, C.B. Whitley, Preclinical studies of lymphocyte gene therapy for mild Hunter syndrome (MPS type II), Hum. Gene Ther. 7 (1996) 283–290.

[29] D.F. Stroncek, A. Hubel, R.A. Shankar, S.R. Burger, D. Pan, J. McCullough, C.B. Whitley, Retroviral transduction and expansion of peripheral blood lymphocytes for the treatment of mucopolysaccharidosis type II, Hunter's syndrome, Transfusion 39 (1999) 343–350.

[30] W. Rommerskirch, A.L. Fluharty, C. Peters, K. von Figura, V. Gieselmann, Restoration of arylsulphatase A activity in human-metachromatic-leucodystrophy fibroblasts via retroviral-vector-mediated gene transfer, Biochem. J. 280 (1991) 459–461.

[31] M S. Sands, C A. Vogler, K K. Ohlemiller, M. Roberts, J H Grubb, B. Levy, W S Sly, Biodistribution, kinetics and efficacy of highly phosphorylated and non-phosphorylated beta-glucuronidase in the murine model of mucopolysaccharidosis VII, J Biol. Chem. 276 (2001) 43160–43165

[32] D S. Anson, J Bielicki, J J Hopwood, Correction of mucopolysaccharidosis type I fibroblasts by retroviral-mediated transfer of the human alpha-L-iduronidase gene, Hum Gene Ther 3 (1992) 371–379

[33] J. Muenzer, Targeted disruption of the mouse iduronate sulfatase gene, 5th International Symposium on Mucopolysaccharide and Related Diseases, Vienna, March 18–21, 1999 (Abstract)

ELSEVIER

Biochimica et Biophysica Acta 1588 (2002) 210–216

BIOCHIMICA ET BIOPHYSICA ACTA

BBA

www.bba-direct.com

Molecular and functional effects of the T14709C point mutation in the mitochondrial DNA of a patient with maternally inherited diabetes and deafness

D. Perucca-Lostanlen [a,*], R.W. Taylor [b], H. Narbonne [c], B. Mousson de Camaret [d], C.M. Hayes [b], A. Saunieres [a], V. Paquis-Flucklinger [a], D.M. Turnbull [b], B. Vialettes [c], C. Desnuelle [a]

[a] *UMR 6549 CNRS/UNSA, Faculté de Médecine, Avenue de Valombrose, 06107 Nice Cedex 02, France*
[b] *Department of Neurology, The Medical School, University of Newcastle upon Tyne, NE2 4HH, UK*
[c] *Service de Nutrition, Maladies Metaboliques et Endocrinologie, Hopital Sainte Marguerite, UPRES EA 2193, Université de la Méditerranée, 13274 Marseille Cedex 09, France*
[d] *Laboratoire de Biochimie, Hopital Debrousse, 29, Rue Sœur Bouvier, 69322 Lyon Cedex 05, France*

Received 27 February 2002; received in revised form 12 July 2002; accepted 31 July 2002

Abstract

A heteroplasmic T to C transition at nucleotide position 14709 in the mitochondrial tRNA glutamic acid (tRNA^{Glu}) gene has previously been associated with maternally inherited diabetes and deafness (MIDD). To investigate the pathogenic mechanism of the T14709C mutation, we have constructed transmitochondrial cell lines by transferring fibroblasts mitochondria from a patient with the mutation into human cells lacking mitochondrial DNA (mtDNA) (rho° cells). Clonal cybrid cell lines were obtained containing various levels of the heteroplasmic mutation, or exclusively mutated or wild-type mtDNA. Measurement of respiratory chain enzymatic activities failed to detect a difference between the homoplasmic mutant and homoplasmic wild-type cybrid cell lines. However, a subtle decrease in the steady-state levels of tRNA^{Glu} transcripts in some mutant clones. Our studies suggest that the T14709C mutation is insufficient to lead impairment of mitochondrial function in homoplasmic osteosarcoma cybrid clones, and that we cannot exclude that the T14709C mutation affects mitochondrial function by a yet unidentified mechanism.

© 2002 Elsevier Science B.V. All rights reserved

Keywords: Mitochondrial diabetes; Mitochondrial DNA; Point mutation; Transmitochondrial cybrid

1. Introduction

Over the last decade, mutations of the mitochondrial genome have become increasingly recognised as important causes of human disease. Many of these abnormalities take the form of mtDNA rearrangements, but an increasing number of mtDNA point mutations have now been described, affecting protein coding, rRNA or tRNA genes (MITOMAP http://www.gen.emory.edu/mitomap.html).

MtDNA abnormalities, including deletions, duplications and point mutations, are a well-recognised cause of diabetes [1–5]. The most commonly described mtDNA defect in patients with maternally inherited deafness and diabetes (MIDD) resides in the tRNA$^{Leu(UUR)}$ gene [2–6], an A to G transition at position 3243 that was first associated with the mitochondrial encephalopathy, lactic acidosis and stroke-like episodes (MELAS) syndrome [7]. Moreover, a point mutation (T14709C) in the mitochondrial tRNA gene for glutamic acid (tRNA^{Glu}) has been identified in some patients with diabetes mellitus [8–11]. In these cases, the T14709C mutation was heteroplasmic and present at high levels in the patient's muscle and white blood cells. Biochemical studies of muscle mitochondria showed reduced complex I and IV activities [8–10], whilst a correlation was also shown between the level of mutation and the activity of cytochrome *c* oxidase in single muscle fibres [9]. In addition, profound alteration of oxidation process was demonstrated in vivo by ^{31}P magnetic spectroscopy [10].

The development of human cell lines lacking mtDNA (rho° cell lines) that can be repopulated with exogenous

---

[*] Corresponding author. Tel.: +33-4-93-37-77-22; fax: +33-4-93-53-30-71.

E-mail address: perucca@unice.fr (D. Perucca-Lostanlen).

0925-4439/02/$ - see front matter © 2002 Elsevier Science B.V. All rights reserved
PII: S0925-4439(02)00167-9

mtDNA by mitochondria-mediated transformation [12] has provided a useful tool to study pathogenic mtDNA mutations, as all cybrids contain the same mtDNA haplotype within the same nuclear background, differing by only the single nucleotide point mutation [13–15]. We have used this methodology to investigate the molecular pathogenic mechanism of the T14709C mutation. Using fibroblasts from a previously characterised patient with this mutation as a source of donor mitochondria [10], we have isolated several clonal cell lines that contained exclusively homoplasmic mutated or wild-type mtDNA and heteroplasmic mtDNA and performed detailed biochemical studies of these cell lines to assess the effect of the T14709C mutation on mitochondrial function.

2. Materials and methods

2.1. Patient

The patient presenting diabetes and severe myopathy was described in detail previously [10]. Briefly, a muscle biopsy revealed ragged red fibers and a decreased activity of respiratory chain complex IV (39% of mean control values). Molecular analysis demonstrated the presence of a heteroplasmic T14709C mutation at a level of 78% mutant load in skeletal muscle and 65% in blood.

2.2. Cell lines and culture conditions

Fibroblasts from skin explant obtained from this patient were cultured in high-glucose DMEM supplemented with 10% foetal bovine serum (FBS), 100 µg/ml pyruvate and 50 µg/ml uridine in 5% CO_2 at 37 °C. The 143B.TK$^-$ osteosarcoma cell line and the daughter 143B.206.TK$^-$ rho° cells were provided by M. King (T. Jefferson University, Philadelphia, PA, USA). 143B.206 rho° cells, completely depleted of mtDNA by long-term exposure to ethidium bromide, were grown in DMEM containing 4.5 g/l glucose and 110 µg/ml pyruvate, supplemented with 10% FBS (Gibco), 50 µg/ml uridine and 100 µg/ml 5-bromo-2′-deoxy uridine (BrdU, Sigma Immunochemicals, Saint Louis, MO).

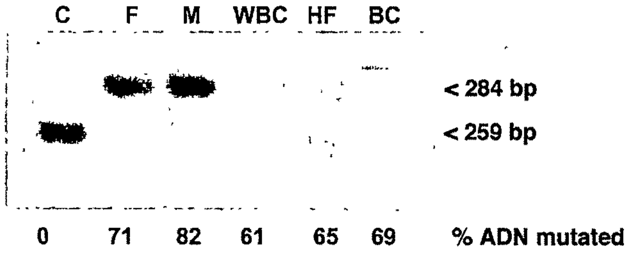

Fig 1 Tissue distribution of T14709C mutation PCR fragments of DNA of fibroblasts (F), muscle (M), white blood cells (WBC), hair follicles (HF) and buccal cells (BC) of the patient were digested with *NdeI* into two fragments of 284 bp (mutated DNA) and 259 bp (wild-type DNA, control C) and separated by electrophoresis through a 15% nondenaturing acrylamide gel.

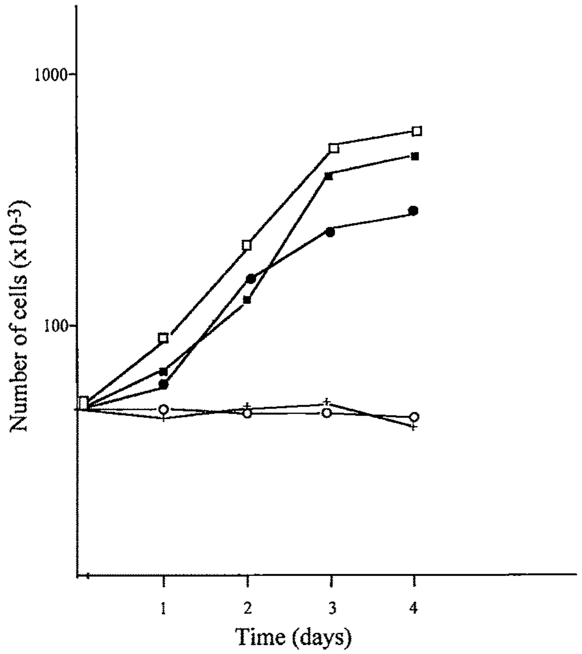

Fig 2 Growth kinetics of the cell types used in complementation experiments Rho° in DMEM+dialysed FBS+BrdU (+—+), rho° in DMEM+dialysed FBS+BrdU+pyruvate+uridine (open squares), fibroblasts from patient in DMEM+dialysed FBS+BrdU (filled circles), fibroblasts from patient in DMEM+dialysed FBS (open circles), cybrid cells in DMEM+dialysed FBS+BrdU (filled squares). Concentrations used dialysed FBS 5% (vol/vol), BrdU, 100 µg/ml; uridine 50 µg/ml, pyruvate, 100 µg/ml.

2.3. Cell fusion

Transmitochondrial cell lines were obtained using the method of King and Attardi [12]. Rho° cells were collected by low-speed centrifugation, resuspended in DMEM, and counted. Fibroblasts (10^6 cells) were mixed with an equal number of rho° cells, and culture medium carefully eliminated by centrifugation. Cells were resuspended for 1 min in 0.2 ml of sterile polyethyleneglycol 1500 (50% w/v) (Roche Diagnostics, Meylan, France). After cell fusions, screening of complemented cells was performed by growing cells in standard DMEM for 24 h and then in selective medium (pyruvate- and uridine-free DMEM supplemented with 5% dialysed FBS and 100 µg/ml BrdU). After 15 days, about 27 independent colonies were observed and selected in the same medium used for the rho° cells.

2.4. DNA analysis

Total DNA from blood cells and from cybrids cells was prepared using standard protocols [10]. Hair follicles and buccal cells were prepared and subjected to PCR amplification as described [16,17]. For the quantitation of the T14709C tRNA^{Glu} mutation, a 284-bp fragment was amplified using the polymerase chain reaction (PCR) method. Conditions were as follows: one cycle at 94 °C for 3 min, followed by 30 cycles at 94 °C for 30 s, 62 °C for 30 s and 72 °C for 30 s; the final extension proceeded for 10 min. Primers for the reaction were 5′ CACGGACTACAACCACGACCAATCATA 3′(nt 14682–14708) and 5′ TTACGTCTCGAGTGATGTGG 3′(nt 14966–14947). The underlined position in the first primer represents a modification from the wild-type sequence to create an *Nde*I restriction site in wild-type mtDNA. The amplification products were digested with *Nde*I, which cleaves the 284-bp fragment into two fragments of 259 and 25 bp. The T14709C mutation abolishes this *Nde*I restriction site. To determine the proportion of normal and mutated mtDNA, the amplified fragment was labeled with [α-^{32}P]dCTP in the last cycle to prevent underestimation of the proportion of mutant mtDNA due to heteroduplex formation. Following digestion, the restriction fragments were submitted to electrophoresis through a 15% polyacrylamide gel, the gel was dried onto a support and exposed to radiographic film. The relative proportions of mutant and wild-type mtDNA were quantified by scanning and analysing a shortly exposed X-ray film with the Image 1.45 software.

Nuclear genotypes were characterised by high polymorphic markers analysis. PCR fragments with CA repeats from chromosome 5 (D5S455) were amplified and sequenced using an ABI Prism automated DNA sequencer (Perkin Elmer) [18]. The highly polymorphic repetitive sequence D11S533 present on chromosome 11q was evidenced in the different cell lines, as described [19].

2.5. Respiratory chain enzyme analysis of transmitochondrial cybrid clones

Mitochondrial fractions were isolated from cultured cells and the activities of the individual respiratory chain complexes and the matrix marker citrate synthase were determined spectrophotometrically as previously described [20,21].

2.6. High-resolution Northern blot analysis

Total cytosolic RNA was isolated from 1 to 2 × 10^6 cells using TRIZOL® Reagent (Life Technologies, UK). Large RNA species were precipitated by the addition of 10 M LiCl, allowing smaller RNAs (5S, tRNA) to be precipitated from the resulting supernatant. Small RNAs (1 μg) were separated through a 13%, 8 M urea denaturing polyacrylamide gel using 1 × TBE as running buffer, electroblotted onto GeneScreen-plus membranes (NEN Dupont) in 0.25 × TBE and immobilised by UV crosslinking. Regions of mtDNA encompassing the tRNA^{Glu} and $\text{tRNA}^{\text{Leu(UUR)}}$

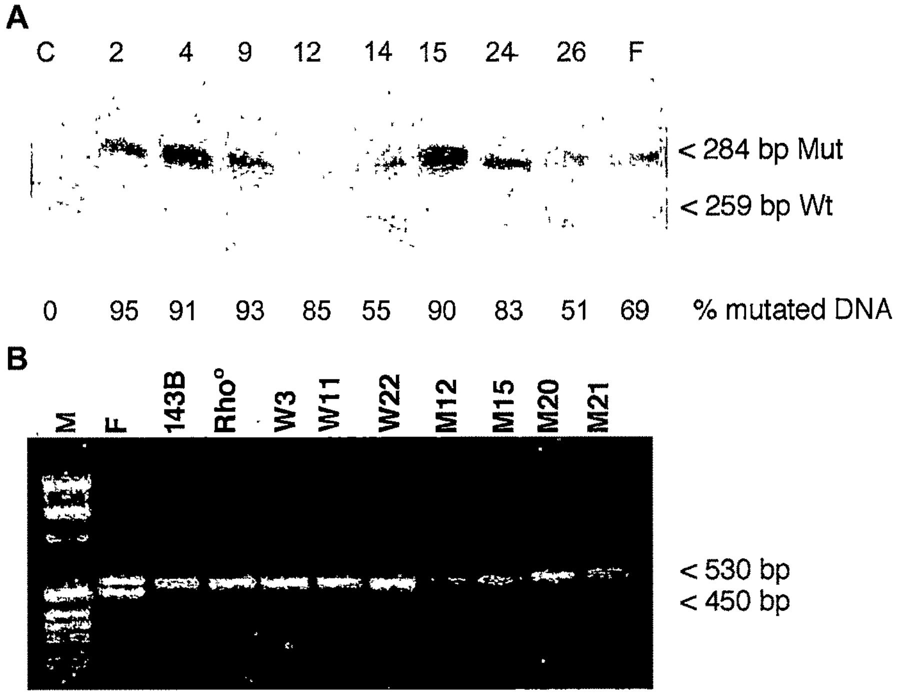

Fig. 3. Genetic characterization of patient's fibroblasts and cybrid cells. (A) Analysis for the presence and quantity of the mutated DNA with the 14709 mutation in DNA isolated from patient's fibroblasts (F) and eight derived heteroplasmic cybrid cells compared to control DNA (C) after *Nde*I digestion of a PCR-amplified fragment containing the tRNA glutamic acid gene The size of the fragments is shown on the right, and the proportion of mutated DNA is indicated below each lane. (B) PCR amplification of the D11S533 locus of patient's fibroblasts, cybrid clones, their nuclear parent 143B and rho° cells Amplification of the nuclear DNA of the donor fibroblasts (F) produces a two-band pattern (530 and 430 bp) which differs from the single band obtained from the nuclear DNA of the other cell lines, including 143B cells, rho° cells, three wild-type (W3, W11, W22) and four mutated transformant cybrid clones (M12, M15, M20 M21)

genes amplified by PCR were used as probes for Northern blots. The tRNA^{Glu} probe (69 bp) was amplified using the forward primer L14635 (positions 14635–14655). 5′TACTAAACCCACACTCAACAG 3′and the reverse primer H14810 (positions 14810–14791) 5′ GGAGGTCGATGAATGAGTGG 3′. The tRNA$^{Leu(UUR)}$ probe (75 bp) was amplified using the forward primer L3200 (positions 3200–3219) 5′ TATACCCACACCCACCCAAG 3′ and the reverse primer H3353 (positions 3353–3334) 5′GCGATTAGAATGGGTACAAT 3′. Purified PCR products were radiolabelled with [α-^{32}P] dCTP (3000 Ci/mmol) (Amersham, UK) by the random-primer method and unincorporated nucleotides were removed by gel filtration through a Sephadex G-50 DNA grade column (Pharmacia, UK). Hybridization was carried out at 42 °C overnight in a solution of 5 × SSPE, 50% formamide, 10% dextran sulphate, 5 × Denhardt's solution, 1% SDS containing 2×10^6 cpm radiolabelled probe. After hybridization, two 15-min washes were performed at room temperature with 2 × SSPE, followed by a 15-min wash at 65 °C with 2 × SSPE and 2% SDS. Blots were subjected to PhosphorImager analysis and the radioactive signal for the tRNA^{Glu} probe (69 bp) normalised to that of the tRNA$^{Leu(UUR)}$ probe (75 bp) for each sample using ImageQuant software (Molecular Dynamics).

3. Results

3.1. *Tissue distribution of the T14709C mutation and respiratory chain activity measurements in fibroblasts*

Fig. 1 shows that the proportion of mutant mtDNA was highest in the muscle of the patient (82%) as compared to the proportion found in white blood cells (61%). The T14709C mutation was found in buccal cells (69 %) and in hair follicles (65%) of the patient. Skin fibroblasts cultures were established from the patient carrying the T14709C mutation. Analysis of fibroblasts established from the patient revealed a mutant load of 71%. Respiratory chain enzyme activities determined from mitochondria-enriched preparations [19] showed a reduced complex I activity (57%) and a slightly decreased complex IV activity (72%) in the patient compared to controls.

3.2 *Cell fusion and characterization of the cybrid cells*

To obtain homoplasmic mutant transmitochondrial cell lines, patients' fibroblasts were fused with rho° cells fully depleted of mtDNA derived from the 143B.TK$^-$ cell line. The growth capacity of the different cell lines in various media was assessed (Fig. 2). The rho° cells exhibited both auxotrophy for pyruvate and uridine and resistance to BrdU, as they were obtained from the thymidine kinase-deficient (TK −) osteosarcoma 143B cell line. Patient's fibroblasts exhibited BrdU sensitivity and were able to grow in DMEM lacking pyruvate and uridine (Fig. 2). After fusion, selection of cybrids was performed in the selective medium containing BrdU but lacking pyruvate and uridine. After 15 days, we collected 27 transformant cybrid clones. The different clones were able to grow in the selective medium with growth kinetics similar to those of rho° cells in a pyruvate- and uridine-supplemented medium.

We analysed the mtDNA genotype of the 27 cybrids clones by PCR-RFLP analysis. Eleven clones were heteroplasmic ranging from 4% to 95% mutated DNA (Fig. 3A). Nine of 27 clones contained 100% mutant mtDNA, whereas seven were judged homoplasmic for wild-type mtDNA (Fig. 4A).We confirmed the presence of normal amounts of mtDNA in each clone by Southern blot analysis (the mtDNA probe was a 15.6-kb purified PCR product amplified with the Expand Long Template PCR system and the nuclear probe was a 18S probe) (data not shown).

Each clone was subsequently examined to verify that the mitochondrial genotype was identical to the donor fibroblasts by sequence analysis [22,23] and that the nuclear genotype was identical to that of the nuclear parent, the 143B cell line. We demonstrated that the DNA of the wild-type and mutated cybrid clones were homozygous for the

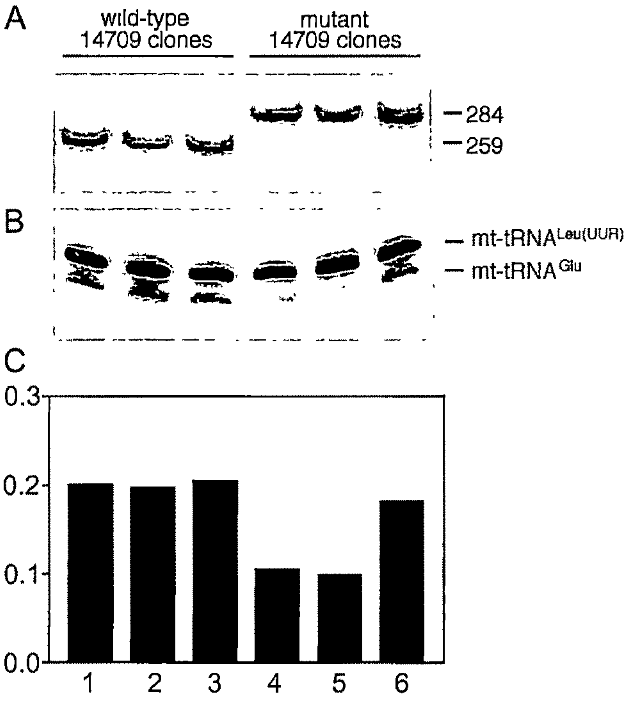

Fig. 4 Molecular analysis of wild-type and mutant 14709 cybrid clones (A) PCR-RFLP analysis of three wild-type (lanes 1–3) and three homoplasmic mutant clones (lanes 4–6) The band at 284 bp represents mutated mtDNA whilst the band at 259 bp represents wild-type mtDNA (B) Determination of steady-state mt-tRNA^{Glu} levels in cybrid clones using high-resolution Northern blots Small RNAs (1 μg) were separated through a denaturing polyacrylamide gel, electroblotted onto membranes and hybridized with radiolabeled probes specific for mt-tRNA^{Glu} and mt-tRNA$^{Leu(UUR)}$ transcripts as described in Materials and Methods (C) The bar chart illustrates the ratio of mt-tRNA^{Glu} signal to mt-tRNA$^{Leu(UUR)}$ signal for each of the six cybrid clones

Table 1
Mitochondrial respiratory chain enzyme activities in transmitochondrial cybrids

	Wild type, $n=4$ (mean ± S.D.)	M5	M7	M8	M20	M21
Complex I/CS	0.145 ± 0.064	0.089	0.162	0.120	0.078	0.125
Complex II/CS	0.292 ± 0.103	0.266	0.276	0.193	0.318	0.415
Complex IV/CS	1.34 ± 0.32	0.821	1.025	2.127	1.230	2.360

Four wild-type and five totally mutated (M5, M7, M8, M20, M21) cybrid clones were analysed. Enzyme activities from mitochondria-enriched preparations are expressed as nanomoles NADH oxidised per minute per unit citrate synthase (CS) activity for complex I, nanomoles DCPIP reduced per minute per unit of citrate synthase for complex II and the apparent first-order rate constant per second per unit citrate synthase for complex IV ($\times 10^3$). DCPIP = 2,6-dichlorophenol-indophenol, S.D. = standard deviation. Assays were performed in triplicate.

same length polymorphism at the D11S533 locus of their nuclear parent, 143B, which differed from the heterozygous pattern found in the donor patient's fibroblasts (Fig. 3B). Moreover, the allelic marker pattern D5S455 found in the rho° cells was evidenced by sequence analysis of the cybrid cells DNA (data not shown). This clearly indicated that the nucleus in cybrid cells originated from rho° cells.

3.3. *Respiratory chain enzyme analysis of transmitochondrial cybrid clones*

The activities of complexes I, II and IV were measured in mitochondrial fractions prepared from four wild-type cybrid clones and five homoplasmic mutant cybrids, and compared to the activity of the mitochondrial matrix marker enzyme, citrate synthase (Table 1). No significant differences in the enzymatic activities between homoplasmic mutant cells and homoplasmic wild-type cybrid clones were observed.

3.4. *tRNA^{Glu} steady-state levels*

To investigate the effect of the T14709C mutation on the processing of tRNA^{Glu} from its precursor, the steady-state level of tRNA^{Glu} was determined by Northern blot hybridization in the three homoplasmic wild-type and three homoplasmic mutant cybrid clones. The tRNA^{Glu} did not show any obvious size change in the mutant form compared to controls, although there appeared to be a decrease in the quantity of the mature tRNA^{Glu} transcripts in two of the three mutant clones to about 50% of the amount present in the wild-type clones (Fig. 4).

4. Discussion

In an attempt to further characterise the pathogenic mechanism of the T14709C tRNA^{Glu} mutation of mitochondrial DNA, we have constructed transmitochondrial cell lines by transferring fibroblast mitochondria from a patient previously shown to be heteroplasmic for this mutation [10], into the 143B.TK$^-$ osteosarcoma rho° cell line. Several clones were isolated that contained either exclusively the wild-type allele (homoplasmic for 14709T) or the mutant allele (homoplasmic for 14709C), and assessed for respiratory chain enzyme activities. No discernible difference in respiratory chain function was noted between the homoplasmic mutant and wild-type cybrids. High-resolution Northern analysis revealed steady-state levels of tRNA^{Glu} transcripts to be subtly decreased in some mutant clones, thus highlighting the limitations of these transmitochondrial cybrids for the investigation of pathogenic mutations.

The T14709C transition was first described in two families in whom the index case presented with an adult-onset myopathy and diabetes mellitus [8,9]; mental retardation and cerebellar ataxia was evident in members of one pedigree [8]. The mutation affects a highly conserved nucleotide flanking the anticodon of the tRNA^{Glu}, a functionally important region of the tRNA structure (Fig. 5). Incidentally, a mutation (A4295G) at the analogous position of the mitochondrial tRNA^{Ile} gene has also been documented as causing disease [24]. The T14709C mutation was shown to be heteroplasmic and present at high levels in skeletal muscle. Muscle biopsy of affected individuals revealed mitochondrial accumulations (ragged-red fibres) and a proportion of fibres expressing focal defects of cytochrome *c* oxidase (COX-negative fibres) [8,9]. Biochemical studies in muscle also revealed a defect in the activities of complexes I and IV [8–10], consistent with an impairment of mitochondrial translation. These data, together with the demonstration that COX-negative fibres harboured significantly higher levels of mutated mtDNA than functionally normal, COX-positive have assigned the mutation as pathogenic in accordance with fulfilled accepted criteria [25]. To elucidate the molecular mechanism of any

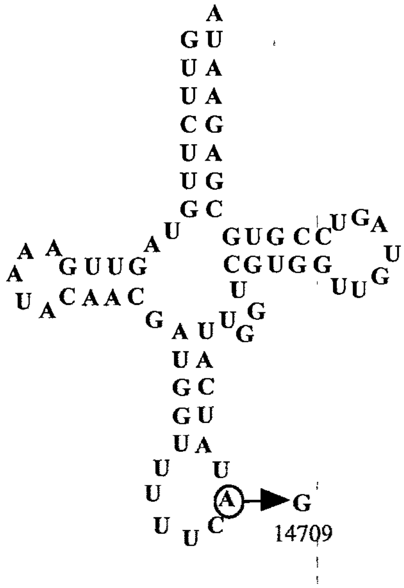

Fig. 5. Location of the T14709C mutation in the mitochondrial tRNA^{Glu} gene, highlighting the nucleotide position that is affected (arrow) within the cloverleaf secondary structure of the molecule

potential pathogenic mutation, however, studying homoplasmic transmitochondrial cybrids remains very much the method of choice [12–15].

The most puzzling aspect of our results is that the studies of the T14709C mutation in cybrids did not reflect the biochemical defect (partial complex IV deficiency) expressed in mature muscle of our patient, or those seen in previously reported cases [8,10]. We believe this may be due to a number of reasons, not least the fact that the expression of mitochondrial DNA variants is dependent upon a combination of nuclear background and mtDNA genotype. Non-random segregation of pathological and wild-type mtDNA molecules in osteosarcoma and lung carcinoma cells has been observed previously in particular for the A3243G mtDNA mutation [26] and partially duplicated mtDNAs [27]. Moreover, Hao et al. [28] have observed that under selective pressure, some transmitochondrial cybrids containing essentially homoplasmic levels of the G5703A mutation could regain normal mitochondrial function, in a process that appears to be associated with changes in the nuclear background. As cells respond to the presence of a mutation that impairs tRNA function by a variety of compensatory mechanisms, this might explain why essentially homoplasmic cybrid clones exhibited slight differences in the level of $\mathrm{tRNA}^{\mathrm{Glu}}$ transcripts.

It is reasonable that the primary molecular consequences of the T14709C mutation might be due to a translation defect by impairing the translation of glutamate codons, or to reduced levels of aminoacylated $\mathrm{tRNA}^{\mathrm{Glu}}$. Recent studies have investigated this possibility in patients with MELAS due to the A3243G mutation, following the isolation of another mutation (at position 12300) in the anticodon of the mitochondrial $\mathrm{tRNA}^{\mathrm{Leu(CUN)}}$ gene that was able to suppress both the protein synthesis defect and respiratory impairment of cells harbouring very high levels of mutant mtDNA in a lung carcinoma line [29]. Although the suppressor tRNA is efficiently aminoacylated in the lung carcinoma cell line, aminoacylation of the $\mathrm{tRNA}^{\mathrm{Leu(UUR)}}$ is severely decreased [15,30]. These data, together with studies in A3243G MELAS biopsy samples that reported decreased amounts of aminocylated $\mathrm{tRNA}^{\mathrm{Leu(UUR)}}$ in some, but not all, biopsy samples suggest that the molecular consequences of the mutation can be as diverse *in vivo* as they are in cultured cells and are dependent upon the nuclear background [31].

The large variation of the clinical phenotype in MIDD associated with the T14709C mutation is striking [8,10]. Although some of this diversity may be accounted for by intra-tissue variability of mutation load, the involvement of additional nuclear factors is likely to contribute to the phenotypic variability of the MIDD disease.

In conclusion, the T14709C mutation currently fulfils all accepted criteria to be documented as pathogenic. It has been detected in several families, is heteroplasmic and is associated with a measurable biochemical defect in patient's muscle. Our studies indicate that T14709C $\mathrm{tRNA}^{\mathrm{Glu}}$ mutation is insufficient to lead impairment of mitochondrial function in these homoplasmic osteosarcoma cybrid clones and although reduced levels of mutant tRNAs were observed, this may highlight a limitation of the cybrid cell system for studying pathogenic mtDNA mutations. More extensive work, including the analysis of further cybrids with different nuclear backgrounds, will be required before the exact correlation between clinical symptoms and state level of $\mathrm{tRNA}^{\mathrm{Glu}}$ is understood.

Acknowledgements

This work was supported by grants from the Association Française contre les Myopathies (AFM), the Programme Hospitalier pour la Recherche Clinique (PHRC Grant 97-606) and the Wellcome Trust (R.W.T. and D.M.T.).

References

[1] S W Ballinger, J M. Shoffner, E.V. Hedaya, I Trounce, M A Polak, D.C. Wallace, Maternally transmitted diabetes and deafness associated with a 10 4 kb deletion, Nat Genet. 1 (1992) 11–15

[2] J.M.W Van Den Ouweland, H.P J. Lemkes, W Ruitenbeek, L A Sandkuijl, M F Vijlder, P A A. Struyvenberg, J.J P Van de Kamp, J.A. Maasen, Mutation in mitochondrial tRNA leu (UUR) gene in a large pedigree with maternally transmitted type 2 diabetes mellitus and deafness, Nat Genet 1 (1992) 368–371

[3] N G. Larsson, D.A. Clayton, Molecular genetic aspects of human mitochondrial disorders, Annu. Rev Genet 29 (1995) 151–178

[4] K D. Gerbitz, J M W Van Den Ouweland, J A. Maassen, M. Jaksch, Mitochondrial diabetes mellitus: a review, Biochim Biophys. Acta 1271 (1995) 253–260.

[5] B Vialettes, V Paquis-Flucklinger, P. Silvestre-Aillaud, D Ben Dahan, J.F Pelissier, F Etchary-Bouyx, D Raccah, H. Gin, P.J Guillausseau, D Vanuxen, F. Orsini, J. Pouget, P Cozzone, C. Desnuelle, Extra-pancreatic manifestations in diabetes secondary to mitochondrial DNA point mutations within the tRNA leu (UUR) gene, Diabetes Care 18 (1995) 1023–1028.

[6] P.J. Guillausseau, P. Massin, D Dubois-Laforgue, J Timsit, M Virally, H Gin, E Bertin, J F Blickle, B Bouhanick, J. Cahe-Versaux, S. Caillat-Zuckman, G Charpentier, P Chedin, C Derrien, P H Duclozeau, A. Grimaldi, B. Guerci, R Kaloustian, A Murat, F. Olivier, M. Pâques, V. Paquis-Flucklinger, V Prokhov, J Samuel-Lajeunesse, B. Vialettes, Maternally inherited diabetes and deafness: a multicenter study, Ann Intern Med 134 (2001) 721–728

[7] Y. Goto, I Nonaka, S Horai, A mutation in the tRNA leu(UUR) gene associated with the MELAS subgroup of mitochondrial encephalopathies, Nature 348 (1990) 651–653.

[8] M.G Hanna, I. Nelson, M G Sweeny, V M. Cooper, P S. Watkins, J.A. Morgan Hugues, A Harding, Congenital encephalopathy and adult-onset myopathy and diabetes mellitus: different phenotypic associations of a new heteroplasmic mtDNA tRNA glutamic acid mutation, Am J Hum. Genet 56 (1995) 1026–1033

[9] H Hao, E. Bonilla, G Manfredi, S. DiMauro, C T. Moraes, Segregation patterns of a novel mutation in the mitochondrial tRNA glutamic acid gene associated with myopathy and diabetes mellitus, Am J Hum Genet 56 (1995) 1017–1025

[10] B Vialettes, V Paquis-Flucklinger, J.F Pelissier, D. Ben Dahan, H Narbonne, P Silvestre-Aillaud, M.F Montfort, M Righini-Chossegros, J Pouget, P.J. Cozzone, C. Desnuelle, Phenotypic expression of diabetes secondary to a T14709C mutation of mitochondrial DNA, Diabetes Care 20 (1997) 1731–1737.

[11] M.E Damore, P.W. Speiser, A E. Slonim, M I New, S. Shanske, W Xia, F.M Santorelli, S. DiMauro, Early onset of diabetes mellitus associated with the mitochondrial DNA T14709C point mutation patient report and literature review, J Pediatr. Endocrinol Metab 12 (1999) 207–213

[12] M P King, G. Attardi, Human cells lacking mtDNA: repopulation with exogenous mitochondria by complementation, Science 246 (1989) 500–503.

[13] M.D. Brown, I.A. Trounce, A.S Jun, J.C. Allen, D C. Wallace, Functional analysis of lymphoblast and cybrid mitochondria containing the 3460, 11778, or 14484 Leber's hereditary optic neuropathy mitochondrial mutation, J. Biol. Chem 275 (2000) 39831–39836.

[14] J.M W Van den Ouweland, P Maechler, C.B Wolheim, G Attardi, J.A Maassen, Functional and morphological abnormalities of mitochondria harboring the $\text{tRNA}^{\text{Leu(UUR)}}$ mutation in mtDNA derived from patients with maternally inherited diabetes and deafness (MIDD) and progressive kidney disease, Diabetologia 42 (1999) 485–492

[15] G M C Janssen, A. Maassen, J.M W. Van den Ouweland, The diabetes-associated mutation in the mitochondrial $\text{tRNA}^{\text{Leu(UUR)}}$ gene causes severe mitochondrial dysfunction without a strong decrease in protein synthesis rate, J Biol. Chem. 274 (1999) 29744–29748

[16] N. Kotsimbos, M.J B Jean-François, M Huizing, R M I. Kapsa, P. Lertrit, N.C Siregar, S. Marzuki, C Sue, E. Byrne, Rapid and non-invasive screening of patients with mitochondrial myopathy, Hum. Mutat 4 (1994) 132–135

[17] H. Narbonne, D. Perucca-Lostanlen, C. Desnuelle, B. Vialettes, A. Saumieres, V. Paquis-Flucklinger, Searching for the A3243G mtDNA mutation in buccal mucosa in order to improve the screening of patients with mitochondrial diabetes, Eur. J Endocrinol. 145 (2001) 541–542

[18] V Procaccio, B Mousson, R. Beugnot, H. Duborjal, F. Feillet, G Putet, I. Pignot-Paintrand, A Lombès, R De Coo, H. Smeets, J. Lunardi, J.P Issartel, Nuclear DNA origin of mitochondrial complex I deficiency in fetal infantile lactic acidosis evidenced by transnuclear complementation of cultured fibroblasts, J Clin. Invest 104 (1999) 83–92.

[19] C Mariotti, V. Tiranti, F Carrara, B Dallapiccola, S Didonato, M Zeviani, Defective respiratory capacity and mitochondrial protein synthesis in transformant cybrids harboring the tRNA Leu (UUR) mutation associated with maternally inherited myopathy and cardiomyopathy, J. Clin. Invest. 93 (1994) 1102–1107

[20] S A Lowerson, L Taylor, H Briggs, D M. Turnbull, Measurement of the activity of individual respiratory chain complexes in isolated fibroblast mitochondria, Anal Biochem 205 (1992) 372–374

[21] R W Taylor, D M Turnbull, Laboratory analysis of mitochondrial disease, in. D A Applegarth, J. Dimmick, J.G. Hall (Eds), Organelle Diseases, Chapman and Hall, London, 1997, pp. 341–350

[22] S Anderson, A.T Bankier, B G Barrell, M.H.L de Bruijn, A R Coulson, J Drouin, I C Eperon, D P Nierlich, B.A Roe, F Sanger, P H Schreier, A.J.H Smith, R Staden, I G. Young, Sequence and organisation of the human mitochondrial genome, Nature 290 (1981) 457–465.

[23] R.M Andrews, I. Kubacka, P F Chinnery, R N. Lightowlers, D.M. Turnbull, N. Howell, Reanalysis and revision of the Cambridge reference for human mitochondrial DNA, Nat. Genet 23 (1999) 147

[24] F Merante, T Myint, I Tein, L Benson, B.H. Robinson, An additional mitochondrial tRNA (Ile) point mutation (A-to-G at nucleotide 4295) causing hypertrophic cardiomyopathy, Hum. Mutat 8 (1996) 216–222

[25] S DiMauro, E.A. Schon, Mitochondrial DNA mutations in human disease, Am. J. Med. Genet 106 (2001) 18–26.

[26] D R Dunbar, P.A Moonie, H.T Jacobs, I.J Holt, Different cellular backgrounds confer a marked advantage to either mutant or wild-type mitochondrial genomes, Proc. Natl. Acad Sci U S A 92 (1995) 6562–6566

[27] I.J. Holt, D R Dunbar, H T Jacobs, Behaviour of a population of partially duplicated mitochondrial DNA molecules in cell culture. segregation, maintenance and recombination upon nuclear background, Hum Mol Genet. 6 (1997) 1251–1260

[28] H Hao, L.E Morrison, C.T Moraes, Suppression of a mitochondrial tRNA gene mutation phenotype associated with changes in the nuclear background, Hum. Mol Genet 8 (1999) 1117–1124

[29] A El Meziane, S K Lehtinen, N. Hance, N.G.J. Nijtmans, D. Dunbar, I.J. Holt, H T Jacobs, A tRNA suppressor mutation in human mitochondria, Nat Genet 18 (1998) 350–353.

[30] A El Meziane, S K Lehtinen, I.J. Holt, H T. Jacobs, Mitochondrial tRNA (Leu) isoforms in lung carcinoma cybrid cells containing the np 3243 mtDNA mutation, Hum. Mol. Genet 7 (1998) 2141–2147

[31] G V Börner, M. Zeviani, V. Tiranti, F Carrara, S Hoffmann, K D Gerbitz, H. Lochmüller, D Pongratz, T Klopstock, A. Melberg, E. Holme, S. Pääbo, Decreased aminoacylation of mutant tRNAs in MELAS but not in MERFF patients, Hum. Mol Genet 9 (2000) 467–475

ELSEVIER

Biochimica et Biophysica Acta 1588 (2002) 217–225

BIOCHIMICA ET BIOPHYSICA ACTA
BBA
www.bba-direct.com

Ethanol-induced augmentation of annexin IV in cultured cells and the enhancement of cytotoxicity by overexpression of annexin IV by ethanol

Hiroko Ohkawa [a,b], Hitoshi Sohma [a,*], Rie Sakai [a,c], Yoshio Kuroki [a], Eri Hashimoto [c], Shinji Murakami [b], Toshikazu Saito [c]

[a] *Department of Biochemistry, Sapporo Medical University School of Medicine, South-1, West-17, Chuo-ku, Sapporo 060-8556, Japan*
[b] *Department of Occupational Therapy, Sapporo Medical University School of Health Sciences, Sapporo 060-8556, Japan*
[c] *Department of Neuropsychiatry, Sapporo Medical University School of Medicine, Sapporo 060-8543, Japan*

Received 19 March 2002; received in revised form 12 July 2002, accepted 31 July 2002

Abstract

The annexins are a family of highly homologous Ca^{2+} and phospholipid binding proteins. The expressive amounts of several annexins have been shown to alter in certain pathological states such as brain ischemia and Alzheimer's disease. It has been demonstrated that ethanol induces cytotoxicity, which results in brain damage. In this study, we examined the relationship between ethanol-induced cytotoxicity and the intrinsic amount of annexins using cell lines (rat glioma C6 cells and human adenocarcinoma A549 cells). A decrease in the mitochondrial enzyme (dehydrogenase) activity, which is widely used to measure cytotoxicity, was observed with a high concentration of ethanol (200 mM or more) after a 24-h exposure in both C6 and A549 cells. Western blot analysis revealed that the amount of annexin IV was augmented in both cells by ethanol, whereas levels of annexins I and V were unchanged. The amount of annexin IV was augmented with increasing concentration of ethanol. The overexpression of annexin IV in C6 cells by transfection with annexin IV-DNA enhanced ethanol-induced cell lesion and was accompanied by NFκB activation. Thus, it might be indicated that the amount of annexin IV is selectively augmented and this augmentation facilitates the development of cell lesion by ethanol

© 2002 Elsevier Science B.V All rights reserved.

Keywords Annexin IV, Ethanol, Cytotoxicity, NFκB; Cell line

1. Introduction

The annexins are a family of proteins that bind to both Ca^{2+} and phospholipids; particularly acidic phospholipids [1]. Annexins are widely distributed among species and tissues, although the precise function of annexins is not fully understood.

Several annexins have been identified in the brain and the patterns of annexin expression have been reported to change during development of the brain and in pathological states. High levels of annexin II are detected in the human fetal brain, but it is not detectable in the adult brain [2,3] The neuronal cytoarchitectural distribution of annexin VI is altered and the expressive amounts of annexins I, II and IV are increased in the hippocampus in pathological states such as brain ischemia and Alzheimer's disease [4]. The amount of annexin I is increased in the astrocytosis of the human brain in other pathological states [5]. Moreover, therapeutic effect of the administration of annexin I to the experimentally ischemic rat brain was reported [6–9]. We have previously shown that the amount of annexin IV was significantly increased in the hippocampus of the postmortem brains of alcoholic patients, compared with controls [10].

Ethanol induces brain damage by unknown mechanisms. It has been reported that exposure of isolated neuronal cells to ethanol (either 120 mM or more) induces Fas/Apo-1 mRNA leading to programmed cell death or apoptosis [11]. Recently, it was demonstrated that Fas-induced apoptosis was accompanied by expressive and locational alterations of increasing amounts of several proteins, including annexin IV, in cytoplasm of Jurkat T cells [12].

Abbreviations XTT, (sodium 3′-[1-(phenylaminocarbonyl)-3,4-tetrazolium]-bis (4-methoxy-6-nitro) benzene sulfonic acid hydrate; PBS, phosphate buffered saline, PVDF, polyvinylidene difluoride, CAPS, cyclohexylaminopropanesulfonic acid, DMEM, Dulbecco's Modified Eagle's Medium

[*] Corresponding author. Tel · +81-11-611-2111x2671; fax: +81-11-611-2236.

E-mail address sohma@sapmed ac.jp (H Sohma)

0925-4439/02/$ - see front matter © 2002 Elsevier Science B.V All rights reserved
PII S0925-4439(02)00168-0

The present study was performed to examine the effect of ethanol on the expression of annexins in cultured cells (rat C6 glioma and human adenocarcinoma A549 cells) and the relationship of this to ethanol-induced cytotoxicity. We show that the expression of annexin IV is augmented by ethanol but that both annexins I and V are unaffected and that overexpression of annexin IV enhances ethanol-induced cytotoxicity.

2. Materials and methods

2.1. Materials

Reagents were purchased from the following sources: restriction enzymes and DNA-modifying enzymes, Gibco BRL (Rockville, MD, USA) and New England Biolabs (Beverly, MA, USA); antibiotics and IPTG, Sigma Chemical (St. Louis, MO, USA); κB oligo nucleotide probe and T4 polynucleotide kinase, Promega (Madison, WI, USA); molecular weight standards and Protein A-Sepharose 4B, Amersham Pharmacia Biotech. (Buckinghamshire, UK); pET3d vector and BL21(3D) cells, Strategene (La Jolla, CA, USA); pcDNA3.1 vector, Invitrogen (Carlsbad, CA, USA); Cell proliferation kit II (XTT), Roche Molecular Biochemicals (Indianapolis, IN, USA); [γ-^{32}P]ATP, Perkin-Elmer Life Science Products (Boston, MA, USA).

2.2 Cell culture

Rat glioma C6 cells (JCRB9096) and human adenocarcinoma A549 cells (JCRB0076) were obtained from the Health Science Research Resources Bank (Osaka, Japan). C6 and A549 cells were maintained in continuous log phase growth in Nutrient Mixture F-10 Ham and RPMI-1640, respectively, containing 10% fetal calf serum at 37 °C in a humidified incubator containing 95% air–5% CO_2 atmosphere. The cells were not allowed to reach confluence at any time since the cell viability decreased after being confluent without adding ethanol. Cells were cultured in serum-free media for 0.5–1 h prior to the addition of ethanol to the culture media and then cultured for the indicated times.

2.3. Preparation of recombinant annexins

Recombinant human annexin IV was prepared as described previously [10]. Rat annexins I and V DNAs were prepared based on polymerase chain reaction. Total RNA was prepared from fresh rat brain with an SV Total RNA Isolation System (Promega). After synthesis of first strand cDNA, annexin I and V genes were amplified by PCR with synthesized primers based on the previously reported sequence of rat annexins I and V [13,14]. *Nco*I and *Bam*HI restriction sites were introduced at the 5′ and 3′ termini of the coding sequence of both annexins I and V DNAs, respectively. *Nco*I/*Bam*HI-digested annexin IV DNA was subcloned into expression vector (pET-3d) by standard techniques. The DNA clone was used to transform *E. coli* strain (BL21 (3D)). Purification of recombinant annexins I and V was based on Ca^{2+}-dependent binding to rat brain lipids by the method of Nelson and Creutz [15], and Sohma et al. [16]. The purified proteins were dialyzed against 10 mM Hepes (pH 7.0) and 0.1 M NaCl and stored at − 40 °C until use and used within a few months.

2.4. Antibodies

Polyclonal antibodies against each annexin were prepared from rabbits. IgG fractions of anti-annexins I and V antisera were then obtained with a Protein-Sepharose 4B column. A specific antibody against annexin IV was prepared with a human recombinant annexin IV-conjugated Sepharose 4B column. Each antibody specifically reacted with each annexin (Fig. 1). Rabbit antibody againt NFκB p65 (sc-372) and goat antibody against actin antibodies (sc-1616) were purchased from Santa Cruz Biotechnology (Santa Cruz, CA, USA).

2.5. Western blotting and densitometric analysis

After ethanol treatment, culture media was replaced with 10 mM phosphate buffered saline (PBS). The cells were harvested by pipetting for C6 cells and by using the cell scraper for A549 cells, washed once with PBS and frozen at − 80 °C. Frozen cells were thawed and 1 mM phenylmethylsulfonyl fluoride (PMSF) was added and homogenized with a pellet mixer (20 strokes) (Treff Lab. Switzerland) in ice and mixed with an equivalent volume of PBS, and then sonicated for 10 s at 20 W to homogeneity with a probe sonicator and stored at − 40 °C until use. Cell lysates containing 20-μg proteins were subjected to polyacrylamide gel electrophoresis in the presence of SDS (0.1% w/v) (SDS-PAGE) by the method of Laemmli [17] and then transferred to polyvinylidene difluoride (PVDF) membrane for 12 h at 12 V with transfer buffer (10 mM cyclohexylaminopropanesulfonic acid (CAPS) (pH 11), and 10% methanol (v/v)). The blots were blocked with 3% skim milk in PBS for 1 h and then probed with affinity-purified rabbit antibody against human annexin IV (1:50 dilution with PBS containing 1 mg/ml BSA), anti-annexins I or V IgG (1:500 dilution) or anti-actin antibody (1 to 400 dilution) for 1–2 h. The blots were then incubated with horseradish peroxidase-conjugated goat anti-rabbit IgG or rabbit anti-goat IgG (1:3000 dilution with PBS containing 1 mg/ml BSA) (Jackson ImmunoResearch Laboratories, West Grove, PA, USA). Finally, after washing, antibody visualization was performed using a SuperSignal West Pico Chemiluminescent Substrate (Pierce, Rockford, IL, USA). Washing between incubations

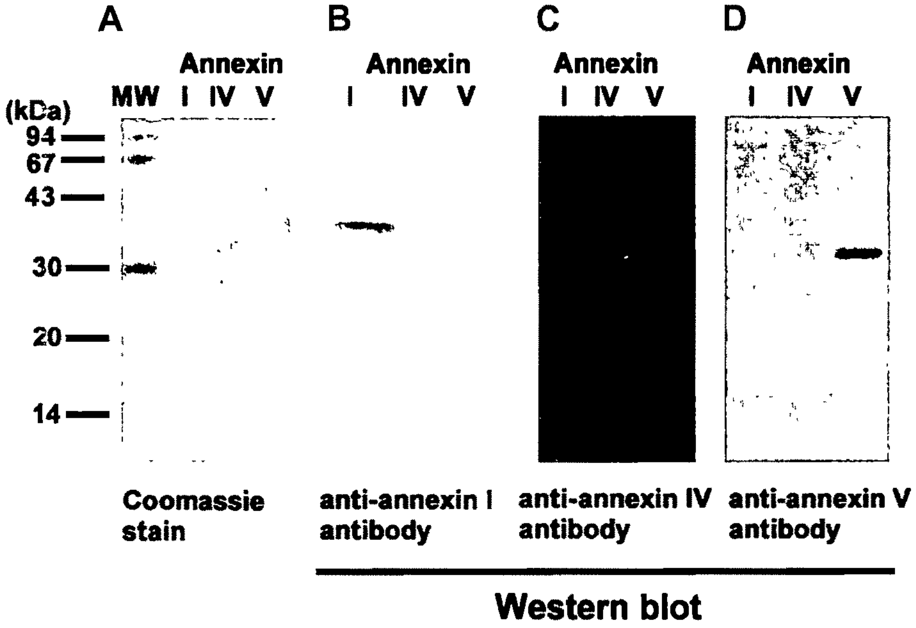

Fig. 1. Specific recognition by antibody to annexins I, IV, or V. Fifty nanograms of recombinant annexins I, IV, and V were resolved in SDS-PAGE and Western blotting was performed with anti-annexins I, IV, or V antibody. (A) Coomassie blue-stained PVDF membrane; (B–D) Western blot with anti-annexins I, IV, and V antibodies, respectively.

was done with PBS containing 2% skim milk and 0.1% Tween 20. Densitometric analysis of the stained bands was performed with an Epi-Light FA500 (Aisin Cosmos R&D, Tokyo, Japan).

2.6. Measurement of cell cytotoxicity (XTT assay)

To analyze cell lesion by ethanol, the mitochondrial dehydrogenase activity that cleaves XTT (sodium 3′-[1-(phenylaminocarbonyl)-3,4-tetrazolium]-bis (4-methoxy-6-nitro) benzene sulfonic acid hydrate) (Cell proliferation kit II) was measured according to the instruction manual. Since only living cells can cleave XTT to form a formazan product, the magnitude of the absorbance at 450 nm is proportional to the number of viable cells. Briefly, 1×10^5 cells were plated in a 35-mm culture dish and cultured for 24 h and culture medium was replaced with serum-free Nutrient Mixture F-10 Ham for C6 cells and serum- and phenol red-free Dulbecco's Modified Eagle's Medium (DMEM) for A549 cells and incubated for 0.5–1 h at 37 °C. Then, ethanol was added to the culture media and incubated for the indicated times at 37 °C. After ethanol treatment, the culture medium was replaced again with 1 ml of serum-free Nutrient Mixture F-10 Ham for C6 cells and serum- and phenol red-free DMEM for A549 cells, and 500 μl of XTT solution was added to each of the culture dishes and incubated for 1–2 h more at 37 °C. Two-hundred-microliter aliquots of the solution were transferred to a 96-well plate and absorbance at 450 nm was measured to detect formazan product.

2.7. Transfection of annexin IV cDNA

Human annexin IV DNA was prepared by polymerase chain reaction as described previously [10], introducing *Nhe*I and *Bam*HI restriction sites at the 5′ and 3′ termini of the coding sequence. The insert (~ 1.1 kb, *NheI/Bam*H1 fragment) was subcloned into a pcDNA3.1(+) expression vector as in the sense orientation. Transfection into C6 cells was performed using FuGENE™ 6 Transfection Reagent (Roche Molecular Biochemicals). One microgram and 5 μg of the plasmid DNA were used for the 35-mm and 100-mm culture dish, respectively, according to the instruction manual.

2.8. Preparation of nuclear extract from cultured cells

Nuclear fractions of cells were prepared by the method of Dignam et al. [18] with a slight modification. All procedures were done on ice. Briefly, 5×10^6 cells were suspended in 1 ml of buffer A (10 mM Hepes, pH 7.5, 1.5 mM $MgCl_2$, 10 mM KCl, 1 mM DTT, and 0.5 mM PMSF) and lysed by passing them through a 27G-needle connected to a 1-ml syringe (10 strokes), and then centrifuged at 800 × *g* for 10 min. The pellet was suspended in 1.5 ml of buffer B (2.2 M sucrose, 20 mM Hepes, pH 7.5, 5 mM $MgCl_2$, and 0.5 mM PMSF) and centrifuged at 40,000 × *g* for 1 h. The pellet containing the nuclei was suspended with 200 ml of nuclear extraction solution (20 mM Hepes, pH 7.5, 0.4 M NaCl, 2 mM EGTA, and 0.5 mM PMSF) and incubated in ice for 30 min. Finally the solution was centrifuged at

80,000 × *g* for 20 min. The supernatant was stored at − 40 °C until use.

2.9. Electrophoretic gel mobility shift assay

Activation of transcription factor NFκB was examined using consensus κB oligonucleotides (5′-AGTTGAGGG-GACTTTCCCAGGC-3′). A probe was labeled with [γ-^{32}P]ATP (3000 Ci/mmol) by T4 polynucleotide kinase. The ^{32}P-labeled probe (1 μl, 20,000 cpm) was added to the reaction mixture (9 μl) containing nuclear extract (1 μg), 10 mM Tris (pH 7.5), 4% glycerol, 0.5 mM EDTA, 1 mM $MgCl_2$, 50 mM NaCl, and 50 μg/ml poly(dI–dC), and incubated for 20 min at room temperature. The mixture was subjected to PAGE (5% gel) for 150 min at 100 V. The

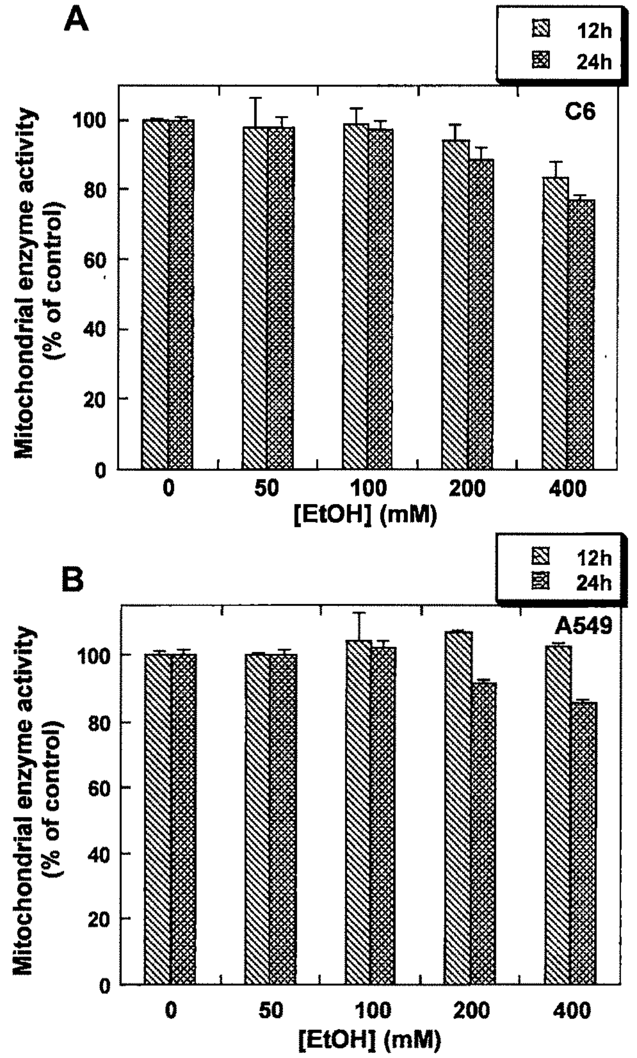

Fig. 2. Effect of ethanol on the mitochondrial dehydrogenase in C6 and A549 cells. The mitochondrial dehydrogenase activity was measured as described in Materials and methods. Relative enzyme activity of the cells (either C6 (A) or A549 cells (B)) after exposure to various concentrations of ethanol for either 12 or 24 h was shown, the magnitude of the enzyme activity of untreated control was regarded as 100%. Data represent mean ± S.D. of three experiments. Hatched bars, 12-h exposure; cross-hatched bars, 24-h exposure.

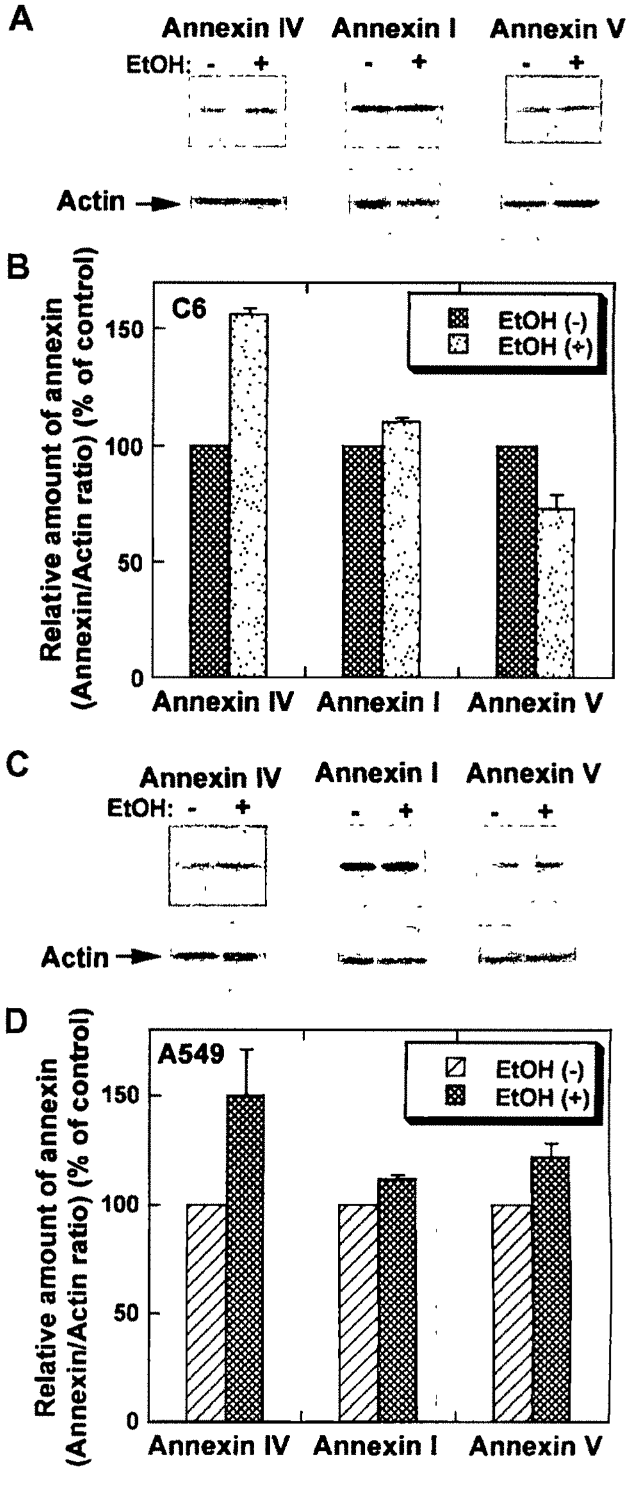

Fig. 3. Effect of ethanol on the expressive amounts of annexins I, IV, and V in C6 and A549 cells. Cells were incubated with 200 mM ethanol for 12 h and the cell lysate containing 20 μg was resolved by SDS-PAGE, and then transferred to PVDF membrane. Western blotting was performed with the specific antibody against each annexin isoform and actin. (A, C) Representative Western blots, (B, D) densitometric analysis of the intensities of the immunostained bands. Relative ratio of annexin to actin was shown. (A, B) C6 cells, (C, D) A549 cells. A, C: −, untreated control, +, ethanol treatment. B, D: hatched bars, untreated controls, cross-hatched bars, ethanol treatment. Data represent mean ± S.D. of three experiments.

gel was dried and exposed to X-ray film overnight at 4 °C. To verify the specificity of the DNA binding of NFκB, competition assay was done by adding a molar excess of unlabeled κB oligonucleotides to the reaction mixture before the addition of labeled probe.

2.10 Others

Protein concentrations were determined by a BCA Protein Assay Reagent Kit (Pierce) using bovine serum albumin as standard. Statistical analysis was performed by using one-way ANOVA, with a value of $P<0.05$ considered as significant.

3. Results

To analyze the cytotoxic effect of ethanol in cultured cells (C6 and A549 cells), we first measured ethanol-induced change in the mitochondrial dehydrogenase activity (XTT assay) (Fig. 2). The magnitude of the enzyme activity was unchanged with either 50 or 100 mM ethanol in both C6 and A549 cells after 12- and 24-h exposure compared with the untreated control, while the activity decreased with 200 or 400 mM of ethanol after either 12- or 24-h exposure in C6 cells (Fig. 2A). In A549 cells, the activity was unchanged after 12-h exposure with either 200 or 400 mM of ethanol but decreased after 24-h exposure (Fig. 2B). These results suggest that C6 cells might be more susceptible to ethanol than A549 cells.

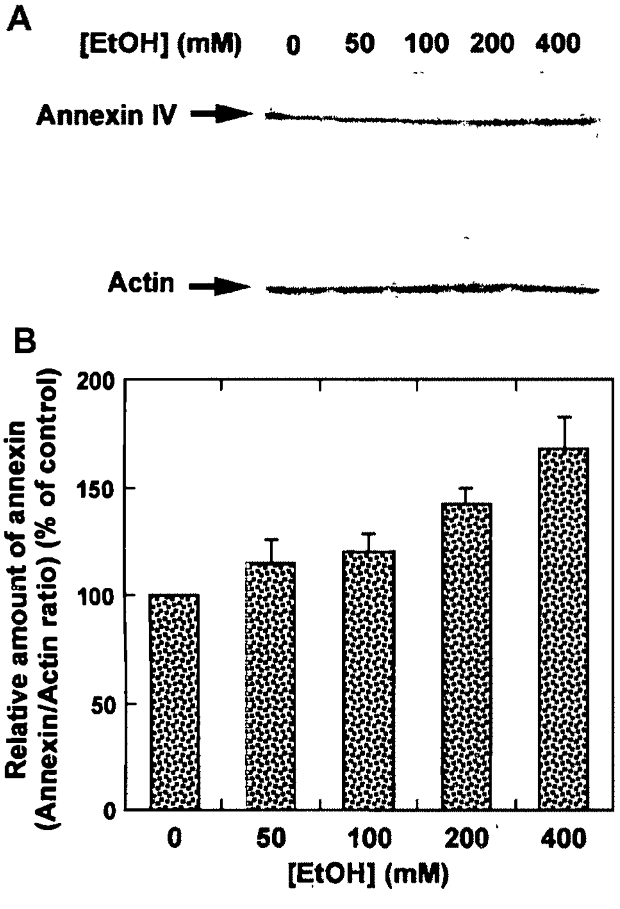

Fig. 4. Ethanol concentration-dependent increase in the amount of annexins IV in C6 cells C6 cell were incubated with various concentrations of ethanol for 12 h and the cell lysate containing 20 μg was resolved by SDS-PAGE and then transferred to PVDF membrane. Western blotting was performed with the specific antibody against annexin IV and actin. (A) Representative Western blots, (B) densitometric analysis of the intensities of the immunostained bands Relative ratio of annexin to actin was shown Data represent mean ± S D of three experiments

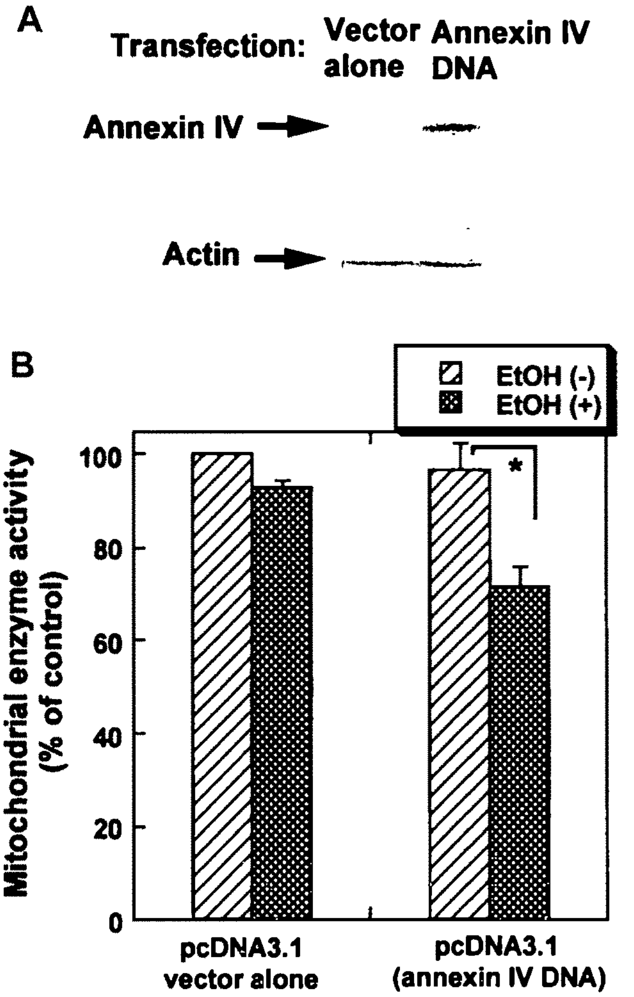

Fig 5 Effect of overexpression of annexin IV on ethanol-induced cell lesion. (A) C6 cells were transfected with either vector alone (pcDNA3 1) or annexin IV DNA After transfection, the cell lysate containing 10 μg was resolved by SDS-PAGE and then transferred to PVDF membrane Western blotting was performed with the specific antibody against annexin IV and actin Representative Western blots are shown (B) After transfection, the cells were incubated with 400 mM ethanol for 12 h. Relative mitochondrial dehydrogenase activity of the cells is shown, the magnitude of the enzyme activity of the control (without ethanol) (transfected with vector alone) was regarded as 100% Data represent mean ± S D of three experiments Hatched bars, no ethanol, cross-hatched bars, incubation with 400 mM ethanol for 12 h –, untreated control, +, ethanol treatment. Data represent mean ± S D. of three experiments *, significantly different ($P<0.05$) when compared between the two groups.

Next, using the antibodies representing specific interaction with each annexin (Fig. 1), we performed Western blot analysis to monitor the amounts of annexins I, IV and V in both C6 and A549 cells (Fig. 3). The relative ratio of each immunostained annexin band to actin band was compared. The intensity of annexin IV band was augmented by a 12-h exposure to 200 mM ethanol in both C6 (Fig. 3A) and A549 cells (Fig. 3C). Densitometric analysis indicated that the amount of annexin IV increased by about 1.5 times, compared with the untreated control (Fig. 3B and D). On the other hand, the extent of the changes in the intensities of the immunostained bands of both annexins I and V was almost comparable with the untreated controls in both C6 and A549 cells (Fig. 3). Thus, it is possible that expression of annexin IV is selectively augmented by ethanol. We next examined ethanol-induced increase of annexin IV in C6 cells after 12-h exposure to varying concentrations of ethanol (0–400 mM). The amount of annexin IV increased in an ethanol concentration-dependent manner (Fig. 4).

To further investigate the properties of annexin IV in ethanol-induced cytotoxicity, we next performed XTT assay using annexin IV-overexpressed C6 cells (Fig. 5). Western blot analysis revealed that the amount of annexin IV in the C6 cells transfected with annexin IV cDNA rose to at least five times (Fig. 5A). After transfection, cells were incubated with 400 mM ethanol for 12 h and XTT assay was performed (Fig. 5B). Interestingly, the ethanol-induced cytotoxicity was enhanced by the overexpression of annexin IV. The extent of the ethanol-induced decrease in the mitochondrial dehydrogenase activity was larger in the annexin IV-overexpressed C6 cells than in the C6 cells transfected with vector alone (Fig. 5B). Thus, increased annexin IV is likely to be involved in the enhancement of ethanol-induced cell lesion in C6 cells.

It has been demonstrated that ethanol augments the transcription factor NFκB activation by cytokines such as tumor necrosis factor-α (TNF-α) and interferon α (IFN α) in primary cultured cells and cell line [19–21]. To investigate if annexin IV modulates the activity of NFκB in the presence of ethanol, we analyzed NFκB binding to specific oligonucleotides encompassing the consensus sequence of κB with the nuclear extracts from the C6 cells by electrophoretic gel mobility shift assay (Fig. 6). It was shown that the amount of DNA binding to NFκB was significantly larger when the cells transfected with annexin IV-DNA were incubated with 400 mM ethanol. In contrast, the amount of DNA binding was only slightly increased in the nuclear extract from the cells transfected with vector alone (Fig. 6). Since the shift bands diminished when an excess amount of unlabeled DNA probe was co-incubated (data not shown), it was concluded that overexpression of annexin IV enhanced NFκB activation by ethanol in C6 cells. Western blot analysis with anti-NFκB (65 kDa-subunit) antibody revealed that the intensity of the immunostained NFκB band with 65 kDa significantly increased in the nuclear extract from the annexin IV-overexpressed C6 cells, while the amount of the 65 kDa band was only slightly increased in the cells transfected with vector alone (Fig. 7). These

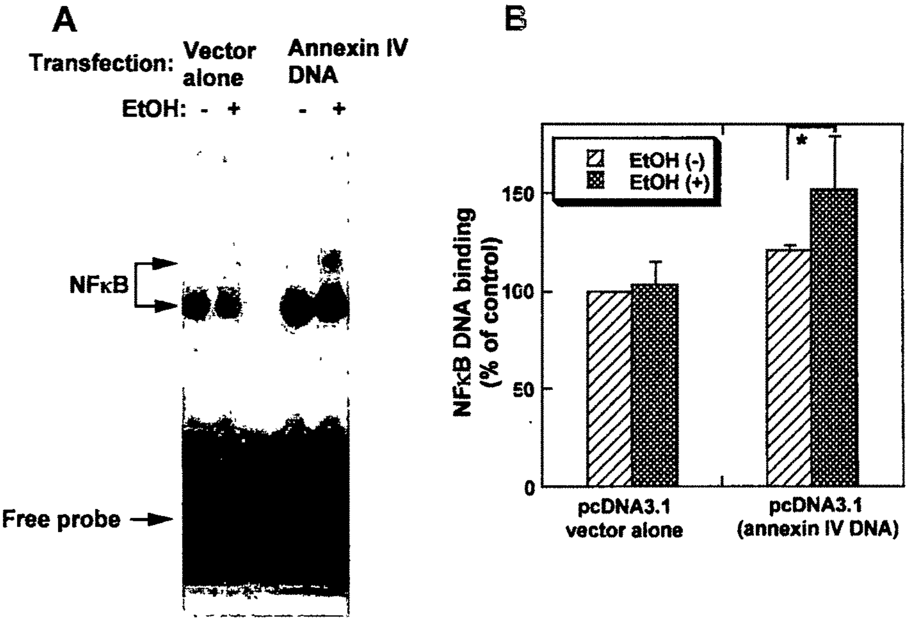

Fig. 6 Effect of overexpression of annexin IV on NFκB activation by ethanol in C6 cells C6 cells were transfected with either vector alone (pcDNA3.1) or annexin IV DNA After transfection, cells were incubated with 400 mM ethanol for 12 h The cells were harvested and nuclear extracts were prepared as described in Materials and methods Equal amounts (1 μg) of protein were evaluated in an electrophoretic gel mobility shift assay by using ^{32}P-labeled NFκB oligonucleotide (A) Autoradiography of the gel; (B) densitometric analysis of NFκB-shift bands. −, untreated control, +, ethanol treatment Data represent mean ± S D of three experiments *, significantly different ($P<0.05$) when compared between the two groups.

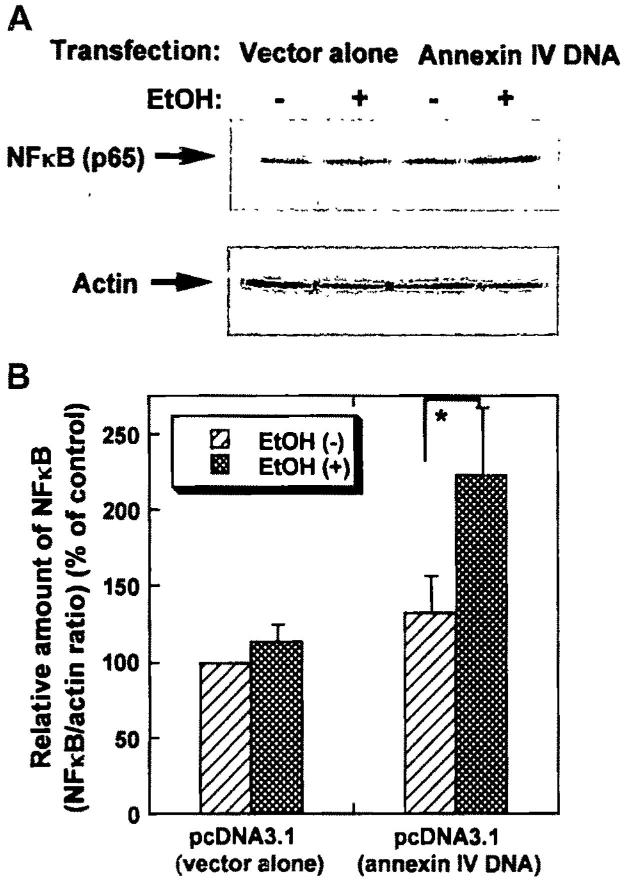

Fig 7 Effect of overexpression of annexin IV in the amount of nuclear NFκB in C6 cells C6 cells were transfected with either vector alone (pcDNA3 1) or annexin IV DNA. After transfection, cells were incubated with 400 mM ethanol for 12 h. The cells were harvested and nuclear extracts were prepared as described in Materials and methods and 10 μg was resolved by SDS-PAGE and then transferred to PVDF membrane. Western blotting was performed with the specific antibodies against NFκB and actin (A) Representative Western blots (B) Densitometric analysis of the intensities of the immunostained bands Relative ratio of NFκB to actin was shown. −, untreated control, +, ethanol treatment Data represent mean ± S.D of three experiments *, significantly different ($P<0.05$) when compared between the two groups.

results are consistent with the electrophoretic gel mobility shift assay. Thus, the augmentation of annexin IV expression by ethanol might facilitate ethanol-induced cell lesion via NFκB activation.

4. Discussion

In the present study, it was demonstrated that the amount of annexin IV was augmented by exposure to ethanol in cultured cells (C6 and A549 cells), whereas the amount of either annexin I or V was unaltered by ethanol (Fig. 3). The increase in the amount of annexin IV was ethanol concentration-dependent in C6 cells (Fig. 4). The amount of annexin IV also increased in an ethanol concentration-dependent manner in A549 cells (data not shown). These results may indicate that annexin IV expression is selectively altered by ethanol.

Mitochondrial dehydrogenase activity measurement has been widely used to monitor detection of cell lesion. Using this method, it was shown that a high concentration of ethanol (>200 mM) induced cell lesion in both C6 and A549 cells (Fig. 2). However, the increased amount of annexin IV was observed with lower concentration of ethanol (50 or 100 mM) than 200 mM (Fig. 3), where the mitochondrial enzyme level was the same as control (Fig. 2). It is plausible that the increase in the expression of annexin IV occurred at the early stage of cell lesion before damage had been induced.

It has been demonstrated that fetal alcohol syndrome and neurological outcome are directly related to the neurotoxic effect of ethanol [22]. We previously reported that the amount of annexin IV was significantly increased in the hippocampus of the postmortem brains of alcoholic patients compared with controls [10]. Since the present study revealed that the expression of annexin IV is augmented by exposure to ethanol in cultured cells, annexin IV might be a biological marker for alcoholism.

The ethanol concentration used in this study seems larger than the concentrations measured in sober alcohol users in an emergency room, who had average concentration with about 60 mM [23]. On the other hand, a high concentration of blood ethanol in woman drinkers (165–330 mM) was also reported [24,25]. The ethanol concentration used in this study is not far from the physiologically relevant concentration.

It has been demonstrated that ethanol augments TNF-α-induced neurotoxicity, and that ethanol enhanced TNF-α- and IFNα-induced activation of NFκB [19,26]. Ethanol exposure itself does not alter NFκB activation, but it does in the HEP G2 cells transfected with cytochrome *P*450 2E1 (CYP2E1) DNA [21]. Since CYP2E1 is involved in the oxidative metabolism of ethanol, it conceivably contributes to ethanol-induced lesion via oxidative stress. In this study, it was shown that 200 mM or more of ethanol was needed to induce cell lesion when ethanol alone was used as the cytotoxic reagent. Since no exogenous cytokine was added in our experimental system, the augmentation of annexin IV might have been caused by the direct effect of ethanol. It is striking that ethanol-induced cytotoxicity was enhanced by overexpression of annexin IV in C6 cells (Fig. 5). Only slightly enhanced NFκB activity was shown with 400 mM of ethanol alone, but overexpression of annexin IV significantly augmented NFκB activity by ethanol (Figs. 6 and 7). Since no enzymatic activity for annexin IV has been identified, the overexpressed annexin IV might affect other unknown enzyme activities that may be involved in oxidative stress.

The role of NFκB is now controversial. It has been reported that NFκB functions to either promote or inhibit apoptosis in cells [27]. The present study suggests a correlation among enhanced annexin IV expression, ethanol-induced cytotoxicity and NFκB activation. Thus, it is possible that NFκB activation might be involved in the cytotoxic effect of ethanol-induced cytotoxicity.

Annexin IV has been shown to translocate from nucleus to cytosol in Jurkat T-lymphocyte during Fas-induced cell death [12]. A strong immunostaining of annexin IV in both the cytosol and nuclear region was observed in C6 cells after 12–24-h exposure to 50 or 100 mM ethanol in C6 cells (Sohma et al., unpublished data). Moreover, nuclear annexin IV diminished after 24-h exposure to 400 mM ethanol and a strong staining was observed in the cytosol, suggesting that annexin IV in the nuclei translocated to cytosol (Sohma et al., unpublished data). These results suggest that annexin IV translocation might be related to cytotoxicity by ethanol. Furthermore, it will be intriguing to investigate whether nuclear annexin IV has a functional role in this process or not.

An antitumor drug or antimitotic compound (A204197) increases annexin IV in HCT15 cells [28]. Interestingly, transfection of annexin IV cDNA into 293T cells imbued the cells with resistance to another antimitotic compound (paclitaxel) [28], indicating that annexin IV contributes to drug resistance. In contrast, our data revealed that overexpression of annexin IV enhanced ethanol-induced cell lesion. Thus, annexin IV involvement in cellular conditions might differ, depending on the use of drugs.

In conclusion, the present study showed that ethanol increased annexin IV expression in C6 and A549 cells, but no increased expression of annexins I or V was seen. Thus, annexin IV expression may be a specific marker for ethanol.

Acknowledgements

We are indebted to Mr. Wataru Ukai of Toyama Chemical for assistance in the cell cytotoxicity assays. We are also grateful to Dr. Tomonobu Shirasaka of Ishibashi hospital and Dr. Hiroki Ozawa of Sapporo Medical University for their valuable contributions. This study was supported by research grants from the Foundation of Sapporo Medical University, a Grant-in-Aid for Scientific Research from the Ministry of Education, Science, Sports and Culture, Japan (grant number 12670950), the Suntory foundation of Japan and the Hokkaido wine foundation.

References

[1] V. Gerke, S.E Moss, Annexins and membrane dynamics, Biochim Biophys Acta 1357 (1997) 129–154

[2] R.D. Burgoyne, M A. Cambray-Deakin, K -M Norman, Developmental regulation of tyrosine kinase substrate p36 (calpactin heavy chain) in rat cerebellum, J Mol Neurosci 1 (1989) 47–54.

[3] S.A. Reeves, C Chavez-Kappel, R Davis, M Rosenblum, M A Israel, Developmental regulation of annexin II (lopocortin-2) in human brain and expression in high grade glioma, Cancer Res 52 (1992) 6871–6876

[4] D.A. Eberhard, M.D. Brown, S R VandenBerg, Alteration of annexin expression in pathological neuronal glial reactions Immunohistochemical localization of annexins I, II (p36 and p11 subunits), IV, and VI in the human hippocampus, Am. J Pathol. 145 (1994) 640–649.

[5] J K Relton, P J L.M Strijbos, C.T. O'Shaughnessy, F. Carey, R A Forder, F.J H Tilders, N J Rothwell, Lipocortin-1 is an endogenous inhibitor of ischemic damage in the rat brain, J Exp Med 174 (1991) 305–310

[6] M D Johnson, J M Kamso-Pratt, J W O. Whetsll, R B. Pepinsky, Lipocortin-1 immunoreactivity in the normal human central nervous system and lesions with astrocytosis, Am J. Clin. Pathol 92 (1989) 424–429.

[7] F. Carey, R.A Forder, M D. Edge, A R Greene, M.A Horan, P J.L M Strijbos, N.J Rothwell, Lipocortin 1 fragment modifies pyrogenic actions of cytokines in rats, Am J. Physiol 259 (1990) R266–R269

[8] J.A McKanna, A Chuncharunee, K A Munger, J A Breyer, S Cohen, R C Harris, Localization of p35 (annexin I, lipocortin I) in normal adult rat kidney and during recovery from ischemia, J Cell. Physiol. 153 (1992) 467–476

[9] S Cuzzocrea, A Taylor, B Zingarelli, A L. Salzman, R.J Flower, C. Szabó, M Perretti, Lipocortin 1 protects against splanchnic artery occlusion and reperfusion injury by affecting neutrophil migration, J Immunol 159 (1997) 5089–5097

[10] H. Sohma, H. Ohkawa, E Hashimoto, S. Toki, H. Ozawa, Y Kuroki, T. Saito, Alteration of annexin IV expression in alcoholics, Alcohol., Clin Exp. Res 25 (2001) 55S–58S.

[11] Z F Cheema, J.R West, R C Miranda, Ethanol induces Fas/Apo [apotosis]-1 mRNA and cell suicide in the developing cerebral cortex, Alcohol , Clin Exp Res 24 (2000) 535–543

[12] C Gerner, U. Froehwein, J Gotzmann, E Bayer, D Gelbmann, W Bursch, R. Schulte-Hermann, The fas-induced apoptosis analysis analyzed by high throughput proteome analysis, J. Biol Chem 275 (2000) 39018–39026.

[13] M Tamaki, E Nakamura, C Nishikubo, T. Sakata, M Shin, H Teraoka, Rat lipocortin I cDNA, Nucleic Acids Res. 15 (1987) 7637

[14] R B. Pepinsky, R Tizard, R J Mattaliano, G T Miller, J L Browning, P E Chow, C Burne, K.-S. Huang, D Pratt, L Wachter, C Hession, A Z Frey, B P Wallner, Five distinct calcium and phospholipid binding proteins share homology with lipocortin I, J. Biol Chem 263 (1988) 10799–10811

[15] M.R. Nelson, C E Creutz, Comparison of the expression of native and mutant bovine annexin IV in *Escherichia coli* using four different expression systems, Protein Expr Purif. 6 (1995) 132–140.

[16] H Sohma, C E. Creutz, M. Saitoh, H Sano, Y Kuroki, D R Voelker, T. Akino, Characterization of the Ca^{2+}-dependent binding of annexin IV to surfactant protein A, Biochem J 341 (1999) 203–209.

[17] U K Laemmli, Cleavage of structural proteins during assembly of the head of bacteriophage T_4, Nature 227 (1970) 680–685

[18] J D Dignam, R.M Lebovitz, R G Roeder, Accurate transcription initiation by RNA polymerase II in a soluble extract from isolated mammalian nuclei, Nucleic Acids Res 11 (1977) 1475–1489

[19] G Szabio, D Catalano, G. Bellerose, P Mandrekar, Interferon α and alcohol augment nuclear regulatory factor-κB activation in HepG2 cells, and interferon α increases pro-inflammatory cytokine production, Alcohol , Clin. Exp Res. 25 (2001) 1188–1197

[20] A -S M Jonsson, J E.W. Palmblad, Effects of ethanol on NF-κB activation, production of myeloid growth factors, and adhesive events in human endothelial cells, J. Infect. Dis 184 (2001) 761–769.

[21] J Roman, A Colell, C Blasco, J. Caballeria, A. Pares, J Rodes, J.C. Fernandez-Checa, Differential role of ethanol and acetaldehyde in the induction of oxidative stress in HEP G2 cells , effect on transcription factors AP-1 and NFκB, Hepatology 30 (1999) 1473–1480

[22] C. Ikonomidou, P. Bittigau, M J Ishimura, D F Wozniak, C Koch, K. Genz, M.T. Price, V. Stefovska, F Hoerster, T. Tenkova, K Dikranian, J W Olney, Ethanol-induced apoptotic neurodegeneration and fetal alcohol syndrome, Science 287 (2000) 1056–1060

[23] T Urso, J.S. Gavaler, D.H. Van Thiel, Blood ethanol levels in sober alcohol users in an emergency room, Life Sci 28 (1981) 1053–1056.

[24] K.B. Hammond, R.H. Rumack, D O. Rodgerson, Blood ethanol. A report of unusually high levels in a living patient, JAMA 226 (1973) 63–64

[25] R A. Johnson, E.C. Noll, W M Rodney, Survival after a serum ethanol concentration of 1 1/2%, Lancet 2 (1982) 1394

[26] W.J. DeVito, S. Stone, M Shamgochian, Ethanol increases the neurotoxic effect of tumor necrosis factor-α in cultured rat astrocytes, Alcohol , Clin. Exp Res 24 (2000) 82–92

[27] M P Mattson, S Camandola, NF-κB in neuronal plasticity and neurodegenerative disorders, J Clin. Invest 107 (2001) 247–254

[28] E K -H Han, S.K. Tahir, S P Cherian, N Collins, S -C Ng, Modulation of paclitaxael resistance by annexin IV in human cancer cell lines, Br J. Cancer 83 (2000) 83–88

ELSEVIER

Biochimica et Biophysica Acta 1588 (2002) 226–231

BIOCHIMICA ET BIOPHYSICA ACTA
BBA
www.bba-direct.com

Expression and regulation by insulin of low-density lipoprotein receptor-related protein mRNA in human skeletal muscle

Philippe Boucher[a,1], Pierre-Henri Ducluzeau[b,c], Paul Davelu[a], Fabrizio Andreelli[b,c], Paulette Vallier[b], Jean-Paul Riou[b,c], Martine Laville[b,c], Hubert Vidal[b,*]

[a]*Department of Biochemistry, E. Herriot Hospital, Lyons, France*
[b]*INSERM U-449 and Centre de Recherche en Nutrition Humaine de Lyon, Faculté de Médecine R.T.H. Laennec, F-69372 Lyons, France*
[c]*Department of Endocrinology, Diabetologia and Nutrition, E. Herriot Hospital, Lyons, France*

Received 18 February 2002; received in revised form 12 July 2002; accepted 31 July 2002

Abstract

Evidence suggests that increased hydrolysis and/or uptake of triglyceride-rich lipoprotein particles in skeletal muscle can be involved in insulin resistance. We determined the steady state mRNA levels of the low-density lipoprotein-related receptor (LRP) and lipoprotein lipase (LPL) in skeletal muscle of eight healthy lean control subjects, eight type 2 diabetic patients and eight nondiabetic obese individuals. The regulation by insulin of LRP and LPL mRNA expression was also investigated in biopsies taken before and at the end of a 3 h euglycemic hyperinsulinemic clamp (insulinemia of about 1 nM). LRP mRNA was expressed in human skeletal muscle (1.3 ± 0.1 amol/μg total RNA in control subjects). Type 2 diabetic patients, but not nondiabetic obese subjects, were characterized by a reduced expression of LRP (0.8 ± 0.2 and 1.3 ± 0.3 amol/μg total RNA in diabetic and obese patients, respectively; $P < 0.05$ in diabetic vs. control subjects). Insulin infusion decreased LRP mRNA levels in muscle of the control subjects but not in muscle of type 2 diabetic and nondiabetic obese patients. Similar results were found when investigating the regulation of the expression of LPL. Taken together, these results did not support the hypothesis that a higher capacity for clearance or hydrolysis of circulating triglycerides in skeletal muscle is present during obesity- or type 2 diabetes-associated insulin resistance.

© 2002 Elsevier Science B.V. All rights reserved.

Keywords: Gene expression; Insulin resistance; Lipoprotein lipase; Triglyceride; Hyperinsulinemic clamp; RT-PCR

1. Introduction

Evidence has been accumulated suggesting that increased lipid availability in skeletal muscle is a cause of insulin resistance in obesity and in type 2 diabetes [1,2]. Based on the initial finding by Randle et al. [3], it has been postulated that the elevation of circulating free fatty acid concentrations, as frequently observed in obese and in diabetic patients, was one of the culprits in the reduced action of insulin [4–6]. A number of observations also suggest that triglyceride availability and hydrolysis in skeletal muscle could be involved in insulin resistance [2]. For instance, infusion of lipid emulsions, composed of triglycerides, reduced insulin action both in humans and animal models [5–8]. However, most of the infused lipids combine with circulating apoproteins to form lipoproteins that are subsequently cleared from the circulation [9]. It has also been demonstrated that high fat feeding induces insulin resistance [10,11]. Dietary fat generally forms chylomicrons that are hydrolyzed by lipoprotein lipase (LPL) in adipose tissue and skeletal muscle capillaries [12]. Thirty-five years ago, it was reported that chylomicrons could inhibit glucose uptake in rat heart [13]. Furthermore, overexpression of LPL in mice skeletal muscle leads to intramuscular lipid accumulation and insulin resistance, without any increase in plasma free fatty acid [14,15]. In humans, recent data also clearly demonstrated that accumulation of intramyocellular triglycerides is strongly associated with insulin resistance [16,17]. All these results therefore suggest that transfer of lipids from

---

Abbreviations: LRP, low-density lipoprotein receptor-related protein, LPL, lipoprotein lipase; RT-cPCR, reverse transcription competitive polymerase chain reaction, BMI, body mass index; NEFA, non-esterified fatty acid

[*] Corresponding author. Tel.: +33-4-7877-8629, fax: +33-4-7877-8762.
E-mail address: vidal@laennec.univ-lyon1.fr (H. Vidal)

[1] Current address: Department of Molecular Genetics, Southwestern Medical Center, University of Texas, Dallas, TX, USA

0925-4439/02/$ - see front matter © 2002 Elsevier Science B.V. All rights reserved.
PII S0925-4439(02)00169-2

triglyceride-rich lipoprotein particles to skeletal muscle can be involved in lipid-induced insulin resistance.

The low-density lipoprotein (LDL) receptor-related protein (LRP) is a large multiligand receptor that belongs to the LDL receptor gene family [18] and that has been shown to play a role, in cooperation with the LDL receptor, in the removal of chylomicron remnants from the circulation [19]. In rat adipose tissue, insulin up-regulates LRP gene expression, and this effect is thought to be involved in the stimulation by insulin of the endocytic uptake of remnant lipoproteins by adipocytes [20]. In addition, fed rats expressed more LRP and accumulated significantly more chylomicrons in adipose tissue than did fasted animals [20]. In adipose tissue, insulin and feeding also increase the expression and activity of LPL, the enzyme that catalyses the hydrolysis of triglycerides and thus controls the rate of entrance of fatty acids into fat cells [12]. Therefore, in a postprandial situation, a coordinate stimulating action on LRP and LPL could lead to an increased uptake of triglycerides and fatty acids from remnant lipoproteins in adipocytes.

Little data is available regarding the regulation of lipid uptake in skeletal muscle and its relationship with insulin resistance in humans. The expression and the regulation of LRP in human skeletal muscle is not known, and only a few studies have investigated the expression of muscle LPL in pathological conditions of insulin resistance [21–23]. As discussed above, increased availability and uptake of lipids from triglyceride-rich lipoproteins could be involved in fat accumulation within the muscle cells. However, it is not clear whether the disturbances in lipid metabolism in skeletal muscle result from elevated circulating levels of lipids or from higher hydrolysis and clearance of plasma lipoproteins and triglycerides in skeletal muscle. According to this latter hypothesis, it might be expected that the expression and activity of LPL and other proteins involved in lipid transfer, such as LRP, are increased in skeletal muscle of insulin-resistant patients. The aim of this study was therefore to determine LRP and LPL mRNA expression in skeletal muscle of insulin-resistant patients. In addition, we have investigated the in vivo regulation by insulin of the expression of these two genes in muscle from healthy lean controls, nondiabetic obese subjects and type 2 diabetic patients.

Table 1
Characteristics of the subjects

	Lean	Obese	Type 2 diabetic
n	8	8	8
M/W	2/6	1/7	4/4
Age (years)	46 ± 4	43 ± 5	52 ± 2
BMI (kg/m^2)	23 ± 1	35 ± 2^a	30 ± 1^a
Glucose (mM)	4.9 ± 0.9	5.0 ± 0.1	11.8 ± 1.1^{a,b}
Insulin (pM)	41 ± 5	83 ± 21^c	55 ± 10
Cholesterol (mM)	5.5 ± 0.3	5.6 ± 0.3	5.0 ± 0.4
NEFA (μM)	436 ± 42	629 ± 61^c	652 ± 53^a
Triglycerides (mM)	0.8 ± 0.1	1.2 ± 0.1^c	1.3 ± 0.1^c
Clamp study^d			
Glucose (mM)	4.4 ± 0.2	4.4 ± 0.1	5.0 ± 0.1^e
Insulin (pM)	1015 ± 67	1157 ± 157	1153 ± 160
Glucose disposal rate (mg/kg/min)	9.5 ± 1.5	4.3 ± 0.8^a	4.1 ± 0.5^a

Plasma metabolite and hormone concentrations were determined after an overnight fast

[a] $P<0.01$ vs lean subjects.

[b] $P<0.01$ vs obese subjects.

[c] $P<0.05$ vs. lean subjects.

[d] Measured during the last hour of the clamp

[e] $P<0.05$ vs obese subjects

2. Materials and methods

2.1. Subjects

Twenty-four subjects (eight lean, eight obese nondiabetic and eight type 2 diabetic subjects) who participated in a study aiming to investigate the regulation of gene expression by insulin in human tissues [24,25], were selected for the present work. Their characteristics are presented in Table 1. None of the healthy lean subjects had a familial or personal history of diabetes, obesity or hypertension. None of the obese subjects had impaired glucose tolerance as assessed by classical oral glucose tolerance test (2 h plasma glucose concentration below 7.8 mM following a 75 g oral glucose test, according to the revised American Diabetes Association criteria). All participants gave their written consent after being informed of the nature, purpose and possible risks of the study. The experimental protocols were approved by the Ethical Committees of the Hospices Civils de Lyon (Lyon, France).

2.2. Euglycemic hyperinsulinemic clamp

To investigate insulin action on gene expression, all subjects were studied using the euglycemic hyperinsulinemic clamp technique after an overnight fast. The clamp was performed as previously described [24,26], with a rate of insulin infusion of 450 pmol/m^2 body surface area/min for 3 h. Serum insulin concentration was measured by commercial radioimmunoassay, and serum metabolite concentrations were determined by enzymatic assays [26].

2.3. Skeletal muscle biopsies

Muscle samples (vastus lateralis) were taken under local anesthesia (2% Lidocain without adrenaline), 3 h before and at the end of the hyperinsulinemic clamp period by percutaneous biopsies using a Weil Blakesley plier, as previously described [24,25]. The average weight of the muscle samples were 51 ± 4 mg wet weight ($n=48$) with no difference between samples from lean, obese and type 2 diabetic subjects or before and after clamp. Possible contamination of the muscle biopsies by fat cells was unlikely since the expression level of leptin mRNA was found to be below the detection limit of a very sensitive RT-competitive PCR (RT-cPCR) assay [27] in these muscle samples (data not shown).

2 4. *Total RNA preparation*

Tissue samples were crushed in liquid nitrogen, and total RNA was prepared according to a modified procedure of Chomczynski and Sacchi [28]. Average yields of total RNA were 25 ± 3 µg/100 mg, and were not significantly different in tissues from lean, obese and type 2 diabetic subjects, before or after the clamp. Integrity of the RNA preparations was checked by electrophoresis in agarose gel stained with ethidium bromide. Total RNA solutions were stored at − 80 °C until quantification of LRP mRNA.

2.5. *Quantification of LRP mRNA*

Human LRP mRNA was quantified by RT-cPCR, which consists of the co-amplification of target cDNA with known amounts of a specific DNA competitor molecule added in the same PCR tube [29]. To generate a specific LRP competitor DNA, a 440-bp-long cDNA fragment was obtained by RT-PCR using 5′-TGGAACAGATGGCCATC-GAC-3′ as sense primer (nucleotides + 1311 to + 1330 of the human LRP cDNA sequence, and 5′-CGAGTTGG-TGGCATAGAGAT-3′ (nucleotides + 1731 to + 1750) as antisense primer. The competitor was obtained by deleting 30 bp (from nucleotide + 1330 to + 1360) using a PCR-based mutagenesis strategy as described by Schneeberger and Zeillinger [30]. The LRP competitor fragment (406 bp) was subcloned (pGEM-T, Promega) and the plasmid was purified, carefully quantified and stored at − 20 °C. Working solutions (20 amol/µl to 10^{-3} amol/µl) were prepared by serial dilutions in 10 mM Tris–HCl (pH 8.3), 1 mM EDTA buffer.

For the assay of LRP mRNA, the reverse transcription reaction was performed from 0.2 µg of tissue total RNA with 2.5 U of thermostable reverse transcriptase (Tth, Promega, Charbonières, France), in the presence of 15 pmol of LRP-specific antisense primer. The conditions of the reaction have been described in detail previously and warranted optimal synthesis of first-strand cDNA [29]. For the competitive PCR amplification, the reverse transcription medium was added to a PCR master mix (10 mM Tris–HCl pH 8.3, 100 mM KCl, 0.75 mM EGTA, 5% glycerol) containing 0.2 mM deoxynucleoside triphosphates, 5 U of Taq polymerase (Life Technologies, Cergy Pontoise, France), 30 pmol of LRP antisense primer and 45 pmol of LRP sense primer. The sense primer was 5′-labeled with the CY-5 fluorescent dye (Eurogentec, Seraing, Belgium). The final volume was 100 µl and four aliquots of 20 µl were transferred to 0 5-ml microtubes containing 5 µl of a defined working solution of the LRP competitor. After 120 s at 94 °C, the PCR mixtures were subjected to 40 cycles of PCR amplification with a cycle profile including denaturation for 60 s at 94 °C, hybridization for 60 s at 58 °C and elongation for 60 s at 72 °C. The PCR products were separated and analyzed by polyacrylamide gel electrophoresis (6%) using a ALFexpress DNA sequencer (Pharmacia, Upsala, Sweden) and the Fragment Manager software (Pharmacia). The RT-cPCR assay of LRP mRNA was validated using known amounts of an in vitro synthesized LRP RNA fragment (Riboprobe System, Promega), as recommended [29]. LPL mRNA levels were determined using a RT-cPCR assay previously described [26].

2.6 *Statistical analysis*

All data are presented as mean ± S.E. between group comparisons were done using Kruskal–Wallis one-way ANOVA followed by Mann–Whitney U-test when the ANOVA indicated a significant difference. Wilcoxon's test for paired values was used when comparing mRNA levels before and after clamp. Correlation coefficients were calculated using Spearman's test. $P < 0.05$ was considered statistically significant.

3. Results

Under basal conditions, after an overnight fast, LRP mRNA is expressed in human skeletal muscle as shown in Fig. 1. When comparing the mRNA levels of LRP in the muscle of healthy lean control, type 2 diabetic and nondiabetic obese subjects, the Kruskal–Wallis test indicated a tendency for a difference ($P = 0.097$). The non-parametric Mann–Whitney U-test showed that type 2 diabetes, but not obesity, was associated with a significant ($P = 0.035$) reduc-

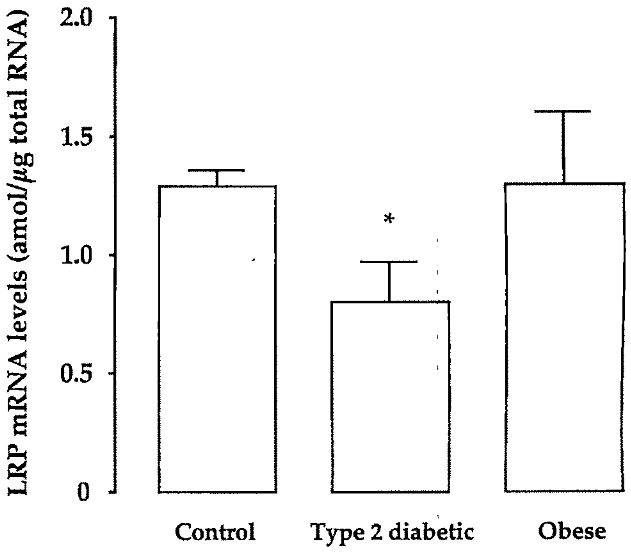

Fig 1 Basal mRNA levels of LRP in skeletal muscle from lean, obese nondiabetic and type 2 diabetic subjects The steady state concentrations of LRP mRNA were determined by RT-cPCR in skeletal muscle biopsies taken after an overnight fast in healthy lean subjects, obese nondiabetic and type 2 diabetic patients as indicated under Materials and methods Data are mean ± S E *P<0 05

tion in the abundance of LRP mRNA (Fig. 1). When the data of the control subjects and the type 2 diabetic patients were analyzed together, there was a trend for a negative correlation between fasting insulinemia and basal LRP mRNA levels ($r = -0.50$, $P = 0.058$). This correlation was not found when the obese subjects were included in the analysis. Skeletal muscle LRP mRNA concentration was not associated with either fasting glycemia, plasma non-esterified fatty acid concentrations, plasma triglyceride concentrations, plasma cholesterol concentrations or insulin-stimulated whole body glucose uptake (data not shown). In the same tissue samples, LPL mRNA expression was significantly lower in type 2 diabetic patients than in control subjects (14 ± 3 vs. 54 ± 6 amol/mg of total RNA, $P = 0.006$). In addition, reduced LPL expression was also observed in the muscle of the nondiabetic obese subjects (23 ± 5 vs. 54 ± 6 amol/mg of total RNA, $P = 0.04$). There was no correlation between LRP and LPL mRNA levels in skeletal muscle. It should be noted that in contrast to LRP and LPL, the mRNA levels of a number of other genes, such as β-actin, insulin receptor and Glut 4, were not different between groups in muscle preparations from the same type 2 diabetic and obese subjects (data not shown), as previously reported [25].

Hyperinsulinemia for 3 h produced a significant ($P = 0.012$) decrease in LRP mRNA levels in the skeletal muscle of lean control subjects (Fig. 2). In contrast, LRP mRNA expression was not modified during the hyperinsulinemic clamp in the muscle of obese nondiabetic subjects or of type 2 diabetic patients. Similar changes were observed in response to insulin for LPL expression (Fig. 3). LPL mRNA levels were significantly reduced during the hyperinsulinemic clamp in control subjects (−21 ± 8%, $P = 0.018$), but not in type 2 diabetic and in obese patients.

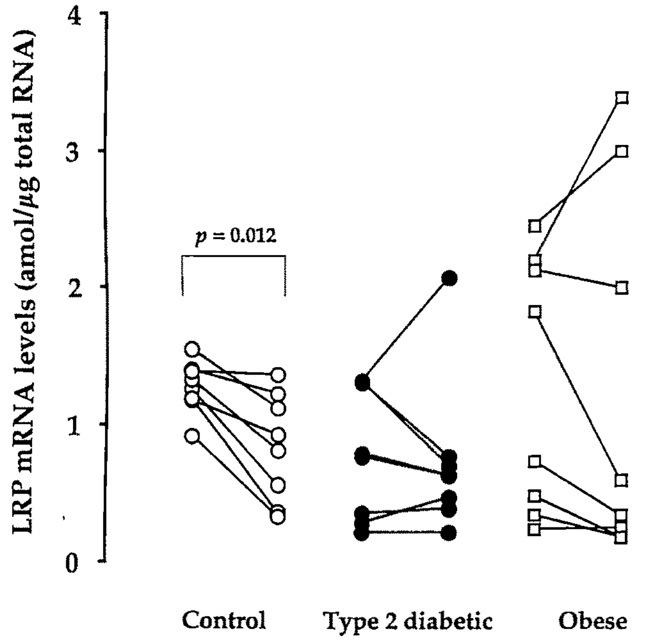

Fig 2 Regulation of LRP mRNA expression by insulin Acute 180 min insulin infusion significantly decreased the expression of LRP mRNA in skeletal muscle of lean subjects ($P = 0.012$) but not of obese nondiabetic ($P = 0.575$) or type 2 diabetic subjects ($P = 0.735$)

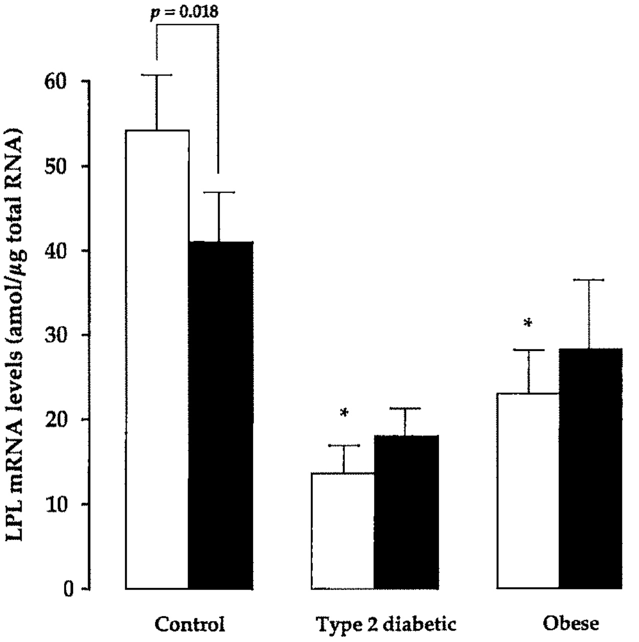

Fig 3 Regulation by insulin of LPL mRNA levels. The concentrations of LPL mRNA were determined by RT-cPCR in skeletal muscle biopsies taken before (open boxes) and at the end (closed boxes) 3 h of hyperinsulinemic clamp in control subjects, obese nondiabetic and type 2 diabetic patients Insulin infusion significantly decreased the expression of LPL mRNA in skeletal muscle of lean subjects ($P = 0.018$) but not of obese nondiabetic ($P = 0.345$) or type 2 diabetic subjects ($P = 0.499$) Data are means ± S.E $*P < 0.05$ vs control subjects

4. Discussion

In this study, it was demonstrated that LRP was expressed in human skeletal muscle and that insulin infusion for 3 h reduced LRP mRNA levels in healthy lean subjects. Furthermore, there was an about 2-fold reduction in the abundance of LRP transcripts, and a lack of response to insulin infusion, in the muscle of type 2 diabetic patients. Similar results were observed for LPL mRNA expression.

LRP has been shown to be involved, among other functions [31], in the removal of chylomicron remnants from the circulation [19]. It is mainly expressed in liver and adipose tissue where most of the clearance of chylomicrons occurs [31]. The presence of LRP mRNA, although at rather low levels (about 10-fold less LRP than LPL transcripts) in human muscle and the fact that its expression was regulated by insulin, suggest that LRP protein might be expressed at the membrane of the myocytes and have a biological function. With respect to liver and adipose tissue, skeletal muscles are not considered as major sites of chylomicron removal but evidence suggests that higher targeting of lipoproteins and increased lipid uptake may play a role in the development of insulin resistance [2]. It is indeed well demonstrated that infusion of lipid emulsions, composed of triglycerides that form lipoproteins in the circulation [9], reduced insulin action both in humans and animal models [5–8]. Furthermore, high fat feeding induces muscle insulin resistance [10,11], and dietary fat generally forms chylomicrons that are hydrolyzed by LPL in adipose tissue and skeletal muscle capillaries [12]. Therefore, an increased capacity for the transfer of lipids from triglyceride-rich lipoprotein particles to the muscle cells can be involved in lipid-induced insulin resistance. We found here that there is no evidence for higher expression of either LRP or LPL, the rate-limiting enzyme for the uptake of fatty acids from circulating triglycerides, in muscle of insulin-resistant subjects. Even more, there was a marked reduction in the mRNA levels of both LRP and LPL in skeletal muscle of type 2 diabetic patients. If the changes in mRNA abundances are translated into a reduction in LRP and LPL proteins and activities, one must thus assume that skeletal muscle of insulin-resistant subjects do not have increased capacity for removal of triglycerides from the circulation. Regarding LPL, the observed reduction in mRNA levels is in keeping with a decreased LPL activity found in muscle of insulin-resistant subjects [21]. For LRP and the other proteins involved in the removal of circulating lipoproteins and the uptake of lipids, further studies are required to verify whether their activity is altered in insulin resistance. Nevertheless, we have recently reported that the mRNA expression of the fatty acid transport protein-1 (FATP-1) is reduced in skeletal muscle of insulin-resistant women [32]. In addition, it has been shown that the uptake of long chain fatty acids in skeletal muscle is reduced in fasting conditions in type 2 diabetic patients [33], and that the uptake of fatty acid across the leg is decreased in women with visceral obesity and insulin resistance [34]. Taken together, these data strongly suggest that insulin resistance is not characterized by higher capacities for the capture and uptake of lipids in skeletal muscle. Therefore, increased availability of triglycerides and fatty acids due to higher circulating concentrations, or altered intracellular lipid metabolism, seem more likely to explain the relationship between lipids and insulin resistance [1,2]. This might in turn down-regulate the expression of the genes coding for the proteins involved in lipid uptake (like LPL and LRP) through mechanisms that are not yet determined.

Previous studies have clearly demonstrated that LRP gene expression was up-regulated by insulin in vivo in rodent adipose tissue [20]. In adipocytes, LRP mRNA increased within minutes after the cells were exposed to physiological concentrations of insulin [20]. In other cells, such as macrophages [35], insulin also increased LRP mRNA levels and LRP activity, in a dose- and time-dependent manner. Moreover, insulin action on LRP expression involved both the PI 3-kinase and Ras/MAPkinase signaling pathways in macrophages [35]. These data demonstrated that LRP gene is a bona fide target gene of insulin. In our study, LRP gene expression also appeared to be regulated during insulin infusion. However, 3 h of hyperinsulinemia reduced LRP mRNA levels in skeletal muscle of the lean control subjects. Similar down-regulation by insulin was observed for LPL mRNA, in agreement with a previous study [26]. Therefore, there is an opposing action of insulin in muscle and in adipocytes on LPL and LRP gene expression. This result is in keeping with the expected biological effects of insulin which promotes an orientation of the flux of lipids to adipose tissue where they are stored and a reduction in lipid utilization in muscles, favoring glucose uptake. Our results showed that the regulation by insulin of the balance between lipid and glucose metabolisms in skeletal muscle also occurs at the transcriptional level. For instance, it has been reported that insulin up-regulates the expression of several genes coding proteins of glucose metabolism, such as Glut 4 [25,26,36,37] or hexokinase II [25,38] and we showed here that insulin down-regulates the expression of genes involved in the uptake of lipids, such as LPL and LRP.

The effect of insulin on LPL and LRP expression is altered in muscle from nondiabetic obese subjects and type 2 diabetic patients. Defective regulation by insulin of gene expression has been previously documented in diabetic patients [25,36–38]. We have demonstrated that the altered regulation of hexokinase II, p85αPI 3-kinase and the transcription factor SREBP1c was encountered in type 2 diabetic patients and not in nondiabetic obese subjects, suggesting that type 2 diabetes is characterized by specific transcriptional alterations which are not directly linked to insulin resistance [25]. In the same group of subjects, however, the regulation by insulin of other gene, such as Glut 4 [25], was found to be impaired both in type 2 diabetic patients and in nondiabetic obese subjects, suggesting that this defect was likely a consequence of insulin resistance. In this study, the effect of insulin on LRP and LPL mRNA expression was also altered in type 2 diabetic patients and in nondiabetic obese subjects, indicating that the defect, as for Glut 4, probably results from the reduced insulin action in the muscle of these subjects.

In conclusion, this study showed that LRP was expressed in human skeletal muscle and that insulin, in vivo, decreased its mRNA levels in muscle of insulin-sensitive control subjects. In type 2 diabetic patients, the expression levels of muscle LRP mRNA was significantly reduced compared to healthy subjects and the regulation by insulin was altered. Similar results were found for LPL transcripts. Taken together, these results did not support the hypothesis that a higher hydrolysis and/or uptake of triglyceride-rich lipoprotein particles in skeletal muscle can be involved in obesity- and type 2 diabetes-associated insulin resistance.

Acknowledgements

The expert technical assistance of C. Urbain-Pellissier and N. Vega is deeply appreciated. This study was supported, at least in part, by grants from Institut de Recherches Servier and from INSERM (progress no. 4P020D). Dr. R.H. Unger is acknowledged for critical reading of the manuscript.

References

[1] G Boden, Diabetes 46 (1997) 3–10.
[2] J D. McGarry, Diabetes 51 (2002) 7–18.
[3] P J Randle, P.B. Garland, E A Newsholme, C N Hales, Ann. N Y. Acad Sci. 131 (1965) 324–333
[4] M A Charles, E Eschwege, N Thibult, J R. Claude, J.M Warnet, G E. Rosselin, J. Girard, B Balkau, Diabetologia 40 (1997) 1101–1106.
[5] E. Ferrannini, E J Barrett, S Bevilacqua, R A. DeFronzo, J Clin. Invest 72 (1983) 1737–1747
[6] G Boden, X Chen, J Clin Invest 96 (1995) 1261–1268
[7] D. Thiebaud, R.A DeFronzo, E Jacot, A. Golay, K. Acheson, E Maeder, E Jequier, J P. Felber, Metabolism 31 (1982) 1128–1136
[8] M. Laville, V Rigalleau, J.P. Riou, M Beylot, Metabolism 44 (1995) 639–644.
[9] K Iriyama, Y.A Carpentier, Nutrition 10 (1994) 252–254
[10] L H Storlien, D E James, K.M Burleigh, D J Chisholm, E W Kraegen, Am. J. Physiol 251 (1986) E576–E583
[11] E.J. Mayer, B Newman, C.P. Quesenberry Jr, J V. Selby, Diabetes Care 16 (1993) 1459–1469
[12] R H. Eckel, N. Engl. J Med 320 (1989) 1060–1068
[13] J.A. Ontko, P.J. Randle, Biochem J 104 (1967) 43C–44C.
[14] L.D Ferreira, L.K. Pulawa, D R. Jensen, R H. Eckel, Diabetes 50 (2001) 1064–1058.
[15] J.K. Kim, J J. Fillmore, Y Chen, C Yu, I.K. Moore, M Pypaert, E.P Lutz, Y Kako, W Velez-Carrasco, I J Goldberg, J L Breslow, G I Shulman, Proc. Natl Acad. Sci. U. S A. 98 (2001) 7522–7527
[16] S Jacob, J Machann, K Rett, K Brechtel, A. Volk, W. Renn, E. Maerker, S Matthaei, F Schick, C D Claussen, H.U Haring, Diabetes 48 (1999) 1113–1119
[17] M. Krssak, K.F Petersen, A Dresner, L. DiPietro, S M. Vogel, D L. Rothman, G.I Shulman, M. Roden, Diabetologia 42 (1999) 113–116
[18] J. Herz, U Hamann, S Rogne, O Myklebost, H. Gausepohl, K K Stanley, EMBO J. 7 (1988) 4119–4127
[19] A Rohlmann, M Gotthardt, R.E. Hammer, J Herz, J Clin. Invest. 101 (1998) 689–695
[20] O. Descamps, D. Bilheimer, J Herz, J Biol Chem. 268 (1993) 974–981.
[21] T Pollare, B Vessby, H Lithell, Arterioscler Thromb 11 (1991) 1192–1203
[22] M R. Taskinen, E.A Nikkila, T Kuusi, K Harmo, Diabetologia 22 (1982) 46–50
[23] F. Andreelli, M. Laville, N. Vega, J P Riou, H Vidal, Diabetologia 43 (2000) 356–363
[24] F. Andreelli, M. Laville, P H Ducluzeau, N Vega, P. Vallier, Y Khalfallah, J P. Riou, H Vidal, Diabetologia 42 (1999) 358–364
[25] P.H. Ducluzeau, N Perretti, M Laville, F Andreelli, N Vega, J P Riou, H Vidal, Diabetes 50 (2001) 1134–1142.
[26] M. Laville, D. Auboeuf, Y. Khalfallah, N Vega, J P Riou, H. Vidal, J. Clin Invest. 98 (1996) 43–49.
[27] H Vidal, D. Auboeuf, P. De Vos, B. Staels, J P Riou, J Auwerx, M Laville, J Clin Invest 98 (1996) 251–255.
[28] P. Chomczynski, N Sacchi, Anal Biochem 162 (1987) 156–159.
[29] D. Auboeuf, H. Vidal, Anal Biochem. 245 (1997) 141–148.
[30] C. Schneeberger, R Zeillinger, BioTechniques 20 (1996) 360–362
[31] J. Herz, D K. Strickland, J Clin Invest. 108 (2001) 779–784.
[32] C. Binnert, H A Koistinen, G Martin, F. Andreelli, P. Ebeling, V A Koivisto, M Laville, J. Auwerx, H. Vidal, Am J Physiol, Endocrinol Metabol 279 (2000) E1072–E1079.
[33] D.E. Kelley, J.A Simoneau, J. Clin. Invest 94 (1994) 2349–2356
[34] S R. Colberg, J.A Simoneau, F L. Thaete, D E Kelley, J. Clin. Invest 95 (1995) 1846–1853
[35] U.K Misra, G Gawdi, M Gonzalez-Gronow, S.V. Pizzo, J Biol Chem. 274 (1999) 25785–25791.
[36] P.H. Andersen, S. Lund, H. Vestergaard, S. Junker, B.B Kahn, O Pedersen, J Clin Endocrinol Metab 77 (1993) 27–32.
[37] C Schalin-Jantti, H. Yki-Jarvinen, L Koranyi, R Bourey, J Lindstrom, P Nikula-Ijas, A Franssila-Kallunki, L C Groop, Diabetologia 37 (1994) 401–407.
[38] M. Pendergrass, J Koval, C Vogt, H Yki-Jarvinen, P Iozzo, R Pipek, H Ardehali, R Printz, D Granner, R.A DeFronzo, L J Mandarino, Diabetes 47 (1998) 387–394

ELSEVIER

Biochimica et Biophysica Acta 1588 (2002) 232–240

BIOCHIMICA ET BIOPHYSICA ACTA

BBA

www.bba-direct.com

Antibacterial peptide PR-39 affects local nitric oxide and preserves tissue oxygenation in the liver during septic shock

Melanie Madhani[a,b], Aaron Barchowsky[c], Linda Klei[c], Chris R. Ross[d], Simon K. Jackson[e], Harold M. Swartz[b], Philip E. James[a,*]

[a]*Department of Cardiology, Wales Heart Research Institute, University of Wales College of Medicine, Cardiff, Wales, CF14 4XN, UK*
[b]*Department of Radiology, EPR Center, Dartmouth Medical School, Hanover, NH, USA*
[c]*Department of Pharmacology and Toxicology, Dartmouth Medical School, Hanover, NH, USA*
[d]*Department of Anatomy and Physiology, College of Veterinary Medicine, University of Manhattan, KS, USA*
[e]*Department of Medical Microbiology, University of Wales College of Medicine, Cardiff, Wales, UK*

Received 5 September 2001; received in revised form 15 July 2002; accepted 31 July 2002

Abstract

The effects of the antibacterial peptide PR-39 on nitric oxide (NO) and liver oxygenation (pO_2) in a mouse model of endotoxaemia have been explored. In vivo electron paramagnetic resonance (EPR) spectroscopy was used to make direct measurements of liver NO and pO_2. Measurements of pO_2 were made at two different anatomical locations within hepatic tissue to assess effects on blood supply (hence oxygen supply) and lobule oxygenation, selectively from the liver sinusoids or an average pO_2 across the liver lobule. PR-39 induced elevated levels of liver NO at 6 h following injection of lipopolysaccharide (LPS) as a result of increased iNOS expression in liver, but had no effect on eNOS or circulatory NO metabolites. Sinusoidal oxygenation was preserved, and pO_2 across the hepatic tissue bed improved with PR-39 treatment. We propose that the beneficial effects of PR-39 on liver in this septic model were mediated by increased levels of local NO and preservation of oxygen supply to the liver sinusoids.

© 2002 Elsevier Science B.V. All rights reserved.

Keywords: PR-39; Endotoxaemia; Liver; NO; pO_2

---

1. Introduction

PR-39, a proline-rich antibacterial peptide was first identified and isolated in pig intestines [1] and later from neutrophils [2]. Unlike most antibacterial peptides that kill bacteria by lysis, PR-39 has been shown to halt protein and DNA synthesis [3] to work as a neutrophil chemoattractant [4] and has also been implicated in wound repair [5]. Recently, Gao et al. [6] demonstrated PR-39 inhibition of NF-κB-dependent gene expression, suggesting that this antibacterial peptide may have a potential role during infection and inflammation. Our interest in PR-39 stems from its potential to inhibit superoxide production by NADPH oxidase [7] and promote cellular adaptation to hypoxia [8]. In particular, whether PR-39 could influence NO availability and tissue oxygenation in septic shock.

Lipopolysaccharide (LPS), a constituent of the Gram-negative bacterial outer membrane, plays a critical role in the pathogenesis of septic shock. Although it has long been recognised that LPS induces a cascade of inflammatory mediators such as cytokines and reactive oxygen and nitrogen species (e.g. superoxide (O_2^-) and nitric oxide (NO)) [9], little is known about the pathophysiological mechanisms underlying the tissue damage that occurs during multiple organ failure (MOF). Microvascular abnormalities [10] and inhibition of oxygen utilization [11] are thought to contribute to this tissue damage, however, the role of excess NO in relation to these mechanisms and the resulting defects in tissue oxygenation remain to be elucidated directly in experimental models of sepsis in vivo.

Conflicting data exists on the putative role of NO during sepsis. Nitric oxide synthase (NOS) inhibitors have been

---

[*] Corresponding author. Tel. +44-2920-743512; fax: +44-2920-743739.
E-mail address: JamesPP@cardiff.ac.uk (P.E. James).

0925-4439/02/$ - see front matter © 2002 Elsevier Science B.V. All rights reserved.
PII S0925-4439(02)00170-9

used in animal models of sepsis [12] although investigators have generally focussed on the preservation of circulatory haemodynamics, and only limited emphasis has been placed on whether inhibition of iNOS actually alleviated tissue damage and improved mortality [13,14]. Contrary to this, it is becoming increasingly apparent that NO itself may have protective functions (including maintenance of vascular tone and neutralising of other reactive oxygen species). Cobb et al. [15] recently demonstrated that wild-type mice show improved survival compared with iNOS knockout mice when subjected to cecal ligation and puncture (CLP). In addition, the work of Saavedra et al. [16] used a liver-specific NO donor to reduce LPS-induced liver injury in mice.

Other oxygen-derived radicals also contribute to localised tissue damage, particularly in liver. Harbrecht et al. [17] demonstrated that when mice were subjected to N^G-monomethyl-L-arginine (L-NMMA) and superoxide dismutase (SOD), the detrimental effects of L-NMMA alone (i.e. lack of NO) were reduced because SOD eliminated hepatic damage by superoxide and peroxynitrite. Thus, both circulatory and local effects on tissue contribute to eventual organ failure, and NO, either directly or indirectly plays a critical role in both. Treatment of any one of these components may not necessarily alter eventual survival.

We have previously described direct in vivo measurements of NO and pO_2 using electron paramagnetic resonance spectroscopy (EPR) during LPS-induced sepsis [18]. Quantification of liver NO was undertaken using diethyldithiocarbamate (DETC) and iron to complex with NO in the liver and give rise to a characteristic (EPR) signal. Measurements of pO_2 were made using gloxy (an oxygen-sensitive paramagnetic material [19]). Direct in vivo measurements of pO_2 can also be made at two different anatomical locations within the liver, either as pO_2 specifically from the sinusoids or as average pO_2 across the hepatic tissue bed [20].

The present study was undertaken to explore the effects of PR-39 in a mouse model of endotoxin (LPS)-induced sepsis which is well characterized in our laboratory and provides a haemodynamic model of sepsis over 6 h. We were specifically interested to evaluate the effects on NO levels (circulating versus local) and tissue oxygenation. Shi et al. [7,21] demonstrated increased iNOS expression and reduced oxidative damage to liver in mice subjected to LPS challenge. The sepsis model utilised in these studies involved priming the mice with galactosamine, providing a liver-specific model in which liver toxicity to LPS is greatly enhanced and the longer term effects of oxidative damage to tissue are brought forward. Based on these results, we hypothesized that PR-39 may influence iNOS expression directly in the liver as well as inhibit superoxide production, resulting in increased availability of NO that might influence liver oxygenation. We report here that PR-39 increased NO levels locally in liver, preserved sinusoidal perfusion and oxygenation across the hepatic bed during an induced septic episode.

2. Materials and methods

2.1. Chemicals

Male Balb/C mice (18–20 g), purchased from Charles River Laboratories were used throughout. The chemicals used in these studies were as follows: LPS (isolated from *Escherichia coli*, serotype 0111:B4), DETC, ferrous sulfate ($FeSO_4$) and sodium citrate were all obtained from Sigma Chemicals Co., St. Louis, USA. PR-39 was synthesised by the solid-phase method, using t-boc chemistry as previously described [21]. Gloxy, coal blend was obtained from Filter Anthracite Ltd., Ammanford, South Wales, UK. Oxygen-sensitive material was selected as previously described [19].

2.2. Treatment groups

To evaluate the effects of PR-39, LPS and the combined effects of PR-39 + LPS, mice were assigned to one of the following treatment groups: (I) LPS 10 mg/ml in saline (intraperitoneally; 40 mg/kg body weight); (II) PR-39 (4.12 mg/ml in saline; 20.6 mg/kg body weight); (III) co-treatment with LPS and PR-39 (given the same dosage as I and II); and (IV) a control group of mice injected with pyrogen-free saline (100 µl). This LPS model is well established in our laboratory and effectively reproduces a haemodynamic model of sepsis [18].

2.3. Direct in vivo measurement of NO and pO_2 in liver

We have previously demonstrated simultaneous measurement of tissue pO_2 and NO in vivo [18]. This is possible because the EPR signal arising from gloxy and that from the trapped NO complex have different positions in the magnetic field and the resulting EPR spectrum. However, where the spectral line width reported from Gloxy is broad (reflecting high tissue pO_2), interference in the spectral signal arising from Gloxy and the trapped NO complex may result in the inability to accurately measure Gloxy line width. In the studies reported here, because Gloxy slurry administered i.v. resided in or close to the liver sinusoids, a broad spectral line width (i.e. high pO_2) was measured. The pO_2 and NO trapping measurements presented in this paper were therefore conducted on separate animals. Ex vivo determination of blood levels of NO derivatives, however, was carried out on animals following EPR oximetry.

2.3.1. In vivo measurements of nitric oxide

The NO trapping agent Fe/DETC was administered by injecting each mouse with DETC (500 mg/kg, i.p.), immediately followed by Fe_2SO_4 and sodium citrate (50 and 250 mg/kg, respectively, subcutaneously, lower leg). This was prepared in a hypoxia chamber (InVivO2 400; Fred Baker Scientific) so as to minimise the possibility of ferric/DETC complex formation that might result in spin trapping nitroxyl anion.

Fifteen minutes after Fe/DETC administration, the mouse was anaesthetised with 1.4% isoflurane. The mouse was restrained in a supine position and then placed inside a "whole-body" resonator of an L-Band EPR spectrometer. The liver was the area of interest so the upper abdomen of the mouse was positioned within the active site of the detecting resonator. EPR spectra were recorded with the following instrumental settings: 100 G field scan; 60 s scan time; 0.1 s time constant; 2.0 G modulation. The NO–Fe–(DETC)$_2$ complex formed gave rise to an EPR triplet signal. This signal was measured 30 min after Fe/DETC administration. For each mouse, we observed an initial accumulation of this triplet signal before equilibrium was established between signal accumulation and decrease. The latter arising from a combination of EPR signal reduction, possible cessation of NO synthesis, and clearance of NO–Fe–(DETC)$_2$ from the tissue. The maximum signal amplitude at the equilibration point of NO–Fe–(DETC)$_2$ was taken as a level of NO for comparison between mice.

Since DETC/Fe was used to complex with NO in vivo in these studies, it was important to consider whether DETC/Fe itself induced changes in the parameters we were measuring. We have previously demonstrated DETC/Fe did not have a significant effect on pO$_2$ [18] in a mouse model of sepsis. Furthermore, administration of DETC/Fe to control mice did not significantly affect mean arterial blood pressure or levels of circulating metabolites.

Although nitroxyl anion (NO$^-$) can react with a related chelator, methyl–glucamine–dithiocarbamate (MGD) and recent evidence suggests that NO$^-$ is the primary reaction product of neuronal NOS [22], these recent findings were obtained in vitro and under conditions where trap concentration was high and NOS/NO production low compared to our in vivo septic model of iNOS overexpression.

2.3.2. *In vivo EPR oximetry*

Measurements of partial pressure of oxygen (pO$_2$) were made using the paramagnetic material gloxy [19]. Gloxy was administered by one of the two following techniques; (I) i.v. administration of a fine slurry of gloxy, or (II) implantation of gloxy particles directly into the liver. Histological examination of tissue slices revealed that the slurry of fine particles injected i.v. distributed mainly to the liver, and was confined within the hepatic sinusoidal capillaries. In contrast, the larger gloxy particles injected directly in the liver apparently localised to the implantation site. Thus, selective measurements of pO$_2$ were possible at two different anatomical locations within hepatic tissue. Measurement of pO$_2$ by the "slurry" method was used to reflect supply of oxygen to the sinusoid, whereas "particle" measurements reflected average pO$_2$ across the liver lobule. The difference in pO$_2$ between these sites was taken to reflect oxygen utilization across the liver lobule.

2.3.2.1. Gloxy slurry. One-hundred microliters was administered intravenously via the lateral tail vein. Slurry was produced by grinding gloxy using a pestle and mortar, suspending it in sterile saline, and filtering it through a 20-μm mesh. The mean particle size in the prepared slurry was found to be 1.1 μm with >80% being smaller than 3 μm. The distribution and inertness of gloxy slurry administered i.v. to mice [19] was similar to that found with administration of India Ink which distributes almost exclusively to Kupffer cells of liver [20]. Histological examination of gloxy slurry in liver shows remarkable homogeneity in micro-particle size with no apparent affect on cells or surrounding tissue [23].

2.3.2.2. Gloxy particles Fifty to two-hundred micrometers, chosen manually using a microscope and cell hemocytometer scale. Mice were anaesthetised with 1.4% isoflurane and a laparotomy was performed. The particles were injected using a 22-gauge needle. This contained a length of wire used to displace the gloxy from the needle directly into the liver tissue.

Forty-eight hours following administration of gloxy, baseline pO$_2$ was measured for each mouse using an L-Band EPR spectrometer with a "whole-body" loop-gap detecting resonator operating at 1.1 GHz. Typical spectrometer settings were: scan range, 10 G; scan time, 60 s; modulation amplitude was kept to one-third of the recorded line width in order to prevent artificial line broadening and potential over-estimation of pO$_2$. The mice were then assigned to one of the treatment groups. We focussed our pO$_2$ studies on 6 h following LPS because this corresponded with the peak in tissue and circulating NO in this model. Mice were anaesthetised and placed into the whole-body-detecting resonator 5 1/2 h after the administration of the different treatments (as for the measurement of NO). pO$_2$ was calculated by measuring peak-to-peak line width of the first derivative spectral signal [19]. A 60-s scan time was used, and spectra were recorded every 3 min for up to a period of 1 1/2 h. The line width was converted to pO$_2$ by comparison with a calibration of either gloxy slurry or particle line width against known O$_2$ tensions. The measured line width at a given pO$_2$ depends on whether a particle or slurry is used. The pO$_2$ values reported in this study reflect true differences in tissue pO$_2$ at specific anatomical locations, since they were calculated from the appropriate calibration curve, rather than differences in slurry versus particle line width or physical properties of the gloxy (such as size and surface area).

2.3.2.3. Blood flow. An ultrasound flow device (Transonic systems) was used to monitor blood flow through the hepatic artery. These measurements were relatively invasive and extremely sensitive to positioning of the flow probe, we therefore measured flow in separate groups of mice (i.e. flow was not measured in animals in which pO$_2$ and NO measurements were made). We ensured that implantation of gloxy itself (particles or slurry) had no effect on flow through the hepatic artery by comparing flow measurements in animals with and without prior gloxy implantation. Typically, in anaesthetised animals, an incision was made in the upper right peritoneal region. This was large enough to allow access to the hepatic vessels and placement of the flow probe. The shaft of the flow probe was 2 mm in diameter and semi-rigid, and was held in position using a micro-manipulation device. The incision was closed and sutured around the probe shaft. Animals were then allowed to equilibrate for 30 min prior to taking flow readings. We focussed our studies to taking flow readings every 5 min between 5.5 and 6.5 h post-saline, LPS, or LPS + PR-39 injection (in order to compare with pO_2 and NO measurements). In order to achieve this, surgery to position the flow probe was initiated 4 h into the septic episode.

2.4. Determination of blood levels of NO derivatives

2.4.1. Measurement of nitrosyl hemoglobin (HbNO)

Binding of NO to deoxyhaemoglobin results in the formation of nitrosylhemoglobin (HbNO) which can be measured by EPR spectroscopy [24]. HbNO levels were determined by cryogenic EPR of a frozen red cell suspension. Briefly, blood samples were obtained by cardiac puncture 6 h after treatment. Approximately 500 μl of blood was collected into an Eppendorf tube containing EDTA. Blood samples were immediately centrifuged and the plasma component was removed and stored at − 70 °C. Approximately 150 μl of the red blood cells were then transferred into a 0.5 ml insulin syringe and immediately placed into liquid nitrogen. The samples were then stored at − 70 °C until analyzed.

X-band EPR analysis of HbNO was carried out by placing the samples in an EPR finger dewar containing liquid nitrogen. Typical instrumental settings were; modulation 4 G; microwave power 10 mW; scan range 200 G, 10 min scan.

2.4.2. Measurement of nitrite and nitrate (NO_x)

Nitrite and nitrate concentration was assayed using a procedure by Misko et al. [25]. Briefly, the plasma samples were filter-centrifuged (Sartorious Vivaspin 500 membranes) at 10,000 × *g* for 30 min at room temperature. For total nitrite and nitrate determination, 50 μl of filtrate was combined with 10 μl of NADPH (10 μM), 40 μl of phosphate buffer. To determine the amount of nitrate, 50 μl of filtrate was combined with 10 μl of NADPH (10 μM) and master mix (equal quantities of glucose-6-phosphate (5 mM), sodium phosphate buffer (14 mM) and nitrate reductase (0.8 U/ml)). Standards for both nitrite and nitrate were prepared from the corresponding sodium salt (standard concentration ranging from 1 to 200 μM). The mixture was incubated at 37 °C for 1 h. After 1 h incubation, 10 μl of naphthylethlene diamine (DAN; 0.62 M) was added to the mixture and was then incubated for a further 10 min at room temperature. After 10 min incubation, the reaction was stopped by adding 5 μl of sodium hydroxide (2.8 M). The fluorescence was read at emission 450 nm and excitation 365 nm, 10 min following the addition of sodium hydroxide. Nitrate concentration was calculated by subtracting the nitrite concentration from the total nitrite and nitrate value obtained after the nitrate reduction process ($NO_x = NO_2^- + NO_3^-$).

2.5. Measurement of eNOS/iNOS protein expression using Western blotting

Mice were treated for 6 h and sacrificed following anaesthetisation with isoflurane. Liver tissues were excised and were frozen in liquid nitrogen and stored at − 80 °C until tissue extraction.

2.5.1. Preparation of liver extracts

Frozen liver tissue was weighed and homogenized (Pierce Tissue Grinder Kit) in boiling lysis buffer (10 mM Tris, pH 7.4, 1.0 mM sodium orthovanadate, 1.0% SDS). Protein was determined with a Micro Bovine Serum Albumin (BSA) Protein Assay Reagent kit (Pierce).

2.5.2. Western blot analysis

Tissue homogenates were heated for 5 min at 95 °C in cracking buffer (1 ml 2–mercaptoethanol, 2 ml glycerol, 0.4 g SDS, 0.2 g PMSF (100 ×), 20 mg bromophenol blue, 20 ml of distilled water). The proteins (40 μg of protein/lane) were then separated by SDS-polyacrylamide gel electrophoresis (PAGE) in 7.5% resolving gels, and blotted onto nitrocellulose membranes (Hybond-ECL) in a semi-dry electrophoretic transfer cell (Trans-Blot; Bio-Rad). Nitrocellulose membranes were incubated in blocking solution (4.5 g NaCl; 0.6 g Tris; 250 μl Tween 20 made up to 500 ml with distilled water) overnight at room temperature. The membranes were incubated for 2 h at room temperature with mouse monoclonal anti-iNOS (N32030, Transduction Laboratories) diluted 1:2500 in blocking solution or rabbit polyclonal anti-eNOS (Transduction Laboratories) diluted 1:1000 in blocking solution. Thereafter, membranes were washed five times for 30 min in washing solution (4.5 g NaCl; 250 μl Tween 20 made up to 500 ml with distilled water). They were then incubated for 2 h at room temperature with the secondary antibody (rabbit anti-mouse HRP conjugate (A9044, Sigma)) diluted 1:10,000 in blocking buffer. The membranes were then washed five times for 30 min in washing buffer and developed using ECL Plus detection kit (Amersham) according to the protocol supplied by Amersham. Finally, the chemiluminescence signal was detected with photographic film (Hyperfilm ECL; Amersham Pharmacia Biotech) and recorded after 5–10 min exposure.

2.6. Electrophoretic mobility shift assays (EMSAs)

Electrophoretic mobility shift assays (EMSAs) were used to demonstrate activation and translocation of proteins

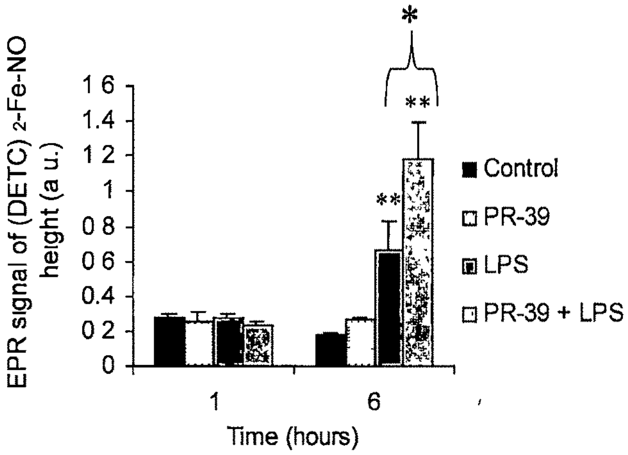

Fig 1 Direct in vivo measurements of liver NO were made in mice treated intraperitoneally with saline (control), LPS (40 mg/kg), PR-39 (20.6 mg/kg) or PR-39 + LPS. NO levels were measured at 1 and 6 h post-treatment (n>six mice per time point) Data are expressed as mean ± S D $*P=0.01$ for LPS versus PR-39+LPS and $**P=0\ 001$ for control versus LPS and control versus PR-39+LPS

that bind to specific consensus DNA sequences for NF-κB. Typically, NF-κB activation occurs early following LPS injection (<2 h). Excised samples of liver tissue were snap frozen in liquid nitrogen. Approximately 50 mg of frozen tissue was pulverized in a pre-cooled mortar and pestle and then transferred to a microfuge tube. Cold stop buffer (10 mM Tris–HCl, pH 7.4, 10 mM EDTA, 5 mM EGTA, 100 mM NaF, 200 mM sucrose, 100 μM Na-orthovanadate, 5 mM pyrophosphate, 4 μg/ml leupeptin, 4 μg/ml soybean trypsin inhibitor, 1 mM benzamidine, 20 μM calpain inhibitor 1, 100 mU/ml aprotinin, and 100 μM phenylmethylonylflouride) was added and mixed with the tissue. The samples were homogenized using 10 strokes in a dounce homogenizer and then centrifuged at 4000 × g. The resulting cell pellets were rinsed twice and the protein content of the nuclear extracts was determined using Coomassie® Plus Reagent (Pierce, Rockford, IL) and BSA as the standard. Equal amounts (5 μg) of nuclear protein was incubated with 5′-[^{32}P] labelled, double-strand oligonucleotide that contains the consensus binding sequence for NF-κB (5′-AGTTGAGGGGACTTTCC-CAGGC-3′) (Promega, Madison, WI). The incubation mixtures were separated by 4% non-denaturing PAGE using high ionic conditions and bands were detected by autoradiography.

2.7. Statistics

Results are expressed as the mean ± S.D. of n animals. Statistical evaluation unless otherwise stated was performed by one-way analysis of variance (ANOVA) followed by the Newman–Keuls test for multiple comparison. $**P<0.001$ and $*P<0.01$. Statistical analysis was undertaken using Prism software.

3. Results

3.1. Levels of liver nitric oxide

Liver NO was measured directly in vivo by EPR spectroscopy. The resultant NO data from mice in each of the treatment groups (control, PR-39, LPS, and LPS+PR-39) are summarised in Fig. 1 and represent NO levels at 1 and 6 h after treatment. There was a significant increase in liver NO in mice treated with LPS compared with controls at 6 h. However, mice treated with LPS and PR-39 had significantly greater amounts of NO in the liver than those treated with LPS alone. Mice treated with saline or PR-39 alone showed similar baseline levels of NO and no significant change with time.

3.2. Levels of NO-derivatives in blood

We analyzed red blood cells for HbNO (same animals as in vivo NO above) using ex vivo EPR at liquid nitrogen temperatures. Mice treated with LPS or LPS and PR-39 had significantly increased levels of HbNO in the blood compared with control animals. However, unlike the liver NO, there was no difference between HbNO levels in the LPS or LPS+PR-39 treated mice. Measurement of plasma nitrite and nitrate levels (NO_x) in these animals showed increased NO_x 6 h following LPS or PR-39+LPS. Significantly more NO_x was found in the plasma of mice treated with PR-39+LPS compared with LPS alone ($P<0.05$) (Table 1). As we have demonstrated previously [28], no significant increase in NO_x was observed 15 min or 1 h after LPS injection (data not shown).

These results agree with our previous measurements of NO_x and mean arterial blood pressure in control and septic animals using similar doses of LPS in this model [18]. LPS (40 mg/kg) typically producing a transient decrease in blood pressure within minutes following i.p. injection, but large increases in NO_x and severe hypotension at 6 h.

Table 1
Summary of the blood flow and NO metabolites in blood from animals in each of the treatment groups

	6 h after treatment			
	Control	LPS	PR-39+LPS	PR-39
NO_x (μm) (n=6)	75.2 ± 22 0	444.4 ± 83.9^a	582.6 ± 136.8^b	67 4 ± 16 3
HbNO (μM) (n=8)	1.08 ± 0 36	5.36 ± 1 44^a	4 76 ± 0.46^a	1.84 ± 2 80
Blood flow (ml/min) (n=8)	5 6 ± 4.0	3 9 ± 5.7^c	4 8 ± 3 9^c	5.1 ± 4.2^c

[a] Represents a significant difference compared to control group (P=0 01).

[b] Represents significant difference from control, and PR-39 (P=0.01), and also compared to LPS alone (P=0.05)

[c] Represents no significant difference from control group

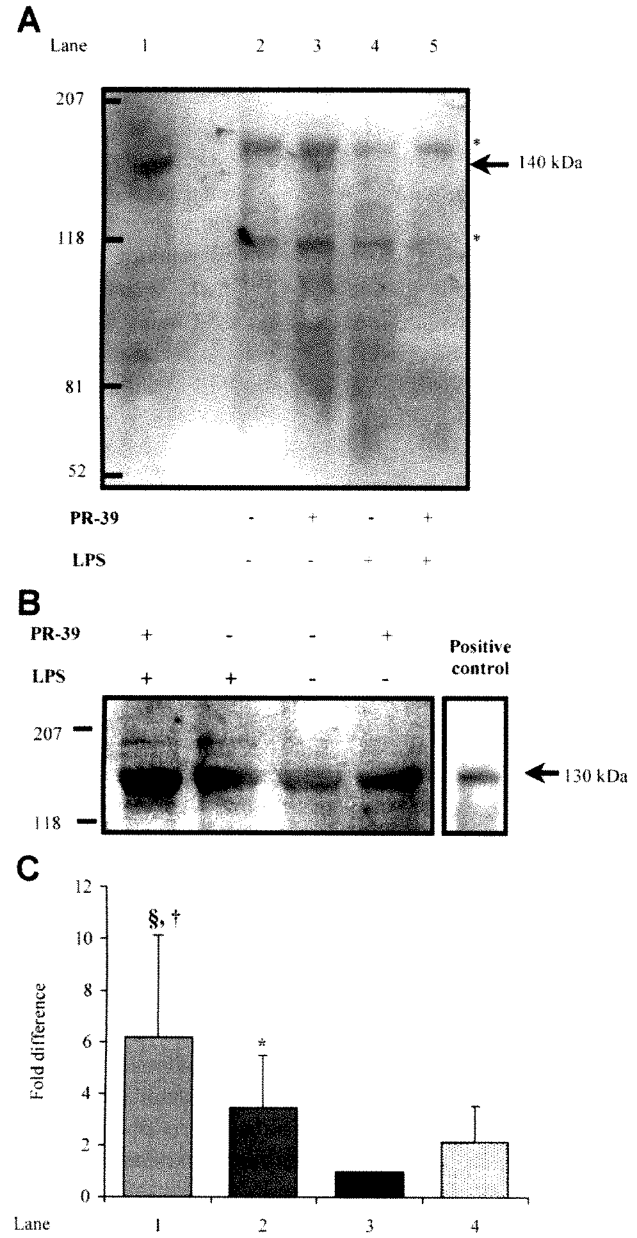

Fig. 2. (A) A representative Western blot for eNOS at 6 h with saline (lane 2), PR-39 (lane 3), LPS (lane 4) and PR-39 + LPS (lane 5). There was no induction of eNOS protein expression (molecular weight of 140 kDa) found in any of the treatment groups. Lane 1, positive control from endothelial cell extract; * denotes non-specific binding. (B) Western blot analysis of iNOS in liver 6 h after administration of PR-39 + LPS (lane1), LPS (lane 2), saline (control; lane 3) and PR-39 (lane 4). Each lane contains 40 μg of protein from separate animals. (C) Densometric analysis from iNOS bands of five gels (five animals in each case). * and †—Represent significant difference from control ($P<0.03$). §—Represents significant difference from LPS ($P<0.04$).

3.3. Expression of NOS protein

NOS protein expression in liver tissue was measured by Western blot analysis 6 h after treatment. Densitometry was carried out on NOS bands ($n=5$ gels from five mice in each treatment group). A typical Western blot for eNOS/iNOS protein expression in livers of control, PR-39, LPS and PR-39 + LPS treated mice at 6 h is shown in Fig. 2 (A and B, respectively). The fold difference between PR-39, LPS or PR-39 + LPS compared with the control group for iNOS expression was calculated. It was found that iNOS protein expression was high following both LPS alone and PR-39 + LPS treatment ($P=0.028$ and $P=0.022$, respectively, compared to controls). Furthermore, there was a significant increase following PR-39 + LPS treatment ($P=0.038$). These results are summarised in Fig. 2(C). There was no up-regulation of eNOS following treatment (compared with the positive control in each case).

3.4. Nuclear factor-κB DNA binding

In separate groups of mice, NF-κB DNA binding by EMSA was measured at 1, 3 and 5 h post-treatment (Fig. 3). Mice treated with LPS showed an approximate 18-fold increase in NF-κB binding at 1 h, typical of early NF-κB activation following LPS injection. A 14-fold increase was observed in mice treated with PR-39 + LPS (not significantly different from LPS treatment alone). NF-κB binding declined at 3 and 5 h for both LPS and with PR-39 + LPS. Both control (saline) and PR-39 showed only baseline NF-κB binding at all time points.

3.5. Direct in vivo measurements of pO_2 at the sinusoids and across the hepatic tissue bed

Liver pO_2 was measured from gloxy EPR line widths at 6 h in mice subjected to saline, LPS, PR-39 and PR-39 + LPS. Liver pO_2 (mm Hg) measured at the sinusoids (from gloxy slurry) or across the liver lobule (from gloxy particles) is summarised in Table 2. In control (saline) mice, the mean pO_2 at the sinusoidal lumen was 44.39 ± 5.13 mm Hg, whereas average liver lobule pO_2 was 4.56 ± 1.28 mm Hg.

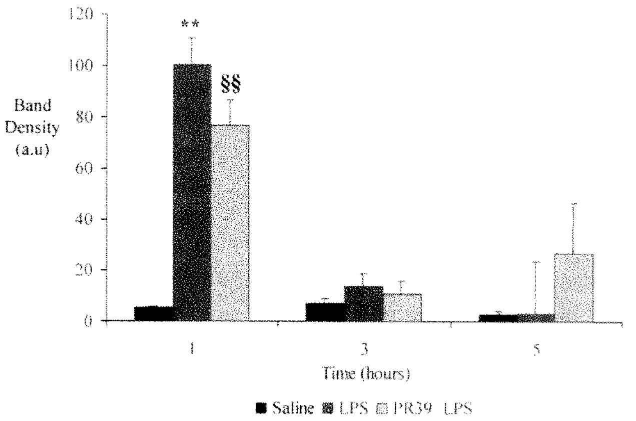

Fig. 3. NF-κB activity measured in mouse liver. Mice were treated with saline, LPS or PR-39 + LPS for 1, 3 or 5 h. Each bar represents the mean value ± S.D. ($n=$three mice for each time point). **—Represents a significant difference where $P<0.001$ and §§ represents a significant difference where $P<0.001$.

Table 2

Summary of in vivo measurements of pO_2 in mouse liver 6 h after treatment with saline (control), LPS or PR-39 + LPS

	Control pO_2 (mm Hg)	LPS pO_2 (mm Hg)	PR39 + LPS pO_2 (mm Hg)
Slurry	44.39 ± 5.13	11.22 ± 2.48^{a}	$23.58 \pm 9.36^{a,b}$
Particles	4.56 ± 1.28^{c}	$1.16 \pm 0.42^{a,c}$	$3.80 \pm 1.34^{a,b,c}$
pO_2 difference (slurry – particles)	39.83	10.05	19.78

The pO_2 experienced by the sinusoidal lumen (slurry) and across the sinusoidal bed (particles), and the difference in pO_2 (slurry – particle) are presented. n = six mice for each treatment group. The data is expressed as the mean ± S.D.

[a] Represents a significant difference compared to control values ($P < 0.01$).

[b] Represents a significant difference compared to LPS values ($P < 0.01$).

[c] Represents a significant difference between particle and slurry values within each respective treatment group ($P < 0.001$).

The difference in pO_2 between these sites was therefore 39.83 mm Hg. When mice were subjected to LPS or PR-39 + LPS, this pO_2 difference was 10.05 and 19.78 mm Hg, respectively. (Measurements of pO_2 in mice subjected to PR-39 alone are not shown because our initial studies indicated that PR-39 had no affect upon liver oxygenation).

Treatment with LPS significantly reduced liver pO_2 by approximately 75% at both the sinusoids and across the lobule tissue (Table 2; LPS). Our data also showed only a 53% decrease in the amount of oxygen being supplied to the sinusoidal capillaries following PR-39 treatment of LPS treated mice (reflected by the slurry pO_2 in controls compared with PR-39 + LPS). This would indicate that oxygen supply to liver sinusoids was preserved by PR-39 in septic animals (Table 2; PR-39 + LPS). There was also a greater pO_2 difference across the liver lobule (pO_2 difference (PR-39 + LPS) = 19.78 mm Hg).

Blood flow through the hepatic artery at 6 h was essentially the same in control, LPS, and PR-39 + LPS-treated animals (Table 1). However, we acknowledge the high degree of variability within the treatment groups and between individual mice. This factor may have made measurement of smaller differences in blood flow difficult to detect.

4. Discussion

Direct measurements of pO_2 and NO in vivo are difficult but are desirable to improve our understanding of organ dysfunction in sepsis. This study has demonstrated the usefulness of the EPR technique for the measurement of these parameters directly in vivo. Measurements of pO_2 were made specifically from liver sinusoids (reflecting supply of blood and oxygen to the liver lobule) and also as average pO_2 across the liver lobule. With this technology, we have shown that the antibacterial peptide PR-39 can preserve sinusoid perfusion and oxygen levels across the hepatic tissue bed in our LPS-induced model of septic shock. Furthermore, PR-39 treatment was seen to increase nitric oxide levels in the liver in LPS-treated animals. This appeared to be the result of increased iNOS expression in liver rather than enhanced systemic production of NO.

We have previously made simultaneous measurements of NO and pO_2 in vivo in mice [18] and demonstrated the usefulness of EPR oximetry for making measurements of pO_2 from selected tissue regions [20,26]. In the present study, we observed increased liver NO (observed as an increase in NO–Fe–$(DETC)_2$ in liver) at 6 h that coincided with LPS induction of iNOS. Expression of iNOS (mRNA and protein) is induced in a variety of cell types during sepsis [27] and is thought to play a critical role in multiple organ failure [30]. PR-39 significantly increased LPS-induced iNOS expression in liver but had only a moderate effect on systemic NO_x and no significant affect on circulating HbNO.

We cannot rule out the possibility that reaction of NO with O_2^- was also prevented as a result of the known inhibitory effects of PR-39 on NADPH-oxidase function. However, injection of a comparatively large LPS bolus provides a model in which to study primarily haemodynamic and physiological dysfunction during a 1–7 h septic episode. It seems unlikely that PR-39 mediated its effects via modulation of superoxide production in these studies, since assessment of oxidative stress to tissue (levels of thiobarbituric acid reactive substances (TBARS) in liver tissue and in plasma) or liver damage (levels of serum aspartate amino transferase (AST)) showed little evidence for the production of large quantities of reactive oxygen intermediates like superoxide or the occurrence of oxidative damage in our model as a result of LPS challenge [28,29]. A variety of sepsis models are available to specifically investigate tissue damage and longer term effects of LPS. These typically involve priming animals with an additional insult (such as galactosamine or BCG) in order to enhance host response and bring forward pathophysiological events, usually observed much later during sepsis. In such a model, we have previously demonstrated PR-39 reduced oxidative damage to liver 8–12 h following galactosamine/LPS [7,21].

Gao et al. [6] reported PR-39 inhibited IκBα degradation and thus inhibited NF-κB-dependent gene expression. We measured NF-κB DNA binding by EMSA in liver tissue homogenates and found mice treated with LPS showed an approximate 18-fold increase in NF-κB binding at 1 h (compared to controls), typical of early NF-κB activation following LPS injection. However, an approximate 14-fold increase was observed in mice treated with PR-39 + LPS (not significantly different from LPS treatment alone). NF-κB binding typically declined at 3 and 5 h for both LPS and with PR-39 + LPS. We can conclude from these experiments that PR-39 is unlikely to affect expression of iNOS or other pro-inflammatory proteins mediated via NF-κB. However, PR-39 significantly increased iNOS expression in liver. PR-

39 administration to septic mice showed an approximate 3-fold increase in iNOS protein expression (compared to LPS alone), but did not enhance eNOS protein expression. Mice treated with PR-39 alone also showed an approximate 1-fold increase in iNOS protein expression when compared to the controls. PR-39 may have induced iNOS protein via an unidentified NF-κB-independent mechanism. For example, activator protein-1 (AP-1) can activate the human iNOS promoter in cells stimulated with LPS/IFN-γ [31].

We concentrated our in vivo measurements of liver pO_2 at the 6 h time point because our previous physiological data indicated that LPS treatment had a significant impact on MABP and organ perfusion at this time [18]. LPS treatment resulted in approximately 75% decrease in pO_2 both at sinusoids and across the hepatic tissue bed. This suggests that LPS-induced hypoxia in this model was primarily the result of defective oxygen supply to liver sinusoids. Decreased sinusoidal perfusion could be due to a number of mechanisms, including LPS-induced arterio-venous shunting of blood and microaggregation of platelets and neutrophils within sinusoidal capillaries [32]. Alternatively, swelling of Kupffer cells within the liver sinusoids may also cause reduction in sinusoidal capillary diameter, partially or completely occluding the sinusoids [33].

We found that PR-39 treatment alleviated the LPS-induced defect in oxygen delivery to sinusoids (an approximate 53% decrease at the sinusoids compared to 75%, respectively). The oxygen difference between sinusoids and across the lobule also increased (20 versus 10 mm Hg in PR-39 + LPS and LPS groups, respectively, reflecting a 25% improvement compared to controls), which most likely reflects the improved delivery of oxygen to sinusoids (also increased by 25% recorded by Gloxy slurry) and increased oxygen availability across the lobule. Elevated NO induced by PR-39 may have reduced sinusoidal blockage by maintaining sinusoid dilatation, eradicating classic inflammatory responses, such as leukocyte activation and recruitment in sinusoids [34] and prevented intravascular coagulation.

In addition, PR-39 apparently preserved hepatic tissue oxygenation almost to the level of controls (approximately 4 mm Hg reported by gloxy particles). Our data strongly implicates that improvement in sinusoidal perfusion results in the normalisation of pO_2 at both tissue sites. There are, however, several other plausible explanations to the maintenance of 4 mm Hg at the level of the particle that warrant further study. The increase in local liver NO in mice subjected to PR-39 + LPS may have contributed to decreased mitochondrial respiration [35,36] resulting in higher pO_2 across the liver lobule. PR-39 inhibition of HIF-1α degradation by the ubiquitin–proteasome system may also have facilitated enhanced glycolytic capacity and reduced mitochondrial activity [37].

In conclusion, we have shown, in a mouse model of endotoxin-induced sepsis, that PR-39 treatment causes a relative increase in local hepatic NO by influencing iNOS expression in liver. Our site-selective pO_2 measurements demonstrate that PR-39 preserved sinusoidal perfusion and lobule oxygenation.

Acknowledgements

This study was supported by NIH Grant PO1 GM51630 and used the facilities of the EPR Center for Viable Biological Studies, supported by NIH Grant P41 RR11602. The Department of Cardiology, Wales Heart Research Institute, is supported by the British Heart Foundation.

We thank Elena Donskaya and Liuqiong Lu for their excellent technical assistance.

References

[1] B. Agerberth, H. Gunne, J. Odeberg, P. Kogner, H.G. Boman, G.H. Gudmundsson, Vet. Immunol. Immunopathol. 54 (1996) 127–131.

[2] J. Shi, C.R. Ross, M.M. Chengappa, F. Blecha, J. Leukoc. Biol. 56 (1994) 807–811.

[3] H.G. Boman, B. Agerberth, A. Boman, Infect. Immun. 61 (1993) 2978–2984.

[4] H.J. Huang, C.R. Ross, F. Blecha, J. Leukoc. Biol. 61 (1997) 624–629.

[5] Y.R. Chan, R.L. Gallo, J. Biol. Chem. 273 (1998) 28978–28985.

[6] Y. Gao, S. Lecker, M.J. Post, A.J. Hietaranta, J. Li, R. Volk, M. Li, K. Sato, A.K. Saluja, M.L. Steer, A.L. Goldberg, M. Simons, J. Clin. Invest 106 (2000) 439–448.

[7] J. Shi, C.R. Ross, T.L. Leto, F. Blecha, Proc. Natl. Acad. Sci. U. S. A. 93 (1996) 6014–6018.

[8] J. Li, M. Post, R. Volk, Y. Gao, M. Li, C. Metais, K. Sato, J. Tsai, W. Aird, R.D. Rosenberg, T.G. Hampton, F. Sellke, P. Carmeliet, M. Simons, Nat. Med. 6 (2000) 49–55.

[9] M.P. Glauser, G. Zanetti, J.D. Baumgartner, J. Cohen, Lancet 338 (1991) 732–736.

[10] J.R. Parratt, J. Antimicrob. Chemother. 41 (Suppl. A) (1998) 31–39.

[11] D. Jacobson, M. Singer, in: J.-L. Vincent (Ed.), The Cell, the Mitochondria, Oxygen and Sepsis, Springer, Berlin, 1996, pp. 263–274.

[12] T.R. Billiar, R.D. Curran, B.G. Harbrecht, D.J. Stuehr, A.J. Demetris, R.L. Simmons, J. Leukoc. Biol. 48 (1990) 565–569.

[13] H. Ruetten, G.J. Southan, A. Abate, C. Thiemermann, Br. J. Pharmacol. 118 (1996) 261–270.

[14] J.A. Scott, D.G. McCormack, J. Appl. Physiol. 86 (1999) 1739–1744.

[15] J.P. Cobb, R.S. Hotchkiss, P.E. Swanson, K. Chang, Y. Qiu, V.E. Laubach, I.E. Karl, T.G. Buchman, Surgery 126 (1999) 438–442.

[16] J.E. Saavedra, T.R. Billiar, D.L. Williams, Y.M. Kim, S.C. Watkins, L.K. Keefer, J. Med. Chem. 40 (1997) 1947–1954.

[17] B.G. Harbrecht, T.R. Billiar, J. Stadler, A.J. Demetris, J. Ochoa, R.D. Curran, R.L. Simmon, J. Leukoc. Biol. 52 (1992) 390–394.

[18] P.E. James, M. Miyake, H.M. Swartz, Nitric Oxide 3 (1999) 292–301.

[19] P.E. James, O.Y. Grinberg, F. Goda, T. Panz, J.A. O'Hara, H.M. Swartz, Magn. Reson. Med. 38 (1997) 48–58.

[20] J. Jiang, T. Nakashima, K.J. Liu, F. Goda, T. Shima, H.M. Swartz, J. Appl. Physiol. 80 (1996) 552–558.

[21] J. Shi, C.R. Ross, M.M. Chengappa, M.J. Sylte, D.S. McVey, F. Blecha, Antimicrob. Agents Chemother. 40 (1996) 115–121.

[22] Y. Xia, A.J. Cardounel, A.F. Vanin, J.L. Zweier, Free Radic. Biol. Med. 29 (2000) 793–797.

[23] M. Miyake, J.A. O'Hara, P.E. James, T. Panz, H.M. Swartz, in: H. Kamada, H. Ohya (Eds.), Proceedings of ESR (EPR) Imaging and In vivo ESR Spectroscopy, Yamagata, Japan, 1998, pp. 252–254.

[24] U. Westenberger, S. Thanner, H.H. Ruf, K. Gersonde, G. Sutter, O. Trentz, Free Radic. Res. Commun. 11 (1990) 167–178.

[25] P. Misko, R.J. Schilling, D. Salvemini, W.M. Moore, M.G. Currie, Anal. Biochem. 214 (1993) 11–16.

[26] P.E. James, G. Bacic, O.Y. Grinberg, F. Goda, J.F. Dunn, S.K. Jackson, H.M. Swartz, Free Radic. Biol. Med. 21 (1996) 25–34.

[27] S.M. Morris Jr., T.R. Billiar, Am. J. Physiol. 266 (1994) E829–E839.

[28] J.D. Mac Micking, C. Nathan, G. Hom, N. Chartrain, D.S. Fletcher, M. Trumbauer, K. Stevens, Q.-W. Xie, K. Sokoi, N. Hutchinson, H. Chen, J.S. Mudgett, Cell 81 (1995) 641–650.

[29] P.E. James, M. Madhani, W. Roebuck, S.K. Jackson, H.M. Swartz, Nitric Oxide: Biol. Chem. 6 (2002) 18–28.

[30] K.D. Kroncke, K. Fehsel, V. Kolb-Bachofen, Nitric Oxide 1 (1997) 107–120.

[31] A.S. Kristof, J. Marks-Konczalik, J. Moss, J. Biol. Chem. 276 (2001) 8445–8452.

[32] E.F. Mammen, J. Antimicrob. Chemother. 41 (Suppl. A) (1998) 17–24.

[33] R.S. McCuskey, Am. J. Anat. 119 (1966) 455–477.

[34] R.J. Korthuis, D.C. Gute, F. Blecha, C.R. Ross, Am. J. Physiol. 277 (1999) H1007–H1013.

[35] P.R. Forfia, T.H. Hintze, M.S. Wolin, G. Kaley, Adv. Exp. Med. Biol. 471 (1999) 381–388.

[36] P.E. James, S.K. Jackson, O.Y. Grinberg, H.M. Swartz, Free Radic. Biol. Med. 18 (1995) 641–647.

[37] G.L. Semenza, J. Lab. Clin. Med. 131 (1998) 207–214.

ELSEVIER

Biochimica et Biophysica Acta 1588 (2002) 241–246

BIOCHIMICA ET BIOPHYSICA ACTA
BBA
www.bba-direct.com

Isolation of differentially expressed genes in human heart tissues

Guifeng Sun[a,*,1], Siu Yuen Chan[b,1], Yihua Yuan[c], Kin Wang Chan[b], Guangrong Qiu[a], Kailai Sun[a], Maurice Ping Leung[b]

[a]*Department of Medical Genetics, Institute of Basic Medicine, China Medical University, Shenyang, PR China*
[b]*Department of Pediatrics, The University of Hong Kong, Queen Mary Hospital, Hong Kong SAR, PR China*
[c]*Department of Cardiovascular Surgery, The First Hospital, China Medical University, Shenyang, PR China*

Received 7 March 2002; received in revised form 16 July 2002; accepted 1 August 2002

Abstract

We applied RNA arbitrarily primed-PCR (RAP-PCR) to screen the genes differentially expressed between common congenital heart defects (CHD) [atrial septal defect, ventricular septal defect, Tetrology of Fallot (TOF)] and normal human heart samples. Three of these differentially amplified fragments matched cDNA sequences coding for proteins of unknown function in humans: hCALO (human homologue of calossin), NP79 (coding for a nuclear protein of 79KD) and SUN2 (Sad-1 unc-84 domain protein 2). The other four fragments were from known human genes: apolipoprotein J, titin, dystrophin and protein kinase C-delta. Northern blot analysis confirmed that all of these genes are expressed in the human heart. The results of RAP-PCR were reconfirmed by quantitative RT-PCR in TOF and control heart samples. Both techniques showed the levels of expression of hCALO, NP79 and SUN2 to be comparable in TOF and control samples and the level of expression of dystrophin and titin, both coding for cytoskeletal proteins, to be significantly upregulated in TOF samples. In summary, we have shown that the RAP-PCR technique is useful in the identification of differentially expressed gene from biopsy samples of human CHD tissues. In this manner, we have identified three novel genes implicated in the normal function of the human heart and two known genes upregulated in TOF samples.

© 2002 Elsevier Science B.V. All rights reserved.

Keywords: RNA arbitrarily primed-PCR; Congenital heart defect; Gene expression; Titin; Dystrophin

1. Introduction

Congenital heart defects (CHD) are the most common form of heart disease in childhood, occurring in about 1% of live births and perhaps 10% of stillbirths [1]. CHD are the clinical manifestation of anomalies in heart development, a complex process requiring cell specification and differentiation, cell migration, morphogenesis and interactions among cells from a variety of embryonic origins. In recent years, studies of heart development in fish, frogs, mice, flies and worms by mutagenesis studies have begun to develop how morphogenesis and hierarchies of developmental control are exerted, and have pointed to the role of genes such as the transcription factors Nkx2-5, GATAs, MEF2s, dHAND and eHAND [2–5]. However, the basic mechanism for CHD in man is still incompletely defined.

The paucity of large CHD human families and the incomplete penetrance of CHD as a phenotype have limited the usefulness of linkage analysis in identifying causal genes. Until now, only a few genes directly related to human CHD have been identified, and most of them are related to a complex syndrome that includes cardiac malformations, such as TBX5 mutations in Holt Oram syndrome [6], TFAP2B mutations in Char syndrome [7], and the haploinsufficiency of one or more genes in 22q11 or 10p13-p14 that cause DiGeorge Syndrome/velocardiofacial syndrome (VCFS), two genetic diseases with overlapping clinical features that include conotruncal defects and abnormal development of other structures derived from the neural crest [8].

While mutations in the homeobox transcription factor NKX2.5 gene have been found in patients with nonsyndromic congenital heart diseases [9], it is likely that new strategies will be required to identify the common nonsyndromic CHD susceptibility genes. The identification of

---

[*] Corresponding author. Present address: Department of Physiology and Biophysics, College of Medicine, University of California, Irvine, Room 288, Joan Irvine Smith Hall, Irvine, CA 92697, USA. Tel.: +1-949-8246638; fax: +1-949-8243143.

E-mail address: guifengs@uci.edu (G. Sun).

[1] These two authors contributed equally to this paper.

0925-4439/02/$ - see front matter © 2002 Elsevier Science B.V. All rights reserved.
PII: S0925-4439(02)00171-0

genes involved in various stages of cardiac development will likely be one important step. Another lead may come from a comparison of gene expression patterns between normal and CHD hearts or among different types of CHD. Identification of those differentially expressed genes in human CHD heart tissues will serve as markers that may point to the molecular mechanisms involved in normal and CHD states, and perhaps provide new insights for the discovery of novel molecular targets for diagnostics and therapeutics.

RNA arbitrarily primed-PCR (RAP-PCR) [10] and mRNA differential display (mRNA DD) [11] are two sensitive PCR-based RNA fingerprinting techniques that have been successfully applied to many areas including carcinogenesis, neurobiology, developmental biology and cardiovascular disease. More than 10 novel genes in cardiovascular functions and diseases have been discovered by application of this method [12]. Compared to RAP-PCR, which preferentially provides internal coding sequences of differentially expressed genes, cDNA fragments obtained from mRNA DD methods are often in the 3′ untranslated region, and therefore difficult to identify by homology in databases. In order to find genes related to the pathogenesis of CHD, we applied RAP-PCR to isolate and characterize the differentially expressed genes in three common forms of CHD: atrial septal defect (ASD), ventricular septal defect (VSD) and Tetrology of Fallot (TOF). We have identified three interesting sequences that are likely to be related to normal functioning of the developing and the mature heart. We also find that the expression of dystrophin and titin, both coding for a cytoskeletal protein, is significantly upregulated in TOF samples.

2. Methods

2.1. Tissue sources and total RNA preparation

For RAP-PCR, ventricle biopsies were obtained from six children with CHD during corrective cardiac surgery. Two of them were with ASD (ages: 6 and 7 years), two with VSD (ages: 3 and 5 years) and two with TOF (ages: 7 months and 2 years). Ventricle tissue from a 32-year-old woman with rheumatic heart disease obtained during her valve-replacement surgery and two biopsies taken from children (age: 5 and 9 years) with acute cardiac infections were taken as non-CHD controls. All procedure conforms to the principles outlined in the Declaration of Helsinki [Cardiovasc. Res. 35 (1997) 2]. The tissues were directly frozen in liquid nitrogen and stored at −70 °C until use. Total RNA was prepared using TRIZOL Reagent (Life Technologies, New York, USA). Normal adult (27 years old) and fetal (27 weeks old) RNA samples were purchased from BioChain Institute, Inc. As very limited amounts of fresh CHD cardiac biopsy material were available, only TOF samples that tend to be larger were chosen to reconfirm the validity of the RAP-PCR technique using quantitative RT-PCR.

2.2. RAP-PCR

The RNA samples were purified by DNase I treatment followed by phenol/chloroform extraction and ethanol precipitation. Two quantities of each total RNA (50 and 100 ng) were reverse transcribed (RT) in a 20 μl reaction mix with 5 pmol arbitrarily chosen primer 5′-AGCCCGTAGGTACCCTGG or 5′-GCAAACCGCGGTGACCACTG to synthesize first-strand cDNA. The RT reaction was performed with AMV reverse transcriptase and reagents in Reverse Transcription System (Promega, WI, USA). Afterwards, 10 μl was used for PCR in a 25 μl reaction volume containing 25 pmol of the same primer as in first-strand synthesis. PCR was performed with one low stringency cycle of 94 °C for 5 min, 40 °C for 5 min and 72 °C for 5 min, followed by 39 high stringency cycles of 94 °C for 1 min, 60 °C for 1 min and 72 °C for 2 min in a PTC-100 Thermal Cycler (MJ Research). For nonradioactive RAP-PCR, the PCR products were electrophoresed in a 6% nondenaturing polyacrylamide gel, and then stained with 10 μl/100 ml SYBR Green (Boehringer Mannheim, Mannheim, Germany) for 30 min. The differentially amplified bands were cut from the gel under long wavelength UV light. For radioactive RAP-PCR, the PCR reactions were performed with ^{33}P end-labeled primers. Then the PCR products were electrophoresed in a 6% denaturing polyacrylamide gel. The gel was dried on a 3M Whatman paper and exposed to Fuji X-ray film for 24–72 h. Differentially expressed cDNA bands of interest were cut from the gel and eluted in 25 μl TE buffer at 65 °C for 2 h. The cDNA bands isolated by either the radioactive or nonradioactive method were reamplified with the same PCR conditions and primer.

2.3. cDNA cloning and sequence analysis

cDNA fragments were ligated into pGEM-4Z vector (Promega) by single-step direct cloning methods [13]. Each ligation reaction (20 μl) included 200 ng uncut vector pGEM4Z, 150 ng PCR product, 2U *Sma*I, 1 unit T4 DNA polymerase, 0.4 mM dNTPs, 1 unit T4 ligase and ligation buffer with ATP. The ligation mixture was left overnight at room temperature, and 5 μl was used for heat shock transformation into the *Escherichia coli* strain DH5α. Plasmid DNA was purified using High Pure Plasmid Isolation kit (Boehinger Mannheim). The presence of insert was tested by digestion with *Eco*RI. Successfully cloned cDNA fragments were sequenced with M13 forward primers in an ABI PRISM 377 automatic sequencing machine (Applied Biosystems, Foster City, CA) using the ABI Prism dRhodamine Terminator Cycle Sequencing kit. Homology search was performed using the BLAST algorithm in the nonredundant database of the National Center for Biotechnology Information.

2.4. Northern blot analysis

The cDNA inserts were released from plasmids with restriction enzymes and purified by QIAEX II Gel Extraction Kit (Qiagen). Then, the DNA fragment was labeled with α-^{32}P-dCTP (3000 Ci/mmol) by random primer labeling [14]. Premade human multiple-tissue blot and fetal multiple-tissue blot II were purchased from Invitrogen (Carlsbad, CA). The manufacturer's information indicated that each lane was loaded with 20 μg of total RNA from eight different male tissues including adult heart, brain, kidney, liver, lung, pancreas, spleen, skeletal muscle for human multiple tissue blot; and from human fetal heart, kidney, stomach and intestine for fetal blot II. Filters were hybridized with the labeled probe, washed and exposed to X-ray film (Fuji) at −70 °C with two intensifying screens. Blots were stripped with 0.5% SDS at 95 °C, and rehybridized with labeled glyceraldehyde-3-phosphate dehydrogenase (GAPDH) probe as a standard to allow calibration for actual mRNA loading difference.

2.5. Relative quantitation of gene expression by RT-PCR

For first-strand cDNA synthesis, 5 μg of total RNA (DNase treated) was reverse transcribed with 250 pmol random hexamers and 400 units Superscript II (Life Technologies) in a 100 μl reaction following manufacturer's instructions. The resulting cDNA (from 50 ng total RNA per μl) was stored at −70 °C until use. Relative quantitation was done using the comparative C_T method with SYBR Green PCR Core Reagents (Applied Biosystems) according to manufacturer's protocol (User Bulletin #2, ABI PRISM 7700 Sequence Detection System, Applied Biosystems). GAPDH was used as the reference internal control. A panel of serially diluted cDNA (50, 5 and 0.5 ng, and 50 pg total RNA) was used to check the consistency of relative amplification efficiency of the target and reference. Quantitative PCR was carried out with an ABI PRISM 7700 Sequence Detector (Applied Biosystems) in a 25 μl reaction with 5 ng of cDNA, 5 pmol each of forward and reverse primer (Table 1), 3 mM $MgCl_2$, 200 μM dATP, dCTP, dGTP, 400 μM dUTP, 0.625 unit AmpliTaq Gold and 0.25 unit AmpErase UNG. The PCR cycling condition was 2 min at 50 °C for AmpErase UNG incubation, 10 min at 95 °C for AmpliTaq Gold activation, followed by 40 cycles of 15 s at 95 °C, 15 s at 60 °C and 30 s at 70 °C. An aliquot of PCR product was checked for a single specific band by electrophoresis.

Table 1
Sequences of primer pairs for PCR

Gene	Primer pair (5′ to 3′)	Amplicon length (bp)
GAPDH (reference)	ACCACAGTCCATGCCATCAC TCCACCACCCTGTTGCTGTA	452
Titin	CAAGGACACCAAGTGCACAG TGGTCCAGGAGTGGTAAAGG	148
Dystrophin	GACCAGCACAACCTCAAGCA TCAGCAGCCAGTTCAGACACA	151
hCALO	CATGGCAATGAGGCAGAAGG CAGCTCTTCCATCTGCTTCAGG	103
NP79	TTCCGCTACTTGACCAATCTGC GCGCTGGAACTCCTTGACAAT	126
SUN2	CCGTTACCTTAGAGCATGTGCC TCGCCGTCCTGATCGTAAGT	148

3. Results

3.1. RAP-PCR

RAP-PCR was performed using total RNA isolated from ASD, VSD, TOF and non-CHD ventricle biopsies. To avoid differential amplification caused by concentration or quality differences among RNA samples, two concentrations of RNA were tested for each RNA sample. Only differentially amplified products present in both concentrations were selected. RAP-PCR with radioisotope-labeled primer produced approximately 200 resolved products in a 40-cm gel. Six well-resolved differentially expressed cDNA fragments (R1–R6) were selected and excised from the gel. Nonradioactive RAP-PCR yielded approximately 100 resolved bands in a 15-cm gel. Nine well-resolved differentially expressed fragments (NR1–NR9) were isolated under direct UV light visualization.

3.2. Sequence analysis of the differentially amplified cDNA fragments

The cDNA fragments were cloned and sequenced. Homology search was performed and the results are summarized in Table 2. The six differentially amplified fragments isolated with the radiolabeled primer were: Human apolipoprotein J mRNA, *Homo sapiens* mRNA for KIAA0462 protein (referred to as hCALO for human homologue of *Drosophila* calossin), *H. sapiens* mRNA for KIAA0668 protein or sad1 unc-84 domain protein 2 (referred to as SUN2). The remaining three were homologous to 28s ribosomal RNA sequence. Using nonradiolabeled primer, nine differentially amplified cDNA fragments were isolated and studied further. Homology search revealed those to be: titin, dystrophin, protein kinase C-delta 13 and HRIHFB2216 mRNA, a sequence recently reported to be a cutaneous T-cell lymphoma-associated antigen. Since we have found HRIHF2216 mRNA encodes a putative nuclear localization protein of predicted molecular weight 79 kDa (see discussion), we referred to it as NP79. The remaining five cDNAs were ribosomal RNA and mitochondrial RNA. In the RAP-PCR fingerprint, hCALO, NP79, SUN2, protein kinase C-delta and apolipoprotein J showed a higher expression in VSD samples. On the other hand, titin and dystrophin showed a higher expression in TOF samples.

Table 2
Homology search results of cloned cDNA fragments from RAP-PCR

Fragment	Size (bp)	Name	Accession number	Description
R1	310	ApoJ	J02908	Human apolipoprotein J mRNA, complete cds (1512 bp)
R2	406	hCALO	AB007931	*Homo sapiens* mRNA for KIAA0462 protein, partial cds (7150 bp)
R3	173	SUN2	AF202723	*Homo sapiens* Sad1 unc-84 domain protein 2 (SUN2) mRNA, partial cds (1323 bp)
			AB014568	*Homo sapiens* mRNA for KIAA0668 protein, partial cds (3767 bp)
R4-R6	–	–	–	Ribosomal RNA
NR1	162	titin	X90568	*Homo sapiens* mRNA for titin protein (81940 bp)
NR2	412	dystrophin	M18533	*Homo sapiens* dystrophin (DMD) mRNA, complete cds (13957 bp)
NR3	300	PKC-δ	L07860	Human protein kinase C-delta 13 mRNA, complete cds (2104 bp)
NR4	388	NP79	AB015345	*Homo sapiens* HRIHFB2216 mRNA, partial cds (1605 bp)
			AF273046	*Homo sapiens* CTCL tumor antigen se20-4 mRNA, complete cds (2830 bp)
NR5–NR9	–	–	–	Ribosomal RNA and mitochondrial RNA

3.3. Northern blot analysis

The expression patterns of the three functionally unknown genes (hCALO, NP79 and SUN2) in adult and fetal tissues were studied using Northern blots (Fig. 1). It can be seen that although equal amounts of total RNA were loaded, as reported by the manufacturer, the GAPDH signal in lung and pancreas was reduced, reflecting tissue differences in these mRNA abundance in these tissues (Invitrogen). hCALO is identical to *H. sapiens* mRNA for KIAA0462 protein, with 7150 bases reported. Northern blot analysis of this novel sequence revealed a transcript longer than 9 kilobases (kb) detected only in adult heart, brain and lung. The transcript of NP79 was 2.8 kb and was strongly expressed in adult heart, moderately in brain, lung and spleen, and weakly in kidney and skeletal muscle. Interestingly, the expression of NP79 in adult heart was stronger than in fetal heart while the converse was observed in kidney. Another differentially amplified gene, SUN2, demonstrated constitutive expression of a 3.8 kb transcript in various tissues, with strongest expression in adult heart, lung and muscle. By Northern blot analysis, protein kinase C-delta 13 and apolipoprotein J were found to be constitutively expressed in various adult and fetal tissues and TOF biopsies (data not shown).

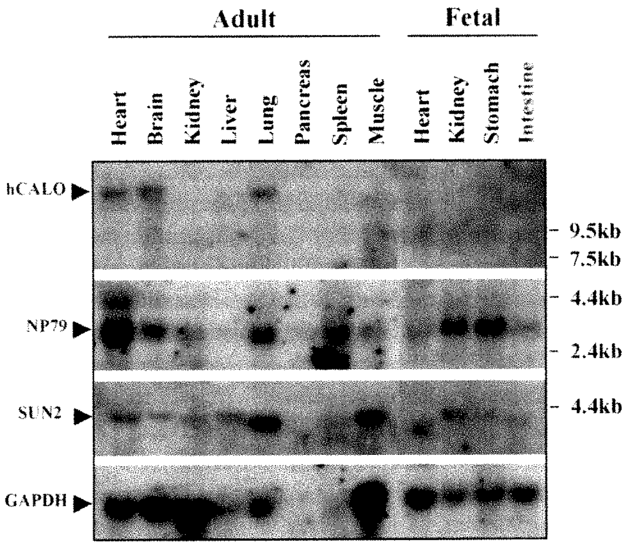

Fig. 1. Northern analysis of the sequences identified by RAP-PCR. RNA (20 μg) from the tissues indicated were loaded. hCALO, NP79 and SUN2 all showed a higher expression in adult than in fetal heart. The same filters were used for all probes. Hybridization with GAPDH was done lastly to indicate RNA loading. Positions of the RNA marker bands were indicated to the right.

3.4. Relative quantitation of gene expression by RT-PCR

Only ventricle biopsies from TOF patients yielded sufficient RNA for further analysis. Amplification curves from serial dilution of cDNA show that the C_T value (threshold cycle) correlated with the concentration of the gene under investigation within the cDNA range from 50 ng to 50 pg total RNA. The amount of cDNA used in quantitative PCR (from 5 ng of total RNA) falls in the mid range, suggesting that PCR should not be saturated in this study (data not shown). The relative expressions of genes in this study are shown in Fig. 2. The relative expression of each gene in the adult heart sample was used for normalization. Both titin and dystrophin showed a higher expression in TOF samples in the RAP-PCR fingerprint. The levels of expression of titin in adult and fetal hearts were similar (1.00 ± 0.03 and 0.94 ± 0.07). Both TOF samples were found to have higher expression of titin when compared to the normal adult sample (1.60 ± 0.12 and 3.00 ± 0.16). For dystrophin, fetal (1.61 ± 0.11) and TOF samples (1.49 ± 0.11 and 2.24 ± 0.12) both had a higher expression relative to the adult sample (1.00 ± 0.04). hCALO, NP79 and SUN2, which were found to be upregulated in VSD samples in the RNA fingerprint, had expression levels similar to that of the adult heart (Fig. 2), but all three genes had different levels of expression in the adult and fetal heart. In agreement with the results of Northern analysis, NP79 and SUN2 were expressed at a higher level in the adult heart than the fetal heart (1.00 ± 0.11 vs. 0.42 ± 0.1; 1.00 ± 0.17 vs. 0.33 ± 0.05, respectively). However, hCALO was found to have a higher level of expression in the fetal heart by RT-PCR (1.00 ± 0.42 vs.

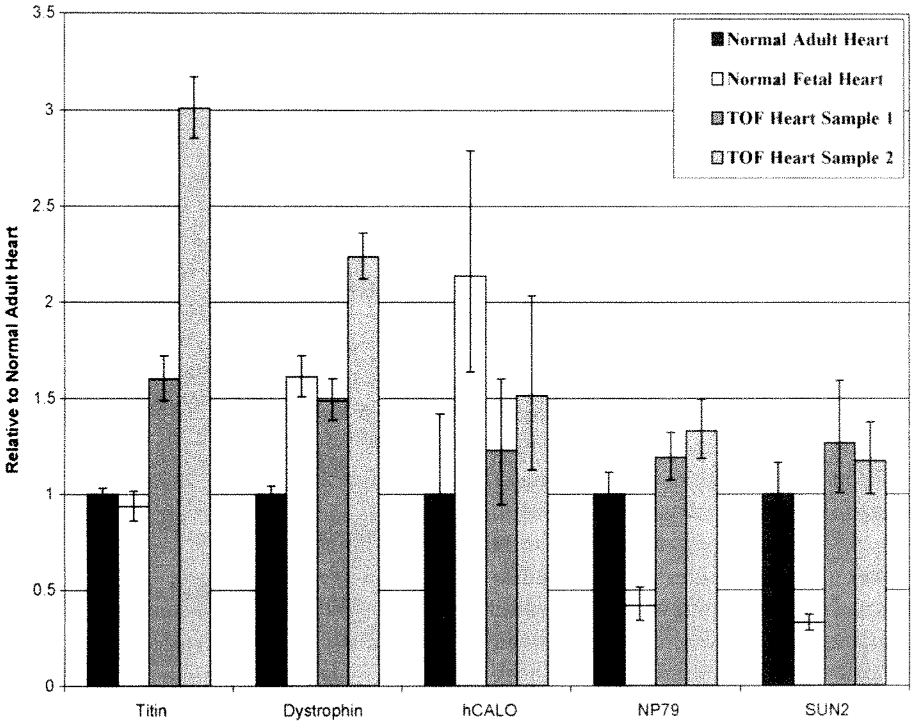

Fig. 2. Quantitative RT-PCR analysis of different genes on adult, fetal and TOF samples. Values are presented in relative expression level to adult tissue, which is normalized with GAPDH ($\Delta\Delta C_T$ method). Height of bars and the error bars represent the mean value and 95% confident intervals based on quadruplicate results.

2.14±0.66). Since the RNA of hCALO is >15 kb, the transcripts might be transferred inefficiently to the filter during northern analysis.

4. Discussion

Defects in heart septation, including ASD, VSD, atrioventricular septal defects and TOF, represent major causes of CHD [10]. They commonly involve ventricular or pressure overload hypertrophy before evolving into compensated congestive heart failure. Since differential gene expression is likely essential for normal heart development and pathological processes [2,10], the discovery of differentially expressed genes may provide a window for understanding the molecular mechanisms involved in normal and pathological states. In an attempt to begin the process of discovering those genes, we investigated a number of the genes that are differentially expressed in RNA samples from ASD, VSD, TOF and non-CHD controls by RAP-PCR. Among these differentially expressed genes resolved, three lack functional characterization (hCALO, NP79 and SUN2), while four are homologous to known genes.

hCALO is identical to *H. sapiens* brain mRNA for KIAA0462 protein, although the complete cDNA sequence has not been characterized yet [15]. The amino acid sequence of KIAA0462 (2276 amino acids) shows 45% identity and 64% similarity to the *pushover* protein of *Drosophila melanogaster*. The pushover gene codes for a large protein of 5322 amino acids that affects synaptic transmission at the neuromuscular junction. Mutations in *pushover* affect both neuronal excitability and the process of transmitter release [16]. Pushover is identical to calossin, a novel calmodulin protein in *Drosophila* retina that is highly conserved through animal phylogeny. The CALO mRNA is of 15–20 kb on Northern blots [17]. We named the gene we found in heart tissue hCALO for human homologue of calossin. The human transcript we identified is also much larger than 9 kb and is detected specifically in adult heart, brain and lung by Northern blotting. Since calmodulin is an important Ca^{2+} sensor and Ca^{2+} influx regulates multiple cellular events, the tissue specificity and sequence conservation of hCALO suggests a possible role in regulating cardiac function.

NP79 is identical to *H. sapiens* HRIHFB2216 mRNA. A partial HRIHFB2216 cDNA of 1605 bases was found to encode a nuclear targeted protein containing nuclear localization signals [18]. As a step towards identifying its function, we have isolated the cDNA by screening a human adult heart cDNA library. Complete sequencing of the 2.8 kb insert indicates that it is identical to a clone for cutaneous T-cell lymphoma-associated antigen isolated from a normal testis cDNA library using the method of 'serological identification of recombinantly expressed genes' [19]. The predicted protein encoded by the complete cDNA sequence has 693 amino acids, a molecular weight of 79 kDa and a nucleosome assembly domain. A fusion protein of our cDNA clone and the green fluorescent protein revealed the same nuclear localization pattern as originally reported for the partial cDNA [18] (not shown). As NP79 is highly expressed in the adult heart, it is a promising candidate for further evaluation of its role in maintaining human cardiac function.

Blast analysis revealed that *H. sapiens* mRNA for KIAA0668 protein is identical to the coding region of *H. sapiens* Sad 1 unc-84 domain protein 2 (SUN2) mRNA (with only 1323 bases being reported) [20]. SUN2 is the human homologue of *C. elegans* unc-84, a gene required for the nuclear migrations that occurs during development of the worm [20]. This sequence is of particular interest since the gene functions of SUN2 in man are still not characterized and because it maps to 22q12-13, a region adjacent to the major chromosome region of microdeletions associated with cardiac and craniofacial defects [21].

The mRNA for titin is 81,940-bp long and codes for the largest protein known [22]. Titin, also known as connectin, is an integral cytoskeletal protein with a molecular weight of approximately 3 million Dalton. It is a relatively abundant protein comprising ~ 10% of the myofibril mass. Titin is essential in the control of the assembly of the highly ordered sacromeres, and mutations in this gene cause autosomal dominant familial dilated cardiomyopathy [23]. The possible function of titin is to hold myosin filaments together at the center of the sarcomere, equidistant from the adjacent *Z* lines, and to provide structural continuity in relaxed myofibrils [24]. An increase in titin mRNA with hypertrophy and loss of titin in heart failure were reported in guinea pigs [25]. Here we report a 1.5- and 3-fold increase in the level of expression of titin in TOF samples compared with normal heart. Dystrophin is also a cytoskeletal protein that is involved in fixation of sarcomeres to the lateral sarcolemma and stabilization of the transverse (T)-tubular system. In adult cardiac muscle, dystrophin is also localized on T-tubules. Like titin, we find an increase in dystrophin expression in TOF samples compared to the adult heart. Altered expression of the membrane-associated protein dystrophin might be associated with cardiac hypertrophy and failure [26]. While it would be ideal to have more perfect matched controls and a larger sample size, our results support the hypothesis that in cardiac hypertrophy and failure, the early and reversible stage is characterized by accumulation of cytoskeletal proteins to counteract the increased strain [26].

In conclusion, we have applied RAP-PCR to identify differentially expressed genes in human normal and CHD heart tissues. We found nonradioactive RAP-PCR a convenient and safe method. The validity of the method was confirmed by our observation that dystrophin and titin were of expressed at increased levels in TOF samples using both RAP-PCR and quantitative PCR. All three functionally unknown genes studied show a higher level of expression in VSD samples in the RAP-PCR fingerprint and have changing level of expression during normal human heart development. The predicted proteins suggest that they may have significant roles in heart development and function. Further investigation of their normal functions is underway using their mouse homologues.

Acknowledgements

We thank Becky Cheung (HKU) for excellent technical assistance, Dr. Mary Waye (CUHK) and Dr. J. Jay Gargus (UC, Irvine) for constructive comments and proofreading on the manuscript. G.F. Sun was a recipient of Dr. Cheng Yu Tung Fellowship, Hong Kong. This work was supported by the National Nature Science Foundation of China (G.F. Sun) and the University of Hong Kong (M.P. Leung).

References

[1] J.I. Hoffman, Pediatr. Cardiol. 16 (1995) 103–113.
[2] D. Srivastava, E.N. Olson, Nature 407 (2000) 221–226.
[3] K.R. Chien, Nature 407 (2000) 227–232.
[4] J.N. Chen, M.C. Fishman, Trends Genet. 16 (2000) 383–388.
[5] D. Srivastava, Trends Cardiovasc. Med. 9 (1999) 11–18.
[6] Q.Y. Li, R.A. Newbury-Ecob, J.A. Terrett, D.I. Wilson, A.R. Curtis, C.H. Yi, T. Gebuhr, P.J. Bullen, S.C. Robson, T. Strachan, D. Bonnet, S. Lyonnet, I.D. Young, J.A. Raeburn, A.J. Buckler, D.J. Law, J.D. Brook, Nat. Genet. 15 (1997) 21–29.
[7] M. Satoda, F. Zhao, G.A. Diaz, J. Burn, J. Goodship, H.R. Davidson, M.E. Pierpont, B.D. Gelb, Nat. Genet. 25 (2000) 42–46.
[8] S. Schiaffino, B. Dallapiccola, R. Di Lisi, Circ. Res. 84 (1999) 247–249.
[9] J.J. Schott, D.W. Benson, C.T. Basson, W. Pease, G.M. Silberbach, J.P. Moak, B.J. Maron, C.E. Seidman, J.G. Seidman, Science 281 (1998) 108–111.
[10] J. Welsh, K. Chada, S.S. Dalal, R. Cheng, D. Ralph, M. McClelland, Nucleic Acids Res. 19 (1992) 4965–4970.
[11] P. Liang, A.B. Pardee, Science 257 (1992) 967–970.
[12] X. Wang, G.Z. Feuerstein, Cardiovasc. Res. 35 (1997) 414–421.
[13] S.E. Chuang, K.C. Wang, A.L. Cheng, Trends Genet. 11 (1995) 7.
[14] A.P. Feinberg, B. Vogelstein, Anal. Biochem. 132 (1983) 6–13.
[15] O. Ohara, DNA Res. 4 (1997) 345–349.
[16] S. Richard, T. Hillman, M. Stern, Genetics 142 (1996) 1215–1523.
[17] X.Z. Xu, P.D. We, H. Chen, H.S. Li, M. Yu, S. Morgan, Y. Liu, C. Montell, J. Biol. Chem. 273 (1998) 31297–31307.
[18] N. Ueki, T. Oda, M. Kondo, K. Yano, T. Noguchi, M. Muramatsu, Nat. Biotechnol. 16 (1998) 1338–1342.
[19] S. Eichmuller, D. Usener, R. Dummer, A. Stein, D. Thiel, D. Schadendorf, Proc. Natl. Acad. Sci. U. S. A. 98 (2001) 629–634.
[20] C. Malone, W. Fixsen, H. Horvitz, M. Han, Development 126 (1999) 3171–3181.
[21] H. Yamagishi, V. Garg, R. Matsuoka, T. Thomas, D. Srivastava, Science 283 (1999) 1158–1161.
[22] S. Labeit, B. Kolmerer, W.A. Linke, Circ. Res. 80 (1997) 290–294.
[23] B. Gerull, M. Gramlich, J. Atherton, M. McNabb, K. Trombitas, S. Sasse-Klaassen, J.G. Seidman, C. Seidman, H. Granzier, S. Labeit, M. Frenneaux, L. Thierfelder, Nat. Genet. 30 (2002) 201–204.
[24] B. Kolmerer, C.C. Witt, A. Freiburg, S. Millevoi, G. Stier, H. Sorimachi, K. Pelin, L. Carrier, K. Schwartz, D. Labeit, C.C. Gregorio, W.A. Linke, S. Labeit, Rev. Physiol., Biochem. Pharmacol. 138 (1999) 19–55.
[25] J.F. Collins, C. Pawloski-Dahm, M.G. Davis, N. Ball , G.W. Dorn II, R.A. Walsh, J. Mol. Cell. Cardiol. 28 (1996) 1435–1443.
[26] S. Hein, S. Kostin, A. Heling, Y. Maeno, J. Schaper, Cardiovasc. Res. 45 (2000) 273–278.

ELSEVIER

Biochimica et Biophysica Acta 1588 (2002) 247–253

BIOCHIMICA ET BIOPHYSICA ACTA
BBA
www.bba-direct.com

Novel mutations (Asn 484 Lys, Thr 500 Ala, Gly 438 Glu) in Morquio B disease

Richard D. Bagshaw[a], Sunqu Zhang[b], Alina Hinek[a], Marie-Anne Skomorowski[a], Donald Whelan[c], Joe T.R. Clarke[d], John W. Callahan[a,b,d,*]

[a] *Department of Pediatric Laboratory Medicine and Pathobiology, The Hospital for Sick Children, University of Toronto, Toronto, Canada*
[b] *Department of Pediatric Laboratory Medicine and Biochemistry, The Hospital for Sick Children, University of Toronto, Toronto, Canada*
[c] *Department of Genetics, McMaster University, Hamilton, ON, Canada*
[d] *Department of Pediatric Laboratory Medicine and Pediatrics, The Hospital for Sick Children, University of Toronto, Toronto, Canada*

Received 30 November 2001; received in revised form 6 September 2002; accepted 6 September 2002

Abstract

Primary deficiency of β-galactosidase results in GM1 gangliosidosis and Morquio B disease. Of the more than 40 disease-causing mutations described in the Gal gene to date, about 75% are of the missense type and are scattered along the length of the gene. No single, major common mutation has been associated with GM1 gangliosidosis. However, a Trp 273 Leu mutation has been commonly found in the majority of patients with Morquio B disease defined genotypically to date.

We now report three new mutations in three Morquio B patients where the Trp 273 Leu mutation is absent. Two of the mutations, C1502G (Asn 484 Lys) and A1548G (Thr 500 Ala), were found in twins (one male, one female) who display a mild form of Morquio B disease and keratan sulfate in the urine. In their fibroblasts, residual activity was 1.9% and 2.1% of controls. On Western blots, the 84-kDa precursor and the 64-kDa mature protein were barely detectable. The occurrence of a 45-kDa degradation product indicates that the mutated protein reached the lysosome but was abnormally processed. In the third case, we identified only a G1363A (Gly 438 Glu) mutation (a major deletion on the second allele has not been ruled out). This female patient too displays a very mild form of the disease with a residual activity of 5.7% of control values. In fibroblasts from this case, the 84-kDa precursor and the 45-kDa degradation product were present, while the mature 64-kDa form was barely detectable. The occurrence of these three mutations in the same area of the protein may define a domain involved in keratan sulfate degradation.

© 2002 Elsevier Science B.V. All rights reserved.

Keywords: β-Galactosidase; Missense mutation; Western blot; Leupeptin

1. Introduction

Morquio disease (MPS IV) occurs in two types (A and B) due to deficiencies in two separate genes. The disorder is characterized as a massive dysostosis multiplex with storage of keratan sulfate but without proven primary central nervous system involvement demonstrable either neuropathologically or biochemically. Patients with type A are generally more severely involved clinically, whereas the B form tends to be milder with a later onset of clinical symptoms [1,2]. Morquio A disease, the more common form of the two, arises from mutations in the gene encoding a 6-sulfate sulfatase that is specific for residues found in keratan sulfate (both galactose 6-sulfate and *N*-acetylglucosamine 6-sulfate) and in chondroitin 6-sulfate (as *N*-acetylgalactosamine 6-sulfate). β-Galactosidase activity is normal in type A patients. Morquio disease, type B (MPS IVB) arises from deficiency in β-galactosidase where the activity of the 6-sulfate sulfatase is normal. A deficiency in the same β-galactosidase arising from the same Gal gene is also the primary defect in GM1 gangliosidosis. The latter is clinically heterogeneous and is characterized as a neuronal lipid storage disease, with GM1 ganglioside as the primary storage product in central nervous system neurons (see Ref. [1] for a recent review of this topic).

---

* Corresponding author. Department of Pediatric Laboratory Medicine, The Hospital for Sick Children, 555 University Avenue, Toronto, ON, Canada M5G 1X8. Tel.: +1-416-813-5754/5154; fax: +1-416-813-8700.
E-mail address: jwc@sickkids.ca (J.W. Callahan).

0925-4439/02/$ - see front matter © 2002 Elsevier Science B.V. All rights reserved.
PII: S0925-4439(02)00172-2

The β-galactosidase gene, located on chromosome 3p21.33 [3–5] is 62.5 kb in length and composed of 16 exons [6,7]. Two related proteins arise by alternative splicing of the primary β-galactosidase transcript. The most abundant product is lysosomal β-galactosidase that we have shown is catalytically active in its precursor form. The second protein, originally called the β-galactosidase-like protein, does not display β-galactosidase activity and has been characterized by us as the elastin binding protein (EBP) of the elastin binding receptor. It arises by alternative splicing whereby the sequence encoded by exons 3, 4 and 6 is missing, a frameshift occurs in exon 5 (which encodes a unique 32-amino-acid sequence) [6] and the reading frame is restored at the start of exon 7. Except for this frameshifted unique sequence, the primary structure of the EBP is identical to β-galactosidase. However, the latter is localized to the cell surface but not to lysosomes [6,8].

Mutations are spread throughout the gene, 70% of which occur simultaneously in both β-galactosidase and the EBP. Most are of the missense type and give rise to GM1 gangliosidosis. Most patients with GM1 gangliosidosis are heteroallelic with different mutations on each parental chromosome and missense mutations affecting some codons (such as those affecting Arg 59, Arg 201, Arg 208, Pro 263, Arg 482) have been noted more frequently than others. In contrast, a major common mutation, Trp 273 Leu, has been found in the majority of the 17 Morquio B patients that have been defined [9,10] to date. It is noteworthy that no patient with one copy of the Trp 273 Leu mutation has presented with GM1 gangliosidosis; all such patients have the clinical and biochemical phenotype of Morquio B disease.

β-Galactosidase cleaves substrates by formation of a galactosylated-amino acid intermediate (the catalytic nucleophile), with subsequent release of the galactose and retention of β-configuration. This mechanism predicts that at least two acidic residues are involved in the catalytic mechanism. We identified the galactosylated residue as Glu 268 [11] and our recent work has identified Asp 332 as a candidate for the second acidic residue in the catalytic mechanism [12]. Because Trp 273 Leu has been the only mutation strictly associated with Morquio B disease to date, it has been postulated to play an essential role in the hydrolysis of keratan sulfate. However, to date, there have been no studies directly examining this question. It has also been proposed that the Trp 273 Leu mutation affects the ability of β-galactosidase to join a lysosomal complex also containing cathepsin A, neuraminidase and GalNAc-6-sulfate sulfatase, the formation and function of which is poorly understood. Thus, the role of Trp 273 in complex binding and hydrolysis of natural substrates, particularly the keratan sulfates, is ill defined.

In the present work, we describe new mutations, Asn 484 Lys and Thr 500 Ala in a set of fraternal twins and Gly 438 Glu in a third unrelated patient, all of whom display the clinical and biochemical features of Morquio B disease. The Trp 273 Leu mutation is absent from these patients. The present data have appeared in abstract form [13].

2. Materials and methods

2.1. Clinical findings

The patients included in this study satisfy the criteria for Morquio disease; namely, systemic bone disease without primary involvement of the central nervous system (defined as retarded developmental milestones, retarded intellectual development, presence of spasticity and seizures). *Family 1.* The first of the twins presented at age 9 years with an abnormal gait and increased fatigability. On examination, he was not dysmorphic, there was no hepatosplenomegaly, and the neurological exam was normal. Some hip weakness was noted. X-rays of the spine revealed platyspondyly with vertebral beaking typical of MPS IV. Keratan sulfate was isolated from his urine at this time. Residual leukocyte β-galactosidase activity was <2.5% of the normal level (in all aspects of this study activity was assayed with the fluorimetric 4-methylumbelliferyl-β-D-galactopyranoside substrate as previously described [14]). By age 11 years, odontoid dysplasia, thoracolumbar scoliosis, and genu valgum typical of the disease were evident. M.S., his twin, was essentially normal at age 9.5 years. Keratan sulfate was isolated from her urine also and again residual leukocyte β-galactosidase activity was <2.5% of the normal level. A mild dorsal scoliosis was noted at age 11 years. At age 18 years, her neurological status was within normal limits, she had an unsteady gait but remained ambulatory, and was otherwise healthy. Their early developmental history was uninformative and the parents (Portuguese) are unrelated. Both patients now in their late-20s are educated both having successfully completed post-secondary education, their neurological status remains within normal limits, but their skeletal abnormalities seriously impair their ambulatory capabilities.

Family 2. This female was diagnosed at the age of 8 years by the presence of keratan sulfate in the urine and a deficiency of leukocyte β-galactosidase (<1% of the normal value) was noted. At 18.5 years, she was short (147.5 cm), had a mild dorsal scoliosis, denied pain in the joints or back, and she had mild limitation of movement of neck, spine, hips and shoulders. Her neurological exam was unremarkable, she was judged to be somewhat dull, and on psychological assessment, her IQ was judged to be borderline normal. Corneal clouding was noted at this time, and the cardiovascular system was normal. This patient married and is now in her early 30s but she and her parents now have been lost to follow-up.

2.2. Fibroblast culture

Fibroblast strains were established for diagnostic studies that were subject to informed consent. Cells from a case of

Morquio disease, type B (GM01602; mutations TG817/8CT; Trp 273 Leu and G1445A; Arg 482 His), and GM1 gangliosidosis (GM05652A; homozygous for mutation C1101T; Arg 351 ter) were from the NIGMS Human Genetic Mutant Cell Repository. In general, skin fibroblasts were grown in α-MEM with penicillin (100 U/ml) and streptomycin (100 mg/ml), supplemented with 10% fetal calf serum (FCS) at 37 °C in 5% CO_2 atmosphere until confluent. All cell cultures used in this work were negative for the presence of mycoplasma contamination, as analysed by a PCR-based method. In the leupeptin experiments, cells were grown in α-MEM medium (in the presence or absence of 20 μM leupeptin) with 10% of FBS at 37 °C in 5% CO_2.

2.3. Isolation of genomic DNA

Genomic DNA was isolated from harvested cultured skin fibroblasts suspended in lysis buffer (100 mM NaCl, 10 mM Tris–Cl pH 8, 25 mM EDTA pH 8, 0.5% SDS, and 0.1 mg/ml proteinase K) by freeze/thawing (10 ×) the cells in a dry ice/ethanol bath. An equal volume of phenol/chloroform was then added, and DNA was precipitated by adding 1/2 volume of 7.5 M ammonium acetate and 2 volumes of 100% ethanol. The DNA pellet was rinsed with 70% ethanol and dissolved in 10 mM Tris pH 8, 0.1 mM EDTA pH 8 (TE buffer).

2.4. PCR and restriction enzyme analysis

Exons 2–16 were amplified from 500 ng of patient or normal genomic DNA. The primers used to amplify the appropriate exons of the β-galactosidase gene and those used for site-directed mutagenesis are based on the published intron/exon junction sequences [7]. DNA amplification reactions were performed in 100 μl total volume containing: 100 ng of each primer, 10 units of *Taq* polymerase (Promega), 0.5 mM each of dCTP, dGTP, dTTP, and dATP, in 10 mM Tris–HCl pH 8.3, 50 mM KCl, 1.5 mM $MgCl_2$. The reaction conditions were 1 min at 94 °C (denaturation), 1 min 10 s at 56 °C (annealing), and 1 min at 72 °C (extension) for 30 cycles using the RoboCycler 40 (Stratagene) thermal cycler. PCR products were run on a 1% agarose gel to check for insertions or deletions before SSCP analysis was performed. To detect the presence of the Trp 273 Leu mutation commonly found in Morquio B disease, we adapted the assay described by Oshima et al. [15]. The upstream primer sequence was 5′-CAATTCTGAATTCTATACAGGC-3′ and the downstream primer was 5′-CATTCTAGCATAAGTTCTACAG-3′. The PCR product (285 bp) containing the mispaired A nucleotide in the upstream primer coupled with the TG817/818CT (Trp 273 Leu) mutation creates a *Stu*1 restriction site where the product is cleaved into 264- and 21-bp fragments. The positive control for this assay were cells from the known case of Morquio disease, type B (from the NIGMS Human Genetic Mutant Cell Repository—GM01602). This cell line was confirmed to be heterozygous for the TG817/818CT (Trp 273 Leu) mutation and for Arg 482 His, a mutation described in patients with GM1 gangliosidosis [16]. To examine the possibility that the mutations found were the result of polymorphic changes, the following primer pairs were used. For exon 13, 5′TAGTGATGTATTTTTCTTAAATCC-3′and 5′-GGACAAAACGCACAGTTCAG, the 183-bp PCR product contains two *Hin*f1 cut sites (generating 116, 40, and 27 bp pieces), one of which is lost in the presence of the G1363A (Gly 484 Glu) mutation (156 bp and 27 bp pieces); for exon 14, the upstream primer 5′-GTAGAGAACATGGGACGTGTTAA-3′was modified (T underlined) to create a new *Hpa*1 site. The downstream primer was 5′-TTAAACCTTAGTCTTGACAGTG-3′. In the presence of the C1502G (Asn 484 Lys) mutation, the new *Hpa*1 site is lost. For exon 15, the upstream and downstream primers were 5′-CAGCTCACTGTGCTCTGTT-3′and 5′-GAATTCAAACCCTTCCCATGA-3′, respectively. In the presence of the A1548G (Thr 500 Ala) mutation, the unique *Hin*f1 site is lost.

2.5. SSCP analysis

SSCP analysis was performed at room temperature and at 4 °C with 6% polyacrylamide gels in 0.5 × TBE running buffer containing 5% glycerol (40 W) as described by Refs. [17,18]. The gels fixed in 50% methanol and 10% acetic acid solution for 1 h were washed three times in distilled water for 15 min and then stained in a solution containing equal volumes of 0.5 M sodium carbonate and 10 mM silver nitrate–25 mM ammonium nitrate–3.5 mM tungstosilicic acid–0.8% formalin for 10–30 min. The reaction was stopped by the addition of 10% acetic acid.

2.6. DNA sequencing

Direct sequencing of PCR products in both directions followed the Amersham ^{33}P-thermosequenase cycle sequencing protocol.

2.7. Western blot analysis

Cells were harvested by scraping in phosphate-buffered saline and lysed by sonication as described earlier. Thirty micrograms of fibroblast protein was analysed using SDS-PAGE. Samples were reduced by boiling for 5 min in 62.5 mM Tris, 3% SDS, 10 mM DTT, and were loaded onto an 8% Bio-Rad Mini Gel SDS-polyacrylamide system as described earlier [12]. Proteins were transferred overnight to nitrocellulose, and the Western blot was probed using a 1:1500 dilution of the polyclonal rabbit IgG (P-Gal) raised against purified human β-galactosidase precursor. This multiepitopic antibody reacts with all known forms of the wild-type and mutant protein including their degradation products [12,19]. Immunoblots were developed using the enhanced chemiluminescence system (ECL-Western Blot, Amersham).

2.8. Immunolocalization of β-galactosidase in intracellular compartments

Histochemical staining was by incubation of fixed permeabilized cells with indolyl-β-galactoside [20]. Cells were grown in α-MEM medium (in the presence or absence of 20 μM leupeptin) with 10% of FBS at 37 °C in 5% CO_2 on glass cover slips, and after 48 h, the cells were fixed and gently permeabilized with 100% cold methanol at −20 °C for 30 min. The fixed cells were then washed in phosphate-buffered saline, blocked with 1% bovine serum albumin, and incubated for 1 h with rabbit IgG raised against purified human β-galactosidase precursor as above (diluted 1:200). The secondary antibody, a green fluorescein-labeled goat-anti-rabbit IgG F(ab′)2, diluted 1:100, was then added for 1 h, either alone or in combination with a 1:10,000 dilution of propidium iodide, which in addition to nuclear DNA also stains cytoplasmic RNA, and RNA bound to the rough ER thereby marking the position of the ER with the red fluorescence. The cells were then washed three times with phosphate-buffered saline and mounted with elvanol [21]. In control cultures, the preimmune rabbit IgG was substituted for the primary antibody.

3. Results

3.1. Identification of the mutations

Direct sequencing of PCR products was used to identify mutations in exons 2–16 using intron/exon primers as described by Morreau et al. [7]. Both patients in Family 1 were found to be heterozygous for two mutations, a C1502→G transversion in exon 14 which converts Asn 484 to Lys (Fig. 1a), and an A1548→G substitution in exon 15 which converts Thr 500 to Ala (Fig. 1b). The patient in Family 2 was homozygous for a G1363→A substitution which converts Gly 438 to Glu in exon 13 (Fig. 1c). We did not detect the nucleotide changes noted in the Morquio patients defined in this study using genomic DNA samples from 30 normal fibroblast lines supporting the assignment of these mutations as disease-causing and not naturally occurring polymorphisms. The Trp 273 Leu mutation commonly found in patients with Morquio B disease was confirmed in the cell repository Morquio B line used as the positive control as was the Arg 482 His mutation. The Trp 273 Leu mutation was not present in any of the current patients.

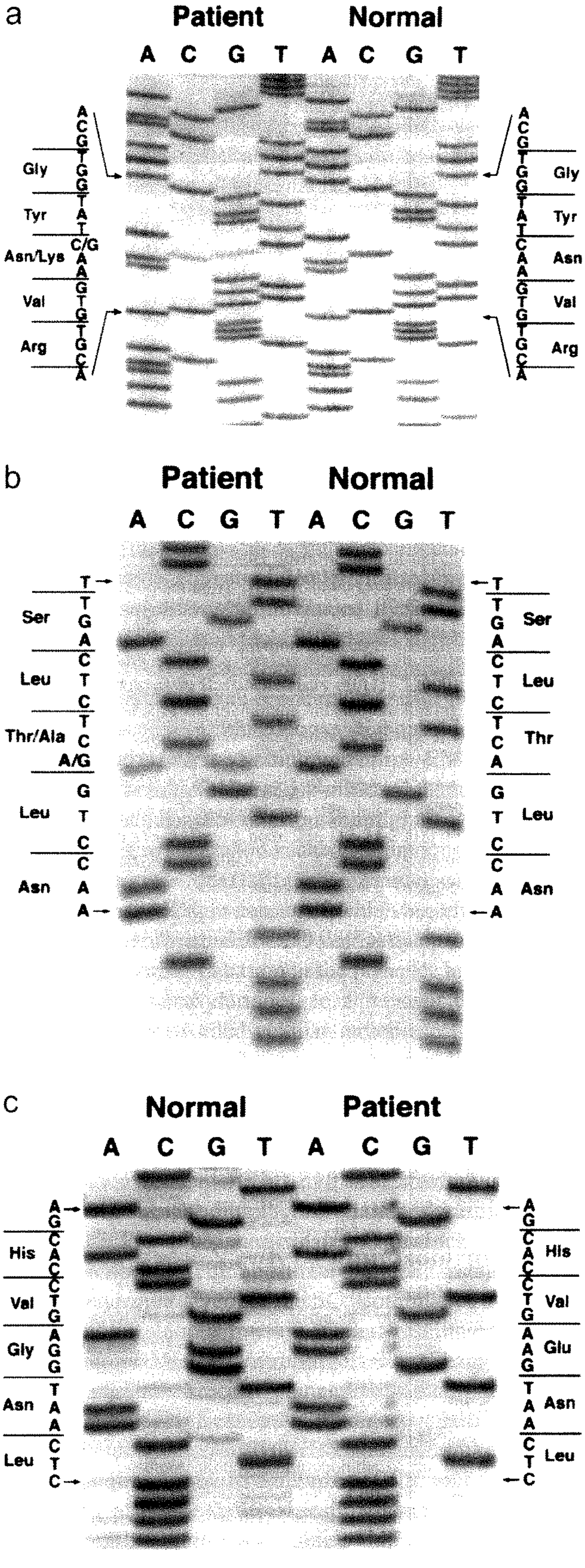

Fig. 1. Identification of mutations in Families 1 and 2. Genomic DNA was isolated as described. One mutation was detected in each of exon 14 and 15 in Family 1 and in exon 13 in Family 2. Genomic fragments were amplified from 500 ng of patient or normal DNA using primers based on intronic/exonic sequences and using the amplification conditions as described in the Materials and Methods. Direct sequencing of PCR products in both directions followed the Amersham ^{33}P-thermosequenase cycle sequencing protocol. In Family 1, we noted in exon 14 a C1502G transversion which changed Asn 484 to Lys (Panel a), and an A1548G substitution converting Thr 500 to Ala (Panel b) in exon 15. In Family 2, the only mutation noted was a G1363A substitution converting Gly 438 to Glu (Panel c) in exon 13.

3.2. Level of β-galactosidase protein

The total β-galactosidase activity in fibroblast extracts from our Morquio B patients was 2.1% and 1.88%, respectively, for the twins in Family 1, and 5.67% in the patient from Family 2 (Table 1). This compares favourably to the values obtained for the positive Morquio B control from the cell repository (1.2%). All of these residual activities are higher than the extremely low level of activity in the GM1 gangliosidosis cells (< 0.5% of the control) included in the study and are consistent with other known cases [12]. To assess the impact of these mutations on the level of β-galactosidase protein in these cells, we used our well-characterized rabbit polyclonal antibody in Western blot analyses. We detected very small but comparable to normal amounts of the 84-kDa precursor in cells from the Family 1 patients (Fig. 2, lanes 1 and 6), and the case from the cell repository (Fig. 2, lane 3), while in the third patient (from Family 2), the precursor was more abundant (Fig. 2, lane 2). The processed, mature 64-kDa polypeptide, the most abundant form of the enzyme, was easily detected as expected in normal cells. The mature protein was decreased in the Family 1 fibroblasts (Fig. 2, lanes 1 and 6) to the levels seen in the GM1 gangliosidosis cells (Fig. 2, lane 5), but was found at a higher level in fibroblasts from Family 2 (Fig. 2, lane 2). On the other hand, fibroblasts from the positive Morquio B control displayed significant amounts of the 64-kDa mature protein (Fig. 2, lane 3). It is noteworthy that in all fibroblasts except those from the patient with the stop codon mutation (Fig. 2, lane 5), prominent degradation products in the range of 45 kDa were detectable. However, the relative abundance of these forms was not constant. For example, as in the normal cell line, Family 1 and 2 cells appeared to have a single major degradation product compared to at least two for the cell repository case and three major bands in one of the GM1 gangliosidosis cases. The relative abundance of all forms of the protein in the Morquio B cases was substantially higher than that found in the case of GM1 gangliosidosis used as a control but was still lower than that noted in the control cell line. Maturation of the precursor to the mature protein and formation of these degradation products arise exclusively from lysosomal digestion since as we have previously shown in I-cell fibroblasts, where the precursors are not localized into lysosomes due to the absence of the mannose 6-phosphate targeting signal, that the enzyme is not

Table 1
Mutations correlated with enzyme activity and Western blots

Cell line mutations		Specific activity[a]		Western blot result
		β-Gal	Hex	
Family 1				
sibling 1	Asn 484 Lys Thr 500 Ala	30	18,220	some precursor, little mature β-gal, degradation products
sibling 2	Asn 484 Lys Thr 500 Ala	27	13,602	some precursor, little mature β-gal, degradation products
Family 2				
Patient 1	Gly 4328 Glu homozygous	81	22,248	abundant precursor, little mature β-gal, degradation products
Cell repository				
	Trp 273 Leu Arg 482 His	17	11,772	some precursor, some mature β-gal, degradation products
GM1 gangliosidosis				
	Arg351STOP	3	21,690	little precursor, little mature β-gal, no degradation products
Normal				
	none known	1429	17,419	some precursor, mature β-gal, some degradation products

[a] Specific activity is nanomoles per hour per milligram of protein.

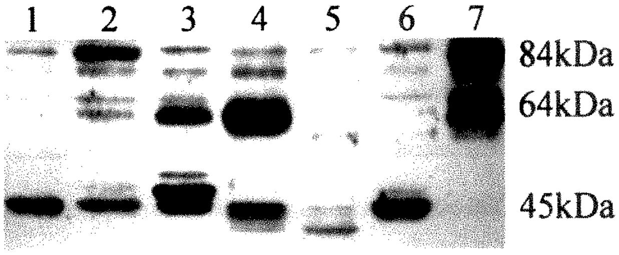

Fig. 2. Western blot of fibroblast lysates from Morquio B and GM1-gangliosidosis patients. Thirty micrograms of total cellular protein was analysed by SDS-PAGE and probed using our well-characterized antibody that cross-reacts with the 84-kDa precursor and the 64-kDa mature forms of β-galactosidase. Lane 1 is Morquio B, sibling 1 of Family 1; Lane 2, is the case from Family 2; Lane 3 is a Morquio B cell line (GM01602) from the NIMCGS repository; Lane 4 is a normal control; Lane 5 is a case of GM1 gangliosidosis, homozygous for an Arg351STOP mutation; Lane 6 is sibling 2 of Family 1; Lane 7 corresponds to wild-type β-galactosidase expressed by CHO cells, as described earlier [14] and demonstrates the location of the 84-kDa precursor and the 64-kDa processed mature form of the enzyme.

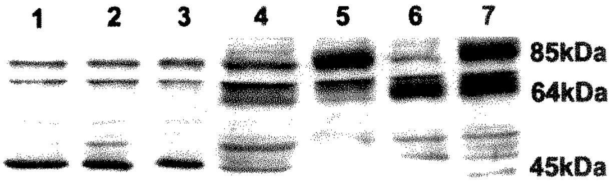

Fig. 3. Western blot of lysates from Morquio B patients incubated in the presence of leupeptin. Thirty micrograms of total cellular protein was analysed by SDS-PAGE and probed using our well-characterized antibody that cross-reacts with the 84-kDa precursor, the 64-kDa mature form and the major degradation product of β-galactosidase at 45 kDa. Lane 1 is Morquio B, sibling 2 of Family 1; Lanes 2 and 3 is Morquio B, Family 2; Lanes 4 and 5 is Morquio B cell line (GM01602) from the NIMCGS repository; Lanes 6 and 7 is a normal control. Lanes 1, 3, 5, and 7 are lysates from cells grown in the presence of leupeptin for 48 h; lanes 2, 4, 6 are from cells grown in the absence of leupeptin.

Table 2
The effect of leupeptin on β-galactosidase in fibroblasts

	Specific activity (nmol/h/mg of protein)	
	No leupeptin	With leupeptin
Control	681.3	994.4
Morquio B, Family 1, Case 1	8.9	7.0
Morquio B, Family 2	19.9	18.1
Morquio B, cell repository	7.8	7.8
GM1 gangliosidosis	0.0	0.0

Cultured skin fibroblasts were incubated for 48 h in the presence of 10 mM leupeptin, after which the cultures were harvested, and processed as described.

processed but rather degraded [19]. These findings are summarized in Table 1. Because it could be argued that the mutant proteins in the Morquio B lines reached the lysosomes in normal abundance but were quickly degraded, we examined the level of β-galactosidase proteins in cells incubated in the presence of leupeptin (Fig. 3). We previously showed in galactosialidosis fibroblasts, where the β-galactosidase deficiency is a secondary manifestation of the primary deficiency in cathepsin A/protective protein, incubating the fibroblasts in the presence of leupeptin restored β-galactosidase to normal levels but did not affect processing to the mature enzyme [19]. In this instance, exposure of Morquio B cells to leupeptin did not effect a rise in β-galactosidase activity regardless of the nature of the mutations (Table 2). No substantial change in the level of β-galactosidase proteins (precursor, mature or degraded forms) were noted in the Morquio B lines with the Asn 484 Lys/Thr 500 Ala or the Gly 438 Glu mutations in the presence of leupeptin. In contrast, in the control lines used (in both the Trp 273 Leu/Arg 482 His Morquio B line and in the normal), leupeptin treatment resulted in a net increase of β-galactosidase proteins. Since leupeptin did not result in a rise of the enzyme protein in the presence of the Asn 484 Lys/Thr 500 Ala or the Gly 438 Glu mutations, it implies that the mutated protein does not reach the lysosome but rather is degraded in a pre-lysosomal compartment. In support of this, we undertook immunofluorescence localization studies. Here, β-galactosidase protein was found primarily in the perinuclear area (i.e. the endoplasmic reticulum) with some immunoreactivity dispersed in organelles distant from the nucleus (data not shown).

4. Discussion

Novel missense mutations (Thr 500 Ala, Asn 484 Lys, and Gly 438 Glu) have been found in three patients in two families who display a mild form of Morquio B disease (primary β-galactosidase deficiency with keratan sulfate storage). Subsequent to our conference report [13], Paschke et al. [10] found the same A1532C, Thr 500 Ala mutation in another mild patient diagnosed at the age of 24 years, but they did not examine the impact on the level of cross-reacting material. In the presence of the Thr 500 Ala and Asn 484 Lys mutations, minimal amounts of precursor (84 kDa) and mature (64 kDa) forms of β-galactosidase were detected, the most abundant form of β-galactosidase protein being a 45-kDa degradation product. With the Gly 438 Glu mutation, both the precursor and the 45-kDa degradation product were noted but again only minimal amounts of the mature form of the enzyme were detected. Incubation of these cells with leupeptin, a potent thiol protease inhibitor, did not affect the level of residual β-galactosidase protein nor did it have any effect on the level of residual activity. On the other hand, with leupeptin treatment, there was a noticeable increase in the level of β-galactosidase precursor protein in control cells and in cells from the Morquio B patient heterozygous for Trp 273 Leu and Arg 482 His mutations, but no change in enzyme activity was observed in the latter. Consistent with this are our initial unpublished findings that show the mutant protein containing the Trp 273 Leu mutation to be catalytically defective at least with synthetic substrates. The failure to alter the level of β-galactosidase protein in the presence of leupeptin suggests that the proteins bearing the Thr 500 Ala, Asn 484 Lys, and Gly 438 Glu mutations do not reach the lysosome and are likely degraded in the endoplasmic reticulum, as we have previously shown for missense mutations causing GM1 gangliosidosis [12].

In normal cells, upon arrival in the endosomal–lysosomal compartment, β-galactosidase associates with Neuraminidase, protective protein (cathepsin A), and *N*-acetylglucosamine 6-sulfate sulfatase [22] to form a stable complex responsible for the hydrolysis of GM1 ganglioside and keratan sulfate. Complex formation is absolutely essential for β-galactosidase stabilization and for its normal posttranslational processing from the precursor to its mature form. Pshezhetsky and Potier [22] demonstrated that the complex also contained *N*-acetylgalactosamine 6-sulfate sulfatase, the enzyme deficient in Morquio disease, type A, and that its activity was reduced in galactosialidosis. This was correlated with elevated levels of keratan sulfate in the urine of galactosialidosis patients. These data indicate that digestion of keratan sulfate is intimately associated with and dependent upon both complex formation and correct processing of the enzyme. In earlier studies using I-cell fibroblasts, we showed that β-galactosidase precursor is degraded to a low molecular weight fragment (about 18 kDa), but no larger intermediate forms were detected. This non-lysosomal proteolysis of β-galactosidase arises due to its mislocalization reflecting the enzyme deficiency in I-cell disease. Because the mutations described here resulted in formation of significant amounts of the 45-kDa degradation products, it is clear that a substantial amount of the mutant enzyme reached the lysosome. However, little productive processing of the precursor to the mature 67-kDa form was noted suggesting that these mutations likely affect the protein's ability to associate correctly with the lysosomal complex, a crucial step for the enzyme's maturation and for keratan sulfate digestion. On the other hand, in the cell line with the Trp 273 Leu mutation, measurable productive processing of the precursor to the mature protein occurred. These differences suggest that keratan sulfate catalysis is impaired in the presence of the Thr 500 Ala, Asn 484 Lys and Gly 438 Glu mutations because formation of the complex is abnormal, whereas with the Trp 273 Leu mutation, complex formation occurs, but the enzyme may be catalytically defective with respect to keratan sulfate degradation. Therefore, the occurrence of these new mutations in an area bounded by Gly 438–Thr 500 may define a region of β-galactosidase that is pivotal in its binding to the complex either alone or in conjunction with keratan sulfate binding and further work is required to examine this.

We have documented that the alternatively spliced form of β-galactosidase is identical to the 67-kDa EBP, the major function of which is to associate with a cell surface elastin binding receptor and to assist in the delivery of tropoelastin to form the extracellular matrix [8,23,24]. The elastin binding receptor is composed of EBP, and two other proteins, which we have shown to be neuraminidase, and protective protein (cathepsin A). Release of newly secreted tropoelastin molecules from the association with EBP occurs upon interaction between it and galactosugar moieties protruding from the carbohydrate chains of glycoproteins thus facilitating formation of the microfibrillar scaffold of elastic fibers. In parallel studies on fibroblasts from the Morquio B patients used in the present work and from patients with GM1 gangliosidosis, we have found that cell lines from patients with Morquio disease type B have decreased capacity to assemble elastic fibers, whereas most GM1 gangliosidosis do not have this impairment [21]. In addition, we have noted that cells from patients with galactosialidosis and sialidosis also do not assemble elastic fibers [21]. These data are in accord with the recent findings that newly synthesized PPCA and neuraminidase associate in the ER are secreted together and reside in the plasma membrane [25,26] and are in agreement with our earlier data [23,24]. The sequences where the three novel missense mutations described here occur are identical between β-galactosidase and its alternatively spliced EBP form. The full impact of these mutations on the pathophysiology of Morquio B disease will only be realized when the respective mutations have been introduced into EBP and their impact on its function directly determined.

Acknowledgements

This work was supported by a grant to J.W.C. from Canadian Institutes for Health Research.

References

[1] J.W. Callahan, Biochim. Biophys. Acta 1455 (1999) 85–103.

[2] Y. Suzuki, A. Oshima, E. Nanba, in: C.R. Scriver, A.L. Beaudet, W.S. Sly, D. Valle (Eds.), Metabolic Basis of Inherited Disease, vol. III, McGraw-Hill, New York, 2001, pp. 3775–3809.

[3] J.H. Sips, H.A. Wit-Verbeek, J. De Wit, A. Westerveld, H. Galjaard, Hum. Genet. 69 (1985) 340–344.

[4] Y. Yamamoto, C.A. Hake, B.M. Martin, K.A. Kretz, A.J. Ahern-Rindell, S.L. Naylor, M. Mudd, J.S. O'Brien, DNA Cell Biol. 9 (1990) 119–127.

[5] T. Takano, Y. Yamanouchi, Hum. Genet. 92 (1993) 403–404.

[6] H. Morreau, N.J. Galjart, N. Gillemans, R. Willemsen, G.T.J. van der Horst, A. D'Azzo, J. Biol. Chem. 264 (1989) 20655–20663.

[7] H. Morreau, E. Bonten, X.Y. Zhou, A. D'Azzo, DNA Cell Biol. 10 (1991) 495–504.

[8] S. Privitera, C.A. Prody, J.W. Callahan, A. Hinek, J. Biol. Chem. 273 (1998) 6319–6326.

[9] I. Milos, B. Jauk, G. Hofler, T. Levade, H.M. Michelakakis, W.J. Kleijer, M. Beck, E. Paschke, Int. Congr. Inborn Errors Metab. 7 (1997) 175.

[10] E. Paschke, I. Milos, H. Kreimer-Erlacher, G. Hoefler, M. Beck, M. Hoeltzenbein, W. Kleijer, T. Levade, H. Michelakakis, B. Radeva, Hum. Genet. 109 (2001) 159–166.

[11] J.D. McCarter, D.L. Burgoyne, S. Miao, S. Zhang, J.W. Callahan, S.G. Withers, J. Biol. Chem. 272 (1997) 396–400.

[12] S. Zhang, R. Bagshaw, W. Hilson, Y. Oho, A. Hinek, J.T. Clarke, J.W. Callahan, Biochem. J. 348 Pt 3 (2000) 621–632.

[13] M.-A. Skomorowski, R. Bagshaw, S. Zhang, W.J. Whelan, J.T. Clarke, J.W. Callahan, J. Inherit. Metab. Dis. 22 (1999) 131.

[14] S. Zhang, J.D. McCarter, Y. Okamura-Oho, F. Yaghi, A. Hinek, S.G. Withers, J.W. Callahan, Biochem. J. 304 (1994) 281–288.

[15] A. Oshima, K. Yoshida, M. Shimmoto, Y. Fukuhara, H. Sakuraba, Y. Suzuki, Am. J. Hum. Genet. 49 (1991) 1091–1093.

[16] G. Mosna, S. Fattore, G. Tubiello, S. Brocca, M. Trubia, E. Gianazza, R. Gatti, C. Danesino, A. Minelli, M. Piantanida, Hum. Genet. 90 (1992) 247–250.

[17] M. Orita, Y. Suzuki, T. Sekiya, K. Hayashi, Genomics 5 (1989) 875–879.

[18] L. Spinardi, R. Mazars, C. Theillet, Nucleic Acids Res. 19 (1991) 4009.

[19] Y. Okamura-Oho, S. Zhang, W. Hilson, A. Hinek, J.W. Callahan, Biochem. J. 313 (1996) 787–794.

[20] B.D. Lake, Histochem. J. 6 (1974) 211–218.

[21] A. Hinek, S. Zhang, A.C. Smith, J.W. Callahan, Am. J. Hum. Genet. 67 (2000) 23–36.

[22] A.V. Pshezhetsky, M. Potier, J. Biol. Chem. 271 (1996) 28359–28365.

[23] A. Hinek, M. Rabinovitch, F. Keeley, Y. Okamura-Oho, J.W. Callahan, J. Clin. Invest. 91 (1993) 1198–1205.

[24] A. Hinek, F.W. Keeley, J. Callahan, Exp. Cell Res. 220 (1995) 312–324.

[25] E.J. Bonten, A. Van der Spoel, M. Fornerod, G. Grosveld, A. D'Azzo, Genes Dev. 10 (1996) 3156–3169.

[26] A. van der Spoel, E. Bonten, A. d'Azzo, EMBO J. 17 (1998) 1588–1597.

ELSEVIER

Biochimica et Biophysica Acta 1588 (2002) 254–260

BIOCHIMICA ET BIOPHYSICA ACTA
BBA
www.bba-direct.com

A regulating element essential for *PDGFRA* transcription is recognized by neural tube defect-associated PRX homeobox transcription factors

Paul H.L.J. Joosten[a], Mascha Toepoel[a], Dirk van Oosterhout[a], Gijs B. Afink[b], Everardus J.J. van Zoelen[a,*]

[a] *Department of Cell Biology, Faculty of Science, University of Nijmegen, Toernooiveld 1, 6525 ED Nijmegen, The Netherlands*
[b] *Department of Genetics and Pathology, Rudbeck Laboratory, S-75185 Uppsala, Sweden*

Received 4 July 2002; received in revised form 5 September 2002; accepted 24 September 2002

Abstract

We have previously shown that deregulated expression of the platelet-derived growth factor α-receptor (*PDGFRA*) can be associated with neural tube defects (NTDs) in both men and mice. In the present study, we have investigated the transcription factors that control the up-regulation of *PDGFRA* expression during differentiation of early embryonic human cells in culture. In Tera-2 embryonal carcinoma cells, *PDGFRA* expression is strongly enhanced upon differentiation induced by retinoic acid and cAMP treatment. Here we show that the corresponding increase in promoter activity is controlled by an ATTA-sequence-containing element located near the transcription initiation site, which is bound by a transcriptional complex that includes PBX and PRX homeobox transcription factors. Mutation of the putative binding sites for these transcription factors results in strong impairment of *PDGFRA* promoter activity in differentiated cells. Since functional inactivation of *Prx* genes has been associated with NTDs in mice, these data support a model in which improper *PDGFRA* expression as a result of mutations in or altered binding of its upstream regulators may be causally related to NTDs.

© 2002 Elsevier Science B.V. All rights reserved.

Keywords: Embryonal carcinoma; Differentiation; Spina bifida; Platelet-derived growth factor alpha-receptor; Promoter analysis

1. Introduction

Neural tube defects (NTDs), including anencephaly and spina bifida, form a major group of congenital malformations with an average incidence of 1 per 1000 pregnancies in the western world. NTDs are multifactorial traits with both genetic and environmental factors contributing to their etiology. Several candidate genes for NTDs have emerged from studies on mouse models, but only few of them have actually been associated with related diseases in humans. Mice with a targeted null mutation in the gene encoding the platelet-derived growth factor α-receptor (*PDGFRA*) and also *Patch* mutant mice, which contain a natural deletion of the chromosomal region that includes *PDGFRA*, both show severe spina bifida combined with embryonic lethality in their homozygous form [1,2]. We have recently shown that this gene also plays a prominent role in the genesis of NTDs in humans. Based on an analysis of naturally occurring single nucleotide polymorphisms in the *PDGFRA* promoter, five different promoter haplotypes could be discriminated which strongly differed in their transcriptional activity. Specific combinations of such haplotypes correlated directly with a predisposition for NTDs in a group of sporadic spina bifida patients [3]. Based on these observations, we have postulated that aberrant transcriptional regulation of *PDGFRA* may also play a central role in the genesis of NTDs in humans.

The above hypothesis suggests that transcription factors that act as upstream regulators of *PDGFRA* expression may also be associated with NTDs. In line with this concept, it has been shown that mice heterozygous for the *Patch* deletion show spina bifida only in combination with the *undulated* mutation in the *Pax1* gene [4]. In a

---

* Corresponding author. Tel.: +31-24-365-2707; fax: +31-24-365-2999.
E-mail address: vzoelen@sci.kun.nl (E.J.J. van Zoelen).

0925-4439/02/$ - see front matter © 2002 Elsevier Science B.V. All rights reserved.
PII: S0925-4439(02)00175-8

previous study, we have shown that Pax1 indeed acts as an upstream transcriptional regulator of *PDGFRA* [5]. Moreover, we have shown that Pax1 carrying the *undulated* mutation, as well as a mutant form of PAX1 found in a patient with spina bifida [6], both show a gain of function in their ability to stimulate *PDGFRA* transcription [5]. Also, other transcription factors that have been associated with NTDs in mouse models, including Pax3 [7], Gli2/Gli3 [8], HoxD4 [9,10] and Mfh1 [11] have been associated directly with *PDGFRA* transcription or at least coexpress with *PDGFRA* during development.

Expression of the *PDGFRA* and thus responsiveness of cells to the various *PDGF* isoforms (PDGF-A, -B, -C and -D) is strictly regulated during embryonic development. Although present in all cells of the pre-implantation embryo from the two-cell stage onwards [12], *PDGFRA* expression becomes limited to mesodermal and certain neural crest-derived structures after implantation [13–17]. Human embryonal carcinoma (EC) cells, which represent the undifferentiated stem cells of non-seminomatous testicular germ cell tumors, are widely used as an in vitro model system for studying differentiation-dependent regulation of gene expression during early human development [18]. In previous studies, we have shown that the Tera-2 cell line in its undifferentiated state (Tera-EC) expresses *PDGFRA* from an internal promoter, giving rise to a set of alternative transcripts that have been used as a specific marker for early detection of testicular germ cell tumors [19,20]. Upon in vitro treatment with retinoic acid (RA), differentiated cell populations are obtained with neuronal and endodermal characteristics, designated Tera-RA, which abundantly express the 6.4 kb *PDGFRA* transcript that encodes the full-length functional *PDGFRA*. Using the cloned 2 kb promoter region of human *PDGFRA* that drives the formation of this 6.4 kb transcript, we have shown [21] in transient transfection assays with a luciferase read-out, that *PDGFRA* transcription is strongly up-regulated upon treatment of Tera-EC cells with RA, particularly in combination with dibutyryl-cAMP (Bt_2cAMP) and theophylline, this in spite of the fact that the promoter neither contains a consensus RA-responsive element nor a consensus cAMP-responsive element (CRE).

Based on the hypothesis that aberrant expression of *PDGFRA* during development can be associated with NTDs, we have investigated the transcription factors that are involved in the up-regulation of *PDGFRA* promoter activity during RA-induced differentiation of Tera-EC cells. Here we show that an ATTA-sequence containing element (parATTA) is essential for *PDGFRA* transcriptional activity by binding a new complex of transcription factors that includes the homeobox proteins PBX2 and PRX2. Intriguingly, in mouse models, *Prx* genes have been found to be associated directly with NTDs [22]. These data underline the hypothesis that improper *PDGFRA* expression during development may be a major cause for the genesis of NTDs.

2. Materials and methods

2.1. Reporter constructs

The construction of the truncated *PDGFRA* promoter-luciferase (LUC) reporter gene vectors − 2120/+ 118 LUC, − 441/+ 118 LUC, − 275/+ 118 LUC, − 197/+ 118 LUC, − 175/+ 118 LUC and − 52/+ 118 LUC has been described previously [21]. Mutant forms of these promoter-luciferase constructs were generated using the Quick Change Site-Directed Mutagenesis Kit (Stratagene).

2.2. Cell culture

The human embryonal carcinoma cell line Tera-2 clone 13 [23] was maintained in α-modification of minimal essential medium lacking nucleosides and deoxynucleosides, supplemented with 10% ES-approved fetal calf serum (Gibco BRL). Undifferentiated cells were seeded 1 day prior to transfection at high density (5.0×10^4 cells/cm^2) in a 0.1% gelatin-coated tissue culture dish. Differentiation was induced by the addition of 5 μM of RA, 12 h after the cells were seeded at low density (5.0×10^3/cm^2), and maintained in this medium for 7 days before further use. Transfections were carried out using the calcium-phosphate method [24] upon addition of 1 μg/well of the promoter-luciferase vector. In addition, 50 ng/well of the lacZ-expressing vector pCH110 (Pharmacia) were cotransfected to correct for differences in transfection efficiency. After the appropriate incubation times, cells were lysed in reporter lysis buffer (Promega). Luciferase activity in the lysate was determined using the luciferase assay kit (Promega), according to the manufacturer's protocol. β-Galactosidase activity was assayed as described [25] using Galacton plus (Tropix) as the substrate.

2.3. Electrophoretic mobility shift assays

Nuclear extracts from Tera-2 cells were prepared as described by Schreiber et al. [26]. Extracts (10–15 μg) were incubated with 3×10^4 cpm ^{32}P-labelled DNA, 2 μg dI–dC and, if necessary, unlabelled competitor DNA in a reaction buffer (20 mM Hepes pH 7.9, 50 mM NaCl, 1 mM EDTA, 0.15 mM EGTA, 1 mM DTT, 0.15 mM PMSF, 4% (w/v) Ficoll and 50 mM KCl) for 5 min at room temperature. The resulting protein–DNA complexes were separated on a 4% polyacrylamide gel using 0.5 × TBE as running buffer [24] and visualized on X-ray film (Kodak X-Omat, Fuji RX).

2.4. Synthetic oligonucleotides

The following synthetic oligonucleotides were obtained in single-stranded form in both the sense and anti-sense direction: parATTA (5′-CTATAACATTGAATCAATTACAA-3′), m-PBX (5′-CTATAACAGGGAAGCAATTACAA-3′), m-

PRX (5′-CTATAACATTGAATCTAGAGCAA-3′), DM (5′-CTATAACAGGGAAGCTAGAGCAA-3′), consensus CRE (5′-AGAGATTGCCTGACGTCAGAGAGAAG-3′), consensus AP1 (5′-CGGATGACTCAGCCGGAA-3′) and consensus AP2 (5′-GATCGAACTGACCGCCCGCGGCCGT-3′).

Equal amounts of the sense and anti-sense oligonucleotides were mixed in distilled water, heated to boiling temperature and slowly cooled to room temperature. If necessary, the resulting double-stranded product was subsequently purified by non-denaturating polyacrylamide gel electrophoresis [24].

2.5. Antibodies

Anti-PBX polyclonal antibodies were directed against the C-terminus of the human protein, recombinantly prepared as a GST fusion protein (a generous gift from Dr. C. Murre, UCSD). Polyclonal antibodies specific for PRX2 (αPrx2) were directed against a synthetic peptide derived from mouse Prx2 (IKSYGQEAAIEQPVAPRPTT), while polyclonal antibodies recognizing both PRX1 and PRX2 (αPrx1 + 2) were generated against the *E. coli* recombinant protein AGRRAAGPVSGPAEARVGAAREPSGGSSGTEAAPQDGDCPSPGRGTKRKKKQRRNRTTFNSSQLQALERVFERTHYPDAFVREELARRVNLSEARVQVWFQNRRAKFRRNERAMLATRSASLLKSYGQEAAIEQPVAPRPTTMSPDYLSWPASSPYSSVPPYSPGGSSPATPGVNMANSIASLRLKAKEFSLHHSQVPTVN. Both antibodies were a generous gift from Dr. F. Meijlink, Hubrecht Laboratory, Utrecht.

3. Results

We have previously shown that the activity of the so-called *PDGFRA* P1-promoter is strongly up-regulated upon RA treatment of undifferentiated Tera-2 human embryonal carcinoma cells. Up-regulation was also observed in the presence of Bt$_2$cAMP, such that synergy in promoter activation was observed by a combination of RA and this cAMP analogue [21]. Since the promoter region tested does not contain sequences corresponding to consensus RA- or cAMP-responsive elements, a panel of progressive 5′-deletion mutants of the promoter, cloned into a luciferase reporter gene vector, was used to map the cis-element(s) involved in the RA- and cAMP-induced promoter activity. Upon transient transfection into undifferentiated Tera-EC cells, the promoter activity of the deletion mutants varied in agreement with previous data [21], but for each mutant, a 9- to 20-fold induction of activity was observed upon treatment of the cells for 48 h with RA alone or with RA in combination with Bt$_2$cAMP and the phosphodiesterase inhibitor theophylline (RACT), as shown in Fig. 1. Interestingly, similar results were obtained when the transfections were performed in Tera-2 cells that had already been differentiated by RA treatment for 7 days (Tera-RA cells). Since these differentiated cells already display a high basal *PDGFRA* promoter activity [21], RA and RACT seem to enhance, rather than induce, promoter activity. The observation that the smallest element tested is still RA- and Bt$_2$cAMP-responsive, suggests that these stimuli mediate their effects through regulating elements within the −52/+118 region of the *PDGFRA* gene.

To characterize the transcription factors that bind to this specific promoter region, electrophoretic mobility shift assays (EMSAs) were performed using the −52/+118 promoter fragment as a probe. As shown in Fig. 2 (lane 1), at least four different complexes were observed upon incubation of this fragment with nuclear extracts of Tera-EC cells. Upon 24 h treatment of these cells with RA, quantitative changes were observed in the three low mobility complexes, while the high mobility complex had disappeared in favour of two new complexes with even higher mobilities. Qualitatively similar differences, although often more pronounced, were observed 24 h after treatment with RACT (data not shown, see also Ref. [21]). These data show that RA treatment of Tera-2 cells results in a complex but

	Tera-2 EC		Tera-2 RA	
construct	**RA**	**RACT**	**RA**	**RACT**
-52/+118LUC	**9.3 ± 0.1**	**16.5 ± 0.0**	**2.5 ± 0.2**	**10.7 ± 0.2**
-175/+118LUC	**7.9 ± 0.1**	**22.4 ± 1.0**	**3.1 ± 0.3**	**11.8 ± 0.3**
-197/+118LUC	**6.1 ± 0.7**	**25.8 ± 0.7**	**2.6 ± 0.0**	**13.6 ± 1.7**
-275/+118LUC	**9.3 ± 0.4**	**16.3 ± 0.9**	**2.2 ± 0.4**	**18.6 ± 0.6**
-441/+118LUC	**9.2 ± 0.7**	**21.9 ± 1.8**	**3.8 ± 0.3**	**8.8 ± 0.2**
-825/+118LUC	**6.2 ± 0.0**	**18.8 ± 2.1**	**3.2 ± 0.1**	**11.9 ± 1.0**

Fig. 1. RA and cAMP-induced activity of *PDGFRA* promoter deletion mutants. Indicated 5′ promoter-luciferase (LUC) deletion mutants were transiently transfected into undifferentiated Tera-EC or differentiated Tera-RA cells. Transfected cells were treated for 48 h with either 5 μM RA or a combination of 5 μM RA, 1 mM Bt$_2$cAMP and 350 μM theophylline (RACT). Subsequently, luciferase activity in the cells was determined and corrected for differences in transfection efficiency. The values represent the fold induction of luciferase activity after treatment relative to that of unstimulated cells, including the sample standard deviation based on two independent experiments. Unstimulated values were in agreement with Afink et al. [21].

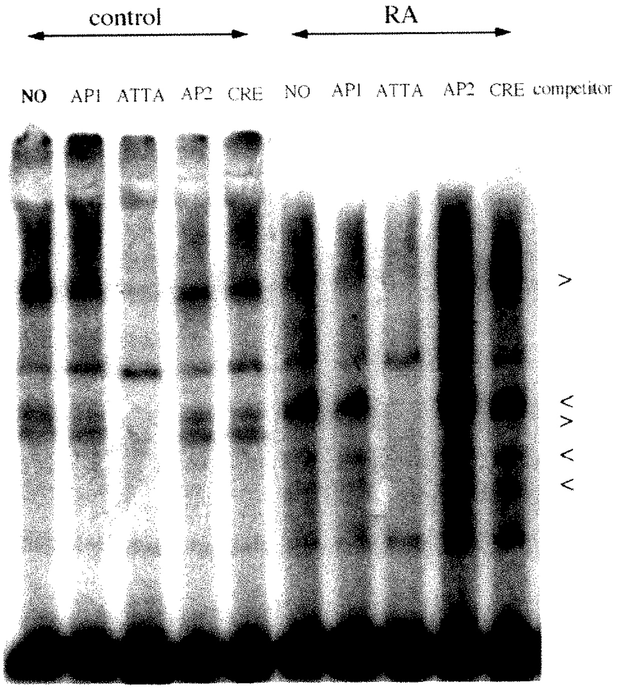

Fig. 2. EMSA on nuclear extracts of Tera-EC cells before (control) and 48 h after incubation with 5 μM RA. Use was made of the ^{32}P-labelled −52/+118 *PDGFRA* promoter fragment, either in the absence of any specific competitor (NO), or in the presence of a 500-fold excess of consensus AP1, parATTA, consensus AP2 or consensus CRE oligonucleotide (see Materials and methods for sequences). The five distinct DNA–protein complexes that can be competed with unlabelled parATTA are indicated by arrows, specified as complexes up-regulated by RA (<) and complexes with decreased intensity following RA treatment (>).

characteristic change in nuclear protein binding to the −52/+118 promoter fragment of *PDGFRA*.

The *PDGFRA* promoter does not contain a consensus RA-responsive element, but it contains various putative binding sites for RA-inducible transcription factors such as AP2 [21], and one such AP2 site (${}^{+97}$GCCGTGGG^{+104}) is located within the −52/+118 region. In addition, an ATTA-containing sequence (${}^{+4}$ATTGAATCAATTA^{+16}), designated here as parATTA, is present which shows some homology to both a cAMP-responsive element (TGACGTCA) and to binding sites for the AP1 transcription factor complex (TGASTCA) [27,28]. In order to investigate the involvement of these sequences in the −52/+118 promoter region in binding of nuclear proteins, we carried out oligonucleotide competition studies, as shown in Fig. 2. Competition with the unlabelled parATTA oligonucleotide resulted in a complete loss of five of the six previously mentioned protein–DNA complexes bound to the −52/+118 probe. This shows that this parATTA element is essential for the formation of protein–DNA complexes in both Tera-EC and Tera-RA cells. No binding competition was observed with a consensus AP1 oligonucleotide, an AP2 oligonucleotide or an oligonucleotide containing a cAMP-responsive element (CRE), which is indicative for the specificity of nuclear protein binding to the parATTA sequence in this promoter element (Fig. 2).

ATTA motifs are known to be involved in the DNA binding of homeobox-containing transcription factors. A search for transcription factor binding sites in the parATTA sequence present in the −52/+118 fragment of the *PDGFRA* promoter (TFSEARCH analysis) revealed the highest correlation with binding sites for members of the PBX and PRX families of homeobox proteins (TTGAAT and AATTA, respectively). In order to identify if such factors indeed bind the parATTA sequence in Tera-2 cells, we used specific antibodies directed against PBX and PRX proteins in EMSA studies. Fig. 3 shows that upon incubation of parATTA with nuclear extracts of Tera-EC cells, a small increase in gel mobility of the DNA–protein complex was observed in the presence of antibodies specific for PBX2. More pronounced, a clear supershift was observed when the experiment was carried out in the presence of antibodies specific for PRX2, while antibodies that recognize both PRX2 and its transcriptional partner PRX1 [22,29,30] strongly reduce DNA–protein complex formation. These data suggest that the parATTA sequence is bound by PRX2, and possibly also PRX1, most likely in a protein complex with PBX2. Similar results were obtained using nuclear extracts from Tera-RA cells (data not shown).

In order to analyse the specific function of the bound nuclear proteins, we introduced inactivating mutations into the parATTA oligonucleotide on positions that are specific for binding of either PBX2 or PRX1/2 (based on TFSEARCH

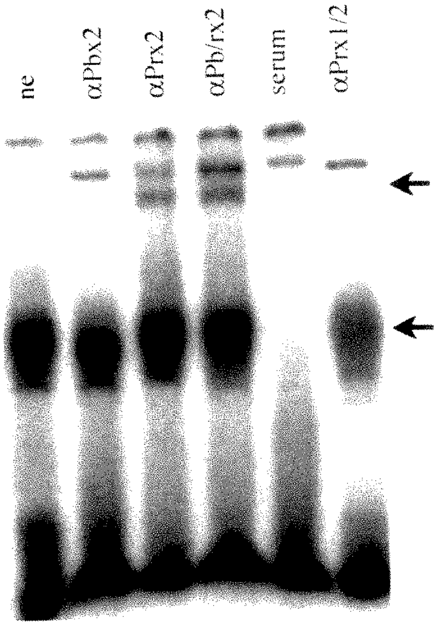

Fig. 3. Identification of parATTA binding proteins in Tera-EC cells. EMSAs were performed on the ^{32}P-labelled *PDGFRA* promoter-derived parATTA oligonucleotide, using nuclear extracts of Tera-EC cells in the presence of anti-PRX and anti-PBX antibodies, as follows: ne, control nuclear extracts; αPbx2, antibodies specific for PBX2; αPrx2, antibodies specific for PRX2; αPb/rx2, a combination of αPbx2 and αPrx2; serum, control rabbit serum in the absence of nuclear extract; αPrx1/2, antibodies recognizing both PRX1 and PRX2. Arrows denote the DNA–protein complexes that are formed or altered upon antibody binding.

analysis). Fig. 4 shows that mutation of the putative PBX binding site in the parATTA oligonucleotide results in a strongly reduced ability to bind Tera-2 nuclear proteins. Similar results were obtained upon mutation of the ATTA site involved in PRX1/2 binding, while no detectable complex formation was observed when both sites were mutated simultaneously. The similarity in effect observed upon mutation of the putative PBX and PRX site suggests that inhibition of binding of one of these factors may already block formation of the entire complex. It has been described that HOX gene products may modulate the DNA binding activity of PBX transcription factors and consequently that removal of either PBX itself or of the homeobox-containing transcription factor is sufficient for dissociation of the DNA–protein complex [31]. In agreement with this observation, we find that PBX2 only forms stable complexes with specific DNA sequences when other homeobox-containing transcription factors, in this case PRX1/2, are bound in addition.

Functional analysis of the wild-type and various mutated parATTA elements was subsequently studied within the context of the highly active −441/+118 promoter-luciferase reporter construct. When transfected into Tera-EC cells, the various mutations in the parATTA element caused a severe reduction in promoter activity compared to the wild-type promoter, as shown in Fig. 5. Mutation of the putative PBX binding site resulted in a more than 5-fold reduction in luciferase activity, both before and after RACT treatment. A similar reduction was observed upon mutation of the ATTA site or when both sets of mutations were combined. A complete loss of promoter activity was observed upon deletion of 11 nucleotides from the palindromic sequence within parATTA which is involved in binding of PBX and PRX1/2. Since this deletion leaves the transcription initiation intact, these data underline the essential role of the parATTA element in the basal transcriptional activity of the *PDGFRA* promoter.

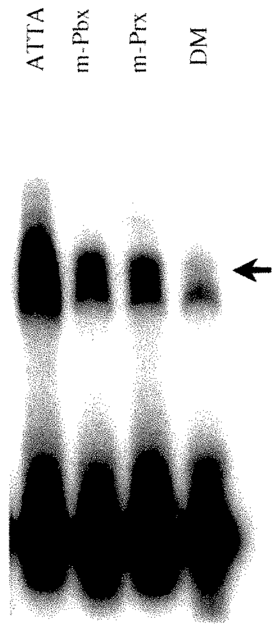

Fig. 4. Effect of mutations in the parATTA sequence on nuclear protein binding. EMSAs were performed with nuclear extracts of Tera-EC cells using ^{32}P-labelled oligonucleotides with different mutations. The sequences of the wild-type parATTA oligonucleotide and of the mutant forms aimed at preventing PBX and PRX binding (designated m-PBX, m-PRX, and the double mutant DM) are shown in Materials and methods. The arrow denotes the major specific DNA–protein complex.

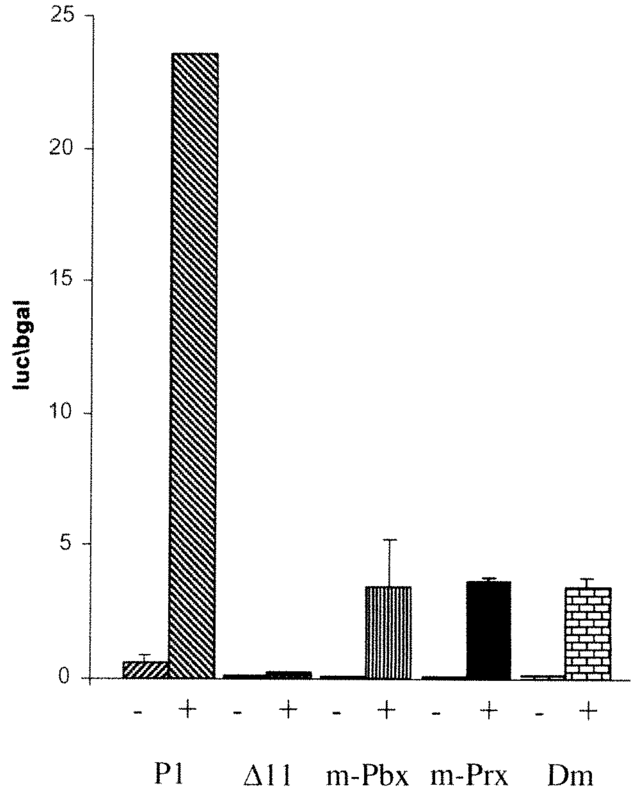

Fig. 5. Effect of mutations in the parATTA element on *PDGFRA* promoter activity. In the −441/+118 PDGFRA promoter construct linked to luciferase, the following mutations were made: P1, no mutation; Δ11, P1 carrying a deletion of the 11 nucleotide inverted repeat $^{+4}$ATTGAATCAAT^{+14}; m-Pbx, P1 carrying the PBX-sensitive mutation similarly as in the m-PBX oligonucleotide; m-Prx, P1 carrying the PRX-sensitive mutation similarly as in the m-PRX oligonucleotide; Dm, P1 carrying both sets of mutations similarly as in the DM oligonucleotide. Constructs were transfected into Tera-EC cells and luciferase (luc) activity was measured in control cells (−) and in cells treated for 48 h with RACT (+). Promoter activity values were corrected for differences in transfection efficiency, expressed in β-galactosidase (bgal) activity. Error bars represent the standard deviation of duplicate independent experiments.

4. Discussion

In the present study, we have shown that the up-regulation of *PDGFRA* expression during differentiation of early embryonic human cells requires a promoter element, designated parATTA, which binds a complex of PRX and PBX proteins. Various studies have shown that improper expression of the *PDGFRA* during embryonic development can result in NTDs, and therefore both *PDGFRA* itself and genes encoding upstream regulators of its expression may be associated with such malformations. We have previously shown that PAX1, as a product of a NTD-associated gene, is an upstream regulator of *PDGFRA* expression, while the current study identifies PBX2, PRX2 and possibly also PRX1 as regulators of PDGFRA expression that are potentially involved in NTDs. These observations are in line with mouse studies, where severe NTDs have been observed, particularly in *Prx1*(−/−); *Prx2*(−/−) mice, with similar vertebrae defects as seen in the *Pdgfra* null mutant [22].

The exact nature of the protein complex that binds the parATTA element in Tera-2 cells is unclear, but the observation that five distinct DNA–protein complexes have been identified in this study that are competed in EMSAs by unlabelled parATTA-containing oligonucleotides, indicates that multiple complexes are formed. This suggests that in addition to PBX2 and PRX1/2, other proteins may also be present in the complexes formed. The EMSAs indicate that PBX2- and PRX1/2-containing complexes can be formed with nuclear extracts from both undifferentiated and differentiated Tera-2 cells, indicating that the increase in *PDGFRA* promoter activity upon RA treatment is most likely not due to the induction of these homeotic genes. These observations suggest that PBX–PRX proteins form the core of a larger complex that is required for transcriptional activation, in agreement with recent data on the binding of such transcription factors to a collagen promoter [32]. The formation of this complex is at most only partly regulated by the mere availability of the transcription factors involved and most likely requires an additional activation step. This is confirmed by the observed synergy between Bt_2AMP and RA, which in comparison with RA alone gives rise to only quantitative, and not to qualitative changes in transcription factor binding to the −52/+118 region [21]. Also the observation that RACT still stimulates *PDGFRA* transcription in Tera-RA cells supports this hypothesis.

The present data indicate that the parATTA binding proteins PBX2 and PRX1/2 are essential for formation of the complex that regulates *PDGFRA* expression during embryonic cell differentiation. Homeobox transcription factors are known to control expression of other homeotic genes, but only few examples are available in which they control expression of non-homeotic genes such as *PDGFRA* [32]. Amino acid alignment reveals that members of the PBX and PRX families are 93–99% conserved between mouse and human, while the parATTA element itself is 100% conserved between rat, mouse and human. This underlines the importance of this mechanism for normal vertebrate development.

Studies on the promoters of the human, mouse and rat *Pdgfra* gene have provided evidence for the involvement of GATA4 [33], PAX3-FKHR [7], Pax1 [5], C/EBPs [34] and Gli1 [35] in transcriptional control. Potentially, the genes encoding these transcription factors can all be involved in the development of NTDs. In mice, *Pdgfra* itself as well as *Pax1*, *Pax3*, *Prx1* and *Prx2*, which all encode upstream regulators of *PDGFRA* expression, have been associated directly with NTDs. In humans, specific combinations of *PDGFRA* promoter haplotypes have been associated with predisposition to NTDs, while mutations in *PAX1* and *PAX3* are also considered to be risk factors for human NTDs. Based on our present results, *PBX2*, *PRX2* and possibly *PRX1* as well should also be considered as candidate genes in the genesis of NTDs in humans. Further studies will have to indicate if mutations in these genes or alterations in their expression levels are indeed observed in patients suffering from anencephaly and spina bifida.

In conclusion, we have shown that *PDGFRA* promoter activity in human Tera-2 cells is strongly up-regulated upon RA and cAMP treatment. The element involved is located in the −52/+118 region of the promoter, and EMSAs show that multiple protein complexes that can bind this region which are all competed by a 23 bp parATTA oligonucleotide. These protein complexes include PRX and PBX, but since these complexes are present in both Tera-EC and Tera-RA cells, RA/cAMP-induced induction of *PDGFRA* promoter activity seems to require an additional, as yet unknown activation step. Point mutations in parATTA reduce binding affinity for PBX–PRX proteins and thereby the induction of promoter activation by RA/cAMP. It is therefore concluded that the parATTA sequence is essential for normal *PDGFRA* transcription regulation and for its activation upon RA/cAMP treatment.

Acknowledgements

The present studies were supported by grants from the Dutch Prinses Beatrix Fonds. We thank Dr. E. Mariman (Department of Anthropogenetics, University of Nijmegen) for fruitful discussion, and Dr. C. Murre and Dr. F. Meijlink for the generous gifts of antibodies.

References

[1] P. Soriano, Development 124 (1997) 2691–2700
[2] J Payne, F Shibasaki, M Mercola, Dev. Dyn. 209 (1997) 105–116.
[3] P H Joosten, M. Toepoel, E.C. Mariman, E J. Van Zoelen, Nat Genet 27 (2001) 215–217.
[4] U Helwig, K. Imai, W Schmahl, B.E. Thomas, D S Varnum, J.H. Nadeau, R Balling, Nat Genet 11 (1995) 60–63
[5] P.H. Joosten, F A Hol, S.E van Beersum, H Peters, B C Hamel, G B. Afink, E J van Zoelen, E.C. Mariman, Proc. Natl. Acad. Sci U S A 95 (1998) 14459–14463.
[6] F A Hol, M.P. Geurds, S Chatkupt, Y.Y. Shugart, R. Balling, C.T Schrander-Stumpel, W G. Johnson, B C. Hamel, E.C Mariman, J Med. Genet 33 (1996) 655–660
[7] J A Epstein, B Song, M. Lakkis, C. Wang, Mol Cell. Biol 18 (1998) 4118–4130
[8] J Aruga, K Mizugishi, H. Koseki, K. Imai, R. Balling, T Noda, K. Mikoshiba, Mech Dev. 89 (1999) 141–150
[9] G S Horan, R Ramirez-Solis, M S Featherstone, D J Wolgemuth, A Bradley, R.R Behringer, Genes Dev. 9 (1995) 1667–1677
[10] G.S. Horan, E.N Kovacs, R R Behringer, M S. Featherstone, Dev. Biol. 169 (1995) 359–372.

[11] T A Furumoto, N. Miura, T Akasaka, Y. Mizutani-Koseki, H. Sudo, K. Fukuda, M. Maekawa, S Yuasa, Y. Fu, H Moriya, M. Taniguchi, K. Imai, E Dahl, R Balling, M. Pavlova, A. Gossler, H Koseki, Dev. Biol. 210 (1999) 15–29

[12] S L. Palmieri, J. Payne, C.D. Stiles, J.D. Biggers, M. Mercola, Mech Dev. 39 (1992) 181–191

[13] A Orr-Urtreger, P Lonai, Development 115 (1992) 1045–1058

[14] A Orr-Urtreger, M.T Bedford, M.S. Do, L. Eisenbach, P Lonai, Development 115 (1992) 289–303.

[15] G C. Schatteman, K Morrison-Graham, A van Koppen, J A Weston, D.F. Bowen-Pope, Development 115 (1992) 123–131.

[16] K. Morrison-Graham, G.C. Schatteman, T Bork, D.F Bowen-Pope, J.A Weston, Development 115 (1992) 133–142.

[17] N Takakura, H. Yoshida, Y Ogura, H. Kataoka, S. Nishikawa, J Histochem. Cytochem. 45 (1997) 883–893

[18] P.W Andrews, Biochim. Biophys Acta 948 (1988) 17–36.

[19] S. Mosselman, L. Claesson-Welsh, J S Kamphuis, E J van Zoelen, Cancer Res. 54 (1994) 220–225

[20] S. Mosselman, L.H Looijenga, A J. Gillis, M.A van Rooijen, H J Kraft, E J van Zoelen, J W. Oosterhuis, Proc. Natl Acad Sci U. S A. 93 (1996) 2884–2888

[21] G.B. Afink, M Nister, B H Stassen, P H Joosten, P J. Rademakers, E. Bongcam-Rudloff, E J. van Zoelen, S Mosselman, Oncogene 10 (1995) 1667–1672

[22] D. Ten Berge, A. Brouwer, J. Korving, J.F Martin, F Meijlink, Development 125 (1998) 3831–3842.

[23] S Thompson, P.L. Stern, M. Webb, F.S. Walsh, W. Engstrom, E P. Evans, W.K Shi, B Hopkins, C F Graham, J. Cell Sci 72 (1984) 37–64

[24] J. Sambrook, E F Fritsch, T Maniatis, Molecular cloning. A Laboratory Manual, 2nd ed., 1989. Cold Spring Harbor Laboratory Press, Plainview, NY.

[25] V.K Jain, I.T Magrath, Anal Biochem 199 (1991) 119–124

[26] E Schreiber, P. Matthias, M M Muller, W. Schaffner, Nucleic Acids Res 17 (1989) 6419

[27] P Angel, M Imagawa, R Chiu, B Stein, R J. Imbra, H.J. Rahmsdorf, C Jonat, P Herrlich, M. Karin, Cell 49 (1987) 729–739

[28] W Lee, P. Mitchell, R. Tjian, Cell 49 (1987) 741–752

[29] M.F. Lu, H T Cheng, M.J. Kern, S.S. Potter, B Tran, T.G. Diekwisch, J F Martin, Development 126 (1999) 495–504

[30] M Bergwerff, A.C. Gittenberger-de Groot, L.J. Wisse, M.C. DeRuiter, A. Wessels, J F Martin, E.N. Olson, M.J. Kern, Virchows Arch. 436 (2000) 12–19.

[31] M A Van Dijk, L T. Peltenburg, C Murre, Mech Dev. 52 (1995) 99–108.

[32] D. Penkov, S. Tanaka, G. Di Rocco, J Berthelsen, F. Blasi, F Ramirez, J. Biol. Chem 275 (2001) 16681–16689.

[33] C Wang, B Song, Mol Cell. Biol. 16 (1996) 712–723

[34] T Fukuoka, Y. Kitami, T Okura, K Hiwada, J Biol Chem 274 (1999) 25576–25582

[35] J Xie, M. Aszterbaum, X Zhang, J.M. Bonifas, C. Zachary, E Epstein, F McCormick, Proc. Natl. Acad. Sci. U. S. A 98 (2001) 9255–9259.

ELSEVIER
Biochimica et Biophysica Acta 1588 (2002) 261–263
BIOCHIMICA ET BIOPHYSICA ACTA
BBA
www bba-direct.com

Molecular Basis of Disease
Author Index

Afink, G.B , see Joosten, P H L.J. (1588) 254
Aktan, F., see Group, T.A.D I C A.D.-I.C.S. (1588) 71
Andreelli, F., see Boucher, P (1588) 226
Anitha, S., see Latha, K.S. (1588) 56
Arthur, J.R., see Miller, S. (1588) 85
Avots, A., see Kneitz, C (1588) 41

Bagshaw, R D., Zhang, S., Hinek, A , Skomorowski, M.-A., Whelan, D , Clarke, J T.R. and Callahan, J.W
  Novel mutations (Asn 484 Lys, Thr 500 Ala, Gly 438 Glu) in Morquio B disease (1588) 247
Barchowsky, A., see Madhani, M. (1588) 232
Barreiro Arcos, M.L., see Gorelik, G (1588) 179
Beckett, G J , see Miller, S. (1588) 85
Beggs, A.H., see Vainzof, M. (1588) 33
Beitia, G., see Montiel-Duarte, C. (1588) 26
Berberat, P O., see Schneider, D. (1588) 1
Bernazzi, B , see Carelli, V (1588) 7
Björntorp, P , see Rosmond, R (1588) 103
Boschero, A.C., see Stoppiglia, L.F. (1588) 113
Bouchard, C., see Rosmond, R. (1588) 103
Boucher, P., Ducluzeau, P -H., Davelu, P., Andreelli, F., Vallier, P., Riou, J.-P., Laville, M and Vidal, H
  Expression and regulation by insulin of low-density lipoprotein receptor-related protein mRNA in human skeletal muscle (1588) 226
Bouscarel, B., see Matsuzaki, Y. (1588) 139
Bucchi, L., see Carelli, V (1588) 7
Büchler, M.W., see Schneider, D. (1588) 1

Callahan, J.W , see Bagshaw, R.D (1588) 247
Camakaris, J., see Lockhart, P J (1588) 189
Cardeal, M., see Tengan, C H. (1588) 65
Carelli, V., Vergani, L., Bernazzi, B., Zampieron, C., Bucchi, L., Valentino, M.L , Rengo, C., Torroni, A and Martinuzzi, A
  Respiratory function in cybrid cell lines carrying European mtDNA haplogroups. implications for Leber's hereditary optic neuropathy (1588) 7
Carneiro, E.M., see Stoppiglia, L.F. (1588) 113
Carpen, O , see Vainzof, M. (1588) 33
Cenarruzabeitia, E., see Montiel-Duarte, C (1588) 26
Ceryak, S , see Matsuzaki, Y. (1588) 139
Chen, Y., see Cheng, K (1588) 48
Cheng, K., Chen, Y., Zimniak, P , Raufman, J.-P , Xiao, Y and Frucht, H.
  Functional interaction of lithocholic acid conjugates with M3 muscarinic receptors on a human colon cancer cell line (1588) 48
Chubinskaya, S., Kumar, B , Merrihew, C., Heretis, K , Rueger, D.C. and Kuettner, K.E.
  Age-related changes in cartilage endogenous osteogenic protein-1 (OP-1) (1588) 126
Clarke, J T R., see Bagshaw, R.D (1588) 247
Clavero, S., Martínez, M.A., Pérez, B., Pérez-Cerdá, C., Ugarte, M. and Desviat, L R
  Functional characterization of *PCCA* mutations causing propionic acidemia (1588) 119
Cremaschi, G A., see Gorelik, G. (1588) 179

Daniele, A., Tomanin, R., Villani, G.R.D., Zacchello, F , Scarpa, M and Di Natale, P
  Uptake of recombinant iduronate-2-sulfatase into neuronal and glial cells in vitro (1588) 203
Das-Evcimen, N , see Group, T A D.I C A D -I C.S. (1588) 71
Davelu, P., see Boucher, P. (1588) 226
De Dios, I., see Uruñuela, A (1588) 159
De Groene, E.M., see Schaaf, G.J (1588) 149
De la Mano, A.M , see Uruñuela, A. (1588) 159
Desnuelle, C , see Perucca-Lostanlen, D (1588) 210
Desviat, L R , see Clavero, S. (1588) 119
Di Natale, P., see Daniele, A. (1588) 203
Doy, M., see Matsuzaki, Y (1588) 139
Ducluzeau, P.-H , see Boucher, P. (1588) 226

Egashira, T., see Obata, T (1588) 173

Faulkner, G., see Vainzof, M. (1588) 33
Ferreiro-Barros, C., see Tengan, C.H. (1588) 65
Fink-Gremmels, J., see Schaaf, G.J (1588) 149
Fireman, M A.T., see Tengan, C.H (1588) 65
Firth, S.D , see Lockhart, P.J. (1588) 189
Friess, H., see Schneider, D. (1588) 1
Frucht, H., see Cheng, K. (1588) 48
Fukuoka, S.-I. and Nyaruhucha, C.M.
  Expression and functional analysis of rat P23, a gut hormone-inducible isoform of trypsin, reveals its resistance to proteinaceous trypsin inhibitors (1588) 106
Fukushima, S., see Matsuzaki, Y (1588) 139

Gabbai, A.A., see Tengan, C.H (1588) 65
Goller, M., see Kneitz, C (1588) 41
Gorelik, G , Barreiro Arcos, M.L., Klecha, A.J and Cremaschi, G.A.
  Differential expression of protein kinase C isoenzymes related to high nitric oxide synthase activity in a T lymphoma cell line (1588) 179
Green, P S. and Leeuwenburgh, C
  Mitochondrial dysfunction is an early indicator of doxorubicin-induced apoptosis (1588) 94
Greenough, M., see Lockhart, P J (1588) 189
Group, T.A D I.C.A.D -I C S., Pekiner, B., Ulusu, N.N., Das-Evcimen, N , Sahilli, M., Aktan, F , Stefek, M , Stolc, S. and Karasu, Ç
  In vivo treatment with stobadine prevents lipid peroxidation, protein glycation and calcium overload but does not ameliorate Ca^{2+}-ATPase activity in heart and liver of streptozotocin-diabetic rats: comparison with vitamin E (1588) 71
Gurgel-Giannetti, J , see Vainzof, M. (1588) 33

PII: S0925-4439(02)00206-5

Hanaoka, K., see Yamamoto, K (1588) 195
Hashimoto, E., see Ohkawa, H (1588) 217
Hayes, C.M., see Perucca-Lostanlen, D. (1588) 210
Heretis, K., see Chubinskaya, S. (1588) 126
Higuchi, W.I., see Liu, C -L. (1588) 15
Hinek, A , see Bagshaw, R.D. (1588) 247
Honda, A., see Matsuzaki, Y (1588) 139
Horii, Y., see Naito, E. (1588) 79
Howie, A F , see Miller, S. (1588) 85

Ikeda, S -i., see Yamamoto, K (1588) 195
Ikegami, T., see Matsuzaki, Y. (1588) 139
Iraburu, M.J., see Montiel-Duarte, C. (1588) 26
Ishikawa, A., see Yamamoto, K. (1588) 195
Ito, M , see Naito, E. (1588) 79

Jackson, S K., see Madhani, M (1588) 232
James, P E , see Madhani, M (1588) 232
Joosten, P.H.L.J , Toepoel, M , Van Oosterhout, D., Afink, G.B. and Van Zoelen, E J.J.
A regulating element essential for PDGFRA transcription is recognized by neural tube defect-associated PRX homeobox transcription factors (1588) 254

Kaneko, K., see Yamamoto, K. (1588) 195
Karasu, Ç., see Group, T.A D.I.C.A.D.-I.C S (1588) 71
Kishikawa, M., Sass, J.O , Sakura, N., Nakanishi, T., Shimizu, A. and Yoshioka, M.
The peak height ratio of *S*-sulfonated transthyretin and other oxidized isoforms as a marker for molybdenum cofactor deficiency, measured by electrospray ionization mass spectrometry (1588) 135
Kitamura, S., see Naito, E. (1588) 79
Kiyomoto, B H., see Tengan, C.H. (1588) 65
Klecha, A.J., see Gorelik, G. (1588) 179
Kleeff, J., see Schneider, D. (1588) 1
Klei, L., see Madhani, M (1588) 232
Kneitz, C., Goller, M., Tony, H.-P., Simon, A., Stibbe, C., König, T., Serfling, E. and Avots, A.
The CD23b promoter is a target for NF-AT transcription factors in B-CLL cells (1588) 41
König, T., see Kneitz, C. (1588) 41
Korc, M., see Schneider, D. (1588) 1
Kuettner, K.E , see Chubinskaya, S (1588) 126
Kumar, B , see Chubinskaya, S. (1588) 126
Kuroda, Y , see Naito, E. (1588) 79
Kuroki, Y., see Ohkawa, H. (1588) 217

La Fontaine, S , see Lockhart, P.J. (1588) 189
Latha, K.S , Anitha, S., Rao, K S J and Viswamitra, M.A
Molecular understanding of aluminum-induced topological changes in $(CCG)_{12}$ triplet repeats: relevance to neurological disorders (1588) 56
Laville, M., see Boucher, P. (1588) 226
Leeuwenburgh, C , see Green, P.S. (1588) 94
Leite, A.R., see Stoppiglia, L.F. (1588) 113
Lewin, M H., see Miller, S (1588) 85
Liu, C.-L. and Higuchi, W.I.
Cholesterol crystallite nucleation in supersaturated model biles from a thermodynamic standpoint (1588) 15
Lockhart, P.J., La Fontaine, S , Firth, S.D., Greenough, M., Camakaris, J. and Mercer, J.F B.
Correction of the copper transport defect of Menkes patient fibroblasts by expression of two forms of the sheep Wilson ATPase (1588) 189
López-Zabalza, M J., see Montiel-Duarte, C. (1588) 26

Maas, R.F.M., see Schaaf, G.J. (1588) 149
Madhani, M , Barchowsky, A., Klei, L., Ross, C.R., Jackson, S.K , Swartz, H.M and James, P E
Antibacterial peptide PR-39 affects local nitric oxide and preserves tissue oxygenation in the liver during septic shock (1588) 232
Manso, M.A., see Uruñuela, A. (1588) 159
Martínez, M.A., see Clavero, S. (1588) 119
Martinuzzi, A., see Carelli, V. (1588) 7
Matsuda, J , see Naito, E. (1588) 79
Matsuzaki, Y , Bouscarel, B., Ikegami, T., Honda, A., Doy, M., Ceryak, S., Fukushima, S., Yoshida, S., Shoda, J. and Tanaka, N
Selective inhibition of CYP27A1 and of chenodeoxycholic acid synthesis in cholestatic hamster liver (1588) 139
Mercer, J F B., see Lockhart, P J (1588) 189
Merrihew, C., see Chubinskaya, S. (1588) 126
Miller, S., Walker, S W., Arthur, J R., Lewin, M.H., Pickard, K., Nicol, F , Howie, A.F. and Beckett, G.J
Selenoprotein expression in endothelial cells from different human vasculature and species (1588) 85
Miyagoe, Y., see Yamamoto, K. (1588) 195
Montiel-Duarte, C., Varela-Rey, M., Osés-Prieto, J A., López-Zabalza, M.J., Beitia, G , Cenarruzabeitia, E. and Iraburu, M.J.
3,4-Methylenedioxymethamphetamine ("Ecstasy") induces apoptosis of cultured rat liver cells (1588) 26
Moreira, E S , see Vainzof, M. (1588) 33
Mousson de Camaret, B., see Perucca-Lostanlen, D. (1588) 210
Murakami, S., see Ohkawa, H. (1588) 217

Naito, E., Ito, M., Yokota, I , Saijo, T., Matsuda, J., Ogawa, Y., Kitamura, S., Takada, E., Horii, Y. and Kuroda, Y
Thiamine-responsive pyruvate dehydrogenase deficiency in two patients caused by a point mutation (F205L and L216F) within the thiamine pyrophosphate binding region (1588) 79
Nakanishi, T., see Kishikawa, M (1588) 135
Narbonne, H., see Perucca-Lostanlen, D. (1588) 210
Nicol, F., see Miller, S. (1588) 85
Nijmeijer, S.M., see Schaaf, G.J. (1588) 149
Nogueira, T.A., see Stoppiglia, L.F. (1588) 113
Nomoto, S., see Yamamoto, K. (1588) 195
Nyaruhucha, C.M., see Fukuoka, S.-I. (1588) 106

Obata, T. and Egashira, T.
Effect of imipramine on 1-methyl-4-phenylpyridinium ion-induced hydroxyl radical generation in rat striatum (1588) 173
Ogawa, Y., see Naito, E. (1588) 79
Ohkawa, H., Sohma, H., Sakai, R., Kuroki, Y., Hashimoto, E., Murakami, S. and Saito, T.
Ethanol-induced augmentation of annexin IV in cultured cells and the enhancement of cytotoxicity by overexpression of annexin IV by ethanol (1588) 217
Oliveira, A S.B., see Tengan, C.H. (1588) 65
Orfao, A , see Uruñuela, A. (1588) 159
Osés-Prieto, J A., see Montiel-Duarte, C. (1588) 26

Paquis-Flucklinger, V , see Perucca-Lostanlen, D (1588) 210
Passos-Bueno, M.R., see Vainzof, M. (1588) 33
Pekiner, B., see Group, T.A D I.C A.D.-I.C.S (1588) 71
Pérez, B , see Clavero, S (1588) 119
Pérez-Cerdá, C , see Clavero, S. (1588) 119
Perucca-Lostanlen, D., Taylor, R W , Narbonne, H , Mousson de Camaret, B., Hayes, C.M., Saunieres, A., Paquis-Flucklinger, V , Turnbull, D.M., Vialettes, B. and Desnuelle, C
Molecular and functional effects of the T14709C point mutation in the mitochondrial DNA of a patient with maternally inherited diabetes and deafness (1588) 210

Pickard, K., see Miller, S. (1588) 85
Ping Leung, M , see Sun, G. (1588) 241

Qiu, G., see Sun, G. (1588) 241

Rao, K.S J., see Latha, K.S. (1588) 56
Raufman, J -P, see Cheng, K (1588) 48
Rengo, C., see Carelli, V. (1588) 7
Ribeiro, A.F., see Vainzof, M. (1588) 33
Riou, J.-P., see Boucher, P. (1588) 226
Roestenberg, P., see Schaaf, G J. (1588) 149
Rosmond, R , Bouchard, C. and Björntorp, P.
Lack of association between the uncoupling protein-2 Ala55Val gene polymorphism and phenotypic features of the Metabolic Syndrome (1588) 103
Ross, C.R., see Madhani, M. (1588) 232
Rueger, D.C., see Chubinskaya, S. (1588) 126

Sahilli, M., see Group, T.A.D.I.C.A.D.-I.C.S (1588) 71
Saijo, T , see Naito, E. (1588) 79
Saito, T , see Ohkawa, H. (1588) 217
Sakai, R., see Ohkawa, H (1588) 217
Sakura, N , see Kishikawa, M. (1588) 135
Sass, J.O , see Kishikawa, M. (1588) 135
Saunieres, A , see Perucca-Lostanlen, D. (1588) 210
Scarpa, M , see Daniele, A. (1588) 203
Schaaf, G.J , Nijmeijer, S.M., Maas, R F M., Roestenberg, P., De Groene, E.M. and Fink-Gremmels, J
The role of oxidative stress in the ochratoxin A-mediated toxicity in proximal tubular cells (1588) 149
Schneider, D., Kleeff, J., Berberat, P.O., Zhu, Z , Korc, M., Friess, H. and Büchler, M.W
Induction and expression of β*ig-h3* in pancreatic cancer cells (1588) 1
Serfling, E., see Kneitz, C (1588) 41
Sevillano, S , see Uruñuela, A (1588) 159
Shimizu, A., see Kishikawa, M. (1588) 135
Shoda, J., see Matsuzaki, Y (1588) 139
Silva, H.C.A., see Vainzof, M. (1588) 33
Simon, A., see Kneitz, C. (1588) 41
Skomorowski, M -A., see Bagshaw, R.D (1588) 247
Sohma, H , see Ohkawa, H. (1588) 217
Stefek, M , see Group, T.A D.I C A.D.-I.C.S. (1588) 71
Stibbe, C., see Kneitz, C. (1588) 41
Stolc, S , see Group, T.A D.I C.A.D.-I C S. (1588) 71
Stoppiglia, L.F, Nogueira, T.A , Leite, A.R., Carneiro, E.M. and Boschero, A.C.
Protective effect of D-glucose, L-leucine and fetal calf serum against oxidative stress in neonatal pancreatic islets (1588) 113
Sun, G., Yuen Chan, S., Yuan, Y., Wang Chan, K., Qiu, G., Sun, K. and Ping Leung, M.
Isolation of differentially expressed genes in human heart tissues (1588) 241
Sun, K., see Sun, G. (1588) 241
Suzuki, O.T., see Vainzof, M. (1588) 33
Swartz, H.M , see Madhani, M. (1588) 232

Takada, E., see Naito, E (1588) 79
Takeda, S , see Yamamoto, K (1588) 195
Tanaka, N., see Matsuzaki, Y (1588) 139
Taylor, R.W., see Perucca-Lostanlen, D. (1588) 210
Tengan, C.H., Ferreiro-Barros, C., Cardeal, M , Fireman, M A T , Oliveira, A.S.B., Kiyomoto, B.H. and Gabbai, A A
Frequency of duplications in the D-loop in patients with mitochondrial DNA deletions (1588) 65
Theocharis, A.D
Human colon adenocarcinoma is associated with specific post-translational modifications of versican and decorin (1588) 165
Toepoel, M., see Joosten, P H.L J (1588) 254
Tomanin, R., see Daniele, A. (1588) 203
Tony, H.-P., see Kneitz, C (1588) 41
Torroni, A , see Carelli, V. (1588) 7
Tsanaclis, A M., see Vainzof, M. (1588) 33
Turnbull, D M , see Perucca-Lostanlen, D. (1588) 210

Ugarte, M., see Clavero, S. (1588) 119
Ulusu, N.N., see Group, T A D.I C A D -I.C.S. (1588) 71
Uruñuela, A , Sevillano, S., De la Mano, A.M., Manso, M.A., Orfao, A. and De Dios, I.
Time-course of oxygen free radical production in acinar cells during acute pancreatitis induced by pancreatic duct obstruction (1588) 159

Vainzof, M., Moreira, E S , Suzuki, O T., Faulkner, G , Valle, G., Beggs, A H , Carpen, O., Ribeiro, A.F., Zanoteli, E., Gurgel-Giannetti, J , Tsanaclis, A M , Silva, H.C.A., Passos-Bueno, M.R. and Zatz, M.
Telethonin protein expression in neuromuscular disorders (1588) 33
Valentino, M L., see Carelli, V. (1588) 7
Valle, G., see Vainzof, M. (1588) 33
Vallier, P., see Boucher, P. (1588) 226
Van Oosterhout, D., see Joosten, P.H L.J (1588) 254
Van Zoelen, E J.J , see Joosten, P.H.L.J. (1588) 254
Varela-Rey, M., see Montiel-Duarte, C. (1588) 26
Vergani, L., see Carelli, V. (1588) 7
Vialettes, B., see Perucca-Lostanlen, D (1588) 210
Vidal, H., see Boucher, P. (1588) 226
Villani, G R D., see Daniele, A (1588) 203
Viswamitra, M.A., see Latha, K.S. (1588) 56

Walker, S.W., see Miller, S. (1588) 85
Wang Chan, K., see Sun, G. (1588) 241
Whelan, D , see Bagshaw, R.D (1588) 247

Xiao, Y , see Cheng, K. (1588) 48

Yamamoto, K , Yoshida, K , Miyagoe, Y., Ishikawa, A., Hanaoka, K., Nomoto, S , Kaneko, K., Ikeda, S.-i and Takeda, S.
Quantitative evaluation of expression of iron-metabolism genes in ceruloplasmin-deficient mice (1588) 195
Yokota, I., see Naito, E. (1588) 79
Yoshida, K., see Yamamoto, K. (1588) 195
Yoshida, S., see Matsuzaki, Y (1588) 139
Yoshioka, M., see Kishikawa, M. (1588) 135
Yuan, Y., see Sun, G (1588) 241
Yuen Chan, S , see Sun, G. (1588) 241

Zacchello, F., see Daniele, A. (1588) 203
Zampieron, C , see Carelli, V. (1588) 7
Zanoteli, E , see Vainzof, M. (1588) 33
Zatz, M., see Vainzof, M. (1588) 33
Zhang, S., see Bagshaw, R.D. (1588) 247
Zhu, Z., see Schneider, D. (1588) 1
Zimniak, P., see Cheng, K (1588) 48

ELSEVIER
Biochimica et Biophysica Acta 1588 (2002) 264–266
BIOCHIMICA ET BIOPHYSICA ACTA
BBA
www.bba-direct.com

Molecular Basis of Disease
Cumulative Contents

Regular papers

Induction and expression of *βig-h3* in pancreatic cancer cells
D. Schneider, J. Kleeff, P.O. Berberat, Z. Zhu, M. Korc, H. Friess and M.W. Büchler (Switzerland, Germany, USA) 1

Respiratory function in cybrid cell lines carrying European mtDNA haplogroups: implications for Leber's hereditary optic neuropathy
V. Carelli, L. Vergani, B. Bernazzi, C. Zampieron, L. Bucchi, M.L. Valentino, C. Rengo, A. Torroni and A. Martinuzzi (Italy) 7

Cholesterol crystallite nucleation in supersaturated model biles from a thermodynamic standpoint
C.-L. Liu and W.I. Higuchi (Taiwan, ROC, USA) 15

3,4-Methylenedioxymethamphetamine ("Ecstasy") induces apoptosis of cultured rat liver cells
C. Montiel-Duarte, M. Varela-Rey, J.A. Osés-Prieto, M.J. López-Zabalza, G. Beitia, E. Cenarruzabeitia and M.J. Iraburu (Spain) 26

Telethonin protein expression in neuromuscular disorders
M. Vainzof, E.S. Moreira, O.T. Suzuki, G. Faulkner, G. Valle, A.H. Beggs, O. Carpen, A.F. Ribeiro, E. Zanoteli, J. Gurgel-Gianneti, A.M. Tsanaclis, H.C.A. Silva, M.R. Passos-Bueno and M. Zatz (Brazil, Italy, USA, Finland) 33

The CD23b promoter is a target for NF-AT transcription factors in B-CLL cells
C. Kneitz, M. Goller, H.-P. Tony, A. Simon, C. Stibbe, T. König, E. Serfling and A. Avots (Germany) 41

Functional interaction of lithocholic acid conjugates with M3 muscarinic receptors on a human colon cancer cell line
K. Cheng, Y. Chen, P. Zimniak, J.-P. Raufman, Y. Xiao and H. Frucht (USA) 48

Molecular understanding of aluminum-induced topological changes in $(CCG)_{12}$ triplet repeats: relevance to neurological disorders
K.S. Latha, S. Anitha, K.S.J. Rao and M.A. Viswamitra (India) 56

Frequency of duplications in the D-loop in patients with mitochondrial DNA deletions
C.H. Tengan, C. Ferreiro-Barros, M. Cardeal, M.A.T. Fireman, A.S.B. Oliveira, B.H. Kiyomoto and A.A. Gabbai (Brazil) 65

In vivo treatment with stobadine prevents lipid peroxidation, protein glycation and calcium overload but does not ameliorate Ca^{2+}-ATPase activity in heart and liver of streptozotocin-diabetic rats: comparison with vitamin E
T.A.D.I.C.A.D.-I.C.S. Group, B. Pekiner, N.N. Ulusu, N. Das-Evcimen, M. Sahıllı, F. Aktan, M. Stefek, S. Stolc and Ç. Karasu (Turkey, Slovak Republic) 71

Thiamine-responsive pyruvate dehydrogenase deficiency in two patients caused by a point mutation (F205L and L216F) within the thiamine pyrophosphate binding region
E. Naito, M. Ito, I. Yokota, T. Saijo, J. Matsuda, Y. Ogawa, S. Kitamura, E. Takada, Y. Horii and Y. Kuroda (Japan) 79

Selenoprotein expression in endothelial cells from different human vasculature and species
S. Miller, S.W. Walker, J.R. Arthur, M.H. Lewin, K. Pickard, F. Nicol, A.F. Howie and G.J. Beckett (UK) 85

PII: S0925-4439(02)00207-7

Mitochondrial dysfunction is an early indicator of doxorubicin-induced apoptosis
P.S. Green and C. Leeuwenburgh (USA) 94

Lack of association between the uncoupling protein-2 Ala55Val gene polymorphism and phenotypic features of the Metabolic Syndrome
R. Rosmond, C. Bouchard and P. Björntorp (Sweden, USA) 103

Expression and functional analysis of rat P23, a gut hormone-inducible isoform of trypsin, reveals its resistance to proteinaceous trypsin inhibitors
S.-I. Fukuoka and C.M. Nyaruhucha (Japan) 106

Protective effect of D-glucose, L-leucine and fetal calf serum against oxidative stress in neonatal pancreatic islets
L.F. Stoppiglia, T.A. Nogueira, A.R. Leite, E.M. Carneiro and A.C. Boschero (Brazil) 113

Functional characterization of *PCCA* mutations causing propionic acidemia
S. Clavero, M.A. Martínez, B. Pérez, C. Pérez-Cerdá, M. Ugarte and L.R. Desviat (Spain) 119

Age-related changes in cartilage endogenous osteogenic protein-1 (OP-1)
S. Chubinskaya, B. Kumar, C. Merrihew, K. Heretis, D.C. Rueger and K.E. Kuettner (USA) 126

The peak height ratio of *S*-sulfonated transthyretin and other oxidized isoforms as a marker for molybdenum cofactor deficiency, measured by electrospray ionization mass spectrometry
M. Kishikawa, J.O. Sass, N. Sakura, T. Nakanishi, A. Shimizu and M. Yoshioka (Japan, Austria) 135

Selective inhibition of CYP27A1 and of chenodeoxycholic acid synthesis in cholestatic hamster liver
Y. Matsuzaki, B. Bouscarel, T. Ikegami, A. Honda, M. Doy, S. Ceryak, S. Fukushima, S. Yoshida, J. Shoda and N. Tanaka (Japan, USA) 139

The role of oxidative stress in the ochratoxin A-mediated toxicity in proximal tubular cells
G.J. Schaaf, S.M. Nijmeijer, R.F.M. Maas, P. Roestenberg, E.M. De Groene and J. Fink-Gremmels (The Netherlands) 149

Time-course of oxygen free radical production in acinar cells during acute pancreatitis induced by pancreatic duct obstruction
A. Uruñuela, S. Sevillano, A.M. De la Mano, M.A. Manso, A. Orfao and I. De Dios (Spain) 159

Human colon adenocarcinoma is associated with specific post-translational modifications of versican and decorin
A.D. Theocharis (Greece) 165

Effect of imipramine on 1-methyl-4-phenylpyridinium ion-induced hydroxyl radical generation in rat striatum
T. Obata and T. Egashira (Japan) 173

Differential expression of protein kinase C isoenzymes related to high nitric oxide synthase activity in a T lymphoma cell line
G. Gorelik, M.L. Barreiro Arcos, A.J. Klecha and G.A. Cremaschi (Argentina) 179

Correction of the copper transport defect of Menkes patient fibroblasts by expression of two forms of the sheep Wilson ATPase
P.J. Lockhart, S. La Fontaine, S.D. Firth, M. Greenough, J. Camakaris and J.F.B. Mercer (Australia) 189

Quantitative evaluation of expression of iron-metabolism genes in ceruloplasmin-deficient mice
K. Yamamoto, K. Yoshida, Y. Miyagoe, A. Ishikawa, K. Hanaoka, S. Nomoto, K. Kaneko, S.-i. Ikeda and S. Takeda (Japan) 195

Uptake of recombinant iduronate-2-sulfatase into neuronal and glial cells in vitro
A. Daniele, R. Tomanin, G.R.D. Villani, F. Zacchello, M. Scarpa and P. Di Natale (Italy) 203

Molecular and functional effects of the T14709C point mutation in the mitochondrial DNA of a patient with maternally inherited diabetes and deafness
D. Perucca-Lostanlen, R.W. Taylor, H. Narbonne, B. Mousson de Camaret, C.M. Hayes, A. Saunieres, V. Paquis-Flucklinger, D.M. Turnbull, B. Vialettes and C. Desnuelle (France, UK) 210

Ethanol-induced augmentation of annexin IV in cultured cells and the enhancement of cytotoxicity by overexpression of annexin IV by ethanol
H. Ohkawa, H. Sohma, R. Sakai, Y. Kuroki, E. Hashimoto, S. Murakami and T. Saito (Japan) 217

Expression and regulation by insulin of low-density lipoprotein receptor-related protein mRNA in human skeletal muscle
P. Boucher, P.-H. Ducluzeau, P. Davelu, F. Andreelli, P. Vallier, J.-P. Riou, M. Laville and H. Vidal (France) 226

Antibacterial peptide PR-39 affects local nitric oxide and preserves tissue oxygenation in the liver during septic shock
M. Madhani, A. Barchowsky, L. Klei, C.R. Ross, S.K. Jackson, H.M. Swartz and P.E. James (UK, USA) 232

Isolation of differentially expressed genes in human heart tissues
G. Sun, S. Yuen Chan, Y. Yuan, K. Wang Chan, G. Qiu, K. Sun and M. Ping Leung (PR China) 241

Novel mutations (Asn 484 Lys, Thr 500 Ala, Gly 438 Glu) in Morquio B disease
R.D. Bagshaw, S. Zhang, A. Hinek, M.-A. Skomorowski, D. Whelan, J.T.R. Clarke and J.W. Callahan (Canada) 247

A regulating element essential for PDGFRA transcription is recognized by neural tube defect-associated PRX homeobox transcription factors
P.H.L.J. Joosten, M. Toepoel, D. van Oosterhout, G.B. Afink and E.J.J. van Zoelen (The Netherlands, Sweden) 254

Author Index 261

Cumulative Contents 264

Information for Contributors can be found in http://www.bba-direct.com

This journal is in the *ADONIS Service*, whereby copies of individual articles can be printed out from CD-ROM on request. An explanatory leaflet can be obtained by writing to: ADONIS B V., P.O. Box 993, 1000 AZ Amsterdam, The Netherlands. Or you can contact ADONIS by e-mail : info@adonis.nl or visit the website at www adonis.nl

OASIS: **O**n-line **A**rticle **S**tatus **I**nformation **S**ystem **(http://www.elsevier.com/oasis)**
Authors of articles which are currently in production at Elsevier can obtain the following information on the status of their article:

- general production status (in preparation, in proof, in issue)
- date of publication and offprints dispatch date
- issue, volume and page numbers

This journal is a part of **ContentsDirect**, the *free* alerting service which sends tables of contents by e-mail for Elsevier Science books and journals. You can register for **ContentsDirect** online at: **http://contentsdirect.elsevier.com**

BIOCHIMICA ET BIOPHYSICA ACTA
MOLECULAR BASIS OF DISEASE

VOL. 1588 NO. 3 12 DECEMBER 2002

(Abstracted/indexed in Biological Abstracts - Chemical Abstract - Current Contents / Life Sciences - EMBASE/Excerpta Medica - Index Chemicus - Index Medicus / MEDLINE - Science Citation Index - Sociedad Iberoamericana de Información Científica (SIIC) Data Bases)

CONTENTS

Regular papers

Quantitative evaluation of expression of iron-metabolism genes in ceruloplasmin-deficient mice
K. Yamamoto, K. Yoshida, Y. Miyagoe, A. Ishikawa, K. Hanaoka, S. Nomoto, K. Kaneko, S.-i. Ikeda and S. Takeda (Japan) 195

Uptake of recombinant iduronate-2-sulfatase into neuronal and glial cells in vitro
A. Daniele, R. Tomanin, G.R.D. Villani, F. Zacchello, M. Scarpa and P. Di Natale (Italy) 203

Molecular and functional effects of the T14709C point mutation in the mitochondrial DNA of a patient with maternally inherited diabetes and deafness
D. Perucca-Lostanlen, R.W. Taylor, H. Narbonne, B. Mousson de Camaret, C.M. Hayes, A. Saunieres, V. Paquis-Flucklinger, D.M. Turnbull, B. Vialettes and C. Desnuelle (France, UK) 210

Ethanol-induced augmentation of annexin IV in cultured cells and the enhancement of cytotoxicity by overexpression of annexin IV by ethanol
H. Ohkawa, H. Sohma, R. Sakai, Y. Kuroki, E. Hashimoto, S. Murakami and T. Saito (Japan) 217

Expression and regulation by insulin of low-density lipoprotein receptor-related protein mRNA in human skeletal muscle
P. Boucher, P.-H. Ducluzeau, P. Davelu, F. Andreelli, P. Vallier, J.-P. Riou, M. Laville and H. Vidal (France) 226

Antibacterial peptide PR-39 affects local nitric oxide and preserves tissue oxygenation in the liver during septic shock
M. Madhani, A. Barchowsky, L. Klei, C.R. Ross, S.K. Jackson, H.M. Swartz and P.E. James (UK, USA) 232

Isolation of differentially expressed genes in human heart tissues
G. Sun, S. Yuen Chan, Y. Yuan, K. Wang Chan, G. Qiu, K. Sun and M. Ping Leung (PR China) 241

Novel mutations (Asn 484 Lys, Thr 500 Ala, Gly 438 Glu) in Morquio B disease
R.D. Bagshaw, S. Zhang, A. Hinek, M.-A. Skomorowski, D. Whelan, J.T.R. Clarke and J.W. Callahan (Canada) 247

A regulating element essential for PDGFRA transcription is recognized by neural tube defect-associated PRX homeobox transcription factors
P.H.L.J. Joosten, M. Toepoel, D. van Oosterhout, G.B. Afink and E.J.J. van Zoelen (The Netherlands, Sweden) 254

Author Index 261

Cumulative Contents 264

Also available on
SCIENCE DIRECT®
www.sciencedirect.com

ALSO AVAILABLE ONLINE:

http://www.bba-direct.com

0925-4439(20021212)1588:3;1-I